生体膜糖鎖異常に起因する
生活習慣病発症機序の解明と臨床への応用

平成 24 年度～平成 28 年度
私立大学戦略的研究基盤形成支援事業
研究成果報告書

平成 29 年 5 月

学校法人名　東北医科薬科大学
大　学　名　東北医科薬科大学
研究組織名　分子生体膜研究所
研究代表者　井ノ口　仁一
（分子生体膜研究所　所長・教授）

－ 目次 －

平成２４年度～２８年度「私立大学戦略的研究基盤形成支援事業」（附属分子生体膜研究所）研究成果報告書発刊にあたって

研究代表者　井ノ口　仁一

本研究プロジェクト「生体膜糖鎖異常に起因する生活習慣病発症機序の解明と臨床への応用」は、平成２２年度までの文部科学省私立大学学術研究高度化推進事業（学術フロンティア推進事業）「生体膜の糖鎖機能と疾患に関する薬学的研究」の後継事業として発足いたしました。この間、レクチンや糖鎖認識受容体を用いた糖鎖情報の解析の基盤技術の確立と疾患に関連している糖鎖機能の解析を推進し、我が国の糖鎖生物学研究の拠点としての研究実績を築いてきました。この研究過程で、 がん、２型糖尿病、アレルギー疾患、難聴あるいは神経疾患などの様々な病態への糖タンパク質および糖脂質などの複合糖質の関与を独自のアプローチで見出してきました。これらの研究成果の発展を期して、機能病態分子、分子認識、がん糖鎖制御、生体膜情報および細胞制御の５部門で構成される分子生体膜研究所は、１） 肥満・糖尿病・アレルギーなどに対する疾患横断的な診断・治療法の開発、２）がん細胞膜糖鎖異常とその制御に基づく診断・治療法の開発の２つのテーマを中心に推進し、多くの研究成果を挙げることができました。

平成２８年度、本学に医学部が設置され、医療系総合大学としての包括的臨床研究へのアプローチが可能になりました。今後、本学の糖鎖生命科学の研究成果の橋渡し研究を医薬融合により推進し、独創的アプローチにより健康寿命の増進を達成することを目指してまいります。

（様式 2）

法人番号	041004
プロジェクト番号	S1201031

平成24年度～平成28年度「私立大学戦略的研究基盤形成支援事業」
研究成果報告書概要

1 学校法人名 東北医科薬科大学 2 大学名 東北医科薬科大学

3 研究組織名 東北医科薬科大学附属分子生体膜研究所

4 プロジェクト所在地 宮城県仙台市青葉区小松島 4 丁目 4 番 1 号

5 研究プロジェクト名 生体膜糖鎖異常に起因する生活習慣病発症機序の解明と臨床への応用

6 研究観点 研究拠点を形成する研究

7 研究代表者

研究代表者名	所属部局名	職名
井ノ口 仁一	分子生体膜研究所・ 機能病態分子学教室	所長・教授

8 プロジェクト参加研究者数 14 名

9 該当審査区分 理工・情報 (生物・医歯) 人文・社会

10 研究プロジェクトに参加する主な研究者

研究者名	所属・職名	プロジェクトでの研究課題	プロジェクトでの役割
箱守 仙一郎	University of Washington 分子生体膜研究所・ 顧問	生体膜糖鎖機能と疾患に関する統合的解析	生体膜糖鎖機能と疾患研究に関するコンサルタント
井ノ口 仁一	分子生体膜研究所・ 機能病態分子学教室・ 教授	肥満･糖尿病･ｱﾚﾙｷﾞｰなどに対する疾患横断的な診断･治療法の開発	ガングリオシドの病態生理学的意義の解明および本研究プロジェクトの統括
東 秀好	分子生体膜研究所・ 生体膜情報学教室・ 教授	肥満･糖尿病･ｱﾚﾙｷﾞｰなどに対する疾患横断的な診断･治療法の開発	肥満関連GPCRの制御による生活習慣病の治療基盤
顧 建国	分子生体膜研究所・ 細胞制御学教室・ 教授	がん細胞膜糖鎖異常とその制御に基づく診断・治療法の開発	がんにおけるN-型糖鎖の機能解明
細野 雅祐	分子生体膜研究所・ 分子認識学教室・ 教授	がん細胞膜糖鎖異常とその制御に基づく診断・治療法の開発	レクチンを用いたがんの治療基盤
宮城 妙子	分子生体膜研究所・ がん糖鎖制御学教室・ 教授	がん細胞膜糖鎖異常とその制御に基づく診断・治療法の開発	シアリダーゼを標的とするがん創薬の実現
鈴木 明身	東北医科薬科大学 客員教授	肥満･糖尿病･ｱﾚﾙｷﾞｰなどに対する疾患横断的な診断･治療法の開発	生活習慣病発症におけるGPCR の構造解析
（共同研究機関等）			

（様式 2）

法人番号	041004
プロジェクト番号	S1201031

矢冨　裕	東京大学大学院医学系研究科・病態診断医学講座・教授	生活習慣病や免疫･ｱﾚﾙｷﾞｰ疾患などに対する新たな疾病横断的な診断	スフィンゴ糖脂質関連新規診断マーカーの開発
平林　義雄	理化学研究所脳科学総合研究センター・チームリーダー	肥満関連 GPCR の機能解析	肥満の機構解明
岩渕　和也	順天堂大学環境医学研究所・教授	マイクロドメイン機能解析	T細胞免疫シナプスにおけるスフィンゴ糖脂質の機能解明
袖岡　幹子	理化学研究所・主任研究員	がん細胞膜糖鎖異常とその制御に基づく診断・治療法の開発	がんで異常亢進するシアリダーゼの阻害剤創製
斎藤　誠一	琉球大学医学部・教授	がん細胞膜糖鎖異常とその制御に基づく診断・治療法の開発	糖鎖を標的とするがん診断マーカーの開発

＜研究者の変更状況（研究代表者を含む）＞

旧

ﾌﾟﾛｼﾞｪｸﾄでの研究課題	所属・職名	研究者氏名	プロジェクトでの役割
がん細胞膜糖鎖異常とその制御に基づく診断・治療法の開	分子生体膜研究所・分子認識学教室・教授	仁田　一雄	レクチンを用いたがんの治療基盤

（変更の時期：平成 26 年 4 月 1 日）

新

変更前の所属・職名	変更（就任）後の所属・職名	研究者氏名	プロジェクトでの役割
分子生体膜研究所 分子認識学教室・准教授	分子生体膜研究所 分子認識学教室・教授	細野　雅祐	レクチンを用いたがんの治療基盤

旧

ﾌﾟﾛｼﾞｪｸﾄでの研究課題	所属・職名	研究者氏名	プロジェクトでの役割
がん細胞膜糖鎖異常とその制御に基づく診断・治療法の開	分子生体膜研究所・がん糖鎖制御学教室・教授	宮城　妙子	シアリダーゼを標的とするがん創薬の実現

（変更の時期：平成 27 年 4 月 1 日）

新

変更前の所属・職名	変更（就任）後の所属・職名	研究者氏名	プロジェクトでの役割
東海大学糖鎖科学研究所 所長	東北医科薬科大学 客員教授	鈴木　明身	生活習慣病発症における GPCR の構造解析

＜研究者の追加状況＞

（追加の時期：平成25年4月1日）

ﾌﾟﾛｼﾞｪｸﾄでの研究課題	所属・職名	研究者氏名	プロジェクトでの役割
肥満･糖尿病･ｱﾚﾙｷﾞｰなどに対する疾患横断的な診断･治療法の開発	分子生体膜研究所・機能病態分子教室・准教授	稲森　啓一郎	視床下部摂食中枢に於けるスフィンゴ糖脂質の機能解明

法人番号	041004
プロジェクト番号	S1201031

11 研究の概要（※ 項目全体を10枚以内で作成）

（1）研究プロジェクトの目的・意義及び計画の概要

東北医科薬科大学附属分子生体膜研究所が発足した平成18年から5年間、文部科学省私立大学学術研究高度化推進事業（学術フロンティア推進事業）に選定され、「生体膜の糖鎖機能と疾患に関する薬学的研究」をテーマとしてレクチンや糖鎖認識受容体を用いた糖鎖情報の解析の基盤技術の確立と疾患に関連している糖鎖機能の解析を推進し、 我が国の糖鎖生物学研究の拠点としての研究実績を築いてきた。この研究過程で、 がん、 2型糖尿病、 アレルギー疾患、難聴あるいは神経疾患などの様々な病態への糖タンパク質および糖脂質などの複合糖質の関与を独自のアプローチで見出してきている。これらの研究成果の発展を期して、 分子生体膜研究所に結集した研究者の総合力を活した「生体膜糖鎖異常に起因する生活習慣病発症機序の解明と臨床への応用」に関する研究を計画した。機能病態分子、分子認識、がん糖鎖制御、生体膜情報および細胞制御の5部門で構成される分子生体膜研究所は、教育研究棟の同一フロアに集合しており、効率的共同研究によるプロジェクトの推進が可能である。また、生体膜複合糖質の生理的・病態的意義の解明を基盤とした臨床応用研究に向けて、包括的アプローチが可能な体制を備えている。本プロジェクトでは、現在までの研究成果をもとに、臨床応用の可能性が高い2つのテーマを中心に推進する。

1） 肥満・糖尿病・アレルギーなどに対する疾患横断的な診断・治療法の開発
2） がん細胞膜糖鎖異常とその制御に基づく診断・治療法の開発

研究テーマ1）肥満・糖尿病・アレルギーに対する疾患横断的な診断・治療法の開発

ガングリオシドはシアル酸を有する酸性スフィンゴ糖脂質の一群であり，トランスメンブランシグナリングの要である細胞膜マイクロドメイン（ラフト）の主要な構成成分である。炎症刺激を受けたリンパ球や肥満脂肪細胞では，細胞膜のガングリオシドレベルの持続的な上昇に基づくラフト構造のリモデリングによって、様々な生活習慣病の病態が惹起されることが以下に述べる事実から明らかになりつつある。特記すべき予備的知見として、井ノ口らは、1）高脂肪食（HFD）を負荷したガングリオシド GM3 合成酵素（GM3S）KO マウスの内臓脂肪組織は、抗炎症状態になっていること。2）GM3S KO を apoE KO と交配させることにより二重 KO マウスでは、血中のコレステロール値は apoE KO マウスの半分に、トリアシルグリセロール値は正常レベルであった。3）血清 GM3 レベルは，肥満による内臓脂肪蓄積に伴う慢性炎症状態を包括的かつ的確に捉える新たな病態マーカーである可能性があること。4）T 細胞サブセットごとに、その機能発現に必要なガングリオシド分子種が異なること。などを見いだしつつあり、これらの研究を推進させることで、スフィンゴ糖脂質および関連代謝産物の生体恒常性維持およびその破綻による病態発症機序を解明し、「マイクロドメイン病」の新たな病態概念と「マイクロドメイン矯正療法」の治療基盤を確立する。また、東らは、グルコース代謝に関与すると考えられる，脳に偏在する GPCR（GPRC5B）について，ノックアウトマウスを作製した[Sano et al., BBRC 2011]。このマウスは，野生型より小型で脂肪の蓄積が少なくエネルギー代謝が盛んであると考えられる形質を示した。最近、ヒトの BMI 値とこの GPCR 遺伝子のコピー数多型が相関している報告がなされ、マウスでの知見とヒトでの知見が合致するとともに、GPRC5B のハエのオルソログである BOSS をノックアウトした個体は小型でエネルギー源貯蔵能が極端に劣るという事実によって、この GPCR の生活習慣病発症における病態生理学的意義の解明を推進する。

研究テーマ2） がん細胞膜糖鎖異常とその制御に基づく診断・治療法の開発

糖鎖は生体において、タンパク質と結合した糖タンパク質あるいは脂質と結合した糖脂質という複合糖質の形で存在する。生命現象の基本である分子間相互作用の実態は、糖鎖付加やリン酸化などの翻訳後修飾を受けた機能分子が働いており，これらの修飾による微細な分子構造の変化が、シグナルの質と量を大きく転換する場合が多い。がん化すると生体膜糖鎖の異常が起こる。特に、重要な生理機能を持つ糖鎖分子のシアル酸異常は、がんの浸潤や転移などの悪性形質に関わっているといわれてきた。しかし、その実体についてはいまだ不明な点が多い。この機構や意義の解明を目的として、N-型糖鎖、シアル酸を脱離するシアリダーゼおよびシアル酸結合レクチン（SBL）に着目して研究を進めてきた。その結果，これまで対象としてきた接着分子インテグリンの N-型糖鎖、シアリダーゼおよびレクチンは、がんの悪性形質に深く関与しており、特に、がんの浸潤・転移あるいはがんの細胞死を制御していることがわかってきた。これらの解析を通じて、がんにおける糖鎖異常機構を解明し，創薬基盤の確立を目指す。具体的には、以下の項目を検討する。

① 細胞接着、上皮-間葉転換（EMT）および Wnt シグナルにおける N-型糖鎖、シアリダーゼ発現の意義と制御機構の解明および SBL の機能解析
② インテグリン糖鎖の機能解析と膜上の超分子複合体形成における糖鎖の役割に関する解析
③ 糖鎖によるがん細胞の複合体形成のダイナミズムの制御に関する解析、特に、炎症およびがんの浸潤・転

法人番号	041004
プロジェクト番号	S1201031

移の微小環境における糖鎖の生合成と複合体の形成との相関に関する研究
④ 実験動物を用いて、それらの糖鎖のがんの浸潤・転移過程における役割を解明すると共に、この結果に基づく新たな治療薬や診断薬基盤の開発

（2）研究組織

研究代表者（分子生体膜研究所 所長 機能病態分子部門教授）井ノ口は、２つの研究テーマを統括し、プロジェクト全体の推進をオーガナイズする。研究支援体制は、学内では中央機器室、実験動物センター、RI センターなどを恒常的に利用しており、それぞれの施設の設備・機器および人員を有効に利用している。共同研究機関として東京大学、理化学研究所、順天堂大学などと緊密な連絡を保ち、プロジェクトの推進に寄与している。

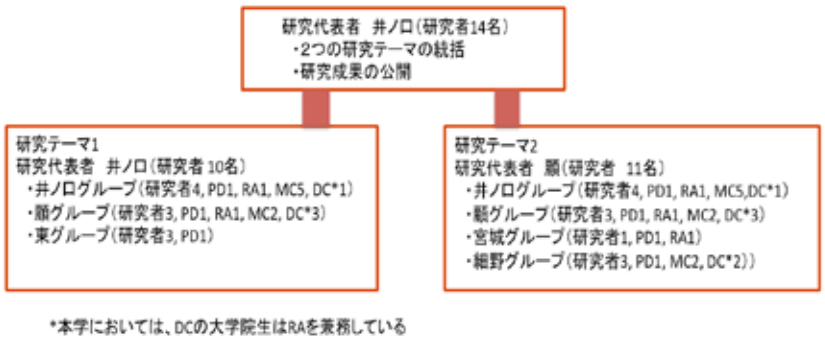

（3）研究施設・設備等

	名称	場所	面積	使用者
研究施設	東北医科薬科大学 附属分子生体膜研究所	東北医科薬科大学 教育研究棟 5 階	1,020 ㎡	37 名

	名称	主な使用目的	利用時間
主な研究装置	Imaging Flow Cytometry (Image Stream X)	多角的な細胞内、細胞間のフローサイトメトリーイメージング	473
主な研究設備	Proteon XPR36 システム	分子間相互作用解析	288
	高速液体クロマトグラフシステム	複合糖質分離分析	10,580
	安定同位体比測定装置	糖・脂質代謝測定	176

（4）研究成果の概要　※下記、13及び14に対応する成果には下線及び＊を付すこと。

－研究成果の概要－

研究テーマ1）肥満・糖尿病・アレルギーなどに対する疾患横断的な診断・治療法の開発
機能病態分子学部門：「炎症性シグナルによる持続的なガングリオシドの発現上昇は，内臓脂肪のインスリン抵抗性や視床下部の摂食中枢機能異常を誘発することにより、全身のメタボリックシンドローム関連病態を悪化させ、さらには、喘息などのアレルギー病態を惹起させる主要因である」という作業仮説および病態概念の確立のための実験的証明が得られつつある。

生体膜情報部門：転写、翻訳等を通じて、細胞環境に応じた細胞のサイズ、分裂、生存などの調節に中心的な役割を果たす mTOR の活性化の新しい経路を見出した。肥満関連 GPCR である GPRC5B がその経路の入口にあり、グルコース枯渇条件においても ATP を消費し、動物細胞を増殖に導いた。GPRC5B の反応では、通常の細胞増殖因子の細胞増殖シグナルと異なり PI3K や Akt は関与せずに、mTOR を活性化した。この際、Gα q が共役していた。GPRC5B は他の GPCR と共役して機能している可能性がある。一方、GPRC5B と同じ Family に属する mGluR2 はガングリオシドによって活性が調節され、その作用部位は特定の塩基性アミノ酸残基を含む領域であることを見出した。

法人番号	041004
プロジェクト番号	S1201031

研究テーマ2） がん細胞膜糖鎖異常とその制御に基づく診断・治療法の開発

がん糖鎖制御学部門：がんで異常に亢進するシアリダーゼ NEU3 は、悪性形質を増強するだけではなく、Wnt や EGFR シグナルを活性化し、がん化能にも深く関与することが明らかになった。この NEU3 を標的とするがん創薬をめざして、抗体医薬の作成や低分子阻害剤の探索を行っている。また、NEU4 の NCAM ポリシアル酸水解活性を見出した。

細胞制御学部門： TGFβ 誘導した上皮−間葉転換(EMT)では,がん転移抑制に働く糖転移酵素 GnT−III の発現が低下することに対して、がん転移促進に働く GnT−V 及び ST6Gal1 が誘導された。また、がん遺伝子 GOLPH3 の発現は細胞表面のシアリル化糖鎖変化を通じてがん細胞の浸潤や悪性度に関与することが明らかとなった）。一方、α 1,6 フコース糖鎖は細胞膜上のアクチビン受容体の複合体の形成に重要で,細胞内のシグナル伝達を制御する(FASEB J, 2013)。野生型に比べα 1,6 フコースの欠損マウスの化学物質による肝がん誘発が著しく抑制されることを見出した。

分子認識部門：ウシガエル卵シアル酸結合性レクチン（SBL）およびナマズ卵由来ラムノース結合性レクチン（SAL）のがん細胞に対する増殖抑制機構の解明に向けて研究を進めており，前者ではヒト白血病細胞において MAPK 系の，また後者ではバーキットリンパ腫細胞において ERK シグナル伝達系の活性化が関与している可能性を明らかにした。

－研究成果・達成度－

研究テーマ1）肥満・糖尿病・アレルギーなどに対する疾患横断的な診断・治療法の開発

機能病態分子学部門：**1)**CD4T細胞とCD8T細胞はTCR依存性の機能発現において異なるガングリオシド分子種の発現を要求することを見いだし、ガングリオシドを標的とした新たなアレルギー治療法を提唱した。*1 **2)** GM3合成酵素（GM3S）KO マウスに高脂肪食を与えると、野生型マウスと同様に肥満になるが、肥満に起因する内臓脂肪組織の慢性炎症が軽減し、インスリン抵抗性が改善した。 また、GM3の脂肪細胞分化と機能の恒常性維持を司る生理的制御因子としての働きを証明した。*2 **3)** GM3SKOとApoE KOのDKOマウスでは、血漿コレステロール値がApoE KOの約50%までに改善していた。*3 **4)**ヒト血清に存在する23種GM3分子種のうち、セラミド部分に極長鎖脂肪酸およびC2位が水酸化された脂肪酸を有する特定のGM3分子種に、BMI,空腹時血糖、TG、LDL，総コレステロール，HOMA−IRと有意な正の相関があり、あらたな病態マーカーの可能性を見いだした。*4 また、この水酸基を有するセラミドは細胞膜流動性を変化させ、ラフトの機能に影響をすることを見いだした。*5 **5)**GM3および関連代謝産物は視床下部の食欲中枢を制御している可能性を見いだした。従って、GM3および関連ガングリオシドの代謝系や免疫系などの生体の高次機能を統合する膜シグナル制御脂質としての意義が明らかになりつつある。*6

最近我々は、極長鎖飽和アシル鎖およびα 位の水酸化修飾をセラミド構造中に有するGM3分子種(C24:0, hC24:0)が、メタボリックシンドローム患者血清および糖尿病肥満モデルマウスの内臓脂肪組織で増加しており、さらにはマクロファージの活性化に際してTNF−α 、IL−6、IL−1β の産生を強力に促進する炎症惹起性GM3であることを見出した。この炎症促進は、リポ多糖(LPS)や炎症組織から放出されるHigh mobility group box 1 (HMGB1) などのTLR4リガンドの存在下でのみ惹起されることから、TLR4/MD2受容体の内因性リガンドとしてGM3分子種が機能する可能性を見出している。一方、メタボリックシンドローム患者血清で減少している短鎖アシル鎖長（C16,C18）または不飽和化GM3分子種は、抗炎症性GM3としてTLR4活性化を抑制することが判明した（論文作成中）。

生体膜情報部門：GPRC5B が ATP 代謝を調節していることを明らかにした。GPCR5B のほ乳類細胞系における機能発現系を見出した。*7 GPRC5B はリガンドが未解明であるが、同じ Family に属し 7 回膜貫通部分の相同性が高い mGluR2 の活性の制御にガングリオシドと特定の塩基性アミノ酸残基間の相互作用が関与していることを見出した。*8 これらの成果を利用して GPRC5B の ATP 代謝制御の分子機構を調べる系を構築できる。

GPRC5B は細胞増殖を亢進させ、特にエネルギー源であるグルコースが枯渇しても ATP を消費して増殖を継続させることを明らかにした。通常の細胞では受容体型チロシンキナーゼが PI3K, Akt を経て mTOR を活性化することで、細胞増殖に至り、グルコースが枯渇すると細胞増殖を停止する。GPCR5B は、Gα q と共役して別の経路から mTOR を活性化しており、この経路はグルコース枯渇の影響を受けなかった。ATP を過剰に消費するため AMP が増加し、AMP キナーゼが活性化していた。mTOR は転写、翻訳等を通じて、環境に応じた細胞のサイズ、分裂、生存などの調節に中心的な役割を果たすとされ、脂質合成を亢進させるなどの機能もある。実際、GPRC5B は、脂肪酸合成関連遺伝子を一括制御して脂肪酸、トリグリセリド合成に導く転写因子 SREBP−1c の誘導を促進した。これらの結果から、GPR5B の高発現が肥満に繋がることを説明できる。

法人番号	041004
プロジェクト番号	S1201031

研究テーマ2）がん細胞膜糖鎖異常とその制御に基づく診断・治療法の開発

がん糖鎖制御学部門：がんで異常に亢進する NEU3 は、ガングリオシドの修飾を介して、悪性形質を増強するだけではなく、Wnt や EGFR シグナルを活性化し、がん化能にも深く関わっていることが明らかになった。一方、がんで上昇する PLD1の産物であるホスファチジン酸によって活性化され、細胞表層への移行が増加するという NEU3 自身の活性化機構の一端を示す証拠も得られた。*9 また、このたび、NEU3 が担がん血清中にも検出されることがわかったので*10、診断マーカーとしての可能性を検討し、さらに、NEU3 を標的とするがん創薬をめざして、抗体医薬の試作や低分子阻害剤の探索を行っている。

分子認識学部門：26 年度までの研究計画に沿い、SBL のアポトーシス誘導機構を検討した。このプロセスにはミトコンドリア障害および小胞体ストレス系が関与していることが示唆されていた。SBL 処理 Jurkat 細胞において p38 や JNK の活性化が確認され、また小胞体分子シャペロンである Bip/GRP78 の発現上昇がみられる一方、この変化にカスパーゼ-9 は影響していないことから、両者はそれぞれ独立して作用していると推察された。*11 SAL の細胞増殖抑制機構に関して、細胞膜レセプターである Gb3 と協働する分子を探索している。新たに行った EMARS 解析より、Raji 細胞膜上では、Gb3 の近傍に膜型受容体 RYK および血管内皮細胞増殖因子受容体 VEGFR-3 の存在が示された。*12 また、Raji 細胞に対する増殖抑制作用（G1 arrest）には，ERK 活性化を介した p21 の発現上昇が重要な要因のひとつであることを明らかにした。さらに、SAL の作用機序として新たに膜結合型 TNF-α および TNFR-1 の発現上昇を介した NF-kB の核移行促進が観察され、細胞死を誘導しない SAL の作用機序の説明となり得る可能性がある。*13

1）Mass 解析により、がん細胞膜上の SBL レセプターがβ アクチンであることが分かった。*1 乳がん細胞における SBL の作用機序として、RNA 分解後 p38→caspase-3/7 の活性化によるアポトーシス誘導経路を明らかにした。*2 悪性中皮腫に対し、ペメトレキセドとの併用により相乗的効果が得られること、また SBL 自身は正常中皮腫細胞に対する毒性が低いことを明らかにした。*3 ヌードマウスを用いた実験で、生体に毒性を及ぼさない投与量で抗腫瘍効果が認められたことから、*in vivo* における有効性について検討を始めた。2）SAL の Burkitt’s リンパ腫 Raji 細胞に対する細胞増殖抑制作用は、Gb3 を介した MEK-ERK 経路の活性化によるものであることを示した。*4 HeLa 細胞において、SAL 処理によりスニチニブの取込み亢進および排出抑制による併用効果を認めた。*5 また SAL は、ヒトセミノーマ JKT-1 細胞に対しインテグリン類の発現上昇をきたし、糖鎖依存的な細胞接着を促進するという新しい知見を得た。*6 3）細胞内において、Gb3 がアポトーシス抑制因子の発現を負に制御することで抗がん剤感受性に影響を及ぼすことを見いだした。*7 また、新規のレクチン活性を検索するなかで、コケ類より糖酸結合性のタンパク質を単離した。*8

細胞制御学部門： 1） TGFβ 誘導した EMT では,がん転移抑制に働く GnT-III の発現が低下することに対して,がん転移促進に働く GnT-V が誘導され,細胞移動が促進された。*14 一方、酸性糖鎖である α 2,6 シアリル化糖鎖もその TGFβ 誘導した EMT において劇的に増加することを見出し、逆に α 2,6 シアリル化を抑制すると EMT が阻害される。*15 さらに、GnT-III のがん転移阻害活性は、細胞に発現する α 2,6 シアリル化のレベルに依存することと新たな作用機序を解明した。*18 3） がん遺伝子 GOLPH3 の発現は細胞表面の糖鎖変化を通じてがん細胞の浸潤性に関与していることが明らかとなった。*16 4)細胞接着分子インテグリン α5 に付加されている 14 カ所糖鎖の中に糖脂質や増殖因子受容体 EGFR と相互作用し，細胞増殖と細胞内シグナル伝達の制御に重要な糖鎖付加部位が特定された。*19, *20 また、インテグリン β1 の糖鎖付加による細胞形態と細胞内シグナルの制御に関わる膜近傍糖鎖の同定及び分子機序を解明した。*21, *22 5)化学誘導性肝がんの実験モデルマウスでは、野生型に比べ Fut8 欠損マウスの肝がん誘発が著しく抑制されることを見出した。コアフコース糖鎖が肝がんの形成に重要な役割を果たすことを証明した。*24 さらに、マウス肝臓の 70%切除モデルを用いて、肝再生においても Fut8 の発現が重要であることを明らかにした。*25 一方、 コアフコースは細胞膜上のアクチビン受容体や AMPA 型グルタミン酸受容体の複合体の形成に重要で、神経形成や長期記憶などに高次機能発現に重要であることを示した。*17, *23

＜優れた成果が上がった点＞

テーマ1）肥満・糖尿病・アレルギーなどに対する疾患横断的な診断・治療法の開発

機能病態分子学部門：我々はTNF-α 刺激によりインスリン抵抗性を獲得した脂肪細胞では、ガングリオシドGM3の発現が増加し、自らが開発したグルコシルセラミド生合成阻害剤（D-PDMP）でGM3の発現を抑制するとインスリン抵抗性が解除されることから、GM3発現制御による新たな糖尿病治療法の可能性を世界に先駆けて示した。この発見を契機として、慢性炎症性病態におけるGM3および関連ガングリオシドの発現異常は、メタボリックシンドロームにおけるインスリン抵抗性やレプチン抵抗性の発症、さらには、アレルギー・喘息・SLEなどにおけるヘルパーT細胞の活性亢進に関与していることを示しつつある。ヒト血清中の主要なガングリオシドはGM3であるが、そのセラミド部分のアシル基は炭素鎖長、2位（α 位）の水酸化および二重結合の有無から多様な分子種が存在している。最近我々は、極長鎖飽和アシル鎖およびα 位の水酸化修飾をセラミド構造中に有するGM3分子種(C24:0, hC24:0)が、メタボリックシンドローム患者血清および糖尿病肥満モデルマウスの内臓脂肪組織で増加しており、さらにはマクロファージの活性化に際してTNF- α、IL-6、IL-1 βの産生を強力に促進する炎症惹起性GM3であることを見出した。この炎症促進は、リポ多糖(LPS)や炎症組織から放出されるHigh mobility group box 1 (HMGB1) などのTLR4リガンドの存在下でのみ惹起されることから、TLR4/MD2受容体の内

法人番号	041004
プロジェクト番号	S1201031

因性リガンドとしてGM3分子種が機能する可能性を見出している。一方、メタボリックシンドローム患者血清で減少している短鎖アシル鎖長（C16,C18）または不飽和化GM3分子種は、抗炎症性GM3としてTLR4活性化を抑制することが判明した。これらの新知見から、「**メタボリックシンドロームなどの慢性炎症性疾患では、炎症惹起性GM3分子種の発現優位によって炎症増悪ループが形成され、自然免疫活性化、さらにはアレルギー性喘息、自己免疫疾患などの発症要因となる**」という新たな病態概念の創出が期待される。

生体膜情報部門： GPCR の class C に属する GPCR5B は、そのノックアウトマウスが小型で脂肪蓄積が少なく、ヒトにおいては BMI 値と遺伝子コピー数多型が相関しているため、エネルギー代謝に関与すると考えられる。ほ乳類の細胞レベルで、GPRC5B を強発現した細胞ではエネルギー源であるグルコースの供給が断たれても ATP を消費して細胞増殖を継続させることを見出した。GPRC5B は、タンパク質合成、脂肪酸合成などを亢進させることで細胞増殖を促進し、結果的に ATP の消費を増加させていた。ヒトの GPRC5B 遺伝子コピー数多型で肥満傾向を示すのは、この増殖シグナルによるものであると考えられる。また、ノックアウトマウスが小型であることは GPRC5B の増殖シグナルが停止したためだと考えられる。また、同じ GPCR の class に属しリガンドが既知であるの mGluR2 が、モデル分子として利用可能となった。

テーマ2）がん細胞膜糖鎖異常とその制御に基づく診断・治療法の開発

がん糖鎖制御学部門： NEU3 ががん幹細胞様形質の発現や、がんの発生や進展に深く関わっていること、NEU3 の発現抑制によって、がん細胞の足場非依存性や in vivo 造腫瘍能が著しく低下することがわかった。がん創薬の優れた標的と期待される。

分子認識学部門：SBL が，悪性中皮腫細胞（H28）に対して Tumor necrosis factor-related apoptosis inducing ligand（TRAIL）と相乗的に作用し、抗腫瘍作用を示すことを明らかにした。この併用効果は，ミトコンドリア異常 → caspase-9 → caspase-3 → caspase-8 → Bid 活性化が回路を形成し、シグナルの増幅をもってアポトーシス誘導に寄与するというメカニズムが推測できた。また、SAL においても同様に腎がん細胞 ACHN に対し、スニチニブとの併用による抗腫瘍作用の増強が確認され、Gb3 陽性がん細胞に対する応用が期待される。
SBL の悪性中皮腫に対する効果は、少なくとも *in vitro* において現在唯一用いられている薬物療法であるペメトレキセド＋シスプラチンの併用効果を凌駕するもので、正常細胞への毒性がより低く、かつ Pem 耐性細胞にも有効であることから、代替薬物としてがん治療への応用が期待できることを明らかにした。同様に SAL もバーキットリンパ腫や HeLa 細胞に対して細胞死を誘導せずに増殖を抑制しつつ、低分子抗腫瘍薬の作用増強させる併用効果を有することを示した。

細胞制御学部門： 1）糖鎖の発現誘導を介して、 細胞−細胞間接着と細胞−ECM 接着との間に cross-talk するという新しい仮説を提唱することができた。EMT において、α 2,6 シアリル化糖鎖が劇的に変化することを見出し、その機序と意義を解明した。2）これまでに不明であったがん遺伝子 GOLPH3 の働きは，シアリル化糖鎖変化を介してがん細胞の転移･浸潤を制御することが分かった。3）細胞接着分子インテグリン α 5β1 に付加されている 26 カ所糖鎖の中に細胞増殖と細胞運動に関わる各々糖鎖部位と糖鎖構造が明らかになった。4）コアフコースの発現が肝がんや肝細胞の増殖に機能的に寄与することを初めて示し,コアフコース糖鎖が肝がんの形成に重要な役割を果たすことを証明した。今後、コアフコースや α 2,6 シアル酸による標的分子の同定及びその機能制御を明らかにすると共に、新たながん治療法の開発に繋がることを目指す。

＜課題となった点＞

テーマ1）肥満・糖尿病・アレルギーなどに対する疾患横断的な診断・治療法の開発
機能病態分子学部門： GM3S阻害剤のスクリーニングを東京大学の化合物ライブラリーで実施したが、有望なリード化合物の同定には至らなかった。今後、天然物ライブラリーも視野にいれ、広範なスクリーニングを実施する予定である。

生体膜情報部門：GPRC5B によるATP 消費による増殖シグナルの亢進作用は、グルコース供給が減少した時に顕著に現れた。GPRC5B のリガンドはまだ不明のままである。グルコース濃度に応じた反応を示すが、これがリガンドであるとする決定的な証拠に欠ける。我々は、B2R と $P2Y_2R$ のようにいくつかの GPCR 分子間でシグナルクロストークが存在することを見出しており、GPRC5B もヒスタミン H1 受容体やアドレナリン β2 受容体と相互作用し、それらの活性に影響を与えるという実験結果を得ている。H1 受容体はそのノックアウトマウスが非活動的である等 GPRC5B ノックアウトマウスと形質の類似性が見られるので、この関係を精査したい。また、アドレナリン β 受容体のうち β3 が熱産生など基礎代謝に関与しているので、β3 についても相互作用があるか検討したい。 また、Glc の取り込みへの GPRC5B の効果は株化細胞では検出できなかったが、Glc 取り込みは個体レベルで制御されていると考えるのが妥当かも知れないので、GPRC5B ノックアウトマウスと野生型マウスの個体間の比較という形で行う。

法人番号	041004
プロジェクト番号	S1201031

テーマ2)がん細胞膜糖鎖異常とその制御に基づく診断・治療法の開発
がん糖鎖制御学部門： NEU3の特異的低分子阻害剤について、合成化合物ライブラリーのスクリーニングによる探索を進めてきたが、複数のSH化合物は得られたものの、現在のところ、特異的阻害活性を示す化合物はまだ見出されていない。天念物ライブラリー等についても探索中である。担がん血清に検出されるNEU3活性については、診断薬としての開発をめざし、病期や浸潤・転移等との関連性の解析を進めており、臨床科との更なる共同研究が必要である。

分子認識学部門：SBL に関しては、がん細胞選択性（正常細胞には作用しない）の要因となる標的分子あるいはそのメカニズムが未だ不明のままである。現在、UV クロスリンカーの原理を応用して細胞膜上の SBL 受容体（もしくは受容体関連分子）を特定する作業を行っている。この方法は、SBL で予測されているレセプターとの弱い結合に対して効力を発揮するもので、サブトラクト法により得られたバンドを Mass 解析して同定する予定である。また、この方法には一定量のリコンビナント SBL が必要であることから、高効率のタンパク質発現系（大腸菌による）も平行して検討している。一方、SAL においては、バーキットリンパ腫の増殖抑制機構において、p21 による細胞周期の制御と NF-kB による抗アポトーシス効果がどのようなバランスをもって機能しているかをつきとめる必要がある。特に TNF-α については，細胞死の誘導に関して異なる作用を有する分子であることから、選択的阻害剤などを利用してより詳細なシグナル伝達経路を明らかにする必要がある。
SBL および SAL ともに、ヒトにとって抗原となるべき異種タンパク質である。したがって、臨床への応用を考える場合、抗体産生あるいは分解酵素による無力化または生体への毒性が予測される。この点については、組換え変異体を作製するなどして構造活性相関を検討、または DDS による効率化を目指す。

細胞制御学部門：糖鎖による糖タンパク質の機能への影響を調べる際には、その特定な糖鎖発現量だけではなく、糖鎖付加部位の同定も大事である。そこで、遺伝子工学の手法を用いて特定な糖鎖付加の有無によるそのタンパク質の動態及び機能を調べ、糖鎖の機能を解析する。また、インテグリン複合体形成の解析には、インテグリンとの非特異的な結合分子を除去することが大事である。対策としては、界面活性剤と塩の濃度を細かくチェックし、適当な条件を見出し、最終的に生細胞の細胞膜上分子間相互作用で確認する。

＜評価体制＞

本プロジェクトの実施状況は、東北医科薬科大学自己評価委員会により、平成 26 年度（3 年度）終了時ならびに平成 28 年度（最終年度）終了時に、詳細な審査に基づき厳正な評価が実施された。また、この時期に研究所顧問の箱守博士、外部評価委員の谷口直之博士および柳澤勝彦博士に各プロジェクトに対する評価を依頼した。紙面の制限上、以下に評価の抜粋を載せた。

（箱守仙一郎顧問）免疫反応の担い手である T リンパ球の内、CD4T 細胞と CD8T 細胞の活性化に異なる種類のガングリシドが関与する事が解明された事は、これらのガングリシドの発現を制御する事により、アレルギー性疾患や自己免疫疾患を治療できる可能性があり、将来が期待される。グルコース代謝に関与し、脳に局在する GPCR5B の研究成果は、最近明らかになりつつある視床下部での摂食中枢機能異常との関連性が示唆され興味深く、更なる研究成果を期待したい。NEU3 ががんの転移や再発に深く関わるがん幹細胞に関与することが判り、がん治療の良い標的になるうることが示された。SBL や SAL のレクチンの抗腫瘍活性機構の解明が進んでいる将来、がん細胞膜表面のこれらレクチンと最初に結合する糖鎖分子の解明を期待したい。がん遺伝子 GOLPH3 の活性機構にシアル化糖鎖変化が関与する事、また Fut8 が肝がんの発生に関与することが見出された。上記の成果を基に実用化にむけての準備もされている。最後に、平成 24 年度より始まった本研究プロジェクトが、かなりの成果が得られている事を評価したいと思う。
（谷口直之外部評価委員）全体として、本プロジェクトのメンバーは国際的にも高い評価をうけている。私立大学としてこれほどの研究所を運営していることに敬意を表したい。分子生体膜研究所としてのホームページなどによる国際的な発信をさらに進めてほしい。
（柳澤勝彦外部評価委員）本プロジェクトにおいては、素晴らしい研究成果が多数あげられていることは高く評価できる。中間報告のこの時期に、以下の 2 点について検討を加えることにより、今後の発展がさらに確かなものになると考えられる。(1)創薬等の実用化への展開にあたっては、本プロジェクトチーム内の研究開発に留まることなく、関連企業との積極的な共同研究を見据た態勢構築を検討して頂きたい。(2)生体膜を介した、あるいは生体膜上での生物作用の解析を基盤としつつも、本プロジェクトの特徴である糖鎖を主軸とする「糖鎖生物学」あるいは「糖鎖病態学」の発展にさらに注力頂きたい。

＜研究期間終了後の展望＞

テーマ 1） 肥満・糖尿病・アレルギーなどに対する疾患横断的な診断・治療法の開発
機能病態分子学部門： 慢性炎症性シグナルによる持続的なスフィンゴ脂質の発現異常は、細胞膜マイクロドメイン（ラフト）構造のリモデリングに起因するシグナル異常により、細胞分化・増殖異常やインスリン抵抗性を誘発し、喘息などのアレルギー病態、メタボリックシンドローム、さらには腫瘍性疾患

法人番号	041004
プロジェクト番号	S1201031

を惹起させる証拠が蓄積されて来ている。本研究の目的は、「マイクロドメイン病」の新たな病態概念と「マイクロドメイン矯正療法」の治療基盤を確立することにある。従って、GM3発現を制御することによる、免疫・アレルギー疾患やメタボリックシンドロームなどの慢性炎症性疾患の新たな治療法開発を目指す。

生体膜情報部門：GPRC5B が ATP 代謝を制御する分子機構を mGluR2 で得られた結果を参考にして、細胞レベルで解明する。その成果を元に、GPCR5B のリガンドの解明に繋げるとともに、個体レベルでのエネルギー代謝制御を理解する実験系を組み立てる。GPRC5B がエネルギーを消費して細胞増殖を亢進する分子機構を他の GPCR との共役の可能性を踏まえて、細胞レベルで解明する。その成果を元に、GPCR5B のリガンドの解明に繋げるとともに、個体レベルでのエネルギー代謝制御を理解する実験系を組み立てる。

テーマ2）がん細胞膜糖鎖異常とその制御に基づく診断・治療法の開発
がん糖鎖制御学部門：（１）さらに、化合物ライブラリーのスクリーニングや合成化学研究者との共同研究を行い、NEU3を標的とするがん創薬を進め、実用化を目指す。（２）担がん血清におけるNEU3分子の同定とELISAによる定量法を構築する。（３）最も悪性度の高く、予後不良のグリオブラストーマにおけるNEU3やNEU4異常とその意義を解析し、適切な治療法開発への方策を探る。（４）シアリダーゼの機能解析を特に遺伝子改変動物を用いて進めた結果、NEU3はNEU4とともにガングリオシド分解の主要な酵素であることが検証された。今後、さらに詳細にその機構を解析、これらを標的とした創薬を目指す。

分子認識学部門：SBL および SAL いずれにおいても、抗腫瘍メカニズムをさらに詳細に明らかにしていく。また、抗腫瘍薬との併用効果について、現在行われている薬物治療スキーム（例えば、悪性中皮腫治療におけるペメトレキセドとシスプラチンとの併用療法など）と比較しつつ検討していく。同時に実用化に向けて *in vivo* における効果についても検討を開始する。
SBL および SAL ともに、がんの治療戦略への参加を企図するものであるが、次の段階として *in vivo* における有効性と安全性を確認する作業が必須である。現在、ヌードマウスを用いた xenograft 実験系の構築を行っており、腫瘍内投与による先行実験では、毒性を示さない濃度域で有意な抗腫瘍効果を確認している。細胞レベルで見られた併用投与の優位性を動物実験でも明らかにする必要がある。

細胞制御学部門：インテグリンの部位特異的な糖鎖構造を明らかにし、特定の糖鎖が細胞膜上で他の受容体との結合・シグナル伝達といった本質的な機能に関わるかを検討する。特に、がんの浸潤･転移などの悪性形質に関わっているシアル酸の発現に注目して解析する。具体的には以下のように検討して行く予定である。1）がん転移・浸潤と深く関わるインテグリン分子などの N 型糖鎖の改変による細胞膜面での受容体間の複合体の形成やその複合体を介したシグナル伝達機構の解明；2）細胞膜上におけるインテグリンを中心とする複合体の形成および機能制御に重要な糖鎖モジュール特定；3）分子間相互作用や相互認識による複合体形成における糖鎖による制御機構の解明；4）α1,6 フコース糖鎖の発現と肝がんおよび他の疾患との関連性解明。

＜研究成果の副次的効果＞

テーマ1）肥満・糖尿病・アレルギーなどに対する疾患横断的な診断・治療法の開発
機能病態分子学部門：本研究構想を実施する上で重要な知的財産であるが、３件の特許（1：ヘルパーT 細胞の選択的機能制御法、2：インスリン抵抗性病態を示す疾患の診断方法、３：高脂血症の治療剤のスクリーニング法、筆頭発明者：井ノ口仁一；　出願：JST）を取得している。これらの知的財産を戦略的に活用した研究を展開し、臨床応用への実質的な社会貢献を目指す。

生体膜情報部門：mGluR2 は細胞からのグルタミン酸の放出を抑制するフィードバック受容体として機能し、疼痛・痛覚過敏、癲癇、統合失調症等の制御を行っていると考えられ、その allosteric modulator が創薬の対象として注目されている。今回、ガングリオシドがこれの negative allosteric modulator としての作用を有することが解明されたので、ガングリオシドが創薬のシード化合物となる可能性が有る。PRC5B が他の GPCR とカップリングしてそれらのシグナルと協調あるいはそれらを制御している可能性が出てきた。そのうち、アドレナリンβ2 受容体は平滑筋の弛緩と糖代謝の活性化作用があり、ヒスタミン H1 受容体は脳において食欲抑制、覚醒の機能を有する。GPRC5B はこれらの情報伝達に直接あるいは間接的に関与していると考えられ、今後、アドレナリンやヒスタミンの作用を理解するためには除外できない分子となるかも知れない。

テーマ2）がん細胞膜糖鎖異常とその制御に基づく診断・治療法の開発
がん糖鎖制御学部門：進行中のNEU3の抗体医薬の試作や特異的阻害剤の探索に成功すれば、特許の申請や創薬開発の実用化へと進めることができる。

法人番号	041004
プロジェクト番号	S1201031

分子認識学部門：SAL 処理細胞において、細胞膜の破綻を伴わずにヨウ化プロピジウム（PI）の取込みが上昇するという現象を利用し、がん細胞の抗腫瘍薬に対する感受性を高められるのではないかと考え、SBL と同様に薬物との併用効果を検討したところ、スニチニブとの併用においてポジティブな結果が得られた。
SBL は、特に Pem 耐性の悪性中皮腫治療に代替薬としての利用できる可能性がある。また SAL は、Gb3 陽性がんに対する既存治療薬（スニチニブなど）の副作用軽減への応用（SAL）に関し、新たな治療戦略の開発に寄与できる。

細胞制御学部門：１）インテグリンの機能発現に必要な最小限の糖鎖付加部位および重要な糖鎖が特定されれば、その立体構造解明に寄与する。インテグリンの高次構造がわかれば、がん浸潤･転移の新医薬品の開発につながる。２）化学肝がん誘発実験では、野生型に比べて Fut8 欠損マウスの肝がん誘発率が著しく抑制されることから、肝がんの新規治療薬の開発に繋がる可能性がある。３）糖鎖の重要性が改めて他の分野の研究者に認識され、領域を超えた融合的な研究が促進される可能性がある。

１２ キーワード（当該研究内容をよく表していると思われるものを8項目以内で記載してください。）

（1） 複合糖質　（2） スフィンゴ糖脂質　（3） N−型糖鎖
（4） 動物レクチン　（5） 生活習慣病　（6） 細胞膜ラフト
（7） がん　（8） 細胞接着

１３ 研究発表の状況（研究論文等公表状況。印刷中も含む。）

上記、11(4)に記載した研究成果に対応するものには＊、本報告書に全文を掲載した主要論文は○で示す。

＜雑誌論文＞

研究テーマ 1）

1. *7 Regulation of ATP production by an obesity-related orphan receptor, GPRC5B, Kuroda, Y., Mitoma, J., Nakagawa, T., Higashi, H. 査読有　in preparation.
2. *8 Modulation by ganglioside of group II metabotropic glutamate receptor activity, Kuroda, Y., Igari, T., Nakagawa, T., Mitoma, J., Higashi, H. 査読有　in preparation.
3. *3 Gangliosides regulate intestinal NPC1L1-mediated cholesterol absorption. Nihei W, Hayamizu H,Odagiri　Y, Nagafuku M, and Inokuchi J.査読有 *Submitted.*
4. *6 Ganglioside GM3 regulates hypothalamic control of food intake by modulating melanocortin signaling. Inamori K, Imazu S, Nihei W, Yang Y, Ito H, Y, Veillon L, Go S, Nagafuku M, and Inokuchi J.査読有　*Submitted.*
5. Altered Expression of Ganglioside GM3 Molecular Species and a Potential Regulatory Role During Myoblast Differentiation. Go S, Veillon L, Ciampa M, Mauri L, Sato C, Kitajima K, Prinetti A, Sonnino S, Inokuchi J. J. Biol. Chem. In press
6. PDMP, a ceramide analogue, acts as an inhibitor of mTORC1 by inducing its translocation from lysosome to endoplasmic reticulum. Takashi O, Katarzyna A. Podyma-Inoue, Kazue T, Jin-ichi I, Toshihide K, Tetsuro W, Yuichi I, Miki Hara-Y. Experimental Cell Research VOL350,査読有 103–114. (2017)
7. ○ N-glycan-dependent cell-surface expression of the $P2Y_2$ receptor and N-glycan-independent distribution to lipid rafts, Nakagawa, T., Takahashi, C., Matsuzaki, H., Takeyama, S., Sato, S., Sato, A., Kuroda, Y., Higashi, H. Biochemical and Biophysical Research Communications 査読有,2017 485,427-31,2017
8. Targeting CERS6-dependent Metastasis-prone Phenotype in Lung Cancer Cells. Suzuki M, Cao K, Kato S, Komizu Y, Tanaka K, Togawa N, Arima C, Chee T-M, Yanagisawa K, Usami N, Taniguchi T, Yokoi K, Mizutani Y, Igarashi Y, Inokuchi J,Iwaki S, Fujii S, Ueoka R, Tamiya-Koizumi K, Murate T, Kyogashima M, Nakamura M, and Takahashi T.J. Clin. Invest. Vol. 126.査読有 254-265,2016
9. ○*2 Control of homeostatic and pathogenic balance in adipose tissue by ganglioside GM3. Nagafuku M, Sato T, Sato S, Shimizu K, Taira T, and Inokuchi J. Glucobiology 25　査読有 303-318,2015
10. ○*4 Identification of Ganglioside GM3 Molecular Species in Human Serum Associated with Risk Factors of Metabolic SyndromeVeillon L, Go S, Suzuki S, Tsuchiya K, Nishimura S, Nagasaki M, Yatomi Y, and Inokuchi J. PLoS ONE,査読有,DOI:10.1371/journal.pone.0129645,2015

法人番号	041004
プロジェクト番号	S1201031

11. *5 Distinct Selectivity of Gangliosides Required for CD4+ T and CD8+ T Cell Activation. Inokuchi J, Nagafuku M, Ohno I, and Suzuki A. Biochim. Biophys. Acta., 1851 査読有 98-106,2015
12. ○Close association of B2 bradykinin receptors with $P2Y_2$ ATP receptors, Yashima, S., Shimazaki, A.,Mitoma, J., Nakagawa, T., Abe, M., Yamada, H., Higashi, H., J. Biochem., 158 査読有 155-163,2015
13. Pain signaling and gangliosides, Watanabe, S., Higashi, H., Trend Glycosci. Glycotechnol. Vol. 27,査読有 37-45,2015
14. The regulation of ER export and Golgi retention of ST3Gal5 (GM3/GM4 synthase) and B4GalNAcT1 (GM2/GD2/GA2 synthase) by arginine/lysine-based motif adjacent to the transmembrane domain. Uemura S, Shishido F, Kashimura M, and Inokuchi J. Glycobiology 25 査読有 1410-1422,2015
15. ○Ganglioside GM3 is essential for the structural integrity and function of cochlear hair cells. Yoshikawa M, Go S, Suzuki S, Suzuki A, Morlet T, Strauss K, Fujiwara M, Iwasaki K, and Inokuchi J. Hum. Mol. Genet. Vol.24 査読有 2796-2807,2015
16. Membrane lipid therapy: Modulation of the cell membrane composition and structure as a molecular base for drug discovery and new disease treatment. Escribá PV, Busquets X, Inokuchi J, Balogh G, Török Z, Horváth I, Harwood JL, Vígh L. Prog. Lipid Res. Vol.59,2015
17. *1 GM3 and Diabetes. Inokuchi, J. *Glycoconj. J.* 査読有 31:193-197, 2014
18. Loss of hydroxyl groups from the ceramide moiety can modify the lateral diffusion of membrane proteins in Saccharomyces cerevisiae.Uemura S, Shisido F, Tani M, Mochizuki T, Abe F, and Inokuchi J. J. Lipid Res. 査読有 55:1343-1356, 2014
19. Functional mapping and implications of substrate specificity of the yeast high-affinity leucine permease Bap2.Usami Y, Uemura S, Michizuki T, Morita A, Sisido F, Inokuchi J, and Abe F. Biochim. Biophys. Acta 査読有 1838:1719-1729, 2014
20. ○Expression machinery of GM4: the excess amounts of GM3/GM4S synthase (ST3GAL5) are necessary for GM4 synthesis in mammalian cells. Uemura S, Go S, Shishido F, and Inokuchi J. Glycoconj. J. 査読有 31:101-108, 2014
21. *1 Heterogeneity of gangliosides among T cell. Inokuchi J, Nagafuku M, Ohno I. and Suzuki A. subsets. Cell. Mol. Life Sci. 査読有 70, 3067-75, 2013
22. *1 The Physiological Significance of Ganglioside Species Selectively Expressed on Individual T Cell Subsets. Nagafuku M, Inokuchi J. Trends in Glycoscience and Glycotechnology 査読有 25, 159-169, 2013
23. ○*1 CD4 and CD8 T cells require different membrane gangliosides for activation.Nagafuku M, Okuyama K., Onimaru Y., Suzuki A., Odagiri Y., Yamashita T., Iwasaki K., Fujiwara M.,Takayanagi M., Ohno I. and Inokuchi J. Proc. Natl. Acad. Sci. USA 査読有 109. E336-E342Author summary 109. 1832-1833, 2012
24. *2 Dissociation of the insulin receptor from caveolae during TNFa-induced insulin resistance and its recovery by D-PDMP. Sekimoto J., Kabayama K., Gohara K., and Inokuchi J. FEBS Lett. 査読有 586, 191-195, 2012
25. ○Involvement of ganglioside GT1b in glutamate release from neuroblastoma cells, Watanabe, S.,Higashi, H., Ogawa, H., Takamori, K., Iwabuchi, K. Neuroscience Letters,査読有, 517,140-3.2012
26. Sialidase NEU4 hydrolyzes polysialic acids of neural cell adhesion molecules and negatively regulates neurite formation by hippocampal neurons, Takahashi, K., Mitoma, J., Hosono, M.,Shiozaki, K., Sato, C., Yamaguchi, K., Kitajima, K., Higashi, H., Nitta, K., Shima, H., Miyagi, T. Journal of Biological Chemistry ,査読有,287,14816-26,2012
27. ○Gangliosides and chondroitin sulfate desensitize and internalize B2 bradykinin receptors,Shimazaki, A., Nakagawa,T.,Mitoma, J., Higashi, H. Biochemical and Biophysical Research Communications, 査読有,420,193-8,2012
28. ○Gangliosides stimulate bradykinin B2 receptors to promote calmodulin kinase II-mediated neuronal differentiation, Kanatsu,Y., Chen, N.H., Mitoma,J., Nakagawa,T., Hirabayashi,Y.,Higashi,H. Journal of Biochemistry (Tokyo) , 査読有,152,63-72, 2012

研究テーマ 2）

1. *12 Receptor tyrosine kinase is a candidate for lectin signaling mediator on Burkitt’s lymphoma Adachi Y., Sugawara S., Im C., Tatsuta T., Nitta K., Hosono M., 査読有, in preparation.
2. *13 Catfish roe lectin-induced cytostatic effect involves in ERK pathway on Burkitt’s lymphoma Raji cells. Sugawara S., Hosono M., Tatsuta T., Masuzaki H., Ozeki Y., Nitta K., 査読有, in preparation.

法人番号	041004
プロジェクト番号	S1201031

3. *3 Synergistic anti-tumor effect of cSBL and pemetrexed against malignant mesothelioma cell lines. Sato T., Tatsuta T., Sugawara S., Hara A., Hosono M., in preparation.
4. *1 Anti-tumor effect of sialic acid-binding lectin is mediated through binding cell surface β-actin. Tatsuta T., Sato T., Sugawara S., Hosono M., in preparation.
5. ○*4 Catfish rhamnose-binding lectin induces G0/1 cell cycle arrest in Burkitt's lymphoma cells via membrane surface Gb3. Sugawara S., Im C., Kawano T., Tatsuta T., Koide Y., Yamamoto D., Ozeki Y., Nitta K., Hosono M., *Glycoconj. J.*, 査読有, 34, 127-138, 2017
6. *5 Combination effect of catfish lectin and sunitinib against HeLa cells. Sugawara S., Takayanagi M., Im C., Tatsuta T., Hosono M., in preparation.
7. *6 The rhamnose-binding lectin increases expression of integrin a2 in human testicular seminoma cell line JKT-1. Sugawara S., Im C., Tatsuta T., Hosono M. in preparation.
8. *7 Cytosolic Gb3 involves apoptosis in HeLa cells. Im C., Sugawara S., Takayanagi M., Tatsuta T., Hosono M. in preparation.
9. *9 Sialidase NEU3 defines invasive potential of human glioblastoma cells by regulating calpain-mediated proteolysis of focal adhesion proteins. Takahashi K., Proshin S,, Yamaguchi K., Yamashita Y., Katakura R., Yamamoto K., Shima, H. Hosono M., and Miyagi T. *BBA General Subjects.* in revision
10. Neuraminidases 3 and 4 Regulate Neuronal Function by Catabolizing Brain Gangliosides. Pan X., De Britto C., De Aragão P., Morales C., Priestman D., Wu H., Takahashi K., Yamaguchi K., Sturiale L., Garozzo D., Platt F., Lamarche-Vane N., Miyagi T., Pshezhetsky AV .*The FASEB Journal* 査読有 in press
11. *8 Purification of two novel sugar acid-binding lectins from Haplomitrium Mnioides (bryophyte, Plantae) and their preliminary characterization. Masuzaki H., Hosono M., Nitta K., *Appl. Biochem. Biotechnol.*, 査読有, 181, 65-82, 2017.
12. A Novel Potent and Highly Specific Inhibitor against Influenza Viral N1-N9 Neuraminidases: Insight into Neuraminidase-Inhibitor Interactions. Sriwilaijaroen N., Magesh S., Imamura A., Ando H., Ishida H., Sakai M., Ishitsubo E., Hori T., Moriya S., Ishikawa T., Kuwata K., Odagiri T., Tashiro, M. Hiramatsu H., Tsukamoto K., Miyagi T., Tokiwa H., Kiso M., and Suzuki Y. *J Med Chem*. 59; 4415-5120, 2016 査読有
13. Positive regulation of myoblast differentiation by medaka Neu3b sialidase through gangliosides esialylation. Shiozaki K, Harasaki Y., Fukuda M., Yoshinaga A., Ryuzono S., Chigwechokha K.P., Komatsu M., Miyagi T. *Biochimie*. 2123:65-72, 2016.
14. *21 Distinct effects of β1 integrin on cell proliferation and cellular signaling in MDA-MB-231 breast cancer cells. Hou, S., Isaji, T., Hang, Q., Im, S., Fukuda, T. and Gu, J. *Sci. Rep.* 査読有 Doi: 10.1038/srep18430, 2016
15. *18 Expression of N-acetylglucosaminyltransferase III suppresses α2,3 sialylation and its distinctive functions in cell migration are attributed to α2,6 sialylation levels. Lu, J., Isaji, T., Im, S., Fukuda, T., Kameyama, A. and Gu, J. *J. Biol. Chem.* 査読有 291, 5708-20, 2016
16. Transforming growth factor (TGF) β1 acted through miR-130b to increase integrin α5 to promote migration of colorectal cancer cells. Yi R., Li Y., Wang F., Gu J., Isaji T., Li J., Qi R., Zhu X. and Zhao Y. *Tumour Biol.* 査読有 37, 10763-73, 2016
17. ○*22 Importance of membrane-proximal N-glycosylation on integrin β1 in its activation and complex formation.Hou, S., Hang, Q., Isaji, T., Lu, J., Fukuda, T. and Gu, J. *FASEB J.*, 査読有 30,4120-31, 2016
18. *20 *N*-Glycosylation of integrin α5 acts as a switch for EGFR-mediated complex formation of integrin α5β1 to α6β4. Hang, Q., Isaji, T., Hou, S., Zhou, Y., Fukuda, T. and Gu, J. *Sci. Rep.* 査読有 doi: 10.1038/srep33507, 2016
19. Disease-associated glycans on cell surface proteins. Takahashi M, Kizuka Y, Ohtsubo K, Gu J, Taniguchi N., *Mol Aspects Med.* 16, 30021-8 2016
20. ○*2 RNase activity of sialic acid-binding lectin from bullfrog eggs drives antitumor effect via the activation of p38 MAPK to caspase-3/7 signaling pathway in human breast cancer cells. Kariya Y., Tatsuta T., Sugawara S., Kariya Y., Nitta K., Hosono M. *Int. J. Oncol.*, 査読有, 49: 1334-1342, 2016.
21. Loss of α1,6-fucosyltransferase Suppressed Liver Regeneration: Implication of Core Fucose In The Regulation of Growth Factor Receptor-mediated Cellular Signaling. Wang, Y., Fukuda, T., Isaji, T., Lu, J., Gu, W., Ohkubo, Y., Kamada, Y., Taniguchi, N., Miyoshi, E. and Gu, J. *Sci. Rep.* 5, 8264; DOI:

法人番号	041004
プロジェクト番号	S1201031

10.1038/srep08264, 2015

22. Loss of α1,6-fucosyltransferase decreased hippocampal long-term potentiation: implications for core fucosylation in the regulation of AMPA receptor heteromerization and cellular signaling. Gu, W., Fukuda, T., Isaji, T., Sakai, S., Morise, J., Higashi, H., Taniguchi, N., Yawo, H., Oka, S. and Gu, J. *J Biol. Chem.* 290, 17566-75, 2015
23. *9 Up-regulation of sialidase NEU3 in head and neck squamous cell carcinoma associated with lymph node metastasis.Shiga K., Takahashi K., Sato I., Kato K., Saijo S., Moriya S., Hosono M. and Miyagi T. Cancer Sci 106,1544-1553 2015.
24. Loss of cellular sialidases does not affect the sialylation status of the prion protein but increases the amounts of its proteolytic fragment C1. Katorcha E., Klimova N., Makarava N., Savtchenko R, PanX., Annunziata I, Takahashi K., Miyagi T., Pshezhetsky A.V., d'Azzo A., and Baskakov IV. PLoS One. 10(11):e0143218., 2015
25. Lysosomal localization of Japanese medaka (Oryzias latipes) Neu1 sialidase and its highly conserve enzymatic profiles with human. Ryuzono S., Takase R., Oishi K., Ikeda A., Chigwechokha K.P., Funahashi A., Komatsu M., Miyagi T., Shiozaki K. *Gene*. 575:513-23.2015
26. ○*10 Increased sialidase activity in serum of cancer patients: Identification of sialidase and inhibitor activities in human serum. Hata K., Tochigi T., Sato I., Shiozaki K., Wada T., Moriya S., Takahashi K., Yamaguchi K., Hosono M., and Miyagi T. *Cancer Sci.* 106:383-389.2015 査読有
27. ○*9 Potentiation of Epidermal Growth Factor-Mediated Oncogenic Transformation by Sialidase NEU3 Leading to Src Activation. Yamamoto K., Takahashi K., Hosono H., Shiozaki K., Yamaguchi K.,Moriya S., Shima H., and Miyagi T. PLoS One. 10:e0120578.2015 査読有
28. ○*9 Phosphatidic acid-mediated activation and translocation to the cell surface of sialidase NEU3, promoting signaling for cell migration. Shiozaki K., Takahashi K., Hosono M., Yamaguchi K., Hata K.,Shiozaki M., Bassi R., Prinetti A., Sonnino S., Nitta K., and Miyagi T. FASEB J. 29:2099-111 2015 査読有
29. ○*9 Sialidase NEU3 contributes neoplastic potential on colon cancer cells as a key modulator of gangliosides by regulating Wnt signaling. Takahashi K., Hosono M., Sato I., Hata, K., Wada T., Yamaguchi K., Nitta K., Shima H., and Miyagi T. Int J Cancer. 137:1560-73. 2015 査読有,
30. Rapid trimming of cell surface polysialic acid (PolySia) by exovesicular sialidase triggers release of preexisting surface neurotrophin. Sumida M., Hane M., Yabe U., Shimoda Y., Pearce T., Kiso M., Miyagi T., Sawada M., Varki A., Kitajima K., Sato C.. J. Biol. Chem. 290, 13202-13214 2015
31. *9 Plasma membrane-associated sialidase confers cancer initiation, promotion and progression. Miyagi T, Takahashi K, Shiozaki K, Yamaguchi K , and Hosono M. *Adv Exp Med Biol,*査読有, 842:139-45.2015 査読有
32. Significance of β-Galactoside α2,6 Sialyltranferase 1 in Cancers. Lu, J. and Gu, J. *Molecules,* 20:7509-7527, 2015
33. *25 Loss of α1,6-fucosyltransferase Suppressed Liver Regeneration: Implication of Core Fucose In The Regulation of Growth Factor Receptor-mediated Cellular Signaling. Wang, Y., Fukuda, T., Isaji, T., Lu, J., Gu, W., Ohkubo, Y., Kamada, Y., Taniguchi, N., Miyoshi, E. and Gu, J. *Sci. Rep.* 査読有 5, 8264; DOI: 10.1038/srep08264, 2015
34. Core fucosylation of IgG-BCR is required for antigen recognition and antibody production. Li, W., Ma, B.,(他 8 名)Fukuda, T., Gu, J., Zhang, J. and Taniguchi, N. *J. Immunol*. 査読有 194, 2596-2606, 2015
35. ○ *24 Loss of α1,6-fucosyltransferase inhibits chemical-induced hepatocellular carcinoma and tumorigenesis by down-regulating several cell signaling pathways. Wang, Y., Fukuda, T., Isaji, T., Lu, J., Im, S., Hang, Q., Gu, W., Hou, S., Ohtsubo, K. and Gu, J. *FASEB J*., 査読有 29, 3217-27, 2015
36. *23 Loss of α1,6-fucosyltransferase decreased hippocampal long-term potentiation: implications for core fucosylation in the regulation of AMPA receptor heteromerization and cellular signaling. Gu, W., Fukuda, T., Isaji, T., Hang, Q., Lee, H., Sakai, S., Morise, J., Mitoma, J., Higashi, H., Taniguchi, N., Yawo, H., Oka, S. and Gu, J. *J. Biol. Chem.* 査読有 290, 17566-75, 2015
37. ○*19 Integrin α5 suppresses the phosphorylation of Epidermal Growth Factor Receptor and Its Cellular Signaling of Cell Proliferation via N-glycosylation. Hang, Q., Isaji, T., Hou, S., Im, S., Fukuda, T. and Gu, J. *J. Biol. Chem.* 査読有 290, 29345-60, 2015
38. ○ *15 β -Galactosideα2, 6-sialyltranferase 1 promotes transforming growth factor-β-mediated epithelial-mesenchymal transition. Lu, J., Isaji, T., Im, S., Fukuda, T., Hashii, N., Takakura, D., Kawasaki, N. and Gu, J. *J Biol. Chem*. 289: 34627-34641, 2014

法人番号	041004
プロジェクト番号	S1201031

39. MytiLec, a Mussel R-Type Lectin, Interacts with Surface Glycan Gb3 on Burkitt's Lymphoma Cells to Trigger Apoptosis through Multiple Pathways. Hasan I, Sugawara S, Fujii Y, Koide Y, Terada D, Iimura N, Fujiwara T, Takahashi KG, Kojima N, Rajia S, Kawsar SM, Kanaly RA, Uchiyama H, Hosono M, Ogawa Y, Fujita H, Hamako J, Matsui T, Ozeki Y. *Marine Drugs,* 査読有, 13, 7377-7389.2015
40. ○*16 An Oncogenic Protein Golgi Phosphoprotein 3 Up-regulates Cell Migration via Sialylation. Isaji, T., Im, S., Gu, W., Wang, Y., Hang, H., Lu, J., Fukuda, T., Hashii, N., Takakura, D., Kawasaki, N., Miyoshi, H. and Gu, J. J Biol. Chem. 査読有 289: 20694-20705, 2014
41. MicroRNA 130b suppresses migration and invasion of colorectal cancer cells through downregulation of integrin. Zhao, Y., Miao, G., Li, Y., Isaji, T., Gu, J., Li, J., Qi, R. PLoS One. 査読有 9(2):e87938, 2014
42. Structural basis for substrate specificity of mammalian neuraminidases.Victoria Smutova V., Albohy A., Pan X., Korchagina E., Miyagi T., Bovin N., Cairo C.W., and Pshezhetsky A.V.*PLoS One*. 9(9):e106320. 2014
43. がんのシアリダーゼ異常．宮城妙子．*化学と生物*、査読有,52, 76-82, 2014
44. A galactose-binding lectin isolated from Aplysia kurodai (sea hare) eggs inhibits streptolysin-induced hemolysis. Hasan I., Watanabe M., Ishizaki N., Sugita-Konishi Y., Kawakami Y., Suzuki J., Dogasaki C., Rajia S., Kawsar S.M.A., Koide Y., Kanaly R.A., Sugawara S., Hosono M., Ogawa Y., Fujii Y., Iriko H., Hamako J., Matsui T., Ozeki Y., *Molecules,* 査読有, 19: 13990-14003, 2014.
45. *11 Cancer-Selective Induction of Apoptosis by Leczyme. Tatsuta T., Sugawara S., Takahashi K., Ogawa Y., Hosono M., Nitta K., *Front Oncol*., doi: 査読有 10.3389/fonc.2014.001392014 (2014)
46. ○*13 Binding profiles and cytokine-inducing effects of fish rhamnose-binding lectins on Burkitt's lymphoma Raji cells. Hosono M., Sugawara S., Matsuda A., Tatsuta T., Koide Y., Hasan I., Ozeki Y., Nitta K., *Fish Physiol. Biochem.,* 査読有 doi: 10.1007/s10695-014-9948-1 .2014
47. *11 Leczyme: A New Candidate Drug for Cancer Therapy. Tatsuta T., Sugawara S., Takahashi K., Ogawa Y., Hosono M., Nitta K., *Biomed Res Int*., 査読有 40, 1559-1572 .2014
48. Sialyl-glycoconjugates in cholesterol-rich microdomains of P388 cells are the triggers for apoptosis induced by *Rana catesbeiana* oocyte ribonuclease. Ogawa Y., Sugawara S., Tatsuta T., Hosono M., Nitta K., Fujii Y., Kobayashi H., Fujimura T., Taka H., Koide Y., Hasan I., Matsumoto R., Yasumitsu H., Kanaly R.A., Kawsar S.M.A, Ozeki Y., *Glycoconj. J.*, 査読有 31, 171-184 .2014
49. ○Sialic acid-binding lectin (leczyme) induces apoptosis to malignant mesothelioma and exerts synergistic antitumor effects with TRAIL . Tatsuta T., Hosono M., Takahashi K., Omoto T., Kariya Y., SugawaraS., Hakomori S., Nitta K., *Int. J. Oncol.*, 査読有 44, 377-384 .2014
50. Down-regulation of Hsp70 inhibits apoptosis induced by sialic acid-binding lectin (leczyme) Tatsuta T., Hosono M., Ogawa Y., Inage K., Sugawara S., Nitta K., *Oncol. Rep.*, 査読有 31, 13-18 .2014
51. Molecular cloning and biochemical characterization of medaka (Oryzias latipes) lysosomal neu4 sialidase. Shiozaki K, Ryuzono S, Matsushita N, Ikeda A, Takeshita K, Chigwechokha PK, Komatsu M, and Miyagi T. *Fish Physiol Biochem.* 40(5):1461-72 2013 査読有
52. *11 Involvement of ER stress in apoptosis induced by sialic acid-binding lectin (leczyme) from bullfrog eggs. Tatsuta T., Hosono M., Miura Y., Sugawara S., Hakomori S., Nitta K., *Int. J. Oncol.*, 査読有 43, 1799-1808 .2013
53. ○Sialic acid-binding lectin (leczyme) induces caspase-dependent apoptosis-mediated mitochondrial perturbation in Jurkat cells. Tatsuta T., Hosono M., Sugawara S., Kariya Y., Ogawa Y., Hakomori S., Nitta K. *Int. J. Oncol.*, 査読有 43, 1402-1412 .2013
54. Domain Composition of Rhamnose-binding Lectin from Shishamo smelt eggs and its Carbohydrate-binding Profiles. Hosono M., Sugawara S., Tatsuta T., Hikita T., Kominami J., Sachiko N.T., Hirabayashi J., Kawsar S.M.A., Ozeki Y., Hakomori S.I., Nitta K., *Fish Physiol. Biochem*., 査読有 39, 1619-1630 .2013
55. シアル酸とがん、宮城妙子、*実験医学*、査読有、31, 1546-1552, 2013
56. Molecular cloning and biochemical characterization of two novel Neu3 sialidases, neu3a and neu3b, from medaka (Oryzias latipes). Shiozaki K, Takeshita K, Ikeda M, Ikeda A, Harasaki Y, Komatsu M, Yamada S, Yamaguchi K, and Miyagi T.: *Biochimie.* 査読有,95, 280-289, 2013
57. *9 Possible association of Neu2 with plasma membrane fraction from mouse thymus exhibited sialidase activity with fetuin at pH 7.0 but not at pH 4.5. Kijimoto-Ochiai1 S, Doi N, Fujii1y F, Go S, Kabayama K, Moriya S, Miyagi T, and Koda T:*Microbiol Immunol* 査読有,57: 569–582, 2013
58. シアリダーゼによる細胞接着の制御、高橋耕太、塩崎一弘、宮城妙子、*生体の科学*. 64,273-278, 2013

法人番号	041004
プロジェクト番号	S1201031

59. *17 α1,6-Fucosylation regulates neurite formation via the activin/phospho-Smad2 pathway in PC12 cells: the implicated dual effects of Fut8 for TGF-β/activin-mediated signaling. Gu, W., Fukuda, T., Isaji, T., Hashimoto, H., Wang., Y and Gu, J. FASEB J., 査読有 27:3947-3958, 2013
60. *14 E-cadherin and adherens-junctions stability in gastric carcinoma: Functional implications of glycosyltransferases involving N-glycan branching biosynthesis, N-acetylglucosaminyltransferases III and V. Pinho, SS., Figueiredo, J., Cabral, J., Carvalho, S., Dourado, J., Magalhães, A., Gärtner, F., Mendonça, AM., Isaji, T., Gu, J., Carneiro, F., Seruca, R., Taniguchi, N., Reis, CA. Biochim. Biophys. Acta, 査読有 1830: 2690-700, 2013
61. Anti-tumor effects of exogenous ganglioside GM3 on bladder cancer in an orthotopic cancer model. Wang, H., Isaji, T., Satoh, M., Li, D., Arai, Y. and Gu, J. Urology 査読有 81, 210.e11-15, 2013
62. *14 Gastric cancer: adding glycosylation to the equation. Pinho, SS., Sandra Carvalho, S., Marcos-Pinto, R., Magalhães, A., Oliveira, C., Gu, J., Dinis-Ribeiro, M., Carneiro, F., Seruca, R. and Reis, CA. Trends in Molecular Medicine 査読有 19: 664-76, 2013
63. Chitosan oligosaccharides suppress production of nitric oxide in lipopolysaccharide- induced N9 murine microglial cells in vitro. Wei, P., Ma, P., Xu, Q., Bai, QH., Gu, J., Xi, H., Du, Y., Yu, C. Glycoconj J. 査読有 29:285-95, 2012
64. *14 Potential roles of N-glycosylation in cell adhesion. Gu, J., Isaji, T., Xu, Q., Kariya, Y., Gu, W., Fukuda, T. and Du, Y. Glycoconj. J. 査読有 29: 599-607,2012
65. *14 Roles of N-acetylglucosaminyltransferase III in epithelial-to-mesenchymal transition induced by TGF-β1 in epithelial cell lines. Xu, Q., Isaji, T., Lu, Y., Gu, W., Kondo, M., Fukuda, T., Du, Y. and Gu, J. J Biol Chem. 査読有 287: 16563-74, 2012
66. Core fucosylation of mu heavy chains regulates the assembly of precursor B cell receptors and its intracellular signaling. Li, W., Liu, Q., Pang, Y., Jin, J., Wang, H., Cao, H., Li, Z., Wang, X., Ma, B., Chi, Y., Wang, R., Kondo, A., Gu, J. and Taniguchi, N. J Biol Chem. 査読有 287: 2500-2508, 2012
67. *9 Human cytosolic sialidase NEU2— low general tissue expression but involvement in PC-3 prostate cancer cell survival. *Koseki K., Wada T., Hosono M., Hata K.,Yamaguchi K.,Nitta K., and Miyagi T.,*Biochem.Biophys.Res.Commun*. 査読有,428, 142–149, 2012
68. Reduced susceptibility to colitis-associated colon carcinogenesis in mice lacking plasma membrane-associated sialidase. *Yamaguchi K, Shiozaki K, Moriya S, Koseki K, Wada T,Tateno H,Sato I, Asano M, Iwakura Y, and Miyagi T. *PLoS One.* 査読有, 7(7) :e41132, 2012
69. Mammalian sialidases: physiological and pathological roles in cellular functions,*Miyagi, T.,and Yamaguchi, K.: *Glycobiology* 査読有,22, 880–896, 2012
70. Sialidase significance for cancer progression, *Miyagi T.,Takahashi K., Hata K., Shiozaki K., and Yamaguchi K., *Glycoconjugate J* 査読有,29, 567–577, 2012.
71. *9Altered expression of sialidases in human cancer. *Miyagi T, Takahashi K, Moriya S, Hata K, Yamamoto K, Wada T, Yamaguchi K, and Shiozaki K. *Adv Exp Med Biol.* 査読有,49:257-267, 2012
72. Sialidase NEU4 Hydrolyzes Polysialic Acids of Neural Cell Adhesion Molecules and Negatively Regulates Neurite Formation by Hippocampal Neurons. Takahashi K., Mitoma J., Hosono M., Shiozaki K.,Sato, C. Yamaguchi K., Kitajima K., Higashi H., Nitta K., Shima H, Miyagi T.: *J Biol Chem.* 287, 14816-14826, 2012
73. ○*9 Plasma membrane-associated sialidase (NEU3) regulates progression of prostate cancer to androgen-independent growth through modulation of androgen receptor signaling. Kawamura S., Sato I.,Wada T., Yamaguchi K., Li Y., Li D., Zhao X.,Ueno S., Aoki H., Tochigi T., Kuwahara M., Kitagawa T. Takahashi K., Moriya S. and Miyagi T. *Cell Death Differ.* 19, 170-179. 2012
74. A lectin from the mussel *Mytilus galloprovincialis* has a highly novel primary structure and induces glycan-mediated cytotoxicity of globotriaosylceramide - expressing lymphoma cells Fujii Y., Dohmae N., Takio K., Kawsar S.M.A., Matsumoto R., Hasan I., Koide Y., Kanaly R.A., Yasumitsu H., Ogawa Y., Sugawara S., Hosono M., Nitta K., Hamako J., Matsui T., Ozeki Y., *J. Biol. Chem*., 査読有 287, 44772-44783 .2012
75. Cytotoxicity and glycan-binding properties of an 18 kDa lectin isolated from the marine sponge *Halichondria okadai* Matsumoto R., Fujii Y., Kawsar S.M.A., Kanaly R.A., Yasumitsu H., Koide Y., Hasan I., Iwahara C., Ogawa Y., Im C.H., Sugawara S., Hosono M., Nitta K., Hamako J., Matsui T., Ozeki Y., *Toxins,*査読有 4, 323-338 .2012
76. MRP1 expressed on Burkitt's lymphoma cells was depleted by catfish egg lectin through Gb3-glycosphingolipid and enhanced cytotoxic effect of drugs. Fujii Y., Sugawara S., Araki D., Kawano

法人番号	041004
プロジェクト番号	S1201031

T., Tatsuta T., Takahashi K., Kawsar S.M., Matsumoto R., Kanaly R.A., Yasumitsu H., Ozeki Y., Hosono M., Miyagi T., Hakomori S.I., Takayanagi M., Nitta K., *Protein J.*, 査読有 31, 15-26 .2012

＜図書＞

研究テーマ1）

1. 2 Sugar Chains (Macrophages govern ganglioside GM3 expression in adipocytes to regulate adipogenesis and insulin signaling in homeostatic and pathogenic conditions) Inokuchi J. Springer Japan 2014
2. *1 Sugar Chains (Gangliosides and T cell immunity) Nagafuku M, and Inokuchi J. Springer Japan 2014
3. *1,2Glycobiology of the Nervous System, Advances in Neurobiology 9 (Synthesis of O-Linked Glycoconjugates in the Nervous System.) Inokuchi J. Go S. and Hirabayashi Y. Springer Science+Business Media New York. Chapter 4, DOI 10.1007/978-1-4939-1154-7_4, 2014
4. Handbook of Glycosyltransferases and Related Genes. Second Edition.(ST3 beta-galactoside alpha-2,3-sialyltransferase 5;ST3GAL5) Inokuchi J. and Uemura S. Springer Japan 2014
5. Handbook of Glycosyltransferases and Related Genes. Second Edition. (Biosynthetic Pathways of Glycosphingolipids) Inokuchi J. and Go S. Springer Japan 2014
6. *2スフィンゴ糖脂質とメタボリックシンドローム、井ノ口仁一、実験医学（羊土社）Vol. 31: 1566-1573, 2013

研究テーマ 2）

1. *9 Glycosignals in Cancer (Differential roles of mammalian sialidases in cancers) Miyagi T. p.35-53 Eds by K. Furukawa, and M. Fukuda, Springer 2016
2. *9 Sugar Chains (Mammalian sialidase and tumor development) Miyagi T, Takahashi K , Shiozaki K, and Yamaguchi K, Eds by T. Suzuki, K Ohtsubo, and N Taniguchi, Capter 10, pp159-176 Springer Japan 2015
3. *9 Topics in Current Chemistry : Sialoglyco-Biology and -Chemistry, (eds Gerardy- Schahn R, Delannoy P, von Itzstein M) (Structure and function of mammalian sialidases) Monti, E. and Miyagi, T. Springer, 366:183-208. 2015
4. Sugar Chains (α1,6-Fucosyltransferase knockout mice and Schizophrenia-like phenotype.), Wei Gu, Tomohiko Fukuda, and Jianguo Gu. Springer Japan, P.267-280, 2015
5. 糖タンパク質—構造・生合成・代謝：N 結合型糖鎖、顧 建国, 糖鎖の新機能開発・応用ハンドブック　創薬・医療から食品開発まで、エヌ・ティー・エス社、13-17, 2015
6. α1,6 フコース転移酵素(Fut8)欠損による行動異常とその機序について、福田友彦、顧 建国,日本生物学的精神医学会誌、26:95-101, 2015
7. Glycoscience: Biology and Medicine (Mammalian Sialidase Assays) Miyagi T, Takahashi K, Shiozaki K, Yamaguchi K. pp1395-1402 Eds by N. Taniguchi, T. Endo, G. Hart, P. Seeberger, C.-H. Wong, Springer Japan , New Delhi. 2014
8. *9 Glycosignals in Cancer (Differential roles of mammalian sialidases in cancers) Miyagi T. Springer 2014
9. *9 がんのシアリダーゼ異常．宮城妙子. 化学と生物（農芸化学会）、52, 76-82, 2014
10. *14 Glycoscience: Biology and Medicine (Integrin α5β1 and its N-glycosylation.), Jianguo Gu, Qinglei Hang, Tomohiko Fukuda, Tomoya Isaji. Springer, 2014
11. Handbook of Glycosyltransferase and related genes (Fucosyltransferase 8 (α1,6-fucosyltransferase, FUT8)), Ihara, H., Tsukamoto, H., Gu, J., Miyoshi, E., Taniguchi, N. and Ikeda, Y. Springer, P.581-596,2014
12. *14 Handbook of Glycosyltransferase and related genes (β1,4-*N*-Acetylglucosaminyltransferase III (GnT-III, GlcNAc-T III)), Ikeda, Y., Ihara, H., Tsukamoto, H., Gu, J. and Taniguchi, N. Springer, P.209-222,2014
13. Sugar Chains (α1,6-Fucosyltransferase knockout mice and Schizophrenia-like phenotype.), Wei Gu, Tomohiko Fukuda, and Jianguo Gu. Springer Japan, 2014
14. Handbook of Glycosyltransferase and related genes (Fucosyltransferase 8 (α1,6-fucosyltransferase, FUT8), Ihara, H., Tsukamoto, H., Gu, J., Miyoshi, E., Taniguchi, N. and Ikeda, Y. Springer, 2014
15. *14 Handbook of Glycosyltransferase and related genes (β1,4-*N*-Acetylglucosaminyltransferase III (GnT-III, GlcNAc-T III)), Ikeda, Y., Ihara, H., Tsukamoto, H., Gu, J. and Taniguchi, N. Springer, 2014
16. Laminins: Structure, Biological Activity and Role in Disease (Laminin-332 and Integrins: Signaling Platform for Cell Adhesion and Migration and its Regulation by *N*-glycosylation.) Kariya, Y., Kariya, Y and Gu, J. Nova Science Publishers Inc., NY, Chapter 2, 1-23, 2013

法人番号	041004
プロジェクト番号	S1201031

17. α1,6-Fucosyltransferase 欠損マウスに見られた統合失調症様行動とその解析、顧 建国、谷口直之、福田友彦、実験医学（羊土社）P34-39, 2013
18. *9 シアル酸とがん、宮城妙子　実験医学(羊土社)31, 1546-1552, 2013
19. *9 シアリダーゼによる細胞接着の制御、高橋耕太、塩崎 一弘、宮城妙子、生体の科学(医学書院) 64,273-278, 2013

＜学会発表＞

研究テーマ１）

1. スフィンゴミエリン発現の微調整は自己反応性 T 細胞の除去に関与するか？豊島かおる、永福正和、岡崎俊郎、井ノ口仁一、日本薬学会第 137 年会、仙台、2017 年 3 月
2. GM3 合成酵素ノックアウトマウスは腸管からのコレステロール吸収制御を介して高コレステロール血症に抵抗性を示す。二瓶渉、永福正和、田村有美、稲森啓一郎、新井健太、樺山一哉、深瀬浩一、井ノ口仁一、日本薬学会第 137 年会、仙台、2017 年 3 月
3. Role of $CD103^+$ dendritic cells in mediating female-predominant Th2 cytokine production in asthma. Chisaki Masuda, Tomomitsu Miyasaka, Jin-ichi Inokuchi, Shunya Iwami, Tasuku Kawano, Motoaki Takayanagi, Tomoko Takahashi, Isao Ohno，第 45 回日本免疫学会学術集会、沖縄、2016 年 12 月
4. Discovery of Novel Inflammation Amplification Loop by Ganglioside GM3 Molecular Species in Metabolic Syndrome. 井ノ口仁一、 狩野裕考、第 45 回日本免疫学会学術集会、沖縄、2016 年 12 月
5. Identification of pro- and anti-inflammatory molecular species of gangliosides GM3 in the progression of metabolic disorders. 狩野裕考、井ノ口仁一、第 45 回日本免疫学会学術集会、沖縄、2016 年 12 月
6. Discovery of Novel Inflammation Amplification Loop by Ganglioside GM3 Molecular Species in Metabolic Syndrome. Jin-ichi Inokuchi, Hirotaka Kanoh, Shinji Go, Masakazu Nagafuku, Kei-ichiro Inamori. SialoGlyco2016, Santabarbara, CA, 2016 年 11 月
7. Altered expression of GM3 molecular species during myoblast differentiation, and its biological significance. 郷慎司、第 4 回若手による骨格筋細胞研究会、名古屋、2016 年 11 月
8. ガングリオシド GM3 のアシル鎖長が制御する自然免疫応答の解析。狩野裕考、郷慎司、新田昴大、ルーカス・ヴェイロン、井ノ口仁一、第 9 回セラミド研究会学術集会、東京、2016 年 10 月
9. Investigation of the roles of gangliosides in leptin and melanocortin signaling. Kei-ichiro Inamori,8th Asian Community of Glycoscience and Glycotechnology Conference, China, 2016 年 10 月
10. Ganglioside GM3 is essential for the structural integrity and function of cochlear hair cells. Misato Yoshikawa, Shinji Go, Shun-ichi Suzuki, Akemi Suzuki, Yukio Katori, Thierry Morlet, Steven M.Gottlieb, Michihiro Fujiwara, Katsunori Iwasaki, Kevin A.Strauss, Jin-ichi Inokuchi, GM3 Synthase Deficiency Research Summit, Pittsburgh, USA, 2016 年 10 月
11. ATP/UTP 受容体 $P2Y_2$ の細胞外システイン残基の機能について、阿部真耶、渡部佳奈恵、黒田喜幸、中川哲人、東 秀好、第 89 回日本生化学会大会、仙台、2016 年 9 月
12. シアリダーゼ Neu3 は Unconventional Pathway で細胞膜に輸送される、渡邉さと子、 黒田喜幸、 中川哲人、大澤幸希光、西森 誠、宮本朋幸、薬師寺宏匡、所司睦文、池脇信直、荒武八起、大野節代、大野英治、三苫純也、東 秀好、第 89 回日本生化学会大会、仙台、2016 年 9 月
13. マウス視床下部由来神経細胞株を用いた受容体シグナルにおけるガングリオシドの機能解析。田村有美、稲森啓一郎、伊藤英樹、千葉ひかる、井ノ口仁一、第 89 回日本生化学会大会、仙台、2016 年 9 月
14. レプチンおよびメラノコルチン受容体の機能におけるガングリオシドの役割の検討。稲森啓一郎、伊藤英樹、田村有美、楊燕華、二瓶渉、突田壮平、山田哲也、片桐秀樹、井ノ口仁一、第 89 回日本生化学会大会、仙台、2016 年 9 月
15. O-GlcNAc 修飾を介したスフィンゴ糖脂質代謝制御機構の解明。郷慎司、井ノ口仁一、第 89 回日本生化学会大会、仙台、2016 年 9 月
16. 極長鎖 GM3 ガングリオシドによる慢性炎症惹起メカニズム。狩野裕考、郷慎司、新田昴大、ルーカス・ヴェイロン、アンナ・カッタニオ、マリレナ・レティッザ、名取良浩、吉村祐一、安藤弘宗、石田秀治、樺山一哉、下山敦史、深瀬浩一、マリア・チャンパ、ラウラ・マウリ、アレッサンドロ・プリネッティ、サンドロ・ソニーノ、鈴木明身、井ノ口仁一、第 89 回日本生化学会大会、仙台、2016 年 9 月
17. B4GalNAcT1 (GM2/GD2/GA2 合成酵素) の新規アイソフォームの同定と、R-based motif による酵素安定性と細胞内輸送機構の解析。宍戸史、上村聡志、樫村まどか、井ノ口仁一、第 89 回日本生化学会大会、仙台、2016 年 9 月
18. スフィンゴミエリンは胸腺における自己反応性 T 細胞の除去に関与するか？豊島かおる、永福正和、岡崎俊郎、井ノ口仁一、第 89 回日本生化学会大会、仙台、2016 年 9 月
19. GM3 合成酵素ノックアウトマウスが示す高コレステロール血症抵抗性と腸管からのコレステロール吸収低下機構。二瓶渉、永福正和、宍戸史、井ノ口仁一、第 89 回日本生化学会大会、仙台、2016 年 9 月
20. 筋分化過程における GM3 分子種変化の分子機構の解析。郷詩織、郷慎司、井ノ口仁一、佐藤ちひろ、北島健、第 89 回日本生化学会大会、仙台、2016 年 9 月
21. マウス視床下部由来神経細胞株を用いた受容体シグナルにおけるガングリオシドの機能解析。田村有美、稲森啓一郎、伊藤英樹、千葉ひかる、井ノ口仁一、第 89 回日本生化学会大会、仙台、2016 年 9 月

法人番号	041004
プロジェクト番号	S1201031

22. ガングリオシド欠損による過食・肥満モデルマウスの肥満病態の改善。伊藤英樹、稲森啓一郎、田村有美、楊燕華、二瓶渉、突田壮平、山田哲也、片桐秀樹、井ノ口仁一、第 89 回日本生化学会大会、仙台、2016 年 9 月
23. インスリン分泌機構における複合糖質の役割。高橋巌、溝上達也、藤井里穂、松山和佳奈、郷慎司、井ノ口仁一、山田修平、那谷耕司、第 89 回日本生化学会大会、仙台、2016 年 9 月
24. ブラジキニン B2 受容体の活性を調節する N 結合型糖鎖とシステイン残基、大関俊範、黒田喜幸、中川哲人、東　秀好、第 35 回日本糖質学会年会、高知、2016 年 9 月
25. レプチンおよびメラノコルチン受容体の機能におけるガングリオシドの役割の検討。稲森啓一郎、伊藤英樹、田村有美、楊燕華、二瓶渉、突田壮平、山田哲也、片桐秀樹、井ノ口仁一、第 35 回日本糖質学会年会、高知、2016 年 9 月
26. N 結合型糖鎖と細胞外システイン残基によるブラジキニン B2 受容体の発現と機能の調節、大関俊範、黒田喜幸、中川哲人、東　秀好、第 10 回東北糖鎖研究会、福島、2016 年 8 月
27. ブラジキニン B2 受容体の細胞膜表面近傍の塩基性アミノ酸残基の機能、阿部真耶、佐藤亜美、黒田喜幸、中川哲人、東　秀好、第 10 回東北糖鎖研究会、福島、2016 年 8 月
28. B4GalNAcT1 (GM2/GD2/GA2 合成酵素) の新規アイソフォームの同定と、R-based motif による酵素安定性と細胞内輸送機構の解析。宍戸史、上村聡志、樫村まどか、井ノ口仁一、第 10 回東北糖鎖研究会、福島、2016 年 8 月
29. ガングリオシドの微細構造変化が制御する筋分化。郷慎司、日本薬学会東北支部第 15 回生物化学若手研究者セミナー、仙台、2016 年 7 月
30. 内因性リガンドとしての極長鎖 GM3 ガングリオシドによる慢性炎症惹起機構。狩野裕考、郷慎司、新田昴大、ルーカス・ヴェイロン、アンナ・カッタニオ、マリレナ・レティッザ、名取良浩、吉村祐一、安藤弘宗、石田秀治、樺山一哉、下山敦史、深瀬浩一、マリア・チャンパ、ラウラ・マウリ、アレッサンドロ・プリネッティ、サンドロ・ソニーノ、鈴木明身、井ノ口仁一、第 56 回日本脂質生化学会、秋田、2016 年 6 月
31. Discovery of Novel Inflammation Amplification Loop by Ganglioside GM3 Molecular Species in Metabolic Syndrome.Inokuchi Jin-ichi, 2016 Koria-Japan Bioactive Lipid Joint Symposium, South Korea, 2016 年 5 月
32. Membrane Microdomain Lipid Therapy for Diabetes.Inokuchi Jin-ichi, Keystone Symposia: New Therapeutics for Diabates and Obesity, California, USA, 2016 年 4 月
33. Control of Homeostatic and Pathogenic Balance in Adipose Tissue by Ganglioside GM3. Inokuchi Jin-ichi.2015 Annual meeting of Consorciam for Functional Glycomics ,Sanfrancisco, USA , 2015 年 12 月
34. mouse ST3Gal5(GM3/GM4 synthase)の arginine/lysine-based motif による細胞内輸送機構の解析、宍戸 史、上村聡志、樫村まどか、井ノ口仁一、BMB2015 第 38 回日本分子生物学会年会・第 88 回日本生化学会大会合同大会、神戸、2015 年 12 月
35. O-GlcNAc 修飾によるスフィンゴ糖脂質代謝制御機構、郷 慎司、井ノ口仁一 BMB2015 第 38 回日本分子生物学会年会・第 88 回日本生化学会大会合同大会、神戸、2015 年 12 月
36. ブラジキニン B2 受容体の細胞外ドメインと N 結合型糖鎖の機能.大関俊範、尾形聡子、黒田喜幸、中川哲人、東　秀好、第 88 回日本生化学会大会・第 38 回日本分子生物学会年会合同大会、神戸、2015 年 12 月
37. ブラジキニン B2 受容体・ATP/UTP 受容体 $P2Y_2$ 間の双方向活性化とコンドロイチン硫酸による調節、阿部真耶、黒田喜幸、中川哲人、東 秀好,第 88 回日本生化学会大会・第 38 回日本分子生物学会年会・合同大会、神戸、2015 年 12 月
38. 代謝型グルタミン酸受容体２（mGluR2）の活性と局在における膜近傍塩基性アミノ酸とガングリオシドの役割、黒田喜幸、林真優子、中川哲人、東 秀好、第 88 回日本生化学会大会・第 38 回日本分子生物学会年会合同大会、神戸、2015 年 12 月
39. $P2Y_2$ 受容体の細胞表面への発現に与える N 型糖鎖の影響、中川哲人、大東昂良、松崎仁美、高橋千央、佐藤愼平、竹山尚平、黒田善幸、三苫純也、東 秀好、第 88 回日本生化学会大会・第 38 回日本分子生物学会年会合同大会、神戸、2015 年 12 月
40. Ablation of the GM3 synthase gene in KK-Ay mice improved the obese phenotype: implication for its role in leptin and melanocortin signaling. Kei-ichiro Inamori, Hideki Ito, Xiaohua Yang, Wataru Nihei, Sohei Tsukita, Tetsuya Yamada, Hideki Katagiri, Jin-ichi Inokuchi 7th Asian Community of Glycoscience and Glycotechnology Conference,Matsushima, Japan, 2015 年 11 月
41. The regulation of ER export and Golgi retention of ST3Gal5 (GM3/GM4 synthase) and B4GalNAcT1 (GM2/GD2/GA2 synthase) by arginine/lysine-based motif adjacent to the transmembrane domain. Uemura Satoshi, Shishido Fumi, Kashimura Madoka, Inokuchi Jin-ichi 7th Asian Community of Glycoscience and Glycotechnology Conference,Matsushima, Japan, 2015 年 11 月
42. Sphingomyelin controls developmental checkpoint of immature T cells by modulating TCR stimulation. Kaoru Toshima, Nagafuku Masakazu, Reimi Jin, Toshiro Okazaki, Jin-ichi Inokuchi 7th ACGG Annual Conference, 2015 年 11 月
43. Gangliosides regulate intestinal cholesterol absorption. Wataru Nihei, Masakazu Nagafuku, Yui Kikuchi, Jin-ichi Inokuchi 7th Asian Community of Glycoscience and Glycotechnology Conference、Matsushima, Japan, 2015 年 11 月

法人番号	041004
プロジェクト番号	S1201031

44. Investigation of the role of gangliosides in leptin and melanocortin signaling. Hideki Ito, Kei-ichiro Inamori, Xiaohua Yang, Wataru Nihei, Sohei Tsukita, Tetsuya Yamada, Hideki Katagiri, Jin-ichi Inokuchi 7th Asian Community of Glycoscience and GlycotechnologyConference,Matsushima, Japan, 2015 年 11 月
45. Analysis of GM3 synthase-gene knockout cell lines generated from mouse hypothalamic neuronal cells. Yumi Tamura, Kei-ichiro Inamori, Hideki Ito, Hikaru Chiba, Jin-ichi Inokuchi 7th Asian Community of Glycoscience and Glycotechnology Conference,Matsushima, Japan, 2015 年 11 月
46. Sphingomyelin is indispensable for successful thymocyte development. Toshima Kaoru, Nagafuku Masakazu, Okazaki Toshiro, Inokuchi Jin-ichi、第 44 回日本免疫学会、札幌、2015 年 11 月
47. Involvement of the N-linked glycosylation of the B2 bradykinin receptor in the receptor oligomerization and activation.Yoshiyuki Kuroda, Maya Abe, Toshinori Oozeki, Tetsuto Nakagawa, and Hideyoshi Higashi.7th Asian Community of Glycoscience and Glycotechnology Conference, Matsushima, 2015 年 11 月
48. Control of Homeostatic and Pathogenic Balance in Adipose Tissue by Ganglioside GM3. Jin-ichi Inokuchi Keystone Symposia Conference,Diabetes: New Insights into Molecular Mechanisms and Therapeutic StrategiesKyoto, Japan, 2015 年 10 月
49. 自然免疫活性化による慢性炎症性疾患発症におけるガングリオシドの役割、井ノ口仁一、永福正和、稲森啓一郎、Lucas Veillon、郷 慎司、狩野裕考、第 8 回セラミド研究会、札幌、2015 年 10 月
50. 糖尿病研究における糖脂質メタボロミクス. 井ノ口仁一、第 37 回日本薬学会、福岡、2015 年 9 月
51. スフィンゴ糖脂質合成酵素欠損 Jurkat T 細胞株の樹立とその機能解析、山本博之、永福正和、稲森啓一郎、宍戸 史、伊藤 英樹、井ノ口仁一、第 9 回東北糖鎖研究会、仙台、2015 年 9 月
52. ガングリオシドは腸管からのコレステロール吸収を制御する、二瓶 渉、永福正和、菊地 唯、井ノ口仁一、第 9 回東北糖鎖研究会、仙台、2015 年 9 月
53. mouse ST3Gal5(GM3/GM4 synthase)の arginine/lysine-based motif による細胞内輸送機構の解析、宍戸 史、上村聡志、樫村まどか、井ノ口仁一、第 54 日本薬学会東北支部大会、矢巾、2015 年 9 月
54. 代謝型グルタミン酸受容体２（mGluR2）の活性と局在における膜近傍塩基性アミノ酸とガングリオシドの役割.林真優子、黒田喜幸、中川哲人、東 秀好、第 9 回東北糖鎖研究会、仙台、2015 年 9 月
55. 肥満関連 GPCR の構造と機能、東 秀好、平成 27 年度　東北薬科大学分子生体膜研究所　戦略的研究基盤形成支援事業シンポジウム「生体膜糖鎖異常に起因する生活習慣病発症機序の解明と臨床への応用」、仙台、2015 年 9 月
56. Control of Homeostatic and Pathogenic Balance in Adipose Tissue by Ganglioside GM3 ; Development of Membrane Microdomain Ortho-Signaling Therapy. Jin-ichi Inokuchi,Bioactive Lipids in Cancer, Inflammation & Related Diseases , Budapest, Hungary July, 2015
57. GM3 governs homeostatic and pathogenic balance in adipose tissue by regulating insulin signaling（GM3 は脂肪組織の恒常性と病態発症のバランスをインスリンシグナルを制御することにより支配している。）井ノ口仁一、第 58 回日本糖尿病学会、下関市、2015 年 7 月
58. mouse ST3Gal5(GM3/GM4 synthase)の arginine/lysine-based motif による細胞内輸送機構の解析、宍戸　史、上村聡志、樫村まどか、井ノ口仁一、第 34 回日本糖質学会年会、東京、2015 年 7 月
59. Membrane Microdomain Ortho-Signaling Therapy、井ノ口仁一、第 10 回スフィンゴテラピー研究会、加賀、2015 年 6 月
60. Rearrangement of raft constituents during T cell development, Nagafuku Masakazu, Toshima Kaoru, Inokuchi Jin-ichi、第 10 回スフィンゴテラピー研究会、加賀、2015 年 6 月
61. Identification of Ganglioside GM3 Molecular Species in Human Serum Associated With Risk Factors of Metabolic Syndrome、Lucas Veillon、郷 慎司、松山和佳奈、鈴木明身、長崎実佳、矢冨 裕、井ノ口仁一、第 57 回日本脂質生化学会、東京、2015 年 5 月
62. 肥満関連 GPCR の構造と機能の解明に向けて、東 秀好、平成 26 年度東北薬科大学分子生体膜研究所戦略的研究基盤形成支援事業シンポジウム「生体膜糖鎖異常に起因する生活習慣病発症機序の解明と臨床への応用」、仙台、2014 年 11 月
63. *8 ガングリオシドによるグループ II 代謝型グルタミン酸受容体の活性調節, 猪狩崇子、黒田喜幸、中川哲人、三苫純也、東 秀好、第 8 回東北糖鎖研究会、盛岡、2014 年 10 月
64. ATP/UTP 受容体 $P2Y_2$ との相互作用と細胞膜発現、不応化におけるブラジキニン B2 受容体の N 結合型糖鎖および第 1 細胞外ドメインの役割, 芳賀邦彦、黒田喜幸、中川哲人、三苫純也、東 秀好、第 8 回東北糖鎖研究会、盛岡、2014 年 10 月
65. シアリダーゼ Neu3 は小胞体-ゴルジ経路を通らずに細胞膜に輸送される、北村泰久、弓田陽菜、渡辺さと子、中川哲人、黒田喜幸、三苫純也、東 秀好、第 8 回東北糖鎖研究会、盛岡、2014 年 10 月
66. ガングリオシド GM3 は蝸牛有毛細胞の構造と機能維持に必須である、井ノ口仁一、吉川弥里、郷 慎司、第 33 回日本糖質学会、名古屋大学、2014 年 8 月
67. O-GlcNAc 修飾によるスフィンゴ糖脂質代謝制御機構。郷 慎司、井ノ口仁一、第 33 回日本糖質学会、名古屋大学、2014 年 8 月
68. 筋分化過程におけるスフィンゴ糖脂質の発現。新井詩織、郷慎司、Lucas veillon、井ノ口仁一、第 33 回日本

法人番号	041004
プロジェクト番号	S1201031

糖質学会、名古屋大学、2014 年 8 月

69. 糖脂質ガングリオシドによる痛覚過敏の惹起。渡辺 俊、東 秀好、田辺光男、第 36 回日本疼痛学会、大阪、2014 年 6 月
70. *2 マクロファージは内臓脂肪細胞のスフィンゴ糖脂質発現を制御し、脂肪細胞の生理的分化成熟と肥満によるインスリン抵抗性を制御している、井ノ口仁一、永福正和、第 56 回日本脂質生化学会、近畿大学、2014 年 6 月
71. 細胞外グルタミン酸レベルの調節を介したガングリオシドによる痛覚過敏。渡辺俊、東 秀好、田辺光男 第 87 回日本薬理学会年会、仙台、2014 年 3 月
72. *1 T 細胞の分化制御および免疫疾患におけるスフィンゴ糖脂質の発現の意義。永福正和、大野勲、鈴木明身、井ノ口仁一、糖鎖免疫シンポジウム、東京、2014 年 2 月
73. *2 GM3 and Diabetes. Inokuchi J. Gordon Research Conference on Glycolipis and Sphingolipid, Ventura, CA, USA ,2014 年 1 月
74. *1 Distinct expression profile of sphingolipid species during T cell development. 永福正和、豊島かおる、神麗美、井ノ口仁一、2013 年度日本免疫学会総会、幕張、2013 年 12 月
75. *2 生体恒常性の破綻とスフィンゴ糖脂代謝 (Involvement of glycosphingolid metabolism in maintenance and breakdown of homeodynamic state) 井ノ口仁一、第 11 回日本糖質科学コンソーシアムシンポジウム（JCGG）仙台、2013 年 10 月
76. The roles of b-series gangliosides in nociceptive responses, Shun Watanabe, Mitsuo Tanabe, Hideyoshi Higashi, 7th International Ceramide Conference, Montauk, New York, 2013 年 10 月
77. マウスシアリダーゼ Neu3 の細胞内輸送。弓田 陽菜、三苫純也、中川哲人、東 秀好、第 7 回東北糖鎖研究会、新潟、2013 年 9 月
78. ブラジキニン B2 受容体の N-結合型糖鎖の機能。川田彰彦、八嶋紗代、三苫純也、中川哲人、黒田喜幸、東秀好、第 7 回東北糖鎖研究会、新潟、2013 年 9 月
79. G M 3 合成酵素欠損マウスの聴覚障害発症機序。（Elucidation on the mechanism of hearing loss in ganglioside GM3 synthase deficient mice）井ノ口仁一、吉川弥里、郷慎司、第7回東北糖鎖研究会、新潟、2013年9月
80. 筋分化過程におけるスフィンゴ糖脂質発現変化とその意義。（Distinct alteration on the expression of glycosphingolipids during myotube differentiation and its significance）新井 詩織、郷 慎司、井ノ口仁一、第7回東北糖鎖研究会、新潟、2013年9月
81. *2 T細胞の分化成熟におけるスフィンゴ脂質の発現と機能的役割。(Expression pattern of sphingolipids and its role in T cell development)豊島 かおる、神 麗美、永福正和、井ノ口仁一、第7回東北糖鎖研究会、新潟、2013年9月
82. *1 CD4 and CD8T cells require different gangliosides for activation. Inokuchi J.The 54nd International Conference on Bioscience of Lipids, Bari, Italy, Sept. 17-22, 2013
83. *4,5,6 炎症性シグナルメディエーターとしてのガングリオシドの脂肪組織。視床下部および免疫疾患における病態生理学的意義（Pathophysiological roles of gangliosides in adipose tissue, hypothalamus and immune diseases as mediator of inflammatory signals）井ノ口仁一、永福正和　第86回日本生化学会大会、横浜、2013年9月
84. 培地交換による細胞からの ATP パラ分泌の分子機構, 佐藤華絵、黒田喜幸、三苫純也、中川哲人、東 秀好、第 86 回日本生化学会大会、横浜、2013 年 9 月
85. ブラジキニン B2 受容体と ATP/UTP 受容体 $P2Y_2$ のヘテロオリゴマー形成における B2 受容体の N 末端ドメインと糖鎖の役割。川田彰彦、八嶋紗代、嶋﨑彩佳、三苫純也、中川哲人、東　秀好、第 86 回日本生化学会大会、横浜、2013 年 9 月
86. *2,3.4 マクロファージは内臓脂肪細胞のガングリオシド発現量を支配し、脂肪細胞の分化成熟とインスリン抵抗性を制御している。（Macrophages govern spatiotemporal expression of gangliosides in adipocytes for regulation of adipogenesis and insulin signaling）井ノ口仁一、永福正和、第32回日本糖質学会年会、大阪、2013年8月
87. 聴覚におけるガングリオシドの役割。井ノ口仁一、吉川弥里、郷 慎司、第 55 回日本脂質生化学会、宮城、2013 年 6 月
88. ブラジキニン B2 受容体と ATP/UTP 受容体 P2Y2 の相互作用における B2 受容体の N 末端ドメインと糖鎖の役割。川田彰彦、八嶋紗代、嶋﨑彩佳、三苫純也、中川哲人、東 秀好、日本生化学会東北支部第 79 回例会・シンポジウム、仙台、2013 年 5 月
89. *1 CD4 and CD8T cells require different gangliosides for activation. Inokuchi J.The 14th International Membrane Research Forum. Kyoto. March　2013.
90. *2,4,5,7 Lipids in Metabolic Syndrome. Inokuchi J and Soulage C (2013) Ely-T lab workshop. To-o-gatta, Miyagi Japan Feb.
91. Gangliosides produce nociceptive behavior and hyperalgesia via glutamate signals, Shun Watanabe, Koichi Tan-No, Takeshi Tadano, Hideyoshi Higashi, International Symposium for Neurosciences 2013　仙台 2013 年 2 月

法人番号	041004
プロジェクト番号	S1201031

92. *2,3 肥満・慢性炎症関連病態とガングリオシド GM3、第 85 回日本生化学会大会、井ノ口仁一、永福正和、福岡、2012 年 12 月
93. O-GlcNAc 修飾を介したスフィンゴ糖脂質代謝制御機構、郷 慎司、井ノ口仁一、第 85 回日本生化学会大会、福岡　2012 年 12 月
94. *1 T細胞サブセットの機能的レパトア選択におけるガングリオシド分子種の役割。第35回日本分子生物学会年会　井ノ口仁一、永福正和、福岡、2012年12月
95. *1,2ガングリオシドのラフトにおける機能発現機構と病態生理学的意義－メタボリックシンドロームとアレルギー疾患との関連－、井ノ口仁一、日本薬学会北海道支部例会、北海道大学、2012年12月
96. *1 A minimal influence of glycosylation of ganglioside on the *in vivo* Th1-dominant responses in mouse. Keiko Udaka, Takeyuki Shimizu, Masakazu Nagafuku, and Jin-ichi Inokuchi. 第 41 回日本免疫学会学術集会、神戸、2012 年 12 月
97. *2,3 スフィンゴ糖脂質代謝と生活習慣病。井ノ口仁一、平成 24 年度東北薬科大学分子生体膜研究所　戦略的研究基盤形成支援事業シンポジウム「生活習慣病発症機序の解明」、東北薬科大学、2012 年 11 月
98. O-GlcNAc 修飾を介したスフィンゴ糖脂質代謝制御機構。郷 慎司、井ノ口仁一、第 6 回東北糖鎖研究会、弘前大学（弘前）、2012 年 10 月
99. *2,3 GM3 合成酵素欠損糖尿病モデルマウスでは体重増加が抑制されインスリン感受性が亢進している。今津進、飯塚正樹、永福正和、井ノ口仁一、エンスィーナス　ジェフリー、第 33 回日本肥満学会、京都、2012 年 10 月
100. *1,2,6 メタボリックシンドロームおよびアレルギー疾患における GM3 ガングリオシドの病態生理学的意義。井ノ口仁一　FCCA セミナー／FCCA グライコサイエンス若手フォーラム 2012、鹿児島、2012 年 9 月
101. O-GlcNAc 修飾を介したスフィンゴ糖脂質代謝制御機構、郷 慎司、井ノ口仁一、第 31 回日本糖質学会、鹿児島、2012 年 9 月
102. *2,3,4,5,6 Ganglioside-dependent membrane microdomain : Involvement of insulin resistance, hearing function and T cell immunity. Jin-ichi Inokuchi. SialoGlyco2012. Academia Sinica (Taipei). Sept. 9-12, 2012.
103. *1 スフィンゴ脂質による T 細胞サブセットの特異的免疫制御、井ノ口仁一、永福正和、スフィンゴテラピィ研究会、金沢、2012 年 7 月
104. *1 ガングリオシドによる T 細胞サブセット特異的免疫制御。井ノ口仁一、永福正和、鈴木明身、奥山香織、大野勲、第 54 回日本脂質生化学会、九州大学（福岡）2012 年 6 月
105. 糖代謝とスフィンゴ糖脂質。郷 慎司、井ノ口仁一、第 78 回日本生化学会東北支部例会、山形大学医学部、2012 年 5 月
106. *1 T 細胞免疫におけるガングリオシド発現の意義。永福正和、奥山香織、鈴木明身、大野勲、井ノ口仁一、第 78 回日本生化学会東北支部例会、山形大学医学部、2012 年 5 月
107. *2,3,4,5,6 Ganglioside GM3 participates in the metabolic symdrome.Jin-ichi Inokuchi, Gordon Research Conference, Lucca, Italy, April, 2012.
108. The role of GM3 in biological membranes.Jin-ichi Inokuchi, 2012 Annual ELyT Workshop. Giens, France, March, 2012.

研究テーマ 2)

1. *9 Regulation mechanism of enhanced EGFR signaling by sialidase NEU3. Koji Yamamoto, Kohta Takahashi, Kazuhiro Shiozaki, Kazunori Yamaguchi, Hiroshi Shima, and Taeko Miyagi. Sialoglyco2016, Santa Barbara, USA,2016 年 11 月
2. *1 悪性中皮腫に対するレクザイムの抗腫瘍効果。立田岳生、佐藤稔之、髙橋耕太、細野雅祐、第 75 回日本癌学会学術総会、横浜、2016 年 10 月
3. *9 形質膜シアリダーゼ NEU3 は肺癌で EGFR を介したチロシンリン酸化を促進する。山本晃司、高橋耕太、塩崎一弘、山口萱範、島 礼、宮城妙子、日本生化学会　2016 年 9 月　仙台
4. *3 悪性中皮腫に対する cSBL とペメトレキセドの相乗的抗腫瘍効果。佐藤稔之, 立田岳生, 菅原栄紀, 原 明義, 細野雅祐, 第 89 回日本生化学会大会合同大会, 仙台, 2016 年 9 月
5. ヒトセミノーマ JKT-1 に対するナマズ卵レクチンの作用、第 55 回日本薬学会東北支部大会、郡山、2016 年 9 月
6. *6 ラムノース結合性レクチンはヒトセミノーマ細胞株 JKT-1 においてインテグリンα 2 の発現を増加させる、菅原栄紀、任彰壎、立田岳生、細野雅祐、第 35 回日本糖質学会年会、高知、2016 年 9 月
7. N-glycosylation on Integrin α5 define active integrin α5β1 internalization to regulate cell migration.杭 慶雷、伊左治知弥、侯 思聡、福田友彦、顧 建国、第 89 回日本生化学会大会、仙台、2016 年 9 月
8. The importance of N-glycosylation on integrin β1 in its activation and complex formation 侯 思聡、伊左治 知弥、杭 慶雷、福田友彦、顧 建国、第 89 回日本生化学会大会、仙台、2016 年 9 月

法人番号	041004
プロジェクト番号	S1201031

9. 細胞接着における N 型糖鎖の機能発現と細胞内シグナル伝達。顧 建国、第 35 回日本糖質学会年会 高知 2016 年 9 月
10. PIKIIα によるインテグリンα3β1 の制御とン N-型糖鎖調節、伊左治知弥、任 翔壎、福田友彦、顧 建国、第 35 回日本糖質学会年会、高知、2016 年 9 月
11. Core fucose in liver and HCC, Jianguo Gu、2016 Annual Symposium of Hubei Province Key Laboratory of Allergy and Immunology, 武漢大学、招待講演、2016 年 8 月,
12. Roles of N-glycan in EMT and cellular signaling, Jianguo Gu、2016 年中国糖生物学学術会議、南通、招待講演、2016 年 8 月
13. *9 形質膜シアリダーゼ NEU3 のリン酸化とその生理的意義、山本晃司、高橋耕太、塩崎一弘、山口壹範、島 礼、宮城妙子、第 10 回東北糖鎖研究会、福島 2016 年 8 月
14. *3 ウシガエル卵由来シアル酸結合性レクチン (cSBL) は悪性中皮腫の治療薬となりうるか？、佐藤稔之、立田岳生、菅原栄紀、原明義、細野雅祐、第 10 回東北糖鎖研究会、福島、2016 年 8 月
15. N-glycans in cell adhesion and EMT, Jianguo Gu, 6th Charles Warren Workshop 2016, 2016年8月, Hokkaido University, 招待講演 福田友彦、王 玉琴、伊左治知弥、顧 建国、第38回日本分子生物学会年会・第88回日本生化学会大会合同大会、神戸、2015年12月
16. がん細胞接着と EMT における糖鎖の機能発現とその制御、顧 建国、東北薬学支部会総会学術講演会、東北大学、招待講演、2016 年 6 月
17. N-glycosylation on Integrin α5 serve as an on/off switch to regulate EGFR signaling.杭 慶雷、伊左治知弥、侯 思聡、福田友彦、顧 建国、日本生化学会東北支部、弘前大学、2016 年 5 月
18. *9 ホスファチジルセリンと Evt-2 および形質膜シアリダーゼ NEU3 の相互作用とその意義、高橋耕太、山口壹範、細野雅祐、宮城妙子、日本脂質生化学会、2016 年 6 月
19. インテグリンのN-型糖鎖修飾の重要性と糖鎖による機能制御、伊左治知弥、日本生化学会東北支部、弘前大学、受賞講演、2016年5月
20. *9 Sialidase research targeted to diagnosis and therapy. Taeko Miyagi. Frontiers in Sialic acid Research Conference. Bad Lauterberg, Germany, 招待講演、2016 年 5 月
21. Functions of N-glycan in cancer cells. 顧 建国、中国科学院上海薬物所セミナー、中国、2016年3月、招待講演
22. N-glycosylation in cancer cells.顧 建国、南通大学薬学国際人材研討会、中国、招待講演 2016年3月
23. *6 悪性中皮腫に対し cSBL とペメトレキセドの併用は相乗的に抗腫瘍効果を示す、佐藤稔之、立田岳生、菅原栄紀、菅野秀一、細野雅祐、日本薬学会第 136 年会、横浜、2016 年 3 月
24. *9 シアリダーゼ研究：がん診療への応用をめざして、宮城妙子、日本女性科学者の会、新春講演会、仙台、2016年1月
25. *5 ヒト子宮頸がん由来細胞株 Hela に対するナマズ卵レクチンとスニチニブの併用効果、高柳 円、 菅原栄紀、任彰壎、立田岳生、細野雅祐、第38回日本分子生物学会年会・第88回日本生化学会大会合同大会、神戸、2015年12月
26. *7 Gb3 ノックアウト細胞の作製および細胞内Gb3のアポトーシスへの関与、Changhun Im、菅原栄紀、 高柳 円、立田岳生、細野雅祐、第38回日本分子生物学会年会・第88回日本生化学会大会合同大会、神戸、2015年12月
27. 肝がんおよび肝再生におけるコアフコースの機能、福田友彦、王 玉琴、伊左治知弥、顧 建国、第38回日本分子生物学会年会、第88回日本生化学会大会 合同大会、神戸、2015年12月
28. PI4K2α によるインテグリン α3β1 の N-型糖鎖の調節とその機能。任 翔壎、伊左治知弥、福田友彦、顧 建国、第 38 回日本分子生物学会年会、第 88 回日本生化学会大会 合同大会、神戸、2015 年 12 月
29. Integrin α5 suppresses the phosphorylation of EGFR and its cellular signaling via N-glycosylation.杭 慶雷、伊左治知弥、侯 思聡、任 翔壎、福田友彦、顧 建国、第 38 回日本分子生物学会年会・第 88 回日本生化学会大会合同大会、神戸、2015 年 12 月
30. Functions of integrin β1 in the cellular signaling for cell proliferation and importance of N-glycosylation. 侯 思聡、伊左治知弥、杭 慶雷、任 翔壎、福田友彦、顧 建国、第 38 回日本分子生物学会年会・第 88 回日本生化学会大会合同大会、神戸、2015 年 12 月
31. *9 Sialidase NEU3 defines invasive potential of human glioblastoma cells by regulating calpain-mediated proteolysis of focal adhesion proteins. Kohta Takahashi , Kazunori Yamaguchi, Setsuko Moriya, Yoji Yamashita, Ryuichi Katakura, Masahiro Hosono, and Taeko Miyagi 7 thACGG matsushima, 2015 年 11 月
32. *4 Rhamnose-binding lectin suppresses cell growth in Burkitt's lymphoma cells via up-regulation of p21, Sugawara S, Im C, Tatsuta T, Hosono M, 7th Asia Community of Glycoscience and Glycotechnology Conference, Matsushima, Miyagi, Nov. 2015
33. Anti-cancer effect induced by cSBL possessing lectin and ribonuclease activities, Tatsuta T, Sato T, Sugawara S, Kanno S, Hosono M, 7th Asia Community of Glycoscience and Glycotechnology Conference, Matsushima, Miyagi, Nov, 2015

法人番号	041004
プロジェクト番号	S1201031

34. *7 Cytosolic Gb3 facilitates apoptotic cell death induced by anti-cancer drugs, Im C, Sugawara S, Takayanagi M, Tatsuta T, Hosono M, 7th Asia Community of Glycoscience and Glycotechnology Conference, Matsushima, Miyagi, Nov. 2015
35. The interplay of N-acetylglucosaminyltransferase III and sialyltransferases in the regulation of cell motility. Jishun Lu, Tomoya Isaji, Sanghun Im, Tomohiko Fukuda, and Jianguo Gu, 7th Asian Community of Glycoscience and Glycotechnology (ACGG), Miyagi, Nov. 2015
36. PI4K2α regulates sialylation on glycoproteins. Sanghun Im, Tomoya Isaji, Tomohiko Fukuda and Jianguo Gu, 7th Asian Community of Glycoscience and Glycotechnology (ACGG), Miyagi, Nov. 2015
37. Roles for glycans in cell adhesion and migration. Jianguo Gu, 7th Asian Community of Glycoscience and Glycotechnology (ACGG), Miyagi, Nov. 2015
38. *2 レクチン活性とリボヌクレアーゼ活性を併せ持つ cSBL による抗腫瘍効果の作用機序解析。立田岳生,、高橋耕太、細野雅祐、第 74 回日本癌学会学術総会, 名古屋, 2015 年 10 月
39. PI4PによるN-型鎖のシアリル化制御。任　翔壎、伊左治知弥、福田友彦、顧 建国 平成２７年度日本薬学会東北支部第４回物理・分析系若手研究者セミナー、宮城、2015年10月
40. N-glycosylation in cancer cells, 顧 建国、2015 年南京腫瘤生物学診断治療国際研討会、南京、招待講演、2015 年 10 月
41. Expression and characterization of recombinant rhamnose-binding lectin with novel domain structure, Hosono M, Masuzaki H, Tatsuta T, Sugawara S, 23th International Symposium on Glycoconjyugate, Split, Croatia, Sep, 2015
42. *5 ヒト子宮頸がん由来細胞 HeLa に対するナマズ卵レクチンと抗癌がん剤との併用作用。高柳　円、菅原栄紀、任彰壎、立田岳生、細野雅祐、第 9 回東北糖鎖研究会、仙台、 2015 年 9 月
43. *3 悪性胸膜中皮腫に対するウシガエル卵由来シアル酸結合性レクチン（cSBL）とペメトレキセドの併用効果について。佐藤稔之、立田岳生、菅原栄紀、菅野秀一、細野雅祐、第 9 回東北糖鎖研究会、仙台、2015 年 9 月
44. Loss of FUT8 inhibits chemical-induced hepatocellular carcinoma and tumorigenesis by down-regulating multiple cellular signaling, 顧 建国、23rd International Symposium on Glycoconjugates、2015 年 9 月、Split, Croatia
45. 肝がん形成におけるコアフコースの機能、顧 建国、第９回東北糖鎖研究会・東北薬科大学分子生体膜研究所シンポジウム、2015 年 9 月、宮城
46. Integrin α5 suppresses the phosphorylation of EGFR and its cellular signaling of cell proliferation via N-glycosylation. 杭 慶雷、伊左治知弥、侯 思聡、任 翔壎、福田友彦、顧 建国 第9回東北糖鎖研究会, 宮城　2015年9月
47. Fut8の機能解析 : 肝臓および脳神経組織におけるコアフコースの重要性。福田友彦, 顧 建国 第9回東北糖鎖研究会,宮城,2015年9月
48. α1,4 ガラクトース転移酵素欠損バーキットリンパ腫 Raji 細胞の表現型解析。菅原栄紀、任彰壎、 髙柳円、立田岳生、細野雅祐、 第 34 回日本糖質学会年会, 東京, 2015 年 8 月
49. Hepatocellular carcinoma and core fucose, 顧 建国 2015 年 8 月,Institute of Biomedical Sciences of Fudan University, 招待講演
50. Importance of N-glycosylation and functions of core fucose in chemical-induced hepatocellular carcinoma, 顧 建国,2015 年 6 月,南通大学医学院, 招待講演
51. Interplay between cell adhesion and N-glycans in cancer cells, 顧 建国,2015 年 6 月,南通大学薬学院, 招待講演
52. バーキットリンパ腫 Ramos 細胞における Gb3 近傍分子の探索および局在解析，安達裕子，菅原栄紀，任彰壎，髙柳円，立田岳生，細野雅祐，日本薬学会第 135 年会,神戸,2015 年 3 月
53. Cell adhesion and glycans, 顧 建国 The Interdisciplinary Ph.D.Studies“Society-Environment-Technology”at Jagiellonian University, Krakow, Poland, May 2015, 招待講演
54. The importance of N-glycosylation and functional analysis of α1,6-fucosyltransferase in liver regeneration and hepatocarcinogenesis、顧 建国, 中国科学院上海薬物所セミナー, 中国, 招待講演,2015 年 3 月
55. The functions of N-glycans in cancer cells, 顧 建国, Institute of Biomedical Sciences of Fudan University, 中国, 招待講演, 2014 年 12 月
56. *7 腫瘍細胞における細胞内 Gb3 の機能解析。任彰壎，菅原栄紀，安達裕子，髙柳円，佐藤稔之，立田岳生，細野雅祐,第 37 回日本分子生物学会年会,横浜,2014 年 11 月
57. N-型糖鎖によるがん細胞の機能制御。顧 建国,平成26年度 東北薬科大学分子生体膜研究所シンポジウム,宮城,2014年11月
58. Functional analysis of the expression of N-glycans in epithelial-mesenchymal transition: Importance of α2,6 sialylation. Jianguo Gu, Jishun Lu, Sanghun Im, Tomohiko Fukuda, Noritaka Hashii, Daisuke Takakura, Nana Kawasaki and Tomoya Isaji, Joint Meeting of the Society for Glycobiology and the Japanese Society of Carbohydrate Research, Hawaii, 2014 年 11 月
59. A leczyme which has both lectin and ribonuclease activity causes a cancer-selective induction of apoptosis, Tatsuta T., Sugawara S., Takahashi K., Hosono M., 19th World Congress on Advances in Oncology and 17th International Symposium on Molecular Medicine, Athens, Greece, October, 2014
60. ヒト腎癌由来細胞株 ACHN に対するナマズ卵レクチンとスニチニブとの併用効果。髙柳円，菅原栄紀，任

法人番号	041004
プロジェクト番号	S1201031

彰壎，安達裕子，立田岳生，高橋耕太，宮城妙子，細野雅祐，第 87 回日本生化学会大会，京都，2014 年 10 月

61. β-Galactoside α2,6 sialyltransferase 1 is required for the sufficient inductionof TGF-β-medated epithelial-mesenchymal transition. Jishun Lu, Tomoya Isaji, Sanghun Im, Tomohiko Fukuda, Noritaka Hashii, Daisuke Takakura, Nana Kawasaki and Jianguo Gu 第 8 回東北糖鎖研究会、岩手、2014 年 10 月
62. レクザイムによるがん細胞選択的なアポトーシス誘導効果について，立田岳生，高橋耕太，細野雅祐，第 73 回日本癌学会学術総会，横浜，2014 年 9 月
63. α1,6 フコース転移酵素欠損による行動異常とその機序について，福田友彦，顧 建国、第 57 回神経化学会 奈良、 2014 年 9 月
64. Raji 細胞に発現する Gb3 にナマズ卵レクチンが結合することの重要性。任彰壎，菅原栄紀，安達裕子，髙栁円，青木美佑紀,立田岳生，細野雅祐，第 36 回日本糖質学会年会，名古屋，2014 年 8 月
65. *9 シアリダーゼは神経膠芽腫の浸潤能を制御する。高橋耕太、森谷節子、細野雅祐 ,宮城妙子:第33回日本糖質学会年会、名古屋、2014年8月
66. *17 α1,6 フコース転移酵素（Fut8）の発現による正負の機能, 顧 建国、福田友彦, 第 33 回日本糖質学会年会、名古屋、2014 年 8 月
67. *17 The importance of N-glycosylation and functional analysis of α1,6-fucosyltransferase (Fut8) in liver and brain tissues. Jianguo Gu,Konkuk University Research Seminar(招待講演),Seoul, Korea 2014 年 7 月
68. *17 Core Fucosylation Is Required for Hepatocarcinogenesis and Liver Regeneration. 9th International Symposium on Glycosyltransferases, Yuqin Wang, Tomohiko Fukuda, Tomoya Isaji, Kazuaki Ohtsubo, Naoyuki Taniguchi, Eiji Miyoshi and Jianguo Gu,Portugal, 2014 年 6 月
69. Impairment of hippocampal long-term potentiation and enhanced AMPA receptor complexes formation in α1,6-fucosyltransferase-deficient mice. 9th International Symposium on Glycosyltransferases, Tomohiko Fukuda, Wei Gu, Tomoya Isaji, Seiichiro Sakai, Jyoji Morise, Hideyoshi Higashi, Naoyuki Taniguchi, Hiromu Yawo, Shogo Oka and Jianguo Gu, Portugal, 2014 年 6 月
70. *9 がんで異常亢進する形質膜型シアリダーゼの特異的阻害剤の開発．宮城妙子、高橋耕太、森谷節子、細野雅祐：第３回シンポジウム、アカデミアからの抗がん剤創薬に向けて.沖縄、2014 年 5 月
71. キュウリウオ卵ラムノース結合性レクチンの構造と組換え体の発現，細野雅祐，齋藤友志，角張祐斗，佐々木孝志，菅原栄紀，立田岳生，枡崎浩亮，仁田一雄，第 134 回日本薬学会年会，熊本, 2014 年 3 月
72. *17 Core fucose and its relationship with diseases. Jianguo Gu,Fudan University Medical School Research Seminar(招待講演),Shanghai, China, 2014 年 3 月
73. *17 Roles of α1,6-fucosyltransferase (Fut8) in brain tissues. Jianguo Gu, Shanghai Center for Systems Biomedicine of Jiaotong University(招待講演), Shanghai, China, 2014 年 3 月
74. *17 Roles of α1,6-fucosyltransferase (Fut8) in liver tissues. Jianguo Gu, Nantong University Medical School Research Seminar(招待講演), China, 2014 年 3 月
75. Impairment of long-term potential and aberrant complex formation of glutamate receptors in α1,6-fucosyltransferase knockout mice. Wei Gu, Tomohiko Fukuda, Tomoya Isaji, Seiichiro Sakai, Jyoji Morise, Hideyoshi Higashi, Naoyuki Taniguchi, Hiromu Yawo, Shogo Oka and Jianguo Gu, International Symposium on Glyco-neuroscience,兵庫, 2014 年 1 月
76. *9 Sialidase confers neoplastic potential by regulating Wnt signaling. Miyagi T, Takahashi K, Hosono M, Hata K, Wada T, Moriya S, Yamaguchi K, Nitta K. on ISCSM 10 “Biochemical Roles of Eukaryotic Cell Surface Macromolecules” Kolkata, India,（招待講演）2014,1.
77. Magmas の機能解析。任 彰壎，菅原栄紀，細野雅祐，立田岳生，仁田一雄，第 36 回日本分子生物学会年会，神戸，2013 年 12 月
78. *14-17 糖タンパク質の糖鎖の機能制御と疾患への関わり。 顧建国、第 35 回東北薬学セミナー（特別講演）、宮城、2013 年 11 月
79. *16Sanghun Im, Tomohiko Fukuda, GOLPH3 regulates integrin-mediated functions via up-regulation of sialylation. Annual Meeting of the Society for Glycobiology, Jianguo Gu, Tomoya Isaji,フロリダ, USA、2013 年 11 月
80. *14-*16 細胞接着における糖転移酵素の発現制御とその意義、伊左治知弥、顧建国、第 39 回日本応用酵素協会研究発表会、大阪、2013 年 11 月
81. *14-*16 がん遺伝子 GOLPH3 による N 型糖鎖および細胞接着の制御とその意義、顧 建国、第１１回糖鎖科学コンソーシアムシンポジウム、宮城、2013 年 10 月
82. *9 がん化におけるシアリダーゼの役割．宮城妙子：第 11 回日本糖鎖科学コンソーシアムシンポジウム、仙台、2013 年 10 月
83. *9 シアリダーゼ NEU3 によるがん化能の制御。宮城妙子、高橋耕太、細野雅祐、山本晃司、和田正、秦敬子、森谷節子、塩崎一弘、山口壹範、仁田一雄: 第 72 回日本癌学会学術総会、横浜、2013 年 10 月

法人番号	041004
プロジェクト番号	S1201031

84. *9 シアリダーゼ NEU3 による Wnt シグナルを介した大腸がん細胞の造腫瘍能制御機構。高橋耕太, 細野雅祐, 和田正,山口壹範, 仁田一雄, 宮城妙子：第 72 回日本癌学会学術総会、横浜、2013 年 10 月
85. レクザイムによる悪性中皮腫細胞に対するアポトーシス誘導効果と TRAIL との併用効果について。立田岳生，高橋耕太，細野雅祐，仁田一雄，第 72 回日本癌学会学術総会，横浜，2013 年 10 月
86. *13 ナマズ卵レクチンは膜結合型 TNF α の発現量を増加させる。菅原栄紀，Im Changhun，安達裕子，細野雅祐，立田岳生，仁田一雄，第 86 回日本生化学会大会，横浜，2013 年 9 月
87. *12 RYK は Gb3 近傍に存在する細胞膜分子である。安達裕子，菅原栄紀，Im Changhun，立田岳生，細野雅祐，仁田一雄，第 86 回日本生化学会大会，横浜，2013 年 9 月
88. *Silurus asotus* lectin (SAL) depresses citric acid cycle in Gb3-expressing Burkitt's lymphoma cells.（ナマズ卵レクチンはバーキットリンパ腫 Raji 細胞の TCA 回路を停止させるか？）。仁田一雄，菅原栄紀，立田岳生，細野雅祐，第 86 回日本生化学会大会，横浜，2013 年 9 月
89. 正常 B 細胞における magmas の発現制御機構の解析。任　彰壎，菅原栄紀，立田岳生，細野雅祐，仁田一雄，第 7 回東北糖鎖研究会・第 65 回 FCCA セミナー，新潟，2013 年 9 月
90. *13 ナマズ卵レクチンで誘導されるバーキットリンパ腫細胞の増殖抑制機構の解析。菅原栄紀，任　彰壎，立田岳生，細野雅祐，仁田一雄，第 7 回東北糖鎖研究会・第 65 回 FCCA セミナー，新潟，2013 年 9 月
91. *12 EMARS 法を用いた Gb3 近傍に存在する分子の探索。安達裕子，菅原栄紀，任　彰壎，立田岳生，細野雅祐，仁田一雄，第 7 回東北糖鎖研究会・第 65 回 FCCA セミナー　新潟　2013 年 9 月
92. ナマズ卵レクチンはバーキットリンパ腫Raji細胞のTCA回路を停止させるか？　仁田一雄，菅原栄紀，立田岳生，細野雅祐，第7回東北糖鎖研究会・第65回FCCAセミナー　新潟　2013年9月
93. *17 肝臓がん形成および肝再生における α1,6 フコシル化の重要性、王玉琴、福田友彦、顧 威、伊左治知弥、三善英知、顧 建国、第 7 回東北糖鎖研究会、新潟、2013 年 9 月
94. *16 GOLPH3 によるインテグリンの機能制御とその糖鎖変化、任翔壎、伊左治知弥、福田友彦、顧 建国、第 7 回東北糖鎖研究会、新潟、2013 年 9 月
95. *16 GOLPH3 による糖鎖修飾を介したインテグリンの機能調節。伊左治知弥、福田友彦、顧 建国、第 86 回日本生化学会大会、横浜、2013 年 9 月
96. *14-*16 細胞接着における N-結合型糖鎖の発現調節とその意義。顧 建国、第 86 回日本生化学会大会　横浜 2013 年 9 月
97. *9 グリオーマにおけるシアリダーゼ異常。高橋耕太、細野雅祐、森谷節子、和田正、仁田一雄、宮城妙子：第 7 回東北糖鎖研究会　長岡　2013 年 9 月
98. *9 形質膜シアリダーゼ NEU3 は EGFR シグナリング活性化を介してがん化能を亢進する。山本晃司, 高橋耕太, 細野雅祐, 森谷節子, 和田正, 秦敬子,仁田一雄, 宮城妙子：第 86 回日本生化学会、横浜、横浜パシフィコ、2013 年 9 月
99. *10 ヒト血清におけるシアリダーゼ活性およびその阻害活性の同定。秦　敬子、森谷節子、細野雅祐、和田正、高橋耕太、塩崎一弘、仁田一雄、宮城妙子：第 86 回日本生化学会、横浜、横浜パシフィコ、2013 年 9 月
100. *9 シアリダーゼ NEU3 によるがん化能の制御。宮城妙子、高橋耕太、細野雅祐、和田正、森谷節子、秦敬子、山本晃司、山口壹範、仁田一雄：第 32 回日本糖質学会年会　大阪国際交流センター、2013 年 8 月
101. ノイラミニダーゼ阻害活性を持つ新規化合物の viNA と huNeu に対する理論的相互作用解析。石坪江梨花、堀 隆典、酒井美帆、Nongluk Sriwilaijaroen, Sadagopan Magesh、 安藤弘宗、石田秀治、 木曽真、宮城妙子、鈴木康夫、常盤広明：第 32 回日本糖質学会年会　大阪国際交流センター、2013 年 8 月
102. *14-*16 インテグリンの糖鎖と癌の悪性形質。顧建国、第 32 回日本糖質学会、大阪、2013 年 8 月
103. Fut8 ノックダウンによるアクチビンシグナル及び神経突起形成の増強。顧 威、福田友彦、伊左治知弥、橋本弘和、王玉琴、顧 建国、第３２回日本糖質学会、大阪、2013 年 8 月
104. 海馬神経細胞における α1,6 fucosylation の機能解析、福田友彦、顧 威、李 和勳、伊左治知弥、岡昌吾、八尾寛、顧 建国、第 32 回日本糖質学会、大阪、2013 年 8 月
105. コアフコースによる神経細胞の受容体の機能制御、顧 建国、新学術領域「神経糖鎖生物学」班会議、滋賀、2013 年 7 月
106. *9 シアリダーゼによる Wnt シグナル経路を介した造腫瘍能の制御. 宮城妙子：第 22 回、日本がん転移学会学術総会　松本 2013 年 7 月
107. *9 Roles of sialidase in cancer initiation and progression. Miyagi T, Takahashi K, Hosono M, Yamamoto K,Nitta K: XXIIth International Symposium on Glycoconjugates, Dalian, China, June 26, 2013
108. *9Plasma membrane-associated sialidase NEU3 confers neoplastic potential on colon cancer cells by regulating Wnt/beta-catenin signaling. Takahashi K, Hosono M, Hata K, Wada T, Yamaguchi K, Nitta K,Miyagi T: XXIIth International Symposium on Glycoconjugates, Dalian, China, June 26, 2013
109. *17 α1,6-fucosylation and its relationship with diseases、顧 建国、北京大学化学研究所セミナー（招待講演）北

法人番号	041004
プロジェクト番号	S1201031

京　2013 年 6 月

110. *17 α1, 6-Fucosylation bidirectionally regulates TGF-β/activin-mediated signaling. Wei Gu, Tomohiko Fukuda, Tomoya Isaji, Hirokazu Hashimoto, Yuqin Wang and Jianguo Gu.22nd International Symposium on Glycoconjugates, Dalian, China. 2013 年 6 月
111. 22nd International Symposium on Glycoconjugates, Tomohiko Fukuda, Wei Gu, Tomoya Isaji, Naoyuki Taniguchi and Jianguo Gu. Mice lacking fucosyltransferase 8 exhibit abnormal behavioral abnormalities associated with a schizophrenia-like phenotype. Dalian, China. 2013 年 6 月
112. *16 GOLPH3 regulates integrin-mediated cell migration via up-regulation of sialylation of β1 integrin. Tomoya Isaji, Wei Gu, Tomohiko Fukuda and Jianguo Gu. 22nd International Symposium on Glycoconjugates, Dalian, China. 2013 年 6 月
113. *14,*16 Functional crosstalk between cell-cell adhesion and cell-ECM adhesion via different expression of N-glycans. Jianguo Gu, 22nd International Symposium on Glycoconjugates,Dalian, China. 2013年6月
114. *16 GOLPH3による糖鎖修飾を介したインテグリンの機能調節、伊左治知弥、福田友彦、顧 建国、第79回生化学会東北支部会、宮城、2013年5月
115. *9 シアリダーゼ NEU3 による Wnt シグナルを介した大腸がん細胞の造腫瘍能制御。高橋耕太、細野雅祐、秦 敬子、和田正、山口壹範、仁田一雄、宮城妙子：第 79 回日本生化学会東北支部会、仙台、東北大学片平さくらホール､2013 年 5 月
116. 抗がん剤との併用によるナマズ卵レクチン，cyclosporin AおよびMK571の併用効果について。新谷香絵、菅原栄紀、任彰壎、細野雅祐、立田岳生、仁田一雄、第133回日本薬学会年会、横浜、2013年3月
117. マキバブラシノキ由来ピセアタンノールの腫瘍細胞に対する効果, 菅原栄紀、小林匡子、 任彰壎、 細野雅祐、立田岳生、吉崎文彦、仁田一雄、第133回日本薬学会年会、横浜, 2013年3月
118. *17 α1,6-Fucosylation plays dual effects on TGFβ- and activin-mediated signaling. Jianguo Gu, Wei Gu, Tomoya Isaji and Tomohiko Fukuda, Gordon Conference on Glycobiology,ロサンゼルス,USA,2013 年 3 月
119. 海馬ニューロンにおけるコアフコースの機能、顧 建国、新学術領域「神経糖鎖生物学」班会議、宮崎、2013 年 1 月
120. Sugar chain and diseases: From glycomics towards glycomedicine. .顧 建国、中国科学院上海薬物所セミナー（招待講演）、上海、2012 年 12 月
121. *14-*17 Functional analysis of N-glycosylation and its related diseases. 顧 建国、上海市薬理学会第十三回学術年会（招待講演）、上海　2012 年 12 月
122. *14-*16 N-glycosylation of integrins and cancer metastasis. 顧 建国、浙江省がんセンターセミナー（招待講演）、杭州、中国　2012 年 12 月
123. *14-*17 Functional analysis of N-glycosylation and related diseases. 顧 建国、 Glycobiology Forum at Jiangnan University（招待講演）、無錫、中国　2012 年 12 月
124. *14 細胞接着における N-結合型糖鎖の発現調節とその意義、顧 建国、第 85 回日本生化学大会、福岡 2012 年 12 月
125. *9 形質膜シアリダーゼ NEU3 による EGFR シグナリング活性化とそのがん化能への影響。山本晃司、高橋耕太、細野雅祐、森谷節子、和田正、秦敬子、仁田一雄、宮城妙子、第 85 回日本生化学会大会、福岡、2012 年 12 月
126. *9 シアリダーゼ NEU3 は大腸がん細胞の Wnt/beta-catenin シグナリングを制御する。高橋耕太、細野雅祐、和田正、秦敬子、山口壹範、仁田一雄、 宮城妙子、 第 85 回日本生化学会大会、福岡、2012 年 12 月
127. 組換えナマズ卵ラムノース結合性レクチンの調製とその糖結合性について。細野雅祐、永久　諒、佐藤真澄、菅原栄紀、立田岳生、仁田一雄、第85回日本生化学会大会、福岡、2012年12月
128. *9 シアリダーゼ異常による癌進展機構、宮城妙子、仙台、東北薬科大学、分子生体膜研究所、戦略的研究基盤形成支援事業シンポジウム　2012 年 11 月
129. *14 N-結合型糖鎖の機能発現・調節機構とその意義に関して、顧 建国、平成 24 年東北薬科大学分子生体膜研究所シンポジウム　宮城　2012 年 11 月
130. The knockdown ofα1,6-fucosyltransferase promotes neurite formation via the activin/phospho-Smad2 pathway in PC12 cells: the implicated dual effects of Fut8 for TGFβ/activin-mediated signaling、顧 建国、顧威、王 玉琴、伊左治知弥、福田友彦、The 4th Asian Communications of Glycobiology and Glycotechnology (ACGG), Jeju, Korea 2011 年 10 月
131. *16 GOLPH3 による N-型糖鎖修飾の調節とインテグリンの機能制御、竹原 雅子花，小林 沙織，伊左治 知弥，福田 友彦，顧 建国、第 6 回東北糖鎖研究会、弘前　2012 年 10 月
132. 脳神経における α1,6 フコースの機能解析、福田友彦、顧威、橋本弘和、酒井 誠一郎、王玉琴、伊左治知弥、八尾寛、東秀好、谷口直之、顧建国　第 6 回東北糖鎖研究会、弘前　2012 年 10 月
133. *17 Fut8 発現は activin/phospho-Smad2 活性経路を負に制御する、顧 威、福田友彦、伊左治知弥、王玉琴、

法人番号	041004
プロジェクト番号	S1201031

顧建国、第 6 回東北糖鎖研究会、弘前　2012 年 10 月

134. Raji細胞に発現しているmagmasの役割について, 任　彰壎，菅原栄紀，細野雅祐，立田岳生，仁田一雄，第6回東北糖鎖研究会，弘前，2012年10月
135. ナマズ卵レクチン処理細胞におけるアクチンの変化, 菊田由香，菅原栄紀，任　彰壎，細野雅祐，立田岳生，仁田一雄，第51回日本薬学会東北支部大会，青森，2012年10月
136. 封入体として得た組換えラムノース結合性レクチンのリフォールドおよび活性について. 永久　諒，佐藤真澄，細野雅祐，菅原栄紀，立田岳生，仁田一雄，第51回日本薬学会東北支部大会，青森，2012年10月
137. 腫瘍細胞に対するレスベラトロールの効果, 菅原栄紀，任 彰壎，細野雅祐，立田岳生，仁田一雄，第51回日本薬学会東北支部大会，青森，2012年10月
138. ヒトシアリダーゼ NEU2 の発現と機能, 小関弘恵知、和田 正、秦 敬子、高橋耕太、山口壹範、宮城妙子、第 6 回東北糖鎖研究会、弘前、2012 年 10 月
139. *9 形質膜シアリダーゼのがん化能への影響、山本晃司, 高橋耕太, 森谷節子, 和田 正, 秦 敬子, 宮城妙子、第 6 回東北糖鎖研究会、弘前、2012 年 10 月
140. *9 シアリダーゼ NEU3 は Wnt/beta-catenin シグナリングの調節を介してがん幹細胞性の維持に関与する．高橋耕太、和田 正、細野雅祐、山口壹範、仁田一雄、宮城妙子．第 7 1 回日本癌学会学術総会、札幌、2012 年 9 月
141. *10 担がん患者血清におけるシアリダーゼ活性の同定と診断への応用．宮城妙子 和田 正、細野雅祐、栃木達夫、川村貞文、佐藤郁郎、塩崎一弘、仁田一雄．第 71 回日本癌学会学術総会　札幌　2012 年 9 月
142. *10 ヒト担がん血清におけるシアリダーゼ活性の同定、秦敬子、森谷節子、細野雅祐、和田正、塩崎一弘、仁田一雄、宮城妙子　第 31 回日本糖質学会年会　鹿児島、2012 年 9 月
143. *9 シアリダーゼ異常による大腸がんの進展機構と治療への応用, 宮城妙子、高橋耕太、細野雅祐、和田 正、森谷節子、秦 敬子、山本晃司、山口壹範、仁田一雄　第 31 回日本糖質学会年会　鹿児島　2012 年 9 月
144. *9Sialidase in cancer progression.　Miyagi T. Sialo-Glyco 2012 Taipei, Taiwan 2012 9.10 (招待講演)
145. *13 ラムノース結合性レクチンはp21の発現上昇によりバーキットリンパ腫細胞の増殖を停止する.菅原栄紀，任彰壎，細野雅祐，立田岳生，仁田一雄，第31回日本糖質学会年会　鹿児島　2012年9月
146. α1,6 フコース転移酵素 Fut8 欠損による海馬機能の変化、福田友彦、顧 威、橋本弘和、酒井誠一郎、王 玉琴、伊左治知弥、八尾 寛、東 秀好、顧 建国、第 31 回日本糖質学会年会、2012 年 9 月、鹿児島
147. *16 GOLPH3 はシアル酸転移酵素と相互作用し糖鎖構造とインテグリンの機能を制御する、伊左治知弥、竹原雅子花、福田友彦、橋井則貴、高倉大輔、川崎ナナ、顧 建国、第 31 回日本糖質学会年会　鹿児島　2012 年 9 月
148. Fut8 ノックダウンによる activin/phospho-Smad2 を介した神経突起形成、顧 威、福田友彦、伊左治知弥、橋本弘和、顧 建国、第 31 回日本糖質学会年会　鹿児島　2012 年 9 月
149. α1,6 フコース転移酵素 Fut8 欠損マウスに認められた脳内神経伝達物質バランスの変化と海馬機能の低下、福田友彦、顧威、伊左治知弥、顧 建国、包括型脳科学研究推進支援ネットワーク夏のワークショップ　宮城　2012 年 7 月
150. コアフコースの機能と神経疾患との関連性について　顧 建国、括型脳科学研究推進支援ネットワーク夏のワークショップ班会議　宮城　2012 年 7 月
151. *14 N-acetylglucosaminyltransferases III and V regulate E-cadherin stability at the cell membrane. Implications in the Epithelial to Mesenchymal Transition, Salomé S. Pinho, Sandra Carvalho, Joana Cabral, Joana Figueiredo, Patricia Oliveira, Fátima Gärtner, Tomoya Isaji, Jianguo Gu, Fátima Carneiro, Raquel Seruca, Carla Oliveira, Naoyuki Taniguchi, Celso A. Reis, 8th International Symposidum on Glycosyltransferases, ハノーファー　ドイツ　2012 年 6 月
152. *14 Molecular mechanism for the regulation of N-acetylglucosaminyltransferase III expression and its roles in epithelial-mesenchymal transition. Jianguo Gu, 8th International Symposium on Glycosyltransferases ハノーファー　ドイツ　2012 年 6 月
153. *16 ラミニン 332 上の Bisecting GlcNAc 糖鎖はガレクチン 3 依存的ケラチノサイトの運動を抑制する、苅谷慶喜、顧 建国、第 44 回日本結合組織学会学術大会　第 59 回マトリックス研究会大会合同学術集会(大高賞受賞記念講演)　東京　2012 年 6 月
154. *10 ヒト担がん血清に於けるシアリダーゼ活性の検出とその性質.秦敬子、森谷節子、和田正、高橋耕太、山本晃司、宮城妙子： 第 78 回日本生化学会東北支部会　山形　山形大学医学部大講義室　2012 年 5 月

法人番号	041004
プロジェクト番号	S1201031

＜研究成果の公開状況＞（上記以外）

シンポジウム・学会等の実施状況、インターネットでの公開状況等

シンポジウム

1. 平成 28 年度（2016 年）第 10 回 東北医科薬科大学附属分子生体膜研究所シンポジウム
「生体膜糖鎖異常に起因する生活習慣病発症機序の解明と臨床への応用」
実施場所・日時　東北医科薬科大学・平成 29 年 3 月 2 日
招待講演　北島　健　先生（名古屋大学）
招待講演　大山　力　先生（弘前大学）
特別公演　川嵜　敏祐　先生（立命館大学）

2.平成 27 年度（2015 年）第 9 回 東北薬科大学附属分子生体膜研究所・第 9 回東北糖鎖研究会合同シンポジウム
実施場所・日時　東北薬科大学・平成 27 年 9 月 4，5 日
招待講演　宮城　妙子　先生（宮城県立がんセンター）
招待講演　山口　芳樹　先生（理化学研究所）
特別公演　谷口　直之　先生（理化学研究所）

3.平成 26 年度（2014 年）第 8 回 東北薬科大学附属分子生体膜研究所シンポジウム
「生体膜糖鎖異常に起因する生活習慣病発症機序の解明と臨床への応用」
実施場所・日時　東北薬科大学・平成 26 年 11 月 22 日
招待講演　門松　健治　先生（名古屋大学）
招待講演　鈴木　匡　先生（理化学研究所）
招待講演　Michael Pierce 先生（ジョージア大学）
招待講演　神奈木　玲児　先生（アカデミアシニカ）

4. 平成 25 年度（2013 年）第 7 回 東北薬科大学附属分子生体膜研究所合同シンポジウム・第 11 回糖鎖科学コンソーシアム（JCGG）
「生命科学に於ける糖鎖の底力―生活習慣病と糖鎖科学」
実施場所・日時　東北薬科大学・10 月 25、26 日
特別公演　片桐　秀樹　先生（東北大学）
特別公演　大隅　典子　先生（東北大学）
URL:http://www.jcgg.jp

5.平成 24 年度（2012 年）東北薬科大学附属分子生体膜研究所シンポジウム
「生体膜糖鎖異常に起因する生活習慣病発症機序の解明と臨床への応用」
実施場所・日時　東北薬科大学・11 月 3 日
招待講演　五十嵐　靖之　先生（北海道大学）
招待講演　柳澤　勝彦　先生（国立長寿医療研究センター）
招待講演　坪井　滋　先生（鷹揚郷腎研究所）
特別公演　箱守　仙一郎　先生（分子生体膜研究所顧問、University of Washington）

セミナー等

1. 第 17 回分子生体膜研究所戦略的研究基盤セミナー　　平成 29 年 3 月 16 日
渡邉　康春　先生（富山大学大学院医学薬学研究部　免疫バイオ・創薬探索研究講座客員講師）
「メタボリック症候群の基盤病態である内臓脂肪組織炎症・線維化を制御する自然免疫センサーと免疫細胞の解析」
館野　浩章　先生（国立研究開発法人　産業技術総合研究所　主任研究員）
「レクチンの再生医療への応用」

法人番号	041004
プロジェクト番号	S1201031

2. 第 16 回分子生体膜研究所戦略的研究基盤セミナー　　平成 28 年 9 月 28 日
   五十嵐　靖之　博士（北海道大学名誉教授　先端生命科学研究院招聘客員教授　東北医科薬科大学　客員教授）
   「アルツハイマーと神経細胞由来のエクソソームの役割－エクソソームによるアルツハイマー病の予防・治療は可能か？－」
3. 第 15 回分子生体膜研究所戦略的研究基盤セミナー　　平成 28 年 5 月 20 日
   Prof. Sandro Sonnino　教授（ミラノ大学）
   「Anti-glycan antibodies」
4. 第 14 回分子生体膜研究所戦略的研究基盤セミナー　　平成 28 年 3 月 23 日
   白井　孝　先生（公益財団法人　野口研究所　常任理事）
   「エンドグリコシダーゼによる糖鎖改変技術開発とそのバイオ医薬品トラスツズマブへの応用」
   松田　昭生　先生（公益財団法人　野口研究所　糖タンパク質工学研究室長）
   「変形性関節炎治療薬の探索研究～新規創薬標的の発掘からリード化合物の創製まで」
5. 第 13 回分子生体膜研究所戦略的研究基盤セミナー　　平成 28 年 2 月 26 日
   Prof. Roger A Raine　(ルイジアナ州立大学)
   「Sialin, a Multifunctional Protein with Potential as a Target for Cancer Therapeutics」
6. 第 12 回分子生体膜研究所戦略的研究基盤セミナー　　平成 26 年 10 月 9 日
   河野　まり　先生（NIDDK（アメリカ国立糖尿病・消化器・腎疾病研究所）・Biologist）
   「目で見る S1P1 受容体の活性化－活性化 S1P1 受容体視覚化マウスモデル」
   「Visualizing S1P1 recepter activation in vivo」
7. 第 11 回分子生体膜研究所戦略的研究基盤セミナー　　平成 26 年 9 月 3 日
   小川　誠一郎　名誉教授（慶應義塾大学理工学部）
   「バリエナミン型シャペロン活性化合物の設計と合成」
   「Design and Synthesis of Bioactive Valienamine-type Chaperones」
8. 第 10 回分子生体膜研究所戦略的研究基盤セミナー　　平成 26 年 8 月 25 日
   大関　泰裕　教授（横浜市立大学大学院生命ナノシステム科学研究科
   「グライコミクス解析に役立つ最新のレクチン研究」
9. 第 9 回分子生体膜研究所戦略的研究基盤形成支援事業セミナー　　平成 26 年 2 月 7 日
   結城　伸泰　教授（シンガポール国立大学医学部内科）
   「糖鎖相同性による自己免疫病の発症機序」
10. 第 8 回分子生体膜研究所戦略的研究基盤セミナー　　平成 26 年 1 月 15 日
    本橋ほづみ　教授（東北大学加齢医学研究所）
    「Keap1-Nrf2 制御系によるストレス応答と代謝リプログラミング」
11. 第 7 回分子生体膜研究所戦略的研究基盤セミナー　　平成 25 年 1 月 21 日
    有山　弘高　博士（静岡大学創造科学技術大学院　協力研究員
    「構造解析に向けた内向き整流性カリウムチャネルの細胞内領域のタンパク質の構築とマガイニン 2 やトランスポータン 10 が誘起する脂質膜中でのポア形成の研究」
12. 第 6 回分子生体膜研究所戦略的研究基盤セミナー　　平成 25 年 1 月 21 日
    黒田　喜幸（弘前大学大学院 保健学研究科　博士後期課程）
    「ヒアルロン酸合成阻害剤によるヒアルロン酸合成酵素のリン酸化への影響」
13. 第 5 回分子生体膜研究所戦略的研究基盤セミナー　　平成 24 年 11 月 16 日
    陸　吉順　博士（北海道大学大学院 生命科学院 P.D.）
    「Alg14 organizes the formation of Alg7/13/14 complex involved in *N*-glycosylation initiation」
14. 第 4 回分子生体膜研究所戦略的研究基盤セミナー　　平成 24 年 10 月 3 日
    Alessandro Prinetti 教授（ミラノ大学）
    「A GLYCOSPHINGOLIPID/CAVEOLIN-1-DEPENDENT SIGNALING COMPLEX CONTROLS THE ADHESION AND MOTILITY OF HUMAN OVARIAN CANCER CELLS」
15. 第 3 回分子生体膜研究所戦略的研究基盤セミナー　　平成 24 年 8 月 16 日
    ELENA CHIRICOZZI（Ph.D student University of Milan）
    「LacCer with long chain fatty acid and cell signaling in neutrophil functions」
    「Use of Pyrimethamine,a pharmacological chaperon, for the treatment of Sendhoff Disease」

法人番号	041004
プロジェクト番号	S1201031

16. 第 2 回分子生体膜研究所戦略的研究基盤セミナー　　平成 24 年 7 月 20 日
　　桝崎浩亮　博士（広島大学大学院生物圏科学研究科　特別研究員
　　「農林水産物からのレクチン本格的探索」
17. 第 1 回分子生体膜研究所戦略的研究基盤セミナー　　平成 24 年 5 月 15 日
　　稲森啓一郎　博士（米国 Iowa 大学 Carver College of Medicine 博士研究員）
　　「ジストログリカンの機能に必要な LARGE の糖転移活性」

＜インターネットでの公開状況＞
本プロジェクトの目的、研究計画概要及び平成 26 年度に提出した「研究進捗状況報告書の概要」をインターネット上に公開している。（http://www.tohoku-mpu.ac.jp/about/a13/）
　また、研究成果報告書概要も公開する。

14　その他の研究成果等

機能病態分子学部門: GM3S阻害剤のHTS（high-throughput screening）を製薬企業と実施中。

生体膜情報部門:我々はマウス足底皮下にガングリオシドGT1bを投与すると疼痛行動を引き起こし、低濃度のホルマリンによる痛みに対し痛覚過敏効果が認められることを見出した。
さらに、ホルマリン投与部位に予めシアリダーゼを投与するとホルマリンによる疼痛が減弱された*。これを根拠にシアリダーゼを新たな鎮痛薬として特許申請し、以下のごとく受諾、登録された。GT1bは神経終末からのグルタミン酸放出を促進することで疼痛反応を引き起こしている証拠が得られた（文献4,5）ので、グルタミン酸放出を抑制するグループII mGluRが関与する可能性が考えられ、GT1bによるmGluR2の活性抑制を検証したところ、上述のようにこの仮説を支持する結果を得た。
*Intraplantar injection of gangliosides produces nociceptive behavior and hyperalgesia via a glutamate signaling mechanism
S. Watanabe, K. Tan-No, T. Tadano H. Higashi
Pain, 152, 327-334 (2011)
特許登録:　特許第5414366号、疼痛治療剤、東秀好、渡辺俊、2013年11月22日登録

がん糖鎖制御学部門:がんの創薬を目的として、NEU3を標的とする抗体医薬と核酸医薬について、ベンチャー企業と連携開発中である。

細胞制御学部門:*Fut8 欠損マウスを用いて、理化学研究所や協和メデックス社と共同研究を行い、バイオマーカーとして有益になる可能性が高い「α1,6 フコースを認識する抗体」が得られそうになって、特許を申請する予定である。一方、3者で「抗コアフコシル化ヒト免疫グロブリンG抗体」特願 2016-179944 として 2016 年 9 月 14 日提出した。

法人番号	041004
プロジェクト番号	S1201031

15 「選定時」及び「中間評価時」に付された留意事項及び対応

＜「選定時」に付された留意事項＞

留意次項：前身の事業からの発展性をより明確にされたい。

＜「選定時」に付された留意事項への対応＞

前身の事業「生体膜の糖鎖機能と疾患に関する薬学的研究」を基盤に現在実施中の「生体膜糖鎖異常に起因する生活習慣病発症機序の解明と臨床への応用」が採択された。本プロジェクトでは、前身の事業の研究成果をもとに、臨床応用の可能性が高い2つのテーマ：

1） 肥満・糖尿病・アレルギーなどに対する疾患横断的な診断・治療法の開発
2） がん細胞膜糖鎖異常とその制御に基づく診断・治療法の開発

を中心に推進している。

具体的な成果：

機能病態分子学部門：GM3SKO マウスとメタボリックシンドロームモデルマウスとの交配実験により、著しい病態の改善を認めつつあること、炎症性サイトカインで刺激した脂肪細胞では選択的に GM3S 発現が上昇していることなどから、GM3S 阻害剤は、慢性炎症状態時に発現が上昇した GM3 を正常レベルに戻すことで治療効果が上がり、安全性の高い医薬創製に繋がる可能性がある。さらに我々は、CD4T 細胞と CD8T 細胞はそれぞれ異なるガングリオシド分子種によって機能が制御されていることを証明し、世界の関連分野の研究者が予想もしなかったアレルギー喘息などに対するＴ細胞サブセット特異的機能制御による治療法開発の可能性に繋がっている。従って、GM3S を分子標的とした画期的新薬の開発基盤を日本に創ることが望まれる。

生体膜情報部門：前身の事業では、生活習慣病の研究の一環としてブラジキニン受容体のガングリオシドによる制御を研究する中でATP/UTP 受容体 $P2Y_2$との共役を見出し、血圧制御や炎症といった似た機能を持つ受容体が共役することで、これらを効率良く制御している可能性を示した。また、ガングリオシドが GPCR を制御することを初めて示すことができたと自負している。現事業においては、肥満関連の GPCR に研究を集約している。肥満に関連するエネルギー代謝においてもこれを制御している GPRC5B 等の GPCR があり、それらが互いに連携、共役する可能性がある。実際、いくつかの代謝関連 GPCR の共役を新たに見出しつつある。GPRC5B については、同じクラス C に属する mGluR2 がその Allosteric modulator との反応において重要なアミノ酸残基が GPRC5B にも保存されていることから、その構造ー活性相関について得られた成果をフィードバックすることで、未だ不明なリガンドや allosteric modulator の解明に繋がると期待している。さらに、mGluR2 のガングリオシドによる活性制御を見出したので、GPRC5B を始めこのクラスの他の GPCR がガングリオシドにより制御されている可能性を検討したい。ガングリオシドの分布は組織によって大きく異なるので、そのために、同じ GPCR であっても発現される組織によって活性が異なるであろう。GPRC5B や mGluR は神経系と非神経系の両方の組織に発現されており、各組織に適合するような制御がガングリオシドによって行われている可能性がある。これを解明し、臨床応用に向けた基礎データを集めたい。

細胞制御学部門：これまでに我々は、インテグリンの N 型糖鎖が増殖因子受容体との複合体形成やその細胞内シグナル伝達の制御に重要であることが解明された。それをもとにして、主に増殖因子受容体を標的とする従来のがん治療薬の開発を加え、新たな糖鎖創薬に繋がる可能性がある。肝がんにおいてはFut8 の発現が上昇し、また Fut8 欠損マウスの肝がん誘発が著しく抑制されたことから、肝がんの治療薬の開発に新たな突破口になる可能性がある。

＜「中間評価時」に付された留意事項＞

該当なし

（様式2）

法人番号	041004
プロジェクト番号	S1201031

16 施設・装置・設備・研究費の支出状況（実績概要）　（千円）

年度・区分		支出額	内訳						
			法人負担	私学助成	共同研究機関負担	受託研究等	寄付金	その他（　　）	備考
平成24年度	施設	0							
	装置	45,329	22,665	22,664					
	設備	57,480	19,160	38,320					
	研究費	41,473	23,512	17,961					
平成25年度	施設	0							
	装置	0							
	設備	0							
	研究費	54,696	39,096	15,600					
平成26年度	施設	0							
	装置	0							
	設備	0							
	研究費	55,321	38,809	16,512					
平成27年度	施設	0							
	装置	0							
	設備	0							
	研究費	51,775	35,080	16,695					
平成28年度	施設	0							
	装置	0							
	設備	0							
	研究費	46,732	31,635	15,097					
総額	施設	0	0	0	0	0	0	0	
	装置	45,329	22,665	22,664	0	0	0	0	
	設備	57,480	19,160	38,320	0	0	0	0	
	研究費	249,997	168,132	81,865	0	0	0	0	
総計		352,806	209,957	142,849	0	0	0	0	

（様式2）

法人番号	041004

17 施設・装置・設備の整備状況 （私学助成を受けたものはすべて記載してください。）

《施　設》（私学助成を受けていないものも含め、使用している施設をすべて記載してください。）　（千円）

施設の名称	整備年度	研究施設面積	研究室等数	使用者数	事業経費	補助金額	補助主体
附属分子生体膜研究所	H18	1,020㎡	5	37 名			

※ 私学助成による補助事業として行った新増築により、整備前と比較して増加した面積

＿＿＿＿＿＿＿＿＿＿㎡

《装置・設備》（私学助成を受けていないものは、主なもののみを記載してください。）　（千円）

装置・設備の名称	整備年度	型　番	台　数	稼働時間数	事業経費	補助金額	補助主体
（研究装置）							
Imaging Flow Cytometry	H24	ImageStreamX	1式	473 h	45,329	22,664	私学助成
（研究設備）							
生体分子間相互作用解析装置	H24	ProteOnXPR36	1式	288 h	29,400	19,600	私学助成
高速液体ｸﾛﾏﾄｸﾞﾗﾌｼｽﾃﾑ	H24	LC-2000Plus	1式	10,580 h	7,500	5,000	私学助成
安定同位体測定装置	H24	INTEGRA2-CN	1式	176 h	20,580	13,720	私学助成
（情報処理関係設備）							

18 研究費の支出状況

【テーマ1】　（千円）

年　度	平成　24　年度			
小科目	支出額	積算内訳		
		主な使途	金額	主な内容
教育研究経費支出				
消耗品費	11,703	薬品	7,849	試薬
		実験材料	3,615	試料，実験用品
		その他	239	文房具，OA用品
通信運搬費	79	郵便･運搬	79	ｻﾝﾌﾟﾙ等配送等
印刷製本費	0	論文等印刷		論文印刷，文献複写
旅費交通費	94	学会･研究発表	94	学会参加，研究打合せ
報酬･委託料	105	委託	8	分析･検査，英文校正
		支払報酬	97	講演料、送金手数料
（賃借料）	19	設備賃借費	19	容器使用料
（修繕費）	212	設備修繕	212	機器修理･ﾒﾝﾃﾅﾝｽ
（諸会費）	0	学会等参加	0	学会，ｼﾝﾎﾟｼﾞｳﾑ
計	12,212			
アルバイト関係支出				
人件費支出（兼務職員）				
教育研究経費支出	0	--		--
計	0			
設備関係支出（1個又は1組の価格が500万円未満のもの）				
教育研究用機器備品	1,788	機械器具	1,788	遺伝子導入装置 Nucleofector 2d 他
図　書	0	和･洋書		
計	1,788			
研究スタッフ関係支出				
リサーチ･アシスタント	0			
ポスト･ドクター	2,498	研究補助	2,498	学内1人
研究支援推進経費	0			--
計	2,498			

（様式2）

法人番号	041004

【テーマ1】 （千円）

年　度	平成　25　年度			
小科目	支出額	積算内訳		
		主な使途	金額	主な内容
教育研究経費支出				
消耗品費	11,051	薬品	6,816	試薬
		実験材料	4,201	試料，実験用品
		その他	35	文房具，OA用品
通信運搬費	3	郵便･運搬	3	ｻﾝﾌﾟﾙ等配送等
印刷製本費	0	論文等印刷		論文印刷，文献複写
旅費交通費	125	学会･研究発表	125	学会参加，研究打合せ
報酬･委託料	134	委託	77	分析･検査，英文校正
		支払報酬	57	講演料、送金手数料
（賃借料）	9	設備賃借費	9	容器使用料
（修繕費）	238	設備修繕	238	機器修理･ﾒﾝﾃﾅﾝｽ
（諸会費）	8	学会等参加	8	学会，ｼﾝﾎﾟｼﾞｳﾑ
計	11,569			
アルバイト関係支出				
人件費支出（兼務職員）	0			
教育研究経費支出	0	--		--
計	0			
設備関係支出（1個又は1組の価格が500万円未満のもの）				
教育研究用機器備品	2,431	機械器具	2,431	等電点電気泳動装置一式 他
図書	0	和･洋書		
計	2,431			
研究スタッフ関係支出				
リサーチ･アシスタント	0			--
ポスト･ドクター	7,939	研究補助	7,939	学内2人
研究支援推進経費	0			--
計	7,939			

【テーマ1】 （千円）

年　度	平成　26　年度			
小科目	支出額	積算内訳		
		主な使途	金額	主な内容
教育研究経費支出				
消耗品費	12,270	薬品	8,165	試薬
		実験材料	4,029	試料，実験用品
		その他	76	文房具，OA用品
通信運搬費	70	郵便･運搬	70	ｻﾝﾌﾟﾙ等配送等
印刷製本費	263	論文等印刷	263	論文印刷，文献複写
旅費交通費	544	学会･研究発表	544	学会参加，研究打合せ
報酬･委託料	1,714	委託	1,630	分析･検査，英文校正
		支払報酬	84	講演料、送金手数料
（賃借料）	24	設備賃借費	24	容器使用料
（修繕費）	332	設備修繕	332	機器修理･ﾒﾝﾃﾅﾝｽ
（諸会費）	0	学会等参加	0	学会，ｼﾝﾎﾟｼﾞｳﾑ
計	15,218			
アルバイト関係支出				
人件費支出（兼務職員）	0			
教育研究経費支出	0	--		--
計	0			
設備関係支出（1個又は1組の価格が500万円未満のもの）				
教育研究用機器備品	1,283	機械器具	1,283	ﾃﾞｰﾀ解析装置 他
図書	0	和･洋書		
計	1,283			
研究スタッフ関係支出				
リサーチ･アシスタント	0			--
ポスト･ドクター	8,192	研究補助	8,192	学内2人（1名平成27年4月1日付採用：専任教員）
研究支援推進経費	0			--
計	8,192			

（様式2）

法人番号	041004

【テーマ1】 （千円）

年　度	平成　27　年度			
小科目	支出額	積算内訳		
		主な使途	金額	主な内容
教育研究経費支出				
消耗品費	9,951	薬品	6,879	試薬
		実験材料	3,071	試料，実験用品
		その他		文房具，OA用品
通信運搬費	237	郵便･運搬	237	ｻﾝﾌﾟﾙ等配送等
印刷製本費	167	論文等印刷	167	論文印刷，文献複写
旅費交通費	63	学会･研究発表	63	学会参加，研究打合せ
報酬･委託料	223	委託	56	分析･検査，英文校正
		支払報酬	167	講演料、送金手数料
（賃借料）	4	設備賃借費	4	容器使用料
（修繕費）	330	設備修繕	330	機器修理･ﾒﾝﾃﾅﾝｽ
（公租公課）	2		2	関税(試料)
計	10,977			
アルバイト関係支出				
人件費支出（兼務職員）	0			
教育研究経費支出	0	---		---
計	0			
設備関係支出（1個又は1組の価格が500万円未満のもの）				
教育研究用機器備品	5,470	機械器具	5,470	自動分注ｼｽﾃﾑ Eppendorf epMotion P5073C 他
図書	53	和･単行本	53	糖鎖の新機能開発･応用ﾊﾝﾄﾞﾌﾞｯｸ
計	5,523			
研究スタッフ関係支出				
リサーチ･アシスタント	0			---
ポスト･ドクター	4,200	研究補助	4,200	学内1人
研究支援推進経費	0			---
計	4,200			

【テーマ1】 （千円）

年　度	平成　28　年度			
小科目	支出額	積算内訳		
		主な使途	金額	主な内容
教育研究経費支出				
消耗品費	13,562	薬品	9,562	試薬
		実験材料	3,989	試料，実験用品
		その他	12	文房具，OA用品
通信運搬費	65	郵便･運搬	65	ｻﾝﾌﾟﾙ等配送等
印刷製本費	0	論文等印刷	0	論文印刷，文献複写
旅費交通費	38	学会･研究発表	38	学会参加，研究打合せ
報酬･委託料	402	委託	364	分析･検査，英文校正
		支払報酬	38	講演料、送金手数料
（賃借料）	22	設備賃借費	22	容器使用料
（修繕費）	250	設備修繕	250	機器修理･ﾒﾝﾃﾅﾝｽ
	0			
計	14,340			
アルバイト関係支出				
人件費支出（兼務職員）	0			
教育研究経費支出	0	---		---
計	0			
設備関係支出（1個又は1組の価格が500万円未満のもの）				
教育研究用機器備品	2,160	機械器具	2,160	ﾌﾟﾚｰﾄﾘｰﾀﾞｰSynergy
図書	0	和･洋書		
計	2,160			
研究スタッフ関係支出				
リサーチ･アシスタント	0			---
ポスト･ドクター	3,787	研究補助	3,787	学内1人(平成29年4月1日付採用:専任教員)
研究支援推進経費	0			---
計	3,787			

（様式2）

法人番号	041004

【テーマ2】 （千円）

年　度	平成　24　年度			
小科目	支出額	積算内訳		
		主な使途	金額	主な内容
教育研究経費支出				
消耗品費	15,400	薬品	11,442	試薬
		実験材料	3,410	試料，実験用品
		その他	548	文房具，OA用品
通信運搬費	291	郵便･運搬	291	ｻﾝﾌﾟﾙ等配送等
印刷製本費	0	論文等印刷		論文印刷，文献複写
旅費交通費	1,290	学会･研究発表	1,290	学会参加，研究打合せ
報酬･委託料	432	委託	302	分析･検査，英文校正
		支払報酬	130	講演料、送金手数料
（賃借料）	2	設備賃借費	2	容器使用料
（修繕費）	192	設備修繕	192	機器修理･ﾒﾝﾃﾅﾝｽ
（諸会費）	8	学会等参加	8	学会，ｼﾝﾎﾟｼﾞｳﾑ
計	17,614			
アルバイト関係支出				
人件費支出（兼務職員）	1,624	ｱｿｼｴｲﾄ･ｽﾀｯﾌ	1,624	学内1人、月給、7ヶ月
教育研究経費支出	0	---		---
計	1,624			
設備関係支出（1個又は1組の価格が500万円未満のもの）				
教育研究用機器備品	3,386	機械器具	3,386	高速冷却遠心機CR21GⅢ 他
図書	0	和･洋書		
計	3,386			
研究スタッフ関係支出				
リサーチ･アシスタント	0			---
ポスト･ドクター	2,351	研究補助	2,351	学内1人
研究支援推進経費	0			---
計	2,351			

【テーマ2】 （千円）

年　度	平成　25　年度			
小科目	支出額	積算内訳		
		主な使途	金額	主な内容
教育研究経費支出				
消耗品費	15,506	薬品	12,041	試薬
		実験材料	3,241	試料，実験用品
		その他	224	文房具，OA用品
通信運搬費	672	郵便･運搬	672	ｻﾝﾌﾟﾙ等配送等
印刷製本費	0	論文等印刷		論文印刷，文献複写
旅費交通費	1,026	学会･研究発表	1,026	学会参加，研究打合せ
報酬･委託料	39	委託	5	分析･検査，英文校正
		支払報酬	33	講演料、送金手数料
（賃借料）	1	設備賃借費	1	容器使用料
（修繕費）	269	設備修繕	269	機器修理･ﾒﾝﾃﾅﾝｽ
（諸会費）	60	学会等参加	60	学会，ｼﾝﾎﾟｼﾞｳﾑ
計	17,573			
アルバイト関係支出				
人件費支出（兼務職員）	0			
教育研究経費支出	0	---		---
計	0			
設備関係支出（1個又は1組の価格が500万円未満のもの）				
教育研究用機器備品	3,427	機械器具	3,427	日立ﾀﾞﾌﾞﾙﾋﾞｰﾑ分光光度計UH5300 他
図書	0	和･洋書		
計	3,427			
研究スタッフ関係支出				
リサーチ･アシスタント	0			---
ポスト･ドクター	11,757	研究補助	11,757	学内3人
研究支援推進経費	0			---
計	11,757			

（様式2）

法人番号	041004

【テーマ2】 （千円）

年　度	平成　26　年度			
小科目	支出見込額	積算内訳		
		主な使途	金額	主な内容
教育研究経費支出				
消耗品費	14,393	薬品	9,519	試薬
		実験材料	4,509	試料，実験用品
		その他	365	文房具，OA用品
通信運搬費	33	郵便･運搬	33	ｻﾝﾌﾟﾙ等配送等
印刷製本費	501	論文等印刷	501	論文印刷，文献複写
旅費交通費	1,272	学会･研究発表	1,272	学会参加，研究打合せ
報酬･委託料	503	委託	467	分析･検査，英文校正
		支払報酬	36	講演料、送金手数料
（賃借料）	3	設備賃借費	3	容器使用料
（修繕費）	730	設備修繕	730	機器修理･ﾒﾝﾃﾅﾝｽ
計	17,434			
アルバイト関係支出				
人件費支出（兼務職員）	0			
教育研究経費支出	0	---		---
計	0			
設備関係支出（1個又は1組の価格が500万円未満のもの）				
教育研究用機器備品	1,066	機械器具	1,066	遠心機用ｱﾝｸﾞﾙﾛｰﾀｰ R-15A 他
図書	0	和･洋書		
計	1,066			
研究スタッフ関係支出				
リサーチ･アシスタント	0			---
ポスト･ドクター	12,128	研究補助	12,128	学内3人
研究支援推進経費	0			---
計	12,128			

【テーマ2】 （千円）

年　度	平成　27　年度			
小科目	支出見込額	積算内訳		
		主な使途	金額	主な内容
教育研究経費支出				
消耗品費	14,012	薬品	8,556	試薬
		実験材料	4,976	試料，実験用品
		その他	480	文房具，OA用品
通信運搬費	12	郵便･運搬	12	ｻﾝﾌﾟﾙ等配送等
印刷製本費	791	論文等印刷	791	論文印刷，文献複写
旅費交通費	997	学会･研究発表	997	学会参加，研究打合せ
報酬･委託料	58	委託	57	分析･検査，英文校正
		支払報酬	1	講演料、送金手数料
（賃借料）	0	設備賃借費		容器使用料
（修繕費）	117	設備修繕	117	機器修理･ﾒﾝﾃﾅﾝｽ
（公租公課）	62		62	関税（試薬）
計	16,049			
アルバイト関係支出				
人件費支出（兼務職員）	0			
教育研究経費支出	0	---		---
計	0			
設備関係支出（1個又は1組の価格が500万円未満のもの）				
教育研究用機器備品	2,397	機械器具	2,397	振とう培養器 他
図書	53	和･単行本	53	糖鎖の新機能開発･応用ﾊﾝﾄﾞﾌﾞｯｸ
計	2,451			
研究スタッフ関係支出				
リサーチ･アシスタント	0			---
ポスト･ドクター	12,575	研究補助	12,575	学内3人
研究支援推進経費	0			---
計	12,575			

（様式2）

法人番号	041004

【テーマ2】 （千円）

年　度	平成　28　年度			
小 科 目	支出見込額	積　算　内　訳		
		主 な 使 途	金　額	主　な　内　容
教　育　研　究　経　費　支　出				
消 耗 品 費	14,119	薬品	9,450	試薬
		実験材料	4,440	試料，実験用品
		その他	229	文房具，OA用品
通信運搬費	114	郵便･運搬	114	ｻﾝﾌﾟﾙ等配送等
印刷製本費	540	論文等印刷	540	論文印刷，文献複写
旅費交通費	616	学会･研究発表	616	学会参加，研究打合せ
報酬･委託料	652	委託	573	分析･検査，英文校正
		支払報酬	79	講演料、送金手数料
（賃借料）	0	設備賃借費		容器使用料
（修繕費）	53	設備修繕	53	機器修理･ﾒﾝﾃﾅﾝｽ
（諸会費）	9	学会等参加費	9	学会･ｼﾝﾎﾟｼﾞｳﾑ
計	16,102			
ア　ル　バ　イ　ト　関　係　支　出				
人件費支出（兼務職員）	0			
教育研究経費支出	0	--		--
計	0			
設 備 関 係 支 出（1個又は1組の価格が500万円未満のもの）				
教育研究用機器備品	2,398	機械器具	2,398	マイクロプレートリーダー
図　書	0	和･洋書		
計	2,398			
研　究　ス　タ　ッ　フ　関　係　支　出				
リサーチ･アシスタント	0			--
ポスト･ドクター	7,945	研究補助	7,945	学内2人
研究支援推進経費	0			--
計	7,945			

研究テーマ①

肥満・糖尿病・アレルギーなどに対する
疾患横断的な診断・治療法の開発

Biochemical and Biophysical Research Communications 485 (2017) 427–431

Contents lists available at ScienceDirect

Biochemical and Biophysical Research Communications

journal homepage: www.elsevier.com/locate/ybbrc

N-glycan-dependent cell-surface expression of the $P2Y_2$ receptor and *N*-glycan-independent distribution to lipid rafts

Tetsuto Nakagawa, Chihiro Takahashi, Hitomi Matsuzaki, Shohei Takeyama, Shinpei Sato, Ayaka Sato, Yoshiyuki Kuroda, Hideyoshi Higashi*

Division of Glyco-Signal Research, Institute of Molecular Biomembrane and Glycobiology, Tohoku Medical and Pharmaceutical University, Sendai, Miyagi 981-8558, Japan

ARTICLE INFO

Article history:
Received 3 February 2017
Accepted 10 February 2017
Available online 14 February 2017

Keywords:
Cell surface expression
ER-associated protein degradation
Lipid raft
N-linked glycosylation
$P2Y_2$ receptor

ABSTRACT

$P2Y_2$ receptor ($P2Y_2R$) is a G-protein-coupled receptor (GPCR) that couples with Gαq/11 and is stimulated by ATP and UTP. $P2Y_2R$ is involved in pain, proinflammatory changes, and blood pressure control. Some GPCRs are localized in lipid rafts for interaction with other signaling molecules. In this study, we prepared *N*-glycan-deficient mutants by mutating the two consensus Asn residues for *N*-glycosylation to Gln to examine intracellular localization and association with lipid rafts. Western blotting of the wild type (WT) protein and mutants (N9Q, N13Q, N9Q/N13Q) in COS-7 cells showed that both Asn residues were glycosylated in the WT. Fluorescent microscopy analysis showed that WT, N9Q and N13Q were expressed in the endoplasmic reticulum (ER), Golgi body, and cell membrane, but N9Q/N13Q was only found in the ER. WT, N9Q and N13Q moved from the cell surface to endosomes within 15 min after UTP stimulation. WT and the N9Q/N13Q glycosylation-deficient mutant appeared in the detergent insoluble membrane fraction, lipid raft. These findings suggest that $P2Y_2R$ is localized in lipid rafts in the ER during biosynthesis, and that *N*-glycosylation is required for subsequent expression in the cell membrane. In the presence of epoxomicin, a proteasome inhibitor, there was a significant increase in the level of N9Q/N13Q, which suggests that *N*-glycan-deficient $P2Y_2R$ undergoes proteasomal degradation.

1. Introduction

The P2Y receptor family consists of G-protein-coupled receptors (GPCRs) that are activated by nucleotides such as adenosine triphosphate (ATP) and uridine triphosphate (UTP) and have various physiological functions. $P2Y_2$ receptor ($P2Y_2R$) is a Gαq/11-coupled receptor that has ATP and UTP as ligands and is expressed in mammalian tissues as a mediator of pain and inflammation. $P2Y_2R$ is associated with chloride secretion upon damage to respiratory tract epithelial cells [1], neuronal protection upon development of inflammation [2], phagocytosis of apoptotic cells by macrophages [3,4], and axonal elongation and differentiation of neurocytes [5]. There are an increasing number of reports on cross talk of signals *via* ATP and bradykinin upon development of inflammation [6–9], and we recently suggested that $P2Y_2R$ may be associated with the bradykinin receptor, B2R [10]. We also showed that sugar chains of B2R in Western blotting have a wide range of sizes, while the sizes of the sugar chains of $P2Y_2R$ are uniformly small.

Glycosylation promotes expression of proteins in the cell membrane [11] and some GPCRs are localized in membrane microdomains such as rafts for interaction with other signaling molecules and regulation of their activity [12–14]. In this study, the cellular localization and distribution to lipid rafts of WT $P2Y_2R$ and its mutants with loss of *N*-glycosylation sites were examined. The results showed that most of WT $P2Y_2R$ localized in lipid rafts and was expressed on the cell surface. Besides, a glycosylation-deficient $P2Y_2R$ mutant remained localized in lipid rafts, was not transferred beyond the ER, and was degraded by proteasomes. These results show that $P2Y_2R$ requires *N*-glycosylation for expression on the cell surface.

2. Materials and methods

Preparation of Plasmids. Human $P2Y_2R$ genes with a C-terminal *c*-Myc epitope tag (EQKLISEEDL) were prepared by PCR and

* Corresponding author.
E-mail address: hhigashi@tohoku-mpu.ac.jp (H. Higashi).

http://dx.doi.org/10.1016/j.bbrc.2017.02.061
0006-291X/

inserted into the pIRES2-EGFP plasmid (Clontech) with *Eco*RI and *Bam*HI sites. The IRES and EGFP gene sequences were removed using *Bam*HI and *Not*I, followed by blunting and ligation. Phusion High-Fidelity DNA Polymerase, restriction enzymes and a Quick Ligation kit were purchased from New England Biolabs. A DNA blunting kit was obtained from Takara Bio.

Cell culture. COS-7 cells were grown in D-MEM supplemented with 10% fetal calf serum and kept in a humidified 5% CO_2 atmosphere at 37 °C. COS-7 cells were transiently transfected using Viafect transfection reagent (Promega). In some experiments, epoxomicin (Peptide Institute Inc.) and bafilomycin A1 (LC Labs) were added at final concentrations of 1 and 0.1 μM, respectively, 12 h before harvesting.

Preparation of membrane fractions. COS-7 cells cultured on a 6-well plate were washed once with PBS and harvested using a cell scraper. After centrifugation at 3000 rpm for 5 min at 4 °C, precipitated cells were suspended in ice-cold TBS and homogenized in 500 μL of TBS containing Protease Inhibitor Cocktail (Nacalai Tesque) with 15 strokes using a teflon homogenizer on ice. The homogenate was centrifuged at 700 g for 5 min at 4 °C, and supernatant was centrifuged at 21,900 g for 90 min at 4 °C. This pellet was used as the total membrane fraction. In some experiment, the pellet was first treated with Peptide-*N*-Glycosidase F (PNGase F, New England Biolabs). The pellet was resuspended in 100 μL of ice-cold TBS containing 0.1% Triton X-100, and the tube was inverted using a rotator for 1 h at 4 °C. The supernatant and pellet from centrifugation at 21,900 g for 90 min at 4 °C were used as the detergent-soluble and detergent-insoluble membrane fractions, respectively.

Chloroform-methanol precipitation of protein. Methanol (400 μL) was added to 100 μL of detergent soluble membrane fraction, followed by 100 μL of $CHCl_3$, and then 300 μL of water. The mixture was vortexed well after each addition. After centrifugation at 17,400 g for 1 min at room temperature, the upper layer was removed while leaving the intermediate protein layer. To eliminate layer separation, 400 μL of methanol was added and the tube was inverted a few times to mix gently. After centrifugation at 17,400 g for 2 min, supernatant was removed and the dried pellet was used as a protein sample for SDS-PAGE.

SDS-PAGE and Western blotting. SDS-PAGE was performed using a Novex NuPAGE SDS-Gel system with 4–12% Bis-Tris gels (Thermo Fisher Scientific). Proteins were electrophoretically transferred to an Immobilon PVDF membrane (Merck Millipore) using a semi-dry blotting system. After blocking with 5% skim milk in PBS, $P2Y_2R$ was detected using *anti*-Myc mouse mAb (9B11; Cell Signaling Technology) followed by Horseradish Peroxidase conjugated anti-mouse IgG goat pAb (Jackson ImmunoResearch Lab.), and a Luminata Forte Western HRP Substrate (Merck Millipore).

Immunocytochemistry. COS-7 cells were cultured on Millicell EZ 8 well slides (Merck Millipore) for 1 day, stimulated with 0.1 mM UTP 15 min before fixation, and fixed by 3% paraformaldehyde after removal of the medium. After blocking with 5% skim milk in PBS, $P2Y_2R$ was detected using *anti*-Myc monoclonal antibodies (9B11 mouse mAb and 71D10 rabbit mAb; Cell Signaling Technology) followed by Alexa Fluor 546 conjugated secondary antibodies (Thermo Fisher Scientific), and observed using an Olympus FV1000 confocal laser scanning microscope. The following antibodies were used to detect organelles: *anti*-KDEL mouse mAb (10C3; Enzo Life Science) for the ER, *anti*-RCAS1 rabbit mAb (D2B6N; Cell Signaling Technology) for Golgi bodies, *anti*-Na^+-K^+ ATPase rabbit mAb (D2B6N; abcam) for plasma membrane, *anti*-hTransferin receptor mouse mAb (H68.4; Thermo Fisher Scientific) for recycling endosomes, *anti*-EEA1 mouse mAb (4/EEA1; BD Biosciences) for early endosomes, and Alexa Fluor 546 conjugated secondary antibodies (Thermo Fisher Scientific).

3. Results

3.1. Preparation of N-glycan-deficient mutants of $P2Y_2$ receptor

$P2Y_2R$ has *N*-glycosylation consensus sequences (Asn-X-Ser/Thr) at three sites, including two (Asn9 and Asn13) in the N-terminal extracellular region and a third (Asn66) located in an intracellular region. For deletion of *N*-glycans, N9Q and N13Q point mutants and the N9Q/N13Q double mutant were made by replacing Asn9, Asn13 or both with Gln residues (Fig. S1). Each $P2Y_2R$ construct had a *c*-Myc epitope tag attached to the C-terminal region for detection in Western blotting and immunostaining. After expressing WT or glycosylation-deficient $P2Y_2R$ in COS-7 cells, Western blotting was performed with *anti*-Myc antibody. Bands were detected at 46 kDa for the WT protein, 42 kDa for N9Q and N13Q, and 38 kDa for the glycosylation-deficient N9Q/N13Q protein, indicating that both Asn9 and Asn13 are glycosylated in $P2Y_2R$ (Fig. 1A). The apparent absence of glycosylation in WT, N9Q and N13Q $P2Y_2R$ (38 kDa bands) may have been due to transient expression. Membrane fractions prepared from COS-7 cells

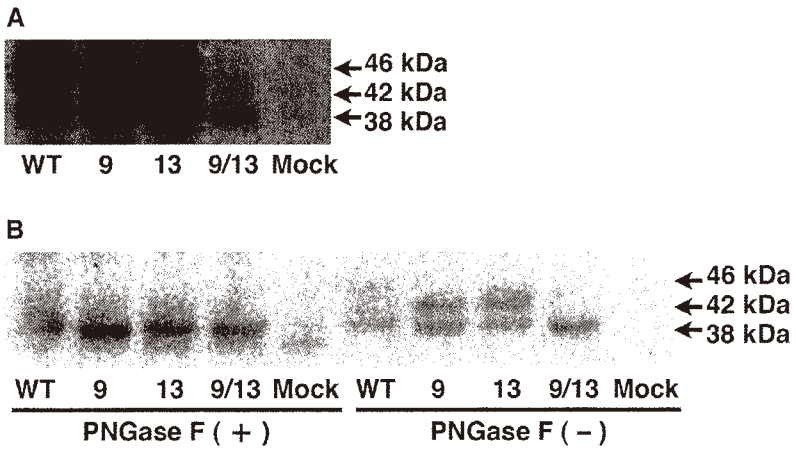

Fig. 1. Confirmation of N-linked glycosylation of $P2Y_2R$. (A) Membrane fractions of COS-7 cells expressing $P2Y_2R$ wild-type (WT) and mutants (N9Q, N13Q, N9Q/N13Q) analyzed by Western blotting using *anti*-Myc antibody. (B) Membrane fractions treated with PNGase F and examined by Western blotting.

expressing WT or mutant $P2Y_2R$ were treated with PNGase F and then subjected to Western blotting. The bands at 46 kDa for WT and 42 kDa for N9Q and N13Q were eliminated by PNGase F and only the 38 kDa band remained, thus confirming that both Asn9 and Asn13 in $P2Y_2R$ undergo *N*-glycosylation (Fig. 1B).

3.2. Subcellular localization of N-glycan deficient $P2Y_2$ receptor

WT and mutant $P2Y_2R$ were expressed in COS-7 cells to observe the distribution using confocal fluorescent microscopy. Except glycosylation-deficient mutant N9Q/N13Q, $P2Y_2R$ appeared to distribute on cell membrane and the distribution disappeared by UTP stimulation (Fig. 2A). Furthermore, WT and N9Q/N13Q were expressed in COS-7 cells for fluorescent double staining of marker proteins for the ER, Golgi body, late endosome, and recycling endosome, and observation by confocal microscopy. The distribution of WT $P2Y_2R$ was consistent with staining of the ER, Golgi body, and cell membrane (Fig. 2B). When the cells expressed WT $P2Y_2R$ were stimulated with UTP, distribution to the cell membrane decreased, and a granulated distribution overlapping early endosomes and recycling endosomes was observed (Fig. 2B). N9Q/N13Q $P2Y_2R$ was distributed only in the ER, and not in the cell membrane or Golgi body (Fig. 2B), and showed no changes in distribution upon stimulation with UTP (Fig. 2A). We examined localization of $P2Y_2R$ in lipid rafts, based on resistance to detergent. Almost all N9Q/N13Q proteins were found in the detergent insoluble membrane fraction, lipid raft (Fig. 3A). While N9Q/N13Q $P2Y_2R$ was not transferred to the Golgi body due to the absence of *N*-glycan, this mutant remained in the detergent insoluble membrane fraction. These results show that $P2Y_2R$ is distributed to lipid rafts in the ER membrane prior to *N*-glycosylation in ER.

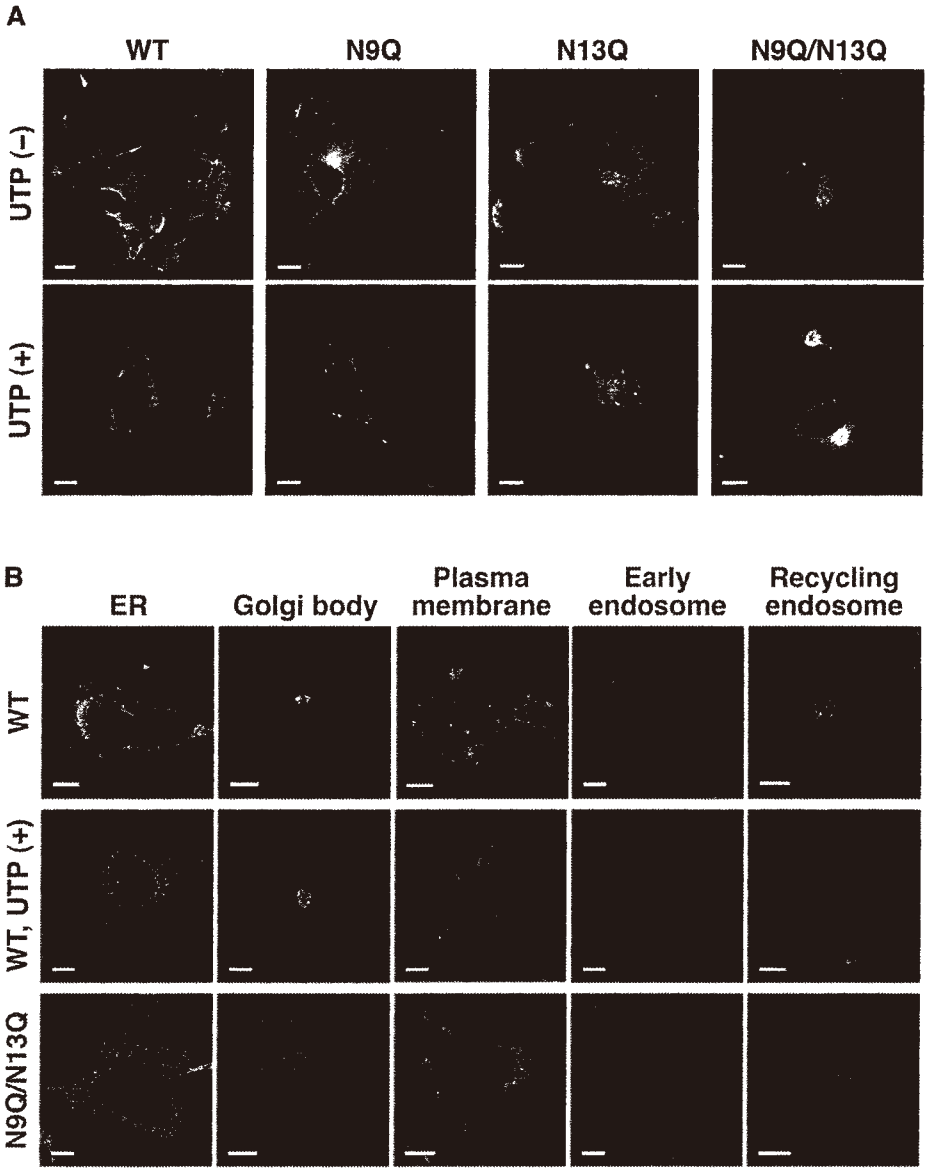

Fig. 2. Localization of $P2Y_2R$ WT and N9Q/N13Q mutant. (A) Intracellular localization in COS-7 cells observed by confocal laser scanning microscopy. In some experiments, cells were treated with 0.1 mM UTP (UTP (+)). (B) Colocalization of $P2Y_2R$ (red) and organelles (green) examined by double staining. Scale bars indicate 10 μm.

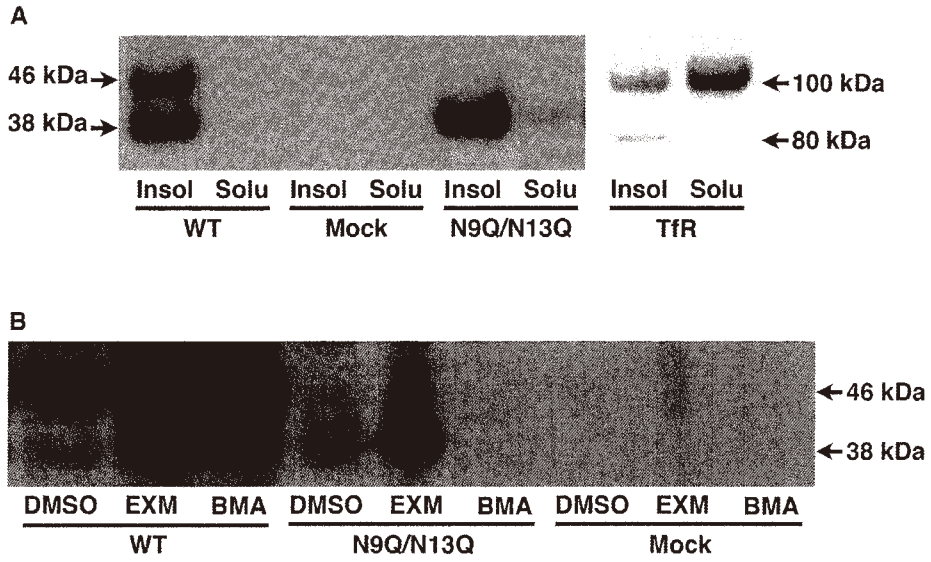

Fig. 3. Distribution to lipid rafts and proteolysis of $P2Y_2R$ mutants. (A) Detergent insoluble (Insol) and soluble (Solu) membrane fractions analyzed by Western blotting using *anti*-Myc antibody. To ensure separation of lipid raft and non-raft proteins, the distribution of transferrin receptor (TfR) in the same sample was examined. (B) COS-7 cells expressing $P2Y_2R$ WT or N9Q/N13Q were treated with the proteasome inhibitor epoxomicin (EXM) or the lysosome inhibitor bafilomycin A1 (BMA) 12 h before harvesting, and total membrane fractions were analyzed by Western blotting.

3.3. ER-associated degradation of N-glycan-deficient $P2Y_2$ receptor

Epoxomicin, a proteasome inhibitor, or bafilomycin A1, a lysosome-autophagy inhibitor, was added 12 h after transfection of WT or N9Q/N13Q $P2Y_2R$ in COS-7 cells. Culture was then performed for an additional 12 h. Western blotting and immunostaining with *anti*-Myc antibody showed significantly increased levels of WT and N9Q/N13Q $P2Y_2R$ in cells treated with epoxomicin (Fig. 3B). This result suggests that $P2Y_2R$ (38 kDa) without glycosylation is degraded by proteasomes. Glycosylated WT $P2Y_2R$ (46 kDa) also significantly increased because of degradation of proteins that were folded or glycosylated incorrectly due to excess expression. The level of WT $P2Y_2R$ was also increased by bafilomycin A1 (Fig. 3B). There was also an increased level of receptors without glycosylation, which were not transferred to the cell membrane, and such receptors may be degraded by autophagy. Collectively, these findings show that *N*-glycan modification at either of the two consensus sequences in the N-terminal domain of $P2Y_2R$ is required for transfer of the receptor to the cell membrane, and that non-glycosylated $P2Y_2R$ is degraded by proteasomes.

4. Discussion

Many GPCRs have *N*-glycosylation consensus sequences in the extracellular region, and most membrane proteins are likely to be glycosylated. Most of the roles of *N*-glycosylation in GPCRs are unclear, but glycosylation is known to be required for expression of angiotensin II receptor (AT_1R) and follicle-stimulating hormone receptor (FSHR) in cell membranes [15–17], and for maintaining a higher level of β_2-adrenaline receptor in the cell membrane, although glycosylation is not essential for this receptor [18]. In contrast, there are many receptors, including α_2-adrenaline receptor, H_2 histamine receptor, and muscarinic receptor, for which loss of *N*-glycosylation has almost no impact on cell surface expression [18–20].

Expression of membrane proteins at a designated site requires formation of the native fold, and misfolded proteins are excluded from transport vesicles by a quality control mechanism in the ER [21,22]. In this mechanism, non-native folds are detected to faciliate refolding or degradation. The mechanism involves molecular chaperones and lectin-like chaperones, which recognize the hydrophobic surface of non-native proteins, unbridged Cys residues, and immature *N*-glycosylation. Calnexin, calreticulin, and BiP are molecular chaperones related to GPCRs [23–28]. Calnexin and calreticulin are homologous lectin-like molecular chaperones that facilitate maturation of glycoproteins by recognizing *N*-glycosylation in an early phase of modification of membrane proteins and secreted proteins during folding [29]. BiP binds to the hydrophobic region on the surface of a protein during folding or to a misfolded protein, and is involved in retrograde trafficking to the ER or membrane transport to the cytoplasm in ER-associated degradation (ERAD) [30,31].

The results of this study show that both *N*-glycosylation consensus sequences in the extracellular region of $P2Y_2R$ are modified, and that the N9Q/N13Q double mutant with complete loss of glycosylation was not transferred to the cell surface and had an extremely low expression level. Since N9Q/N13Q $P2Y_2R$ cannot remain in the ER with lectin-like chaperones such as calnexin and calreticulin, molecular chaperones such as BiP that recognize hydrophobic surfaces may be involved. The expression level of N9Q/N13Q $P2Y_2R$ was low because the absence of *N*-glycosylation may prevent proper folding and quality control by calnexin and calreticulin, causing lower folding efficiency. Thus, the expressed protein is degraded by proteasomes as a misfolded protein, rather than remaining in the ER.

Lipid rafts mature in the Golgi body through synthesis of glycolipid and sphingomyelin structural components, and signaling proteins associate with the rafts during the course of maturation. However, the *N*-glycan-deficient $P2Y_2R$ existed in the detergent insoluble membrane fraction when the lipid raft was fractionated, while $P2Y_2R$ remained in the ER. Since the detergent insoluble membrane fraction is product in the experiment, these results may be an artifact, but it is possible that $P2Y_2R$ may associate with lipid rafts in the ER because glucosylceramide synthases are also present

in the ER, and retrograde traffic of vesiles can be observed from the *cis* Golgi. Prevously, we demonstrated that B2 bradykinin receptor is closely associated with $P2Y_2R$ and has heterogeneous glycans differ from $P2Y_2R$ [10]. If localization of $P2Y_2R$ in lipid rafts occurs before glycosylation, this may lead to uniform and short sugar chains. $P2Y_2R$ forms hetero-oligomers with various GPCRs [10,32,33], and $P2Y_2R$ localized in lipid rafts may recruit interacting GPCRs.

This study shows that *N*-glycosylation of $P2Y_2R$ is involved in receptor cell surface expression, and that $P2Y_2R$ is distributed to lipid rafts before *N*-glycosylation. $P2Y_2R$ lacking *N*-glycosylation at one site was transferred to the cell surface but the effect of partial loss of *N*-glycosylation on the receptor function of $P2Y_2R$ and association with other GPCRs are unclear.

Acknowledgements

Funding: This study was supported by the Strategic Study Base Formation Support Project for Private Universities, Japan.

Appendix A. Supplementary data

Supplementary data related to this article can be found at http://dx.doi.org/10.1016/j.bbrc.2017.02.061.

Transparency document

Transparency document related to this article can be found online at http://dx.doi.org/10.1016/j.bbrc.2017.02.061.

References

[1] V.L. Cressman, E. Lazarowski, L. Homolya, R.C. Boucher, B.H. Koller, B.R. Grubb, Effect of loss of $P2Y_2$ receptor gene expression on nucleotide regulation of murine epithelial Cl^- transport, J. Biol. Chem. 274 (1999) 26461–26468.
[2] G.A. Weisman, D. Ajit, R. Garrad, T.S. Peterson, L.T. Woods, C. Thebeau, J.M. Camden, L. Erb, Neuroprotective roles of the $P2Y_2$ receptor, Purinergic Signal 8 (2012) 559–578.
[3] M.R. Elliott, F.B. Chekeni, P.C. Trampont, E.R. Lazarowski, A. Kadl, S.F. Walk, D. Park, R.I. Woodson, M. Ostankovich, P. Sharma, J.J. Lysiak, T.K. Harden, N. Leitinger, K.S. Ravichandran, Nucleotides released by apoptotic cells act as a find-me signal to promote phagocytic clearance, Nature 461 (2009) 282–286.
[4] M. Kronlage, J. Song, L. Sorokin, K. Isfort, T. Schwerdtle, J. Leipziger, B. Robaye, P.B. Conley, H.C. Kim, S. Sargin, P. Schon, A. Schwab, P.J. Hanley, Autocrine purinergic receptor signaling is essential for macrophage chemotaxis, Sci. Signal 3 (2010) ra55.
[5] D.B. Arthur, K. Akassoglou, P.A. Insel, $P2Y_2$ receptor activates nerve growth factor/TrkA signaling to enhance neuronal differentiation, Proc. Natl. Acad. Sci. U. S. A. 102 (2005) 19138–19143.
[6] A. Luckhoff, R. Zeb, R. Busse, Desensitization of the bradykinin-induced rise in intracellular free calcium in cultured endothelial cells, Pflugers. Arch. 412 (1988) 654–658.
[7] G. Reetz, G. Reiser, Cross-talk of the receptors for bradykinin, serotonin, and ATP shown by single cell Ca^{2+} responses indicating different modes of Ca^{2+} activation in a neuroblastoma x glioma hybrid cell line, J. Neurochem. 62 (1994) 890–897.
[8] U. Czubayko, G. Reiser, Desensitization of P2U receptor in neuronal cell line. Different control by the agonists ATP and UTP, as demonstrated by single-cell Ca^{2+} responses, Biochem. J. 320 (Pt 1) (1996) 215–219.
[9] H.E. Lopez-Valdes, L. Beltran-Parrazal, K.C. Brennan, A.C. Charles, Bradykinin increases resensitization of purinergic receptor signaling in glioma cells, Cancer Cell Int. 10 (2010) 35.
[10] S. Yashima, A. Shimazaki, J. Mitoma, T. Nakagawa, M. Abe, H. Yamada, H. Higashi, Close association of B2 bradykinin receptors with $P2Y_2$ ATP receptors, J. Biochem. 158 (2015) 155–163.
[11] K. Ohtsubo, S. Takamatsu, C. Gao, H. Korekane, T.M. Kurosawa, N. Taniguchi, N-Glycosylation modulates the membrane sub-domain distribution and activity of glucose transporter 2 in pancreatic beta cells, Biochem. Biophys. Res. Commun. 434 (2013) 346–351.
[12] R. Shamri, V. Grabovsky, S.W. Feigelson, O. Dwir, Y. Van Kooyk, R. Alon, Chemokine stimulation of lymphocyte alpha 4 integrin avidity but not of leukocyte function-associated antigen-1 avidity to endothelial ligands under shear flow requires cholesterol membrane rafts, J. Biol. Chem. 277 (2002) 40027–40035.
[13] A.M. Navratil, S.P. Bliss, K.A. Berghorn, J.M. Haughian, T.A. Farmerie, J.K. Graham, C.M. Clay, M.S. Roberson, Constitutive localization of the gonadotropin-releasing hormone (GnRH) receptor to low density membrane microdomains is necessary for GnRH signaling to ERK, J. Biol. Chem. 278 (2003) 31593–31602.
[14] E.M. Hur, Y.S. Park, B.D. Lee, I.H. Jang, H.S. Kim, T.D. Kim, P.G. Suh, S.H. Ryu, K.T. Kim, Sensitization of epidermal growth factor-induced signaling by bradykinin is mediated by c-Src. Implications for a role of lipid microdomains, J. Biol. Chem. 279 (2004) 5852–5860.
[15] S. Jayadev, R.D. Smith, G. Jagadeesh, A.J. Baukal, L. Hunyady, K.J. Catt, N-linked glycosylation is required for optimal AT_{1a} angiotensin receptor expression in COS-7 cells, Endocrinology 140 (1999) 2010–2017.
[16] B. Deslauriers, C. Ponce, C. Lombard, R. Larguier, J.C. Bonnafous, J. Marie, N-glycosylation requirements for the AT_{1a} angiotensin II receptor delivery to the plasma membrane, Biochem. J. 339 (Pt 2) (1999) 397–405.
[17] D. Davis, X. Liu, D.L. Segaloff, Identification of the sites of N-linked glycosylation on the follicle-stimulating hormone (FSH) receptor and assessment of their role in FSH receptor function, Mol. Endocrinol. 9 (1995) 159–170.
[18] D.G. Sawutz, S.M. Lanier, C.D. Warren, R.M. Graham, Glycosylation of the mammalian alpha 1-adrenergic receptor by complex type N-linked oligosaccharides, Mol. Pharmacol. 32 (1987) 565–571.
[19] Y. Fukushima, Y. Oka, T. Saitoh, H. Katagiri, T. Asano, N. Matsuhashi, K. Takata, E. van Breda, Y. Yazaki, K. Sugano, Structural and functional analysis of the canine histamine H2 receptor by site-directed mutagenesis: *N*-glycosylation is not vital for its action, Biochem. J. 310 (Pt 2) (1995) 553–558.
[20] C.J. van Koppen, N.M. Nathanson, Site-directed mutagenesis of the m2 muscarinic acetylcholine receptor. Analysis of the role of *N*-glycosylation in receptor expression and function, J. Biol. Chem. 265 (1990) 20887–20892.
[21] L. Ellgaard, A. Helenius, Quality control in the endoplasmic reticulum, Nat. Rev. Mol. Cell Biol. 4 (2003) 181–191.
[22] B. Kleizen, I. Braakman, Protein folding and quality control in the endoplasmic reticulum, Curr. Opin. Cell Biol. 16 (2004) 343–349.
[23] J.P. Morello, A. Salahpour, U.E. Petaja-Repo, A. Laperriere, M. Lonergan, M.F. Arthus, I.R. Nabi, D.G. Bichet, M. Bouvier, Association of calnexin with wild type and mutant AVPR2 that causes nephrogenic diabetes insipidus, Biochemistry 40 (2001) 6766–6775.
[24] P.M. Lanctot, P.C. Leclerc, E. Escher, G. Guillemette, R. Leduc, Role of N-glycan-dependent quality control in the cell-surface expression of the AT_1 receptor, Biochem. Biophys. Res. Commun. 340 (2006) 395–402.
[25] D. Mizrachi, D.L. Segaloff, Intracellularly located misfolded glycoprotein hormone receptors associate with different chaperone proteins than their cognate wild-type receptors, Mol. Endocrinol. 18 (2004) 1768–1777.
[26] S. Siffroi-Fernandez, A. Giraud, J. Lanet, J.L. Franc, Association of the thyrotropin receptor with calnexin, calreticulin and BiP. Efects on the maturation of the receptor, Eur. J. Biochem. 269 (2002) 4930–4937.
[27] P.M. Lanctot, P.C. Leclerc, M. Clement, M. Auger-Messier, E. Escher, R. Leduc, G. Guillemette, Importance of *N*-glycosylation positioning for cell-surface expression, targeting, affinity and quality control of the human AT_1 receptor, Biochem. J. 390 (2005) 367–376.
[28] A. Anukanth, H.G. Khorana, Structure and function in rhodopsin. Requirements of a specific structure for the intradiscal domain, J. Biol. Chem. 269 (1994) 19738–19744.
[29] D.B. Williams, Beyond lectins: the calnexin/calreticulin chaperone system of the endoplasmic reticulum, J. Cell. Sci. 119 (2006) 615–623.
[30] B.D. Hamman, L.M. Hendershot, A.E. Johnson, BiP maintains the permeability barrier of the ER membrane by sealing the lumenal end of the translocon pore before and early in translocation, Cell 92 (1998) 747–758.
[31] B. Meusser, C. Hirsch, E. Jarosch, T. Sommer, ERAD: the long road to destruction, Nat. Cell Biol. 7 (2005) 766–772.
[32] K. Yoshioka, O. Saitoh, H. Nakata, Heteromeric association creates a P2Y-like adenosine receptor, Proc. Natl. Acad. Sci. U. S. A. 98 (2001) 7617–7622.
[33] T. Suzuki, K. Namba, H. Tsuga, H. Nakata, Regulation of pharmacology by hetero-oligomerization between A_1 adenosine receptor and $P2Y_2$ receptor, Biochem. Biophys. Res. Commun. 351 (2006) 559–565.

Glycobiology, 2015, vol. 25, no. 3, 303–318
doi: 10.1093/glycob/cwu112
Advance Access Publication Date: 9 October 2014
Original Article

Original Article

Control of homeostatic and pathogenic balance in adipose tissue by ganglioside GM3

Masakazu Nagafuku[2], Takashige Sato[2,3], Saya Sato[2], Kyoko Shimizu[4], Toshio Taira[4], and Jin-Ichi Inokuchi[1,2]

[2]Division of Glycopathology, Institute of Molecular Biomembrane and Glycobiology, Tohoku Pharmaceutical University, 4-4-1, Komatsushima, Aoba-ku, Sendai, Miyagi 981-8558, Japan, [3]Cosmo Bio Co., Ltd., Tokyo 135-0016, Japan, and [4]Primary Cell Co., Ltd., Sapporo 001-0021, Japan

[1]To whom correspondence should be addressed: Tel: +81-22-727-0117; Fax: +81-22-727-0076; e-mail: jin@tohoku-pharm.ac.jp

Received 6 August 2014; Revised 26 September 2014; Accepted 3 October 2014

Abstract

Ganglioside GM3 (Siaα2-3Galβ1-4Glcβ1-1Cer) has been known to participate in insulin signaling by regulating the association of the insulin receptor in caveolae microdomains (lipid rafts), which is essential for the execution of the complete insulin metabolic signaling in adipocytes. Macrophage-secreted factors including proinflammatory cytokines, tumor necrosis factor-α and interleukin-1β, in adipose tissues have been known to limit the local adipogenesis and induce insulin resistance; however, the interplay between adipocytes and macrophages upon regulation of GM3 expression is not clear. GM3 was virtually absent in primary adipocytes differentiated from macrophage-depleted mesenteric stromal vesicular cells, which accompanies enhancement of insulin signaling and adipogenesis. We found that the expression of GM3 is governed by soluble factors including steady-state levels of proinflammatory cytokines secreted from resident macrophages. The direct involvement of GM3 in insulin signaling is demonstrated by the fact that embryonic fibroblasts obtained from GM3 synthase (*GM3S*)-deficient mice have increased insulin signaling, when compared with wild-type embryonic fibroblasts, which in turn leads to enhanced adipogeneis. In addition, GM3 expression in primary adipocytes is increased under proinflammatory conditions as well as in adipose tissue of diet-induced obese mice. Moreover, *GM3S*-deficient mice fed high-fat diets become obese but are resistant to the development of insulin resistance and chronic low-grade inflammatory states. Thus, GM3 functions as a physiological regulatory factor of the balance between homeostatic and pathological states in adipocytes by modulating insulin signaling in lipid rafts.

Key words: adipogenesis, GM3 ganglioside, inflammatory cytokines, insulin resistance, macrophages

Introduction

Glycosphingolipids (GSLs), and their sialic acid (SA)-containing derivatives, gangliosides, are components of membrane lipids in which the lipid portion is embedded in the outer leaflet of the plasma membrane with the sugar chain extending to the extracellular space; the structural features of GSLs affect membrane fluidity and allow for microdomain formation, contributing to cell–cell interaction and receptor-mediated signal transduction (Hakomori 2002). We have previously shown that in cultured adipocytes in a state of tumor necrosis factor (TNF)-α-induced insulin resistance, removal of GSLs by the inhibition of glucosylceramide (GlcCer) synthase, the first step enzyme for the biosynthesis of all of GSLs, results in nearly complete recovery of insulin receptor (IR) signaling (Tagami et al. 2002). A number of studies in animal models demonstrate that pharmacological inhibition of GSLs ameliorates insulin resistance and prevents some manifestations of metabolic syndrome (Aerts et al. 2007; Zhao et al. 2007; Bijl et al. 2009; van Eijk et al. 2009; Yew et al. 2010). Further, we have shown

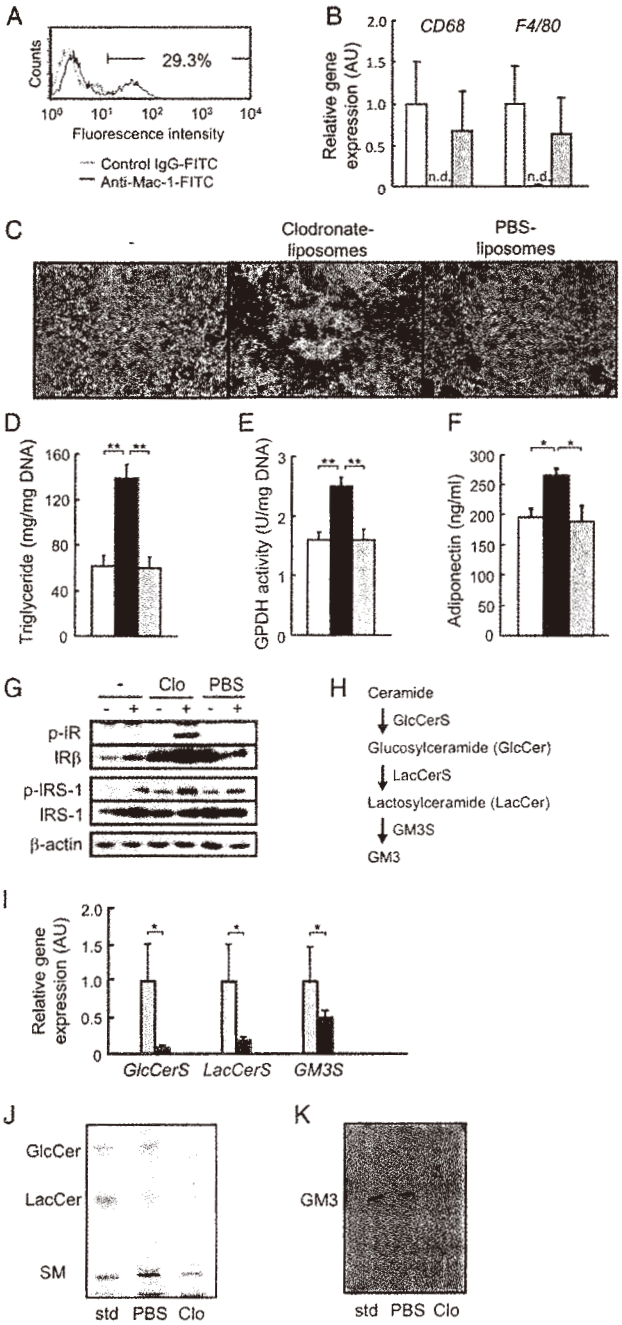

Fig. 1. Adipogenic efficiency of mesenteric preadipocytes is enhanced by macrophage depletion using clodronate-liposomes. (**A**) Freshly isolated mSVCs were stained with PE-conjugated anti-Mac-1 mAb or PE-conjugated isotype control mAb and then analyzed by flow cytometry. The number in the histogram represents the percentages of cells exhibiting positive staining for the macrophage marker Mac-1. One representative experiment of three similar experiments is shown. (**B**) Total mSVCs were untreated (–) or treated with 1/100 clodronate- or PBS-liposomes. After 48-h treatment of total mSVCs, mRNA expression of CD68 or F4/80 was determined by quantitative RT-PCR analysis. Data represent the relative gene expression in treated cells compared with that in untreated cells (set to 1.0 separately for each target gene). n.d., not detectable. White, black and gray bars represent untreated and clodronate-liposome and PBS-liposome-treated mSVCs, respectively. (**C–G**) Isolated mSVCs, untreated or clodronate-liposome- or PBS-liposome-treated were cultured in adipogenic medium. After 8 days, lipid-laden cells were stained with Oil-Red O solution and visualized under a phase-contrast microscope (C). The cultured mSVCs were harvested, lysed and analyzed to determine intracellular triglyceride content (D) and GPDH activity (E). Adiponectin concentrations in culture media of the cultured mSVCs were determined at day 8 (F). White, black and gray bars (**I**) in (D)–(F) represent untreated and clodronate-liposome and PBS-liposome-treated mSVCs, respectively. The cultured mSVCs were stimulated with insulin (30 nM) for 5 min and lysed for immunoblot analysis of components of IR signaling pathways (G). GM3 biosynthetic pathway (**H**). (**I–K**) Total mSVCs were left untreated or treated with 1/100 clodronate- or PBS-liposomes. After 48 h of treatment,

that expression of ganglioside GM3 (Siaα2-3Galβ1-4Glcβ1-1Cer), which is the simplest ganglioside species synthesized by GM3 synthase (GM3S; also called SAT-I/ST3Gal-5; Inokuchi and Uemura 2014), is increased in metabolic diseases (Tagami et al. 2002; Sato et al. 2008). *GM3S* gene expression and GM3 content are upregulated in visceral adipose tissue of obese model animals and serum GM3 levels are 2-fold higher in obese patients with type 2 diabetes and/or dyslipidemia. Moreover, *GM3S*-deficient mice exhibit enhanced insulin signaling and less susceptibility to insulin resistance induced by a high-fat diet (HFD; Yamashita et al. 2003). These results imply that GM3 is responsible for insulin homeostasis.

We have postulated a working hypothesis "insulin resistance as a membrane microdomain disorder" (Inokuchi 2010, 2011, 2014) because of the fact that the abnormal increase of membrane GM3 in adipocytes induced by inflammatory cytokine TNFα resulted in the elimination of the IR from caveolae (Kabayama et al. 2005, 2007). The association of IR in caveolae is essential to execute the complete insulin metabolic signaling (Couet et al. 1997).

Visceral adipose tissues are composed of not only adipocytes but also immune cells including resident macrophages and T lymphocytes, and other types of cells (Suganami and Ogawa 2011; Chalwa et al. 2011; Samaan 2011; Sun et al. 2012). Although the interplay between adipocytes and resident macrophages is well documented (Suganami and Ogawa 2011; Chalwa et al. 2011; Samaan 2011), their effect on raft-mediated insulin signaling in adipose tissue is not studied. Here we demonstrate the biosynthesis of the raft resident molecule GM3 in adipocytes is strictly controlled by soluble factors including proinflammatory cytokines secreted from resident macrophages under not only proinflammatory states but also steady-state conditions. Furthermore, obese *GM3S*-deficient mice fed HFDs are resistant to developing proinflammatory states in adipose tissues. These results indicate that GM3 functions as a homeostatic and pathogenic regulatory factor in adipose tissue.

Results

Adipogenesis of mesenteric preadipocytes is increased following depletion of the resident macrophages

Mesenteric stromal vascular cells (mSVCs) isolated from adipose tissue consist of preadipocytes, fibroblasts, endothelial cells, mesenchymal stem cells and macrophages. Fluorescence-activated cell sorting (FACS) analysis for the macrophage markers Mac-1 and CD163 indicated that, of the total mSVCs, ~30% were macrophages (Figure 1A). To examine whether these resident macrophages had any regulatory function for the adipogenesis of preadipocytes, the macrophages were removed from the total mSVCs using clodronate-liposomes. Many reports have repeatedly demonstrated that clodronate-liposomes, liposomes containing dichloromethylene diphosphonate, efficiently and selectively deplete phagocytic macrophages by apoptosis, while other non-phagocytic immune cells such as T cells, B cells and dendritic cells are not eliminated (van Rooijen and van Kesteren-Hendrik 2002; Dupasquier et al. 2004; Sunderkotter et al. 2004). PBS-liposomes were used as a control, which were prepared with PBS in place of clodronate. First, we evaluated the efficiency of clodronate-liposomes on macrophage depletion by measuring the expression of macrophage-specific genes. The mSVCs treated with clodronate-liposomes did not express macrophage marker genes such as *CD68* and *F4/80* (Figure 1B). We next examined the effect of clodronate-liposomes on adipogenic events. The mSVCs were left untreated or treated with clodronate- or clodronate-liposomes and were cultured in adipogenic differentiation conditions for 8 days. The cultures were stained with Oil-Red O to observe lipid-laden cells (Figure 1C). The number of lipid-laden cells had increased in the macrophage (M)-depleted mSVCs compared with the total mSVCs. These results indicate that, in adipogenic cultures, macrophage depletion results in enhancement of formation of new adipocytes. In addition, triglyceride accumulation, glycerol 3-phosphate dehydrogenase (GPDH) activity and adiponectin production, which are indicators of adipogenesis, were all enhanced in mSVCs treated with clodronate-liposomes (Figure 1D–F). The increased adiponectin production indicates that, in the absence of macrophages, more mesenteric preadipocytes are functionally differentiated into mature adipocytes. As adiponectin has been shown to be a key regulator of insulin sensitivity, we therefore examined whether increased adiponectin production had an impact on insulin-mediated signal transduction of differentiated mesenteric adipocytes. Phosphorylation levels of both IR and insulin receptor substrate 1 (IRS-1) after insulin stimulation were dramatically increased by depleting macrophages and protein levels of IR per se were increased in the mSVCs treated with clodronate-liposomes, at the same time (Figure 1G).

Resident macrophages are involved in regulation of GSL expression in visceral adipocytes

GSLs are built on a ceramide backbone comprising a long-chain amino alcohol, sphingosine and an amide-linked fatty acid. Gangliosides are SA-containing GSLs that are largely concentrated in lipid rafts (Figure 1H). GM3, the simplest of the gangliosides, is synthesized by GM3S, which catalyzes the transfer of SA to the nonreducing terminal galactose of lactosylceramide (LacCer). GM3S levels are markedly increased in cultured 3T3-L1 adipocytes in insulin-resistant states induced by TNFα treatment, as well as in adipose tissues of obese *ob/ob* mice (Tagami et al. 2002). Furthermore, we demonstrated previously that the state of insulin resistance in 3T3-L1 adipocytes treated with TNFα was almost completely normalized by inhibition of the synthesis of GM3 by an inhibitor of GlcCer synthase, D-threo-1-phaenyl-2-decanoylamino-3-morpholino-1-propanol (Inokuchi and Radin 1987; Tagami et al. 2002). Thus, a tight relationship between cellular levels of GM3 and inflammatory states, including insulin resistance, in adipocytes is strongly suggested. It is known that macrophages participate in adipogenesis (Constant et al. 2006) and the development of chronic low-grade inflammatory states in adipose tissues (Chalwa et al. 2011; Samaan 2011; Suganami and Ogawa 2011; Sun et al. 2012). Indeed, after removal of resident macrophages from mSVCs, the adipogenic potential was significantly increased (Figure 1C) with concomitant

mRNA expression of *GlcCerS*, *LacCerS* or *GM3S* was determined by quantitative RT-PCR analysis (I). Data represent the relative gene expression in treated cells compared with that in untreated cells (set to 1.0 separately for each target gene). White and black bars in (I) represent PBS-liposome- and clodronate-liposome-treated mSVCs, respectively. After 48 h of treatment, neutral and acidic lipids were obtained, separated on TLC plates and then visualized with orcinol-sulfuric acid (J) or stained with anti-GM3 mAb followed by HRP-conjugated anti-mouse Ig (K). Std, standard lipids; PBS, PBS-liposomes; Clo, clodronate-liposomes. The same results were obtained in three independent experiments. $*P<0.05$, $**P<0.01$.

increase of insulin sensitivity (Figure 1G), suggesting that the expression of GM3 in adipocytes may be regulated by factors secreted from resident macrophages. So, we analyzed the expression of GSLs in mature adipocytes differentiated from mSVCs treated with or without clodronate-liposomes. Notably, in adipocytes differentiated from M-depleted mSVCs, the expression levels of GSL synthase genes, such as *GlcCer synthase (GlcCerS)*, *LacCer synthase (LacCerS)* and *GM3synthase (GM3S)*, were significantly decreased (Figure 1I). In addition, the cellular GlcCer and LacCer in M-depleted cells were greatly decreased confirmed by thin-layer chromatography (TLC) with $CuSO_4$ staining (Figure 1J). Moreover, the almost complete absence of GM3 in the macrophage-depleted cells was confirmed by TLC-immunostainining using an anti-GM3 antibody (Figure 1K).

Suppression of adipogenisis of mesenteric preadipocytes by the steady-state levels of proinflammatory cytokines secreted from macrophages with concomitant decrease of GSL content

The above data raised the question of whether cell–cell contact between preadipocytes and macrophages or soluble factors secreted from macrophages were required for suppression of adipogenesis and decrease of GSL content. In order to gain more insight into the role of resident macrophages on adipogenesis, we used an indirect coculture system (transwell culture and a magnetic sorting system, to deplete macrophages from mSVCs) (Figure 2A). Consistent with the above results using clodronate-liposomes (Figure 1A–G), the M-depleted mSVCs showed increased adiposity and hyperinsulin sensitivity; the number of lipid-laden cells (Figure 2B), triglyceride accumulation (Figure 2C), GPDH activity (Figure 2D), adiponectin secretion (Figure 2E) and IR phosphorylation in response to insulin (Figure 2F) all increased in the M-depleted mSVCs compared with the total mSVCs. After 8 days in the differentiation culture, the enhanced adipogenesis observed in M-depleted mSVCs was returned to the same level as total mSVCs when M-depleted mSVCs were indirectly cocultured with macrophages (Figure 2B–D). Taken together, these results indicate that soluble factors which are secreted from resident macrophages are enough to suppress the adipogenesis of mesenteric preadipocytes. In this situation, the expression levels of *GlcCerS*, *LacCerS* and *GM3S* genes were markedly decreased in adipocytes differentiated from M-depleted mSVCs (Figure 2G). We also found that, the resident macrophages at steady-state conditions produced TNFα (41 pg/mL), interleukin (IL)-1β (18 pg/mL) and IL-6 (338 pg/mL) by total mSVCs but not M-depleted SVCs (Figure 2H). Taken together, GSL levels of preadipocytes and mature adipocytes are tightly maintained by soluble factors including steady-state levels of proinflammatory cytokines secreted from resident macrophages.

Inflammatory cytokines exert an anti-adipogenic effect toward mesenteric preadipocytes

It is possible that soluble anti-adipogenic factors produced by macrophages are inflammatory cytokines, since many studies have revealed that proinflammatory cytokines such as TNFα, IL-6 and IL-1β inhibit adipogenesis of preadipocytes and macrophages are a major source of such cytokines (Feve 2005). We examined whether these cytokines suppressed adipogenesis of the mesenteric preadipocytes. Thioglycollate (TGM) or lipopolysaccharide (LPS) treatment-induced gene expression of *TNFα* and *IL-6* (Figure 3A and B) in total mSVCs. In accordance with this, these cells produced marked amounts of TNFα and IL-6 as well as IL-1β following TGM or LPS treatment (Figure 3C–E). Notably, the M-depleted mSVCs did not produce TNFα and IL-1β, even when treated with TGM or LPS (Figure 3C and E); on the contrary much lower amounts of IL-6 were produced in the M-depleted mSVCs compared with total mSVCs in response to TGM or LPS (Figure 3D). These results demonstrate that TGM and LPS mainly stimulate macrophages, but not preadipocytes or other cell populations in mSVCs.

In accordance with these results, adipogenesis of mSVCs was prevented by the addition of TNFα or IL-1β to the adipogenic medium (Figure 4). TNFα and IL-1β are known to act on macrophages and induce the synthesis of other inflammatory cytokines in the macrophages (Neta et al. 1992). However, it is notable that adipogenesis of M-depleted mSVCs was also suppressed by these cytokines (Figure 4). These data negated the possibility that TNFα or IL-1β directly induced the inflammatory responses of the macrophages, which resulted in anti-adipogenesis of mSVCs. Together, these data suggest that proinflammatory cytokines produced by resident macrophages suppress adipogenesis of mesenteric preadipocytes.

It has been reported that the expression levels of proinflammatory cytokines were increased in the adipose tissues of diabetic obese model animals, *ob/ob*, *db/db* and diet-induced obese mice (Hotamisligil et al. 1993; Ye et al. 2007). So, we examined the effects of TNFα and/or IL-1β (0.2 ng/mL each) on the gene expression of *GlcCerS*, *LacCerS* and *GM3S* using primary cultured rat primary adipocytes. Among the three genes responsible for GSL synthesis, the selective enhancement of the *GM3S* gene was observed when the adipocytes were treated with a combination of these proinflammatory cytokines (Figure 4E). There is an especially synergistic effect between TNFα and IL-1β.

Enhanced adipogenesis of GM3S-deficient mouse embryonic fibroblasts

Since the expression of GSLs, including GM3, was suppressed in M-depleted mSVCs that acquired a higher adipogenic potential (Figures 1I–K and 2G), we examined the adipogenesis of *GM3S*-deficient mouse embryonic fibroblasts (MEFs) (Figure 5). MEFs obtained from wild-type B6 mice and *GM3S* null mice were cultured in adipogenic culture medium containing dexamethasone and isobutylmethyxanthine for 8 days and their adiposity and the representative genes involved in adipocyte differentiation were compared. *GM3S*-deficient MEFs acquired higher adipogenic potential (Figure 5A) with enhanced expression of marker genes for mature adipocytes such as *C/EBPα*, *GLUT4*, *adiponectin* and *PPARγ* (Figure 5B). Since GM3 was virtually absent in M-depleted mSVCs (Figure 1J) which accompanied enhanced insulin signaling (Figures 1G and 2F), we compared the insulin signaling between wild-type MEFs and *GM3S*-deficient MEFs after adipogenic treatment. As shown in Figure 5C, the insulin-dependent tyrosine phosphorylations in both IR and IRS-1 were significantly upregulated in *GM3S*-deficient MEFs.

Increased expression of GM3 in epididymal fat of diet-induced (HFD) obese mouse

Previously, we observed a significant increase of GM3 in the epididymal fats of *ob/ob* mouse compared with their lean counterparts (Tagami et al. 2002). Here we examined whether the expression of GM3 is also affected in diet-induced obese mice. Eight-week-old B16 mice (mean BW 25.3 ± 0.4 g) were divided into two groups, HFD and standard diet (SD). After feeding for 12 weeks, mean BW of SD and HFD groups were 31.0 ± 0.6 and 46.0 ± 0.8 g, respectively. Fasted blood glucose levels of SD and HFD groups were 137 and 203 mg/dL, respectively

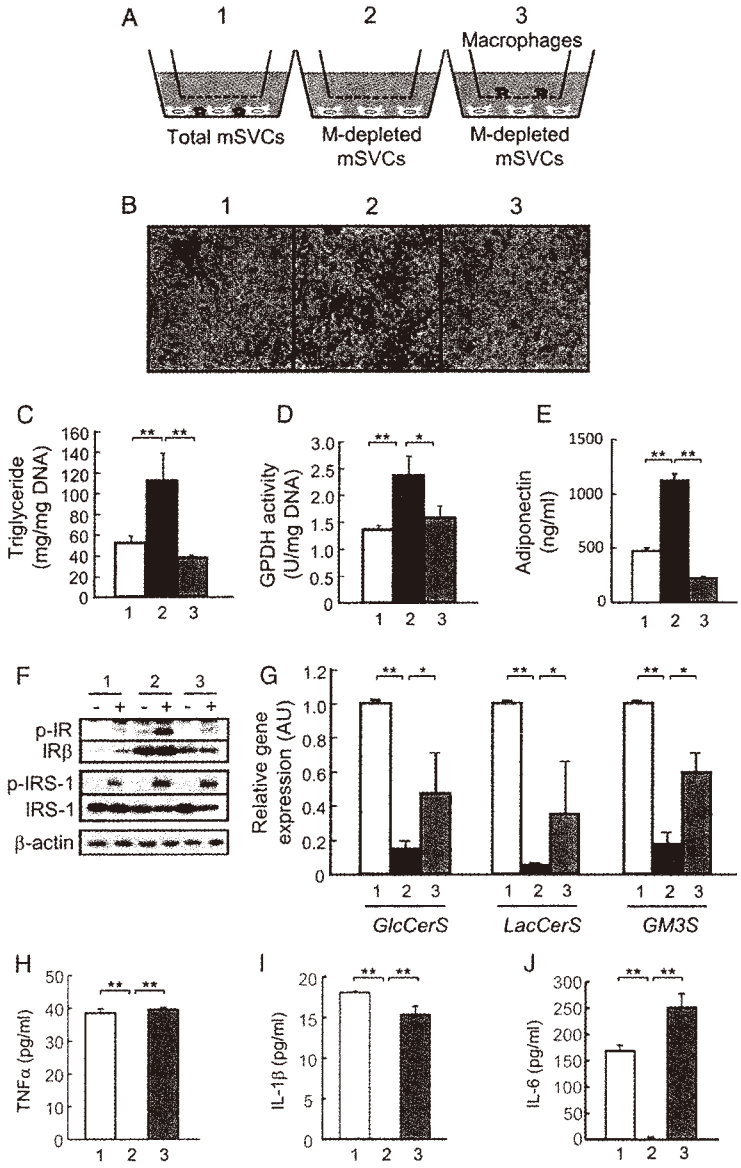

Fig. 2. Non-contact transwell coculture of mesenteric preadipocytes with resident macrophages. (**A**) Diagram of the transwell culture system used in this study. Total mSVCs were placed in the lower chamber of a transwell and no cell in the upper insert (1), and macrophage (M)-depleted mSVCs were placed in the lower chamber with no cell or macrophages in the upper insert (2, 3). (**B**) Oil-Red O staining was performed, and (**C**) intracellular triglyceride content and (**D**) GPDH activity was determined after 8 days in the differentiation culture. (**E**) Adiponectin concentrations in culture media of the cultured mSVCs were determined at day 8. (**F**) After 8 days, the cultured mSVCs were stimulated with insulin (30 nM) for 5 min and lysed for immunoblot analysis of components of IR signaling pathways. (**G**) mRNA expression of *GlcCerS*, *LacCerS* or *GM3S* using cultures in the lower chamber was determined by RT-PCR analysis. The culture media were collected to measure concentrations of TNF-α (**H**), IL-1β (**I**) and IL-6 (**J**) and by ELISA. White, black and gray bars represent total mSVCs, M-depleted mSVCs, and M-depleted mSVCs + M (C–E, G–J). $^{*}P < 0.05$, $^{**}P < 0.01$.

(Figure 6A). As shown in Figure 6B and C, the GM3 levels in epididymal fat of the HFD group was 3-fold higher than that of the SD group. In addition, the mRNA levels of the *GM3S* gene in the HFD group were also increased 3-fold (Figure 6D). These results strongly suggest the possibility that the increased expression of GM3 in abdominal adipose tissues might contribute to the induction of adipose tissue malfunction such as the chronic low grade-inflammatory states observed in obesity.

GM3S-deficient mice are resistant to the development of HFD-induced proinflammatory states in adipose tissue

It has been reported that the severity of HFD-induced insulin resistance was ameliorated in *GM3S*-deficient mice compared with wild-type mice (Yamashita et al. 2003). The authors demonstrated that the reason for the amelioration of insulin resistance in *GM3S*-deficient mice could be due to the absence of downregulation of insulin signaling in muscle and liver under obese conditions. Considering the

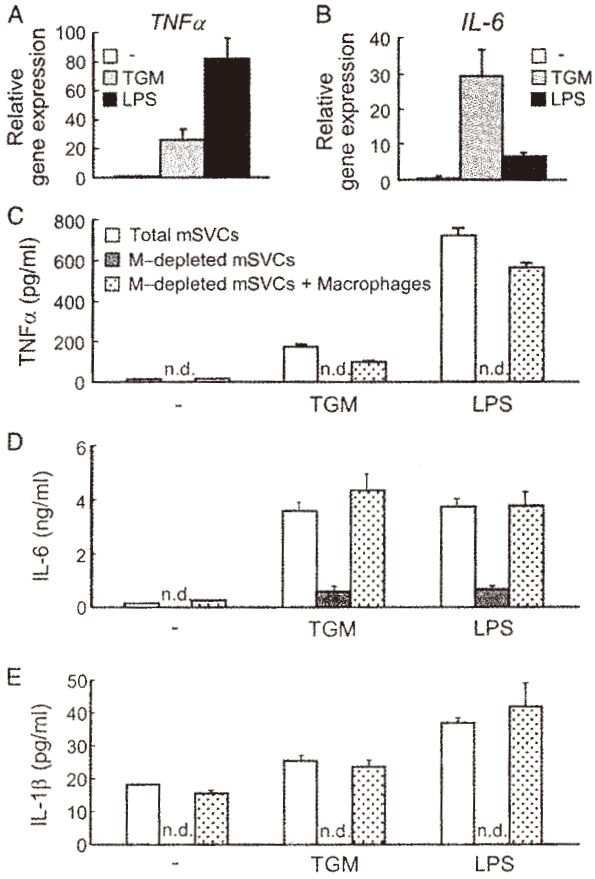

Fig. 3. Macrophages in the mSVCs are capable of expressing inflammatory cytokines. Total mSVCs were untreated (–) or treated with 1/10 TGM solution or 10 ng/mL LPS for 1 h. Gene expression of *TNF-α* (**A**) or *IL-6* (**B**) was determined by RT-PCR analysis. Data represent the relative gene expression in treated cells compared with that in untreated cells (set to 1.0 separately for each target gene). (**C–E**) Isolated mSVCs, unsorted (total mSVCs), macrophage-depleted (M-depleted mSVCs) and macrophage-depleted and replenished (M-depleted mSVCs + M (macrophages)), were untreated (–) or treated with 1/10 TGM solution or 10 ng/mL LPS. Culture media were collected at day 3, concentrations of TNF-α (C), IL-6 (D) and IL-1β (E) were determined by ELISA. Not detectable (n.d.) indicates that measurements were under the lower detection limit of the ELISA system.

contribution of chronic inflammatory states in adipose tissue on the development of systemic insulin resistance, we measured various factors including inflammatory cytokines, adipokines, lipid metabolism and macrophage phenotypes in adipose tissues related to obesity and diabetes. After 12 weeks of feeding HFD, the mean body weight in the GM3S-deficient mice (null, –/–) was slightly smaller than that of the heterozygote (+/–) mice (Figure 7A). Simultaneous measurements of adipose tissues showed that the epididymal and subcutaneous adipose tissues of *GM3S* null mice were significantly smaller than those of *GM3S* hetero mice in SD condition. In the HFD condition, the mesenteric and subcutaneous adipose tissues of *GM3S* null mice were significantly smaller than those of *GM3S* hetero mice (Figure 7B). Next, insulin resistance of these mice was evaluated by a glucose tolerance test (GTT) (Figure 7C) and an insulin tolerance test (ITT) (Figure 7D). Both GTT and ITT showed significant improvements of insulin resistance in the HFD condition as expected (Yamashita et al. 2003).

As shown in Figure 8, after performing both GTT and ITT, the epididymal fat tissues of *GM3S* hetero and null mice were removed and subjected to measurement of the mRNA expression of the pro- and anti-inflammatory cytokines (TNFα, IL-1-β, IL-6 and IL-10), adiponectin and leptin, diacylglycerol acyltransferase (DGAT1) and fatty acid synthase (FASN), macrophage galactose-type C-type lectin (Mgl-1) and arginase 1 (Arg1) by quantitative real-time (RT)-PCR analysis. Interestingly, we found thought-provoking expression profiles of the abovementioned genes in *GM3S* null mice under the HFD condition but not in the SD condition as follows: inflammatory cytokine *TNFα* was significantly decreased, while anti-inflammatory cytokine *IL-10* was increased compared with the *GM3S* hetero mice (Figure 8A). Expression level of adiponectin was significantly increased (Figure 8B). *DGAT1* and *FASN*, which are the essential enzymes for fat synthesis, are significantly suppressed (Figure 8C). The downregulation of *DGAT1* and *FASN* could be the cause of the observed decreased fat mass in *GM3S* null mice (Figure 8B). As shown in Figure 8D and E, M2 signature genes such as *MGL1* and *Arg1* tend to increase in *GM3S* null mice; however, FACS analysis of the M1($F4/80^+CD11b^+CCR2^+$) to M2($F4/80^+CD11b^+MMR^+$) ratios was the same in the adipose tissues of the homo- and heterozygotes (data not shown).

These results indicate that *GM3S* null mice were resistant to the development of chronic and low-grade inflammatory states in visceral fat

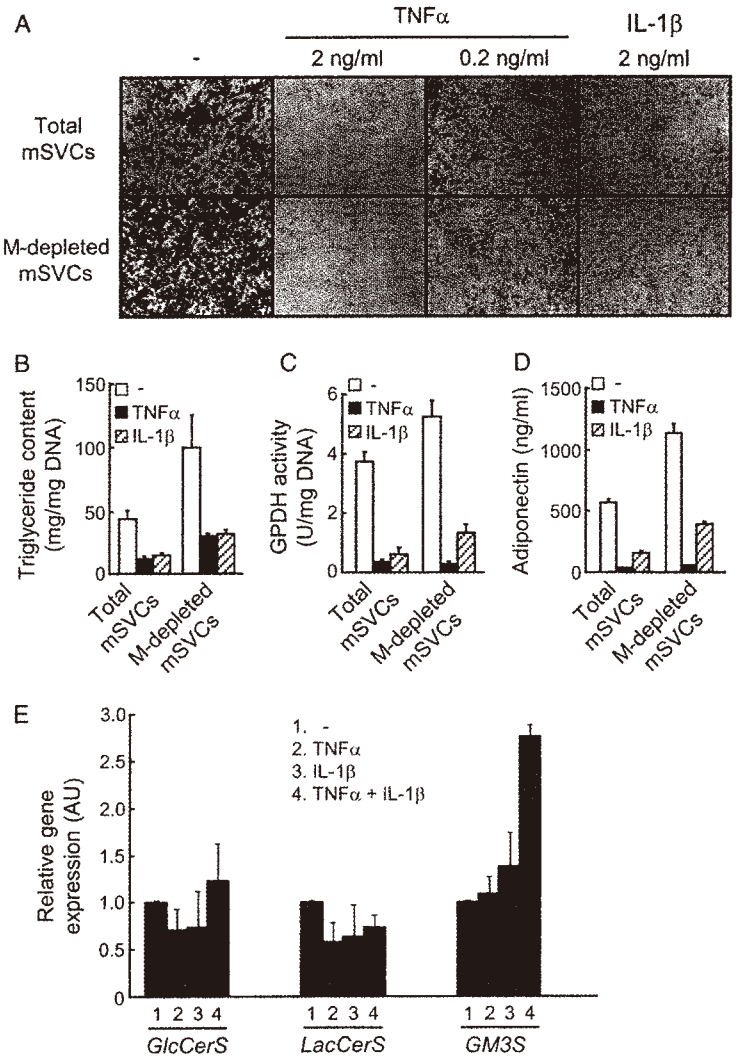

Fig. 4. Inflammatory cytokines inhibit mesenteric adipogenesis and enhance GM3S expression. Total mSVCs and M-depleted mSVCs were untreated (–) or treated with TNF-α (2 or 0.2 ng/mL or IL-1β (2 ng/mL), during adipogenic differentiation. (**A**) At day 8, Oil-Red O staining was performed, and (**B**) intracellular triglyceride content and (**C**) GPDH activity, as well as (**D**) adiponectin concentrations in the culture media, were determined. (**E**) At the same time, mRNA expression of *GlcCerS*, *LacCerS* or *GM3S* treated with TNF-α (0.2 ng/mL) and/or IL-1β (0.2 ng/mL) was determined by RT-PCR analysis. $*P<0.05$, $**P<0.01$.

tissues under obese conditions with a propensity for an M2-like phenotype through amelioration of insulin resistance. This conclusion is also supported by the improvement of GTT and ITT scores in *GM3S* null mice under HFD conditions (Figure 7C and D).

Discussion

It is well established that the proinflammatory TNFα (Torti et al. 1985) and IL1-β (Suzawa et al. 2003) are potent inhibitors of adipocyte differentiation. Of note, it is also known that both of these cytokines induce insulin resistance in adipocytes (Stephens et al. 1992; Jager et al. 2007). Moreover, TNFα expression is induced in adipose tissue of obese diabetic rodents (Hotamisligil et al. 1993) and humans (Hotamisligil et al. 1995). It is now largely accepted that TNFα expression in adipose tissue comes mainly from macrophages (Weisberg et al. 2003). Together, these studies suggest that macrophages in adipose tissue produce TNFα and IL1-β, which can inhibit differentiation of preadipocytes and induce insulin resistance in mature adipocytes (Constant et al. 2006). However, the ability of these cytokines to induce insulin resistance by inhibiting adipogenesis has not been considered. Nonetheless, there are new model systems that clearly suggest that limitations in adipose tissue expansion are associated with insulin resistance. Mice that are very obese but have unlimited adipose tissue expansion are metabolically healthy and insulin sensitive (Kim et al. 2007). Overall, these studies largely support the idea that adequate numbers of preadipocytes that are differentiation competent allow for hyperplastic growth with the effect being to preserve metabolic function in the face of obesity.

Here we have demonstrated that these intercellular interactions are functionally involved in the spatiotemporal expression of GSLs, especially GM3, in adipocytes. The critical roles of GM3 focusing on a

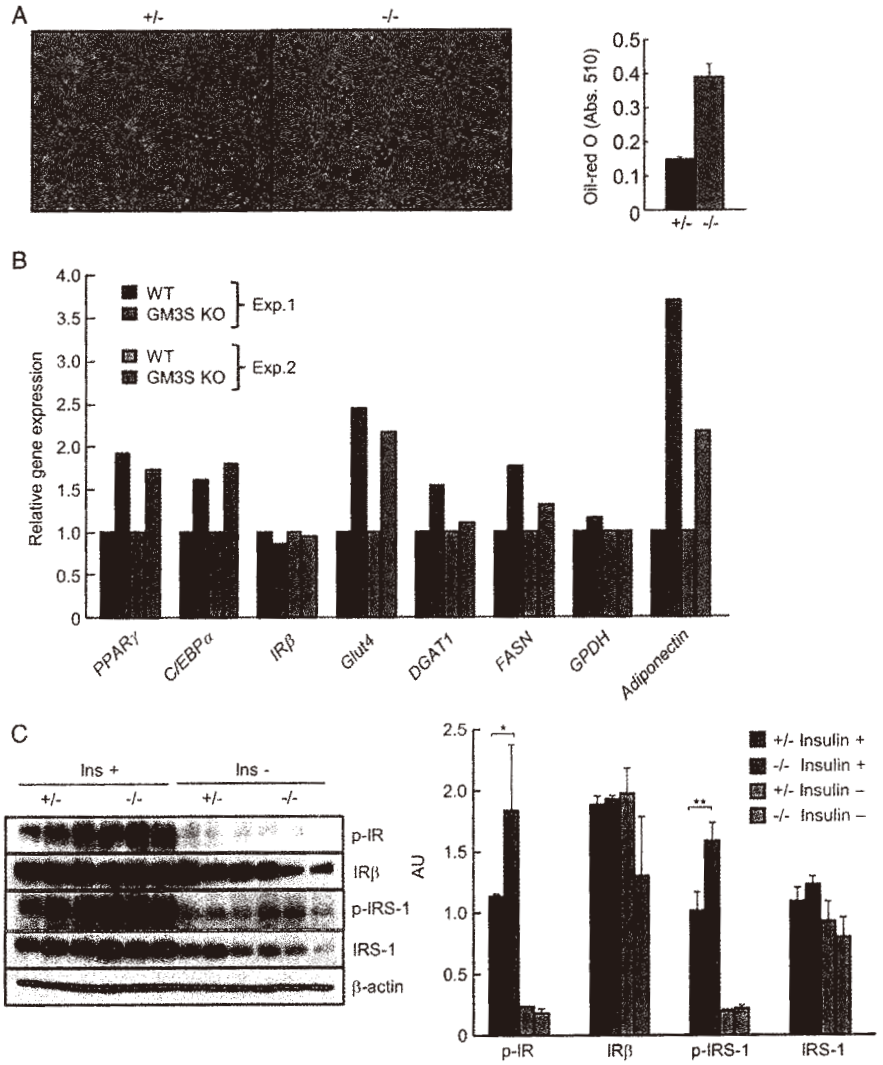

Fig. 5. Evidence for the direct involvement of GM3 in adipogenesis. Enhanced adipogenesis of *GM3S*-deficient MEFs (**A**) accompanying increased expression of adipogenic markers was observed (**B**). Phosphorylation levels of both IR and IRS-1 after insulin stimulation in adipocytes derived from *GM3S*-deficient MEFs were increased (**C**).

novel interplay between macrophages and adipocytes in adipose tissue under homeostatic and pathogenic conditions are discussed in the next section "GM3 functions as a physiological regulatory factor for insulin signaling".

GM3 functions as a physiological regulatory factor for insulin signaling

Visceral adipose tissue, particularly mesenteric adipose tissue, is important in the pathogenesis of metabolic syndrome (Wellen and Hotamisligil 2005; Ailhaud, 2006; Xu et al. 2013). To investigate the fundamental characteristics of mesenteric adipocytes, we established a physiologically relevant differentiation system of mSVC to mesenteric visceral adipocytes (Sato et al. 2008). We optimized the insulin concentration at levels comparable with those in vivo (0.85 ng/mL) by including physiological concentrations of IGF-1 (200 ng/mL). We found that IGF-1 and insulin worked synergistically, because IGF-1 alone could enhance CCAAT/enhancer-binding protein α (C/EBPα) and adipocyte lipid-binding protein (aP2) mRNA expression; however, IGF-1 could not induce lipid droplet accumulation associated adipocyte maturation without the physiological concentration of insulin.

Using this culture system, we have explored the commitment of resident macrophages in mSVCs on physiological adipogenesis. Adipogenesis of mSVCs was increased following removal of resident macrophages, which was accompanied by enhanced insulin signaling and concomitant decrease of GSLs including GlcCer, LacCer and GM3. Of note, GM3 could not be detected in the primary adipocytes differentiated from macrophage-depleted mSVCs (Figure 1). Phosphorylation levels of both IR and IRS-1 after insulin stimulation were markedly increased by depleting macrophages and protein level of IR per se was increased in the mSVCs (Figures 1G and 2F). Thus,

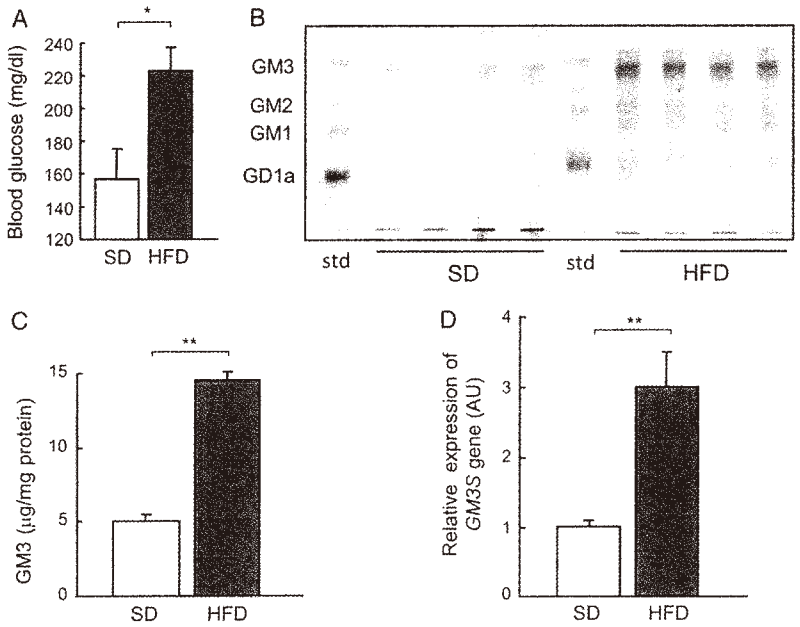

Fig. 6. GM3 expression in visceral adipose tissue is augmented in diet-induced obese mice. Eight-week-old C57BL/6 mice were fed a SD or a HFD for 12 weeks. (**A**) Fasting blood glucose levels were determined. (**B**) Acidic lipids were obtained from epididymal adipose tissue of mice fed an SD or HFD, separated on TLC plates and then visualized with orcinol-sulfuric acid. Std, standard lipids. (**C**) The intensity of the band corresponding to GM3 in (C) was quantitated. Data are means ± SEM. (**D**) mRNA expression of *GM3S* in epididymal adipose tissue of mice fed an SD or HFD was determined by RT-PCR analysis. Data represent the relative gene expression in HFD mice compared with that in SD mice (set to 1.0 separately for each target gene). $*P<0.05$, $**P<0.01$.

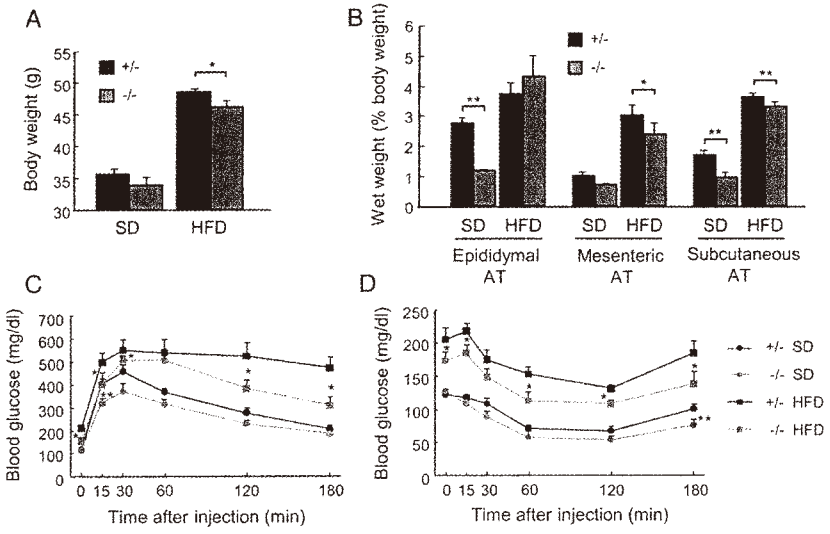

Fig. 7. *GM3S*$^{-/-}$ mice exhibit improvement of impaired glucose tolerance caused by high-fat feeding. *GM3S*$^{+/+}$ and *GM3S*$^{-/-}$ mice were fed an SD or HFD for 12 weeks. (**A**) Body weight (*GM3S*$^{+/+}$ SD; $n=12$, *GM3S*$^{+/+}$ HFD; $n=12$, *GM3S*$^{-/-}$ SD; $n=16$, *GM3S*$^{-/-}$ HFD; $n=17$). (**B**) Wet weights of various adipose tissues (AT) were expressed as a percentage of the animals' total body weights ($n=8$ for each). (**C**) Glucose tolerance test. Glucose (2 g/kg) was intraperitoneally injected into the fasted mice and blood glucose level was serially monitored ($n=4$ for each). (**D**) Insulin tolerance test. Insulin (0.6 U/kg) was intraperitoneally injected into the fasted mice and blood glucose level was serially monitored ($n=4$ for each). $*P<0.05$.

GSL levels, especially GM3, of adipocytes are tightly maintained by soluble factors (physiological levels of proinflammatory cytokines) secreted from resident macrophages to execute physiological adipogenesis (Figure 9). In addition, MEFs prepared from *GM3S*-deficient mice have activated insulin signaling, and as a result, accelerated adipogenesis (Figures 5 and 9B). Taken together, we propose that GM3 is a homeostatic mediator for adipogenesis and insulin signaling (Figure 9).

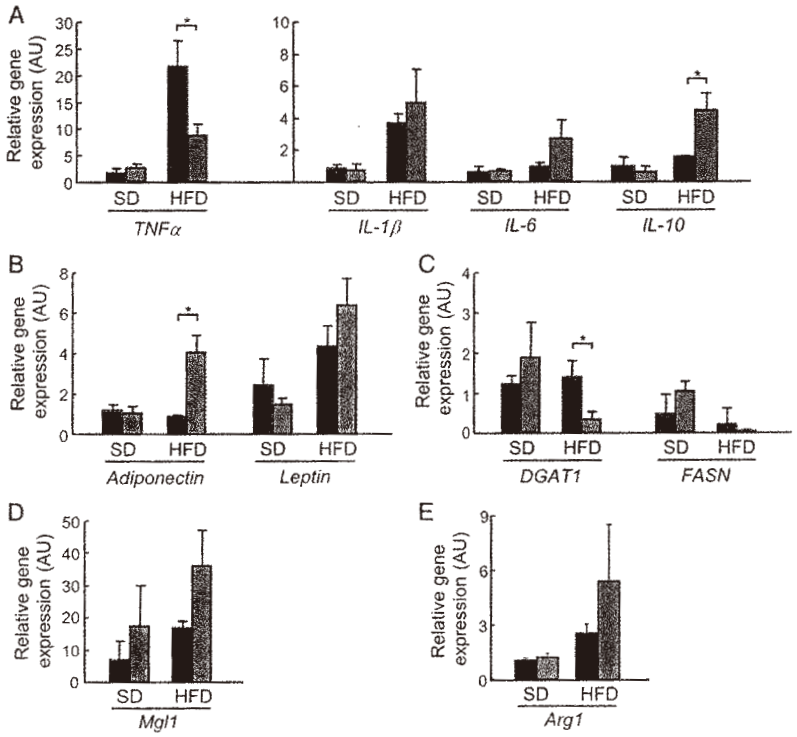

Fig. 8. Obese *GM3S*$^{-/-}$ mice showed anti-inflammatory phenotypes in visceral adipose tissue. Epididymal fat tissues of *GM3S*$^{-/-}$ and *GM3S*$^{+/-}$ mice fed with HFD and SD for 10 weeks were exercised and subjected to measurement of mRNA expression of (**A**) (anti-)inflammatory cytokines, (**B**) *adiponectin* and *leptin*, (**C**) *DGAT1* and *FASN*, (**D**) *Mgl1* and (**E**) *Arg1* by quantitative RT-PCR analysis. *$P < 0.05$, **$P < 0.001$.

Pathogenic control of adipocytes by the increased expression of GM3 caused by proinflammatory cytokines

Adipose tissue macrophages are present in two main subtypes. A concept of M1/M2 polarization has been developed for macrophages according to patterns of expression of cytokines, surface markers and metabolic enzymes (Lumeng et al. 2007; Odegaard and Chalwa 2011). M1 macrophages are potent effector cells that produce inflammatory cytokines such as TNFα, IL1-β and IL-6. In contrast, M2 macrophages exert anti-inflammatory functions by producing IL-10. IL-10 potentiates insulin signaling in adipocytes (Lumeng et al. 2007; Odegaard and Chawla 2011). M2 macrophages upregulate production of Arginase I enzyme (Arg1), reducing nitric oxide synthesis and inflammation via metabolizing arginine to ornithine (Gordon 2007; Martinez et al. 2009). Under normal physiological states, 5–10% of adipose tissue cells are resident M2 macrophages. Consumption of an HFD shifts cytokine expression of murine adipose tissue macrophages from M2- to M1-like patterns by decreasing expression of IL-10 and Arg1 and increasing TNFα (Lumeng et al. 2007). Although segregating macrophages into these two states in experimental context is very useful, it also has its limitation, as macrophage phenotypes in vivo exhibit plasticity across the entire spectrum of activation states that are encompassed by the M1 and M2 nomenclature (Stout and Shuttles 2004; Shaul et al. 2010). Macrophages very likely exist in multiple intermediate phenotypes depending on local tissue microenvironment (Gordon 2007), and are able to respond to local cues and shift their phenotype to maintain local tissue homeostasis.

Obese *GM3S*-deficient mice showed significant increases of *adiponectin* and *IL-10* in adipose tissue compared with obese wild-type mice (Figure 8). This observation was supported by the improvement of GTT and ITT in obese *GM3S*-deficient mice (Figure 7C and D). Reportedly, IL-10 (Odegaard and Chawla, 2011) and adiponectin (Kadowaki *et al.* 2006) have crucial roles in maintaining the insulin sensitivity of adipocytes. Alternatively, insulin signaling upregulates adiponectin secretion (Blüher et al. 2008). Since the insulin signaling of *GM3S*-deficient adipocytes is upregulated significantly (Figure 5C), the resistance to the development of diet-induced inflammatory conditions in GM3S-deficient visceral adipose tissue (Figure 8) and the improvements of GTT and ITT (Figure 7C and D) could be due to the enhancement of insulin signaling through lipid rafts depleted of GM3 (Yamashita et al. 2003; Kabayama et al. 2007; Wang et al. 2014).

Dynamic remodeling of the adipose tissue architecture occurs with its expansion. During a positive caloric balance, the development of metabolic disease is more closely related to how fat is stored through adipocyte hypertrophy versus hyperplasia than simply the amount of fat that is stored (Figure 10). In the past, it was widely hypothesized that inhibitors of adipogenesis were potential anti-obesity therapeutics. However, evidence from a variety of experiments in mice and humans suggests that inhibitors of adipogenesis are a poor choice for amelioration of metabolic disease states because limiting fat cell expansion is associated with insulin resistance. As proposed more than a decade ago, a failure in adipocyte differentiation can cause type 2 diabetes (Danforth 2000), and this hypothesis is generally recognized and supported by independent lines of investigation in adipocyte

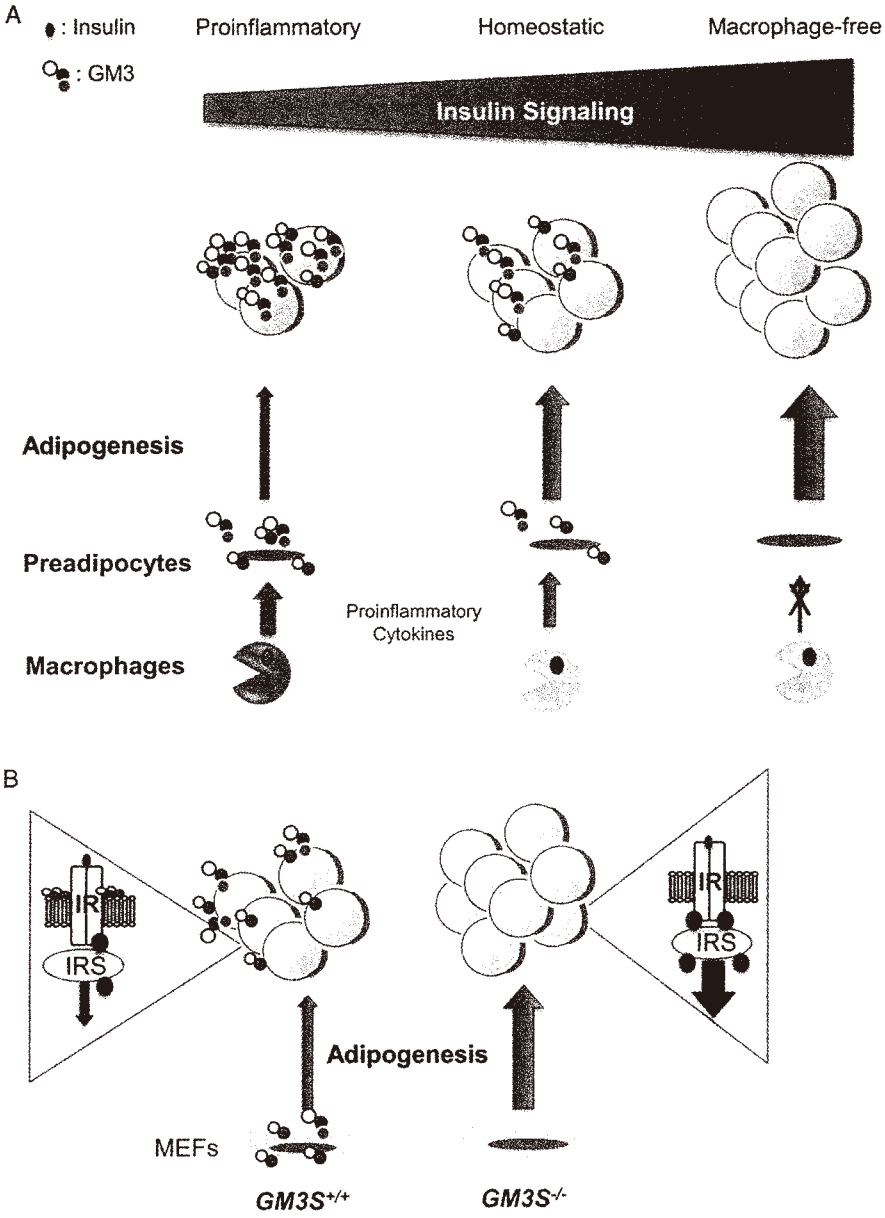

Fig. 9. Control of homeostatic and pathogenic balance in adipose tissue by ganglioside GM3. (**A**) Adipogenesis of mesenteric preadipocytes is increased following depletion of resident macrophages. The expression of GSLs including GM3 in mesenteric preadipocytes and adipocytes could be maintained by soluble factors secreted from resident macrophages to execute physiological adipogenesis. Thus, surprisingly primary adipocytes themselves are not capable of making GSLs without macrophages. Adequate adipogenesis with proper insulin signaling in the presence of resident macrophages is shown in the middle, while acceleration of adipogenesis with enhanced insulin signaling in the absence of resident macrophages is depicted on the right. Phosphorylation levels of both insulin receptor (IR) and IRS-1 after insulin stimulation were dramatically increased and protein levels of IR per se was increased by depleting macrophages (Figures 1G and 2F). On the other hand, the activation of macrophages by proinflammatory cytokines suppresses adipogenesis (Figure 4A and B) and enhances *GM3S* gene expression (Figure 4C) which results in the development of the state of insulin resistance (Tagami et al. 2002; Inokuchi 2014). (**B**) Evidence for the direct involvement of GM3 in adipogenesis. MEFs were prepared from E14 embryos of wild-type C57/BL6 mice and *GM3S*-deficient mice, and subjected to adipogenesis. Enhanced adipogenesis of *GM3S*-deficient MEF which accompanied with the increased insulin signaling was observed. Phosphorylation levels of both IR and IRS-1 after insulin stimulation were increased (Figure 5).

biology. *GM3S* null mice were resistant to the development of chronic and low-grade inflammatory states in visceral fat tissues under obese conditions with a propensity for an M2-like phenotype accompanied by amelioration of insulin resistance (Figure 10).

Collectively, the normalization of elevated levels of GM3 in adipose tissue under proinflammatory states could lead to a new intervention to treat metabolic syndrome. Currently, inhibitors of GlcCerS proved to be active for the treatment of metabolic diseases using

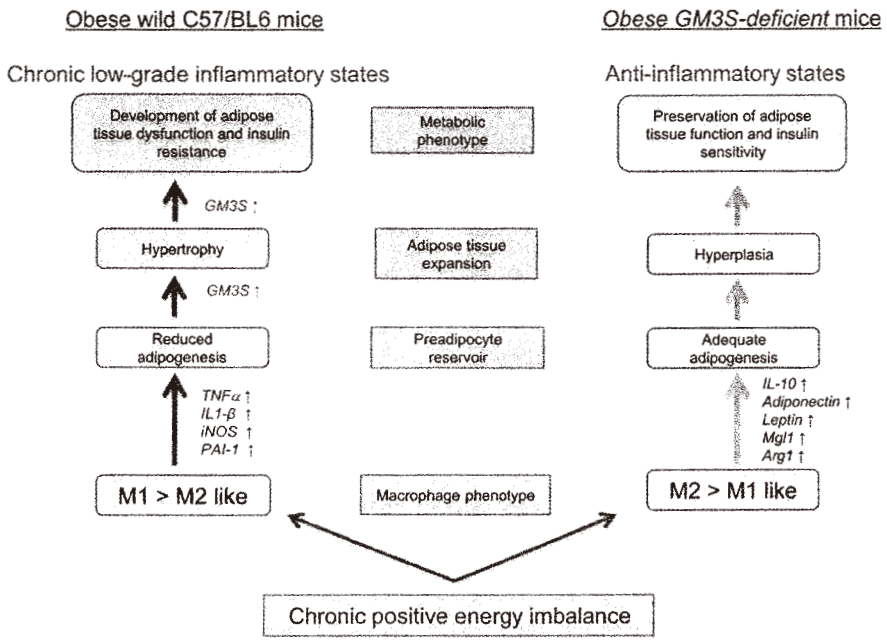

Fig. 10. A model of how GM3 regulates adipose tissue remodeling during chronic positive energy imbalance. Chronic positive energy imbalance (HFD) leads to obesity, and macrophage phenotype may influence the mechanism by which adipose tissue expands. During obesity, the mass of adipose tissue increases by hyperplasia and hypertrophy, and the latter is associated with the activation of stress signaling. When proinflammatory M1 macrophages dominate, an inadequate preadipocyte reservoir may exist due to reduced preadipocyte survival, proliferation and/or adipogenic capacity. Energy storage will occur via exaggerated adipose hypertrophy, resulting in dysfunctional adipose tissue and contributing to an inflamed, insulin-resistant state. Chronic increase of GM3 through the upregulation of the *GM3S* gene by proinflammatory cytokines such as TNF-α and IL-1β could participates in the development of insulin resistance (Tagami et al. 2002; Kabayama et al. 2007). In contrast, *GM3S*-deficient mice improves insulin action without exerting a significant impact on diet-induced obesity (Figure 7). Obese *GM3S*-deficient mice showed anti-inflammatory M2-like phenotypes in visceral adipose tissue (epidydimal fat) (Figure 8). Significant increases of adiponectin and IL-10 compared with obese wild-type mice were observed. IL-10 (Chalwa et al. 2011) and adiponectin (Fantuzzi 2005) have a crucial role in maintaining the insulin sensitivity of adipocytes.

rodent diabetic models. Considering the embryonic lethality of systemic *GlcCerS* KO mice (Yamashita et al. 1999), the targeted inhibition of GM3S might exhibit a better intervention rather depleting all GSLs.

Materials and methods

Animals and feeding conditions

C57BL/B6J mice were obtained from Japan SLC Inc. (Hamamatsu, Japan). The *GM3S*-deficient mice were generated as previously described (Tsukamoto et al. 2005; Yoshikawa et al. 2009) and were backcrossed with C57BL/6 mice >11 generations. Mice were analyzed for the *GM3S* gene genotype by PCR as described previously (Shimizu et al. 2006). Male Sprague-Dawley rats obtained from Japan Clea Inc. at 3–5 weeks of age were housed in individual stainless-steel metabolic cages. The cages were placed in a room with controlled temperature (21–23°C) and lighting (light 0800–2000 hours). The animals had free access to tap water and a solid laboratory diet (CE-2, Japan Clea, Tokyo, Japan) for >1 week before the collection of tissues. All animals were maintained in accordance with Tohoku Pharmaceutical University guidelines for the care and use of laboratory animals.

At 8 weeks of age, one group of mice was transferred to an HFD (D12492, Research Diet, New Brunswick, NJ), providing 60% of energy as fat. The control group remained on the SD (Research Diet), which provides 10% of energy as fat, for the duration of the diet trial. All mice were weighed every week during the studies. After 12 weeks, mice were denied food for 14 h then blood was collected from the abdominal aorta. The mice were sacrificed and tissues were removed and rinsed with PBS. The isolated tissues were weighed and used in the experiments described.

To examine glucose metabolism GTT and ITT were performed after a 14-h fast and 6-h fast, respectively. Glucose (2 g/kg) or insulin (0.6 U/kg) was intraperitoneally injected into the fasted mice and blood glucose level was serially monitored with a Glucose Pilot (Aventir Biotech, LLC, Carlsbad, CA) which uses technology based on a biosensor.

Isolation of mSVCs and removal of macrophages

The isolation of mSVCs from rats was performed as described previously (Shimizu et al. 2006). To deplete macrophages from the mSVCs, we took two approaches: one utilized a magnetic sorting system and the other clodronate encapsulated liposomes. For the former approach, total mSVCs were suspended in HBSS with 0.1% BSA and incubated for 25 min with biotinylated anti-Mac-1 antibody (Cedarlane Labs, Hornby, ON, Canada) then with streptavidin-coupled magnetic beads (BD Biosciences). Macrophages with attached beads were magnetically removed, and the remaining cells were defined as M-depleted mSVCs. Purity of the M-depleted mSVCs obtained was ~99.5% by FACS analysis (data not shown). To examine whether the magnetic sorting steps affect adipogenesis of mSVCs, depleted macrophages were reintroduced into M-depleted mSVCs. A depleted macrophage

suspension and M-depleted mSVC suspension was mixed to provide a suspension with the same macrophage number as estimated by FACS analysis of the total mSVCs. For the latter approach, clodronate- and control-liposomes were prepared as described previously (van Rooijen and van Kesteren-Hendrik 2002; Dupasquier et al. 2004; Sunderkotter et al. 2004). Clodronate-liposomes were prepared from 1 g of clodronate (dichloromethylene diphosphonate; Sigma-Aldrich, St. Louis, MO) and were finally resuspended in 1 mL PBS. Control-liposomes were prepared with PBS in place of clodronate. Total mSVCs were cultured in an adipogenic medium (described below) for 24 h and then were treated with 1/100 dilution of clodronate- or PBS-liposomes for 48 h.

Adipogenic conditions for mSVCs

mSVCs were cultured in an adipogenic medium (DMEM/F-12 containing 10% newborn bovine serum, 100 units/mL penicillin, 100 μg/mL streptomycin, 17 μM pantothenic acid, 33 μM biotin, 100 μM ascorbic acid, 1 mM octanoic acid, 50 nM triiodothyronine, 2.5 μM niacinamide, 200 ng/mL IGF-1 and 0.85 ng/mL insulin (Sato et al. 2008). Cells were maintained in a humidified 5% CO_2 atmosphere, and the culture media were changed every 2 days until the end of the experimental periods. A 3% TGM solution, a source for advanced glycation end products (AGEs), was prepared by dissolving dehydrated Brewer's TGM (Sigma-Aldrich) in deionized water and autoclaving it for 20 min. The autoclaved TGM was kept in the dark at room temperature for 2–4 months, because the aging generates AGEs, which, compared with fresh TGM, enhance the activity of macrophages (Li *et al.* 1997). Autoclaved TGM solution (1/10 dilution of 3% stock), LPS (10 ng/mL; Sigma-Aldrich), rat TNFα (2 or 0.2 ng/mL; eBioscience, San Diego, CA) or rat IL-1β (0.2 ng/mL; eBioscience) was added after the seeded cells had adhered to the culture plate. Each treatment was continued throughout the adipogenic culture. On Days 8–10, Oil Red O staining was performed to observe lipid-laden cells. The cultured cells were washed with PBS and fixed with 10% formaldehyde for 10 min. Fixed cells were rinsed and stained for 15 min with a filtered solution of Oil Red O (Sigma-Aldrich) in 60% isopropanol. Cells were washed then visualized and photographed under a phase-contrast microscope.

Measurement of triglyceride biosynthesis

Cultured mSVCs were rinsed with PBS, combined with the extraction buffer included in the GPDH activity assay kit (Cell Garage Co., Ltd, Tokyo, Japan), harvested with a cell scraper and sonicated vigorously. The sonicated samples were used to measure triglyceride content and GPDH activity using commercially available enzymatic kits, a TG-EN Kainos kit and a GPDH activity assay kit from Kainos Laboratories (Tokyo, Japan), according to the manufacturer's instructions.

Immunoblotting analysis

Seven days after adipogenic culture, cultured mSVCs were preincubated for 18 h with low glucose DMEM (Sigma-Aldrich) containing 1% BSA, 0.5% FCS, 10 ng/mL insulin and 25 mM HEPES (pH 7.4). The culture medium was then changed into KRBH buffer (Krebs-Ringer bicarbonate HEPES) with 1% BSA to starve insulin and serum for 2 h before insulin stimulation. After addition of insulin (30 nM) for 5 min, the cells were washed with ice-cold PBS containing 5 mM Na_3VO_4 and 5 mM EDTA, then lysed in lysis buffer (20 mM Tris–HCl, pH 7.6, 120 mM NaCl, 1% NP-40, 0.5% sodium deoxycholate, 5 mM EDTA, 5 mM Na_3VO_4, 1 mM phenylmethylsulfonyl fluoride and Complete Protease Inhibitor Cocktail Tablets (Roche). Cell lysates were resolved by SDS–PAGE and transferred onto PVDF membranes (Immobilon-P; Millipore, Bedford, MA) that were subsequently probed with the following antibodies: anti- IR® (Santa Cruz Biotechnology, Inc.), anti-insulin IRS-1 (Santa Cruz Biotechnology, Inc.), anti-phospho-IR (Tyr1146; Cell Signaling), anti-phospho-IRS-1 (Tyr612; Biosource), and anti-®-actin (Sigma-Aldrich).

Flow cytometry

Cells were suspended in cytometry buffer (HBSS with 0.1% BSA and 0.01% NaN_3), incubated with normal mouse serum to block nonspecific binding, and stained with the appropriate fluorochrome-conjugated antibodies for 30 min at 4°C. Stained cells were analyzed using an FACS Caliber with CELLQuest™ software (BD Biosciences). Fluorochrome-conjugated anti-mouse monoclonal antibodies were purchased from Biolegend (San Diego, CA), except for anti-B220 (SouthernBiotech). FITC-conjugated CTx-B was purchased from Sigma. PE-conjugated anti-rat CD11b mAb (clone M1.70) was purchased from Immunotech (Marseille, France).

Quantitative real-time PCR

Total RNA was extracted from cultured cells using the TRIZOL reagent (Invitrogen Corporation) following the instructions of the manufacturer. cDNA was prepared from total RNA using a first-strand cDNA synthesis kit for RT-PCR (AMV; Roche Diagnostics Corporation), according to the manufacturer's protocol. RT-PCR was performed on an Applied Biosystems 7500 Real Time PCR System (Applied Biosystems) using a standard TaqMan® PCR kit protocol. TaqMan universal PCR master mix, primers and probes of rodent *GAPDH* as well as mouse *GlcCerS*, *LacCerS* and *GM3S* were purchased from Applied Biosystems. PCR reaction mixtures included RT product, 2× TaqMan® Universal PCR Master Mix, 0.25 μM TaqMan probe, 0.9 μM forward primer and 0.9 μM reverse primer. The reactions were incubated in a 96-well plate at 95°C for 10 min, followed by 40 cycles of 95°C for 15 s and 60°C for 1 min. All reactions were run in triplicate.

Other genes were quantitated by SYBR Green I (TaKaRa Bio) according to the manufacturer's instructions. Primers used are shown in Table 1. These primers spanned more than one intron to avoid amplification of any contaminating DNA. After amplification, a melting curve (0.1°C/s) was used to confirm product purity, and only one peak for each sample was observed. The threshold cycle value was taken as the fractional cycle number at which the emitted fluorescence of the sample passed a fixed threshold above the baseline. Relative quantification was calculated using a standard curve, which was produced to demonstrate linearity (correlation coefficient; >0.98), and to determine amplification efficiency (90–110%). Each sample expression level was normalized to that of *GAPDH*.

Lipid analysis

Lipid analysis was performed as described previously (Ladisch and Gillard, 1985). Briefly, in order to extract cell pellets of the cultured adipocytes they were incubated with a chloroform/methanol solution. The lipid extract was separated into neutral and acidic lipid fractions by using a DEAE-Sephadex A-25 column (GE Healthcare, Piscataway, NJ). The fractions were dried and subjected to methanolic 0.1 M NaOH for ester cleavage. After neutralization, the solutions were desalted with Sep-Pak C18 reverse-phase cartridges (Waters, Milford, MA) and lipids were eluted.

Ganglioside purification from the adipose tissues was performed by Ladisch's methods with only minor modification (Ladisch and

Table I. Primers for RT-PCR

Target gene	Forward	Reverse
GAPDH	AAATGGTGAAGGTCGGTGTG	TGAAGGGGTCGTTGATGG
TNFα	ACCCTCACACTCAGATCATCTTC	TGGTGGTTTGCTACGACGT
IL-1β	CTCCATGAGCTTTGTACAAGG	TGCTGATGTACCAGTTGGGG
IL-6	CCAGAGATACAAAGAAATGATGG	ACTCCAGAAGACCAGAGGAAAT
IL-10	GGTTGCCAAGCCTTATCGGA	ACCTGCTCCACTGCCTTGCT
Adiponectin	GCTCCTGCTTTGGTCCCTCCAC	GCCCTTCAGCTCCTGTCATTCC
Leptin	GGAAGCCTCACTCTACTCCA	GAATGTCCTGCAGAGAGCCC
DGAT1	TATTACTTCATCTTTGCTCC	AAAGTAGGTGACAGACTCAG
FASN	GAGGACACTCAAGTGGCTGA	GTGAGGTTGCTGTCGTCTGT
Mgl1	TGAGAAAGGCTTTAAGAACTGGG	GACCACCTGTAGTGATGTGGG
Arg1	CTCCAAGCCAAAGTCCTTAGAG	AGGAGCTGTCATTAGGGACATC

Gillard, 1985). Briefly, tissue samples were minced with scissors and extracted several times with a chloroform/methanol solution. The extracts were combined, reduced in volume, freed of material insoluble upon cooling to −20°C, and taken to dryness under N_2. The dried total lipid extract was then partitioned in diisopropyl ether/1-butanol/50 mM NaCl (6 : 4 : 5). The ganglioside-containing aqueous phase was repartitioned with fresh organic phase, and the final aqueous phase was desalted with Sep-Pak C18 reverse-phase cartridges and lipids were eluted.

Neutral lipid fractions were separated by silica gel high-performance thin-layer chromatography (HPTLC) plates (Merck, Darmstadt, Germany) half-developed with chloroform/methanol/water (65 : 25 : 4), dried and redeveloped with hexane/diethyl ether/acetic acid (50 : 50 : 1), and neutral GSLs were detected with orcinol-sulfuric acid reagent. The gangliosides purified with Ladisch's methods were separated by HPTLC with chloroform, dried and redeveloped with chroloform/methanol/0.5% $CaCl_2$ (50 : 50 : 10), and detected with orcinol-sulfuric acid reagent. TLC immunostaining was performed to detect GM3 in the acidic lipid fraction (Suzuki et al. 1986; Nakamura et al. 1991). Acidic lipids were separated on TLC plates with aluminum backing (Merk, Darmstadt, Germany) with chroloform/methanol/0.5% $CaCl_2$ (50 : 50 : 10). After soaked in 0.1% polyisobutylmethacrylate in cyclohexane, dried and blocked with 1% BSA–PBS, the plates were incubated with anti-GM3 mAb (Seikagaku Corporation, Tokyo, Japan) followed by HRP-conjugated anti-mouse Ig antibody (NXA931, GE Healthcare). After washing with PBS, the plates were developed by enhanced chemiluminescence with Lumi-Light PLUS (Roche Applied Science, Mannheim, Germany) and detected using a Fujifilm LAS-3000 imaging system (Fujifilm, Tokyo, Japan).

Statistical analysis

Values in the text are means ± SD. Data were compared using Student's *t*-test for two-group comparison or ANOVA for multigroup comparison. Significant differences were post hoc analyzed using Scheffé's test. Differences were considered significant at $P < 0.05$.

Acknowledgements

We thank Dr. Lucas Veillon for their critical review of this manuscript. We also thank Yukari Tamekawa and Masumi Toyosawa for assistance with mouse breeding and genotyping and finally, Dr. Masaki Saito for providing the GM3S gene targeting mice.

Conflict of interest statement

None declared.

Funding

This work was supported by research grants for a Grant-in-Aid for Scientific Research (B) (to J.-I.I.) and for Scientific Research on Innovative Areas (No. 23110002 to K.K.) from MEXT, Japan (J.-I.I.), the Mizutani Research Foundation for Glycoscience (J.-I.I.), The Naito Foundation (J.-I.I.), the ONO Medical Research Foundation (J.-I.I.) and the Uehara Memorial Foundation (J.-I.I.). This work was also supported by MEXT-Supported Program for the Strategic Research Foundation at Private Universities.

Abbreviations

AGEs, advanced glycation end products; Arg1, arginase 1; DGAT1, diacylglycerol acyltransferase; FACS, Fluorescence-activated cell sorting; FASN, fatty acid synthase; GlcCer, glucosylceramide; *GM3S*, GM3 synthase; GPDH, glycerol 3-phosphate dehydrogenase; GSLs, Glycosphingolipids; GTT, glucose tolerance test; HFD, high-fat diet; HPTLC, high-performance thin-layer chromatography; IR, insulin receptor; IRS-1, insulin receptor substrate 1; ITT, insulin tolerance test; LacCer, lactosylceramide; LPS, lipopolysaccharide; LPS, lipopolysaccharide; mAbs, monoclonal antibodies; MEFs, mouse embryonic fibroblasts; Mgl1, macrophage galactose-type C-type lectin; mSVCs, Mesenteric stromal vascular cells; NCS, newborn bovine serum; SA, sialic acid; SD, standard diet; TGM, Thioglycollate; TGM, thioglycollate; TLC, thin-layer chromatography; TNF, tumor necrosis factor

References

Aerts JM, Ottenhoff R, Powlson AS, Grefhorst A, van Eijk M, Dubbelhuis PF, Aten J, Kuipers F, Serlie MJ, Wennekes T, et al. 2007. Pharmacological inhibition of glucosylceramide synthase enhances insulin sensitivity. *Diabetes*. 56:1341–1349.

Ailhaud G. 2006. Adipose tissue as a secretory organ: from adipogenesis to the metabolic syndrome. *C R Biol*. 329:570–577 (discussion 653–5).

Bijl N, Sokolović M, Vrins C, Langeveld M, Moerland PD, Ottenhoff R, van Roomen CP, Claessen N, Boot RG, Aten J, et al. 2009. Modulation of glycosphingolipid metabolism significantly improves hepatic insulin sensitivity and reverses hepatic steatosis in mice. *Hepatology*. 50:1431–1441.

Blümer RM, van Roomen CP, Meijer AJ, Houben-Weerts JH, Sauerwein HP, Dubbelhuis PF. 2008. Regulation of adiponectin secretion by insulin and amino acids in 3T3-L1 adipocytes. *Metabolism*. 57:1655–1662.

Chalwa A, Nguen KD, Goh YPS. 2011. Macrophage-mediated inflammation in metabolic disease. *Nat Rev Immunol*. 11:738–749.

Constant VA, Gagnon A, Landry A, Sorisky A. 2006. Macrophage-conditioned medium inhibits the differentiation of 3T3-L1 and human abdominal preadipocytes. *Diabetologia*. 49:1402–1411.

Couet J, Li S, Okamoto T, Ikezu T, Lisanti MP. 1997. Identification of peptide and protein ligands for the caveolin-scaffolding domain. Implications for the interaction of caveolin with caveolae-associated proteins. *J Biol Chem*. 272:6525–6533.

Danforth E Jr. 2000. Failure of adipocyte differentiation causes type II diabetes mellitus? *Nat Genet.* 26:13.

Fantuzzi G. 2005. Adipose tissue, adipokines, inflammation. *J Allergy Clin Immunol.* 115:911–919.

Feve B. 2005. Adipogenesis: cellular and molecular aspects. *Best Pract Res Clin Endocrinol Metab.* 19:483–499.

Dupasquier M, Stoitzner P, van Oudenaren A, Romani N, Leenen PJ. 2004. Macrophages and dendritic cells constitute a major subpopulation of cells in the mouse dermis. *J Invest Dermatol.* 123:876–879.

Gordon S. 2007. Macrophage heterogeneity and tissue lipids. *J Clin Invest.* 117:89–93.

Hakomori SI. 2002. Inaugural article: The glycosynapse. *Proc Natl Acad Sci USA.* 99:225–232.

Hotamisligil GS, Arner P, Caro JF, Atkinson RL, Spiegelman BM. 1995. Increased adipose tissue expression of tumor necrosis factor-α in human obesity and insulin resistance. *J Clin Invest.* 195:2409–2415.

Hotamisligil GS, Shargill NS, Spiegelman BM. 1993. Adipose expression of tumor necrosis factor-alpha: Direct role in obesity-linked insulin resistance. *Science.* 259:87–91.

Inokuchi J. 2010. Membrane microdomains and insulin resistance. *FEBS Lett.* 584:1864–1871.

Inokuchi J. 2011. Physiopathological function of hematoside (GM3 ganglioside). *Proc Jpn Acad Ser B.* 87:179–198.

Inokuchi J. 2014. GM3 and diabetes. *Glycoconj J.* 31:193–197.

Inokuchi J, Radin NS. 1987. Preparation of active isomer of 1-phenyl-2-decanoylamino-3-morpholino-1-propanol, inhibitor of murine glucocerebroside synthetase. *J Lipid Res.* 28:565–571.

Inokuchi J, Uemura S. 2014. ST3 beta-galactoside alpha-2,3-sialyltransferase 5 (ST3GAL5). In: Taniguchi N, editor. *Handbook of Glycosyltransferaes and Related Genes.* Japan: Springer. p. 675–684.

Jager J, Gremeaux T, Cormont M, Le Marchand-Brustel Y, Tanti JF. 2007. Interleukin-1β-induced insulin resistance in adipocytes through down-regulation of insulin receptor. *Endocrinology.* 148:241–251.

Kabayama K, Sato T, Kitamura F, Uemura S, Kang BW, Igarasgi Y, Inokuchi J. 2005. TNFalpha-induced insulin resistance in adipocytes as a membrane microdomain disorder: Involvement of ganglioside GM3. *Glycobiology.* 15:21–29.

Kabayama K, Sato T, Saito K, Loberto N, Prinetti A, Sonnino S, Kinji M, Igarashi Y, Inokuchi J. 2007. Dissociation of the insulin receptor and caveolin-1 complex by ganglioside GM3 in the state of insulin resistance. *Proc Natl Acad Sci USA.* 104:13678–13683.

Kadowaki T, Yamauchi T, Kubota N, Hara K, Ueki K, Tobe K. 2006. Adiponectin and adiponectin receptors in insulin resistance, diabetes, and the metabolic syndrome. *J Clin Invest.* 116:1784–1792.

Kim JY, van de Wall E, Laplante M, Azzara A, Trujillo ME, Hofmann SM, Schraw T, Durand JL, Li H, Li G, et al. 2007. Obesity-associated improvements in metabolic profile through expansion of adipose tissue. *J Clin Invest.* 117:2621–2637.

Ladisch S, Gillard B. 1985. A solvent partition method for microscale ganglioside purification. *Anal Biochem.* 146:220–231.

Li YM, Baviello G, Vlassara H, Mitsuhashi T. 1997. Glycation products in aged thioglycollate medium enhance the elicitation of peritoneal macrophages. *J Immunol Methods.* 201:183–188.

Lumeng CN, Bodzin JL, Saltiel AR. 2007. Obesity induces a phenotypic switch in adipose tissue macrophage polarization. *J Clin Invest.* 117: 175–184.

Martinez FO, Helming L, Gordon S. 2009. Alternative activation of macrophages: An immunologic functional perspective. *Annu Rev Immunol.* 27:451–483.

Nakamura K, Suzuki M, Taya C, Inagaki F, Yamakawa T, Suzuki A. 1991. A sialidase-susceptible ganglioside, IV3 alpha(NeuGc alpha 2–8NeuGc)-Gg4Cer, is a major disialoganglioside in WHT/Ht mouse thymoma and thymocytes. *J Biochem.* 110:832–841.

Neta R, Sayers TJ, Oppenhaim JJ. 1992. Relationship of TNF to interleukins. *Immunol Ser.* 56:499–566.

Odegaard JI, Chawla A. 2011. Alternative macrophage activation and metabolism. *Annu Rev Pathol.* 6:275–297.

Samaan MC. 2011. The macrophage at the intersection of immunity and metabolism in obesity. *Diabetol Metab Syndr.* 3:29.

Sato T, Nagafuku M, Shimizu K, Taira T, Igarashi Y, Inokuchi J. 2008. Physiological levels of insulin and IGF-1 synergistically enhance the differentiation of mesenteric adipocytes. *Cell Biol Int.* 32:1397–1404.

Shaul ME, Bennett G, Strissel KJ, Greenberg AS, Obin MS. 2010. Dynamic, M2-like remodeling phenotypes of CD11+ adipose tissue macrophages during high-fat diet-induced obesity in mice. *Diabetes.* 59:1171–1181.

Shimizu, Sakai M, Ando M, Chiji H, Kawada T, Mineo H, Taira T. 2006. Newly developed primary culture of rat visceral adipocytes and their in vitro characteristics. *Cell Biol Int.* 30:381–388.

Stephens JM, Butts MD, Pekala PH. 1992. Regulation of transcription factor mRNA accumulation during 3T3-L1 preadipocyte differentiation by tumour necrosis factor-α. *J Mol Endocrinol.* 9:61–72.

Stout RD, Suttles J. 2004. Functional plasticity of macrophages: reversible adaptation to changing microenvironments. *J Leukoc Biol.* 76:509–513.

Suganami T, Ogawa Y. 2011. Adipose tissue macrophages: Their role in adipose tissue remodeling. *J Leucocyte Biol.* 88:33–39.

Sun S, Ji Y, Qi L. 2012. Mechanisms of inflammatory responses in obese adipose tissue. *Annu Rev Nutr.* 32:261–286.

Sunderkotter C, Nikolic T, Dillon MJ, Van Rooijen N, Stehling M, Drevets DA, Leenen PJ. 2004. Subpopulations of mouse blood monocytes differ in maturation stage and inflammatory response. *J Immunol.* 172:4410–4417.

Suzawa T, Takada I, Yanagisawa J, Ohtake F, Ogawa S, Yamauchi T, Kadowaki T, Takeuchi Y, Shibuya H, Gotoh Y, et al. 2003. Cytokines suppress adipogenesis and PPAR-γ function through the TAK1/TAB1/NIK cascade. *Nat Cell Biol.* 5:224–230.

Suzuki M, Nakamura K, Hashimoto Y, Suzuki A, Yamakawa T. 1986. Mouse liver gangliosides. *Carbohydr Res.* 151:213–223.

Tagami S, Inokuchi J, Kabayama K, Yoshimura H, Kitamura F, Uemura S, Ogawa C, Ishii A, Saito M, Ohtsuka Y, et al. 2002. Ganglioside GM3 participates in the pathological conditions of insulin resistance. *J Biol Chem.* 277:3085–3092.

Torti FM, Dieckmann B, Beutler B, Cerami A, Ringold GM. 1985. A macrophage factor inhibits adipocyte gene expression: An in vitro model of cachexia. *Science.* 229:867–869.

Tsukamoto K, Kohda T, Mukamoto M, Takeuchi K, Ihara H, Saito M, Kozaki S. 2005. Binding of Clostridium botulinum type C and D neurotoxins to ganglioside and phospholipid. Novel insights into the receptor for clostridial neurotoxins. *J Biol Chem.* 280:35164–35171.

van Eijk M, Aten J, Bijl N, Ottenhoff R, van Roomen CP, Dubbelhuis PF, Seeman I, Ghauharali-van der Vlugt K, Overkleeft HS, Arbeeny C, et al. 2009. Reducing glycosphingolipid content in adipose tissue of obese mice restores insulin sensitivity, adipogenesis and reduces inflammation. *PLoS ONE.* 4:e4723.

van Rooijen N, van Kesteren-Hendrik E. 2002. Clodronate liposomes: perspectives in research and therapeutics. *J Liposome Res.* 12:81–94.

Wang X-Q, Lee S, Wilson H, Seeger M, Iordanov H, Gatla N, Whittngton A, Bach D, Lu J, Paller A. 2014. Ganglioside GM3 deletion reverses impaired wound healing in diabetic mice by activating IGF-1 and insulin receptors. *J Invest Dermatol.* 134:1446–1455.

Weisberg SP, McCann D, Desai M, Rosenbaum M, Leibel RL, Ferrante AW Jr. 2003. Obesity is associated with macrophage accumulation in adipose tissue. *J Clin Invest.* 112:1796–1808.

Wellen KE, Hotamisligil GS. 2005. Inflammation, stress, and diabetes. *J Clin Invest.* 115:1111–1119.

Xu H, Barnes GT, Yang Q, Tan G, Yang D, Chou CJ, Sole J, Nichols A, Ross JS, Tartaglia LA, et al. 2013. Chronic inflammation in fat plays a crucial role in the development of obesity-related insulin resistance. *J Clin Invest.* 112:1821–1830.

Yamashita T, Hashiramoto A, Haluzik M, Mizukami H, Beck S, Norton A, Kono M, Tsuji S, Daniotti JL, Werth N, et al. 2003. Enhanced insulin sensitivity in mice lacking ganglioside GM3. *Proc Natl Acad Sci USA.* 100:3445–3449.

Yamashita T, Wada R, Sasaki T, Deng C, Bierfreund U, Sandhoff K, Proia RL. 1999. A vital role for glycosphingolipid synthesis during development and differentiation. *Proc Natl Acad Sci USA.* 96:9142–9147.

Ye J, Gao Z, Yin J, He Q. 2007. Hypoxia is a potential risk factor for chronic inflammation and adiponectin reduction in adipose tissue of ob/ob and dietary obese mice. *Am J Physiol Endcrinol Metab*. 293: E111–1128.

Yew NS, Zhao H, Hong EG, Wu IH, Przybylska M, Siegel C, Shayman JA, Arbeeny CM, Kim JK, Jiang C, et al. 2010. Inhibiting glycosphingolipid synthesis ameliorates hepatic steatosis in obese mice. *Hepatology*. 50:85–93.

Yoshikawa M, Go S, Takasaki K, Kakazu Y, Ohashi M, Nagafuku M, Kabayama K, Sekimoto J, Suzuki S, Takaiwa K, et al. 2009. Mice lacking ganglioside GM3 synthase exhibit complete hearing loss due to selective degeneration of the organ of Corti. *Proc Natl Acad Sci USA*. 106:9483–9488.

Zhao H, Przybylska M, Wu IH, Zhang J, Siegel C, Komarnitsky S, Yew NS, Cheng SH. 2007. Inhibiting glycosphingolipid synthesis improves glycemic control and insulin sensitivity in animal models of type 2 diabetes. *Diabetes*. 56:1210–1218.

PLOS | ONE

RESEARCH ARTICLE

Identification of Ganglioside GM3 Molecular Species in Human Serum Associated with Risk Factors of Metabolic Syndrome

Lucas Veillon[1], Shinji Go[1], Wakana Matsuyama[1], Akemi Suzuki[2], Mika Nagasaki[3], Yutaka Yatomi[4], Jin-ichi Inokuchi[1]*

1 Division of Glycopathology, Institute of Molecular Biomembrane and Glycobiology, Tohoku Pharmaceutical University, Sendai, Japan, **2** Institute of Glycoscience, Tokai University, Kanagawa, Japan, **3** Department of Cardiovascular Medicine, Graduate School of Medicine, The University of Tokyo, Tokyo, Japan, **4** Department of Clinical Laboratory Medicine, Graduate School of Medicine, The University of Tokyo, Tokyo, Japan

* jin@tohoku-pharm.ac.jp

Citation: Veillon L, Go S, Matsuyama W, Suzuki A, Nagasaki M, Yatomi Y, et al. (2015) Identification of Ganglioside GM3 Molecular Species in Human Serum Associated with Risk Factors of Metabolic Syndrome. PLoS ONE 10(6): e0129645. doi:10.1371/journal.pone.0129645

Academic Editor: Howard Riezman, University of Geneva, SWITZERLAND

Received: February 22, 2015

Accepted: April 18, 2015

Published: June 23, 2015

Data Availability Statement: All relevant data are within the paper and its Supporting Information files.

Funding: This work was supported by research grants for a Grant-in-Aid for Scientific Research (B) (J.-i.I.) (No. 23370064) from MEXT, Japan, http://www.jsps.go.jp/english/e-grants/, The Mizutani Research Foundation for Glycoscience (J.-i.I.), http://www.mizutanifdn.or.jp, The Naito Foundation (J.-i.I.), https://www.naito-f.or.jp/en/, The Uehara Memorial Foundation (J.-i.I.),http://www.ueharazaidan.or.jp, and MEXT-Supported Program for the Strategic Research Foundation at Private Universities (J.-i.I., L.V. A.S., W.

Abstract

Serum GM3 molecular species were quantified in 125 Japanese residents using tandem mass spectrometry multiple reaction monitoring. Individuals were categorized by the presence or absence of metabolic disease risk factors including visceral fat accumulation, hyperglycemia and dyslipidemia. A total of 23 GM3 molecular species were measured, of these, eight were found to be significantly elevated in individuals with visceral fat accumulation and metabolic disease, defined as the presence of hyperglycemia and dyslipidemia. All of the GM3 molecular species were composed of the sphingoid base sphingosine (d18:1 (Δ4)) and, interestingly, six of the eight elevated GM3 molecular species contained a hydroxylated ceramide moiety. The hydroxylated GM3 species were, in order of decreasing abundance, d18:1-h24:0 ≈ d18:1-h24:1 > d18:1-h22:0 » d18:1-h20:0 > d18:1-h21:0 > d18:1-h18:1. Univariate and multiple linear regression analyses were conducted using a number of clinical health variables associated with obesity, type 2 diabetes, metabolic disease, atherosclerosis and hypertension. GM3(d18:1-h24:1) was identified as the best candidate for metabolic screening, proving to be significantly correlated with intima-media thickness, used for the detection of atherosclerotic disease in humans, and a number of metabolic disease risk factors including autotaxin, LDL-c and homeostatic model assessment insulin resistance (HOMA-IR).

Introduction

Type 2 diabetes is generally regarded as a lifestyle related disease, associated with a chronic caloric surplus, lack of exercise, obesity and high serum levels of LDL-c [1] and characterized by insulin resistance, hyperglycemia and relative insulin deficiency where the severity of each factor varies on a case by case basis [2].

M., S.G.) http://www.jsps.go.jp/english/e-grants/. The funders had no role in study design, data collection and analysis, decision to publish, or preparation of the manuscript.

Competing Interests: The authors have declared that no competing interests exist.

In normal subjects, insulin triggers an array of biological activities that fall in to either mitogenic or metabolic changes. Upon insulin binding to the insulin receptor (IR), internal-tyrosine kinase activity is activated and phosphorylates IR. At this point, Shc may be phosphorylated, which in turn induces mitogenic signaling through activation of the Ras-MAPK pathway. Alternatively, the activated IR may stimulate metabolic signaling by recruiting and phosphorylating adaptor proteins including the insulin receptor substrate (IRS) protein. Phosphorylation of IRS leads to PI3-kinase activation which induces translocation of the GLUT-4 to the plasma membrane facilitating cellular glucose uptake [3]. It is known that the association of IR in caveolae microdomains (lipid rafts) in adipocytes is essential to execute complete insulin metabolic signaling [4].

Glycosphingolipids (GSLs) and their sialic acid-containing derivatives, gangliosides, are components of membrane lipids in which the lipid portion is embedded in the outer leaflet of the plasma membrane with the sugar chain extending to the extracellular space. The structural features of GSLs affect membrane fluidity and allow for microdomain formation, contributing to cell-cell interaction and receptor-mediated signal transduction [5]. We have previously shown that in cultured adipocytes in a state of tumor necrosis factor (TNF)α-induced insulin resistance, the depletion of GSLs by the inhibition of glucosylceramide synthase, which is the first step enzyme for the biosynthesis of all of GSLs, results in nearly complete recovery from the resistance of insulin receptor signaling [6]. A number of studies in animal models demonstrate that pharmacological inhibition of GSLs ameliorates insulin resistance and prevents some manifestations of metabolic syndrome [7–11]. Further, we have shown that expression of ganglioside GM3, which is the simplest ganglioside species synthesized by GM3 synthase (GM3S; also called SAT-I/ST3Gal-5), is increased in metabolic diseases [6,12]. *GM3S* gene expression and GM3 content are upregulated in visceral adipose tissue of obese model animals and serum GM3 levels are approximately 2-fold higher in obese patients with type 2 diabetes and/or dyslipidemia [12]. Moreover, *GM3S* deficient mice exhibit enhanced insulin signaling and less susceptibility to insulin resistance induced by a high fat diet [13,14]. These results imply that GM3 is responsible for insulin homeostasis.

We have postulated a working hypothesis "insulin resistance as a membrane microdomain disorder" [3,15,16] because of the fact that the abnormal increase of membrane GM3 in adipocytes induced by inflammatory cytokine TNFα resulted in the elimination of the IR from caveolae microdomains [17].

In 2008, we examined serum GM3 concentrations of patients with hyperlipidemia or type 2 diabetes, and found that serum GM3 concentrations were increased in type 2 diabetes with severe visceral fat accumulation (VFA) [12] and a patent was issued for the use of GM3 measurement as a method for detecting insulin-resistant diseases [18]. It is with this information in mind that we set out to determine which specific GM3 molecular species are implicated in metabolic disease. In this study, twenty three GM3 molecular species were quantified in individuals with or without VFA, hyperglycemia and dyslipidemia and, for the first time, the relationships between numerous metabolic disease risk factors and serum GM3 molecular species are reported. Our results indicate that levels of hydroxylated GM3 species in human serum correlate with a number of risk factors for metabolic and cardiovascular diseases (CVD).

Research Design and Methods

Study participants

One hundred and twenty five Japanese residents were recruited for the study. Twenty six subjects were healthy and without metabolic disease risk factors, 39 had VFA, 15 had VFA with hyperglycemia, 28 had VFA with accompanying dyslipidemia and 17 had VFA, hyperglycemia

Table 1. Subject Characteristics.

	Control subjects	Patients with VFA	Patients with VFA + hyperglycemia	Patients with VFA + dyslipidemia	Patients with VFA + hyperglycemia + dyslipidemia
n	26	39	15	28	17
Sex	8 men/18 women	29 men/10 women	13 men/2 women	25 men/3 women	16 men/1 women
Age (years)	51.8 ± 1.8	52.1 ± 1.5 ns	59.9 ± 2.1 **	50.1 ± 1.6 ns	54.4 ± 2.4 ns
BMI (kg/m^2)	24.3 ± 0.2	27.5 ± 0.4 ****	27.3 ± 0.8 ****	28.1 ± 0.6 ****	28.8 ± 0.8 ****
Height (cm)	159.6 ± 1.5	168.2 ± 1.5 ***	167.4 ± 1.6 **	169.0 ± 1.5 ****	168.8 ± 1.8 ***
Weight (kg)	62.1 ± 1.1	78.0 ± 1.7 ****	76.5 ± 2.7 ****	80.3 ± 2.2 ****	82.3 ± 2.8 ****
Waist (cm)	83.3 ± 0.7	95.1 ± 1.0 ****	96.0 ± 2.2 ****	95.5 ± 1.5 ****	97.3 ± 1.7 ****
SBP (mmHg)	110.1 ± 1.9	113.7 ± 2.0 ns	121.0 ± 4.7 *	114.4 ± 2.5 ns	128.4 ± 3.1 ****
DBP (mmHg)	71.4 ± 1.1	72.2 ± 1.3 ns	74.8 ± 2.9 ns	75.4 ± 1.7 ns	82.6 ± 2.1 ****
TG neutral lipids (mg/dL)	85.1 ± 5.4	101.6 ± 3.8 *	96.9 ± 7.0 ns	266.5 ± 33.5 ****	275.7 ± 35.0 ****
HDL-c (mg/dL)	66.4 ± 2.5	54.2 ± 1.8 ***	57.0 ± 2.9 *	46.0 ± 1.8 ****	43.0 ± 2.3 ****
LDL-c (mg/dL)	121.4 ± 5.0	122.4 ± 4.5 ns	130.3 ± 5.8 ns	128.3 ± 7.5 ns	132.8 ± 8.9 ns
Fasting blood glucose (mg/dL)	92.2 ± 1.4	94.6 ± 1.2 ns	143.6 ± 8.4 ****	96.3 ± 1.2 *	127.2 ± 4.3 ****
Total cholesterol (mg/dL)	201.6 ± 5.3	192.6 ± 4.7 ns	204.5 ± 7.1 ns	208.6 ± 7.6 ns	210.7 ± 7.9 ns
Free fatty acids (μEq/L)	540.6 ± 53.8	470.3 ± 38.1 ns	444.5 ± 49.5 ns	527.7 ± 32.8 ns	410.8 ± 43.2 ns
Insulin (mIU/L)	5.0 ± 0.5	7.2 ± 0.7 *	9.5 ± 2.0 **	10.7 ± 1.7 **	12.8 ± 1.2 ****
HOMA-IR (mU/L)	1.1 ± 0.1	1.7 ± 0.2 *	3.4 ± 0.7 ***	2.5 ± 0.4 **	4.0 ± 0.4 ****
HOMA-β (%)	64.5 ± 6.8	93.0 ± 16.0 ns	46.4 ± 9.7 ns	121.3 ± 21.6 *	77.2 ± 8.2 ns

Means ± SE are presented. SBP, systolic blood pressure; DBP, diastolic blood pressure; TG, triglycerides; HOMA-IR and β, homeostatic model assessment insulin resistance and beta-cell function, respectively.

ns $P > 0.05$,

* $P \leq 0.05$,

** $P \leq 0.01$,

*** $P \leq 0.001$,

**** $P \leq 0.0001$

doi:10.1371/journal.pone.0129645.t001

and dyslipidemia (metabolic disease). Data describing these individuals are found in Table 1. Hyperglycemia was defined as having a fasting blood glucose level greater than 126 mg/dL. Subjects were categorized as having dyslipidemia if any one of the following diagnostic values were above or below normal levels; triglycerides > 150 mg/dL, LDL-c > 140 mg/dL or HDL-c < 40 mg/dL. Serum lipids, glucose, insulin, renal, and liver enzymatic levels were measured in fresh blood samples obtained after more than 6 hr fasting. VFA was measured as previously reported [19]. All participants gave their written informed consent prior to their inclusion in the study. The experimental protocol was in agreement with international norms and approved by the ethics committee of The University of Tokyo.

Measurement of GM3

Total lipid extraction. One hundred, 1500 and 20 ng of GM3(d18:1-[^{13}C]16:0), sphingomyelin(d18:1–17:0) and ceramide(d18:1–17:0) were added for internal standards to 50 μL of serum, respectively, the solution was lyophilized then dissolved in 5 mL of chloroform:methanol (1:1). The mixture was sonicated, incubated at 40°C for 1 h then centrifuged at 15,000 x g

at 4°C for 30 min. The supernatant was retained and the pellet was subjected to the same extraction procedure. The first and second supernatants were combined and evaporated. Sphingolipid molecular species lipoform designations such as d18:1-h24:0 indicate a sphingosine (d = dihydroxy, 1 = number of double bonds) of 18 carbons and a 2-hydroxy (h) nervonic acid (24:1) residue within the ceramide portion.

Mass spectrometry. GM3, ceramide and sphingomyelin molecular species were quantified using HPLC coupled with electrospray ionization tandem mass spectrometry (MS/MS) in multiple reaction monitoring (MRM) negative ionization mode. The Thermo Fisher triple stage quadrupole (TSQ) Vantage AM (Waltham, MA) instrument was calibrated by directly infusing a mixture of GM3 species extracted from milk, all ion source parameters and ionization conditions were optimized to improve sensitivity. Total lipid extracts from 50 μL of serum were dissolved in 50 μL of methanol and 6 μL were injected onto a Thermo Fisher Accela 1250 HPLC pump (Waltham, MA) and separated using a Develosil carbon 30 column (C30-UG-3-1 x 50 mm, Nomura Co. Ltd, Japan). The gradient program employed started with 100% solvent A (20% H_2O / 50% 2-propanol / 30% methanol containing 0.1% acetic acid and 0.1% ammonia) for 5 min then ramped to 100% solvent B (2% H_2O / 50% 2-propanol / 48% methanol containing 0.1% acetic acid and 0.1% ammonia) over 30 min. One hundred percent solvent B was maintained for 4 min, then the solvent was returned to 100% solvent A over 1 min and held there for 10 min. The flow rate throughout the duration of the chromatographic run was 50 μL/min. A potential of -2500 V was applied between the ion source and the electrospray needle and nitrogen gas was used. The vaporizer temperature was 373°C, sheath gas pressure was 50 (arbitrary units), ion sweep gas pressure was 0 (arbitrary units), the auxiliary gas pressure was 15 (arbitrary units), the capillary temperature was 204°C, the declustering voltage was 0, the collision pressure was 1.0 mTor, the S-lens RF amplitudes were 276, 204 and 171 and the collision energies were 53, 29 and 46 eV for GM3, ceramide and sphingomyelin molecular species, respectively. A 0.01 s scan time was used, data were collected in profile mode and peak widths were Q1 full width at half maximum (FWHM) 0.7 and (FWHM) 0.7. MS/MS transitions are listed in S1 Table. The abundance of each molecular species was compared based on its relative percentage of the internal standards GM3(d18:1-[^{13}C]16:0), ceramide(d18:1–17:0), and sphingomyelin(d18:1–17:0), of which 12, 0.4 and 30 ng were injected, respectively. Total GM3 values were calculated by taking the sum of the 23 molecular species detected. The following evaluation comes with a caveat: that all molecular species do not share identical ionization efficiencies. In this case, due to limited availability of pure molecular species standards, all species are assumed to have ionization efficiencies comparable to the internal standards used. Therefore, when evaluating the abundance of molecular species, detected amounts are compared that may not necessarily represent absolute amounts.

Statistical analysis

Data are presented as mean ± SD. For all tests, $P < 0.05$ was deemed statistically significant. GM3 molecular species comparisons between groups were performed using the Mann-Whitney *U* test and Spearman's rank correlation coefficients were calculated. For all other comparisons two-sample *t* tests were employed. All GM3 molecular species were subjected to multiple regression analyses where age, BMI, abdominal circumference, calcaneus stiffness, diastolic and systolic blood pressure, Brinkman index, ejection fraction, homeostatic model assessment insulin resistance (HOMA-IR), hemoglobin, platelets, aspartate aminotransferase (glutamic oxaloacetic transaminase) (AST (GOT)), alanine transaminase (glutamate-pyruvate transaminase) ((ALT (GPT)), γ-glutamyl transpeptidase (γ-GTP), triglycerides, creatinine, uric acid, HDL-c, C-reactive protein, LDL-c, free fatty acids, total adiponectin, autotaxin,

Table 2. Serum GM3 Molecular Species Multivariate Analysis.

	C24:0	C16:0	C24:1	C22:0	C23:0	C20:0	C22:1	C18:0	hC24:0	hC24:1	hC22:0	C18:1
All	LPC***	SM***	SM***		EF***	SM***	PLT***	BP****	LDL-c**	Age	ATX**	BP****
			LPC***		SM***	LPC***		SM***	LPC***	ATX**		SM***
					LPC***			LPC***		SM***		
Male		SM***	LPC***		LPC***	SM***	LPC***	BP****	LDL-c**	BP****		BP****
						LPC***		SM***		HOMA-IR**		SM***
								LPC***		SM***		
										LPC***		
Female				TG***	BP****	CRP***	LDL-c**	PLT***	AST**	Age	BMI*	
					Age				ALT**	HOMA-IR**	AST**	
									CR*****	Hb**	ALT**	
										AST**		
										ALT**		
										CRP***		

Clinical variables found to be significantly ($P < 0.05$) correlated with 12 most abundant GM3 molecular species by multiple regression analysis. LPC, lysophosphatidylcholine; SM, sphingomyelin; EF, ejection fraction; BP, blood pressure; ATX, autotaxin; CRP, C-reactive protein; HOMA-IR, homeostatic model assessment insulin resistance; AST, aspartate aminotransferase; ALT, alanine aminotransferase; TG, triglyceride; CR, Creatinine; PLT, platelets; Hb, hemoglobin.

Risk factors associated with

* obesity,

** metabolic disease,

*** atherosclerosis,

**** hypertension and

***** nephropathy.

doi:10.1371/journal.pone.0129645.t002

sphingomyelin, phosphotidylcholine, lysophosphatidylcholine, and intima-media thickness (IMT) were investigated as explanatory variables (Table 2). All statistical analyses were conducted using GraphPad Prism 6.04 (GraphPad Software Inc., La Jolla, CA, USA) except multiple linear regression analyses when XLSTAT version 2014.4.02 (Addinsoft, New York, NY, USA) was utilized.

Results

Subject characteristics

Individuals in the VFA, VFA with hyperglycemia, VFA with dyslipidemia and VFA with metabolic disease groups all had significantly higher BMI, height, weight, waist circumference, insulin levels, HOMA-IR scores and lower HDL-c values (Table 1). Individuals in the VFA, VFA with dyslipidemia and VFA with metabolic disease groups all had elevated triglyceride levels when compared to controls, however only the VFA with dyslipidemia and VFA with metabolic disease had values deemed pathological (>150 mg/dL) with averages of 266.5 ± 33.5 and 275.7 ± 35.0 mg/dL, respectively (Table 1). Fasting blood glucose was elevated to the point of a type 2 diabetes diagnosis (>126 mg/dL) in both the VFA with hyperglycemia and VFA with metabolic disease groups, average values of 143.6 ± 8.4 and 127.2 ± 4.3 mg/dL, respectively (Table 1).

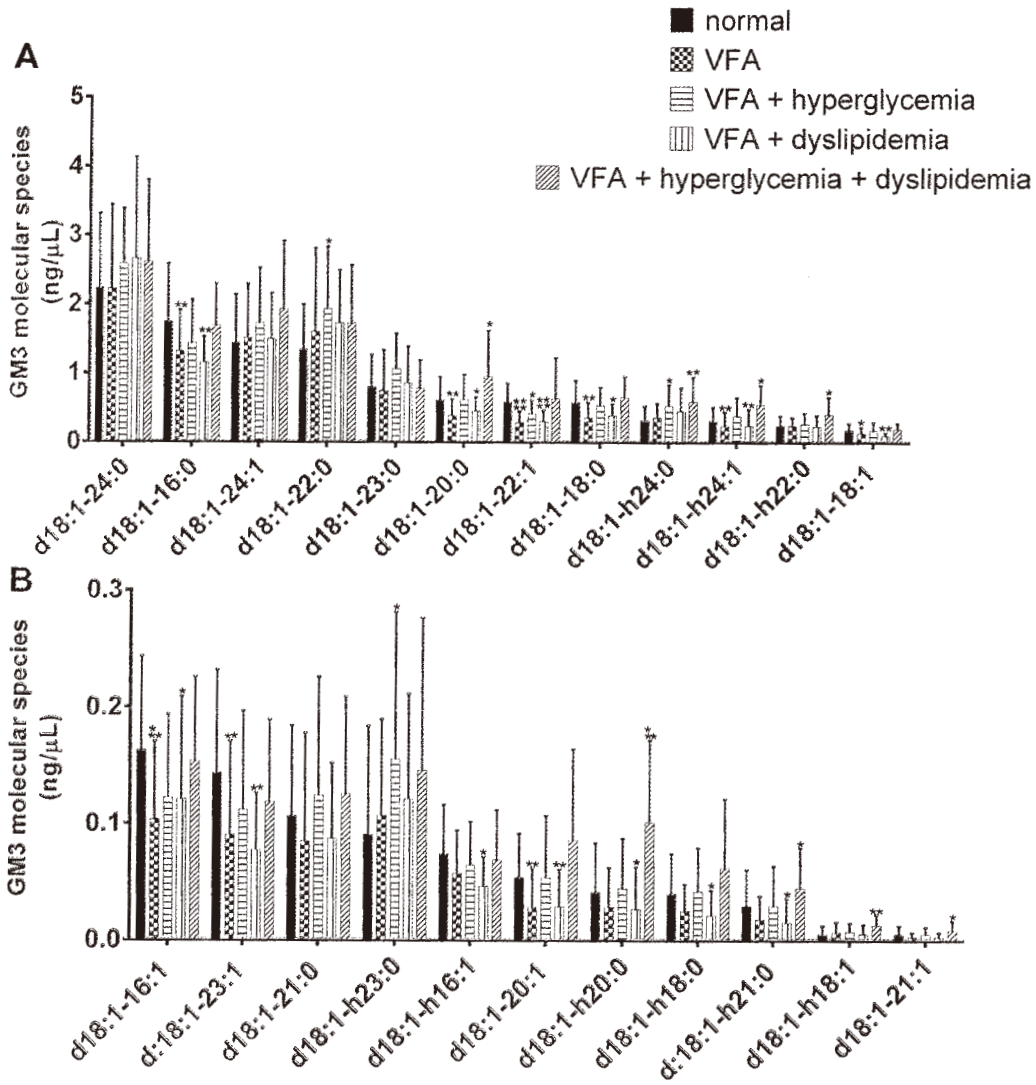

Fig 1. GM3 molecular species levels in human serum. Twelve most abundant (A) and eleven least abundant (B) GM3 molecular species detected in serum of patients with visceral fat accumulation (VFA) (n = 39), VFA with hyperglycemia (n = 15), VFA with dyslipidemia (n = 28) and VFA with both hyperglycemia and dyslipidemia (n = 17) compared with healthy lean control individuals (n = 26). Species were determined using LC-MS/MS MRM. Data are reported as means ± SD. * $P \leq 0.05$, ** $P \leq 0.01$, *** $P \leq 0.001$, **** $P \leq 0.0001$ metabolic risk factor groups vs. control; Mann-Whitney unpaired test.

doi:10.1371/journal.pone.0129645.g001

Serum GM3 molecular species levels in patients with risk factors for metabolic disease

The four most abundant molecular species of GM3 detected in control subjects were GM3 (d18:1–24:0), GM3(d18:1–16:0), GM3(d18:1–24:1) and GM3(d18:1–22:0) (Fig 1A). Eight GM3 molecular species were elevated in a statistically significant fashion ($P < 0.05$) in the individuals of VFA with metabolic disease, in order of decreasing abundance they were GM3(d18:1–20:0) (control, 0.610 ± 0.336 ng/μL vs metabolic disease, 0.956 ± 0.662 ng/μL), GM3 (d18:1-h24:0) (control, 0.317 ± 0.204 ng/μL vs metabolic disease, 0.588 ± 0.357 ng/μL), GM3

(d18:1-h24:1) (control, 0.316 ± 0.192 ng/μL vs metabolic disease, 0.546 ± 0.283 ng/μL), GM3 (d18:1-h22:0) (control, 0.238 ± 0.145 ng/μL vs metabolic disease, 0.400 ± 0.252 ng/μL), GM3 (d18:1-h20:0) (control, 0.041 ± 0.042 ng/μL vs metabolic disease, 0.101 ± 0.070 ng/μL), GM3 (d18:1-h21:0) (control, 0.029 ± 0.031 ng/μL vs metabolic disease, 0.044 ± 0.035 ng/μL), GM3 (d18:1-h18:1) (control, 0.005 ± 0.007 ng/μL vs metabolic disease, 0.013 ± 0.009 ng/μL) and GM3(d18:1–21:1) (control, 0.005 ± 0.007 ng/μL vs metabolic disease, 0.009 ± 0.008 ng/μL), (Fig 1A and 1B). Additionally, the individuals of VFA with hyperglycemia exhibited elevated levels of GM3(d18:1–22:0) (control, 1.339 ± 0.651 ng/μL vs VFA with hyperglycemia, 1.927 ± 0.906 ng/μL), GM3(d18:1-h24:0) (control, 0.317 ± 0.204 ng/μL vs VFA with hyperglycemia, 0.527 ± 0.311 ng/μL) and GM3(d18:1-h23:0) (control, 0.091 ± 0.093 ng/μL vs VFA with hyperglycemia, 0.155 ± 0.126 ng/μL) (Fig 1A and 1B). Total GM3 values were elevated in the VFA with hyperglycemia and VFA with metabolic disease groups with average values of 12.814 ± 4.509 ng/μL and 13.972 ± 5.237 ng/μL respectively, compared with the control group's average value of 11.468 ± 3.771 ng/μL (Fig 2A). However, this difference was not deemed statistically significant due to variation within the groups. Total hydroxylated GM3 species were elevated, and this increase observed in the VFA with metabolic disease group was statistically significant (control, 1.508 ± 0.651 ng/μL vs metabolic disease, 2.316 ± 1.041 ng/μL) with a P value of 0.0073 (Fig 2B).

Correlation between GM3 molecular species and metabolic disease risk factors

The results of multiple regression (Table 2) and univariate analyses indicated GM3 (d18:1-h24:1) is significantly correlated with the largest number of metabolic disease risk factors. Spearman's rank correlations were used to assess relationships between GM3 molecular species and clinical variables relevant to metabolic disease. Clinical variables associated with type 2 diabetes and atherosclerosis and correlated with GM3(d18:1-h24:1) include, but are not limited to, fasting blood glucose $r_s = 0.2633$ (mg/dL, Fig 3A), insulin $r_s = 0.3923$ (mIU/L, Fig 3B), HOMA-IR $r_s = 0.4226$ (Fig 3C), HbA1c $r_s = 0.2803$ (% glycated hemoglobin, Fig 3D), total cholesterol $r_s = 0.2045$ (mg/dL, Fig 3E), LDL-c $r_s = 0.1899$ (mg/dL, Fig 3F), autotaxin $r_s = 0.2934$ (mg/L, Fig 3G) and mean IMT $r_s = 0.3709$ (mm, Fig 3H).

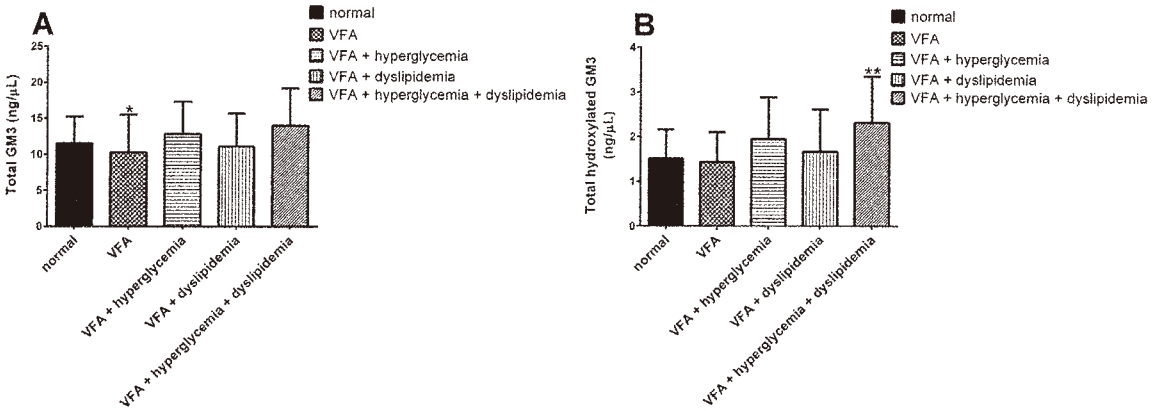

Fig 2. The sum of GM3 molecular species. Total GM3 (A) and total hydroxylated GM3 (B) detected in serum of patients with visceral fat accumulation (VFA) (n = 39), VFA with hyperglycemia (n = 15), VFA with dyslipidemia (n = 28) and VFA with both hyperglycemia and dyslipidemia (n = 17) compared with healthy lean control individuals (n = 26). Species were determined using LC-MS/MS MRM. Data are reported as means ± SD. * $P \leq 0.05$, ** $P \leq 0.01$, *** $P \leq 0.001$, **** $P \leq 0.0001$ metabolic risk factor groups vs. control; Mann-Whitney unpaired test.

doi:10.1371/journal.pone.0129645.g002

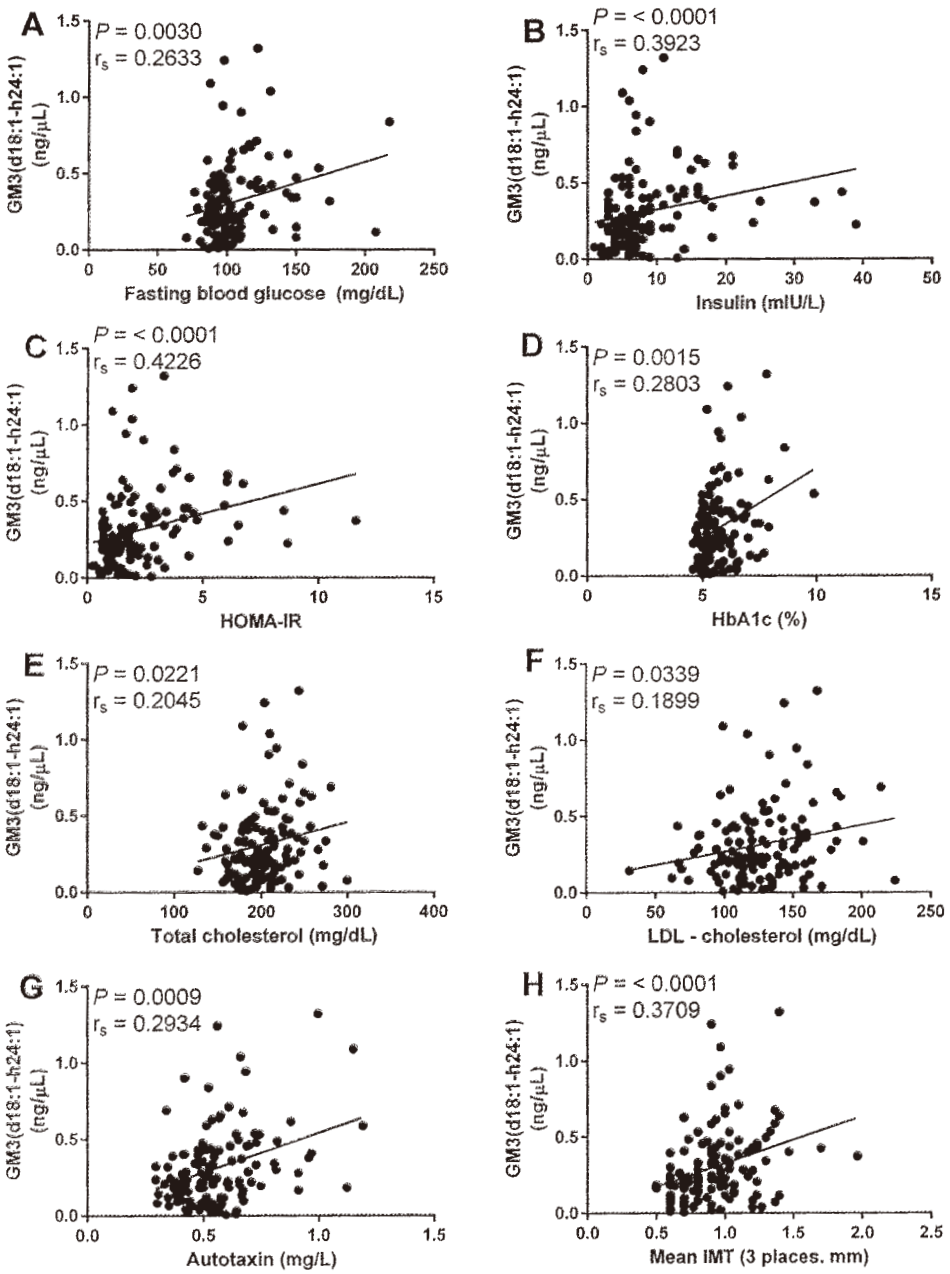

Fig 3. Association between metabolic disease risk factors and GM3(d18:1-h24:1). Correlation of GM3(d18:1-h24:1) with fasting blood glucose (A), insulin (B), HOMA-IR (C), HbA1c (D), total cholesterol (E), LDL-c (F), autotaxin (G) and mean IMT (H). Spearman's rank correlation was used to access correlation between GM3(d18:1-h24:1) and metabolic disease risk factors. All correlations were deemed significant with *P* values below 0.05.

doi:10.1371/journal.pone.0129645.g003

In addition to GM3(d18:1-h24:1) it was found that total GM3 and total hydroxylated GM3 molecular species were correlated with risk factors for type 2 diabetes and CVD. Total GM3 was significant correlated with fasting blood glucose $r_s = 0.2793$ (mg/dL, Fig 4A), Hba1c $r_s = 0.1820$ (% glycated hemoglobin, Fig 4D), total cholesterol $r_s = 0.5046$ (mg/dL, Fig 4E), LDL-c r_s

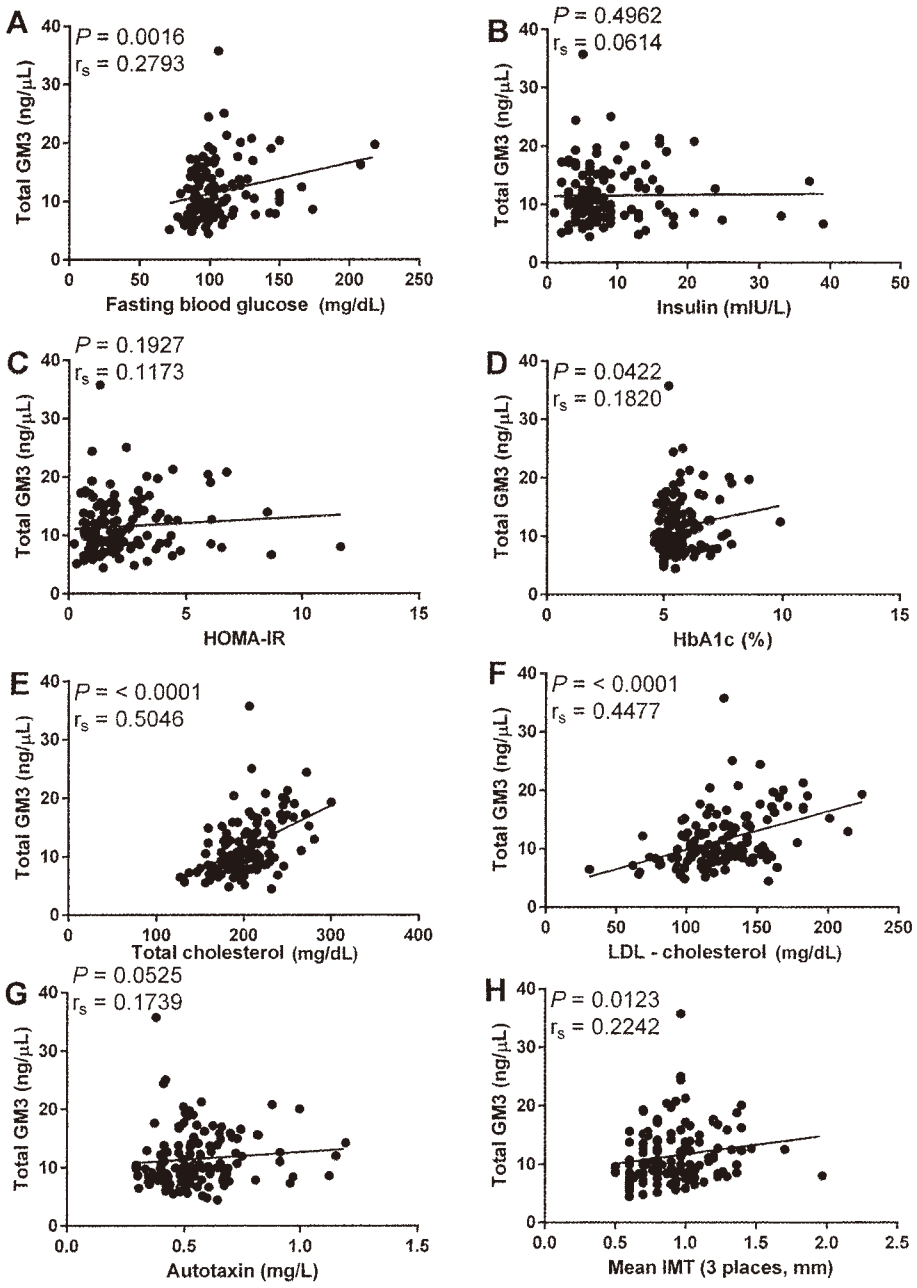

Fig 4. Association between metabolic disease risk factors and total GM3. Correlation of total GM3 with fasting blood glucose (A), insulin (B), HOMA-IR (C), HbA1c (D), total cholesterol (E), LDL-c (F), autotaxin (G) and mean IMT (H). Spearman's rank correlation was used to access correlation between total GM3 and metabolic disease risk factors. Correlations of fasting blood glucose, HbA1c, total cholesterol, LDL-c and mean IMT with total GM3 were deemed significant with *P* values below 0.05.

doi:10.1371/journal.pone.0129645.g004

= 0.4477 (mg/dL, Fig 4F) and mean IMT r_s = 0.2242 (mm, Fig 4H). While total hydroxylated GM3 molecular species were significantly correlated with fasting blood glucose r_s = 0.3273 (mg/dL, Fig 5A), insulin r_s = 0.2766 (mIU/L, Fig 5B), HOMA-IR r_s = 0.3223 (Fig 5C), HbA1c r_s = 0.2975 (% glycated hemoglobin, Fig 5D), total cholesterol r_s = 0.4293 (mg/dL, Fig 5E), LDL-c r_s = 0.3958 (mg/dL, Fig 5F), autotaxin r_s = 0.3188 (mg/L, Fig 5G) and mean IMT r_s = 0.2987 (mm, Fig 5H).

Relative abundance of GM3(d18:1-h24:1)

In individuals of VFA with metabolic disease, the ratio of GM3(d18:1-h24:1) to GM3(d18:1–24:1) was significantly greater than that of sphingomyelin and ceramide. GM3(d18:1-h24:1) existed at 35.8 ± 22.9% of GM3(d18:1–24:0), whereas sphingomyelin(d18:1-h24:1) and ceramide(d18:1-h24:1) presented at 0.6 ± 0.3% and 0.4 ± 0.5%, respectively (Fig 6A). The total amount of GM3(d18:1-h24:1) in serum was also found to be greater than the same species in sphingomyelin and ceramide, measuring 0.546 ± 0.283 ng/μL compared to 0.426 ± 0.406 ng/μL and 0.011 ± 0.013 ng/μL, respectively (Fig 6B). To put the relative amounts of d18:1-h24:1 molecular species into perspective, the sums of the 12 most abundant GM3, sphingomyelin and ceramide molecular species were calculated. The amounts were 12.697 ± 4.713 ng/μL, 391.538 ± 161.703 ng/μL and 11.135 ± 3.281 ng/μL for GM3, sphingomyelin and ceramide, respectively (Fig 6C).

Discussion

The pathogenesis of obesity induced type 2 diabetes and CVD has been reported to correspond with increased plasma sphingolipids such as ceramide and sphingomyelin [20]. Previous studies have also found human serum GM3 concentrations to be increased in type 2 diabetes accompanied by severe visceral fat accumulation [12]. In addition to increased GM3 levels a positive correlation with LDL-c in serum of patients with type 2 diabetes (r_s = 0.403, p = 0.012) has been observed [12]. Serum GM3 levels were also found to be elevated in patients with high levels (> 10 mg/dL) of small dense LDL, a form of LDL that is known to be especially atherogenic [21–23], a finding significant to our discovery that GM3 molecular species are correlated with CVD risk factors. Because GM3 exists as a prominent ganglioside in blood and has a negative influence on insulin signaling [6,17,24], this information is important. However, GM3 is not a single entity but rather a number of molecular species with varying ceramide moieties, each with unique biophysical properties and, presumably, physiological functions. With the fact in mind that total GM3 is elevated in metabolic syndrome we set out to explicitly determine which GM3 molecular species are implicated in metabolic disease.

Our results confirmed the finding by Sato, et al. [12] that individuals of VFA with hyperglycemia, and even more so in individuals of VFA with metabolic disease, have increased total serum GM3 (Fig 2A), however variation within groups resulted in an alpha level greater than 0.05. Further, we also confirmed that total GM3 levels are correlated with LDL-c (Fig 4F), a finding in line with previous reports that lipoprotein associated gangliosides are increased in hyperlipidemic patients [25] and that approximately 98% of human serum gangliosides are transported by lipoproteins [26].

Upon comparing total GM3 (Fig 4) and GM3(d18:1-h24:1) (Fig 3), the advantage to monitoring individual GM3 molecular species over total GM3 becomes clear. While both total GM3 and GM3(d18:1-h24:1) are correlated with total cholesterol, LDL-c and fasting blood glucose (Figs 4E, 3E, 4F, 3F, 4A and 3A, respectively), only GM3(d18:1-h24:1) is significantly correlated with autotaxin (Fig 3G), insulin (Fig 3B) and HOMA-IR (Fig 3C); adipose-derived autotaxin contributes to adipose tissue expansion and insulin resistance in diet-induced obesity [27].

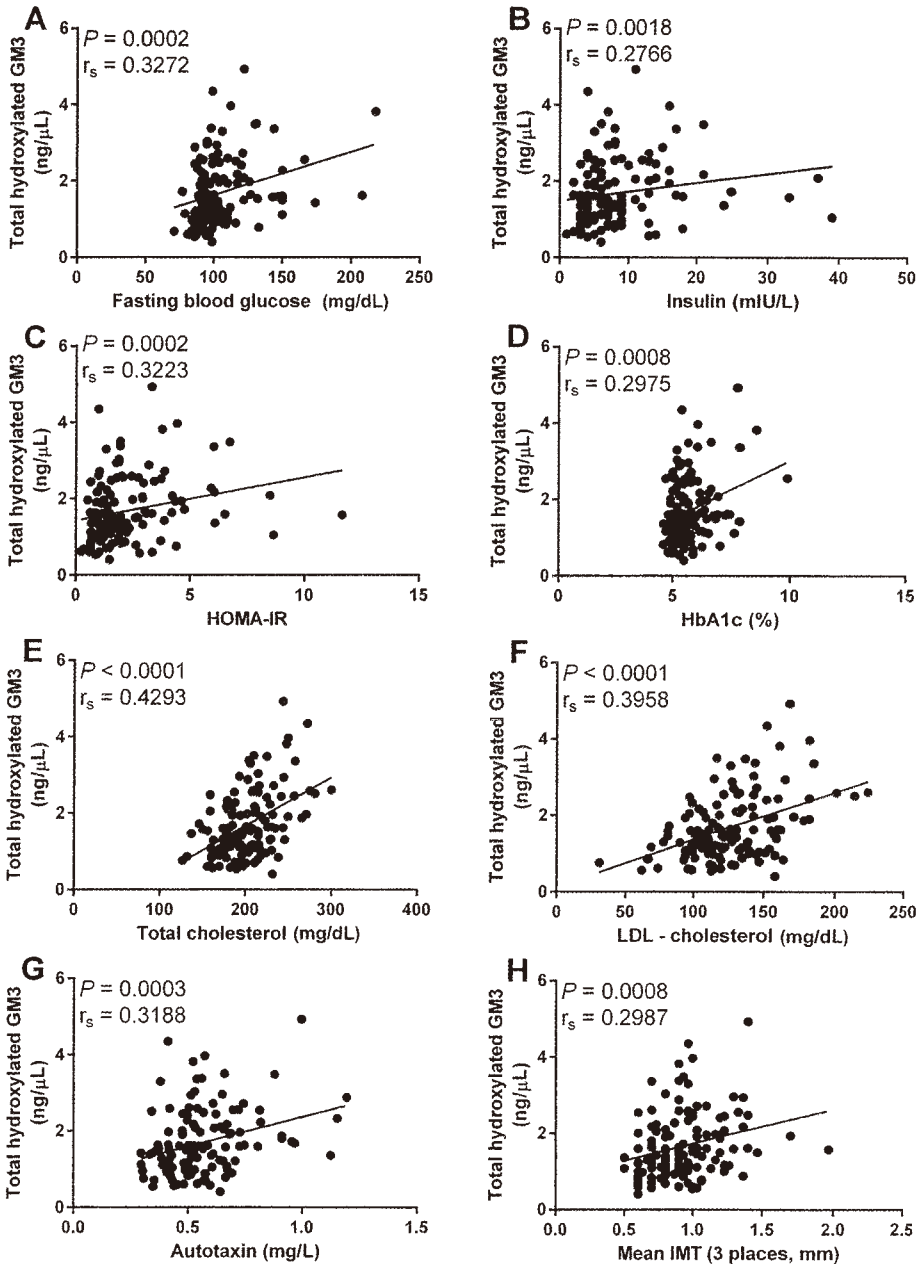

Fig 5. Association between metabolic disease risk factors and total hydroxylated GM3. Correlation of total hydroxylated GM3 molecular species with fasting blood glucose (A), insulin (B), HOMA-IR (C), HbA1c (D), total cholesterol (E), LDL-c (F), autotaxin (G) and mean IMT (H). Spearman's rank correlation was used to access correlation between total hydroxylated GM3 molecular species and metabolic disease risk factors. All correlations were deemed significant with *P* values below 0.05.

doi:10.1371/journal.pone.0129645.g005

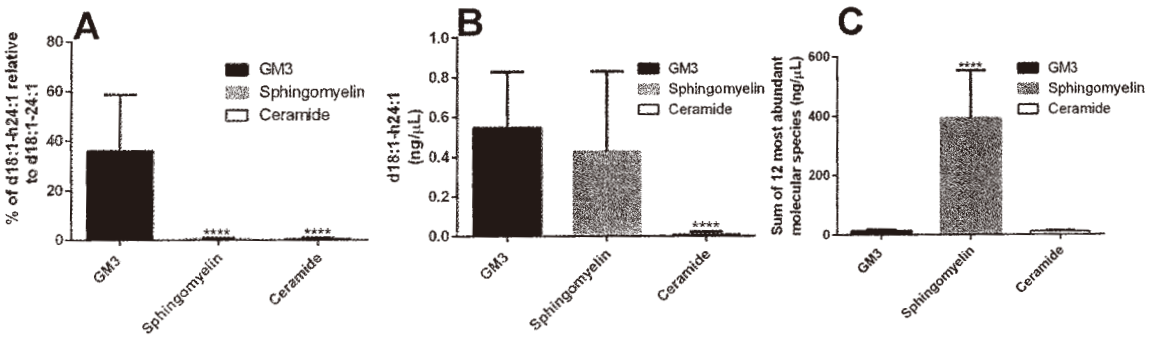

Fig 6. The relative abundance of d18:1-h24:1 molecular species. Percent of d18:1-h24:1 relative to d18:1–24:1 in GM3, sphingomyelin and ceramide in individuals with metabolic disease (A). The average amounts of d18:1-h24:1 (B) and the sum of the 12 most abundant molecular species (C) of GM3, sphingomyelin and ceramide in six microliters of human serum from individuals with metabolic disease. Data are reported as means ± SD. **** $P \leq 0.0001$ sphingomyelin and ceramide vs. GM3; Mann-Whitney unpaired test.

doi:10.1371/journal.pone.0129645.g006

Additionally, GM3(d18:1-h24:1) is more strongly correlated with both mean IMT (total GM3 $r_s = 0.2242$ (Fig 4H) vs GM3(d18:1-h24:1) $r_s = 0.3709$ (Fig 3H)), a risk factor for atherosclerotic disease, and the diabetic indicator HbA1c (total GM3 $r_s = 0.1820$ (Fig 4D) vs GM3 (d18:1-h24:1) $r_s = 0.2803$ (Fig 3D)).

It is important to note that all GM3 molecular species are not always correlated with metabolic disease risk factors (Fig 4B, 4C and 4G). Because of this, simply measuring total GM3 values to infer information about a patient's propensity for type 2 diabetes or CVD may be misleading and result in a false positive or a missed diagnosis, *e.g.* in the event that elevated total GM3 levels are due to molecular species not associated with risk factors or the situation where GM3 levels are within the normal range but high levels of the risk factor associated hydroxylated species are present. Moving forward it will be essential to target specific GM3 molecular species, namely hydroxylated molecular species, to provide the most accurate and reliable biomarker information to patients and health care providers.

The molecular species containing ceramide(d18:1-h24:1) is present in GM3, sphingomyelin and ceramide and relative abundances are variable. However, the absolute and relative abundance of GM3(d18:1-h24:1) makes it the most attractive target for metabolic screening, *e.g.* the relative abundance of GM3(d18:1-h24:1) to GM3(d18:1–24:0) 35.8 ± 22.9%, that of sphingomyelin and ceramide 0.6 ± 0.3% and 0.4 ± 0.5%, respectively (Fig 6A) and the absolute amount of each GM3(d18:1-h24:1), sphingomyelin(d18:1-h24:1) and ceramide(d18:1-h24:1) in human serum is 0.546± 0.283 ng/μL, 0.426 ± 0.406 ng/μL and 0.011 ± 0.013 ng/μL, respectively (Fig 6B). The finding that the molecular species GM3(d18:1-h24:1) is most abundant is quite remarkable, considering the degree that total serum sphingomyelin outweighs total serum GM3. For example, the 12 most abundant sphingomyelin molecular species total 391.538 ± 161.703 ng/μL, over thirty times more than the same measure of GM3 which is 12.697 ± 4.713 ng/μL (Fig 6C). This underscores the significant and specific upregulation of GM3(d18:1-h24:1) in individuals with risk factors for type 2 diabetes and CVD.

The formation of hydroxylated sphingolipids begins with fatty acid 2-hydroxylase (FA2H) converting acyl-CoAs to 2-hydroxylated-CoAs and 2-hydroxylted-CoAs are transferred to dihydrosphingosine by an isoform of ceramide synthase, of which there are six capable. Des-1 desaturase then converts hydroxy fatty acid (hFA)-dihydroceramide to hFA-ceramide which acts as a precursor for complex hFA-sphingolipids [28]. Another possible means for the formation of hydroxylated sphingolipids, that is FA2H independent, involves the enzyme phytanoyl-CoA-2-hydroxylase (PHYH) of the α-oxidation pathway. In this scenario hFA would be

synthesized in peroxisomes and transported to the endoplasmic reticulum (ER) where hFA-ceramide is formed. Or, alternatively, PHYH would be trafficked to the ER to participate in the synthesis of hFA-ceramide [28]. A third possibility that does not involve hFA-ceramide serving as the precursor for hFA-sphingolipid synthesis is that of direct hydroxylation of non-hydroxy fatty acid-containing sphingolipids, a possibility supported by studies examining the formation of hFA-sphingolipids in tetrahymena [29]. Although we presently do not have enough evidence to indicate the means by which hydroxylated GM3 molecular species are enriched in the individuals of VFA with metabolic disease, the observation that hydroxylated GM3 molecular species are far more abundant than hydroxylated ceramide molecular species seems to point to the mechanism of direct hydroxylation. It is interesting to note that a linear correlation has been reported between GM3 molecular species containing hydroxylated acyl chains and aging in the human liver [30], the site of excretion of gangliosides into mammalian sera [25,31].

The observation that GM3 treatment of 3T3-L1 adipocytes induces a fourfold increase in IL-6, PAI-1 and TNF-α mRNA suggests that gene expression of proteins involved in obesity induced thrombosis and inflammation may be dependent on its abundance [20]. Moving forward we will explore the idea that a specific increase in hydroxylated GM3 molecular species (Fig 2B), particularly GM3(d18:1-h24:1) (Fig 1A), may influence the regulation of membrane-associated signal transduction events. An idea that seems plausible in light of the finding that hFA derivatives have been shown to regulate microdomain structure by modulating the composition of ordered microdomain components [32] and membrane lateral diffusion [33]. Future investigations will aim to elucidate potential underlying mechanisms linking hydroxylated GM3 molecular species with the progression of insulin resistance and atherosclerosis. Planned experiments involve examining the impact that synthetic hydroxylated GM3 molecular species have on signaling events associated with IR activation. Additionally, owing to the fact that the GM3 precursor ceramide has been reported to be positively correlated with obesity and metabolic disease [34], to obtain a more global view of sphingolipid metabolism, it will be important to analyze full profiles covering ceramide, glucosylceramide, lactosylceramide and sphingomyelin molecular species for these patients in the future.

Supporting Information

S1 Table. Mass spectrometer settings and MRM transition pairs.
(PDF)

Acknowledgments

The authors would like to thank Kaori Tsuchiya for her assistance in isolation and purification of sphingolipids from serum samples.

Author Contributions

Conceived and designed the experiments: J-iI. Performed the experiments: LV AS WM SG MN YY. Analyzed the data: LV AS WM SG MN YY. Contributed reagents/materials/analysis tools: MN YY. Wrote the paper: J-iI LV.

References

1. Chen L, Magliano DJ, Zimmet PZ (2012) The worldwide epidemiology of type 2 diabetes mellitus—present and future perspectives. Nat Rev Endocrinol 8: 228–236. doi: 10.1038/nrendo.2011.183 PMID: 22064493
2. Maitra A, Abbas AK (2005) Endocrine systems. In: Kumar V, Fauston N, Abbas AK, editors. Robbins and Cotran Pathologic basis of diease (7th ed). Philadelphia, U.S.A.: Saunders. pp. 1156–1226.

3. Inokuchi J (2011) Physiopathological function of hematoside (GM3 ganglioside). Proc Jpn Acad Ser B Phys Biol Sci 87: 179–198. PMID: 21558756

4. Couet J, Li S, Okamoto T, Ikezu T, Lisanti MP (1997) Identification of peptide and protein ligands for the caveolin-scaffolding domain. Implications for the interaction of caveolin with caveolae-associated proteins. J Biol Chem 272: 6525–6533. PMID: 9045678

5. Hakomori SI (2002) The glycosynapse. Proc Natl Acad Sci U S A 99: 225–232. PMID: 11773621

6. Tagami S, Inokuchi J, Kabayama K, Yoshimura H, Kitamura F, Uemura S, et al. (2002) Ganglioside GM3 participates in the pathological conditions of insulin resistance. J Biol Chem 277: 3085–3092. PMID: 11707432

7. Zhao H, Przybylska M, Wu IH, Zhang J, Siegel C, Komarnitsky S, et al. (2007) Inhibiting glycosphingolipid synthesis improves glycemic control and insulin sensitivity in animal models of type 2 diabetes. Diabetes 56: 1210–1218. PMID: 17470562

8. Aerts JM, Ottenhoff R, Powlson AS, Grefhorst A, van Eijk M, Dubbelhuis PF, et al. (2007) Pharmacological inhibition of glucosylceramide synthase enhances insulin sensitivity. Diabetes 56: 1341–1349. PMID: 17287460

9. van Eijk M, Aten J, Bijl N, Ottenhoff R, van Roomen CP, Dubbelhuis PF, et al. (2009) Reducing glycosphingolipid content in adipose tissue of obese mice restores insulin sensitivity, adipogenesis and reduces inflammation. PLoS One 4: e4723. doi: 10.1371/journal.pone.0004723 PMID: 19305508

10. Zhao H, Przybylska M, Wu IH, Zhang J, Maniatis P, Pacheco J, et al. (2009) Inhibiting glycosphingolipid synthesis ameliorates hepatic steatosis in obese mice. Hepatology 50: 85–93. doi: 10.1002/hep.22970 PMID: 19444873

11. Bijl N, Sokolovic M, Vrins C, Langeveld M, Moerland PD, Ottenhoff R, et al. (2009) Modulation of glycosphingolipid metabolism significantly improves hepatic insulin sensitivity and reverses hepatic steatosis in mice. Hepatology 50: 1431–1441. doi: 10.1002/hep.23175 PMID: 19731235

12. Sato T, Nihei Y, Nagafuku M, Tagami S, Chin R, Kawamura M, et al. (2008) Circulating levels of ganglioside GM3 in metabolic syndrome: A pilot study. Obes Res Clin Pract 2: I–II.

13. Yamashita T, Hashiramoto A, Haluzik M, Mizukami H, Beck S, Norton A, et al. (2003) Enhanced insulin sensitivity in mice lacking ganglioside GM3. Proc Natl Acad Sci U S A 100: 3445–3449. PMID: 12629211

14. Nagafuku M, Sato T, Sato S, Shimizu K, Taira T, Inokuchi J (2014) Control of homeostatic and pathogenic balance in adipose tissue by ganglioside GM3. Glycobiology doi: 10.1093/glycob/cwu112

15. Inokuchi J (2014) GM3 and diabetes. Glycoconj J 31: 193–197. doi: 10.1007/s10719-013-9516-4 PMID: 24399479

16. Inokuchi J (2010) Membrane microdomains and insulin resistance. FEBS Lett 584: 1864–1871. doi: 10.1016/j.febslet.2009.10.012 PMID: 19822143

17. Kabayama K, Sato T, Saito K, Loberto N, Prinetti A, Sonnino S, et al. (2007) Dissociation of the insulin receptor and caveolin-1 complex by ganglioside GM3 in the state of insulin resistance. Proc Natl Acad Sci U S A 104: 13678–13683. PMID: 17699617

18. Inokuchi J (2013) Method for detection of disease having insulin-resistant conditions. Google Patents.

19. Nemoto M, Yeernuer T, Masutani Y, Nomura Y, Hanaoka S, Miki S, et al. (2014) Development of automatic visceral fat volume calculation software for CT volume data. J Obes 2014: 495084. doi: 10.1155/2014/495084 PMID: 24782922

20. Samad F, Hester KD, Yang G, Hannun YA, Bielawski J (2006) Altered adipose and plasma sphingolipid metabolism in obesity: a potential mechanism for cardiovascular and metabolic risk. Diabetes 55: 2579–2587. PMID: 16936207

21. Austin MA, Breslow JL, Hennekens CH, Buring JE, Willett WC, Krauss RM (1988) Low-density lipoprotein subclass patterns and risk of myocardial infarction. JAMA 260: 1917–1921. PMID: 3418853

22. De Graaf J, Hak-Lemmers HL, Hectors MP, Demacker PN, Hendriks JC, Stalenhoef AF (1991) Enhanced susceptibility to in vitro oxidation of the dense low density lipoprotein subfraction in healthy subjects. Arterioscler Thromb 11: 298–306. PMID: 1998647

23. Tribble DL, Krauss RM, Lansberg MG, Thiel PM, van den Berg JJ (1995) Greater oxidative susceptibility of the surface monolayer in small dense LDL may contribute to differences in copper-induced oxidation among LDL density subfractions. J Lipid Res 36: 662–671. PMID: 7616114

24. Kabayama K, Sato T, Kitamura F, Uemura S, Kang BW, Igarashi Y, et al. (2005) TNFalpha-induced insulin resistance in adipocytes as a membrane microdomain disorder: involvement of ganglioside GM3. Glycobiology 15: 21–29. PMID: 15306563

25. Senn HJ, Orth M, Fitzke E, Koster W, Wieland H, Gerok W (1992) Human serum gangliosides in hypercholesterolemia, before and after extracorporeal elimination of LDL. Atherosclerosis 94: 109–117. PMID: 1632864

26. Senn HJ, Orth M, Fitzke E, Wieland H, Gerok W (1989) Gangliosides in normal human serum. Concentration, pattern and transport by lipoproteins. Eur J Biochem 181: 657–662. PMID: 2731542

27. Nishimura S, Nagasaki M, Okudaira S, Aoki J, Ohmori T, Ohkawa R, et al. (2014) ENPP2 Contributes to Adipose Tissue Expansion and Insulin Resistance in Diet-Induced Obesity. Diabetes 63: 4154–4164. doi: 10.2337/db13-1694 PMID: 24969110

28. Hama H (2010) Fatty acid 2-Hydroxylation in mammalian sphingolipid biology. Biochim Biophys Acta 1801: 405–414. doi: 10.1016/j.bbalip.2009.12.004 PMID: 20026285

29. Kaya K, Ramesha CS, Thompson GA Jr. (1984) On the formation of alpha-hydroxy fatty acids. Evidence for a direct hydroxylation of nonhydroxy fatty acid-containing sphingolipids. J Biol Chem 259: 3548–3553. PMID: 6423633

30. Riboni L, Acquotti D, Casellato R, Ghidoni R, Montagnolo G, Benevento A, et al. (1992) Changes of the human liver GM3 ganglioside molecular species during aging. Eur J Biochem 203: 107–113. PMID: 1730216

31. Senn HJ, Sellin S, Fitzke E, Stehle T, Haussinger D, Wieland H, et al. (1992) Biosynthesis and excretion of gangliosides by the isolated perfused rat liver. Eur J Biochem 205: 809–814. PMID: 1572373

32. Ibarguren M, Lopez DJ, Encinar JA, Gonzalez-Ros JM, Busquets X, Escriba PV (2013) Partitioning of liquid-ordered/liquid-disordered membrane microdomains induced by the fluidifying effect of 2-hydroxylated fatty acid derivatives. Biochim Biophys Acta 1828: 2553–2563. doi: 10.1016/j.bbamem.2013.06.014 PMID: 23792066

33. Uemura S, Shishido F, Tani M, Mochizuki T, Abe F, Inokuchi JI (2014) Loss of hydroxyl groups from the ceramide moiety can modify the lateral diffusion of membrane proteins in S. cerevisiae. J Lipid Res 55: 1343–1356. PMID: 24875539

34. Chavez JA, Summers SA (2012) A ceramide-centric view of insulin resistance. Cell Metab 15: 585–594. doi: 10.1016/j.cmet.2012.04.002 PMID: 22560211

J. Biochem. 2015;158(2):155–163 doi:10.1093/jb/mvv022

JB THE JOURNAL OF BIOCHEMISTRY

Close association of B2 bradykinin receptors with $P2Y_2$ ATP receptors

Received December 22, 2014; accepted February 10, 2015; published online February 20, 2015

Sayo Yashima, Ayaka Shimazaki, Junya Mitoma, Tetsuto Nakagawa, Maya Abe, Hiroyuki Yamada and Hideyoshi Higashi*

Division of Glyco-Signal Research, Institute of Molecular Biomembrane and Glycobiology, Tohoku Pharmaceutical University, Sendai, Miyagi 981-8558, Japan

*Hideyoshi Higashi, Division of Glyco-Signal Research, Institute of Molecular Biomembrane and Glycobiology, Tohoku Pharmaceutical University, 4-4-1 Komatsushima, Aoba-ku, Sendai Miyagi 981-8558, Japan. Tel.: +81-22-727-0119, Fax: +81-22-727-0077, email: hhigashi@tohoku-pharm.ac.jp

Two G-protein-coupled receptors (GPCRs) that couple with Gαq/11, B2 bradykinin (BK) receptor (B2R) and ATP/UTP receptor $P2Y_2$ ($P2Y_2R$), are ubiquitously expressed and responsible for vascular tone, inflammation, and pain. We analysed the cellular signalling of $P2Y_2Rs$ in cells that express B2Rs. B2R desensitization induced by BK or B2R internalization-inducing glycans cross-desensitized the $P2Y_2R$ response to ATP/UTP. Fluorescence resonance energy transfer from $P2Y_2R$-AcGFP to B2R-DsRed was detected in the cells and on the cell surfaces, showing the close association of these GPCRs. BK- and ATP-induced cross-internalization of $P2Y_2R$ and B2R, respectively, was shown in a β-galactosidase complementation assay using $P2Y_2R$ or B2R fused to the H31R substituted α donor peptide of a β-galactosidase reporter enzyme ($P2Y_2R$-α or B2R-α) with coexpression of the FYVE domain of endofin, an early endosome protein, fused to the M15 acceptor deletion mutant of β-galactosidase (the ω peptide, FYVE-ω). Arrestin recruitment to the GPCRs by cross-activation was also shown with the similar way. Coimmunoprecipitation showed that B2R and $P2Y_2R$ were closely associated in the cotransfected cells. These results indicate that B2R couples with $P2Y_2R$ and that these GPCRs act together to fine-tune cellular responsiveness. The collaboration between these receptors may permit rapid onset and turning off of biological events.

Keywords: ATP/bradykinin/crosstalk/G-protein-coupled receptor/hetero oligomer.

Abbreviations: BSS, balanced salt solution receptor; BK, bradykinin; B2R, B2 bradykinin; CSC, chondroitin sulfate C; FRET, fluorescence resonance energy transfer; GT1b, Neu5Acα3Galβ3GalNAcβ4(Neu5Acα8Neu5Acα3)Galβ4GlcCer; GPCR, G-protein–coupled receptor; MEM, minimum essential medium; $P2Y_2R$, $P2Y_2$ receptor.

Tissue damage associated with infection, inflammation and ischemia produces an array of chemical mediators such as ATP, bradykinin (BK) and histamine (*1*). BK is a key regulator of vascular tone that is implicated in pathological disorders such as inflammation, pain and cancer (*2*). The BK B2 receptor (B2R) is distributed ubiquitously in cells throughout the body, including neuronal tissues. Expression of an ATP receptor, $P2Y_2$ receptor ($P2Y_2R$) is upregulated in response to stress and injury in a variety of tissues (*3–6*). $P2Y_2R$ is a dominant regulator of Cl^- transport and a mediator of mechanical stress-induced intercellular Ca^{2+} waves in airway epithelia (*7*, *8*). $P2Y_2R$ is also the receptor responsible for modulating the ATP-mediated transmission of Ca^{2+} waves from normal human epidermal keratinocytes to dorsal root ganglia neurons (*9*). Both receptors couple with Gαq/11, activate phospholipase C with agonist stimulation to produce IP3, and induce release of Ca^{2+} from intracellular stores. There is no evidence of a direct interaction between $P2Y_2Rs$ and B2Rs, but an increasing number of reports have described crosstalk between BK and ATP signalling (*10–13*). Reiser and colleagues suggested that BK may interact with the ATP-activated mechanism by cross-desensitization (*11*) and demonstrated that $P2Y_2R$ plays a main role in this mechanism (*12*). However, different reactivities of ATP and UTP to the receptor(s) in the NG108-15 cells used in these studies are inconsistent with authentic features of $P2Y_2R$.

In this study, the interaction of $P2Y_2R$ with B2R was examined in CHO-K1 cells, which endogenously express authentic $P2Y_2R$ (*14*), but little if any B2Rs. Formation of heterooligomers between B2R and $P2Y_2R$ and investigation of the effects of B2R expression on $P2Y_2R$ activity were examined by transiently expressing B2Rs in CHO-K1 cells. Coimmunoprecipitation suggested a close interaction between B2R and $P2Y_2R$.

Materials and Methods

Reverse transcriptase-PCR of $P2Y_2R$ and B2R

Total RNA was isolated from cultured CHO-K1 cells with Sepasol RNA-I (Nacalai Tesque, Kyoto, Japan) and then treated with DNase I (Invitrogen) to digest genomic DNA. First-strand complementary DNA (cDNA) was synthesized with PrimeScript Reverse Transcriptase (RT) (Takara Bio Inc., Otsu, Japan) using oligo $(dT)_{12\text{-}18}$ as a primer. To obtain cDNAs of $P2Y_2R$ and B2R, PCR was performed by KOD-Plus-Neo, a high fidelity thermostable DNA polymerase (Toyobo Co. Ltd., Osaka, Japan), with 200 nM each of the following specific primers: $chP2Y_2$-5, GTG CAC AGG TGC CTG GGA GT; $chP2Y_2$-3, CAG TGG CCG GGT GAT CTT GT (designed using the registered partial sequence of Chinese hamster $P2Y_2R$ receptor, GenBank accession number GI:20450942); mB2-597-616, ACC ATG TCC ATG GGC CGG AT; mB2-1197-1216c, CCC ATG GAG TTC TCC ATC TG (designed using

the sequence common among mouse B2R [GI:31560615], rat B2R [GI:27465530] and human B2R [GI:168480073]).

Plasmids and constructs

Plasmids encoding human long variant B2R (hB2R) and rat short variant B2R fused with DsRed (rB2R-DsRed) were prepared as described previously (*15*). Plasmids encoding human $P2Y_2R$ were prepared by inserting $P2Y_2R$ cDNA between the EcoRI and BamHI sites of pIRES2-EGFP (Clontech). Plasmids encoding $P2Y_2R$-AcGFP fusion proteins were prepared by inserting $P2Y_2R$ cDNA (without a stop codon) between the EcoRI and BamHI sites of pAcGFP-N1 vector (Clontech). Rat B2R with a C-terminal HA epitope tag (YPYDVPDYA) and human $P2Y_2R$ with an N-terminal Myc epitope tag (EQKLISEEDL) (*16*) were prepared by PCR. HA epitope was positioned immediately after the B2R gene (without a stop codon). Myc epitope was positioned immediately before the first methionine of the $P2Y_2R$ gene. cDNA of each gene was subcloned into pIRES2-EGFP. The identity of the constructs was confirmed by DNA sequencing.

Cell culture

CHO-K1 cells were grown in alpha minimum essential medium (α-MEM) supplemented with 10% (v/v) fetal calf serum and kept in a humidified 5% CO_2/95% air atmosphere at 37°C. CHO-K1 cells were transiently transfected with plasmids using GeneJuice (Merck). Transfection efficiency was 15–25%. HEK293, HEK293T and 1321N1 cells were grown in Dulbecco's Modified Eagle's Medium with 5.5 mM glucose supplemented with 10% (v/v) foetal calf serum and kept in a humidified 5% CO_2/95% air atmosphere at 37°C. The cells were transiently transfected with plasmids using Lipofectamine 2000 (Invitrogen). Transfection efficiency was 90% or more. Cell membranes for immunoprecipitation and Western blotting were prepared from the cells 48 h after the transfection.

Ca^{2+} imaging

Cells cultured on glass-bottom dishes were loaded with the Ca^{2+} indicator Fura-2 and exposed to stimulants using the bath application method (*17*, *18*). Images were acquired and analysed using balanced salt solution (BSS, pH 7.3) consisting of 130 mM NaCl, 5.4 mM KCl, 20 mM HEPES, 5.5 mM glucose, 0.8 mM $MgSO_4$, and 1.8 mM $CaCl_2$ for the extracellular media (*15*, *17*).

Fluorescence resonance energy transfer image analysis

1321N1 cells cultured on a glass-bottom dish were transiently transfected with $P2Y_2R$-AcGFP and rB2R-DsRed. After 48 h cultivation, the media was replaced with BSS and the dish was placed on a fluorescence microscope at 35°C. Fluorescence images were obtained at excitation and emission wavelengths of 485 nm and 525–531 nm, respectively, for AcGFP; and at 560 and 607–623 nm, respectively, for DsRed. Fluorescence resonance energy transfer (FRET) images were obtained at excitation and emission wavelengths of 485 and 607–623 nm, respectively.

β-galactosidase complementation assay

The C-terminal of $P2Y_2R$ or B2R was fused to the H31R-substituted α donor peptide of a β-galactosidase reporter enzyme (*19*) ($P2Y_2R$-α or B2R-α), and the C-terminal of β-arrestin-2 (*20*) or the FYVE domain of endofin (*21*) was fused to the M15 acceptor deletion mutant of β-galactosidase (the ω peptide, β-arrestin-ω or FYVE-ω). Plasmid encoding fusion proteins were generated by sub-cloning PCR products into pAlpha-N1 or pOmega-N1 vectors, which were constructed from pAcGFP-N1 vector (Clontech) by substitution of α or ω peptide for AcGFP using AgeI and NotI restriction sites. β-arrestin-2 was generated by RT-PCR from a human liver cDNA library and cloned into pOmega-N1 using XhoI and KpnI restriction sites. The FYVE domain of endofin was generated by RT-PCR from a mouse brain cDNA library and cloned into pOmega-N1 using KpnI and BamHI restriction sites.

HEK293T cells were cultured in a six-well cell culture plate for 24 h. Cells in a well were transfected with a mixture of 0.2 μg of each plasmid DNA coding GPRC-α and the ω-fused target protein in 250 μl Opti-MEM, and 2.5 μL Lipofectamine 2000 in 250 μl Opti-MEM. After 24 h, transfected cells were washed once with phosphate-buffered saline (PBS) (137 mM NaCl, 2.7 mM KCl, 1.5 mM KH_2PO_4 and 8.1 mM Na_2HPO_4) and harvested by digestion with 0.4 ml of 0.05 % trypsin/ethylenediaminetetraacetic acid for 30 s at room temperature. Digestion was stopped by adding 0.5 ml of the culture media. The harvested cells were spun down (700 g, 5 min) and washed with 3 ml PBS by spinning down. The cells were then suspended in 2 ml Hank's balanced salt solution with Mg^{2+} and Ca^{2+} (HBSS) and incubated in white tissue culture 96-well plate (Corning 3917) (90 μl/well) at 37°C for 180 min. After stimulation of the cells with 10 μl of 10× concentrated BK for 1 h at 37°C, the supernatant (50 μl) was discarded and 50 μl of Gal Screen (B, Applied Biosystems) was added, followed by incubation at room temperature. Luminescence of the wells was read after about 40 min. For apyrase treatment, the enzyme was added after 30 min and incubated for 3.5 h at 37°C.

Immunoprecipitation and Western blot analysis

HEK293 cells were transfected using Lipofectamine 2000 with plasmids for expressing rat B2R with a C-terminal HA epitope tag (YPYDVPDYA) and human $P2Y_2R$ with an N-terminal Myc epitope tag (EQKLISEEDL), as described above. Transfected cells (approximately 5×10^6 cells) were collected and washed twice with PBS. Cells were then disrupted by sonication using Handy Sonic UR-20P (Tomy Seiko, Tokyo, Japan) in hypotonic lysis buffer (50 mM Tris-acetate, pH 7.4) containing protease inhibitors (Protease Inhibitor Cocktail for use with mammalian cell and tissue extracts; Nacalai Tesque, Kyoto, Japan). After centrifugation at 17,400 g for 30 min, the cell membranes were solubilized by incubation with 300 μl of Tx buffer (50 mM Tris-acetate, pH 7.4, 300 mM NaCl, and 1% Triton X-100) containing protease inhibitors and incubated for 1 h with end-over-end mixing at 4°C. In some instances, the extracted cell membrane lysate was treated with 0.7 units N-glycosidase F for 1 h at 37°C. The supernatant containing the solubilized membranes was precleared by incubation for 30 min at 4°C with 30 μl of 50% Ab-Capcher (ProteNova, Naruto, Tokushima, Japan) in Tx buffer with end-over-end mixing, followed by centrifugation at 17,400 g for 1 min. The supernatant was collected, mixed with 1 μg of anti-HA 3F10 or anti-Myc 9E10 antibody (Roche Diagnostics, Basel, Switzerland), and incubated for 2 h at 4°C with end-over-end mixing, followed by incubation for 2 h with 30 μl of 50% Ab-Capcher. The immune complex was washed twice with 300 μl of Tx buffer, after which bound proteins were eluted with 20 μl SDS-PAGE sample buffer. The solubilized proteins were separated by SDS-PAGE and then electrophoretically transferred to an Immobilon PVDF membrane (Millipore). After blocking with 5% skim milk in PBS-T, the receptors were detected using anti-HA, anti-Myc or anti-$P2Y_2R$ (APR-010; Alomone Labs Ltd., Jerusalem, Israel) antibody, followed by horseradish peroxidase conjugated anti-rat IgG antibody (Invitrogen), anti-mouse IgG antibody (115-035-062; Jackson Immunoresearch Lab.) or anti-rabbit IgG antibody (Zymed). Immunoreactive proteins were detected with Immobilon Western Chemiluminescent HRP Substrate (Millipore).

Other materials

Gangliosides were kindly provided by Dr. Yoshio Hirabayashi (Laboratory for Molecular Membrane Neuroscience, RIKEN Brain Science Institute, Wako, Saitama, Japan). Chondroitin sulfates were purchased from Seikagaku Co., Tokyo, Japan. BK was purchased from Peptide Institute Co., Osaka, Japan. ATP was purchased from Wako Pure Chemical Industries, Ltd., Osaka, Japan. UTP and apyrase (from potato) were purchased from Nacalai Tesque, Kyoto, Japan.

Statistical analysis

Results are presented as means ± SEM. The statistical significance between groups was assessed by two-tailed unpaired Student *t*-tests.

Results

Response to chemical mediators and expression of B2R and $P2Y_2R$ mRNA in CHO-K1 cells

CHO-K1 cells responded equivalently to 10 μM ATP and 10 μM UTP by transiently increasing intracellular Ca^{2+} concentrations (Fig. 1, control), indicating that endogenous $P2Y_2R$ is expressed (*14*). Using RT-PCR,

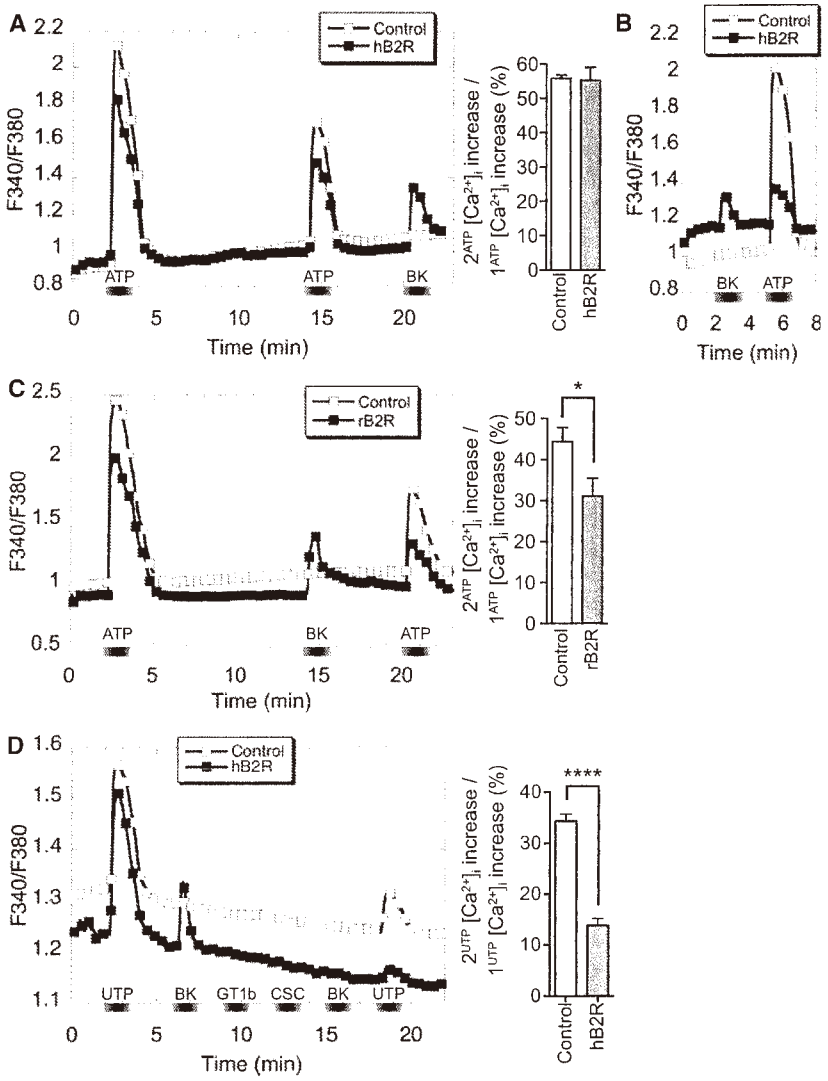

Fig. 1 P2Y$_2$R desensitization via BK stimulation and B2R internalization. CHO-K1 cells expressing human B2R (hB2R) (**A**, **B**, **D**) or DsRed-fused rat B2R (rB2R-DsRed) (**C**) were exposed to 10 μM ATP, 10 μM UTP, 10 nM BK, 10 ng/ml GT1b and 1 μg/ml CSC as indicated, and intracellular Ca^{2+} concentrations were monitored by fluorescence microscopy with Fura-2 as an indicator. Relative Ca^{2+} levels are expressed as a ratio of fluorescence at an excitation wavelength of 340 nm to that at an excitation wavelength of 380 nm. Plots of the averaged ratios derived from B2R- and non-B2R-expressing cells (control) (B and left panels of A, C, D) are shown. Bar graphs (A, C, D) show the percentage of peak increases in $[Ca^{2+}]_i$ induced by the second ATP or UTP treatment over those induced by the first ATP or UTP treatment. $^{****}P<0.0001$; $^{*}P<0.05$. The numbers of B2R-expressing and control cells examined were 11 and 22 (A), 20 and 31 (B), 15 and 28 (C) and 19 and 19 (D), respectively.

we confirmed P2Y$_2$R mRNA expression in CHO-K1 cells and determined its partial sequence (959 residues from 77 bases upstream of the start codon). This sequence included the registered partial sequence of CHO P2Y$_2$R (GenBank, AF314034). In contrast, exposing CHO-K1 cells to 10 nM (Fig. 1, control) to 1 μM BK (data not shown) failed to affect intracellular Ca^{2+} concentrations. Moreover, these cells expressed undetectable levels of B2R mRNA (data not shown).

Effects of B2R expression and BK stimulation on P2Y$_2$R activity

In these experiments, we used human (hB2R) and rat (rB2R) B2Rs. The latter was fused with DsRed (rB2R-DsRed) to confirm proper membrane expression. The fusion protein responded to BK and became internalized upon repeated BK treatment, as did the original unfused B2R (*15*). CHO-K1 cells that transiently expressed B2R responded to 10 nM BK by increasing intracellular Ca^{2+} levels (Fig. 1). BK stimulation significantly reduced the P2Y$_2$R response to ATP (Fig. 1B, C), while expression of B2R itself did not affect this response (Fig. 1A).

Desensitization of B2R cross-desensitized P2Y$_2$R

We recently showed that treatment with Neu 5Acα3Galβ3GalNAcβ4(Neu5Acα8Neu5Acα3) Galβ4 GlcCer (GT1b) ganglioside and chondroitin sulfate C

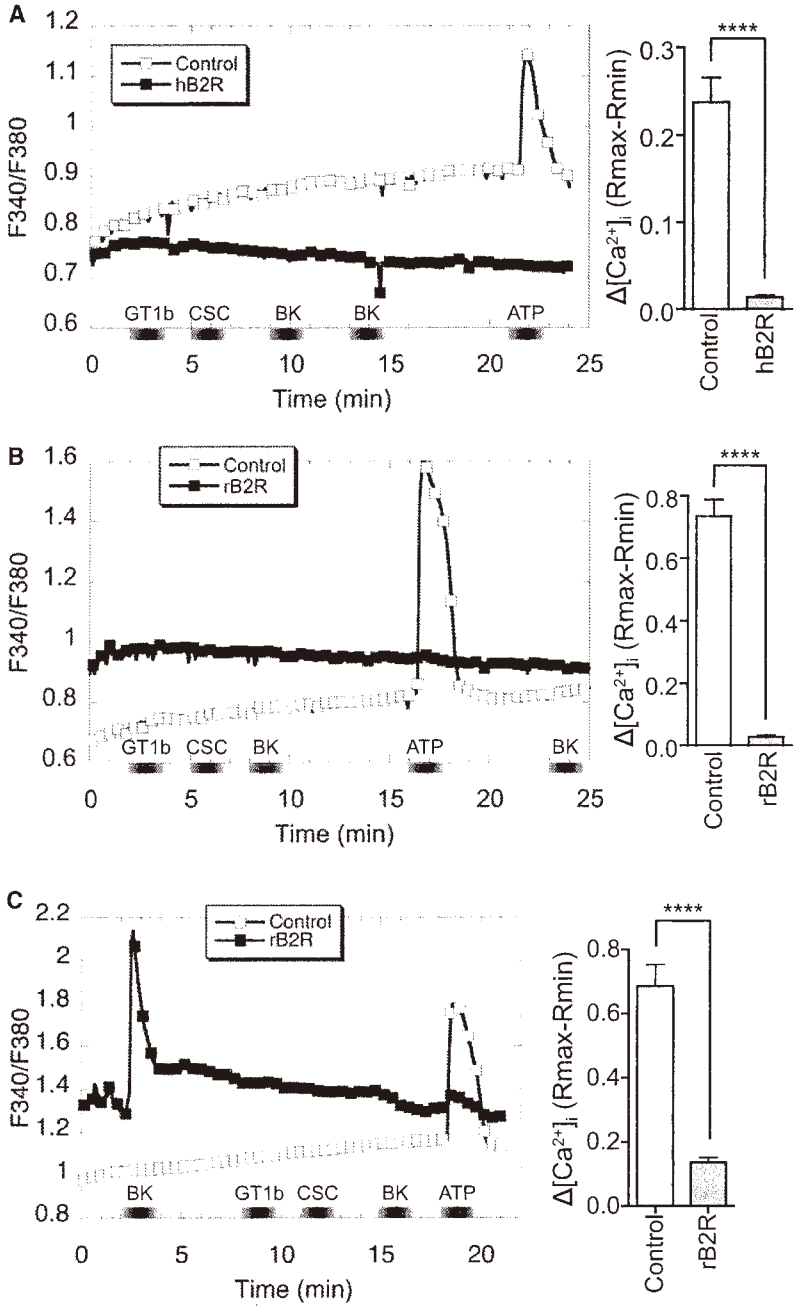

Fig. 2 $P2Y_2R$ desensitization via B2R internalization. Human B2R (hB2R) (**A**) or rB2R-DsRed (**B**, **C**) was expressed in CHO-K1 cells that were exposed to 10 nM BK, 10 ng/ml GT1b, 1 μg/ml CSC and 1 μM ATP, as indicated. Plots of the averaged ratios of B2R-expressing cells (A, B), BK-responding cells (C), and control cells are shown on the left. Bar graphs (A–C) show peak increases in $[Ca^{2+}]_i$ induced by 10 μM ATP. $^{****}P<0.0001$. The numbers of B2R-expressing and control cells examined were 7 and 10 (A), and 8 and 15 (B), respectively; and those of BK-responding and control cells were 15 and 27 (C), respectively.

(CSC) desensitizes and internalizes B2Rs expressed in CHO-K1 cells without inducing Ca^{2+} release (*15*). GT1b-CSC treatment reduced the response of B2R-expressing cells to BK and to UTP and ATP (Figs 1D and 2). GT1b-CSC treatment also desensitized BK-responding/B2R-expressing cells to BK and to ATP and UTP (Figs 1D and 2C), but failed to desensitize cells that did not express B2R to ATP and UTP (Figs 1 and 2; control). Thus, $P2Y_2R$ and B2R act together in cells that coexpress $P2Y_2R$ and B2R.

FRET analysis of B2R–$P2Y_2R$ interactions

FRET analysis was used to confirm the close association between B2Rs and $P2Y_2Rs$, using AcGFP-fused

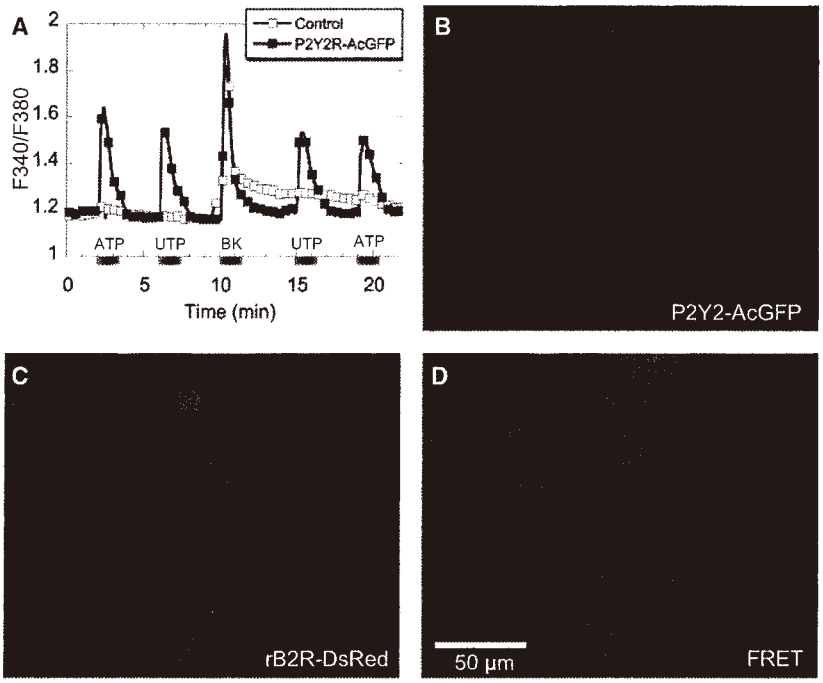

Fig. 3 FRET from P2Y$_2$R-AcGFP to B2R-DsRed in HEK293 cells. (**A**) Reactivity of P2Y$_2$R-AcGFP fusion protein to ATP and UTP. AcGFP-fused human P2Y$_2$R (P2Y$_2$R-AcGFP) was expressed in 1321N1 cells that were exposed to 10 μM ATP, 10 μM UTP and 1 μM BK, as indicated. Plots of the averaged ratios of P2Y$_2$R-AcGFP-expressing cells (n = 22) and control cells (n = 4) are shown. (**B–D**) Cells coexpressing P2Y$_2$R-AcGFP and rB2R-DsRed. Fluorescence images were obtained at excitation and emission wavelengths of 485 and 525–531 nm, respectively, for AcGFP (B), and at 560 and 607–623 nm, respectively, for DsRed (C). FRET images were obtained at excitation and emission wavelengths of 485 and 607–623 nm, respectively (D). Scale bar, 50 μm.

P2Y$_2$R. Human astrocytoma 1321N1 cells are unresponsive to extracellular nucleotides (*22*) and do not express P2Y receptors. We transiently expressed P2Y$_2$R-AcGFP fusion protein in 1321N1 cells and confirmed that they do respond to ATP and UTP (Fig. 3A). In contrast to native P2Y$_2$R, P2Y$_2$R-AcGFP was minimally desensitized and internalized, even after repeated treatment with ATP and UTP (Fig. 3A). FRET was used to investigate the interaction between P2Y$_2$R-AcGFP and B2R-DsRed in live HEK293 cells that transiently coexpressed these proteins. FRET was detected in the cells and on the cell surfaces, indicating a close relationship of B2R and P2Y$_2$R (Fig. 3).

Activation and internalization of P2Y$_2$R by BK and B2R by ATP

We examined whether BK stimulates P2Y$_2$R activation and internalization using a β-galactosidase complementation assay (*21*). The GPCR fused to the H31R substituted α peptide of β-galactosidase (GPCR-α) was coexpressed with the target protein, β-arrestin or the FYVE domain of endofin fused to the M15 deletion mutant of β-galactosidase (the ω peptide, protein-ω), and stimulated with BK. As shown in Fig. 4A, BK of ≥20 nM induced significant β-galactosidase complementation with β-arrestin-ω recruitment to P2Y$_2$R-α, indicating activation of P2Y$_2$R by BK. BK of ≥10 nM induced significant β-galactosidase complementation with P2Y$_2$R-α sorting to endosomes expressing FYVE-ω, indicating internalization of P2Y$_2$R by BK. Overexpression of B2R increased both reactions (data not shown). Likewise, ATP, which is released into culture media by a cultivation-stimulated autocrine mechanism (*23*), was shown to induce β-arrestin recruitment to B2R and B2R sorting to endosomes by apyrase treatment of the cells (Fig. 4B). Thus, B2R and P2Y$_2$R were shown to be coactivated, codesensitized and cointernalized by BK as well as ATP.

Association of B2R and P2Y$_2$R in coexpressed HEK293 cells

The above results provide a possible close association of B2R and P2Y$_2$R likely forming a heteromeric complex. To test this possibility, we examined coimmunoprecipitation of B2R-HA and Myc-P2Y$_2$R using solubilized membranes from B2R-HA/Myc-P2Y$_2$R-cotransfected HEK293 cells. B2R-HA and Myc-P2Y$_2$R showed the same behavior in SDS-PAGE or reactivity to the ligand, as their native GPCR molecules. In Western blots using anti-HA of B2R-HA expressing cell membranes, HA positive bands were detected at the positions of the reported molecular weight (B2R, 40–80 kDa; (*24*, *25*)), in addition to a band at 36 kDa (Fig. 5A). The 36 kDa band is possibly an underglycosylated form of B2R since N-glycosidase F treatment shifted most HA-positive bands to this position (Fig. 5D). In

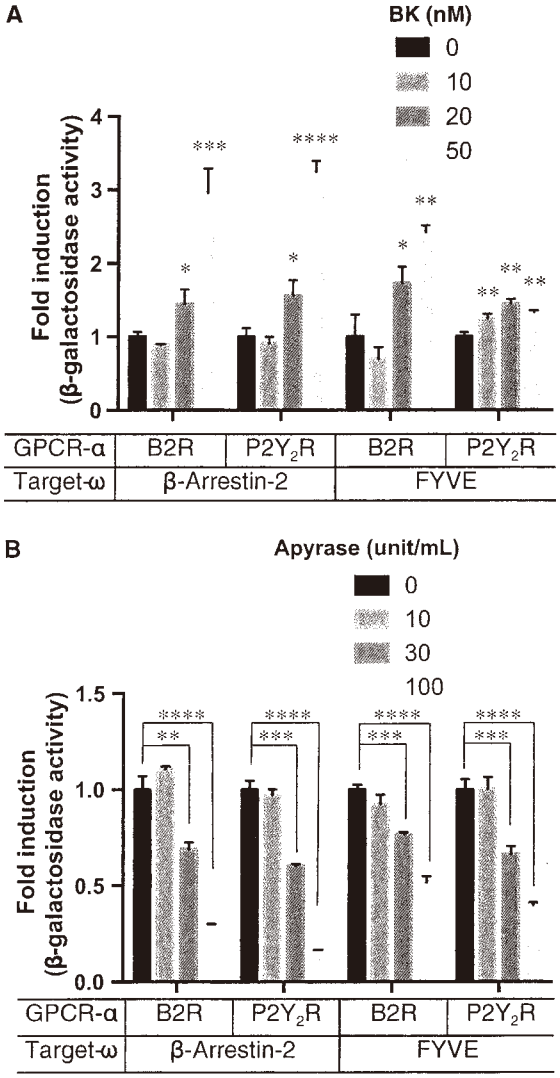

Fig. 4 Coactivation and internalization of B2R and $P2Y_2R$. The GPCR fused to the H31R substituted α donor peptide of β-galactosidase reporter enzyme (B2R-α or $P2Y_2R$-α) was co-expressed with the target protein, β-arrestin or FYVE domain of endofin fused to the M15 acceptor deletion mutant of β-galactosidase (the ω peptide, β-arrestin-ω or FYVE-ω), and stimulated with BK (**A**) or autocrine ATP was degraded by apyrase (**B**). Recruitment of β-arrestin to the GPCR-α or endosome sorting of the GPCR-α was detected by β-galactosidase activity produced with complementation of H31R-substituted α donor peptide and the M15 acceptor deletion mutant of β-galactosidase, the ω peptide. The activity is expressed as a multiple of the control activity measured without the reagents. $^{****}P<0.0001$; $^{***}P<0.001$; $^{**}P<0.01$; $^{*}P<0.05$.

Western blots using anti-Myc of Myc-$P2Y_2R$ expressing cell membranes, Myc positive bands were detected at 42 kDa (Fig. 5B–D) that was shifted to 36 kDa by N-glycosidase F treatment (Fig. 5D).

As shown in Fig. 5A, B2R-HA was coprecipitated with Myc-$P2Y_2R$ by anti-Myc antibody from cells coexpressing B2R-HA and Myc-$P2Y_2R$. The major band of coprecipitated B2R-HA at 36 kDa is likely to be the underglycosylated form. Conversely, Myc-$P2Y_2R$ was coprecipitated with B2R-HA by anti-HA antibody from cells coexpressing B2R-HA and Myc-$P2Y_2R$ (Fig. 5B), and the coprecipitated Myc-$P2Y_2R$ at 42 kDa is likely to be the glycosylated form. Such coimmunoprecipitation did not occur when the two membrane fractions were mixed after the individual expression of each receptor (data not shown). Furthermore, as HEK293 cells express $P2Y_2R$ (*26*) endogenously, anti-HA antibody precipitated endogenous $P2Y_2R$ with a molecular weight of 42 kDa, along with B2R-HA, from B2R-HA single-transfected cells (Fig. 5C). The anti-HA antibody did not immunoprecipitate Myc-$P2Y_2R$ or vice versa for B2R-HA from cell membrane extracts expressing only Myc-$P2Y_2R$. These findings demonstrated heterooligomer formation by B2R and $P2Y_2R$ when expressed simultaneously in HEK293 cells.

Discussion

This study shows a novel close association and functional coupling between two GPCRs (B2R and $P2Y_2R$) that mediate the effects of two humoral factors (BK and ATP). These GPCRs modulate vascular tone and induce inflammation and pain (*2*, *27*, *28*). BK stimulation and internalization of B2Rs desensitized and probably internalized $P2Y_2Rs$.

Several reports have shown crosstalk between BK and ATP signalling. Repetitive ATP stimulation causes Ca^{2+} release from intracellular stores by PLC activation and desensitizes B2R in cultured endothelial cells (*10*). The mediating GPCR is $P2Y_2R$ or $P2Y_{11}R$. ATP and UTP desensitize B2R, probably through $P2Y_2R$, in neuronal cells (*11*, *12*), and BK also releases ATP (*29–32*) in smooth muscle cells and astrocytes as an autacoid. Here, we found crosstalk between B2R and $P2Y_2R$, in which BK stimulation is accompanied by codesensitization of B2R and $P2Y_2R$ in CHO-K1 cells coexpressing $P2Y_2R$ and B2R. B2R and $P2Y_2R$ are expressed in most cultured cells and in cells in neural and non-neural tissues, such as Purkinje cells, cerebellar nuclei and hippocampal neurons (*33*, *34*) and airway epithelia (*35*, *36*).

Receptor interaction such as heterodimer formation is often accompanied by receptor co-internalization (*37–39*). The close association between B2R and $P2Y_2R$ was shown by FRET from $P2Y_2R$-AcGFP to B2R-DsRed (Fig. 3). However, since $P2Y_2R$-AcGFP is resistant to desensitization, we were not able to use this fusion protein as a reporter of internalization. The two GPCRs may associate at the biosynthetic sites because FRET was observed in cells, as well as on the cell surface. Instead of FRET analysis, we evaluated arrestin recruitment and endosome sorting of the receptors using a β-galactosidase complementation assay. BK promoted arrestin recruitment and endosome sorting of $P2Y_2R$ in HEK293T cells, which endogenously express B2R. Likewise, ATP promoted arrestin recruitment and endosome sorting of B2R in HEK293T cells, which endogenously express $P2Y_2R$.

We also showed a close association between B2R and $P2Y_2R$ by coimmunoprecipitation in B2R/$P2Y_2R$-cotransfected HEK293 cells (Fig. 5). The major band of B2R-HA that precipitated with

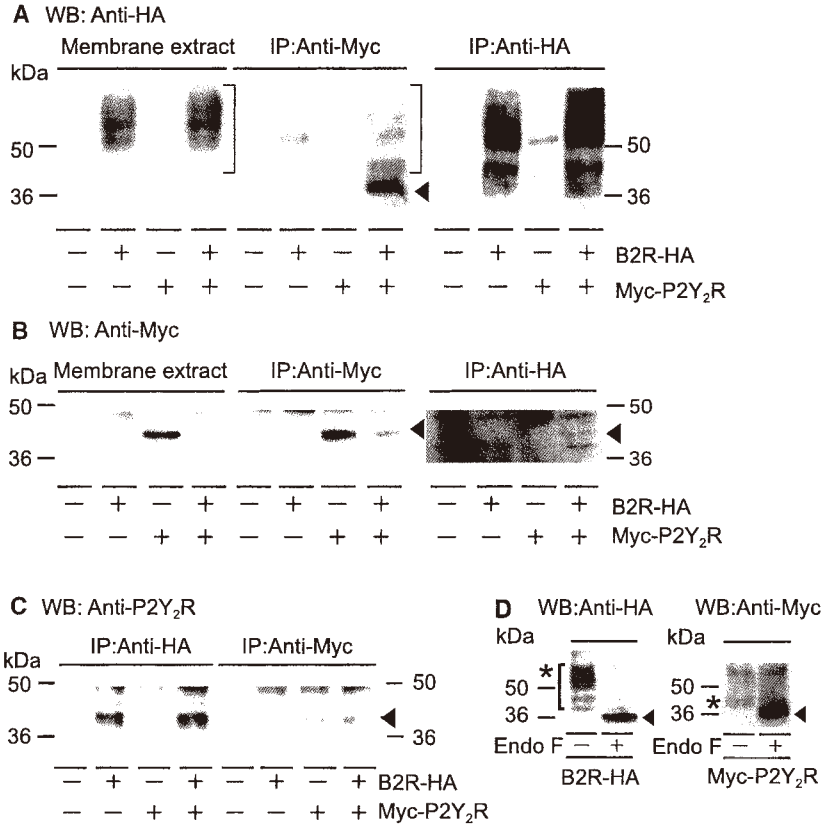

Fig. 5 Association of B2R and P2Y$_2$R in B2R/P2Y$_2$R-transfected HEK293 cells. (**A**, **B**) Coimmunoprecipitation of B2R-HA and Myc-P2Y$_2$R. Cell lysates were immunoprecipitated with anti-Myc (center panels) or anti-HA (right panels), and precipitates were analysed by Western blotting with anti-HA and anti-Myc antibodies in A and B, respectively. Anti-HA antibody precipitated B2R-HA (panel A, lanes 10 and 12) and Myc-P2Y$_2$R coimmunoprecipitated with B2R-HA (panel B, lane 12, arrowhead). Anti-Myc antibody precipitated Myc-P2Y$_2$R (panel B, lanes 7 and 8, arrowhead), and B2R-HA coimmunoprecipitated with Myc-P2Y$_2$R (panel A, lane 8). The major band of coprecipitated B2R-HA was 36 kDa (arrowhead) and most of the highly glycosylated B2R-HA (see panel A, lanes 10 and 12) was not associated with Myc-P2Y$_2$R (panel A, lane 8). (**C**) Coimmunoprecipitation of B2R-HA and P2Y$_2$R. Cell lysates were immunoprecipitated with anti-HA (left panel) or anti-Myc (right panel), and precipitates were analysed by Western blotting with anti-P2Y$_2$R antibodies. Anti-HA antibody precipitated endogenous P2Y$_2$R (lane 2) and endogenous and Myc-tagged P2Y$_2$R (lane 4), and anti-Myc antibody immunoprecipitated Myc-P2Y$_2$R (lanes 7 and 8), as indicated by arrowheads. (**D**) Western blot analysis of cell membranes expressing B2R-HA (Left) and Myc-P2Y$_2$R (Right). Cell lysates that had been treated by N-glycosidase F (Endo F+) for 3 h at 37°C were subjected to Western blotting. B2R-HA and Myc-P2Y$_2$R were detected by anti-HA and anti-Myc antibodies, respectively. The control (Endo F-; no treatment with N-glycosidase F) was also subjected to Western blotting. The apparent molecular weights of the glycosylated (*) and deglycosylated (arrowheads) B2R-HA are 40-100 and 36 kDa, respectively. The apparent molecular weights of the glycosylated and deglycosylated Myc-P2Y$_2$R are 42 kDa (*) and 36 kDa (arrowheads), respectively. Membrane extract, solubilized membrane extract; IP, immunoprecipitate; sup, supernatant following immunoprecipitation. Approximate molecular weights are shown in kDa. Data are representative of 2–4 independent experiments.

Myc-P2Y$_2$R had a molecular weight of 36 kDa, the same as that of non-glycosylated B2R, although most B2R is heavily glycosylated in HEK293 cells and other cells, including CHO-K1 cells (*25*). Coimmunoprecipitation requires high affinity binding between two molecules. In this study, the non-glycosylated form and several glycosylated forms of B2R were coprecipitated with P2Y$_2$R. This suggests that less glycosylated forms of B2R have higher binding affinity with P2Y$_2$R and are preferably coprecipitated. In rat B2R, there are at least 3 N-glycosylation sites at N3, N14, and N182, and the first two of these sites are located in the first extracellular domain. AbdAlla *et al.* (*40*) and Michineau *et al.* (*25*) found that B2R homodimerization requires the first extracellular domain, which possesses two N-glycosylation sites, and N-glycosylation, respectively. Thus, the preference for homodimer and heterooligomer formation is probably related to the degree of glycosylation of B2R, and bulky glycans at these sites in B2R may regulate the interaction between B2R and P2Y$_2$R.

P2Y$_2$Rs show crosstalk with β-adrenergic receptors, adenosine A$_1$ receptors, and CXC chemokine receptors (*41–43*), and the responses of these receptors to ligand stimulation are modulated by each other. B2Rs form homodimers and heterodimers with angiotensin II receptor AT1a (*44*, *45*), and show crosstalk with β-adrenergic receptors (*46*) and with B1 kinin receptor (*47*). These GPCRs may compete with each other for coupling in a cell.

Repeated treatment of non-neuronal cells with gangliosides and chondroitin sulphate desensitizes B2R

and $P2Y_2R$ without activating an authentic PLC-activating pathway. Since receptor desensitization protects against both acute and chronic receptor overstimulation (*48*), gangliosides and chondroitin sulphate may prove to be effective anti-inflammatory and analgesic agents.

Acknowledgements

We thank Dr. Yoshio Hirabayashi (Laboratory for Molecular Membrane Neuroscience, RIKEN Brain Science Institute, Wako, Saitama, Japan) for the generous gift of gangliosides.

Funding

This study was supported by the Strategic Study Base Formation Support Project for Private Universities, Japan.

Conflict of Interest

None declared.

References

1. Sawynok, J. (2003) Topical and peripherally acting analgesics. *Pharmacol. Rev.* **55**, 1–20
2. Leeb-Lundberg, L.M., Marceau, F., Muller-Esterl, W., Pettibone, D.J., and Zuraw, B.L. (2005) International union of pharmacology. XLV. Classification of the kinin receptor family: from molecular mechanisms to pathophysiological consequences. *Pharmacol. Rev.* **57**, 27–77
3. Koshiba, M., Apasov, S., Sverdlov, V., Chen, P., Erb, L., Turner, J.T., Weisman, G.A., and Sitkovsky, M.V. (1997) Transient up-regulation of $P2Y_2$ nucleotide receptor mRNA expression is an immediate early gene response in activated thymocytes. *Proc. Natl Acad. Sci. USA.* **94**, 831–836
4. Peterson, T.S., Camden, J.M., Wang, Y., Seye, C.I., Wood, W.G., Sun, G.Y., Erb, L., Petris, M.J., and Weisman, G.A. (2010) $P2Y_2$ nucleotide receptor-mediated responses in brain cells. *Mol. Neurobiol.* **41**, 356–366
5. Seye, C.I., Gadeau, A.P., Daret, D., Dupuch, F., Alzieu, P., Capron, L., and Desgranges, C. (1997) Overexpression of $P2Y_2$ purinoceptor in intimal lesions of the rat aorta. *Atertio. Thromb. Vasc. Biol.* **17**, 3602–3610
6. Turner, J.T., Park, M., Camden, J.M., and Weisman, G.A. (1998) Salivary gland nucleotide receptors. Changes in expression and activity related to development and tissue damage. *Ann. N. Y. Acad. Sci* **842**, 70–75
7. Cressman, V.L., Lazarowski, E., Homolya, L., Boucher, R.C., Koller, B.H., and Grubb, B.R. (1999) Effect of loss of $P2Y_2$ receptor gene expression on nucleotide regulation of murine epithelial Cl^- transport. *J. Biol. Chem.* **274**, 26461–26468
8. Homolya, L., Steinberg, T.H., and Boucher, R.C. (2000) Cell to cell communication in response to mechanical stress via bilateral release of ATP and UTP in polarized epithelia. *J. Cell Biol.* **150**, 1349–1360
9. Koizumi, S., Fujishita, K., Inoue, K., Shigemoto-Mogami, Y., and Tsuda, M. (2004) Ca^{2+} waves in keratinocytes are transmitted to sensory neurons: the involvement of extracellular ATP and $P2Y_2$ receptor activation. *Biochem. J.* **380**, 329–338
10. Luckhoff, A., Zeh, R., and Busse, R. (1988) Desensitization of the bradykinin-induced rise in intracellular free calcium in cultured endothelial cells. *Pfluegers Arch./Eur. J. Physiol.* **412**, 654–658
11. Reetz, G. and Reiser, G. (1994) Cross-talk of the receptors for bradykinin, serotonin, and ATP shown by single cell Ca^{2+} responses indicating different modes of Ca^{2+} activation in a neuroblastoma x glioma hybrid cell line. *J. Neurochem.* **62**, 890–897
12. Czubayko, U. and Reiser, G. (1996) Desensitization of P_{2U} receptor in neuronal cell line. Different control by the agonists ATP and UTP, as demonstrated by single-cell Ca^{2+} responses. *Biochem. J* **320**, 215–219
13. Lopez-Valdes, H.E., Beltran-Parrazal, L., Brennan, K.C., and Charles, A.C. (2010) Bradykinin increases resensitization of purinergic receptor signaling in glioma cells. *Cancer Cell Int.* **10**, 35
14. Iredale, P.A. and Hill, S.J. (1993) Increases in intracellular calcium via activation of an endogenous P2-purinoceptor in cultured CHO-K1 cells. *Br. J. Pharmacol.* **110**, 1305–1310
15. Shimazaki, A., Nakagawa, T., Mitoma, J., and Higashi, H. (2012) Gangliosides and chondroitin sulfate desensitize and internalize B2 bradykinin receptors. *Biochem. Biophys. Res. Commun.* **420**, 193–198
16. Yoshioka, K., Saitoh, O., and Nakata, H. (2001) Heteromeric association creates a P2Y-like adenosine receptor. *Proc. Natl Acad. Sci. USA.* **98**, 7617–7622
17. Chen, N., Furuya, S., Doi, H., Hashimoto, Y., Kudo, Y., and Higashi, H. (2003) Ganglioside/calmodulin kinase II signal inducing cdc42-mediated neuronal actin reorganization. *Neuroscience.* **120**, 163–176
18. Higashi, H. and Chen, N.H. (2004) Ganglioside/protein kinase signals triggering cytoskeletal actin reorganization. *Glycoconj. J.* **20**, 49–58
19. Wehrman, T.S., Casipit, C.L., Gewertz, N.M., and Blau, H.M. (2005) Enzymatic detection of protein translocation. *Nat. Methods.* **2**, 521–527
20. von Degenfeld, G., Wehrman, T.S., Hammer, M.M., and Blau, H.M. (2007) A universal technology for monitoring G-protein-coupled receptor activation in vitro and noninvasively in live animals. *FASEB J.* **21**, 3819–3826
21. Hammer, M.M., Wehrman, T.S., and Blau, H.M. (2007) A novel enzyme complementation-based assay for monitoring G-protein-coupled receptor internalization. *FASEB J.* **21**, 3827–3834
22. Parr, C.E., Sullivan, D.M., Paradiso, A.M., Lazarowski, E.R., Burch, L.H., Olsen, J.C., Erb, L., Weisman, G.A., Boucher, R.C., and Turner, J.T. (1994) Cloning and expression of a human P_{2U} nucleotide receptor, a target for cystic fibrosis pharmacotherapy. *Proc. Natl Acad. Sci. USA.* **91**, 3275–3279
23. Lazarowski, E.R., Shea, D.A., Boucher, R.C., and Harden, T.K. (2003) Release of cellular UDP-glucose as a potential extracellular signaling molecule. *Mol. Pharmacol.* **63**, 1190–1197
24. AbdAlla, S., Godovac-Zimmermann, J., Braun, A., Roscher, A.A., Muller-Esterl, W., and Quitterer, U. (1996) Structure of the bradykinin B2 receptors' amino terminus. *Biochemistry.* **35**, 7514–7519
25. Michineau, S., Alhenc-Gelas, F., and Rajerison, R.M. (2006) Human bradykinin B2 receptor sialylation and N-glycosylation participate with disulfide bonding in surface receptor dimerization. *Biochemistry.* **45**, 2699–2707
26. Schachter, J.B., Sromek, S.M., Nicholas, R.A., and Harden, T.K. (1997) HEK293 human embryonic kidney cells endogenously express the $P2Y_1$ and $P2Y_2$ receptors. *Neuropharmacology.* **36**, 1181–1187

27. Guns, P.J., Korda, A., Crauwels, H.M., Van Assche, T., Robaye, B., Boeynaems, J.M., and Bult, H. (2005) Pharmacological characterization of nucleotide P2Y receptors on endothelial cells of the mouse aorta. *Br. J. Pharmacol.* **146**, 288–295
28. Guns, P.J., Van Assche, T., Fransen, P., Robaye, B., Boeynaems, J.M., and Bult, H. (2006) Endothelium-dependent relaxation evoked by ATP and UTP in the aorta of P2Y$_2$-deficient mice. *Br. J. Pharmacol.* **147**, 569–574
29. Tamesue, S., Sato, C., and Katsuragi, T. (1998) ATP release caused by bradykinin, substance P and histamine from intact and cultured smooth muscles of guinea-pig vas deferens. *Naunyn-Schmiedeberg's Arch. Pharmacol.* **357**, 240–244
30. Verderio, C. and Matteoli, M. (2001) ATP mediates calcium signaling between astrocytes and microglial cells: modulation by IFN-gamma. *J. Immunol.* **166**, 6383–6391
31. Zhao, Y., Migita, K., Sato, C., Usune, S., Iwamoto, T., and Katsuragi, T. (2007) Endoplasmic reticulum is a key organella in bradykinin-triggered ATP release from cultured smooth muscle cells. *J Pharmacol. Sci.* **105**, 57–65
32. Zhao, Y., Migita, K., Sun, J., and Katsuragi, T. (2010) MRP transporters as membrane machinery in the bradykinin-inducible export of ATP. *Naunyn Schmiedebergs Arch. Pharmacol.* **381**, 315–320
33. Chen, E.Y., Emerich, D.F., Bartus, R.T., and Kordower, J.H. (2000) B2 bradykinin receptor immunoreactivity in rat brain. *J. Comp. Neurol.* **427**, 1–18
34. Namba, K., Suzuki, T., and Nakata, H. (2010) Immunogold electron microscopic evidence of in situ formation of homo- and heteromeric purinergic adenosine A$_1$ and P2Y$_2$ receptors in rat brain. *BMC Res. Notes.* **3**, 323
35. Al-Bazzaz, F.J. (1986) Regulation of salt and water transport across airway mucosa. *Clin. Chest Med* **7**, 259–272
36. Homolya, L., Watt, W.C., Lazarowski, E.R., Koller, B.H., and Boucher, R.C. (1999) Nucleotide-regulated calcium signaling in lung fibroblasts and epithelial cells from normal and P2Y$_2$ receptor (-/-) mice. *J. Biol. Chem.* **274**, 26454–26460
37. Hillion, J., Canals, M., Torvinen, M., Casado, V., Scott, R., Terasmaa, A., Hansson, A., Watson, S., Olah, M.E., Mallol, J., Canela, E.I., Zoli, M., Agnati, L.F., Ibanez, C.F., Lluis, C., Franco, R., Ferre, S., and Fuxe, K. (2002) Coaggregation, cointernalization, and codesensitization of adenosine A2A receptors and dopamine D2 receptors. *J. Biol. Chem.* **277**, 18091–18097
38. Barki-Harrington, L., Luttrell, L.M., and Rockman, H.A. (2003) Dual inhibition of β-adrenergic and angiotensin II receptors by a single antagonist: a functional role for receptor-receptor interaction in vivo. *Circulation.* **108**, 1611–1618
39. Quitterer, U., Pohl, A., Langer, A., Koller, S., and Abdalla, S. (2011) A cleavable signal peptide enhances cell surface delivery and heterodimerization of Cerulean-tagged angiotensin II AT1 and bradykinin B2 receptor. *Biochem. Biophys. Res. Commun.* **409**, 544–549
40. AbdAlla, S., Zaki, E., Lother, H., and Quitterer, U. (1999) Involvement of the amino terminus of the B2 receptor in agonist-induced receptor dimerization. *J. Biol. Chem.* **274**, 26079–26084
41. Suh, B.C., Kim, J.S., Namgung, U., Han, S., and Kim, K.T. (2001) Selective inhibition of β$_2$-adrenergic receptor-mediated cAMP generation by activation of the P2Y$_2$ receptor in mouse pineal gland tumor cells. *J. Neurochem.* **77**, 1475–1485
42. Suzuki, T., Namba, K., Tsuga, H., and Nakata, H. (2006) Regulation of pharmacology by hetero-oligomerization between A$_1$ adenosine receptor and P2Y$_2$ receptor. *Biochem. Biophys. Res. Commun.* **351**, 559–565
43. Werry, T.D., Wilkinson, G.F., and Willars, G.B. (2003) Cross talk between P2Y$_2$ nucleotide receptors and CXC chemokine receptor 2 resulting in enhanced Ca^{2+} signaling involves enhancement of phospholipase C activity and is enabled by incremental Ca^{2+} release in human embryonic kidney cells. *J. Pharmacol. Exp. Ther.* **307**, 661–669
44. AbdAlla, S., Zaki, E., Lother, H., and Quitterer, U. (1999) Involvement of the amino terminus of the B(2) receptor in agonist-induced receptor dimerization. *J. Biol. Chem.* **274**, 26079–26084
45. AbdAlla, S., Lother, H., and Quitterer, U. (2000) AT1-receptor heterodimers show enhanced G-protein activation and altered receptor sequestration. *Nature* **407**, 94–98
46. Hanke, S., Nurnberg, B., Groll, D.H., and Liebmann, C. (2001) Cross talk between β-adrenergic and bradykinin B2 receptors results in cooperative regulation of cyclic AMP accumulation and mitogen-activated protein kinase activity. *Mol. Cell. Biol.* **21**, 8452–8460
47. Barki-Harrington, L., Bookout, A.L., Wang, G., Lamb, M.E., Leeb-Lundberg, L.M., and Daaka, Y. (2003) Requirement for direct cross-talk between B1 and B2 kinin receptors for the proliferation of androgen-insensitive prostate cancer PC3 cells. *Biochem. J.* **371**, 581–587
48. Ferguson, S.S. (2001) Evolving concepts in G protein-coupled receptor endocytosis: the role in receptor desensitization and signaling. *Pharmacol. Rev.* **53**, 1–24

OXFORD

Human Molecular Genetics, 2015, Vol. 24, No. 10 2796–2807

doi: 10.1093/hmg/ddv041
Advance Access Publication Date: 4 February 2015
Original Article

ORIGINAL ARTICLE

Ganglioside GM3 is essential for the structural integrity and function of cochlear hair cells

Misato Yoshikawa[1,6,†], Shinji Go[1,†], Shun-ichi Suzuki[1], Akemi Suzuki[2], Yukio Katori[3], Thierry Morlet[4], Steven M. Gottlieb[5], Michihiro Fujiwara[6], Katsunori Iwasaki[6], Kevin A. Strauss[7,8,9] and Jin-ichi Inokuchi[1,*]

[1]Division of Glycopathology, Institute of Molecular Biomembranes and Glycobiology, Tohoku Pharmaceutical University, 4-4-1 Aoba-ku, Sendai, Miyagi 981-8558, Japan, [2]Institute of Glycoscience, Tokai University, Kanagawa 259-1292, Japan, [3]Department of Otorhinolaryngology, Head and Neck Surgery, Tohoku University School of Medicine, 1-1 Seiryo-machi, Aoba-ku, SendaiCity, Miyagi 980-8574, Japan, [4]Department of Biomedical Research, Nemours, Wilmington, DE 19803, USA, [5]Division of Pediatric Neurology, Nemours Alfred I. DuPont Hospital for Children, Wilimington, DE 19803, USA, [6]Department of Neuropharmacology, Faculty of Pharmaceutical Sciences, Fukuoka University, Fukuoka 814-0180, Japan, [7]Clinic for Special Children, Strasburg, PA 17579, USA, [8]Biological Foundations of Behavior Program, Franklin and Marshall College, Lancaster, PA 17602, USA and [9]Lancaster General Hospital, Lancaster, PA 17602, USA

*To whom correspondence should be addressed at: Division of Glycopathology, Institute of Molecular Biomembranes and Glycobiology, Tohoku Pharmaceutical University, 4-4-1 Aoba-ku, Sendai, Miyagi 981-8558, Japan. Tel: +81 227270117; Fax: +81 227270076; Email: jin@tohoku-pharm.ac.jp

Abstract

GM3 synthase (ST3GAL5) is the first biosynthetic enzyme of a- and b-series gangliosides. Patients with GM3 synthase deficiency suffer severe neurological disability and deafness. Eight children (ages 4.1 ± 2.3 years) homozygous for *ST3GAL5* c.694C>T had no detectable GM3 (a-series) or GD3 (b-series) in plasma. Their auditory function was characterized by the absence of middle ear muscle reflexes, distortion product otoacoustic emissions and cochlear microphonics, as well as abnormal auditory brainstem responses and cortical auditory-evoked potentials. In *St3gal5*$^{-/-}$ mice, stereocilia of outer hair cells showed signs of degeneration as early as postnatal Day 3 (P3); thereafter, blebs devoid of actin or tubulin appeared at the region of vestigial kinocilia, suggesting impaired vesicular trafficking. Stereocilia of *St3gal5*$^{-/-}$ inner hair cells were fused by P17, and protein tyrosine phosphatase receptor Q, normally linked to myosin VI at the tapered base of stereocilia, was maldistributed along the cell membrane. *B4galnt1*$^{-/-}$ (GM2 synthase-deficient) mice expressing only GM3 and GD3 gangliosides had normal auditory structure and function. Thus, GM3-dependent membrane microdomains might be essential for the proper organization and maintenance of stereocilia in auditory hair cells.

Introduction

The organ of Corti is the auditory sensory organ of the cochlea, comprised of hair cells, supporting cells and the tectorial membrane. Inner hair cells (IHCs) are directly involved in sound transduction, whereas outer hair cells (OHCs) amplify the vibrations. Cochlear fluids in scala tympani cause to drive the deflection of the stereocilia on apical surfaces of IHCs and OHCs. Movement of stereocilia opens mechanotransduction

† These authors contributed equally.

Received: November 11, 2014. Revised: January 9, 2015. Accepted: February 2, 2015

potassium channels located at their tips and triggers hair cell depolarization (1,2).

Sialic acid-containing glycosphingolipids (GSLs), also called gangliosides, are enriched in the central nervous system and vital to normal brain development and function (3–5). Gangliosides localize to the outer leaflet of membranes to form microdomains called lipid rafts, which regulate membrane organization, transmembrane signaling and cell adhesion (6). GM3 synthase (a.k.a lactosylceramide sialyltransferase; ST3GAL5) is the first enzyme mediating biosynthesis of complex a- and b-series gangliosides. The second enzyme, B4GALNT1, transfers GalNAc to LacCer, GM3 or GD3 to form GA2, GM2 or GD2, respectively (Fig. 1A).

Various patterns of ganglioside deficiency have been modeled in genetically engineered mice (7). GD3 synthase null (*Siat8*$^{-/-}$) mice lack b-series gangliosides and have thermal hyperalgesia and mechanical allodynia (8). *B4galnt1*$^{-/-}$ mice, which express only two ganglioside species (GM3 and GD3), have reduced neural conduction velocity, ataxia and progressive axonal degeneration (9,10). Mice that express only GM3 (*B4galnt1*$^{-/-}$; *Siat8*$^{-/-}$ double knockout) have audiogenic seizures and sudden death (5,11). Mice lacking all a- and b-series ganglioside species, generated by double knockout of both *St3gal5* and *B4galnt1*, have a severe neurodegenerative disease characterized by reduced brain weight, aberrant axon-glial interactions, axonal degeneration and decreased survival (12).

In humans, homozygous or compound heterozygous loss-of-function mutations of *ST3GAL5* cause systemic a- and b-series ganglioside deficiency and are associated with infantile-onset epileptic encephalopathy, slow brain growth, stagnant psychomotor development, growth failure, blindness, dyspigmentation and deafness (13–17). *St3gal5*$^{-/-}$ mice produce no GM3 and also have severe hearing loss manifest at the time of normal hearing onset accompanied by degeneration of cochlear hair cells (18). Based on the auditory phenotype of human and murine GM3 synthase-deficiency, we hypothesized that GM3 plays an essential role in the postnatal maturation and function of the organ of Corti (18). Here, we study auditory function of human patients with homozygous *ST3GAL5* c.694C>T mutations and explore mechanisms of hearing loss using *St3gal5*$^{-/-}$ and *B4galnt1*$^{-/-}$ transgenic mice. Our results implicate a specific and indispensable role for GM3 ganglioside in development and viability of cochlear hair cells.

Results

GM3 synthase (ST3GAL5) deficiency in humans

Eight children (ages 4.1 ± 2.3 years, 4 female) from the Old Order Amish community of Pennsylvania were homozygous for *ST3GAL5* c.694C>T mutations. As reported by Simpson *et al.* (13), we confirmed that plasma of affected children had undetectable GM3 and its downstream biosynthetic derivatives as well as elevated lactosylceramide (LacCer; the proximate), globoside and paragloboside metabolites (data not shown). All eight children had the characteristic phenotype of systemic a- and b-series ganglioside deficiency, including slow postnatal head growth, intractable epileptic encephalopathy, severe psychomotor delay, visual impairment and hearing loss. Patient electroencephalograms (EEGs) revealed slow (2–4 Hz), high voltage (>300 μV), chaotic background activity. Sleep–wake variation, posterior rhythm, and photic driving response were consistently absent. Multifocal spike-slow wave discharges at a frequency of 1.5–3 Hz lasting 3–10 s were seen in all children, and electrographic seizures of similar frequency and duration were captured on 29% of EEG (Fig. 2). Magnetic resonance images from a subgroup of patients showed normal brain size and structure at birth, but evidence of hypomyelination and delayed brain maturation with advancing age (Fig. 2).

Auditory phenotype of humans with ST3GAL5 deficiency

Children homozygous for *ST3GAL5* c.694C>T had absent middle ear muscle reflexes (MEMRs) at all frequencies in most ears tested (Table 1). Thresholds were normal in only one ear of one patient, but responses were absent for two out of four frequencies in that subject's other ear. Another patient had elevated responses in one ear, but absent responses at all frequencies in the other ear. Distortion product otoacoustic emissions (DPOAEs) were absent bilaterally in all subjects, consistent with the observation that all *ST3GAL5* c.694C>T homozygotes who were tested failed the newborn hearing screen.

Auditory brainstem responses (ABRs) had abnormal thresholds in all ears and cochlear microphonics (CM) was consistently absent (Table 2). One child had no reproducible ABR waves. Wave I was observed in one subject, questionable in another, and absent in remaining patients. In six children, only Waves III and V could be clearly defined. Wave latencies were normal (80 dB) in the majority of patients. In most ears, comparison of condensation and rarefaction responses revealed waveform phase reversals (Fig. 2). Cortical auditory-evoked potentials (CAEPs) were detectable in all *ST3GAL5* c.694C>T homozygotes (Table 2), but their morphology was abnormal in 7 (88%) and P2/N2 latency was delayed in 6 (75%) patients.

Postnatal GSL expression in wild-type murine cochlea

Healthy mice begin to recognize sound by postnatal Day 12 (P12), designated the 'onset of hearing' (Fig. 1D). We investigated the expression of GSLs in wild-type murine cochlea during the postnatal maturation period from P1 to P17. As shown in Figure 1B, GM3 is the dominant cochlear GSL at P1. After P3, there is marked increase of GM3 as well as other GSLs, including glucosylceramide, complex gangliosides (GM1, GD1a, GD3, GD1b, GT1b) and sulfatides (SM3 and SM4) (Fig. 1B). The structures of each ganglioside species were examined by liquid chromatography mass spectrometry (LC-MS) (Fig. 1C).

It has been reported that ganglioside GM1 is present on the surface of the cochlea of the chinchilla using FITC-labeled cholera toxin B subunits (19). Table 3 summarizes the distinctive membrane distributions of GM1 and GM3 in wild-type organ of Corti. In OHC stereocilia, GM3 was high but GM1 was undetectable (Fig. 3C and D), and neither ganglioside species was expressed on the basolateral cell body (Fig. 3E). In IHC stereocilia, both GM1 and GM3 were expressed from the taper region to the top (Fig. 3C and D), but GM3 was absent from the IHC body. Expression of GM1 (but not GM3) was especially high on the surface of supporting Deiters cells and pillar cells expressed only GM1 (Fig. 3E).

GSL expression in cochlea of St3gal5 and B4galnt1 null mice

Cochlea of *St3gal5*$^{-/-}$ mice were devoid of a- and b-series gangliosides, replaced by compensatory o-series gangliosides (GM1b and GD1α) (Fig. 3A, left panel) and a high content of LacCer, the proximate substrate of GM3 synthase (Fig. 3A right panel). In *B4galnt1*$^{-/-}$ mice, the only other ganglioside detected was GD3 (Fig. 3A). Neutral glycolipid composition of *B4galnt1*$^{-/-}$ cochlea was similar to wild type.

Auditory system morphology and function in St3gal5 and B4galnt1 null mice

To better define the role of various ganglioside species in hearing, we compared auditory function between *St3gal5*$^{-/-}$ and

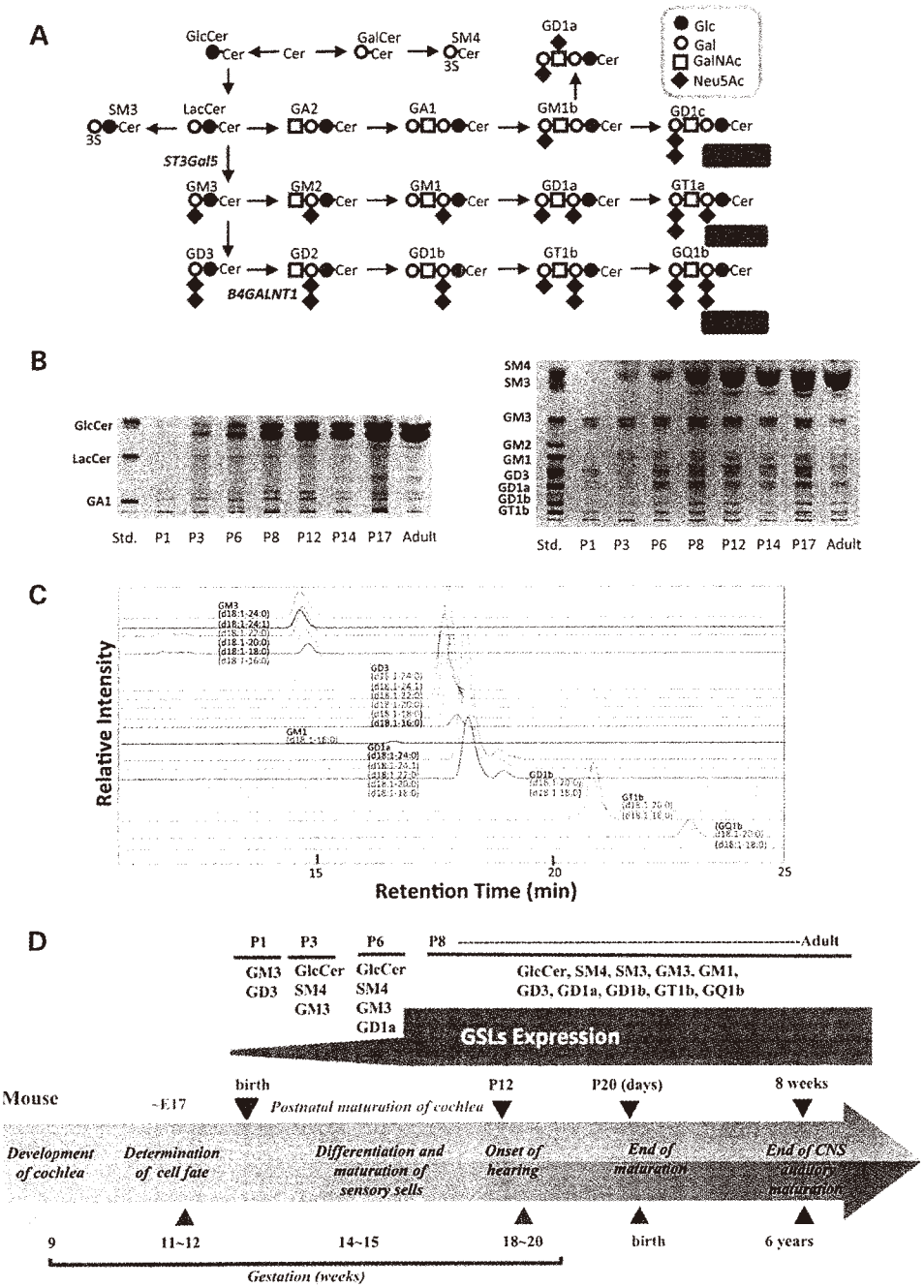

Figure 1. Marked increase of GSLs in cochlea during postnatal maturation period. (A) Schematic presentation of GSL biosynthesis. (B) High performance-thin-layer chromatograms (HPTLC analysis of gangliosides in cochlea of wild-type mice during the postnatal maturation period. Left panel is neutral glycolipids and right panel is acidic glycolipids. Cochlea were isolated and subjected for the purification of GSL analysis as described in Materials and Methods. Each purified fraction was spotted as 2 mg protein per lane. (C) Mass chromatograms of gangliosides prepared from cochlea of the wild mice at P17. The acidic fraction was analyzed by liquid chromatography-ion trap-mass spectrometry with a NH2 column under the conditions described in the Materials and Methods. The MS^1 chromatogram was monitored with theoretical values of $[M-H]^{-1}$ or $[M-2H]^{-2}$ for each ganglioside. The structures indicated in the figure is tentative, and based on information with only molecular related ions indicated with black and, in addition, carbohydrate-related fragment ions indicated with red, and requires the consideration of possibility of d20:1 sphingosine. (D) Summary of stage-specific expression of GSLs during postnatal maturation of cochlea based on the information of Figure 1B and C. Comparative development of the cochlea of both humans and mice are also shown.

B4galnt1$^{-/-}$ mice. At age 4 weeks, hearing ability of *B4galnt1*$^{-/-}$ mice was comparable to that of wild-type mice at all frequencies tested (Fig. 3B). In contrast, ABRs were absent in 4-week-old *St3gal5*$^{-/-}$ mice (Fig. 3B).

We used confocal laser microscopy with phalloidin staining to examine hair cell morphology in transgenic animals. In *B4galnt1*$^{-/-}$ mice, OHC and IHC morphology were normal at 4 weeks-old (Fig. 3C and D). In contrast, *St3gal5*$^{-/-}$ mice had

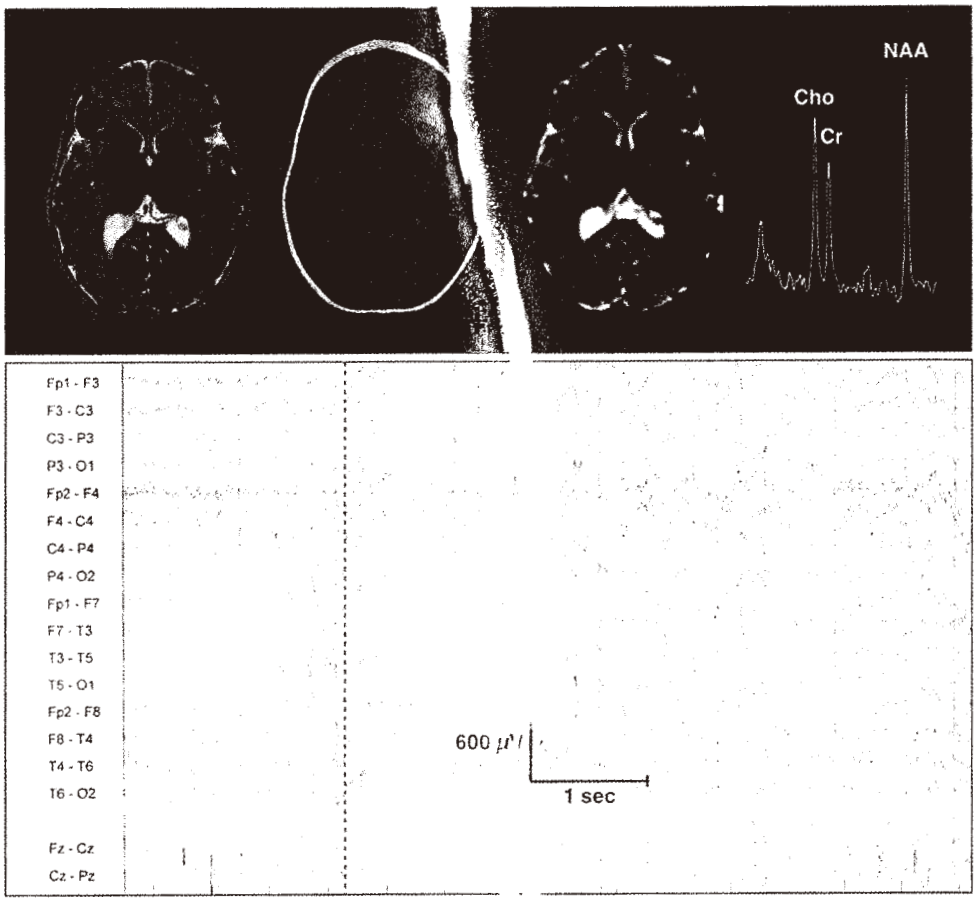

Figure 2. Upper panel from left to right, T2, fluid-attenuated inversion recovery, diffusi · eigh l, and ^{1}H-MR spectroscopy at 1.5 T show normal cortical and subcortical structure, but severe hypomyelination and increased water diffusion throughout the c· na rad a, as well as elevated choline (Cho) relative to creatine-phosphocreatine (Cr) and N-acetylaspartate ^{1}H signals (single voxel PRESS, TE 144/TR 1500). (Lower pan· EG of ·year-old child homozygous for ST3GAL5 c.694C>T shows a slow, chaotic background, absent posterior rhythm and no discernable change through a behavior· eep– :e cycle. Beginning at the dashed red line, there is a burst of generalized, frontal predominant, spike-slow wave discharges at 3 Hz in excess of 450 μV (note v ge se tivity).

Table 1. Middle ear muscle reflexes in children homozygous f· ST3GAL5 c.694C>T

Age (years)	Middle ear muscle reflexes							
	0.5 kHz		1 kHz		2 kHz		4 kHz	
	Left	Right	Left	Right	Left	Right	Left	Right
1.6	NR	90	NR	95	95	95	95	90
2.0	NR	NR	NR	NR	100	NR	100	NR
2.8	NR	NR	NR	NR	NR	100	NR	NR
3.1	NR	95	NR	NR	NR	NR	NR	NR
3.6	100	100	100	95	100	NR	NR	NR
4.5	85	NR	NR	NR	NR	NR	NR	NR
7.2	100	NR	NR	NR	100	NR	NR	NR
7.9	95	NR	NR	NR	NR	NR	NR	NR

NR, no response; 85, 90, 95 or 100 dB hearing level.

structural derangements of both OHCs and IHCs that progressed over time (Figs 4 and 5). At P1, hair bundles of *St3gal5*$^{-/-}$ mice resembled those of wild-type mice, but by P3 abnormal OHC hair bundle morphology was evident in most regions of the basal cochlea (Fig. 4A). By P8, scanning electron microscopy (SEM) reve: ed blebs along both apical and basal coils of vestigial kinocilia (Fig. 4B, left panel), but these disappeared by P17 (Fig. 4B, righ panel). As depicted in Figure 4C, OHC blebs in P8 *St3gal5*$^{-/-}$ m e did not stain with anti-acetylated tubulin, suggesting they di not derive from tubulin-based kinocilia. Negative phalloidin st ning indicated that these blebs contained neither cytoplasm nor cortical actin. Blebs generally indicate cellular injury and subsequent necrosis or apoptosis (20–22), but TUNEL staining showed no signs of apoptosis in cochlea of P8 *St3gal5*$^{-/-}$ mice (Fig. 4D). In this vestigial kinocilia region of the cuticular plate, actin filaments were depleted and connections between the actin cortical layer and plasma membrane were weak (23), but membrane recycling, endocytosis, and exocytosis appeared active (24). Transmission electron microscopy (TEM) revealed the appearance of intracellular vesicles in OHCs of *St3gal5*$^{-/-}$ mice (Fig. 4E). Magnified view clearly showed that these vesicles contained the intracellular membranous structures. Taken together, these observations suggest that blebs and intracellular vesicles seen in OHCs of *St3gal5*$^{-/-}$ mice might reflect an imbalance of endocytosis and exocytosis.

We next examined the morphology of IHC hair bundles using both SEM (Fig. 5A) and TEM (Fig. 5B). Until P10, IHC stereocilia of

Table 2. Auditory brainstem responses and CAEPs in children homozygous for ST3GAL5 c.694C>T

Age (years)	Auditory brainstem responses												CAEPs			
	CM		Morphology		Waves (80 dB)		Thresholds		Latency (80 dB)		Phase reversal		Morphology		Latency	
	Left	Right	Left	Right	Left	Right	Left	Right	Left	Right	Left	Right	Left	Right	Left	Right
1.6	Abs	Abs	–	–	Abs	Abs	–	–	–	–	–	–	Abn	Abn	D	D
2.0	Abs	Abs	Abn	Abn	I, III, V	I, III,V	50	50	N	N	No	Yes	Abn	Abn	D	D
2.8	Abs	Abs	Abn	Abn	III, V	III, V	70	70	D	D	Yes	Yes	Abn	Abn	D	D
3.1	Abs	Abs	Abn	Abn	III, V	III, V	80	80	N	N	No	Yes	Abn	Abn	D	D
3.6	Abs	Abs	Abn	Abn	III, V	III, V	80	80	N	N	Yes	Yes	Abn	Abn	D	D
4.5	Abs	Abs	Abn	Abn	I[a], III, V	I[a], III, V	DNT	DNT	N	N	Yes	Yes	Abn	Abn	N	N
7.2	Abs	Abs	Abn	Abn	III, V	III, V	60	50	N	N	No	Yes	N	N	N	N
7.9	Abs	Abs	Abn	Abn	III[a], V[a]	III[a], V[a]	80	80	N	D	No	[a]	Abn	Abn	D	D

Abn, abnormal; Abs, absent; CM, cochlear microphonic; D, delayed, N, normal; DNT, did not test.
[a]Equivocal result.

Table 3. Comparison of GM3 and GM1 expression of specific regions in the organ of Corti at P14

	OHC			IHC			DC		PC
	Stereocilia	Cuticular plate	Cell body	Stereocilia	Cuticular plate	Cell body	Cell surface	Cell body	Cell body
GM3	++	+	–	++	+	–	–	+	–
GM1	–	–	–	++	+	+	++	+	+

OHC, outer hair cell; IHC, inner hair cell; DC, Deiters cell; PC, pillar cell.

St3gal5$^{-/-}$ mice were structurally normal. However, by P12 some IHC stereocilia were stuck together and bent (Fig. 5A, arrows). Most degenerated by P14. TEM at P17 revealed giant and fused stereocilia with thick, long rootlets that penetrated the cuticular plate (Fig. 5B).

Irregular expression of PTPRQ and myosin VI in stereocilia of St3gal5 null mice

Myosin VI is normally concentrated at the base of stereocilia, where it interacts with protein tyrosine phosphatase receptor Q (PTPRQ) to maintain organization of the cell surface coat and structure of the overall hair bundle (25). We used immunostaining to evaluate involvement of gangliosides in the formation of this basal PTPRQ-myosin VI complex (Fig. 6). As shown in Figure 6B, PTPRQ was exclusively localized to the base of stereocilia in wild-type mice, but in *St3gal5*$^{-/-}$ mice, PTPRQ was maldistributed along the fused stereocilia.

In fused IHC stereocilia of *St3gal5*$^{-/-}$ mice, myosin VI was present from the base to the midshaft but absent from top regions (Fig. 6A), suggesting loss of normal ciliary motor action. In *St3gal5*$^{-/-}$ OHCs, expression of myosin VI was concentrated on the surface of the cuticular plate, close to vestigial kinocilia (Fig. 6A). Our observations suggest that membrane domain enriched with GM3 are crucial to the formation and proper localization of the stereocilia PTPRQ-myosin VI complex. In the absence of GM3, localization of this complex is disrupted (Fig. 6C), and this may have important structural and functional consequences for both inner and outer hair cells.

Discussion

Gangliosides and mammalian auditory development

Humans lacking all a- and b-series gangliosides have a profound disturbance of auditory function, described here as the neonatal onset hearing impairment, weak or absent MEMRs and DPOAEs, abnormal ABR morphology and thresholds, absent CMs, and delayed CAEPs. Absent DPOAEs and CMs indicate severe OHC impairment. Although the presence of ABRs in seven of eight patients indicates at least partial IHC function, numerous abnormalities revealed by MEMR and ABR testing suggest there is significant dysfunction of IHCs, central auditory pathways or both. As further evidence of this, ABR thresholds are generally higher than expected if OHC dysfunction alone explain hearing loss. Wave reversal observed in many patients indicates that hearing is more impaired at high versus low and middle frequencies (26).

In contrast, humans with autosomal recessive *B4GALNT1* deficiency have no hearing loss, visual impairment or epileptic encephalopathy, but suffer from progressive spastic paraplegia (13–17,27). This suggests that (i) each ganglioside has a particular distribution and functional relevance within the nervous system; (ii) there may be limited functional redundancy among various ganglioside species; and (iii) GM3 is indispensable to both the cochlear and neural phases of sound processing in mammals.

In this study, we exploited differential patterns of GSL expression among wild-type, *St3gal5*$^{-/-}$ and *B4galnt1*$^{-/-}$ mice to explore cochlear mechanisms of hearing loss that could be specifically attributed to deficiency of GM3 (18). Wild-type mice have a marked increase of gangliosides and other GSLs in the cochlea during early postnatal maturation (Fig. 1D), suggesting these molecules contribute to hearing onset. After auditory maturation, GM3 and GM1 show a distinctive distribution among cellular elements of the organ of Corti (i.e. IHC, OHC, Dieters cell, pillar cell) as summarized in Table 3. Both IHCs and OHCs express GM3, which is preferentially distributed to the apical surface, cuticular plate and stereocilia, whereas only IHCs express GM1, which is localized to their apical surface. In *St3gal5*$^{-/-}$ mice, degeneration of OHCs precedes that of IHCs, and this may reflect relative enrichment of GM3 in OHCs.

St3gal5$^{-/-}$ and *B4galnt1*$^{-/-}$ mice have predictable patterns of GSL expression within the organ of Corti. Cochlea of *B4galnt1*$^{-/-}$

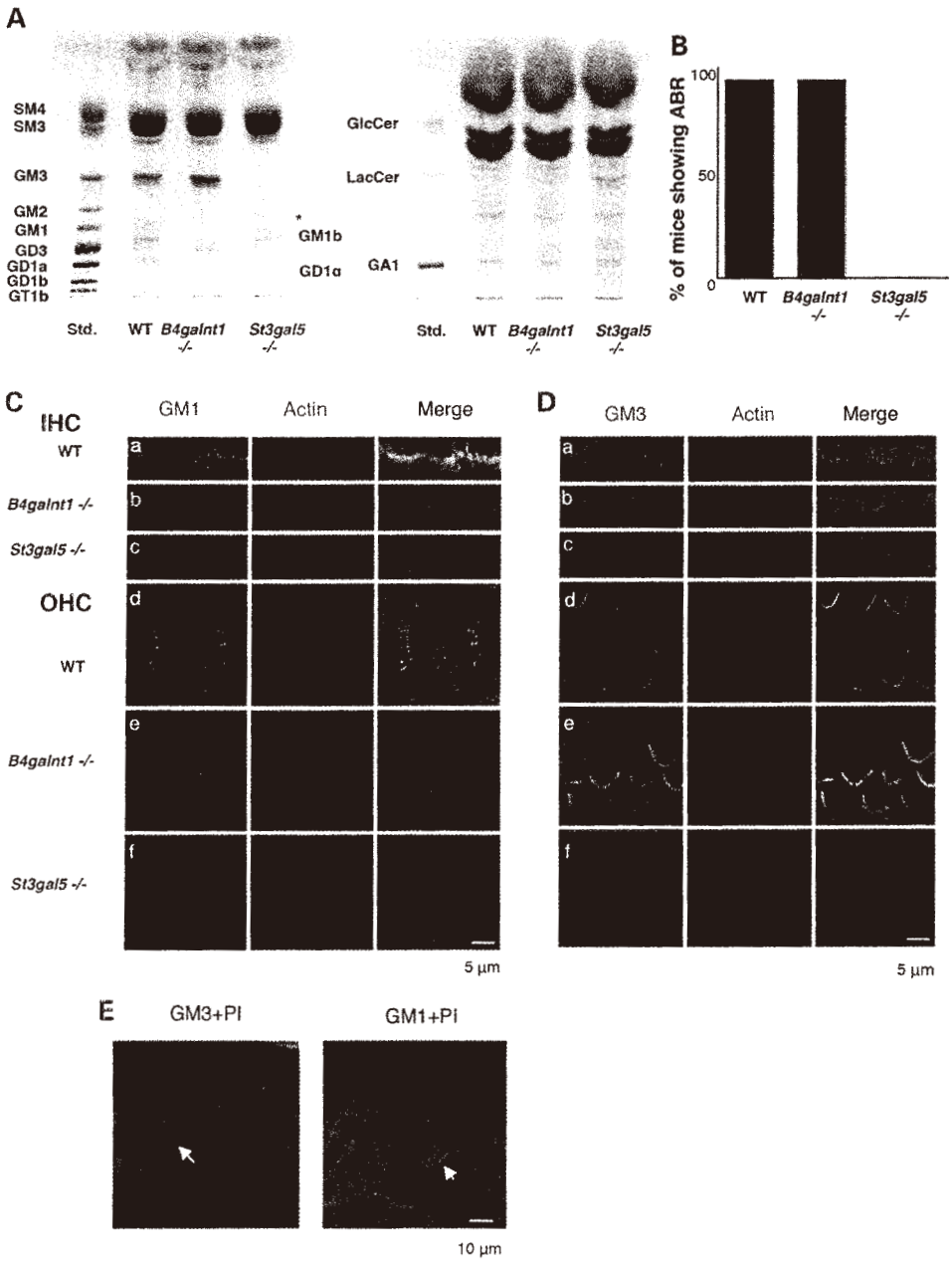

Figure 3. Identification of GM3 as an essential molecule for hair cell function. (A) HP-TLC of acidic (left) and neutral (right) GSLs from the cochlea of 4-week-old wild-type (WT), *B4galnt1*$^{-/-}$ and *St3gal5*$^{-/-}$ mice. The cochlea of *B4galnt1*$^{-/-}$ mice were mainly expressed GM3 and GD3. Each purified fraction was spotted 2 mg protein per lane. (B) Auditory-evoked brainstem response (ABR) of wild-type, *B4galnt1*$^{-/-}$ and *St3gal5*$^{-/-}$ mice at 4 weeks old. (C and D) Comparison of gangliosides expression in hair cells among wild-type, *B4galnt1*$^{-/-}$ and *St3gal5*$^{-/-}$ mice aged 4 weeks. Whole-mount immunostaining was performed. GM1 (C, green) and GM3 (D, green) of IHC (a–c) and OHC (d–f) stereocilia in wild-type (a and d), *B4galnt1*$^{-/-}$ (b and e) and *St3gal5*$^{-/-}$ (c and f) mice. In IHC, both GM1 and GM3 were expressed along the stereocilium from the taper region to top (Ca and Da). On the other hand, only GM3 was highly enriched in OHC stereocilia (Dd) without staining of GM1 (Cd). The stereocilia of IHC and OHC in *B4galnt1*$^{-/-}$ mice were expressed GM3 but not GM1 (Cb and Db). In *St3gal5*$^{-/-}$ mice, fused stereocilia was observed in IHC (Cc and Dc) and irregular phalloidin staining was observed in OHC (Cf and Df). Notably, the expression levels of GM1 but not GM3 was especially high on the surface of supporting cells (Deiters cell) (Cd and Dd). (E) Confocal images of cross sections of the cochleae in wild-type mice stained for GM3 (green, left panel), GM1 (green, right panel) and propidium iodide to label cell nuclei. (Arrow) Deiters cell, (arrow head) pillar cell. The red color of phalloidin staining (C and D) and propidium iodide (E) has been converted to magenta using Adobe Photoshop CC2014 software.

mice have high GM3 content, intact hair bundle structure and support normal hearing. In contrast, cochlea of *St3gal5*$^{-/-}$ mice are devoid of GM3, develop microstructural and degenerative changes as early as P3, and do not support auditory function. *B4galnt1/Siat8* double null mice that express only GM3 have an acoustic startle response (28), and we confirmed that *Siat8*$^{-/-}$

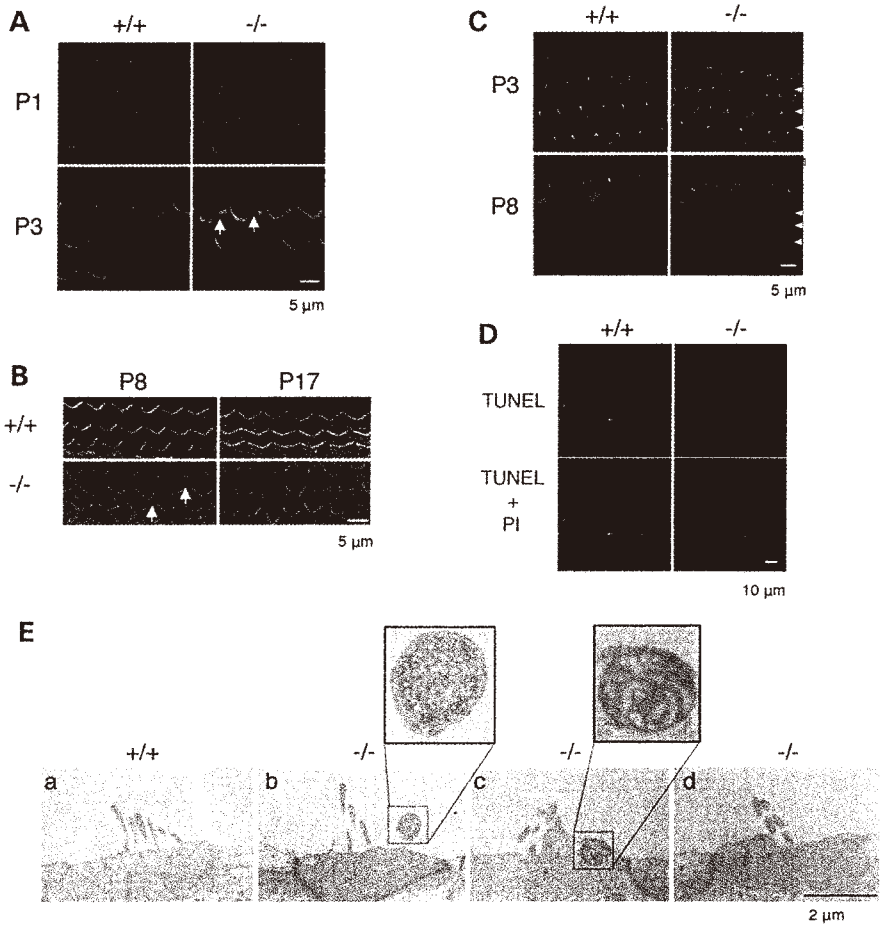

Figure 4. Degeneration of OHC in *St3gal5* null mice. (A) Confocal images of the basal coil of phalloidin-stained cochlear whole mounts from *St3gal5*$^{+/+}$ and $^{-/-}$ mice at P1 and P3. Defects in structure of hair bundle are first in the outer hair cells (arrows) at P3. (B) SEM images of OHC of *St3gal5*$^{+/+}$ and *St3gal5*$^{-/-}$ mice at P8 and 17. At P8, the blebs at the vestigial kinocilium location were observed (arrows), but disappeared at P17. (C) Expression of acetylated tubulin. Confocal images from showing stereocilia of *St3gal5*$^{+/+}$ and $^{-/-}$ mice stained for acetylated tubulin (green) and F-actin (phalloidin, magenta) at P3 and P8. At P3, hair cells of *St3gal5*$^{+/+}$ and $^{-/-}$ mice were expressed kinocilia with or without degeneration of stereocilia. At P8, kinocilia were disappeared from OHC in both *St3gal5*$^{+/+}$ and $^{-/-}$ mice. Three rows of OHCs are indicated by the white arrowheads. (D) TUNEL staining. Apoptotic cell was not detected in both *St3gal5*$^{+/+}$ and $^{-/-}$ mice at P8. (E) TEM images of OHC in *St3gal5*$^{+/+}$ and $^{-/-}$ mice at P17. The red color of phalloidin staining (C) and propidium iodide (D) has been converted to magenta using Adobe Photoshop CC2014 software.

mice lacking b-series gangliosides (e.g. GD3) hear normally (unpublished data).

All GM3 synthase-deficient patients tested with a newborn hearing screen failed, confirming that auditory deficits in humans with GM3 deficiency are present early in life. However, no structural abnormality of OHC or IHC stereocilia is evident in *St3gal5*$^{-/-}$ mice at P0. Thus GM3 may play its most critical role in postnatal maturation rather than embryogenesis of the auditory system. Consistent with this, auditory function of *St3gal5*$^{-/-}$ mice, although impaired at the onset of hearing, is completely abolished by P17 (18), at which time TEM reveals pathological remodeling of stereocilia (Fig. 5B).

Glycocalyx integrity and membrane cycling in GM3-deficient mice

Apical membranes of stereocilia are covered with a glycocalyx composed of acidic glycoproteins and glycolipids (including gangliosides) that contain sialic acid (29). This creates a dense negative charge distribution within the glycocalyx that normally prevents fusion of adjacent stereocilia. In experimental animals, aminoglycoside administration reduces the expression of sialoglycoconjugates in the OHC glycocalyx (30) and is associated with fusion of stereocilia (31). Fused stereocilia in *St3gal5*$^{-/-}$ mice may similarly reflect loss of the normal repulsive charge barrier between adjacent stereocilia, mediated in part by GM3 and its a- and b-series derivatives.

In the cuticular plate region of *St3gal5*$^{-/-}$ OHCs, we observed depletion of actin filaments, weak connections between the plasma membrane and actin cortical layer (23) and numerous membrane blebs. Abundant blebs are also seen in aminoglycoside-treated organ of Corti (32,33). In both cases, blebs may arise from imbalance of endocytosis and exocytosis (24,34,35). Since endocytosis in OHCs is clathrin-independent, mediated by caveolae and glycolipid rafts (24,36,37), the depletion of GM3 from ganglioside-dependent membrane organization may disrupt membrane recycling or vesicle transport to cause bleb formation (Fig. 4).

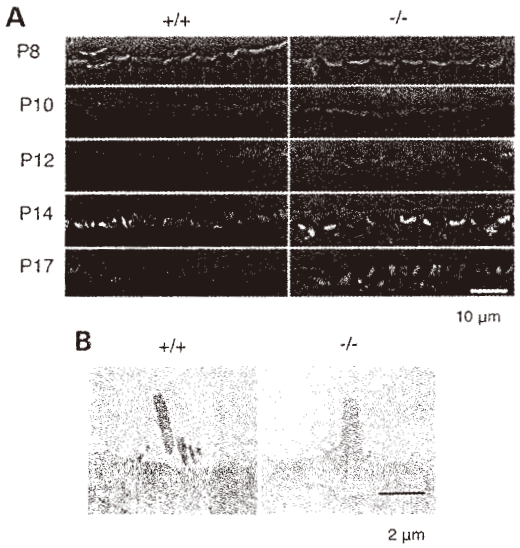

Figure 5. Fused stereocilia formation of IHC in *St3gal5* null mice. (**A**)The stereocilia of the IHCs of *St3gal5*$^{-/-}$ mice were fused after P12. Arrows indicate the fused stereocilia. (**B**) TEM images of the IHC stereocilia in *St3gal5*$^{+/+}$ and $^{-/-}$ mice at P17.

GM3-enriched membrane organization, PTPRQ-myosin VI complex localization and hair cell morphology

In the normal organ of Corti, functional PTPRQ-myosin VI complexes at the base of stereocilia appear critical to maintaining hair cell morphology and function (25). PTPRQ is a shaft connector located at the tapered base of stereocilia, with an extracellular domain containing 18 fibronectin III (FNIII) repeats, a membrane spanning domain, and a cytoplasmic domain that has both phosphatidylinositol and tyrosine phosphatase activities (38,39). Myosin VI is an actin-based motor protein that controls interactions between the plasma membrane and actin cytoskeleton (40). Mice lacking PTPRQ are deaf and lack tapering at the base of stereocilia, which become fused (25). In deaf, myosin VI-deficient mice, comparable structural changes of stereocilia are accompanied by maldistribution of PTPRQ along the length of the stereocilia membrane (25,41,42). We observed a similar morphological disruption of stereocilia and maldistribution of PTPRQ in *St3gal5*$^{-/-}$ mice (Fig. 6B), indicating a common underlying mechanism.

In renal membranes, myosin VI has a regulatory association with Na^+/H^+ exchanger three within microdomains called lipid rafts (43). These lipid rafts, enriched in cholesterol, gangliosides and other GSLs, are important for the maintenance of brush border microvilli architecture and function, and also influence the activity of many transmembrane proteins (44–50). Furthermore, the existence of ganglioside-rich membrane domains colocalized with PTPRQ has been observed in the basal tapers of bull frog hair cells (51). Based on observations from GM3-deficient humans and mice, we postulate that membrane organization enriched with GM3 are essential to the functional interactions among PTPRQ, myosin VI, actin and the cytoskeleton of inner and outer hair cell stereocilia (Fig. 6C).

Taken together, our results show that normal spatial and temporal expression of GM3 is critical to the structural integrity and function of auditory hair cells. These findings provide a foundation for understanding mechanisms of hearing loss in humans with GM3 synthase deficiency, but are not sufficient to explain the full constellation of neurological findings in these patients. Clearly, systemic GM3 deficiency also interferes with cerebral myelination and electrical activity (Fig. 2). This certainly affects central auditory function and also explains the severe psychomotor delay, epilepsy and visual impairment seen in children homozygous for *ST3GAL5* c.694C>T. Future studies should more carefully delineate the role of lipid rafts generally, and GM3 specifically, in the development and physiology of the central nervous system.

Although hearing is already impaired at birth in humans with GM3 synthase deficiency, our observations of *St3gal5*$^{-/-}$ mice suggest that a critical postnatal window may exist during which hair cell remodeling and degeneration could be rescued by ganglioside repletion therapy. This will prove challenging for at least three reasons: (i) purified GM3 is prohibitively expensive, and not currently available in sufficient quantities to offer human subjects; (ii) bioavailability of intestinal GM3 is unknown but may be quite limited, making enteral GM3 therapy impractical; and (iii) even if GM3 is successfully delivered to the circulation, it may not efficiently cross biological barriers into the organ of Corti or central nervous system. Cochlear and neural tissues are believed to make their own GSLs, and it is not clear that gangliosides from the circulation could be routed in adequate abundance to their proper location to restore function of OHCs, IHCs, neurons and oligodendrocytes. Nevertheless, these are soluble questions and the answers are important; we have experiments underway to answer them.

Materials and Methods

Study subjects

Study of human subjects was approved by the Lancaster General Hospital Institutional Review Board and parents consented in writing on behalf of their children. We studied eight children, ages 4.1 ± 2.3 years (four females), all of whom were members of the Old Order Amish community of Pennsylvania and homozygous for c.694C>T mutations of *ST3GAL5*. All patients received longitudinal pediatric care at the Clinic for Special Children (Strasburg, PA).

Auditory testing

We performed tympanometry testing with a 226-Hz probe tone, and ipsilateral MEMRs were measured between 80–100 dB HL at 0.5, 1, 2 and 4-kHz (Titan, Interacoustics). Distortion product otoacoustic emissions were obtained using the ILO (Otodynamic) 'eight points/octave' function. 2f1–f2 were recorded for f2 varying from 842 Hz to 7996 Hz and intensities of the primaries were kept constant across the frequency range (f1 = 65 dB SPL, f2 = 55 dB SPL). The f1/f2 frequency ratio was 1.22.

ABRs were elicited using 100 μs air-conduction clicks and recorded from a two-channel four-electrode montage (mastoid-high forehead-mastoid) with the Eclipse system (Interacoustics). Responses were first obtained at 80 dB normal hearing level (nHL). The intensity was increased by 10 dB when deemed appropriate to better visualize a response. When responses were present, intensities were then decreased in 10 dB steps to obtain a response threshold.

Condensation and rarefaction clicks were used to distinguish the CM from the compound action potential. The rate of stimulation was 27.7/s, low pass filter was 1500 Hz and high pass filter was 100 Hz, with gain set at 20 K. The presence of a wave was only established when at least two different recordings (for each polarity of the click) were available at the same or different intensity to verify reproducibility.

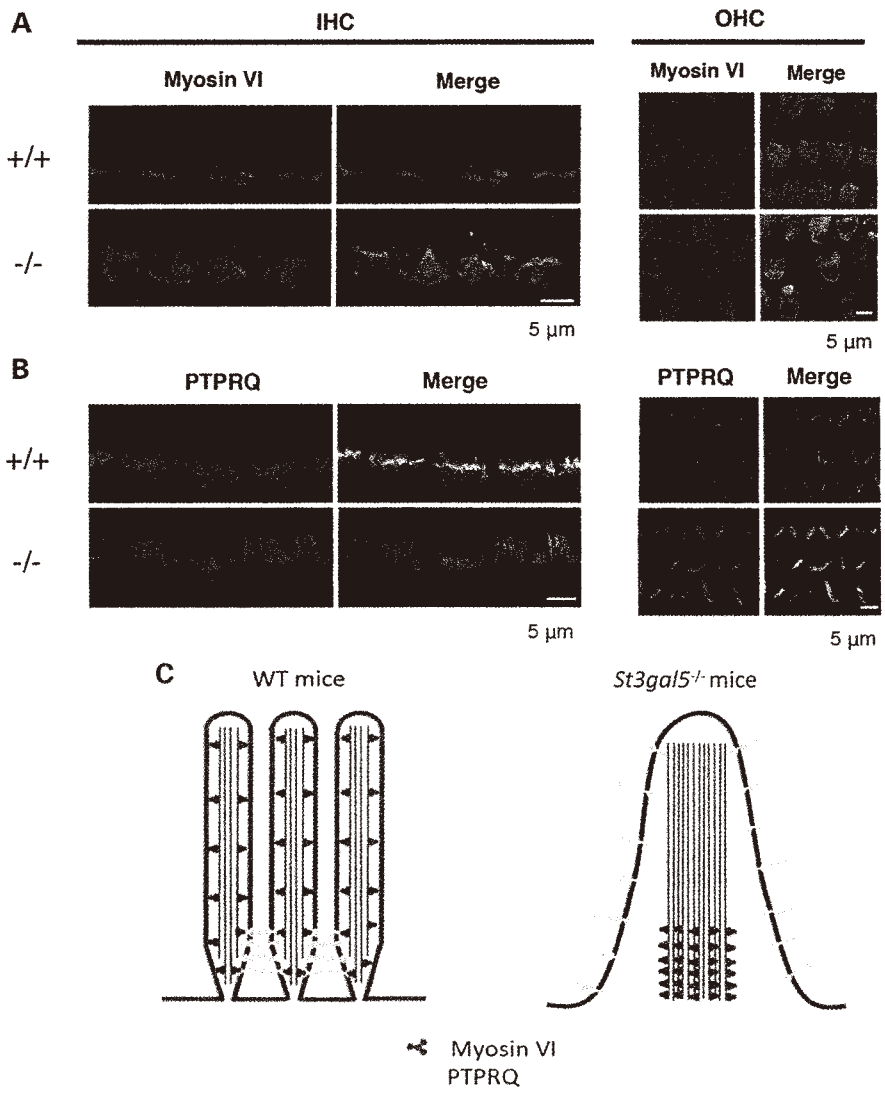

Figure 6. Dislocalization of PTPRQ and myosinVI in the stereocilia of *St3gal5* null mice. Confocal images showing stereocilia of IHCs and OHCs of *St3gal5*$^{+/+}$ and $^{-/-}$ mice stained for myosinVI (A) PTPRQ (B) (green) and F-actin (phalloidin, magenta). (C) Schematic images for dislocalization of PTPRQ and myosin VI in the IHC stereocilia of *St3gal5*$^{-/-}$ mouse. The red color of phalloidin staining (A and B) has been converted to magenta using Adobe Photoshop CC2014 software.

CAEPs were recorded with the Intelligent Hearing System device following the delivery of the stimulus/da/. Stimuli were delivered at 80 dB SPL to each ear separately through insert earphones. Responses were recorded using a two-channel, four-electrode montage (mastoid-high forehead-mastoid). The recording window was 400 ms. For each ear, 60 responses were averaged three times to calculate a grand average.

Mice

All animal studies were approved by Institutional Review Boards of Tohoku Pharmaceutical University. *St3gal5*$^{-/-}$ mice were generated as previously described (18,52). Mutant mice were maintained on a C57BL6 background by heterozygous mating to generate littermate controls and PCR genotyping of *St3gal5* alleles was performed as previously described (18). Briefly, *St3gal5* genotypes were determined by Southern blot and PCR analysis of genomic DNA isolated from embryonic stem cells and tail biopsies. Primer pairs used for genotyping included 5′-GGAATC CATCCCTTTTCTCACAGAG-3′ and 5′-TGAACTCACTTGGCATTG CTGG-3′ for detection of the wild-type allele (exon 2) and 5′-ACTGGGCACAACAGACAATCGG-3′ and 5′-TGGATACTTTCTCG GCAGGAGC-3′ for the knockout allele (neomycin resistance gene). *B4galnt1*$^{-/-}$ mice were established from *B4galnt1* and *B4galnt2* double null mice supplied by the Consortium for Functional Glycomics (www.functionalglycomics.org). Genotypes were using PCR from tail-tissue DNA (53). Both types of null mice were backcrossed with C57BL/6 mice over >11 generations.

Immunohistochemistry

Animals were kept under deep anesthesia and briefly perfused with physiological saline and 4% paraformaldehyde in 0.1 M phosphate buffer (PB; pH 7.4). Each cochlea was rapidly removed

from the temporal bones and fixed in 4% paraformaldehyde in 0.1 M PB for 1 h at room temperature or overnight at 4°C. For whole mounts, the organ of Corti was dissected out of the cochlea and the Reissner's membrane and tectorial membrane removed to expose the sensory epithelium. For sectioning, cochlea were decalcified in 10% ethylenediamine tetraacetic acid in Tris buffer (pH 7.4) and washed in PB, equilibrated overnight in 40% sucrose and then embedded and rapidly frozen in a mixture of equal parts 40% sucrose in PB and Tissue-Tek OCT compound (Sakura Finetechnical Co.). Cochlea were cryosectioned at 5 μm thickness. Sections and dissected cochlea were immunostained with anti-ganglioside GM3 (GMR6, Seikagaku Co. Ltd.), FITC-conjugated cholera toxin B-subunit (SIGMA), anti-myosin VI (Proteus BioSciences), anti-PTPRQ (gifted by Drs Sakaguchi and Kachar). Alexa 488-conjugated secondary antibodies, Alexa 594-conjugated phalloidin and propidium iodide were from Invitrogen. FITC-conjugated secondary anti-IgM antibody was from Vector Laboratories. Images were collected using Olympus FLUOVIEW confocal microscope.

TUNEL staining

Apoptotic cells in the cochlea were detected using In Situ Cell Death Detection Kit, POD (Roche). Apoptotic cleavage of genomic was identified by TUNEL, following the manufacturer's instructions. Positive controls for apoptosis were obtained by treating cochlear sections with DNase I.

Scanning and TEM

For SEM, cochlea were dissected to expose the organ of Corti and were fixed in 2.5% glutaraldehyde and 2% paraformaldehyde in 30 mM HEPES buffer (pH 7.3) for 2 h at room temperature. Post-fixation was performed by rotating tissues in 1% osmium tetroxide in 0.1 M sodium cacodylate buffer for 1 h at 4°C. Samples were dehydrated through a graded series of ethanol, substituted with t-butyl alcohol, freeze-dried, coated with platinum, and viewed in a JEOL JSM-T330A scanning microscope at 20 kV. For TEM, cochlea were fixed in 2.5% glutaraldehyde in 0.1 M PB (pH 7.4) for 2 h at room temperature. Postfixation was performed by rotating tissues in 1% osmium tetroxide in 0.1 M PB for 1 h at 4°C. Samples were dehydrated through a graded series of ethanol, equilibrated with propylene oxide and imbedded in Quetol-812 resin. Blocks were cured for 2 d at 60°C and sectioned with glass and diamond knives at 90–200 nm thickness. Sections were mounted on copper grids, double stained with uranyl acetate followed by lead citrate, and viewed in a JEOL transmission electron microscope at 70 kV.

Auditory brainstem responses

Mice (4 weeks of the age) were anesthetized with ketamine hydrochloride and xylazine hydrochloride. ABRs were recorded by using stainless steel electrodes placed at the vertex (positive), behind the bilateral ears (negative), and at the lower back (ground). Tone burst stimuli (rise/fall time: 0.2 ms; plateau time: 1 ms; repetitive rate: 11 Hz) were applied from the speaker (PT-R100; Pioneer) by using a function generator (DPS-725; Dia Medical) for which the system could provide 100 dB SPL at each frequency. Evoked responses were filtered with a band pass of 200 to 3 kHz, and the average 200 sweeps was recorded by using a single processor (Neuropack Micro; Nihon Kohden). ABR waveforms were recorded in decreasing 5 dB SPL intervals from a maximum amplitude until no waveforms could be visualized.

GSL (ganglioside) analysis

Cochlea were dissected from wild-type, *B4galnt1*$^{-/-}$, and *St3gal5*$^{-/-}$ mice after perfusion with PBS, then lyophilized. Dried tissues were crushed, and lipids were extracted from the tissues with the following solvent mixtures: chloroform/methanol, 1:1, 1:2 (v/v). After evaporation, the residue was dissolved in chloroform/methanol/water (30:60:8, v/v). The sample was allowed to absorb to the column packing with DEAE-Sephadex A25 (GE Healthcare). Chloroform/methanol/water (30:60:8, v/v) was applied to a column of same material and then chloroform/methanol/1 N sodium acetate aqueous (30:60:8, v/v). Neutral and acidic lipid fractions were eluted and spotted 2 mg/protein on the high performance-thin-layer chromatogram (HPTLC) plates. The plate of acidic fraction was developed in chloroform/methanol/0.2%$CaCl_2$ (55:45:10, v/v) and the plate of neutral fraction was developed in chloroform/methanol/water (65:25:4, v/v). Glycolipids were detected by spraying the plate with orcinol-sulfuric acid reagent.

LC-MS analysis

The acidic fraction was analyzed by liquid chromatography-ion trap-mass spectrometry with a NH2 column (Inertsil NH2, 3 mm, 1 × 50 mm, GL Science, Japan), flow rate (50 μl/min), a linear gradient made with solvent A: 1 mM ammonium formate in acetonitrile–water (95:5, v/v), solvent B: 50 mM ammonium formate in acetonitrile–water (50:50, v/v), and a time program: at 0 and 5 min (5% of B), 20 min (75% of B), 25 min (90% of B) and 30 min (90% of B) (54). The MS^1 chromatogram was monitored with theoretical values of $[M - H]^{-1}$ or $[M - 2H]^{-2}$ for each ganglioside (54). The structures indicated in the figure is tentative, and based on information with only molecular related ions indicated with black and, in addition, carbohydrate-related fragment ions obtained by MS^2 analysis indicated with red, and requires the consideration of possibility of d20:1 sphingosine instead of d18:1 in the ceramides.

Statistical analysis

Values in the text are the means ± SD. Data were compared using Student's t-test for two-group comparison or ANOVA for multi-group comparison. Significant differences were post hoc analyzed using Scheffé's test. Differences were considered significant at $P < 0.05$.

Conflict of Interest statement. None declared.

Funding

This work was supported by research grants for a Grant-in-Aid for Scientific Research (B) (to J.-i.I.) and for Scientific Research on Innovative Areas (no. 23110002, Deciphering sugar chain-based signals regulating integrative neuronal functions) from MEXT, Japan, the Mizutani Research Foundation for Glycoscience (J.-i.I.), The Naito Foundation (J.-i.I.), the ONO Medical Research Foundation (J.-i.I.), the Uehara Memorial Foundation (J.-i.I.), and by Grant-in-Aid for Japan Society for the Promotion of Science Fellows (M.Y.). This work was also supported by MEXT-Supported Program for the Strategic Research Foundation at Private Universities. The Clinic for Special Children is supported by generous charitable contributions from the Amish and Mennonite communities it serves.

References

1. Roberts, W.M., Howard, J. and Hudspeth, A.J. (1988) Hair cells: transduction, tuning, and transmission in the inner ear. *Annu. Rev. Cell Biol.*, **4**, 63–92.
2. Hudspeth, A.J. (1997) How hearing happens. *Neuron*, **19**, 947–950.
3. Hakomori, S. (1981) Glycosphingolipids in cellular interaction, differentiation, and oncogenesis. *Annu. Rev. Biochem.*, **50**, 733–764.
4. Schengrund, C.L. (1990) The role(s) of gangliosides in neural differentiation and repair: a perspective. *Brain. Res. Bull.*, **24**, 131–141.
5. Kawai, H., Allende, M.L., Wada, R., Kono, M., Sango, K., Deng, C., Miyakawa, T., Crawley, J.N., Werth, N., Bierfreund, U., Sandhoff, K. and Proia, R.L. (2001) Mice expressing only monosialoganglioside GM3 exhibit lethal audiogenic seizures. *J. Biol. Chem.*, **276**, 6885–6888.
6. Hakomori, S.I. (2002) The glycosynapse. *Proc. Natl. Acad. Sci. U.S.A.*, **99**, 225–232.
7. Proia, R.L. (2004) Gangliosides help stabilize the brain. *Nat. Genet.*, **36**, 1147–1148.
8. Handa, Y., Ozaki, N., Honda, T., Furukawa, K., Tomita, Y., Inoue, M., Furukawa, K., Okada, M. and Sugiura, Y. (2005) GD3 synthase gene knockout mice exhibit thermal hyperalgesia and mechanical allodynia but decreased response to formalin-induced prolonged noxious stimulation. *Pain*, **117**, 271–279.
9. Takamiya, K., Yamamoto, A., Furukawa, K., Yamashiro, S., Shin, M., Okada, M., Fukumoto, S., Haraguchi, M., Takeda, N., Fujimura, K. *et al.* (1996) Mice with disrupted GM2/GD2 synthase gene lack complex gangliosides but exhibit only subtle defects in their nervous system. *Proc. Natl. Acad. Sci. U.S.A.*, **93**, 10662–10667.
10. Chiavegatto, S., Sun, J., Nelson, R.J. and Schnaar, R.L. (2000) A functional role for complex gangliosides: motor deficits in GM2/GD2 synthase knockout mice. *Exp. Neurol.*, **166**, 227–234.
11. Inoue, M., Fujii, Y., Furukawa, K., Okada, M., Okumura, K., Hayakawa, T., Furukawa, K. and Sugiura, Y. (2002) Refractory skin injury in complex knock-out mice expressing only the GM3 ganglioside. *J. Biol.Chem.*, **277**, 29881–29888.
12. Yamashita, T., Wu, Y.P., Sandhoff, R., Werth, N., Mizukami, H., Ellis, J.M., Dupree, J.L., Geyer, R., Sandhoff, K. and Proia, R.L. (2005) Interruption of ganglioside synthesis produces central nervous system degeneration and altered axon-glial interactions. *Proc. Natl. Acad. Sci. U.S.A.*, **102**, 2725–2730.
13. Simpson, M.A., Cross, H., Proukakis, C., Priestman, D.A., Neville, D.C., Reinkensmeier, G., Wang, H., Wiznitzer, M., Gurtz, K., Verganelaki, A. *et al.* (2004) Infantile-onset symptomatic epilepsy syndrome caused by a homozygous loss-of-function mutation of GM3 synthase. *Nat. Genet.*, **36**, 1225–1229.
14. Farukhi, F., Dakkouri, C., Wang, H., Wiztnitzer, M. and Traboulsi, E.I. (2006) Etiology of vision loss in ganglioside GM3 synthase deficiency. *Ophthalmic Genet.*, **27**, 89–91.
15. Boccuto, L., Aoki, K., Flanagan-Steet, H., Chen, C.F., Fan, X., Bartel, F., Petukh, M., Pittman, A., Saul, R., Chaubey, A. *et al.* (2013) A mutation in a ganglioside biosynthetic enzyme, ST3GAL5, results in salt & pepper syndrome, a neurocutaneous disorder with altered glycolipid and glycoprotein glycosylation. *Hum. Mol. Genet.*, **23**, 418–433.
16. Wang, H., Bright, A., Xin, B., Bockoven, J.R. and Paller, A.S. (2013) Cutaneous dyspigmentation in patients with ganglioside GM3 synthase deficiency. *Am. J. Med. Genet. Part A*, **161A**, 875–879.
17. Fragaki, K., Ait-El-Mkadem, S., Chaussenot, A., Gire, C., Mengual, R., Bonesso, L., Bénéteau, M., Ricci, J.E., Desquiret-Dumas, V., Procaccio, V. *et al.* (2013) Refractory epilepsy and mitochondrial dysfunction due to GM3 synthase deficiency. *Eur. J. Hum. Genet.*, **21**, 528–534.
18. Yoshikawa, M., Go, S., Takasaki, K., Kakazu, Y., Ohashi, M., Nagafuku, M., Kabayama, K., Sekimoto, J., Suzuki, S., Takaiwa, K. *et al.* (2009) Mice lacking ganglioside GM3 synthase exhibit complete hearing loss due to selective degeneration of the organ of Corti. *Proc. Natl. Acad. Sci .U. S. A.*, **106**, 9483–9488.
19. Santi, P.A., Mancini, P. and Barnes, C. (1994) Identification and localization of the GM1 ganglioside in the cochlea using thin-layer chromatography and cholera toxin. *J. Histochem. Cytochem.*, **42**, 705–716.
20. Casciola-Rosen, L., Rosen, A., Petri, M. and Schlissel, M. (1996) Surface protrusions on apoptotic cells are sites of enhanced procoagulant activity: implications for coagulation events and antigenic spread in systemic lupus erythematosus. *Proc. Natl. Acad. Sci. U. S. A.*, **93**, 1624–1629.
21. Barros, L.F., Kanaseki, T., Sabirov, R., Morishima, S., Castro, J., Bittner, C.X., Maeno, E., Ando-Akatsuka, Y. and Okada, Y. (2003) Apoptotic and necrotic protrusions in epithelial cells display similar neck diameters but different kinase dependency. *Cell Death Differ.*, **10**, 687–697.
22. Morelli, A., Chiozzi, P., Chiesa, A., Ferrari, D., Sanz, J.M., Falzoni, S., Pinton, P., Rizzuto, R., Olson, M.F. and Di Virgilio, F. (2003) Extracellular ATP causes ROCK I-dependent protrusion formation in P2X7-transfected HEK293 cells. *Mol. Biol. Cell*, **14**, 2655–2664.
23. Shi, X., Gillespie, P.G. and Nuttall, A.L. (2005) Na+ influx triggers protrusion formation on inner hair cells. *Am. J. Physiol. Cell Physiol.*, **288**, C1332–C1341.
24. Griesinger, C.B., Richards, C.D. and Ashmore, J.F. (2004) Apical endocytosis in outer hair cells of the mammalian cochlea. *Eur. J. Neurosci.*, **20**, 41–50.
25. Sakaguchi, H., Tokita, J., Naoz, M., Bowen-Pope, D., Gov, N.S. and Kachar, B. (2008) Dynamic compartmentalization of protein tyrosine phosphatase receptor Q at the proximal end of stereocilia: implication of myosin VI-based transport. *Cell. Motil. Cytoskeleton*, **65**, 528–538.
26. Coats, A.C. and Martin, J.L. (1977) Human auditory nerve action potentials and brain stem evoked responses: effects of audiogram shape and lesion location. *Arch. Otolaryngol.*, **103**, 605–622.
27. Harlalka, G.V., Lehman, A., Chioza, B., Baple, E.L., Maroofian, R., Cross, H., Sreekantan-Nair, A., Priestman, D.A., Al-Turki, S., McEntagart, M.E. *et al.* (2013) Mutations in B4GALNT1 (GM2 synthase) underlie a new disorder of ganglioside biosynthesis. *Brain*, **136**, 3618–3624.
28. Tajima, O., Egashira, N., Ohmi, Y., Fukue, Y., Mishima, K., Iwasaki, K., Fujiwara, M., Inokuchi, J., Sugiura, Y., Furukawa, K. *et al.* (2009) Reduced motor and sensory functions and emotional response in GM3-only mice: emergence from early stage of life and exacerbation with aging. *Behav. Brain. Res.*, **198**, 74–82.
29. Luft, J.H. (1971) Ruthenium red and violet. II. Fine structural localization in animal tissues. *Anat. Rec.*, **171**, 369–415.
30. de Groot, J.C., Hendriksen, E.G. and Smoorenburg, G.F. (2005) Reduced expression of sialoglycoconjugates in the outer hair cell glycocalyx after systemic aminoglycoside administration. *Hear. Res.*, **205**, 68–82.
31. Takumida, M., Wersäll, J., Bagger-Sjöbäck, D. and Harada, Y. (1989) Observation of the glycocalyx of the organ of Corti:

an investigation by electron microscopy in the normal and gentamicin-treated guinea pig. *J. Laryngol. Otol.*, **103**, 133–136.
32. Goodyear, R.J., Gale, J.E., Ranatunga, K.M., Kros, C.J. and Richardson, G.P. (2008) Aminoglycoside-induced phosphatidylserine externalization in sensory hair cells is regionally restricted, rapid, and reversible. *J. Neurosci.*, **28**, 9939–9952.
33. Gale, J.E., Marcotti, W., Kennedy, H.J., Kros, C.J. and Richardson, G.P. (2001) FM1–43 dye behaves as a permeant blocker of the hair-cell mechanotransducer channel. *J. Neurosci.*, **21**, 7013–7025.
34. Richardson, G.P. and Russell, I.J. (1991) Cochlear cultures as a model system for studying aminoglycoside induced ototoxicity. *Hear. Res.*, **53**, 293–311.
35. Forge, A. and Richardson, G. (1993) Freeze fracture analysis of apical membranes in cochlear cultures: differences between basal and apical-coil outer hair cells and effects of neomycin. *J. Neurocytol.*, **22**, 854–867.
36. Grati, M., Schneider, M.E., Lipkow, K., Strehler, E.E., Wenthold, R.J. and Kachar, B. (2006) Rapid turnover of stereocilia membrane proteins: evidence from the trafficking and mobility of plasma membrane Ca(2+)-ATPase 2. *J. Neurosci.*, **26**, 6386–6395.
37. Kaneko, T., Harasztosi, C., Mack, A.F. and Gummer, A.W. (2006) Membrane traffic in outer hair cells of the adult mammalian cochlea. *Eur. J .Neurosci.*, **23**, 2712–2722.
38. Wright, M.B., Hugo, C., Seifert, R., Disteche, C.M. and Bowen-Pope, D.F. (1998) Proliferating and migrating mesangial cells responding to injury express a novel receptor protein-tyrosine phosphatase in experimental mesangial proliferative glomerulonephritis. *J. Biol. Chem.*, **273**, 23929–23937.
39. Oganesian, A., Poot, M., Daum, G., Coats, S.A., Wright, M.B., Seifert, R.A. and Bowen-Pope, D.F. (2003) Protein tyrosine phosphatase RQ is a phosphatidylinositol phosphatase that can regulate cell survival and proliferation. *Proc. Natl. Acad. Sci. U. S. A.*, **100**, 7563–7568.
40. Nambiar, R., McConnell, R.E. and Tyska, M.J. (2010) Myosin motor function: the ins and outs of actin-based membrane protrusions. *Cell. Mol. Life Sci.*, **67**, 1239–1254.
41. Self, T., Sobe, T., Copeland, N.G., Jenkins, N.A., Avraham, K.B. and Steel, K.P. (1999) Role of myosin VI in the differentiation of cochlear hair cells. *Dev. Biol.*, **214**, 331–341.
42. Hertzano, R., Shalit, E., Rzadzinska, A.K., Dror, A.A., Song, L., Ron, U., Tan, J.T., Shitrit, A.S., Fuchs, H., Hasson, T. *et al.* (2008) A Myo6 mutation destroys coordination between the myosin heads, revealing new functions of myosin VI in the stereocilia of mammalian inner ear hair cells. *PLoS Genet.*, **4**, e1000207.
43. Riquier, A.D., Lee, D.H. and McDonough, A.A. (2009) Renal NHE3 and NaPi2 partition into distinct membrane domains. *Am. J. Physiol. Cell Physiol.*, **296**, C900–C910.
44. Hauser, H., Howell, K., Dawson, R.M. and Bowyer, D.E. (1980) Rabbit small intestinal brush border membrane preparation and lipid composition. *Biochim. Biophys. Acta*, **602**, 567–577.
45. Christiansen, K. and Carlsen, J. (1981) Microvillus membrane vesicles from pig small intestine. Purity and lipid composition. *Biochim. Biophys. Acta*, **647**, 188–195.
46. Simons, K. and van Meer, G. (1988) Lipid sorting in epithelial cells. *Biochemistry*, **27**, 6197–6202.
47. Simons, K. and Ikonen, E. (1997) Functional rafts in cell membranes. *Nature*, **387**, 569–572.
48. Simons, K. and Toomre, D. (2000) Lipid rafts and signal transduction. *Nat. Rev. Mol. Cell Biol.*, **1**, 31–39.
49. Zonta, B. and Minichiello, L. (2013) Synaptic membrane rafts: traffic lights for local neurotrophin signaling? *Front. Synaptic. Neurosci.*, **5**, 9.
50. Head, B.P., Patel, H.H. and Insel, P.A. (2014) Interaction of membrane/lipid rafts with the cytoskeleton: impact on signaling and function: membrane/lipid rafts, mediators of cytoskeletal arrangement and cell signaling. *Biochim. Biophys. Acta*, **1838**, 532–545.
51. Zhao, H., Williams, D.E., Shin, J.B., Brügger, B. and Gillespie, P.G. (2012) Large membrane domains in hair bundles specify spatially constricted radixin activation. *J. Neurosci.*, **32**, 4600–4609.
52. Tsukamoto, K., Kohda, T., Mukamoto, M., Takeuchi, K., Ihara, H., Saito, M. and Kozaki, S. (2005) Binding of Clostridium botulinum type C and D neurotoxins to ganglioside and phospholipid. Novel insights into the receptor for clostridial neurotoxins. *J. Biol. Chem.*, **280**, 35164–35171.
53. Sun, J., Shaper, N.L., Itonori, S., Heffer-Lauc, M., Sheikh, K.A. and Schnaar, R.L. (2004) Myelin-associated glycoprotein (Siglec-4) expression is progressively and selectively decreased in the brains of mice lacking complex gangliosides. *Glycobiology*, **14**, 851–857.
54. Ikeda, K. and Taguchi, R. (2010) Highly sensitive localization analysis of gangliosides and sulfatides including structural isomers in mouse cerebellum sections by combination of laser microdissection and hydrophilic interaction liquid chromatography/electrospray ionization mass spectrometry with theoretically expanded multiple reaction monitoring. *Rapid Commun. Mass Spectrom.*, **24**, 2957–2965.

Glycoconj J
DOI 10.1007/s10719-013-9499-1

Expression machinery of GM4: the excess amounts of GM3/GM4S synthase (ST3GAL5) are necessary for GM4 synthesis in mammalian cells

Satoshi Uemura · Shinji Go · Fumi Shishido · Jin-ichi Inokuchi

Received: 1 July 2013 / Revised: 31 July 2013 / Accepted: 20 August 2013

Abstract The ganglioside GM4 is a sialic acid-containing glycosphingolipid mainly expressed in mammalian brain and erythrocytes. GM4 is synthesized by the sialylation of galactosylceramide (GalCer), while the ganglioside GM3 is synthesized by the sialylation of lactosylceramide (LacCer). Recently, the enzyme GM3 synthase was found to be responsible for the synthesis of GM4 *in vitro* and *in vivo*, yet the mechanism behind GM4 expression in cells remains unclear. In this study, we attempted to establish GM4-reconstituted cells to reveal the regulation of GM4 synthesis. Interestingly, GM4 was not detected in RPMI 1846 cells expressing LacCer, GalCer, and GM3. Similarly, GM4 was not detected in CHO-K1 cells, even when such cells expressing LacCer and GM3 were stably transfected with the GalCer synthase (GalCerS) gene. GM4 became detectable only when the GM3/GM4 synthase (GM3/GM4S, ST3GAL5) gene was overexpressed in either RPMI 1846 or CHO-K1/GalCerS cells. A mutant of the B16 melanoma cell line, GM-95, lacks GlcCer and LacCer, due to an absence of GlcCer synthase, but carries endogenous LacCer synthase and GM3/GM4S. GalCer became detectable after transfection of GalCerS into GM95 cells, but the GM95/GalCerS reconstituted cells did not express GM4, indicating that competition between the substrates LacCer and GalCer for GM3/GM4S does not cause the failure of GM4 synthesis. These results suggest that the expression machinery of GM4 under physiological conditions is independent from that of GM3.

Keywords Gangliosides · GM4 · GM3 · Glycosyltransferase · Sialyltransferase · ST3GAL5

Abbreviations

GalCer	Galactosylceramide
LacCer	Lactosylceramide
GalCerS	GalCer synthase
GM3/GM4S	GM3/GM4 synthase
ER	Endoplasmic reticulum
GlcCer	Glucosylceramide
GlcCerS	GlcCer synthase
LacCerS	LacCer synthase
TLC	Thin-layer chromatography

Introduction

Gangliosides, glycosphingolipids containing sialic acids, exist in the outer leaflet of the plasma membrane and are involved in a variety of cell processes. For example, the ganglioside GM3 is involved in the insulin resistance of type 2 diabetes [1–4], and GM3 levels are increased in the adipose tissue in a typical rodent model of obesity [1]. GM3 accumulation results in the dissociation of the insulin receptor from caveolae and leads to the insulin resistance [5, 6]. Another ganglioside, GM4, is expressed on the epithelial cells of the intestinal tract in red sea bream (Pagrus major) where it functions as a receptor for the pathogen that causes vibriosis [7]. In mammals, GM4 is reportedly expressed in the white matter,

Highlights - First establishment of GM4-reconstituted cells by overexpression of ST3Gal5 gene.

S. Uemura · S. Go · F. Shishido · J.-i. Inokuchi (✉)
Division of Glycopathology, Institute of Molecular Biomembrane and Glycobiology, Tohoku Pharmaceutical University, 4-4-1, Komatsushima, Aoba-ku, Sendai, Miyagi 981-8558, Japan
e-mail: jin@tohoku-pharm.ac.jp

S. Uemura (✉)
Molecular Genetic Research Department of Chemistry and Biological Science College of Science, Engineering Aoyama Gakuin University, 5-10-1 Fuchinobe, Chuo-ku, Sagamihara 252-5258, Japan
e-mail: uemura@chem.aoyama.ac.jp

Published online: 03 September 2013

myelin, and astrocytes of human brain [8–10], but in general, the function and physiological significance of GM4 is still not clear.

Glycosphingolipid synthesis begins with ceramide formed in the endoplasmic reticulum (ER) (Fig. 1). In the GM3 synthesis pathway, the glucosylation of ceramide by glucosylceramide synthase (GlcCerS) occurs on the cytosolic leaflet of the cis-Golgi membrane, forming glucosylceramide (GlcCer). GlcCer is transported to the trans-Golgi compartment by FAPP2, and then translocated to the luminal leaflet [11]. GlcCer is then converted to lactosylceramide (LacCer), which is the acceptor substrate for GM3 synthesis. Thus, the sequential biosynthesis of GM3 from GlcCer is believed to occur in the lumen of the trans-Golgi compartment. In contrast, in the GM4 synthesis pathway, the galactosylation of ceramide by galactosylceramide synthase (GalCerS) occurs in the lumen of the ER, forming galactosylceramide (GalCer) (Fig. 1). GalCerS is a type I membrane protein that has an ER retention signal in its cytoplasmic tail and localizes in the ER [12]. UDP-galactose, the donor substrate for GalCer synthesis, is imported into the ER lumen as the UDP-galactose transporter localizes in the ER by interacting with GalCerS [12]. Subsequently, GalCer is transported to the trans-Golgi compartment from the ER, although the detailed mechanism for this step is unknown.

In mammals, ST3Gal5 is a common sialyltransferase active in generating GM3 and GM4 from LacCer and GalCer, respectively [13], so here we designate this enzyme GM3/GM4 synthase (GM3/GM4S, ST3GAL5). GM3/GM4S is a type II membrane protein with three isoforms (M1-, M2-, M3-GM3/GM4S) [14]. M2- and M3-GM3/GM4S are localized in the Golgi apparatus, whereas M1-GM3/GM4S is mainly localized in the ER due to a retrograde transport signal (Arginine [R]-based motif) in its cytoplasmic tail [14]. However, unlike GalCer synthesis, both GM3 and GM4 synthesis should occur in the trans-Golgi since the CMP-sialic acid transporter localizes exclusively in the Golgi and not in the ER [15].

In the presented study, to examine the expression machinery of GM3 and GM4 in cells, we have attempted to establish GM4-reconstituted cells using several cell lines. Interestingly, overexpression of the GM3/GM4S gene was necessary to detect GM4 in cells expressing GalCer and endogenous GM3/GM4S. These results suggest that the regulation of the production and/or degradation of GM4 are different from those of GM3.

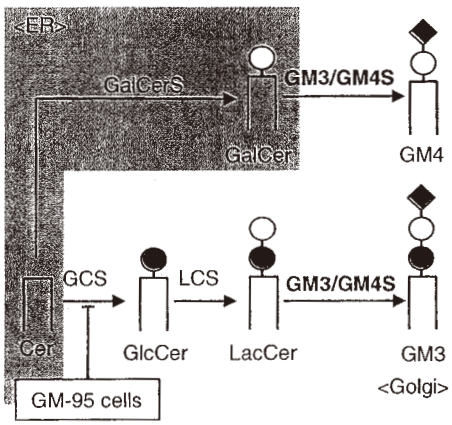

Fig. 1 The biosynthesis pathways of GM3 and GM4. GM3/GM4S transfers a sialic acid to LacCer and GalCer to generate GM3 and GM4, respectively. Mouse B16 melanoma GM-95 cells are glycosphingolipid-deficient mutants that lack GlcCerS (GCS) activity. A blue circle, yellow circle, and purple diamond indicate glucose, galactose, and a sialic acid, respectively. LCS denotes galactosyltransferase (LacCerS), which catalyzes LacCer synthesis

Material and methods

Materials

RPMI 1846 and GM-95 cells were kindly provided by Dr. M. Ito (Kyushu University, Hukuoka, Japan) and Dr. Y. Hirabayashi (Riken Brain Science Institute, Wako, Japan), respectively. Anti-GM4 antibody (rabbit IgG), LacCer, GalCer, and GlcCer were purchased from Matoreya (Pleasant Gap, PA). GM3 was also purchased from Matoreya. GM4 (d18:1-C18:0) was purchased from Wako (Osaka, Japan). Thin-layer chromatography (TLC) plates were purchased from Merck (Darmstadt, Germany). CSII-CMV-MCS, pCAG-HIVgp, and pCMV-VSV-G-RSV-Rev plasmids were provided by the DNA Bank, RIKEN BioResource Center (Ibaraki, Japan).

Plasmids

The pNF4 plasmid encoding GalCer synthase GalCerS was constructed using cDNA prepared from mouse kidney and primers 5′-GGATCCACCATGAAGTCTTACACTC CATATTTCATGC-3′ and 5′-TCATCTCACCTTCTT TTCGTGTTTAACAC-3′. The resulting fragments were cloned into a pGEM-T Easy vector (Promega, Madison, WI) to generate pNF2. The 1.6-kb BamHI-NotI fragment of pNF2 was then cloned into the BamHI-NotI site of a pcDNA3.1 Zeo(+) vector (Life Technologies, Carlsbad, CA) to generate pNF4.

To produce a lentivirus, the pFS311 (GM3/GM4S/CSII-CMV-RfA) was constructed using pcDNA3.1 Zeo(+)-GM3/GM4S [16] and primers 5′-CACCATGAGAAGAC CCAGCTTGTTAATAAAAGA-3′ and 5′-TTCAGTGG ATGCCGCCGCTGAGGTCCTC-3′. The resulting fragments were cloned into a pENTR/D-TOPO vector (Life Technologies) to generate pSU212. The CSII-CMV-MCS plasmid was converted to a Gateway® destination vector (CSII-CMV-RfA) using the Gateway® vector conversion system (Life Technologies). The GM3/GM4S gene of pSU212 was inserted into

the lentiviral expression vector, CSII-CMV-RfA, using the LR clonase reaction to generate pFS311.

Cell culture

Hamster melanoma RPMI 1846 cells, Chinese hamster ovary CHO-K1 (CHO) cells, mouse melanoma GM-95 cells, and human kidney 297 T cells were cultured in RPMI 1640 (Wako), F-12 HAM (Wako), low-glucose DMEM (Wako), and high-glucose DMEM (Life Technologies) medium, respectively, each supplemented with 10 % fetal bovine serum, 100 U/ml penicillin, and 100 μg/ml streptomycin. CHO-K1 and GM-95 cells were transfected using Lipofectamine 2000 (Life Technologies) according to the manufacturer's instructions. Stable transfectants were selected in the same medium used for culture in the presence of zeocin (Life Technologies).

Preparation of lentiviral vectors

Twenty-four hours before transfection, 293 T cells (0.5×10^6) were seeded in a poly-lysine coated 60-mm dish. The 293 T cells were transfected with 3 μg of pFS311 (GM3/GM4 synthase/CSII-CMV-RfA), 1.5 μg of pCAG-HIVgp, and 1.5 μg of pCMV-VSV-G-RSV-Rev plasmids using Lipofectamine 2000. The cells were incubated for 24 h at 37 °C, then the medium was replaced with 4 mL of high-glucose DMEM containing 10 μM Forskolin. Approximately 32 h after transfection, the culture temperature was shifted from 37 °C to 32 °C to maintain virus stability. The lentivirus-containing supernatant was harvested 48 h after transfection and centrifuged at 200 x *g* for 3 min to remove living cells. The lentiviral supernatant was either used immediately for experiments or snap-frozen in liquid nitrogen and stored at −80 °C for later applications. For the lentiviral transduction of RPMI 1846, CHO-K1/GalCerS, or GM-95/GalCerS cells, 4 ml of the lentiviral supernatant was added to 0.25×10^6 cells in a 60-mm dish, and the cells were cultured at 32 °C. After 24 h, the culture temperature was shifted from 32 °C to 37 °C, and the cells were incubated for 48 h.

Lipid analysis

Cells were washed twice with PBS, and total lipids were extracted from the cells with chloroform/methanol (1/1 and 1/2 v/v, successively). Samples were equalized for protein concentration, which was determined using a BCA kit (Pierce Chemical, Rockford, IL). Briefly, the total lipid extract was dissolved in chloroform/methanol/water (30/60/8, v/v/v), passed through a DEAE-Sephadex A-25 column (0.8 × 4.5 cm, acetate form), and eluted with another five volumes each of the 30/60/8 (neutral lipid fraction) and chloroform/methanol/1 M aqueous Na acetate (30/60/8) (acidic lipid fraction). The solvent was evaporated to dryness, and esters were cleaved with methanolic 0.5 M NaOH for 1 h 40 °C. The solution was neutralized with 1 M acetic acid in methanol and diluted with 6 ml 50 mM NaCl solution then desalted using a Sep-Pack C18 reverse-phase cartridge (Waters). Neutral lipid and acidic lipid fractions were separated by TLC using chloroform/acetone/methanol/acetic acid/water (50/20/10/10/5, v/v/v/v/v) and chloroform/methanol/0.5 % $CaCl_2$ (55/45/10, v/v/v), respectively, then detected with orcinol-sulfuric acid reagent.

TLC immunostaining

TLC immunostaining was performed as described [17] with slight modifications. Briefly, GM4 (standard) and the acidic lipid fraction were spotted on a TLC plate and separated with chloroform/methanol/0.2 % $CaCl_2$ (55/45/10, v/v/v). The dry plate was dipped in cyclohexane containing 0.1 % (w/v) polyisobutylmethacrylate for 60 s to air-dry and then blocked by incubation in PBS containing 1 % bovine serum albumin at room temperature for 1 h. The plate was incubated with a polyclonal anti-GM4 antibody (rabbit IgG) in PBS at room temperature for 2 h. The plate was then washed five times with PBS, and the plate was incubated with horseradish peroxidase-conjugated anti-rabbit Fab fragment at room temperature for 1 h. Labeling was detected using an ECL kit (GE Healthcare Bio-Sciences, Piscataway, NJ). The polyclonal antibody specifically recognizes GM4 but not other GSLs such as GM3 and GalCer.

Immunofluorescence microscopy

GM3/GM3S overexpressed cells were cultured on coverglass and then fixed for 15 min with 3.7 % formaldehyde in PBS at room temperature. After rinsing with PBS, the cells were permeabilized by 0.5 % SDS in PBS, treated with Image-iT FX Signal Enhancer (Life Technologies) for 30 min, and then incubated for 1 h with 1:100 dilutions of anti-GM3/GM4S (9129) [14] and anti-GM130 (BD Bioscience, Franklin Lakes, NJ) antibodies. After washing three times in PBS, the cells were incubated for 30 min with 1:200 dilutions of Alexa 488-conjugated anti-rabbit IgG antibodies (Life Technologies) and Alexa 594-conjugated anti-mouse IgG antibodies (Life Technologies). Coverslips were washed in PBS three times, mounted on glass slides using ProLong Gold antifade reagent (Life Technologies), and analyzed by fluorescence microscopy FV1000 (Olympus, Tokyo, Japan).

Results

GM4 synthesis in cell lines expressing LacCer, GalCer, and endogenous GM3/GM4 synthase

Hamster melanoma RPMI 1846 cells reportedly express GalCer on their cell surface [13]. However, since GM3 and

GM4 synthesis activities *in vitro* are barely detectable in the lysates of these cells [13], we had assumed that RPMI 1846 cells express only the neutral glycosphingolipids GlcCer, LacCer, and GalCer (Fig. 1). To confirm the glycosphingolipid composition of RPMI 1846 cells, we performed a lipid analysis using TLC. Neutral and acidic lipid fractions were separated from the total lipid extracts of RPMI 1846 cells using DEAE-Sephadex A-25 column, and each fraction was analyzed by TLC (Fig. 2a). As expected, GlcCer, LacCer, and GalCer were detected in the neutral lipid fraction. Surprisingly, GM3 and unidentified bands were also detected in the acidic lipid fraction. These bands reacted with an anti-GM3 antibody (M2590) by TLC-immunostaining (data not shown), suggesting that the unidentified bands might be sialylparaglobosides. GM4 was not detected in RPMI 1846 cells although the cells express GalCer and endogenous GM3/GM4S.

Next, we attempted to establish GM4-reconstituted cells using Chinese hamster CHO-K1 cells expressing GlcCer, LacCer and GM3, but not expressing GalCer due to the lack of GalCerS. When CHO-K1 cells were stably transfected with the GalCerS gene, bands corresponding to GalCer appeared during TLC analysis (Fig. 2b left panel). However, as observed in RPMI 1846 cells, GM4 was not detected in the acidic lipid fraction of the CHO-K1/GalCer (Fig. 2b right panel). These results suggest that the expression of both the GalCer substrate and endogenous GM3/GM4S is not sufficient to induce GM4 expression in cultured cells.

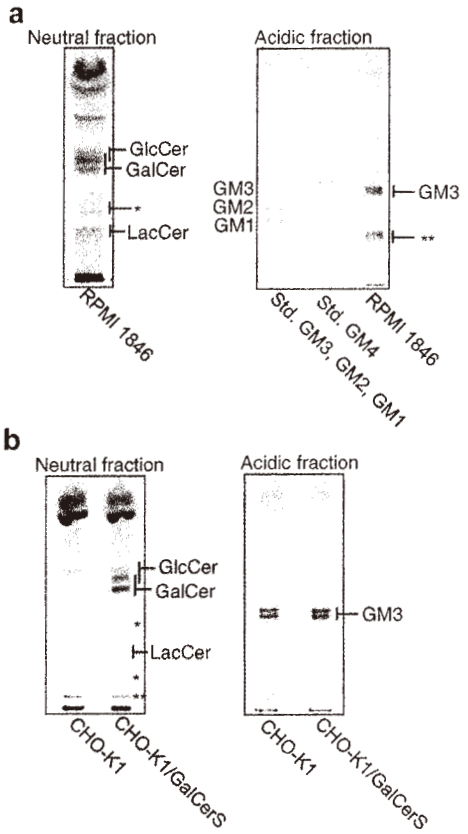

Fig. 2 Endogenous GM3/GM4S is not sufficient for GM4 expression *in vivo*. **a**. Glycosphingolipids (neutral and acidic fractions) extracted from RPMI 1846 cells, corresponding to 2 mg of protein, were separated on TLC plates and stained with orcinol-sulfuric acids. **b**. CHO cells were stably transfected with GalCerS using Lipofectamine 2000. Glycosphingolipids (neutral and acidic fractions) extracted from CHO or CHO/GalCerS cells, corresponding to 1.5 mg of protein, were separated on TLC plates and stained with orcinol-sulfuric acid reagent. A *single asterisk* indicates unidentified neutral glycosphingolipids. A *double asterisk* indicates unidentified acidic glycosphingolipids, which were M2590 (anti-GM3 monoclonal antibody)-positive

The effect of GM3/GM4S overexpression on GM4 synthesis

The cell surface expression of GM4 detected by anti-GM4 antibody is markedly increased in RPMI 1846 cells upon transient transfection of the GM3/GM4S gene [13]. We analyzed the cellular levels of GM4 in RPMI 1846 cells stably transfected with GM3/GM4S (using a lentivirus expression system) by separating lipids on TLC plates and detecting them with orcinol-sulfuric acid reagent and by TLC immunostaining (Fig. 3a and b). In the neutral fraction, the amounts of GalCer, GlcCer, and LacCer in RPMI 1846 cells expressing GM3/GM4S (RPMI 1846/GM3/GM4S cells) were similar to those in the original RPMI 1846 cells (Fig. 3a left panel). In the acidic fraction, faint bands were apparent that corresponded to GM4 (just above the GM3) in RPMI 1846/GM3/GM4S cells, while the amount of GM3 was unchanged (Fig. 3a right panel). TLC immunostaining with anti-GM4 antibodies confirmed the presence of GM4 (Fig. 3b).

We next investigated whether the overexpression of GM3/GM4S affects the GM4 synthesis in CHO-K1/GalCerS cells. The lipid composition of the CHO-K1/GalCerS/GM3/GM4S cells was similar to that of the CHO-K1/GalCerS cells. Although GM4 bands were not detected using orcinol-sulfuric acid reagent in the acidic fraction from the CHO-K1/GalCerS/GM3/GM4S cells (Fig. 3c), TLC immunostaining with anti-GM4 antibodies did reveal GM4 in the transfected cells (Fig. 3d). Taken together, these results indicate that overexpression of the GM3/GM4S gene is required to express GM4 in both RPMI 1846 and CHO-K1/GalCerS cells.

GalCer, which is an acceptor in GM4 synthesis, is produced in ER. However, since CMP-sialic acid, which is a donor in GM4 synthesis, is transported into lumenal side at Golgi apparatus by CMP-sialic acid transporter, GM4 synthesis would also occur in Golgi apparatus such as GM3 synthesis. Thus, the GalCer synthesis ought not to affect the localization of overexpressed GM3/GM4S in Golgi apparatus. Accordingly, we performed indirect immunofluorescence microscopic analysis to determine the subcellular localization of M3-GM3/GM4S expressed in RPMI1846, CHO-K1 and

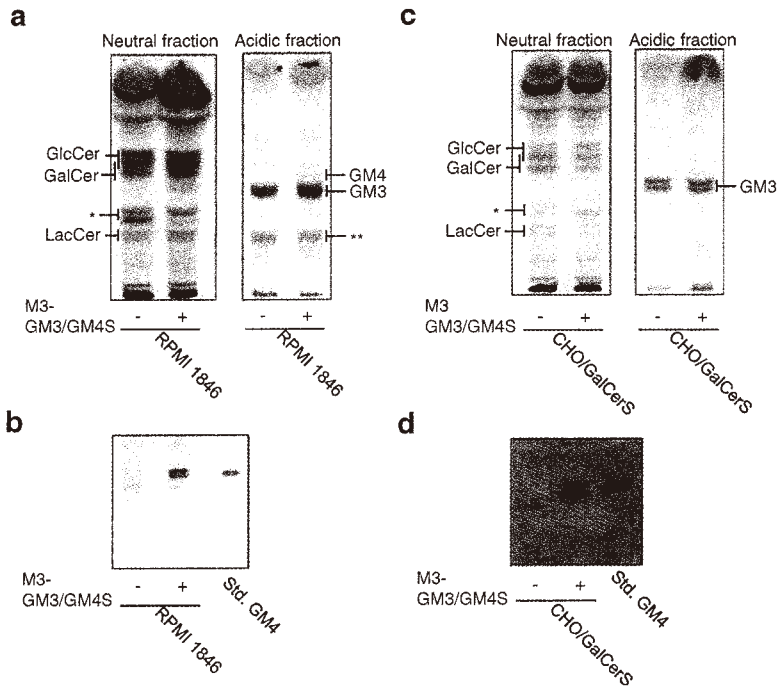

Fig. 3 Overexpression of the GM3/GM4S gene induces GM4 expression in RPMI 1846 and CHO/GalCerS cells. RPMI 1846 and CHO/GalCerS cells were transfected with (+) GM3/GM4S using a lentivirus expression system. A *minus sign* indicates no transfection. **a**. Glycosphingolipids (neutral and acidic fractions) extracted from RPMI 1846 (−) or RPMI 1846 (+) cells, corresponding to 2 mg of protein, were separated on TLC plates and stained with orcinol-sulfuric acid reagent. A *single asterisk* indicates unidentified neutral glycosphingolipids. The *double asterisk* indicates unidentified acidic glycosphingolipids (M2590-positive bands). **b**. The acidic lipid fractions from cells in A were analyzed by immunostaining with using an anti-GM4 polyclonal antibody. **c**. Glycosphingolipids (neutral and acidic fractions) extracted from CHO/GalCerS (−) or CHO/GalCerS (+) cells, corresponding to 1.5 mg of protein, were separated on TLC plates and stained with orcinol-sulfuric acid reagent. The *asterisk* indicates unidentified neutral glycosphingolipids. **d**. The acidic lipid fractions from cells in C were analyzed by immunostaining with anti-GM4 polyclonal antibody

CHO-K1/GalCerS cells. In all cell lines, M3-GM3/GM4S localized to a compact juxtanuclear reticulum and partially colocalized with GM130, a cis-Golgi marker proteins (Fig. 4), suggesting that GM4 synthesis occurs in Golgi apparatus.

Possibility of competition between the substrates LacCer and GalCer in GM4 synthesis

Since GM3 and GM4 are produced by the same enzyme (GM3/GM4S), differences in the affinity of GM3/GM4S toward the two substrates, LacCer and GalCer, may be responsible for the amounts of GM3 and GM4 produced in RPMI 1846 and CHO/GalCerS cells. If the failure of GM4 expression in these cells is caused by the competition of LacCer and GalCer for the enzyme, then cells expressing only GalCer and not LacCer, should synthesize GM4 more efficiently. We employed GM-95 cells, a mutant clone derived from mouse B16 melanoma cells [18], to examine this possibility. While GM-95 cell lysates exhibit LacCer and GM3 synthesis activity *in vitro*, the intact cells do not express GlcCer, LacCer, or GM3 due to a deletion of GlcCer synthase (GlcCerS) (Fig. 1). Indeed, studies have shown that GM-95 cells express LacCer and GM3 after introduction of the GlcCerS gene [19]. Accordingly, to establish cells expressing a single substrate, GalCer, GM-95 cells were stably transfected with the GalCerS gene, and the lipid composition of the resultant GM-95/GalCerS cells was analyzed by TLC. As shown Fig. 5a, the GM-95/GalCerS cells expressed only GalCer and not GlcCer or LacCer. As a result, GM4 was not detectable in the acidic fraction of the GM-95/GalCerS cells, although endogenous GM3/GM4S is present in these cells. This result indicates that the failure of GM4 synthesis observed in RPMI 1846 and CHO-K1/GalCerS cells is not caused by a competition between substrates. Moreover, overexpression of the GM3/GM4S gene by the lentivirus expression system induced GM4 synthesis in GM-95/GalCer cells similar to that observed in RPMI 1846 and CHO-K1/GalCer cells (Fig. 5a and b), suggesting that an excess amount of GM3/GM4S is required to detect GM4 in mammalian cells.

Discussion

In mammals, small amounts of GM4 are known to be expressed in brain and erythrocytes [8–10, 20], but the

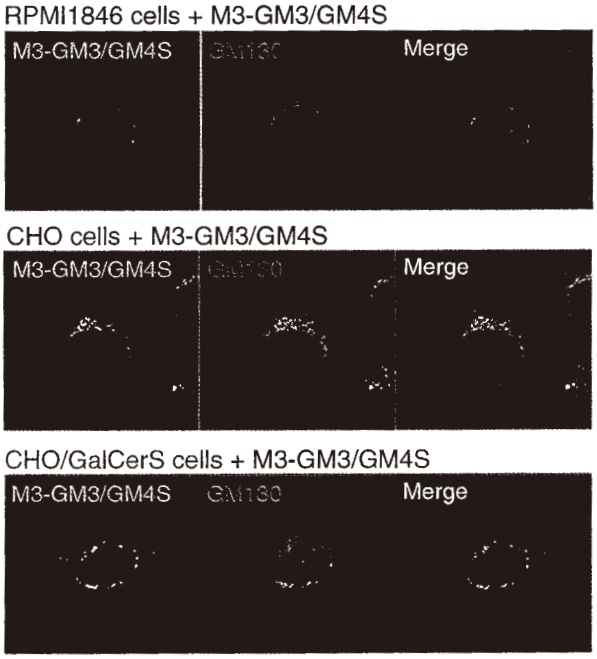

Fig. 4 Subcellular localization of overexpressed M3-GM3/GM4S in RPMI1846, and CHO, and CHO/GalCerS cells. The cells were fixed, permeabilized with 0.5 % SDS in PBS, and stained with anti-GM3/GM4S antibodies and Alexa 488-conjugated anti-rabbit IgG. Cells were visualized by confocal laser-scanning microscopy. For colocalization studies, cells were incubation with antibodies against GM130 for 1 h, followed by incubation with Alexa 594-conjugated anti-mouse IgG for 30 min. Merged images are shown in the right panels

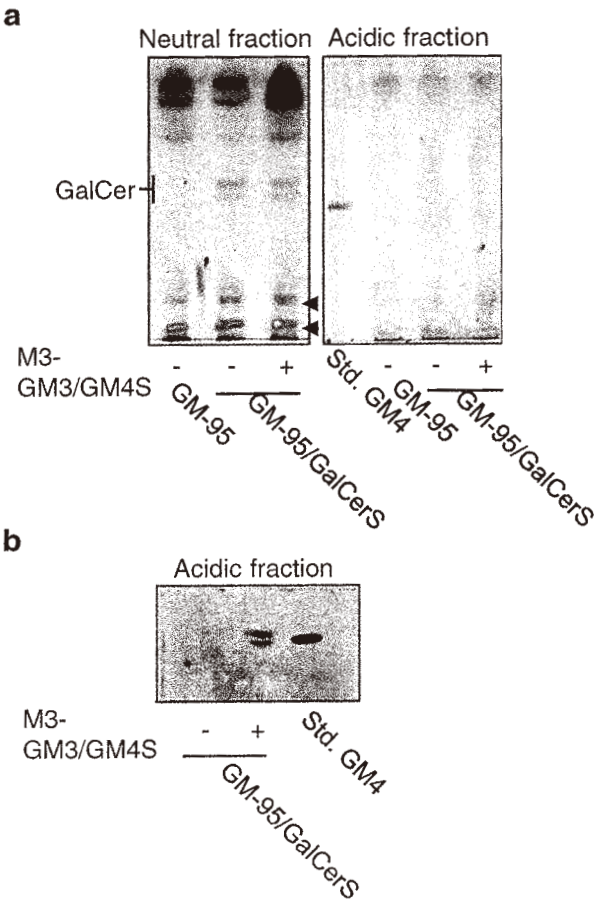

Fig. 5 GM4 expression is not affected by GM3 synthesis machinery. GM-95 cells were stably transfected with GalCerS using Lipofectamine 2000, and the resultant GM-95/GalCer cells were transfected with (+) GM3/GM4S using a lentivirus expression system. A *minus sign* indicates no transfection. **a**. Glycosphingolipids (neutral and acidic fractions) extracted from GM-95 (−), GM-95/GalCerS (−), or GM-95/GalCerS (+) cells, corresponding to 1 mg of protein, were separated on TLC plates and stained with orcinol-sulfuric acid reagent. The *arrowheads* indicate unidentified neutral glycosphingolipids. **b**. TLC immunostaining of GM-95/GalCerS (−) or GM-95/GalCerS (+) cells using anti-GM4 polyclonal antibody

regulation of GM4 synthesis remains unknown. Recently, several groups, including ours, independently found that GM3S is also involved in GM4 synthesis [13, 21]. Accordingly, we have investigated how the production and degradation of GM4 are regulated at the cellular level. In the presented study, we attempted to establish GM4-reconsituted cells using hamster melanoma RPMI 1846, Chinese hamster CHO-K1, and mouse melanoma GM-95 cells. Interestingly, GM4 was not detected by TLC immunostaining with anti-GM4 antibody in RPMI 1846 or CHO-K1/GalCerS cells, both of which express GalCer, LacCer, and GM3. Since GM4 was not detected in GM-95/GalCerS cells expressing GalCer and GM3/GM4S but not LacCer, the lack of GM4 synthesis is not caused by the competition between the acceptor substrates LacCer and GalCer. GM4 was detectable only when excess amounts of the GM3S/GM4S gene were introduced in these cells.

What is implied by these results regarding the expression mechanisms of GM4? One possibility is that GM4 synthesis is not efficient compared with GM3 synthesis. Since GM3/GM4S forms a complex with LacCer synthase (LacCerS) in the Golgi apparatus [22], GlcCer transported by FAPP2 is rapidly converted to GM3 *via* LacCer. If GlcCer is selectively transported to the compartment of the LacCerS-GM3/GM4S complex, these synthase complexes will proceed to synthesize GM3 more effectively. On the other hand, GalCer, which is a substrate in GM4 synthesis by GM3/GM4S, is produced in the ER and transported to the Golgi apparatus [12]. It is not clear whether GalCer is transported efficiently to the compartment of GM4 synthesis since the details behind the mechanism of transporting GalCer into Golgi have not been determined. Moreover, overexpression of GM3/GM4S was necessary to detect GM4 in several cell lines expressing GalCer. Under this condition, the amount of free-GM3/GM4S, which is not associated with LacCerS, may have increased. Therefore, this result may suggest that GM4 is synthesized only by

free GM3/GM4S and that the expression machinery of GM4 is independent from that of GM3.

Another possibility is that the stability of GM4 is remarkably lower than that of GM3. GM3 and the ganglioside GM1, which are generally regarded as microdomain markers, exist in distinct microdomians in the native cell membrane [23]. Since the mechanisms behind the formation of these heterogeneous microdomains are at present completely unknown, it is unclear whether GM4 and GM3 are clustering independently. If GM4 molecules in the plasma membrane localize distinctly from the other gangliosides, including GM3, then the degradation rate of the GM4 cluster during the endocytic pathway from the plasma membrane to the lysosome might be much faster than that of GM3. This hypothesis should be clarified by future studies.

GM3/GM4S knock out mice reportedly exhibit several phenotypes, including enhanced insulin sensitivity in skeletal muscle and liver [2], complete hearing loss [24], and deficient $CD4^+$ T-cell activation [25]. GalCer is not expressed in skeletal muscle, liver, or $CD4^+$ T-cells, so GM4 is also not synthesized. In the mouse inner ear, however, not only a-series gangliosides (GM3, GM1, GD1a, GD1b, and GT1b) but also sulfatides (SM3 and SM4), which are synthesized from LacCer and GalCer, respectively, are highly expressed [24]. Although the expression of GalCer was not confirmed in that report, the data nevertheless indicate that GalCer are abundant in the mouse inner ear. Thus, GM4 may also be synthesized in that structure and may be involved in the functional maturation of the cochlea, which is essential for the acquisition and maintenance of hearing function. Consequently, it will be an important subject for future studies to clarify the biological functions of GM4 at the cellular level, and the GM4-reconsituted cells (GM-95/GalCerS/GM3/GM4S cells) established in this study could be useful tools.

Acknowledgments We thank Dr. A. Sweeney for critical reading of this manuscript, Dr. M. Ito for providing RPMI 1846 cells and Dr. Y. Hirabayashi for providing GM-95 cells. This work was supported by Grant-in-Aid for Scientific Research (B; 23370064) (J.I.) and Mizutani Glycoscience Foundation (J.I.).

References

1. Tagami, S., Inokuchi Ji, J., Kabayama, K., Yoshimura, H., Kitamura, F., Uemura, S., Ogawa, C., Ishii, A., Saito, M., Ohtsuka, Y., Sakaue, S., Igarashi, Y.: Ganglioside GM3 participates in the pathological conditions of insulin resistance. J. Biol. Chem. **277**, 3085–3092 (2002)
2. Yamashita, T., Hashiramoto, A., Haluzik, M., Mizukami, H., Beck, S., Norton, A., Kono, M., Tsuji, S., Daniotti, J.L., Werth, N., Sandhoff, R., Sandhoff, K., Proia, R.L.: Enhanced insulin sensitivity in mice lacking ganglioside GM3. Proc. Natl. Acad. Sci. U. S. A. **100**, 3445–3449 (2003)
3. Aerts, J.M., Ottenhoff, R., Powlson, A.S., Grefhorst, A., van Eijk, M., Dubbelhuis, P.F., Aten, J., Kuipers, F., Serlie, M.J., Wennekes, T., Sethi, J.K., O'Rahilly, S., Overkleeft, H.S.: Pharmacological inhibition of glucosylceramide synthase enhances insulin sensitivity. Diabetes **56**, 1341–1349 (2007)
4. Zhao, H., Przybylska, M., Wu, I.H., Zhang, J., Siegel, C., Komarnitsky, S., Yew, N.S., Cheng, S.H.: Inhibiting glycosphingolipid synthesis improves glycemic control and insulin sensitivity in animal models of type 2 diabetes. Diabetes **56**, 1210–1218 (2007)
5. Kabayama, K., Sato, T., Kitamura, F., Uemura, S., Kang, B.W., Igarashi, Y., Inokuchi, J.: TNFalpha-induced insulin resistance in adipocytes as a membrane microdomain disorder: Involvement of ganglioside GM3. Glycobiology **15**, 21–29 (2005)
6. Kabayama, K., Sato, T., Saito, K., Loberto, N., Prinetti, A., Sonnino, S., Kinjo, M., Igarashi, Y., Inokuchi, J.: Dissociation of the insulin receptor and caveolin-1 complex by ganglioside GM3 in the state of insulin resistance. Proc. Natl. Acad. Sci. U. S. A. **104**, 13678–13683 (2007)
7. Chisada, S., Horibata, Y., Hama, Y., Inagaki, M., Furuya, N., Okino, N., Ito, M.: The glycosphingolipid receptor for Vibrio trachuri in the red sea bream intestine is a GM4 ganglioside which contains 2-hydroxy fatty acids. Biochem. Biophys. Res. Commun. **333**, 367–373 (2005)
8. Kuhn, R., Wiegandt, H.: Furthre gangliosode from the human brain. Z. Naturforsch. **19**, 256–257 (1964)
9. Ueno, K., Ando, S., Yu, R.K.: Gangliosides of human, cat, and rabbit spinal cords and cord myelin. J. Lipid Res. **19**, 863–871 (1978)
10. Chiba, A., Kusunoki, S., Obata, H., Machinami, R., Kanazawa, I.: Ganglioside composition of the human cranial nerves, with special reference to pathophysiology of Miller Fisher syndrome. Brain Res. **745**, 32–36 (1997)
11. D'Angelo, G., Polishchuk, E., Di Tullio, G., Santoro, M., Di Campli, A., Godi, A., West, G., Bielawski, J., Chuang, C.C., van der Spoel, A.C., Platt, F.M., Hannun, Y.A., Polishchuk, R., Mattjus, P., De Matteis, M.A.: Glycosphingolipid synthesis requires FAPP2 transfer of glucosylceramide. Nature **449**, 62–67 (2007)
12. Sprong, H., Degroote, S., Nilsson, T., Kawakita, M., Ishida, N., van der Sluijs, P., van Meer, G.: Association of the Golgi UDP-galactose transporter with UDP-galactose:ceramide galactosyltransferase allows UDP-galactose import in the endoplasmic reticulum. Mol. Biol. Cell **14**, 3482–3493 (2003)
13. Chisada, S., Yoshimura, Y., Sakaguchi, K., Uemura, S., Go, S., Ikeda, K., Uchima, H., Matsunaga, N., Ogura, K., Tai, T., Okino, N., Taguchi, R., Inokuchi, J., Ito, M.: Zebrafish and mouse alpha2,3-sialyltransferases responsible for synthesizing GM4 ganglioside. J. Biol. Chem. **284**, 30534–30546 (2009)
14. Uemura, S., Yoshida, S., Shishido, F., Inokuchi, J.: The cytoplasmic tail of GM3 synthase defines its subcellular localization, stability, and in vivo activity. Mol. Biol. Cell **20**, 3088–3100 (2009)
15. Eckhardt, M., Muhlenhoff, M., Bethe, A., Gerardy-Schahn, R.: Expression cloning of the Golgi CMP-sialic acid transporter. Proc. Natl. Acad. Sci. U. S. A. **93**, 7572–7576 (1996)
16. Uemura, S., Kabayama, K., Noguchi, M., Igarashi, Y., Inokuchi, J.: Sialylation and sulfation of lactosylceramide distinctly regulate anchorage-independent growth, apoptosis, and gene expression in 3LL Lewis lung carcinoma cells. Glycobiology **13**, 207–216 (2003)
17. Watarai, S., Kushi, Y., Shigeto, R., Misawa, N., Eishi, Y., Handa, S., Yasuda, T.: Production of monoclonal antibodies directed to Hanganutziu-Deicher active gangliosides, N-glycolylneuraminic acid-containing gangliosides. J. Biochem. **117**, 1062–1069 (1995)
18. Ichikawa, S., Nakajo, N., Sakiyama, H., Hirabayashi, Y.: A mouse B16 melanoma mutant deficient in glycolipids. Proc. Natl. Acad. Sci. U. S. A. **91**, 2703–2707 (1994)
19. Ichikawa, S., Sakiyama, H., Suzuki, G., Hidari, K.I., Hirabayashi, Y.: Expression cloning of a cDNA for human ceramide glucosyltransferase

that catalyzes the first glycosylation step of glycosphingolipid synthesis. Proc. Natl. Acad. Sci. U. S. A. **93**, 4638–4643 (1996)
20. Nakamura, K., Hashimoto, Y., Moriwaki, K., Yamakawa, T., Suzuki, A.: Genetic regulation of GM4(NeuAc) expression in mouse erythrocytes. J. Biochem. **107**, 3–7 (1990)
21. Berselli, P., Zava, S., Sottocornola, E., Milani, S., Berra, B., Colombo, I.: Human GM3 synthase: a new mRNA variant encodes an NH2-terminal extended form of the protein. Biochim. Biophys. Acta **1759**, 348–358 (2006)
22. Giraudo, C.G., Maccioni, H.J.: Ganglioside glycosyltransferases organize in distinct multienzyme complexes in CHO-K1 cells. J. Biol. Chem. **278**, 40262–40271 (2003)
23. Fujita, A., Cheng, J., Hirakawa, M., Furukawa, K., Kusunoki, S., Fujimoto, T.: Gangliosides GM1 and GM3 in the living cell membrane form clusters susceptible to cholesterol depletion and chilling. Mol. Biol. Cell **18**, 2112–2122 (2007)
24. Yoshikawa, M., Go, S., Takasaki, K., Kakazu, Y., Ohashi, M., Nagafuku, M., Kabayama, K., Sekimoto, J., Suzuki, S., Takaiwa, K., Kimitsuki, T., Matsumoto, N., Komune, S., Kamei, D., Saito, M., Fujiwara, M., Iwasaki, K., Inokuchi, J.: Mice lacking ganglioside GM3 synthase exhibit complete hearing loss due to selective degeneration of the organ of Corti. Proc. Natl. Acad. Sci. U. S. A. **106**, 9483–9488 (2009)
25. Nagafuku, M., Okuyama, K., Onimaru, Y., Suzuki, A., Odagiri, Y., Yamashita, T., Iwasaki, K., Fujiwara, M., Takayanagi, M., Ohno, I., Inokuchi, J.: CD4 and CD8 T cells require different membrane gangliosides for activation. Proc. Natl. Acad. Sci. U. S. A. **109**, E336–E342 (2012)

CD4 and CD8 T cells require different membrane gangliosides for activation

Masakazu Nagafuku[a,b], Kaori Okuyama[c], Yuri Onimaru[d], Akemi Suzuki[e], Yuta Odagiri[a], Tadashi Yamashita[f], Katsunori Iwasaki[d,g], Michihiro Fujiwara[d], Motoaki Takayanagi[c], Isao Ohno[c], and Jin-ichi Inokuchi[a,b,g,1]

[a]Division of Glycopathology, Institute of Molecular Biomembrane and Glycobiology, and [c]Department of Pathophysiology, Tohoku Pharmaceutical University, Sendai 981-8558, Japan; [b]Core Research for Evolutional Science and Technology, Japan Science and Technology Agency, Saitama 332-0012, Japan; [d]Department of Neuropharmacology, Faculty of Pharmaceutical Sciences, and [g]Academic, Industrial and Governmental Institute for Aging and Brain Sciences, Fukuoka University, Fukuoka 814-0180, Japan; [e]Institute of Glycoscience, Tokai University, Kanagawa 259-1292, Japan; and [f]Division of Integrated Life Science, Faculty of Advanced Life Science, Hokkaido University, Sapporo 001-0021, Japan

Edited* by Sen-itiroh Hakomori, Pacific Northwest Research Institute, Seattle, WA, and approved December 19, 2011 (received for review September 17, 2011)

Initial events of T-cell activation involve movement of the T-cell receptor into lipid rafts. Gangliosides are major components of lipid rafts. While investigating T-cell activation in ganglioside-deficient mice, we observed that CD4$^+$ and CD8$^+$ T cells required different ganglioside subsets for activation. Activation of CD4$^+$ T cells from GM3 synthase-null mice, deficient in GM3-derived gangliosides, is severely compromised, whereas CD8$^+$ T-cell activation is normal. Conversely, in cells from GM2/GD2 synthase-null mice, expressing only GM3 and GD3, CD4$^+$ T-cell activation is normal, whereas CD8$^+$ T-cell activation is deficient. Supplementing the cells with the corresponding missing gangliosides restores normal activation. GM3 synthase-null mice do not develop experimental asthma. Distinct expression patterns of ganglioside species in CD4$^+$ T and CD8$^+$ T cells, perhaps in uniquely functional lipid rafts, define immune functions in each T-cell subset. Control of ganglioside expression would offer a strategy targeting for specific T-cell subpopulations to treat immune diseases.

glycosphingolipids | repertoire selection

The initial events of T-cell activation involve movement of the T-cell receptor into specialized membrane microdomains known as lipid rafts. The term "lipid rafts" was introduced by Kai Simons and Elina Ikonen, on the basis of the close association of sphingolipids and cholesterol as the detergent resistant complex of signaling molecules present in the membrane microdomains (1). In T lymphocytes, lipid rafts are implicated in signaling from T-cell antigen receptor (TCR) and in localization and function of proteins residing proximal to the receptor, such as coreceptors CD4 and CD8, Src family kinases Lck and Fyn, transmembrane adaptor linker for activation for T cells (LAT), and protein kinase Cθ (2, 3). Gangliosides, sialic acid (SA)-containing glycosphingolipids (GSLs) associated with lipid rafts, are thought to be involved in T-cell activation. For example, following TCR clustering induced by anti-CD3 and anti-CD28 antibodies, polarization of GM1a ganglioside occurs in CD4$^+$ T cells but not in CD8$^+$ T cells (4). In polarized human T cells, asymmetric redistribution results in ganglioside GM3- and GM1a-enriched raft domains segregating to the leading edge and uropod, respectively (5). Additionally, major differences in GM1a expression levels are apparent among cell types or stages of cellular development (6), and at times GM1a expression in certain cell types is much lower than that of other gangliosides (7). Thus, to understand the role of lipid rafts in the differentiation, maturation, and activation of CD4$^+$ T and CD8$^+$ T cells in vivo, it is necessary to understand the ganglioside composition in each respective T-cell subset. To date, however, there has been no report detailing the ganglioside structures in naive or primary T-cell subsets.

In the present study, we analyzed the expression of gangliosides during T-cell differentiation and investigated whether the activation of individual T-cell subsets requires distinct species of gangliosides (Fig. 1*A*). We used two kinds of gene-targeted mice, one carrying disrupted GM3 synthase (GM3S), and so lacking GM3-derived gangliosides (a- and b-series gangliosides) (8), and the other with an altered GM2/GD2 synthase (GM2/GD2S) and expressing only GM3 and GD3 gangliosides while lacking the o-series (9). We found distinct and dramatic changes in ganglioside profiles between primary thymocytes and resting CD4$^+$ T and CD8$^+$ T cells. In particular, CD4$^+$ T cells preferentially express a-series gangliosides, whereas CD8$^+$ T cells express very high levels of o-series gangliosides. Likewise, TCR-dependent activation of CD4$^+$ T cells selectively requires a-series gangliosides, yet for similar activation of CD8$^+$ T cells, o-series gangliosides and not a-series gangliosides are indispensable. Distinct expression patterns of gangliosides in CD4$^+$ T and CD8$^+$ T cells in unique functional lipid rafts may define immune functions in each T-cell subset.

We propose that the repertoire selection from immature thymocytes to mature T-cell subsets is accompanied by selective GSL expression in individual T-cell subsets. This GSL selection process may be indispensable in the formation of distinct and functional lipid rafts in mature T cells.

Results

Distinct Selectivity of Gangliosides Required for CD4$^+$ T- and CD8$^+$ T-Cell Activation. GSLs are built on a ceramide backbone comprising a long-chain amino alcohol, sphingosine, and an amide-linked fatty acid. Gangliosides are SA-containing GSLs (Fig. 1*A*). GM3, the simplest of the "a-series" gangliosides, is synthesized by GM3S, which catalyzes the transfer of SA to the nonreducing terminal galactose (Gal) of lactosylceramide (LacCer). GM3 is altered by GM2/GD2S to form GM2, a downstream a-series ganglioside, or by GD3 synthase to form GD3, the simplest of the "b-series" gangliosides. GM2/GD2S also elongates LacCer to form GA2, the simplest of the "o-series" ganglio-series GSLs. Each branch of GSL biosynthesis is a committed pathway (Fig. 1*A*), so competition between enzymes at a key branch point determines the relative expression levels of o-, a-, and b-series gangliosides.

To investigate functional roles of gangliosides in T-cell development and immunity, we used two types of gene-targeted mice with interrupted ganglioside biosynthesis (Fig. 1*A*). GM3S null mice presumably lack all a- and b-series gangliosides, resulting in LacCer accumulation and compensatory increase of o-series GSLs (8). GM2/GD2S null mice lack all o-series GSLs and all elongated a- and b-series gangliosides, so they accumu-

Author contributions: M.N., A.S., T.Y., K.I., M.F., M.T., I.O., and J.-i.I. designed research; M.N., K.O., Y. Onimaru, A.S., Y. Odagiri, I.O., and J.-i.I. performed research; M.N., K.O., A.S., I.O., and J.-i.I. analyzed data; and M.N., A.S., I.O., and J.-i.I. wrote the paper.

The authors declare no conflict of interest.

*This Direct Submission article had a prearranged editor.

[1]To whom correspondence should be addressed. E-mail: jin@tohoku-pharm.ac.jp.

See Author Summary on page 1832.

This article contains supporting information online at www.pnas.org/lookup/suppl/doi:10.1073/pnas.1114965109/-/DCSupplemental.

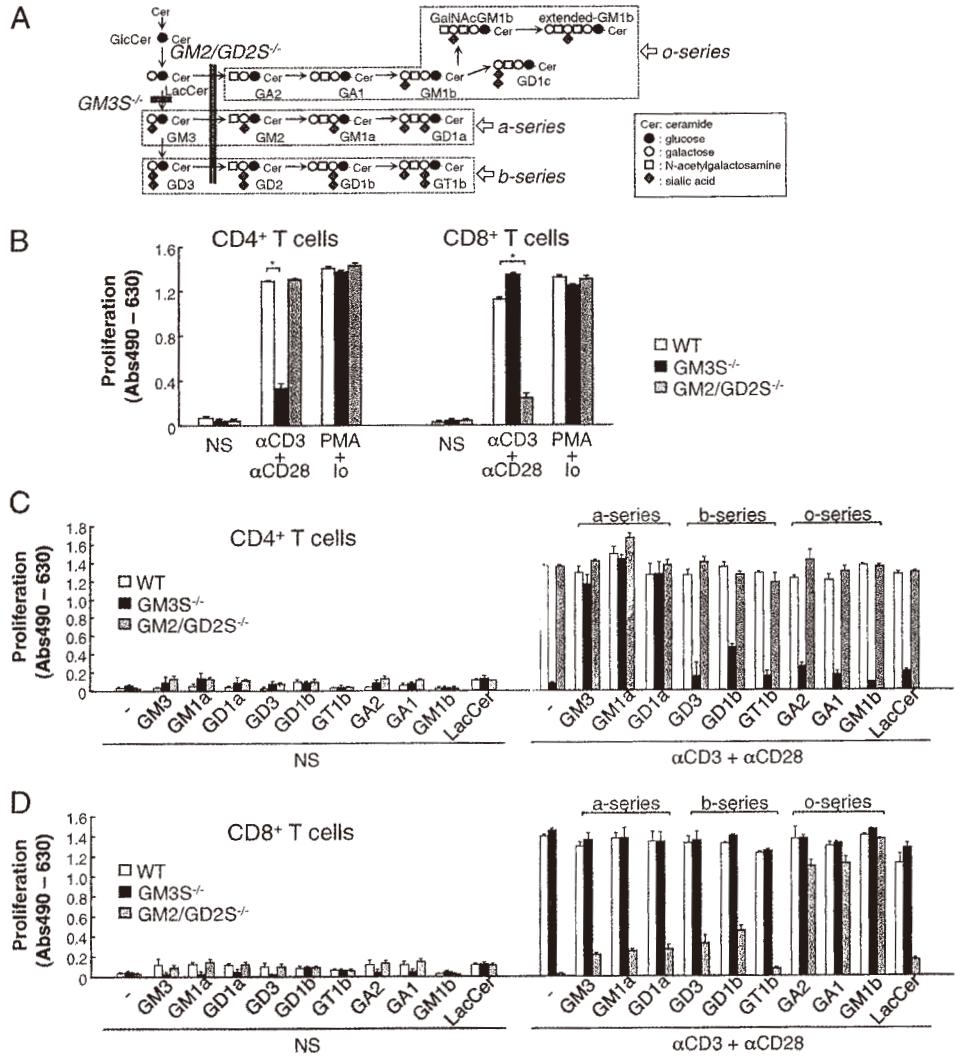

Fig. 1. Distinct selectivity of ganglioside species for CD4$^+$ T and CD8$^+$ T activation. Ganglio-series glycosphingolipids are synthesized from ceramide and are divided into o-, a-, and b-series species. (*B*) Activation of CD4$^+$ T and CD8$^+$ T cells upon TCR-mediated stimulation. Purified peripheral CD4$^+$ T and CD8$^+$ T cells from WT, GM3S null, and GM2/GD2S null mice (20–25 mice each) were left unstimulated (NS) or were stimulated for 72 h with anti-CD3 antibody plus anti-CD28 antibody or with PMA plus ionomycin (Io). Proliferative responses were determined after an 8-h pulse with XTT reagent. One representative of three experiments is presented. *$P < 0.01$. (*C* and *D*) Functional rescue experiments by supplementation of gangliosides. Purified peripheral CD4$^+$ T (*C*) and CD8$^+$ T (*D*) cells from WT, GM3S null, and GM2/GD2S null mice were pretreated for 2 h with the indicated GSL (5 μg/mL). The cells were left unstimulated (NS) or were stimulated for 72 h with anti-CD3 antibody plus anti-CD28 antibody. Proliferative responses were determined after an 8-h pulse with XTT reagent. Data are representative of more than three experiments.

late LacCer and express only GM3 and GD3 gangliosides (9), as described later in detail.

Initial analysis of GM3S null and GM2/GD2S null mice did not reveal any obvious alteration in the cellularity of the lymphoid organs (Fig. S1*A*). To assess T-cell development, we performed flow cytometry for CD4 and CD8 on thymocytes and found similar distribution patterns in the thymocyte populations of the null and wild-type (WT) mice (Fig. S1*B*). In the spleen and lymph nodes, there was no obvious alteration in relative distribution within the T-cell and B-cell populations (Fig. S1*C*) and the CD4$^+$ T- and CD8$^+$ T-cell populations (Fig. S1*D*). These data indicate no gross defects in T-cell development despite the altered ganglioside expression. Then we examined the T-cell activation in purified peripheral CD4$^+$ T and CD8$^+$ T cells of the two null mice (Fig. 1*B*). Remarkably, CD4$^+$ T cells (but not CD8$^+$ T cells) from GM3S null mice exhibited severe defects in their proliferative response to the anti-CD3/anti-CD28 antibody mixture, but maintained a normal response to phorbol myristate acetate (PMA) plus ionomycin (Io). Conversely, CD8$^+$ T cells (but not CD4$^+$ T cells) from GM2/GD2S null mice exhibited similar severe defects in TCR-mediated activation when stimulated with the antibody mixture. Following TCR stimulation with the antibody mixture, both IL-2 production and IFN-γ production were severely reduced in both GM3S null CD4$^+$ T cells and GM2/GD2S null CD8$^+$ T cells (Fig. S2). Responses to an alloantigen, a superantigen, and a specific antigen peptide were similar to those observed with the anti-CD3/anti-CD28 mixture (Fig. 2). In contrast to T cells, splenic B cells isolated from GM3S null and GM2/GD2S null mice exhibited no obvious alterations in proliferative responses to various concentrations of anti-IgM antibody and lipopolysaccharide (Fig. S3). In experiments to determine which gangliosides have an essential role in

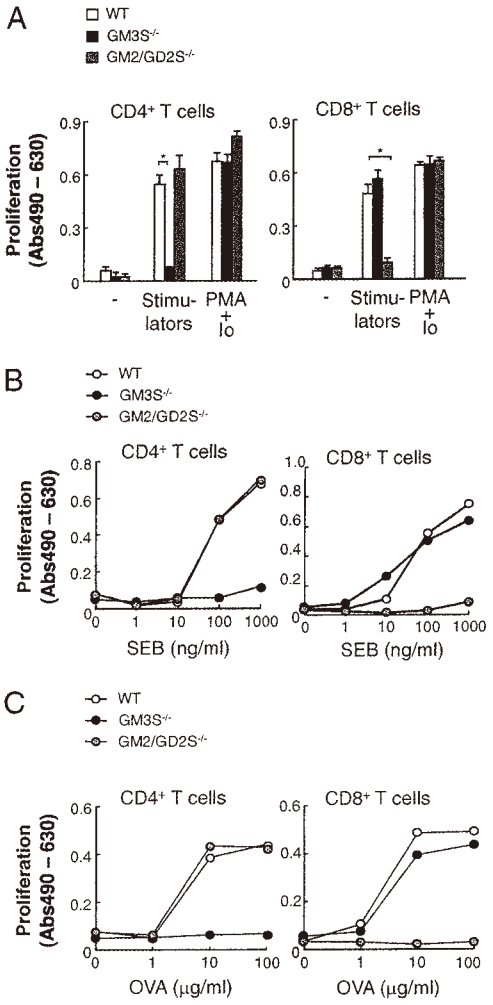

Fig. 2. Antigen-specific responses of $CD4^+$ T and $CD8^+$ T cells of GM3S null and GM2/GD2S null mice. (*A* and *B*) Peripheral $CD4^+$ T and $CD8^+$ T cells were purified from WT, GM3S null, and GM2/GD2S null mice. (*A*) Mixed lymphocyte reaction. The cells were left untreated (–), mixed with MMC-treated MHC-mismatched splenocytes from BALB/c as stimulators, or treated with PMA plus ionomycin (Io) for 72 h. (*B*) Superantigen-induced activation. The indicated cells were stimulated with indicated amounts of *Staphylococcal* enterotoxin B (SEB) and MMC-treated WT splenocytes as APCs. (*C*) Antigen-specific T-cell responses. Purified $CD4^+$T and $CD8^+$T cells from WT, GM3S null and GM2/GD2S null mice were obtained 7 d after immunization with TNP-OVA. The resulting cells were cocultured with MMC-treated WT splenocytes as APCs, together with the indicated amounts of OVA peptide. Proliferative responses were determined after an 8-h pulse with XTT reagent. Data are representative of three experiments. $*P < 0.01$ vs. WT.

TCR-mediated activation of T-cell subsets, $CD4^+$ T cells and $CD8^+$ T cells from WT, GM3S null, or GM2/GD2S null mice were pretreated with gangliosides followed by anti-CD3/anti-CD28 stimulation. Proliferative responses of GM3S null $CD4^+$ T cells were restored following pretreatment with any of the a-series species (GM3, GM1, and GD1a), but were not restored with any o- or b-series species (Fig. 1*C*). Conversely, the proliferative responses of GM2/GD2S null $CD8^+$ T cells were restored following pretreatment with any of the o-series species (GA2, GA1, and GM1b), but not with any of the a- or b-series species (Fig. 1*D*). Importantly, the gangliosides themselves had no effect in the absence of stimulation. These results indicate that o-series ganglioside expression is essential for TCR-mediated activation of $CD8^+$ T cells and a-series ganglioside expression is indispensable for that of $CD4^+$ T cells. Data from these lipid-restoring experiments demonstrate that a different series of gangliosides is necessary in each T-cell subset for proper T-cell activation following TCR stimulation. These data suggest that different species of gangliosides are essential in TCR-mediated activation of $CD4^+$ T cells vs. $CD8^+$ T cells.

We compared ganglioside profiles among thymocytes and peripheral $CD4^+$ T and $CD8^+$ T cells from WT, GM3S null, and GM2/GD2S null mice using TLC (Fig. 3). Acidic lipid fractions from thymocytes and $CD4^+$ T and $CD8^+$ T cells were separated by TLC, and lipids were stained with HRP-conjugated cholera toxin B subunit (CTx-B) (Fig. 3*A*). CTx-B recognizes a monosialo-ganglio-triose moiety, Galβ1-3GalNAcβ1-4 (SAα2-3)Galβ1-, which is found in GM1a, fucosylated GM1a, and GalGalNAcGM1b (extended-GM1b) (6). In WT $CD4^+$ T cells, GM1a was dominantly expressed, but extended-GM1b was expressed much more than GM1a in WT $CD8^+$ T cells. The thymocytes and peripheral $CD4^+$ T and $CD8^+$ T cells of GM3S null mice lacked a-series GM1a and expressed o-series extended GM1b, whereas the cells from GM2/GD2S null mice did not express either one (Fig. 3*A*). GM2/GD2S null cells also did not express complex gangliosides but did express GM3 and GD3 (Fig. 3*B*). None of the cells from GM3S null mice exhibited any accumulation of LacCer (Fig. 3*C*). In contrast, the cells from GM2/GD2S null mice exhibited an absence of GA1 and an accumulation of LacCer (Fig. 3*C*). Taken together, these results indicate that the ganglioside expression patterns of GM3S null mice, compared with those of WT cells, switch from an a-series–rich pattern to an o-series–rich pattern. GM2/GD2S null mice express LacCer, GM3, and GD3 in thymocytes and peripheral $CD4^+$ T cells, but only LacCer in $CD8^+$ T cells.

Differentiation from Thymocytes to Mature T-Cell Subsets Is Accompanied by Selective GSL Expression. We examined the expression of *GM3S* and *GM2/GD2S* genes in thymocytes and peripheral $CD4^+$ T and $CD8^+$ T cells from WT mice. *GM3S* expression was increased to 180% in $CD4^+$ T cells and was decreased to 30% in $CD8^+$ T cells compared with expression in thymocytes (Fig. 4*A*, *Left*). *GM2/GD2S* expression was markedly increased in both $CD4^+$ T and $CD8^+$ T cells compared with thymocytes (Fig. 4*A*, *Right*). These gene expression patterns suggest that $CD4^+$ T cells dominantly express a-series gangliosides due to up-regulation of *GM3S* and $CD8^+$ T cells would carry o-series GSLs due to down-regulation of *GM3S* and up-regulation of *GM2/GD2S* expression.

Liquid chromatography (LC)-MS analysis demonstrated that thymocytes and peripheral $CD4^+$ T and $CD8^+$ T cells predominantly express GM1, GD1, GalNAcGM1b, and extended GM1b. Whereas GM1 and GD1 levels were comparable in all three cell types, GalNAcGM1b and extended-GM1b levels were dramatically increased in the $CD8^+$ T-cell subset (Fig. 4*B*, and Fig. S4 *A* and *B*). MS^2 analysis distinguished positional isomers of GM1 (GM1a and GM1b) and GD1 (GD1b and GD1c) and their ratios (Fig. S4 *C*–*E*, and Fig. S5). GD1a was not detectable in any of the three cell types. Consistent with CTx-B TLC staining (Fig. 3*A*), LC-MS indicates that the expression pattern of ganglioside species is altered during T-cell development, and o-series and a-series gangliosides are dominantly expressed in $CD8^+$ T and $CD4^+$ T cells, respectively (Fig. 4*B*).

Airway Inflammatory Responses in GM3S Null Mice. Allergic airway inflammation is tightly regulated by adaptive immunity, in which $CD4^+$ T cells play a crucial role via Th2 cytokine production. We examined allergic airway responses induced by inhalation of ovalbumin (OVA) in OVA-sensitized mice (experimental asthma). OVA challenge induced extensive mucus hypersecretion, a cardinal feature of asthma, in WT but not in the GM3S null

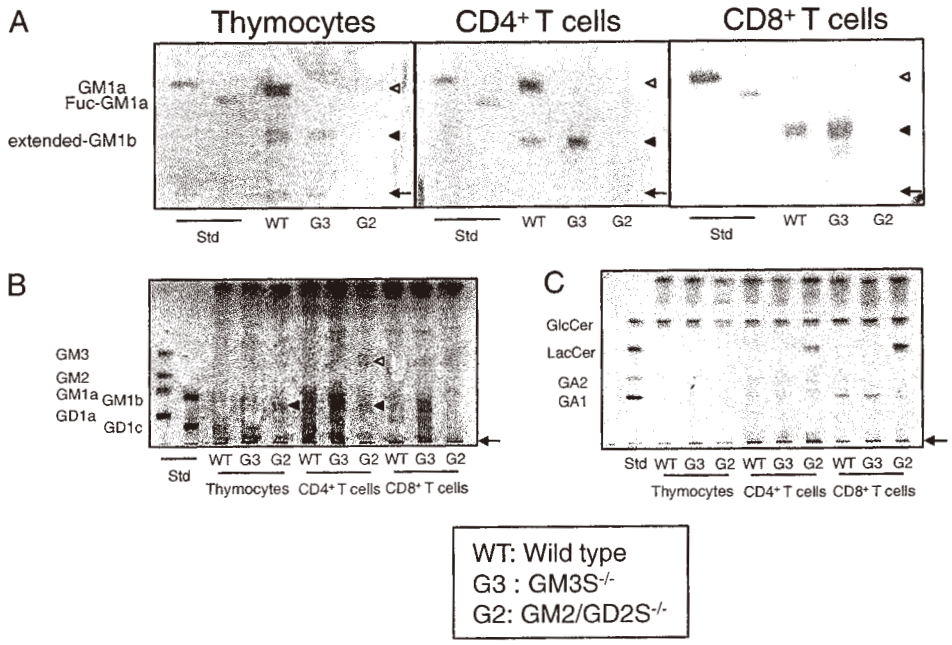

Fig. 3. Glycosphinogolipid expression patterns in thymocytes and peripheral primary CD4$^+$ T and CD8$^+$ T cells in WT, GM3S$^{-/-}$, and GM2/GD2S$^{-/-}$ mice. Neutral and acidic lipids were obtained from thymocytes, CD4$^+$ T cells, and CD8$^+$ T cells of WT, GM3S$^{-/-}$ (G3), and GM2/GD2S$^{-/-}$ (G2) mice. (*A*) The acidic lipids were separated on HPTLC plates and were stained with HRP-conjugated choleragenoid (CTx-B). An arrow indicates the origin for TLC. White and black arrowheads indicate GM1a and extended-GM1b bands, respectively. (*B* and *C*) Acidic (*B*) and neutral (*C*) lipids were separated on HPTLC plates and visualized with orcinol-sulfuric acid. White and black arrowheads in (*B*) indicate GM3 and GD3 bands, respectively. Fuc-GM1a, fucosylated GM1a; std, standard lipids.

mice (Fig. 5*A*). Although both types of mice challenged with OVA exhibited airway infiltration of inflammatory cells including eosinophils and lymphocytes, the numbers of infiltrating cells were significantly lower in GM3 null mice (Fig. 5*B*). Serum OVA-specific IgE levels were greatly increased on days 3 and 5 after OVA challenge in WT mice, but not in GM3S null mice (Fig. 5*C*). Decreased levels of Th2 cytokines in the bronchoalveolar lavage (BAL) fluids were also observed in GM3S null mice (Fig. 5*D*). In adoptive transfer experiments, CD4$^+$ T cells isolated from OVA-sensitized WT and GM3S null mice were transferred into naive WT mice, and the recipient mice were challenged with OVA. Infiltration of inflammatory cells, particularly eosinophils and lymphocytes, was suppressed in the recipient mice of CD4$^+$ T cells from GM3S null mice (Fig. 5*E*). In the recipient mice of CD4$^+$ T cells from GM2/GD2 synthase null mice, there was no difference in the numbers of infiltrated cells compared with those of recipient mice of CD4$^+$ T cells from WT mice (Fig. 5*F*). These results indicate that the immune function of CD4$^+$ T cells in vivo is selectively deficient in GM3S null mice.

Discussion

In the present study, we determined in great detail the ganglioside expression patterns of primary T cells, specifically those of immature thymocytes and mature peripheral CD4$^+$ T cells and CD8$^+$ T cells. Our most important finding was that distinct expression of gangliosides exists in CD4$^+$ T cells and CD8$^+$ T cells, and defines the immune function of each T-cell subset. CD4$^+$ T cells preferentially express a-series gangliosides, and cells isolated from GM3S null mice exhibit severe impairments in TCR-mediated cytokine production and clonal expansion, but can be rescued by reintroducing a-series gangliosides. Similarly, CD8$^+$ T cells preferentially express o-series GSLs, and cells isolated from GM2/GD2S null mice exhibit severe impairments in TCR-mediated cytokine production and clonal expansion. They can be rescued by reintroducing o-series gangliosides. These results suggest that CD4$^+$ T-cell and CD8$^+$ T-cell subsets require a-series and o-series ganglioside expression, respectively, to undergo activation upon TCR ligation.

Why are CD4$^+$ T cells and CD8$^+$ T cells dependent on expression of distinct gangliosides for proper immune function?

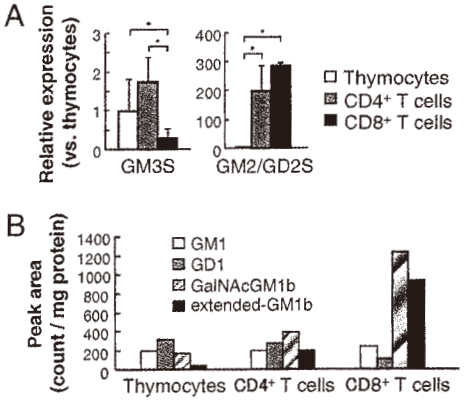

Fig. 4. Distinct expression of ganglioside species during T-cell repertoire selection. (*A*) Gene expression of GM3S and GM2/GD2S was determined by quantitative real-time PCR analysis. Data represent the relative gene expression in peripheral T-cell subsets compared with that in thymocytes (set to 1.0 separately for each target gene). *$P < 0.05$. (*B*) Gangliosides of mouse thymocytes and CD4$^+$ and CD8$^+$ T cells analyzed by LC-MS. Peak areas of GM1, GD1, GalNAcGM1b, and extended-GM1b were determined in the mass chromatograms obtained by C30 column chromatography-MS with GM3 (NeuAc, d18:1–14:0) as an internal standard. GM1 includes GM1a [*N*-glycolylneuraminic acid (NeuGc)] and GM1b (NeuGc), each carrying d18:1–16:0, –18:0, –20:0, –22:0, –24:1, and –24:0. GD1 includes GD1b (NeuGc) and GD1c (NeuGc) each carrying d18:1–16:0, –18:0, –20:0, –22:0, –24:1, and –24:0. GD1a was not detectable in any of the three cell types.

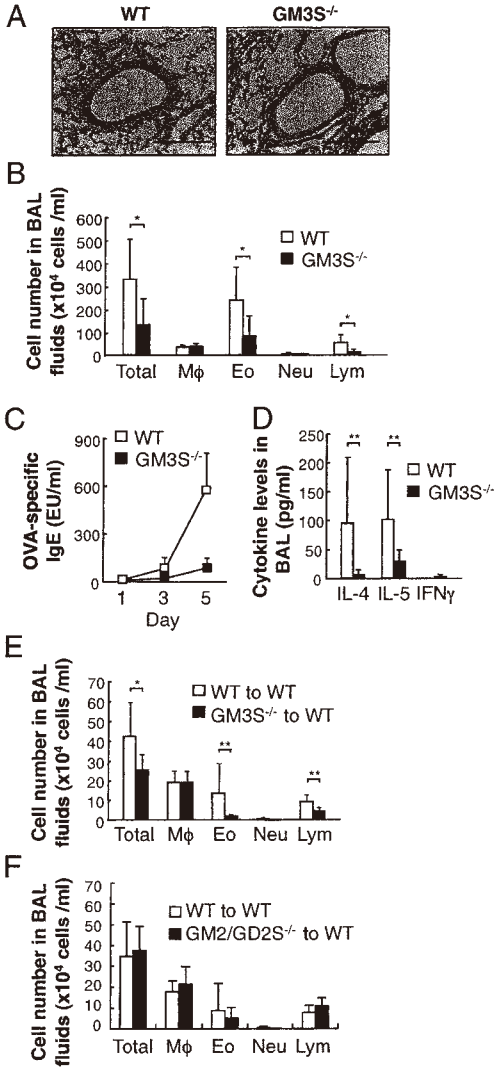

Fig. 5. Allergic airway inflammation in GM3S null mice. (*A* and *B*) Sensitized WT and GM3S null mice were challenged with OVA. Five days after the challenge, BAL fluid and lung tissues were collected. The representative lung sections stained with PAS (*A*) and the numbers of total cells (Total), macrophages (Mϕ), eosinophils (Eo), neutrophils (Neu), and lymphocytes (Lym) in BAL fluids (*B*) are shown. (WT, $n = 7$; GM3S null, $n = 9$). (Scale bar in *A*, 200 μm.) (*C*) Sera from sensitized WT and GM3S null mice were obtained at 1 (WT, $n = 6$; GM3S null, $n = 6$), 3 (WT, $n = 6$; GM3S null, $n = 6$) and 5 d (WT, $n = 6$; GM3S null, $n = 6$) after OVA challenge. OVA-specific IgE in the sera was measured. (*D*) Cytokine levels in BAL fluid (WT, $n = 6$; GM3S null, $n = 6$) were measured 1 d after challenge. (*E* and *F*) Cell numbers in BAL fluid of mice adoptively transferred with $CD4^+$ T cells. $CD4^+$ T cells from sensitized WT and GM3S null mice (*E*) or GM2/GD2S null mice (*F*) were transferred to naive WT mice. BAL fluid was obtained from the recipient mice 5 d after OVA challenge [(*E*) WT recipient, $n = 6$; GM3S null recipient, $n = 7$; (*F*) WT recipient, $n = 10$; GM2/GD2S null recipient, $n = 6$]. The numbers of total cells (Total), macrophages (Mϕ), eosinophils (Eo), neutrophils (Neu), and lymphocytes (Lym) in BAL fluid were counted. $^*P < 0.05$, $^{**}P < 0.01$.

Although there are some commonalities between the mechanisms of TCR-mediated signaling in $CD4^+$ T cells and $CD8^+$ T cells, the two subsets do have different cellular and molecular modifications. CD4 and CD8 can localize to lipid rafts by palmitoylation in their juxtamembrane region (10, 11), yet raft localization seems not to be determined by lipid modification alone (11, 12). To ensure that CD4 and CD8 undergo proper intracellular trafficking and successful localization on the plasma membrane, it might be vital for CD4/CD8 to interact with rafts carrying a specific ganglioside. CD28, a B7-type costimulatory molecule, provides functional differences between $CD4^+$ T cells and $CD8^+$ T cells (13, 14). In human and mouse $CD4^+$ T cells, CD28 promotes the clustering of CTx-B–detectable rafts at the immunological synapse through its downstream signaling molecule protein kinase Cθ (15). However, $CD8^+$ T cells do not reorient CTx-B–detectable rafts to the T-cell/antigen-presenting cell (APC) interface during activation (4, 16). Considering the combined information, we speculate that ganglioside compositions in rafts necessary for signaling events mediated by TCR and costimulatory molecules differ between $CD4^+$ T cells and $CD8^+$ T cells.

Ganglioside expression in primary T cells has previously been studied using biochemical analyses (TLC and HPLC) of whole T-cell populations. However, whole T-cell populations are truly a "mixed population," so any such results would be of limited value to study specific T-cell subsets. In contrast, we separated $CD4^+$ T cells and $CD8^+$ T cells from cell mixtures isolated from lymph nodes and spleen and then performed TLC and LC-MS analyses. Previously, FACS analyses with monoclonal antibodies (mAbs) against several ganglioside species determined that mature peripheral $CD4^+$ T cells and $CD8^+$ T cells express differential species of gangliosides (17, 18). Our LC-MS analysis (Fig. 4*B* and Figs. S4 and S5) demonstrated that expression of GalNAcGM1b and extended-GM1b is much higher in $CD8^+$ T cells than in $CD4^+$ T cells. $CD4^+$ T cells express a larger amount of GD1c than $CD8^+$ T cells do.

Staining with CTx-B, commonly used to detect GM1a and visualize rafts, has demonstrated that $CD8^+$ T cells express higher levels of GM1a in the rafts than $CD4^+$ T cells (19). However, this toxin also reacts to other gangliosides including fucosylated-GM1a and extended-GM1b, both of which have a monosialo-ganglio-triose structure, Galβ1-3GalNAcβ1-4(SAα2-3)Galβ1- (6). In fact, we were able to detect two CTx-B–reactive gangliosides, GM1a and extended GM1b in T cells with different quantities in individual T-cell subsets (Fig. 3*A*). The presence in a single cell of a variety of rafts with different gangliosides has been suggested (4, 5). Cross-linking gangliosides using CTx-B or a homolog, the heat-labile enterotoxin of *Escherichia coli*, can induce apoptosis in $CD8^+$ T cells but not in $CD4^+$ T cells (20), which results from the induction of caspase-dependent signaling caused by activation of NF-κB and c-Myc (20). Although this process is known to proceed in a Fas- and p55 tumor necrosis factor receptor-independent pathway (21), the events in rafts following the ganglioside cross-linking remain undetermined. Considering the differences in the expression of CTx-B–binding ganglioside species between $CD4^+$ T cells and $CD8^+$ T cells (Fig. 3*A*), it seems possible that apoptosis by CTx-B cross-linking may involve extended-GM1b rafts and not GM1a rafts. This result strongly suggests that each T-cell subset has unique rafts in the plasma membrane and that these rafts provide distinct functions in different intracellular events following receptor-mediated stimulation.

FACS analyses have revealed that $CD4^+$ T cells and $CD8^+$ T cells each include subpopulations expressing a particular GSL not observed in the rest of the population. GA1-positive $CD8^+$ T cells exhibit more robust activation via the TCR and play a critical role in CD40/CD28 costimulated and blockade-resistant allograft rejection, compared with GA1-negative $CD8^+$ T cells (22, 23). These findings imply that each subpopulation of $CD4^+$ T cells and $CD8^+$ T cells has a unique ganglioside expression pattern in its rafts, which may be responsible for exerting specific functions of Th and Tc effector cells. GA1-positive mouse $CD8^+$ T cells produce higher levels of IFN-γ in vitro upon TCR stimulation than GA1-negative $CD8^+$ T cells, and both clonal expansion of $CD8^+$ T cells and cytotoxic T-cell–

dependent allograft rejection are suppressed by administration of anti-GA1 mAb in vivo (22). It remains unclear whether, in addition to GA1, the other o-series species expressed in primary $CD8^+$ T cells are essential for TCR-mediated activation. In mouse $CD4^+$ T cells, few studies have addressed whether expression of a-series gangliosides is indispensable for TCR-mediated activation. Human $CD4^+$ T cells isolated from peripheral blood mainly express GM3 (24), which would form GM3-containing rafts available as a platform for TCR signal transduction. The importance of GM3-containing rafts may be corroborated by the observation that GM3 forms a complex with CD4 and Lck on plasma membranes and is coimmunoprecipitated with ZAP-70 after cross-linking with anti-CD3 plus anti-CD28 mAb (24, 25). Consequently, the future challenge will be to examine immune responses in primary T-cell subpopulations separated on the basis of ganglioside species.

Mouse $CD4^+$ T cells and $CD8^+$ T cells activated by anti-CD3 antibody exhibit different profiles for *N*-linked glycans (26). In addition, differentially *N*-glycosylated TCR complexes have been observed in $CD4^+$ T cells compared with $CD8^+$ T cells, which might affect the functional avidity of TCR-transduced T cells (27, 28). The CD4 and CD8 coreceptors, which enhance the TCR–MHC interaction upon binding, have also been shown to be glycosylated (29). These findings, combined with multiple lines of evidence that gangliosides interact with *N*-linked glycans of glycoproteins (30), suggest that a specific ganglioside species expressed on the plasma membrane of $CD4^+$ T and $CD8^+$ T cells might be responsible for the interaction between the TCR and CD4/CD8, to ensure the induction of proper TCR signaling.

Roles of GSLs in TCR signaling and T-cell activation have also been studied using inhibitors of GSL biosynthesis (31). We previously demonstrated that treatment of Jurkat cells with D-*threo*-1-phenyl-2-decanoylamino-3-morpholino-1-propanol (D-PDMP), an inhibitor of GlcCerS (32), preferentially reduces the levels of GSLs in rafts without affecting SM or cholesterol levels. The alteration of raft lipid content results in the up-regulation of TCR signaling via GPI-anchored protein (31). In contrast, treatment of human peripheral blood lymphocytes with this inhibitor attenuated TCR signaling and T-cell activation, indicated by reduction in the expression of markers for T-cell activation and IFN-γ secretion (33).

Activated human T cells are increased in GM1a levels (34, 35). Studies in cells from patients with systemic lupus erythematosus, an autoimmune rheumatic disease characterized by abnormalities in T-cell activation, have determined that the expression of a raft-associated ganglioside, GM1a, is increased in $CD4^+$ T cells, but not in $CD8^+$ T cells, compared with controls (36, 37). It is thought that GM1a expression is enhanced in self-reactive $CD4^+$ T cells, which causes persistence of abnormal cell activation (37, 38). We demonstrated that allergic airway responses caused by OVA inhalation were improved in GM3S null mice, which lack GM1a, resulting in dysfunction of $CD4^+$ T cells. This finding, as well as a recent report in which airway inflammation is suppressed by administration of antisense oligonucleotides against GM3S (39), suggests that inhibition of a-series ganglioside synthesis would be a powerful choice for a treatment of allergic airway diseases.

Recently, novel $CD4^+$ T-cell subsets, in addition to Th1 and Th2 cells, Th17 and regulatory T (Treg), have been described. In allergic airway inflammation, the balance between effector Th2 cells and suppressive Treg cells is skewed toward Th2 predominance (40). Th17 cells have been suggested to contribute to neutrophilic, steroid-resistant severe asthma and to enhance Th2-mediated airway inflammation, although a role for the cells in asthma remains to be determined (41). Reportedly, GM3S null mice exhibit a decreased number of Th17 cells skewed by in vitro culture (42). Because the adoptive transfer experiments confirmed the marked reduction of allergic responses in WT mice that received a whole $CD4^+$ T-cell population from sensitized GM3S null mice (Fig. 5*E*), we are underway to identify which $CD4^+$ T-cell subset is affected in GM3S null mice in vivo.

The present study demonstrates that the functional repertoire selection from double-positive ($CD4^+CD8^+$) to single-positive cells is accompanied by selective GSL expression in individual T-cell subsets and this GSL selection process would be critical for the formation of a functional microcluster and/or lipid rafts in mature T cells. These findings may open up a strategy for targeting specific T-cell subpopulations to treat immune diseases by controlling ganglioside expression in lipid rafts.

Materials and Methods

Experimental Animals. All animals were maintained in accordance with the guidelines of the Tohoku Pharmaceutical University for the care and use of laboratory animals. C57BL/6 mice were obtained from Japan SLC. The GM3S null and GM2/GD2S null mice were generated as previously described (8, 43). Both types of null mice were backcrossed with C57BL/6 mice over >11 generations. Mice were analyzed for the *GM3S* and *GM2/GD2S* genotypes by PCR as described previously (8, 43).

T-Cell Purification. Thymus, spleen, and lymph nodes were collected from WT, GM3S null, and GM2/GD2S null mice. Detailed methods can be found in *SI Materials and Methods*.

T-Cell Activation. For antibody-mediated activation, T-cell subsets purified by negative selection were incubated with 0.1 μg/mL of anti-CD3ε antibody (145-2C11) in the presence of 0.2 μg/mL of anti-CD28 (PV-1) antibody for 72 h. For GSL supplementation experiments the cells were pretreated with the indicated GSLs for 2 h before TCR-mediated stimulation. For the antigen-specific proliferative response assays, $CD4^+$ T cells and $CD8^+$ T cells were prepared from the spleen 7 d after immunization with OVA conjugated with trinitrophenyl (TNP) (Biosearch Technologies). The cells were cocultured with mitomycin C (MMC)-treated WT splenocytes for 72 h in the presence or absence of TNP-OVA antigen. For mixed lymphocyte reactions (MLR), $CD4^+$ T and $CD8^+$ T cells were cocultured for 72 h with MMC-treated splenocytes from BALB/c mice. Cell proliferation was measured by 2,3-bis-(2-methoxy-4- nitro-5-sulfophenyl)-2H-tetrazolium-5-carboxanilide (XTT) assay with a cell proliferation kit (MD Biosciences), according to the manufacturer's instructions.

Allergen-Induced Airway Inflammation. Airway inflammation was generated as previously described (44). Detailed methods can be found in *SI Materials and Methods*.

Preparation of $CD4^+$ T Cells for Adoptive Transfer. On day 17, spleens collected from sensitized WT, GM3S null, and GM2/GD2S null mice were excised, and the splenocytes were disaggregated. The washed splenocytes were resuspended and cultured in the presence of 200 μg/mL OVA. Three days after the culture, $CD4^+$ T cells were purified by positive selection on an autoMACS separator (Miltenyi Biotec), using anti-mouse CD4 (L3T4) MicroBeads (Miltenyi Biotec) according to the manufacturer's protocol. The $CD4^+$ T cells (2×10^6 cells/ 200 μL in saline) were transferred to naive WT mice by tail vein injection. Three days after the injection, the recipient mice were aerosol challenged; BAL fluids were collected 5 d after the challenge as described above.

ELISA. Concentrations of IL-2 and IFN-γ in culture supernatants were measured by ELISA as described elsewhere (45), using two types of anti-mouse IL-2 mAbs and anti-mouse IFN-γ mAb. Serum levels of OVA-specific IgE were measured with ELISA according to published methods (42). IL-4 and IL-5 contents in BAL fluid were measured using an ELISA kit (R&D Systems) according to the manufacturer's protocol.

Lipid Analysis. Lipid analysis was performed as described previously (31). Detailed methods can be found in *SI Materials and Methods*.

Liquid Chromatography–Mass Spectrometry (LC-MS). LC-MS analyses of ganglioside species were performed as described previously (46) with modifications as follows. Detailed methods can be found in *SI Materials and Methods*.

Quantitative Real-Time PCR. Total RNA was isolated using TRI Reagent (Molecular Research Center). Detailed information can be found in *SI Materials and Methods*.

Statistics. Values in the text are the means ± SD. Data were compared using Student's *t* test for two-group comparison or ANOVA for multigroup comparison. Significant differences were post hoc analyzed using Scheffé's test. Differences were considered significant at $P < 0.05$.

ACKNOWLEDGMENTS. We thank Shiro Ono and Yoshiko Mori for helpful technical advice and Elizabeth A. Sweeney and James C. Paulson for critical review of the manuscript. We also thank Yukari Tamekawa and Masumi Toyosawa for assistance with mouse breeding and genotyping and Masaki Saito for providing the gene-targeting mice. This work was supported by research grants from the Core Research for Evolutional Science and Technology division of the Japan Science and Technology Agency (to J.-i.I. and M.N.), a Grant-in-Aid for Scientific Research (B) (to J.-i.I.), the Mizutani Research Foundation for Glycoscience (J.-i.I.), The Naito Foundation (J.-i.I.), and the ONO Medical Research Foundation (J.-i.I.).

1. Simons K, Ikonen E (1997) Functional rafts in cell membranes. *Nature* 387:569–572.
2. Dykstra M, Cherukuri A, Sohn HW, Tzeng SJ, Pierce SK (2003) Location is everything: Lipid rafts and immune cell signaling. *Annu Rev Immunol* 21:457–481.
3. Harder T, Rentero C, Zech T, Gaus K (2007) Plasma membrane segregation during T cell activation: Probing the order of domains. *Curr Opin Immunol* 19:470–475.
4. Kovacs B, et al. (2002) Human CD8$^+$ T cells do not require the polarization of lipid rafts for activation and proliferation. *Proc Natl Acad Sci USA* 99:15006–15011.
5. Gómez-Móuton C, et al. (2001) Segregation of leading-edge and uropod components into specific lipid rafts during T cell polarization. *Proc Natl Acad Sci USA* 98: 9642–9647.
6. Nakamura K, Suzuki M, Inagaki F, Yamakawa T, Suzuki A (1987) A new ganglioside showing choleragenoid-binding activity in mouse spleen. *J Biochem* 101:825–835.
7. Degroote S, Wolthoorn J, van Meer G (2004) The cell biology of glycosphingolipids. *Semin Cell Dev Biol* 15:375–387.
8. Yoshikawa M, et al. (2009) Mice lacking ganglioside GM3 synthase exhibit complete hearing loss due to selective degeneration of the organ of Corti. *Proc Natl Acad Sci USA* 106:9483–9488.
9. Takamiya K, et al. (1996) Mice with disrupted GM2/GD2 synthase gene lack complex gangliosides but exhibit only subtle defects in their nervous system. *Proc Natl Acad Sci USA* 93:10662–10667.
10. Balamuth F, Brogdon JL, Bottomly K (2004) CD4 raft association and signaling regulate molecular clustering at the immunological synapse site. *J Immunol* 172: 5887–5892.
11. Pang DJ, Hayday AC, Bijlmakers MJ (2007) CD8 raft localization is induced by its assembly into CD8alpha beta heterodimers, not CD8alpha alpha homodimers. *J Biol Chem* 282:13884–13894.
12. Popik W, Alce TM (2004) CD4 receptor localized to non-raft membrane microdomains supports HIV-1 entry. Identification of a novel raft localization marker in CD4. *J Biol Chem* 279:704–712.
13. Kroczek RA, Mages HW, Hutloff A (2004) Emerging paradigms of T-cell co-stimulation. *Curr Opin Immunol* 16:321–327.
14. Greenwald RJ, Freeman GJ, Sharpe AH (2005) The B7 family revisited. *Annu Rev Immunol* 23:515–548.
15. Bi K, et al. (2001) Antigen-induced translocation of PKC-theta to membrane rafts is required for T cell activation. *Nat Immunol* 2:556–563.
16. O'Keefe JP, Blaine K, Alegre ML, Gajewski TF (2004) Formation of a central supramolecular activation cluster is not required for activation of naive CD8+ T cells. *Proc Natl Acad Sci USA* 101:9351–9356.
17. Marusić A, Markotić A, Kovacić N, Müthing J (2004) Expression of glycosphingolipids in lymph nodes of mice lacking TNF receptor 1: Biochemical and flow cytometry analysis. *Carbohydr Res* 339:77–86.
18. Nakamura K, Suzuki H, Hirabayashi Y, Suzuki A (1995) IV3 alpha (NeuGc alpha 2-8NeuGc)-Gg4Cer is restricted to CD4+ T cells producing interleukin-2 and a small population of mature thymocytes in mice. *J Biol Chem* 270:3876–3881.
19. de Mello Coelho V, et al. (2004) Quantitative differences in lipid raft components between murine CD4+ and CD8+ T cells. *BMC Immunol*, 10.1186/1471-2172-5-2.
20. Nashar TO, Williams NA, Hirst TR (1996) Cross-linking of cell surface ganglioside GM1 induces the selective apoptosis of mature CD8+ T lymphocytes. *Int Immunol* 8: 731–736.
21. Salmond RJ, et al. (2002) CD8+ T cell apoptosis induced by Escherichia coli heat-labile enterotoxin B subunit occurs via a novel pathway involving NF-kappaB-dependent caspase activation. *Eur J Immunol* 32:1737–1747.
22. Trambley J, et al. (1999) Asialo GM1(+) CD8(+) T cells play a critical role in costimulation blockade-resistant allograft rejection. *J Clin Invest* 104:1715–1722.
23. Sorice M, et al. (1997) Evidence for the existence of ganglioside-enriched plasma membrane domains in human peripheral lymphocytes. *J Lipid Res* 38:969–980.
24. Garofalo T, et al. (2002) Association of GM3 with Zap-70 induced by T cell activation in plasma membrane microdomains: GM3 as a marker of microdomains in human lymphocytes. *J Biol Chem* 277:11233–11238.
25. Barbat C, et al. (2007) p56lck, LFA-1 and PI3K but not SHP-2 interact with GM1- or GM3-enriched microdomains in a CD4-p56lck association-dependent manner. *Biochem J* 402:471–481.
26. Comelli EM, et al. (2006) Activation of murine CD4+ and CD8+ T lymphocytes leads to dramatic remodeling of N-linked glycans. *J Immunol* 177:2431–2440.
27. Rossi NE, et al. (2008) Differential antibody binding to the surface alphabetaTCR.CD3 complex of CD4+ and CD8+ T lymphocytes is conserved in mammals and associated with differential glycosylation. *Int Immunol* 20:1247–1258.
28. Kuball J, et al. (2009) Increasing functional avidity of TCR-redirected T cells by removing defined N-glycosylation sites in the TCR constant domain. *J Exp Med* 206: 463–475.
29. Marth JD, Grewal PK (2008) Mammalian glycosylation in immunity. *Nat Rev Immunol* 8:874–887.
30. Hakomori SI (2008) Structure and function of glycosphingolipids and sphingolipids: Recollections and future trends. *Biochim Biophys Acta* 1780:325–346.
31. Nagafuku M, et al. (2003) Reduction of glycosphingolipid levels in lipid rafts affects the expression state and function of glycosylphosphatidylinositol-anchored proteins but does not impair signal transduction via the T cell receptor. *J Biol Chem* 278: 51920–51927.
32. Inokuchi J, Radin NS (1987) Preparation of the active isomer of 1-phenyl-2-decanoylamino-3-morpholino-1-propanol, inhibitor of murine glucocerebroside synthetase. *J Lipid Res* 28:565–571.
33. Blank N, Schiller M, Gabler C, Kalden JR, Lorenz HM (2005) Inhibition of sphingolipid synthesis impairs cellular activation, cytokine production and proliferation in human lymphocytes. *Biochem Pharmacol* 71:126–135.
34. Tani-ichi S, et al. (2005) Structure and function of lipid rafts in human activated T cells. *Int Immunol* 17:749–758.
35. Tuosto L, et al. (2001) Organization of plasma membrane functional rafts upon T cell activation. *Eur J Immunol* 31:345–349.
36. Jury EC, Kabouridis PS, Flores-Borja F, Mageed RA, Isenberg DA (2004) Altered lipid raft-associated signaling and ganglioside expression in T lymphocytes from patients with systemic lupus erythematosus. *J Clin Invest* 113:1176–1187.
37. Dong L, et al. Increased expression of ganglioside GM1 in peripheral CD4+ T cells correlates soluble form of CD30 in systemic lupus erythematosus patients. *J Biomed Biotechnol*, 10.1155/2010/569053.
38. Kabouridis PS, Jury EC (2008) Lipid rafts and T-lymphocyte function: Implications for autoimmunity. *FEBS Lett* 582:3711–3718.
39. Karman J, et al. (2010) Reducing glycosphingolipid biosynthesis in airway cells partially ameliorates disease manifestations in a mouse model of asthma. *Int Immunol* 22:593–603.
40. Shalaby KH, Martin JG (2010) Overview of asthma; the place of the T cell. *Curr Opin Pharmacol* 10:218–225.
41. Lloyd CM, Hessel EM (2010) Functions of T cells in asthma: More than just T(H)2 cells. *Nat Rev Immunol* 10:838–848.
42. Zhu Y, et al. (2011) Lowering glycosphingolipid levels in CD4+ T cells attenuates T cell receptor signaling, cytokine production, and differentiation to the Th17 lineage. *J Biol Chem* 286:14787–14794.
43. Yamashita T, et al. (2005) Interruption of ganglioside synthesis produces central nervous system degeneration and altered axon-glial interactions. *Proc Natl Acad Sci USA* 102:2725–2730.
44. Okuyama K, Wada K, Chihara J, Takayanagi M, Ohno I (2008) Sex-related splenocyte function in a murine model of allergic asthma. *Clin Exp Allergy* 38:1212–1219.
45. Takeuchi N, et al. (2004) Anti-HER-2/neu immune responses are induced before the development of clinical tumors but declined following tumorigenesis in HER-2/neu transgenic mice. *Cancer Res* 64:7588–7595.
46. Ikeda K, Taguchi R (2010) Highly sensitive localization analysis of gangliosides and sulfatides including structural isomers in mouse cerebellum sections by combination of laser microdissection and hydrophilic interaction liquid chromatography/electrospray ionization mass spectrometry with theoretically expanded multiple reaction monitoring. *Rapid Commun Mass Spectrom* 24:2957–2965.

Supporting Information

Nagafuku et al. 10.1073/pnas.1114965109

SI Materials and Methods

Mice. Mice were maintained in accordance with the guidelines of the Tohoku Pharmaceutical University for the care and use of laboratory animals. C57BL/6 mice were obtained from Japan SLC. The GM3S null and GM2/GD2S null mice were generated as previously described (1, 2). Both types of null mice were backcrossed with C57BL/6 mice over >11 generations. Mice were analyzed for the GM3S and GM2/GD2S genotypes by PCR as described previously (1, 2).

T-Cell Purification. For T-cell isolation, antigen-presenting cells (APCs) were depleted from cell suspensions prepared from spleen and lymph nodes, by incubating with 10 μg/mL anti-MHC class II antibody (SouthernBiotech) at 4 °C for 30 min, followed by BioMag anti-rat IgG and anti-mouse IgG secondary antibodies (Polyscience) for 45 min. $CD4^+$ T and $CD8^+$ T cells were positively selected using anti-CD4 and anti-CD8 Magnetic Particles (BD Biosciences) or negatively selected using column kits for $CD4^+$ and $CD8^+$ T-cell subsets from R&D Systems. T cells isolated using the positive selection methods were used for lipid analysis and gene expression assay. The purity of the populations was assessed by flow cytometry and was found to be at least 95%.

T-Cell Activation. For antibody-mediated activation, T-cell subsets purified by negative selection were incubated with 0.1 μg/mL of anti-CD3ε antibody (145-2C11) in the presence of 0.2 μg/mL of anti-CD28 (PV-1) antibody for 72 h. For glycosphingolipid (GSL) add-back experiments the cells were pretreated with the indicated GSLs for 2 h before T-cell antigen receptor (TCR)-mediated stimulation. For the antigen-specific proliferative response assays, $CD4^+$ T cells and $CD8^+$ T cells were prepared from the spleen 7 d after immunization with ovalbumin (OVA) conjugated with trinitrophenyl (TNP) (Biosearch Technologies). The cells were cocultured with mitomycin C (MMC)-treated WT splenocytes for 72 h in the presence or absence of TNP-OVA antigen. For mixed lymphocyte reactions (MLR), $CD4^+$ T and $CD8^+$ T cells were cocultured for 72 h with MMC-treated splenocytes from BALB/c mice. Cell proliferation was measured by 2,3-bis-(2-methoxy-4-nitro-5-sulfophenyl)-2H-tetrazolium-5-carboxanilide (XTT) assay with a cell proliferation kit (MD Biosciences), according to the manufacturer's instructions.

Allergen-Induced Airway Inflammation. Female WT and GM3S null mice, 6–8 wk old, were sensitized by i.p. injections of OVA (8 μg/mouse) adsorbed with aluminum hydroxide on days 0 and 5. On day 17, mice were challenged with aerosolized OVA (5% in saline) or saline as a control for 1 h on two occasions 4 h apart. At time points indicated after the challenge, peripheral blood, bronchoalveolar lavage (BAL) fluids, and lung tissues were collected. Total cell numbers in the BAL fluids were counted with a hemocytometer. Smears of BAL cells prepared with a Cytospin IV (Shandon) were stained with Diff-Quik solution (International Reagents) for differential cell counting. The percentages of cell differentials were determined by counting at least 200 cells under a light microscope. After centrifugation of the BAL fluid, supernatants were collected for cytokine measurements. Lung tissues were fixed with 10% buffered formaldehyde, embedded in paraffin, and sectioned at 4-μm thickness. The resulting sections were stained with periodic acid Schiff (PAS) and counterstained with hematoxylin for evaluation of mucus inclusions in bronchial epithelium. Slides were examined in a blinded fashion.

Preparation of $CD4^+$ T Cells for Adoptive Transfer. On day 17, spleens collected from sensitized WT, GM3S null, and GM2/GD2S null mice were excised, and the splenocytes were disaggregated. The washed splenocytes were resuspended and cultured in the presence of 200 μg/mL OVA. Three days after the culture, $CD4^+$ T cells were purified by positive selection on an auto-MACS separator (Miltenyi Biotec), using anti-mouse CD4 (L3T4) MicroBeads (Miltenyi Biotec) according to the manufacture's protocol. The $CD4^+$ T cells (2×10^6 cells/200 μL in saline) were transferred to naive WT mice by tail vein injection. Three days after the injection, the recipient mice were aerosol challenged; BAL fluids were collected 5 d after the challenge as described above.

Flow Cytometry. Cells from thymus, spleen, and lymph nodes of C57BL/6 mice, GM3S null mice, and GM2/GD2S null mice were resuspended in FACS buffer (HBSS with 0.1% BSA and 0.01% NaN3) and stained with the appropriate fluorochrome-conjugated antibodies for 30 min at 4 °C. Stained cells were analyzed using a FACS Caliber with CELLQuest software (BD Biosciences). Fluorochrome-conjugated mAbs were all purchased from Biolegend, except for the anti-B220 antibody, which was from SouthernBiotech. FITC-conjugated CTx-B was purchased from Sigma.

Lipid Analysis. Total lipids were extracted from cell pellets with chloroform/methanol and were separated into neutral and acidic lipid fractions, using a diethylaminoethyl (DEAE)-Sephadex A-25 column (GE Healthcare). The fractions were dried and subjected to methanolic 0.1 M NaOH for ester cleavage. After neutralization, solutions were desalted with Sep-Pak C18 reverse-phase cartridges (Waters). Acidic lipids were separated on silica gel high-performance TLC plates (Merck) with chloroform: methanol:0.5% $CaCl_2$ (50:50:10), and gangliosides were detected with resorcinol-HCl reagent. Neutral lipids were separated on TLC by half-developing with chloroform:methanol:water (65:25:4) and then drying and redeveloping with hexane:diethyl ether:acetic acid (50:50:1); GSLs were detected with orcinol-sulfuric acid reagent.

TLC immunostaining was performed as described previously (3). Acidic lipids were separated on TLC plates with aluminum backing (Merck). Plates were soaked in 0.1% polyisobutylmethacrylate in cyclohexane, dried, and blocked with 1% BSA-PBS. The plates were incubated with HRP-conjugated CTx-B (Sigma) followed with HRP-conjugated anti-mouse Ig antibody (NXA931; GE Healthcare). After a PBS wash, the plates were developed by enhanced chemiluminescence, using Lumi-Light PLUS (Roche Applied Science), and detected using a Fujifilm LAS-3000 imaging system.

Liquid Chromatography–Mass Spectrometry (LC-MS). Gangliosides were dissolved in methanol, mixed with GM3 [*N*-acetylneuraminic acid (NeuAc), d18:1–14:0] as an internal standard, and separated by LC with a Develosil C30 column (1 mm i.d. × 50 mm; Nomura Chemical) and elution solvents, solvent A (12.5% water, 10 mM ammonium formate, and 0.1% formic acid in methanol) and solvent B (2.5% water, 10 mM ammonium formate, 0.1% formic acid, and 50% isopropyl alcohol in methanol), using a gradient elution of 20% B in A for 5 min, from 20% to 100% B in A for 20 min, and 100% B for 5 min. Another separation was performed with a Unison NH2 column (1 mm i.d. × 50 mm; Impakt) and elution solvents, solvent C (1 mM

ammonium formate in acetonitrile:water 83:17, vol/vol) and solvent D (50 mM ammonium formate in acetonitrile:water 50:50, vol/vol), using a gradient elution of 0% D in C for 5 min, 76% D in C for 15 min, 90% D in C for 5 min, and 90% D in C for 5 min. Flow rate for both modes of LC was 50 μL/min.

MS was performed by a Shimadzu LC-IT-MS in the negative ion mode with mass range from *m/z* 200–2,000, detector voltage at 1.9 kV, MS^2 mass range from *m/z* 200–2,000, and collision-induced dissociation (CID) energy for MS^2 at 50% arbitrary value. Analysis of the ratios between GM1a [*N*-glycolylneuraminic acid (NeuGc)] and GM1b (NeuGc) and between GD1b (NeuGc) and GD1c (NeuGc) was performed by MS^2 with manual detection, selecting *m/z* 765.91 and 820.97 for GM1 (NeuGc) containing d18:1–16:0 and d18:1–24:1, respectively, and 919.46 and 974.51 for GD1 (NeuGc) containing d18:1–16:0 and d18:1–24:1, respectively.

Quantitative Real-Time PCR. Total RNA was isolated using TRI Reagent (Molecular Research Center). Reverse transcription was performed using a PrimeScript RT reagent Kit (TaKaRa Bio), according to the manufacturer's protocol. Quantitative real-time PCR was performed using an Applied Biosystems 7500 Real Time PCR System and SYBR Green I (TaKaRa Bio), according to the manufacturers' instructions. Primers were as follows: for *GM3S* forward, 5′-AGTCCCACTCCAGCCAAAG-3′, and *GM3S* reverse, 5′-CCAAGACAACGGCAATGAC-3′; for *GM2/GD2S* forward, 5′-ACCCACCATCATCCCTACCC-3′, and *GM2/GD2S* reverse, 5′-GAACCAACCCTTGCCGAAG-3′; and for *GAPDH* forward, 5′-AAATGGTGAAGGTCGGTGTG-3′, and *GAPDH* reverse, 5′-TGAAGGGGTCGTTGATGG-3′. These primers spanned more than one intron to avoid amplification of any contaminating DNA. After amplification, a melting curve (0.1 °C/s) was used to confirm product purity, and only one peak for each sample was observed. The threshold cycle value was taken as the fractional cycle number at which the emitted fluorescence of the sample passed a fixed threshold above the baseline. Relative quantification was calculated using a standard curve, which was produced to demonstrate linearity (correlation coefficient >0.98) and to determine amplification efficiency (90–110%). Each expression level of samples was normalized to those of *GAPDH*.

1. Yoshikawa M, et al. (2009) Mice lacking ganglioside GM3 synthase exhibit complete hearing loss due to selective degeneration of the organ of Corti. *Proc Natl Acad Sci USA* 106:9483–9488.
2. Yamashita T, et al. (2005) Interruption of ganglioside synthesis produces central nervous system degeneration and altered axon-glial interactions. *Proc Natl Acad Sci USA* 102:2725–2730.
3. Nakamura K, et al. (1991) A sialidase-susceptible ganglioside, IV3 alpha(NeuGc alpha 2-8NeuGc)-Gg4Cer, is a major disialoganglioside in WHT/Ht mouse thymoma and thymocytes. *J Biochem* 110:832–841.

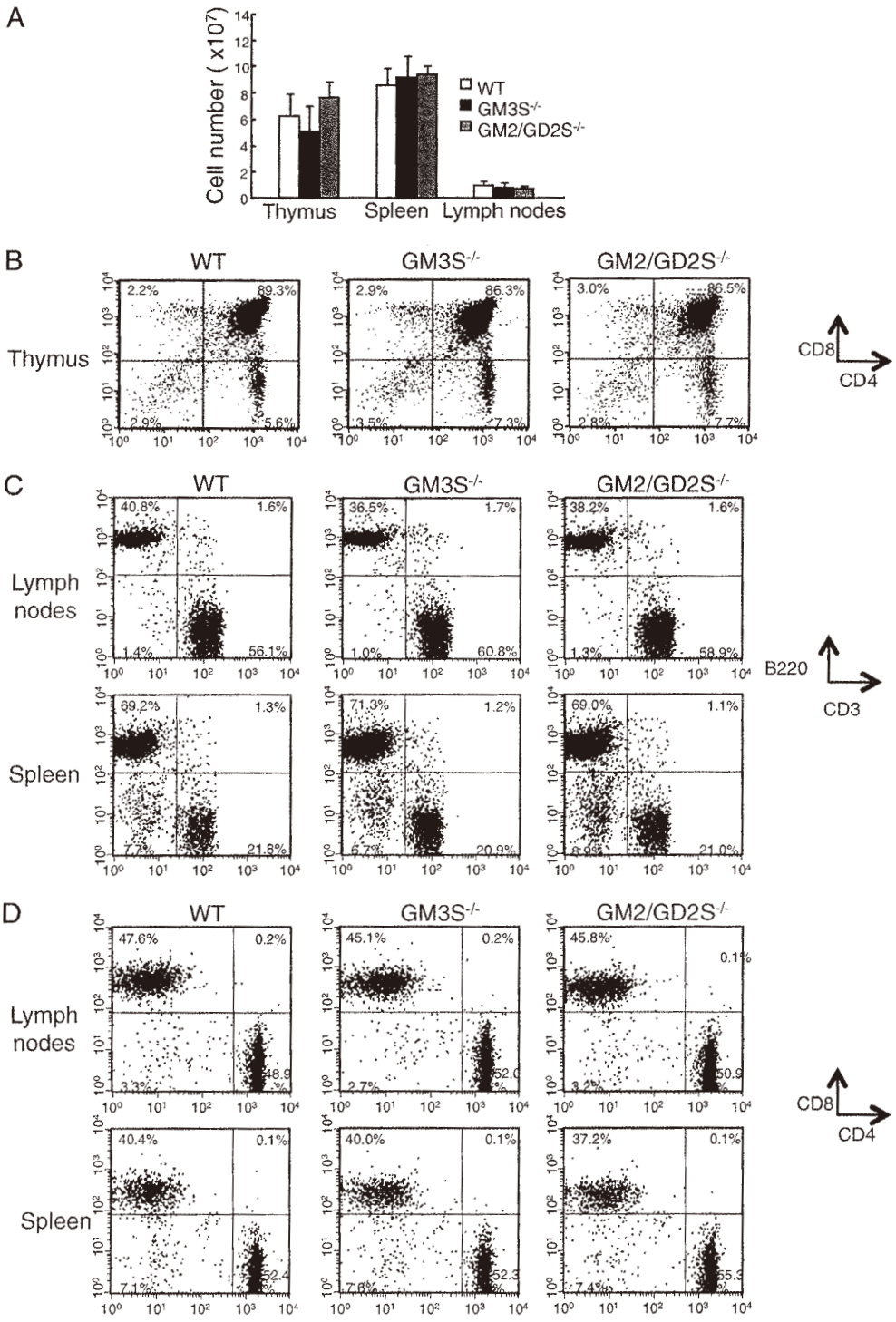

Fig. S1. Cellularity and distribution of lymphocytes in GM3S$^{-/-}$ and GM2/GD2S$^{-/-}$ mice. Thymocytes, splenocytes, and lymph node cells were collected from WT, GM3S$^{-/-}$, and GM2/GD2S$^{-/-}$ mice at 8–10 wk old. (*A*) Cells of the lymphoid organs were counted ($n = 4$ per group). GM3S null and GM2/GD2S null mice did not reveal any obvious alteration in the cellularity of the lymphoid organs. (*B*) Thymocytes were stained with anti-CD4 and anti-CD8 antibodies and analyzed by flow cytometry. Similar distribution patterns in the thymocyte populations of the null and WT mice were obseved. (*C* and *D*) Lymph node cells and splenocytes were stained with anti-B220/CD3, anti-CD4, and anti-CD8 antibodies and analyzed by flow cytometry. In the spleen and lymph nodes, there was no obvious alteration in relative distribution within the T-cell and B-cell populations (*C*) and the CD4$^+$ T and CD8$^+$ T-cell populations (*D*). Numbers in the quadrants indicate percentage of different cell populations.

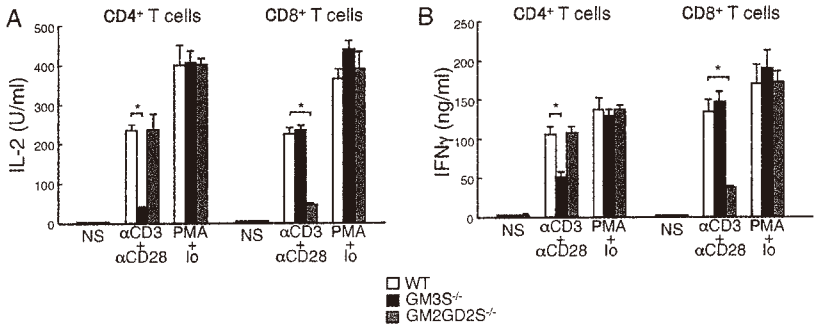

Fig. S2. Cytokine production in GM3S$^{-/-}$ and GM2/GD2S$^{-/-}$ mice. (*A*) IL-2 production and (*B*) IFN-γ production were evaluated by ELISA of culture supernatants. All values represent the means (±SEM) of triplicate cultures and are representative of three independent experiments. Data are representative of three experiments. *$P < 0.01$.

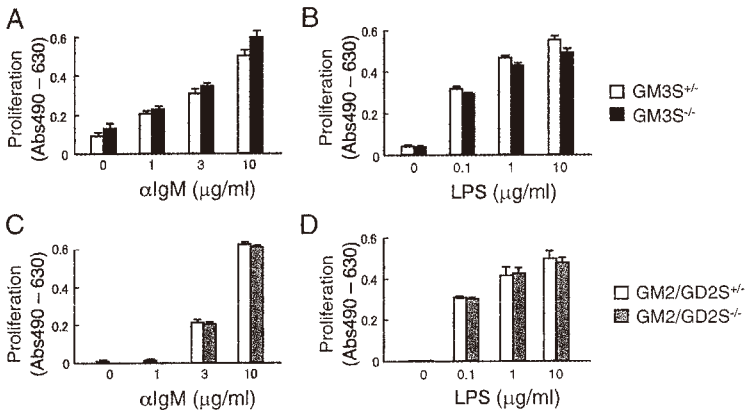

Fig. S3. B-cell responses in GM3S$^{-/-}$ and GM2/GD2S$^{-/-}$ mice. Purified splenic B cells from WT, GM3S$^{-/-}$, and GM2/GD2S$^{-/-}$ mice were stimulated for 48 h with the indicated concentrations of anti-IgM antibody (*A* and *C*) or LPS (*B* and *D*). Proliferative responses were determined after an 8-h pulse with XTT reagent.

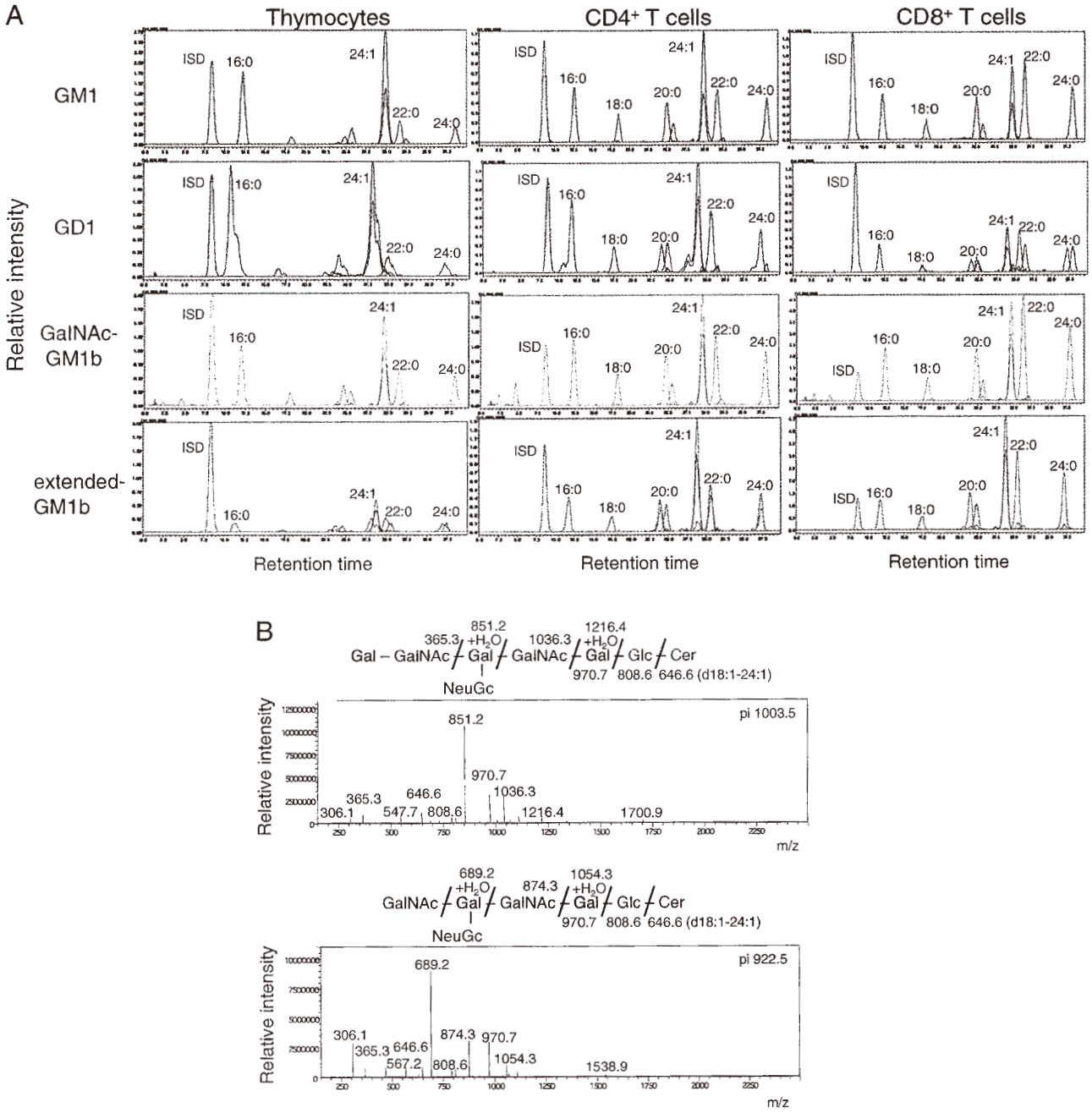

Fig. S4. (Continued)

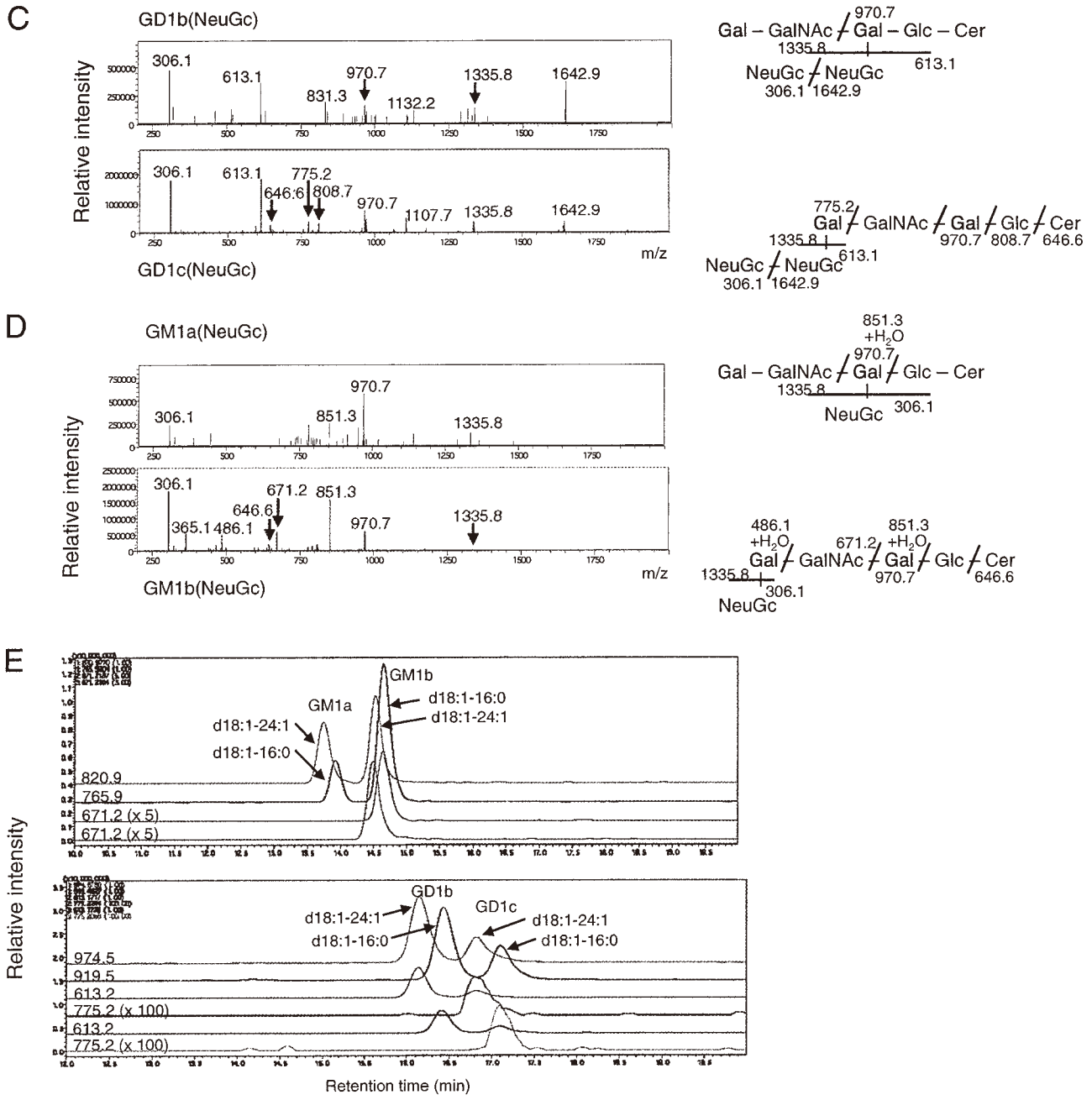

Fig. S4. LC-MS/MS analysis of ganglioside species in thymocytes and primary $CD4^+$ T and $CD8^+$ T cells obtained from WT mice. (*A*) Mass chromatograms of GM1, GD1, GalNAcGM1b, and extended GM1b in thymocytes and $CD4^+$ T and $CD8^+$ T cells. The gangliosides were separated by a C30 reverse-phase column, and mass chromatograms monitored molecular species containing d18:1–16:0, –18:0, –20:0, –22:0, –24:1, and –24:0. All gangliosides monitored contained *N*-glycolylneuraminic acid (NeuGc). Fig. 3*B* shows the integrated peak area obtained from these chromatograms. (*B*) MS^2 spectra of extended GM1b and GalNAcGM1b in $CD8^+$ T cells. Ions at *m/z* 1003.5 and 922.5 were selected as precursor ions. (*C*) MS^2 spectra of GD1b and GD1c in $CD4^+$ T cells. Ions at *m/z* 974.5 were selected as precursor ions. Reporter signals were detected at *m/z* 613.1 for NeuGc-NeuGc structure in GD1b and GD1c and at 775.2 for NeuGc-NeuGc-Gal fragment in GD1c. (*D*) MS^2 spectra of GM1a and GM1b1c in $CD4^+$ T cells. The ion at *m/z* 820.9 was selected as a precursor ion. Reporter signals were detected at *m/z* 486.1 for NeuGc-Gal in GM1b and 671.2 for NeuGc-Gal-GalNAc in GM1b. (*E*) Mass chromatograms showing the separation between GM1a and GM1b and between GD1b and GD1c. GM1 (NeuGc) containing d18:1–16:0 and d18:1–24:1 was monitored using *m/z* 765.9 and 820.9 as $[M - 2H]^{-2}$, respectively, and the reporter ion at *m/z* 671.2 is the fragment ion of $[NeuGc\text{-}Gal\text{-}GalNAc]^{-1}$ for GM1b. GD1 (NeuGc) containing d18:1–16:0 and d18:1–24:1 was monitored using *m/z* 919.5 and 974.5 as $[M - 2H]^{-2}$, respectively, and the reporter ions at 613.2 and 775.2 are $[NeuGc\text{-}NeuGc]^{-1}$ specific to GD1b and GD1c and $[NeuGc\text{-}NeuGc\text{-}Gal\text{-}GalNAc]^{-1}$ specific to GD1c, respectively.

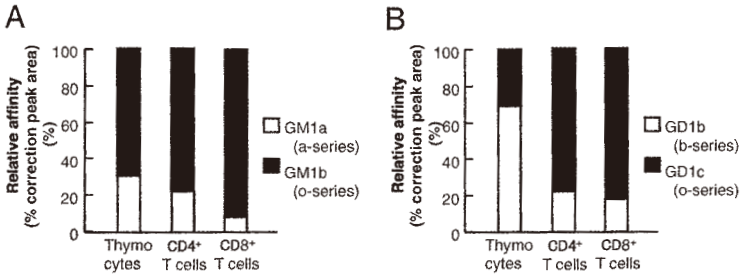

Fig. S5. LC-MS analysis of positional isomers of gangliosides of mouse thymocytes and $CD4^+$ and $CD8^+$ T cells. (*A*) Percentage of distributions of GM1a (NeuGc) and GM1b (NeuGc). Both include GM1 (NeuGc) carrying d18:1–16:0 and d18:1–24:1, which are the major components, as shown in Fig. S4. (*B*) Percentage of distributions of GD1b (NeuGc) and GD1c (NeuGc). Both include GD1 (NeuGc) carrying d18:1–16:0 and d18:1–24:1, which are the major components, as shown in Fig. S4.

Neuroscience Letters 517 (2012) 140–143

Contents lists available at SciVerse ScienceDirect

Neuroscience Letters

journal homepage: www.elsevier.com/locate/neulet

Involvement of ganglioside GT1b in glutamate release from neuroblastoma cells

Shun Watanabe[a], Hideyoshi Higashi[b], Hideoki Ogawa[a], Kenji Takamori[a], Kazuhisa Iwabuchi[a,*]

[a] Institute for Environmental and Gender-Specific Medicine, Juntendo University School of Medicine, 2-1-1 Tomioka, Urayasu-shi, 279-0021 Chiba, Japan
[b] Division of Glyco-signal Research, Institute of Molecular Biomembrane and Glycobiology, Tohoku Pharmaceutical University, 4-4-1 Komatsushima, Aoba-ku, Sendai-shi, 981-8558 Miyagi, Japan

ARTICLE INFO

Article history:
Received 4 February 2012
Received in revised form 28 March 2012
Accepted 20 April 2012

Keywords:
Ganglioside
Glutamate
Neuroblastoma
Neurotransmitter

ABSTRACT

Since gangliosides play many important roles in neural systems, we investigated whether gangliosides are involved in glutamate release from neural cells. Differentiated neruro2a cells were treated with gangliosides, including GM3, GM1, GD1a, GD3, GD1b, or GT1b, for 30 min, and glutamate concentration in the culture media was measured using o-phthalaldehyde derivatization. Among the tested gangliosides, GT1b significantly increased the glutamate concentration when compared with untreated cells. Moreover, GT1b increased the glutamate concentration in the culture media of neuroblastoma × dorsal root ganglion neuron hybrid F11 cells. These results suggested that gangliosides are important in regulating extracellular glutamate concentration in the nervous system.

1. Introduction

Gangliosides are sialic acid containing glycosphingolipids synthesized from sphinganine/sphingosine. These compounds can be divided into four groups according to their biosynthetic pathway: the asialo-, a-, b-, and c-series gangliosides. Gangliosides are abundant in the nervous system, and are thought to be involved in axonal elongation [4,17]; synaptic transmission [26]; and neuron–glia interactions [16,24]. Gangliosides have also been reported to be components of lipid rafts, acting as key assemblers and regulators of the sorting of other molecules into lipid rafts that regulate cell–cell interactions and signal transduction complexes [20].

Gangliosides also function in synaptic transmission and long-term potentiation (LTP). For example, the accumulation of exogenous or endogenous GM1 by sialidase treatment has been found to enhance synaptic transmission and LTP [8,27], and exogenous addition of the b-series ganglioside GQ1b has been found to enhance ATP-induced LTP [6]. In addition, LTP was attenuated in β1,4 GalNAc-T transgenic mice, which have an increase in a-series and a decrease in b-series gangliosides [9].

All of these synaptic transmission pathways utilize glutamate a major excitatory neurotransmitter. Moreover, the extracellular concentration of glutamate is regulated by its release and uptake via several pathways, such as those involving synaptic vesicles and transporters in neuron and glial cells [21]. In contrast, membrane proteins involved in synaptic transmission, including glutamate signaling, have been localized into lipid rafts [1,15], which consist of cholesterol and sphingolipids including gangliosides. We have reported that exogenous GT1b enhances extracellular glutamate concentrations in subdermal tissues [25], in which nerve fibers are regarded as the major source of glutamate [2,5,12]. To determine whether gangliosides induce glutamate release from neuronal cells, we examined the effects of exogenously added gangliosides on glutamate concentration in the supernatants of differentiated neuroblastoma cell cultures. We found that the b-series ganglioside GT1b, not the a-series ganglioside GM1, enhanced extracellular glutamate release from these cells.

2. Materials and methods

2.1. Cell cultures

Neuro2a cells, the kind gift of Dr. Masami Takahashi (Mitsubishi Kagaku Institute of Life Sciences, Machida, Tokyo, Japan) were grown in DMEM supplemented with 10% fetal bovine serum (FBS) and 2 mM glutamine at 37 C in an atmosphere of 5% CO_2 and 95% air. For differentiation, 1.0×10^4 cells/cm^2 were plated onto poly-D-lysine coated 24 well plates in DMEM plus 10% FBS and incubated overnight, after which they were grown in DMEM plus 1% FBS, 2 mM glutamine, and 20 μM retinoic acid for 72 h.

Neuroblastoma × dorsal root ganglion neuron hybrid F-11 cells [19] were grown in DMEM plus 10% FBS and 2 mM glutamine at 37 C in 5% CO_2 and 95% air. For differentiation, 0.25×10^4 cells/cm^2 were plated onto poly-D-lysine coated 24 well plates in DMEM plus 10% FBS and incubated overnight, after which they were cultured

Abbreviations: D-PDMP, D-threo-1-phenyl-2-decanoylamino-3-morpholino-1-propanol; MTT, 3-(4,5-dimethylthiazol-2-yl)-2,5-diphenyltetrazolium bromide.

* Corresponding author. Tel.: +81 47 353 3171; fax: +81 47 353 3178.
E-mail address: iwabuchi@juntendo.ac.jp (K. Iwabuchi).

0304-3940/$ – see front matter © 2012 Elsevier Ireland Ltd. All rights reserved.
http://dx.doi.org/10.1016/j.neulet.2012.04.049

for 7–8 days in DMEM plus 0.5% FBS, 2 mM glutamine, and 10 μM forskolin.

To measure glutamate released by cells, each plate was washed with 500 μl HEPES-buffered saline (130 mM NaCl, 5.4 mM KCl, 1.8 mM $CaCl_2$, 4.5 mM glucose, 20 mM HEPES–NaOH pH 7.4), and the cells were incubated at 37 C in the same buffer containing 5–50 μM various gangliosides for 10–60 min. To inhibit ganglioside biosynthesis, cells were incubated for 24 h with 4 μM D-threo-1-phenyl-2-decanoylamino-3-morpholino-1-propanol (D-PDMP), the kind gift of Prof. Jin-ichi Inokuchi (Tohoku Pharmaceutical University, Sendai, Miyagi), before glutamate was assayed. To assess their viability, the D-PDMP-treated cells were incubated with 0.5 mg/ml 3-(4,5-dimethylthiazol-2-yl)-2,5-diphenyltetrazolium bromide (MTT) for 90 min at 37 C. The resultant formazan crystals were dissolved in 100 μl DMSO, and absorbance at 570 nm was determined with a microplate reader.

2.2. Amino acid analysis

Amino acids in the HEPES-buffered saline (50 μl) were analyzed by high-performance liquid chromatography (HPLC) following *o*-phthalaldehyde derivatization and fluorescence detection. Amino acids were quantified by reverse-phase chromatography using a ZORBAX Eclipse AAA column (5 μm, 75 mm × 4.6 mm I.D., Agilent Technology, Santa Clara, CA) attached to an HPLC system consisting of a pump connected to a degasser, a fluorescence HPLC monitor, and a chromato-integrator. The samples were eluted using the following program: 0–1.0 min with solvent A (40 mM NaH_2PO_4, pH 7.8); 1.0–9.8 min with a linear gradient of 0–57% solvent B (methanol:acetonitrile:water, 45:45:10); 9.8–10.0 min with a linear gradient of 57–100% solvent B; 10.0–12.0 min with 100% solvent B; 12.0–12.5 min linear gradient with 100–0% solvent B; and 12.5–14.0 min with solvent A. The flow rate and temperature were kept constant at 2.0 ml/min and 40 C, respectively.

2.3. Drugs

GM1, GD1b, GD1a, and GT1b were purchased from Wako Pure Chemical Industries Ltd. (Osaka, Japan), and GM3 and GD3 were purchased from ENZO Life Sciences (Farmingdale, NY, USA). All gangliosides were derived from bovine brain.

2.4. Statistical analysis

Results are presented as means ± S.E.M. The statistical significance between groups was assessed by two-tailed unpaired Student's *t* tests, two-way repeated-measures ANOVA followed by Bonferroni post-tests, and means of one-way analysis of variance followed by Dunnett's multiple comparison test, as appropriate. All statistical analyses were performed using GraphPad software (San Diego, CA, USA), with *P*-values less than 0.05 ($P < 0.05$) considered statistically significant.

3. Results

To identify which gangliosides enhance extracellular glutamate concentration in the supernatants of differentiated neuroblastoma cells, we incubated cells with 50 μM of each ganglioside and measured glutamate concentrations in the culture media (Fig. 1). We found that GT1b significantly enhanced glutamate concentration, whereas the other gangliosides (GM3, GM1, GD1a, GD3 and GD1b) did not. Assessment of the dose–response relationship showed that 50 μM GT1b maximally and significantly enhanced glutamate concentration (Fig. 2). Moreover, this increase was time-dependent, becoming significant after incubation for 30 min (Fig. 3).

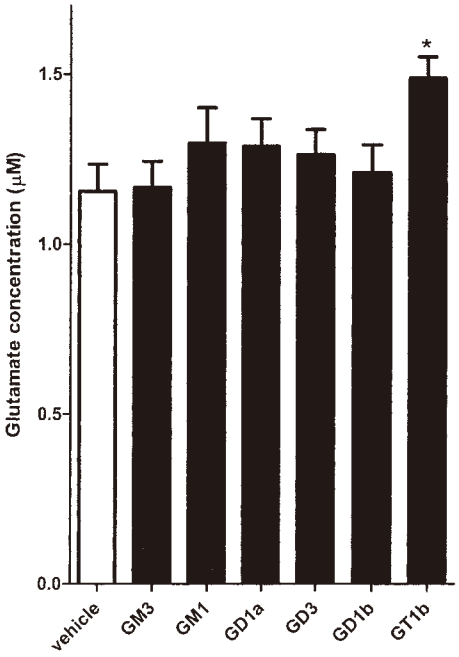

Fig. 1. The effects of gangliosides of different structures on glutamate release by differentiated neuro2a cells. Cells were treated with 50 μM gangliosides for 30 min at 37 C and glutamate concentrations in the culture supernatants were measured using HPLC. Results are expressed as means ± S.E.M. of 5 experiments. *$P < 0.05$ compared with vehicle by one-way ANOVA followed by Dunnett's test.

During nociception, glutamate acts as a nociceptive agent in the epidermis, and as an important neurotransmitter between dorsal root ganglion cells and dorsal horn neurons in the spinal cord. Since the free nerve endings of dorsal root ganglion cells are thought to be the primary sources of glutamate in subdermal tissues [12,13], we assessed the effects of GT1b on glutamate release from neuroblastoma × dorsal root ganglion F-11 neuron hybrid cells. GT1b also increased glutamate concentration in the supernatants of differentiated F-11 cells (Fig. 4), suggesting that gangliosides influence not only the central but the peripheral nervous system. To

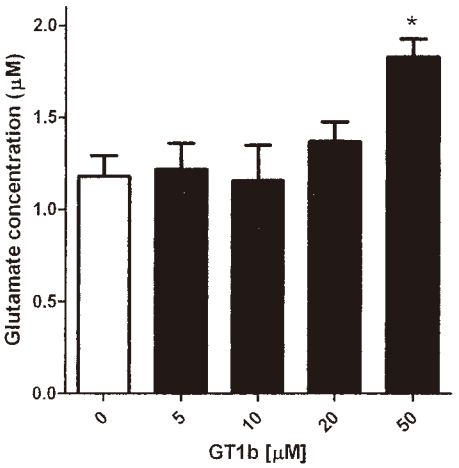

Fig. 2. Dose–response relationship between GT1b concentration and glutamate concentration in supernatants of differentiated neuro2a cells. Cells were treated with various concentrations of gangliosides for 30 min at 37 C and glutamate concentrations in the culture supernatants were measured using HPLC. Data are expressed as means ± S.E.M. of 4 experiments. *$P < 0.05$ compared with vehicle by one-way ANOVA followed by Dunnett's test.

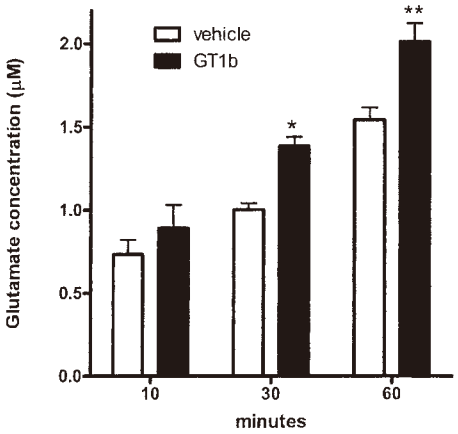

Fig. 3. Time course of the effects of gangliosides on glutamate concentration in supernatants of differentiated neuro2a cells. Cells were treated with gangliosides for 10, 30, and 60 min at 37 °C and glutamate concentrations in the culture supernatants were measured using HPLC. Data are expressed as means ± S.E.M. of 8 experiments.: $^{*}P < 0.05$ and $^{**}P < 0.01$ compared with vehicle by two-way repeated-measures ANOVA followed by Bonferroni post-tests.

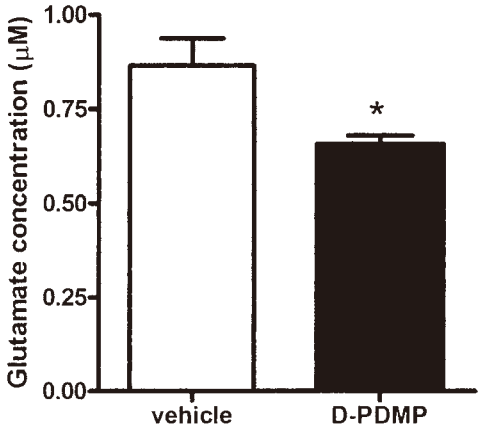

Fig. 5. Effects of D-PDMP on glutamate concentration in supernatants of differentiated neuro2a cells. Cells were treated with D-PDMP for 24 h, washed with HEPES-buffered saline, and incubated at 37 °C in the same buffer. Glutamate concentrations in the culture supernatants were measured using HPLC. Data are expressed as means ± S.E.M. of 4 independent experiments. $^{*}P < 0.05$ compared with vehicle by two-tailed unpaired Student's *t* tests.

assess whether endogenous gangliosides are involved in glutamate release, we tested the effects of D-PDMP, an inhibitor of glucosylceramide synthase [10,22], the enzyme catalyzing the synthesis of glucosylceramide, a precursor of most glycosphingolipids including gangliosides, on extracellular glutamate concentration. We found that the maximum nontoxic concentration of D-PDMP under our experimental conditions was 4 μM, since the mean ± S.E.M. viability of cells ($n = 3$) incubated with 4 μM and 10 μM D-PDMP was 98.1 ± 3.3% and 74.5 ± 4.65%, respectively, relative to control cells, as shown by MTT assays. Incubation of cells with 4 μM D-PDMP decreased glutamate concentration in supernatants, suggesting that endogenous glycosphingolipids including gangliosides are involved in glutamate release (Fig. 5).

4. Discussion

We have assessed whether gangliosides induce glutamate secretion by neuroblastoma cells in culture. We found that the b-series ganglioside GT1b enhanced extracellular glutamate release by these cells, whereas the glucosylceramide synthase inhibitor, D-PDMP, reduced extracellular glutamate concentration, suggesting that GT1b is involved in glutamate release from neuro2a cells.

Gangliosides have been found to be important in synaptic transmission and LTP [8,9,28]. In addition, glutamate receptors play pivotal roles in synaptic plasticity, and glutamate release is also involved in LTP production. We found that the b-series ganglioside GT1b but not the a-series ganglioside GM1 enhanced extracellular glutamate concentration in the supernatants of neuroblastoma cells. However, GM1 has been shown to enhance LTP [8,28]. Thus, GT1b may influence presynaptic mechanisms such as glutamate release from synaptic vesicles, whereas GM1 may be involved in postsynaptic mechanisms such as those involving glutamate receptors.

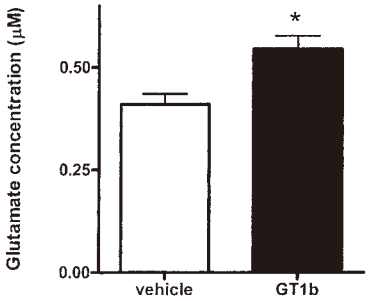

Fig. 4. The effects of GT1b on glutamate concentration in supernatants of differentiated F11 cells. Cells were treated with gangliosides for 30 min at 37 °C and glutamate concentrations in the culture supernatants were measured using HPLC. Data are expressed as means ± S.E.M. of 3 experiments. $^{*}P < 0.05$ compared with vehicle by two-tailed unpaired Student's *t* tests.

Gangliosides form lipid rafts and play essential roles in cell adhesion, differentiation, and protein trafficking in neural systems [4,16,17,24,26]. Synaptic vesicle proteins have been reported to localize to lipid rafts consisting of cholesterol and sphingolipids, including gangliosides; these rafts are important in synaptic vesicle transport and release [3,11]. In addition, cholesterol depletion by methyl-beta-cyclodextrin and lovastatin reduced neurotransmitter release by PC12 cells [3], suggesting that GT1b may contribute to glutamate release via a raft-dependent mechanism.

The gangliosides GM3 and GM1 have been shown to form independent clusters on plasma membranes [7], suggesting that each type of lipid raft may have different lipid and protein compositions and that these differences may cause specific ganglioside–protein interactions. Protein–ganglioside interactions have been found to be dependent on the sugar moiety on gangliosides (e.g. GT1b-NgR1 [23], GM3-insulin receptor [14], GM1-TrkA [17]). Thus, glutamate release-related proteins may specifically interact with GT1b, although further studies are needed to clarify these molecular mechanisms.

We recently reported that GT1b induced the accumulation of extracellular glutamate in subdermal tissues, activating glutamate receptors and resulting in hyperalgesia and nociception. Glutamate is released in subdermal tissues by heat, formalin, and capsaicin cream [12,18], and stimulation of A and/or C fibers can result in the peripheral release of glutamate [5]. Moreover, recent immunohistochemical studies have shown that vesicular glutamate transporters localize to free nerve endings [2]. Taken together, these results indicate that the accumulation of glutamate into vesicles, followed by exocytosis, is an important glutamate releasing mechanism in sensory neurons. We found that GT1b promoted glutamate release, not only from neuro2a cells but from dorsal root ganglia-derived F-11 cells, suggesting that GT1b directly modulates glutamate release from nerve endings. Additional studies, however,

are required to determine the molecular mechanisms underlying GT1b-induced glutamate release.

Acknowledgments

We thank Prof. Jin-ichi Inokuchi (Division of Glycopathology, Institute of Molecular Biomembrane and Glycobiology, Tohoku Pharmaceutical University Graduate School of Pharmaceutical Sciences) for the generous gift of D-PDMP. This study was supported in part by a Grant-in-Aid from the Foundation of Strategic Research Projects in Private Universities from the Ministry of Education, Culture, Sports, Science, and Technology (Japan) and Grant-in-Aid for Young Scientist (No. 23790647) from the Japan Society for Promotion of Science (Japan). F-11 cells were purchased from ECACC (No. 08062601).

References

[1] J.A. Allen, R.A. Halverson-Tamboli, M.M. Rasenick, Lipid raft microdomains and neurotransmitter signalling, Nature Reviews 8 (2007) 128–140.
[2] P. Brumovsky, M. Watanabe, T. Hokfelt, Expression of the vesicular glutamate transporters-1 and -2 in adult mouse dorsal root ganglia and spinal cord and their regulation by nerve injury, Neuroscience 147 (2007) 469–490.
[3] L.H. Chamberlain, R.D. Burgoyne, G.W. Gould, SNARE proteins are highly enriched in lipid rafts in PC12 cells: implications for the spatial control of exocytosis, Proceedings of the National Academy of Sciences of the United States of America 98 (2001) 5619–5624.
[4] J.S. Da Silva, T. Hasegawa, T. Miyagi, C.G. Dotti, J. Abad-Rodriguez, Asymmetric membrane ganglioside sialidase activity specifies axonal fate, Nature Neuroscience 8 (2005) 606–615.
[5] J. deGroot, S. Zhou, S.M. Carlton, Peripheral glutamate release in the hindpaw following low and high intensity sciatic stimulation, Neuroreport 11 (2000) 497–502.
[6] S. Fujii, K. Igarashi, H. Sasaki, H. Furuse, K. Ito, K. Kaneko, H. Kato, J. Inokuchi, H. Waki, S. Ando, Effects of the mono- and tetrasialogangliosides GM1 and GQ1b on ATP-induced long-term potentiation in hippocampal CA1 neurons, Glycobiology 12 (2002) 339–344.
[7] A. Fujita, J. Cheng, T. Fujimoto, Segretation of GM1 and GM3 clusters in the cell membrane depends on the intact actin cytoskeleton, Biochimica et Biophysica Acta (2009).
[8] H. Furuse, H. Waki, K. Kaneko, S. Fujii, M. Miura, H. Sasaki, K.I. Ito, H. Kato, S. Ando, Effect of the mono- and tetra-sialogangliosides, GM1 and GQ1b, on long-term potentiation in the CA1 hippocampal neurons of the guinea pig, Experimental Brain Research – Experimentelle Hirnforschung 123 (1998) 307–314.
[9] K. Ikarashi, H. Fujiwara, Y. Yamazaki, J. Goto, K. Kaneko, H. Kato, S. Fujii, H. Sasaki, S. Fukumoto, K. Furukawa, H. Waki, K. Furukawa, Impaired hippocampal long-term potentiation and failure of learning in beta1,4-N-acetylgalactosaminyltransferase gene transgenic mice, Glycobiology 21 (2011) 1373–1381.
[10] J. Inokuchi, N.S. Radin, Preparation of the active isomer of 1-phenyl-2-decanoylamino-3-morpholino-1-propanol, inhibitor of murine glucocerebroside synthetase, Journal of Lipid Research 28 (1987) 565–571.
[11] J.Y. Jia, S. Lamer, M. Schumann, M.R. Schmidt, E. Krause, V. Haucke, Quantitative proteomics analysis of detergent-resistant membranes from chemical synapses: evidence for cholesterol as spatial organizer of synaptic vesicle cycling, Molecular and Cellular Proteomics 5 (2006) 2060–2071.
[12] Y.H. Jin, H. Nishioka, K. Wakabayashi, T. Fujita, N. Yonehara, Effect of morphine on the release of excitatory amino acids in the rat hind instep: Pain is modulated by the interaction between the peripheral opioid and glutamate systems, Neuroscience 138 (2006) 1329–1339.
[13] Y.H. Jin, F. Yamaki, M. Takemura, Y. Koike, A. Furuyama, N. Yonehara, Capsaicin-induced glutamate release is implicated in nociceptive processing through activation of ionotropic glutamate receptors and group I metabotropic glutamate receptor in primary afferent fibers, Journal of Pharmacological Science 109 (2009) 233–241.
[14] K. Kabayama, T. Sato, K. Saito, N. Loberto, A. Prinetti, S. Sonnino, M. Kinjo, Y. Igarashi, J. Inokuchi, Dissociation of the insulin receptor and caveolin-1 complex by ganglioside GM3 in the state of insulin resistance, Proceedings of the National Academy of Sciences of the United States of America 104 (2007) 13678–13683.
[15] T. Lang, SNARE proteins and 'membrane rafts', The Journal of Physiology 585 (2007) 693–698.
[16] P.H. Lopez, R.L. Schnaar, Gangliosides in cell recognition and membrane protein regulation, Current Opinion in Structural Biology 19 (2009) 549–557.
[17] T. Mutoh, A. Tokuda, T. Miyadai, M. Hamaguchi, N. Fujiki, Ganglioside GM1 binds to the Trk protein and regulates receptor function, Proceedings of the National Academy of Sciences of the United States of America 92 (1995) 5087–5091.
[18] K. Omote, T. Kawamata, M. Kawamata, A. Namiki, Formalin-induced release of excitatory amino acids in the skin of the rat hindpaw, Brain Research 787 (1998) 161–164.
[19] D. Platika, M.H. Boulos, L. Baizer, M.C. Fishman, Neuronal traits of clonal cell lines derived by fusion of dorsal root ganglia neurons with neuroblastoma cells, Proceedings of the National Academy of Sciences of the United States of America 82 (1985) 3499–3503.
[20] A. Regina Todeschini, S.I. Hakomori, Functional role of glycosphingolipids and gangliosides in control of cell adhesion, motility, and growth, through glycosynaptic microdomains, Biochimica et Biophysica Acta 1780 (2008) 421–433.
[21] A.V. Tzingounis, J.I. Wadiche, Glutamate transporters: confining runaway excitation by shaping synaptic transmission, Nature Reviews 8 (2007) 935–947.
[22] K. Uemura, E. Sugiyama, T. Taketomi, Effects of an inhibitor of glucosylceramide synthase on glycosphingolipid synthesis and neurite outgrowth in murine neuroblastoma cell lines, Journal of Biochemistry 110 (1991) 96–102.
[23] M. Vinson, P.J. Strijbos, A. Rowles, L. Facci, S.E. Moore, D.L. Simmons, F.S. Walsh, Myelin-associated glycoprotein interacts with ganglioside GT1b. A mechanism for neurite outgrowth inhibition, The Journal of Biological Chemistry 276 (2001) 20280–20285.
[24] S. Watanabe, S. Endo, E. Oshima, T. Hoshi, H. Higashi, K. Yamada, K. Tohyama, T. Yamashita, Y. Hirabayashi, Glycosphingolipid synthesis in cerebellar Purkinje neurons: roles in myelin formation and axonal homeostasis, Glia 58 (2010) 1197–1207.
[25] S. Watanabe, K. Tan-No, T. Tadano, H. Higashi, Intraplantar injection of gangliosides produces nociceptive behavior and hyperalgesia via a glutamate signaling mechanism, Pain 152 (2011) 327–334.
[26] A. Wieraszko, W. Seifert, Evidence for a functional role of gangliosides in synaptic transmission: studies on rat brain striatal slices, Neuroscience Letters 52 (1984) 123–128.
[27] A. Wieraszko, W. Seifert, Evidence for the functional role of monosialoganglioside GM1 in synaptic transmission in the rat hippocampus, Brain Research 371 (1986) 305–313.
[28] A. Wieraszko, W. Seifert, The role of monosialoganglioside GM1 in the synaptic plasticity: in vitro study on rat hippocampal slices, Brain Research 345 (1985) 159–164.

Biochemical and Biophysical Research Communications 420 (2012) 193–198

Contents lists available at SciVerse ScienceDirect

Biochemical and Biophysical Research Communications

journal homepage: www.elsevier.com/locate/ybbrc

Gangliosides and chondroitin sulfate desensitize and internalize B2 bradykinin receptors ☆

Ayaka Shimazaki, Tetsuto Nakagawa, Junya Mitoma, Hideyoshi Higashi *

Division of Glyco-Signal Research, Institute of Molecular Biomembrane and Glycobiology, Tohoku Pharmaceutical University, 4-4-1 Komatsushima, Aoba-ku, Sendai, Miyagi 981-8558, Japan

ARTICLE INFO

Article history:
Received 20 February 2012
Available online 3 March 2012

Keywords:
Bradykinin
B2 receptor
Ganglioside
Chondroitin sulfate
GRK
Calcium mobilization

ABSTRACT

Prolonged or repeated agonist activation of G-protein-coupled receptors (GPCRs) initiates their desensitization and internalization, rendering them unresponsive to agonist activation. We analyzed how gangliosides and chondroitin sulfate affect B2 bradykinin (BK) receptors (B2Rs). Gangliosides and chondroitin sulfate did not stimulate intracellular Ca^{2+} release from B2R-expressing CHO-K1 cells, but repeated exposure desensitized B2Rs to BK stimulation. Microscopic observation of DsRed-fused B2Rs revealed that several gangliosides and chondroitin sulfate C (CSC) effectively internalized B2Rs. Ganglioside-CSC treatment of B2R mutant-expressing cells failed to desensitize and internalize the mutant receptors. As this mutant lacks the first extracellular domain and cannot activate GPCR kinase (GRK), gangliosides and CSC likely initiate B2R desensitization and endocytosis through GRK-mediated B2R phosphorylation.

1. Introduction

Bradykinin (BK) is a key regulator of vascular tone that has been implicated in pathological disorders such as inflammation, pain, and cancer (for review see [1]). BK stimulation of bradykinin B2 receptors (B2Rs) leads to activation of the Gαq/11 family of heterotrimeric G proteins in many cell types, which in turn stimulates the activity of phosphatidylinositol-specific phospholipase C (PLC) to yield PI hydrolysis and increase intracellular Ca^{2+}. Glycans of glycolipids, glycoproteins, and proteoglycans all are exposed to cell surfaces and contribute to intercellular recognition.

Gangliosides are acidic glycolipids that are major components of glycoconjugates in the brain. Exposure of neuronal cells to nanomolar concentrations of b-series gangliosides, such as GT1b, stimulate the transient increase of intracellular Ca^{2+} concentrations, activation of cdc42, and formation of filopodia [2], suggesting that gangliosides stimulate a cell surface glycan receptor. Since neuronal cells ubiquitously express B2Rs [3], and because BK is one of the known ligands for a G-protein-coupled receptor (GPCR) that activates cdc42 [4], we analyzed the interaction between gangliosides and B2Rs. For this purpose, we introduced B2R to CHO-K1 cells, which express undetectable levels of endogenous B2R and the response to the ganglioside was examined. We also analyzed chondroitin sulfate, another major acidic glycan in whole body since glycoconjugates other than gangliosides should contribute to early morphological brain development whereas morphological development of the brain is apparently normal in ganglioside deficient mice [5]. We found that chondroitin sulfate C (CSC) stimulated neuronal cells to release Ca^{2+} from intracellular store in the similar way as GT1b and that CSC activated B2R expressing in yeast cells. However, in CHO-K1 cells expressing transfected B2R, gangliosides and chondroitin sulfate did not induce Ca^{2+} release, instead they did stimulate desensitization to BK and endocytosis of B2Rs.

2. Materials and methods

2.1. Plasmids and constructs

Plasmids encoding human long variant (hB2R) and rat short variant B2R, starting at the second initiating ATG coding Met31 (rsB2R), were prepared by insertion of B2R cDNA between EcoRI and BamHI sites of pIRES2-EGFP (Clontech). Plasmids encoding B2R-DsRed fusion proteins were prepared by insertion of B2R cDNA (without stop codon) between EcoRI and AgeI sites of pDsRed-Monomer-N1 vector (Clontech). The cDNAs encoding the rat

Abbreviations: BK, bradykinin; B2R, B2 bradykinin receptor; CSC, chondroitin sulfate C; CSE, chondroitin sulfate E; GRK, G-protein-coupled receptor kinase; GM1, Galβ3GalNAcβ4(Neu5Acα3)Galβ4GlcCer; GD1a, Neu5Acα3Galβ3GalNAcβ4(Neu5Acα3)Galβ4GlcCer; GD1b, Galβ3GalNAcβ4(Neu5Acα8Neu5Acα3)Galβ4GlcCer; GT1b, Neu5Acα3Galβ3GalNAcβ4(Neu5Acα8Neu5Acα3)Galβ4GlcCer; GPCR, G-protein-coupled receptor; BSS, balanced salt solution.

☆ This study was supported by the "Academic Frontier" Project for Private Universities, Japan.

* Corresponding author. Fax: +81 22 727 0077.
E-mail address: hhigashi@tohoku-pharm.ac.jp (H. Higashi).

0006-291X/$ - see front matter © 2012 Elsevier Inc. All rights reserved.
http://dx.doi.org/10.1016/j.bbrc.2012.02.142

B2R variants, starting at amino acid Gln65 (B2R-ΔE1) [6], were constructed by polymerase chain reaction (PCR) and subcloned into pDsRed-Monomer-N1. For B2R-ΔE1, an initiating ATG was introduced to start translation at Gln65. The identity of the constructs was confirmed by DNA sequencing.

2.2. Cell culture

NG108-15 neuroblastoma-glioma hybridoma cells were cultured as described previously [2].

CHO-K1 cells were grown in alpha minimum essential medium (α-MEM) supplemented with 10% (v/v) fetal calf serum and kept in a humidified 5% CO_2/95% air atmosphere at 37 °C. CHO-K1 cells were transiently transfected with plasmids using GeneJuice (Merck) per the manufacturer's instructions. Transfection efficiency was 15–25%.

HEK293 cells were grown in Dulbecco's modified Eagle's medium with 5.5 mM glucose supplemented with 10% (v/v) fetal calf serum and kept in a humidified 5% CO_2/95% air atmosphere at 37 °C. HEK293 cells were transiently transfected with plasmids using Lipofectamine 2000 (Invitrogen) per the manufacturer's instructions. Transfection efficiency was 90% or more.

2.3. Yeast strain, manipulations and Gα expression and Ste2p deletion construct

Saccharomyces cerevisiae strain YKG005 (MATa ura3-52 lys2-801 ade2-101 his3-200 leu2-3 sst2Δ1 far1Δ1 ste2Δ1 gpa1Δ3:: GPA1-Gαq-c5 pep4Δ2 trp1-901 fus1::FUS1-HIS3 can1Δ::FUS1-CAN1 FUS2::FUS2-lacZ) was derived from YPH499 (MATa ura3-52 lys2-801 ade2-101 trp1-Δ63 his1-Δ200 leu2-Δ1) by a series of one-step gene replacements [7]. The FUS1-HIS3 reporter gene was integrated at the FUS1 locus. The FUS2-lacZ reporter gene was integrated for the β-galactosidase reporter assay. A yeast/mammalian G protein αq-subunit chimera, GPA1-Gq-c5, was constructed by replacing the C-terminal five amino acids of Gpa1p with those of a mammalian Gαq protein [8].

2.4. Plasmid for yeast transformation

Plasmid pYSF1 was derived from pYES2 (Invitrogen) by replacing the GAL1 promoter and the T7 promoter/primer sites with a STE2 promoter (0.42 kb), α factor leader (0.26 kb), FLAG tag, and a polylinker (EcoRI, XhoI, SmaI, BglII, BanIII, BamHI, ApaI, SalI, and SacII) at the position between the SpeI and NotI sites of pYES2. To express the human B2R, plasmid pYSF-B2R was created by inserting the B2R open reading frame into the EcoRI site of pYSF1. To express the murine B2R, plasmid pYSF-B2R was created by inserting the B2R open reading frame between the EcoRI and BamHI sites of pYSF1. To express the human AT1a angiotensin II receptor, plasmid pYSF-AT1a was created by inserting the AT1a open reading frame between the EcoRI and SalI sites of pYSF1. Preparation of the yeast competent cells and transformation was performed using a Fast-Yeast Transformation Kit (Geno Tech, Mo) according to the manufacturer's manual. Yeast expressing the two GPCRs was prepared by a co-transformation of the plasmids.

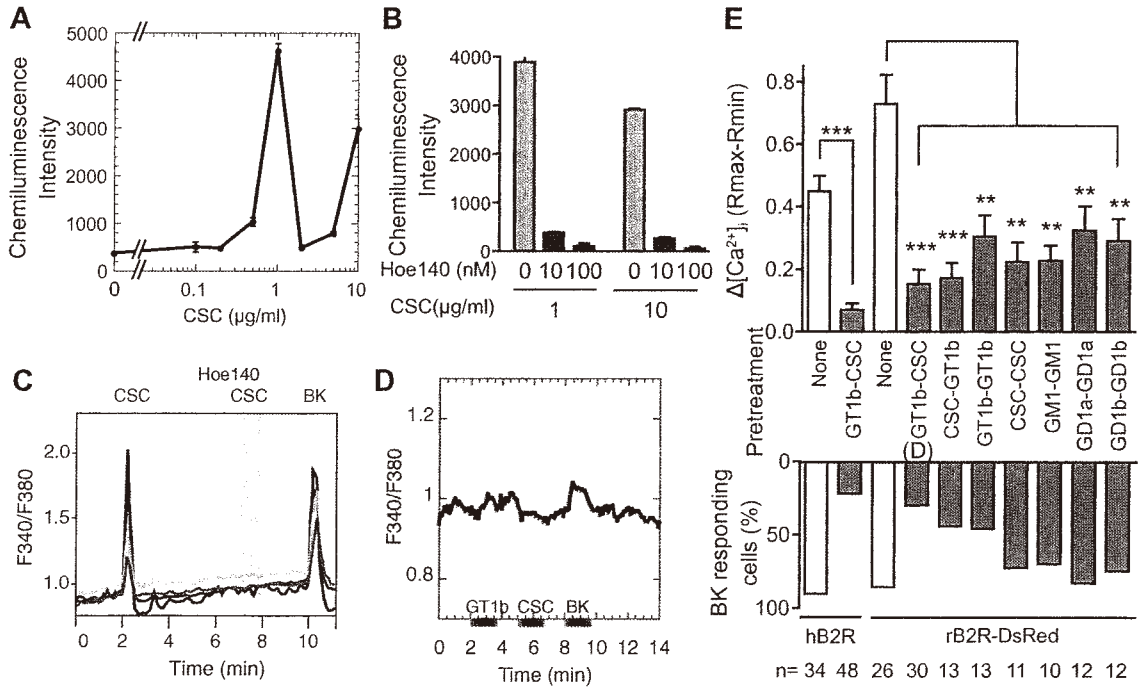

Fig. 1. B2R desensitization in non-neuronal cells after repeated treatment with gangliosides and CSC which stimulate B2R in neuronal cells and yeast cells. A, Activation of B2R signal by exogenously applied CSC in yeast reporter assay. Intensities of chemiluminescence produced by reporter β-galactosidase are shown as the reactivity. Error bar, standard error of three samples. B, Reactivity of 1 or 10 μg/ml of CSC to yeast expressing B2R was determined with or without Hoe140 at indicated concentrations. Blank value (without CSC) = 734 was subtracted from each value. Hoe140 significantly ($P < 0.05$) inhibited CSC induced B2R activities. C, NG108-15 neuroblastoma-glioma hybridoma cells were exposed to 1 μg/ml of CSC and 1 nM of B2 antagonist Hoe140 followed by CSC and 1 μM BK as indicated. Intracellular Ca^{2+} concentrations were monitored by fluorescence microscopy with Fura-2 as an indicator. Relative Ca^{2+} levels are expressed as a ratio of fluorescence at excitation wavelengths of 340–380 nm. D, CHO-K1 cells expressing DsRed-fused rat B2R (rB2R-DsRed) were exposed to 10 ng/ml GT1b, 1 μg/ml CSC, and 10 nM BK as indicated and intracellular Ca^{2+} concentrations were monitored as C. The average ratios of 30 individual cells are plotted. E, top, Peak increases in $[Ca^{2+}]_i$ of human B2R (hB2R) or rB2R-DsRed expressing CHO-K1 cells induced by 10 nM BK after indicated treatment as shown in D for example and without glycan treatment (None). Bottom, Percentage of BK-responding cells in among cells expressing EGFP or DsRed. *n*, numbers of cells analyzed. $^{***}P < 0.001$; $^{**}P < 0.01$.

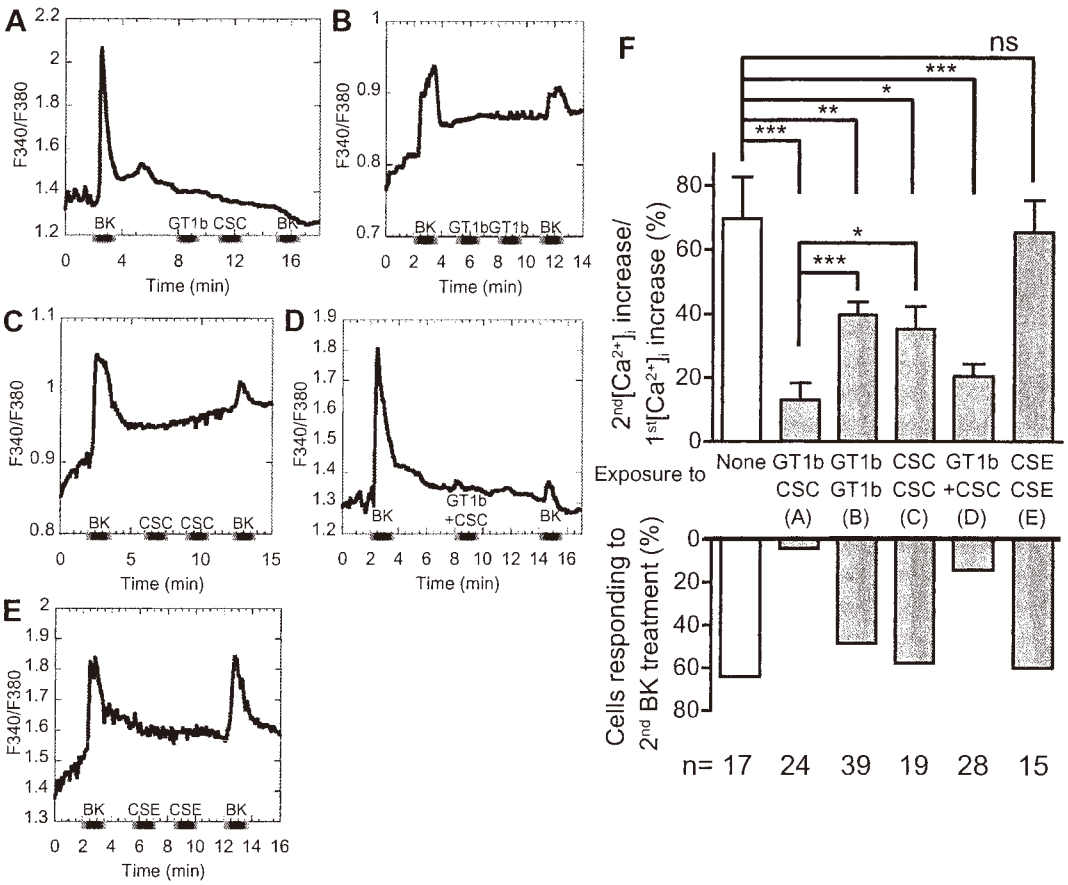

Fig. 2. B2R desensitization caused by repeated exposure to gangliosides and CSC. rB2R-DsRed was expressed in CHO-K1 (A, C, D, and E) and HEK293 (B) cells. The cells were exposed to 10 nM BK, 10 ng/ml GT1b, 1 μg/ml CSC, and 1 μg/ml CSE as indicated. The average ratios of individual cells that responded to the first BK treatment are plotted. Numbers of cells analyzed (n) are indicated in F. F, top, Percentage of peak increases in $[Ca^{2+}]_i$ induced by the second BK treatment. The percentage was calculated by dividing the peak increases in $[Ca^{2+}]_i$ induced by the second BK treatment by the peak increases in $[Ca^{2+}]_i$ induced by the first BK treatment (see A–E) and without glycan treatment (None). Bottom, Percentage of second BK-responding cells in among the first BK-responding cells. $^{***}P < 0.001$; $^{**}P < 0.01$; $^{*}P < 0.05$.

2.5. Yeast reporter assay for mammalian GPCR and ligand binding

The yeast cells (1×10^5) were suspended with ligands in a 40 μl SD-ura medium, pH 7.0, in 96-well flat-bottom white microplates. After incubation, (5 h at 30 °C), 40 μl of chemiluminescent substrate solution for the reporter β-galactosidase, and a Gal-Screen System for the yeast cell culture (Applied Biosystems) was added to the reaction mixture and incubated an additional 1 h. The chemiluminescence was determined using an Applied Biosystems TR717 Microplate Luminometer.

2.6. Ca^{2+} imaging

The Ca^{2+} indicator Fura-2 was loaded into cells as its acetoxymethyl ester (AM) derivative. A stock solution of 1 mM Fura-2-AM (Dojindo Labs., Kumamoto, Japan) in DMSO was diluted 400-fold into culture media and added to cells cultured on glass-bottom dishes (Asahi Glass Co., Tokyo, Japan). Cells were then incubated at 37 °C for 1–2 h to load and sensitize the Ca^{2+} probe through the cleaving of its AM group with cytosolic esterase. Images were acquired at emission wavelengths between 490 and 530 nm while exciting sequentially at 340 and 380 nm (exposure time: 0.1–2 s). The images were then analyzed as described previously [9,10] using an image processor (Aqua Q, Hamamatsu Photonics, Hamamatsu, Japan) connected to a cooled CCD camera (Orca, Hamamatsu Photonics).

Cells were exposed to stimulants by using the bath application method. Fura-2-loaded cells were conditioned with a flow of balanced salt solution (BSS), pH 7.3, consisting of 130 mM NaCl, 5.4 mM KCl, 20 mM HEPES, 5.5 mM glucose, 0.8 mM $MgSO_4$, and 1.8 mM $CaCl_2$ (1.75 ml/min) at 34 °C. The extracellular media in the assay dish was maintained at 1 ml. Thereafter, the cells were exposed to the stimulating reagent by changing the BSS flow to the reagent-containing BSS flow. After 1 min of exposure, the media was exchanged with BSS by changing the flow to BSS without the reagent. Thus, through this bath application method, the concentration of applied reagents reached maximum levels about 40 s after starting the application of the reagent and almost completely washed out about 40 s after the end of the application.

2.7. Other materials

Gangliosides were kindly provided by Dr. Yoshio Hirabayashi (Laboratory for Molecular Membrane Neuroscience, RIKEN Brain Science Institute, Wako, Saitama, Japan). Chondroitin sulfates were purchased from Seikagaku Co., Tokyo, Japan. BK and Hoe140, a B2-selective antagonist, were purchased from Peptide Institute Co., Osaka, Japan.

2.8. Statistical analysis

Results are presented as means ± SEM. The statistical significance between groups was assessed by 2-tailed unpaired Student's *t*-tests.

3. Results

3.1. Effects of chondroitin sulfates on B2R signaling in yeast and neuronal cells

We previously found that nanomolar levels of b-series gangliosides such as GT1b and GD1b induce Ca^{2+} release in neuronal cells [2] and we recently have found that around 10 nM of these gangliosides stimulate B2R signals in neuronal cells as well as in yeast cells expressing mammalian B2R [11]. As chondroitin sulfate is another acidic glycan widely distributed in mammalian body and plays neuro-regulatory roles like gangliosides, we first screened if chondroitin sulfate activate B2R in yeast reporter assay in which a yeast pheromone receptor, Ste2, was replaced with mammalian GPCR and the mammalian GPCR signal was linked via a chimeric yeast/mammalian Gα protein to the yeast pheromone receptor signaling pathway constructed to express reporter β-galactosidase. We tested commercially obtained chondroitin sulfate samples and found that chondroitin sulfate C and E activate B2R signals in all the B2R expressing yeast clones being CSC most potent (Fig. S1). Yeast coexpressing B2R and AT1a angiotensin II receptor, which form heterodimers with B2R [12], reacted better than yeast expressing solely B2R. Using one of the coexpressing clones, GqAB14, we examined dose–response of CSC and found that CSC showed at least two peaks of effective concentrations, around 1 μg/ml and over 10 μg/ml (Fig. 1A). CSC induced activation was inhibited by B2 antagonist Hoe140. Hoe140 at 10 and 100 nM reduced 1 and 10 μg/ml of CSC activities in similar degrees (Fig. 1B) suggesting that CSC is unlikely to compete with Hoe140 for B2R binding. Thus, we decided to use 1 μg/ml of CSC for the further experiments to avoid unexpected physicochemical effects by the strong acidity of the sulfate groups possibly brought by higher concentrations of CSC. We then examined the effect of CSC on a neuronal cell line, NG108-15 neuroblastoma-glioma hybridoma cells, which respond to GT1b by releasing Ca^{2+} [2]. CSC induced transient increase of intracellular Ca^{2+} levels as seen in ganglioside exposure and the reaction was inhibited when the cells were pretreated with Hoe140 (Fig. 1C). Thus, the effects of CSC on NG108-15 cells were similar to GT1b.

3.2. Reduced response of B2R to BK after repeated treatment with gangliosides and CSC

As shown previously [2] and above, neuronal cells respond to gangliosides and CSC in a similar way, we examined effects of those glycans on B2R exogenously introduced to CHO-K1 cells, which express undetectable levels of endogenous B2R, or to HEK293 cells, around 10% of which express endogenous B2R. As effective concentration ranges observed with neuronal cells and yeast reporter assay is around 10 ng/ml for GT1b and GD1b [2,11], and 1 μg/ml for CSC, we tested the effects of the glycans at these concentrations.

Treating B2R-overexpressing CHO-K1 and HEK293 cells with 10 nM BK transiently increased intracellular Ca^{2+} levels. Repeated treatment with BK caused the cells to become desensitized to BK. Human B2R, rat B2R, and DsRed-fused rat B2R were activated and desensitized. When the cells were pretreated sequentially with 10 ng/ml GT1b and 1 μg/ml CSC, 70–78% of the cells stopped responding to 10 nM BK (Fig. 1D, E). However, when the cells were exposed once to either of these two glycans, the cells still responded to BK and displayed increased Ca^{2+} levels (data not shown). The reversed sequential treatment—exposing the cells first to CSC and then to GT1b—also caused the cells to become desensitized to BK (Fig. 1E). The same occurred with repeated treatments with either GT1b or CSC (Fig. 1E). These results indicated that

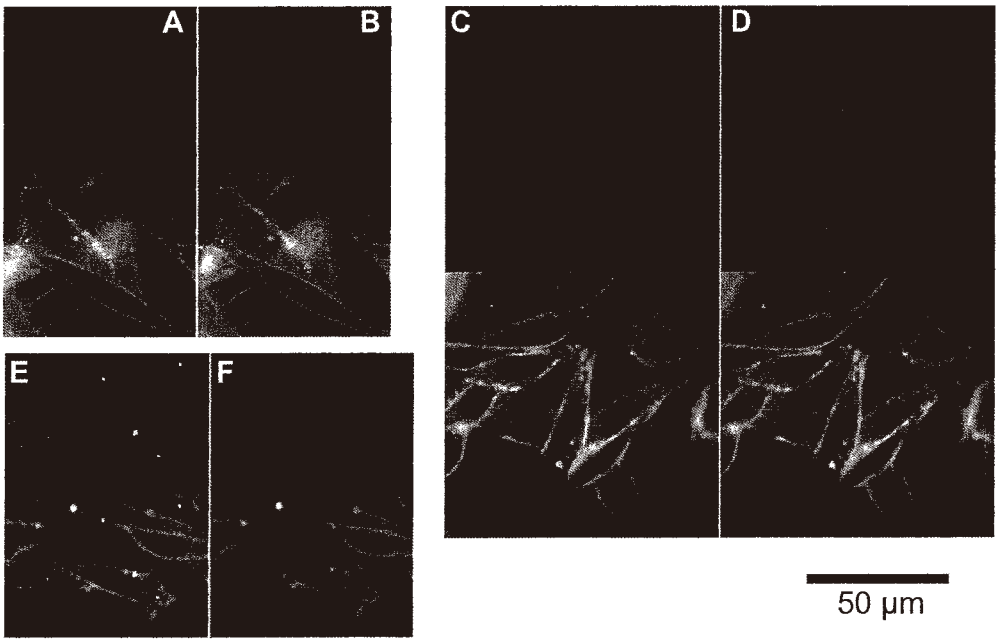

Fig. 3. Expression pattern of rat B2R-DsRed in CHO-K1 cells before and after B2R desensitization. Cells before (A, C, and E) and after sequential exposure to 10 nM BK, 10 ng/ml GT1b, and 1 μg/ml CSC (B, D, and F) of DsRed images. Plasma membrane was stained with a lipophilic styryl dye MF43-1FX (Molecular Probes) after the treatment per the manufacturer's instructions. Fluorescence images were obtained at an excitation wavelength of 560 nm for the DsRed and of 485 nm for MF43-1FX. Top and bottom of each figures are DsRed image (red) and DsRed image merged with MF43-1FX image (green), respectively. Scale bar, 50 μm.

repeated treatment with glycans induced B2R desensitization. We also examined the effects of other related glycans and found that GM1, GD1a, and GD1b affected the cells similarly to GT1b (Fig. 1E).

To verify that the B2R-expressing cells are capable of responding to BK before glycan treatment, we exposed the cells first to 10 nM BK, treated them sequentially with glycans (GT1b and CSC), and then exposed them a second time to BK (Fig. 2). More than 95% of the cells failed to respond to BK after the sequential GT1b–CSC treatment (Fig. 2A, F). Exposing the cells to the GT1b–CSC mixture similarly reduced BK reactivity (Fig. 2D, F). Exposing the cells twice to either GT1b or CSC also reduced BK reactivity, but the effects were weaker than those observed when cells were exposed sequentially to each glycan (Fig. 2B, C, F). In contrast to CSC, chondroitin sulfate E (CSE) was not effective in reducing BK reactivity (Fig. 2E, F), indicating that glycan structure, not acidity, determines whether a glycan desensitizes B2Rs to BK.

3.3. Internalization of B2R by ganglioside or CSC treatment

Fluorescent microscopic images of cells expressing rat B2R-DsRed revealed that some B2R-DsRed were distributed across cell surfaces (Fig. 3A, C, E). After desensitization with gangliosides and CSC, cell-surface fluorescence disappeared; however, the fluorescence intensity of small vesicle-like structures in the cytosol increased (Fig. 3B, D, F). These results suggested that the repeated glycan treatment caused B2R-DsRed to be internalized.

3.4. Glycan-induced internalization probably depends on GPCR receptor kinase (GRK)

Truncated rat B2R mutant (B2RΔE1), which lacks the first extracellular domain, cannot be desensitized and internalized, as it cannot be phosphorylated by GRK [6]. All the cells expressing B2RΔE1-DsRed responded to BK stimulation and released Ca^{2+}, even after repeated GT1b and CSC treatment, without significant reduction of the response (Fig. 4). Thus, gangliosides and CSC desensitized B2R most likely by stimulating GRK-mediated B2R phosphorylation.

4. Discussion

We here demonstrated that ganglioside and CSC application to non-neuronal cells that express the BK B2 receptor desensitizes and internalizes B2Rs without inducing Gαq/11 protein-mediated Ca^{2+} release.

GPCRs constitute the largest family of proteins that convert external stimuli into intracellular activity [13]. Signal transduction of GPCRs is tightly controlled: Prolonged or repeated agonist stimulation desensitizes and internalizes these receptors such that ligands cannot access the receptors [14,15]. This modulatory process seems to involve agonist-induced receptor phosphorylation [16–18]. In the present study, although gangliosides and CSC stimulated the desensitization and internalization of B2R, they

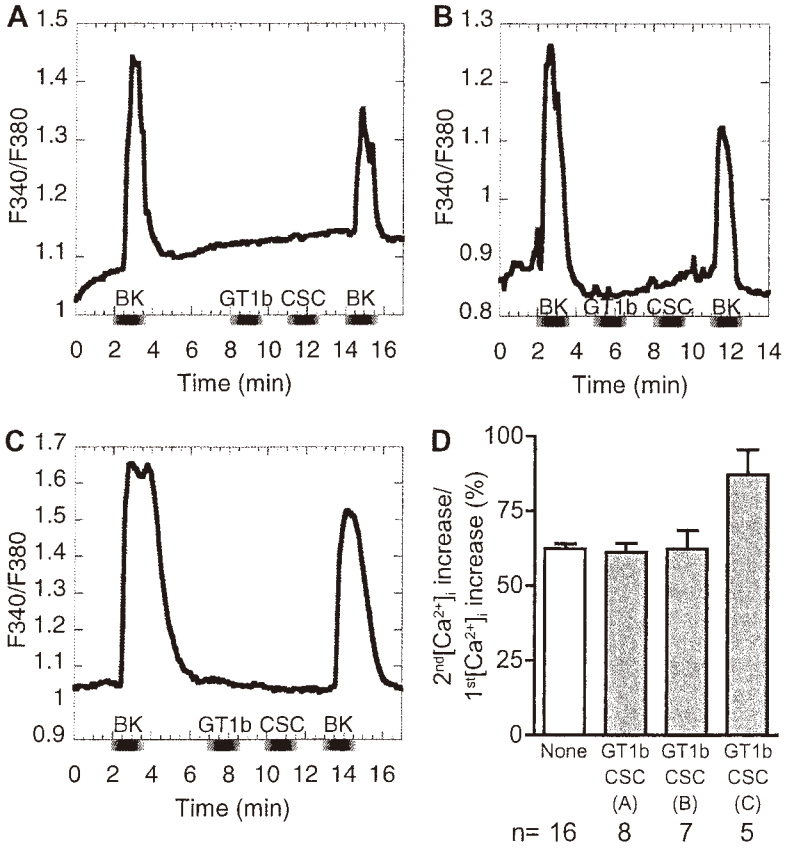

Fig. 4. Sequential glycan treatment failed to desensitize a B2R mutant lacking the first extracellular domain. A DsRed-fused rat B2R mutant lacking the first extracellular domain (B2RΔE1-DsRed) was expressed in CHO-K1 (A, B) and HEK293 (C) cells. The cells were exposed to 10 nM BK, 10 ng/ml GT1b, and 1 μg/ml CSC as indicated. The average ratios of individual cells are plotted. Numbers of cells analyzed (*n*) are indicated in D. All the cells that responded to the first BK stimulation also responded to the second BK stimulation. D, Percentage of peak increases in $[Ca^{2+}]_i$ induced by the second BK treatment over those induced by the first BK treatment of A–C (GT1b/CSC) and without glycan treatment (None).

failed to activate G-protein-coupled phospholipase and subsequent Ca^{2+} release (Figs. 1 and 2). Because a B2R mutant unable to activate GRK was not desensitized and internalized by gangliosides and CSC (Fig. 4), the glycan-stimulated desensitization and internalization of B2R seems to involve B2R phosphorylation followed by β-arrestin recruitment, as in the case of agonist-induced receptor desensitization and internalization.

Among the glycans we tested, the GT1b and CSC combination seemed to be the most potent and effective in desensitizing and internalizing B2Rs. However, even though we examined the individual effects of several glycans, we tested only a few glycan combinations.

The B2 antagonist Hoe140 (at 100 nM) showed little, if any, effects on glycan-stimulated desensitization and internalization (data not shown), also suggesting that the glycan-induced B2R desensitization was not accompanied by B2R activation.

B2R participates in the regulation of blood pressure, inflammation, and pain. B2Rs are distributed ubiquitously in cells throughout the body, including neuronal tissues. Gangliosides and chondroitin sulfates also are distributed not only in neuronal tissues but also throughout the body. These glycans probably regulate B2R function. Recently, we determined that b-series gangliosides such as GT1b and GD1b generate and enhance pain [19]. Unlike b-series gangliosides, a-series gangliosides such as GM1 and GD1a do not generate and enhance pain [19]. As GM1 and GD1a stimulated B2R desensitization in the present study, these gangliosides and CSC may play a role in pain relief through B2R desensitization.

We previously found that b-series gangliosides induce Ca^{2+} release in neuronal cells [2] and we recently have found that ganglioside GT1b stimulate B2R signals in neuronal cells as well as in yeast cells expressing mammalian B2R [11]. The present study using B2R-expressing non-neuronal cells did not produce such results. Thus, it remains unclear whether B2Rs directly participate in ganglioside-mediated neuronal cell excitation. This issue will be addressed in a future study. In neuronal cells, another factor may mediate ganglioside-associated regulation of G-protein-coupled signaling.

Acknowledgments

We thank Dr. Yoshio Hirabayashi (Laboratory for Molecular Membrane Neuroscience, RIKEN Brain Science Institute, Wako, Saitama, Japan) for the generous gift of various gangliosides.

Appendix A. Supplementary data

Supplementary data associated with this article can be found, in the online version, at doi:10.1016/j.bbrc.2012.02.142.

References

[1] L.M. Leeb-Lundberg, F. Marceau, W. Muller-Esterl, D.J. Pettibone, B.L. Zuraw, International union of pharmacology. XLV. Classification of the kinin receptor family: from molecular mechanisms to pathophysiological consequences, Pharmacol. Rev. 57 (2005) 27–77.
[2] N. Chen, S. Furuya, H. Doi, Y. Hashimoto, Y. Kudo, H. Higashi, Ganglioside/calmodulin kinase II signal inducing cdc42-mediated neuronal actin reorganization, Neuroscience 120 (2003) 163–176.
[3] E.Y. Chen, D.F. Emerich, R.T. Bartus, J.H. Kordower, B2 bradykinin receptor immunoreactivity in rat brain, J. Comp. Neurol. 427 (2000) 1–18.
[4] R. Kozma, S. Ahmed, A. Best, L. Lim, The Ras-related protein Cdc42Hs and bradykinin promote formation of peripheral actin microspikes and filopodia in Swiss 3T3 fibroblasts, Mol. Cell. Biol. 15 (1995) 1942–1952.
[5] T. Yamashita, Y.P. Wu, R. Sandhoff, N. Werth, H. Mizukami, J.M. Ellis, J.L. Dupree, R. Geyer, K. Sandhoff, R.L. Proia, Interruption of ganglioside synthesis produces central nervous system degeneration and altered axon-glial interactions, Proc. Natl. Acad. Sci. USA 102 (2005) 2725–2730.
[6] S. AbdAlla, E. Zaki, H. Lother, U. Quitterer, Involvement of the amino terminus of the B(2) receptor in agonist-induced receptor dimerization, J. Biol. Chem. 274 (1999) 26079–26084.
[7] R. Rothstein, Targeting, disruption, replacement, and allele rescue: integrative DNA transformation in yeast, Methods Enzymol. 194 (1991) 281–301.
[8] A.J. Brown, S.L. Dyos, M.S. Whiteway, J.H. White, M.A. Watson, M. Marzioch, J.J. Clare, D.J. Cousens, C. Paddon, C. Plumpton, M.A. Romanos, S.J. Dowell, Functional coupling of mammalian receptors to the yeast mating pathway using novel yeast/mammalian G protein alpha-subunit chimeras, Yeast 16 (2000) 11–22.
[9] Y. Kudo, A. Ogura, Glutamate-induced increase in intracellular Ca^{2+} concentration in isolated hippocampal neurons, Br. J. Pharmacol. 89 (1986) 191–198.
[10] N. Chadborn, B. Eickholt, P. Doherty, S. Bolsover, Direct measurement of local raised subplasmalemmal calcium concentrations in growth cones advancing on an N-cadherin substrate, Eur. J. Neurosci. 15 (2002) 1891–1898.
[11] Y. Kanatsu, N.H. Chen, J. Mitoma, T. Nakagawa, Y. Hirabayashi, H. Higashi, Gangliosides stimulate bradykinin B2 receptors to promote calmodulin kinase II-mediated neuronal differentiation, J. Biochem. in press.
[12] S. AbdAlla, H. Lother, U. Quitterer, AT1-receptor heterodimers show enhanced G-protein activation and altered receptor sequestration, Nature 407 (2000) 94–98.
[13] E.J. Neer, Heterotrimeric G proteins: organizers of transmembrane signals, Cell 80 (1995) 249–257.
[14] S.S. Ferguson, Evolving concepts in G protein-coupled receptor endocytosis: the role in receptor desensitization and signaling, Pharmacol. Rev. 53 (2001) 1–24.
[15] R.J. Lefkowitz, G protein-coupled receptors. III. New roles for receptor kinases and beta-arrestins in receptor signaling and desensitization, J. Biol. Chem. 273 (1998) 18677–18680.
[16] S.K. Bohm, E.F. Grady, N.W. Bunnett, Regulatory mechanisms that modulate signalling by G-protein-coupled receptors, Biochem. J. 322 (Pt 1) (1997) 1–18.
[17] N.J. Freedman, R.J. Lefkowitz, Desensitization of G protein-coupled receptors, Recent Prog. Horm. Res. 51 (1996) 319–353.
[18] J.G. Krupnick, J.L. Benovic, The role of receptor kinases and arrestins in G protein-coupled receptor regulation, Annu. Rev. Pharmacol. Toxicol. 38 (1998) 289–319.
[19] S. Watanabe, K. Tan-No, T. Tadano, H. Higashi, Intraplantar injection of gangliosides produces nociceptive behavior and hyperalgesia via a glutamate signaling mechanism, Pain 152 (2011) 327–334.

J. Biochem. 2012;152(1):63–72 doi:10.1093/jb/mvs055

JB THE JOURNAL OF BIOCHEMISTRY

Gangliosides stimulate bradykinin B2 receptors to promote calmodulin kinase II-mediated neuronal differentiation

Received February 12, 2012; accepted March 8, 2012; published online May 9, 2012

Yoshinori Kanatsu[1,2,*], Nai Hong Chen[3], Junya Mitoma[1,2], Tetsuto Nakagawa[1,2], Yoshio Hirabayashi[2,4] and Hideyoshi Higashi[1,2,†]

[1]Division of Glyco-Signal Research, Institute of Molecular Biomembrane and Glycobiology, Tohoku Pharmaceutical University, Sendai, Miyagi 981-8558; [2]Core Research for Evolutional Science and Technology Program (CREST) of Japan Science and Technology Corporation, Kawaguchi, Saitama 332-0012, Japan; [3]Institute of Materia Medica, Chinese Academy of Medical Sciences and Peking Union Medical College, Beijing 100050, China; and [4]Laboratory for Molecular Membrane Neuroscience, Brain Science Institute, RIKEN, Wako, Saitama 351-0198, Japan

[†]Hideyoshi Higashi, Division of Glyco-Signal Research, Institute of Molecular Biomembrane and Glycobiology, Tohoku Pharmaceutical University, 4-4-1 Komatsushima, Aoba-ku, Sendai, Miyagi 981-8558, Japan. Tel: +81-22-727-0119, Fax: +81-22-727-0077, email: hhigashi@tohoku-pharm.ac.jp

*Present address: Department of Anatomy, Akita University School of Medicine, Hondo 1-1-1, Akita 010-8543, Japan.

Gangliosides mediate neuronal differentiation and maturation and are indispensable for the maintenance of brain function and survival. As part of our ongoing efforts to understand signaling pathways related to ganglioside function, we recently demonstrated that neuronal cells react to exogenous gangliosides GT1b and GD1b. Both of these gangliosides are enriched in the synapse-forming area of the brain and induce Ca^{2+} release from intracellular stores, activation of Ca^{2+}/calmodulin-dependent protein kinase II (CaMKII) and activation of cdc42 to promote reorganization of cytoskeletal actin and dendritic differentiation. Here, we show that bradykinin B2 receptors transduce these reactions as a mediator for ganglioside glycan signals. The B2 antagonist Hoe140 inhibited ganglioside-induced CaMKII activation, actin reorganization and early development of axon- and dendrite-like processes of primary cultured hippocampal neurons. Furthermore, we confirmed by yeast reporter assay that major b-series gangliosides, GT1b, GD1b and GD3, stimulated B2 bradykinin receptors. We hypothesize that this B2 receptor-mediated ganglioside signal transduction pathway is one mechanism that modulates neuronal differentiation and maturation.

Keywords: bradykinin receptor/Ca^{2+} signal/cdc42/ganglioside/neuritogenesis.

Abbreviations: AM, acetoxymethyl ester; AS2, acrylodan-CPLARTLSVAGLPGKK; ATII, angiotensin II; AT1a, angiotensin II receptor 1a; B1R, bradykinin B1 receptor; B2R, bradykinin B2 receptor; BSS, balanced salt solution; CaMKII, Ca^{2+}/calmodulin-dependent protein kinase II; CNS, central nervous system; DIV, days *in vitro*; GD1a, Neu5Acα3Galβ3GalNAcβ4(Neu5Acα3)Galβ4GlcCer; GD1b, Galβ3GalNAcβ4(Neu5Acα8Neu5Acα3)Galβ4GlcCer; GD3, Neu5Acα8Neu5Acα3Galβ4GlcCer; GM1, Galβ3GalNAcβ4(Neu5Acα3)Galβ4GlcCer; GM2, GalNAcβ4(Neu5Acα3)Galβ4GlcCer; GM3, Neu5Acα3Galβ4GlcCer; GPCR, G-protein-coupled receptor; Hoe140, D-arginyl-[Hyp[3], Thi[5], D-Tic[7], Oic[8]]-bradykinin; GT1b, Neu5Acα3Galβ3GalNAcβ4(Neu5Acα8Neu5Acα3)Galβ4GlcCer; Oic, (3aS,7aS)-octahydroindolyl-2-carboxylic acid; PBS, phosphate-buffered saline; Tic, 1,2,3,4-tetrahydroisoquinoline-3-carboxylic acid; Thi, L-thienylalanine.

Glycans of glycolipids, glycoproteins and proteoglycans are all exposed to cell surfaces and contribute to intercellular recognition. Gangliosides are acidic glycolipids that are major components of glycoconjugates in the brain. We found that exposure of neural cells to nanomolar levels of gangliosides GD1b and GT1b stimulates several reactions: Ca^{2+} release from intracellular stores, Ca^{2+}/calmodulin-dependent protein kinase II (CaMKII) activation, cdc42-mediated cytoskeletal actin reorganization and dendritic differentiation (*1*). Mice lacking ganglioside synthesis die soon after birth, with degradation of their central nervous system (CNS) (*2*). The ganglioside signal transduction pathway that we identified is purported to mediate CNS differentiation and maintenance. The cell surface portion of the glyco-receptor has been suggested to recognize glycans, because cdc42 activation is rapid and the oligosaccharide portion of GT1b ganglioside is active as the ganglioside itself (*1*). Moreover, because ganglioside-induced release of Ca^{2+} may be mediated through phospholipase C activation via Gαq protein, trimeric G proteins are suggested to contribute to this reaction.

The present study sought to identify the molecule that transduces cell-surface glyco-signals from the extracellular ganglioside glycan into intracellular signals. As bradykinin is one of the known ligands for a G-protein-coupled receptor (GPCR) that activates cdc42 (*3–5*), we used bradykinin antagonists to determine whether bradykinin receptors may be involved in glycan-related signal transduction. We found that a bradykinin B2 antagonist did indeed inhibit glyco-signals. The gangliosides GD1b and GT1b stimulated both axon- and dendrite-like neuritogenesis in primary cultured hippocampal neurons. In addition, the B2 antagonist Hoe140 inhibited part of

the stimulating effects of the gangliosides. Using a reporter assay system constructed in budding yeast, which has a far simpler GPCR system than mammalian cells, we confirmed that the B2 bradykinin receptor (B2R) acted as a cell surface glyco-signal mediator or transducer. We propose that glyco-signals serve as a mechanism for regulating neuronal development and differentiation.

Materials and Methods

Cell culture

NG108-15 neuroblastoma-glioma hybridoma cells were cultured as described previously (*1*). Primary cultures of rat hippocampal cells were prepared from 19-day-old embryonic rat brains and cultured as described previously (*6*, *7*). Cells were plated on glass-bottom dishes at low density (8,000–10,000 cells/cm^2) and cultivated in a N2 medium as described by Clement *et al.* (*7*). The cultures consisted of a minimal Eagle's medium supplemented with N2 mixture, 0.1 mM pyruvate, 0.1% (w/v) ovalbumin and 0.01% (w/v) apo-transferrin. The B2 antagonist Hoe140 was added to the culture media at the time of plating. The cultures were then kept in a humidified atmosphere of 5% CO_2 at 37°C.

Cell culturing onto ganglioside-coated glass culture plates and neurite staining

Preparation of the culture substrates and staining of the neurites were performed as described by Clement *et al.* (*7*). Glass-bottom dishes (35 mm; Asahi Glass Co., Tokyo, Japan) were pre-coated with 15 μg/ml poly-DL-ornithine in 0.1 M borate buffer (pH 8.1) for 1 h, washed three times with H_2O and coated with 1 μg/ml ganglioside in phosphate-buffered saline (PBS) overnight at 37°C. Afterwards, the culture dishes were washed three times with PBS and flooded with N2 medium containing cells. The cells cultured were fixed, permeabilized and stained with a tubulin monoclonal antibody. The amount of ganglioside coated onto the glass culture dishes was determined by measuring the amount of sialic acids released from the ganglioside immobilized on the glass surface by heating at 80°C in 0.1 N H_2SO_4 for 1 h. The released sialic acids were quantified by fluorometric thiobarbituric acid assay (*8*).

Imaging of CaMKII activity in cells

CaMKII activity in the living cells was monitored by fluorescence imaging as described previously (*9*) using a fluorescent-labeled peptide substrate of CaMKII, acrylodan-CPLARTLSVAGLPGKK (AS2). A balanced salt solution (BSS, pH 7.3) consisting of 130 mM NaCl, 5.4 mM KCl, 20 mM HEPES, 5.5 mM glucose, 1.8 mM $CaCl_2$ and 0.8 mM $MgSO_4$ was used as the extracellular media. Calpeptin (1 μM) was added to protect the peptide substrate. Cells were cultured on poly-lysine-coated glass-bottom dishes (35 mm; MatTek, MA, USA). The cells were loaded with the substrate through incubation with 150 μM AS2 in BSS for 30 min at 25°C. The substrate-loaded cells were exposed to ganglioside and antagonist via a bath application method as described (*1*, *10*). Cell fluorescence was measured at 360 nm excitation and then subjected to image analysis using an image processor (Argus 50, Hamamatsu Photonics, Shizuoka, Japan).

Ca^{2+} imaging

Ca^{2+} indicators (Fura-2) were loaded into the cells as their acetoxymethyl ester (AM) derivatives. A stock solution of 1 mM Fura-2-AM (Dojindo Labs, Kumamoto, Japan) in DMSO was diluted 1000- or 200-fold into BSS and added to the cells cultured on the poly-lysine-coated glass-bottom dishes. The cells were then incubated at 37°C for 30 min to load and sensitize the Ca^{2+} probe by cleaving its AM group with cytosolic esterase. Images were acquired at emission wavelengths between 490 and 530 nm while exciting sequentially at 340 and 380 nm (exposure time: 1–2 s). The images were subjected to image analysis using an image processor (Aqua-C Imaging, Hamamatsu Photonics) connected to a cooled CCD camera (Orca-ER, Hamamatsu Photonics). Cells were exposed to stimulants by bath application as described previously (*1*, *10*).

Detection of polymerized actin

Cultured cells were washed three times with BSS, exposed to a stimulator in BSS with or without inhibitors for 2 min and then fixed with 4% paraformaldehyde/100 mM phosphate buffer (pH 7.4) for 15 min at 25°C. The polymerized cytoskeletal actin was visualized with rhodamine–phalloidin using the method of Ono *et al.* (*11*) with modifications (*1*).

Yeast strain, manipulations and Gα expression and Ste2p deletion constructs

Saccharomyces cerevisiae strain YKG005 (*MATa ura3-52 lys2-801 ade2-101 his3-200 leu2-3 sst2Δ1 far1Δ1 ste2Δ1 gpa1Δ3::GPA1-Gαq-c5 pep4Δ2 trp1-901 fus1::FUS1-HIS3 can1Δ::FUS1-CAN1 FUS2::FUS2-lacZ*) was derived from YPH499 (*MATa ura3-52 lys2-801 ade2-101 trp1-Δ63 his1-Δ200 leu2-Δ1*) through a series of one-step gene replacements (*12*). The *FUS1–HIS3* reporter gene was integrated at the *FUS1* locus. The *FUS2-lacZ* reporter gene was integrated for the β-galactosidase reporter assay. A yeast/mammalian G protein αq-subunit chimera, GPA1-Gq-c5, was constructed by replacing the C-terminal five amino acids of Gpa1p with those of a mammalian Gαq protein (*13*).

Plasmid for yeast transformation

Plasmid pYSF1 was derived from pYES2 (Invitrogen) by replacing the *GAL1* promoter and the T7 promoter primer sites with a *STE2* promoter (0.42 kb), α factor leader (0.26 kb), FLAG tag and a polylinker (EcoRI, XhoI, SmaI, BglII, BanIII, BamHI, ApaI, SalI and SacII) at the position between the SpeI and NotI sites of pYES2. To express human B2R, we created plasmid pYSF-B2R by inserting the B2R open reading frame into the EcoRI site of pYSF1. To express murine B2R, we created plasmid pYSF-B2R by inserting the B2R open reading frame between the EcoRI

and BamHI sites of pYSF1. To express human angiotensin II receptor 1a (AT1a) receptor, we created plasmid pYSF-AT1a by inserting the AT1a open reading frame between the EcoRI and SalI sites of pYSF1. To express rat B1 bradykinin receptor (B1R), we created plasmid pYSF-B1 by inserting the B1R open reading frame between the BglII and BamHI sites of pYSF1. Preparation of competent yeast cells and transformation was performed using a Fast-Yeast Transformation Kit (Geno Tech, Maryland Heights, MO, USA) according to the manufacturer's manual. Yeasts expressing the two GPCRs were prepared by a co-transformation of the plasmids.

Yeast reporter assay for mammalian GPCR and ligand binding

The yeast cells (1×10^5) were suspended with ligands in 40 µl of SD-ura medium (pH 7.0) in white 96-well flat-bottom microplates. After incubation, (5 h at 30°C), 40 µl of chemiluminescent substrate solution for the reporter β-galactosidase and a Gal-Screen System for yeast cell cultures (Applied Biosystems) was added to the reaction mixture and incubated an additional 1 h. Chemiluminescence was determined using an Applied Biosystems TR717 Microplate Luminometer.

Other materials

Gangliosides GT1b, GD1b, GD1a, GD3 and GM1 were purchased from Iatron Co. (Japan). The oligosaccharide portion of the ganglioside was prepared by EGCase digestion as described (*14*). Bradykinin, human ATII, B2R-selective antagonist Hoe140 and B1-selective antagonist Des-Arg^9-[Leu^8]-bradykinin were purchased from the Peptide Institute Co. (Japan).

Results

Bradykinin antagonist-associated inhibition of GT1b-mediated intracellular Ca^{2+} release, CaMKII activation and filopodia formation

We have previously shown that the oligosaccharide portion of GT1b ganglioside stimulates cdc42-mediated reorganization of cytoskeletal actin through the rapid release of Ca^{2+} from intracellular stores and through the activation of CaMKII (*1*). These findings suggest that oligosaccharides trigger cdc42 upregulation via a cell-surface receptor-like component, most likely GPCR. Although several downstream signals of cdc42 have been identified, only a few extracellular stimulators are known to activate cdc42 via GPCRs, one of which is bradykinin (*3–5*).

To determine whether bradykinin receptors act as oligosaccharide receptors, we investigated the effects of bradykinin antagonists on GT1b-induced CaMKII activation. We detected GT1b-induced CaMKII activation using a fluorescence microscopic imaging system and a fluorescent-labeled peptide substrate, AS2, as described previously (*1*, *9*). As shown in Fig. 1A, when GT1b was added to the extracellular media of primary cultured rat hippocampal neurons, a rapid increase in the fluorescence signal was detected in the cytosol, indicating that the substrate was

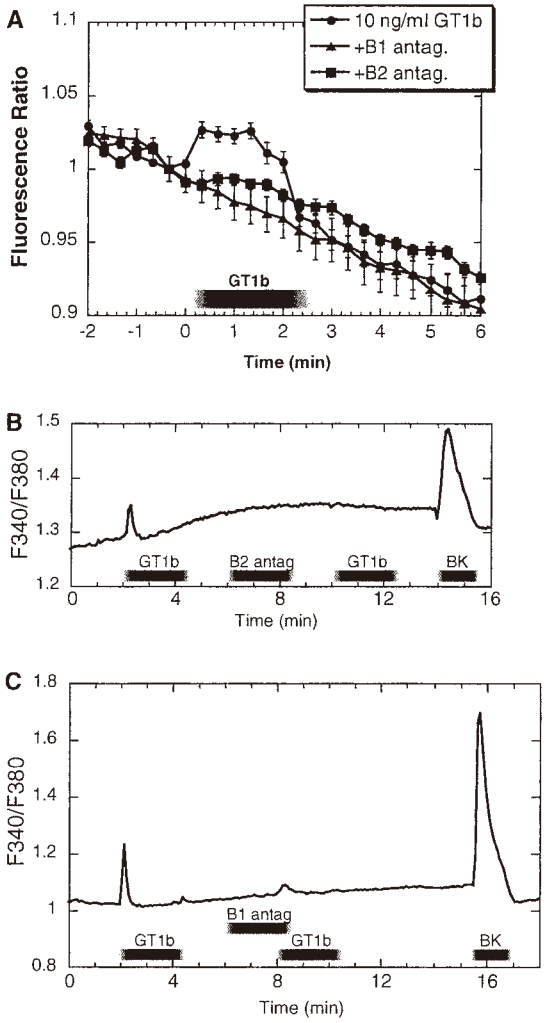

Fig. 1 Prevention of GT1b-mediated activation of intracellular CaMKII and Ca^{2+} release by bradykinin B1 and B2 antagonists. (**A**) Primary cultured rat hippocampal cells were preloaded with a fluorescent peptide substrate, AS2, and were exposed to 10 ng/ml GT1b for 2 min and 40 s as indicated. AS2 fluorescence increases as it becomes phosphorylated. The time course of the averaged fluorescence ratios in cytosolic areas of 28, 24 and 26 cells without an antagonist, with a B1 antagonist, and with a B2 antagonist, respectively, were plotted every 20 s. The ratio was calculated by dividing the fluorescence intensity at each time by that at −20 s. CaMKII activation by 10 ng/ml GT1b was undetectable in the presence of 100 nM B1 antagonist (Des-Arg^9-[Leu^8]-bradykinin) or 10 nM B2 antagonist (Hoe140) in the extracellular media. Error bars, standard error. (**B** and **C**) NG108-15 cells were preloaded with Fura-2-AM and were exposed to 20 ng/ml GT1b as in (A). The time course of the averaged fluorescence ratios excited at wavelengths of 340/380 nm (F340/F380) in cytosolic areas of 15 cells for (B) and 11 cells for (C) were plotted every 5 s. GT1b-induced elevation of intracellular Ca^{2+} levels were undetectable after exposure to 10 nM Hoe140 (B) and were inhibited after exposure to 100 nM B1 antagonist (C).

phosphorylated by CaMKII in accordance with a previous report (*1*). This reaction was inhibited when either a bradykinin B1 antagonist (100 nM Des-Arg^9-[Leu^8]-bradykinin) or a B2 antagonist (10 nM Hoe140) was present in the media. This result indicated that

GT1b-induced CaMKII activation was mediated by bradykinin B1 and/or B2 receptors. Since the upstream reaction of CaMKII is Ca^{2+} release from intracellular stores, we analyzed the effects of the antagonists on GT1b-induced elevation of intracellular Ca^{2+} levels. As shown in Fig. 1B and C, GT1b-induced Ca^{2+} release was inhibited after treating NG108-15 cells with B2 or B1 antagonists.

We then investigated how the antagonists affected filopodia formation, a downstream reaction of CaMKII activation. As shown in Fig. 2B and C, exposing NG108-15 cells to GT1b for 2 min induced filopodia formation in a CaMKII-dependent manner. The GT1b-mediated filopodia formation was partially blocked by the B1 antagonist and completely blocked by the B2 antagonist (Fig. 2D and E), indicating that the GT1b signal for filopodia formation was mainly mediated by B2Rs.

Neurite outgrowth on ganglioside-containing culture substrates and effects of B2 antagonist

We previously observed that the oligosaccharide portion of GT1b, when introduced to culture media, promoted dendritic outgrowth in primary cultured hippocampal and cerebellar Purkinje neurons by at least 4 days *in vitro* (DIV) (*1*). In the present study, we sought to determine whether these gangliosides coated on culture dishes affect early neurite development by contact with the cell surface. We prepared the ganglioside-containing culture substrate according to the method used for preparing chondroitin sulfate-containing culture substrates (*7*). The efficiency of ganglioside-coating was determined to be approximately 30%, meaning that about 300 ng of gangliosides was immobilized onto the glass surface (27 mm diameter) of a culture dish ($\approx$50 ng/cm^2). The ganglioside-containing culture substrate promoted neuritogenesis in primary cultured rat hippocampal neurons (Fig. 3). The longest neurite of cells was denoted axon-like neurites, whereas the remaining neurites were denoted dendrite-like neurites, according to Dotti *et al.* (*15*). GT1b was the most potent promoter of axon- and dendrite-like neuritogenesis followed by GD1b and GM1 (Fig. 4). When added to the culture medium, the B2 antagonist Hoe140 maximally inhibited GD1b- and GT1b-induced neuritogenesis at concentrations of 10 and 100 nM, respectively. The B1 antagonist also inhibited the neuritogenic effects of GT1b. These results indicate that gangliosides can potentially promote the growth of both axon- and dendrite-like neurites and that ganglioside signals are transduced via B2Rs and perhaps via B1Rs.

Gangliosides and their oligosaccharides stimulate B2Rs in a yeast reporter assay

To confirm the stimulatory effects of glycans on B2Rs, we used a yeast reporter system in which a yeast pheromone receptor, Ste2, was replaced with mammalian GPCR. In addition, the mammalian GPCR signal was linked via a chimeric yeast/mammalian Gα protein to the yeast pheromone receptor signaling pathway constructed to express the reporter β-galactosidase. The yeast/mammalian Gαq chimeric protein, GPA1-Gαq-c5, was constructed by replacing five amino acid residues in the Gpa1p C-terminal with those of Gαq. We examined glycan binding by either expressing B2R (GqB2) or coexpressing B2R with AT1a receptor (GqAB) in the yeast system. As shown in Fig. 5A, the oligosaccharide portion of GT1b reacted to both the B2R-expressing clones and the B2R/AT1a receptor coexpressing clones to activate the pheromone-signaling pathway. Yeast coexpressing B2R and AT1a reacted better than yeast expressing

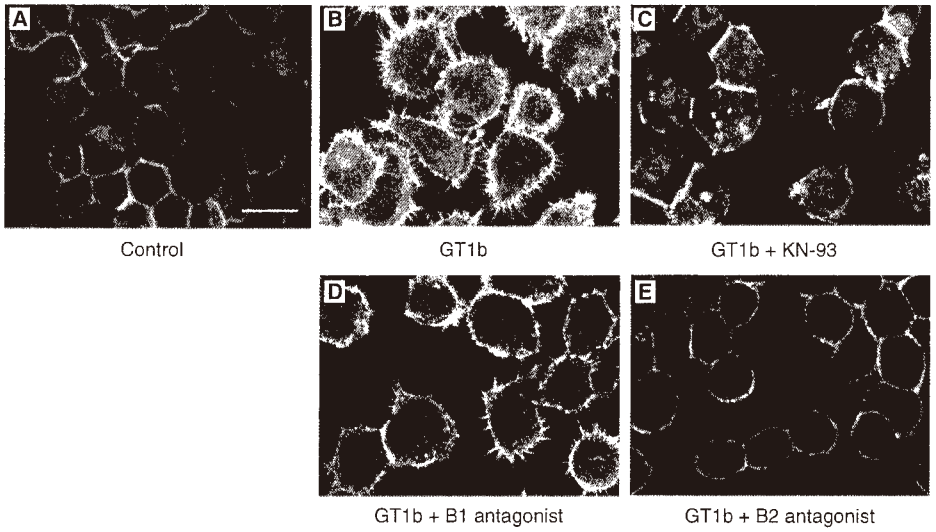

Fig. 2 Effects of CaMKII and bradykinin receptor inhibitors on GT1b-induced filopodia formation. NG108-15 cells were exposed to 10 ng/ml GT1b (**B–E**) without any inhibitors (**B**); or with 10 μM KN-93, a CaMKII inhibitor (**C**); 100 nM Des-Arg^9-[Leu^8]-bradykinin, a B1 antagonist (**D**); or 10 nM Hoe140, a B2 antagonist (**E**) for 2 min at 37°C. The cells were then fixed and stained with rhodamine–phalloidin and observed with a confocal fluorescence microscope. For the control, cells were untreated (A). Scale bar, 10 μm.

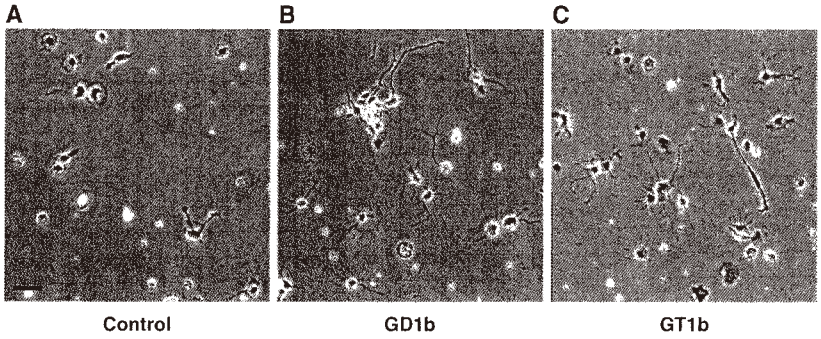

Fig. 3 Differentiation of primary cultured hippocampal neurons on glycan-containing substrate in the defined media. Axon- and dendrite-like neurites of neurons cultured on substrates containing GD1b (**B**) and GT1b (**C**) were more elongated than those cultured on the control poly-ornithine substrate (**A**). Defined culture media were used as described in 'Materials and Methods'. Scale bar, 50 μm.

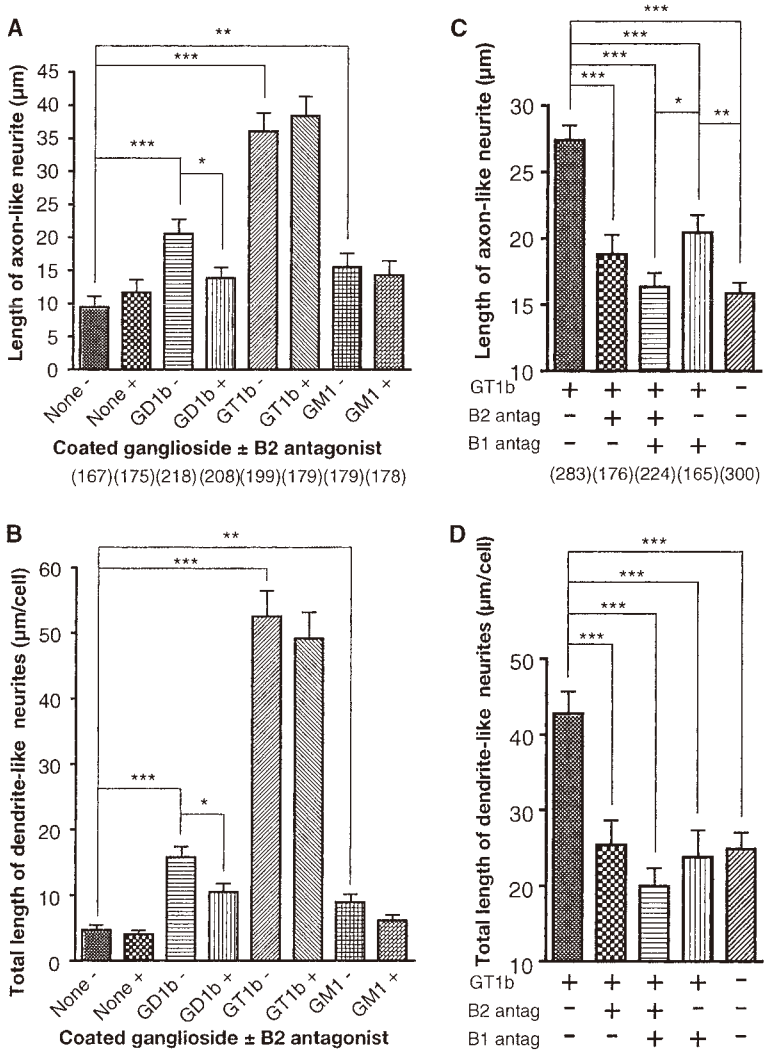

Fig. 4 Neurite outgrowth on glycan-containing culture substrates and effects of B2 antagonist. Hippocampal neurons were grown on substrates composed of the indicated gangliosides in culture media (see Fig. 3). (**A** and **B**) Effects of a B2 antagonist were examined by adding (+) 10 nM Hoe140 to the media. (**C** and **D**) The effects of a higher concentration (100 nM) of Hoe140 and 100 nM Des-Arg^9-[Leu^8]-bradykinin (a B1 antagonist) on GT1b-mediated neuritogenesis were examined in a separate experiment. A '+' or '−' denotes the presence or absence of GT1b coating or antagonist in the media, as indicated. The mean lengths ± SE of the longest neurites (termed 'axon-like neurites') (A and C) or the sum of lengths of other neurites (termed 'dendrite-like neurites') of single neurons (B and D) are plotted. Numbers of neurons analyzed are shown in parentheses in (**A**) and (**C**). Statistical significance of neurite length relative to different substrates and effects of antagonists were compared using a Student's *t* test. $^{***}P<0.001$; $^{**}P<0.01$; $^{*}P<0.05$.

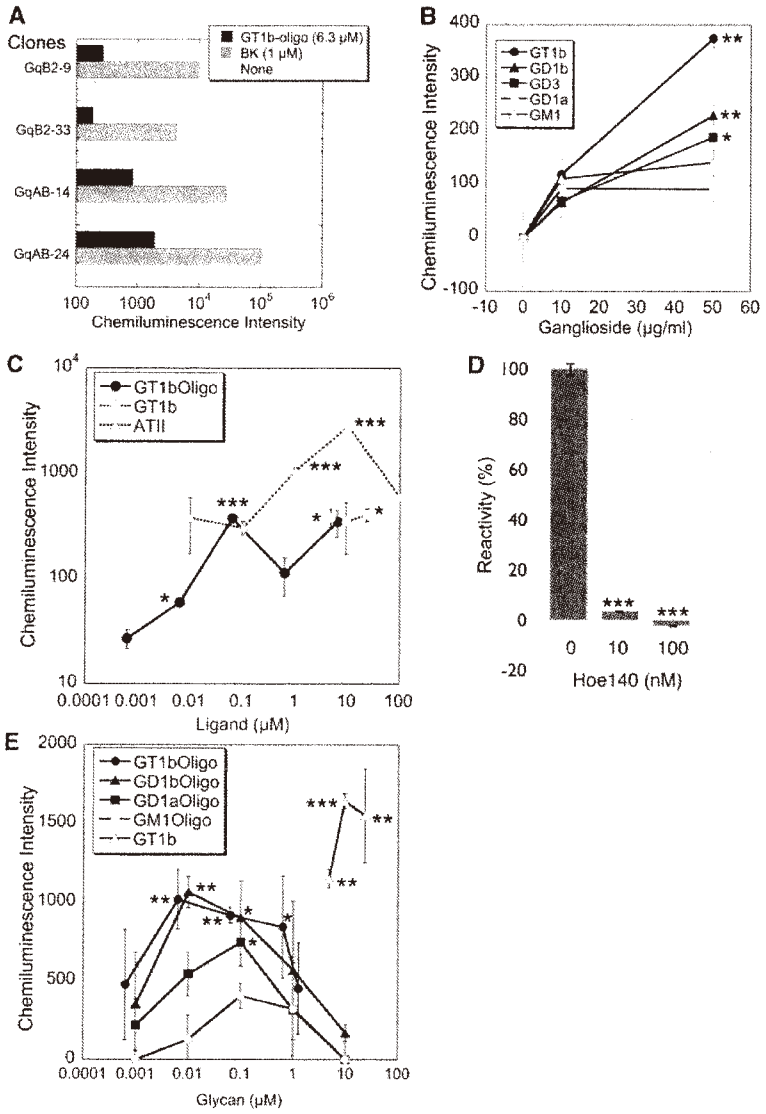

Fig. 5 Activation of B2R signal by exogenously applied glycans in yeast reporter assay. (**A**) Different yeast clones that expressed only human B2R (GqB2) or coexpressed B2R with human AT1a (GqAB) were used. Clone numbers are shown after the yeast names. Reactivity of the oligosaccharide portion of GT1b (GT1b oligo) and reactivity of 1 μM bradykinin (BK) are shown. (**B**) Reactivity of gangliosides GT1b, GD1b, GD3, GD1a and GM1 were determined using the yeast clone GqB2-9. Intensities of chemiluminescence produced by the β-galactosidase reporter represent reactivity. Error bars, standard error of three samples. (**C**) Reactivity of different concentrations of GT1b, GT1b oligosaccharide and human ATII to yeast clone GqAB-14 (A) were determined. Chemiluminescence intensities of assay mixture without ligand were subtracted from those with ligand. (**D**) Reactivity of 63 nM of the oligosaccharide portion of GT1b to yeast clone GqAB-14 was determined in the absence or presence of the B2 antagonist Hoe140 at the indicated concentrations. Relative activities (%) based on samples lacking the antagonist are shown. Similar results were obtained when another yeast clone (GqAB-24) was used. (**E**) Reactivity of GT1b and oligosaccharide portions of gangliosides in yeast expressing mouse B2R. Error bars, standard error of three samples. Significant differences of reactivity compared with reactivity at zero ligand concentration are shown as $^{***}P<0.001$; $^{**}P<0.01$; $^{*}P<0.05$ (Student's *t*-test).

solely B2R. The oligosaccharide did not react to yeast clones that solely expressed either B1R or AT1a (data not shown). Moreover, the oligosaccharide portion of GM1 ganglioside did not react to B2R/AT1a- or B2R-expressing clones (data not shown). These results indicate that B2Rs mediated the glycan signal of GT1b.

Using a yeast reporter assay, we then examined the reactivity of various gangliosides. As shown in Fig. 5B, GT1b, GD1b and GD3 reacted to B2R, with GT1b exhibiting the most potent reactivity. GD1b and GD3 showed moderate and slight reactivity, respectively, corresponding to their efficiency for stimulating CaMKII and cdc42-mediated actin reorganization (*1*). Similar results were obtained with yeast clone GqAB-14 (data not shown).

Since in the yeast reporter assay system the effective ganglioside concentration was above the micromolar range (Fig. 5B), which is 2–3 orders of magnitude higher than that in experiments using mammalian

cells, we assumed that, by interacting with the yeast cell wall, the hydrophobic ceramide portion of the gangliosides should influence how the gangliosides affect the receptor in the yeast cell membrane. Thus, we examined the reactivity of GT1b and its oligosaccharide portion to B2R-expressing yeast. As shown in Fig. 5C, in GqAB yeast the oligosaccharide portion of GT1b reacted at a concentration range of 6.3–63 nM, reaching nearly maximal reactivity at 63 nM. To determine whether bradykinin antagonists inhibit this reaction in the yeast assay system, we examined the reactivity of the oligosaccharide portion of GT1b to GqAB yeast in the presence of the B2 antagonist Hoe140. Hoe140 completely abolished oligosaccharide reactivity (Fig. 5D), confirming that B2R is a potential mediator of glycan signaling related to the oligosaccharide portion of GT1b ganglioside.

Next, we analyzed the reactivity of other ganglioside-derived oligosaccharides using yeasts that only express B2R. As shown in Fig. 5E, the oligosaccharide portion of GT1b reacted significantly to these yeasts at a concentration range of 6.3–630 nM in the same way as it reacted to GqAB yeast, with a maximal reactivity at 6.3 nM. In the same fashion as GT1b oligosaccharide, the oligosaccharide portion of GD1b reacted to B2R significantly at a concentration range of 10–100 nM, and the oligosaccharide portion of GD1a reacted significantly at a concentration of 0.1 μM. However, although the oligosaccharide portion of GM1 reacted to these yeast cells, the reactions were not statistically significant at a concentration range of 1 nM to 10 μM. Nonetheless, these results show that the oligosaccharides reacted to B2Rs on yeast cells as well as on mammalian cells at a concentration of less than 1 μM.

Discussion

The present study demonstrated that B2Rs modulate neuritogenesis by serving as mediators for the glycan signal of GT1b and GD1b gangliosides. GT1b and GD1b have been shown to stimulate B2Rs to activate the Ca^{2+}/CaMKII signal transduction pathway (*1*). This is supported by the finding that a B2 antagonist inhibited several GT1b-induced reactions in neuronal cells, such as Ca^{2+} release, CaMKII activation and cdc42-mediated actin reorganization (*1*). We then demonstrated that at least part of the modulatory effects of these glycans on neuritogenesis resulted from the stimulation of B2Rs by GT1b and GD1b gangliosides. To analyze the functional interaction between B2Rs and the glycans of these two gangliosides, we performed a yeast reporter assay, which showed that GT1b, GD1b and GD3 stimulate B2Rs. B2Rs are ubiquitously and selectively expressed in neurons (*16*) and probably contribute to neuronal differentiation as glycan-signal mediators in addition to their role as a peptide receptor.

The budding yeast *S.cerevisiae* has only two species of GPCRs, and their signaling pathways are well characterized. For the present study, we utilized an assay system in which yeast pheromone GPCRs were replaced with mammalian B2Rs. This assay system was much simpler to use than those involving mammalian cells. Mammalian cells are not suitable for analyzing the functions of a single GPCR because mammals have more than 300 species of GPCRs, some of which function by forming heterodimers (*17–25*), making it difficult to clarify which specific GPCRs are expressed in a cell. Moreover, it is difficult to clarify the output of the signals because sometimes more than two Gα proteins work as partners of a single GPCR (*26*). In the yeast reporter assay used here, we were able to observe bradykinin activity clearly (Fig. 5A). Moreover, yeast coexpressing B2R and AT1a, but not yeast expressing solely AT1a, reacted with ATII (Fig. 5C), which was expected since B2R/AT1a dimer formation is essential for ATII signal transduction via AT1a (*22*).

In this assay, we demonstrated preference of b-series gangliosides over a-series gangliosides in the stimulation of B2R. This is consistent with the preference observed in neuronal cells. In the yeast reporter assay, the effective concentration of a ganglioside was much higher than that of its oligosaccharide portion (Fig. 5), as the cell wall of yeast may interfere with hydrophobic ligand access to B2Rs. GT1b and GD1b stimulated B2Rs at the same concentration ranges (Fig. 5B). GD3 also showed weak, but significant reactivity to B2Rs consistent with our previous findings that GD3 also activates CaMKII and promotes CaMKII-dependent filopodia formation (*1*). Oligosaccharide portions of GD1a and GM1 showed reactivity at concentrations of 0.1 μM in the yeast reporter assay (Fig. 5E), whereas GM1 but not GD1a ganglioside stimulates slight elevation of cytosolic Ca^{2+} of NG108-15 cells (*1*). This discrepancy may be caused by the different accessibility of the gangliosides and oligosaccharides to the plasma membranes and different physicochemical nature of plasma membranes between yeast and mammalian cells. In our yeast reporter assay, specificity of glycan reactivity was the same for yeast expressing solely B2R and those coexpressing B2R and AT1a (Fig. 5A). However, yeast expressing either B1R or AT1a as the sole GPCR did not react with the glycans. Moreover, the B1 agonist Des-Arg^{10}-Kallidin failed to stimulate reporter production in B1R-expressing yeast (data not shown), suggesting that another factor, such as heterodimer formation, is necessary for the functional expression of B1R. The reaction of the glycans with B2R was completely inhibited by the B2 antagonist Hoe140. Thus, we concluded that glycans stimulate B2R. B2R stimulation by the glycans tended to be more intensive when B2R was coexpressed with AT1a. This may be due to heterodimer formation by these receptors (*22*).

In the present study, to confirm that the gangliosides target cell surface molecules in order to induce activities such as neuronal differentiation, we investigated how the gangliosides affect hippocampal neurons cultured on a ganglioside-coated surface. This method mimics cell–cell or cell–extracellular environment interactions. In this experiment, GD1b and GT1b stimulated the formation of both axon-like and dendrite-like processes. Hoe140 significantly inhibited

these effects (Fig. 4). In this analysis, GD1b-induced effects were inhibited significantly by 10 nM Hoe140, but GT1b-induced effects were not and 100 nM Hoe140 was needed for the inhibition. It is probable that the efficiency of GT1b is too high to compete with 10 nM Hoe140 since the actual densities of the gangliosides coated on the culture surface ($\approx 50\,ng/cm^2$) were relatively higher than that added as a solution (10 ng/ml). We previously found that the oligosaccharide portion of GT1b stimulates dendritogenesis in primary cultured rat hippocampal neurons 4–7 DIV after exposure to the oligosaccharide (*1*). The present results are consistent with this phenomenon, which we surmise to be also mediated by B2Rs. The GT1b effect was also significantly inhibited by 100 nM B1 antagonist (Fig. 4C, D), suggesting that another signaling cascade via B1R was involved. This premise was corroborated by the findings that the B1 antagonist inhibited GT1b-induced Ca^{2+} release, CaMKII activation and filopodia formation in other experiments using neuronal cells (Fig. 1 and 2D).

Mice lacking all ganglio-series gangliosides, which are characteristically found in the brain, are born as double null mutants of GM3 and GM2 synthases (*2*). They die soon after birth due to impaired CNS maturation and exhibit axon degradation and altered axon–glial interactions. This indicates that gangliosides mediate neuronal maturation and maintenance of neuronal architecture and function. In the literature, there is a plethora of functional studies that have investigated gangliosides at the cell or tissue level (*10*). We previously identified an additional cdc42-mediated neuritogenesis pathway triggered by GM2 ganglioside (*27*). In a cell-free system, gangliosides interact directly with calmodulin and calmodulin-dependent enzymes, including CaMKII, to regulate enzymatic activity (*28*, *29*). Gangliosides and oligosaccharides applied extracellularly, as in the present study, have difficulty in rapidly accessing cytosolic proteins like calmodulin and calmodulin-dependent enzymes. Since gangliosides bind to unique amphiphilic peptide structures of these proteins (*30*), it is likely that they may also bind such structures in B2R protein.

Gangliosides account for a large part of brain glycoconjugates and are characteristically found in the brain. Different species of gangliosides are distributed differentially in the brain. GD1b and GT1b, which activate cdc42 via CaMKII activation, distribute in the area of synapses (*31*, *32*). B2Rs are ubiquitously and selectively expressed in brain neurons. In the cerebellum, Purkinje cells are enriched with B2Rs more than other neurons such as granular neurons (*16*). GD1b and GT1b are not expressed in Purkinje cells but are well expressed in granular neurons (*31*). Purkinje cells and granular neurons expand their dendrites and their axons, respectively, to form synapses in the molecular layer. Thus, B2Rs and ganglioside ligands may play roles in synapse formation between Purkinje cell dendrites and granular neuron axons. Consistent with this notion is the finding that adding the oligosaccharide portion of GT1b into the extracellular medium stimulated dendritogenesis in primary cultured Purkinje and hippocampal neurons (*1*). In the present study, we demonstrated that adding either GT1b or GD1b to the culture substrate stimulated early neuritogenesis in primary cultured hippocampal neurons. The effects of the gangliosides were mediated by B2Rs. The same signal may play a role in dendritogenesis in Purkinje cells.

Generally, GT1b is expressed during a late developmental stage in the brain. However, in rat cerebellar cortex, GT1b expression starts at birth first in the molecular and internal granular layers and then with development in other layers, except the Purkinje cell layer (*33*). Moreover, GT1b expression in the molecular and internal granular layers continues throughout adulthood (*33*). GD1b expression occurs in all layers of the cerebellar cortex, except the Purkinje cell layer, starting at birth and continuing throughout adulthood. Thus, these gangliosides may affect neurite outgrowth during brain development.

B2R-deficient mice are born, mature normally and are fertile (*34*). They do, however, exhibit some disorders such as Na^+-dependent hypertension (*35*), short life span, abnormal mitochondrial physiology, abnormal morphology of Leydig cells in testes and reduced bone density (*36*). At present, with the exception of altered nociceptive responses (*37*), no neurological abnormalities have been reported in these mice. However, since B2Rs are ubiquitously and selectively expressed in neurons (*16*), the effects of B2R deficiency on neural systems should be analyzed carefully. As the B2R-mediated glyco-signal system mediates at least some of the differentiation and maturation processes in the CNS, gangliosides, B2 antagonists and B2 agonists, therefore may be useful in regenerative therapy.

Recent reports have shown that B2Rs sense fluid shear stress (*38*), suggesting that dynamic changes in membrane structure due to environmental influences affect the spatial conformation of GPCRs and their activation. Oligosaccharide portions of GT1b and GD1b modulate the conformation of B2Rs in membranes for activation either by binding to the receptors themselves or by interacting with an environmental component of B2R-containing membranes, the micro-domain 'raft'.

Acknowledgements

The authors are grateful to Dr. Yasunori Kozutsumi at Kyoto University for valuable discussions.

Funding

This study was supported by grants from the Core Research for Evolutional Science and Technology Program (CREST) of the Japan Science and Technology Corporation (JST) and by the Academic Frontier Project for Private Universities, Japan.

Conflict of interest

None declared.

References

1. Chen, N., Furuya, S., Doi, H., Hashimoto, Y., Kudo, Y., and Higashi, H. (2003) Ganglioside/calmodulin kinase II

signal inducing cdc42-mediated neuronal actin reorganization. *Neuroscience* **120**, 163–176
2. Yamashita, T., Wu, Y.P., Sandhoff, R., Werth, N., Mizukami, H., Ellis, J.M., Dupree, J.L., Geyer, R., Sandhoff, K., and Proia, R.L. (2005) Interruption of ganglioside synthesis produces central nervous system degeneration and altered axon-glial interactions. *Proc. Natl. Acad. Sci. U.S.A.* **102**, 2725–2730
3. Kozma, R., Ahmed, S., Best, A., and Lim, L. (1995) The Ras-related protein Cdc42Hs and bradykinin promote formation of peripheral actin microspikes and filopodia in Swiss 3T3 fibroblasts. *Mol. Cell. Biol.* **15**, 1942–1952
4. Wilk-Blaszczak, M.A., Singer, W.D., Quill, T., Miller, B., Frost, J.A., Sternweis, P.C., and Belardetti, F. (1997) The monomeric G-proteins Rac1 and/or Cdc42 are required for the inhibition of voltage-dependent calcium current by bradykinin. *J. Neurosci.* **17**, 4094–4100
5. Feoktistov, I., Goldstein, A.E., and Biaggioni, I. (2000) Cyclic AMP and protein kinase A stimulate Cdc42: role of A2 adenosine receptors in human mast cells. *Mol. Pharmacol.* **58**, 903–910
6. Kudo, Y. and Ogura, A. (1986) Glutamate-induced increase in intracellular Ca^{2+} concentration in isolated hippocampal neurons. *Br. J. Pharmacol.* **89**, 191–198
7. Clement, A.M., Nadanaka, S., Masayama, K., Mandl, C., Sugahara, K., and Faissner, A. (1998) The DSD-1 carbohydrate epitope depends on sulfation, correlates with chondroitin sulfate D motifs, and is sufficient to promote neurite outgrowth. *J. Biol. Chem.* **273**, 28444–28453
8. Hammond, K.S. and Papermaster, D.S. (1976) Fluorometric assay of sialic acid in the picomole range: a modification of the thiobarbituric acid assay. *Anal. Biochem.* **74**, 292–297
9. Higashi, H., Sato, K., Omori, A., Sekiguchi, M., Ohtake, A., and Kudo, Y. (1996) Imaging of Ca2+ / calmodulin-dependent protein kinase II activity in hippocampal neurons. *Neuroreport.* **7**, 2695–2700
10. Higashi, H. and Chen, N.H. (2004) Ganglioside/protein kinase signals triggering cytoskeletal actin reorganization. *Glycoconj. J.* **20**, 49–58
11. Ono, S., Abe, H., and Obinata, T. (1996) Stimulus-dependent disorganization of actin filaments induced by overexpression of cofilin in C2 myoblasts. *Cell Struct. Funct.* **21**, 491–499
12. Rothstein, R. (1991) Targeting, disruption, replacement, and allele rescue: integrative DNA transformation in yeast. *Methods Enzymol.* **194**, 281–301
13. Brown, A.J., Dyos, S.L., Whiteway, M.S., White, J.H., Watson, M.A., Marzioch, M., Clare, J.J., Cousens, D.J., Paddon, C., Plumpton, C., Romanos, M.A., and Dowell, S.J. (2000) Functional coupling of mammalian receptors to the yeast mating pathway using novel yeast/ mammalian G protein alpha-subunit chimeras. *Yeast.* **16**, 11–22
14. Higashi, H., Ito, M., Fukaya, N., Yamagata, S., and Yamagata, T. (1990) Two-dimensional mapping by the high-performance liquid chromatography of oligosaccharides released from glycosphingolipids by endoglycoceramidase. *Anal. Biochem.* **186**, 355–362
15. Dotti, C.G., Sullivan, C.A., and Banker, G.A. (1988) The establishment of polarity by hippocampal neurons in culture. *J. Neurosci.* **8**, 1454–1468
16. Chen, E.Y., Emerich, D.F., Bartus, R.T., and Kordower, J.H. (2000) B2 bradykinin receptor immunoreactivity in rat brain. *J. Comp. Neurol.* **427**, 1–18
17. White, J.H., Wise, A., Main, M.J., Green, A., Fraser, N.J., Disney, G.H., Barnes, A.A., Emson, P., Foord, S.M., and Marshall, F.H. (1998) Heterodimerization is required for the formation of a functional GABA(B) receptor. *Nature* **396**, 679–682
18. Jones, K.A., Borowsky, B., Tamm, J.A., Craig, D.A., Durkin, M.M., Dai, M., Yao, W.J., Johnson, M., Gunwaldsen, C., Huang, L.Y., Tang, C., Shen, Q., Salon, J.A., Morse, K., Laz, T., Smith, K.E., Nagarathnam, D., Noble, S.A., Branchek, T.A., and Gerald, C. (1998) GABA(B) receptors function as a heteromeric assembly of the subunits GABA(B)R1 and GABA(B)R2. *Nature* **396**, 674–679
19. Kaupmann, K., Malitschek, B., Schuler, V., Heid, J., Froestl, W., Beck, P., Mosbacher, J., Bischoff, S., Kulik, A., Shigemoto, R., Karschin, A., and Bettler, B. (1998) GABA(B)-receptor subtypes assemble into functional heteromeric complexes. *Nature* **396**, 683–687
20. Jordan, B.A. and Devi, L.A. (1999) G-protein-coupled receptor heterodimerization modulates receptor function. *Nature* **399**, 697–700
21. Liu, F., Wan, Q., Pristupa, Z.B., Yu, X.M., Wang, Y.T., and Niznik, H.B. (2000) Direct protein-protein coupling enables cross-talk between dopamine D5 and gamma-aminobutyric acid A receptors. *Nature* **403**, 274–280
22. AbdAlla, S., Lother, H., and Quitterer, U. (2000) AT1-receptor heterodimers show enhanced G-protein activation and altered receptor sequestration. *Nature* **407**, 94–98
23. Nelson, G., Hoon, M.A., Chandrashekar, J., Zhang, Y., Ryba, N.J., and Zuker, C.S. (2001) Mammalian sweet taste receptors. *Cell* **106**, 381–390
24. Nelson, G., Chandrashekar, J., Hoon, M.A., Feng, L., Zhao, G., Ryba, N.J., and Zuker, C.S. (2002) An amino-acid taste receptor. *Nature* **416**, 199–202
25. Suzuki, T., Namba, K., Tsuga, H., and Nakata, H. (2006) Regulation of pharmacology by hetero-oligomerization between A1 adenosine receptor and P2Y2 receptor. *Biochem. Biophys. Res. Commun.* **351**, 559–565
26. Liebmann, C., Graness, A., Ludwig, B., Adomeit, A., Boehmer, A., Boehmer, F.D., Nurnberg, B., and Wetzker, R. (1996) Dual bradykinin B2 receptor signalling in A431 human epidermoid carcinoma cells: activation of protein kinase C is counteracted by a GS-mediated stimulation of the cyclic AMP pathway. *Biochem. J.* **313**, 109–118
27. Chen, N., Furuya, S., Shinoda, Y., Yumoto, M., Ohtake, A., Sato, K., Doi, H., Hashimoto, Y., Kudo, Y., and Higashi, H. (2003) Extracellular carbohydrate-signal triggering cAMP-dependent protein kinase-dependent neuronal actin-reorganization. *Neuroscience* **122**, 985–995
28. Fukunaga, K., Miyamoto, E., and Soderling, T.R. (1990) Regulation of Ca2+/calmodulin-dependent protein kinase II by brain gangliosides. *J. Neurochem.* **54**, 102–109
29. Higashi, H. and Yamagata, T. (1992) Mechanism for ganglioside-mediated modulation of calmodulin-dependent enzyme. Modulation of calmodulin-dependent cyclic nucleotide phosphodiesterase activity through the binding of gangliosides to calmodulin and the enzyme. *J. Biol. Chem.* **267**, 9839–9843

30. Higashi, H., Yoshida, S., Sato, K., and Yamagata, T. (1996) Interaction of ganglioside with specific peptide sequences as a mechanism for the modulation of calmodulin-dependent enzymes. *J. Biochem.* **120**, 66–73
31. Kotani, M., Kawashima, I., Ozawa, H., Terashima, T., and Tai, T. (1993) Differential distribution of major gangliosides in rat central nervous system detected by specific monoclonal antibodies. *Glycobiology* **3**, 137–146
32. Kotani, M., Kawashima, I., Ozawa, H., Ogura, K., Ishizuka, I., Terashima, T., and Tai, T. (1994) Immunohistochemical localization of minor gangliosides in the rat central nervous system. *Glycobiology* **4**, 855–865
33. Kotani, M., Terashima, T., and Tai, T. (1995) Developmental changes of ganglioside expressions in postnatal rat cerebellar cortex. *Brain Res.* **700**, 40–58
34. Borkowski, J.A., Ransom, R.W., Seabrook, G.R., Trumbauer, M., Chen, H., Hill, R.G., Strader, C.D., and Hess, J.F. (1995) Targeted disruption of a B2 bradykinin receptor gene in mice eliminates bradykinin action in smooth muscle and neurons. *J. Biol. Chem.* **270**, 13706–13710
35. Alfie, M.E., Yang, X.P., Hess, F., and Carretero, O.A. (1996) Salt-sensitive hypertension in bradykinin B2 receptor knockout mice. *Biochem. Biophys. Res. Commun.* **224**, 625–630
36. Kakoki, M., Kizer, C.M., Yi, X., Takahashi, N., Kim, H.S., Bagnell, C.R., Edgell, C.J., Maeda, N., Jennette, J.C., and Smithies, O. (2006) Senescence-associated phenotypes in Akita diabetic mice are enhanced by absence of bradykinin B2 receptors. *J. Clin. Invest.* **116**, 1302–1309
37. Ferreira, J., Campos, M.M., Araujo, R., Bader, M., Pesquero, J.B., and Calixto, J.B. (2002) The use of kinin B1 and B2 receptor knockout mice and selective antagonists to characterize the nociceptive responses caused by kinins at the spinal level. *Neuropharmacology* **43**, 1188–1197
38. Chachisvilis, M., Zhang, Y.L., and Frangos, J.A. (2006) G protein-coupled receptors sense fluid shear stress in endothelial cells. *Proc. Natl. Acad. Sci. U.S.A.* **103**, 15463–15468

研究テーマ②

がん細胞膜糖鎖異常と
その制御に基づく診断・治療法の開発

Glycoconj J (2017) 34:127–138
DOI 10.1007/s10719-016-9739-2

ORIGINAL ARTICLE

Catfish rhamnose-binding lectin induces $G_{0/1}$ cell cycle arrest in Burkitt's lymphoma cells via membrane surface Gb3

Shigeki Sugawara[1] · Changhun Im[1] · Tasuku Kawano[1] · Takeo Tatsuta[1] · Yasuhiro Koide[2] · Daiki Yamamoto[2] · Yasuhiro Ozeki[2] · Kazuo Nitta[1] · Masahiro Hosono[1]

Received: 15 June 2016 / Revised: 24 August 2016 / Accepted: 3 October 2016 / Published online: 28 October 2016

Abstract *Silurus asotus* egg lectin (SAL), an α-galactoside-binding protein isolated from the eggs of catfish, is a member of the rhamnose-binding lectin family that binds to Gb3 glycan (Galα1–4Galβ1–4Glc). We have previously demonstrated that SAL reduces the proliferation of Gb3-expressing Burkitt's lymphoma Raji cells and confirm here that it does not reduce their viability, indicating that unlike other lectins, it is not cytotoxic. The aim of this study was to determine the signal transduction mechanism(s) underlying this novel SAL/Gb3 binding-mediated effect profile. SAL/Gb3 interaction arrested the cell cycle through increasing the $G_{0/1}$ phase population of Raji cells. SAL suppressed the transcription of cell cycle-related factors such as c-MYC, cyclin D3, and cyclin-dependent protein kinase (CDK)-4. Conversely, the CDK inhibitors p21 and p27 were elevated by treatment with SAL. In particular, the production of p27 in response to SAL treatment increased steadily, whereas p21 production was maximal at 12 h and lower at 24 h. Activation of Ras-MEK-ERK pathway led to an increase in expression of p21. Notably, treatment of Raji cells with anti-Gb3 mAb alone did not produce the above effects. Taken together, our findings suggest that Gb3 on the Raji cell surface interacts with SAL to trigger sequential GDP-Ras phosphorylation, Ras-MEK-ERK pathway activation, p21 production, and cell cycle arrest at the $G_{0/1}$ phase.

Keywords Cell cycle arrest · Extracellular signal-regulated kinase · Globotriaosylceramide · p21 · SUEL/rhamnose-binding lectin

Abbreviations

BrdU	Bromodeoxy uridine
CCND3	Cyclin D3
CDK	Cyclin-dependent protein kinase
ERK	Extracellular signal-regulated kinase
FBS	Fetal bovine serum
FITC	Fluorescein isothiocyanate
Gb3	Galα1–4Galβ1–4Glc-Cer
GDP	Guanosine diphosphate
GEM	Glycosphingolipid-enriched microdomains
GTP	Guanosine triphosphate
GSL	Glycosphingolipid
mAb	Monoclonal antibody
JNK	c-Jun N-terminal kinase
MAPK	Mitogen-activated protein kinase
MEK	MAPK/ERK kinase
PVDF	Polyvinylidene difluoride
qRT-PCR	Quantitative reverse transcription-polymerase chain reaction
SAL	*Silurus asotus* egg lectin
SDS-PAGE	Sodium dodecyl sulfate-polyacrylamide gel electrophoresis
SUEL	Sea urchin egg lectin

Electronic supplementary material The online version of this article (doi:10.1007/s10719-016-9739-2) contains supplementary material, which is available to authorized users.

✉ Masahiro Hosono
mhosono@tohoku-mpu.ac.jp

[1] Division of Cell Recognition Study, Institute of Molecular Biomembrane and Glycobiology, Tohoku Medical and Pharmaceutical University, 4-4-1 Komatsushima, Aoba-ku, Sendai 981-8558, Japan

[2] Laboratory of Glycobiology and Marine Biochemistry, Department of Life and Environmental System Science, Graduate School of NanoBio Sciences, Yokohama City University, 22-2 Seto, Kanazawa-ku, Yokohama 236-0027, Japan

Introduction

Rhamnose-binding lectins (RBLs) have been found in the eggs (oocytes) of various fish species [1–3] and are capable of binding to L-rhamnose and α-D-galactosides. The primary structure of rhamnose-binding lectins is similar to that of a D-galactose-binding lectin termed SUEL that was purified from sea urchin (*Anthocidaris crassispina*) eggs and is composed of 105 amino acid residues [4]. The symbolic term "RBLs" is named after their carbohydrate-binding specificity against L-rhamnose. Indeed, it shows the highest affinity among common saccharides, however, actual ligands of RBL are thought to be α-galactosyl sugar chains such as human type B oligosaccharide and globotriaosylceramide (Gb3) being on the cell surface. *Silurus asotus* egg lectin (SAL) is a 32-kDa protein comprised of three tandem repeats of 95 amino acid residues [5]. Previously, we demonstrated that SAL agglutinated Raji Burkitt's lymphoma cells (which express glycosphingolipids [GSLs] containing Gb3 (or CD77; Galα1–4Galβ1–4Glc) in GSL-enriched microdomains on the cell surface) but does not agglutinate erythroleukemia K562 cells (which do not express Gb3 on the cell surface) [6]. Additionally, SAL caused a reduction in cell size and increased annexin-V binding to and propidium iodide incorporation into Raji cells. Although this effect on Raji cells might represent damage at the late apoptosis or necrosis stage, the SAL-treated Raji cells remained viable [7]. In contrast, the lectin CSL3 purified from the eggs of the chum salmon (*Oncorhynchus keta*) was found to induce cell death of Gb3-displaying Caco-2 cells via an apoptotic pathway [8]. Watanabe *et al.* reported that Gb3-expressing HeLa cells were killed by pierisin, a toxic lectin isolated from cabbage butterfly (*Pieris rapae*) wings [9]. Pierisin contains a triple tandem repeat of ricin B-like domains and an ADP-ribosyltransferase domain in the polypeptide [10]. Treatment of HeLa cells with pierisin caused a delay in the cell cycle as well as apoptosis [11]. Therefore, SAL appears to have a different biological function as compared to CSL3 and pierisin.

Much research has focused on Gb3 because it comprises one of the components of glycosphingolipid-enriched microdomains (GEMs) on the cell surface, which has been shown to function as trigger of signal transduction. The glycosphingolipids including Gb3 in GEM were reported to associate with signal transducers such as Src family kinases and small G-proteins localized in the cytosol through the lipid bilayer [12]. Therefore, in this study we focused on identifying the signal transduction pathways stimulated by the SAL-Gb3 interaction. We found that the interaction between SAL and Gb3 enhanced the expression level of cyclin-dependent protein kinase inhibitors. This enhancement promoted Raji cell cycle arrest at the $G_{0/1}$ phase through phosphorylation of GDP-Ras, mitogen-activated protein kinase (MAPK)/extracellular signal-regulated kinase (ERK) kinase (MEK), and ERK. Taken together, these findings suggest that Gb3 plays an important role in cell signal regulation through its ability to bind to lectins. Elucidation of the mechanism of cell cycle arrest by SAL and Gb3 might lead to the discovery of novel lectin-based cell regulatory systems.

Materials and methods

Materials SAL was purified by sequential chromatography on DE23 (Whatman, Little Chalfont, UK) anion exchange and D-galactose-Sepharose 6B columns as described previously [13].

Cell lines Burkitt's lymphoma Raji cells from the Cell Resource Center of Biomedical Research, Institute of Development, Aging and Cancer, Tohoku University (Sendai, Japan) were cultured in RPMI-1640 medium (Nissui Pharmaceutical Co., Tokyo, Japan) supplemented with 10 % v/v fetal bovine serum (FBS) and antibiotic-antimycotic solution (penicillin [100 IU/ml], streptomycin [100 μg/ml], and amphotericin B [0.25 μg/ml], Life Technologies, Carlsbad, CA, USA) and maintained at 37 °C in a 95 % air/5 % CO_2 atmosphere.

Cytotoxicity and cell viability assays Raji cells (1×10^6 /ml) were seeded in 6-well plates and incubated with various concentrations of SAL (0–100 μg/ml) for 24, 36, 48, 72, 96, or 120 h. Cytotoxic activity and cell growth were determined by trypan blue (0.5 % w/v) exclusion assay [14]. Cell proliferation was determined by WST-8 assay using a Cell Counting Kit-8 (Dojindo Laboratories; Kumamoto, Japan). After plating the cells into a 96-well flat-bottom plate at 5×10^4 cells/well (90 μl), the cells were treated with 100 μg/ml SAL (final concentration) for 24 or 48 h. Then, 10 μl WST-8 solution was added into each well and the cells were incubated for 4 h at 37 °C. The absorbance was measured at a wavelength of 450 nm using the GloMax Multi Detection System (Promega, Madison, WI, USA). Cells were treated with rat anti-Gb3 monoclonal antibody (mAb) (clone 38.13; Beckman Coulter, Miami, FL, USA) in flat-bottom plastic plates for 24, 48, 72, 96, or 120 h at 37 °C. Cytotoxic activity and cell growth were determined as described above. Bright-field images were acquired using an inverted microscope (model IX71; Olympus Co., Tokyo, Japan) with a 10× objective lens.

Detection of cell cycle arrest by SAL Cell cycle arrest was assayed using a fluorescein isothiocyanate (FITC) bromodeoxy uridine (BrdU) flow kit (BD Biosciences, San Jose, CA, USA) according to the manufacturer's protocol. In brief, cells (5×10^5) were treated with SAL (100 μg/l) for 24 h, fixed with 4 % paraformaldehyde, and permeabilized by saponin for 1 h at 37 °C in the presence of 1 U DNase. Cell division was estimated as the ratio of BrdU incorporation into cells (detected using a FITC-conjugated anti-BrdU antibody after incubation for 20 min at room temperature) to total

DNA amount in the cells (detected with 7-aminoactinomycin D) using a FACSCalibur (BD Biosciences) with single laser emitting excitation at 488 nm and analyzed with Cell Quest pro software (BD Biosciences).

Expression levels of mRNA encoding cell cycle-related molecules Raji cells (5×10^5) were cultured for 12 or 24 h in RPMI-1640 medium containing SAL (100 μg/ml), SAL (100 μg/ml)/saccharide (20 mM), or without SAL at 37 °C in 95 % air/5 % CO_2. Total RNA was extracted from cells using an AllPrep RNA/Protein Kit (Qiagen, Valencia, CA, USA). cDNA was synthesized from the total RNA (1 μg) using a SuperScript VILO cDNA Synthesis Kit (Invitrogen, San Diego, CA, USA). Quantitative reverse transcription-polymerase chain reaction (qRT-PCR) assays were performed using a LightCycler 480 system with the LightCycler 480 Probes Master Kit (Roche Diagnostics, Indianapolis, IN, USA). PCR primers for amplification of *CDK4*, *c-MYC*, cyclin D3 (*CCND3*), *p21*, and *p27* using a TaqMan/probe library assay were designed by the Universal Probe Library Assay Design Center (https://www.roche-applied-science.com/sis/rtpcr/upl/acenter.jsp). The expression levels of these genes were standardized relative to the mRNA expression level of *GAPDH* (as a housekeeping gene) based on their average crossing point values.

Protein expression of signal transduction molecules, their phosphorylated forms, and cell cycle-related molecules Raji cells (5×10^5) were cultured for 12 or 24 h in RPMI-1640 with or without SAL (100 μg/ml) at 37 °C in 95 % air/5 % CO_2. Cell lysate was prepared using an AllPrep RNA/Protein Kit (Qiagen), subjected to sodium dodecyl sulfate-polyacrylamide gel electrophoresis (SDS-PAGE) (10 % separation gel), and electrotransferred onto a polyvinylidene difluoride (PVDF) membrane (pore size 0.45 μm) (Hybond-P; GE Healthcare Bio-Sciences AB, Uppsala, Sweden) according to the manufacturer's protocol [15–17]. The membrane was treated with blocking buffer (Blocking One; Nacalai Tesque Inc., Kyoto, Japan) for 1 h at room temperature and washed with Tris-buffered saline (TBS) containing 0.05 % Tween-20. The primary antibodies used were directed to $p21^{Waf1/Cip1}$ (1:1000, rabbit mAb, clone 12D1; Cell Signaling Technology Inc., Danvers, MA, USA [CST]), $p27^{Kip1}$ (1:1000, rabbit mAb; clone D69C12; CST), c-MYC (1:1000, rabbit polyclonal antibody; CST), CDK4 (1:2000, mouse mAb; clone DCS156; CST), cyclin D3 (1:2000, mouse mAb; clone DCS22; CST), phospho-$MEK_{1/2}$ (1:1000, rabbit mAb; CST), MEK1 (1:1000, rabbit mAb; CST), phospho-$ERK_{1/2}$ (1:1000, mouse mAb; BD Biosciences), ERK1 (1:5000, mouse mAb; BD Biosciences), phospho-p38 MAPK (1:2500, mouse mAb; BD Biosciences), p38 MAPK (1:5000, mouse mAb; BD Biosciences), phospho-JNK (1:250, mouse mAb; BD Biosciences), JNK (1:250, mouse mAb; BD Biosciences), and GAPDH (1:20,000, mouse mAb; clone 6C5; Ambion/Invitrogen, Carlsbad, CA, USA). These antibodies were applied in immunoreaction enhancer solution (Can Get Signal Solution 1; Toyobo Co., Osaka, Japan). The membrane was incubated for 16 h at 4 °C. The secondary antibody, horseradish peroxidase (HRP)-conjugated anti-mouse or anti-rabbit IgG (Chemicon International Inc., Temecula, CA, USA), was diluted 1:20,000 in immunoreaction enhancer solution. The membrane was incubated for 1 h at room temperature and then exposed to X-ray film (Fuji Film Co., Tokyo, Japan) using enhanced chemical luminescence and western blotting with ECL Prime detection reagent (GE Healthcare Bio-Sciences AB). A synthetic inhibitor of $MEK_{1/2}$, 1,4-diamino-2,3-dicyano-1,4-bis (2-aminophenylthio) butadiene (U0126) (1 μg) (Calbiochem; San Diego, CA, USA) was dissolved in 247 μl dimethylsulfoxide to create a 10 mM stock solution. Cells were incubated with U0126 (10 μM) in RPMI-1640 with FBS for 2 h, supplemented with SAL (100 μg/ml), and incubated for another 12 h. Whole cell extracts were separated by SDS-PAGE on a 10 % gel and blotted onto PVDF membranes. Phosphorylated kinases were identified by western blotting with anti-phospho-$MEK_{1/2}$, anti-$MEK_{1/2}$, anti-phospho-$ERK_{1/2}$, anti-ERK_1, and HRP-conjugated anti-mouse IgG antibodies. Signals were detected by X-ray film exposure and western blotting as described above. Proteins were quantified by densitometry using NIH ImageJ software (version 1.440, Bethesda, MD, USA). The optical densities of phosphorylated $MEK_{1/2}$ (P-$MEK_{1/2}$) and phosphorylated $ERK_{1/2}$ (P-$ERK_{1/2}$) were measured and normalized to the optical densities of $MEK_{1/2}$ and ERK_1, respectively.

Detection of GTP-Ras The active form of Ras exchanged through GDP to GTP as a result of SAL stimulation was assayed by affinity precipitation using a Ras activation assay kit (Upstate Biotechnology; Lake Placid, NY, USA). Raji cells (1×10^6) were cultured for 0.5, 3, 6, 12, or 24 h in RPMI-1640 containing SAL (100 μg/ml) at 37 °C in 95 % air/5 % CO_2, lysed with Mg^{2+} lysis buffer (125 mM 4-(2-hydroxyethyl)-1-piperazineethanesulfonic acid [HEPES], pH 7.5, 750 mM NaCl, 5 % Igepal® CA-630, 50 mM $MgCl_2$, 5 mM ethylenediaminetetraacetic acid, and 10 % glycerol), and incubated with the agarose-conjugated Ras-binding domain of Raf-1 (5 μl) for 30 min at 4 °C. The agarose-coated beads were boiled in sample buffer and the cell lysate was then subjected to SDS-PAGE on a 10 % separation gel and transferred onto a PVDF membrane. The GTP-Ras formed following SAL stimulation was detected by anti-Ras mAb (0.05 μg/ml) and HRP-conjugated polyclonal antibodies (1:1000) [18, 19]. Activated Ras was detected using ECL Prime (GE Healthcare Bio-Sciences AB).

RNA interference-mediated knockdown of alpha-1,4-galactosyltransferase (A4GALT) Raji cells (1.2×10^6) cells were centrifuged and resuspended in 100 μl nucleofection V solution (Lonza, Basel, Switzerland) containing 20 μM A4GALT siRNA (Dharmacon, Lafayette, CO, USA) and electroporated with a Nucleofector (Lonza) using the M-13 program. After nucleofection, the cells were transferred to a 12-well plate containing 1 ml fresh complete medium (RPMI 1640 containing 10 % FBS and antibiotic-antimycotic solution) and incubated at 37 °C for 120 h. After incubation, the expression of Gb3 was detected by flow cytometry.

Flow cytometric analysis of Gb3 expression Cells (2×10^5) were treated with or without anti-Gb3 mAb (BGR23, mouse IgG2b; Tokyo Kasei Co. Ltd., Tokyo, Japan) at a dilution of 1:1000 in PBS (100 μl) at 4 °C for 30 min and washed three times with PBS. The cells were then treated with Alexa Fluor (AF) 488-conjugated goat anti-mouse IgG (H + L) (Molecular Probes, Invitrogen AG, Basel, Switzerland) at a dilution of 1:2500 in PBS (100 μl) at 4 °C for 30 min. The degree of Gb3 expression on the cell surface was analyzed using the FACSCalibur as described above.

Statistical analysis Experimental results are presented as the means ± standard error (SE). Differences in means were evaluated using the two-tailed Student's *t*-test with P values <0.05 considered to be statistically significant.

Results

Effects of SAL on cell proliferation and viability In the current study, we further expand upon our previous findings following exposure of Raji cells to SAL (100 μg/ml) for 24 h by examining the concentration- and time-dependent effect of SAL. According to the trypan blue exclusion assay, SAL did not reduce the viability of Raji cells even at the concentration of 100 μg/ml for 120 h (Fig. 1a and S1). Proliferation was

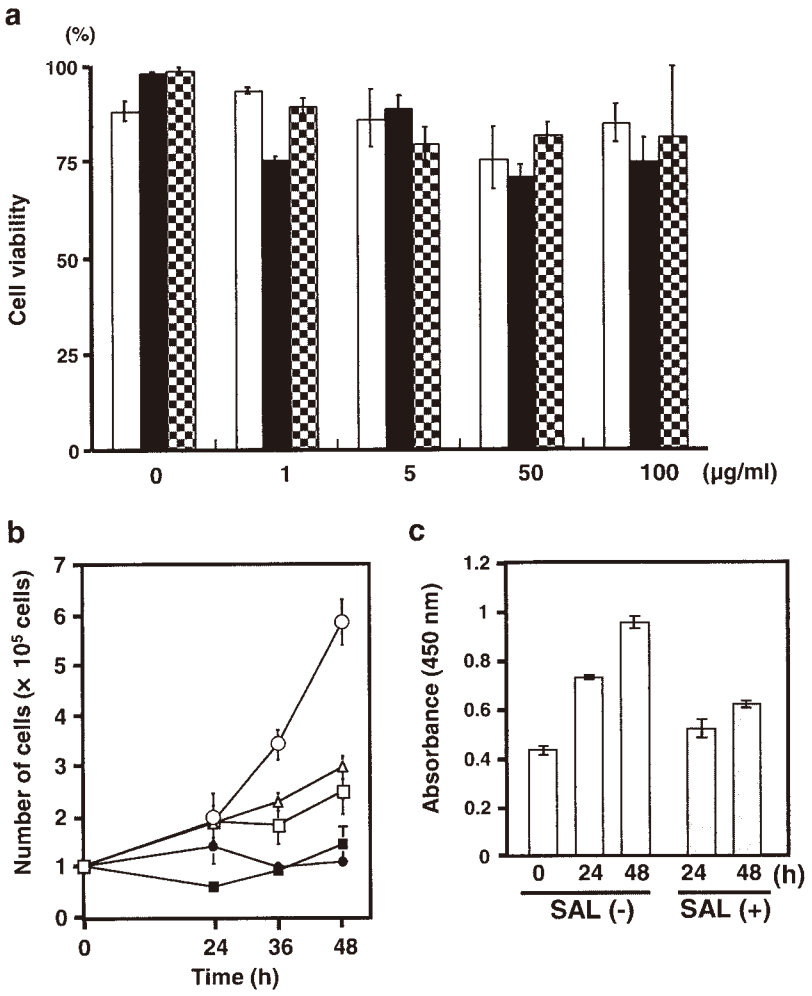

Fig. 1 SAL reduces the proliferation but has no effect on the viability of Raji cells. **a.** Time- and dose-dependent effects of SAL treatment on cell viability. Cells were treated with SAL (0, 1, 5, 50, or 100 μg/ml) for 24 h (white columns), 36 h (black columns), or 48 h (gray columns) at 37 °C. Cell viability was evaluated by trypan blue exclusion assay. The values shown are the means of triplicate experiments. Error bars: standard error (SE). **b.** Cells were treated with SAL (0, 1, 5, 50, or 100 μg/ml) for 24, 36, or 48 h at 37 °C. The number of living cells was assessed by trypan blue exclusion assay. ○: 0 μg/ml (control). △: 1 μg/ml. □: 5 μg/ml. ■: 50 μg/ml. ●: 100 μg/ml. **c.** Cells were treated with (+) or without (−) SAL (100 μg/ml) for 24 or 48 h at 37 °C. Proliferation was evaluated by the WST-8 assay. The values shown are the means of triplicate experiments. Error bars: SE

reduced further at higher concentrations and was abolished completely at 50 μg/ml (Fig. 1b). The WST-8 assay showed that SAL reduced cell proliferation in a time-dependent manner (Fig. 1c). On the other hand, Gb3-binding monoclonal antibody, anti-Gb3, had no such effects to Raji cells including cell-agglutination (Fig. 2a~c, S2 and S3). Stimulation with SAL (100 μg/ml) for 72 h caused a 6-fold decrease in the number of cells compared with control cells (Fig. 3). When the medium was replaced by SAL-free medium, the cells completely recovered their proliferation activity after 48 h (Fig. 3, column "SAL free"). These results suggest that SAL reduced the proliferation of Raji cells but was not cytotoxic.

G_1 cell cycle arrest by SAL To gain insight into the mechanism of SAL-induced growth inhibition in Raji cells, we analyzed the SAL-dependent changes in cell cycle distribution. Flow cytometric analysis showed that stimulation with SAL (100 μg/ml) for 24 h caused a substantial increase of the ratio of the $G_{0/1}$ phase to the whole Raji cell population of 20 % with a consequent decrease of the proportion of cells in S phase by 20 % (Fig. 4 and Table 1). The $G_{0/1}$ cell cycle arrest no longer occurred when SAL was removed from the medium. In contrast, the $G_{2/M}$ phase was not shifted by SAL treatment (Table 1). These findings suggest that SAL arrests the $G_{0/1}$ phase of the cell cycle by binding to Gb3, followed by the loss of cell proliferation.

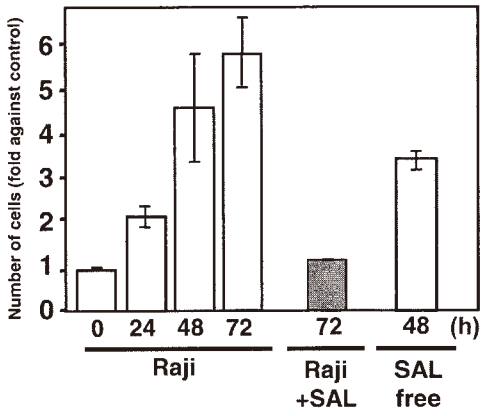

Fig. 3 Removal of SAL restores cell proliferation. Cells were cultured without SAL at 37 °C for 0, 24, 48, or 72 h (Raji). Other cells were treated with SAL (100 μg/ml) for 72 h (Raji + SAL) or with SAL followed by SAL-free medium for 48 h (SAL free). The number of living cells was assessed by trypan blue exclusion assay. The values shown are the means of triplicate experiments. Error bars: SE

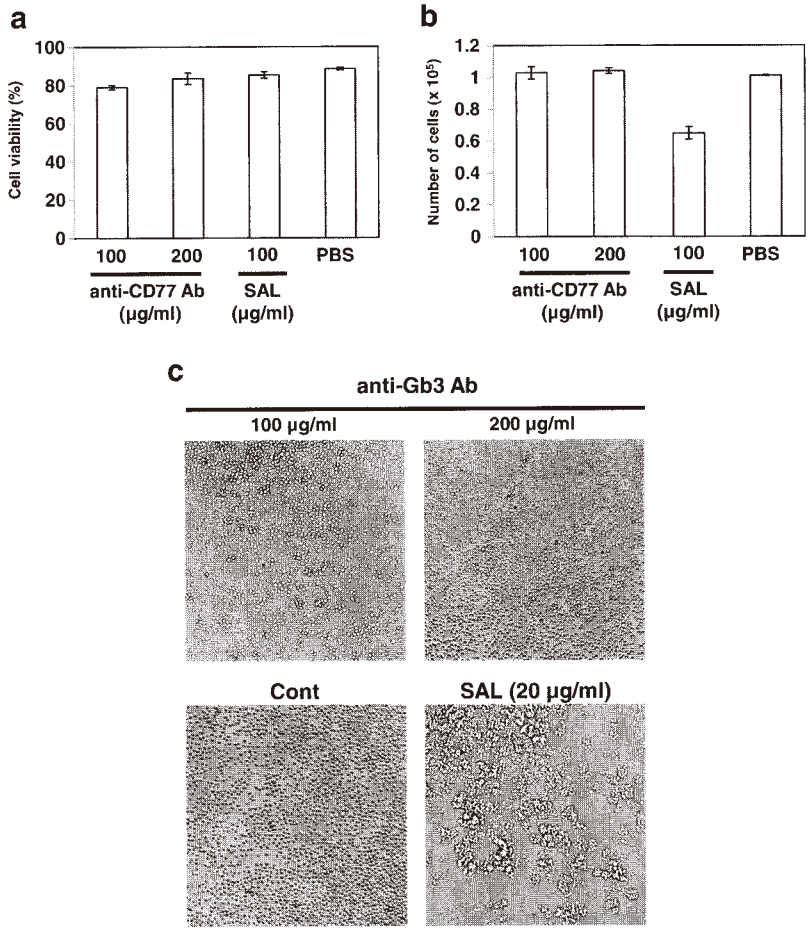

Fig. 2 Anti-Gb3 mAb does not induce apoptosis or inhibit cell proliferation. Cells were treated with anti-Gb3 mAb (100 or 200 μg/ml) or SAL (100 μg/ml) for 24 h at 37 °C. Cell viability (a) and proliferation (b) were evaluated by trypan blue exclusion and WST-8 assays, respectively. The values shown are the means of triplicate experiments. Error bars: SE. **c.** Cell agglutination induced by treatment with anti-Gb3 mAb (100 or 200 μg/ml) or SAL (20 μg/ml). Negative control (Cont): addition of PBS instead of lectin or antibody. The images are from bright-field microscopy at 100× magnification

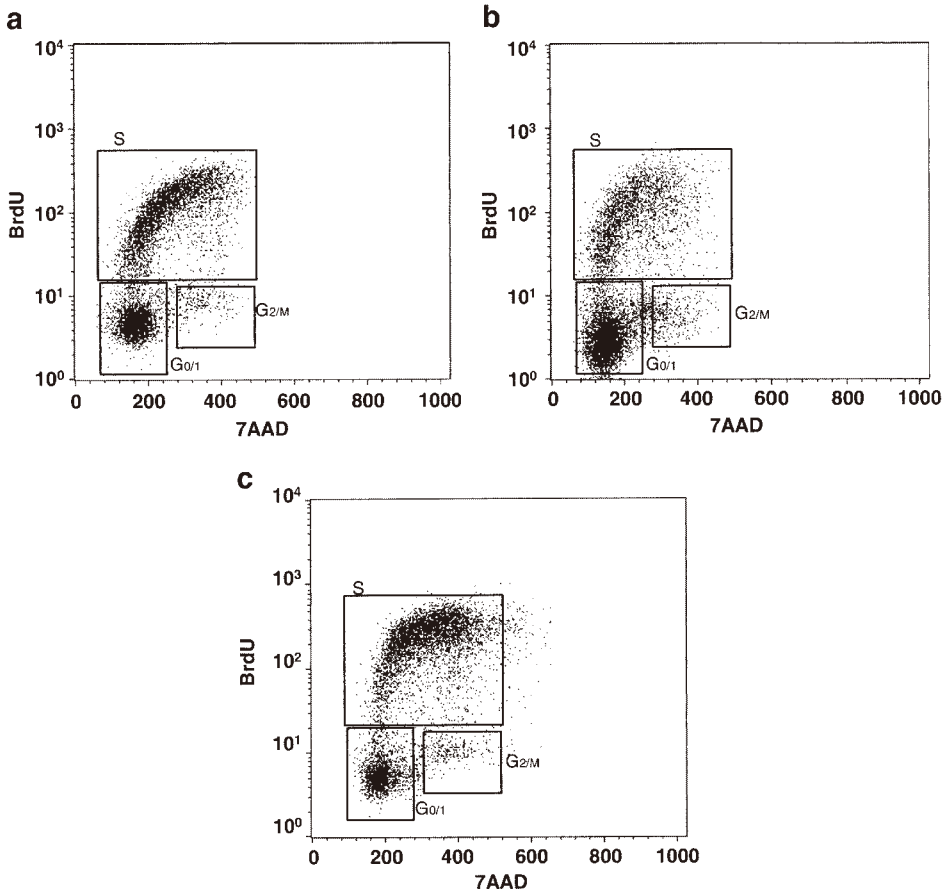

Fig. 4 Alteration of cell cycle distribution in SAL-treated Raji cells. Cells were cultured without SAL at 37 °C for 72 h (SAL-untreated) (**a**). Other cells were treated with SAL (100 μg/ml) for 72 h (SAL-treated) (**b**) or subsequently with SAL-free medium for 48 h (SAL-removed) (c). The distribution of cells in each cell cycle phase ($G_{0/1}$, S, and $G_{2/M}$) was determined by FACSCalibur analysis

Down-regulation of *c-MYC, CDK4*, and *CCND3* gene expression levels and the induction of mRNA and protein expression levels of the CDK inhibitors p21 and p27 by SAL Numerous studies have shown that CDK acts as an accelerating factor of the cell cycle [20, 21]. In Raji cells treated with SAL for 24 h, *CDK4* mRNA levels were down-regulated in comparison with those of untreated cells (Fig. 5a). However, SAL had no effect on the mRNA expression levels of *CDK2* (data not shown). The expression of *CDK4* is regulated by c-Myc. In addition, mammalian cyclin D3 is a member of the G_1/S cyclin family and functions as a key protein to transition the cell cycle to the next phase [22–24]. Therefore, the alteration of protein expression levels of c-MYC and cyclin D3 in Raji cells were examined following SAL treatment. As shown Fig. 5a, SAL treatment for 24 h reduced the expression level of *c-MYC* by 40 % and that of *CCND3* by 30 %. Western blotting confirmed the coordinate decreased expression levels of the c-Myc, CDK4, and cyclin D3 proteins (Fig. 5b). In addition, the inhibitory effects of SAL on gene expression were partially eliminated in the presence of 10 mM melibiose or rhamnose (Fig. 5c). These findings indicate that the interaction between SAL and Gb3 reduced the expression of *CDK4*, *c-MYC*, and *CCND3* mRNAs.

Table. 1 Effect of SAL on cell cycle distribution. The percentages of cells in each cell cycle phase ($G_{0/1}$, S, or $G_{2/M}$) were determined by FACSCalibur analysis. The values shown are the means ± SE from two or more independent experiments

	G0/1	S	G2/M (%)
SAL-untreated	34.3 ± 2.5	62.0 ± 2.9	2.7 ± 0.4
SAL-treated	53.5 ± 3.2	35.1 ± 2.5	7.5 ± 1.7
SAL-removed	27.0 ± 0.7	67.5 ± 1.1	3.7 ± 0.5

p21 and p27 have been shown to inhibit CDK activity and cell cycle progression [25–27]. We therefore examined whether the expression of p21 and p27 was changed by treatment with SAL. qRT-PCR analysis showed increases of 130 % and 70 % in the mRNA expression levels of *p21* and *p27*, respectively, in SAL-treated Raji cells (Fig. 5a). In addition, western blotting analysis showed corresponding increases of p21 and p27 protein expression levels (Fig. 5b). Furthermore, up-regulation of *p21* was specifically inhibited in the presence of rhamnose or melibiose (10 mM) but not by glucose and lactose. Notably, however, elevation of *p27* was not blocked by these saccharides (Fig. 5c).

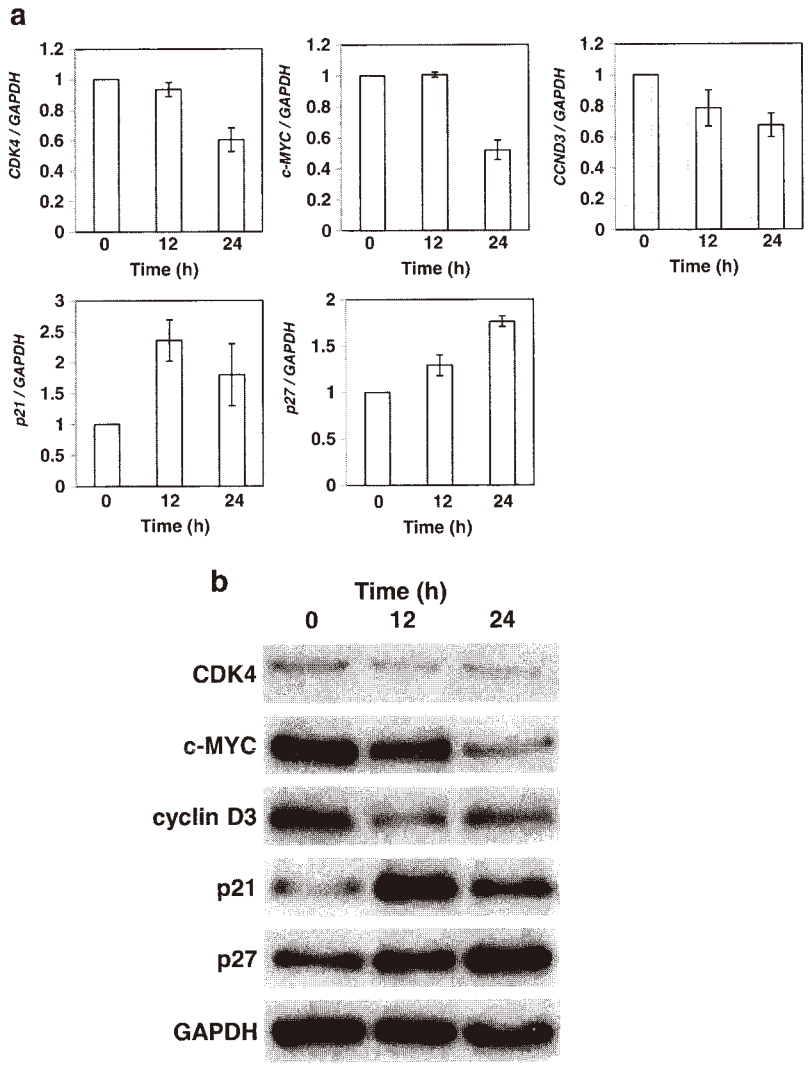

Fig. 5 SAL treatment alters the gene and protein expression of CDK4, c-MYC, cyclin D3, p21, and p27. **a.** Cells (1×10^6) were treated with SAL (100 μg/ml) at 37 °C for 12 or 24 h. Total RNAs extracted from SAL-untreated and -treated cells were analyzed by qRT-PCR using specific primers for *CDK4*, *c-MYC*, *CCND3*, *p21*, *p27*, and *GAPDH*, respectively. The control value was defined as one. Fold increases in the target genes relative to the control were normalized to *GAPDH*. Results are expressed as n-fold increase over the control; means ± SE of three independent triplicate experiments. **b.** Cells (1×10^6) were treated with SAL (100 μg/ml) at 37 °C for 12 or 24 h. Whole cell extracts obtained from SAL-untreated and -treated cells were subjected to western blotting using anti-CDK4, anti-c-MYC, anti-cyclinD3, anti-p21, anti-p27, and anti-GAPDH antibodies. **c.** Cells (1×10^6) were exposed to SAL (100 μg/ml) and SAL/saccharide (20 mM) co-treatment for 24 h. Total RNAs extracted from SAL-treated, SAL/saccharide co-treated, and untreated Raji cells were analyzed by qRT-PCR using the specific primers for *CDK4*, *c-MYC*, *CCND3*, *p21*, *p27*, and *GAPDH*, respectively. The control value was defined as one. Fold increases in the target genes relative to the control were normalized to *GAPDH*. Results are expressed as n-fold increase over the control; means ± SE of three independent triplicate experiments

These findings suggest that the up-regulation of the CDK inhibitors p21 and p27 by SAL treatment induced $G_{0/1}$ phase cell cycle arrest.

Activation of the MEK-ERK signaling pathway by Gb3/lectin interaction at the cell surface The MEK-ERK signaling pathway has been reported to participate in the regulation of cell growth [28]. Treatment with SAL resulted in the formation and accumulation of GTP-Ras in Raji cells in a time-dependent manner as indicated by enhanced phosphorylation of $MEK_{1/2}$ and $ERK_{1/2}$ (Fig. 6). Conversely, SAL treatment had no enhancing effect on the phosphorylation of p38 MAPK or c-Jun N-terminal kinase, which are MAPK family members in the broad sense (Fig. S4). A4GALT siRNA-treatment of Raji cells suppressed Gb3 cell surface expression (Fig. 7a and b). Consequently, A4GALT-knockdown abolished SAL-induced cell agglutination and also inhibited the phosphorylation of $MEK_{1/2}$ and $ERK_{1/2}$ following SAL treatment (Fig. 7c

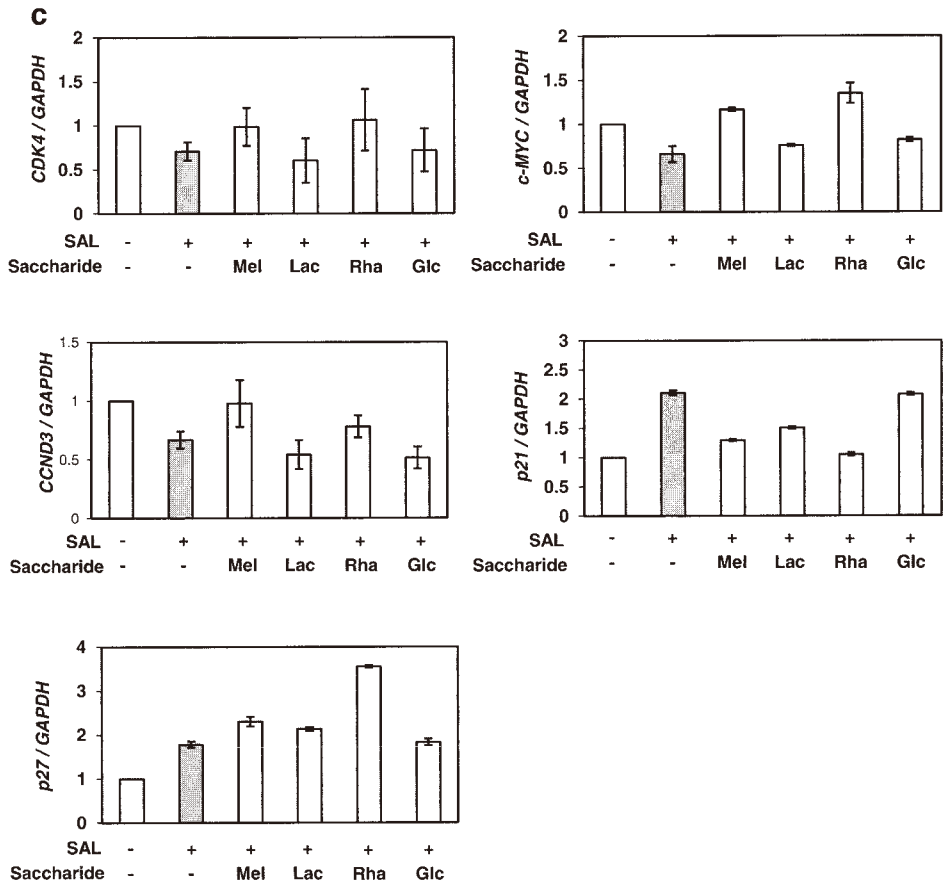

Fig. 5 (continued)

and d). Specifically, the levels of $MEK_{1/2}$ and $ERK_{1/2}$ phosphorylation were significantly increased by about 2 and 2.5-fold following SAL treatment in A4GALT siRNA-untreated Raji cells, whereas only 1.1 and 1.2-fold increases were observed upon SAL treatment in A4GALT siRNA-treated Raji cells (data not shown). These results suggest that the direct interaction between Gb3 and SAL induced the MEK-ERK signaling pathway.

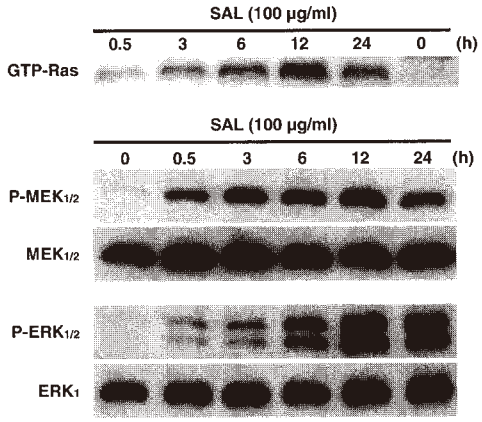

Fig. 6 SAL treatment causes activation of Ras and phosphorylation of MEK, and ERK. Cells (1×10^6) were treated with SAL (100 μg/ml) at 37 °C for various durations from 0 to 24 h. Whole cell extracts were subjected to western blotting using antibodies directed to GTP-Ras, P-$MEK_{1/2}$, $MEK_{1/2}$, P-$ERK_{1/2}$, and ERK_1. Representative results from triplicate experiments are shown

Up-regulation of p21 by SAL via phosphorylation of the Ras-MEK-ERK signaling pathway We tested whether $ERK_{1/2}$ phosphorylation was associated with the increase of p21 expression. Treatment with SAL in combination with the MEK inhibitor U0126 down-regulated *p21* mRNA expression (Fig. 8a) and restored cell growth (Fig. 8b). U0126 by itself had no significant effect on cell growth (Fig. 8b). Pre-incubation with U0126 significantly decreased SAL-induced phosphorylation of $ERK_{1/2}$ (Fig. 8c). SAL-induced enhancement of p21 protein expression was also inhibited in the presence of U0126 (Fig. 8c).

Discussion

Taken together, the results from this study indicate that the SAL/Gb3 interaction on the surface of Raji cells promotes activation of Ras (to form GTP-Ras) and phosphorylation of

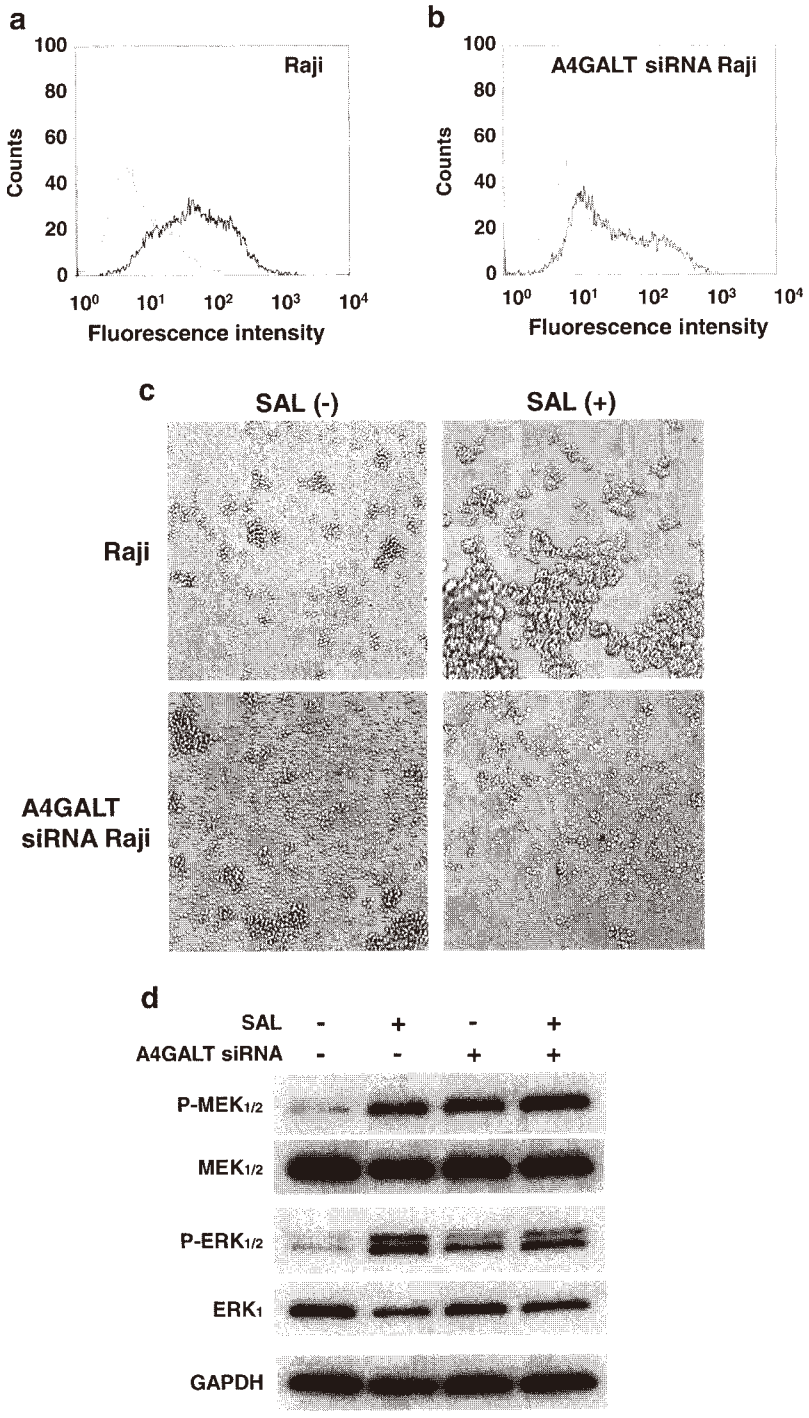

Fig. 7 Gb3 knockdown inhibits the phosphorylation of MEK and ERK. For the detection of Gb3, untreated Raji cells (**a**) and A4GALT siRNA-treated Raji cells (**b**) were stained with anti-Gb3 mAb and AF488-conjugated goat anti-mouse Ab (black line). The degree of Gb3 expression on Raji cell membranes was determined by FACSCalibur. Fluorescence intensity of control cells: gray line. **c.** Cell agglutination induced by treatment with SAL (100 μg/ml). The images are from bright-field microscopy at 100× magnification. **d.** Degrees of expression and phosphorylation of MEK and ERK proteins were detected by western blotting as described in Materials and Methods

$MEK_{1/2}$ and $ERK_{1/2}$. The suppression of cell growth by SAL was likely due to the enhancement of p21 expression caused by the phosphorylation of $ERK_{1/2}$, which derived from the Ras-MEK-$ERK_{1/2}$ pathway. In addition, SAL reduced the protein expression levels of CDK4, c-myc, and cyclin D3. These results therefore indicate that SAL treatment induced cell cycle arrest at the $G_{0/1}$ phase.

Gb3 is the key structure in globo-series GSLs, which contain a galactosyl α1–4 linkage to lactosylceramide. Cell surface Gb3 is involved in the transmission of various signals into the cytoplasm via α-galactoside-binding lectins such as SAL, pierisin, and the mussel *Mytilus galloprovincialis* lectin (MytiLec) [9–11, 29]. Park *et al.* elucidated that the other globo-series GSL, globotetoraosylceramide (Gb4), interacts

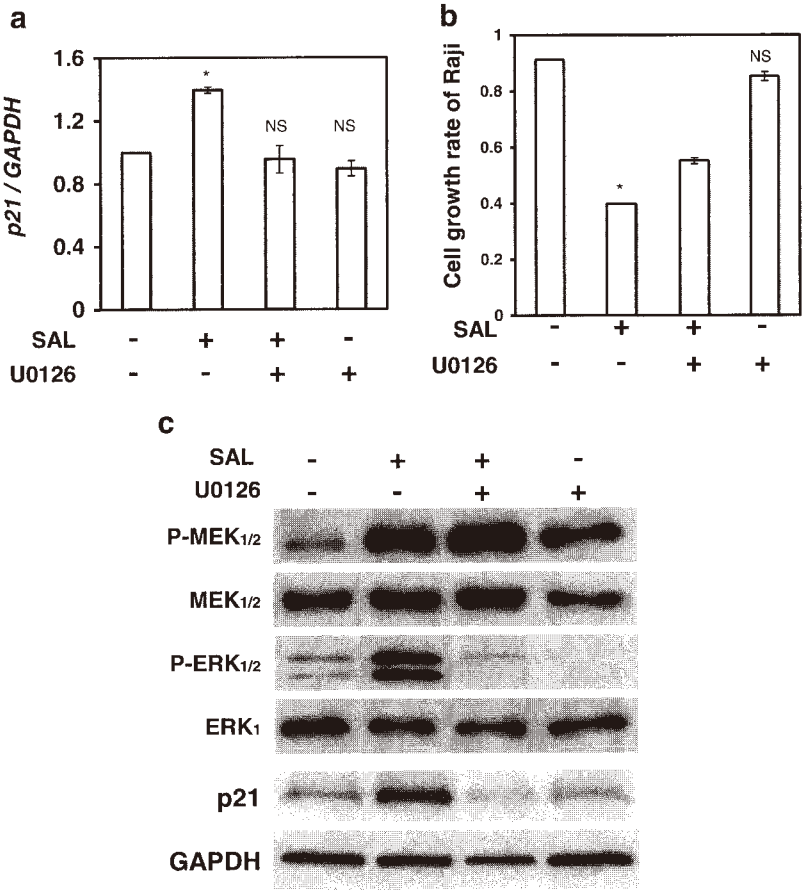

Fig. 8 SAL treatment enhances p21 protein expression levels through a Ras-MEK-ERK pathway. **a.** Quantitative RT-PCR showing *p21* expression, normalized relative to *GAPDH*, following treatment with SAL (100 μg/ml) and/or the MEK inhibitor U0126 (10 μM). The values shown are the means of triplicate experiments. Asterisk denotes $P < 0.05$ versus untreated control cells. NS denotes not significant versus untreated control cells. **b.** Growth of cells treated or untreated with SAL and/or U0126, measured by the WST-8 assay. The values shown are the means of triplicate experiments. Asterisk denotes $P < 0.05$ versus untreated control cells. NS denotes not significant versus untreated control cells. **c.** Degrees of expression and phosphorylation of Ras-MEK-ERK pathway-related proteins as detected by western blotting as described in Materials and Methods

with the epidermal growth factor receptor to promote activation of the MAPK pathway [30]. However, it has not yet been clarified whether Gb3 is involved in the activation of such a pathway. In the present study, direct interaction between Gb3 and SAL was found to transmit a regulatory signal in Raji cells through the MEK-ERK signaling pathway (Figs. 6 and 7). Phosphorylation of ERK initiates synthesis of the CDK inhibitor p21, which induces cell cycle arrest at the $G_{0/1}$ phase. External stimulation through p21 prevents damage to cellular DNA by irradiation and harmful toxins by arresting the cell cycle at the G_1/S phase transition. In comparison, p27 is involved in cell differentiation and proliferation in addition to cell cycle arrest [31]. p21 binds to the cyclin D3-CDK4 complex and suppresses cell growth. Conversely, recent reports have shown that the induction of p21 phosphorylation by ERK2 promotes cell proliferation [32]. Consistent with these properties, it has been reported that kinase-deficient forms of ERK1/2 were able to up-regulate the expression of p21 and subsequently induce $G_{0/1}$ phase cell cycle arrest [33]. Previous studies have suggested that Ras undergoes post-translational processing to be able to associate with cell membranes [34]. Thus, GDP-Ras might be located in the vicinity of GEMs on which Gb3 molecules are present. It is therefore important to elucidate the mechanism of SAL/Gb3 interaction in the initiation of Ras activation to understand the cellular functions of lectin-induced, glycan-mediated signal transduction.

Previous reports have indicated that Ras is activated by the exchange of GTP for GDP, leading to the GTP-dependent binding of target proteins to Ras [35]. In analogy to the present findings, the activation of Ras is caused by binding between galectin-1 and the *N*-acetyllactosamine of α5β1 integrin, which is followed by the induction of cell cycle arrest at the $G_{0/1}$ phase [36]. Thus, Ras activation might involve multiple pathways associated with various glycans and lectins. Several types of rhamnose-binding lectins having distinctive domain architectures are known [37, 38]. SAL has a unique domain construction with 9 binding sites based on a trimer of polypeptides, each consisting of triple tandem repeat domains [39]. For example, mAb raised against Gb3, which has divalent high-affinity binding sites, did not cause phosphorylation of GDP-Ras-MEK-$ERK_{1/2}$ or induce Raji cell cycle arrest (Fig. 2). Binding of inadequate ligands to Gb3 therefore evidently do not cause the transmission of a phosphorylation signal to GDP-Ras. Studies of the cell regulatory effects of various Gb3-binding lectins will likely help to elucidate the novel mechanisms whereby multiple lectins are able to

transmit different growth-regulatory signals through the same glycan. This phenomenon is highlighted by our recent discoveries regarding MytiLec, which has a completely different primary sequence than SAL and causes direct apoptosis by binding to Gb3 [29]. This report raises the possibility that these lectins lead to different cell-regulatory signals [29].

In the current study, phosphorylated $ERK_{1/2}$ increased the expression of the CDK inhibitor p21. This protein contains CDK-binding domains at its N-terminus and interacts with CDK to inhibit its activity, resulting in cell cycle arrest at the $G_{0/1}$ phase [40]. In general, the expression of CDK inhibitors is regulated by the tumor suppressor p53, a transcription factor that is expressed consequent to DNA damage [41]. The p21 and p27 peptides have differing molecular masses of 21 and 27 kDa, respectively, and their C-terminal domains also play different roles. We observed that the time-dependent up-regulation of p27 occurred simultaneously with the down-regulation of cyclin D3 during a 24-h period to promote cell cycle arrest at the G_1 phase. In contrast, p21 was strongly up-regulated during a 12-h period following treatment with SAL and then decreased slightly during the subsequent 24-h period (Fig. 5).

Consistently with the phenomena described above, we found that SAL treatment is affected by the up-regulation of p21 (Fig. 5) and that production of p21 interfered with cyclin D3/CDK4 complex formation. Oligosaccharides containing α-galactoside are not a common type of glycan in human cells. Gb3 has been identified as the target of hemorrhagic toxins (*e.g.*, verotoxin secreted by pathogenic bacteria, O157 strain) and has been proposed as a rejection antigen of pig organs that carry an α-galactose residue 1–3 linked to lactosylceramide following xenotransplantation into humans. The present results, using a lectin isolated from a fish, indicate a novel role of Gb3 as the trigger for activation of signal transduction molecules to induce cell cycle arrest of human lymphoma cells. Notably, α-galactoside-binding lectins (with diverse primary structures) are isolated more frequently from lower vertebrates and invertebrates than from higher vertebrates (mammals and birds) [42–47]. The physiological functions of these "primitive" lectins remain to be clarified in almost all cases. However, it is becoming increasingly clear that such knowledge will greatly promote biomedical studies focused on novel regulatory systems in human cells.

Acknowledgments This study was supported by the "Academic Frontier" Project for Private Universities and the "Strategic Project to Support the Formation of Research Bases at Private Universities (SENRYAKU)" from the Ministry of Education, Culture, Sports, Science, and Technology (MEXT), Japan. We would like to thank Editage (www.editage.jp) for English language editing.

Compliance with ethical standards

Conflict of interest The authors declare that there are no conflicts of interest regarding the publication of this paper.

Ethical approval This article does not contain any studies with human participants or animals performed by any of the authors.

References

1. Krajhanzl A., Horejsi V., Kocourek K.: Studies on lectins. XLI. Isolation and characterization of a blood group B specific lectin from the role of the powan (*Coregonus lavaretus maraena*). Biochem. Biophys Acta. **532**, 209–214 (1978)
2. Krajhanzl A., Horejsi V., Kocourek K.: Studies on lectins. XLII. Isolation, partial characterization and comparison of lectins from the roe of five fish species. Biochem. Biophys. Acta. **532**, 215–224 (1978)
3. Sakakibara F., Kawauchi H., Takayanagi G.: Blood group B-specific lectin of *Plecoglossus altivelis* (Ayu fish) eggs. Biochim Biophys Acta. **841**, 103–111 (1985)
4. Ozeki Y., Matsui T., Suzuki M., Titani T.: Amino acid sequence and molecular characterization of a D-galactoside-specific lectin purified from sea urchin (*Anthocidaris crassispina*) eggs. Biochemistry. **30**, 2391–2394 (1991)
5. Hosono M., Ishikawa K., Mineki R., Murayama K., Numata C., Ogawa Y., Takayanagi Y., Nitta K.: Tandem repeat structure of rhamnose-binding lectin from catfish (*Silurus asotus*) eggs. Biochim Biophys Acta. **1472**, 668–675 (1999)
6. Kawano T., Sugawara S., Hosono M., Tatsuta T., Nitta K.: Alteration of gene expression induced by *Silurus asotus* lectin in Burkitt's lymphoma cells. Biol Pharm Bull. **31**, 998–1002 (2008)
7. Sugawara S., Hosono M., Ogawa Y., Takayanagi M., Nitta K.: Catfish egg lectin causes rapid activation of multidrug resistance 1 P-glycoprotein as a lipid translocase. Biol Pharm Bull. **28**, 434–441 (2005)
8. Shirai T., Watanabe Y., Lee M.S., Ogawa T., Muramoto K.: Structure of rhamnose-binding lectin CSL3: unique pseudo-tetrameric architecture of a pattern recognition protein. J Mol Biol. **391**, 390–403 (2009)
9. Watanabe M., Kono T., Matsushima-Hibiya Y., Kanazawa T., Nishisaka N., Kishimoto T., Koyama K., Sugimura T., Wakabayashi K.: Molecular cloning of an apoptosis-inducing protein, pierisin, from cabbage butterfly: possible involvement of ADP-ribosylation in its activity. Proc Natl Acad Sci U S A. **96**, 10608–10613 (1999)
10. Shiotani B., Kobayashi M., Watanabe M., Yamamoto K., Sugimura T., Wakabayashi K.: Involvement of the ATR- and ATM-dependent checkpoint responses in cell cycle arrest evoked by pierisin-1. Mol Cancer Res. **4**, 125–133 (2006)
11. Matsushima-Hibiya Y., Watanabe M., Hidari K.I., Miyamoto D., Suzuki Y., Kasama T., Kanazawa T., Koyama K., Sugimura T., Wakabayashi K.: Identification of glycosphingolipid receptors for pierisin-1, a guanine-specific ADP-ribosylation toxin from the cabbage butterfly. J Biol Chem. **278**, 9972–9978 (2003)
12. Katagiri Y.U., Mori T., Nakajima H., Katagiri C., Taguchi T., Takeda T., Kiyokawa N., Fujimoto J.: Activation of Src family kinase yes induced by Shiga toxin binding to globotriaosyl ceramide (Gb3/CD77) in low density, detergent-insoluble microdomains. J Biol Chem. **274**, 35278–35282 (1999)
13. Hosono M., Kawauchi H., Nitta K., Takayanagi Y., Shiokawa H., Mineki R., Murayama K.: Purification and characterization of Silurus Asotus (catfish) roe lectin. Biol Pharm Bull. **16**, 1–5 (1993)
14. Tennant J.R.: Evaluation of the trypan blue technique for determination of cell viability. Transplantation. **2**, 685–694 (1964)

15. Laemmli U.K.: Cleavage of structural proteins during the assembly of the head of bacteriophage T4. Nature. **227**, 680–685 (1970)
16. Lowry O.H., Rosebrough N.J., Farr A.L., Randall R.J.: Protein measurement with the Folin phenol reagent. J Biol Chem. **193**, 265 (1951)
17. Matsudaira P.T.: Sequence from picomole quantities of proteins electroblotted onto polyvinylidene difluoride membranes. J Biol Chem. **262**, 10035–10038 (1987)
18. Taylor S.J., Shalloway D.: Cell cycle-dependent activation of ras. Curr Biol. **6**, 1621–1627 (1996)
19. Taylor S.J., Resnick R.J., Shalloway D.: Nonradioactive determination of ras-GTP levels using activated ras interaction assay. Methods Enzymol. **333**, 333–342 (2001)
20. Yamauchi N., Takezawa T., Kizaki K., Herath C.B., Hashizume K.: Proliferative potential of endometrial stromal cells, and endometrial and placental expression of cyclin in the bovine. J Reprod Dev. **49**, 553–560 (2003)
21. Schmidt B.A., Rose A., Steinhoff C., Strohmeyer T., Hartmann M., Ackermann R.: Up-regulation of cyclin-dependent kinase 4/cyclin D2 expression but down-regulation of cyclin-dependent kinase 2/cyclin E in testicular germ cell tumors. Cancer Res. **61**, 4214–4221 (2001)
22. Mateyak M.K., Obaya A.J., Sedivy J.M.: c-Myc regulates Cyclin D-Cdk4 and -Cdk6 activity but affects cell cycle progression at multiple independent points. Mol Cell Biol. **19**, 4672–4683 (1999)
23. Colo M.D., Mcmahon S.B.: The myc oncoprotein: a critical evaluation of transactivation and target gene regulation. Oncogene. **18**, 2916–2924 (1999)
24. Pines J.: Cyclins and cyclin-dependent kinases: a biochemical view. Biochem J. **308**, 697–711 (1995)
25. Sherr C.J.: Cancer cell cycles. Science. **274**, 1672–1677 (1996)
26. Eguchi H., Carpentier S., Kim S.S., Moss S.F.: p27kip1 regulates the apoptotic response of gastric epithelial cells to *Helicobacter pylori*. Gut. **53**, 797–804 (2004)
27. Russo A.A., Jeffrey P.D., Patten A.K., Massagué J., Pavletich N.P.: Crystal structure of the p27Kip1 cyclin-dependent-kinase inhibitor bound to the cyclin A-Cdk2 complex. Nature. **382**, 325–331 (1996)
28. McCubrey J.A., Steelman L.S., Chappell W.H., Abrams S.L., Wong E.W., Chang F., Lehmann B., Terrian D.M., Milella M., Tafuri A., Stivala F., Libra M., Basecke J., Evangelisti C., Martelli A.M., Franklin R.A.: Roles of the Raf/MEK/ERK pathway in cell growth, malignant transformation and drug resistance. Biochim Biophys Acta. **1773**, 1263–1284 (2007)
29. Fujii Y., Dohmae N., Takio K., Kawsar S.M., Matsumoto R., Hasan I., Koide Y., Kanaly R.A., Yasumitsu H., Ogawa Y., Sugawara S., Hosono M., Nitta K., Hamako J., Matsui T., Ozeki Y.: A lectin from the mussel *Mytilus galloprovincialis* has a highly novel primary structure and induces glycan-mediated cytotoxicity of globotriaosylceramide-expressing lymphoma cells. J Biol Chem. **287**, 44772–44783 (2012)
30. Park S.Y., Kwak C.Y., Shayman J.A., Kim J.H.: Globoside promotes activation of ERK by interaction with the epidermal growth factor receptor. Biochim Biophys Acta. **1820**, 1141–1148 (2012)
31. Nadeem L., Brkic J., Chen Y.F., Bui T., Munir S., Peng C.: Cytoplasmic mislocalization of p27 and CDK2 mediates the anti-migratory and anti-proliferative effects of nodal in human trophoblast cells. J Cell Sci. **126**, 445–453 (2013)
32. Hong S.K., Kim J.H., Lin M.F., Park J.I.: The Raf/MEK/extracellular signal-regulated kinase 1/2 pathway can mediate growth inhibitory and differentiation signaling via androgen receptor downregulation in prostate cancer cells. Exp Cell Res. **317**, 2671–2682 (2011)
33. Hwang C.Y., Lee C., Kwon K.S.: Extracellular signal-regulated kinase 2-dependent phosphorylation induces cytoplasmic localization and degradation of p21Cip1. Mol Cell Biol. **29**, 3379–3389 (2009)
34. Hancock J.F.: Ras proteins: different signals from different locations. Nat Rev Mol Cell Biol. **4**, 373–385 (2003)
35. Avruch J., Zhang X.F., Kyriakis J.M.: Raf meets ras: completing the framework of a signal transduction pathway. Trends Biochem Sci. **19**, 279–283 (1994)
36. Fischer C., Sanchez-Ruderisch H., Welzel M., Wiedenmann B., Sakai T., André S., Gabius H.J., Khachigian L., Detjen K.M., Rosewicz S.: Galectin-1 interacts with the α5β1 fibronectin receptor to restrict carcinoma cell growth via induction of p21 and p27. J Biol Chem. **280**, 37266–37277 (2005)
37. Ogawa T., Watanabe M., Naganuma T., Muramoto K.: Diversified carbohydrate-binding lectins from marine resources. J Amino Acids. **2011**(838914), (2011)
38. Tateno H.: SUEL-related lectins, a lectin family widely distributed throughout organisms. Biosci Biotechnol Biochem. **74**, 1141–1114 (2010)
39. Murayama K., Taka H., Kaga N., Fujimura T., Mineki R., Shindo N., Morita M., Hosono M., Nitta K.: The structure of Silurus Asotus (catfish) roe lectin (SAL): identification of a noncovalent trimer by mass spectrometry and analytical ultracentrifugation. Anal Biochem. **247**, 319–326 (1997)
40. Harper J.W., Adami G.R., Wei N., Keyomarsi K., Elledge S.J.: The p21 Cdk-interacting protein Cip1 is a potent inhibitor of G1 cyclin-dependent kinases. Cell. **75**, 805–816 (1993)
41. Jänicke R.U., Sohn D., Essmann R., Shulze-Osthoff K.: The multiple battles fought by anti-apoptotic p21. Cell Cycle. **6**, 407–413 (2007)
42. Franchi N., Schiavon F., Carletto M., Gasparini F., Bertoloni G., Tosato S.C., Ballarin L.: Immune roles of a rhamnose-binding lectin in the colonial ascidian *Botryllus schlosseri*. Immunobiology. **216**, 725–736 (2011)
43. Kawsar S.M.A., Matsumoto R., Fujii Y., Matsuoka H., Masuda N., Chihiro I., Yasumitsu H., Kanaly R.A., Sugawara S., Hosono M., Nitta K., Ishizaki N., Dogasaki C., Hamako J., Matsui T., Ozeki Y.: Cytotoxicity and glycan-binding profile of a D-galactose-binding lectin from the eggs of a Japanese sea hare (*Aplysia kurodai*). Protein J. **30**, 509–519 (2011)
44. Watanabe Y., Tateno H., Nakamura-Tsuruta S., Kominami J., Hirabayashi J., Nakamura O., Watanabe T., Kamiya H., Naganuma T., Ogawa T., Naudé R.J., Muramoto K.: The function of rhamnose-binding lectin innate immunity by restricted binding to Gb3. Dev Comp Immunol. **33**, 187–197 (2009)
45. Kawsar S.M., Matsumoto R., Fujii Y., Yasumitsu H., Dogasaki C., Hosono M., Nitta K., Hamako J., Matsui T., Kojima N., Ozeki Y.: Purification and biochemical characterization of a D-galactose binding lectin from Japanese sea hare (*Aplysia kurodai*) eggs. Biochemistry (Mosc). **74**, 709–716 (2009)
46. Naganuma T., Ogawa T., Hirabayashi J., Kasai K., Kamiya H., Muramoto K.: Isolation, characterization and molecular evolution of a novel pearl shell lectin from a marine bivalve. *Pteria penguin* Mol Divers. **10**, 607–618 (2006)
47. Lee J.K., Buckhaults P., Wilkes C., Teilhet M., King M.L., Moremen K.W., Pierce M.: Cloning and expression of a *Xenopus laevis* oocyte lectin and characterization of its mRNA levels during early development. Glycobiology. **7**, 367–372 (1997)

THE FASEB JOURNAL • RESEARCH • www.fasebj.org

Importance of membrane-proximal *N*-glycosylation on integrin β1 in its activation and complex formation

Sicong Hou, Qinglei Hang, Tomoya Isaji, Jishun Lu, Tomohiko Fukuda, and Jianguo Gu[1]

Division of Regulatory Glycobiology, Institute of Molecular Biomembrane and Glycobiology, Tohoku Medical and Pharmaceutical University, Miyagi, Japan

ABSTRACT: ***N*-Glycosylation of integrin α5β1 plays important roles in cell biologic functions; however, the mechanisms that underlie those roles remain poorly understood. Here, we present evidence that the membrane-proximal *N*-glycosylation on integrin β1 could positively regulate cell migration by promoting β1 activation. The S4-6 β1 mutant contains only 3 *N*-glycosylation sites, which are essential for α5 and β1 heterodimer formation, and despite only a small difference in expression levels of α5β1 between wild-type and S4-6 mutant, cell spreading and migration of the S4-6 mutant was significantly decreased compared with that of control. Consistent with these phenotypes, β1-mediated cellular signaling and its activation were clearly suppressed in the S4-6 mutant. Of note, these developments could be rescued by restoration of *N*-glycosylation sites in the membrane-proximal domain. Further study on the regulatory mechanisms suggested that membrane-proximal *N*-glycosylation is critical for intermolecular interactions between integrin β1 and other cell membrane proteins, such as syndecan-4 and epidermal growth factor receptor. Moreover, α2,6-sialylation is required for β1 activation. These data suggest a novel regulatory mechanism wherein *N*-glycosylation near the cell membrane on β1 may serve as a platform that facilitates its complex formation on the cell membrane, thereby affecting integrin-mediated functions.—Hou, S., Hang, Q., Isaji, T., Lu, J., Fukuda, T., Gu, J. Importance of membrane-proximal *N*-glycosylation on integrin β1 in its activation and complex formation. FASEB J. 30, 4120–4131 (2016). www.fasebj.org**

KEY WORDS: cell migration · cell signaling · sialylation

Integrins are a large family of heterodimeric glycoproteins that function as adhesion molecules and play key roles in many biologic processes, such as cell spreading, adhesion, and migration, by connecting the extracellular matrix to the cytoskeleton (1). Integrin β1, the largest subgroup of integrins, has received much attention as it forms heterodimers with 12 different α subunits and binds with multiple extracellular ligands, such as collagen, fibronectin, and laminin (2). Recently, the binding affinities of integrin β1 to these ligands have been shown to depend mainly on the structure of its extracellular domain (3–5). The low affinity structure undergoes rapid, reversible conformational changes to increase ligand affinity, which is referred to as activation. This process could be triggered by cytoplasmic factors (inside-out activation) or by extracellular events (outside-in activation) (6, 7), and has been shown to play critical roles in tumor metastasis. Therefore, blockade of integrin activation is considered a potential anticancer therapy (8, 9). In fact, β1-mediated cellular events depend not only on its activation, but also on the effective assembly of surrounding signaling molecules. Several studies point to vital roles for the sophisticated networks of integrin β1 and other membrane receptors, including growth factor receptors, syndecans, and IL receptors in tumor cell behavior (10, 11). Complex formation with these coreceptors further regulates integrin β1–mediated function and cell signal transduction (12, 13). For example, syndecans that are associated with β1 regulate signaling complex formation and activate internal signaling cascades, which promotes cell spreading and migration (14–16). Of note, these studies focus mainly on the role of the inner membrane domains of integrin β1 in the interaction with cytoplasmic coactivators, whereas the function of outer membrane domains in integrin-mediated cellular events remains unknown.

A growing body of studies shows that cell surface oligosaccharides are important for the interaction between cells and the extracellular matrix (17, 18). Glycosylation is one of the key regulators and plays important roles in modulating protein activity. Integrin β1 is a major carrier of *N*-glycans, and alterations in *N*-linked glycosylation on β1 have been observed in various cancer cells (19–21). For example, introduction of bisecting *N*-acetylglucosamine

ABBREVIATIONS: BSA, bovine serum albumin; DKO, double knockout; EGFR, epidermal growth factor receptor; FAK, focal adhesion kinase; FBS, fetal bovine serum; FN, fibronectin; GlcNAc, *N*-acetylglucosamine; GnT-III, *N*-acetylglucosaminyltransferase III; KO, knockout; PSI, plexin-semaphorin-integrin domain; ST6GAL1, β-galactoside 2,6-sialyltranferase 1; WT, wild-type

[1] Correspondence: Tohoku Medical and Pharmaceutical University, 4-4-1 Komatsushima, Aobaku, Sendai, Miyagi, 981-8558, Japan. E-mail: jgu@tohoku-mpu.ac.jp

doi: 10.1096/fj.201600665R

0892-6638/16/0030-4120 © FASEB

(GlcNAc) into β1—by enhancing the expression of *N*-acetylglucosaminyltransferase III (GnT-III)—inhibits cell adhesion and migration (22). An increase in β1-6-GlcNAc branching structures on the β1 subunit, which is catalyzed by *N*-acetylglucosaminyltransferase V, correlates with increases in tumor metastasis (23). α2,6-Galactoside sialyltransferase 1 (ST6GAL1)–mediated hypersialylation of β1 primarily contributes to tumor migration (20). These results suggest that *N*-glycosylation modification of the β1 subunit is closely associated with its function. To investigate the distinct role of the *N*-glycosylation site on integrins, our group has reported that 3 *N*-glycosylation sites on the β-propeller domain of the α5 subunit and the I-like domain of the β1 subunit, respectively, are essential for α5β1 heterodimer formation and its biologic functions (18, 24). In addition, there is a specific *N*-glycosylation site on the α5 subunit (site 4) that is pivotal and can be specifically modified by GnT-III (25). These results highlight the importance of individual *N*-glycans on α5β1. Given the fact that β1 contains 12 potential *N*-glycosylation sites and little is known about the biologic functions of these *N*-glycans, if the importance of individual *N*-glycosylation sites can be identified, this will facilitate an understanding of the molecular mechanisms that underlie integrin function alterations by *N*-glycans.

In the present study, we focused on elucidating the mechanisms by which *N*-glycans regulate integrin functions. We established a β1-null human breast cancer MDA-MB-231 cell line *via* a knockout (KO) of the β1 gene, and then reintroduced wild-type (WT) or various types of *N*-glycosylation mutant β1 into the cells. We found that activation of β1 and β1-mediated complex formation and cellular signaling were strictly regulated by *N*-glycosylation on the membrane-proximal region of β1. In addition, structures of *N*-glycans were also important for function, as the silence of α2,6-sialylation significantly decreased β1 activation and cell membrane complex formation.

MATERIALS AND METHODS

Antibodies and reagents

Experiments were performed by using the following antibodies: antibody against human integrin β1 subunit (P5D2; Developmental Studies Hybridoma Bank, University of Iowa, Iowa City, IA, USA); rabbit mAbs against AKT, p-AKT, and epidermal growth factor receptor (EGFR; Cell Signaling Technology, Danvers, MA, USA); goat antibody against integrin α3 (Santa Cruz Biotechnology, Santa Cruz, CA, USA); integrin α5, focal adhesion kinase (FAK), and p-FAK (BD Biosciences, San Jose, CA, USA); mouse mAbs against human integrin α5β1, rabbit mAbs against integrin β1, and mouse antibody against active integrin β1 (HUTS-4; Millipore, Billerica, MA, USA); rabbit mAbs against syndecan 4 (Novus Biologicals, Littleton, CO, USA); mAb against α-tubulin (Sigma-Aldrich, St. Louis, MO, USA); and Alexa Fluor 488 and 647 goat anti-mouse IgG (Thermo Fisher Scientific Life Sciences, Waltham, MA, USA). Peroxidase-conjugated goat antibodies against mouse, rabbit, and goat were obtained from Promega (Madison, WI, USA), Cell Signaling Technology, and Santa Cruz Biotechnology, respectively. Sambucus sieboldiana agglutinin agarose was from J-Oil Mills (Tokyo, Japan), fibronectin (FN) from Sigma-Aldrich, To-Pro-3 from Thermo Fisher Scientific, and Ab-Capcher ExTra from ProteNova (Takamatsu, Japan). Sulfo-NHS-SS Biotin for cell surface biotinylation and streptavidin-conjugated agarose were from Thermo Fisher Scientific and Millipore, respectively.

Cell lines and cell culture

MDA-MB-231, a human breast cancer cell line, was obtained from American Type Culture Collection (Manassas, VA, USA). 293T and HeLa cell lines were provided from RIKEN cell bank (Tokyo, Japan). β1-KO MDA-MB-231 cells were previously established in our laboratory (26). All cell lines were maintained at 37°C in DMEM (Thermo Fisher Scientific) supplemented with 10% fetal bovine serum (FBS) under a humidified atmosphere that contained 5% CO_2, except for virus production.

Generation of CRISPR/Cas9-based integrin β1-KO HeLa cells and integrin β1/ST6GAL1 double KO MDA-MB-231 cells

CRISPR/Cas9-based integrin β1-KO HeLa and double-KO (DKO) MDA-MB-231 cells were established as described previously (27). In brief, the integrin β1-KO– and ST6GAL1-KO–specifying pSpCas9 (BB)-2A-GFP vectors, which were established previously in our laboratory (26, 28), were transfected into parent HeLa cells and β1-KO MDA-MB-231 cells, respectively, by using Cell Line Nucleofector TM kits (Lonza, Basel, Switzerland) according to manufacturer instructions. After 72 h of transfection, GFP highly expressed cells were sorted by using the FACSAria II (BD Biosciences). After ~10 d of culture, β1- and GFP-negative Hela cells or ST6GAL1- and GFP-negative MDA-MB-231 cells were sorted another 7 or 2 times, respectively. β1-KO HeLa and DKO MDA-MB-231 cells were defined *via* flow cytometry and Western blot analyses as described below.

ST6GAL1 and integrin β1 expression vectors

WT or S4-6 mutant integrin β1- and ST6GAL1-overexpressing lentiviral vectors—CSII-EF-Rfa-WT-β1, CSII-EF-Rfa-S4-6-β1, CSII-EF-Rfa-D4-6-β1, CSII-EF-Rfa-D9-12-β1, and CSIV-TRE-CMV-3xFLAG-ST6GAL1—were previously established in our laboratory (18, 29). Other integrin β1 mutation vectors—S4-6 + 1-3, S4-6 + 7-8, and S4-6 + 9-12—were constructed by using the In-Fusion kit (Takara Bio, Tokyo, Japan) according to manufacturer instructions. The resultant cDNAs were sequenced to confirm the presence of the desired mutations, then cloned into the CSII-EF-Rfa vector by using a Gateway Cloning System kit (Thermo Fisher Scientific) to acquire all expression vectors.

Virus production and infection

Virus production and infection were performed as described previously (18). In brief, the CSII-EF-Rfa—related β1- or CSIV-TRE-CMV-3×FLAG-ST6GAL1-overexpressing lentiviral vectors were cotransfected with pCAG-HIVgp and pCMV-VSV-G-RSV-Rev into 293T cells. After transfection for 48 h, lentivirus supernatants were collected. β1-KO MDA-MB-231 or HeLa cells and DKO MDA-MB-231 cells were infected with the indicated lentiviruses. β1- or ST6GAL1-positive cells were sorted 3 times by using FACSAria II after infection for 72 h. Stable cell lines were used in subsequent studies.

Western blot and Immunoprecipitation

For Western blot, indicated cells were seeded in 10-cm dishes overnight, then washed with ice-cold PBS and lysed in lysis buffer (20 mM Tris-HCl, pH 7.4; 150 mM NaCl; 1% Triton X-100) with protease inhibitors and phosphatase inhibitors (Nacalai Tesque, Kyoto, Japan) for 30 min. After centrifugation, supernatants were collected and protein concentrations were determined by using a bicinchoninic acid protein assay kit (Pierce, Rockford, IL, USA). Protein lysates were subjected to SDS-PAGE. After electrophoresis, proteins were transferred to a PVDF membrane (Millipore). Membrane was detected with primary and secondary antibodies, and proteins were visualized by Immobilon Western Chemiluminescent horseradish peroxidase substrate (Millipore) according to manufacturer instructions.

For immunoprecipitation, cells were lysed with lysis buffer (20 mM Tris-HCl, pH 7.4; 150 mM NaCl; 1% Triton X-100) with protease inhibitors and phosphatase inhibitors (Nacalai Tesque) for 30 min. After centrifugation at 13,000 rpm for 10 min, supernatant was collected and protein concentrations were determined by using a bicinchoninic acid protein assay kit. Equivalent amounts (600 μg) of supernatants were immunoprecipitated by Ab-Capcher ExTra with anti-P5D2 antibody or streptavidin-conjugated agarose for 1 h at 4°C, with rotation, then immunoprecipitates were washed twice with Tris-buffered saline buffer (20 mM Tris-HCl, pH 7.4; 150 mM NaCl) and subjected to SDS-PAGE. Lectin precipitations were performed by using sambucus sieboldiana agglutinin agarose, which specifically recognized α2,6-sialylation. Precipitated glycoproteins were subjected to SDS-PAGE.

Cell surface biotinylation

Cells were gently washed with PBS, and then incubated with ice-cold PBS that contained 0.2 mg/ml Sulfo-NHS-SS Biotin for 1 h at 4°C. After incubation, cells were washed 3 times with ice-cold PBS, then harvested by lysis buffer. Biotinylated proteins were precipitated with streptavidin-conjugated agarose, and then subjected to SDS-PAGE.

Flow cytometric analysis

Cells were grown to ~90% confluency, then detached from culture dishes by using trypsin that contained 1 mM EDTA, washed with ice-cold PBS, and stained with the primary antibodies, followed by incubation with Alexa Fluor 647 goat anti-mouse IgG for 60 min on ice. Finally, cells were washed 3 times with PBS and analyzed *via* FACSCalibur flow cytometry (BD Biosciences).

Immunofluorescence staining

Cells were cultured on a glass-bottom dish, washed with PBS, fixed with ice-cold methanol, and permeabilized with 0.1% Triton X-100. Antibody against active β1 was used, followed by incubation with anti-mouse Alexa Fluor 488 secondary antibodies and Alexa Fluor 546 phalloidin (Thermo Fisher Scientific). Fluorescence images were observed *via* confocal microscopy by using a FluoView FV1000 (Olympus, Tokyo, Japan).

Cell migration

For wound-healing assay, cells were seeded in a 6-well plate and grown to a confluent monolayer. A scratch with a p200 pipette tip was made through the cell layer. After washing with PBS, DMEM that contained 3% FBS was added in each well. Wounded areas were photographed under a light microscope with ×10 objective after 24 h. All experiments were repeated 3 times.

For Transwell migration assay, each Transwell (BD BioCoat TM control inserts, 8.0 mm; BD Biosciences) was coated on the bottom side with 10 μg/ml FN at 4°C overnight. Cells were starved in serum-free medium overnight, trypsinized, and suspended in DMEM that contained 10% FBS. Suspended cells were centrifuged and supernatants were removed. Cells were resuspended with serum-free DMEM and diluted to 0.8×10^5 cells/ml. To each FN-coated Transwell, 500-μl aliquots of cell suspension were added, then cells were incubated at 37°C for 3 h (MDA-MB-231 cells) and 4 h (HeLa cells). After incubation, cells on the upper side were removed by scraping with a cotton swab. The membranes of each Transwell were fixed with 4% paraformaldehyde and stained with 0.5% crystal violet for 2 h. Cells that had migrated to the lower side were counted by using a phase-contrast microscope.

Cell-spreading assays

Cell-spreading assays were performed as described previously (24). In brief, 6-well plates were coated with FN (10 μg/ml) in PBS at 4°C overnight and then blocked with 1% bovine serum albumin (BSA) in DMEM for 1 h at 37°C. Indicated cells were detached and suspended in serum-free DMEM with 0.1% BSA at 4×10^4 cells/ml. After 20-min incubation, nonadherent cells were removed by washing with PBS, attached cells were fixed with 4% paraformaldehyde in PBS, and representative photos were then taken by phase-contrast microscopy.

Video microscope

A glass-bottom dish (Asahi Glass, Shizuoka, Japan) was precoated with FN (10 μg/ml) in PBS at 4°C overnight, then blocked with 1% BSA in DMEM for 1 h at 37°C. Cells (4×10^4) were suspended in 2 ml growth medium, and then added to each FN-coated glass-bottom dish, which was followed by monitoring for 16 h by using time-lapse video equipment (Carl Zeiss, Jena, Germany). Images were acquired by using inverted microscopes (Axio Observer.D1; Carl Zeiss) every 10 min with 5% CO_2 at 37°C in a heated chamber with temperature and CO_2 controller (Onpu-4 and CO_2; AR Brown, Tokyo, Japan) during time-lapse imaging. Cell motility was evaluated by using Chemotaxis and Migration Tool 2.0 (Ibidi GmbH, Planegg/Martinsried, Germany).

Statistical analyses

Statistical analyses were performed *via* Student's *t* test using GraphPad Prism5 (GraphPad Software, La Jolla, CA, USA). Results are presented as means ± SEM. Statistical significance was defined as $P < 0.05$.

RESULTS

Effects of β1 underglycosylation on its heterodimer formation and FN-mediated cell spreading

Given the important role of *N*-glycosylation sites on the I-like domain of the β1 subunit in α5β1 heterodimer formation and cell adhesion (18), we hypothesized that the other *N*-glycosylation sites on the β1 subunit may also have unique functions. After establishing the β1-null MDA-MB-231 cells, we reconstituted with WT, a *N*-glycosylation

mutant on the β1 I-like domain, S4-6, that represents the minimal *N*-glycosylation required for α5β1 function in GE11 cells (18), or with *N*-glycosylation sites on the I-like domain-deleted mutant, D4-6 (**Fig. 1*A***). To determine the effects of *N*-glycosylation on β1 expression on the cell surface, we performed flow cytometric analysis and a biotinylation assay. As shown in Fig. 1*B*, *C*, those 3 cells exhibited similar β1 expression levels on the cell surface and in whole-cell lysates, which suggests that the *N*-glycosylation of β1 had little influence on its expression in MDA-MB-231 cells. It seems to be inconsistent with a previous study that showed that D4-6 reduced expression levels of β1 in GE11 cells (18). In fact, the α5 subunit is a main constituent in β1 integrin–containing dimers in GE11 cells (30), and, therefore, the inhibition of α5β1 heterodimer formation in D4-6 cells greatly reduced expression levels of β1. However, MDA-MB-231 cells highly expressed either α5 or α3, α2, and α6 integrin subunits (31). Therefore, we wondered whether D4-6 β1 forms heterodimers with other α subunits, such as α3. As shown in Fig. 1*D*, α5 subunits were consistently clearly detected in immunocomplexes of WT or S4-6 mutant, but not the D4-6 mutant. Of interest, the α3β1 heterodimer was observed in all 3 cell types, which indicated that α3 integrin is different from α5 and requires different *N*-glycosylation for αβ dimer formation. Of note, the expression level of integrin α5β1 on the cell surface in

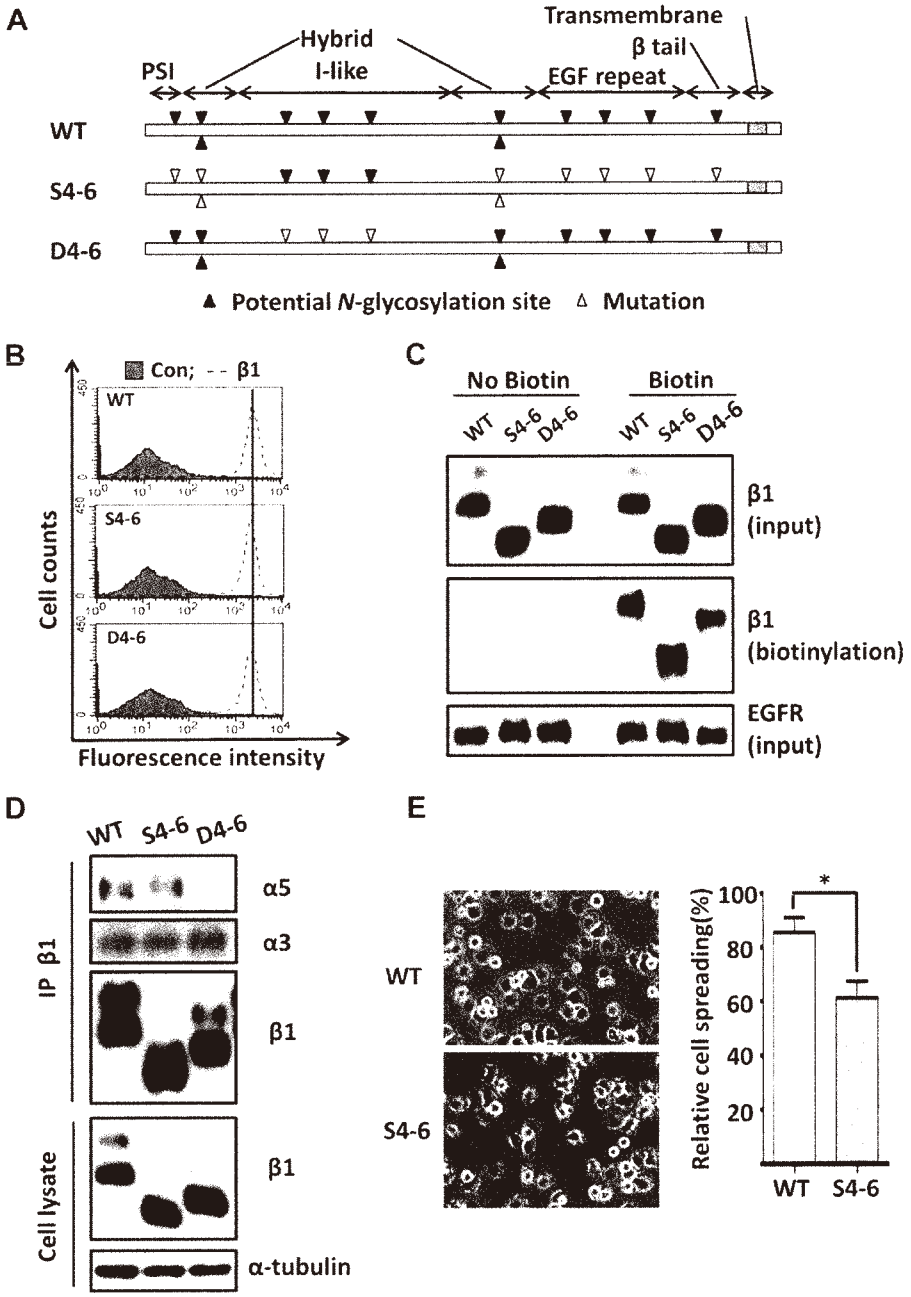

Figure 1. Comparison of β1 expression, its association with α subunits, and FN-mediated cell spreading among WT and *N*-glycosylation mutants of integrin β1. *A*) Schematic diagram of potential *N*-glycosylation sites on integrin β1 subunit (Asn50, Asn94, Asn97, Asn212, Asn269, Asn363, Asn406, Asn417, Asn481, Asn520, Asn584, and Asn669). *N*-Glycosylation sites are indicated by closed triangles, and point mutations are indicated by open triangles. *B*) WT, S4-6, and D4-6 cells exhibited the same expression levels as β1 on the cell surface. Cells were collected and incubated with (dotted line) or without (gray shadow) anti-β1 antibody, followed by incubation with Alexa Fluor 647 goat anti-mouse IgG, then were subjected for flow cytometric analysis. *C*) Expression levels of β1 on cell surfaces (biotinylation) and in total cell lysates were immunoblotted with anti-β1 antibody. EGFR was used as a loading control. *D*) Cell lysates from WT, S4-6, and D4-6 cells were immunoprecipitated (IP) with anti-β1 antibody (P5D2) and blotted with anti–α3, anti–α5, and anti–β1 antibodies. *E*) WT and S4-6 cells were detached and then replated on the FN-coated (10 μg/ml) dishes. After incubation for 20 min, cells were fixed with paraformaldehyde and images were taken. Percentages of spread cells were statistically analyzed as means ± SEM of 3 independent experiments. $^*P < 0.05$ by 2-tailed unpaired Student's *t* test.

S4-6 cells was comparable to that of WT cells, but the cell-spreading ability was significantly decreased in S4-6 cells compared with WT cells (Fig. 1*E*). Collectively, these results suggest that *N*-glycosylation on domains other than the I-like domain of the β1 subunit may be involved in the regulation of its various cellular functions.

Removal of *N*-glycosylation sites on β1 suppressed FN-mediated cell migration

N-Glycans on β1 integrin play important roles in the regulation of its biologic functions. Our wound healing assay and boyden chamber analysis showed that S4-6 cells exhibited a significant decrease in cell migration compared with WT cells (**Fig. 2*A, B***). To check whether underglycosylation of β1 also suppresses FN-mediated migration of other cells, integrin β1 was knocked out in Hela cells by using a CRISPR/Cas9 system, and WT or S4-6 of β1 was restored in the KO cells. In similar manner, decreased cell migration was also observed in S4-6 mutant HeLa cells (Fig. 2*A, B*). To further confirm the phenotype of S4-6 cells, cell motilities of WT and S4-6 mutant cells were examined and compared by using *in vitro* time-lapse imaging. Consistently, WT cells seemed to move faster than the underglycosylated S4-6 mutant cells (Fig. 2C). Taken together, these results demonstrate that *N*-glycosylation on the β1 subunit is capable of promoting cell migration.

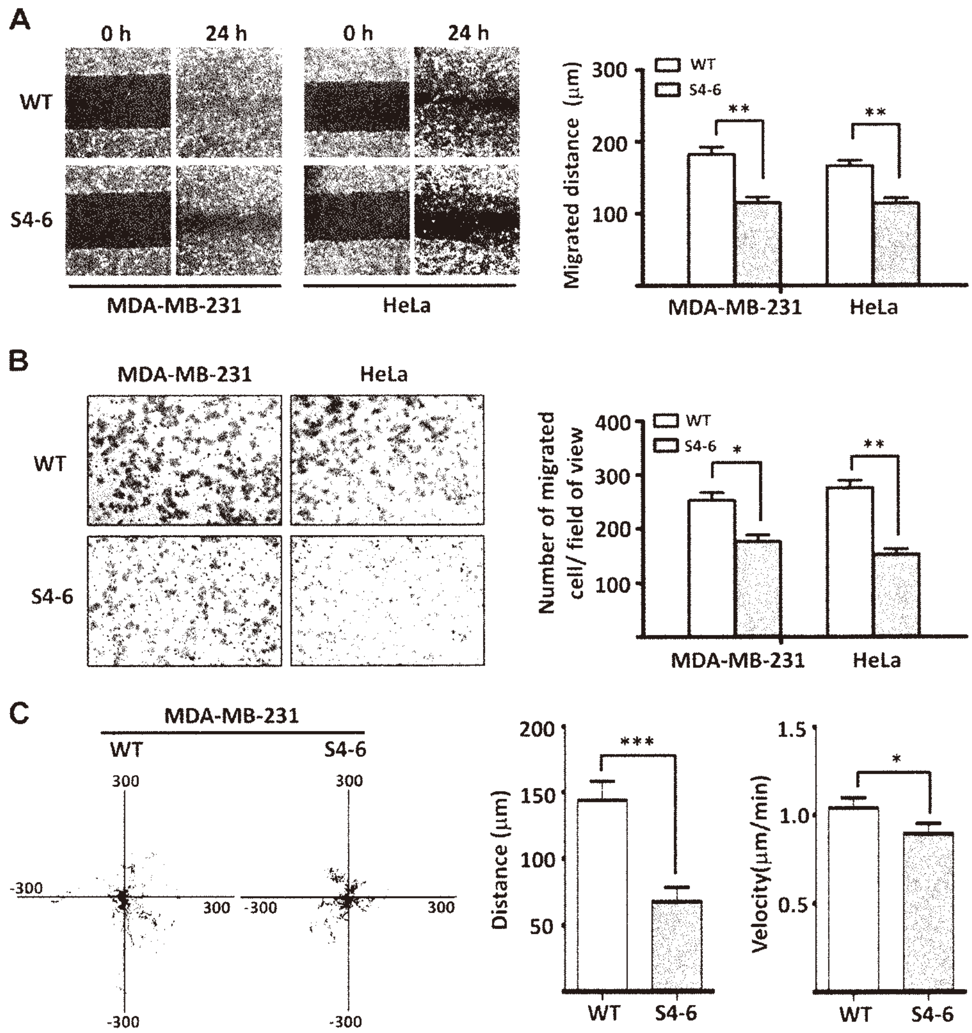

Figure 2. Removal of *N*-glycosylation sites on β1 suppressed FN-mediated cell migration in MDA-MB-231 and HeLa cells. *A*) Indicated cells were cultured until >90% confluence. A scratch was made with a p200 pipette in each well, and photographs were taken at 0 and 24 h (left). Quantitative data of migrated distances were expressed as means ± SEM from 3 independent experiments (right). *B*) Migration ability was also analyzed by Transwell assay. In brief, cells that migrated through the Transwell membrane were stained with 0.5% crystal violet. Representative photos were recorded by phase-contrast microscopy (left). Migrated cells were counted and quantitative data were obtained from 3 independent experiments (right). *C*) Individual migration tracks of WT and S4-6 cells were monitored by time-lapse microscopy as described in Materials and Methods (left). Values for the distance and velocity of cell migration were analyzed and each bar represents means ± SEM of 16 cells. $^{*}P < 0.05$, $^{**}P < 0.01$, $^{***}P < 0.001$ by 2-tailed unpaired Student's *t* test (right).

Depletion of *N*-glycosylation on β1 affects integrin-mediated classic signaling on FN and its activation

Activation of FAK is an important step for β1-mediated intracellular signaling and cell migration (32, 33). To determine whether *N*-glycosylation of the β1 subunit could also affect integrin signaling, the phosphorylation level of FAK was assessed by using cell lysates that were collected at indicated times. As shown in **Fig. 3*A***, response of the FN-induced activation of FAK was attenuated in S4-6 cells compared with WT cells. In addition, there were more lamellipodia formation and membrane protrusions in WT than in S4-6 cells, as detected by phalloidin staining. These observations provided molecular support for the decreased motility of S4-6 cells (Fig. 3*B*). Consistent with phosphorylated levels of FAK, p-AKT levels were also decreased in S4-6 cells compared with WT cells (Fig. 3C). These data indicate that *N*-glycosylation on the β1 subunit might affect the status of integrin activation. To test this idea, β1 activation was examined by flow cytometry analyses and immunofluorescence staining with anti-active β1 antibodies. As expected, loss of *N*-glycosylation resulted in a significant decrease in expression level of active β1 both in the intracellular domain and on the cell surface (Fig. 3*D*, *E*).

N-Glycosylation on the membrane-proximal domain of β1 (9-12) is required for integrin-mediated cellular signaling and its biologic function

The question arose as to which of the *N*-glycosylation sites on β1 were important for its function in cell migration. To address this, we established several mutant cell lines that expressed β1 with the restoration of *N*-glycosylation sites on its plexin-semaphorin-integrin domain (PSI)

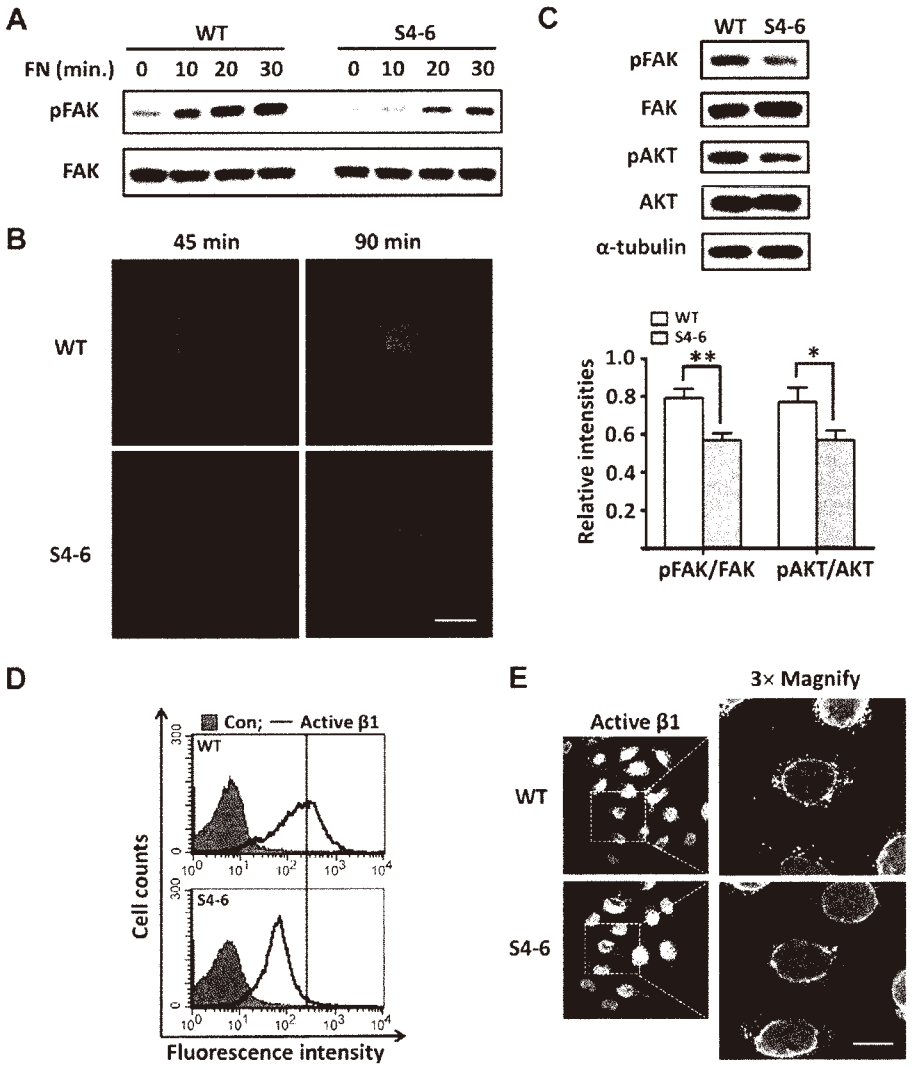

Figure 3. *N*-Glycosylation on β1 was essential for integrin-mediated cellular signaling and its activation. *A*) WT and S4-6 cells were detached and then replated on the FN-coated (10 μg/ml) dishes for the indicated times. Cell lysates were collected and then immunoblotted by anti–p-FAK, anti-FAK antibodies. *B*) Indicated cells were detached and kept in suspension for 30 min before seeding. Cells were then plated on FN-coated (10 μg/ml) glass bottom dishes for 45 min (left) or 90 min (right) in serum-free medium. Localization of F-actin was examined by staining with Alexa Fluor 546 phalloidin. *C*) Cell lysates from WT and S4-6 cells were immunoblotted with anti–p-FAK, anti-FAK, anti–p-AKT, and anti-AKT antibodies. α-Tubulin was used as a loading control (top). Quantitative data are presented as means ± SEM from 3 independent experiments (bottom). *D*) WT and S4-6 cells were collected and incubated with (bold line) or without (gray shadow) anti-active β1 antibody (HUTS-4), followed by Alexa Fluor 647 goat anti-mouse IgG, then subjected to flow cytometry. *E*) Immunofluorescence staining patterns of active integrin β1 in WT and S4-6 cells. Cells were stained with anti-active β1 antibody (HUTS-4), followed by incubation with fluorescent secondary antibody. Con, control. Scale bar, 20 μm. $^*P < 0.05$, $^{**}P < 0.01$ by 2-tailed unpaired Student's *t* test.

containing 2 conserved disulfide motifs, an upstream region of the hybrid domains (S4-6 + 1-3), the downstream region of the hybrid domain (S4-6 + 7-8), and EGF repeat and β-tail domains (S4-6 + 9-12; **Fig. 4*A***). All *N*-glycosylation–restored cells exhibited similar expression levels of α5β1 on the cell surface (Fig. 4*B*); however, among these, only S4-6 + 9-12 mutant cells showed comparable abilities of cell spreading and migration on FN to

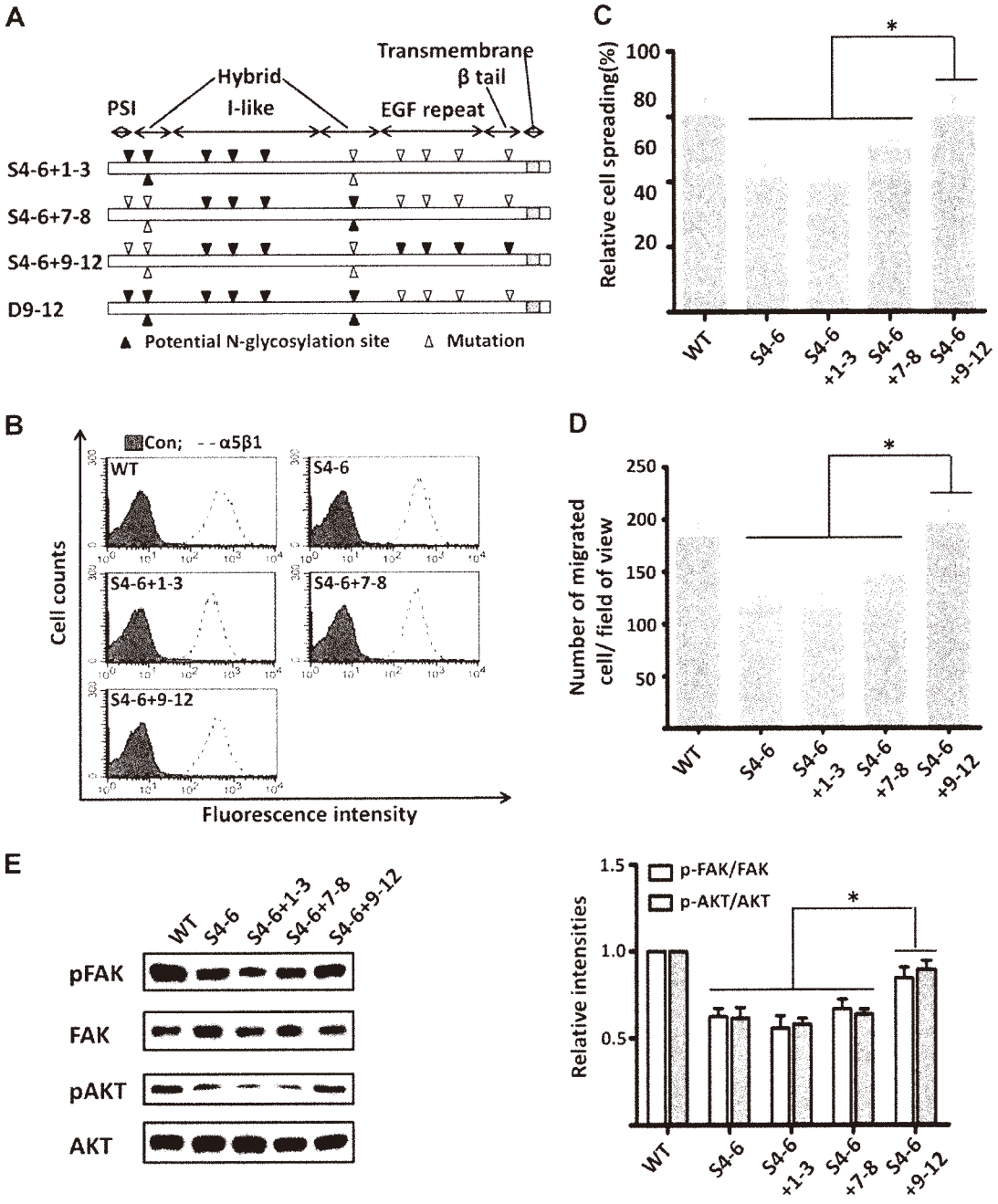

Figure 4. *N*-Glycosylation on the membrane-proximal domain played important roles in β1-mediated signal transduction and cell migration. *A*) Schematic diagram of potential *N*-glycosylation mutant on β1 (S4-6 + 1-3, S4-6 + 7-8, S4-6 + 9-12, and D9-12). *N*-Glycosylation sites are indicated by closed triangles and point mutations are indicated by open triangles. *B*) Expression levels of integrin α5β1 on cell surface analyzed by flow cytometry. Cells were collected and incubated with (dotted line) or without (gray shadow) anti-α5β1 antibody, followed by incubation with Alexa Fluor 647 goat anti-mouse IgG. *C*) Indicated cells were detached and replated on FN-coated dishes. Cell spreading was monitored as described in Materials and Methods. Percentages of the spread cells were statistically analyzed and presented as means ± SEM of 3 independent experiments. *D*) Cell migration was determined by Transwell assay. Cells that migrated through the Transwell membrane were stained with 0.5% crystal violet. Representative photos were recorded and migrated cells were counted. Quantitative data were obtained from 3 independent experiments. *E*) Cell lysates from these mutant cells were immunoblotted by anti–p-FAK, anti-FAK, anti–p-AKT, and anti-AKT antibodies. Con, control. Quantitative data were presented as means ± SEM from 3 independent experiments. $^*P < 0.05$, by 2-tailed unpaired Student's *t* test.

WT cells (Fig. 4*C*, *D*). Consistently, levels of p-FAK and p-AKT were also rescued by restoration of *N*-glycosylation on the EGF repeat and β-tail domain (sites 9–12), instead of other domains (Fig. 4*E*). Taken together, these results clearly suggest that *N*-glycosylation located in the vicinity of the cell membrane domain of β1 plays a crucial role in integrin β1–mediated cell signaling and cell migration.

α2,6-Sialylation plays critical roles in integrin activation

To compare expression levels of active β1 integrin in these mutant cells, we chose flow cytometric analysis and immunofluorescence staining by using the confocal mid-section, which only shows intracellular compartments, to check the expression of active β1 on the cell membrane and in the intracellular domain, respectively. Expression levels of active β1 on the intracellular and cell surface were clearly increased in S4-6 + 9-12 cells compared with S4-6 and S4-6 + 1-3 cells (**Fig. 5*A*, *B***). Unexpectedly, expression levels were also rescued in S4-6 + 7-8 cells (Fig. 5*A*, *B*), although cell migration could not be rescued as described above; therefore, the question arose as to what could affect β1 activation. We considered the fact that ST6GAL1-mediated sialylation plays vital roles in β1 function and tumor progression (20, 34, 35), and a bioinformatics study estimated that sialylation on the I-like domain of β1 might regulate its activation *via* altering binding of FN to β1 (4). Therefore, we checked the α2,6-sialylation levels in these mutants. As shown in Fig. 5*C*, levels of sialylated β1 and α5 were clearly higher in S4-6 + 7-8 and S4-6 + 9-12 mutant cells than in S4-6 cells, whereas levels of sialylated α3 showed no significant difference in any of the mutant cells. In contrast, S4-6 + 1-3 cells showed the lowest α2,6-sialylation levels of α5β1 among these cells, which suggested that *N*-glycosylation on PSI and on the upstream region of the hybrid may have a negative impact on the α2,6-sialylation of α5β1 integrin. To further confirm that rescue of integrin activation observed above was a result of the increased sialylation level on β1, the ST6GAL1 gene was knocked out in WT, S4-6 + 7-8, or S4-6 + 9-12 mutant cells, and similar assays for β1 activation were performed. As expected, ST6GAL1-KO cells showed a clear decrease in expression of active β1 on the cell surface, and this phenotype could be rescued in ST6GAL1 restored cells (Fig. 5*D*). Collectively, these findings suggest that α2,6-sialylated *N*-glycans are crucial for integrin β1 activation.

N-Glycosylation of β1 on the membrane-proximal domain is important for the signaling complex with other receptors

The question of why only S4-6 + 9-12 *N*-glycosylation mutants could rescue both cell migration and cellular signaling remains unclear. Considering that integrin-mediated cellular events are thought to be regulated not only by a conformational change caused by integrin activation, but also by coordination between integrin and other membrane proteins (10), we further investigated β1-mediated complex formation. Here, we chose 2 representative membrane proteins, syndecan-4 and EGFR, which have a vital influence on integrin-mediated cellular functions. On one hand, syndecan-4 is known to synergize with the FN-specific integrin α5β1 to regulate its activation, adhesion-complex formation, and cell spreading and migration (36, 37). On the other hand, it is also well known that EGFR cooperation with integrin β1 has important implications for regulation of diverse cell events (10, 38). As shown in **Fig. 6*A***, immunoprecipitation assay showed little difference in the interaction of integrin β1 with EGFR or syndecan-4 between S4-6 + 9-12 and WT cells, but those interactions were clearly inhibited in mutant cells, such as S4-6, S4-6 + 1-3, and even S4-6 + 7-8 cells. To further confirm this result, we established D9-12 cells that expressed β1 without *N*-glycosylation sites on EGF repeat and β-tail domains (Fig. 4*A*) and found the interactions between D9-12 integrin and EGFR or syndecan-4 were clearly decreased compared with those in WT and S4-6 + 9-12 cells (Fig. 6*B*). As described above, *N*-glycosylation on the EGF repeat and β-tail domain (sites 9–12) regulated cell membrane signaling complex formation, and we also detected an up-regulated overall level of sialylated α5β1 in this mutant. Therefore, we wondered whether α2,6-sialylation on β1 participates in its association with other membrane receptors. Attenuated interactions of β1 with EGFR or syndecan-4 were observed in ST6GAL1-KO in both WT and S4-6 + 9-12 cells (Fig. 6*C*), which indicated that sialylation on β1 was required for its cooperation with EGFR and syndecan-4. Taken together, these results strongly suggest that *N*-glycosylation of β1 on the membrane-proximal domain regulates cell migration and cellular signaling by promoting β1 activation and complex formation.

DISCUSSION

N-Glycosylation of integrin β1 is involved in diverse biologic functions, including cell adhesion, cell migration, and transmembrane signaling; however, most studies have focused mainly on the entire alteration in *N*-glycosylation and little is known about the function of individual *N*-glycans on integrin β1. The present study is the first, to our knowledge, to show that different *N*-glycosylations of β1 have distinct functions and participate in different cell biologic processes. In detail, although both *N*-glycosylation sites on 7-8 and 9-12 play important roles in β1 activation, only the membrane-proximal *N*-glycosylation on the EGF repeat and β-tail domain (9-12) rescued cell migration and β1-mediated complex formation. Furthermore, *N*-glycosylation on the PSI and upstream region of the hybrid domain (sites 1–3) suppressed α2,6-sialylation and β1 activation. In addition, our data clearly suggest that α2,6-sialylated *N*-glycans on the β1 membrane-proximal domain play essential roles in promoting cell migration, which provides new insights into the molecular mechanisms for aberrant *N*-glycosylation in tumors.

Structural and functional studies have shown that integrins undergo rapid conformational changes that increase the affinity for ligand binding, referred to as

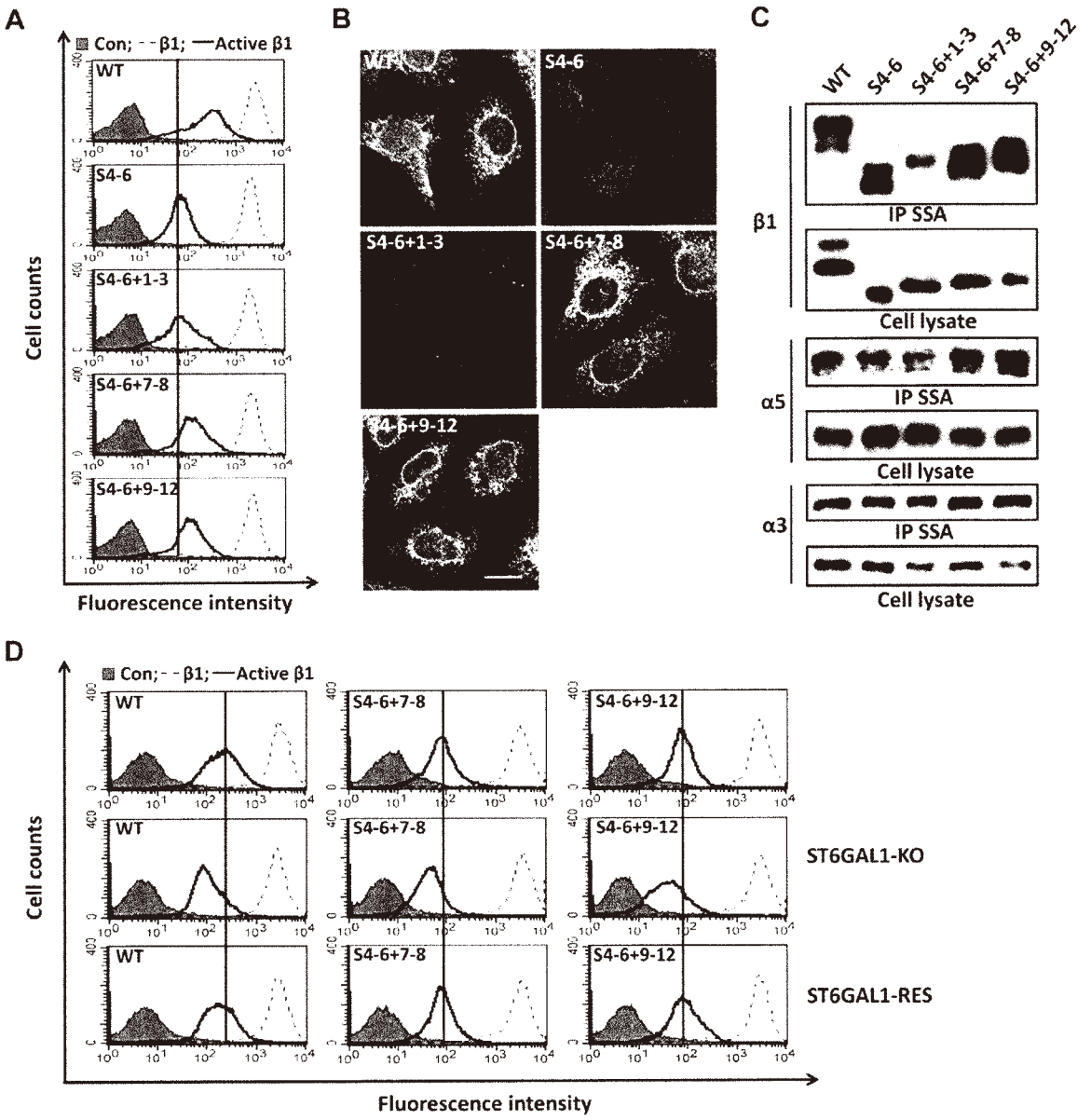

Figure 5. Effects of *N*-glycosylation on different domains on β1 activation. *A*) Expression levels of total integrin β1 and active β1 on the cell surface were measured by flow cytometry. Cells were collected and incubated with anti-β1 (dotted line) and anti-active β1 (bold line) antibodies or without (gray shadow) primary antibody, followed by incubation with Alexa Fluor 647 goat anti-mouse IgG. *B*) Expression levels of active β1 in different mutants, which were immunostained with antibody against active β1, followed by incubation with fluorescent secondary antibody. *C*) Comparison of sialylation levels in these mutant cells. Cell lysates were immunoprecipitated (IP) by sambucus sieboldiana agglutinin (SSA) agaroses, which specifically recognized α2,6-sialylation, and probed with antibodies against integrin α3, α5, or β1. *D*) Effects of sialylation on β1 activation. Derivative cell lines as indicated were incubated with anti-β1 antibody (dotted line), anti-active β1 antibody (bold line), or without (gray shadow) primary antibody, followed by incubation with appropriate Alexa Fluor 647 goat anti-mouse IgG, and then subjected to flow cytometry. Con, control; ST6GAL1-RES, ST6GAL1-KO cells rescued by overexpression of ST6GAL1. Scale bar, 20 μm.

activation. Activation is an important mechanism by which cells regulate integrin function (5, 39). Previous studies were primarily focused on the cytoplasmic domains of integrin, as talin binding to the integrin β tail is the last common step either during inside-out or outside-in activation (5, 40). There are 2 important cytoplasmic NPxY (Asn-Pro-X-Tyr) motifs in the integrin β1 tail: one is the membrane-proximal NPxY motif, which can associate with talin and is crucial for connecting integrin to the actin cytoskeleton; the other is the membrane-distal NPxY motif, which can bind with kindlin and is responsible for integrin α5β1 expression and degradation (8). However, recent studies have indicated that the extracellular domain is also important for its activation process by regulating ligand binding ability and the interaction with cytoplasmic domain molecules during integrin activation (41, 42).

The FASEB Journal Vol.30, No.12 , pp:4120-4131, December, 2016

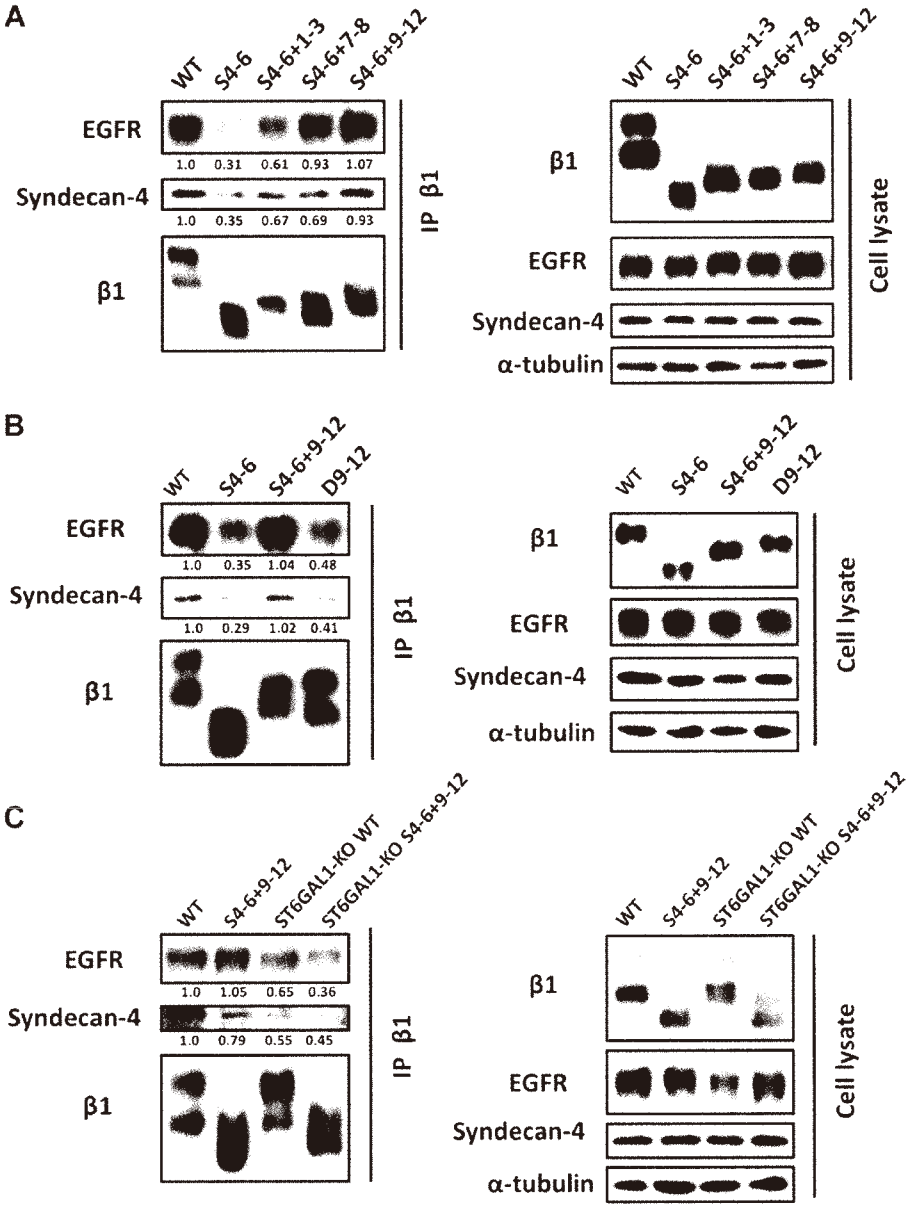

Figure 6. *A*) Cell lysates obtained from WT and the 4 indicated *N*-glycosylation mutants were immunoprecipitated (IP) with anti-β1 antibody (P5D2), and these immunoprecipitants were then subjected to Western blotting with anti-EGFR, anti-syndecan-4, or anti-β1 antibodies (left panel). The whole cell lysates were also subjected to Western blotting with the indicated antibodies (right panel; as an input). *B*) The cell lysates of WT and the 3 indicated mutants were immunoprecipitated with anti-β1 antibody, and these immunoprecipitants were blotted with the indicated antibodies as described above (left panel). The total expression levels of these proteins were blotted with the indicated antibodies (right panel). *C*) The cell lysates of WT and the indicated 3 mutants were immunoprecipitated with anti-β1 antibody, and these immunoprecipitants were blotted with the indicated antibodies (left panel). The total expression levels of these proteins were blotted with the indicated antibodies (right panel). The ratio of band density of EGFR or syndecan-4 *vs.* band density of β1 in WT cells was set as 1.0.

Consistent with a molecular modeling study that has shown that *N*-glycosylation surrounding the RGD-binding pocket of integrin α5β1 affects its binding to FN (43), our data here also support the notion that *N*-glycosylation of integrin is involved in its activation process. Furthermore, we showed that either the re-expression of *N*-glycans on the downstream region of the hybrid domain (sites 7–8) or the EGF repeat and β-tail domain (sites 9–12), but not S4-6 or S4-6 + 1-3 mutants, could rescue β1 activation. Although the detailed mechanisms remain unclear, it is reasonable to postulate that *N*-glycosylation on these 2 domains may exhibit some specific *N*-glycans and/or localizations, which contribute to integrin activation, and may also regulate the internalization of integrin α5β1.

Given the terminal location of sialic acids and their relatively strong electronegative charge, it is reasonable to assume that ST6GAL1-mediated sialylation plays crucial roles in the regulation of β1 conformation, activation, and its mediated functions (20, 44). In addition to effects of overall sialylation of integrin β1, sialylation on some specific domain, such as the I-like domain, is thought to affect its binding ability to FN and α5β1-mediated cellular activities (4). Here, our results clearly show that different *N*-glycosylation sites exhibited different patterns of α2,6-sialylation. As shown in Fig. 5, the α2,6-sialylated level in the S4-6 + 1-3 mutant was even lower than that in S4-6 mutants, which indicated that some *N*-glycosylations might be involved in the regulation of the sialylation level of integrin β1. One possibility for its regulatory mechanism is that *N*-glycosylation on the PSI, an upstream region of the hybrid domain, regulates integrin conformation, which may block the accessibility of ST6GAL1 to

modify *N*-glycosylation sites 4–6, as we previously demonstrated that GnT-III could modify the specific *N*-glycosylation of the α5 subunit (25).

Of note, integrin activation is crucial for its functions but is insufficient for full biologic functions. In the present study, we observed that although 2 *N*-glycosylation mutants could rescue β1 activation, only 1 mutant could fully rescue β1-mediated cell migration and cellular signaling. Given the evidence that sophisticated networks of extracellular signals control diverse aspects of cell fate (38, 45), it is reasonable to think that cooperation of integrin with other membrane proteins may serve as a possible explanation for this phenomenon. Actually, α2,6-sialylation on the membrane-proximal domain of the β1 mutant could greatly facilitate the interaction with syndecan-4 and EGFR, which plays key roles in cell migration and cell signaling. Similar to β1, we recently found that *N*-glycosylation on the calf-1,2 domain of integrin α5 suppresses the phosphorylation of EGFR and cell signaling (46). Matthew *et al.* (47) reported that a bulky glycocalyx can influence integrin clustering and activity and facilitate focal adhesion assembly and integrin-dependent growth factor signaling. Eric *et al.* (20) described β1 hypersialylation that can promote the association with talin, which is the final step of integrin activation, and then contribute to up-regulation of cell migration in the colon adenocarcinomas. Taken together, these studies strongly support the notion that integrin-mediated cellular functions can be regulated by *N*-glycans and that the importance of *N*-glycosylation is reflected in either the specific domain or the structure of *N*-glycans. On the basis of the results of the present study, *N*-glycosylation on the membrane-proximal domain of β1 was essential for FN-mediated cell migration, and it is highly possible that specific *N*-glycans may exist in different conformations, which would place different influences on diverse cell behaviors. A question arises, then, regarding how *N*-glycosylation on β1 mediated its association with EGFR and syndecan-4. One possibility could be that some lectins and glycosphingolipids may act as a linker for interaction between *N*-glycosylation on β1 and other membrane proteins. It has been previously reported that galectin-3, one kind of animal lectin with affinity for β-galactosides, could associate with both β4 integrin and EGFR and thereby cross-link the 2 molecules (48, 49). In addition to galectins, gangliosides are also involved in the interaction with integrin-EGFR complex formation (46, 50); however, we could not exclude the possibility of a direct interaction between β1 and membrane proteins, as an unknown lectin-like domain may exist on EGFR, as a lectin domain on integrin αMβ2 has been reported to mediate its association with GlcNAc on platelets (51).

Aberrant glycan structures on integrin are closely associated with malignant cell behaviors. These alterations in glycosylation are part of a long-term process, from maturation and cell surface localization to recycling until degradation (18, 23, 46). Our previous study showed that *N*-glycosylation on β1 I-like domain plays essential roles in α5β1 heterodimer formation. As part of a continuing study, the present investigation demonstrated that *N*-glycosylation on the membrane-proximal region of β1 is crucial for the regulation of cell migration and complex formation. Our sequential analysis of the *N*-glycosylation of integrin is important for elucidating the molecular mechanisms that underlie integrin-mediated biologic processes, which could provide insights for cancer treatment. FJ

ACKNOWLEDGMENTS

This work was supported in part by a Grant-in-Aid for Scientific Research (15H04354; to J.G.), a grant for Challenging Exploratory Research (15K14408; to J.G.) from the Japan Society for the Promotion of Science, and by a Strategic Research Foundation Grant-aided Project for Private Universities from the Ministry of Education, Culture, Sports, Science, and Technology of Japan.

AUTHOR CONTRIBUTIONS

S. Hou performed all experiments; Q. Hang, T. Isaji, and J. Lu assisted with experiments; T. Isaji, J. Lu, and T. Fukuda constructed the virus expression and knockout vectors; Q. Hang analyzed protein expression levels using flow cytometry; J. Gu designed the experiment; S. Hou and J. Gu analyzed the data, prepared the figures, and wrote the manuscript; and all authors discussed the results and commented on the manuscript.

REFERENCES

1. Campbell, I. D., and Humphries, M. J. (2011) Integrin structure, activation, and interactions. *Cold Spring Harb. Perspect. Biol.* **3**, a004994
2. Hynes, R. O. (2002) Integrins: bidirectional, allosteric signaling machines. *Cell* **110**, 673–687
3. Calderwood, D. A., Campbell, I. D., and Critchley, D. R. (2013) Talins and kindlins: partners in integrin-mediated adhesion. *Nat. Rev. Mol. Cell Biol.* **14**, 503–517
4. Pan, D., and Song, Y. (2010) Role of altered sialylation of the I-like domain of beta1 integrin in the binding of fibronectin to beta1 integrin: thermodynamics and conformational analyses. *Biophys. J.* **99**, 208–217
5. Margadant, C., Monsuur, H. N., Norman, J. C., and Sonnenberg, A. (2011) Mechanisms of integrin activation and trafficking. *Curr. Opin. Cell Biol.* **23**, 607–614
6. Shattil, S. J., Kim, C., and Ginsberg, M. H. (2010) The final steps of integrin activation: the end game. *Nat. Rev. Mol. Cell Biol.* **11**, 288–300
7. Kim, C., Ye, F., and Ginsberg, M. H. (2011) Regulation of integrin activation. *Annu. Rev. Cell Dev. Biol.* **27**, 321–345
8. Margadant, C., Kreft, M., de Groot, D. J., Norman, J. C., and Sonnenberg, A. (2012) Distinct roles of talin and kindlin in regulating integrin α5β1 function and trafficking. *Curr. Biol.* **22**, 1554–1563
9. Petrich, B. G., Fogelstrand, P., Partridge, A. W., Yousefi, N., Ablooglu, A. J., Shattil, S. J., and Ginsberg, M. H. (2007) The antithrombotic potential of selective blockade of talin-dependent integrin alpha IIb beta 3 (platelet GPIIb-IIIa) activation. *J. Clin. Invest.* **117**, 2250–2259
10. Streuli, C. H., and Akhtar, N. (2009) Signal co-operation between integrins and other receptor systems. *Biochem. J.* **418**, 491–506
11. Guo, W., and Giancotti, F. G. (2004) Integrin signalling during tumour progression. *Nat. Rev. Mol. Cell Biol.* **5**, 816–826
12. Pillozzi, S., Brizzi, M. F., Bernabei, P. A., Bartolozzi, B., Caporale, R., Basile, V., Boddi, V., Pegoraro, L., Becchetti, A., and Arcangeli, A. (2007) VEGFR-1 (FLT-1), beta1 integrin, and hERG K^+ channel for a macromolecular signaling complex in acute myeloid leukemia: role in cell migration and clinical outcome. *Blood* **110**, 1238–1250
13. Assoian, R. K., and Schwartz, M. A. (2001) Coordinate signaling by integrins and receptor tyrosine kinases in the regulation of G1 phase cell-cycle progression. *Curr. Opin. Genet. Dev.* **11**, 48–53
14. Beauvais, D. M., and Rapraeger, A. C. (2004) Syndecans in tumor cell adhesion and signaling. *Reprod. Biol. Endocrinol.* **2**, 3

15. Bendas, G., and Borsig, L. (2012) Cancer cell adhesion and metastasis: selectins, integrins, and the inhibitory potential of heparins. *Int. J. Cell Biol.* **2012**, 676731
16. Wang, H., Jin, H., Beauvais, D. M., and Rapraeger, A. C. (2014) Cytoplasmic domain interactions of syndecan-1 and syndecan-4 with α6β4 integrin mediate human epidermal growth factor receptor (HER1 and HER2)-dependent motility and survival. *J. Biol. Chem.* **289**, 30318–30332
17. Gu, J., Isaji, T., Sato, Y., Kariya, Y., and Fukuda, T. (2009) Importance of *N*-glycosylation on alpha5beta1 integrin for its biological functions. *Biol. Pharm. Bull.* **32**, 780–785
18. Isaji, T., Sato, Y., Fukuda, T., and Gu, J. (2009) *N*-glycosylation of the I-like domain of beta1 integrin is essential for beta1 integrin expression and biological function: identification of the minimal *N*-glycosylation requirement for alpha5beta1. *J. Biol. Chem.* **284**, 12207–12216
19. Pocheć, E., Janik, M., Hoja-Łukowicz, D., Link-Lenczowski, P., Przybyło, M., and Lityńska, A. (2013) Expression of integrins α3β1 and α5β1 and GlcNAc β1,6 glycan branching influences metastatic melanoma cell migration on fibronectin. *Eur. J. Cell Biol.* **92**, 355–362
20. Seales, E. C., Jurado, G. A., Brunson, B. A., Wakefield, J. K., Frost, A. R., and Bellis, S. L. (2005) Hypersialylation of beta1 integrins, observed in colon adenocarcinoma, may contribute to cancer progression by up-regulating cell motility. *Cancer Res.* **65**, 4645–4652
21. Asada, M., Furukawa, K., Segawa, K., Endo, T., and Kobata, A. (1997) Increased expression of highly branched *N*-glycans at cell surface is correlated with the malignant phenotypes of mouse tumor cells. *Cancer Res.* **57**, 1073–1080
22. Isaji, T., Gu, J., Nishiuchi, R., Zhao, Y., Takahashi, M., Miyoshi, E., Honke, K., Sekiguchi, K., and Taniguchi, N. (2004) Introduction of bisecting GlcNAc into integrin alpha5beta1 reduces ligand binding and down-regulates cell adhesion and cell migration. *J. Biol. Chem.* **279**, 19747–19754
23. Guo, H. B., Lee, I., Kamar, M., Akiyama, S. K., and Pierce, M. (2002) Aberrant *N*-glycosylation of beta1 integrin causes reduced alpha5beta1 integrin clustering and stimulates cell migration. *Cancer Res.* **62**, 6837–6845
24. Isaji, T., Sato, Y., Zhao, Y., Miyoshi, E., Wada, Y., Taniguchi, N., and Gu, J. (2006) *N*-glycosylation of the beta-propeller domain of the integrin alpha5 subunit is essential for alpha5beta1 heterodimerization, expression on the cell surface, and its biological function. *J. Biol. Chem.* **281**, 33258–33267
25. Sato, Y., Isaji, T., Tajiri, M., Yoshida-Yamamoto, S., Yoshinaka, T., Somehara, T., Fukuda, T., Wada, Y., and Gu, J. (2009) An *N*-glycosylation site on the beta-propeller domain of the integrin alpha5 subunit plays key roles in both its function and site-specific modification by beta1,4-*N*-acetylglucosaminyltransferase III. *J. Biol. Chem.* **284**, 11873–11881
26. Hou, S., Isaji, T., Hang, Q., Im, S., Fukuda, T., and Gu, J. (2016) Distinct effects of β1 integrin on cell proliferation and cellular signaling in MDA-MB-231 breast cancer cells. *Sci. Rep.* **6**, 18430
27. Ran, F. A., Hsu, P. D., Wright, J., Agarwala, V., Scott, D. A., and Zhang, F. (2013) Genome engineering using the CRISPR-Cas9 system. *Nat. Protoc.* **8**, 2281–2308
28. Lu, J., Isaji, T., Im, S., Fukuda, T., Kameyama, A., and Gu, J. (2016) Expression of *N*-acetylglucosaminyltransferase III suppresses α2,3-sialylation, and its distinctive functions in cell migration are attributed to α2,6-sialylation levels. *J. Biol. Chem.* **291**, 5708–5720
29. Isaji, T., Im, S., Gu, W., Wang, Y., Hang, Q., Lu, J., Fukuda, T., Hashii, N., Takakura, D., Kawasaki, N., Miyoshi, H., and Gu, J. (2014) An oncogenic protein Golgi phosphoprotein 3 up-regulates cell migration *via* sialylation. *J. Biol. Chem.* **289**, 20694–20705
30. Danen, E. H., Sonneveld, P., Brakebusch, C., Fassler, R., and Sonnenberg, A. (2002) The fibronectin-binding integrins alpha5beta1 and alphavbeta3 differentially modulate RhoA-GTP loading, organization of cell matrix adhesions, and fibronectin fibrillogenesis. *J. Cell Biol.* **159**, 1071–1086
31. Morini, M., Mottolese, M., Ferrari, N., Ghiorzo, F., Buglioni, S., Mortarini, R., Noonan, D. M., Natali, P. G., and Albini, A. (2000) The alpha 3 beta 1 integrin is associated with mammary carcinoma cell metastasis, invasion, and gelatinase B (MMP-9) activity. *Int. J. Cancer* **87**, 336–342
32. Frisch, S. M., Vuori, K., Ruoslahti, E., and Chan-Hui, P. Y. (1996) Control of adhesion-dependent cell survival by focal adhesion kinase. *J. Cell Biol.* **134**, 793–799
33. Mitra, S. K., and Schlaepfer, D. D. (2006) Integrin-regulated FAK-Src signaling in normal and cancer cells. *Curr. Opin. Cell Biol.* **18**, 516–523
34. Christie, D. R., Shaikh, F. M., Lucas IV, J. A., Lucas III, J. A., and Bellis, S. L. (2008) ST6Gal-I expression in ovarian cancer cells promotes an invasive phenotype by altering integrin glycosylation and function. *J. Ovarian Res.* **1**, 3
35. Büll, C., Stoel, M. A., den Brok, M. H., and Adema, G. J. (2014) Sialic acids sweeten a tumor's life. *Cancer Res.* **74**, 3199–3204
36. Fiore, V. F., Ju, L., Chen, Y., Zhu, C., and Barker, T. H. (2014) Dynamic catch of a Thy-1-α5β1+syndecan-4 trimolecular complex. *Nat. Commun.* **5**, 4886
37. Saito, Y., Imazeki, H., Miura, S., Yoshimura, T., Okutsu, H., Harada, Y., Ohwaki, T., Nagao, O., Kamiya, S., Hayashi, R., Kodama, H., Handa, H., Yoshida, T., and Fukai, F. (2007) A peptide derived from tenascin-C induces beta1 integrin activation through syndecan-4. *J. Biol. Chem.* **282**, 34929–34937
38. Schwartz, M. A., and Ginsberg, M. H. (2002) Networks and crosstalk: integrin signalling spreads. *Nat. Cell Biol.* **4**, E65–E68
39. Vial, D., and McKeown-Longo, P. J. (2012) Epidermal growth factor (EGF) regulates α5β1 integrin activation state in human cancer cell lines through the p90RSK-dependent phosphorylation of filamin A. *J. Biol. Chem.* **287**, 40371–40380
40. Byron, A., and Frame, M. C. (2016) Adhesion protein networks reveal functions proximal and distal to cell-matrix contacts. *Curr. Opin. Cell Biol.* **39**, 93–100
41. Luo, B. H., Springer, T. A., and Takagi, J. (2003) Stabilizing the open conformation of the integrin headpiece with a glycan wedge increases affinity for ligand. *Proc. Natl. Acad. Sci. USA* **100**, 2403–2408
42. Takagi, J., and Springer, T. A. (2002) Integrin activation and structural rearrangement. *Immunol. Rev.* **186**, 141–163
43. Nagae, M., Re, S., Mihara, E., Nogi, T., Sugita, Y., and Takagi, J. (2012) Crystal structure of α5β1 integrin ectodomain: atomic details of the fibronectin receptor. *J. Cell Biol.* **197**, 131–140
44. Zhuo, Y., Chammas, R., and Bellis, S. L. (2008) Sialylation of beta1 integrins blocks cell adhesion to galectin-3 and protects cells against galectin-3-induced apoptosis. *J. Biol. Chem.* **283**, 22177–22185
45. Larsen, M., Artym, V. V., Green, J. A., and Yamada, K. M. (2006) The matrix reorganized: extracellular matrix remodeling and integrin signaling. *Curr. Opin. Cell Biol.* **18**, 463–471
46. Hang, Q., Isaji, T., Hou, S., Im, S., Fukuda, T., and Gu, J. (2015) Integrin α5 suppresses the phosphorylation of epidermal growth factor receptor and its cellular signaling of cell proliferation *via* *N*-glycosylation. *J. Biol. Chem.* **290**, 29345–29360
47. Paszek, M. J., DuFort, C. C., Rossier, O., Bainer, R., Mouw, J. K., Godula, K., Hudak, J. E., Lakins, J. N., Wijekoon, A. C., Cassereau, L., Rubashkin, M. G., Magbanua, M. J., Thorn, K. S., Davidson, M. W., Rugo, H. S., Park, J. W., Hammer, D. A., Giannone, G., Bertozzi, C. R., and Weaver, V. M. (2014) The cancer glycocalyx mechanically primes integrin-mediated growth and survival. *Nature* **511**, 319–325
48. Danguy, A., Camby, I., and Kiss, R. (2002) Galectins and cancer. *Biochim. Biophys. Acta* **1572**, 285–293
49. Kariya, Y., Kawamura, C., Tabei, T., and Gu, J. (2010) Bisecting GlcNAc residues on laminin-332 down-regulate galectin-3-dependent keratinocyte motility. *J. Biol. Chem.* **285**, 3330–3340
50. Yoon, S. J., Nakayama, K., Hikita, T., Handa, K., and Hakomori, S. I. (2006) Epidermal growth factor receptor tyrosine kinase is modulated by GM3 interaction with *N*-linked GlcNAc termini of the receptor. *Proc. Natl. Acad. Sci. USA* **103**, 18987–18991
51. Josefsson, E. C., Gebhard, H. H., Stossel, T. P., Hartwig, J. H., and Hoffmeister, K. M. (2005) The macrophage alphaMbeta2 integrin alphaM lectin domain mediates the phagocytosis of chilled platelets. *J. Biol. Chem.* **280**, 18025–18032

Received for publication May 23, 2016.
Accepted for publication August 15, 2016.

RNase activity of sialic acid-binding lectin from bullfrog eggs drives antitumor effect via the activation of p38 MAPK to caspase-3/7 signaling pathway in human breast cancer cells

YUKIKO KARIYA[1], TAKEO TATSUTA[1], SHIGEKI SUGAWARA[1], YOSHINOBU KARIYA[2], KAZUO NITTA[1] and MASAHIRO HOSONO[1]

[1]Division of Cell Recognition Study, Institute of Molecular Biomembrane and Glycobiology, Tohoku Pharmaceutical University, Sendai 981-8558; [2]Department of Biochemistry, Fukushima Medical University School of Medicine, Fukushima City, Fukushima 960-1295, Japan

Received March 18, 2016; Accepted July 20, 2016

DOI: 10.3892/ijo.2016.3656

Abstract. Sialic acid-binding lectin obtained from bullfrog eggs (SBL) induces cell death in cancer cells but not in normal cells. This antitumor effect is mediated through its ribonuclease (RNase) activity. However, the underlying molecular mechanisms remain unclear. We found that the p38 mitogen-activated protein kinase (MAPK) signaling pathway was activated when SBL induced cell death in three human breast cancer cell lines: SK-BR-3, MCF-7, and MDA-MB231. The suppression of p38 MAPK phosphorylation by a p38 MAPK inhibitor as well as short interference RNA knockdown of p38 MAPK expression significantly decreased cell death and increased the cell viability of SBL-treated MDA-MB231 cells. H103A, an SBL mutant lacking in RNase activity, showed decreased SBL-induced cell death compared with native SBL. However, the loss of RNase activity of SBL had no effect on its internalization into cells. The H103A mutant also displayed decreased phosphorylation of p38 MAPK. Moreover, SBL promoted caspase-3/7 activation followed by a cleavage of poly (ADP-ribose)-polymerase, whereas the SBL mutant, H103A, lost this ability. The SBL-induced caspase-3/7 activation was suppressed by the p38 MAPK inhibitor, SB203580, as well as pan-caspase inhibitor, zVAD-fmk. In the presence of zVAD-fmk, the SBL-induced cell death was decreased. In addition, the cell viability of SBL-treated MDA-MB231 cells recovered by zVAD-fmk treatment. Taken together, our results suggest that the RNase activity of SBL leads to breast cancer cell death through the activation of p38 MAPK followed by the activation of caspase-3/7.

Correspondence to: Professor Masahiro Hosono, Division of Cell Recognition Study, Institute of Molecular Biomembrane and Glycobiology, Tohoku Medical and Pharmaceutical University, 4-4-1 Komatsushima, Aoba-ku, Sendai 981-8558, Japan
E-mail: mhosono@tohoku-mpu.ac.jp

Abbreviations: CBB, Coomassie Brilliant Blue; DMSO, dimethyl sulfoxide; Gb3, globotriaosylceramide 3; IPTG, isopropyl 1-thio-β-D-galactoside; mAb, monoclonal antibody; MAPK, mitogen-activated protein kinase; PARP, poly (ADP-ribose)-polymerase; PBS, phosphate-buffered saline; RNase, ribonuclease; SBL, sialic acid-binding lectin; SD, standard deviation; siRNA, short interference RNA

Key words: antitumor, cell death, p38 MAPK, RNase, sialic acid-binding lectin

Introduction

Sialic acid-binding lectin is a lectin from *Rana catesbeiana* oocytes (SBL). SBL preferentially binds to cancer cells rather than normal cells (1) because cancer cells often overexpress sialylated glycans on their surface, which is usually associated with poor prognosis (2). SBL shows an agglutination activity toward cancer cells by binding to the sialylated glycans on the surface of cancer cells (1).

SBL also exhibits a prominent antitumor effect on many types of cancer and tumor cells, such as breast, cervical, oral cancer, glioblastoma, and T-cell leukemia, but not normal cells, such as keratinocytes, fibroblasts, and lymphocytes (3-6). Moreover, the treatment of cancer cells with SBL ultimately leads to cell death (7). In mice with ascites tumor cells, the injection of SBL inhibits tumor growth and prolongs the life span, and sialidase protects cancer cells from SBL toxicity (8). Therefore, this selective antitumor effect of SBL is due to the sialylated glycans on the surface of tumors or cancer cells.

SBL is homologous with various members of the ribonuclease (RNase) A superfamily and is also known as RC-RNase (9,10). The RNase A superfamily exhibits RNA-cleavage activity and has three catalytic amino acid residues. Therefore, SBL also has RNase activity and the conserved catalytic amino acid residues (His^{10}, Lys^{35}, and His^{103}). Huang *et al* demonstrated that the three amino acid residues in the SBL molecule are required for inducing cancer cell death as well as RNase activity using recombinant SBL mutants with these amino acid residues replaced with alanine residues (11).

The internalization of SBL into cancer cells causes the degradation of ribosomal RNA, which leads to the inhibition of protein synthesis and, in turn, induces cell death (8,12,13).

SBL-induced cell death is accompanied by mitochondrial dysfunction (14), endoplasmic reticulum stress (15), autophagocytosis (16), and caspase activation (3,5). Our previous studies showed that mitogen-activated protein kinases (MAPKs) were phosphorylated in two SBL-treated cell lines, human T-cell leukemia Jurkat cells and malignant mesothelioma NCI-H28 cells (14,17). However, it remains unclear whether MAPK activation is related to SBL-induced cell death and how SBL activates MAPKs.

In this study, we found that SBL-induced cell death and activation of p38 MAPK signaling in human breast cancer cell lines. The analyses using p38 MAPK-specific inhibitors and short interference RNA (siRNA) showed that p38 MAPK activation and expression were associated with SBL-induced cell death. Furthermore, RNase activity of SBL was required for the observed SBL-induced cell death. SBL mutant lacking RNase activity indicated that such RNase activity of SBL was important for SBL-induced p38 MAPK activation and subsequent caspase-3/7 activation. Together, these data demonstrate that the RNA degradation by SBL triggers the SBL-induced p38 MAPK activation that leads to cell death mediated by caspase-3/7 activation.

Materials and methods

Antibodies and reagents. Mouse mAbs against p38 MAPK (no. 612168) and phospho-p38 MAPK (no. 612280) were obtained from BD Biosciences. A mouse mAb against β-actin (clone AC-74) was obtained from Sigma. A rabbit polyclonal antibody against PARP was obtained from Roche (no. 11835238001). A rabbit polyclonal SBL antibody was established in our laboratory. Alexa Fluor 488-conjugated goat anti-rabbit IgG (no. A11008) and Alexa Fluor 546-conjugated Phalloidin (no. A22283) were obtained from Invitrogen. Native SBL was isolated by sequential chromatography on Sephadex G-75, DEAE-cellulose, hydroxyapatite, and SP-Sepharose as described previously (1). Two types of p38 MAPK inhibitor (SB203580, no. 559389; and SB239063, no. 559404) and a JNK inhibitor (SP600125, no. 420119) were from Calbiochem. A pan-caspase inhibitor [zVAD-fmk, benzyloxycarbonyl-Val-Ala-Asp(OMe)-fluoromethylketone] was from MBL. Signal Silence p38 MAPK siRNA (no. 6564) and Signal Silence control siRNA (no. 6568) were from Cell Signaling Technology, Inc.

Cell culture. Human breast cancer cell lines, SK-BR-3, MCF-7, and MDA-MB231 were cultured in Dulbecco's modified Eagle's medium supplemented with 10% fetal bovine serum, penicillin, and streptomycin.

Cell viability. Cells were plated to each well of 96-well microtiter plates before treatment with test samples. After the treatment at 37°C for indicated time, WST-8 (Dojindo) was added to each well to detect viable cells. Color development was recorded at 450 nm using the PowerScan HT (DS Pharma Biomedical).

Expression vector encoding an SBL mutant. The full-length cDNA of SBL was prepared from a bullfrog liver. To prepare the expression vector of the SBL mutant lacking RNase activity, we replaced His^{103} of SBL with Ala by a PCR method using the SBL cDNA in pET11d with a *pel B* sequence of the pET22b vector as a template. The cycle protocol for PCR was as follows: one cycle of 94°C for 2 min; 25 cycles of 94°C for 1 min, 51°C for 30 sec, and 68°C for 6 min; and one cycle of 68°C for 4 min. The primer set for H103A was 5'-GTAGCGT TTGCTGGAATAGGACGA-3' and 5'-GGGATATTGATT CTCACATTTTAC-3'. The cDNA sequence was verified by DNA sequencing.

Purification of recombinant SBL. E. coli BL21 (DE) pLysS was transformed with SBL cDNA expression vector and then selected with carbenicillin and chloramphenicol. The transformed cells were grown at 34°C in Terrific Broth medium containing 50 μg/ml carbenicillin and 34 μg/ml chloramphenicol until the A600 reached 0.6 before isopropyl 1-thio-β-D-galactoside (IPTG) induction. After IPTG induction at a final concentration of 0.4 mM for 2 days, the culture supernatant was collected and then concentrated with 80% saturated ammonium sulfate. Pellet containing proteins were dissolved in 20 mM HEPES buffer (pH 7.0) and then dialyzed against the same buffer. The crude sample was loaded onto a DEAE-Sepharose 6B column (GE Healthcare), and the flow-through fraction was collected. The fraction was loaded on a Heparin-Sepharose 6 column (GE Healthcare) and eluted with 10 mM Tris-HCl (pH 7.5) containing 0.1-0.5 M NaCl. The fractions containing H103A were loaded on a hydroxyapatite column after a threefold dilution with 10 mM Tris-HCl (pH 7.5) and then the flow-through fraction was collected. The purified protein was resolved by SDS-PAGE and then stained with CBB. The purified protein concentration was determined by DC protein assay (Bio-Rad Laboratories).

Knockdown of p38 MAPK by siRNA. Double-stranded siRNAs were transfected into MDA-MB231 cells using X-treme GENE siRNA Transfection Reagent (Roche) according to the instruction manual. After transfection for 24 h, the cells were used for the following assays.

Analysis of RNA degradation. For analysis of intracellular RNA degradation, cells ($2x10^4$ cells) were grown in the medium containing SBL. After incubation for 24, 48, or 72 h, total RNA of the cells was extracted with TRIzol reagent (Gibco BRL) according to the instruction manual. A volume of 2 μg RNA was run on a 2% agarose gel containing formaldehyde, and the RNA bands were visualized by ethidium bromide.

Immunoblot analysis. Cells were washed twice with cold phosphate-buffered saline (PBS) and then lysed with lysis buffer (1% Triton X-100, 20 mM Tris-HCl, pH 7.4, 150 mM NaCl, 5 mM EDTA) containing protease and phosphatase inhibitor cocktails (Roche). After incubation for 10 min on ice, the cell lysates were clarified by centrifugation at 20,400 g for 10 min at 4°C. The resultant supernatant was used in the following experiments. The protein concentration was determined using a Protein Quantification Kit-Rapid (Dojindo). For immunoblot analysis, proteins resolved by SDS-PAGE were transferred to nitrocellulose membranes. The blots were blocked with 5% fat-free skim milk in TBS (20 mM Tris-HCl, 150 mM NaCl, pH 7.4) for 1 h. Then

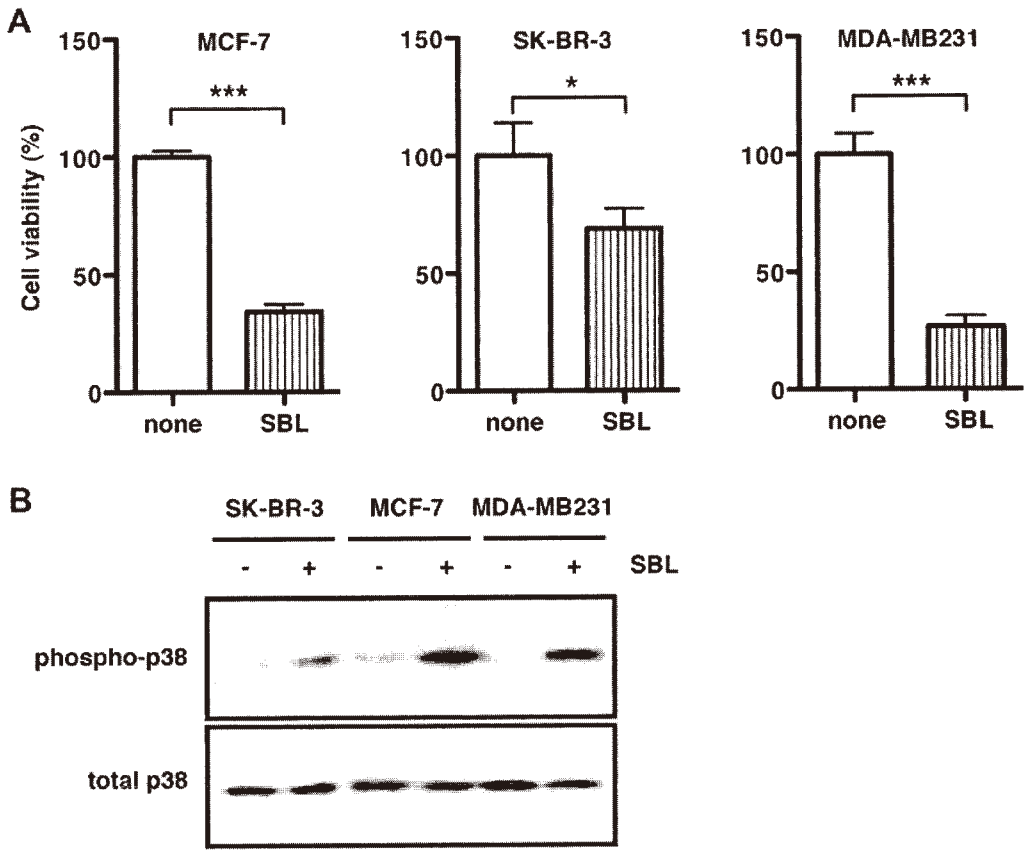

Figure 1. SBL induces cell death and activation of p38 MAPK in human breast cancer cell lines. (A) Cell viability of the indicated human breast cancer cell lines after treatment with 2 μM SBL for 72 h. The relative cell viability of cells with no treatment with SBL (none) was set at 100%. Results are means ± SD from three independent experiments conducted in triplicate for each experiment. *P<0.05. ***P<0.001. (B) Cell lysates after treatment with or without 2 μM SBL for 72 h were subjected to immunoblotting to detect phosphorylated p38 MAPK (upper panel) and total p38 MAPK (lower panel).

the membranes were probed with each specific antibody. Immunoreactive bands were detected using an ECL Western blotting detection reagent (GE Healthcare).

Immunofluorescence analysis. Cells were cultured in growth medium containing test samples. Cells were then fixed with 4% paraformaldehyde in PBS for 10 min and permeabilized with 0.2% Triton X-100 in PBS for 10 min. Cells were blocked with 1.2% BSA in PBS before staining with appropriate primary and secondary antibodies. After labeling with the indicated antibodies, labeled slides were analyzed using a fluorescent microscope, TIRFM (Olympus Corp.).

Caspase-3/7 activity. Caspase-3/7 activity was quantified using SensoLyte® Homogeneous AMC Caspase-3/7 Assay kit (AnaSpec Inc., no. 7118), according to the instruction manual.

Statistical analysis. Results are expressed as means ± SD and are representative of at least two or three independent experiments conducted in triplicate for each experiment. Statistical comparisons between two groups were made using an unpaired Student's t-test and among groups using one-way ANOVA followed by a Tukey's multiple comparison test, with GraphPad Prism Version 5.0 software. A P-value of <0.05 was considered statistically significant.

Results

SBL induces cell death through p38 MAPK activation and expression in human breast cancer cell lines. SBL induces cell death in various types of human cancer cells (7). To examine the antitumor effect of SBL on breast cancer cells, we used one estrogen-positive cell line (MCF-7) and two estrogen-negative cell lines (SK-BR-3 and MDA-MB231) for a cell viability assay. After treatment with SBL for 72 h, the cell viability of MCF-7, SK-BR-3, and MDA-MB231 was significantly reduced to 30.4, 65.3 and 25.5% of control levels (none, 100%), respectively (Fig. 1A). As shown in our previous study using T-cell leukemia Jurkat cells and malignant mesothelioma NCI-H28 cells (14,17), treatment with SBL markedly induced phosphorylation of p38 MAPK in all the three breast cancer cell lines, indicating that SBL activated the p38 MAPK signaling pathway (Fig. 1B).

The p38 MAPK inhibitor SB203580, sufficiently blocked SBL-induced phosphorylation of p38 MAPK (Fig. 2A, SB). In contrast, neither JNK inhibitor, SP600125 (Fig. 2A, SP), nor the pan-caspase inhibitor, VAD (Fig. 2A, VAD), had an effect on p38 MAPK phosphorylation. To investigate whether SBL-induced cell death was mediated by p38 MAPK activation, we tested the inhibitory effect of the p38 MAPK inhibitor SB203580, on SBL-induced cell death using MDA-MB231

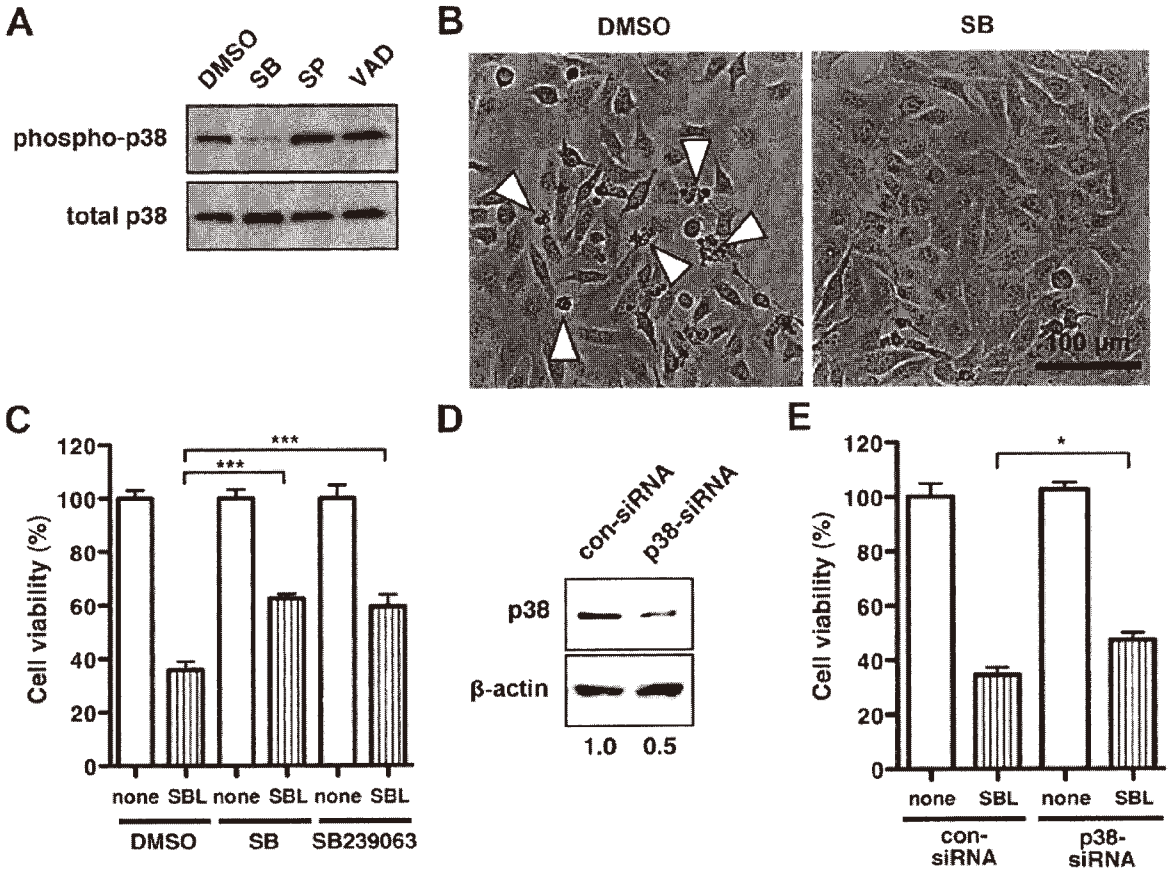

Figure 2. Inhibition of p38 MAPK activation and expression suppresses SBL-induced cell death in MDA-MB231 cells. (A) Immunoblot analysis of phosphorylated p38 MAPK (upper panel) and total p38 MAPK (lower panel) in MDA-MB231 cells treated with 2 μM SBL in the presence of 1% (v/v) solvent (DMSO), 10 μM SB203580 (SB), 10 μM SP600125 (SP), or 100 μM zVAD-fmk (VAD) for 72 h. (B) Cell morphology of MDA-MB231 cells after treatment with 2 μM SBL for 72 h in the presence of DMSO or 10 μM SB. Arrowheads indicate dying or dead cells. (C) Cell viability after treatment with or without SBL for 72 h in the presence of DMSO, 10 μM SB or 10 μM SB239063. The relative cell viability of cells with no treatment with SBL (none) in each sample, was set at 100%. ***P<0.001. (D) Cell lysates treated with control siRNA (con-siRNA) or p38 MAPK-specific siRNA (p38-siRNA) were subjected to immunoblotting to detect endogenous p38 MAPK and β-actin. The numbers at the bottom indicate the ratio of the intensity of p38 MAPK to the intensity of β-actin in each sample, which was 1.0 for con-siRNA-treated cells. (E) The viability of cells treated with con-siRNA or p38-siRNA. The relative cell viability of cells with no treatment with SBL for 48 h (none) in each sample was set at 100%. Results are the means ± SD for three independent experiments conducted in triplicate. *P<0.05.

cells. When treated with SBL, some MDA-MB231 cells shrank and were dying or dead [Fig. 2B, dimethyl sulfoxide (DMSO)]. The SBL-induced cell death was markedly inhibited by the addition of SB203580 (Fig. 2B, SB). The p38 MAPK inhibitors, SB203580 and SB239063 improved the cell viability in SBL-treated cells from 36% (Fig. 2C, DMSO/SBL) to 63% (Fig. 2C, SB/SBL) and 59% (Fig. 2C, SB239063/SBL), respectively.

To further investigate the relationship between SBL-induced cell death and the p38 MAPK signaling pathway, we performed a cell viability assay using a specific siRNA to p38 MAPK (p38-siRNA). The expression of the endogenous p38 MAPK molecule was assessed after 96 h transfection of p38-siRNA or scrambled control siRNA (con-siRNA). When MDA-MB231 cells were treated with p38-siRNA, the expression level of the p38 MAPK molecule was suppressed to a half of that treated with con-siRNA (Fig. 2D). After treating with siRNA for 24 h, cells were further treated with SBL for 48 h. The cell viability in the presence of SBL was partially rescued by the knockdown of p38 MAPK molecule (Fig. 2E). These results suggest that SBL induces cell death of the cancer cells through activation of p38 MAPK.

RNase activity is required for SBL-induced cell death. SBL exhibits RNase activity. When cells were treated with SBL, 28S and 18S ribosomal RNA bands decreased in a time-dependent manner, and some degraded RNA bands were detected via formaldehyde-agarose gel electrophoresis (Fig. 3A). RNase activity has been shown to be necessary for SBL to degrade RNA, as well as to cause cell death of cancer cells (11). However, it remains unclear how the SBL-induced RNA degradation leads to cell death. To clarify the relationship between RNase activity and SBL-induced cell death, we prepared a recombinant SBL mutant that lacks RNase activity by replacing His^{103} (important for its RNase and cell death-induced activities) with Ala (Fig. 3B, H103A). *Escherichia coli* BL21 (DE) pLysS was transformed with H103A cDNA expression vector, and then the recombinant protein was purified from the culture medium of H103A-expressing BL21 (DE) pLysS using several columns.

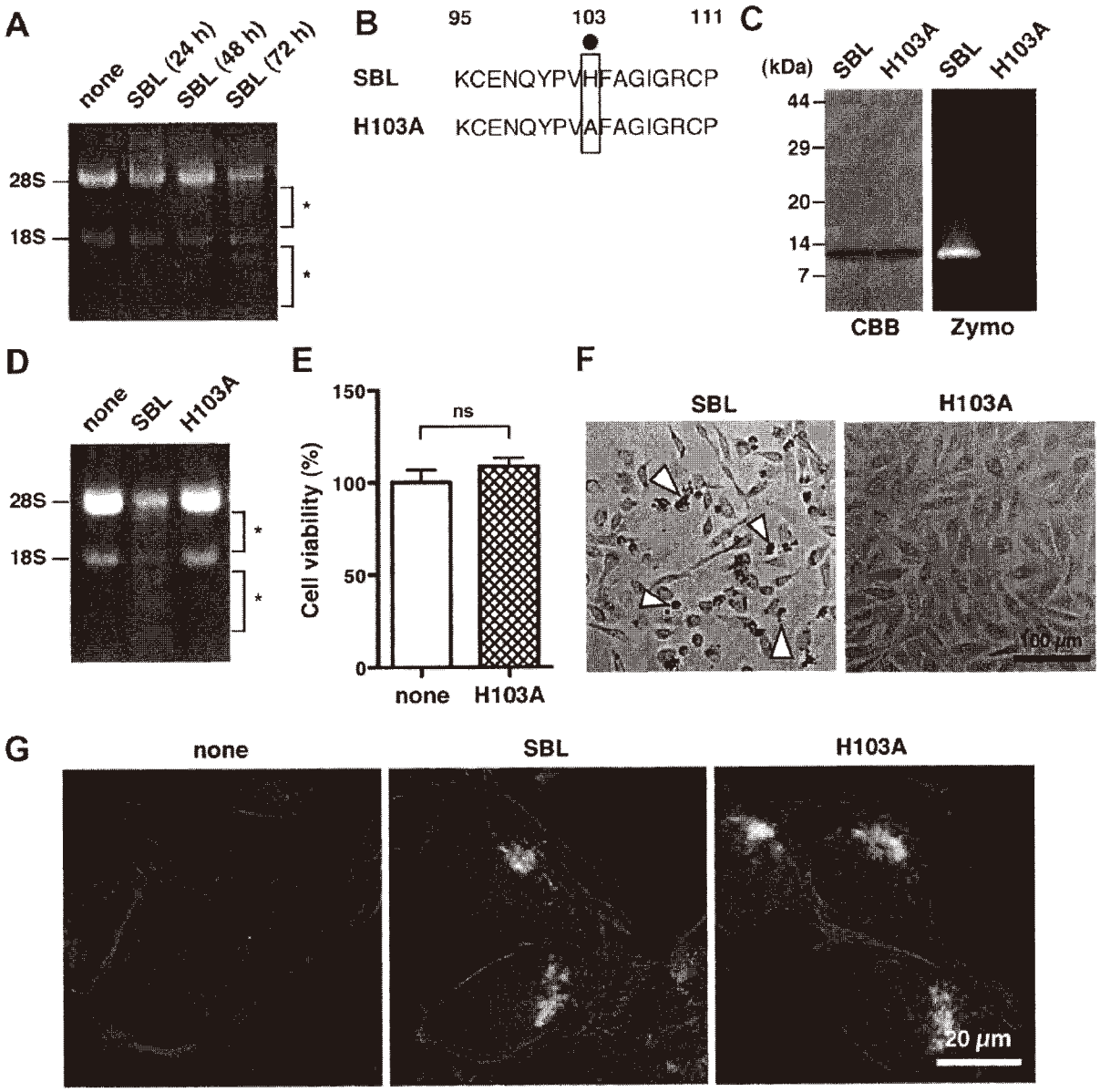

Figure 3. RNase activity of SBL is required for SBL-induced cell death. (A) RNA was extracted from MDA-MB231 cells treated with or without SBL for the indicated times and then analyzed on a formaldehyde-agarose gel. Asterisks indicate degraded RNA. None, no SBL treatment for 72 h. SBL, 2 μM SBL treatment. (B) For preparing an SBL mutant lacking RNase activity (H103A), the histidine residue at position 103 essential for its catalytic activity was replaced with an alanine residue (black dot). Numbers indicate the number of amino acid residues. (C) Purified proteins were run on 15% SDS-PAGE gel under reducing conditions and stained with CBB (left panel). RNase activity of the purified proteins was analyzed by RNA substrate zymography under non-reducing conditions (right panel, Zymo). (D) MDA-MB231 cells were treated with 10 μM SBL or 10 μM H103A for 72 h. None, no SBL treatment for 72 h. Total RNA was analyzed by formaldehyde-agarose gel electrophoresis. Asterisks indicate degraded RNA. (E) Cell viability after treatment with 10 μM H103A for 72 h. The relative cell viability of cells with no treatment with SBL (none) was set at 100%. Results are the means ± SD for three independent experiments conducted in triplicate. ns, not significant. (F) Cell morphology of MDA-MB231 cells after treatment with 2 μM SBL or 10 μM H103A for 72 h. Arrowheads indicate dying or dead cells. (G) MDA-MB231 cells treated with 4 μM SBL (middle), 4 μM H103A (right), or without SBL (left, none) for 6 h were fixed with 4% paraformaldehyde, permeabilized with 1% Triton X-100/PBS, and then stained with anti-SBL antibody (green), phalloidin (red), and Hoechst 33342 (blue).

The quality of the purified H103A protein was assessed by Coomassie Brilliant Blue (CBB) staining, and its molecular mass was estimated to be 13 kDa, which was the same as that of native SBL protein (Fig. 3C, CBB). In a zymographic assay using an RNA-containing gel, native SBL exhibited RNase activity, but H103A did not (Fig. 3C, Zymo). The cellular RNA from the treated cells with native SBL was considerably degraded at 72 h while H103A and no SBL treatment did not induce the cellular RNA degradation (Fig. 3D). Furthermore, H103A had no effect on cell viability (Fig. 3E). In agreement with the result of cell viability, the H103A mutant did not initiate a cell death phenotype as observed with the native SBL (Fig. 3F). These results indicate that RNase activity is closely related to SBL-induced cell death.

The internalization of SBL into cells is required for SBL to degrade cellular RNA (12). To exclude the possibility

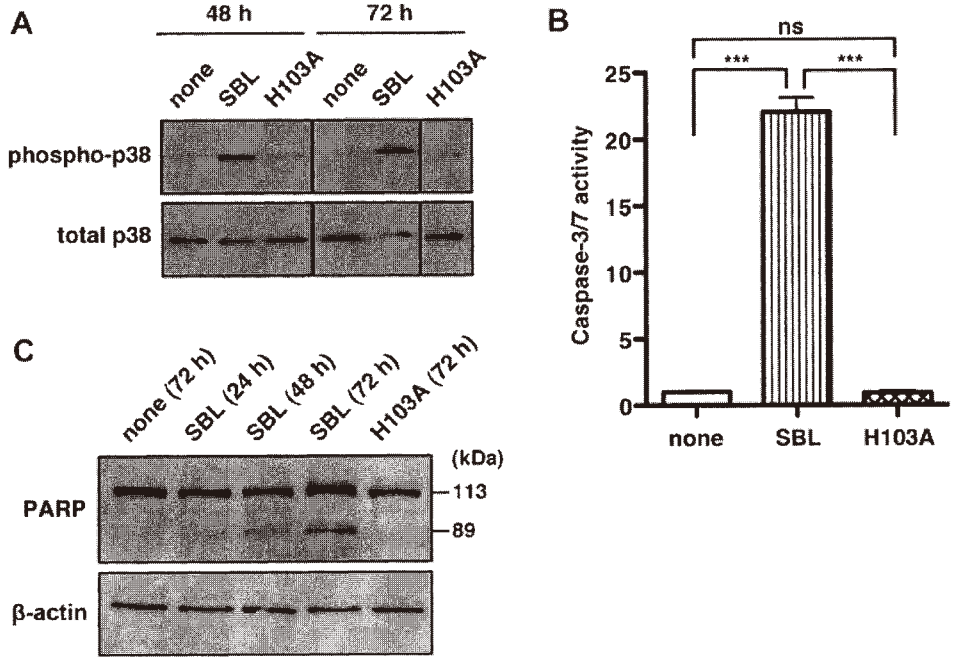

Figure 4. RNase activity of SBL is essential for SBL-induced p38 MAPK and caspase-3/7 activation. (A) Cell lysates of MDA-MB231 treated with 2 μM SBL or 2 μM H103A for the indicated times were subjected to immunoblotting to detect phosphorylated p38 MAPK (upper panel) and total p38 MAPK (lower panel). Thin vertical lines indicate the removal of an intervening lane for presentation purposes. (B) Caspase-3/7 activity in MDA-MB231 cells treated with 2 μM SBL or 10 μM H103A for 72 h was assessed using SensoLyte Homogeneous AMC Caspase-3/7 assay kit. Results are the means ± SD for three independent experiments conducted in triplicate. ***P<0.001. ns, not significant. None, no SBL treatment. (C) Cell lysates of MDA-MB231 cells treated with 2 μM SBL or 10 μM H103A for the indicated times were subjected to immunoblotting to detect PARP and β-actin. The smaller size of PARP, approximately 89 kDa, is a cleaved form of PARP, which is correlated to caspase-3/7 activation.

that H103A is not capable of cellular internalization, the intracellular localization of H103A was observed. H103A and native SBL were localized to the perinuclear region in MDA-MB231 cells at 6 h (Fig. 3G), indicating that H103A is internalized.

As shown in Figs. 1 and 2, p38 MAPK activation was associated with SBL-induced cell death. Therefore, it is likely that the RNase activity of SBL may be of relevance to p38 MAPK activation. We then examined the activation of p38 MAPK after treatment with native SBL and the H103A mutant. Native SBL increased the phosphorylation of p38 MAPK both at 48 and 72 h. In contrast, H103A, as well as the untreated controls, did not promote the phosphorylation of p38 MAPK even at 72 h (Fig. 4A). These results revealed that the RNase activity of SBL is required for SBL-induced p38 MAPK activation.

RNA degradation by SBL leads to activation of caspase-3/7. Although SBL has been reported to activate caspase-3/7 (3,5,18), known as the major executioner caspases, the molecular mechanism remains unclear. Indeed, the caspase-3/7 activity in SBL-treated MDA-MB231 cells was 22-fold higher than that in the untreated cells (Fig. 4B, none vs. SBL). This upregulated caspase-3/7 activity by SBL was completely ablated in the H103A mutant (Fig. 4B, H103A).

Active caspase-3/7 cleaves a full-length poly (ADP-ribose)-polymerase (PARP; 113 kDa) into two fragments: a) 89 kDa and b) 24 kDa. Therefore, we also examined SBL-induced caspase-3/7 activation by checking the fragments of PARP. The immunoblot analysis using an anti-PARP antibody showed that SBL treatment caused an increase in the 89-kDa PARP fragment in a time-dependent manner, whereas only a 113-kDa PARP band was detected when H103A was treated for 72 h (Fig. 4C). These results indicate that RNase activity of SBL is required for SBL-induced caspase-3/7 activation.

Activation of p38 MAPK signaling induced by SBL leads to activation of caspase-3/7. Since RNA degradation by SBL remarkably induced p38 MAPK and caspase-3/7 activation, we speculated that SBL-induced p38 MAPK activation might be related to caspase-3/7 activation. To test this hypothesis, we examined caspase-3/7 activity after treatment with SBL in the presence of a p38 MAPK inhibitor. Caspase-3/7 activity after co-treatment of the p38 MAPK inhibitor, SB203580, with SBL was suppressed by 41.8% compared with that after co-treatment with the solvent, DMSO and SBL (Fig. 5A, SB). These results indicate that the activation of p38 MAPK by SBL leads to caspase-3/7 activation.

A pan-caspase inhibitor, zVAD-fmk, completely inhibited the caspase-3/7 activation induced by SBL (Fig. 5A, VAD). Furthermore, zVAD-fmk treatment inhibited the cleavage of PARP increased by SBL (Fig. 5B). Using zVAD-fmk, we then studied how active caspase-3/7 contributes to SBL-induced cell death. In the presence of zVAD-fmk, SBL-induced cell death decreased (Fig. 5C). In addition, zVAD-fmk increased the cell viability of SBL-treated MDA-MB231 cells compared with the control (Fig. 5D). These results suggest that SBL induces cell death of cancer cells through p38 MAPK-mediated activation of caspase-3/7.

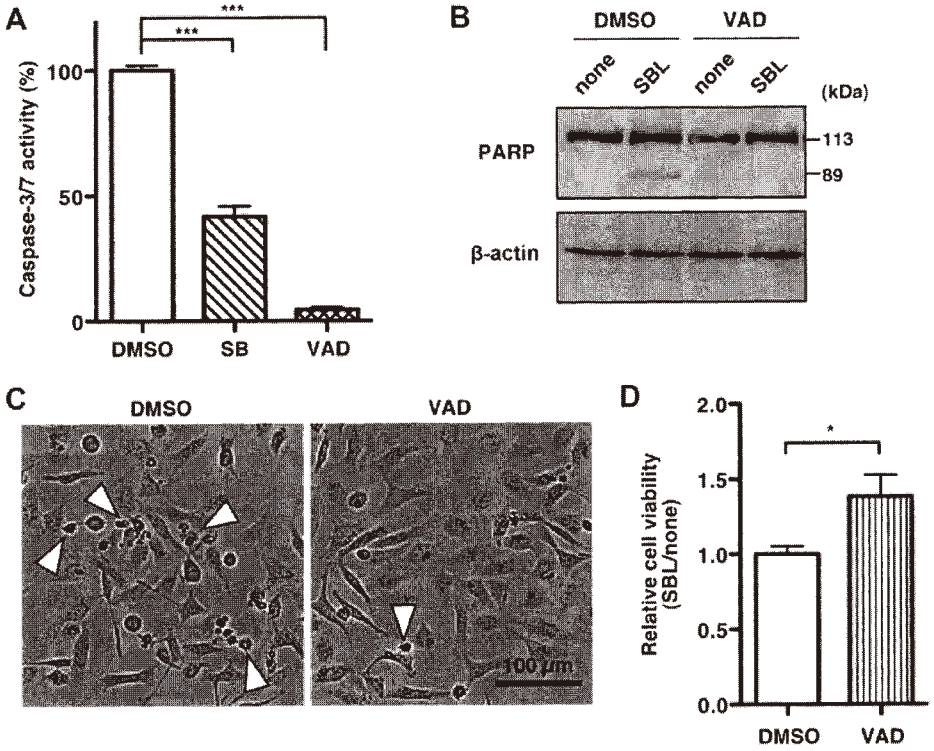

Figure 5. SBL induces caspase-3/7 activation. (A) Caspase-3/7 activity in MDA-MB231 cells treated with or without 2 μM SBL in the presence of solvent DMSO, 10 μM p38 MAPK inhibitor SB203580 (SB) or 100 μM pan-caspase inhibitor zVAD-fmk (VAD) was assessed using SensoLyte Homogeneous AMC Caspase-3/7 assay kit. Each bar indicates the ratio of caspase-3/7 activity of the cells with SBL treatment to without SBL treatment. Results are means ± SD for two independent experiments conducted in triplicate. ***P<0.001. (B) Cell lysates of MDA-MB231 cells treated with or without 2 μM SBL in the presence of DMSO or 100 μM zVAD-fmk (VAD) for 72 h were subjected to immunoblotting to detect PARP and β-actin. The smaller size of PARP, approximately 89 kDa, is a cleaved form of PARP, which is correlated to caspase-3/7 activation. (C) Cell morphology of MDA-MB231 cells after treatment with SBL for 72 h in the presence of solvent DMSO or 100 μM zVAD-fmk (VAD). Arrowheads indicate dying or dead cells. (D) MDA-MB231 cells were treated with or without 2 μM SBL in the presence of DMSO or 100 μM zVAD-fmk (VAD) for 72 h. Each bar indicates the ratio of cell viability with or without SBL treatment. *P<0.05.

Discussion

Our previous study showed that SBL induced MAPK phosphorylation. However, it remains unclear whether the MAPK activation is related to SBL-induced cell death and RNase activity of SBL. In this study, we demonstrate that SBL induces the phosphorylation of p38 MAPK, due to RNA degradation by the RNase activity of SBL. We also find that SBL-induced p38 MAPK activation leads to caspase-3/7 activation and subsequent cell death.

In this study, the p38 MAPK inhibitor, SB inhibited caspase-3/7 activity (Fig. 5A) but caspase-3/7 inhibitor, VAD did not show any inhibitory effect on p38 MAPK phosphorylation (Fig. 2A). This suggests that p38 MAPK is an upstream regulator of caspase-3/7. However, SB did not completely inhibit caspase-3/7 activity (Fig. 5A). These results indicate that caspase-3/7 may be also activated by a signaling pathway other than p38 MAPK. Iordanov *et al* showed that both JNK and p38 MAPK are activated by onconase, which is an RNase isolated from *Rana pipiens* oocytes, and that JNK is related to the cleavage of PARP and onconase-induced cell death (19). Since SBL also activates JNK (14,17), JNK activation may also contribute to capase-3/7 activation resulting in SBL-induced cell death.

Although the p38 MAPK inhibitor, SB significantly inhibited SBL-induced cell death (Fig. 2C), approximately two-fifths of SB-treated cells still induced SBL-dependent cell death. Given that H103A efficiently abrogated SBL-induced cell death (Fig. 3E), there could also be p38 MAPK-independent signaling pathways for SBL-induced cell death. Inhibition of protein synthesis is most likely related to this pathway because RNA damage leads to an inhibition of protein synthesis in addition to p38 MAPK activation, and inhibition of protein synthesis was observed in SBL-treated cells (8).

SBL-induced cell death and p38 MAPK phosphorylation in SK-BR-3 cells were much weaker than those of MCF-7 and MDA-MB231 cells. SBL requires at least three steps to induce cell death: binding to cell surface via sialic acid, entering into cells, followed by the activation of cell death-related signaling. From the immunoblot analysis of cell lysate of SBL-treated cells, the amount of SBL entered into the cells was lower in SK-BR-3 cells than in MDA-MB231 and MCF-7 cells, suggesting that SBL inefficiently enters into SK-BR-3 cells compared to MDA-MB231 and MCF-7 cells (data not shown). Therefore, the weak reactivity against the SBL-induced cell death and p38 MAPK phosphorylation in SK-BR-3 cells might be due to the problem in the low binding of SBL to cell surface of SK-BR-3 cells. Further studies such as sialylation state and unidentified receptors in the cells are required to address the question.

Shiga toxin, also known as verotoxin 1, acts as a protein synthesis inhibitor within target cells. Shiga toxin cleaves a

specific adenine from 28S rRNA by its RNA *N*-glycosidase activity, thereby inhibiting protein synthesis (20,21). Moreover, Shiga toxin activates p38 MAPK or JNK (22,23). The ability of Shiga toxin to activate p38 MAPK and JNK was lost by heat denaturation or substituted mutation in the active site, indicating that the p38 MAPK and JNK activation by Shiga toxin depend on its RNA *N*-glycosidase activity (22). Since an inhibitor of the p38 MAPK was demonstrated to block the cytotoxicity of Shiga toxin (23), Shiga toxin induces cell death via the p38 MAPK signaling pathway. Thus, the molecular mechanisms of Shiga toxin-induced cell death are mediated in large part by the ribotoxic stress response and are very similar to that of SBL-induced cell death presented in this study. The B subunit of Shiga toxin binds to globotriaosylceramide 3 (Gb3) on the host cells, followed by the RNA *N*-glycosidase activity containing A subunit internalizing into cells. Although the mechanism of the internalization of SBL into cells is still unknown, sialoglycoproteins may work as a receptor for SBL-internalization, like Gb3 for the B subunit of Shiga toxin.

Onconase strongly induces cell death depending on its RNase activity (24,25) by leading to the suppression of cell cycle progression, followed by apoptosis (26). Onconase has also been shown to have effective anticancer activity in animal models (27). Moreover, onconase has been studied in advanced phase IIIb clinical trials against malignant mesothelioma (28). Similar to onconase, SBL also shows high toxicity against some cancer cells and has antitumor effects in mouse models (3,8). Moreover, SBL does not kill primary or normal cells because SBL recognizes and selectively binds to sialoglycoproteins on tumor and cancer cells (1,7,18). Therefore, SBL may work as a potential antitumor drug as well as onconase.

In conclusion, our findings demonstrate an important role for RNase activity-dependent p38 MAPK activation and the subsequent caspase-3/7 activation in SBL-induced cancer cell death. Further studies regarding the molecular mechanism of SBL-induced cancer cell death may be helpful to the development of anticancer therapies in the future.

Acknowledgements

We appreciate Ms. Yuki Miura and Dr Kohta Takahashi (Tohoku Pharmaceutical University, Sendai) for their assistance. We also appreciate Dr Takashi Sugino (Shizuoka Cancer Center, Shizuoka) for his kind gift of breast cancer cell lines. This study was supported by the grant-in-aid for the 'Academic Frontier' Project (2006-2011) for Private Universities from the Ministry of Education, Culture, Sports, Science and Technology of Japan; and a Grant-in-Aid for Young Scientists (B) [grant no. 20790073 (to Yukiko Kariya)].

References

1. Nitta K, Takayanagi G, Kawauchi H and Hakomori S: Isolation and characterization of *Rana catesbeiana* lectin and demonstration of the lectin-binding glycoprotein of rodent and human tumor cell membranes. Cancer Res 47: 4877-4883, 1987.
2. Dall'Olio F and Chiricolo M: Sialyltransferases in cancer. Glycoconj J 18: 841-850, 2001.
3. Hu CC, Tang CH and Wang JJ: Caspase activation in response to cytotoxic *Rana catesbeiana* ribonuclease in MCF-7 cells. FEBS Lett 503: 65-68, 2001.
4. Liao YD, Huang HC, Chan HJ and Kuo SJ: Large-scale preparation of a ribonuclease from *Rana catesbeiana* (bullfrog) oocytes and characterization of its specific cytotoxic activity against tumor cells. Protein Expr Purif 7: 194-202, 1996.
5. Chen JN, Yiang GT, Lin YF, Chou PL, Wu TK, Chang WJ, Chen C and Yu YL: *Rana catesbeiana* ribonuclease induces cell apoptosis via the caspase-9/-3 signaling pathway in human glioblastoma DBTRG, GBM8901 and GBM8401 cell lines. Oncol Lett 9: 2471-2476, 2015.
6. Ogawa Y, Sugawara S, Tatsuta T, Hosono M, Nitta K, Fujii Y, Kobayashi H, Fujimura T, Taka H, Koide Y, *et al*: Sialylglycoconjugates in cholesterol-rich microdomains of P388 cells are the triggers for apoptosis induced by *Rana catesbeiana* oocyte ribonuclease. Glycoconj J 31: 171-184, 2014.
7. Tatsuta T, Sugawara S, Takahashi K, Ogawa Y, Hosono M and Nitta K: Cancer-selective induction of apoptosis by leczyme. Front Oncol 4: 139, 2014.
8. Nitta K, Ozaki K, Ishikawa M, Furusawa S, Hosono M, Kawauchi H, Sasaki K, Takayanagi Y, Tsuiki S and Hakomori S: Inhibition of cell proliferation by *Rana catesbeiana* and *Rana japonica* lectins belonging to the ribonuclease superfamily. Cancer Res 54: 920-927, 1994.
9. Liao YD: A pyrimidine-guanine sequence-specific ribonuclease from *Rana catesbeiana* (bullfrog) oocytes. Nucleic Acids Res 20: 1371-1377, 1992.
10. Titani K, Takio K, Kuwada M, Nitta K, Sakakibara F, Kawauchi H, Takayanagi G and Hakomori S: Amino acid sequence of sialic acid binding lectin from frog (*Rana catesbeiana*) eggs. Biochemistry 26: 2189-2194, 1987.
11. Huang HC, Wang SC, Leu YJ, Lu SC and Liao YD: The *Rana catesbeiana* rcr gene encoding a cytotoxic ribonuclease. Tissue distribution, cloning, purification, cytotoxicity, and active residues for RNase activity. J Biol Chem 273: 6395-6401, 1998.
12. Nitta K, Ozaki K, Tsukamoto Y, Furusawa S, Ohkubo Y, Takimoto H, Murata R, Hosono M, Hikichi N, Sasaki K, *et al*: Characterization of a *Rana catesbeiana* lectin-resistant mutant of leukemia P388 cells. Cancer Res 54: 928-934, 1994.
13. Nitta K, Ozaki K, Tsukamoto Y, Hosono M, Ogawakonno Y, Kawauchi H, Takayanagi Y, Tsuiki S and Hakomori S: Catalytic lectin (leczyme) from bullfrog (*Rana catesbeiana*) eggs. Int J Oncol 9: 19-23, 1996.
14. Tatsuta T, Hosono M, Sugawara S, Kariya Y, Ogawa Y, Hakomori S and Nitta K: Sialic acid-binding lectin (leczyme) induces caspase-dependent apoptosis-mediated mitochondrial perturbation in Jurkat cells. Int J Oncol 43: 1402-1412, 2013.
15. Tatsuta T, Hosono M, Miura Y, Sugawara S, Kariya Y, Hakomori S and Nitta K: Involvement of ER stress in apoptosis induced by sialic acid-binding lectin (leczyme) from bullfrog eggs. Int J Oncol 43: 1799-1808, 2013.
16. Yiang GT, Yu YL, Chou PL, Tsai HF, Chen LA, Chen YH, Su KJ, Wang JJ, Bau DT and Wei CW: The cytotoxic protein can induce autophagocytosis in addition to apoptosis in MCF-7 human breast cancer cells. In Vivo 26: 403-409, 2012.
17. Tatsuta T, Hosono M, Takahashi K, Omoto T, Kariya Y, Sugawara S, Hakomori S and Nitta K: Sialic acid-binding lectin (leczyme) induces apoptosis to malignant mesothelioma and exerts synergistic antitumor effects with TRAIL. Int J Oncol 44: 377-384, 2014.
18. Tang CH, Hu CC, Wei CW and Wang JJ: Synergism of *Rana catesbeiana* ribonuclease and IFN-gamma triggers distinct death machineries in different human cancer cells. FEBS Lett 579: 265-270, 2005.
19. Iordanov MS, Wong J, Newton DL, Rybak SM, Bright RK, Flavell RA, Davis RJ and Magun BE: Differential requirement for the stress-activated protein kinase/c-Jun NH(2)-terminal kinase in RNAdamage-induced apoptosis in primary and in immortalized fibroblasts. Mol Cell Biol Res Commun 4: 122-128, 2000.
20. Endo Y, Tsurugi K, Yutsudo T, Takeda Y, Ogasawara T and Igarashi K: Site of action of a Vero toxin (VT2) from *Escherichia coli* O157:H7 and of Shiga toxin on eukaryotic ribosomes. RNA *N*-glycosidase activity of the toxins. Eur J Biochem 171: 45-50, 1988.
21. Saxena SK, O'Brien AD and Ackerman EJ: Shiga toxin, Shiga-like toxin II variant, and ricin are all single-site RNA *N*-glycosidases of 28 S RNA when microinjected into *Xenopus* oocytes. J Biol Chem 264: 596-601, 1989.
22. Smith WE, Kane AV, Campbell ST, Acheson DW, Cochran BH and Thorpe CM: Shiga toxin 1 triggers a ribotoxic stress response leading to p38 and JNK activation and induction of apoptosis in intestinal epithelial cells. Infect Immun 71: 1497-1504, 2003.

23. Ikeda M, Gunji Y, Yamasaki S and Takeda Y: Shiga toxin activates p38 MAP kinase through cellular Ca(2+) increase in Vero cells. FEBS Lett 485: 94-98, 2000.
24. Wu Y, Mikulski SM, Ardelt W, Rybak SM and Youle RJ: A cytotoxic ribonuclease. Study of the mechanism of onconase cytotoxicity. J Biol Chem 268: 10686-10693, 1993.
25. Lee JE and Raines RT: Contribution of active-site residues to the function of onconase, a ribonuclease with antitumoral activity. Biochemistry 42: 11443-11450, 2003.
26. Juan G, Ardelt B, Li X, Mikulski SM, Shogen K, Ardelt W, Mittelman A and Darzynkiewicz Z: G1 arrest of U937 cells by onconase is associated with suppression of cyclin D3 expression, induction of p16INK4A, p21WAF1/CIP1 and p27KIP and decreased pRb phosphorylation. Leukemia 12: 1241-1248, 1998.
27. Rybak SM, Pearson JW, Fogler WE, Volker K, Spence SE, Newton DL, Mikulski SM, Ardelt W, Riggs CW, Kung HF, *et al*: Enhancement of vincristine cytotoxicity in drug-resistant cells by simultaneous treatment with onconase, an antitumor ribonuclease. J Natl Cancer Inst 88: 747-753, 1996.
28. Pavlakis N and Vogelzang NJ: Ranpirnase - an antitumour ribonuclease: Its potential role in malignant mesothelioma. Expert Opin Biol Ther 6: 391-399, 2006.

Cancer Science
Japanese Cancer Association JCA
Open Access

Increased sialidase activity in serum of cancer patients: Identification of sialidase and inhibitor activities in human serum

Keiko Hata,[1] Tatsuo Tochigi,[2] Ikuro Sato,[3] Sadafumi Kawamura,[2] Kazuhiro Shiozaki,[4] Tadashi Wada,[1] Kohta Takahashi,[1,5] Setsuko Moriya,[1] Kazunori Yamaguchi,[6] Masahiro Hosono[5] and Taeko Miyagi[1]

[1]Division of Cancer Glycosylation Research, Institute of Molecular Biomembrane and Glycobiology, Tohoku Pharmaceutical University, Sendai; [2]Department of Urology, Miyagi Cancer Center, Natori; [3]Division of Pathology, Miyagi Cancer Center Research Institute, Natori; [4]Faculty of Fisheries and The United Graduate School of Agricultural Science, Kagoshima University, Kagoshima; [5]Division of Cell Recognition Study, Institute of Molecular Biomembrane and Glycobiology, Tohoku Pharmaceutical University, Sendai; [6]Division of Molecular and Cellular Oncology, Miyagi Cancer Center Research Institute, Natori, Japan

Key words

Cancer serum, diagnostic marker, ganglioside, prostate cancer, sialidase

Correspondence

Taeko Miyagi, Division of Cancer Glycosylation Research, Institute of Molecular Biomembrane and Glycobiology, Tohoku Pharmaceutical University, 4-4-1 Komatsushima, Aoba-ku, Sendai 981-8558, Japan.
Tel: +81-22-727-0157; Fax: +81-22-275-2013;
E-mail: tmiyagi@tohoku-pharm.ac.jp

Funding Information

This research supported in part by Grants-in-Aid for Scientific Research on FS A-Step (241FT0338) and by CREST of Japan Science and Technology Agency.

Received December 9, 2014; Revised January 22, 2015; Accepted January 31, 2015

Cancer Sci **106** (2015) 383–389

doi: 10.1111/cas.12627

Aberrant sialylation in glycoproteins and glycolipids is a characteristic feature of malignancy. Human sialidases, which catalyze the removal of sialic acid residues from glycoconjugates, have been implicated in cancer progression. They have been detected in a wide variety of human cells and tissues, but few studies have focused on their existence in human serum. Among the four types identified to date, we previously demonstrated that plasma membrane-associated ganglioside sialidase (NEU3) is markedly upregulated in various human cancers, including examples in the colon and prostate. Here, using a sensitive assay method, we found a significant increase of sialidase activity in the serum of patients with prostate cancer compared with that in healthy subjects having low activity, if any. Activity was apparent with gangliosides as substrates, but only to a very limited extent with 4-methylumbelliferyl sialic acid, a good synthetic substrate for sialidases other than human NEU3. The serum sialidase was also almost entirely immunoprecipitated with anti-NEU3 antibody, but not with antibodies for other sialidases. Interestingly, sera additionally contained inhibitory activity against the sialidase and also against recombinant human NEU3. The sialidase and inhibitor activities could be separated by exosome isolation and by hydrophobic column chromatography. The serum sialidase was assessed by a sandwich ELISA method using two anti-NEU3 antibodies. The results provide strong evidence that the serum sialidase is, in fact, NEU3, and this subtype may, therefore, be a potential utility for novel diagnosis of human cancers.

Alterations in glycosylation occur during tumorigenesis, and aberrant sialylation in particular has been implicated in the malignant phenotype with reference to metastatic potential and invasiveness.[1,2] Mammalian sialidases are the key enzymes controlling cellular sialic acid contents, through catalyzing the initial step of degradation of glycoproteins and glycolipids by removing sialic acid residues from their carbohydrate portions. Four types of human sialidases have been identified to date, designated as NEU1, NEU2, NEU3 and NEU4, and characterized as differing in major subcellular localization and enzymatic properties, including substrate specificity, as well as in chromosomal sites.[3] They appear to behave in different independent manners during carcinogenesis.[4] NEU1, NEU3 and NEU4 have been detected in various cells and tissues as major human sialidases,[5,6] but no details on serum sialidase have been reported, except for the activity toward 4-methylumbelliferyl sialic acid (4MU-NeuAc) as a substrate, found to be associated with immunoglobulin IgG in the serum of multiple myeloma patients.[7]

Among the four human sialidases, the plasma membrane-associated sialidase, NEU3, is unique in substrate preference for gangliosides, co-existing at the cell surface, therefore being suggested to participate in transmembrane signaling.[8] NEU3 is markedly upregulated in various human cancers, including colon,[9] renal,[10] ovarian[11] and prostate[12], and contributes to augmentation of malignant properties of cancer cells, probably by causing disturbance of transmembrane signaling. In contrast, NEU1[13] and NEU4[14] may be downregulated in colon cancer. In the present study, we found ganglioside sialidase activity detectable in the serum of prostate cancer patients applying a sensitive method with fluorometric high-performance liquid chromatography (HPLC) using malononitrile,[15] with significant elevation as compared to normal subjects. We obtained evidence of NEU3 identity for the sialidase, and additionally, demonstrated the presence of inhibitory activity for the sialidase. Although the functional significance and the mechanisms of appearance in serum remain to be elucidated, this is the first report describing the existence of serum siali-

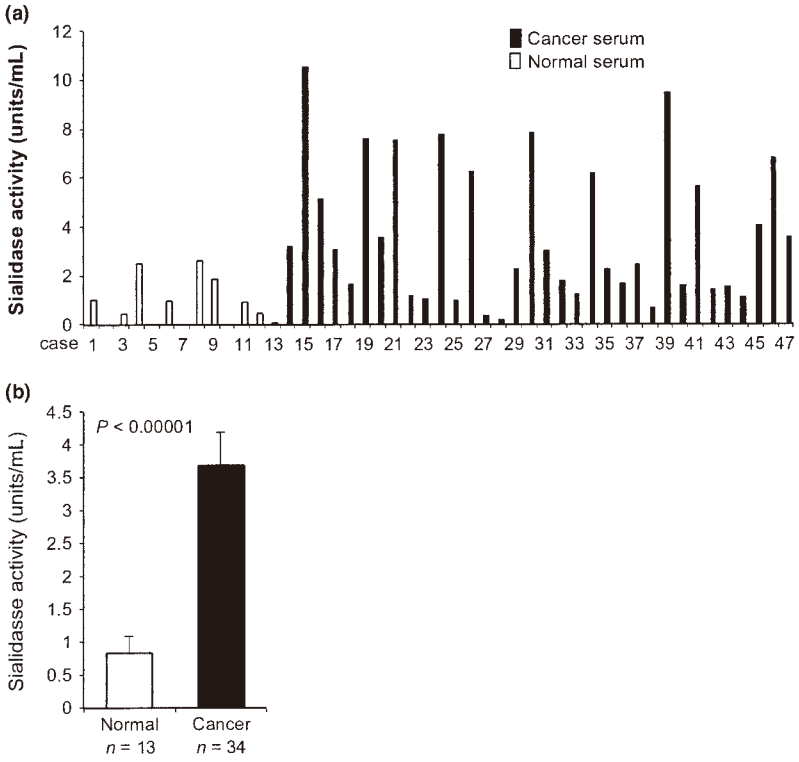

Fig. 1. Determination of ganglioside sialidase activity in human serum and increase in the serum of prostate cancer patients. (a) Note significantly higher levels of sialidase activity toward the ganglioside GM3 substrate in serum of prostate cancer patients than in normal subjects. (b) Statistical significance of increased sialidase activity in the serum of prostate cancer patients compared with normal subjects.

dase of human origin and increase in cancer patients, providing a pointer to a new diagnostic tool.

Materials and Methods

Serum samples. Human sera were obtained from 3 female and 10 male healthy adults, and from 34 patients diagnosed with prostate cancer at various clinical stages in the Urology Department of Miyagi Cancer Center. Non-hemolytic blood samples, drawn from the cubital vein, were allowed to coagulate at room temperature for 30 min and were subsequently centrifuged at 2000 *g* for 10 min. Supernatants were carefully collected to avoid contamination by blood cells. Informed consent was obtained from each subject to allow use of the blood for research purposes, and the study was approved by the Committee on Human Rights in Research at Miyagi Cancer Center.

Sialidase activity assays. Human sera were used for sialidase assays using gangliosides GM3 (NeuAc α2-3Galβ1-4Glcβ1-1Cer) (Alexis Biochemicals, Lansen, Switzerland) or 4MU-NeuAc as the routine substrates in 25 μL of reaction mixture. Activities for NEU1, NEU2 and NEU4 were measured with mixtures containing 2.5 μmol sodium acetate buffer (pH 4.6 for NEU1 and NEU4; pH 5.5 for NEU2), 10 μg bovine serum albumin (BSA) and 20 nmol 4MU-NeuAc. After incubation for 30 to 60 min at 37°C, the 4-methylumbelliferone released was determined fluorometrically.[15] The reaction mixture for assays of NEU3 activity contained 2.5 μmol sodium acetate buffer (pH 4.5), 10 μg BSA, 5 nmol GM3 and 25 μg Triton X-100. The sialic acids released from GM3 were measured by fluorometric HPLC with malononitrile.[15] On occasion, NEU4 activity was also assayed with GM3 as the substrate in the same manner, because of its potential hydrolytic ability toward GM3 as well as 4MU-NeuAc. Protein concentrations were determined by dye-binding assay (Bio-Rad Laboratories, Hercules, CA, USA). One unit was defined as the amount of enzyme cleaving 1 nmol of sialic acid/h.

Preparation of recombinant sialidases. HK-293 T cells (2~5 × 10^7) were transfected with FLAG-tagged sialidase cDNA using Effectene reagent (QIAGEN). At 48 h after transfection, the cells were collected, washed with PBS, and sonicated on ice in 9 volume of ice-cold lysis buffer. The lysates were centrifuged at 1000 *g* for 10 min at 4°C and the resultant supernatants (homogenates) were then used for measurement of sialidase activity. For the NEU1 enzyme, a cDNA for a protective protein (carboxypeptidase A), which is known to be associated with NEU1 protein and β-galactosidase as a complex in the lysosomes to maintain the sialidase activity,[16] was co-transfected. The lysis buffer for NEU1 and NEU2 contained 20 mM potassium phosphate pH 6.8, 0.15 M NaCl, 1 mM phenymethylsulfonyl fluoride (PMSF), and Protease Inhibitor Cocktail (Roche, Basel, Switzerland), while that for NEU3 and NEU4 contained 1 mM EDTA and 1% Triton X-100. The detailed procedures were as described previously.[5]

Preparation of antibodies. Anti-human NEU1 antibody was prepared by immunizing rabbits with keyhole limpet hemocyanin-conjugated oligopeptides corresponding to amino acid residues 201–216 and 392–410 of human NEU1. Anti-rat NEU2 polyclonal antibody (cross-reactive with human recombinant NEU2) was obtained as described earlier.[17] Anti-human NEU3 monoclonal antibody was prepared as detailed previously.[18] Preparation of anti-human NEU4 antibody was accomplished by immunizing rabbits with keyhole limpet hemocyanin-coupled oligopeptides (amino acid residues 347–363) of human NEU4. Immunoprecipitation studies with serum sialidase were performed using the respective sialidase antibodies. Serum (2.5–5.0 μL) or recombinant sialidase protein (0.9–1.2 units) was immunoprecipitated with anti-sialidase antibody at 4°C for 4 h, and then with protein A Sepharose beads (GE Healthcare Life Sciences, Little Chalfont,UK) for

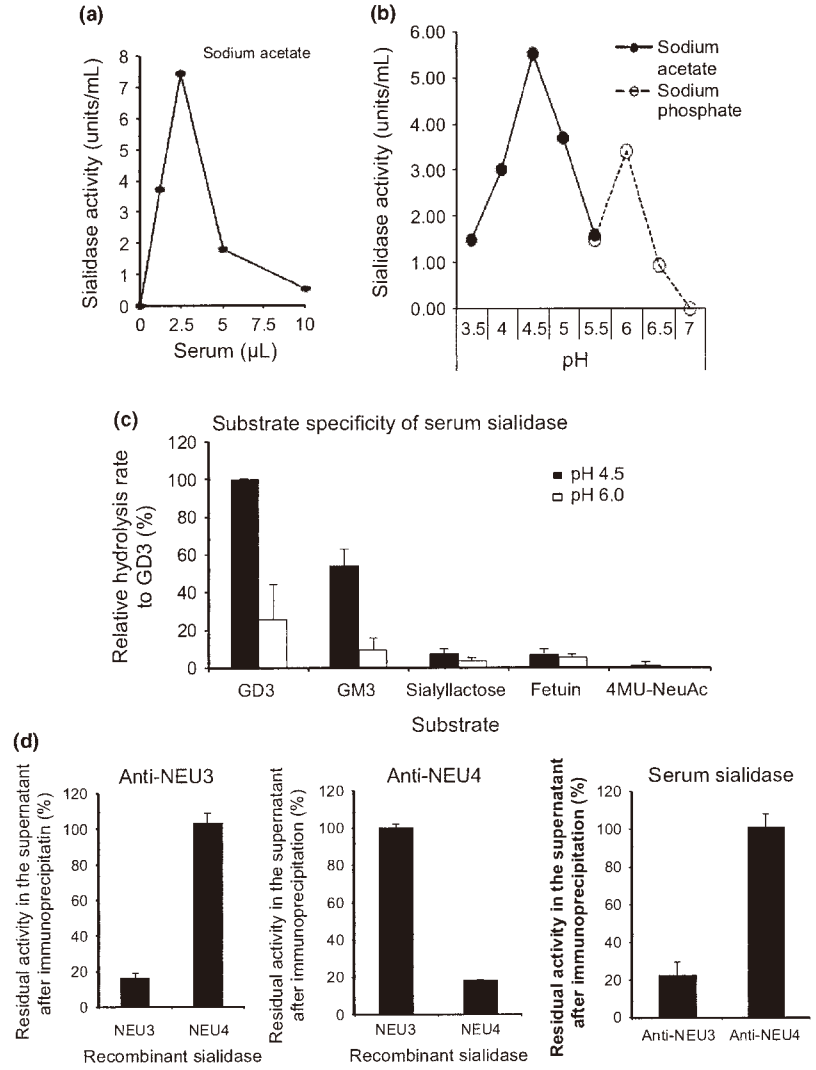

Fig. 2. Characterization of a ganglioside sialidase activity in human serum. (a) Sialidase activity toward GM3 gangliosides with various serum amounts. Note that with 5 μL of serum decreased sialidase activity was observed. (b) Effect of pH on the sialidase activity. Sialidase activitity was assayed using GM3 substrate in sodium acetate buffer at pH 3.5–5.5 and sodium phosphate buffer at pH 5.5–7.0. (c) Substrate specificity of the serum sialidase. Various natural substrates and a synthetic substrate, 4MU-NeuAc, were examined. (d) Immunoprecipitation studies of the serum sialidase using anti-NEU3 and NEU4 antibodies. Anti-NEU3 and anti-NEU4 antibodies precipitated recombinant NEU3 (left panel) and NEU4 (middle), respectively. The serum sialidase was precipitated only with anti-NEU3 antibody (right panel).

2 h. The immunocomplexes were then centrifuged and the resulting supernatant was assayed for sialidase activity.

Inhibitor activity determination. Serum was fractionated with ammonium sulfate, and the fraction precipitating between 50 and 80% of saturation was collected by centrifugation, and dialyzed. Serum (5.0 μL) or the dialyzed fraction of the ammonium precipitates was routinely used as the inhibitor source. Alternatively, serum was fractionated by ExoQuick (System Biosciences, Mountain View, CA, USA) according to the manufacturer's recommended procedure, and the resulting exosome fractions were also used as a sialidase inhibitor source. Serum, ammonium sulfate precipitates or exosome fractions were determined for sialidase inhibitory activity by incubating with recombinant sialidase (0.9–1.2 units) and substrate for 30–60 min in the same assay system as that for sialidase activity. The inhibitory activity was defined as the percentage of residual sialidase activity relative to the control value without inhibitor.

ELISA for NEU3 sialidase. To measure NEU3 protein concentrations in human serum, a sandwich ELISA method was developed using two anti-NEU3 monoclonal antibodies prepared previously.[18] Serum (10 μL) was added to each well of anti-NEU3 (clone 7) antibody-coated plates (1:100 dilution with 1% BSA in PBS), which were then incubated overnight at 4°C. After washing three times with PBS-T (PBS containing 0.05% Tween20), peroxidase-conjugated anti-NEU3 (clone 11) antibody was added to each well, and the plates were incubated at room temperature for 1 h. After washing three times with PBS-T, and following treatment with TMB reagent (Sigma-aldrich, St. Louis, MO) for 10 min at room temperature, the reaction was stopped by the addition of 1 N H_2SO_4. Color intensity was determined at 450 nm.

Statistical analysis. The results are expressed as mean ± SD. Values were compared using Student's *t*-test.

Results

Identification of ganglioside sialidase acitivity in serum of prostate cancer patients with significantly higher levels than in healthy subjects. We previously demonstrated marked increase in sialidase NEU3 expression in tumor specimens of prostate cancer compared with non-tumor prostate tissues with reference to mRNA levels and immunohistochemistry staining.[12] Human NEU3 has been found to be almost specific for gangliosides with hardly any action on glycoproteins, glycopeptides, or 4MU-NeuAc that are considered as good substrates

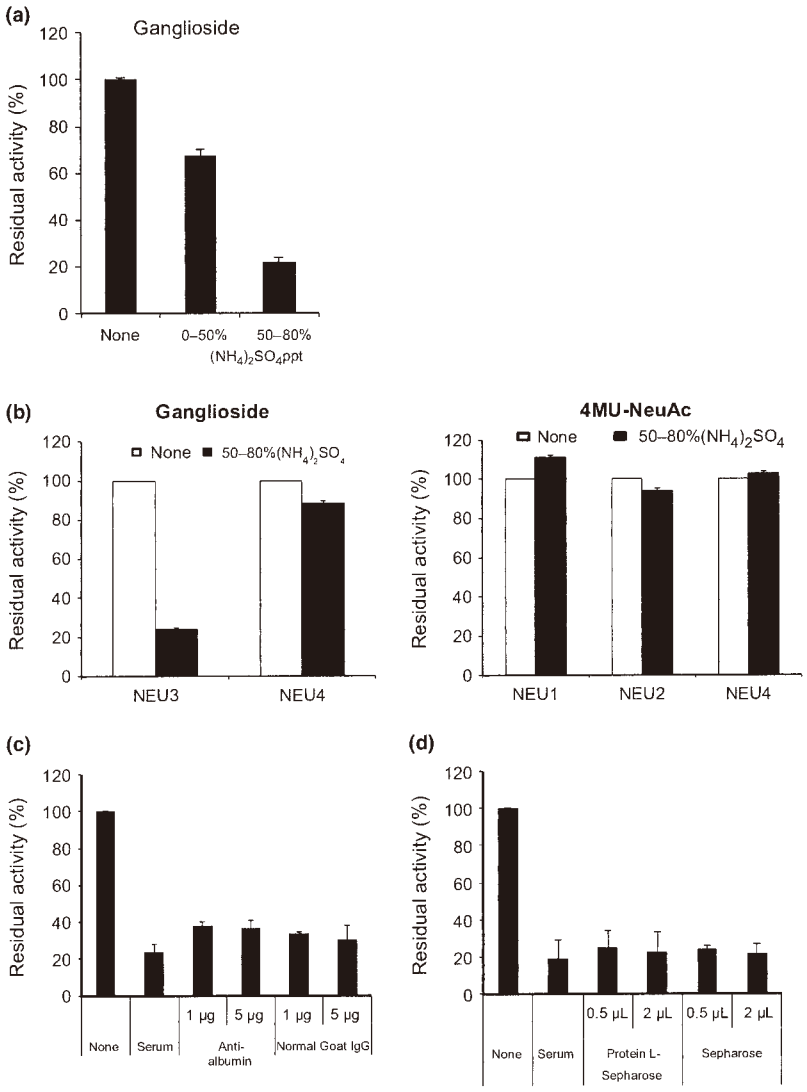

Fig. 3. Characterization of the inhibitor activity in human serum. (a) Inhibitory effects of human serum on ganglioside sialidase activity. The inhibitory activity was defined as the percentage of residual sialidase activity relative to the controls without inhibitor. Ammonium sulfate fractions of whole serum were examined for inhibitory activity against recombinant NEU3 or NEU4 sialidase activity (0.8–1.2 units of each) with the GM3 substrate. The results here were obtained only with NEU3 but not with NEU4. (b) The 50–80% ammonium sulfate fractions were tested for inhibitory activity against recombinant sialidase (0.9–1.3 units of each) NEU3 or NEU4 with ganglioside GM3 (left panel), and NEU1, NEU2 and NEU4 with 4MU-NeuAc as the substrate (right panel). (c, d) Immunoprecipitation studies of the serum inhibitory activity with anti-human albumin goat antibody (Bethyl Laboratories, Montgomery) (c) or protein L-Sepharose (1.5 × 3 cm, BioVision Inco.) (d). As controls, goat IgG and Sepharose beads were used instead of anti-albumin antibodies and protein L-Sepharose, respectively. Recombinant NEU3 (1.5 units) was preincubated with human serum (5 μL) or serum treated with anti-albumin antibodies (c) or protein L-Sepharose (d), and each supernatant after immunoprecipitation was assayed for sialidase activity with GM3 as the substrate.

for other sialidases in *in vitro* activity assays.[19,20] Based on previous results, our attempts were made to measure the sialidase activity in the serum of prostate cancer patients. For the present assays with 2.5 μL of serum, ganglioside GM3 was first used as the substrate. As shown in Figure 1(a), sialidase activity was evident in serum of prostate cancer patients, even though the level was extremely low (approximately 1/20–1/50) compared with those of prostate cancer tissues per milligram of protein. When compared with healthy subjects, however, sera of the patients showed significantly higher levels of sialidase activity toward GM3 (Fig. 1b). Although our previous results demonstrated that NEU3 mRNA levels in prostate cancer tissues positively correlated with cancer grades (e.g. Gleason score [$P < 0.001$]) and, furthermore, immunohistochemistry with anti-NEU3 monoclonal antibody exhibited strong positive staining in the cancer tissues with a high score,[12] the serum sialidase activities toward GM3 showed no statistically significant correlation with the cancer grade in the present study.

Characterization of serum sialidase activity. To facilitate optimum activity for the sialidase, influence of various times of incubation and serum volumes was assessed in the assays with GM3 as the substrate. As shown in Figure 2(a), linearity in activity up to 2.5 μL was obtained, but a dramatic decrease in the activity at over 5 μL serum, and especially the 80–90% reduction with 10 μL, suggested the existence of some components for activity inhibition or degradation of released sialic acids. The inhibitory component(s) will be described in the next section. The time course of the sialidase activity with 2.5 μL serum was confirmed to be linear for up to 60 min.

First, using 2.5 μL serum as an enzyme source, we examined which type of sialidase was responsible for the activity. Regarding substrate specificity, 4MU-NeuAc is capable of being used as a substrate to determine NEU1, NEU2 and NEU4 activities, and as a ganglioside for NEU3 and NEU4 in the presence of Triton X-100, although NEU3 and NEU4 cannot be clearly distinguished because of both acting on gangliosides at acidic pH. As shown in Figure 2(b), with GM3 as the substrate, the pH dependence of the serum silaidase showed two peaks in the pH curve, a large one at pH 4.5–4.8 and with a smaller one at pH 5.8–6.0, similar to the case with human NEU3.[20] When the substrate specificity was investigated with various substrates, the serum sialidase hydrolyzed GD3 and GM3 efficiently but there was only a little activity on oligosaccharides such as sialyllactose, glycoproteins including fetuin and 4MU-NeuAc (Fig. 2c), as would be expected with

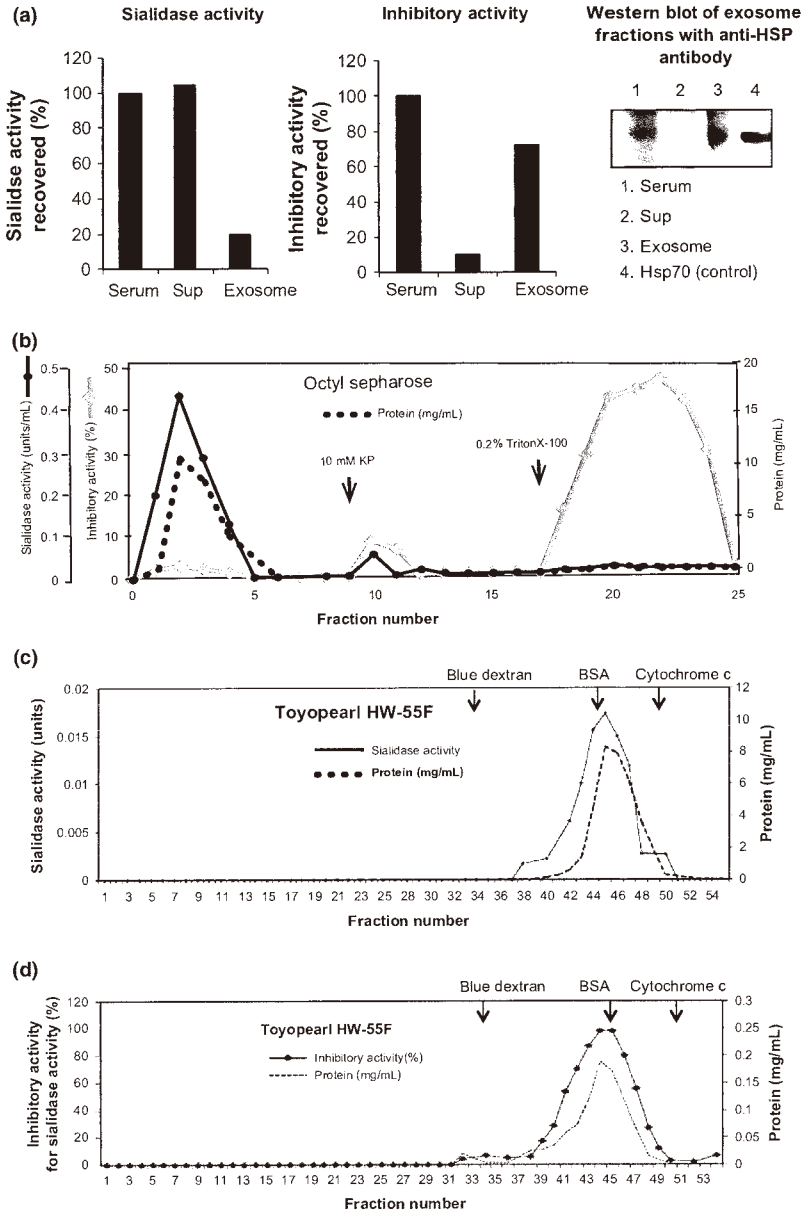

Fig. 4. Separation of the sialidase from the inhibitory activities. (a) Separation of the two activities by exosome isolation kit (ExoQuick, System Biociences). Resulting supernatants after exosome isolation retained most of the sialidase activity, whereas the exosome fraction had enriched inhibitory activity. The western blot with anti-HSP70 antibody is shown for each exosome fraction to verify the fractionation. (b) Separation of the two activities on Octyl-Sepharose chromatography. Ammonium sulfate fractions (40–80%, containing sialidase and inhibitory activities) of cancer patient serum (3 mL) were dissolved in 0.1 M phosphate buffer (pH 6.8) containing 0.5 M NaCl and 0.2 mM PMSF, and loaded on a Octyl-Sepharose column (1.5 × 3 cm, GE health care) equilibrated with the same buffer. After washing the column with the same buffer, the sialidase activity was eluted with 10 mM phosphate buffer containing 0.2 mM PMSF, and then the inhibitory activity followed with 0.2% Triton X-100 in the buffer. (c,d) The each activity fractions from the Octyl-Sepharose column were concentrated and separately applied to the Toyopearl HW-55F column (1.5 × 45 cm, Tosoh Bioscience) to estimate the apparent molecular size. BSA, bovine serum albumin.

NEU3.[20] To obtain the results showing a strong possibility of NEU3 identity, we purified the enzyme from pooled sera (60 mL) of cancer patients with affinity chromatography immobilized anti-NEU3 antibodies followed by gel electrophoresis and liquid chromatography coupled to mass spectrometry for analyses of the protein obtained. However, the attempts failed probably due to insufficient volume of the serum as the enzyme source. Studies were then undertaken to address the issues by immunoprecipitation studies using anti-sialidase antibodies. Because the results for the substrate specificity suggested the serum sialidase to be a ganglioside-hydrolyzing sialidase, as described above, anti-NEU3 or anti-NEU4 antibodies were employed. As references, recombinant sialidases NEU3 and NEU4 were applied to verify that the antibodies could immunoprecipitate their respective sialidases. Figure 2(d) (left and middle) clearly shows that the antibodies cross-react and immunoprecipitate the corresponding recombinant sialidases, whereas no mutual reactions occurred between the antibodies. Under the conditions used, the serum sialidase was evidently precipitated with only the anti-NEU3 antibody (Fig. 2d, right panel). It should be noted that no significant precipitation of the serum sialidase occurred with anti-NEU1 or NEU2 antibodies (data not shown). These results together indicate that the serum sialidase should, indeed, be considered as NEU3.

Characterization of sialidase inhibitor activity in serum. Next, we investigated the properties of the inhibitor activity against sialidase. When whole serum (5 μL) of the prostate cancer patients was incubated with NEU3 or NEU4 recombinant sialidase using GM3 as substrate, the serum was found to suppress only NEU3 recombinant enzyme activity. The inhibitory activity was then fractionated in precipitates of 0–50 and 50–80% ammonium sulfate, and was detected mainly in the latter fractions (Fig. 3a). To determine specificity for any other type of sialidase, the 50–80% ammonium sulfate fractions were incubated with equal amount of each recombinant sialidases with

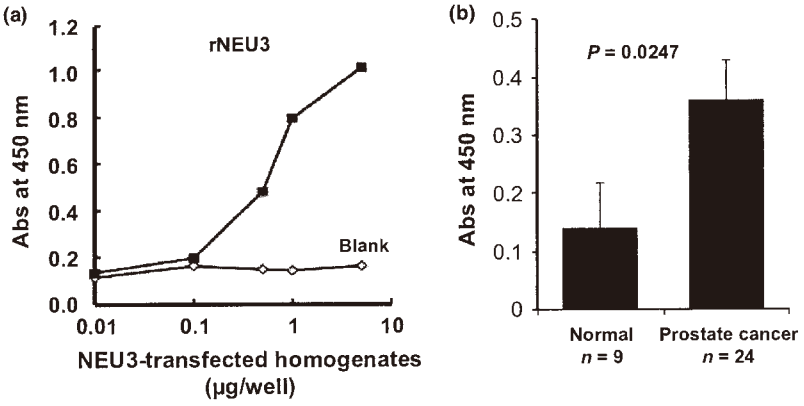

Fig. 5. Sialidase NEU3 assay by ELISA. (a) Standard curve of sialidase NEU3 concentrations using recombinant NEU3 protein in the sandwich ELISA. Homogenates of vector-transfected and NEU3-transfected 293T cells were used as the control and NEU3 standard, respectively. (b) The results of increased sialidase NEU3 in the serum of prostate cancer patients (n = 24) compared with normal sera (n = 9) as assessed by the ELISA method.

ganglioside GM3 (Fig. 3b, left) or 4MU-NeuAc (Fig. 3b, right) as substrates at an appropriate pH. NEU4 was tested with GM3 and 4MU-NeuAc substrates, based on its substrate preference. The results clearly confirm that the inhibition occurred specifically with NEU3, and not other sialidases, even the ganglioside sialidase NEU4. The inhibitory activity was stable after boiling for 2 min, and not affected by proteases inhibitors, including PMSF, leupeptin, pepstatin and aprotinin. Furthermore, the fraction did not contain measurable activity of N-acetylneuraminic aldolase, a degradation enzyme for released sialic acids. To exclude the possibility of albumin itself, because of its enrichment in 50–80% ammonium sulfate fraction, and of production of auto-antibodies to NEU3 protein, immunoprecipitation studies with anti-human albumin antibody and protein L-Sepharose (binding to all human immunoglobulins, Fab and k light chains), respectively, were performed by pre-incubating with the inhibitor fractions (Fig. 3c,d). However, the inhibitor activity was not suppressed by these treatments. When assessed in the serum of healthy adults in the same way as for cancer serum, it was detected to a similar extent. Unlike the case with the sialidase activity, the inhibitor activity did not show a statistically significant difference between the values of cancer and healthy subjects. However, interestingly, there was a negative correlation between the sialidase and inhibitory activities (correlation coefficient, $r = -0.58$) only in serum of the cancer patients. Hence, it seems likely that serum of cancer patients with relatively low sialidase activity tends to contain higher inhibitory activity than the case with high sialidase activity, even though the serum (2.5 μL) used for sialidase activity assays did not exhibit apparent inhibitory activity. The molecular basis of the correlation of the two activities is unclear at present.

Separation of sialidase and inhibitory activities. To further characterize the two activities, separation by exosome isolation kit and hydrophobic chromatography was undertaken. Exosome isolation yielded most of the ganglioside sialidase activity in the supernatant and, in contrast, the inhibitory activity in the pellet (exosome fraction), in line with distribution pattern of an exosome marker, HSP70 (Fig. 4a). These results also suggest that sialidase activity assays with 2.5 μL serum would be appropriate for obtaining the correct sialidase activity, because the value in the same volume of serum was similar to that in the supernatant when the inhibitor activity was removed by exosome isolation. To separate the two activities by column chromatography, the 40–80% ammonium sulfate fractions of cancer patient serum (3 mL), containing sialidase and inhibitory activities, were loaded on Octyl-Sepharose (1.5 × 3 cm) (Fig. 4b). The sialidase activity was detected in the pass-through fractions, and the inhibitory activity was eluted with 0.2% Triton X-100, indicating that they are different proteins distinguished by differing hydrophobic properties. When each of the activity fractions from the column were concentrated and separately applied to Toyopearl HW-55F column (1.5 × 45 cm; Tosoh Bioscience Tokyo, Japan), the sialidase activity emerged a little behind the position of the BSA marker, with an apparent molecular weight of 58 KDa (Fig. 4c), which is similar to that for recombinant NEU3, and inhibitor activity was detected at the position similar to BSA, with an apparent molecular weight of 65–70 kDa (Fig. 4d).

Quantification of serum NEU3 by sandwich ELISA. For the purpose of quantitation of serum NEU3, sandwich ELISA was performed using two anti-NEU3 monoclonal antibodies prepared previously. The standard curve showed linearity at the 0.1 to 10 μg protein concentrations of the homogenates of NEU3-transfected HK-293T as a standard (Fig. 5a). Under the conditions adopted, the serum NEU3 concentrations of each prostate cancer patient and normal adult were calculated. As with sialidase activity shown in Figure 1(b), the ELISA tests showed the levels of NEU3 in serum of prostate cancer patients to be higher than those in normal subjects with statistical relevance (Fig. 5b), validating the results of sialidase activity assays.

Discussion

We previously demonstrated remarkable upregulation of sialidase NEU3 in various human cancers, including prostate cancer, showing an apparent acceleration of tumor progression mostly by disturbance of cellular signaling at the cell surface.[4] Based on these results, the aim of the present study was to investigate whether NEU3 could be detected in the serum of cancer patients. We focused on prostate cancer for development of a new diagnosis marker, because measurement of serum PSA as the most frequently used tool is often associated with substantial false-positives.[21] Although our previous results on prostate cancer suggested that the NEU3 expression level in tissue specimens could be a more sensitive marker than PSA for early diagnosis to discriminate non-cancer from malignant prostate lesions,[12] it is definitely preferable to use a non-invasive diagnostic method. As was hoped, sialidase activity considered due to NEU3 was identified in the serum with significantly higher levels than in normal subjects. This is the first evidence for the existence of a mammalian sialidase in serum.

At present, the functional significance of the sialidase and the reason for its appearance in serum are uncertain, but it

may be associated with the existence of gangliosides in serum. There have been reports of gangliosides in human serum,[22–24] and it has been suggested that their shedding by some tumor cells may occur at strikingly high rates, correlated with tumorigenicity and cell density.[22] Serum gangliosides in cancer patients have been described to undergo pronounced changes with relatively high amounts, probably contributing to the suppression of the immune system that is frequently evident in tumor-bearing hosts.[24] To compensate for the high amounts of gangliosides in serum of cancer patients, NEU3 may be secreted from the cell surface. Alternatively, it could be just a reflection of tumor breakdown. In this context, the inhibitor activity for NEU3 was expected to be attributed to one of the low density lipoproteins,[23,24] known to be major ganglioside binding proteins *in vivo*, but their molecular sizes were clearly distinct, although the possibility cannot be completely excluded. The presence of the inhibitor may also have some relevance to the modulation of amounts of gangliosides. In preliminary experiments, we additionally found higher sialidase activities in the serum of cancer patients, including examples with bladder, testes and renal cancers (data to be published). The values so far obtained from the ELISA as well as the sialidase activity assays did not show any statistically significant correlation with pathological stage, but more detailed examinations will be necessary to clarify this issue in the future. Further work along these lines should make an important contribution to the determination of whether the serum sialidase is a potential target for new diagnosis tests for human cancers.

Acknowledgments

We thank the technologists at the Clinical Laboratory of Miyagi Cancer Center for their great help in storage of collected serum. This research was supported in part by Grants-in-Aid for Scientific Research on FS A-Step (241FT0338) and by CREST of the Japan Science and Technology Agency.

Disclosure Statement

The authors have no conflict of interest to declare.

References

1 Lau KS, Dennis JW. N-Glycans in cancer progression. *Glycobiology* 2008; **18**: 750–60.
2 Hakomori SI. Glycosynaptic microdomains controlling tumor cell phenotype through alteration of cell growth, adhesion, and motility. *FEBS Lett* 2010; **584**: 1901–6.
3 Miyagi T, Yamaguchi K. Mammalian sialidases: physiological and pathological roles in cellular functions. *Glycobiology* 2012; **22**: 880–96.
4 Miyagi T, Takahashi K, Hata K, Shiozaki K, Yamaguchi K. Sialidase significance for cancer progression. *Glycoconj J* 2012; **29**: 567–77.
5 Hata K, Koseki K, Yamaguchi K *et al.* Limited inhibitory effects of oseltamivir and zanamivir on human sialidases. *Antimicrob Agents Chemother* 2008; **52**: 3484–91.
6 Koseki K, Wada T, Hosono M *et al.* Human cytosolic sialidase NEU2-low general tissue expression but involvement in PC-3 prostate cancer cell survival. *Biochem Biophys Res Commun* 2012; **428**: 142–9.
7 Bilyy R, Tomin A, Mahorivska I *et al.* Antibody-mediated sialidase activity in blood serum of patients with multiple myeloma. *J Mol Recognit* 2011; **24**: 576–84.
8 Miyagi T, Wada T, Yamaguchi K, Hata K, Shiozaki K. Plasma membrane-associated sialidase as a crucial regulator of transmembrane signaling. *J Biochem* 2008; **144**: 279–85.
9 Kakugawa Y, Wada T, Yamaguchi K *et al.* Up-regulation of plasma membrane-associated ganglioside sialidase (Neu3) in human colon cancer and its involvement in apoptosis suppression. *Proc Natl Acad Sci USA* 2002; **99**: 10718–23.
10 Ueno S, Saito S, Wada T *et al.* Plasma membrane-associated sialidase is up-regulated in renal cell carcinoma and promotes interleukin-6-induced apoptosis suppression and cell motility. *J Biol Chem* 2006; **281**: 7756–64.
11 Nomura H, Tamada Y, Miyagi T *et al.* Expression of NEU3 (plasma membrane-associated sialidase) in clear cell adenocarcinoma of the ovary: its relationship with T factor of pTNM classification. *Oncol Res* 2006; **16**: 289–97.
12 Kawamura S, Sato I, Wada T *et al.* Plasma membrane-associated sialidase (NEU3) regulates progression of prostate cancer to androgen-independent growth through modulation of androgen receptor signaling. *Cell Death Differ* 2012; **19**: 170–9.
13 Uemura T, Shiozaki K, Yamaguchi K *et al.* Contribution of sialidase NEU1 to suppression of metastasis of human colon cancer cells through desialylation of integrin beta4. *Oncogene* 2009; **28**: 1218–29.
14 Yamanami H, Shiozaki K, Wada T *et al.* Down-regulation of sialidase NEU4 may contribute to invasive properties of human colon cancers. *Cancer Sci* 2007; **98**: 299–307.
15 Li K. Determination of sialic acids in human serum by reversed-phase liquid chromatography with fluorimatric detection. *J Chromatogr* 1992; **579**: 209–13.
16 Galjart NJ, Gillemans N, Harris A *et al.* Expression of cDNA encoding the human "protective protein" associated with lysosomal β-galactosidase and neuraminidase: homology to yeast proteases. *Cell* 1988; **54**: 755–64.
17 Miyagi T, Konno K, Emori Y *et al.* Molecular cloning and expression of cDNA encoding rat skeletal muscle cytosolic sialidase. *J Biol Chem* 1993; **268**: 26435–40.
18 Wang Y, Yamaguchi K, Wada T *et al.* A close association of the ganglioside-specific sialidase Neu3 with caveolin in membrane microdomains. *J Biol Chem* 2002; **277**: 26252–9.
19 Miyagi T, Wada T, Iwamatsu A *et al.* Molecular cloning and characterization of a plasma membrane-associated sialidase specific for gangliosides. *J Biol Chem* 1999; **274**: 5004–11.
20 Wada T, Yoshikawa Y, Tokuyama S, Kuwabara M, Akita H, Miyagi T. Cloning, expression, and chromosomal mapping of a human ganglioside sialidase. *Biochem Biophys Res Commun* 1999; **261**: 21–7.
21 Lumen N, Fonteyne V, De Meerleer G *et al.* Population screening for prostate cancer: an overview of available studies and meta-analysis. *Int J Urol* 2012; **19**: 100–8.
22 Katopodis N, Hirshaut Y, Geller NL, Stock CC. Lipid-associated sialic acid test for the detection of human cancer. *Cancer Res* 1982; **42**: 5270–5.
23 Senn H-J, Orth M, Fitzke E, Wieland H, Gerock W. Gangliosides in normal human serum concentration, pattern and transport by lipoproteins. *Eur J Biochem* 1989; **181**: 657–62.
24 Bergelson LD. Serum gangliosides as endogenous immunomodulators. *Immunol Today* 1995; **16**: 483–6.

PLOS | ONE

RESEARCH ARTICLE

Potentiation of Epidermal Growth Factor-Mediated Oncogenic Transformation by Sialidase NEU3 Leading to Src Activation

Koji Yamamoto[1,5☯], Kohta Takahashi[1☯], Kazuhiro Shiozaki[2], Kazunori Yamaguchi[3], Setsuko Moriya[1], Masahiro Hosono[4], Hiroshi Shima[5], Taeko Miyagi[1]*

1 Departments of Cancar Glycosylation Research, Institute of Molecular Biomembrane and Glycobiology, Tohoku Pharmaceutical University, Sendai, Japan, **2** Faculty of Fisheries and The United Graduate School of Agricultural Science, Kagoshima University, Kagoshima, Japan, **3** Molecular and Cellular Oncology, Miyagi Cancer Center Research Institute, Natori, Japan, **4** Departments of Cell Recognition Study, Institute of Molecular Biomembrane and Glycobiology, Tohoku Pharmaceutical University, Sendai, Japan, **5** Division of Cancer Molecular Biology, Graduate School of Medicine, Tohoku University, Sendai, Japan

☯ These authors contributed equally to this work.
* tmiyagi@tohoku-pharm.ac.jp

OPEN ACCESS

Citation: Yamamoto K, Takahashi K, Shiozaki K, Yamaguchi K, Moriya S, Hosono M, et al. (2015) Potentiation of Epidermal Growth Factor-Mediated Oncogenic Transformation by Sialidase NEU3 Leading to Src Activation. PLoS ONE 10(3): e0120578. doi:10.1371/journal.pone.0120578

Academic Editor: Laszlo Buday, Hungarian Academy of Sciences, HUNGARY

Received: October 21, 2014

Accepted: January 24, 2015

Published: March 24, 2015

Data Availability Statement: All relevant data are within the paper.

Funding: This study was supported in part by Grants-in-Aid for Scientific Research on Innovative Areas (No. 23110002) from the Ministry of Education, Culture, Sports, Science and Technology of Japan. The funders had no role in study design, data collection and analysis, decision to publish, or preparation of the manuscript.

Competing Interests: The authors have declared that no competing interests exist.

Abstract

We previously demonstrated that sialidase NEU3, a key glycosidase for ganglioside degradation, is up-regulated in various human cancers, leading to increased cell invasion, motility and survival of cancer cells possibly through activation of EGF signaling. Its up-regulation is also important for promotion of the stage of colorectal carcinogenesis *in vivo* in human NEU3 transgenic mice treated with azoxymethane for the induction of aberrant crypt foci in the colon mucosa, accompanied by enhanced phosphorylation of EGF receptor (EGFR). To address whether the activation of EGF signaling by the sialidase is associated with oncogenic transformation, we here analyzed the effects of overexpression of NEU3 and EGFR in NIH-3T3 cells. When NEU3 was stably transfected with or without EGFR, it was associated with significant increases in clonogenic growth, clonogenicity on soft agar and *in vivo* tumor growth in nude mice either with or without the receptor overexpression in the presence of EGF, compared with the levels in their vector controls. Despite the fact that the endogenous level of EGFR is known to be extremely low in these cells, NEU3 significantly enhanced the phosphorylation of Akt and ERK, as well as that of the receptor. The NEU3-mediated activation was largely abrogated by the EGFR inhibitor AG1478 or PD153035, but significant clonogenic growth still remained. NEU3 was then found to activate Src kinase, and the clonogenicity was completely suppressed by an Src inhibitor, PP2. The activity-null mutants failed to activate Src and EGFR, indicating that ganglioside modulation by NEU3 may be necessary for the activation. NEU3 and Src were co-immunoprecipitated with EGFR in NEU3- and EGFR- transfected cells. These findings identify NEU3 as an essential participant in tumorigenesis through the EGFR/Src signaling pathway and a potential target for inhibiting EGFR-mediated tumor progression.

Introduction

Sialidases catalyze the removal of sialic acid residues from the terminal positions of the carbohydrate groups of glycoproteins and glycolipids, which is the initial step in the degradation of these glycoconjugates. The sialidase reaction, therefore, is considered to influence many biological processes through alteration of the conformation and recognition of the biological sites of functional molecules. During malignant transformation, aberrant glycosylation has been observed as a characteristic feature of cancer cells [1, 2], and altered sialylation in particular is closely associated with metastatic potential and invasiveness. To shed light on the causes and consequences of such aberrant sialylation, our studies have focused on mammalian sialidases, which regulate the cellular sialic acid contents and function of glycoconjugates by desialylation [3].

Among four mammalian sialidases identified to date, the plasma membrane- associated and ganglioside-specific sialidase NEU3 appears to play particular roles in controlling transmembrane signaling by the modulation of gangliosides [4], and its aberrant expression is closely related to the pathogenesis of cancer [5]. We previously demonstrated that NEU3 is up-regulated in tumor compared with that in adjacent non-tumor tissues in colon, renal, prostate and ovarian cancers [6–9], which may be regulated by Sp1/Sp3 transcriptional factors [10]. NEU3 enhances cancer cell survival [6,11], cell migration and attachment [12], whereby it stimulates Ras activation with a consequent influence on ERK1/2 and Akt and actually enhances the EGF-stimulated tyrosine-phosphorylation of EGFR [11]. *NEU3* transgenic mice have also provided evidence of the involvement of this sialidase in carcinogenesis, in terms of an increase in azoxymethane- induced aberrant crypt foci [13], whereas *Neu3*- knock out mice exhibited reduction of tumor incidence in a colitis-associated colon carcinogenesis model induced by azoxymethane and dextran sodium sulfate [14]. These observations suggest the possibility that up-regulation of NEU3 is involved in not only augmentation of the malignant phenotype of cancer cells, but also in the process of malignant transformation.

EGFR is often found overexpressed or mutated in a wide variety of human cancers, and these events are closely linked to enhanced tumorigenicity [15]. The non-receptor tyrosine kinase, c-Src is also overexpressed in many of these same cancers, but is non-oncogenic in normal cells [16], implying that the two tyrosine kinases may functionally interact. In this context, it is assumed that co-overexpression of EGFR, c-Src and NEU3 in cancers is not just coincident but probably an essential event in tumorigenesis. To address this issue, we prepared stable transfectants of NIH-3T3 cells overexpressing NEU3 and/or EGFR, and examined them for their growth and tumorigenic properties. Here, we found that NEU3 potentiates EGFR-mediated tumorigenesis through the stimulation of EGFR phosphorylation and Src activity, and these findings should provide a new tool for the development of cancer therapy by the suppression of NEU3 that activates EGFR-signaling.

Materials and Methods

Cell culture and transfection

NIH-3T3 mouse fibroblast cells were obtained from Riken BRC Cell Bank (Tsukuba, Japan). The cells were cultured in Dulbecco's modified Eagle's medium (DMEM) supplemented with 10% fetal bovine serum (Invitrogen) at 37°C in a 5% CO_2 atmosphere. For NEU3 overexpression, the entire open reading frame of the human *NEU3* gene [17] was inserted into the EcoRI site of a retrovirus vector pMXs-puro and the plasmid was introduced into PlatA. The target cells were then incubated with the culture media containing infectious viruses for two days and selected by cultivation in the presence of 2 μg/ml puromycin for 10–14 days, as previously

described [18]. Null-activity mutants of NEU3, N88D and Y370C, were prepared as described previously [19] and subcloned into the EcoRI site of pMXs-puro. For EGFR overexpression, the human wild- type gene, which was kindly provided by Dr. M. Shibuya (Institute of Medical Science, University of Tokyo), was inserted into a retroviral vector pMXs-neo, and for selection, 800 μg/ml neomycin was used to obtain stable transfectants.

Antibodies

Phospho-EGFR (Cell Signaling, Y-845, Y-1068), EGFR (Santa Cruz), phospho-ERK, ERK, phospho-Akt, Akt, phosphor-Src (Y416), Src, Fyn, Yes (Cell Signaling), and monoclonal anti-NEU3, prepared as described previously [20], were used in immunoprecipitation, or immunoblotting analysis.

Quantitative RT-PCR analysis

Total RNA was prepared using an RNeasy mini kit (Qiagen) and reverse transcribed with SuperScript II (Invitrogen). Real-time PCR was performed with a QuantiTect SYBR Green PCR kit (Qiagen) and a Light Cycler PCR system (Roche). The primers for EGFR and NEU3 were as follows: mouse EGFR sense 5'-TTGGCCTATTCATGCGAA GAC-3', and antisense 5'-GAGGTTCCACGAGCTCTCTCTCT-3'; human EGFR sense 5'-GACCTCCATGCCTTT-GAGAA-3', and antisense 5'-GCTGACGACT GCAAGAGAAA-3'; mouse NEU3 sense 5'-CTCAGTCAGAGATGAGGATGCT-3', and antisense 5'- GTGAGACATAGTAGGCA-TAGGC-3'; and human NEU3 sense 5'-AGGTCAGTCTCCAGTACCTTC-3' and antisense 5'-ACATCCAGCATCC TGACTGTAG-3'. The expression of glyceraldehyde- 3-phosphate dehydrogenase (GAPDH) was determined as an internal control.

Sialidase activity assays

Crude extracts were used for sialidase assays using bovine brain ganglioside GM3 (Alexis Biochemicals, Lausen, Switzerland) as the substrate in the presence of 0.1%Triton X-100. After incubation at 37°C for 30 min, the amount of sialic acid released was determined by a modified thiobarbituric acid method or by fluorometric high-performance liquid chromatography with malononitrile [11]. One unit of activity was defined as the amount of enzyme that cleaved 1 nmol sialic acid from the substrates. Protein concentrations were determined by dye-binding assay (Bio-Rad Laboratories).

Cell growth, colony formation and anchorage-independent growth assays

Cell growth rate was determined by 3-(4,5-dimethylthiazol-2-yl)-2,5- diphenyltetrazolium bromide assay using the WST-1 Cell Proliferation Assay System (Takara, Tokyo) on 96 well culture plates. For colony formation, cells were plated at 1000 cells/well in six-well dishes, cultured for 10–14 days and the colonies were counted using Gel-Doc (Bio-Rad) after staining with 0.1% crystal violet. Assays of colony formation in soft agar were performed as described previously [21]. Briefly, 1- mL underlayers consisting of 0.5% agar medium were prepared in six-well dishes by combining equal volumes of 1.0% Noble agar (Difco, Detroit, MI) with 2 x DMEM and 20% FBS. A total of 1 x10^5 cells were suspended in 0.33% agar medium and then plated onto the previously prepared underlayers. After two to three 2–3 weeks, the colonies in five fields per sample were counted and the sizes per colony number were measured under a microscope.

In vivo xenograft assays

Forty male athymic BALB/c nu/nu male mice (8–9 weeks old, SLC, Shizuoka, Japan) were used in this study. Animals were kept in rooms maintained at constant temperature (22±2 C) and humidity (60%±15%) under a 12 h light- dark cycle, and were housed in ten groups (n = 3 or 4) in isolated ventilates cages and allowed free access to water and standard food. Mice were injected subcutaneously with the cells ($1x10^7$) under ether anesthesia and then given either subcutaneous doses of murine EGF (Nacalai Tesque, 5 μg/day) every two days or no additional treatment. Tumor growth was measured every three days once tumors became visible. Tumor volume was estimated as follows: (length x width x thickness)/2. After 35–55 days of the cell injection, tumor-bearing mice were sacrificed under ether anesthesia. All animal experiments were performed in compliance with the Guidelines of Laboratory Animal Research, Tohoku Pharmaceutical University. The protocol was approved by the Animal Care and Use Committee of Tohoku Pharmaceutical University (Permit Number: A-13015-cn).

Immunoprecipitation and immunoblotting

After culturing under serum-starved conditions for 16–24 h, cells were treated with EGF (20 ng/ml) for 15 min, washed with PBS and homogenized and solubilized by sonication for 10 sec in cold lysis buffer [50mM HEPES (pH7.5), 150 mM NaCl, 1% Nonidet P40, 2 mM EDTA, 7.5 μg/mL aprotinin, 10 μg/mL leupeptin, 10 mM NaF, 2 mM orthovanadate, and 2 mM PMSF]. After clarification by centrifugation (12,000 x g for 15 min), cellular lysates were immunoprecipitated with anti-EGFR antibody overnight, and then with protein A/G Sepharose beads (GE Healthcare Life Sciences) for 3 h. The immunocomplexes were then washed with cold lysis buffer, resuspended in SDS sample buffer, and subjected to SDS-PAGE and immunoblotting with the respective antibodies using ECL Plus Western blotting reagent (Amersham Biosciences). For the EGFR or Src inhibition, the cells were treated with specific inhibitor, AG1478 or PP2 (Calbiochem), respectively.

Thin-layer chromatography

Glycolipids were extracted from cells as described elsewhere [7], fractionated by thin-layer chromatography on high-performance thin-layer chromatography plates (Baker, Phillipsburg, NJ, USA, or Merck, Darmstadt, Germany) and visualized with orcinol-H_2SO_4.

Statistical analysis

The results are expressed as mean ± SD. All values were compared using Student's t test.

Results

NEU3 promotes cell growth and colony formation of NIH-3T3 cells

To examine the effects of NEU3 on the cell proliferation and transformation, NIH-3T3 cells were utilized, since the cells were often employed in transfection assays for transforming genes [22]. We generated stable transfectants of the cells by the introduction of human NEU3 and/or EGFR cDNA using a retroviral vector system, and analyzed the clones (Vec-, NEU3-, EGFR-, and EGFR/NEU3-cells) for NEU3 and EGFR by western blotting with anti-NEU3 and anti-EGFR antibodies, respectively. A high level of NEU3 protein was detected in the NEU3-, and EGFR/NEU3-cells, but not in the vector controls or in the EGFR- cells (Fig. 1A), which is consistent with the data showing an approximately 25-fold increase in activity levels towards ganglioside substrates by NEU3 transfection compared with those in the controls (Fig. 1B). Such a potent increase of NEU3 expression is not unusual, but often seen in cancer compared with

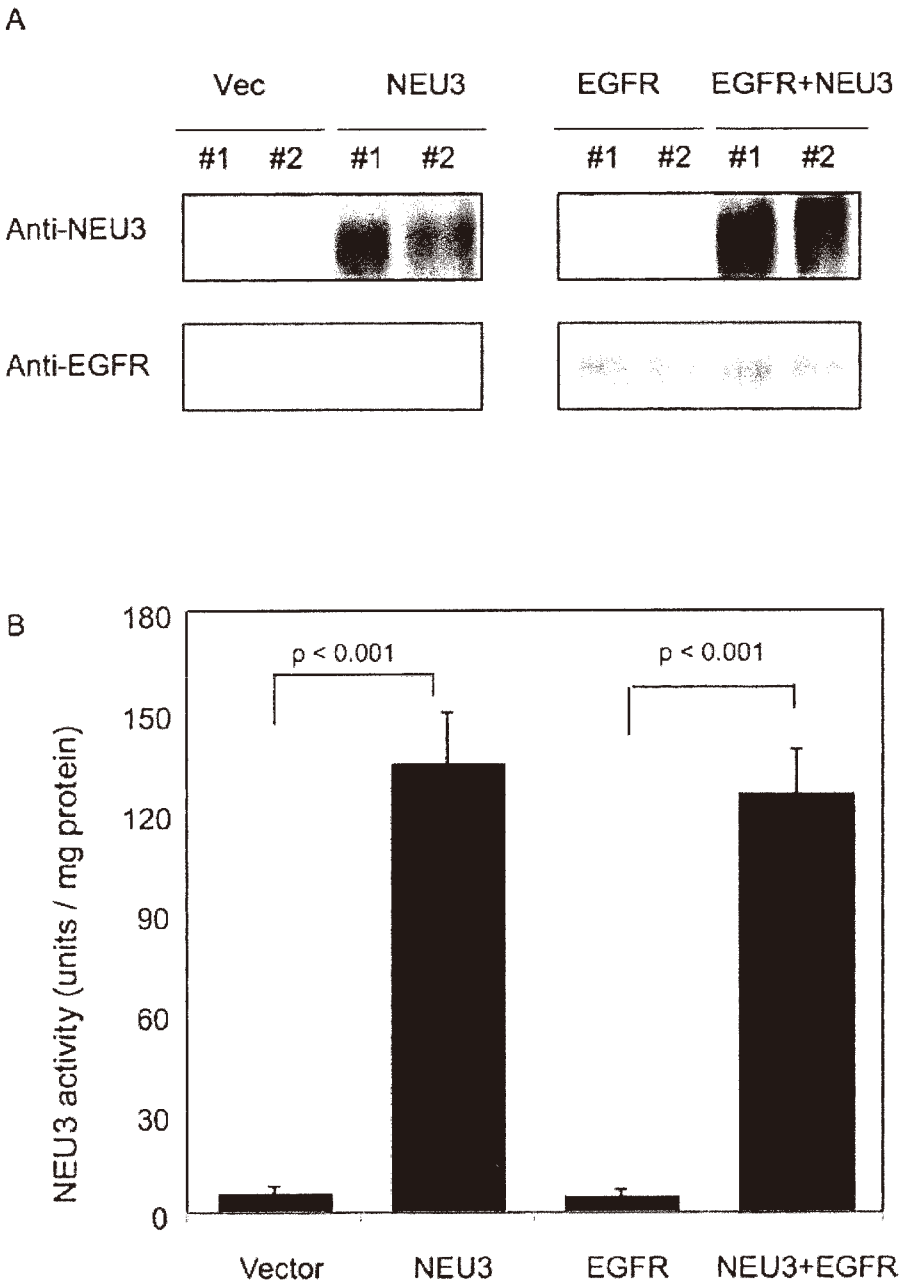

Fig 1. Measurement of NEU3 and EGFR levels in NEU3- and/or EGFR- transfected NIH-3T3 cells. (A) NEU3 and EGFR protein levels were analyzed by western blotting using antibodies for NEU3 and EGFR, respectively. The proteins were hardly detectable in the cells without the transfection of NEU3 and EGFR genes. Relative mRNA levels for murine EGFR/GAPDH were 0.7–0.9 in the controls and all the clones generated, and those for human EGFR/GAPDH were 0.1–0.2 in controls and NEU3-cells and 5,000–6,000 in the EGFR- and EGFR/NEU3-cells. (B) The sialidase activity levels toward mixed gangliosides (Bovine brain, Sigma) as a substrate were estimated. Only a slight sialidase activity was shown in vector controls and in EGFR-transfected cells.

doi:10.1371/journal.pone.0120578.g001

that in adjacent normal tissues, as we reported in the case of colon cancer [6]. The EGFR- and EGFR/NEU3- cells showed significant EGFR protein expression, whereas the controls and NEU3-cells did not, because of extremely low level of the endogenous EGFR in 3T3-NIH cells [23], confirmed by assessment of EGFR mRNA (Fig. 1A legend). The level of EGFR protein was hardly affected by NEU3 overexpression.

We first determined the cell growth in NEU3-cells by MTT assays. NEU3 showed a growth rate higher than that of the vector controls, which was further enhanced in the presence of EGF (Fig. 2A); similar effects were also observed in the EGFR-cells (Fig. 2B). These clones were then examined in colony formation assays. As expected from the results of the MTT assays, NEU3 caused a significant increase in colony formation compared with that in the controls, even without EGF, which was markedly potentiated in combination with EGFR. Much greater enhancement of the above effects was observed upon EGF addition in all of these cells (Fig. 2C). The total colony numbers shown in Fig. 2D indicate that NEU3 and EGFR increased colony formation in monolayer culture and the overexpression of both had synergistic effects. Interestingly, the number of large colonies (over 3 mm in size) was increased by NEU3 to the same extent as by EGFR overexpression (Fig. 2D, right panel). These results indicate that NEU3 promotes colony formation in terms of size as well as number.

NEU3 promotes anchorage-independent growth and *in vivo* tumorigenicity

To determine the effects of NEU3 overexpression on the tumorigenic ability of the respective clones, we examined anchorage-independent growth. The NEU3-, EGFR- and NEU3/EGFR-cells apparently formed colonies in soft agar in the presence of EGF, but vector controls failed to do so (Fig. 3A). As observed in the monolayer culture, NEU3 potentiated the colony formation in soft agar to a considerable extent, similar to the case of EGFR, and led to a further increase when in combination with EGFR, although it had only a small effect in the absence of EGF (Fig. 3B). This is consistent with a previous report describing that EGF-induced growth in agar for human EGFR-transfected cells [23]. To determine further the effect of NEU3 expression on tumorigenesis *in vivo*, we injected the respective cells (1×10^7 cells) subcutaneously into the flanks of male nude mice. The mice were given either subcutaneous doses of murine EGF (5μg) every two days or no additional treatment, although mature male mice have been shown to produce EGF [24]. As shown in Fig. 3C (left graph), 30 days after inoculation, interestingly, the NEU3-cells produced progressively growing tumors whereas the control cells did not form any visible tumors. In the mice injected with EGFR- and EGFR/NEU3- cells, the tumor growth was faster, the latency period was just less than half as long, and the average tumor volume was also greater than that of those received only the NEU3- cells (Fig. 3C, right graph). In particular, however, it is interesting that NEU3 markedly accelerated the tumor growth in volume and shortened the latency period in the mice injected with the EGFR/NEU3 cells compared with those with the EGFR-cells. As shown by the three experiments using independent clones (Fig. 3D), these results indicate that NEU3 potentiates the transformation of NIH-3T3 cells, and probably even possesses transformative ability alone, along with confirmation that EGFR is capable of transforming these cells. The transformation ability of NEU3- and/or EGFR- overexpressing cells was evident even in the case of no EGF injection, probably due to endogenous EGF in the male mice sufficient for the transformation. It would be also interesting to elucidate the cause of the results that NEU3- cells injected into some of the mice did not show *in vivo* tumorigenic potential.

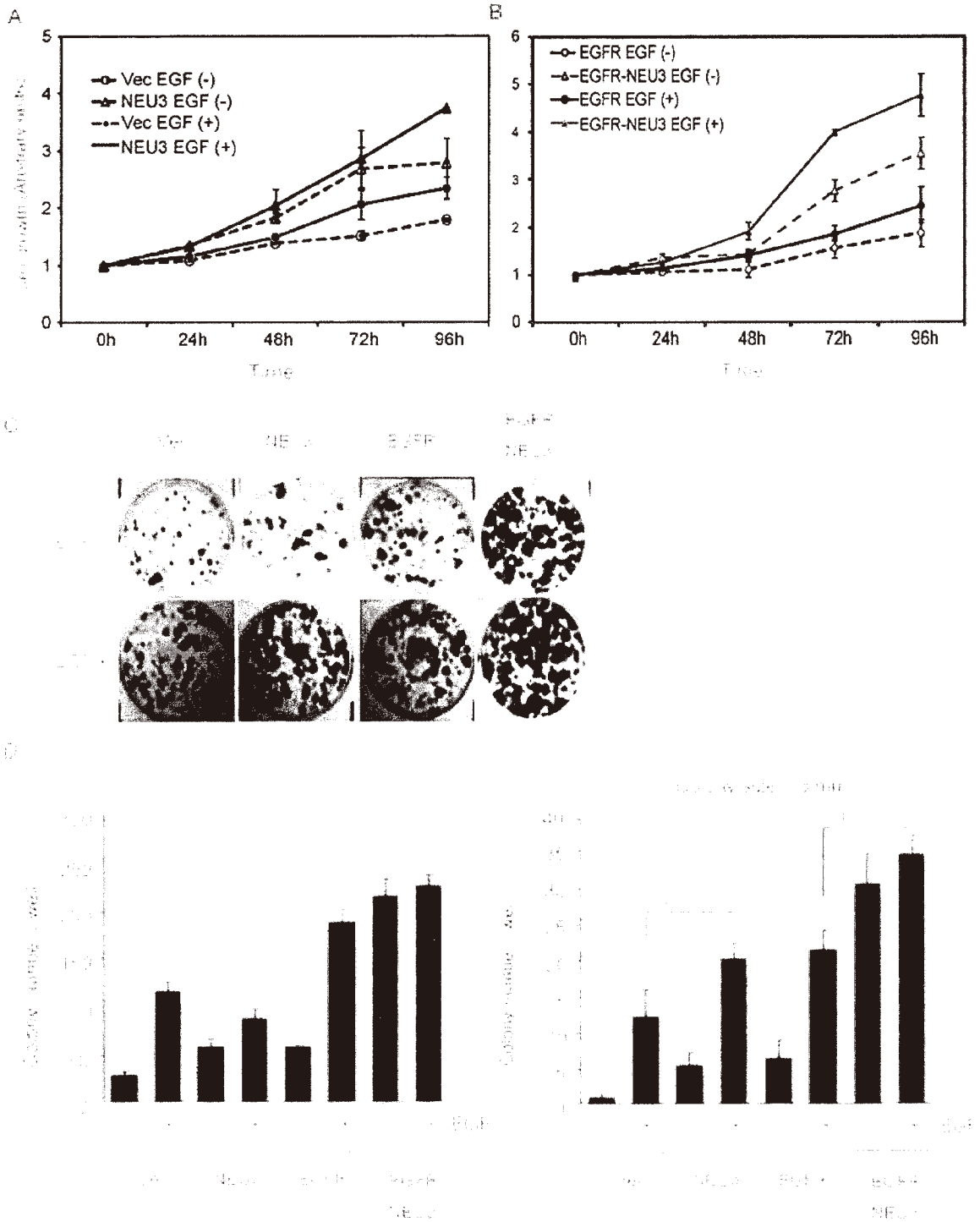

Fig 2. NEU3-mediated potentiation of cell growth assessed by MTT assays and colony formation assays. (A) The cell growth curves of NEU3-transfected cells were compared with those of vector controls in the absence and presence of murine EGF (20 ng/ml). Three independent experiments were performed (mean ±SD). (B) The cell growth curves of EGFR- and EGFR/NEU3-transfected cells are shown with or without EGF in independent experiments performed in triplicate (mean ±SD). (C) Colony formation assays in the transfectants. The cells were plated at 1000 cells/well in six-well dishes with or without EGF, and the colonies were quantified after 7–14 days of culture. Representative images are shown. (D) Values represent means with

standard deviations obtained from three independent experiments. In the right graph, the number of colonies over 3.0 mm in size was counted in independent experiments performed in triplicate (mean ±SD).

doi:10.1371/journal.pone.0120578.g002

NEU3 activates EGFR signaling

To understand how NEU3 affects EGF- dependent tumorigenesis and potentiates EGFR-mediated effects, we next examined EGFR signaling pathways in the respective cells. Consistent with our previous findings for HeLa cells [11], at 15min after EGF treatment, NEU3 increased EGFR phosphorylation even in the non-EGFR- transfected cells (Fig. 4A), presumably because of expression of a low number of analogous murine receptors in parent NIH-3T3 cells [23] and, besides, NEU3 transfection hardly changed the expression of the receptor (Fig. 1A legend). The effects of NEU3 were further potentiated by EGFR overexpression. The level of EGFR phosphorylation was higher at Tyr-845 than at Tyr-1068 in NEU3- transfected cells, as previously observed [11]. Stimulation of ERK and Akt phosphorylation was also observed by the forced NEU3 expression in the NEU3- and EGFR/NEU3- cells compared with that in the respective controls (Fig. 4B, C), although Akt phosphorylation was not notable in NEU3-cells compared to the controls. These cells were then examined to determine whether endogenous Src undergoes activation by NEU3, because the biological synergy between EGFR and c-Src has been reported [25]. The phosphorylation of Src was indeed increased by NEU3 overexpression as well as EGF addition (Fig. 4D) as quantified in the lower graph, suggesting the NEU3-dependent activation of both EGFR and Src. To verify that the NEU3-mediated activation occurs through the interaction of these molecules, we performed immunoprecipitation studies using anti-EGFR antibodies. NEU3 was found in the immunoprecipitates together with endogenous Src, and interestingly, EGF stimulation yielded a higher level of immunoprecipitable NEU3 and Src. These results suggest that NEU3 facilitates the activation of EGFR signaling by forming a complex with EGFR and Src (Fig. 4E). It should be noted here that endogenous c-Src in the complex with EGFR and NEU3 might be Src but not Fyn or Yes, ubiquitously expressed among the Src family kinases [26], based on our immunoprecipitation studies using antibodies specific to the respective proteins (data not shown).

Inhibitors for EGFR and Src suppress colony formation

To study the effects of EGFR and Src on colony formation in NEU3- and/or EGFR- overexpressing NIH-3T3 cells, the cells were treated with EGFR inhibitor AG1478 or PD153035, or with Src inhibitor PP2. With AG1478 (15 μM), EGFR phosphorylation was abrogated even in the cells forced to express EGFR, although ERK phosphorylation still remained to a certain extent (Fig. 5A). Under these conditions, NEU3 reduced the number of colonies but a considerable number still remained (Fig. 5B). Another EGFR inhibitor, PD153035 (5 μM), also caused the complete inhibition of EGFR phosphorylation (data not shown), but NEU3 resulted in the continued formation of some colonies (Fig. 5B). On the other hand, PP2 (10 μM) treatment resulted in entire suppression of colony formation, suggesting the importance of Src activity for the clonogenic growth. However, colony formation in soft agar was completely blocked by either AG1478 (15 μM) or PP2 (10 μM) in all of the cells (Fig. 5C), indicating that the activation of EGFR and Src is essential for anchorage-dependent cell growth.

Ganglioside modulation by NEU3 is required for activation of EGFR signaling

To investigate further the molecular mechanism behind the NEU3-mediated activation of EGFR and Src in the cell system, we generated NEU3 activity mutants and determined the

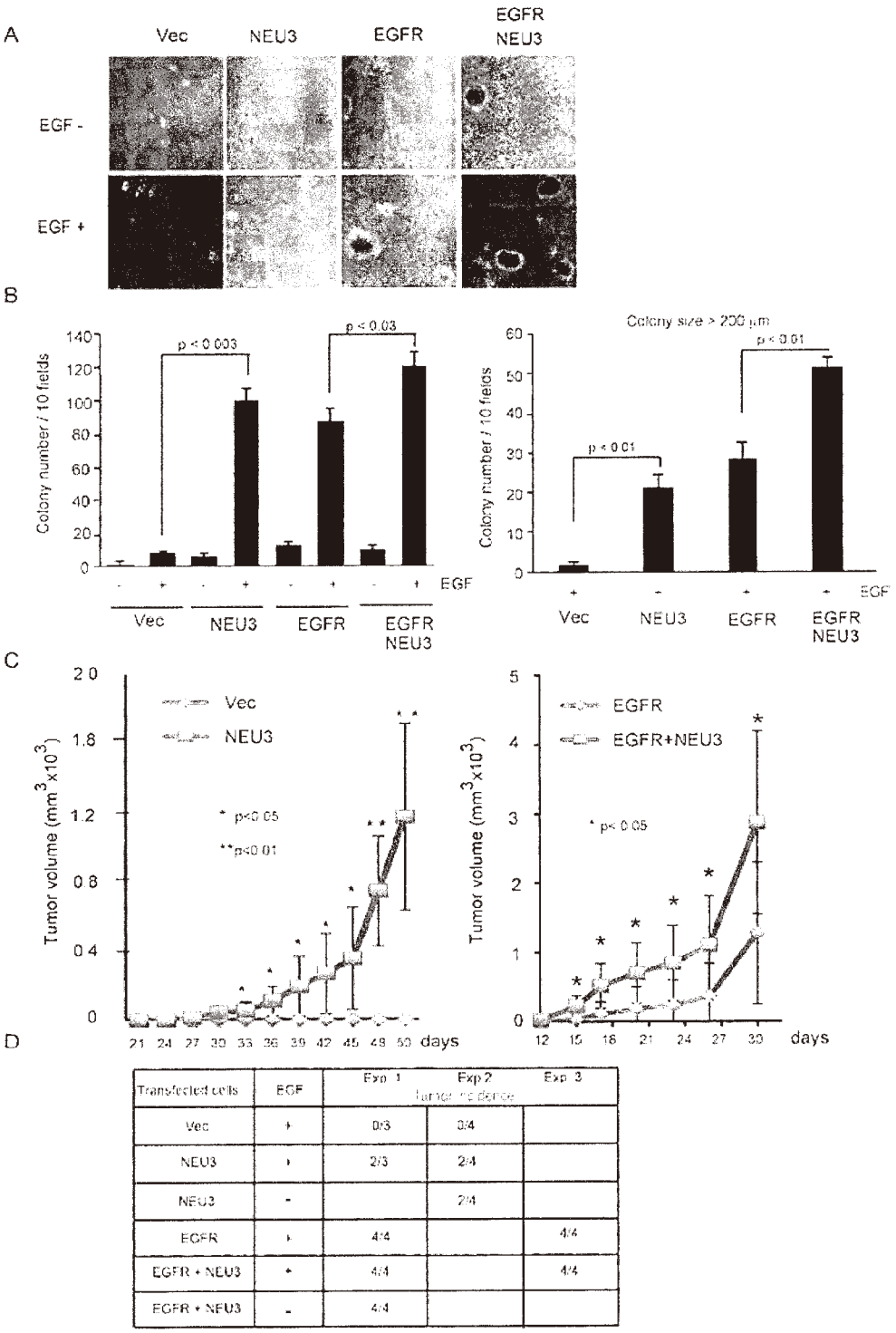

Transfected cells	EGF	Exp 1	Exp 2	Exp 3
		Tumor formation		
Vec	+	0/3	0/4	
NEU3	+	2/3	2/4	
NEU3	-		2/4	
EGFR	+	4/4		4/4
EGFR + NEU3	+	4/4		4/4
EGFR + NEU3	-	4/4		

Fig 3. NEU3-mediated potentiation of anchorage- independent growth and in *vivo* growth in nude mice. (A) Anchorage-independent growth in soft agar. The cells (1 x 10^5) were plated on soft agar with or without EGF, and two to three weeks later, the colony number and size were measured. Representative images are shown. (B) In the graph, the colony number on soft agar was calculated. The values are means with standard deviations obtained from three independent experiments. The graph in the right indicates the number of colonies over 200 μm in size. (C) *In vivo* growth in nude mice. Respective

cells were subcutaneously transplanted into nude mice with injection of murine EGF (5 μg/ml) every two days, and the measured tumor weights are indicated. The results of experiments with the vector controls and NEU3-transfected cells (left graph) and those with EGFR- and EGFR/NEU3-transfected cells (right graph) are shown in the four groups (n = 3 or 4). (D) Tumor incidence in the mice transplanted with the cells. To confirm the results, other six groups (n = 4) of these cells were further examined with or without injection of EGF, as indicated in the lower table.

doi:10.1371/journal.pone.0120578.g003

phosphorylation of EGFR and Src in the wild-type NEU3/EGFR- or mutant NEU3/EGFR- cells. Mutations of the residues (N88D, Y370C) have been proposed to reduce the enzymatic activity markedly as the key catalytic residues [19, 27]. With ganglioside GM3 as a substrate, clones of the two mutants showed only a slight activity in the assays (Fig. 6A). In comparison of the phosphorylation levels among the cells, the wild-type NEU3 significantly increased the phosphorylation of EGFR together with that of ERK (Fig. 6B), whereas this failed in the mutants. It is particularly interesting that Src phosphorylation was enhanced only by the wild-type NEU3. These results indicate that NEU3-mediated activation of EGFR signaling requires NEU3 sialidase activity.

As we previously demonstrated that human NEU3 is almost exclusively specific for gangliosides, alteration of the endogenous ganglioside pattern of NEU3-transfected NIH-3T3 cells was examined by thin layer chromatography (Fig. 7A). In the acidic fractions of the products, the level of the glycolipid with mobility similar to that of GM3 was reduced, whereas in the neutral fractions, the level of the glycolipid with mobility similar to that of lactosylceramide (Lac-cer) was increased. We have reported that Lac-cer stimulates EGFR phosphorylation [11], and other investigators have shown the evidence that GM3 reduces the phosphorylation [28–30]. To confirm the effects of the altered possible products, EGFR-transfected NIH-3T3 cells were treated with Lac-cer or GM3 under serum-depleted conditions. EGFR phosphorylation was increased by Lac-cer (Fig. 7B) and decreased by GM3 (Fig. 7C). All of the data together indicate that ganglioside- specific sialidase NEU3 potentiates EGF-mediated oncogenic transformation through EGFR and Src activation by ganglioside modulation.

Discussion

The observation that the overexpression of both sialidase NEU3 and EGFR occurs in various human cancers suggested that they might functionally interact and contribute to cancer progression in a synergistic manner. Consistent with this idea, our previous results showed that NEU3 regulates the phosphorylation of EGFR and its dimerization in HeLa cells, leading to stimulation of the Ras cascade subsequent to the promotion of cell survival [11]. In the present study, using stable lines of NIH-3T3 cells that contain overexpressed wild- type human NEU3 and/or EGFR, we found that NEU3 is required for the biological synergy with the receptor as well as its phosphorylation, and additionally, for the activation of cellular Src, which has also been shown to be overexpressed in many of these same cancers. In the presence of EGF, NEU3 indeed accelerated cell growth, colony formation in soft agar and *in vivo* tumorigenicity in synergy with EGFR and Src through enhancing their phosphorylation. It has been reported that lung cancer- derived EGFR active- site mutants are constitutively active and thus oncogenic, even without EGF [31], and that this activation is probably caused by interaction with Src [32]. In this context, it is particularly interesting that the overexpression of NEU3 might give rise to cellular conditions similar to those for the mutant EGFR in terms of the promotion of anchorage independence and even *in vivo* tumorigenicity through enhancing the association with EGFR and Src, if EGF is present. The detection of NEU3 together with Src in the EGFR immunoprecipitates was more evident in the presence of EGF, indicating that the signal complex may facilitate the EGFR phosphorylation subsequent to the activation of downstream

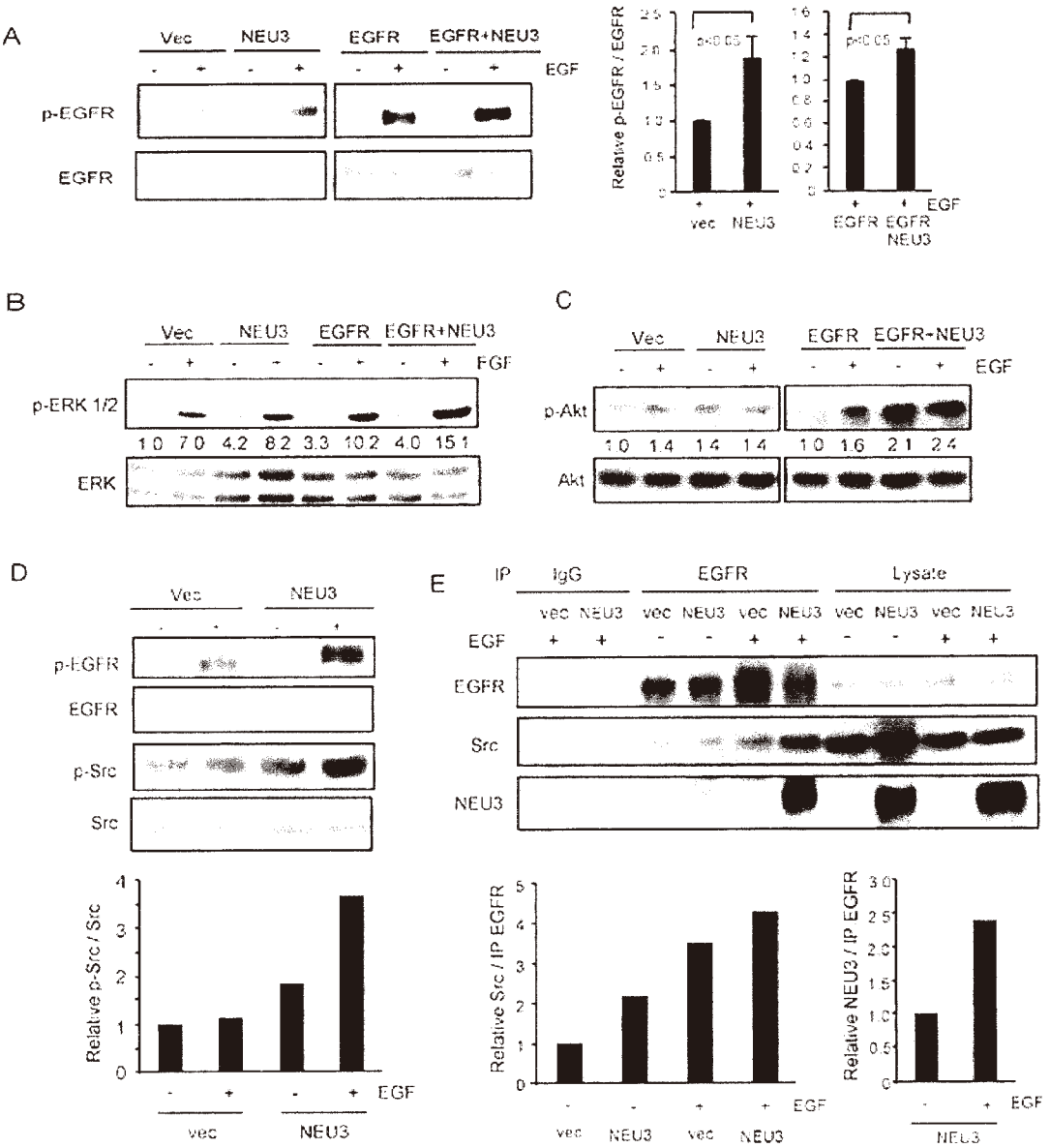

Fig 4. NEU3-mediated activation of EGFR/Src signaling. Phosphorylation of EGFR at Tyr-845 (A), ERK1/2 (B) and Akt (C) was determined with or without EGF by western blotting using respective antibodies. (A) Enhanced phosphorylation of EGFR at Tyr-845 in response to EGF and further synergistically by NEU3 overexpression. Results on immunoblotting are representative of three independent experiments, and the relative values for phospho-EGFR/EGFR in the presence of EGF were quantified in the right graph. (B, C) Enhanced phosphorylation of ERK1/2 (B) and Akt (C) with EGF and NEU3 overexpression. Each value shown under the blot represents as a value relative to that in the vector controls without EGF. (D) Enhanced Src activity by NEU3 overexpression. Results are representative of two independent experiments. The values for phospho-Src/Src relative to the vector controls without EGF are shown in the lower graph. (E) Immunoprecipitation of NEU3 and endogenous Src with anti-EGFR antibody and its promotion with EGF stimulation. Results are representative of two independent experiments. The values for the amounts of Src and NEU3, respectively, in the immunoprecipitates relative to those for the vector controls without EGF are shown in the graphs.

doi:10.1371/journal.pone.0120578.g004

signaling. However, the detailed mechanisms behind the physical interaction of the three molecules remain to be elucidated.

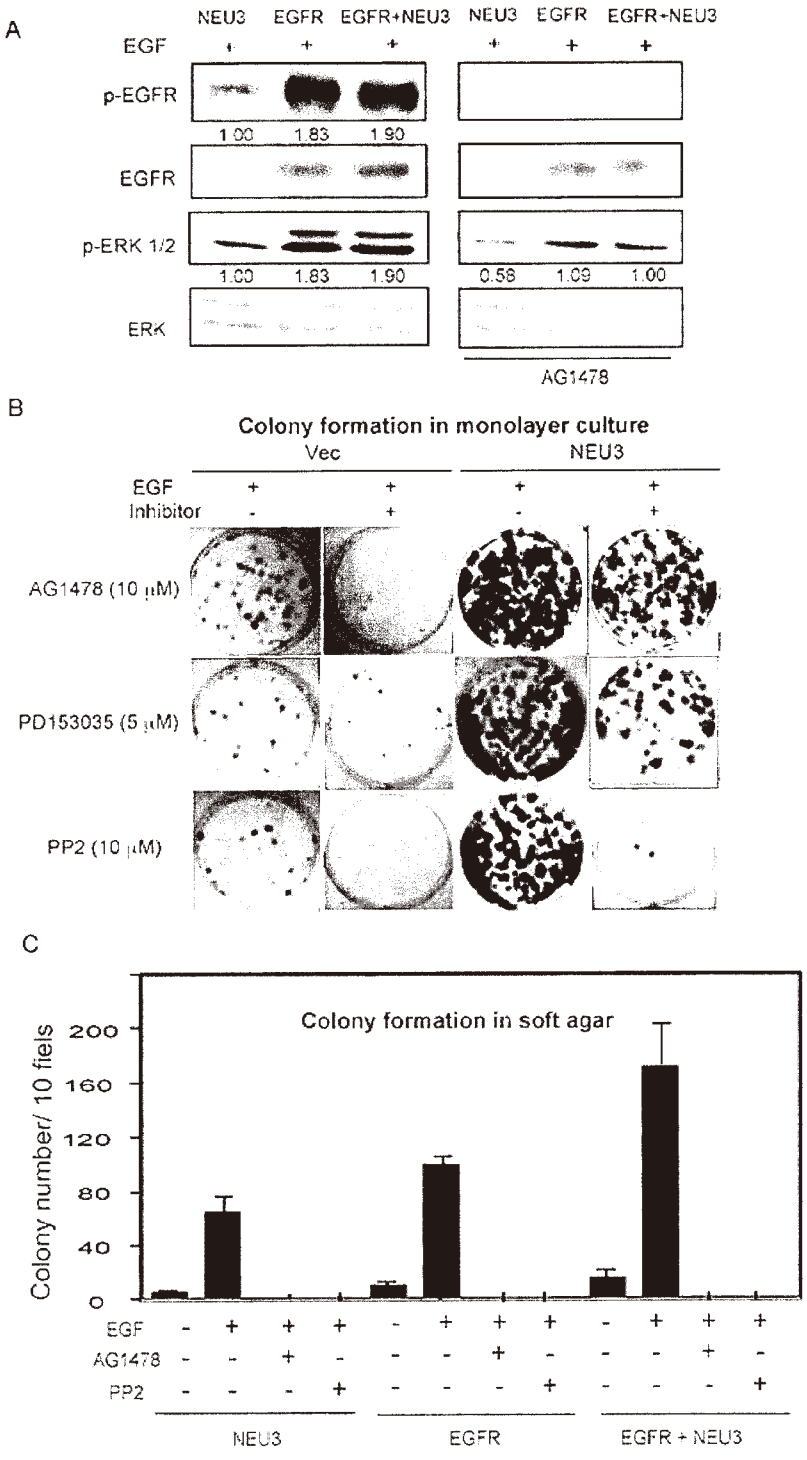

Fig 5. Suppression of colony formation and anchorage-independent growth by inhibitors. (A) Phosphorylation of EGFR and ERK1/2 was suppressed by an EGFR inhibitor, AG1478. Each value shown under the blot represents as a value relative to that in the vector controls. (B) Colony formation assays were performed in the presence of AG1478 (15 μM), PD153035 (5 μM) or an Src inhibitor, PP2 (10 μM). Representative images are shown. (C) Colony formation in soft agar was tested in the presence of AG1478 or PP2. Values are means with standard deviations obtained from three independent experiments (in graph)

doi:10.1371/journal.pone.0120578.g005

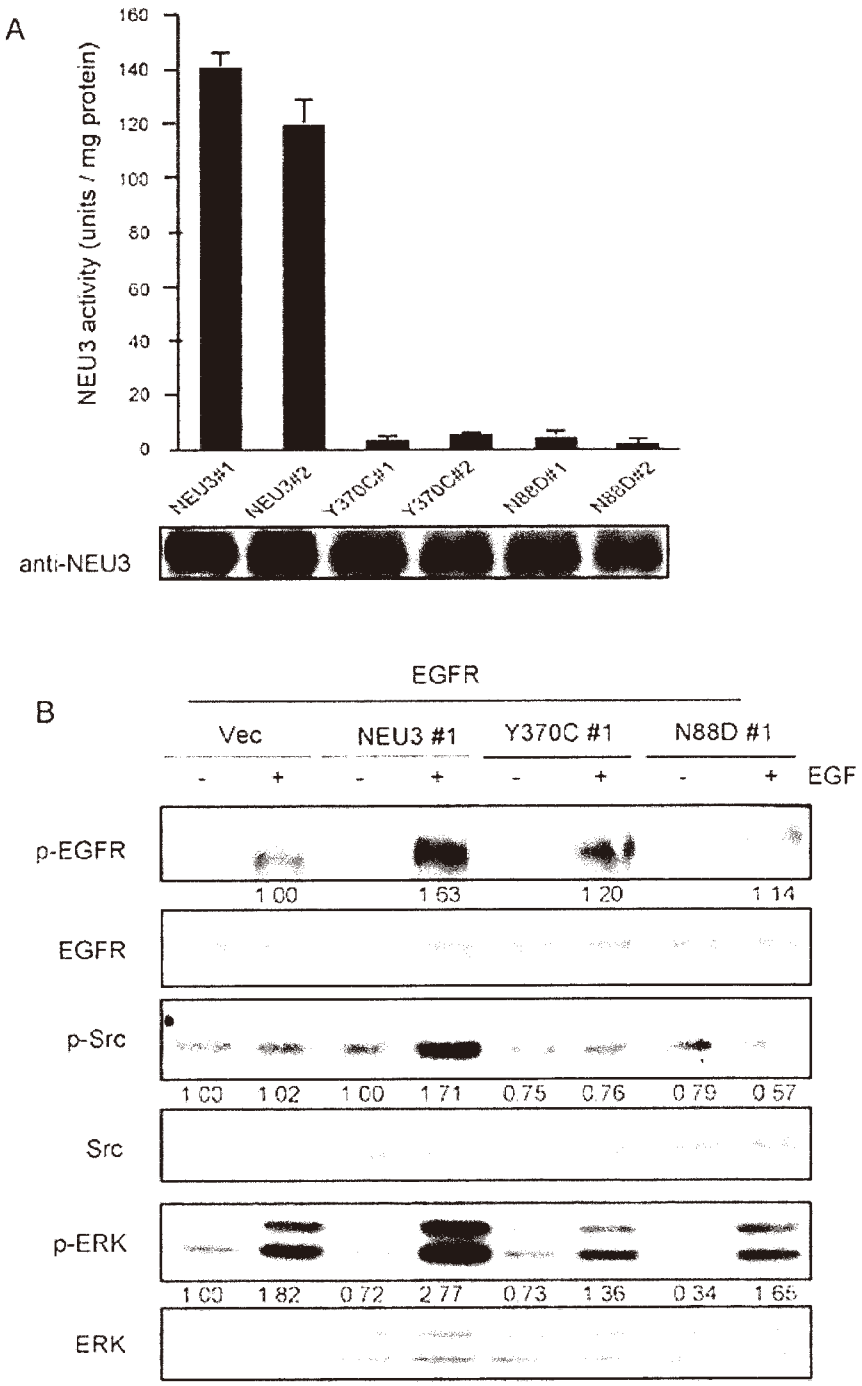

Fig 6. Requirement of NEU3 sialidase activity for enhanced phosphorylation of EGFR and Src. (A) The sialidase activities of NEU3 wild type and the mutant (Y370 or N88D) in the EGFR-overexpressing clones were assayed with ganglioside as a substrate in independent experiments performed in triplicate (mean ±SD). (B) The phosphorylation levels of EGFR, Src and ERK1/2 in the NEU3 wild and mutant clones in EGFR-cells were measured by western blotting using the respective antibodies. Each value shown under the blot represents as a value relative to that in the vector controls.

doi:10.1371/journal.pone.0120578.g006

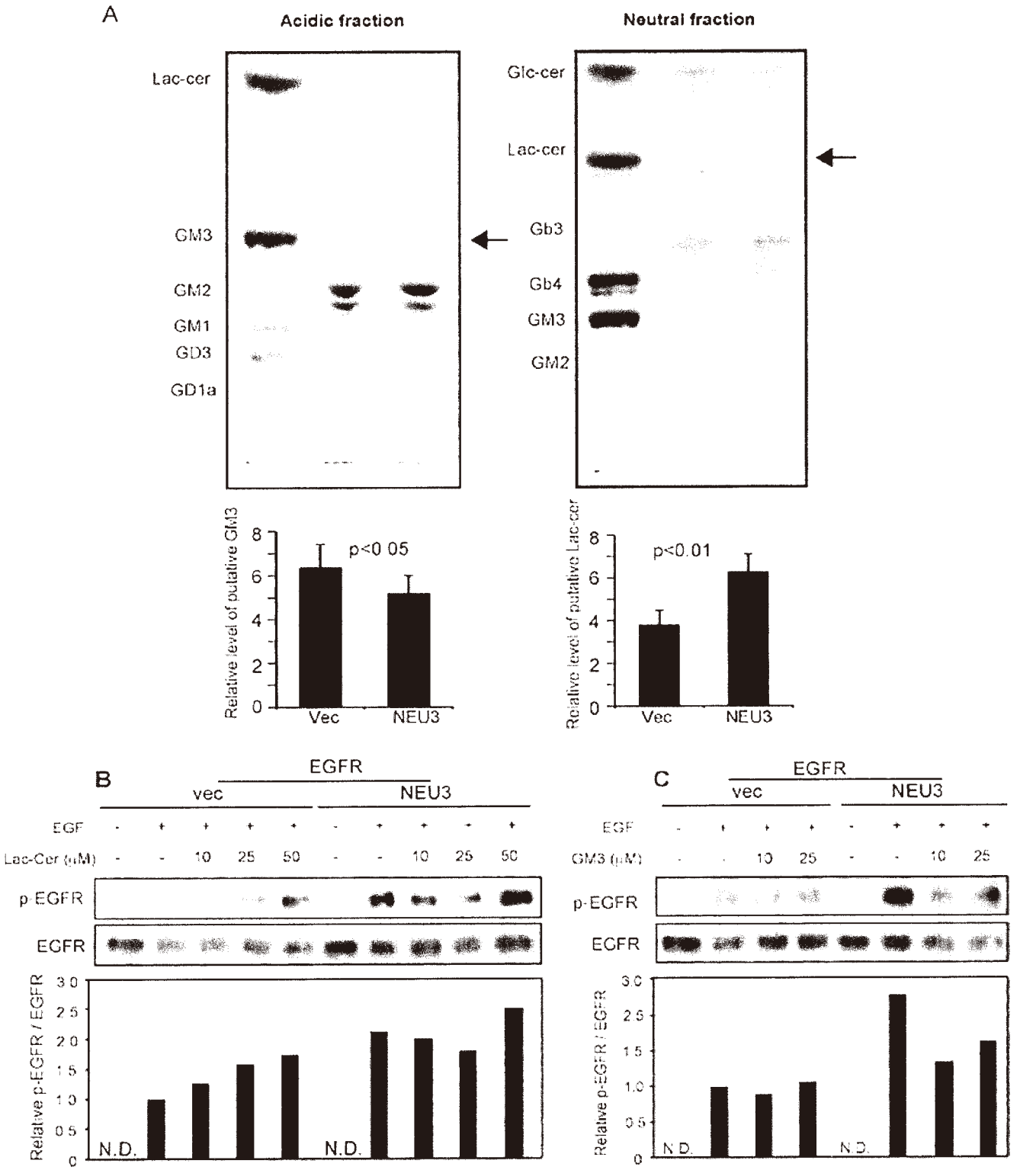
A
Acidic fraction
Neutral fraction
Lac-cer
GM3
GM2
GM1
GD3
GD1a
Glc-cer
Lac-cer
Gb3
Gb4
GM3
GM2
Relative level of putative GM3
p<0 05
Vec
NEU3
Relative level of putative Lac-cer
p<0.01
Vec
NEU3
B
EGFR
vec
NEU3
EGF
Lac-Cer (μM)
p-EGFR
EGFR
Relative p-EGFR / EGFR
N.D.
N.D.
C
EGFR
vec
NEU3
EGF
GM3 (μM)
p-EGFR
EGFR
Relative p-EGFR / EGFR
N.D.
N.D.

Fig 7. Alteration of glycolipids as a result of NEU3 catalytic reaction. Glycolipid changes due to NEU3 transfection were analyzed by thin- layer chromatography (A) in acidic (left panel) and neutral (right panel) fractions, and the relative changes in putative GM3 and Lac-cer were quantified in independent experiments performed in triplicate, as shown in the graphs below. (B, C) The effects of exogenously added Lac-cer (B) and GM3 (C) on EGFR phosphorylation in EGFR- and EGFR/NEU3-NIH-3T3 cells. Results are representative of two independent experiments. The values for phosphor-EGFR/EGFR relative to those for the vector controls with EGF are shown in the lower graphs.

doi:10.1371/journal.pone.0120578.g007

The NEU3-mediated effects were dependent on the sialidase catalytic reaction, with the putative product Lac-cer possibly affecting the EGFR phosphorylation, as shown in the experiments with exogenously administered Lac-cer. On the other hand, in terms of the studies of EGFR regulation by GM3 to date, the evidence demonstrates GM3-mediated inhibition of EGFR phosphorylation by interaction of GM3 with N-glycan in the ectodomain of EGFR through carbohydrate- to -carbohydrate interactions [28–30], but there is a report showing the low binding ability of Lac-cer to the ectodomain [33]. We do not currently know whether glycolipids such as Lac-cer generated by the NEU3 reaction interact directly with EGFR. In contrast to the ectodomain inhibiting EGFR phosphorylation, the intracellular juxtamembrane region has been described as acting as an activation domain [34, 35]. Therefore, it is possible that Lac-cer interacts with this region, although the connection of Lac-cer, located in the external leaflet of the bilayer, with Src and the domain of EGFR, located in a cytoplasmic site of the membrane, is unclear. Alternatively, it is feasible that NEU3 could participate in the regulation of EGFR/Src signaling in the glycosphingolipid- enriched membrane microdomains, because of evidence for these three molecules being located in microdomains such as caveolae [20, 36].

In conclusion, the overexpression of NEU3 could cause the constitutive activation of EGFR together with Src activation in the presence of EGF, and subsequently potentiation of the tumorigenicity of cancer cells. This is in good agreement with our previous observations on NEU3 transgenic mice showing an involvement of NEU3 in colon carcinogenesis in terms of an increase in azoxymethane- induced aberrant crypt foci together with enhanced phosphorylation of EGFR in the colon mucosa [13], although some other such as Wnt-related molecules should also confer the tumorigenic potential in the case of colon cancer [37]. Furthermore, NEU3- dependent ERK activation would bring about NEU3 transcriptional activation, leading to positive feedback activation of EGFR signaling, because of ERK signaling elevating sp1 and sp3 transcription factor expression, which is responsible for NEU3 transcription [10]. To prevent the potentiation of tumorigenicity, suppression of the up-regulated NEU3 in cancer is particularly important. Thus, NEU3 may be a potential target for cancer therapy as a molecule upstream of the EGFR/Src pathway, since the therapeutic efficacies of inhibitors for EGFR and Src have not been so encouraging despite many clinical trials for current anticancer therapies.

Acknowledgments

We appreciate Dr. M Shibuya (Institute of Medical Science, University of Tokyo) for his generous gift for pEGFR. We are also grateful to Mr. T Wada (Tohoku Pharmaceutical University) for his valuable technical assistance. This study was supported in part by Grants-in-Aid for Scientific Research on Innovative Areas (No. 23110002) from the Ministry of Education, Culture, Sports, Science and Technology of Japan.

Author Contributions

Conceived and designed the experiments: K. Yamamoto KT TM. Performed the experiments: K. Yamamoto KT KS SM. Analyzed the data: K. Yamamoto KT TM. Contributed reagents/materials/analysis tools: K. Yamaguchi. Wrote the paper: TM. Helpful discussion: MH K. Yamaguchi HS.

References

1. Lau KS, Dennis JW. N-Glycans in cancer progression. Glycobiology. 2008; 18:750–760. doi: 10.1093/glycob/cwn071 PMID: 18701722
2. Hakomori SI. Glycosynaptic microdomains controlling tumor cell phenotype through alteration of cell growth, adhesion, and motility. FEBS Lett. 2010; 584:1901–1906. doi: 10.1016/j.febslet.2009.10.065 PMID: 19874824
3. Miyagi T, Yamaguchi K. Mammalian sialidases: physiological and pathological roles in cellular functions. Glycobiology. 2012; 22:880–896. doi: 10.1093/glycob/cws057 PMID: 22377912
4. Miyagi T, Wada T, Yamaguchi K, Hata K, Shiozaki K. Plasma membrane- associated sialidase as a crucial regulator of transmembrane signaling. J Biochem. 2008; 144, 279–285. doi: 10.1093/jb/mvn089 PMID: 18632803
5. Miyagi T, Takahashi K, Hata K, Shiozaki K, Yamaguchi K. Sialidase significance for cancer progression. Glycoconjugate. 2012; J 29:567–577. doi: 10.1007/s10719-012-9394-1 PMID: 22644327
6. Kakugawa Y, Wada T, Yamaguchi K, Yamanami H, Ouchi K, Sato I, et al. Up-regulation of plasma membrane-associated ganglioside sialidase (Neu3) in human colon cancer and its involvement in apoptosis suppression. Proc Natl Acad Sci USA. 2002; 99:10718–10723. PMID: 12149448
7. Ueno S, Saito S, Wada T, Yamaguchi K, Satoh M, Arai Y, et al. Plasma membrane-associated sialidase is up-regulated in renal cell carcinoma and promotes interleukin-6-induced apoptosis suppression and cell motility. J Biol Chem. 2006; 281:7756–7764. PMID: 16428383
8. Kawamura S, Sato I, Wada T, Yamaguchi K, Li Y, Li D, et al. Plasma membrane-associated sialidase (NEU3) regulates progression of prostate cancer to androgen-independent growth through modulation of androgen receptor signaling. Cell Death Differ. 2012; 19:170–179. doi: 10.1038/cdd.2011.83 PMID: 21681193
9. Nomura H, Tamada Y, Miyagi T, Suzuki A, Taira M, Suzuki N, et al. Expression of NEU3 (plasma membrane-associated sialidase) in clear cell adenocarcinoma of the ovary: its relationship with T factor of pTNM classification. Oncol Res 2006; 16: 289–297. PMID: 17476974
10. Yamaguchi K., Koseki K., Shiozaki M., Shimada Y., Wada T, et al. Regulation of plasma membrane-associated sialidase NEU3 gene by Sp1/Sp3 transcription factors. Biochem, J. 2010; 430: 107–117. doi: 10.1042/BJ20100350 PMID: 20518744
11. Wada T, Hata K, Yamaguchi K, Shiozaki K, Koseki K, Moriya S, et al. A crucial role of plasma membrane-associated sialidase in the survival of human cancer cells. Oncogene. 2008; 26:2483–2490.
12. Kato K, Shiga K, Yamaguchi K, Hata K, Kobayashi T, Miyazaki K, et al. Plasma membrane-associated sialidase (NEU3) differentially regulates integrin-mediated cell proliferation through laminin- and fibronectin-derived signalling. Biochem J. 2006; 394: 647–56. PMID: 16241905
13. Shiozaki K, Yamaguchi K, Sato I, Miyagi T. Plasma membrane-associated sialidase (NEU3) promotes formation of colonic aberrant crypt foci in azoxymethane-treated transgenic mice. Cancer Sci. 2009; 100:588–594. doi: 10.1111/j.1349-7006.2008.01080.x PMID: 19215228
14. Yamaguchi K, Shiozaki K, Moriya S, Koseki K, Wada T, Tateno H, et al. Reduced susceptibility to colitis-associated colon carcinogenesis in mice lacking plasma membrane-associated sialidase. PLoS One. 2012; 7:e41132 doi: 10.1371/journal.pone.0041132 PMID: 22815940
15. Baselga J1, Arteaga CL. Critical update and emerging trends in epidermal growth factor receptor targeting in cancer. J Clin Oncol. 2005; 23:2445–59 PMID: 15753456
16. Ishizawar R, Parsons S. c-Src and cooperating partners in human cancer. Cancer Cell. 2004; 6, 209–214 PMID: 15380511
17. Wada T., Yoshikawa Y., Tokuyama S., Kuwahara M., Akita H., Miyagi T. Cloning, expression and chromosomal mapping of a human ganglioside sialidase. Biochem Biophys Res Commun. 1999; 261, 21–27. PMID: 10405317
18. Kitamura T, Koshino Y, Shibata F, Oki T, Nakajima H, Nosaka T, et al. Retrovirus-mediated gene transfer and expression cloning: powerful tools in functional genomics. Exp Hematol. 2003; 31: 1007–1014. PMID: 14585362
19. Wang Y, Yamaguchi K, Shimada Y, Zhao X, Miyagi T. Site-directed mutagenesis of human membrane-associated ganglioside sialidase: identification of amino-acid residues contributing to substrate specificity. Eur J Biochem. 2001; 268: 2201–2208. PMID: 11298736
20. Wang Y, Yamaguchi K, Wada T, Hata K, Zhao X, Fujimoto T, et al. A close association of the ganglioside-specific sialidase Neu3 with caveolin in membrane microdomains. J Biol Chem. 2002; 277:26252–26259. PMID: 12011038

21. Kato T, Wang Y, Yamaguchi K, Milner CM, Shineha R, Satomi S, et al. Overexpression of lysosomal-type sialidase leads to suppression of metastasis associated with reversion of malignant phenotype in murine B16 melanoma cells. Int J Cancer. 2001; 92:797–804. PMID: 11351298

22. Shih C, Padhy LC, Murray M, Weinberg RA. Transforming genes of carcinomas and neuroblastomas introduced into mouse fibroblasts. Nature. 1981; 290: 261–264. PMID: 7207618

23. Velu TJ1, Beguinot L, Vass WC, Willingham MC, Merlino GT, Pastan I, et al. Epidermal-growth-factor-dependent transformation by a human EGF receptor proto-oncogene. Science. 1987; 238:1408–1410. PMID: 3500513

24. Tsutsumi O, Kurachi H, Oka T. A physiological role of epidermal growth factor in male reproductive function. Science. 1986; 233: 975–977. PMID: 3090686

25. Tice DA, Biscardi JS, Nickles AL, Parsons SJ. Mechanism of biological synergy between cellular Src and epidermal growth factor receptor. Proc Natl Acad Sci U S A. 1999; 96:1415–1420. PMID: 9990038

26. Parsons SJ, Parsons JT. Src family kinases, key regulators of signal transduction. Oncogene. 2004; 23; 7906–7909. PMID: 15489908

27. Albohy A, Li MD, Zheng RB, Zou C, Cairo CW. Insight into substrate recognition and catalysis by the human neuraminidase 3 (NEU3) through molecular modeling and site-directed mutagenesis. Glycobiology. 2010; 20:1127–1138. doi: 10.1093/glycob/cwq077 PMID: 20511247

28. Yoon SJ, Nakayama K, Hikita T, Handa K, Hakomori SI. Epidermal growth factor receptor tyrosine kinase is modulated by GM3 interaction with N-linked GlcNAc termini of the receptor. Proc Natl Acad Sci U S A. 2006; 103:18987–18991. PMID: 17142315

29. Kawashima N1, Yoon SJ, Itoh K, Nakayama K. Tyrosine kinase activity of epidermal growth factor receptor is regulated by GM3 binding through carbohydrate to carbohydrate interactions. J Biol Chem. 2009; 284:6147–6155. doi: 10.1074/jbc.M808171200 PMID: 19124464

30. Coskun Ü, Grzybek M, Drechsel D, Simons K. Regulation of human EGF receptor by lipids. Proc Natl Acad Sci U S A. 2011; 108:9044–8. doi: 10.1073/pnas.1105666108 PMID: 21571640

31. Greulich H, Chen TH, Feng W, Jänne PA, Alvarez JV, Zappaterra M, et al. Oncogenic transformation by inhibitor-sensitive and-resistant EGFR mutants. PLoS Med. 2005; 2:e313. PMID: 16187797

32. Chung BM, Dimri M, George M, Reddi AL, Chen G, et al. The role of cooperativity with Src in oncogenic transformation mediated by non-small cell lung cancer-associated EGF receptor mutants. Oncogene. 2009; 28:1821–1832. doi: 10.1038/onc.2009.31 PMID: 19305428

33. Miljan EA, Meuillet EJ, Mania-Farnell B, George D, Yamamoto H, Simon HG, et al. Interaction of the extracellular domain of the epidermal growth factor receptor with gangliosides. J Biol Chem. 2002; 277:10108–10113. PMID: 11796728

34. Red Brewer M, Choi SH, Alvarado D, Moravcevic K, Pozzi A, Lemmon MA, et al. The juxtamembrane region of the EGF receptor functions as an activation domain. Mol Cell. 2009; 34:641–651. doi: 10.1016/j.molcel.2009.04.034 PMID: 19560417

35. Jura N, Endres NF, Engel K, Deindl S, Das R, Lamers MH, et al. Mechanism for activation of the EGF receptor catalytic domain by the juxtamembrane segment. Cell. 2009; 137:1293–1307. doi: 10.1016/j.cell.2009.04.025 PMID: 19563760

36. Wang XQ, Sun P, Paller AS. Ganglioside induces caveolin-1 redistribution and interaction with the epidermal growth factor receptor. J Biol Chem. 2002; 277: 47028–47034. PMID: 12354760

37. Clevers H. Wnt/beta-catenin signaling in development and disease. Cell. 2006; 127: 469–480. PMID: 17081971

The FASEB Journal • Research Communication

Phosphatidic acid-mediated activation and translocation to the cell surface of sialidase NEU3, promoting signaling for cell migration

Kazuhiro Shiozaki,* Kohta Takahashi,† Masahiro Hosono,‡ Kazunori Yamaguchi,§ Keiko Hata,† Momo Shiozaki,§ Rosaria Bassi,¶ Alessandro Prinetti,¶ Sandro Sonnino,¶ Kazuo Nitta,‡ and Taeko Miyagi†,[1]

*Faculty of Fisheries and The United Graduate School of Agricultural Science, Kagoshima University, Kagoshima, Kagoshima, Japan; †Division of Cancer Glycosylation Research and ‡Division of Cell Recognition Study, Tohoku Pharmaceutical University, Sendai, Miyagi, Japan; §Miyagi Cancer Center Research Institute, Natori, Miyagi, Japan; and ¶Department of Medical Biotechnology and Translational Medicine, University of Milan, Segrate, Milan, Italy

ABSTRACT **The plasma membrane-associated sialidase NEU3 plays crucial roles in regulation of transmembrane signaling, and its aberrant up-regulation in various cancers contributes to malignancy. However, it remains uncertain how NEU3 is naturally activated and locates to plasma membranes, because of its Triton X-100 requirement for the sialidase activity *in vitro* and its often changing subcellular location. Among phospholipids examined, we demonstrate that phosphatidic acid (PA) elevates its sialidase activity 4 to 5 times at 50 μM *in vitro* at neutral pH and promotes translocation to the cell surface and cell migration through Ras-signaling in HeLa and COS-1 cells. NEU3 was found to interact selectively with PA as assessed by phospholipid array, liposome coprecipitation, and ELISA assays and to colocalize with phospholipase D (PLD) 1 in response to epidermal growth factor (EGF) or serum stimulation. Studies using tagged NEU3 fragments with point mutations identified PA- and calmodulin (CaM)-binding sites around the N terminus and confirmed its participation in translocation and catalytic activity. EGF induced PLD1 activation concomitantly with enhanced NEU3 translocation to the cell surface, as assessed by confocal microscopy. These results suggest that interactions of NEU3 with PA produced by PLD1 are important for regulation of transmembrane signaling, this aberrant acceleration probably promoting malignancy in cancers.—Shiozaki, K., Takahashi, K., Hosono, M., Yamaguchi, K., Hata, K., Shiozaki, M., Bassi, R., Prinetti, A., Sonnino, S., Nitta, K., Miyagi, T. Phosphatidic acid-mediated activation and translocation to the cell surface of sialidase NEU3, promoting signaling for cell migration. *FASEB J.* 29, 2099–2111 (2015). www.fasebj.org**

Key Words: sialic acid · phospholipids · gangliosides · PLD1 · cancer

MAMMALIAN SIALIDASES ARE THE key enzymes for control of cellular sialic acid contents, through catalyzing the initial step in degradation of glycoproteins and glycolipids. There are 4 types, designated as NEU1, NEU2, NEU3, and NEU4, according to their subcellular localization and enzymatic properties (1). Among the forms, the human sialidase NEU3 is mainly located at the plasma membranes and hydrolizes almost specifically gangliosides and therefore plays crucial roles as a transmembrane signaling modulator (2). We previously demonstrated that NEU3 is up-regulated in tumor as compared with the adjacent nontumor tissues in colon, renal, prostate, and ovary cancers (3–6), possibly regulated by Sp1/Sp3 transcriptional factors (7). NEU3 enhances cancer cell survival (3, 8), cell migration (5, 9), and attachment (10). NEU3 transgenic mice also provided evidence of involvement of this sialidase in carcinogenesis in the form of increase in azoxymethane-induced aberrant crypt foci (11), whereas Neu3 knockout mice exhibited reduction of tumor incidence in a colitis-associated colon carcinogenesis model (12). In certain cells, aberrant expression of NEU3 has been shown to disturb transmembrane signaling and activate epidermal growth factor receptor (EGFR) signaling, accompanied with ERK and AKT activation (8, 11). In neural cells, NEU3 enhances cell differentiation (13, 14) and activates Trk-signaling (15).

Although NEU3 has been considered as a crucial signaling regulator due to its modulation of gangliosides coexisting at the cell surfaces, mechanisms underlying NEU3 activation are not fully understood. Chemical detergents, such as Triton X-100, are necessary to detect its

Abbreviations: BSA, bovine serum albumin; CaM, calmodulin; DAG, diacylglycerol; EGF, epidermal growth factor; EGFR, epidermal growth factor receptor; FBS, fetal bovine serum; GFP, green fluorescent protein; HA, hemagglutinin; HPTLC, high-performance thin-layer chromatography; HRP, horseradish peroxidase; Lac-Cer, lactosylceramide; *n*-BuOH, *n*-butyl alcohol; PA, phosphatidic acid; PBST, PBS containing 0.05% Tween 20; PC, phosphatidylcholine; PE,

(*continued on next page*)

[1] Correspondence: Tohoku Pharmaceutical University, 4-4-1, Komatsushima, Aoba-ku, Sendai, 981-8558, Japan. E-mail: tmiyagi@tohoku-pharm.ac.jp

doi: 10.1096/fj.14-262543

This article includes supplemental data. Please visit *http://www.fasebj.org* to obtain this information.

sialidase activity *in vitro* (16, 17), because natural activators for NEU3 have not been identified. NEU3 possesses a long hydrophobic stretch in the molecule, but is not always detected on cell surfaces, unlike mouse and bovine NEU3 (1), often changing its subcellular localization to plasma membranes through the action of specific stimuli (9). In this study, we aimed to identify any NEU3 natural activator required for catalytic activity and to clarify regulation mechanisms for translocation to the cell surface. First, we paid attention to various phospholipids as potential activators, because of their detergent properties and recent increasing recognition as important signaling lipids regulating cell growth, membrane trafficking, and cytoskeletal reorganization (18). Among the phospholipids examined, we discovered PA to be a possible activator for the sialidase at neutral pH and a regulator of its translocation to and functions at plasma membranes. Here we also present an evidence of the possible mechanism for NEU3 activation and translocation with PLD1 selective involvement.

MATERIALS AND METHODS

Cell culture and reagents

COS-1 cells were obtained from the RIKEN Cell Bank (Tsukuba, Japan), and HeLa cells from the Cell Resource Center for Biomedical Research, Tohoku University (Sendai, Japan). All were maintained in DMEM supplemented with 10% fetal bovine serum (FBS) (Sigma-Aldrich, St. Louis, MO, USA) at 37°C in a humidified atmosphere containing 5% CO_2. Phospholipids [phosphatidylinositol (PI), phosphatidylserine (PS), phosphatidylethanolamine (PE), PA, phosphatidylcholine (PC), lyso-PI, lyso-PC, lyso-PA, sphingomyelin, ceramide, PI 3-phosphate, PI 4-phosphate, PI 5-phosphate, PI 3,4-bisphosphate, PI 4,5-bisphosphate, PI 3,5-bisphosphate, PI 3,4,5-triphosphate, and diacylglycerol (DAG)] were purchased from Sigma-Aldrich. Dioctanoyl-PA and DAG kinase inhibitor (R59949) were also from Sigma-Aldrich, and selective inhibitors of PLD1 (CAY10593) and PLD2 (CAY10594) were from Cayman Chemicals (Ann Arbor, MI, USA).

Plasmid, siRNA, and transfection

Hemagglutinin (HA)-tagged NEU3 cDNA and its fragments or point mutants (described below) were inserted into pcDNA3.1 plasmid (Invitrogen, Carlsbad,CA, USA). NEU3 siRNA was synthesized by Dharmacon Incorporated (Thermo Fisher Scientific, Waltham, MA, USA) as described elsewhere (8). Expression plasmids were transfected into cells using Effectene (Qiagen, Germantown, MD, USA) as recommended by the manufacture. siRNA was transfected using Lipofectamine RNAiMAX (Invitrogen). Efficacy of knockdown was evaluated by real-time PCR (Roche, Basel, Switzerland) according to the methods described in a previous publication (8). siRNAs for human PLD1 (M-009413) and PLD2 (M-005064) were from Dharmacon. PLD1 expression vector, pCGN-hPLD1b-HA, was kindly provided by Dr. Frohman MA (Stony Brook University, New York, NY, USA). As a plasma membrane marker, cDNA for Aequorea coerulescens GFP1-F (AcGFP1-F, Clontech, Mountain View, CA, USA) encoding farnesylation signal from c-Ha-Ras fused to EGFP was cotransfected used for immunofluorescent staining.

Sialidase activity

Sialidase activity was measured as described previously with or without 0.1% Triton X-100. Cell homogenates or purified FLAG-tagged NEU3 (19) were used for the measurement of sialidase activity toward GM3 at pH4.6 in 50 mM sodium acetate buffer and 6.5 in 50 mM PIPES buffer or 2-(*N*-morpholino) ethanesulfonic acid buffer. Released sialic acids were determined by HPLC with fluorescence derivation using malononitrile as described elsewhere (6, 8). One unit of activity was defined as the amount of enzyme that cleaved 1 nmol sialic acid from the substrates in 1 hour. Protein concentrations were determined by dye-binding assay (Bio-Rad, Hercules, CA, USA) for the crude enzymes and by quantification of electrophoresis bands with standard bovine serum albumin (BSA) for the purified sialidase. To investigate the effects of phospholipids on sialidase activity, indicated amounts of phospholipid were dried under nitrogen gas in the glass test tubes, and then reaction mixtures without Triton X-100 were prepared in the same tubes. A mixture without phospholipid preparation was used as a control.

Phospholipid spot arrays

Recombinant FLAG-tagged NEU3 was used to investigate NEU3 binding to phospholipids. Recombinant NEU3 (20 ng) was purified from NEU3-overexpressing HEK293T cells as described previously (19). PIP strips (Echelon Bioscience, Salt Lake City, UT, USA) were blocked with 3% BSA (fatty acid free) in PBS containing 0.05% Tween 20 (PBST) for 60 minutes at room temperature and incubate with NEU3 in 3% BSA/0.6% heptylthioglucoside/0.05% Tween 20 for 60 minutes at room temperature. The strips were then washed 3 times with PBST for 10 min, incubated with anti-FLAG antibody (clone M2; Sigma-Aldrich) overnight at 4°C, washed with PBST and incubated with horseradish peroxidase (HRP)-conjugated anti-mouse IgG_1. Lipid-bound NEU3 was detected by chemiluminescence with ECL reagent (GE Healthcare, Little Chalfont, United Kingdom).

Liposome-binding assays

Phosphatidylcholine and PA were dissolved in chloroform/methanol (1:2). Preparation of liposomes was conducted as described elsewhere (20). In brief, 250 μg aliquots of total mixtures of phospholipids were dried under N2 gas in glass tubes, suspended in 500 μl PBS, mixed for 1 minute and sonicated for 1 minute, repeated 3 times, then frozen and thawed 3 times with liquid nitrogen. The prepared phospholipid mixtures were used as liposomes. Recombinant FLAG-tagged NEU3 was incubated with 500 μl liposomes for 60 minutes at room temperature, and centrifuged at 100,000 *g* for 30 minutes. The supernatants (liposome unbound fraction) and the precipitates (liposome bound fraction) were separated and NEU3 amounts in each fraction were analyzed by Western blotting.

Indirect immunofluorescence microscopy

Cells grown on coverslips were transfected with pcDNA3.1 NEU3-HA or -FLAG plasmid, or pCGN-hPLD1-HA plasmid and used for the indirect immunofluorescence microscopic analysis as described previously (9). Cells were fixed with 4%

(*continued from previous page*)
phosphatidylethanolamine; PI, phosphatidylinositol; PLD, phospholipase D; PS, phosphatidylserine; PLD, phospholipase D; *t*-BuOH, *t*-butyl alcohol

paraformaldehyde in PBS for 15 minutes at 37°C, permeabilized with 0.1% Triton X-100 in PBS, blocked with 1% BSA for 30 min at 37°C, and then incubated with primary antibodies for 60 min at 37°C. Primary antibodies used were anti-HA (clone 3F10; Roche), anti-FLAG (M2, Sigma-Aldrich), anti-PLD (clone SKB2; Upstate Biotechnology, Lake Placid, NY, USA), anti-PLD1 (Cell Signaling Technology, Danvers, MA, USA) and anti-phospho-PLD1 (Thr147; Cell Signaling). Cells were then incubated with the Alexa Fluor 488-conjugated anti-rat IgG, Alexa Fluor 594-conjugated anti-mouse IgG, or Alexa Fluor 594 anti-rat IgG and phalloidin-tetramethylrhodamine β-isothiocyanate (Sigma-Aldrich) for 60 minutes at room temperature. Preparations were mounted on glass slides using PermaFluor (Shandon Immunon, Thermo Fisher Scientific, Cheshire, United Kingdom) and examined by confocal microscopy (LSM5; Carl-Zeiss, Oberkochen, Germany). Translocated cells were counted at least 5 times from 5 randomly chosen fields.

Cell motility assays

Cell motility assays were carried out with cell culture inserts (BD Biosciences, San Jose, CA, USA). At 24 hours after transfection, cells were seeded at 2.5×10^5/well onto their upper surface membranes and the upper chambers were filled with medium containing 200 μM PA. After 24 hours, the cells were fixed and stained with Wright-Giemsa solution and all those present on the lower surfaces of the membranes were counted under a microscope.

Western blotting

Antibodies for phospho-ERK (Thr202/Tyr204), ERK, and phospho-paxillin (Tyr118) were purchased from Cell Signaling Technology. Antibodies for phospho-EGFR (Tyr845), EGFR, and paxillin (H-114) were from Santa Cruz Biotechnology (Santa Cruz, CA, USA). Western blotting was carried out as described elsewhere (8). To assess *in vitro* Ras activation, affinity precipitation assays for active (GTP-bound form) Ras were performed using Raf-1 RBD-agarose (Upstate Biotechnology) according to the manufacturer's recommendations. Bound Ras-GTP protein was resolved by SDS-PAGE followed by immunoblotting with anti-Ras antibodies.

Construction of green fluorescent protein- and GST-fusion NEU3 fragments

To obtain green fluorescent protein (GFP)-and GST-fusion NEU3 fragments, PCR was carried out using NEU3 ORF as template. The primers for NEU3 fragments, #21 (amino acid 2–130), #24 (amino acid 131–224), #27 (amino acid 225–340), #30 (amino acid 341–427), #33 (amino acid 2–224), #36 (amino acid 131–340), and #41 (amino acid 256–428) are listed in Supplemental Table 1. PCR products were digested with *Sal*I or *Eco*RI, and inserted into pBluescript. After confirming the sequence, products were inserted into pEGFP-C1 (Clontech) or pGEX-6P-1 vector (GE Healthcare). To prepare recombinant GST-tagged NEU3 fragments, expression plasmids were transfected into BL21 *Escherichia coli*. Fusion protein production was induced by adding 0.1 mM isopropyl-β-D-thiogalactoside for 5 hours at 20°C, and bacteria were then lysed with 1% Triton X-100/0.1% deoxycholic acid/1 mM DTT/PBS. Fusion proteins were purified with glutathione-Sepharose 4B (GE Healthcare) as recommended by the supplier.

Estimation of phospholipid binding using ELISA

To estimate the interaction between GST-tagged recombinant proteins and phospholipids, ELISA assays were carried out. First, indicated amounts of phospholipid dissolved in chloroform/methanol were fixed in 96-well plates and blocked with 5% BSA in PBS. Recombinant proteins were applied to each well, and incubated for 45 minutes at room temperature. After washing with PBS/0.05% Tween-20, wells were incubated with anti-GST polyclonal antibody (MBL, Nagoya, Japan) for 60 minutes at room temperature. Wells were washed 8 times with PBS/Tween 20, and then incubated with HRP-conjugated anti-rabbit IgG antibodies. Lipid-bound proteins were estimated with the TMB liquid substrate system (Sigma-Aldrich).

Construction of NEU3 mutants

To construct mutant NEU3 or NEU3 fragments, PCR was carried out using pBluescript-NEU3 or fragment #21 as the templates. Mutant primers for H84E, R85E, and K96E mutants are shown in Supplemental Table 2. PCR products were digested with *Eco*RI, and inserted into the pcDNA3.1 vector.

CaM-binding assays of NEU3 protein

NEU3 or its mutant (H84E) cDNA was transfected into HeLa cells, and after 48 hours they were lysed in cold lysis buffer [50 mM HEPES (pH 7.5), 150 mM NaCl, 1% Triton X-100, 1 mM DTT, 7.5 μg/ml aprotinin, 10 μg/ml leupeptin, and 2 mM PMSF]. After clarification by centrifugation (12,000 *g* for 15 minutes), the cellular lysates were added to 60 μl CaM-agarose (Sigma-Aldrich), with 2 mM $CaCl_2$ or 2 mM EGTA and incubated for 2 hours at 4°C. The mixtures were then washed 3 times with the lysis buffer containing 2 mM $CaCl_2$ or 2 mM EGTA. Pellets obtained by centrifugation were subjected to Western blotting as the CaM-bound fractions.

Sialidase activity in living cells

Radioactive GM3 containing *erythro*-C18-sphingosine, isotopically tritium-labeled at position 3, [3-^{3}H(*Sph18*)] GM3, was prepared previously (21) and used as a substrate for the assay (22). HeLa cells (70% confluence in 6 multiwells plate) were transfected with pCAGGS-NEU3 (8) or empty vector. After 36 hours, Mock- and NEU3-transfected cells were cultured with serum-free medium and incubated for 1 hour in the presence of 50 μM chloroquine. [3-^{3}H(*Sph18*)]GM3 (specific radioactivity, 2.3 Ci/mmole) was then administered at 2 μCi/ml (0.9 nmol/well) for 4 hours in the presence of 50 μM chloroquine. At the end of incubation, pulse medium was removed and cells were submitted or not (time 0) to 15–30 minutes chase with or without 200 μM dioctanoyl-PA. After washing with PBS, cells were immediately subjected to total lipid extraction. High-performance thin-layer chromatography (HPTLC) was performed using chloroform/methanol/water (55/20/3 by volume) as solvent system. [^{3}H]Sphingolipids were identified and quantified by radiochromatoscanning (Digital Autoradiography BIOESPACE; Nesles la Vallee, France).

Statistical analysis

Results are expressed as means ± SD. All values were compared using Student's *t* test or Welch's *t* test.

RESULTS

PA stimulates NEU3 sialidase activity

To search for the natural activators of NEU3, we examined various phospholipids because they possess detergent

properties and are known to activate several proteins (18). Because the pH curve of the NEU3 sialidase activity is biphasic, with a first peak at about pH4.6 and a small second peak at pH 6.5, as shown in our previous study (8), phospholipids were first evaluated at these 2 pH values. In the assays, purified NEU3 recombinant proteins obtained from NEU3-transfected HEK293T as reported elsewhere (19) were used to remove the effect of endogenous phospholipids. Several phospholipids (PI, PS, PE, PA, PC, lyso-PI, lyso-PC, lyso-PA, sphingomyelin, ceramide, PI 3-phosphate, PI 4-phosphate, PI 5-phosphate, PI 3,4-bisphosphate, PI 4,5-bisphosphate, PI 3,5-bisphosphate, PI 3,4,5-triphosphate, and DAG) were tested for influence on NEU3 sialidase activity. As a result, PI, PS, and PA were found to activate NEU3 at pH 4.6 with a statistical significance (**Fig. 1*A***, left), although other phospholipids hardly showed any significant effects that the activity changes were less than one and half times of the controls at either pH 4.5 or 6.5. On the other hand, interestingly, at pH 6.5, only PA showed a marked increase in NEU3 sialidase activity (Fig. 1*A*, middle) and 4 to 5 times at 50 μM (Fig. 1*A*, right). Because NEU3 is considered as a sialidase associated with plasma membranes where the pH was almost neutral, we mainly focused on PA in the following experiments.

To clarify the mechanism of the activation induced by PA, interactions were investigated using phospholipid spot array and liposome coprecipitation assays using purified recombinant NEU3 enzyme. Evaluation of lipid-bound NEU3 on spot arrays indicated that PA clearly interacted with NEU3, whereas other phospholipids showed no or only slight interaction (Fig. 1*B*). This was confirmed in the liposome coprecipitation assays. Liposomes consisting of PC and PA (1:1) showed coprecipitation with NEU3, whereas PC alone did not (Fig. 1*C*). These results suggest that PA enhanced NEU3 sialidase activity, possibly through interaction with the enzyme itself. In addition to the *in vitro* sialidase activity assays, we evaluated the PA effects on sialidase activity using intact living HeLa cells. When transfected cells were administered with tritium-labeled GM3 {[3-^{3}H(Sph18)] GM3} as substrate (21, 22) and PA in the presence of chloroquine, a condition under which the activity of the lysosomal compartment is strongly reduced, the radiolabeled lactosylceramide (Lac-Cer) product was significantly increased over 2 times in the PA-treated cells as shown by HPTLC and quantitatively in graph (Fig.1*D* and Supplemental Table 3), suggesting hydrolysis of GM3 by NEU3 translocated to the cell surface and affirming a possible role of PA in promotion of its sialidase activity even in intact living cells at a neutral pH.

PA enhances NEU3 translocation to the plasma membrane

It has been reported that phospholipids activate a phospholipid-bound enzyme and also change its subcellular localization (18). Our previous report presented evidence that NEU3 was translocated to plasma membranes in response to stimulation with serum or EGF, increasing the cell motility (9). The mechanism of this NEU3 translocation, however, was not clear, although EGF or serum stimulation is known to rapidly induce PA synthesis (23). When the localization of NEU3 was examined using NEU3-transfected HeLa cells with serum conditions (10% FBS) after serum depletion, NEU3 was found to colocalize with a plasma membrane marker, AcGFP1-F (**Fig. 2*A***), consistent with our previous results (9). To verify the possibility of regulation of NEU3 translocation, effects of exogenously administered PA were investigated. Under serum depletion conditions, NEU3 was hardly observed around plasma membranes in COS as well as HeLa cells, but on PA stimulation, NEU3 translocation to plasma membranes was gradually increased, to a maximum after about 15 minutes (Fig. 2*B*). When various amounts of PA were tested in HeLa cells, exogenous 200 μM PA was associated with the highest translocation (Fig. 2*C*). A similar phenomenon was observed in COS-1 cells, and the concentration seems to be nearly optimum at 100 to 200 μM in the cell level assays. Treatment with 0.5% of *n*-butyl alcohol (*n*-BuOH), known as a pan PLD inhibitor (24), significantly inhibited EGF-induced NEU3 translocation to plasma membrane at 5 min compared with 0.5% *t*-butyl alcohol (*t*-BuOH, used as a control) in HeLa cells (Fig. 2*D*), under which conditions PLD gene (PLD1 and PLD2) expression was not affected by NEU3 overexpression (95% and 89% of controls in mRNA level, respectively). It should be noted here that PC did not give any stimulation on the translocation at the same concentration as PA (data not shown).

Identification of a PA-binding site in the NEU3 molecule

Many enzymes, including Raf (25), SHP-1 (26), and mTOR (27), are known to bind to PA and also to be activated by PA (18). As shown in Figs. 1 and 2, our results suggested the possibility that interaction between NEU3 and PA might be involved in stimulation of the enzyme activity and also in translocation to the cell surface. We then investigated whether any PA-binding site exists in the NEU3 molecule. Although alignment of the NEU3 primary sequence using prediction programs did not reveal any apparent PA-binding regions, so-called phospholipid-binding motifs including PH, PX, and C1 domains, and no clearly defined binding motif has been reported to which PA-binding ability could be ascribed (28), we tried to identify a possible PA-binding site with NEU3 fragments designed as GFP- or GST-fusion. Four GFP-NEU3 fragments (GFP #21, #33, #36, #41, in **Fig. 3*A***) and the control (GFP only) were prepared and evaluated for effects on NEU3 translocation induced by PA stimulation in HeLa cells. No NEU3 fragments showed localization to plasma membranes without stimulation. After 200 μM PA exposure, however, transfection of fragments #21 and #33 resulted in translocation to plasma membrane (Fig. 3*B*), suggesting involvement of the N-terminal region of NEU3. To examine further the binding ability of NEU3 fragments to PA, the 4 GST-tagged NEU3 fragments (GST #21, #24, #27, #30, in Fig. 3*C*) and the control (GST) were expressed in BL21 *E. coli* and purified with glutathione-sepharose columns. PA-NEU3 fragment-binding assays were then performed by ELISA assay. First, PA was fixed at indicated amounts on the ELISA plates, and 2 μg aliquots of each GST-NEU3 fragment were loaded into wells for analysis. As shown in Fig. 3*B*, GST #21 showed significant binding to

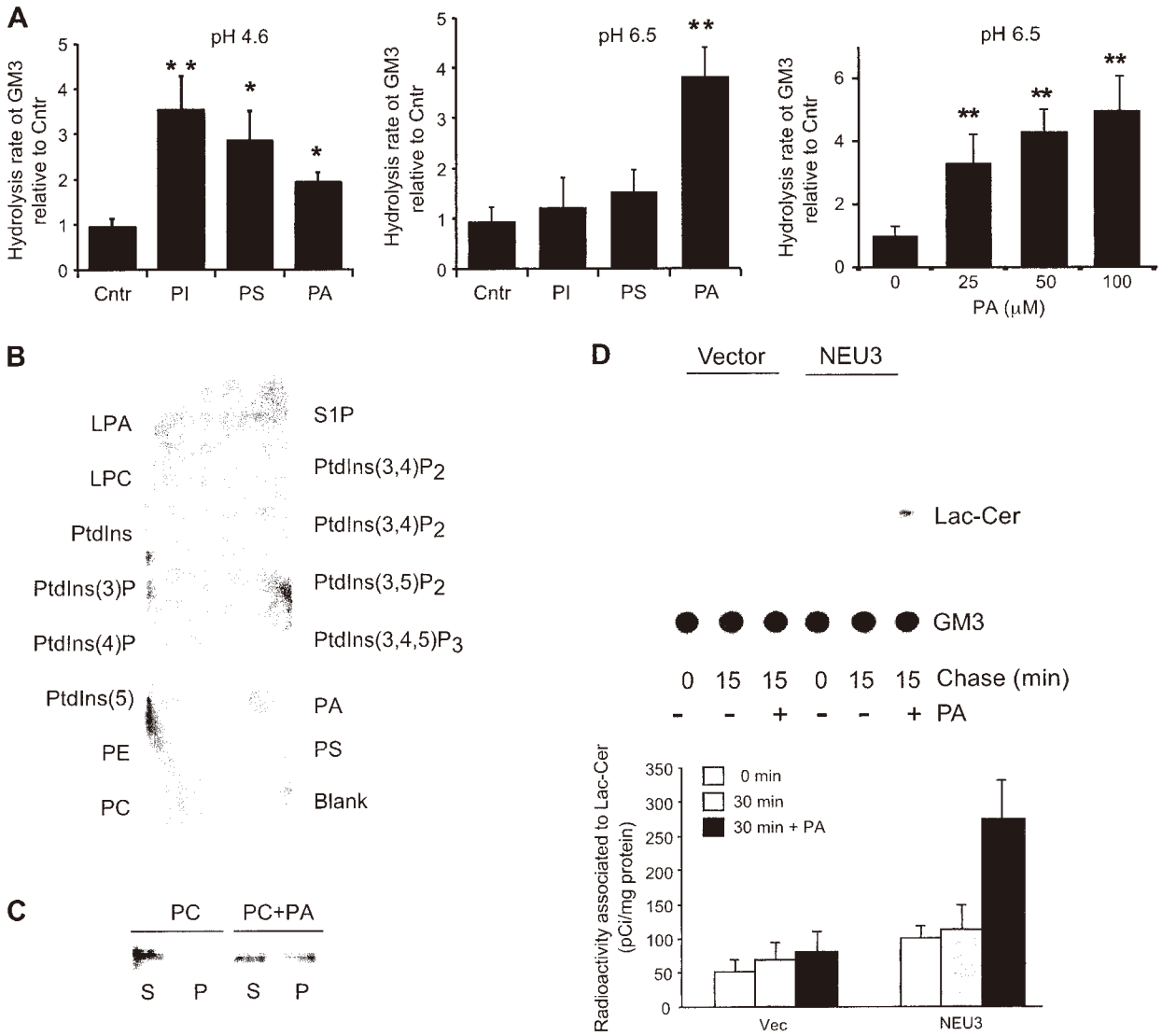

Figure 1. Assessment of the effects of phospholipids on NEU3 sialidase activity and molecular interactions. *A*) Effects of PI, PS, and PA on NEU3 sialidase activity at pH 4.6 (left) and at pH 6.5 (middle) with each phospholipid at 50 μM, and effects of various concentrations of PA on the activity at pH 6.5 (right). Released sialic acids were assessed by HPLC with fluorescence derivation. The sialidase activity levels of the purified NEU3 used here were 13.3 and 3.4 U/μg protein at pH 4.6 and 6.5, respectively, without Triton X-100 in the assays. $^*P < 0.05$, and $^{**}P < 0.01$ compared with controls (Cntr). *B*) Phospholipid spot array findings with NEU3. Purified NEU3 was incubated with a BSA-blocked PIP strip, and then interacting NEU3 was detected by immunochemistry. *C*) Liposome-binding assay findings for NEU3. Liposomes consisting of PC only (control) or the mixture of PC and PA (1:1, PC + PA) were incubated with purified NEU3. After centrifugation, interacting NEU3 was detected by immunoblotting with anti-NEU3 monoclonal antibodies as described previously (30). *D*) PA effects on sialidase activity in the living HeLa cells. NEU3-transfected HeLa cells were administered with PA and tritium-labeled GM3 as substrate in the presence of chloroquine, and the radiolabeled Lac-Cer product was observed by HPTLC (upper) as described in the Materials and Methods and in Supplemental Table 3. Results are representative of 3 independent experiments, and the values for 30-minute chase with and without PA were quantitatively shown in graph (lower).

PA, but this was not seen with other fragments (Fig. 3*D*, upper). Next, 1.5 μM PA was fixed in each well, and indicated amounts of GST-NEU3 fragments were loaded. As expected, only GST #21 demonstrated increased binding in a dose-dependent manner (Fig. 3*D*, lower). These results revealed that the fragment #21 encoding amino acids 2–130 probably contain the region binding to PA as well as that involved in translocation.

For further understanding of the functional significance of this region, our study extended by a search for motifs with a prediction program (CaM target database: *http://calcium.uhnres.utoronto.ca/ctdb/ctdb/motifs/iq_motif.html*) and identified a possible IQ-like motif, similar to the IQ motif defined as the binding site for CaM, in the region corresponding to amino acids 81–103 in GFP #21 (**Fig. 4*A***). It was recently proposed that the IQ motif in neurogranin could bind to PA (20). Because basic amino acids in IQ and IQ-like motifs might be important for PA binding, point mutations were introduced into each basic amino acid (converted to glutamic acid) (29), of 84 (histidine),

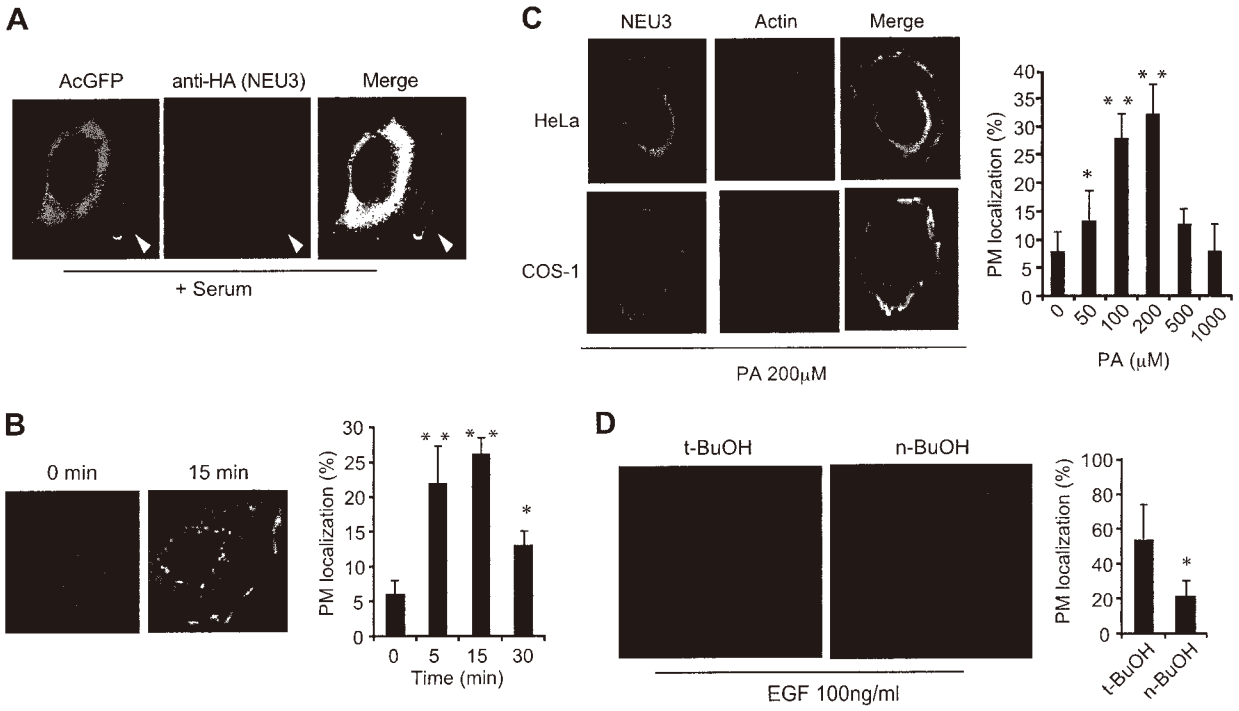

Figure 2. Involvement of PA and PLD in NEU3 translocation to plasma membranes. *A*) Colocalization of NEU3 with a plasma membrane marker in 10% FBS-treated HeLa cells. NEU3 and the marker were detected with anti-HA and GFP, respectively, by indirect immunofluorescence microscopy. *B*) PA-induced PM translocation (200 μM) in COS-1 cells at the indicated time points. $^*P < 0.05$, and $^{**}P < 0.01$ compared with 0 minutes. *C*) PM translocation of NEU3 induced by various concentration of PA in HeLa cells. The cells were serum-depleted for overnight and stimulated with PA, and the percentages of the cells with NEU3 translocation were counted as indicated in the Materials and Methods. Cells showing NEU3 translocation were counted as indicated. $^*P < 0.05$, and $^{**}P < 0.01$ compared with no stimulation. *D*) Effects of PLD inhibition with *n*-BuOH (a pan PLD inhibitor) on NEU3 translocation. HeLa cells were starved overnight and treated with 0.5% of *n*-BuOH for 30 minutes before EGF treatment. *t*-BuOH was used as a control. After 100 ng/ml EGF treatment for 10 min, NEU3 was assessed by indirect immunofluorescence microscopy. Cells with NEU3 translocation were counted as indicated. $^*P < 0.05$ compared with *t*-BuOH.

85 (arginine), and 96 (lysine) in the NEU3 IQ-like motif. When the wild and mutant fragments were tested for the translocation to plasma membranes, GFP #21 provided positive with PA stimulation. Two NEU3 mutant fragments H84E and R85E, however, did not support PA-induced translocation, although another mutant fragment K96E was almost without effect (Fig. 4*B*). When purified GST fragments for H84E and R85E mutants were tested for PA binding, they decreased the affinity to a significant extent compared to wild-type # 21 fragment but kept some of the ability, indicating the importance of the mutations but also other effects such as their conformation (Fig. 4*C*). To confirm further the influence of mutations at H84 and R85, whole NEU3 protein mutants were generated and compared with wild-type NEU3. PA-induced translocation to plasma membrane was significantly decreased in H84E and R85E NEU3 mutants (Fig. 4*D*), indicating His84 and Arg85 to be necessary for translocation. We then examined whether NEU3 possesses any CaM-binding capability using CaM-agarose beads and Western blotting, because the IQ motif may bind to PA (20). As shown in Fig. 4*E*, NEU3 protein was detected in the precipitates with CaM-agarose in the presence of $CaCl_2$ but hardly with EGTA, suggesting that the enzyme is a CAM-binding protein and can bind to PA through the IQ-like motif. Lesser binding to CaM-agarose was seen for NEU3 mutant even in the presence of $CaCl_2$, as expected. We and others have shown apparent active sites in NEU3 by site-directed mutagenesis (30, 31). Given the locations of His84 and Arg85 near active sites (Met87, Asn88), we tested sialidase activity of H84E and R85E mutants with homogenates of cDNA-transfected HEK293T cells. The mutants showed the only slight sialidase activity as compared with wild-type NEU3 at pH 4.6 (Fig. 4*F*, upper), although the proteins were expressed (Fig. 4*F*, lower). It should be noted here that at neutral pH, sialidase activity was almost 0 in the H84E and R85E cases, with or without PA addition. These results imply that binding to PA may change the conformation of NEU3, leading to enhancement of sialidase activity.

PLD1 is involved in NEU3 translocation to the plasma membrane

As observed in Fig. 2, PA-mediated NEU3 translocation was significantly inhibited by the treatment with *n*-BuOH, a pan PLD inhibitor. To know whether PLD1 or/and PLD2 are involved in the PA-mediated effects, isoform-specific inhibitors were added to the cell culture. Each of the PLD1- and PLD2-specific inhibitors used at 10 μM exerted different effects on NEU3 translocation, as assessed by confocal microscopy in HA-tagged NEU3-transfected HeLa cells. The PLD1 inhibitor caused profound inhibition even in the presence of serum (**Fig. 5*A***, cell image and graph),

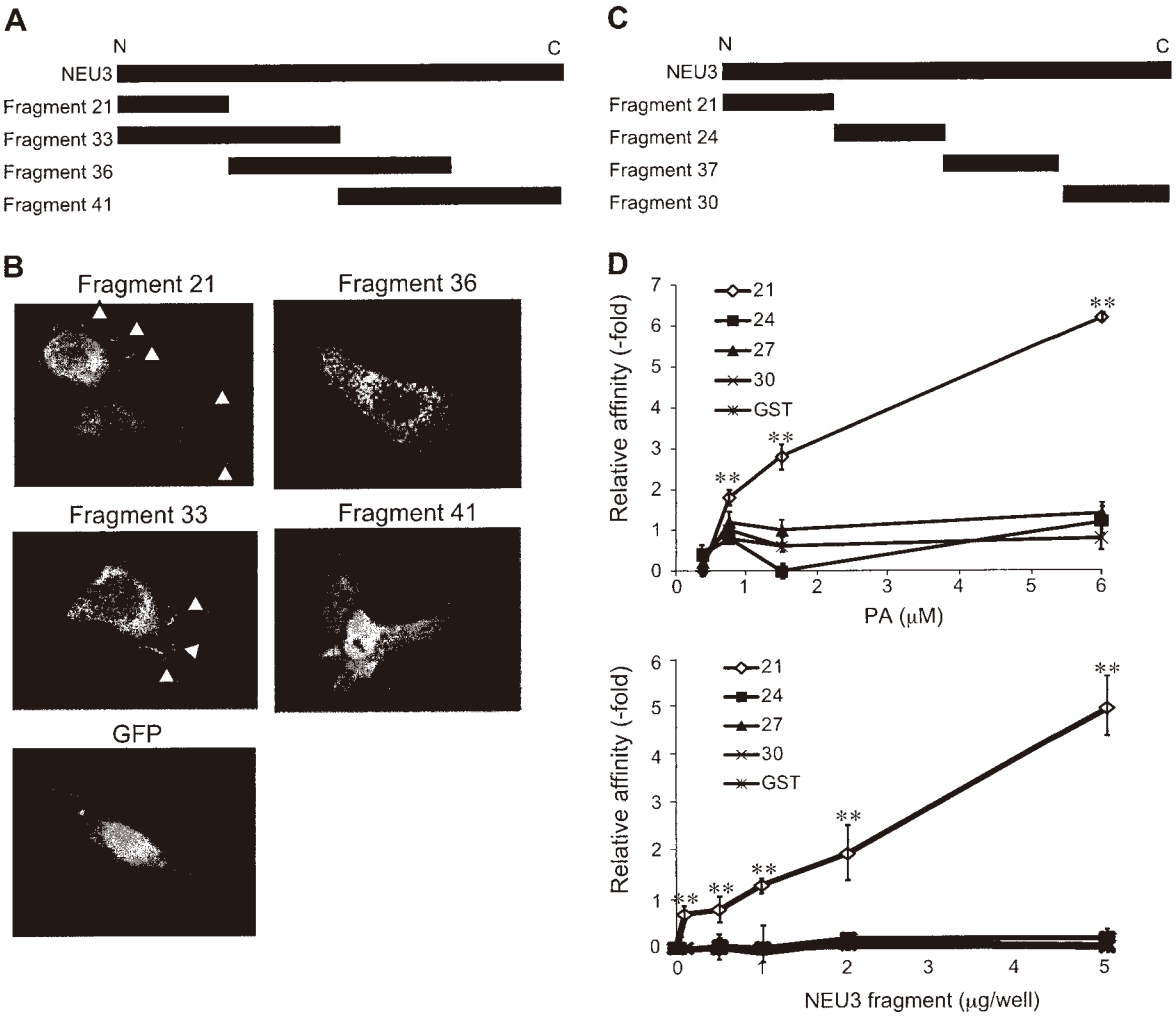

Figure 3. Binding assay for PA with NEU3 fragments. *A*) Construction of GST-fusion NEU3 fragments is illustrated. *B*) Translocation of NEU3 fragments after 200 μM PA treatment. NEU3 fragment cDNA-transfected HeLa cells were stimulated with PA, and PM localization brought about by the NEU3 fragments was assessed by fluorescence microscopy. *C*) Illustration of GST-fusion NEU3 fragments constructed. *D*) Binding assay for PA with purified GST-fusion NEU3 fragments by the ELISA method. Indicated amounts of PA were fixed on 96 well plates, and 2 μg aliquots of each recombinant GST-fusion NEU3 fragment were applied for each well. Amounts of bound NEU3 fragments were estimated using anti-GST antibodies (upper). Aliquots (1.5 μM) of PA were fixed on 96-well plates, and then indicated amounts of each GST-fusion NEU3 fragment were applied (lower). $^{**}P < 0.001$ compared with the fragments other than #21.

and also with serum addition after depletion (Fig. 5*B*, cell image and graph), as compared with DMSO control and with the PLD2 inhibitor, suggesting the involvement of PLD1 in NEU3 translocation. PLD1-transfected HeLa cells were then observed, to verify the PLD1 selectivity responsible for the translocation. In response to either EGF or serum, PLD1 was actually colocalized with NEU3 at the cell surface (Fig. 5*C*). The effects of PLD1 inhibitor were rescued by addition of exogenous PA (Fig. 5*D*), and silencing with siRNA for both PLD isoforms further confirmed that NEU3 translocation was significantly reduced by PLD1 siRNA (65–70% knockdown as compared with control siRNA) (Fig. 5*E*), but there were no effects (data not shown) with PLD2 silencing (over than 90% knockdown of controls). Furthermore, to examine a possible involvement of DAG kinase, another enzyme for PA synthesis, in the NEU3 translocation, a DAG kinase inhibitor (10 μM R59949) was added to the cells and the treatment did not give a significant reduction, although showing a tendency of slight decreasing (Fig. 5*F*). These results indicate that PA synthesis by PLD1 is important for regulation of NEU3 translocation, although it does not seem to affect all the translocation.

Next, we investigated possible mechanisms for translocation of NEU3 and PLD1 to the cell surface. It has been reported that PLD1 is identified in diverse subcellular organelles, including the endoplasmic reticulum, Golgi, endosomes, lysosomes, and plasma membrane, and that EGF stimulates PLD1 activity and induces phosphorylation and localization in the plasma membrane (32, 33). In this context, translocation of both the proteins to the cell surface was analyzed before and after EGF treatment in PLD1- and NEU3-transfected COS1 cells. Figure 6 shows that in response to EGF at 0.5 min, under the conditions that

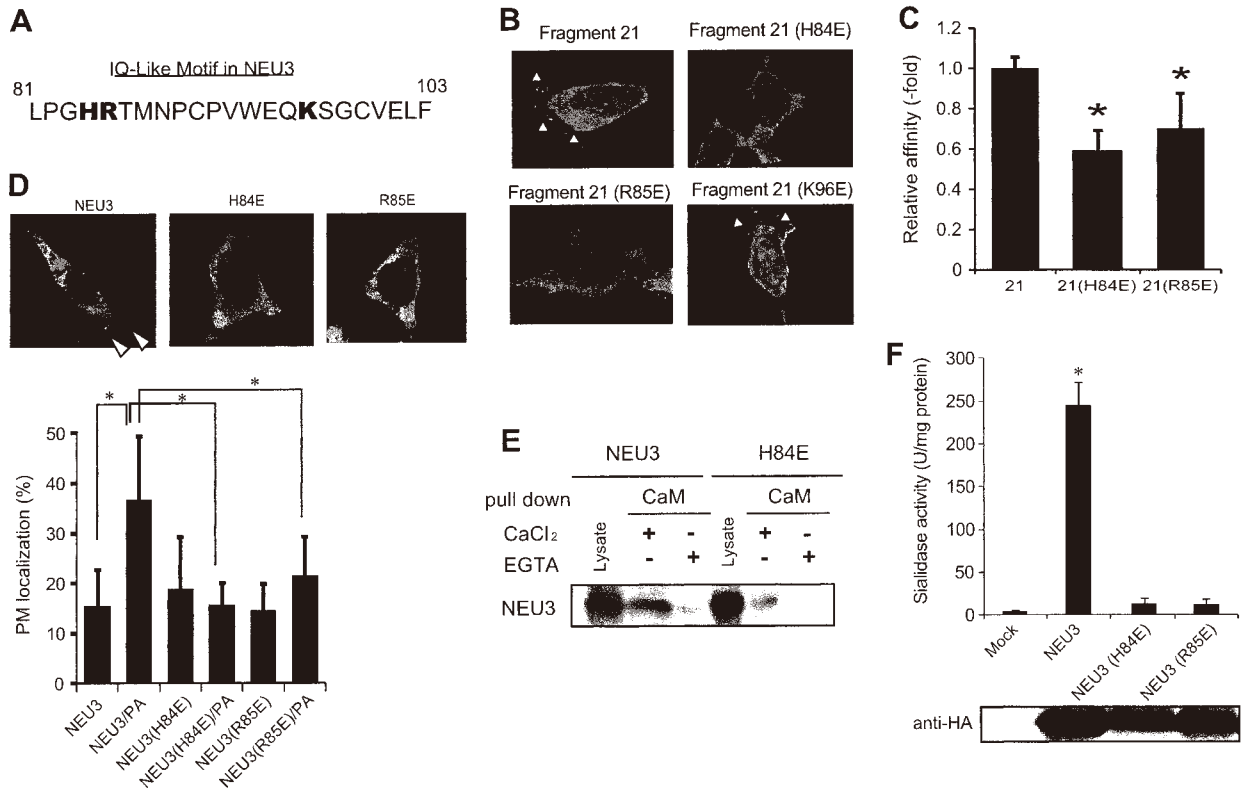

Figure 4. Identification of PA-binding site in NEU3. *A*) A predicted IQ-like motif in NEU3 fragment #21. *B*) Effect of point mutation in the NEU3 fragment #21 on translocation. The sequence in the upper box indicates a predicted IQ-like motif in NEU3 fragment #21. GFP-fusion NEU3 fragment #21, with or without point mutation, was expressed in HeLa cells, and PA-stimulated cells showing the translocation were assessed by fluorescence microscopy. *C*) Effects of NEU3 point mutation on PA binding. GST-fusion NEU3 fragments were purified and assessed for PA binding with PA by the ELISA method as described in Fig. 3*D*. $*P < 0.05$ compared with the wild-type fragment #21. *D*) Effect of NEU3 point mutation on translocation. Whole NEU3 proteins with or without point mutation were overexpressed in HeLa cells, and PA-stimulated cells were examined for the effects on NEU3 translocation by indirect immunomicroscopy. Cells with translocation were counted from 5 randomly chosen fields as quantitatively shown in graph. $*P < 0.05$ compared with NEU3 with or without PA treatment. *E*) CaM-binding ability of NEU3 protein. The binding ability to CaM of wild-type NEU3 and the H84E mutant was assessed using CaM beads in precipitation experiments. CaM-agarose (Sigma-Aldrich) was incubated with the cell lysates in the presence of $CaCl_2$ or EGTA as described in Materials and Methods. *F*) Suppression of NEU3 sialidase activity by point mutations. Each protein was expressed in HEK293T cells, and homogenates were measured for sialidase activity toward GM3 as substrate at pH 4.6 in the presence of 0.1% TritonX-100 (upper). The homogenates were also used for immunoblotting with anti-HA antibodies (lower). $*P < 0.001$ compared with NEU3 mutants.

PLD1 activation occurs at maximum, PLD1 phosphorylation was remarkable at the cell surface and indeed accompanied by NEU3 translocation, consistent with those in HeLa cells in Fig. 5*C*. The EGF-induced effects were gradually diminished as EGFR phosphorylation level was lowered. At 0.5 min, 90% of the NEU3-stained cells at the cell surface exhibited phospho-PLD1 staining, and at 5 min these double-staining cells decreased to 40%. The results suggest that EGF-induced PLD1 activation leads to NEU3 translocation.

NEU3 enhances PA-mediated cell motility

PA has long been proposed to regulate cell motility and invasion through Ras activation (34). Our previous study also indicated NEU3 to activate cell motility induced by EGF stimulation with Rac activation (9). Similar to this case, NEU3 was colocalized with Rac at plasma membrane by PA stimulation (**Fig. 7*A***). To investigate whether NEU3 is involved in PA-induced cell motility, assays were carried out using the Boyden chamber method. HeLa cells showed only slight locomotion without PA stimulation even after NEU3 transfection, but PA treatment showed significant migration to the lower side of Boyden chambers and NEU3 further promoted cell motility (Fig. 7*B*, left). At the same time, PA-induced cell motility was evidently decreased in NEU3-silenced cells (80% knockdown as compared with control siRNA). When transfected the recombinant NEU3 cDNA to HeLa cells, the mutation with H84E resulted in decreased cell motility compared to the wild-type (Fig. 7*B*, right), indicating an influence of the mutation on cell motility as well as on translocation to the cell surface.

To observe whether Ras signaling was involved in regulation of cell motility by NEU3, Ras activity and phosphorylation levels of ERK and paxillin were evaluated by Western blotting. NEU3 enhanced Ras activity as compared with vector control and further activation was apparent with PA treatment (Fig. 7*C*). Phosphorylation of

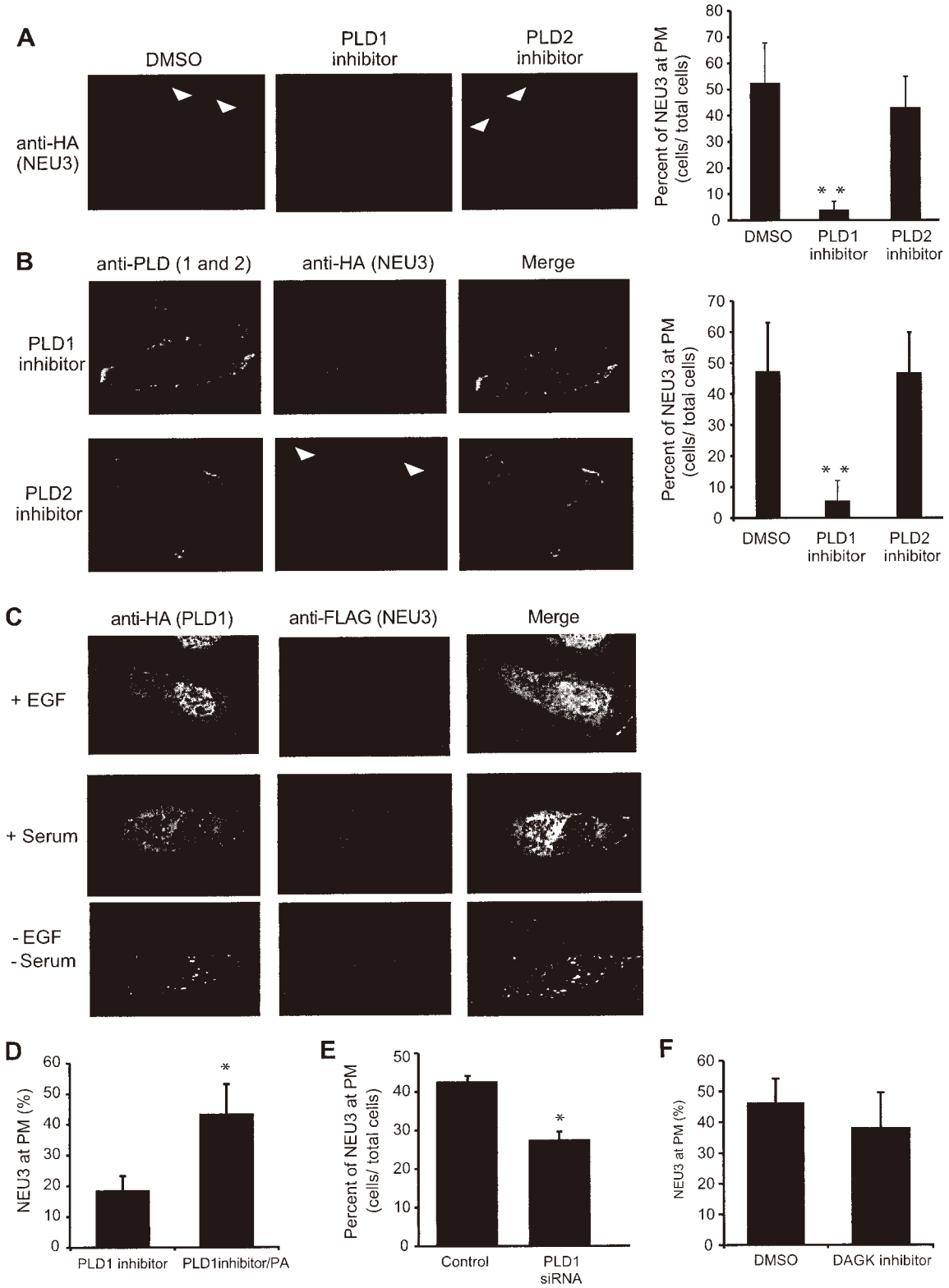

Figure 5. Selective involvement of PLD1 in NEU3 translocation to plasma membranes. *A*) Effects of PLD1 or PLD2 inhibitors on NEU3 translocation in HeLa cells treated with 10% FBS. NEU3-transfected HeLa cells were exposed to selective inhibitors of PLD1 (CAY10593) or PLD2 (CAY10594) after 16-hour culture and NEU3 translocation was assessed with anti-HA antibody after 24-hour culture. Cells showing NEU3 translocation were counted as indicated (right graph). $^{**}P < 0.01$ compared with the control. *B*) Effects of PLD1 or PLD2 inhibitors on NEU3 translocation after serum stimulation. HeLa cells were observed subsequent to 10 minutes of serum stimulation after 24-hour culture under serum-depleted conditions in the presence of PLD1 or PLD2 inhibitor.

(*continued on next page*)

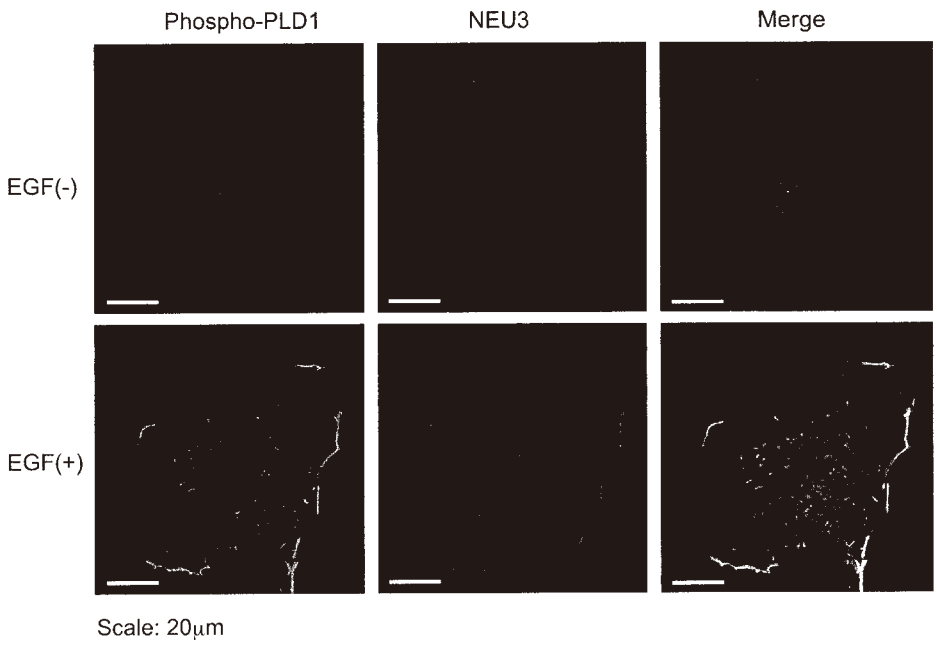

Figure 6. EGF-induced colocalization of NEU3 with activated PLD1 at the cell surface. COS-1 cells were cotransfected with PLD1 and NEU3, and after 40-hour culture, the cells were observed subsequent to EGF stimulation (100 ng/ml) for 0.5 minutes after overnight culture under serum-depleted conditions. The cells were fixed and PLD1 phosphorylation and NEU3 proteins were examined with anti-phospho-PLD1 and anti-Flag-antibodies, respectively, by counting at least 50 cells on immunofluorescence microscopy.

ERK and paxillin was also increased by NEU3 and with PA, especially in NEU3 overexpressing cells, but the H84E mutant confirmed to show almost no effects with or without PA (Fig. 7*D*). In contrast, NEU3 silencing clearly inhibited PA-mediated ERK phosphorylation (Fig. 7*E*). Some studies suggested that PA or PLD stimulates EGFR signaling especially through EGFR-induced endocytosis (33), and our previous article documented NEU3 activation of EGFR signaling (8). When the phosphorylation level of ERK and paxillin was assessed with EGF, the levels were enhanced by NEU3 but the effects were abrogated in the presence of PLD1 inhibitor (Fig. 7*F*), suggesting the NEU3 effects in response to EGF may be mediated through PLD1, if not all. These results indicate that NEU3 regulates PA-induced cell migration possibly by PLD1 *via* EGF signaling.

DISCUSSION

Until now, the sialidase activity assays for NEU3 have required chemical detergents such as Triton X-100, because NEU3 is a membrane-bound enzyme and a natural activator has hitherto not been identified. In the present study, we obtained evidence that PA is one natural activator of NEU3 in living cells, confirming results from an activity assay system *in vitro*. Among phospholipids possessing detergent action as general characteristics, we found selectivity for PA for the activation of NEU3 sialidase activity and for the translocation to the cell surface. Not a few enzymes are known to bind to PA and also to be activated by PA (18), but the actual mechanisms do not seem to be similar. As there is no defined amino acid sequence for PA binding, it was very difficult to identify binding sites, despite the report of an IQ (or IQ-like) motif as on possibility. Our study here revealed interaction between PA and NEU3 and its involvement in enhanced sialidase catalytic activity. Our results also suggested that His84 and Arg85 in NEU3 could be included in the binding site for PA. Given their close proximity to Met87 and Asn88 active sites in NEU3, which are predicted to interact with the 5-*N*-acetyl group of sialic acid (30, 31, 35), it is feasible that the point mutations caused the drastic decrease of sialidase activity shown in Fig. 4*F*, indicating a crucial role in NEU3 sialidase activity. Active sites are well preserved in mammalian sialidases, but interestingly, our preliminary study showed NEU4, with the highest homology to NEU3 in primary sequence among the types, did not demonstrate any interaction with PA (data not shown). Use of the IQ-motif prediction program pointed to a greater likelihood of a IQ-like motif in NEU3 than in other sialidases, consistent with our finding of a capacity of NEU3 for CaM binding (Fig. 4*E*).

Our previous study revealed that EGF or serum stimulation alters NEU3 subcellular localization in HeLa and

Endogenous PLD and transfected NEU3 were assessed by anti-PLD (PLD1 plus PLD2) and anti-HA antibodies, respectively. Percentages of HeLa cells with NEU3 translocation were determined as indicated (right graph). $^{**}P < 0.01$ compared with the control. *C*) Colocalization of PLD1 and NEU3 at the cell surface by EGF or serum stimulation. HeLa cells were transfected with PLD1 and NEU3, and NEU3 translocation was assessed subsequent to 10 minutes of EGF or serum stimulation after overnight culture under serum-depleted conditions. PLD1 and NEU3 were observed with anti-HA and anti-Flag antibodies. *D*) Restoration of PLD1 inhibitor-induced reduction of NEU3 translocation by exogenous addition of PA. $^{*}P < 0.05$ compared with no PA. *E*) Effects of PLD1 silencing on NEU3 translocation in HeLa cells. Cells were transfected with PLD1-specific siRNA and NEU3 translocation was assessed after 40 hours under 10% serum conditions. Percentages of cells with NEU3 translocation were counted as indicated. $^{*}P < 0.01$ compared with the control. The gene-silencing efficiency was nearly 65–80%. Results are representative of 3 independent experiments. *F*) No significant reduction of NEU3 translocation with a DAG kinase inhibitor. $P = 0.268$ compared with the DMSO control. All the results were obtained by counting at least 100 cells in each experiment.

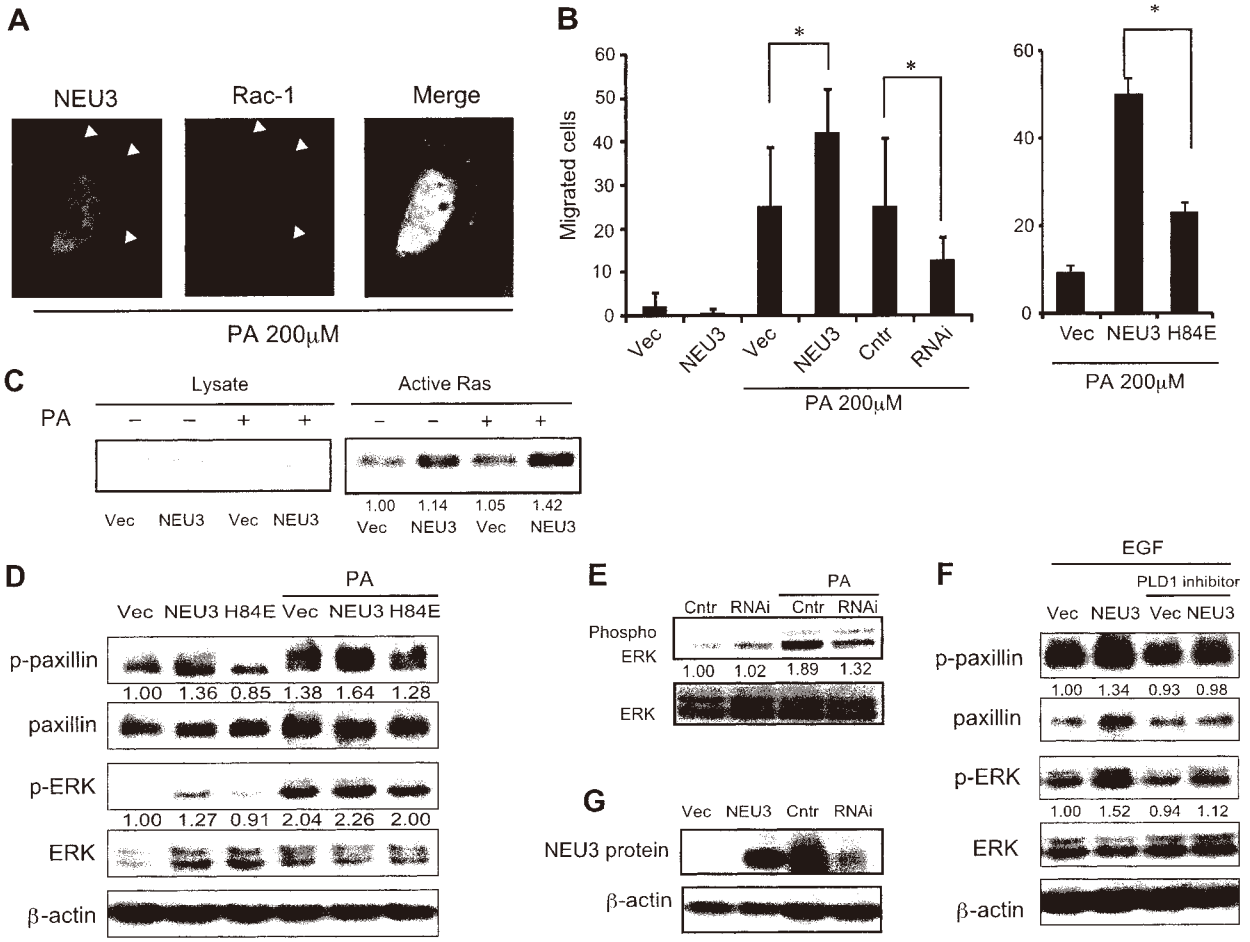

Figure 7. Regulation of PA-induced cell motility by NEU3. *A*) Rac and NEU3 colocalization in HeLa cells. After 200 μM PA stimulation, NEU3 and Rac-1 localization was assessed by immunofluorescence microscopy. *B*) Regulation of PA-induced cell motility by NEU3. HeLa cells were stimulated with 200 μM PA, and migrating cells were fixed and counted at 24 hours after stimulation. $*P < 0.05$ compared with vector or control siRNA (left panel), and with H84E mutant (right panel). *C*) Regulation of PA-induced Ras activation by NEU3. HeLa cells were stimulated with 200 μM PA, and the bound Ras-GTP protein was resolved by SDS-PAGE followed by immunoblotting with anti-Ras antibodies in NEU3-transfected cells. *D*) Regulation of PA-induced phosphorylation of ERK and paxillin by NEU3. Phospho-ERK and ERK and phospho-paxillin and paxillin were detected by immunoblotting in NEU3-transfected with or without 200 μM PA. *E*) Phospho-ERK and ERK were assessed by immunoblotting in NEU3-silenced cells with or without PA. *F*) Regulation of EGF-induced ERK and paxillin phosphorylation by NEU3. The cells were observed subsequent to EGF stimulation (100 ng/ml) for 20 min after overnight culture under serum-depleted conditions. Phospho-ERK and ERK and phospho-paxillin and paxillin were detected by immunoblotting in NEU3-transfected and vector control cells with or without 10 μM PLD1 inhibitor. Results on immunoblotting are representative of 3–4 independent experiments. *G*) NEU3 protein amounts were measured by immunoblotting with anti-NEU3 monoclonal antibody in NEU3-overexpressing or -silencing HeLa cells used in this study. Cell homogenates (10 and 50 μl) were loaded on Western blotting for the former and the latter, respectively. The homogenates showed reasonable amounts of NEU3 protein by Western blotting, although endogenous PLD1 protein level was not determined because of too low expression for detection by the antibody available at present.

A549 cells (9). Here we showed that PA regulates NEU3 translocation to plasma membranes, where the enzyme alters Ras signaling. Consistent with the report by others describing rapid induction of PA by a PLD reaction after EGF stimulation (33), NEU3 translocation in response to EGF stimulation was diminished by a PLD inhibitor and by a specific PLD1 inhibitor (Fig. 5*A*, *B*), suggesting that PA may play an essential role in NEU3 translocation induced by EGF or other stimuli. We also proposed a possible mechanism of this PLD1-dependent NEU3 translocation using the cells treated with EGF. In response to EGF, PLD1 activation and translocation occurred concomitantly with a significant increase in NEU3 at the cell surface (Fig. 6) probably through the binding to PA produced by PLD1.

Promotion of cell migration and invasion may occur through PA induction (36). Our results also showed increased cell migration on PA stimulation in HeLa cells, and NEU3 enhanced the PA-induced cell migration, while its silencing abrogated the effects, suggesting an involvement of both PA and NEU3 in enhancement of cell motility. In the PA case, as reported to be accompanied with expression of Rac (34), we also showed NEU3 to enhance cell motility with Rac-1 translocation to the cell surface. Furthermore, we found Ras activation and

subsequent increase in phosphorylation of ERK and paxillin, after PA stimulation and more so with NEU3 but reduced by NEU3 silencing. Recently it was documented that PLD2, mainly localized at plasma membranes, acts as a downstream effector of EGFR signaling and also as a direct activator for Ras (26, 34). PA binds to the PH domain of Sos, recruiting it to the plasma membranes and converting Ras-GDP to Ras-GTP. We therefore examined whether siRNA-mediated PLD2 silencing and a specific inhibitor might influence NEU3 translocation and Ras activation, but neither exerted any effect. In contrast, PLD1 silencing and the PLD1 inhibitor suppressed the activation events, indicating that PLD1 is mainly involved in the present cell system. PA can be converted to other signaling lipids, especially lyso-PA by phospholipase A2 or DAG by PA phosphatase. DAG is known to play a crucial role in Ras activation and to be required for the activation by lymphocyte function-associated antigen-1 (37), and NEU3 activity was, however, hardly affected by DAG or lyso-PA in our experiments. All the data together suggest that NEU3 activation and translocation to the cell surface occurs, if not all, in a PA-dependent manner *via* PLD1 activation induced by growth factors such as EGF.

We previously demonstrated that NEU3 is markedly up-regulated in various cancers, associated with augmentation of malignant phenotypes (3–6). Up-regulation of PLD is also present in a wide variety of cancers and contributes to cancer progression (20, 38, 39). Our previous studies revealed that ganglioside modulation by NEU3 causes activation of EGFR or integrins (8, 10) and their direct interaction with NEU3 also elevates cancer cell migration, invasion, and survival (5, 8). Our present findings point to a new mechanism of NEU3 activation by PA through direct interaction and provide new insights into a crucial role for NEU3 as a signaling regulator at cell surfaces *via* PLD1-generated PA. As PLD activation in cancer is well known to up-regulate various signaling pathways, we can surmise that NEU3 not only responds to PA but acts in coordination, the end result being enhanced malignancy in cancers. FJ

The authors are grateful to Dr. M. A. Frohman, Stony Brook University, for a kind gift of PLD1 expression vector, pCGN-hPLD1b, and also to Mr. T. Wada and Ms. S. Moriya, Tohoku Pharmaceutical University, for their valuable technical assistance. This study was supported in part by Grants-in-Aid for Scientific Research on Innovative Areas (No. 23110002) from the Ministry of Education, Culture, Sports, Science and Technology of Japan.

REFERENCES

1. Miyagi, T., and Yamaguchi, K. (2012) Mammalian sialidases: physiological and pathological roles in cellular functions. *Glycobiology* **22**, 880–896
2. Miyagi, T., Wada, T., Yamaguchi, K., Hata, K., and Shiozaki, K. (2008) Plasma membrane-associated sialidase as a crucial regulator of transmembrane signalling. *J. Biochem.* **144**, 279–285
3. Kakugawa, Y., Wada, T., Yamaguchi, K., Yamanami, H., Ouchi, K., Sato, I., and Miyagi, T. (2002) Up-regulation of plasma membrane-associated ganglioside sialidase (Neu3) in human colon cancer and its involvement in apoptosis suppression. *Proc. Natl. Acad. Sci. USA* **99**, 10718–10723
4. Nomura, H., Tamada, Y., Miyagi, T., Suzuki, A., Taira, M., Suzuki, N., Susumu, N., Irimura, T., and Aoki, D. (2006) Expression of NEU3 (plasma membrane-associated sialidase) in clear cell adenocarcinoma of the ovary: its relationship with T factor of pTNM classification. *Oncol. Res.* **16**, 289–297
5. Ueno, S., Saito, S., Wada, T., Yamaguchi, K., Satoh, M., Arai, Y., and Miyagi, T. (2006) Plasma membrane-associated sialidase is up-regulated in renal cell carcinoma and promotes interleukin-6-induced apoptosis suppression and cell motility. *J. Biol. Chem.* **281**, 7756–7764
6. Kawamura, S., Sato, I., Wada, T., Yamaguchi, K., Li, Y., Li, D., Zhao, X., Ueno, S., Aoki, H., Tochigi, T., Kuwahara, M., Kitamura, T., Takahashi, K., Moriya, S., and Miyagi, T. (2012) Plasma membrane-associated sialidase (NEU3) regulates progression of prostate cancer to androgen-independent growth through modulation of androgen receptor signaling. *Cell Death Differ.* **19**, 170–179
7. Yamaguchi, K., Koseki, K., Shiozaki, M., Shimada, Y., Wada, T., and Miyagi, T. (2010) Regulation of plasma-membrane-associated sialidase NEU3 gene by Sp1/Sp3 transcription factors. *Biochem. J.* **430**, 107–117
8. Wada, T., Hata, K., Yamaguchi, K., Shiozaki, K., Koseki, K., Moriya, S., and Miyagi, T. (2007) A crucial role of plasma membrane-associated sialidase in the survival of human cancer cells. *Oncogene* **26**, 2483–2490
9. Yamaguchi, K., Hata, K., Wada, T., Moriya, S., and Miyagi, T. (2006) Epidermal growth factor-induced mobilization of a ganglioside-specific sialidase (NEU3) to membrane ruffles. *Biochem. Biophys. Res. Commun.* **346**, 484–490
10. Kato, K., Shiga, K., Yamaguchi, K., Hata, K., Kobayashi, T., Miyazaki, K., Saijo, S., and Miyagi, T. (2006) Plasma-membrane-associated sialidase (NEU3) differentially regulates integrin-mediated cell proliferation through laminin- and fibronectin-derived signalling. *Biochem. J.* **394**, 647–656
11. Shiozaki, K., Yamaguchi, K., Sato, I., and Miyagi, T. (2009) Plasma membrane-associated sialidase (NEU3) promotes formation of colonic aberrant crypt foci in azoxymethane-treated transgenic mice. *Cancer Sci.* **100**, 588–594
12. Yamaguchi, K., Shiozaki, K., Moriya, S., Koseki, K., Wada, T., Tateno, H., Sato, I., Asano, M., Iwakura, Y., and Miyagi, T. (2012) Reduced susceptibility to colitis-associated colon carcinogenesis in mice lacking plasma membrane-associated sialidase. *PLoS ONE* **7**, e41132
13. Hasegawa, T., Yamaguchi, K., Wada, T., Takeda, A., Itoyama, Y., and Miyagi, T. (2000) Molecular cloning of mouse ganglioside sialidase and its increased expression in Neuro2a cell differentiation. *J. Biol. Chem.* **275**, 8007–8015
14. Rodriguez, J. A., Piddini, E., Hasegawa, T., Miyagi, T., and Dotti, C. G. (2001) Plasma membrane ganglioside sialidase regulates axonal growth and regeneration in hippocampal neurons in culture. *J. Neurosci.* **21**, 8387–8395
15. Da Silva, J. S., Hasegawa, T., Miyagi, T., Dotti, C. G., and Abad-Rodriguez, J. (2005) Asymmetric membrane ganglioside sialidase activity specifies axonal fate. *Nat. Neurosci.* **8**, 606–615
16. Miyagi, T., Wada, T., Iwamatsu, A., Hata, K., Yoshikawa, Y., Tokuyama, S., and Sawada, M. (1999) Molecular cloning and characterization of a plasma membrane-associated sialidase specific for gangliosides. *J. Biol. Chem.* **274**, 5004–5011
17. Wada, T., Yoshikawa, Y., Tokuyama, S., Kuwabara, M., Akita, H., and Miyagi, T. (1999) Cloning, expression, and chromosomal mapping of a human ganglioside sialidase. *Biochem. Biophys. Res. Commun.* **261**, 21–27
18. Stace, C. L., and Ktistakis, N. T. (2006) Phosphatidic acid- and phosphatidylserine-binding proteins. *Biochim. Biophys. Acta* **1761**, 913–926
19. Hata, K., Koseki, K., Yamaguchi, K., Moriya, S., Suzuki, Y., Yingsakmongkon, S., Hirai, G., Sodeoka, M., von Itzstein, M., and Miyagi, T. (2008) Limited inhibitory effects of oseltamivir and zanamivir on human sialidases. *Antimicrob. Agents Chemother.* **52**, 3484–3491
20. Domínguez-González, I., Vázquez-Cuesta, S. N., Algaba, A., and Díez-Guerra, F. J. (2007) Neurogranin binds to phosphatidic acid and associates to cellular membranes. *Biochem. J.* **404**, 31–43
21. Sonnino, S., Nicolini, M., and Chigorno, V. (1996) Preparation of radiolabeled gangliosides. *Glycobiology* **6**, 479–487
22. Papini, N., Anastasia, L., Tringali, C., Croci, G., Bresciani, R., Yamaguchi, K., Miyagi, T., Preti, A., Prinetti, A., Prioni, S., Sonnino, S., Tettamanti, G., Venerando, B., and Monti, E. (2004) The plasma membrane- associated sialidase Neu3 modifies the

cell surface ganglioside pattern through cell-to-cell interactions. *J. Biol. Chem.* **279**, 16989–16995
23. Kaszkin, M., Seidler, L., Kast, R., and Kinzel, V. (1992) Epidermal-growth-factor-induced production of phosphatidylalcohols by HeLa cells and A431 cells through activation of phospholipase D. *Biochem. J.* **287**, 51–57
24. Itoh, T., Hasegawa, J., Tsujita, K., Kanaho, Y., and Takenawa, T. (2009) The tyrosine kinase Fer is a downstream target of the PLD-PA pathway that regulates cell migration. *Sci. Signal.* **2**, ra52
25. Rizzo, M. A., Shome, K., Watkins, S. C., and Romero, G. (2000) The recruitment of Raf-1 to membranes is mediated by direct interaction with phosphatidic acid and is independent of association with Ras. *J. Biol. Chem.* **275**, 23911–23918
26. Frank, C., Keilhack, H., Opitz, F., Zschörnig, O., and Böhmer, F. D. (1999) Binding of phosphatidic acid to the protein-tyrosine phosphatase SHP-1 as a basis for activity modulation. *Biochemistry* **38**, 11993–12002
27. Fang, Y., Vilella-Bach, M., Bachmann, R., Flanigan, A., and Chen, J. (2001) Phosphatidic acid-mediated mitogenic activation of mTOR signaling. *Science* **294**, 1942–1945
28. Lemmon, M. A. (2008) Membrane recognition by phospholipid-binding domains. *Nat. Rev. Mol. Cell Biol.* **9**, 99–111
29. Zhao, C., Du, G., Skowronek, K., Frohman, M. A., and Bar-Sagi, D. (2007) Phospholipase D2-generated phosphatidic acid couples EGFR stimulation to Ras activation by Sos. *Nat. Cell Biol.* **9**, 706–712
30. Wang, Y., Yamaguchi, K., Shimada, Y., Zhao, X., and Miyagi, T. (2001) Site-directed mutagenesis of human membrane-associated ganglioside sialidase: identification of amino-acid residues contributing to substrate specificity. *Eur. J. Biochem.* **268**, 2201–2208
31. Albohy, A., Li, M. D., Zheng, R. B., Zou, C., and Cairo, C. W. (2010) Insight into substrate recognition and catalysis by the human neuraminidase 3 (NEU3) through molecular modeling and site-directed mutagenesis. *Glycobiology* **20**, 1127–1138
32. Han, J. M., Kim, Y., Lee, J. S., Lee, C. S., Lee, B. D., Ohba, M., Kuroki, T., Suh, P. G., and Ryu, S. H. (2002) Localization of phospholipase D1 to caveolin-enriched membrane via palmitoylation: implications for epidermal growth factor signaling. *Mol. Biol. Cell* **13**, 3976–3988
33. Lee, C. S., Kim, K. L., Jang, J. H., Choi, Y. S., Suh, P. G., and Ryu, S. H. (2009) The roles of phospholipase D in EGFR signaling. *Biochim. Biophys. Acta* **1791**, 862–868
34. Zhang, Y., and Du, G. (2009) Phosphatidic acid signaling regulation of Ras superfamily of small guanosine triphosphatases. *Biochim. Biophys. Acta* **1791**, 850–855
35. Magesh, S., Suzuki, T., Miyagi, T., Ishida, H., and Kiso, M. (2006) Homology modeling of human sialidase enzymes NEU1, NEU3 and NEU4 based on the crystal structure of NEU2: hints for the design of selective NEU3 inhibitors. *J. Mol. Graph. Model.* **25**, 196–207
36. Mazie, A. R., Spix, J. K., Block, E. R., Achebe, H. B., and Klarlund, J. K. (2006) Epithelial cell motility is triggered by activation of the EGF receptor through phosphatidic acid signaling. *J. Cell Sci.* **119**, 1645–1654
37. Mor, A., Campi, G., Du, G., Zheng, Y., Foster, D. A., Dustin, M. L., and Philips, M. R. (2007) The lymphocyte function-associated antigen-1 receptor costimulates plasma membrane Ras via phospholipase D2. *Nat. Cell Biol.* **9**, 713–719
38. Joseph, T., Wooden, R., Bryant, A., Zhong, M., Lu, Z., and Foster, D. A. (2001) Transformation of cells overexpressing a tyrosine kinase by phospholipase D1 and D2. *Biochem. Biophys. Res. Commun.* **289**, 1019–1024
39. Zhang, Y., and Frohman, M. A. (2014) Cellular and physiological roles for phospholipase D1 in cancer. *J. Biol. Chem.* **289**, 22567–22574

Received for publication August 18, 2014.
Accepted for publication January 11, 2015.

IJC
International Journal of Cancer

Sialidase NEU3 contributes neoplastic potential on colon cancer cells as a key modulator of gangliosides by regulating Wnt signaling

Kohta Takahashi[1,2], Masahiro Hosono[3], Ikuro Sato[4], Keiko Hata[1], Tadashi Wada[1], Kazunori Yamaguchi[5], Kazuo Nitta[2], Hiroshi Shima[2] and Taeko Miyagi[1]

[1] Division of Cancer Glycosylation Research, Institute of Molecular Biomembrane and Glycobiology, Tohoku Pharmaceutical University, Sendai
[2] Division of Cancer Molecular Biology, Graduate School of Medicine, Tohoku University, Sendai, Japan
[3] Division of Cell Recognition Study, Institute of Molecular Biomembrane and Glycobiology, Tohoku Pharmaceutical University, Sendai
[4] Division of Pathology, Miyagi Cancer Center Research Institute, Natori
[5] Division of Molecular and Cellular Oncology, Miyagi Cancer Center Research Institute, Natori

Cancer Cell Biology

The plasma membrane-associated sialidase NEU3 is a key enzyme for ganglioside degradation. We previously demonstrated remarkable up-regulation of NEU3 in various human cancers, with augmented malignant properties. Here, we provide evidence of a close link between NEU3 expression and Wnt/β-catenin signaling in colon cancer cells by analyzing tumorigenic potential and cancer stem-like characteristics. NEU3 silencing in HT-29 and HCT116 colon cancer cells resulted in significant decrease in clonogenicity on soft agar and *in vivo* tumor growth, along with down-regulation of stemness and Wnt-related genes. Analyses further revealed that NEU3 enhanced phosphorylation of the Wnt receptor LRP6 and consequently β-catenin activation by accelerating complex formation with LRP6 and recruitment of GSK3β and Axin, whereas its silencing exerted the opposite effects. NEU3 activity-null mutants failed to demonstrate the activation, indicating the requirement of ganglioside modulation by the sialidase for the effects. Under sphere-forming conditions, when stemness genes are up-regulated, endogenous NEU3 expression was found to be significantly increased, whereas NEU3 silencing suppressed sphere-formation and *in vivo* tumor incidence in NOD-SCID mice. Increased ability of clonogenicity on soft agar and sphere formation by Wnt stimulation was abrogated by NEU3 silencing. Furthermore, NEU3 was found to regulate phosphorylation of ERK and Akt via EGF receptor and Ras cascades, thought to be additionally required for tumor progression. The results indicate an essential contribution of NEU3 to tumorigenic potential through maintenance of stem-like characteristics of colon cancer cells by regulating Wnt signaling at the receptor level, in addition to tumor progression via Ras/MAPK signaling.

Aberrant glycosylation is a characteristic feature of cancer cells.[1,2] In particular, altered sialylation is closely related to malignant properties, including invasiveness and metastatic potential. To elucidate the underlying molecular mechanisms, our studies have focused on mammalian sialidases (EC 3.2.1.18), which catalyze the removal of sialic acid residues from glycoproteins and glycolipids.[3] The four types of mammalian sialidase (NEU1-4) identified to date all show altered expression and behave in different manners during carcinogenesis.[4] We previously demonstrated remarkable up-regulation of the plasma membrane- associated sialidase, NEU3, in various human cancers, including examples in the colon,[5] kidney,[6] ovary,[7] and prostate.[8] Because of its unique substrate preference for gangliosides co-existing at the cell surface, this sialidase appears to play particular roles in regulation of transmembrane signaling at cell surface by the modulation of gangliosides, and its aberrant expression is closely associated with promotion of cell invasion and motility and cell survival of cancer cells. [6,9,10] Our recent reports further suggest important roles of NEU3 in promotion of colon carcinogenesis as well as in progression: we have documented *in vivo* participation of NEU3 in formation of azoxymethane-induced colonic aberrant crypt foci (ACF) in transgenic mice,[11] and showed *Neu3*-deficient mice to exhibit reduced susceptibility to colitis-associated colon carcinogenesis

Key words: sialidase, Wnt signaling, colon cancer, stem cells, gangliosides

Abbreviations: DMEM: Dulbecco's modified Eagle's medium; GSK: glycogen synthase kinase; shRNA: small hairpin RNA; TLC: Thin-layer chromatography; TR: tetracycline repressor

Additional Supporting Information may be found in the online version of this article.

Grant sponsor: Grants-in-Aid for Scientific Research on Innovative Areas from the Ministry of Education, Culture, Sports, Science and Technology of Japan; Grant number: 23110002
DOI: 10.1002/ijc.29527
History: Received 20 Nov 2014; Accepted 12 Mar 2015; Online 21 Mar 2015

Correspondence to: Taeko Miyagi, Division of Cancer Glycosylation Research, Institute of Molecular Biomembrane and Glycobiology, Tohoku Pharmaceutical University, 4-4-1 Komatsushima, Aoba-ku, Sendai 981-8558, Japan, Tel.: +8-22-727-0157, Fax: +8-22-275-2013, E-mail: tmiyagi@tohoku-pharm.ac.jp

What's new?

Although abnormal up-regulation of the sialidase NEU3 may play a role in colon cancer promotion and progression, the mechanisms behind its malignant activity remain unclear. This study shows that NEU3 expression is closely associated with Wnt/β-catenin signaling. In colon cancer cells, NEU3 expression was linked to tumorigenic potential and was found to influence the expression of stem- and Wnt-related genes. NEU3 activation of Wnt signaling was mediated via LRP6 phosphorylation and β-catenin activation. Wnt-mediated sphere formation was abrogated by NEU3 silencing, indicating that regulation of Wnt/β-catenin signaling by NEU3 is critical for colon carcinogenesis.

induced by azoxymethane and dextran sodium sulfate,[12] although the detailed mechanisms remained unclear.

Wnt/β-catenin signaling plays a critical role in cell fate determination and tissue development[13] and maintains pluripotency in embryonic stem cells.[14] Constitutive activation is implicated in the maintenance of cancer stem cells and initiation of the process of colon carcinogenesis,[15] and certain members of the Wnt family interact with co-receptors, Frizzled and LRP5/6, leading to inhibition of β-catenin degradation by the ubiquitin/proteasome pathway, within a large cytoplasmic complex including glycogen synthase kinase-3β (GSK-3β), disheveled, APC and Axin.[16] Inhibition of β-catenin degradation results in its accumulation, then β-catenin-dependent transactivation. There is an increasing body of evidence that inactivation of the tumor suppressor gene *APC* and mutation of the oncogene *KRAS* result in constitutive activation of Wnt/β catenin signaling and MAPK signaling, respectively, both being required for progression of colon cancer.[17–19] High Wnt activity is likely to be correlated with a coincident activation of Ras/MAPK signaling caused by KRAS mutations in colon cancers.[19] However, the upstream molecules involved in this activation and the crosstalk between the two pathways are not fully understood. To elucidate the detailed basis of the roles of NEU3 with the aim of developing an effective cure for cancer, we investigated NEU3 effects on Wnt pathway and found the sialidase to regulate the critical stem cell Wnt pathway at the ligand and receptor level even in colon cancer cells with mutations in APC or β-catenin, as well as Ras/MAPK signaling. NEU3, therefore, may be a pivotal upstream molecule regulating both of the pathways closely related to tumor initiation and progression.

Material and Methods

Patient samples

Surgical specimens were obtained from colon cancer patients who underwent resection of their tumors at Miyagi Cancer Center. Informed consent was obtained from each patient to allow the use of portions of tissue for research purposes, and the study was approved by the Committee on Human Rights in Research at Miyagi Cancer Center.

Cell culture

HT-29, HCT116 and 293 T cells were obtained from the ATCC (Manassas, VA). Cells were cultured in Dulbecco's modified Eagle's medium (DMEM) supplemented with 10% fetal bovine serum (Invitrogen) at 37 °C in a 5% CO_2 atmosphere. Wnt3a-producing L cells and control L cells from the ATCC were cultured in accordance with the manufacturer's instructions.

Plasmids and cells expressing doxycycline-inducible small hairpin RNAs

Sialidase expression vectors were constructed by subcloning NEU3 cDNA into an expression vector pCAGGS vector. Null-activity mutants of NEU3, N88D and Y370C, were prepared as described previously[20] and subcloned into pCAGGS. pCS2-FLAG-LRP6 and pCS2-LRP6-EGFP were kindly provided by Dr. C. Niehers (German Cancer Research Center, Heidelberg). pCS2-DKK1-FLAG was obtained from Addgene (16690). pCDNA-dominant negative TCF4 was a kind gift by Dr. Bert Vogelstein (Johns Hopkins University School of Medicine). To generate HT-29 and HCT116 cell lines harboring doxycycline-inducible small hairpin RNAs (shRNA), the Block-iT Lentiviral expression system (Invitrogen) was used, driven by the H1 promoter. HT-29 and HCT116 cell lines constitutively expressing high levels of the tetracycline repressor (TR) were firstly obtained by infection of lentiviruses containing the pLenti6/TR expression plasmid. After selection with blastcidin (6 and 5 μg/mL, respectively), constitutive expression of TR was assessed by immunoblotting with an anti-TR rabbit antibody (MoBiTec, Göttingen). Several clones showing high TR expression for each cell line (designed HT-29/TR and HCT116/TR) were chosen for the subsequent experiments. The target shRNA sequences for NEU3 oligonucleotides (top: CACCGCTGGAACACCGTCA GAAT CACGAATGATTCTGAC GGTGTTCCAGC, bottom: AAAAGCTGGAACACCGTCAGAATCATTCGTGATTCT GA CGGTGT TCCAGC), and the second shRNAv2 (top: CACC GCCCATGGTTACAGTAGAAT GCGAACATTCTACTGTAA CCATGGGC, bottom: AAAAGCCCATGGTTACAG TAGAAT GTTCGCATTCTACTGTAACCATGGGC), annealed were inserted into the pENTR-BLOCK-iT plasmid. After sequence verification, the H1/shRNA cassette was then transferred by recombination to the pLenti4-BLOCK-iT plasmid. HT-29/TR and HCT116/TR cells were then infected with lentiviruses containing the pLenti4-shRNAs and selected with Zeocin (100 or 200 μg/mL, respectively). After selection, cells were stimulated with Dox (2 μg/mL) and mRNA knockdown was assessed by RT-PCR using specific primers (Supporting Information Table

1). Clones displaying higher levels of mRNA knockdown were chosen.

Cells expressing ecdyson-inducible NEU3

The ecdyson-inducible NEU3 expression vector (pIND-NEU3) was constructed as described previously[5] and cotransfected with a pVgRXR vector into HCT116 cells. Positive clones were selected under G418 (800 μg/mL) and zeocin (200 μg/mL), and the cells (HCT116/Ecdy) were treated with ponasterone A (5 μM) for 24 h to induce NEU3.

Chemoresistance, colony formation and anchorage-independent growth assays

HT-29/TR and HCT116/TR cell were plated at 3,000 cells/well in 6-well dishes with or without Dox. To evaluate the effect of NEU3 silencing on chemoresistance, the cells were treated with 1 μM oxaliplatin (Sigma Aldrich) for 48 h. After 7–14 days of incubation, the colonies were quantified by Quantity One 4.5.2 (Bio-Rad Laboratories). Assays of colony formation in soft agar were performed as described previously.[21] Briefly, 1 mL underlayers consisting of 0.5% agar medium were prepared in 6-well dishes by combining equal volumes of 1.0% Noble agar (Difco, Detroit, MI) with 2× DMEM with 20% FBS. 2.5 × 10^4 cells were suspended in 0.33% agar medium with or without 2 μg/mL doxycycline and then plated onto the previously prepared underlayers. The cells were kept wet by adding a small amount of medium. After 3-4 weeks, the colonies were stained with 0.005% crystalviolet. Colonies in five fields per each sample were counted and sizes per colony number were measured under a microscope.

Quantitative RT-PCR analysis

Total RNA prepared using an RNeasy mini kit (Qiagen) was reverse transcribed with SuperScript II (Invitrogen). RT-PCR was performed with a QuantiTect SYBR Green PCR kit (Qiagen) and a Light Cycler PCR system (Roche) as described previously.[10] The primers are listed in the Supporting Information Table 1, and glyceraldehyde-3-phosphate dehydrogenase expression was determined as an internal control.

TCF reporter assays

HT-29/TR or HCT116/TR cells were plated at 3 × 10^5/well in 12-well dishes with or without Dox. After 24 h incubation, the cells were transfected with 300 ng of TOP-FLASH luciferase construct by using the effectene or lipofectamine 2000 reagents. A renilla luciferase construct (pRL-TK) was included as an internal control for transfection efficiency. After 48 h, cells were lysed, and luciferase activity was determined by using the dual-luciferase reporter assay system (Promega). For 293T cells, 20-50 ng of NEU3 cDNA plasmid was transfected with 100 ng of TOP-FLASH reporter construct.

Immunoprecipitation and immunoblotting

Cells were treated with either Wnt3a or control-conditioned medium, washed with PBS and lysed in cold lysis buffer [50 mM HEPES (pH7.5), 150 mM NaCl, 1% Nonidet P40, 2 mM EDTA, 7.5 μg/mL aprotinin, 10 μg/mL leupeptin, 10 mM NaF, 2 mM orthvanadate and 2 mM PMSF]. After centrifugation at 12, 000*g* for 15 min, cell lysates were immunoprecipitated with anti-FLAG M2 agarose beads (Sigma aldrich) or anti-GFP and protein A Sepharose beads (GE Healthcare Life Sciences). The immunoprecipitates were washed, resuspended in SDS sample buffer, and subjected to immunoblotting.

Thin-layer chromatography (TLC)

Glycolipids were extracted from cells as described elsewhere,[6] fractionated by TLC on HPTLC plates (Baker, Phillipsburg, NJ) and visualized with orcinol-H_2SO_4.

Cell fractionation

293T cells were lysed in buffer [20 mM HEPES, 250 mM sucrose, 10 mM KCl, 1.5 mM $MgCl_2$, 1 mM EDTA, 1 mM DTT and protease inhibitor cocktail (Roche)] and passed through 25G needle for 10 times and left on ice for 20 min. Cell lysates were centrifuged at 4 °C, 720*g* for 5 min and pellets were collected as nuclear fractions. The resultant supernatants were centrifuged at 10,000*g* for 1 h and collected as cytosolic fraction.

Sphere-forming assays

Cells (1000/mL) were grown in suspension culture using ultra-low attachment plates (Corning) and serum-free DMEM supplemented with B27 (Invitrogen), 20 ng/mL EGF and 20 ng/mL bFGF (Invitrogen). For the quantification of sphere-forming activity, 100 or 500 or 1000 cells were plated on 96 well ultra-low-attachment plates with or without 2 μg/mL Dox. After 7-14 days of incubation, the spheres with a diameter over 50 μm were counted.

In vivo xenograft assays

BALB/c nu/nu mice (SLC, Shizuoka, Japan) were injected subcutaneously with 3 × 10^6 HT-29/TR cells and divided into two groups, one provided with and the other without, 2 mg/mL Dox in the drinking water. Tumor growth was measured every three day once tumors become visible, and estimated as (length × width × thickness)/2. For *in vivo* tumor incidence assays, NOD/SCID mice (CREA, Tokyo) were injected subcutaneously with 10^3-10^4 HT-29/TR cells derived from monolayer culture or spheres in 100 μL of a mixture of DMEM/Matrigel (1:1). The mice injected with sphere-derived cells were also divided into two groups, one group provided with 2 mg/mL Dox in the drinking water. Tumorigenicity was evaluated at 6 weeks after transplantation. All animal experiments were performed in compliance with the guidelines of Laboratory Animal Research, Tohoku Pharmaceutical University. The protocol was approved by the Animal Care and Use Committee of Tohoku Pharmaceutical University.

Immunohistochemistry

Removed tissues were fixed in 10% neutral buffered formaldehyde 3 days, routinely processed for embedding in paraffin,

and sectioned 2.5-mm thickness. To assess NEU3 and ki-67 expression, the sections were pretreated for antigen recovery in 0.01M citrate (pH 6.0) by heating in microwave oven, and incubated with the respective antibodies.

Bromodeoxyuridine (BrdU) incorporation assay

BrdU incorporation assays were performing using the BrdU cell proliferation assay kit (Cell Signaling) according to the manufacturer's instructions.

Statistical analysis

Results are expressed as mean ± SD. All values were compared using the Student's *t test* or the Welch's *t* test.

Results

NEU3 expression is associated with tumorigenic potential of colon cancer cells

We first analyzed NEU3 by immunostaining in human colon cancer tissue specimens with anti-NEU3 monoclonal antibodies. A high level of NEU3 staining was evident in the carcinomas, but not adjacent normal mucosa (Fig. 1a), consistent with our previous data showing higher levels of NEU3 mRNA in colon cancer tissues compared with those in non-cancerous mucosa.[5] To investigate the association of NEU3 with tumorigenicity, we generated doxycycline (Dox)-inducible NEU3 shRNA transfectants in clones of HT-29/TR and HCT116/TR colon cancer cells, and examined tumorigenic potential. The gene-silencing efficiency of the Dox-induced shRNA was approximately 75 and 71% relative to non-induced HT-29/TR and HCT116/TR cells, respectively (Supporting Information Fig. 1a). These cells showed sialidase activities toward ganglioside GM3 consistent with the mRNA levels (Supporting information Fig. 1b). The increased sialidase activities were also shown in transient NEU3-transfected cells and in ecdyson-inducible NEU3-transfected cells (Supporting Information Fig. 1c). NEU3 silencing significantly reduced clonogenic growth and sensitized HT-29/TR and HCT116/TR cells to oxaliplatin-induced growth inhibition (Fig. 1b). NEU3-silenced HT-29/TR cells also showed reduction of colony formation in soft agar, both in terms of number and size (Fig. 1c). Furthermore, the silencing significantly suppressed *in vivo* tumor growth in nude mice, tumor volumes and weights being approximately half of the controls at 30 days after inoculation (Fig 1d). These results indicate that NEU3 is essential for clonogenic expansion, chemoresistance and tumorigenicity of cancer cells.

NEU3 influences expression of stem cell pluripotency marker genes and Wnt signaling related genes

To explore the mechanisms of how NEU3 expression is associated with tumorigenic potential, we next examined genes influenced by NEU3 silencing. We found down-regulation of pluripotency marker genes (Nanog, Oct4 and Sox2), epithelial-to-mesenchymal transition- genes (Snail and Twist) and Wnt signal-related genes (Wnt1, Wnt3a and EGFR) (Fig. 2a). In agreement with down-regulation of Wnt genes, expression of its target genes, Lgr5, also known as an intestinal stem cell marker,[22] and Axin2 was suppressed (Fig. 2a). It has been proposed that Nanog, Oct4 and Sox2, known as target genes of Wnt-signaling, contribute to maintenance of self-renewal and pluripotency,[14] and Snail, Twist and EGFR, also Wnt target genes, promote malignant properties such as invasion, metastasis and tumorigenicity of cancer cells.[23–26] Immunoblotting analyses showed that NEU3 silencing reduced expression of Wnt1 and its target genes including cyclinD1 and EGFR (Fig. 2b), whereas its overexpression resulted in the opposite (Fig. 2c). These results show that NEU3 actually modulates expression of Wnt and the target genes including EGFR at protein as well as mRNA levels, suggesting that this sialidase might contribute to maintenance of an undifferentiated and tumorigenic state of cancer cells.

NEU3 activates the Wnt pathway through enhanced LRP6 phosphorylation and formation of signaling complex

To understand how NEU3 regulates expression of Wnt-related genes, we then investigated molecules in the Wnt pathway by transfection of NEU3 into 293T cells. The cells showed accelerated phosphorylation of the Wnt receptor LRP6 especially in the presence of exogenous Wnt3a, and subsequently β-catenin activation (Fig. 2d). Active β-catenin was detected with an antibody recognizing active form of β-catenin non-phosphorylated.[27] LRP6 phosphorylation became evident at 1–4 h after treatment with Wnt3a, and continued up to 8 h, more clearly by NEU3 overexpression (Fig. 2e). Unlike 293T cells, known to carry an intact Wnt signaling cascade, HT-29 and HCT116 cells feature activating mutations of APC (truncated APC) and β-catenin (Ser45 deletion in one β-catenin allele and one WT allele), respectively. In these cells, the Wnt pathway is thought to be locked in the "on" state. However, other experimental observations have provided the evidence that the Wnt signaling can further be affected at the ligand and receptor level even in colon cancer cells carrying mutations in APC and β-catenin.[28–30] For example, such as secreted Frizzled -related proteins (SFRPs)[28] attenuates and Evenness interrupted/Wntless/GPR177 (Evi/Wls)[30] activates Wnt pathway even in the mutant cells *via* regulation of Wnt secretion. Opposite to the observations in 293T cells, HT-29/TR cells exhibited that the LRP6 phosphorylation and β-catenin activation were suppressed by Dox-induced NEU3 silencing either with or without Wnt, although the phosphorylation level was prominent by Wnt stimulation (Fig. 2f). HT-29/TR cells with a second NEU3 shRNA (70% silencing efficiency) and HCT116/TR cells also showed a similar tendency to suppress activation of LRP6 and β-catenin by Dox treatment (Figures 2g and 2h). These results indicate that the two colon cancer cells were affected by altered NEU3 expression and also have ability to further respond to Wnt. It should be noted here that similar results were obtained with Wnt3a recombinant protein (100 ng/mL) instead of Wnt3a conditioned medium, and the effects were

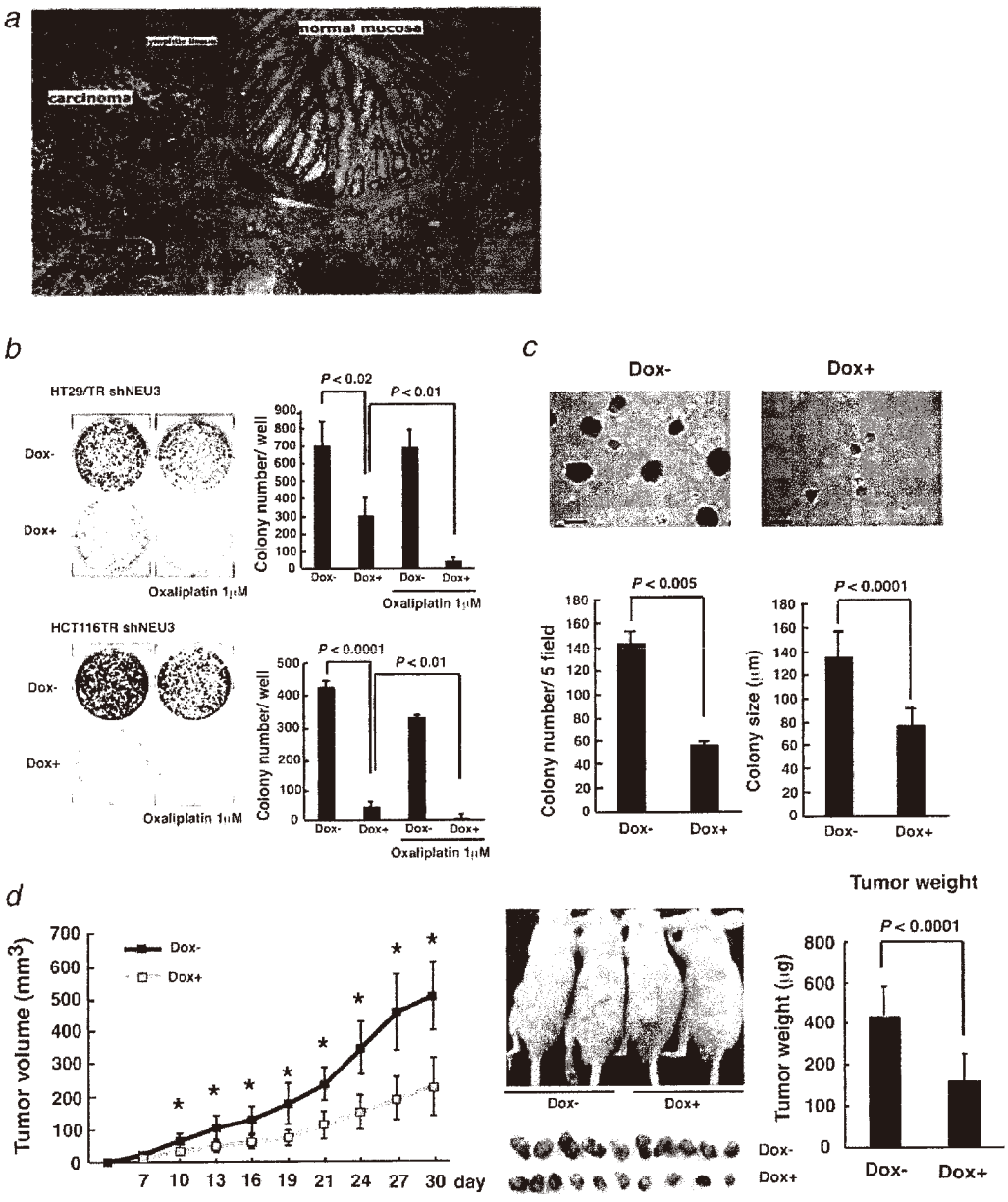

Figure 1. NEU3 is up-regulated in human colon carcinomas and the silencing inhibits clonogenicity, chemoresistance and tumorigenicity of the carcinoma cells. (*a*) Immunohistochemistry of human colon cancer tissues with anti-NEU3 monoclonal antibody. (*b*) Colony formation and chemoresistance assays in Dox-inducible NEU3 shRNA transfectants. HT-29/TR and HCT116/TR cells were plated at 3,000 cells/well in 6-well dishes with or without Dox and oxaliplatin, and the colonies were quantified after 7–14 days of culture. Representative images are shown. Values represent means with standard deviations (SD) obtained from three independent experiments. (c) Anchorage-independent growth in soft agar. 2.5×10^4 HT-29/TR cells were plated on soft agar with or without Dox, and 3–4 weeks later the colony number and size were measured (scale bar, 100 μm). Representative images are shown (upper panel), and values are means ± SD from three independent experiments (lower graph). (d) *In vivo* growth in nude mice. 3×10^7 HT-29/TR cells were subcutaneously transplanted and the mice were divided into two groups ($n = 10$), one provided with, and the other without Dox in the drinking water. Macroscopic appearance of xenotransplanted tumors (left panel) and tumor weights (right panel) is indicated.

hardly impacted by Dox treatment in case of the wild type cells (Supporting Information Figs. 2a and 2b, respectively). To confirm a close relation of NEU3 with β-catenin expression, we analyzed specimens from human colon cancer patients by immunohistochemistry with antibodies for β-catenin and NEU3, and detected strong positive staining

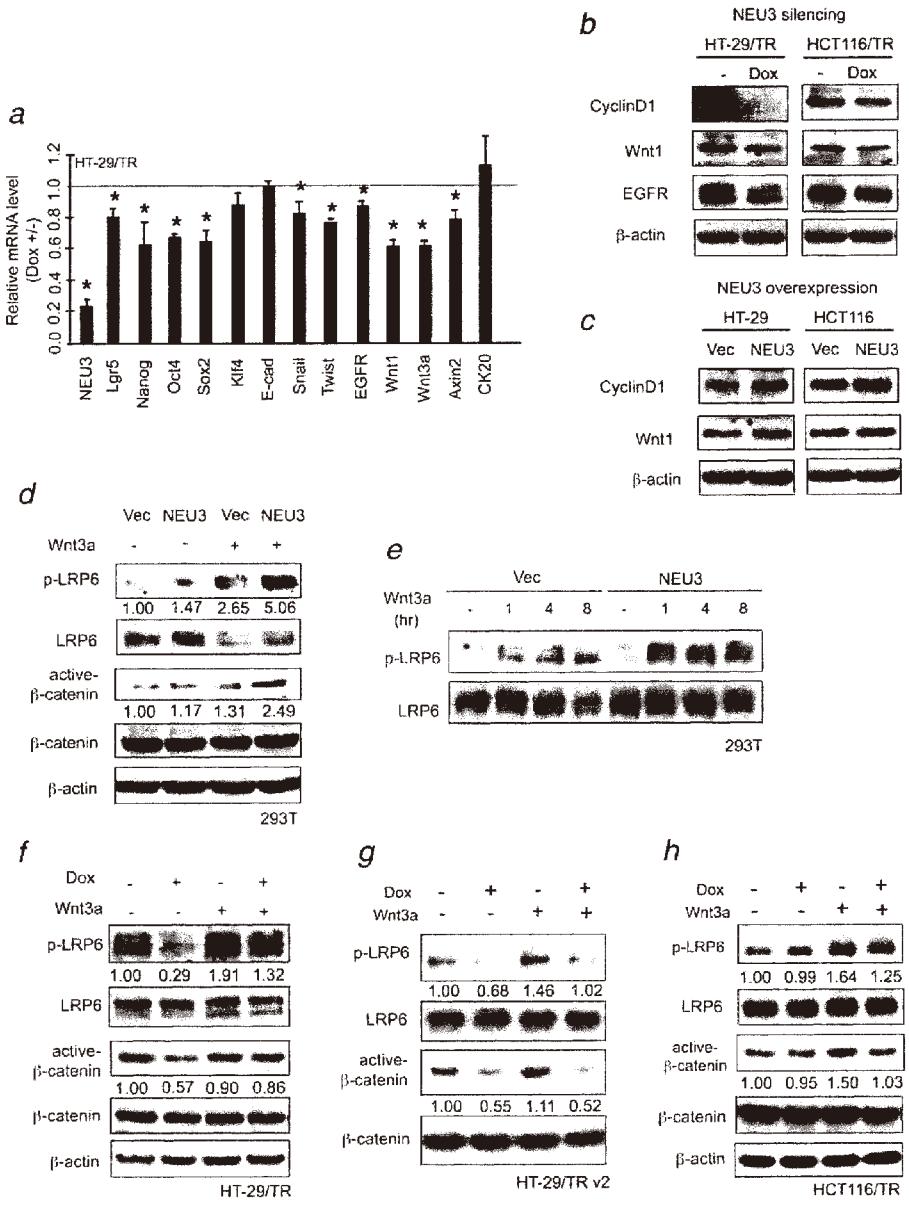

Figure 2. NEU3 alters expression of stemness and Wnt-related genes and regulates Wnt signaling through LRP6 phosphorylation. (a) Altered mRNA levels for stemness, EMT and Wnt-related genes in NEU3-silenced HT-29/TR cells assessed by RT-PCR. Data were derived from three independent experiments and presented as mean values ± SD. *$p > 0.05$ by t test. (b,c) Immunoblotting analyses for cyclin D1 (Sigma Aldrich, DCS-6), Wnt1 (Invitrogen) and EGFR (Santa Cruz) from the lysates of NEU3-silenced (Dox-induced) HT-29/TR and HCT116/TR cells (*b*) and NEU3 overexpressing-HT-29 and -HCT116 cells (*c*) with the indicated antibodies. (*d*) Effects of NEU3 overexpression on LRP6 phosphorylation and β-catenin activation. 293T cells were transfected with NEU3 or a vector control and after 48 h, treated with Wnt3a conditioned or control-conditioned medium for 1 h. Phosphorylated LRP6 (Cell Signaling, S1490) and active β-catenin (Millipore, 8E7) were assayed by immunoblotting. (*e*) Time course of LRP6 phosphorylation after treatment with Wnt3a in NEU3-transfected 293T cells. (*f, g, h*) Effects of NEU3 silencing on LRP6 phosphorylation and β-catenin activation. Phosphorylated LRP6 and activated β-catenin were examined in two HT-29/TR cells bearing different shRNAs (*f, g*) and HT116/TR cells (*h*) by immunoblotting after Dox for three days.

overlapping in areas of tumor tissues with Ki67 labeling, whereas non-tumor tissues were almost negative (Supporting Information Fig. 3).

Since it has been reported that Axin-LRP6 complexes, induced by Wnt stimulation, are required for LRP6 phosphorylation *via* their ability to recruit GSK,[31] we then examined

whether NEU3 affects complex formation. When FLAG-LRP6 was expressed in 293T cells, β-catenin, axin and GSK3β were detected in FLAG-LRP6 immunoprecipitates, and the complexes were augmented by Wnt3a stimulation (Fig. 3a). When NEU3 was co-expressed with FLAG-LRP6, β-catenin, Axin1 and GSK3β in FLAG-LRP6 immunoprecipitates were increased compared to control cells either with or without exogenous Wnt3a stimulation (Fig. 3a). Simultaneously, NEU3 was detected in the immunoprecipitates with greater amounts of the protein on Wnt3a stimulation. LRP6-EGFP was also detected in NEU3-FLAG immunoprecipitates (Fig. 3b), confirming the presence of NEU3 in LRP6-associated complexes. NEU3-transfected HCT116 cells also showed a significant increase in β-catenin, Axin1 and GSK3β in the LRP6 immunoprecipitates (Fig. 3c). It may be reasonable for the cells to enhance Axin-LRP-6 complex formation, since there remains one wild type allele of β-catenin and wild type APC. We then studied the effect of null-activity NEU3 mutants, N88D and Y370, on LRP6 phosphorylation, to determine whether enzymatic activity is essential for the effects. Unlike the case of the wild type, the phosphorylation level was not increased in either the N88D or Y370C mutant, which is not significantly different from that of vector control (Fig. 3d, left panel). The quantitative data in the graph from the four independent experiments (right panel) confirmed that the relative level was the highest in wild NEU3, different from vector and the two mutants. The results indicate that the glycolipid change by NEU3 catalysis is probably required for LRP6 phosphorylation. Glycolipid patterns of wild type NEU3-, or the N88D mutant-transfected 293T cells were then analyzed by TLC (Fig. 3e). In the neutral fractions, wild type NEU3 revealed a significant increase in the glycolipid with similar mobility to lactosylceramide (Lac-Cer), and decrease in that to GM3 in the acidic fraction as compared with those of vector and the mutant. The glycolipid changes are attributable to the results of NEU3 catalytic reaction, because of these glycolipids possibly to be the product and substrate, respectively, for the sialidase. Glycolipid analyses of HT-29 cells also revealed a slight but significant decrease in the glycolipid with similar mobility to Lac-Cer in NEU3-silenced HT-29/TR cells, and an apparent increase in NEU3 overexpressing HT-29 cells (Supporting Information Fig. 4a), although the difference in glycolipid patterns shown between stable HT29/TR cells and transient NEU3- transfected cells is possibly due to the dependence of transfection mode. The glycolipid alterations were validated by quantitative data from the five independent experiments with statistical relevance (right panel). On the other hand, NEU3-silenced HCT116/TR cells showed only a significant increase in GM3 in the acidic fractions as confirmed by TLC-immunostaining with anti-GM3 antibody (Supporting Information Fig. 4b), whereas NEU3 overexpression yielded tendency of a subtle increase in putative Lac-Cer in HCT116 cells (data not shown). These results are not contradictory to our previous observations in human colon cancer tissues,[5] demonstrating that most characteristic changes of the cancer tissues were a marked increase of Lac-Cer in the several cases tested as compared with non-tumor mucosa. Although a small amount of other glycolipids involved in the phenomena cannot be excluded, the glycolipid changes may be related to the NEU3-mediated enhanced LRP6 phosphorylation. To verify the effects, Lac-Cer or GM3 was added exogenously to 293T cells. Wnt-induced LRP6 phosphorylation was accelerated by Lac-Cer (Fig. 3f), and suppressed by GM3 (Fig. 3g), suggesting a positive involvement of Lac-Cer and the opposite effects of GM3 as the glycolipids altered by NEU3 in LRP6 phosphorylation. It is interesting to note here that even without Wnt3a, the phosphorylation increase was observed with Lac-Cer at higher concentration, which may be feasible because endogenous NEU3 in colon cancer cells and overexpressing NEU3 in 293T cells often exhibited higher LRP-6 phosphorylation without Wnt than those in the control cells.

NEU3 regulates β-catenin/T cell factor transcriptional activity and contributes to anchorage-independent growth *via* Wnt/β-catenin/TCF-dependent pathway

We then examined the effects of NEU3 on β-catenin nuclear localization and on β-catenin-dependent TCF transcriptional activity. Subcellular localization of β-catenin was assessed by immunoblotting in NEU3-silenced 293T cells. β-catenin was present in the cytoplasm at a relatively low level, and in response to Wnt3a, was detected at high levels in the cytoplasm and nucleus. However, NEU3 silencing reduced the levels in both compartment (Fig. 4a). The subcellular localization of β-catenin was confirmed by immunofluorescence confocal microscopy in HCT116 cells. As shown in Figure 4b, in response to Wnt3a, accumulation of β-catenin in the nucleus was observed, and NEU3 overexpression showed a greater effect, suggesting that NEU3 enhances β-catenin nuclear localization. We next determined TCF-dependent transcriptional activity in NEU3-transfected 293T cells and HT-29/TR and HCT116/TR cells. NEU3 transfection in 293T cells increased the transcriptional activity in response to Wnt3a, although the increase was only modest without Wnt3a (Fig. 4c). On the other hand, the two Dox-induced HT-29/TR and HCT116/TR cells decreased TCF activity as a consequence of NEU3 silencing (Fig. 4d). These results indicate that NEU3 regulates β-catenin/TCF transcriptional activity.

We further examined whether NEU3-mediated stimulation of TCF activity actually contributes to anchorage-independent growth of colon cancer cells. In ecdyson- inducible NEU3-transfectd HCT116 cells (HCT116/Ecdy),[5] ponasterone- induced NEU3 significantly enhanced colony formation in soft agar as compared in non-induced cells, which was abolished by dominant negative TCF4 and also by LGK974, a porcupine inhibitor causing disturbance of autocline Wnt signaling (Fig. 4e).[30,32] In HT-29/TR cells, colony formation in soft agar was increased in the presence of recombinant Wnt3a and the increase was attenuated by

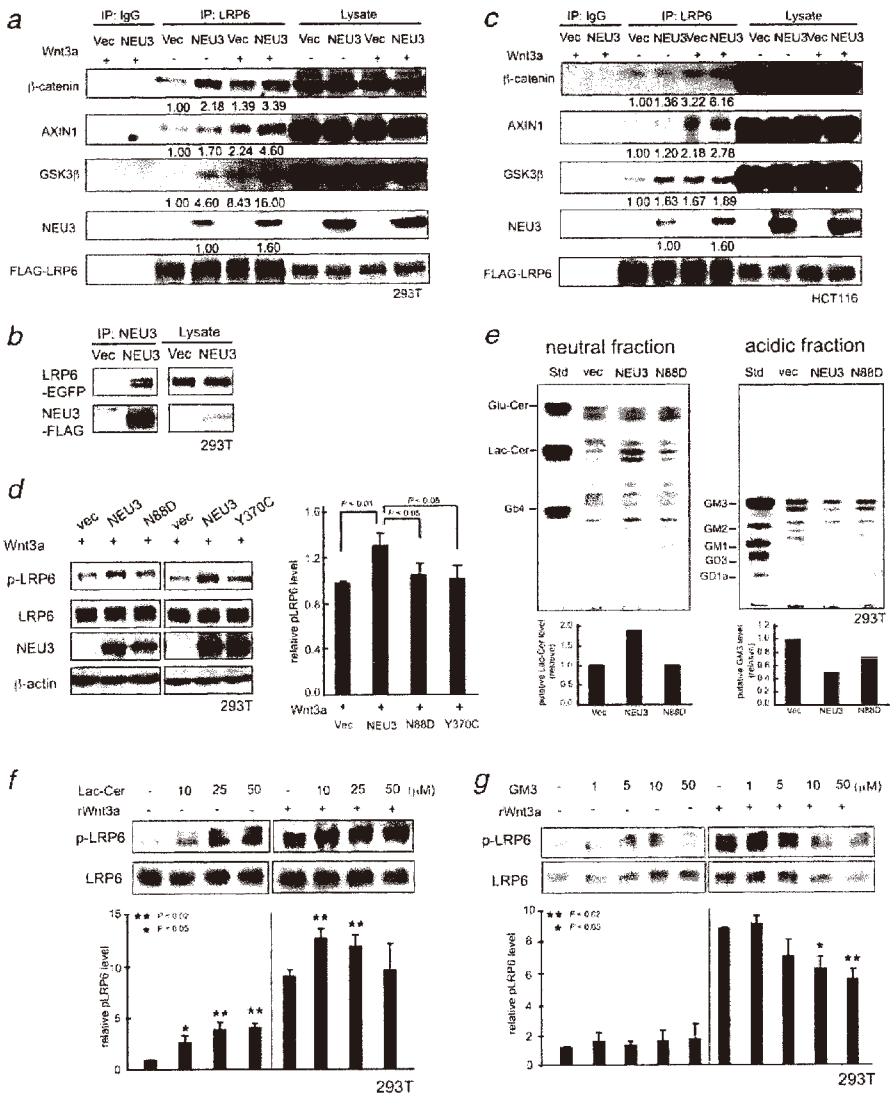

Figure 3. NEU3 regulates LRP6 phosphorylation through acceleration of signaling complex formation and ganglioside modulation. (*a*) Effects of NEU3 on formation of signaling complexes in 293T cells. The cells were co-transfected with NEU3 and FLAG-LRP6 and treated with Wnt3a-conditioned medium for 1 h. Lysates were subjected to immunoprecipitation using FLAG M2 agarose beads and subjected to immunoblotting. Each value shown under the blot represents as a value relative to that in the vector control. (*b*) Co-immunoprecipitation of NEU3 with LRP6 in complexes. For immunoprecipitation assays with NEU3-FLAG, 293T cells were transfected with LRP6-EGFP together with NEU3-FLAG. (*c*) Effects of NEU3 on formation of signaling complexes in HCT116 cells. The cells were co-transfected with NEU3 and FLAG-LRP6 and treated with Wnt3a-conditioned medium for 1 h. Lysates were subjected to immunoprecipitation using FLAG M2 agarose beads and subjected to immunoblotting. Each value shown under the blot represents as a value relative to that in the vector control. (*d*) Effects of NEU3 sialidase activity on LRP6 phosphorylation. 293T cells were transfected with null-activity mutants of NEU3, N88D and Y370C, and treated with Wnt3a-conditioned medium for 1 h. The level of LRP-6 phosphorylation in NEU3-transfected cells was compared with those of vector control and of the mutants N88D and Y370C by immunoblotting (left panel). The graph (right panel) indicates relative LRP6 phosphorylation level in the wild type NEU3 and the mutants, N88D and Y370C. Data are mean values ± SD obtained from four independent experiments (*e*) Alteration of glycolipids in NEU3- and N88D mutant-transfected 293T cells. The neutral and acidic fractions of the glycolipids extracted from the cells were separated by a DEAE- Sephadex A25 column and developed on TLC plates in chloroform-methanol-water (60:40:9, v:v:v) containing 0.02% $CaCl_2$ and in chloroform-methanol-water (60:35:8: v:v:v), respectively. Results are representative of two independent experiments. (*f, g*), Effect of exogenously added Lac-Cer (*f*) or GM3 (*g*) on LRP6 phosphorylation. The glycolipid in a 2:1 chloroform/methanol solution and then in ethanol was dried and sonicated in serum-free DMEM for 10 min. 293T cells (5×10^5) were cultured in 6-well plates in DMEM containing 10% FBS for 24 h at 37 °C, incubated with Lac-Cer or GM3 at final concentrations of 1–50 μM for 16 h, and then with or without recombinant human Wnt3a protein (100 ng/mL, R&D Systems) for an additional 1 h before immunoblotting. The graph indicates LRP6 phosphorylation level relative to those without exogenous glycolipid and Wnt3a protein. Data are mean values ± SD from three independent experiments.

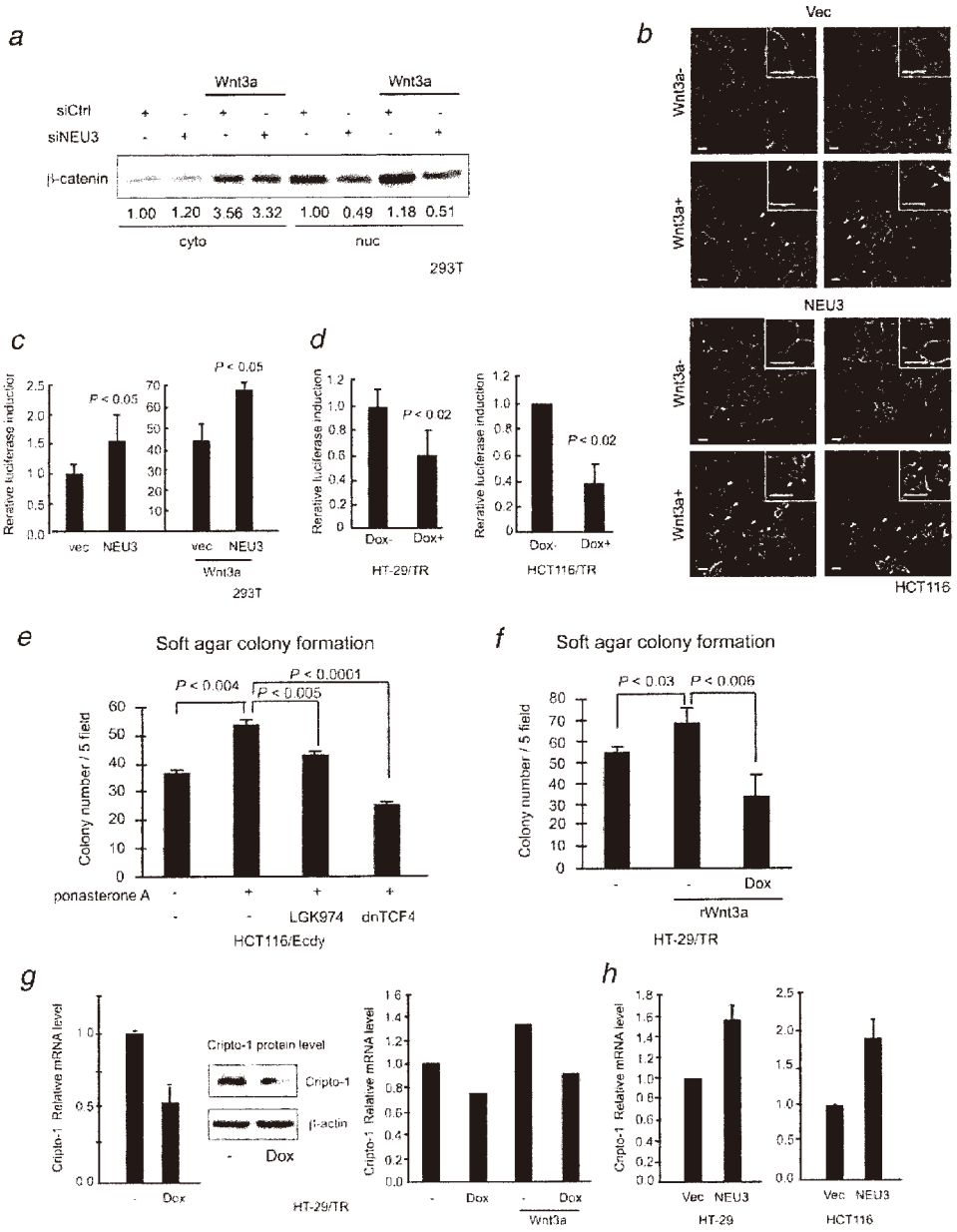

Figure 4. NEU3 regulates TCF-dependent transcriptional activity and contributes to anchorage-independent growth and Cripto-1 expression *via* Wnt/β-catenin/TCF- dependent pathway. (*a*) Effects of NEU3siRNA transfection on the amount of β-catenin in the cytosol and nucleus of 293T cells treated with and without Wnt3a-conditioned medium for 1 h. Each value shown under the blot represents as a value relative to that in the control. (*b*) Subcellular localization of β-catenin in NEU3-transfected HCT116 cells, assessed by immunofluorescence confocal microscopy. The cells grown on glass coverslips were transfected with pCAGGS-vector or -NEU3, incubated for 24 h, treated with Wnt3a conditioned medium for 16 h, and accumulation of β-catenin in the nucleus was observed. Cells were fixed, permeabilized and treated with anti-β-catenin antibody followed by secondary conjugated antibody. The cells washed were mounted on under Fluoromount/Plus (Diagnostic BioSystems) as an anti-fading agent. Fluorescent images were obtained using a confocal laser-scanning microscope (FluoView FV1000, Olympus). Small white arrows indicate accumulated β-catenin. (*c*) The transcriptional activity in the NEU3-transfected 293T cells treated with and without Wnt3a. Data are mean values ± SD from four independent experiments. (*d*) The transcriptional activity in Dox-induced HT-29/TR and HCT116/TR cells. Data are mean values ± SD from four independent experiments. (*e*) Effects of NEU3 activity induction on colony formation in soft agar with and without LGK974 (an inhibitor of Wnt secretion) or dominant negative TCF4. The stable ecdyson-inducible NEU3 transfected HCT116 cells (HCT116/Ecdy) generated as described previously[5] were supplemented with 5 μM ponasterone A for NEU3 induction and treated with or without 1 nM LGK974. For the ectopic expression of dominant negative TCF4, the cells were transiently transfected with dnTCF4 plasmid before the growth assay. (*f*) Effects of NEU3 silencing on Wnt-dependent increase of colony formation in soft agar. HT-29/TR cells were treated with or without Dox and recombinant human Wnt3a protein (100 ng/mL) for 3-4 weeks. (*g,h*), NEU3-mediated alteration of Cripto-1 expression, known to undergo direct regulation by Nanog and Oct4. Down-regulation of cripto-1 expression at mRNA and protein (Cell Signaling) levels in Dox-induced HT-29/TR (*g*), and increased level of Cript-1 mRNA in NEU3 overexpressing HT-29 and HCT-116 cells (*h*).

NEU3 silencing (Fig. 4f). These results strongly suggest that NEU3 plays an essential role in determining anchorage-independent growth of the colon cancer cells *via* Wnt pathway in a β-catenin/TCF-dependent manner and in concert with autocrine secretion of Wnts.

To investigate whether NEU3-mediated TCF activity actually affects transcription of molecules downstream the signaling and what target genes are mostly influenced, we carried out microarray analysis of gene expression in NEU3-silenced HT-29/TR cells using affymetrix Human Gene 1.0 ST Arrays. A total 182 genes were influenced by NEU3 silencing (by ≧1.3-fold), and among those, interestingly Cripto-1 was the one of the most down-regulated. We confirmed that NEU3 silencing down-regulated cripto-1 expression at mRNA and protein levels (Fig. 4g), while its overexpression resulted in the opposite effects (Fig. 4h). Since Cripto-1 has been described to undergo direct regulation by the transcription factors, Nanog and Oct4[33,34] and to drive tumor growth through maintenance of tumor initiating cells bearing stem-like characteristics,[35,36] it may be a key molecule related to NEU3 expression contributing to self-renewal and tumorigenic potential.

NEU3 expression is closely linked to sphere-forming capacity and tumorigenic potential

Tumorigenic undifferentiated cancer cell populations can grow as floating aggregates, called spheres, when placed on non-adhesive plates under serum-free conditions.[37] We therefore used sphere-forming assays to investigate whether NEU3 actually contributes to maintenance of the undifferentiated and tumorigenic state of cancer cells. After 7 days under the culture conditions, HT-29 and HCT116 cells were able to resist anoikis and clustered in multicellular spheroids (Fig. 5a). In these cells, endogenous NEU3 was markedly up-regulated compared to the case in monolayer culture in mRNA and protein levels along with β-catenin activation (Fig. 5b). When colon spheres derived from HT-29 cells were placed on adhesive plates with medium containing 1% FBS, NEU3 expression was decreased down to the same level as in monolayer culture (Figs. 5a and 5b), and in HCT116 spheres NEU3 was further up-regulated after a second generation of sphere dissociation and regrowth (Fig. 5c). We next determined whether the sphere cells express stem cell marker genes. The pluripotency marker genes Nanog, Oct4 and Sox2 were up-regulated, and Lgr5, Wnt1 and Wnt3a were also enriched (Figs. 5d and 5e), indicating a close association of NEU3 expression with tumorigenic undifferentiated cell populations. To confirm effects of NEU3 on sphere-forming ability, we silenced NEU3 in HT-29/TR and HCT116/TR cells and evaluated sphere formation. NEU3 depletion indeed inhibited the formation (Figs. 5f and 5g). In response to Wnt3a, which has been reported as the most essential signal for stem cell maintenance in culture,[38] the cells showed an increase in sphere formation but a significant reduction by Dox-induced NEU3 silencing in two HT-29/TR cells bearing different shRNAs (Fig. 5h) and HCT116/TR cells (Fig. 5i), indicating NEU3 depletion affects Wnt-activated sphere formation. Similar to the results for endogenous NEU3 levels, sphere formation up-regulated Nanog, Oct4 and Sox2 as well as Wnt1 and Wnt3a, but NEU3 depletion induced by Dox treatment dramatically reduced the expression of these genes in HT-29/TR cells (Fig. 5j).

We further evaluated *in vivo* tumorigenicity of the cells derived from spheres. $1x10^3$ or $1x10^4$ cells derived from monolayer or sphere culture were injected subcutaneously into NOD/SCID mice with or without 2 mg/mL Dox in their drinking water, and tumor incidence was evaluated at 6 weeks after inoculation (Figs. 5k and 5l). Cells derived from spheres showed the highest tumorigenic potential, with six of six animals developing tumors when injected with as few as 10^3 cells, whereas with cells from monolayer culture tumors developed in only two of five animals. However, surprisingly, no tumor development was noted with NEU3-silencing of cells derived from spheres in five animals injected with 10^3 cells, probably due to down-regulation of not only stemness but some growth- related genes by NEU3 depletion, under spheroid culture conditions containing growth factors such as EGF and FGF. These results suggest that NEU3 essentially participates in colon sphere tumorigenicity in association with Wnt signaling pathway.

NEU3 activates ras/ERK and akt pathway in response to EGF

Recent observations have proposed that aberrant Wnt signaling does not signify particular tumorigenic potential since promoting adenoma progression to carcinomas requires the additional activation of the KRAS/MAPK pathway.[17–19] We previously demonstrated NEU3 to stimulate Ras activation with consequent influence on ERK and Akt in response to EGF in HeLa cells.[10] We therefore examined whether NEU3 alters the Ras/ERK pathway in colon cancer cells and whether NEU3 is involved in cross-talk between Wnt/β-catenin and MAPK signaling. Similar to the case of HeLa cells, NEU3 silenced HT-29/TR cells clearly showed reduced phosphorylation of EGFR, ERK and Akt with EGF (Fig. 6a, left), together with a marked reduction of the Ras activity even without EGF (lower panel), and HCT116/TR cells even bearing KRAS mutation also gave similar results (Fig. 6a, right), indicating that NEU3 activates the Ras/MAPK pathway.

To cast light on possible pathway relevant to NEU3-mediated activation of LRP6 and ERK, an antagonist of Wnt/β-catenin pathway, DKK1, was overexpressed into 293T cells. DKK1 profoundly reduced phosphorylation of LRP6 but with little effect on NEU3-mediated ERK and c-Jun activation (Fig. 6b). These data confirmed that NEU3 increased LRP6 phosphorylation through canonical pathway. Although there is a report suggesting that MAP-kinases such as p38, ERK1/2 and JNK promote Wnt/β-catenin signaling *via* phosphorylation of proline directed-PPPS/TP motifs of LRP6,[39] it is not the case for NEU3 in the present study. However, NEU3-

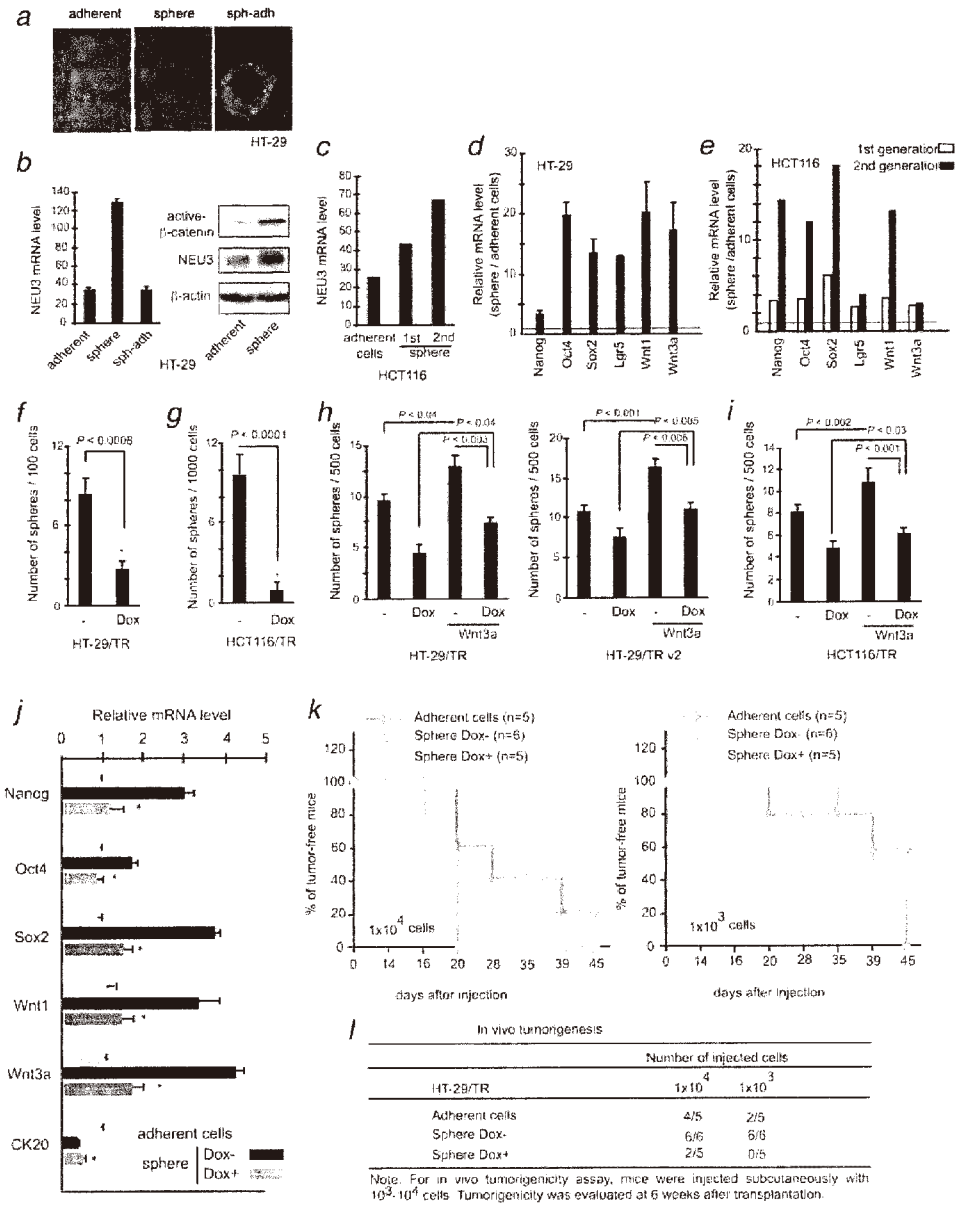

Figure 5. NEU3 expression is closely associated with sphere-forming capacity and tumorigenic potential. (*a*) Representative images for spheres from HT-29 cells. The cells were grown in serum-free medium on non-adhesive plates (scale bar, 100 μm). (*b*) Up-regulation of endogenous NEU3 expression in spheres and its down-regulation on adhesive plates in 1% FBS in HT-29 cells. Data are mean values ± SD from three independent experiments. In the right panel, increased active-β-catenin and up-regulation of NEU3 protein were observed in spheres as compared to adherent cells by immunoblotting. (*c*) Further up-regulation of NEU3 mRNA level after a second generation of sphere in HCT116 cells. Data are mean values ± SD from three independent experiments. (*d*, *e*) Gene expression analyses of spheres compared to adherent cultures, quantitated by RT-PCR in HT-29 (*d*) and HCT116 (*e*) cells. Data are mean values ± SD from three independent experiments (*d*) and mean values from two experiments (*e*). (*f*, *g*) Reduction of sphere-forming ability by NEU3 silencing in. HT-29/TR cells (100 cells) (*f*) or HCT116/TR cells (*g*) (100 or 500 or 1000 cells) on 96 well ultra-low-attachment plates with or without Dox. The values represent means ± SD from six wells. (*h*, *i*) Effects of NEU3 silencing on sphere-forming ability of the cells supplemented with or without Wnt3a recombinant protein (200 ng/mL). Two HT-29/TR cells bearing different shRNAs (*h*) and HCT116/TR cells (*i*) were incubated with or without Dox. The values represent means ± SD from six wells. (*j*) Reduced expression of Nanog, Oct4 and Sox2 as well as Wnt1 and Wnt3a in the spheres in HT29/TR cells with Dox treatment assessed by RT-PCR. The values represent means ± SD from three experiments. *$p > 0.05$ by t test. (*k*, *l*) Reduced *in vivo* tumorigenicity of the cells derived from spheres. 1×10^3 or 1×10^4 cells derived from monolayer or sphere culture were injected subcutaneously into NOD/SCID mice with or without Dox in their drinking water, and tumor incidence was evaluated at 6 weeks after inoculation as shown in graph (*k*) and in Supporting Information Table 1.

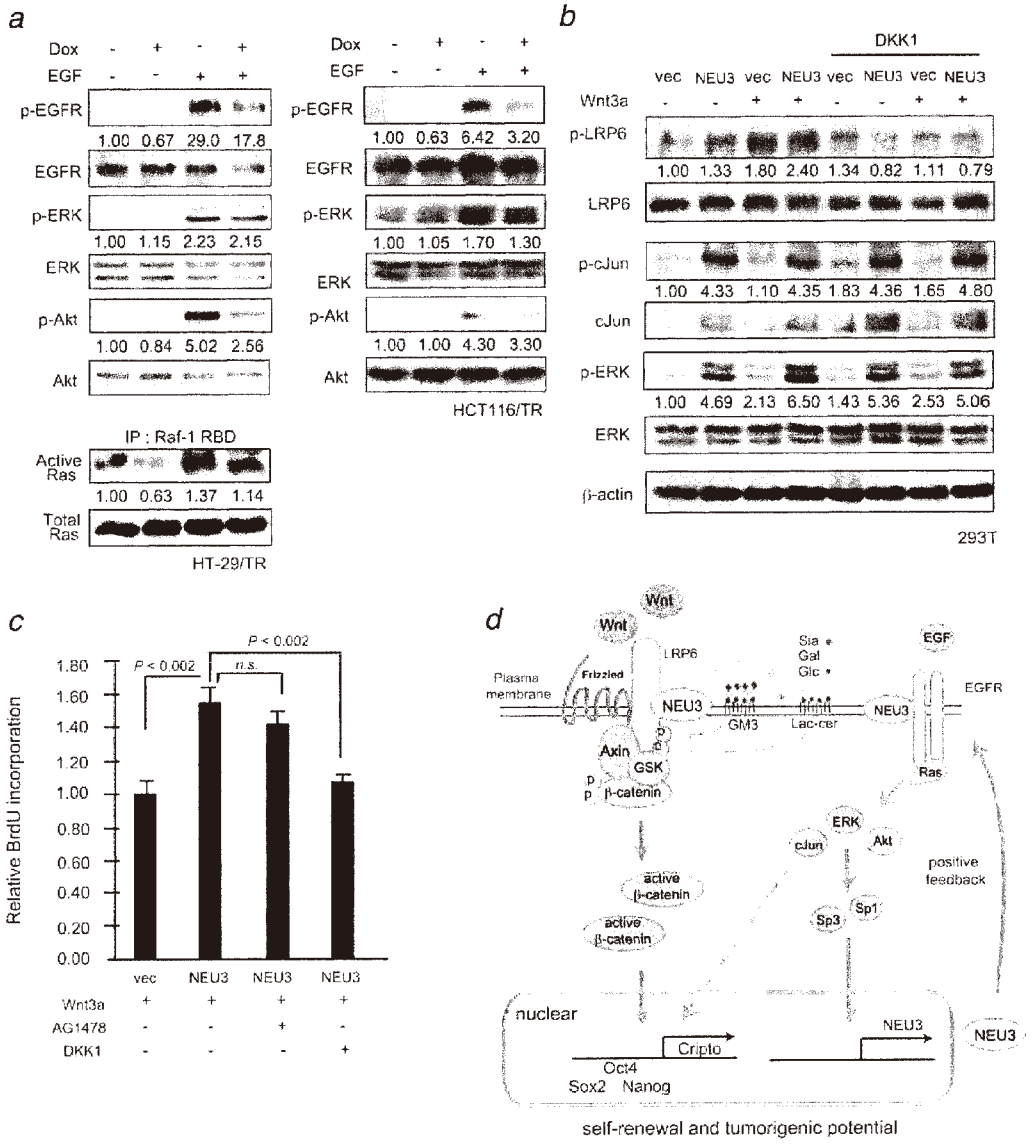

Figure 6. NEU3 regulates Ras/ERK pathway in response to EGF. (*a*) Reduced phosphorylation of EGFR(Santa Cruz), ERK1/2 (Cell Signaling)and Akt (Cell Signaling) by NEU3 silencing with EGF treatment for 15 min in Dox-induced HT-29/TR cells (left panel). Concomitant down-regulation of Ras activity by NEU3 silencing was also shown in the lower panel. To assess Ras activation, affinity precipitation assays for active (GTP-bound form) Ras were performed using Raf-1 RBD-agarose (Upstate). In the right panel, reduced EGFR signaling by NEU3 silencing in Dox-induced HCT116/TR cells. (*b*) Effects of DKK1 (an antagonist of Wnt/βcatenin pathway) on phosphorylation of LRP6 (Cell Signaling), c-Jun (Cell Signaling) and ERK1/2 in the absence or presence of Wnt3a for 1 h in NEU3 overexpressing 293T cells. In this experiment, human DKK1 cDNA was transfected, and in another experiment, human recombinant DKK1 protein (200 ng, R&D Systems) was added to the cell culture medium. In (*a*) and (*b*), Results are representative of two and four independent experiments, respectively. (*c*) BrdU incorporation in Wnt-treated HCT116 cells in the presence of an EGFR inhibitor, AG1478, or DKK1. (*d*) Regulation of Wnt signaling by NEU3 in a positive feedback manner in concert with RAS/MAPK signaling. NEU3 regulates Wnt signaling and Wnt expression through ganglioside modulation, and Wnt treatment promotes expression of endogenous NEU3 and its transcription factors, Sp1 and Sp3, as shown in Supporting Information Figure 5, probably through activation of EGFR and other signaling pathways. Thus, NEU3-mediated Wnt pathway activation could occur in a positive feedback manner especially in colon carcinomas.

mediated stimulation of ERK, Akt and c-Jun may also give some influence on activation of Wnt signaling through transactivation of β-catenin as described in recent reports.[40–42] Not only phosphorylation of c-Jun but also its protein level were increased by NEU3, probably due to autotransactivation by the phosphorylation.[43] To observe whether

NEU3-mediated EGFR activation influences on Wnt-induced effects, cell proliferation was assessed by BrdU incorporation in the presence of an EGFR inhibitor, AG1478, or DKK1 in Wnt-treated HCT116 cells. As shown in Figure 6c, blocking of EGFR activation by AG1478 hardly affected NEU3-mediated increase of cell proliferation, but DKK1 reduced significantly. These results suggest that NEU3-mediated promotion of cell growth subsequent to activation of Wnt signaling may mainly occur through canonical pathway but only partly through MAPK signaling in the cells.

NEU3 regulates Wnt signaling in a positive feedback manner

We then determined whether endogenous NEU3 expression is altered by Wnt stimulation. Consistent with the data in Figure 2b, Wnt expression was down-regulated in the NEU3-silenced cells (Supporting Information Fig. 5a), and on the other hand, Wnt treatment yielded 2.5-fold increase in NEU3 expression in protein as well as mRNA levels, together with increased Sp1 and Sp3 mRNA levels (Supporting Information Figs. 5b and 5c) by which NEU3 undergoes transcriptional activation.[44] These transcriptional factors are positively regulated by several kinases including ERK[45] and are involved in transcriptional regulation of genes implicated in cell growth and tumorigenesis including EGFR.[46] The results suggest that NEU3 dependent activation of Wnt and Ras/MAPK signaling would bring about NEU3 transcriptional activation, possibly leading to positive feedback activation of Wnt and EGFR signaling. As shown in Figure 6d, all the results together suggest that NEU3 regulates Wnt/β-catenin pathway at the ligand and receptor level by promoting LRP6 phosphorylation and formation of Axin-LRP6 complexes, and additionally ERK and Akt pathways, in response to Wnt and EGF, through alteration of gangliosides in a positive feedback manner. This modulates the downstream genes, including Nanog, Oct4 and Crypto-1, essential to maintain the self-renewal and tumorigenic potential of colon cancer cells.

Discussion

Inactivation of APC or activation of β-catenin initiates the process of colon carcinogenesis,[47] and this causes constitutive activation of Wnt signaling.[13] In particular, Wnt activity defines colon cancer stem cells and its down-regulation decreases self-renewal and growth of colon spheres.[37] Recent reports have also proposed that colon cancer development is likely to require additional activation of RAS/MAPK signaling[18] and Wnt activity actually correlates with a coincident activation of MAPK signaling.[19] Our previous studies demonstrated sialidase NEU3 to be aberrantly up-regulated in many human cancers, causing acceleration of cellular invasion and survival by activating EGFR signaling,[10] and also suggested the possible roles of NEU3 in the process of colon carcinogenesis in *NEU3*-expressing transgenic mice[11] and *Neu3*-deficient mice,[12] although the detailed basis of the roles of NEU3 in cancer remained unclear.

In our study, we found NEU3 to be a unique molecule regulating Wnt/β-catenin signaling and participating in crosstalk with Ras/MAPK and Akt pathways, which was expected by the results of Wnt and EGFR protein levels altered by NEU3 expression (Fig. 2b). Firstly, NEU3 was found to regulate Wnt/β-catenin signaling at the receptor level by promoting LRP6 phosphorylation and complex formation with LRP6, for which NEU3 catalytic activity was required. We further found that enhancement of anchorage-independent growth by NEU3 was abolished by dominant negative TCF4 and by an inhibitor for autocline Wnt signaling, LGK974 (Fig. 4e) and that Wnt- stimulated spheroid formation was suppressed by NEU3 silencing of the colon cancer cells (Figs. 5h and 5i). These results all together imply that NEU3 contributes to driving tumor growth through maintenance of tumor initiating cells bearing stem-like characteristics, and thus tumorigenic potential is likely defined at least partly by cell surface glycolipid components altered by NEU3 up-regulation in cancers.

Furthermore, the present study revealed that NEU3 activates Wnt/β-catenin signaling and also ERK and Akt pathways, which are thought to be essential for initiation and progression of colon cancers. Wnt and EGFR pathways have been proposed to apparently crosstalk and transactivate one another.[48] NEU3 is not likely to influence only in one way but may play a role directly as a signaling molecule upstream of the pathways including Wnt/β-catenin signaling and, as a consequence, be involved in regulation of downstream molecules such as Cripto-1. In this context, NEU3 may critically participate in re-expression of embryonic genes such a Nanog, Oct4 and cripto-1 in cancer cells through modulation of autocline and expression of Wnts. Our previous results suggested NEU3 to activate EGFR signaling in a positive-feedback manner by EGF stimulation through Ras/ERK signals elevating Sp1 and Sp3 expression,[10,43] but at present it is uncertain the detailed mechanism how NEU3 to regulate Wnt expression and how itself to be regulated by a pulse of exogenous Wnt. All together, our present study uncovered a pivotal role of NEU3 in maintenance of self-renewal and tumorigenic potential of colon cancer cells probably through alteration of gangliosides. Thus, NEU3 may represent an attractive target for treatment, conceivably leading to the elimination of undifferentiated stem-like tumor initiating cells.

Acknowledgements

The authors appreciate Dr. G. Fischer (Institute of Pathology, Academic Hospital of the University Gottingen) for his great guidance in immunohistochemical analysis, Dr. C. Niehers (German Cancer Research Center, Heidelberg) and Dr. B. Vogelstein (Johns Hopkins University School of Medicine) for their generous gifts for pCS2-FLAG-LRP6 and pCS2-LRP6-EGFP, and pCDNA-dnTCF4, respectively, and Dr. K. Iwabuchi (Juntendo University) for his helpful discussion. We are also grateful to Ms. S. Moriya (Tohoku Pharmaceutical University) for her valuable technical assistance.

References

1. Lau KS, Dennis JW. NGlycans in cancer progression. *Glycobiology* 2008;18:750–60.
2. Hakomori SI. Glycosynaptic microdomains controlling tumor cell phenotype through alteration of cell growth, adhesion, and motility. *FEBS Lett* 2010;584:1901–6.
3. Miyagi T, Yamaguchi K. Mammalian sialidases: physiological and pathological roles in cellular functions. *Glycobiology* 2012;22:880–96.
4. Miyagi T, Takahashi K, Hata K, et al. Sialidase significance for cancer progression. *Glycoconjug J* 2012; 29:567–77.
5. Kakugawa Y, Wada T, Yamaguchi K, et al. Up-regulation of plasma membrane-associated ganglioside sialidase (neu3) in human colon cancer and its involvement in apoptosis suppression. *Proc Natl Acad Sci U S A* 2002;99:10718–23.
6. Ueno S, Saito S, Wada T, et al. Plasma membrane-associated sialidase is up-regulated in renal cell carcinoma and promotes interleukin-6-induced apoptosis suppression and cell motility. *J Biol Chem* 2006;281:7756–64.
7. Nomura H, Tamada Y, Miyagi T, et al. Expression of neu3 (plasma membrane-associated sialidase) in clear cell adenocarcinoma of the ovary: its relationship with T factor of pTNM classification. *Oncol Res* 2006;16:289–97.
8. Kawamura S, Sato I, Wada T, et al. Plasma membrane-associated sialidase (neu3) regulates progression of prostate cancer to androgen-independent growth through modulation of androgen receptor signaling. *Cell Death Differ* 2011;19:170–9.
9. Kato K, Shiga K, Yamaguchi K, et al. Plasma-membrane-associated sialidase (neu3) differentially regulates integrin-mediated cell proliferation through laminin- and fibronectin-derived signalling. *Biochem J* 2006;394:647–56.
10. Wada T, Hata K, Yamaguchi K, et al. A crucial role of plasma membrane-associated sialidase in the survival of human cancer cells. *Oncogene* 2008;26:2483–90.
11. Shiozaki K, Yamaguchi K, Sato I, Miyagi T. Plasma membrane-associated sialidase (neu3) promotes formation of colonic aberrant crypt foci in azoxymethane-treated transgenic mice. *Cancer Sci* 2009;100:588–94.
12. Yamaguchi K, Shiozaki K, Moriya S, et al. Reduced susceptibility to colitis-associated colon carcinogenesis in mice lacking plasma membrane-associated sialidase. *PLoS One* 2012;7: e41132
13. Clevers H. Wnt/beta-catenin signaling in development and disease. *Cell* 2006;127:469–80.
14. Wray J, Hartmann C. WNTing embryonic stem cells. *Trends Cell Biol* 2012;22:159–68.
15. Segditsas S, Tomlinson I. Colorectal cancer and genetic alterations in the wnt pathway. *Oncogene* 2006;25:7531–37.
16. Niehrs C, Shen J. Regulation of lrp6 phosphorylation. *Cell Mol Life Sci* 2010;67:2551–62.
17. Janssen KP, Alberici P, Fsihi H, et al. APC and oncogenic KRAS are synergistic in enhancing wnt signaling in intestinal tumor formation and progression. *Gastroenterology* 2006;131:1096–109.
18. Phelps RA, Chidester S, Dehghanizadeh S, et al. A two step model for colon adenoma initiation and progression caused by APC loss. *Cell* 2009; 137:623–34.
19. Horst D, Chen J, Morikawa T, et al. Differential WNT activity in colorectal cancer confers limited tumorigenic potential and is regulated by MAPK signaling. *Cancer Res* 2012;72:1547–56.
20. Wang Y, Yamaguchi K, Shimada Y, et al. Site-directed mutagenesis of human membrane-associated ganglioside sialidase: identification of amino-acid residues contributing to substrate specificity. *Eur J Biochem* 2001;268:2201–08.
21. Kato T, Wang Yamaguchi K, et al. Overexpression of lysosomal-type sialidase leads to suppression of metastasis associated with reversion of malignant phenotype in murine b16 melanoma cells. *Int J Cancer* 2001;92:797–804.
22. Barker N, van Es JH, Kuipers J, et al. Identification of stem cells in small intestine and colon by marker gene lgr5. *Nature* 2007;449:1003–7.
23. Howe LR, Watanabe O, Leonard J, Brown AM. Twist is up-regulated in response to wnt1 and inhibits mouse mammary cell differentiation. *Cancer Res* 2003;63:1906–13.
24. Mani SA, Guo W, Liao MJ, et al. The epithelial-mesenchymal transition generates cells with properties of stem cells. *Cell* 2008;133:704–15.
25. Tan X, Apte U, Micsenyi A, et al. Epidermal growth factor receptor: a novel target of the wnt/beta-catenin pathway in liver. *Gastroenterology* 2005;129:285–302.
26. Ten Berge D, Koole W, Fuerer C, et al. Wnt signaling mediates self-organization and axis formation in embryoid bodies. *Cell Stem Cell* 2008;3: 508–18.
27. van Noort M, Meeldijk J, van der Zee R, et al. Wnt signaling controls the phosphorylation status of beta-catenin. *J Biol Chem* 2002;277: 17901–05.
28. Suzuki H, Watkins DN, Jair KW, et al. Epigenetic inactivation of SFRP genes allows constitutive WNT signaling in colorectal cancer. *Nat Genet* 2004;36:417–22.
29. Baehs S, Herbst A, Thieme SE, et al. Dickkopf-4 is frequently down-regulated and inhibits growth of colorectal cancer cells. *Cancer Lett* 2009;276: 152–9.
30. Voloshanenko O, Erdmann G, Dubash TD, et al. Wnt secretion is required to maintain high levels of wnt activity in colon cancer cells. *Nat Commun* 2013;4:2610.
31. Zeng X, Huang H, Tamai K, et al. Initiation of wnt signaling: control of wnt coreceptor lrp6 phosphorylation/activation via frizzled, dishevelled and axin functions. *Development* 2008;135: 367–75.
32. Liu J, Pan S, Hsieh MH, et al. Targeting Wnt-driven cancer through the inhibition of porcupine by lgk974. *Proc Natl Acad Sci U S A* 2013;110: 20224–29.
33. Loh YH, Wu Q, Chew JL, et al. The oct4 and nanog transcription network regulates pluripotency in mouse embryonic stem cells. *Nat Genet* 2006;38:431–40.
34. Babaie Y, Herwig R, Greber B, et al. Analysis of Oct4-dependent transcriptional networks regulating self-renewal and pluripotency in human embryonic stem cells. *Stem Cells* 2007;25:500–10.
35. Bianco C, Rangel MC, Castro NP, et al. Role of Cripto-1 in stem cell maintenance and malignant progression. *Am J Pathol* 2010;177:532–40.
36. Watanabe K, Meyer MJ, Strizzi L, et al. Cripto-1 is a cell surface marker for a tumorigenic, undifferentiated subpopulation in human embryonal carcinoma cells. *Stem Cells* 2010;28:1303–14.
37. Vermeulen L, De Sousa E Melo F, van der Heijden M, et al. Wnt activity defines colon cancer stem cells and is regulated by the microenvironment. *Nat Cell Biol* 2010;12:468–76.
38. Červenka I, Wolf J, Mašek J, et al. Mitogen-activated protein kinases promote WNT/beta-catenin signaling via phosphorylation of lrp6. *Mol Cell Biol* 2011;31:179–89.
39. Sato T, van Es JH, Snippert HJ, et al. Paneth cells constitute the niche for lgr5 stem cells in intestinal crypts. *Nature* 2011;469:415–8.
40. Ji H, Wang J, Nika H, et al. EGF-induced ERK activation promotes CK2-mediated disassociation of alpha-catenin from beta-catenin and transactivation of beta-catenin. *Mol Cell* 2009;36: 547–59.
41. Fang D, Hawke D, Zheng Y, et al. Phosphorylation of beta-catenin by AKT promotes beta-catenin transcriptional activity. *J Biol Chem* 2007; 282:11221–9.
42. Nateri AS, Spencer-Dene B, Behrens A. Interaction of phosphorylated c-jun with tcf4 regulates intestinal cancer development. *Nature* 2005;437: 281–5.
43. Angel P, Hattori K, Smeal T, Karin M. The jun proto-oncogene is positively autoregulated by its product, jun/ap1. *Cell* 1988;55:875–85.
44. Yamaguchi K, Koseki K, Shiozaki M, et al. Regulation of plasma membrane-associated sialidase neu3 gene by Sp1/Sp3 transcription factors. *Biochem J* 2010;430:107–17.
45. Wierstra I. Sp1: emerging roles–beyond constitutive activation of TATA-less housekeeping genes. *Biochem Biophys Res Commun* 2008;372:1–13.
46. Safe S, Abdelrahim M. Sp transcription factor family and its role in cancer. *Eur J Cancer* 2005; 41:2438–48.
47. Kinzler KW, Vogelstein B. Lessons from hereditary colorectal cancer. *Cell* 1996;87:159–70.
48. Hu T, Li C. Convergence between Wnt-β-catenin and EGFR signaling in cancer. *Mol Cancer* 2010; 9:236.

The FASEB Journal • Research Communication

Loss of α1,6-fucosyltransferase inhibits chemical-induced hepatocellular carcinoma and tumorigenesis by down-regulating several cell signaling pathways

Yuqin Wang,* Tomohiko Fukuda,* Tomoya Isaji,* Jishun Lu,* Sanghun Im,* Qinglei Hang,* Wei Gu,* Sicong Hou,* Kazuaki Ohtsubo,† and Jianguo Gu*,[1]

*Division of Regulatory Glycobiology, Tohoku Pharmaceutical University, Sendai, Miyagi, Japan; and †Department of Analytical Biochemistry, Faculty of Life Sciences, Kumamoto University, Japan

ABSTRACT **Up-regulation of core fucosylation catalyzed by α1,6-fucosyltransferase (Fut8) has been observed in hepatocellular carcinoma (HCC). Here, to explore the role of Fut8 expression in hepatocarcinogensis, we established the chemical-induced HCC models in the male wild-type (WT; *Fut8*$^{+/+}$), hetero (*Fut8*$^{+/-}$), and knockout (KO; *Fut8*$^{-/-}$) mice by use of diethylnitrosamine (DEN) and pentobarbital (PB). In the *Fut8*$^{+/+}$ and *Fut8*$^{+/-}$ mice, multiple large and vascularized nodules were induced with an increased expression of *Fut8* after DEN and PB treatment. However, the formation of HCC in *Fut8*$^{-/-}$ mice was suppressed almost completely. This potent inhibitory effect of *Fut8* deficiency on tumorigenesis was also confirmed by the abolished tumor formation of *Fut8* KO human hepatoma cell line cells by use of a xenograft tumor model. Furthermore, loss of the *Fut8* gene resulted in attenuated responses to epidermal growth factor (EGF) and hepatocyte growth factor (HGF) in the HepG2 cell line, which provides the possible mechanisms for the contribution of Fut8 to hepatocarcinogensis. Taken together, our study clearly demonstrated that core fucosylation acts as a critical functional modulator in the liver and implicated Fut8 as a prognostic marker, as well as a novel, therapeutic target for HCC.—Wang, Y., Fukuda, T., Isaji, T., Lu, J., Im, S., Hang, Q., Gu, W., Hou, S., Ohtsubo, K., Gu, J. Loss of α1,6-fucosyltransferase inhibits chemical induced hepatocellular carcinoma and tumorigenesis by down-regulating several cell signaling pathways. *FASEB J.* 29, 3217–3227 (2015). www.fasebj.org**

Key Words: N-*glycosylation* · *glycosyltransferase* · *cell proliferation*

N-LINKED GLYCOSYLATION IS A COMMON type of glycosidic bond. It has been shown to be important for folding, stability, and a vast degree of biologic functions of glycoproteins. These different effects on glycoproteins mainly result from the different *N*-linked glycan structures, determined by various glycosyltransferases (1). Among these, Fut8 is the only enzyme that catalyzes the transfer of a fucose from guanosine 5′-diphosphate (GDP)-fucose to the innermost *N*-acetylglucosamine (GlcNAc) residue *via* α1,6-linkage in mammals. The resulting core fucosylated *N*-glycans are widely distributed in a variety of glycoproteins. It has been reported that core fucosylation is crucial for the ligand-binding affinity of TGF-β1 receptor (2), EGF receptor (EGFR) (3), and integrin α3β1 (4). The lack of the core fucose leads to a marked reduction in ligand-binding ability and downstream signaling. Recently, we found that loss of core fucose on activin receptors also resulted in an enhancement of the formation of activin receptor complexes, which constitutively activated intracellular signaling (5). Those studies clearly suggest that Fut8 plays important roles in cell signal transduction.

HCC is the third leading cause of cancer-related mortality worldwide (6), and hepatocarcinogenesis is a complicated process associated with the accumulation of pathologic changes during the initiation, promotion, and progression of the disease (7, 8). The identification of these changes may provide an avenue to develop a new generation of potential biomarkers, as well as therapeutic targets for HCC. It has been shown that altered expressions of growth factors, such as EGF, TGF-α, TGF-β, and HGF, as well as their receptors during the development of HCC, influence the survival of cancerous cells by suppressing apoptosis and regulating the cell cycle (8–11). The small molecule tyrosine kinase inhibitors and specific antibodies targeting those receptor-mediated signaling pathways have been developed successfully and used to improve the survival of patients with HCC (9). However, the therapeutic resistance also develops (12, 13). Recently, an inhibition of *N*-linked glycosylation had been reported as a novel, therapeutic strategy for the treatment of gliomas and other malignant tumors (14). In contrast, the role of *N*-glycosylation in HCC is largely unknown. It has been shown that Fut8 expression is up-regulated in liver and

Abbreviations: AAL, aleuria aurantia lectin; ALP, alkaline phosphatase; ALT, alanine aminotransferase; BA, bile acids; DEN, diethylnitrosamine; EGF, epidermal growth factor; EGFR, epidermal growth factor receptor; FBS, fetal bovine serum; Fut8, α1,6-fucosyltransferase; *Fut8*$^{+/+}$, wild-type α1,6-fucosyltransferase; *Fut8*$^{+/-}$, hetero α1,6-fucosyltransferase; *Fut8*$^{-/-}$,

(*continued on next page*)

[1] Correspondence: Division of Regulatory Glycobiology, Institute of Molecular Biomembrane and Glycobiology, Tohoku Pharmaceutical University, 4-4-1 Komatsushima, Aoba-ku, Sendai Miyagi, 981-8558, Japan. E-mail: jgu@tohoku-pharm.ac.jp

doi: 10.1096/fj.15-270710

This article includes supplemental data. Please visit *http://www.fasebj.org* to obtain this information.

0892-6638/15/0029-3217 © FASEB

serum during the process of hepatocarcinogenesis (15, 16), and the fucosylated α-fetoprotein is a reliable marker that can be used to distinguish patients with HCC from those with chronic hepatitis and liver cirrhosis (17–19). The HCC cases with high Fut8 expression are associated with poor prognosis (20). However, the pathologic role of high Fut8 expression in HCC progression and whether Fut8 could serve as a potential therapeutic target are still unknown.

To address these questions here, the typical HCC model was established in the *Fut8*$^{+/+}$, *Fut8*$^{+/-}$, and *Fut8*$^{-/-}$ mice by administration of DEN, which induces hepatocyte DNA damage, in conjunction with PB, a well-known promoter of liver carcinogenesis (21–23). DEN and PB effectively induced tumor formation in *Fut8*$^{+/+}$ mice, whereas tumor formation was inhibited almost completely in *Fut8*$^{-/-}$ mice. The inhibitory effects of Fut8 were confirmed further by use of the human hepatoma cell line, HepG2. KO of the *Fut8* gene abolished tumorigenesis of the xenograft tumors formed by HepG2 cells in nonobese diabetic (NOD)/SCID mice. These results clearly demonstrate the importance of Fut8 in hepatocarcinogenesis and implicate Fut8 as a novel, therapeutic approach for HCC treatment.

MATERIALS AND METHODS

Mice

The Fut8-deficient mice line used for these studies has been described previously (2, 24). Male mice, on an Institute of Cancer Research background at 6 weeks of age, were used for the experiments in the present study, comparing *Fut8*$^{-/-}$ animals with *Fut8*$^{+/+}$ littermates. Mice were housed in a temperature-controlled room with a 12 hour dark/12 hour light cycle. Food and water were provided *ad libitum*. The present study was approved by the Institutional Animal Care and Use Committee of Tohoku Pharmaceutical University (Sendai, Miyagi, Japan).

Chemical HCC induction

Six-week-old *Fut8*$^{-/-}$, *Fut8*$^{+/-}$, and *Fut8*$^{+/+}$ male mice were divided into 2 groups. The experimental group ($n > 10$) received a single intraperitoneal injection of DEN (100 mg/kg; Sigma-Aldrich, St. Louis, MO, USA) and was provided 0.05% phenobarbital (Tokyo Chemical, Japan) in water after 4 weeks. The serum and livers were harvested after 40 weeks. Meanwhile, the control group received the same operation without agents. A blood chemical analysis was performed by use of a VetScan VS2 automated analyzer (Abaxis, Union City, CA, USA) with a mammalian liver profile multirotor.

(*continued from previous page*)

knockout α1,6-fucosyltransferase; GDP, guanosine 5′-diphosphate; GlcNAc, *N*-acetylglucosamine; H&E, hematoxylin and eosin; HCC, hepatocellular carcinoma; HepG2, human hepatoma cell line; HGF, hepatocyte growth factor; HRP, horseradish peroxidase; KO, knockout; Mgmt, O^6-methylguanine-DNA methyltransferase; mTOR, mammalian targets of rapamycin; NOD, nonobese diabetic; P450, cytochrome P450; PABA, 4-(2-pyridylamino)-butylamine; PB, pentobarbital; PhoSL, mushroom *Pholiota squarrosa* lectin; qRT-PCR, quantitative real-time PCR; TBS, Tris-buffered saline; WT, wild-type, ZFN, zinc finger nuclease

Liver histology and immunostainings

The hepatic lobules were assessed based on 4 μm hematoxylin and eosin (H&E)-stained paraffin sections. Masson's trichrome staining was performed to show collagen fiber deposition. Immunostaining for mushroom *Pholiota squarrosa* lectin (PhoSL), which specifically recognizes core fucose (25), was used to detect changes in core fucosylation during HCC induction. An *in situ* cell death kit (Roche, Laval, Canada) was used for TUNEL staining with frozen sections (10 μm), according to the manufacturer's instructions. Proliferative cells in the liver were detected through immunostaining with a mAb recognizing Ki-67 (Abcam, Cambridge, MA, USA), and the liver sinusoidal endothelial cells were labeled with anti-CD31 antibody (BD Biosciences, San Jose, CA, USA).

Quantitative and semiquantitative real-time PCR

Total RNA from livers was extracted with TRI Reagent (MRC, Cincinnati, OH, USA). cDNA synthesis was carried out with the PrimeScript RT reagent Kit (TaKaRa Bio, Shiga, Japan), according to the manufacturer's instructions. Quantitative real-time PCR (qRT-PCR) reactions were performed with SYBR Premix Ex Taq II Kit (TaKaRa Bio), and semi-qPCR reactions were carried out by use of TaKaRa Bio Ex Taq. Primers are listed in Supplemental Table 1. Values of qPCR reactions were quantified by use of the comparative threshold method and normalized to GAPDH mRNA.

Cell culture and transfection

Human hepatoma HepG2 cells were grown in DMEM with 10% (v/v) fetal bovine serum (FBS), 100 IU/ml penicillin, and 100 μg/ml streptomycin. The *Fut8* KO CompoZr zinc finger nuclease (ZFN) plasmids (Sigma-Aldrich) and green fluorescent protein control plasmid were transfected into the cell lines *via* a TransIT-2020 Transfection Reagent Kit (Mirus Bio, Madison, WI, USA), and stable cell lines were selected *via* PhoSL staining by FACSAria II (BD Biosciences). The cells were incubated for 6 hours at 37°C in a humidified atmosphere with 95% air and 5% CO_2, allowing for cell attachment to the plate. The medium was then changed, which involved replacement by 0.1% FBS containing DMEM, with or without EGF or HGF for stimulation at indicated times.

Genomic PCR to detect *Fut8*

Genomic DNA was extracted from WT and *Fut8* KO HepG2 cells, and the KO efficiency was confirmed by PCR by use of the special primers provided by a the ZFN kit (Sigma-Aldrich). ZFN primer forward: 5′-TGTCAGGTGAAGTGAAGGACA-3′ and primer reverse: 5′-ATCAGATTCTTACCCAATAACTGG-3′.

Western blotting and lectin blot analyses

Total protein was isolated from frozen liver tissue and cultured cells with Tris-buffered saline (TBS) containing 1% Triton X-100. Protein concentration was measured by use of a bicinchoninic acid protein assay kit (Thermo Fisher Scientific, Wilmington, DE, USA). Equal protein samples were separated by SDS-PAGE and then transferred onto nitrocellulose or PVDF (Millipore, Billerica, MA, USA) membranes. After blocking with 5% skim milk or 3% bovine serum albumin, the membranes were incubated with specific antibodies against the indicated antibodies and lectins at 4°C overnight, followed by incubation with horseradish peroxidase (HRP)-conjugated secondary antibody. Immunoreactivity

was visualized by HRP substrate peroxide solution (Millipore). The related antibodies that are used included ERK1 (BD Biosciences), phospho-ERK, phospho-AKT, AKT, phospho-c-Met (Tyr1234/5), c-Met, phospho-EGFR (Tyr1068), EGFR, β-actin, rabbit IgG (Cell Signaling Technology, Beverly, MA, USA), α-tubulin, and mouse IgG (Sigma-Aldirch).

Immunoprecipitation and cell-surface biotinylation

Cell lysates (500 μg total protein) were incubated with 10 μl FG streptavidin beads (Tamagawa Seiki, Nagano Prefecture, Japan) containing 2 μg PhoSL for 2 hours at 4°C, followed by washing 3 times with lysis buffer. The immunoprecipitate was dissolved in a 20 μl SDS-PAGE sample solution. For cell-surface biotinylation, cells were incubated with 0.2 mg/ml sulfosuccinimidobiotin (Thermo Fisher Scientific) on ice for 2 hours and then were solubilized in lysis buffer. The biotinylated proteins were precipitated with 50 μl streptavidin agarose beads (2 hours, 4°C; Millipore) and visualized by Western blot analysis.

Enzyme activity assays for Fut8

Frozen liver tissues were homogenized in TBS containing 1% protease inhibitor cocktail (Nacalai Tesque, Kyoto, Japan). After centrifugation at 900 *g* for 10 minutes, the supernatant was collected. Each sample containing 800 μg total protein was centrifuged at 105,000 *g* for 1 hour, and then the pellet was resuspended in 0.1 M 2-(*N*-morpholino)ethanesulfonic acid-NaOH (PH 7.0) for reactions. Equal amounts of protein were used in Fut8 activity assays. The specific activities of endogenous Fut8 were determined by use of the substrate, 4-(2-pyridylamino)-butylamine (PABA)-labeled GlcNAcβ1–2Manα1–6 (GlcNAcβ1-2Manα1-3) Manβ1–4GlcNAcβ1–4GlcNAc-Asn (GnGn-Asn-PABA). Each assay used 2 mM acceptor substrate and 2 mM GDP-L-fucose as a donor. After incubation at 37°C for 2 hours, the reactions were terminated by boiling. Then, the reaction mixtures were centrifuged at 10,000 *g* for 10 minutes. The resulting supernatants were analyzed by HPLC for the determination of Fut8 enzyme activity, expressed as the picomoles of fucose transferred per hour per milligrams of proteins (26).

Established tumors originating from HepG2 cells

Six-week-old male NOD/SCID mice were purchased from Charles River Laboratories (Wilmington, MA, USA). The mice were inoculated subcutaneously with 5×10^6 HepG2 WT and *Fut8* KO cells into the dorsal flanks, and the tumor tissues were harvested after 4 weeks.

Statistical analysis

Results are given as the means ± SEM. The data were analyzed by use of Prism 5.0 software (GraphPad Software, La Jolla, CA, USA). Comparisons were carried out by use of 2-tailed Mann-Whitney tests and/or a Tukey's multiple comparison test. A P value < 0.05 was considered significant.

RESULTS

Loss of the *Fut8* gene inhibited DEN/PB-induced tumor formation

To assess the effects of Fut8 on the development of HCC, 6-week-old $Fut8^{+/+}$, $Fut8^{+/-}$, and $Fut8^{-/-}$ male mice were exposed to the carcinogen DEN and liver tumor promoter PB. The absence of *Fut8* significantly decreased HCC formation in response to DEN and PB when compared with $Fut8^{+/+}$ mice. Interestingly, the $Fut8^{+/-}$ mice showed an intermediate incidence of tumors compared with the $Fut8^{+/+}$ and $Fut8^{-/-}$ mice (**Fig. 1*B***). Morphologic examination revealed that livers of $Fut8^{+/+}$ model mice showed multiple, large, vascularized nodules at the 40th week, whereas this phenomenon was rarely observed in $Fut8^{-/-}$ mice (Fig. 1*A*). Consistently, Masson's trichrome staining showed much more collagen deposition in the DEN/PB-treated $Fut8^{+/+}$ group compared with the control and $Fut8^{-/-}$ mice. Meanwhile, in agreement with the tumor incidence, a significant increase in liver/body weight ratios after DEN/PB treatment was observed for the $Fut8^{+/+}$ model mice but not the $Fut8^{-/-}$ mice (Fig. 1*C*). The ratio for $Fut8^{+/-}$ mice showed a decreased tendency when compared with that of $Fut8^{+/+}$, albeit not as compared with that of $Fut8^{-/-}$ mice (Fig. 1*C*). Furthermore, the serum biochemical analysis for ALT, ALP, and BA showed that DEN and PB induction destroyed liver functions of $Fut8^{+/+}$ and $Fut8^{+/-}$ mice but not the $Fut8^{-/-}$ mice (Fig. 1*D*). These results strongly suggest that the expression of Fut8 plays an important role in pathologic functions.

Chemical treatment induced the expression of Fut8

The expression of Fut8 and its products are elevated in liver and serum during the process of human hepatocarcinogenesis (15, 27). The increase in core-fucosylated *N*-glycans has also been observed in DEN-induced HCC rat models (27). To confirm whether it is also the case in mice, here, we tested the activities of Fut8 in $Fut8^{+/+}$ mice. As shown in **Fig. 2*A*, *B***, the Fut8 enzyme activities were remarkably enhanced in DEN/PB treatment models compared with the control. The mRNA expression of *Fut8* also showed a dual-phase elevation during the process of hepatocarcinogenesis, which reached a plateau after 36 weeks (Fig. 2*C*). The underlying molecular mechanism for the dual-phase reaction is unclear. Immunostaining analysis that uses PhoSL, which specifically recognizes core fucose, showed that the increases in Fut8 expression and enzyme activities were accompanied by the enhancement of its enzymatic products (Fig. 2*D*), and these core fucose did not localize in the liver sinusoidal endothelial cells, which were stained by an anti-CD31 antibody (Fig. 2*E*). Thus, we believed that it might localize mainly in hepatocytes. Taken together, these results indicate that Fut8 is expressed at lower levels under physiologic conditions in the liver, which could be up-regulated after stimulus and thereby affect subsequent pathologic processes.

Comparison of the acute-phase responses for DEN injection between $Fut8^{+/+}$ and $Fut8^{-/-}$ mice

DEN itself does not exert carcinogenicity. It needs to be bioactivated by cytochrome P450 (P450) enzymes in the liver (28). For instance, CYP2e1-deficient mice showed lower tumor incidence and multiplicity compared with WT mice for DEN-induced hepatocarcinogenesis (29). After activation, DEN formed DNA adducts through an

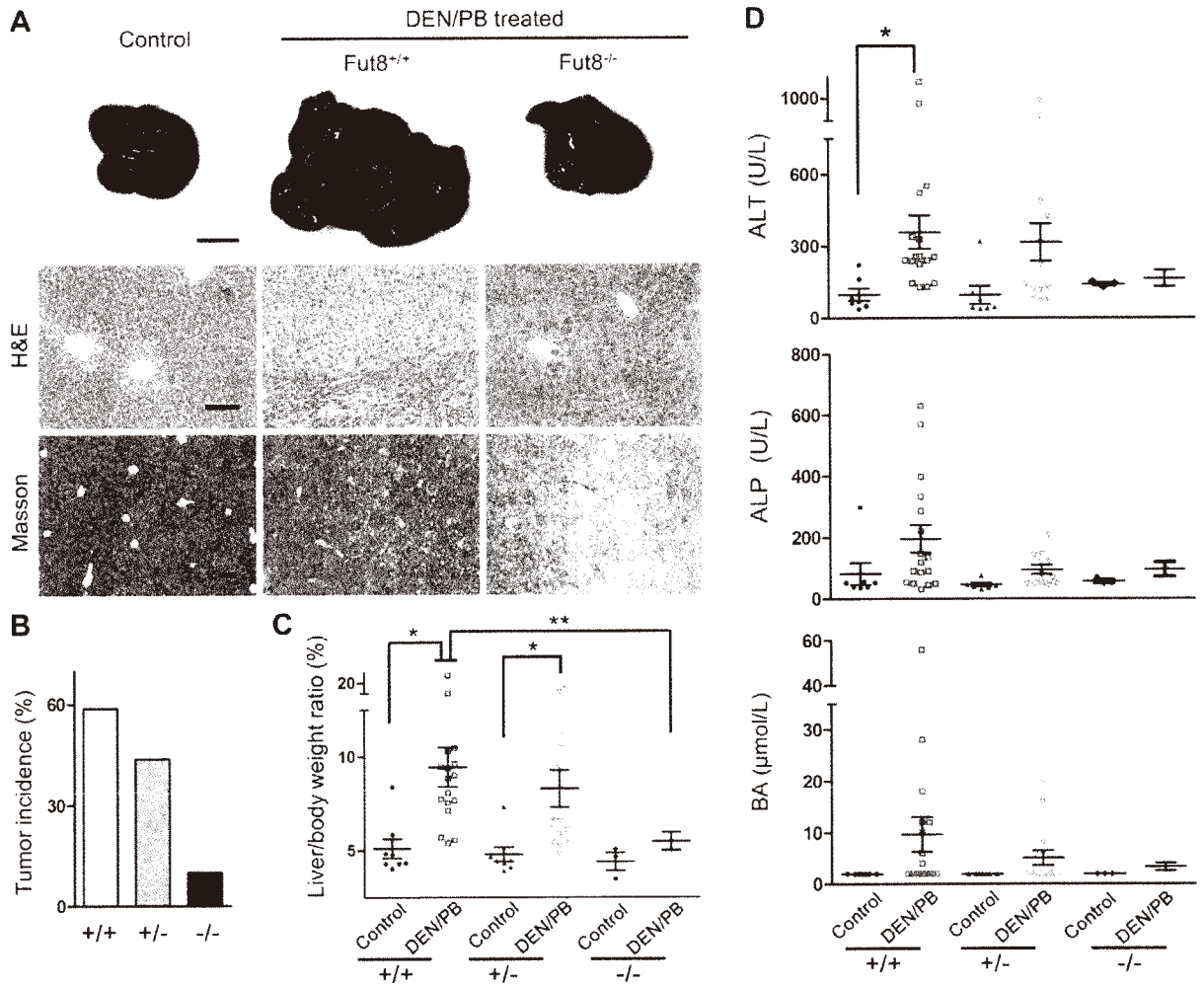

Figure 1. Hepatocarcinogenesis was inhibited in *Fut8*$^{-/-}$ mice. *A*) The DEN/PB-treated *Fut8*$^{+/+}$ mice showed multiple large, vascularized nodules at the 40th week compared with the control group, whereas this phenomenon was rarely observed in *Fut8*$^{-/-}$ mice (top; scale bar, 1 cm). Sections (4 μm thick) from formalin-fixed, paraffin-embedded liver lobe of control and DEN/PB-treated *Fut8*$^{+/+}$ and *Fut8*$^{-/-}$ male mice were used for histologic analysis by H&E (middle; scale bar, 1 mm) and Masson's trichrome staining (bottom; scale bar, 1 mm). *B*) Tumor incidence in different groups after DEN/PB-treatment ($n > 10$). *C*) relative liver weight in different groups after 40 weeks. *$P < 0.05$ compared with control mice; **$P < 0.05$ compared with the DEN/PB-treated *Fut8*$^{-/-}$ mice. *D*) The expression levels of alanine aminotransferase (ALT), alkaline phosphatase (ALP), and bile acids (BA) in the serum were analyzed by use of a VetScan VS2 automated analyzer, as described in Materials and Methods. *$P < 0.0$, compared with *Fut8* $^{+/+}$ control mice.

alkylation mechanism. The alkylated DNA adducts can be removed by the DNA repair gene O^6-methylguanine-DNA methyltransferase (Mgmt) (30). To check the early effects of DEN in *Fut8*$^{+/+}$ and *Fut8*$^{-/-}$ mice, semi-qPCR or qPCR analysis of mRNAs encoding the P450 enzyme (**Fig. 3*A***) and Mgmt (Fig. 3*B*) genes was performed 2 hours after DEN injection. There was no significant difference in the transcriptional levels of P450 genes or the DNA repair gene between *Fut8*$^{+/+}$ and *Fut8*$^{-/-}$ mice. DEN-induced tumor formation was associated further with substantial and marked induction of proinflammatory chemokines within the livers of mice. After DEN injection, IL-6 and TNF-α were induced, resulting in cytokine-driven, compensatory proliferation (31). qPCR analysis of livers after DEN injection revealed an increase in IL-6 expression in *Fut8*$^{+/+}$ and *Fut8*$^{-/-}$ mice, although the expression level in *Fut8*$^{+/+}$ control mice was lower than that in *Fut8*$^{-/-}$ controls. The mRNA expression levels of TNF-α were also increased after DEN injection, but there was no significant difference between the *Fut8*$^{+/+}$ and *Fut8*$^{-/-}$ mice (Fig. 3*C*). Moreover, a TUNEL assay for the livers showed the similar results (Fig. 3*D*). These data demonstrate that the expression of Fut8 may not affect the acute-phase response to DEN.

Cell proliferation induced by DEN/PB treatment is inhibited in the *Fut8*$^{-/-}$ mice

Cell proliferation plays important roles in the HCC process (8, 32, 33). To find the possible mechanisms for the differences in tumorigenesis described above, we carried out

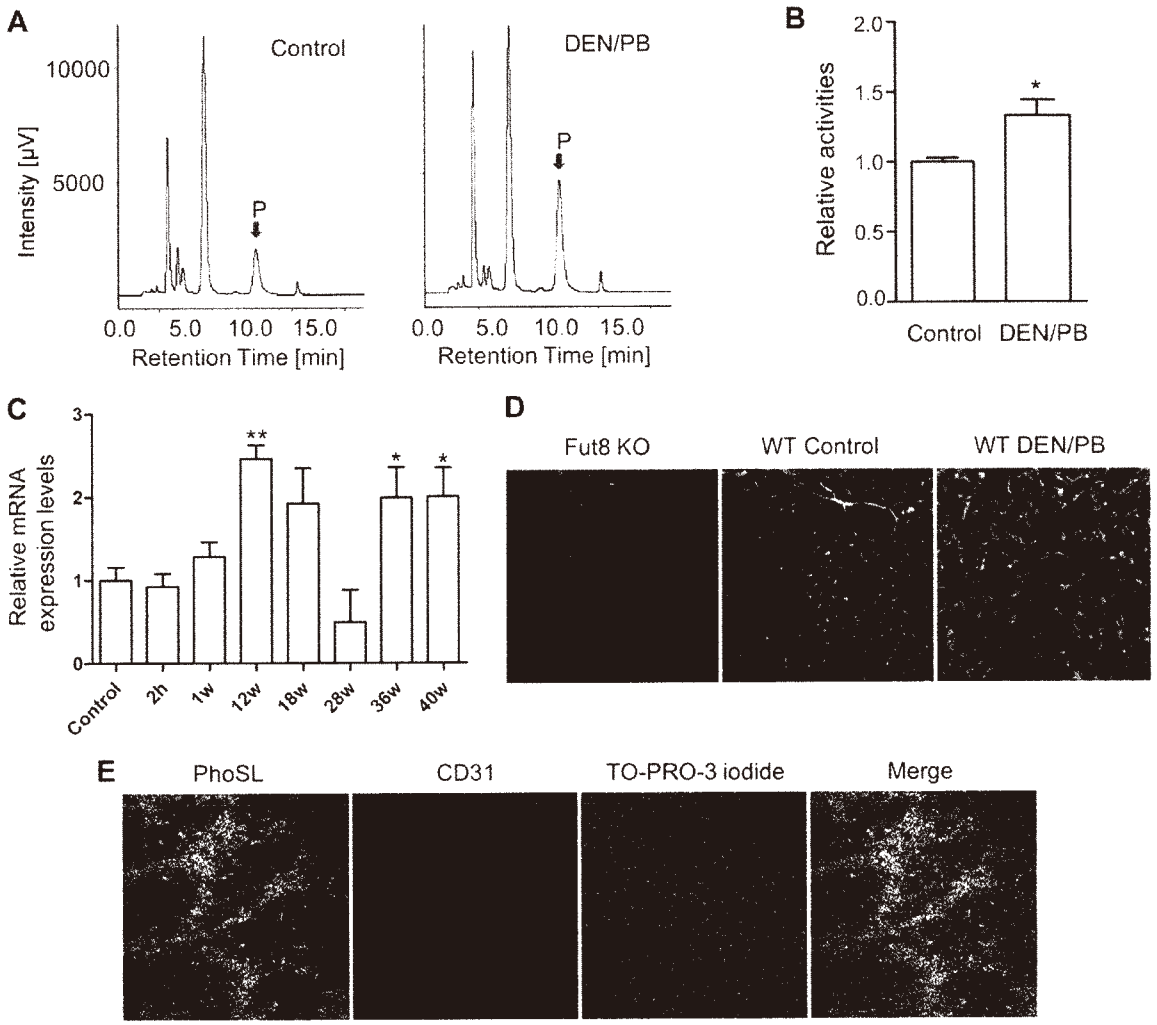

Figure 2. The expression of Fut8 and its reaction product was induced after DEN/PB treatment. *A*) The HPLC elution patterns were determined, as described in Materials and Methods. The red arrows show the products (P) of Fut8 after the reaction. *B*) The quantitative assay for enzyme activities in $Fut8^{+/+}$ mice, with or without the DEN/PB treatment. $^{*}P < 0.05$ compared with the control group without the treatment. *C*) The expression of *Fut8* mRNA showed a dual-phase increase during the DEN/PB-induced tumorigenesis. $^{*}P < 0.05$; $^{**}P < 0.01$ compared with the control group without the treatment ($n = 3$–4). *D*) PhoSL immunostaining for paraffin-embedded sections (4 μm thick) of liver tissues. The immunostaining for $Fut8^{-/-}$ mice was used as a negative control. *E*) The frozen liver sections (10 μm thick) of $Fut8^{+/+}$ mice treated with DEN/PB were coimmunostained with PhosSL (green) and anti-CD31 antibody (red), which is a marker for the sinusoidal endothelial cells. The nuclei were labeled by TO-PRO-3 iodide (blue).

Ki-67 immunostaining for the frozen liver tissues of $Fut8^{+/+}$ and $Fut8^{-/-}$ mice. Without DEN/PB treatment, $Fut8^{+/+}$ and $Fut8^{-/-}$ mice showed few positive cells in the liver, and there was no significant difference between the control groups. After chemical induction, the $Fut8^{+/+}$ mice showed a significant increase by more than ~6.5-fold in positive immunostaining compared with the untreated control. However, only a 2-fold increase was observed in $Fut8^{-/-}$ mice (**Fig. 4A, B**). To confirm further the difference in cell proliferation after DEN/PB induction between $Fut8^{+/+}$ and $Fut8^{-/-}$ mice, qPCR analysis of mRNAs encoded by cell-cycle control genes was performed. DEN/PB treatment induced the transcription levels of cyclin B1, cyclin D1, and cyclin E2 in $Fut8^{+/+}$ mice. This induction was attenuated by ablation of the *Fut8* gene, although the expression levels of cyclin genes were not lower in the $Fut8^{-/-}$ mice compared with the $Fut8^{+/+}$ controls (Fig. 4*C*). These results indicate that Fut8 may influence the progress of DEN/PB-induced HCC by affecting cell proliferation.

Cell proliferation and tumor growth were inhibited in the *Fut8* gene KO HepG2 cell line

To confirm further the observation *in vitro*, we established the stable *Fut8* KO HepG2 cell line by ZFN technique. The KO efficiency was verified, not only by lectin blotting with aleuria aurantia lectin (AAL), which recognizes core fucosylation on *N*-glycans, but also by genomic DNA PCR

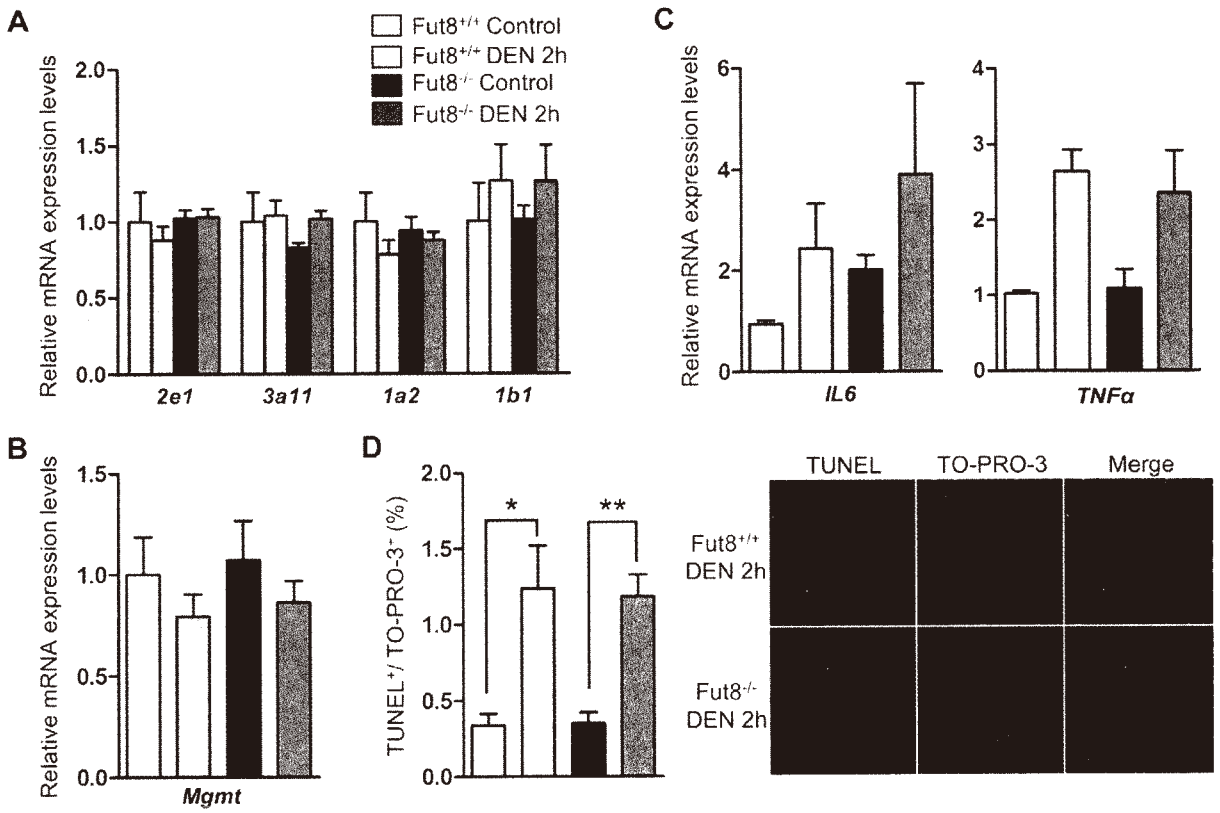

Figure 3. No significant differences in acute response were observed between the *Fut8*$^{+/+}$ and *Fut8*$^{-/-}$ mice after DEN injection. *A*) Semi-qPCR analysis of P450 enzymes (drug metabolism-related enzymes, such as *2e1*, *3a11*, *1a2*, *etc.*) after DEN injection ($n = 3$–5). *B*) qPCR analysis of the DNA-repairing gene (*Mgmt*) after DEN injection ($n = 3$–5). *C*) The mRNA expression levels of *IL-6* and *TNF-α* in the liver were detected by qPCR after DEN injection at 2 hours ($n = 3$–5). *D*) TUNEL analysis was performed by use of the frozen liver tissues (10 μm thick; green), which showed increased apoptosis in *Fut8*$^{+/+}$ and *Fut8*$^{-/-}$ mice after DEN treatment, and the nuclei were labeled by TO-PRO-3 iodide (blue). The quantitative data were obtained from at least 3 mice. $^{**}P < 0.01$; $^{*}P < 0.05$ compared with the control mice.

(**Fig. 5*A***; top and bottom, respectively). *Fut8* KO in HepG2 cells led to a significant inhibition of cell growth (Fig. 5*B*), indicating that the cell proliferation induced by DEN/PB could be suppressed by the loss of Fut8. To evaluate further the impact of Fut8 on tumor growth *in vivo*, a xenograft tumor model was established in NOD/SCID mice. The WT and *Fut8* KO HepG2 cells were implanted subcutaneously into NOD/SCID mice to allow tumor formation. At 4 weeks postinjection, in contrast to the clear tumors in the WT group, the xenograft tumor formation in the *Fut8* KO group was abolished almost completely (Fig. 5*C*), which indicates that *Fut8* gene KO suppresses tumorigenesis *in vivo*.

The responses to EGF and HGF stimulus were attenuated in the Fut8 KO cells

It has been reported that EGF- and HGF-mediated signaling pathways are important for cell proliferation (9, 32). There is also evidence that core fucosylation is capable of regulating the functions of certain receptors (2, 3). Thus, we wondered whether core fucosylation could affect the responses to EGF or HGF stimulation in HepG2 and its *Fut8* KO cell line. To address this question, first, we confirmed that EGFR and c-Met were modified by Fut8 in HepG2 cells by immunoprecipitation analysis with PhoSL (**Fig. 6*A*, *B***; top and second panels). Furthermore, we found that there was no difference in the expression levels of EGFR and c-Met between *Fut8* KO HepG2 cells and the parent cells, either on cell surface or in total cell lysates (Fig. 6*A*, *B*; third panels). The treatments with EGF or HGF significantly increased the phosphorylation levels of EGFR, c-Met, ERK, and AKT in WT cells. However, these increases were greatly suppressed in *Fut8* KO HepG2 cells (Fig. 6*C*, *D*). With the consideration of our previous reports that core fucosylation was required for the binding of EGF to EGFR (2, 3), it is reasonable to conclude that the lack of the core fucosylation on both receptors may decrease their biologic functions *in vitro* or *in vivo*.

DISCUSSION

In the present study, we used a well-established HCC model—DEN/PB-induced hepatocarcinogenesis—to investigate the functions of Fut8 in HCC and found the following: 1) tumor incidence was greatly inhibited in

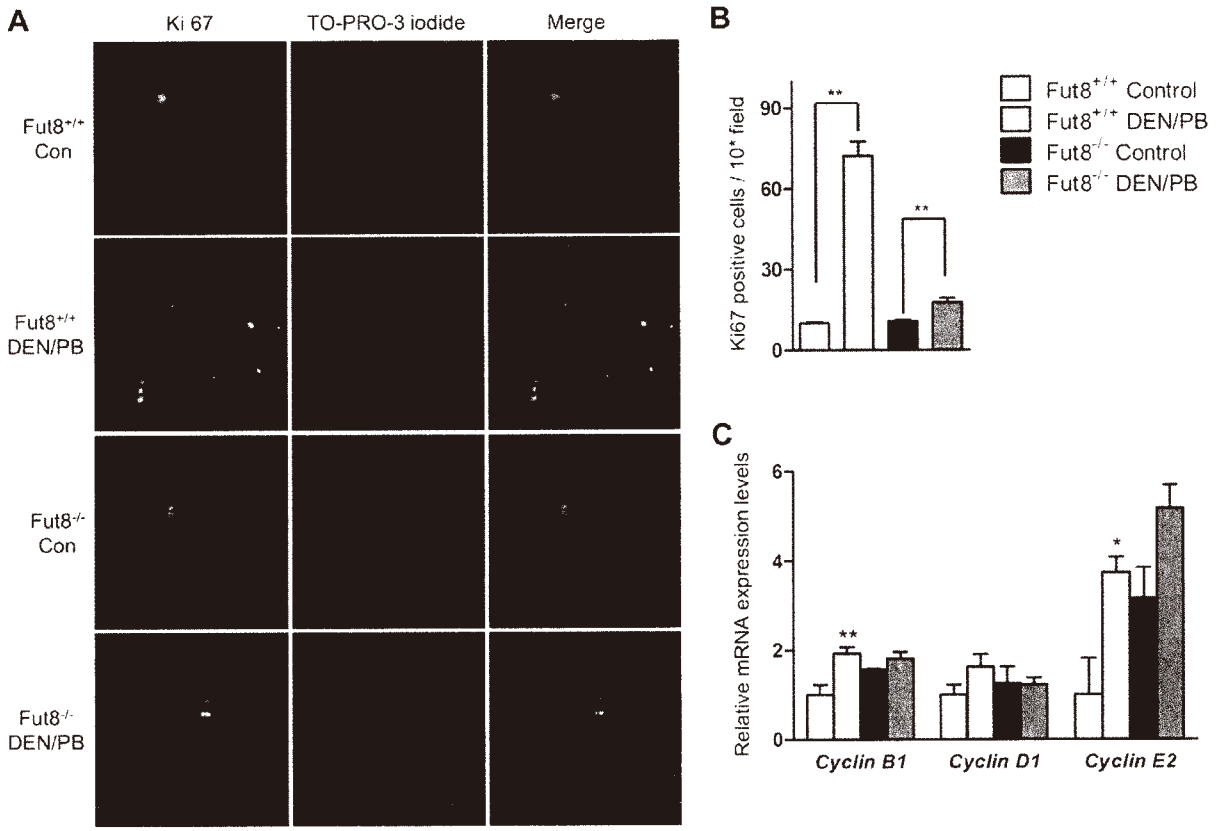

Figure 4. KO of *Fut8* led to suppression of cell proliferation. *A*) Immunostaining for liver tissues of $Fut8^{+/+}$ and $Fut8^{-/-}$ mice by use of anti-Ki-67 antibody (×40 field). The positive cells of the immunostaining were labeled with the green spots (left), and the nuclei were labeled by TO-PRO-3 iodide (red spots, middle). *B*) The quantitative data were obtained from at least 3 mice in each group (×10 field). $^{**}P < 0.01$ compared with the $Fut8^{+/+}$ mice. *C*) qPCR analysis of cell-cycle control gene-encoded mRNAs. $^{**}P < 0.01$; $^{*}P < 0.05$ compared with the control mice; $n = 3$–4.

$Fut8^{-/-}$ mice compared with $Fut8^{+/+}$ mice; 2) the expression of *Fut8* was markedly up-regulated during the DEN/PB-induced hepatocarcinogenesis of $Fut8^{+/+}$ mice; 3) *Fut8* KO abolished HepG2 xenograft tumor formation in NOD/SCID mice; 4) the responses to growth factors, such as EGF and HGF, were decreased in *Fut8*-deficient cells compared with WT cells. Overall, this study marks the first clear demonstration of the biologic functions of Fut8 in HCC, suggesting that the levels of core fucosylation do not only serve as biomarkers for HCC but also function as important signaling modulators during the progression of hepatocarcinogenesis, which provides insight into the development of promising glycotherapeutic methods for HCC.

As far as can be ascertained, inflammation-induced mutagenesis in normal cells is regarded as the initiation of HCC, and there is evidence that DNA damage can lead to inflammation and thereby, promote tumorigenesis (34), for instance, the carcinogen DEN-induced HCC model, in which DNA damage results in an inflammatory reaction and promotes tumor development (31, 35). In our study, acute responses to DEN were also detected. However, no significant difference was observed in the expression of cytokines and dead cells induced by DEN between the $Fut8^{+/+}$ and $Fut8^{-/-}$ mice (Fig. 3*C*, *D*). Meanwhile, the alterations of body weight showed a similar tendency within 2 weeks after DEN injection in $Fut8^{+/+}$ and $Fut8^{-/-}$ mice (data not shown). These results clearly indicated that Fut8 did not influence the initial step of hepatocarcinogenesis.

Increased cell proliferation is essential for initial tumor growth. It is often accompanied by the enhanced expression of some growth factors, leading to the activation of RAS/MAPKK signaling, c-Met signaling, or Akt/mammalian targets of rapamycin (mTOR) signaling and consequently, influences the survival of cancerous cells by suppressing apoptosis and regulating the cell cycle (8, 9). In fact, Fut8, which controls the core fucosylation status on cell-surface molecules globally, plays important roles in cell-signal transduction. Here, we showed that the absence of *Fut8* reduced EGF and c-Met signaling in the HepG2 cell line, and consistently, $Fut8^{-/-}$ mice showed decreased *cyclin B1* and *cyclin D1* expression compared with $Fut8^{+/+}$ mice when treated with DEN/PB. However, interestingly, this reduction was not observed between the $Fut8^{-/-}$ and $Fut8^{+/+}$ control mice without DEN/PB treatment. This observation could be a result of different expression levels of the regulators of cyclin transcription under different conditions. With the consideration that the process of HCC is accompanied by the activation of EGF and c-Met signaling, it is reasonable to think that the expression of cyclin B1 and cyclin D1 is mainly determined by these 2 pathways *in vivo*. However, under normal conditions, the basal signaling

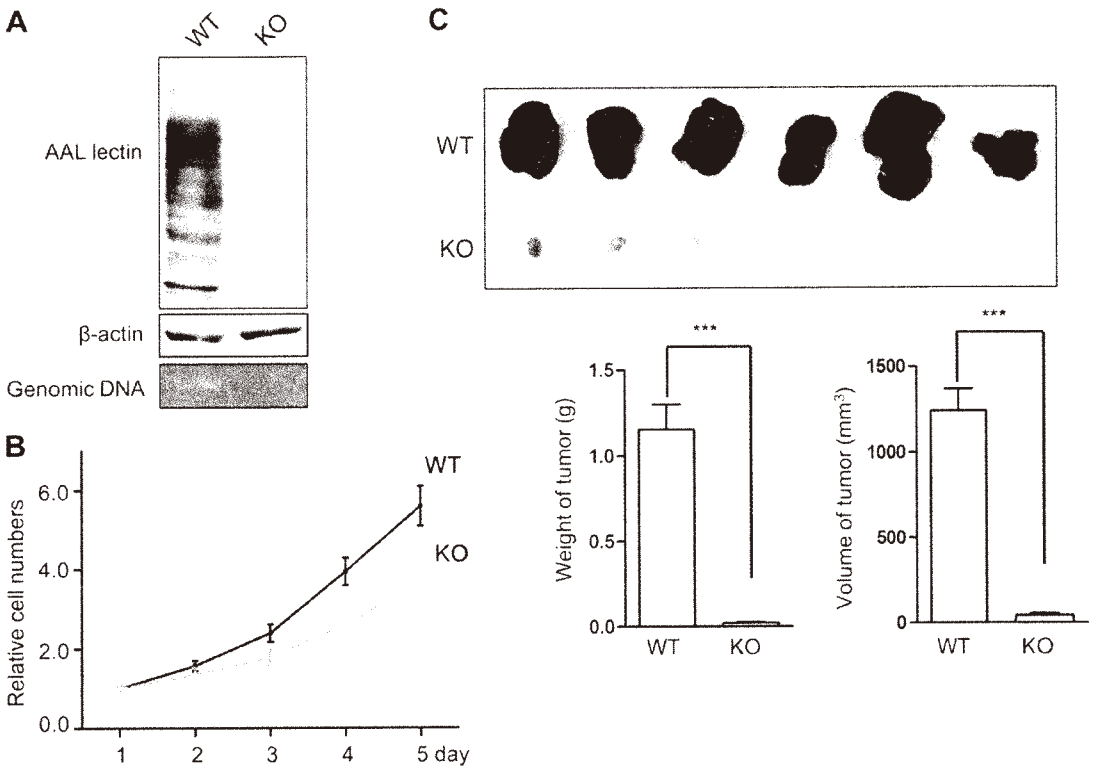

Figure 5. KO *Fut8* gene in HepG2 cells suppressed cell proliferation *in vitro* and xenograft tumor growth *in vivo*. *A*) The *Fut8* gene in HepG2 cells was knocked out by use of a ZFN technique, as described in Materials and Methods. As shown in the figure, AAL staining, which specifically recognized core fucose, disappeared in the *Fut8* KO cells (top), and this result was also confirmed by the genomic DNA PCR (bottom). *B*) The cell proliferation of *Fut8* KO HepG2 cells was slower than that of control cells. The relative cell numbers are shown as the ratios of cell numbers after culture *versus* numbers of the first day in the same area. Each set of the reported data was acquired from at least 3 independent experiments ($n > 8$). *C*) KO of *Fut8* remarkably reduced the volumes and weights of the tumors, which were formed by HepG2 WT or HepG2 *Fut8* KO stable cells in NOD/SCID mice and were measured at 4 weeks after injection. $***P < 0.001$ compared with the control group ($n = 6$).

above is very low. Therefore, the expression of cyclin B1 and cyclin D1 could be affected by many other Fut8-related factors in addition to the EGF- and c-Met-mediated cascades. Consistent with this idea, our previous study showed that the lack of core fucose also led to a marked reduction in the ligand-binding ability of the TGF-β1 receptor and its downstream signaling (2), which negatively controls the expression of cyclin genes (36). It may also partly explain why the basal expression levels of cyclin genes were higher in the $Fut8^{-/-}$ mice compared with the $Fut8^{+/+}$ controls. It is clear that further evidence is needed to support this hypothesis.

We reported previously that core fucosylation was required for the binding of EGF to its receptor and for the regulation of EGFR-mediated intracellular signaling in embryonic fibroblast cells (3). With the consideration also of the reduced response to EGF stimulation in *Fut8* KO HepG2 cells, it is reasonable to conclude that the inhibition of tumor formation in $Fut8^{-/-}$ mice is, at least partially, mediated by the attenuated EGFR-mediated signaling. On the other hand, HGF and its receptor also play a critical role in HCC, and the HGF/c-Met pathway serves as a promising target for HCC treatment (9, 32). Our results showed that the lack of the *Fut8* gene also attenuated the response to an HGF stimulus in HepG2 cells (Fig. 6*D*). So, the reduced HGF/c-Met-mediated signaling could be another reason for the suppressed tumorigenesis in $Fut8^{-/-}$ mice. Nonetheless, we still cannot exclude the possibility that Fut8 may influence the functions of some other glycoproteins, as core fucose widely exists on the cell surface. Overall, it could be postulated that a loss of the *Fut8* gene may affect the biological functions of some target membrane proteins and their subsequent downstream signaling, thereby inhibiting the hepatocarcinogenesis (**Fig. 7**).

Despite the well-established link between core fucosylation and the function of glycoproteins, such as EGFR (3), TGF-β1 receptor (2), and others, the underlying molecular mechanisms still remain poorly understood. Recently, the complex structures of glycosylated low-affinity type 3 receptor for Fc portion of IgG and human core fucosylated or afucosylated Fc of IgG have been determined, which indicated that core fucose depletion increased the incidence of the active conformation of the Tyr-296 of Fc and thereby, accelerated the formation of the high-affinity complex with its receptor (37, 38). These studies clearly explained why the lack of a core fucose on IgG could greatly enhance antibody-dependent cellular cytotoxicity (39, 40). From a more general viewpoint, these studies provide evidence that core fucose on a glycoprotein may

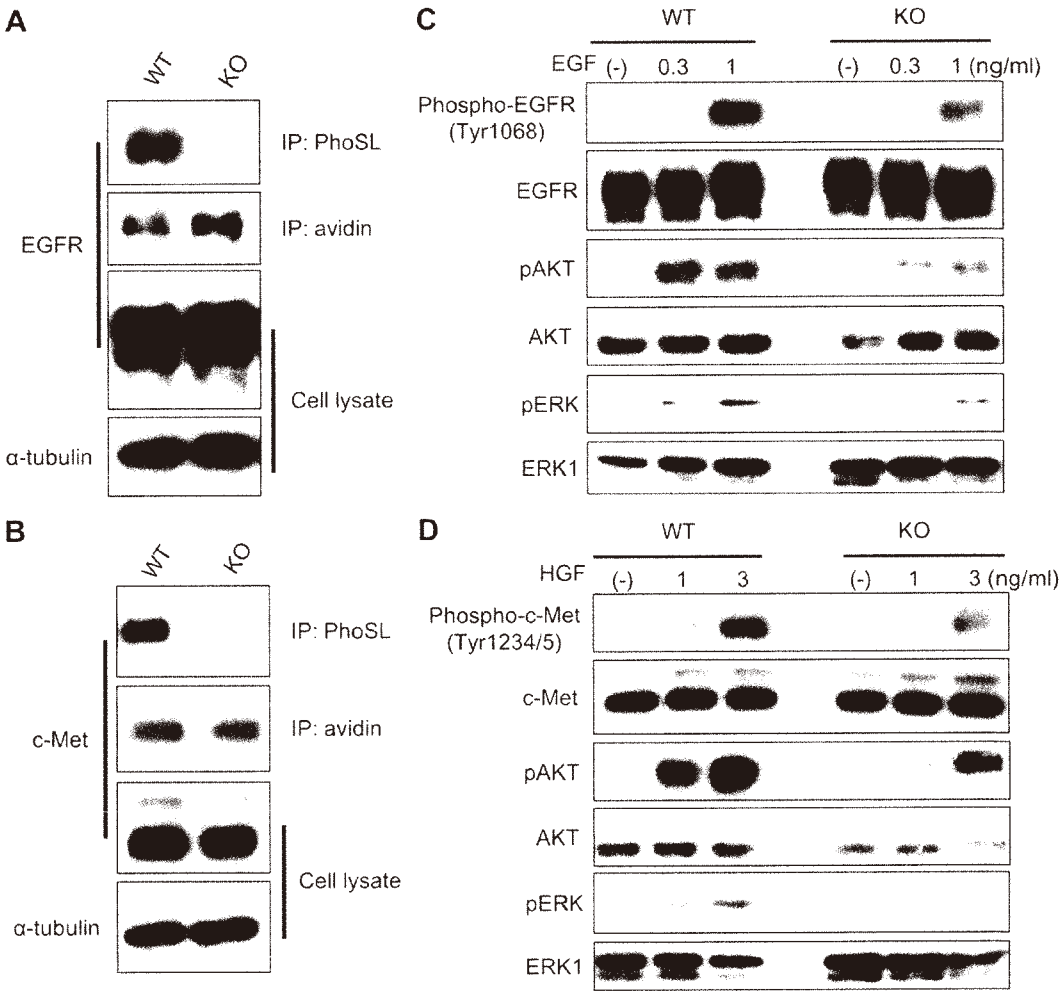

Figure 6. The phospho-AKT and -ERK levels upon EGF and HGF stimulation were suppressed in *Fut8* KO HepG2 cells. *A*) Comparison of the core fucosylation of EGFR [immunoprecipitated (IP) with PhoSL, which specifically recognizes core fucose] and its expression levels on the cell-surface labeled with biotin, as described in Materials and Methods (immunoprecipitated with avidin), between control and *Fut8* KO HepG2 cells. *B*) Comparison of the core fucosylation of c-Met (HGF receptor) and its expression levels on the cell surface between control and *Fut8* KO HepG2 cells. *C*) Cell lysates obtained from the cells, with or without EGF treatment, were immunoblotted with anti-phospho-AKT (pAKT) and AKT and phospho-ERK (pERK) and ERK1 antibodies. *D*) The control and *Fut8*-KO HepG2 cells were stimulated by HGF, and their cell lysates were collected and used for immunoblotting, as described above.

affect its conformation, complex formation, and protein dynamics, coupled with the selection of protein–protein interactions, then positively or negatively regulating intracellular signaling pathways. So, possible mechanisms for the aberration of EGF and HGF signaling in $Fut8^{-/-}$ mice could be that loss of core fucosylation affects the steric structure of EGFR and c-Met, which then impairs dimeric formation and the complex formation between receptor and ligand. Taken together, our study thereby emphasizes that Fut8 is not only an important diagnostic marker but also plays pathologic roles in hepatocarcinogenesis, which sheds light on a novel therapy for HCC.

In the past few years, small molecule receptor tyrosine kinase inhibitors and receptor-specific mAb that target receptor-mediated multiple strategies have been used successfully for HCC patients (41). However, compensatory resistance mediated through other receptors also developed. For instance, c-Met has been reportedly implicated in acquired resistance to gefitinib or erlotinib, which have been proven to be useful in a series of anti-cancer therapies by inhibiting EGFR kinase (42). Because Fut8 has the advantage of affecting multiple cell-signal pathways, mediated by a series of receptors, inhibition of Fut8 could effectively block the DEN/PB-induced HCC, as shown in the current study (Fig. 1*A*). In addition, abnormal expression of Fut8 was observed with diverse carcinomas, including ovarian (43), lung (44), and colorectal cancers (45), and a recent study showed that microRNA-198, which targets Fut8, could suppress the proliferation and invasion of colorectal cancer (46). With the consideration also of our data presented here—that loss of Fut8 has no influence on the normal functions of the liver—we believe that Fut8 might serve as an effective therapeutic target for HCC and possibly other cancers. FJ

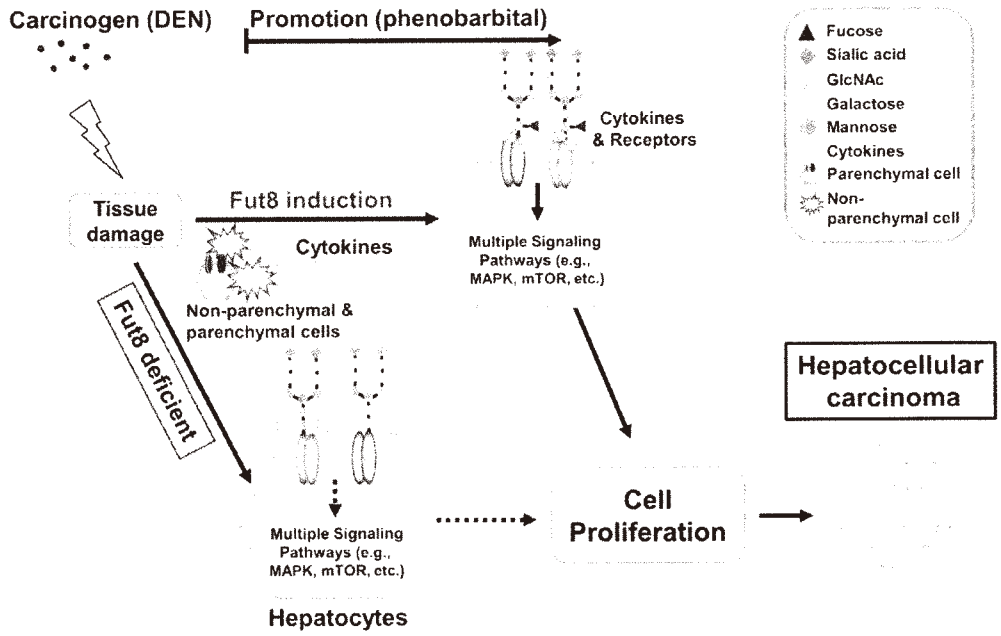

Figure 7. Proposed molecular mechanism for the inhibition of HCC in *Fut8* KO mice. It is well known that cytokines, such as EGF and HGF, could up-regulate cell proliferation by activating several associated signaling pathways, including Ras/MAPKK signaling, c-Met signaling, and Akt/mTOR signaling, and finally lead to HCC. Core fucosylation on growth factor receptors, such as EGFR and c-Met, plays an important role in the interaction between ligands and receptors. Loss of core fucosylation may alter their interactions and then down-regulate their intracellular signaling and inhibit cell proliferation (dash lines). Overall, loss of the *Fut8* gene results in a decrease in hepatocarcinogenesis.

The authors thank Dr. Yuka Kobayashi (J-Oil Mills, Tokyo, Japan) for providing the PhoSL, Dr. Maeda Kento (Kumamoto University, Japan) for technical assistance, and Dr. Lucas Revillon (Tohoku Pharmaceutical University) for the language modification of this manuscript. This work was partially supported by a Grant-in-Aid for Scientific Research 15H04354 to J.G. and 24590087 to T.F.; Challenging Exploratory Research Grant 15K14408 to J.G.; Young Scientists (B) Grant 23790363 to K.O.; Japan Society for the Promotion of Science; and Strategic Research Foundation Grant-aided Project for Private Universities from the Ministry of Education, Culture, Sports, Science and Technology of Japan.

REFERENCES

1. Haltiwanger, R. S., and Lowe, J. B. (2004) Role of glycosylation in development. *Annu. Rev. Biochem.* **73**, 491–537
2. Wang, X., Inoue, S., Gu, J., Miyoshi, E., Noda, K., Li, W., Mizuno-Horikawa, Y., Nakano, M., Asahi, M., Takahashi, M., Uozumi, N., Ihara, S., Lee, S. H., Ikeda, Y., Yamaguchi, Y., Aze, Y., Tomiyama, Y., Fujii, J., Suzuki, K., Kondo, A., Shapiro, S. D., Lopez-Otin, C., Kuwaki, T., Okabe, M., Honke, K., and Taniguchi, N. (2005) Dysregulation of TGF-beta1 receptor activation leads to abnormal lung development and emphysema-like phenotype in core fucose-deficient mice. *Proc. Natl. Acad. Sci. USA* **102**, 15791–15796
3. Wang, X., Gu, J., Ihara, H., Miyoshi, E., Honke, K., and Taniguchi, N. (2006) Core fucosylation regulates epidermal growth factor receptor-mediated intracellular signaling. *J. Biol. Chem.* **281**, 2572–2577
4. Zhao, Y., Itoh, S., Wang, X., Isaji, T., Miyoshi, E., Kariya, Y., Miyazaki, K., Kawasaki, N., Taniguchi, N., and Gu, J. (2006) Deletion of core fucosylation on alpha3beta1 integrin down-regulates its functions. *J. Biol. Chem.* **281**, 38343–38350
5. Gu, W., Fukuda, T., Isaji, T., Hashimoto, H., Wang, Y., and Gu, J. (2013) α1,6-Fucosylation regulates neurite formation *via* the activin/phospho-Smad2 pathway in PC12 cells: the implicated dual effects of Fut8 for TGF-β/activin-mediated signaling. *FASEB J.* **27**, 3947–3958
6. Jemal, A., Bray, F., Center, M. M., Ferlay, J., Ward, E., and Forman, D. (2011) Global cancer statistics. *CA Cancer J. Clin.* **61**, 69–90
7. Farazi, P. A., and DePinho, R. A. (2006) Hepatocellular carcinoma pathogenesis: from genes to environment. *Nat. Rev. Cancer* **6**, 674–687
8. Aravalli, R. N., Steer, C. J., and Cressman, E. N. (2008) Molecular mechanisms of hepatocellular carcinoma. *Hepatology* **48**, 2047–2063
9. Llovet, J. M., and Bruix, J. (2008) Molecular targeted therapies in hepatocellular carcinoma. *Hepatology* **48**, 1312–1327
10. Binamé, F., Lassus, P., and Hibner, U. (2008) Transforming growth factor beta controls the directional migration of hepatocyte cohorts by modulating their adhesion to fibronectin. *Mol. Biol. Cell* **19**, 945–956
11. Giordano, S., and Columbano, A. (2014) Met as a therapeutic target in HCC: facts and hopes. *J. Hepatol.* **60**, 442–452
12. Engelman, J. A., and Jänne, P. A. (2008) Mechanisms of acquired resistance to epidermal growth factor receptor tyrosine kinase inhibitors in non-small cell lung cancer. *Clin. Cancer Res.* **14**, 2895–2899
13. Wheeler, D. L., Huang, S., Kruser, T. J., Nechrebecki, M. M., Armstrong, E. A., Benavente, S., Gondi, V., Hsu, K. T., and Harari, P. M. (2008) Mechanisms of acquired resistance to cetuximab: role of HER (ErbB) family members. *Oncogene* **27**, 3944–3956
14. Contessa, J. N., Bhojani, M. S., Freeze, H. H., Ross, B. D., Rehemtulla, A., and Lawrence, T. S. (2010) Molecular imaging of N-linked glycosylation suggests glycan biosynthesis is a novel target for cancer therapy. *Clin. Cancer Res.* **16**, 3205–3214
15. Hutchinson, W. L., Du, M. Q., Johnson, P. J., and Williams, R. (1991) Fucosyltransferases: differential plasma and tissue alterations in hepatocellular carcinoma and cirrhosis. *Hepatology* **13**, 683–688
16. Noda, K., Miyoshi, E., Gu, J., Gao, C. X., Nakahara, S., Kitada, T., Honke, K., Suzuki, K., Yoshihara, H., Yoshikawa, K., Kawano, K., Tonetti, M., Kasahara, A., Hori, M., Hayashi, N., and Taniguchi, N. (2003) Relationship between elevated FX expression and increased production of GDP-L-fucose, a common donor substrate for fucosylation in human hepatocellular carcinoma and hepatoma cell lines. *Cancer Res.* **63**, 6282–6289

17. Sato, Y., Nakata, K., Kato, Y., Shima, M., Ishii, N., Koji, T., Taketa, K., Endo, Y., and Nagataki, S. (1993) Early recognition of hepatocellular carcinoma based on altered profiles of alpha-fetoprotein. *N. Engl. J. Med.* **328**, 1802–1806
18. Block, T. M., Comunale, M. A., Lowman, M., Steel, L. F., Romano, P. R., Fimmel, C., Tennant, B. C., London, W. T., Evans, A. A., Blumberg, B. S., Dwek, R. A., Mattu, T. S., and Mehta, A. S. (2005) Use of targeted glycoproteomics to identify serum glycoproteins that correlate with liver cancer in woodchucks and humans. *Proc. Natl. Acad. Sci. USA* **102**, 779–784
19. Wang, M., Long, R. E., Comunale, M. A., Junaidi, O., Marrero, J., Di Bisceglie, A. M., Block, T. M., and Mehta, A. S. (2009) Novel fucosylated biomarkers for the early detection of hepatocellular carcinoma. *Cancer Epidemiol. Biomarkers Prev.* **18**, 1914–1921
20. Yamashita, F., Tanaka, M., Satomura, S., and Tanikawa, K. (1996) Prognostic significance of Lens culinaris agglutinin A-reactive alpha-fetoprotein in small hepatocellular carcinomas. *Gastroenterology* **111**, 996–1001
21. Kalinichenko, V. V., Major, M. L., Wang, X., Petrovic, V., Kuechle, J., Yoder, H. M., Dennewitz, M. B., Shin, B., Datta, A., Raychaudhuri, P., and Costa, R. H. (2004) Foxm1b transcription factor is essential for development of hepatocellular carcinomas and is negatively regulated by the p19ARF tumor suppressor. *Genes Dev.* **18**, 830–850
22. Matsumoto, K., Huang, J., Viswakarma, N., Bai, L., Jia, Y., Zhu, Y. T., Yang, G., Borensztajn, J., Rao, M. S., Zhu, Y. J., and Reddy, J. K. (2010) Transcription coactivator PBP/MED1-deficient hepatocytes are not susceptible to diethylnitrosamine-induced hepatocarcinogenesis in the mouse. *Carcinogenesis* **31**, 318–325
23. Lanaya, H., Natarajan, A., Komposch, K., Li, L., Amberg, N., Chen, L., Wculek, S. K., Hammer, M., Zenz, R., Peck-Radosavljevic, M., Sieghart, W., Trauner, M., Wang, H., and Sibilia, M. (2014) EGFR has a tumour-promoting role in liver macrophages during hepatocellular carcinoma formation. *Nat. Cell Biol.* **16**, 972–981, 1–7
24. Fukuda, T., Hashimoto, H., Okayasu, N., Kameyama, A., Onogi, H., Nakagawasai, O., Nakazawa, T., Kurosawa, T., Hao, Y., Isaji, T., Tadano, T., Narimatsu, H., Taniguchi, N., and Gu, J. (2011) Alpha1,6-fucosyltransferase-deficient mice exhibit multiple behavioral abnormalities associated with a schizophrenia-like phenotype: importance of the balance between the dopamine and serotonin systems. *J. Biol. Chem.* **286**, 18434–18443
25. Kobayashi, Y., Tateno, H., Dohra, H., Moriwaki, K., Miyoshi, E., Hirabayashi, J., and Kawagishi, H. (2012) A novel core fucose-specific lectin from the mushroom *Pholiota squarrosa*. *J. Biol. Chem.* **287**, 33973–33982
26. Uozumi, N., Yanagidani, S., Miyoshi, E., Ihara, Y., Sakuma, T., Gao, C. X., Teshima, T., Fujii, S., Shiba, T., and Taniguchi, N. (1996) Purification and cDNA cloning of porcine brain GDP-L-Fuc:*N*-acetyl-beta-D-glucosaminide alpha1—>6fucosyltransferase. *J. Biol. Chem.* **271**, 27810–27817
27. Fang, M., Dewaele, S., Zhao, Y. P., Stärkel, P., Vanhooren, V., Chen, Y. M., Ji, X., Luo, M., Sun, B. M., Horsmans, Y., Dell, A., Haslam, S. M., Grassi, P., Libert, C., Gao, C. F., and Chen, C. C. (2010) Serum *N*-glycome biomarker for monitoring development of DENA-induced hepatocellular carcinoma in rat. *Mol. Cancer* **9**, 215
28. Verna, L., Whysner, J., and Williams, G. M. (1996) *N*-Nitrosodiethylamine mechanistic data and risk assessment: bioactivation, DNA-adduct formation, mutagenicity, and tumor initiation. *Pharmacol. Ther.* **71**, 57–81
29. Kang, J. S., Wanibuchi, H., Morimura, K., Gonzalez, F. J., and Fukushima, S. (2007) Role of CYP2E1 in diethylnitrosamine-induced hepatocarcinogenesis in vivo. *Cancer Res.* **67**, 11141–11146
30. Jacinto, F. V., and Esteller, M. (2007) MGMT hypermethylation: a prognostic foe, a predictive friend. *DNA Repair (Amst.)* **6**, 1155–1160
31. Sakurai, T., He, G., Matsuzawa, A., Yu, G. Y., Maeda, S., Hardiman, G., and Karin, M. (2008) Hepatocyte necrosis induced by oxidative stress and IL-1 alpha release mediate carcinogen-induced compensatory proliferation and liver tumorigenesis. *Cancer Cell* **14**, 156–165
32. Goyal, L., Muzumdar, M. D., and Zhu, A. X. (2013) Targeting the HGF/c-MET pathway in hepatocellular carcinoma. *Clin. Cancer Res.* **19**, 2310–2318
33. Fausto, N., Campbell, J. S., and Riehle, K. J. (2006) Liver regeneration. *Hepatology* **43** (2 Suppl 1), S45–S53
34. Grivennikov, S. I., Greten, F. R., and Karin, M. (2010) Immunity, inflammation, and cancer. *Cell* **140**, 883–899
35. Maeda, S., Kamata, H., Luo, J. L., Leffert, H., and Karin, M. (2005) IKKbeta couples hepatocyte death to cytokine-driven compensatory proliferation that promotes chemical hepatocarcinogenesis. *Cell* **121**, 977–990
36. Taub, R. (2004) Liver regeneration: from myth to mechanism. *Nat. Rev. Mol. Cell Biol.* **5**, 836–847
37. Ferrara, C., Grau, S., Jäger, C., Sondermann, P., Brünker, P., Waldhauer, I., Hennig, M., Ruf, A., Rufer, A. C., Stihle, M., Umaña, P., and Benz, J. (2011) Unique carbohydrate-carbohydrate interactions are required for high affinity binding between FcgammaRIII and antibodies lacking core fucose. *Proc. Natl. Acad. Sci. USA* **108**, 12669–12674
38. Mizushima, T., Yagi, H., Takemoto, E., Shibata-Koyama, M., Isoda, Y., Iida, S., Masuda, K., Satoh, M., and Kato, K. (2011) Structural basis for improved efficacy of therapeutic antibodies on defucosylation of their Fc glycans. *Genes Cells* **16**, 1071–1080
39. Okazaki, A., Shoji-Hosaka, E., Nakamura, K., Wakitani, M., Uchida, K., Kakita, S., Tsumoto, K., Kumagai, I., and Shitara, K. (2004) Fucose depletion from human IgG1 oligosaccharide enhances binding enthalpy and association rate between IgG1 and FcgammaRIIIa. *J. Mol. Biol.* **336**, 1239–1249
40. Shinkawa, T., Nakamura, K., Yamane, N., Shoji-Hosaka, E., Kanda, Y., Sakurada, M., Uchida, K., Anazawa, H., Satoh, M., Yamasaki, M., Hanai, N., and Shitara, K. (2003) The absence of fucose but not the presence of galactose or bisecting *N*-acetylglucosamine of human IgG1 complex-type oligosaccharides shows the critical role of enhancing antibody-dependent cellular cytotoxicity. *J. Biol. Chem.* **278**, 3466–3473
41. Zhu, A. X. (2010) Systemic treatment of hepatocellular carcinoma: dawn of a new era? *Ann. Surg. Oncol.* **17**, 1247–1256
42. Engelman, J. A., Zejnullahu, K., Mitsudomi, T., Song, Y., Hyland, C., Park, J. O., Lindeman, N., Gale, C. M., Zhao, X., Christensen, J., Kosaka, T., Holmes, A. J., Rogers, A. M., Cappuzzo, F., Mok, T., Lee, C., Johnson, B. E., Cantley, L. C., and Jänne, P. A. (2007) MET amplification leads to gefitinib resistance in lung cancer by activating ERBB3 signaling. *Science* **316**, 1039–1043
43. Takahashi, T., Ikeda, Y., Miyoshi, E., Yaginuma, Y., Ishikawa, M., and Taniguchi, N. (2000) alpha1,6Fucosyltransferase is highly and specifically expressed in human ovarian serous adenocarcinomas. *Int. J. Cancer* **88**, 914–919
44. Chen, C. Y., Jan, Y. H., Juan, Y. H., Yang, C. J., Huang, M. S., Yu, C. J., Yang, P. C., Hsiao, M., Hsu, T. L., and Wong, C. H. (2013) Fucosyltransferase 8 as a functional regulator of nonsmall cell lung cancer. *Proc. Natl. Acad. Sci. USA* **110**, 630–635
45. Muinelo-Romay, L., Vázquez-Martín, C., Villar-Portela, S., Cuevas, E., Gil-Martín, E., and Fernández-Briera, A. (2008) Expression and enzyme activity of alpha(1,6)fucosyltransferase in human colorectal cancer. *Int. J. Cancer* **123**, 641–646
46. Wang, M., Wang, J., Kong, X., Chen, H., Wang, Y., Qin, M., Lin, Y., Chen, H., Xu, J., Hong, J., Chen, Y. X., Zou, W., and Fang, J. Y. (2014) MiR-198 represses tumor growth and metastasis in colorectal cancer by targeting fucosyl transferase 8. *Sci. Rep.* **4**, 6145

Received for publication January 15, 2015.
Accepted for publication March 31, 2015.

THE JOURNAL OF BIOLOGICAL CHEMISTRY VOL. 290, NO. 49, pp. 29345–29360, December 4, 2015

Integrin α5 Suppresses the Phosphorylation of Epidermal Growth Factor Receptor and Its Cellular Signaling of Cell Proliferation via *N*-Glycosylation*

Received for publication, July 29, 2015, and in revised form, October 14, 2015 Published, JBC Papers in Press, October 19, 2015, DOI 10.1074/jbc.M115.682229

Qinglei Hang, Tomoya Isaji, Sicong Hou, Sanghun Im, Tomohiko Fukuda, and Jianguo Gu[1]

From the Division of Regulatory Glycobiology, Institute of Molecular Biomembrane and Glycobiology, Tohoku Pharmaceutical University, 4-4-1 Komatsushima, Aoba-ku, Sendai, Miyagi, 981-8558, Japan

Background: The functions of integrin α5 on cell proliferation and the underlying mechanisms remain unclear.
Results: Loss of *N*-glycosylation on α5 increased the phosphorylation and internalization of EGFR and abolished its inhibitory effects on cell proliferation.
Conclusion: Integrin α5 regulates EGFR-mediated signaling through *N*-glycosylation.
Significance: *N*-Glycosylation plays important roles in the cross-talk between integrins and growth factor receptors.

Integrin α5β1-mediated cell adhesion regulates a multitude of cellular responses, including cell proliferation, survival, and cross-talk between different cellular signaling pathways. Integrin α5β1 is known to convey permissive signals enabling anchorage-dependent receptor tyrosine kinase signaling. However, the effects of integrin α5β1 on cell proliferation are controversial, and the molecular mechanisms involved in the regulation between integrin α5β1 and receptor tyrosine kinase remain largely unclear. Here we show that integrin α5 functions as a negative regulator of epidermal growth factor receptor (EGFR) signaling through its *N*-glycosylation. Expression of WT integrin α5 suppresses the EGFR phosphorylation and internalization upon EGF stimulation. However, expression of the *N*-glycosylation mutant integrin α5, S3–5, which contains fewer *N*-glycans, reversed the suppression of the EGFR-mediated signaling and cell proliferation. In a mechanistic manner, WT but not S3–5 integrin α5 forms a complex with EGFR and glycolipids in the low density lipid rafts, and the complex formation is disrupted upon EGF stimulation, suggesting that the *N*-glycosylation of integrin α5 suppresses the EGFR activation through promotion of the integrin α5-glycolipids-EGFR complex formation. Furthermore, consistent restoration of those *N*-glycans on the Calf-1,2 domain of integrin α5 reinstated the inhibitory effects as well as the complex formation with EGFR. Taken together, these data are the first to demonstrate that EGFR activation can be regulated by the *N*-glycosylation of integrin α5, which is a novel molecular paradigm for the cross-talk between integrins and growth factor receptors.

Epidermal growth factor receptor (EGFR),[2] a member of the ErbB receptor tyrosine kinase family, converts extracellular cues into intracellular effectors to trigger appropriate cellular responses (1–3), which play a key role in normal epithelial developmental biology and in tumor metastasis (4). A dysregulation of EGFR signaling, including receptor overexpression and/or activation, is a common feature in tumorigenesis (5). Due to this aberrant activity in the pathology of cancer, EGFR has emerged as an attractive candidate for anticancer therapy (6), which prompted us to examine the underlying molecular mechanisms for EGFR activation.

EGFR activation forms a complex signaling network with several regulators, including related cytoplasmic proteins, microRNAs, tyrosine kinase inhibitors, and other coupled receptors (7–9). However, studies that address these direct or indirect regulations of EGFR have focused mainly on the inner membrane, particularly the cytoplasmic kinase domain of EGFR. The underlying mechanisms of the outer membrane remain unknown.

Current insight into this regulation derives largely from studies around EGFR-related microdomains, so-called lipid rafts (10–13), which are thought to act as platforms for EGFR signaling (14, 15). These molecules are localized in the microdomains of the cell membrane and are usually rich in cholesterol, glycosphingolipids, and glycoproteins (15–17). Several studies have associated glycosphingolipids, including gangliosides GM1, GM3, and GD3, with the regulation of EGFR signaling (18–20). In addition to glycosphingolipids, some glycoproteins that are located in the EGFR-related lipid rafts play important roles in the regulation of EGFR signaling (12, 13, 21–23). These limited results highlight the possibility that glycosylation might act as a "linker" in lipid rafts for the regulation of EGFR. However, little is known about how glycosylation controls regulation. Therefore, elucidation of the underlying mechanisms involved in the glycosylation-mediated regulation of EGFR is

* This work was supported in part by Grants-in-Aid for Scientific Research 15H04354 (to J. G.) and 24570169 (to T. I.) and for Challenging Exploratory Research 15K14408 (to J. G.) from the Japan Society for the Promotion of Science and by a Strategic Research Foundation Grant-aided Project for Private Universities from the Ministry of Education, Culture, Sports, Science, and Technology of Japan. The authors declare that they have no conflicts of interest with the contents of this article.

[1] To whom correspondence should be addressed: Division of Regulatory Glycobiology, Institute of Molecular Biomembrane and Glycobiology, Tohoku Pharmaceutical University, 4-4-1 Komatsushima, Aoba-ku, Sendai Miyagi 981-8558, Japan. E-mail: jgu@tohoku-pharm.ac.jp. Tel.: 81-22-727-0216; Fax: 81-22-727-0078.

[2] The abbreviations used are: EGFR, epidermal growth factor receptor; FN, fibronectin; WB, Western blot; EGF-555, Alexa Fluor® 555-conjugated EGF; GM1, Galβ1,3GalNAcβ1,4(NeuAcα2,3)-Galβ1,4Glc-ceramide; GM3, NeuAcα2,3Galβ1,4Glc-ceramide; GD3, Neu5Acα2,8Neu5Acα2,3Galβ1,4Glc-ceramide.

very important for a complete view of the biological functions of EGFR.

Integrins are important members of the EGFR lipid raft-related glycoproteins, as mentioned above, and are major carriers of *N*-glycans, which are thought to play crucial roles in many biological functions. In response to cell adhesion, integrins not only directly initiate certain cytoplasmic signals for cell spreading but also indirectly modulate the transmission of EGFR signaling, which is referred to as cross-talk (24–30). The integrins mediate cooperation with EGFR mainly through α-cytoplasmic domains (31), which are also restricted to the inner membrane. Until recently, integrin α5β1, a major fibronectin receptor, was believed to be a well characterized integrin, with *N*-glycosylation functions in cell adhesion (32, 33). However, the function of *N*-glycosylation on cell proliferation and cellular signaling remains unclear. In fact, there have been several controversial reports about the regulation of EGFR-mediated signaling by integrin α5 (34, 35).

To resolve these issues, we have examined the relationship between integrin α5 and EGFR and found that the expression of integrin α5 negatively regulates EGFR-mediated cellular signaling and cell proliferation. We used *N*-glycosylation mutants of integrin α5 to clarify the roles of the *N*-glycosylation of α5 in EGFR-mediated signaling and cross-talk with EGFR and found that the regulation was strictly controlled via the *N*-glycans of integrin α5, particularly the *N*-glycans on the Calf-1,2 domain. Our results clearly demonstrate the importance of the *N*-glycans of integrin in the regulation of EGFR-mediated cellular signaling and provide new insights into the cross-talk between growth factor receptors and integrins.

Experimental Procedures

Antibodies and Reagents—The experiments were performed using the following antibodies: mAbs against integrin α5 (catalog no. 610634), ERK1 (catalog no. 610031), and caveolin-1 (catalog no. 610407) obtained from BD Biosciences; mAb against human α5β1 (MAB1999) from Millipore; the supernatant of the hybridoma of hamster integrin β1 subunit (7E2) from the Developmental Studies Hybridoma Bank, University of Iowa; mouse polyclonal antibody to EGFR (sc-120) from Santa Cruz Biotechnology, Inc.; rabbit mAbs to EGFR (catalog no. 4267), phospho-EGFR (catalog no. 3777), phospho-ERK1/2 (catalog no. 4370), AKT (catalog no. 9272), and phospho-AKT (catalog no. 4060) from Cell Signaling Technology; and mAb against α-tubulin from Sigma. Alexa Fluor® 647 goat anti-mouse IgG was obtained from Invitrogen. The peroxidase-conjugated goat against mouse and rabbit IgG antibodies were obtained from Promega and Cell Signaling Technology, respectively. The methyl-β-cyclodextrin, biotin-conjugated cholera toxin B subunit, primaquine, MesNa, iodoacetamide, and fibronectin (FN) were from Sigma; EGF (AF-100) was from PeproTech; EGF-Alexa Fluor® 555 was from Invitrogen; the control mouse IgG1 was from TONBO biosciences; sulfo-NHS-SS-biotin was from Thermo Scientific; and TO-PRO-3 was from Molecular Probes. The agarose-conjugated anti-GFP antibody (RQ2) and the Streptavidin-conjugated agarose were obtained from Medical & Biological Laboratories Co. Ltd. (Nagoya, Japan) and Millipore, respectively.

Cell Lines and Cell Culture—The 293T and HeLa cell lines were provided by the RIKEN cell bank (Japan). The phoenix and MDA-MB-231 cell lines were purchased from ATCC. The integrin α5 subunit-deficient CHO-K1 cell line (CHO-B2) and the U-251MG cell line were gifts from Dr. Rudolf Juliano (School of Medicine, University of North Carolina, Chapel Hill, NC) (36) and Prof. Jun Nakayama (Shinshu University Graduate School of Medicine, Japan), respectively. The stable cell lines used in this study were established as mentioned below. All cell lines were maintained at 37 °C in Dulbecco's modified Eagle's medium (DMEM), supplemented with 10% fetal bovine serum (FBS), under a humidified atmosphere containing 5% CO_2, except for the virus production.

Generation of CRISPR/Cas9-based Integrin α5-knock-out (KO) Cells—The CRISPR/Cas9-based integrin α5-KO cells were established as described previously (37). Briefly, the sgRNA-specifying oligonucleotide sequences spanning human integrin α5 exon 3 (5′-CACCGGGGCAACAGTTCGAGCCCA-3′ and 5′-AAACTGGGCTCGAACTGTTGCCCC-3′) were chosen from the human KO library sgRNAs (38). After annealing, the double-stranded guide oligonucleotides were cloned into the pSpCas9(BB)-2A-GFP (Addgene plasmid ID: 48138) vector. The expression vector was transfected into the indicated cell lines by electroporation according to the manufacturer's instructions. The GFP-positive cells were sorted by FACSAria II (BD Bioscience) after culture for 3 days. The integrin α5-positive but GFP-negative cells were then sorted three times during the following 2-week culture. The α5-KO cells were confirmed by flow cytometry and Western blot analyses as described below.

EGFR and Integrin α5 Expression Vectors—The cDNA of human EGFR (a generous gift from Dr. Motoko Takahashi, Sapporo Medical University, Japan) was inserted into a cloning entry vector (pENTR1A, Invitrogen) according to the manufacturer's protocol for the In-Fusion kit (Takara Bio) using the following primers: 5′-ATCCGGTACCGAATTCACCATGCGACCCTCCGG-3′ and 5′-TCTAGATATCTCGAGTGCTCCAATAAATTC-3′. The vectors of GFP and GFP-tagged integrin α5 with altered *N*-glycosylation sites (WT, S3–5, and Δ10–14) were previously established in our laboratory (33). The S3–5,10–14 mutation vector was also constructed according to the in-fusion kit using the following primers: 5′-TACATTATCAGAGCAAGAGCCG-3′, 5′-ATCCAACTCCAGGCCCTTTGGG-3′, 5′-CAAAGGGCCTGGAGTTGGAT-3′, and 5′-GCTCTTGCTCTGATAATGTAGG-3′. The resultant cDNAs were sequenced to confirm the presence of the desired mutations. We used the Gateway™ cloning system kit (Invitrogen) to acquire all of the expression vectors. Briefly, the LR clonase enzyme (Invitrogen) was used to transfer the cDNAs of EGFR and integrin α5 from the entry vectors into pBABE-puro-Rfa (32) and CSII-CMV-Rfa (kindly provided by Dr. H. Miyoshi (RIKEN, Tokyo, Japan)), respectively.

Virus Production and Infection—The virus production and infection were performed as described previously (32, 39). In brief, the pBABE-puro-Rfa-based retrovirus vectors and pLP/VSVG (Invitrogen) were transfected into Phoenix cells with Lipofectamine 2000 (Invitrogen). The CSII-CMV-Rfa-based lentivirus vectors were cotransfected with pCAG-HIVgp and

pCMV-VSV-G-RSV-Rev into 293T cells. After transfection for 48 h, the retrovirus and lentivirus supernatants were collected. The CHO-B2 cells were infected with the resultant viral supernatant containing 10 μg/ml Polybrene (Sigma) at 32 °C overnight and then selected in the presence of 2.0 mg/ml puromycin (Nacalai Tesque, Kyoto, Japan) for 7 days. The antibiotic-resistant positive colonies (CHO-B2/EGFR) were picked up as a control. In the case of integrin α5-KO cells expressing GFP, WT, or mutant integrin α5, the GFP-positive cells were sorted three times using FACSAria II after lentivirus infection for 72 h. The stable cell lines were used in subsequent studies.

Western Blot (WB) and Immunoprecipitation—For WB, the indicated cells were washed with ice-cold PBS and then lysed in the cell lysate (20 mM Tris-HCl, pH 7.4, 150 mM NaCl, 1% Triton X-100) with protease and phosphatase inhibitors (Nacalai Tesque, Kyoto, Japan) for 30 min. After centrifugation at 1,000 × *g* for 10 min, the supernatant was collected, and protein concentrations were determined using a BCA protein assay kit (Pierce). The protein lysates were resolved by non-reducing SDS-PAGE for integrin α5 and β1 or reducing SDS-PAGE for other proteins. After electrophoresis, the proteins were transferred to a PVDF membrane (Millipore) and detected with the indicated primary and secondary antibodies using an Immobilon Western Chemiluminescent HRP Substrate (Millipore), according to the manufacturer's instructions. For immunoprecipitates, cells were lysed with detergent-free TBS buffer (20 mM Tris-HCl, pH 7.4, 150 mM NaCl) by being passed through a 21-gauge needle as described previously (18). Briefly, cells were resuspended in the TBS with protease and phosphatase inhibitors and lysed by being passed through a 21-gauge needle 30 times. After centrifugation at 1,000 × *g* for 10 min, the supernatant was collected. The remaining pellet was again syringed 30 times. After centrifugation at 1,000 × *g* for 10 min, the second postnuclear supernatant was combined with the first, and protein concentrations were determined using a BCA protein assay kit. Equivalent amounts (600 μg) of the supernatants were immunoprecipitated with anti-GFP-agarose, anti-EGFR antibody, or cholera toxin B subunit-biotin and Streptavidin-conjugated agarose for 1 h at 4 °C with rotation, and then the immunoprecipitates were washed twice with lysis buffer and subjected to 6% SDS-PAGE.

Cell Growth and Colony Formation Analysis—The growth of the indicated cells was estimated by determination of cell growth curves or colony formation assays. To assay the cell growth curves, the cells (3×10^4) were seeded in 6-cm dishes overnight and then serum-starved for either 24 or 48 h (for MDA-MB-231 cells). After starvation, the cells were supplied with DMEM containing 10% FBS with or without EGF (0.1 ng/ml), control IgG (10 μg/ml), or anti-EGFR-blocking Ab (10 μg/ml). The photographs of the same areas on the cultured dishes were taken at the indicated times (0, 24, 48, and 72 h), and the cell numbers were counted. Cell numbers were normalized to those at 0 h and statistically analyzed.

To assay the colony formation, the control, GFP, WT, and S3–5 group cells (0.6×10^3) were seeded in the 6-cm dishes. Cells were incubated for 14 days to allow colony formation, cells were stained with 0.25% crystal violet for 15 min, and images were taken. Quantification of the colonies was obtained by measuring the OD_{595} after digesting the colonies in each dish with 1 ml of 10% acetic acid. The OD_{595} values from GFP, WT, and S3–5 were normalized to that of the control cells.

Cell Surface Biotinylation—Cell surface biotinylation was performed as described previously with minor modifications (33). Briefly, cells were gently washed twice with PBS and then incubated with ice-cold PBS containing 0.2 mg/ml sulfo-NHS-SS-biotin for 1 h at 4 °C. After incubation, cells were washed three times with ice-cold PBS, and the cells were harvested and lysed in the lysis buffer. The biotinylated proteins were precipitated with Streptavidin-conjugated agarose and then detected by WB, as described above.

Flow Cytometry Analysis of Cells—Flow cytometric analysis was performed as described previously (32). Briefly, the indicated semiconfluent cells were detached from the 10-cm culture dishes using trypsin containing 1 mM EDTA and were subsequently stained with either the mouse IgG or primary mouse anti-α5β1 or anti-EGFR antibody for 1 h on ice, followed by incubation with Alexa Fluor® 647 goat anti-mouse IgG for 1 h. During the incubation, the cells were mixed gently every 10 min by flicking. After incubation, cells were washed three times with PBS and then analyzed using a FACSCalibur flow cytometer and Cell Quest Pro software (BD Biosciences).

Isolation of Detergent-free Lipid Raft Fractions—Preparation of detergent-free lipid raft fractions was preformed as described previously, with minor modifications (18). Briefly, 150-mm dishes of the indicated CHO-B2 cells were washed twice with PBS and then lysed twice with a total of 1 ml (each time 0.5 ml) of detergent-free base buffer (20 mM Tris·HCl, 250 mM sucrose, pH 7.8, containing 1 mM $CaCl_2$ and 1 mM $MgCl_2$) with protease and phosphatase inhibitors by being passed through a 21-gauge needle as described above. After centrifugation at 1,000 × *g* for 10 min, the postnuclear supernatant (~1 ml) was mixed with the same volume of the base buffer containing 50% (v/v) OptiPrep and then added to the bottom of a 5-ml ultracentrifuge tube. Subsequently, each 0.6 ml of 20, 15, 10, 5, and 0% of OptiPrep in the base buffer was sequentially overlaid to the ultracentrifuge tube. The gradient was centrifuged at 5.2×10^4 rpm for 18 h at 4 °C, using an ultracentrifuge (Hitachi himac CS100GX). A total of 12 fractions (0.4 ml for each) were carefully collected from top to bottom of the gradient and analyzed by WB, as described above.

Cell-spreading Assay—The cell-spreading assay was performed as described previously with minor modifications (33). Briefly, 6-well plates were coated with FN (10 μg/ml) in PBS overnight at 4 °C and then blocked with 1% bovine serum albumin (BSA) in DMEM for 1 h at 37 °C. The indicated CHO-B2 cells were detached and suspended in serum-free DMEM with 0.1% BSA at 3×10^4 cells/ml. After replating on the FN-coated dishes for 20 min, non-adherent cells were removed by washing with PBS, and the attached cells were fixed with 4% paraformaldehyde in PBS, and representative photographs were then taken by phase-contrast microscopy.

Immunofluorescence—To assay the EGF-Alexa 555-based EGFR endocytosis, the indicated CHO-B2 cells were grown on coverslips (MatTek Corp., Ashland, MA) and starved for 24 h, followed by stimulation with a serum-free medium containing 50 ng/ml Alexa Fluor® 555-conjugated EGF (EGF-555) and 0.3

mM primaquine, a recycling inhibitor, for the indicated times (0, 2.5, 5, 10, and 15 min). Cells were washed and fixed in 4% paraformaldehyde for 20 min at room temperature, followed by two rinses with PBS. A nonspecific blocking solution was applied (PBS, 0.1% Triton X-100, 10% BSA) at room temperature for 1 h followed by incubation with TO-PRO-3 for 1 h in the dark. Cells were washed three times with PBS and were then immediately mounted using a fluorescent mounting medium (Dako). The confocal images were acquired using a ×60/1.35 numerical aperture oil immersion objective lens (FV1000; Olympus). The numbers of internalized EGF-555 puncta per cell in random fields were quantified.

Biotinylation-based EGFR Internalization Assay—The indicated CHO-B2 cells grown on 15-cm dishes were serum-starved for 5 h prior to the assay and washed in ice-cold PBS, and surface proteins were biotinylated with 0.2 mg/ml sulfo-NHS-SS-biotin in cold PBS for 1 h, followed by washing in TBS and placement on ice. For internalization, cells were then incubated in prewarmed DMEM containing 0.1 ng/ml EGF and 0.3 mM primaquine at 37 °C for the indicated duration (0, 2.5, 5, 10, and 15 min), whereas the control groups (without MesNa) remained on ice. Surface biotin was then stripped from the cells with a 10-min incubation in 50 mM MesNa in TBS (pH 8.6) twice, followed by washing and quenching of the MesNa with 20 mM iodoacetamide in TBS for 10 min. The control group cells were not subjected to surface reduction (no MesNa) in order to obtain total surface-labeled EGFR. After quenching, the cells were lysed, precipitated with Streptavidin-conjugated agarose, and subjected to WB. The percentage of internalized EGFR was calculated from the signal intensity of MesNa-resistant (internalized) EGFR at each time point relative to the control groups (no MesNa), which was the total EGFR on the cell surface in the three independent experiments.

Xenograft Assay—The left flank of NOD/SCID mice (5-week-old female mice; Charles River Laboratories, Japan) were injected subcutaneously with the indicated CHO-B2 cells (1×10^6). After 21 days of growth, tumors were dissected, and their volumes and weights were noted. Tumor volumes were calculated using the formula, $V = (L \times W^2) \times 0.5$ (where V is volume, L is length, and W is width). All animal procedures were carried out according to experimental protocols approved by the Tohoku Pharmaceutical University Research Ethics Board.

Statistical Analysis—Results are presented as the mean ± S.E. Statistical analyses were performed using Student's t test using GraphPad Prism version 5. Statistical significance was defined as $p < 0.05$ (not significant (*n.s*), $p > 0.05$; *, $p < 0.05$; **, $p < 0.01$; ***, $p < 0.001$).

Results

Inhibition of Cell Proliferation and Tumor Formation by the Expression of Integrin α5 via N-Glycosylation—Given the evidence that integrin α5 cooperates with EGFR to drive cell cycle progression (40), we established a simple cell model to clarify the underlying molecular mechanism for the cooperation between integrin α5 and EGFR. First, human EGFR cDNA was transfected into the CHO-B2 cell line that lacks the α5 subunit, in order to establish a stable EGFR-overexpressed CHO-B2 cell line (CHO-B2/EGFR). The CHO-B2/EGFR cells then were respectively reconstituted with either a GFP-tagged wild-type (WT) or a *N*-glycosylation mutant α5 subunit, S3–5, which contained only three of the 14 *N*-glycosylation sites (Fig. 1*A*). The three sites on the β-propeller domain of integrin α5 are essential for α5β1 heterodimerization, cell surface expression, and cell adhesion in CHO-B2 cells (33). As shown in Fig. 1*B*, when analyzed by flow cytometry analysis and biotinylation, these cells exhibited almost the same expression levels of EGFR and α5β1 on the cell surface and in the whole-cell lysates, suggesting that the level of α5 subunits had no effect on the expression of EGFR. Unexpectedly, the expression of WT, but not S3–5 α5 subunits, significantly suppressed cell proliferation, compared with those found in control cells with or without overexpression of a GFP tag only (Fig. 1*C*). The colony formation consistently included colony numbers (Fig. 1*D*) and sizes (data not shown) that were clearly decreased in the WT, compared with those in the S3–5 and control cells.

These *in vitro* observations encouraged us to investigate the effects of α5 expression on tumorigenicity *in vivo*. As shown in Fig. 1*E*, the control, GFP, and S3–5 cells permitted vigorous tumor formation. Tumor formation was significantly suppressed, however, in the WT cells, as reflected by both the tumor volume and weight. Taken together, these results suggested that the remaining *N*-glycosylation sites, with the noted exception of sites 3–5 of integrin α5, play an important role in the inhibition of cell growth and tumorigenicity.

EGFR-mediated Cellular Signaling Is Suppressed by the Expression of Wild-type Integrin α5—Considering the overexpression of EGFR in these cells, we wondered whether EGFR-mediated cellular signaling was modulated by α5. Surprisingly, under normal culture conditions, the phosphorylation levels of EGFR and its downstream molecules ERK and AKT were significantly decreased in WT cells compared with those in other cells (Fig. 2*A*). Furthermore, the responses for exogenous EGF-induced cell proliferation (Fig. 2*B*) and cellular signaling (Fig. 2*C*) were also significantly suppressed in WT cells but neither in S3–5 cells nor in the other control cells.

Integrin α5 also is known to cooperate with other growth factor receptors, such as c-Met or VEGFR (41); thus, we next investigated the contributions of EGFR to cell growth. Both the phosphorylation levels of EGFR and ERK were completely blocked in the presence of anti-EGFR blocking antibody (Fig. 2*D*); meanwhile, the abilities and differences among cells for cell proliferation were largely cancelled (Fig. 2*E*). Together, these results supported our hypothesis that the *N*-glycosylation-mediated inhibitory effects of α5 on cell growth happen primarily thorough EGFR signaling.

Inhibitory Effects of Integrin α5 on Cell Growth and EGFR Cellular Signaling Are Also Observed in Several Human Cancer Cell Lines—As described above, α5 negatively regulated EGFR-mediated signaling via *N*-glycosylation in CHO-B2/EGFR cells. Therefore, we selected several human cancer cell lines, such as HeLa, U-251MG, and MDA-MB-231 cells, which express relatively high levels of endogenous EGFR, in order to assess whether the phenomenon is common to other mammalian cells. To eliminate influences from endogenous α5, that gene was deleted by using a CRISPR/Cas9 knock-out system. The knock-out efficiencies were assessed by flow cytometry analysis

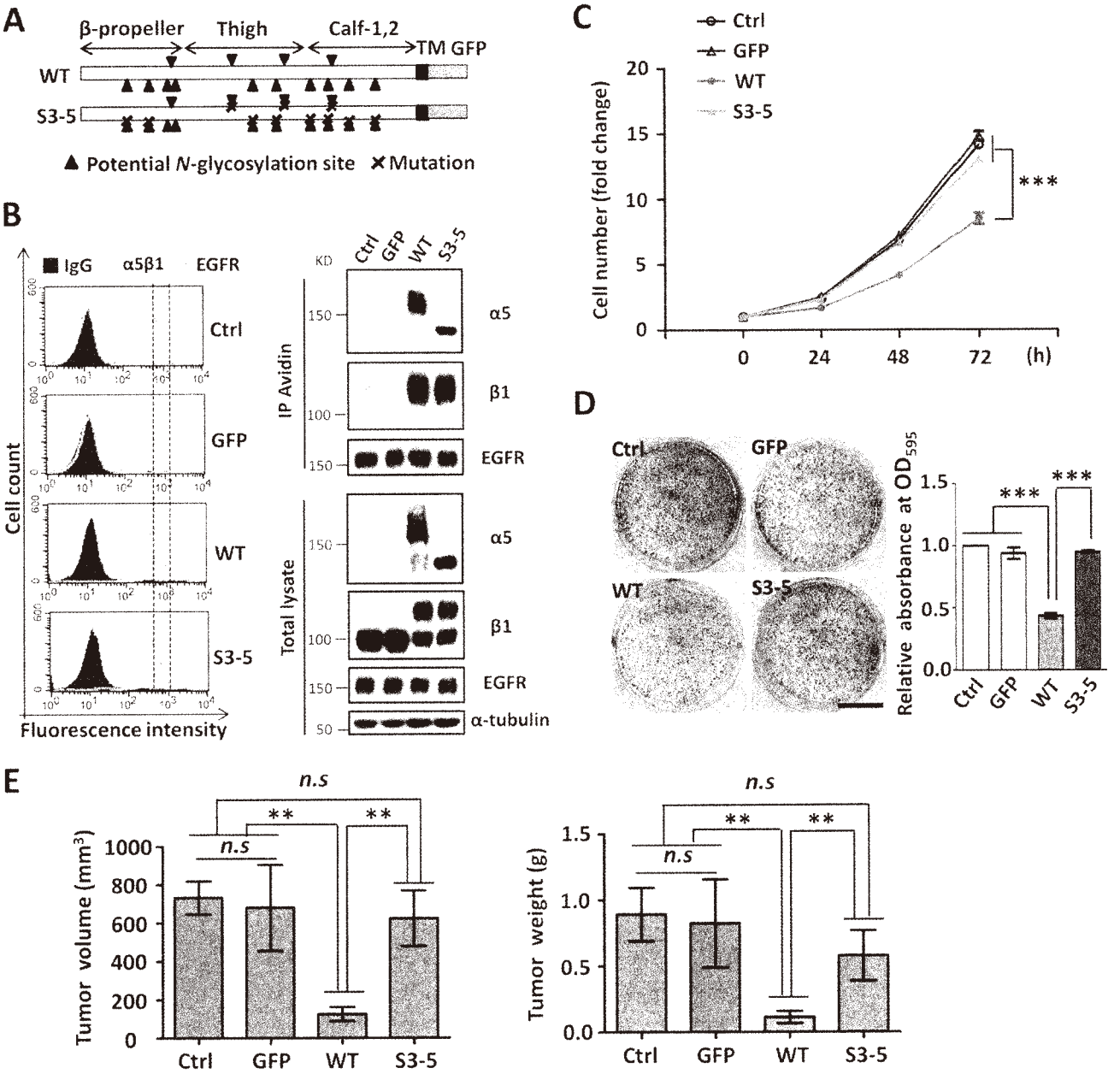

FIGURE 1. **Effects of WT and S3–5 mutant α5 subunit expression on cell growth in CHO cells.** *A*, schematic diagram of potential *N*-glycosylation sites on the WT and S3–5 integrin α5 subunit. Putative *N*-glycosylation sites (N84Q, N182Q, N297Q, N307Q, N316Q, N524Q, N530Q, N593Q, N609Q, N675Q, N712Q, N724Q, N773Q, and N868Q) are indicated by *triangles*, and point mutations are indicated by *crosses*. *B*, the control, GFP, WT, and S3–5 cells exhibited same expression levels of EGFR and integrin α5β1. The stable cell lines were established as described under "Experimental Procedures" section. The expression levels of integrin α5β1 and EGFR on the cell surfaces and in total cell lysates were analyzed by flow cytometry analysis (*left*) or biotinylation (*top right*) and WB with the indicated antibodies (*bottom right*), respectively. The IgG and α-tubulin were used as controls. *C*, the WT but not S3–5 transfectants exhibited a decrease in cell growth. After starvation for 24 h, cells were supplied with DMEM containing 10% FBS, and then cell numbers were counted and statistically analyzed at the indicated times ($n = 3$ individual experiments). *D*, colony formation ability was inhibited in WT but not S3–5 cells. Images of cell colonies are shown on the *left*. Colonies were stained with crystal violet after 14 days of seeding on plastic dishes. The OD_{595} values of GFP, WT, and S3–5 groups were normalized to that of the control group ($n = 3$ individual experiments). *E*, WT but not S3–5 cells showed a decrease in the tumorigenicity *in vivo*. The indicated cells (1×10^6) were injected subcutaneously into the left flank. Tumors were dissected, and their volumes (*left*) and weights (*right*) were noted after 21 days ($n = 4$). All values are means ± S.E. (*error bars*), Student's *t* test; n.s, not significant ($p > 0.05$); **, $p < 0.01$; ***, $p < 0.001$. *Scale bar*, 1 cm (*D*).

and Western blot in HeLa, U-251MG, and MDA-MB-231 cells (Figs. 3 (*A* and *B*) and 4 (*A* and B)). As shown in Fig. 3*C*, the KO HeLa cells exhibited an increased proliferation ability compared with the parent cells, indicating that α5 also acts as a proliferation suppressor in HeLa cells. Furthermore, the α5-KO cells were reconstituted with a GFP tag, WT or S3–5, and each cell line showed similar expression levels of EGFR (Figs. 3*D* and 4*C*). Consistent with the data of CHO-B2 cells, the expression of WT cells had an inhibitory effect on cell proliferation (Figs. 3*E* and 4 (*D* and *G*)) and phospho-EGFR as well as

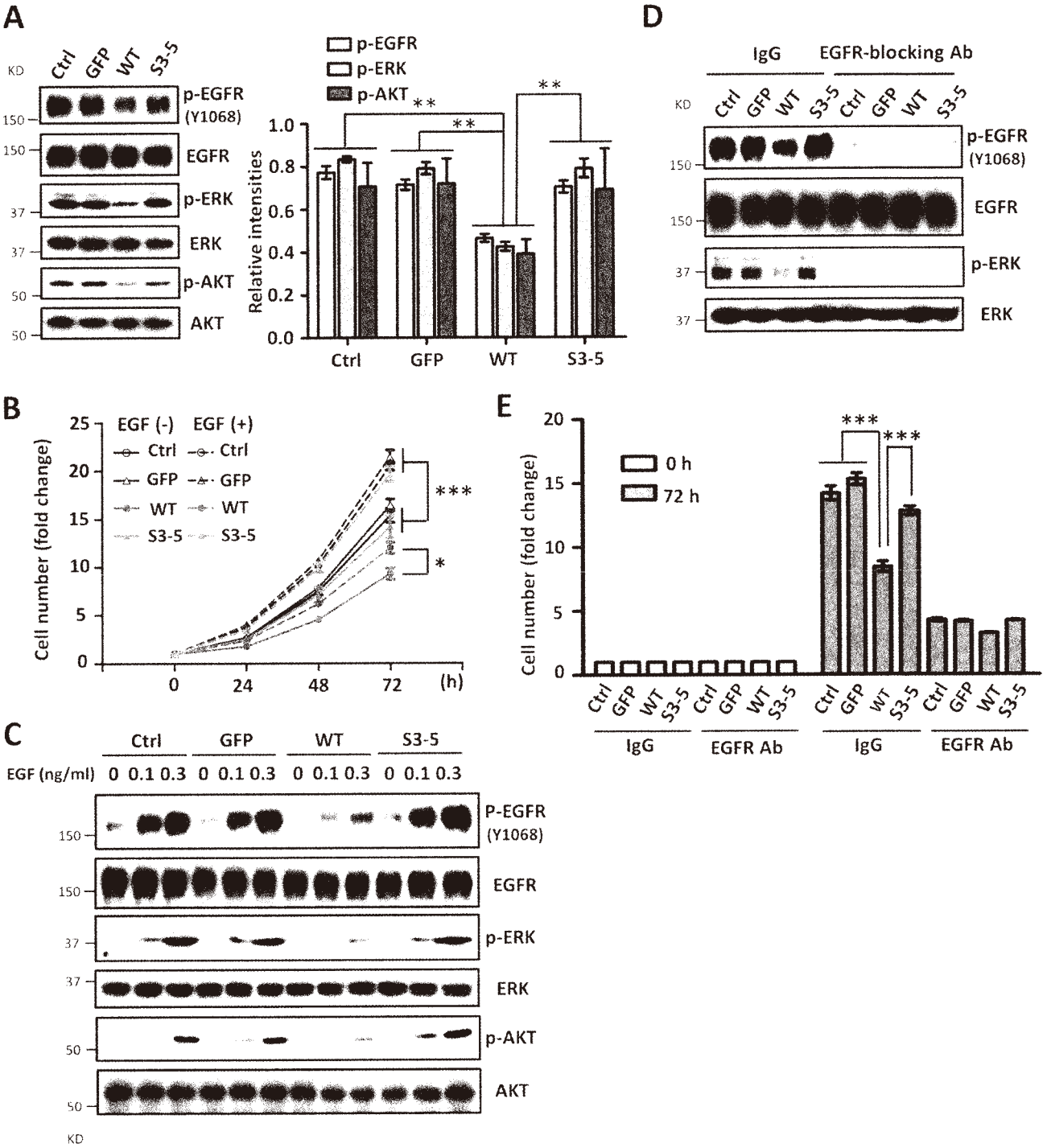

FIGURE 2. **Expression of WT but not S3–5 integrin α5 inhibits EGFR-mediated cellular signaling.** *A*, EGFR-related cellular signaling was inhibited in the WT cells. Cell lysates from the indicated cells were subjected to WBs with the indicated antibodies (*left*). The relative ratios (phospho-EGFR, phospho-ERK, and phospho-AKT *versus* EGFR, ERK, and AKT, respectively) are shown on the *right* ($n = 3$ individual experiments). *B*, comparison of cell growth among WT, S3–5, and control cells upon EGF stimulation. After starvation, cells were supplied with complete medium with or without EGF (0.1 ng/ml). Cell numbers were counted at the indicated times and statistically analyzed ($n = 3$ individual experiments). *C*, expression of WT α5 decreased responses for EGF. After starvation for 24 h, cells were treated with EGF at the indicated concentrations for 5 min. WB analysis was performed with the indicated antibodies. *D* and *E*, effects of the treatment with anti-EGFR-blocking antibody on EGFR-related cellular signaling (*D*) and cell growth (*E*) under normal culture conditions (without EGF stimulation). Cells were cultured with complete medium containing 10 μg/ml IgG (control) or anti-EGFR-blocking Ab for 72 h, the resultant cell extracts were subjected to WB with the indicated antibodies (*Ab*) (*D*), and the cell numbers were counted and statistically analyzed ($n = 3$ individual experiments) (*E*), respectively. All values are the means ± S.E. (*error bars*), Student's *t* test; *, $p < 0.05$; **, $p < 0.01$; ***, $p < 0.001$.

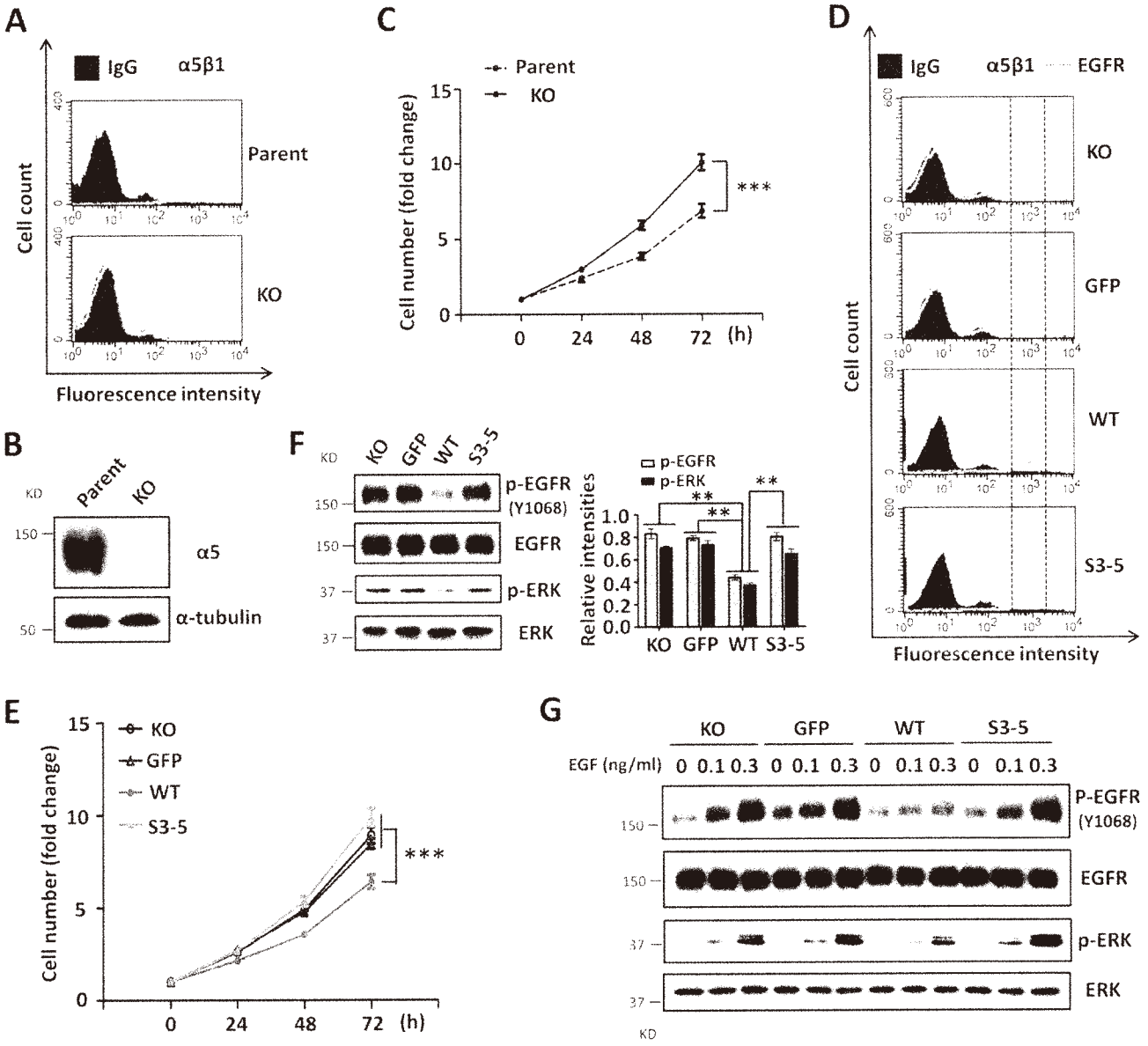

FIGURE 3. **Expression of integrin α5 inhibits cell growth and EGFR cellular signaling in HeLa cells.** *A* and *B*, the efficiency of the knock-out of the α5 gene using the CRISP/Cas9 system was assessed by flow cytometry analysis (*A*) and WB (*B*). The integrin α5-KO HeLa cells were established as described under "Experimental Procedures." *C*, the α5 KO-HeLa cells exhibited an increased cell growth ability. An analysis of cell growth was performed as described in the legend to Fig. 1*C* ($n = 3$ individual experiments). *D*, expression levels of integrin α5β1 and EGFR on the cell surface were assessed by flow cytometry analysis among revived cells with WT and S3–5 mutant of α5 in the α5 KO-HeLa cells. *E*, comparison of cell growth among those transfectants. An analysis of the KO, GFP, WT, and S3–5 HeLa cell growth was performed as described above ($n = 3$ individual experiments). *F*, the phosphorylation levels of EGFR and ERK were significantly suppressed in the WT cells, compared with the other cells. *Left*, WB pattern; *right*, quantitative analysis ($n = 3$ individual experiments). *G*, the WT cells also exhibited attenuated EGFR responses upon EGF stimulation. The responses to the indicated concentrations of EGF were performed by WB as described in Fig. 2*C*. All values are means ± S.E. (*error bars*), Student's *t* test; **, $p < 0.01$; ***, $p < 0.001$.

subsequent downstream phospho-ERK (Figs. 3*F* and 4 (*E* and *H*)), which differed from the expression of S3–5 integrin α5 cells. Moreover, the responses to EGF were also attenuated in WT, compared with that in other cells (Fig. 3*G*). Almost the same tendencies were observed in the U-251MG and MDA-MB-231 cells (Fig. 4, *F* and *I*). Together, these results further suggest that integrin α5 is a negative regulator for EGFR-mediated signaling through *N*-glycosylation. To clarify the underlying molecular mechanism, we further employed CHO-B2/EGFR cells in subsequent experiments.

Expression of Integrin α5 Delays EGFR Internalization upon EGF Stimulation—Upon EGF binding, EGFR is involved in a series of trafficking events, including internalization, degradation, and recycling, which ultimately regulate its signal amplification and propagation (42). Also, integrins are known to regulate the trafficking of some membrane proteins (43). Therefore, we conducted a biotinylation-based internalization assay (Fig. 5*A*) and an EGF-555-based EGFR endocytosis assay (Fig. 5*B*) in order to determine if the kinetics of EGFR internalization are affected by α5. To increase sensitivity for detection,

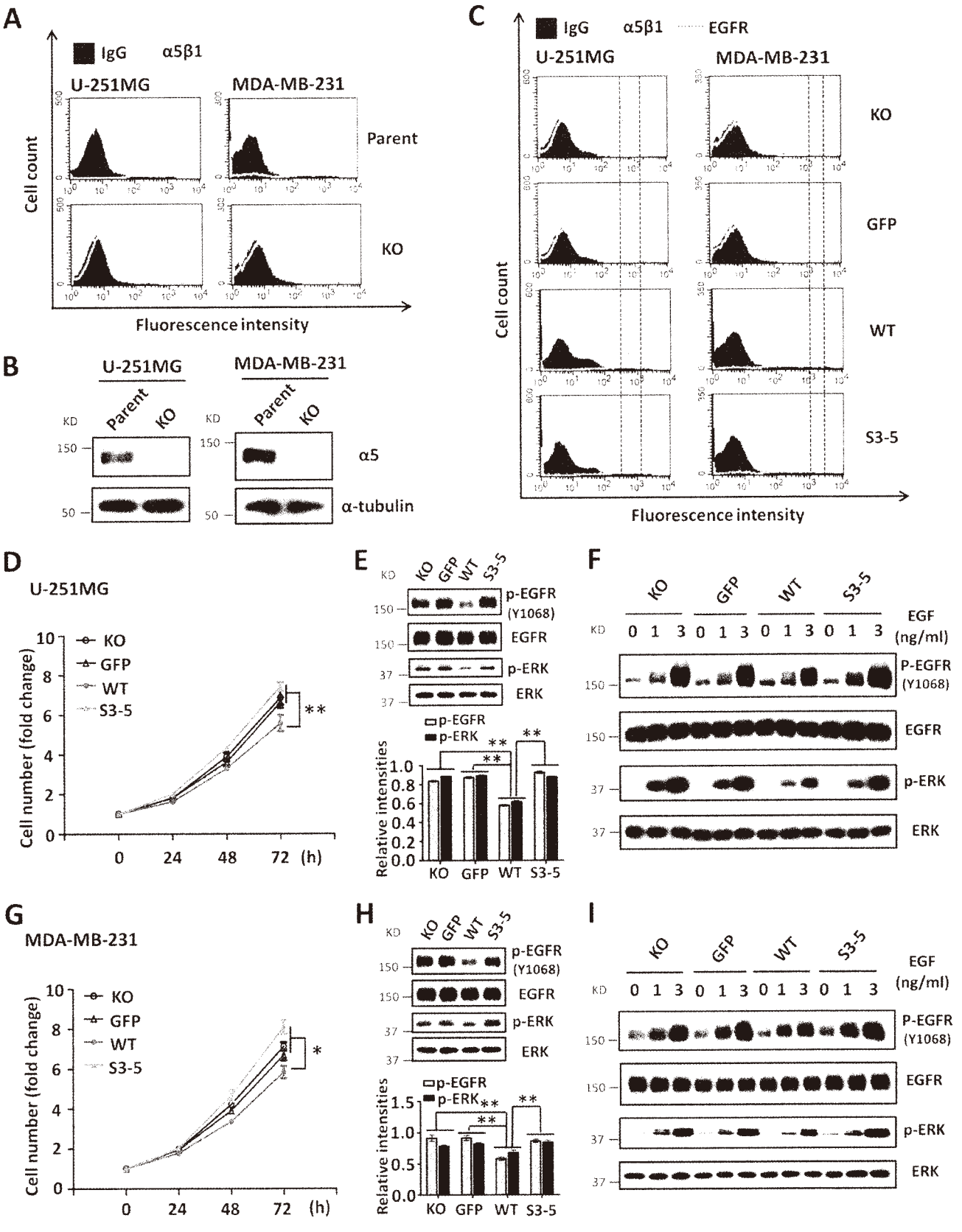

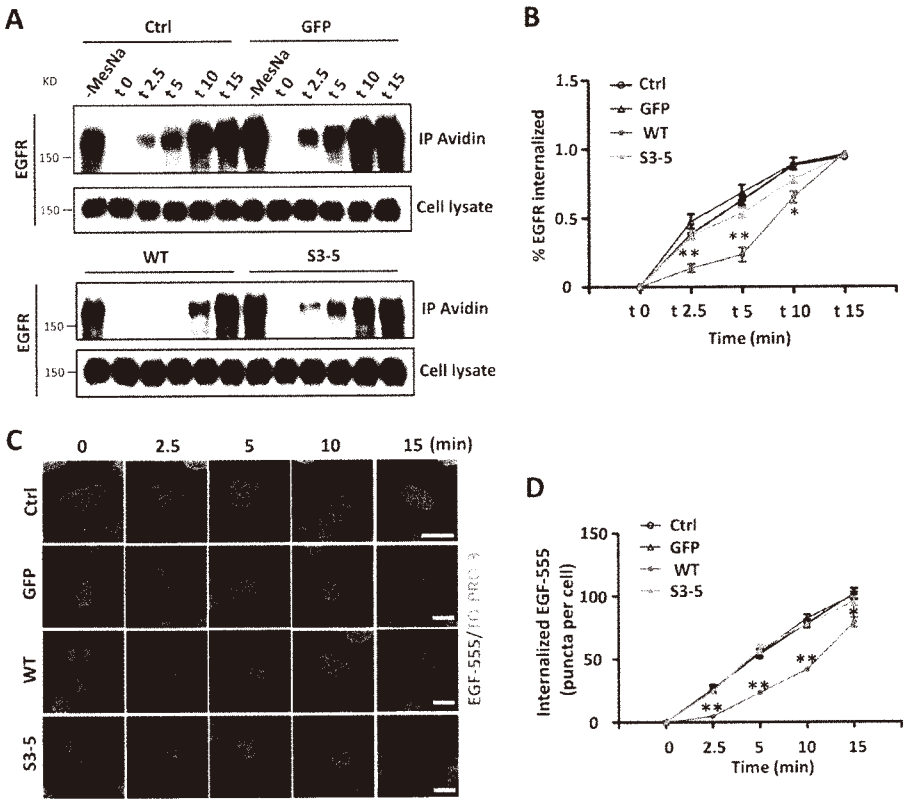

FIGURE 5. **Integrin α5 decreases EGFR internalization upon EGF stimulation in CHO-B2 cells.** *A*, the internalization of EGFR was inhibited in WT cells, compared with the other cells. A biochemical internalization assay of EGFR was performed, as described under "Experimental Procedures." The internalized EGFRs at indicated times were immunoprecipitated by avidin-agarose and then subjected to WB for detection of EGFR. The cell lysates were used as controls to show similar expression levels of EGFR among these cells. *B*, the rates of internalized EGFR were statistically analyzed (*right*; $n = 3$ individual experiments). *C*, EGFR endocytosis was inhibited in the WT but not S3–5 cells upon EGF stimulation. Shown is a representative image for EGFR endocytosis after 50 ng/ml EGF-555 treatment at the indicated times. The image was merged with EGF-555 and TO-PRO-3 staining. *D*, the numbers of internalized EGF-555 puncta/cell in random fields were quantified ($n = 9$, from triplicate experiments). All values are means ± S.E. (*error bars*), Student's *t* test; *, $p < 0.05$; **, $p < 0.01$; ***, $p < 0.001$. *Scale bar*, 10 μm (*C*).

primaquine, a receptor recycling inhibitor, was added to the culture medium to block the recycling of internalized EGFR to the cell membrane. For the EGF-555-based EGFR endocytosis assay, the cells were stimulated by EGF-555 at 10, 30, and 50 ng/ml concentrations, which are approximately equal to 1, 3, and 5 ng/ml EGF, respectively, because the molecular mass of EGF-555 (~63 kDa) is about 10 times higher than that of EGF (6 kDa). We found that the treatment at 50 ng/ml provided clear signals (Fig. 5*B*), and this concentration was also used in other cells (18). A lower concentration, such as 10 or 30 ng/ml, showed no, or only marginal, endocytosis signals (data not shown). Of particular interest, the EGFR internalization after EGF treatment during the first 10-min duration was greatly retarded in the WT cells, compared with that in both the S3–5 and control cells, although the levels of the internalized EGFR were similar at the 15-min chase point. These results clearly indicated that EGFR internalization was delayed by α5 via *N*-glycosylation, which might explain why the EGFR signaling was inhibited in the WT cells.

Integrin α5 Interacts with EGFR and Plays a Critical Role in EGFR Localization in Lipid Rafts—As described above, the *N*-glycosylation of integrin α5 regulated EGFR internalization and activation. Therefore, we wondered how *N*-glycosylation participates in regulation and whether integrin α5 is associated with EGFR through the *N*-glycosylation of α5. Reciprocal immunoprecipitates with anti-GFP-agarose and anti-EGFR antibody showed that integrin α5 indeed interacted with EGFR (Fig. 6*A*), which was consistent with previous reports (44). This interaction was significantly decreased in the S3–5 cells by comparison with WT (Fig. 6*A*). The decreased interactions between S3–5 integrin and EGFR were also observed in HeLa, U-251MG, and MDA-MB-231 cells (Fig. 6*B*). These results suggest that the *N*-glycosylation of integrin α5 is required for the interaction between integrin α5 and EGFR. Next, we wondered

FIGURE 4. **Expression of integrin α5 also inhibits cell growth and EGFR cellular signaling in U-251MG and MDA-MB-231 cells.** The relevant integrin α5-KO cells were established as described under "Experimental Procedures." The established α5-KO U-251MG and MDA-MB-231 cells were assessed by flow cytometry analysis (*A*) and WB (*B*). *C*, the expression levels of integrin α5β1 and EGFR in the relevant integrin α5-rescued U-251MG and MDA-MB-231 cells were assessed by flow cytometry analysis. IgG and α-tubulin were used as controls. *D–I*, these rescued cells with WT, but not S3–5, α5 also exhibited growth retardations, decrease in EGFR signaling, and attenuated EGF responses. These phenomena were similar to those observed in HeLa cells, as shown in Fig. 3. All values are the means ± S.E. (*error bars*), Student's *t* test; *, $p < 0.05$; **, $p < 0.01$ ($n = 3$ individual experiments).

whether this interaction is also modulated by EGF stimulation. As shown in Fig. 6*C*, the interaction was decreased following EGF stimulation both in WT and S3–5 cells. Additionally, the interaction was enhanced when those cells were attached to FN-coated dishes, but it was decreased upon EGF stimulation. These results strongly suggested that the interaction of EGFR and integrin α5 restricts EGFR activation and decreases EGFR responsiveness upon EGF treatment.

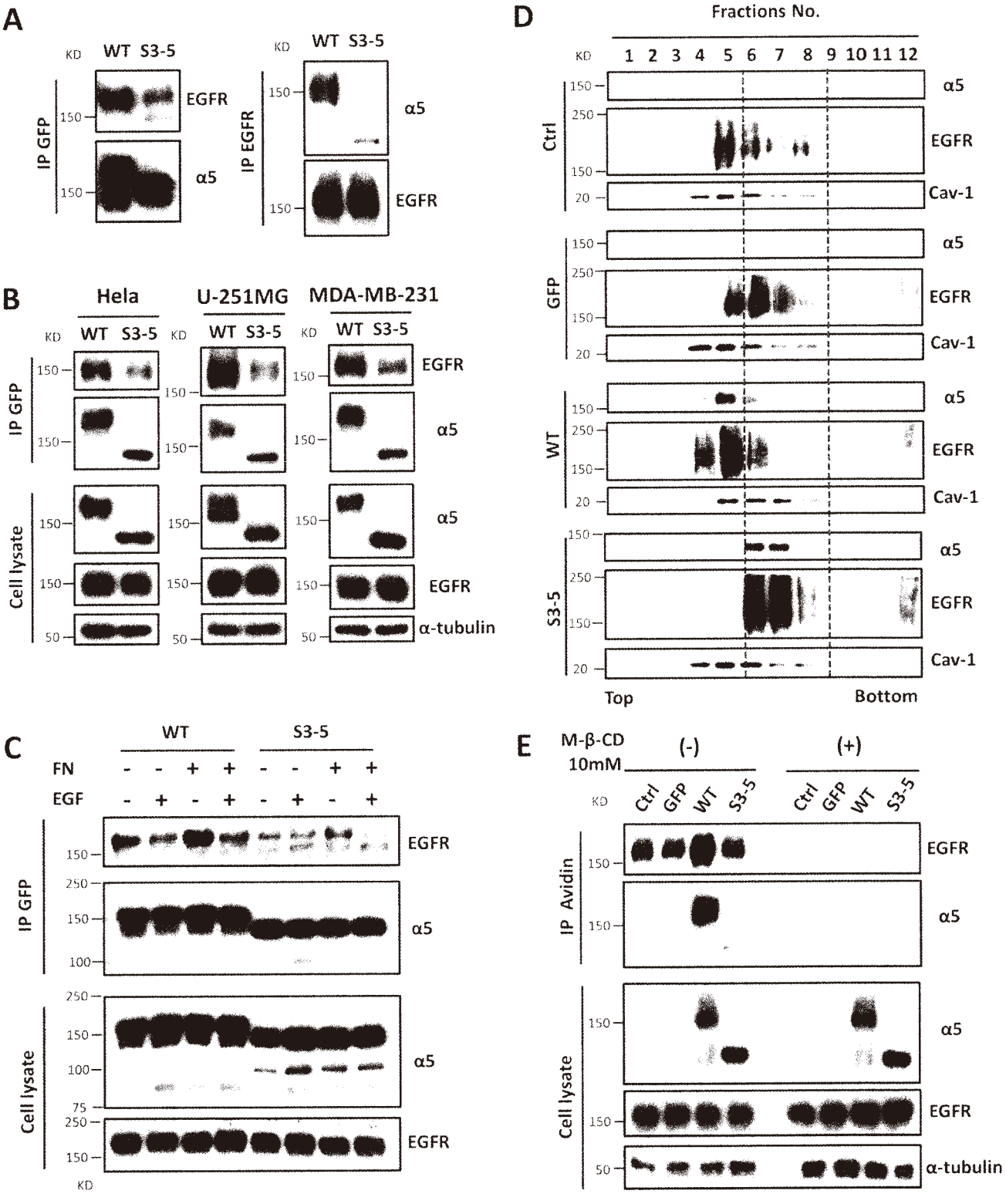

Given the evidence that EGFR localizes in the lipid rafts, which results in its signal transduction (10, 18, 45), we speculated that the *N*-glycans on integrin α5 might affect the distribution of EGFR in the lipid rafts on a cell membrane. When using the OptiPrep density gradient ultracentrifugation method for lipid raft fractions, the EGFR and integrin α5 from each of the cell lines were basically distributed in the fractions ranging from 4 to 8, in which caveolin-1, a marker for lipid raft, could be detected (Fig. 6*D*). Interestingly, the distribution of EGFR and α5 was shifted from the low-density fractions (fractions 4 and 5) in the WT cells to higher density fractions (fractions 6–8) in the S3–5 and control cells, indicating that the *N*-glycans on integrin α5 may be a switch that influences EGFR and integrin α5 localization on the cell membrane.

The glycosylation of integrin α5 could affect its translocation into or out of a glycosphingolipid-enriched microdomain (46); thus, we tested its association with ganglioside GM1 and EGFR in these cells. Co-immunoprecipitation using biotinylated cholera toxin subunit B, which specifically binds ganglioside GM1, showed that the association of EGFR and α5 was much higher in the WT cells than it was in either the S3–5 or the control cells (Fig. 6*E*). These interactions among GM1, EGFR, and α5 were completely disrupted in the presence of methyl-β-cyclodextrin, a cholesterol depletion reagent. Taken together, these results clearly showed that the *N*-glycosylation of α5 plays a crucial role in its localization and complex formation with other receptors on the cell membrane.

N-Glycosylation on the Calf-1,2 Domain of Integrin α5 Is Important for Its Inhibitory Functions—The data provided above led us to seek the *N*-glycosylation site(s) of α5 that was essential for its growth inhibitory effect. To address this, we focused on the *N*-glycosylation of the Calf domain (sites 10–14) (Fig. 7*A*), which happens in the vicinity of the cell membrane. Therefore, we restored *N*-glycosylation on the Calf domain in the S3–5 mutant cells (S3–5,10–14). Both of the *N*-glycosylation-rescued cell lines (Δ10–14 and S3–5,10–14) exhibited similar expression levels of EGFR and α5β1 on the cell surface (Fig. 7*B*) and abilities for cell spreading on FN (Fig. 7*C*), compared with those in the S3–5 cells. Restoration of *N*-glycosylation on the Calf domain in the S3–5 mutant, S3–5,10–14, decreased cell proliferation, which was similar to that in WT cells (Fig. 7*D*). Furthermore, deletion of the *N*-glycosylation sites on the Calf domain (Δ10–14) of α5 abolished its inhibitory effects on cell growth (Fig. 7*D*). These results indicated that *N*-glycosylation on sites 10–14 of α5 plays a crucial role in its inhibitory functions. Consistently, the levels of phospho-EGFR, phospho-ERK, and phospho-AKT in S3–5,10–14 cells were similar to those in the WT but different from those in S3–5 or Δ10–14 cells (Fig. 7*E*). The attenuated response to EGF in WT cells was also observed in S3–5,10–14 but not Δ10–14 cells (Fig. 7*F*). The decreased association with EGFR (Fig. 7*G*) and the aberrant localization of EGFR and α5 in lipid rafts (Fig. 7*H*) in S3–5 cells could be reversed in the S3–5,10–14 cells, which was similar to the situation in the WT cells. Taken together, these results clearly showed that the *N*-glycosylation on the Calf-1,2 domain of integrin α5 plays a crucial role in the regulation of EGFR-mediated cell signaling, which demonstrates a novel regulator for EGFR inhibition.

Discussion

We describe here how cell growth could be down-regulated by integrin α5 and clearly demonstrate how the *N*-glycosylation of α5 is a key factor for α5 regulation of EGFR signaling. Among 14 potential *N*-glycosylation sites of α5, sites on the Calf domain played a crucial role in the inhibitory effect on EGFR-mediated signaling, through regulation of the complex formation between EGFR and α5, localization in lipid rafts, and internalization (Fig. 8). Thus, the present study outlines the novel underlying mechanism responsible for the inhibition of EGFR and also provides new insight into the role of *N*-glycosylation in the regulation of cellular signaling to maintain cell properties via a cross-talk manner among glycoproteins on the cell surface.

Integrin α5 is thought to play crucial roles in many biological functions, but there are several controversial reports concerning the functions of integrin α5 in cancer. Low expression levels of α5 have been linked to the growth of tumors in gastric, colorectal, colon, and breast cancers (47), whereas the overexpression of integrin α5 inhibited cell growth in several cell lines, such as 4T1, HT29, and CHO (48–52). Furthermore, integrin α5 has been used to down-regulate the HER2 pathway in Caco-2 and HT-29 cells (34). However, these findings are contradicted by other studies showing that integrin α5 functions as an oncogene and was associated with several instances of tumorigenesis (53, 54) as well as promoting EGFR activation in some cancer cells (35, 44, 55). The reasons for the contradictions in the functioning of α5 in cancers remain unclear. Of course, it could be spec-

FIGURE 6. **Integrin α5 associates with EGFR and regulates EGFR localization in lipid rafts.** *A*, the association of integrin α5 with EGFR was decreased in S3–5 cells compared with the WT cells. The indicated CHO-B2 cell extracts were immunoprecipitated (*IP*) with anti-GFP agarose (*left panels*) or anti-EGFR antibody (*right panels*), and then subjected to WB, reciprocally followed by anti-EGFR and integrin α5 antibodies for detection. *B*, the interaction between integrin α5 and EGFR was also decreased in the HeLa, U-251MG, and MDA-MB-231 S3–5 mutant cells. The indicated cell extracts were immunoprecipitated as described in *A*. Crude cell extracts were also subjected to WB as "input" using the indicated antibodies (*bottom panels*). *C*, the interaction between integrin α5 and EGFR was decreased upon EGF stimulation. The indicated CHO-B2 cells were cultured on dishes coated with or without 10 μg/ml FN for 24 h and then stimulated with or without EGF at 0.1 ng/ml for 5 min. The resultant cell lysates (as an input; *bottom panels*) were directly blotted with anti-EGFR and integrin α5 antibodies or immunoprecipitated with anti-GFP agarose (*top panels*) and then blotted with anti-EGFR antibody. *D*, comparison of localization of EGFR and integrin α5 in the lower density lipid rafts in the indicated CHO-B2. Distributions of integrin α5 and EGFR from the indicated cell lysates in the lipid raft fractions were prepared as described under "Experimental Procedures." Fraction 1 is the top fraction of the gradient, and fraction 12 is the bottom fraction. The localization shifts of the integrin α5 and EGFR are highlighted with *gray dotted lines*. Caveolin-1 (*Cav-1*) was used to act as a marker for lipid rafts. *E*, the complex of EGFR and integrin α5 is mediated by GM1. The indicated CHO-B2 cells were pretreated with or without methyl-β-cyclodextrin (*M-β-CD*) (10 mM) for 1 h. After the treatment, cell lysates were incubated with biotinylated cholera toxin B subunit (*CTB*) for another 1 h and then immunoprecipitated with avidin-agarose beads. The immunoprecipitates were subjected to WB detected with anti-EGFR and integrin α5 antibodies (*top panels*). The whole cell lysates were also subjected to WB with the indicated antibodies (*bottom panel*; as an input).

ulated that α5 might differentially affect cellular signaling in different cell types or may exhibit intrinsic limitations in different cell models. However, based on our observation, integrin α5 inhibits cell proliferation through a negative regulation of EGFR via *N*-glycosylation and shows tumor suppressor-like activity. Coincidently, similar to integrin α5,

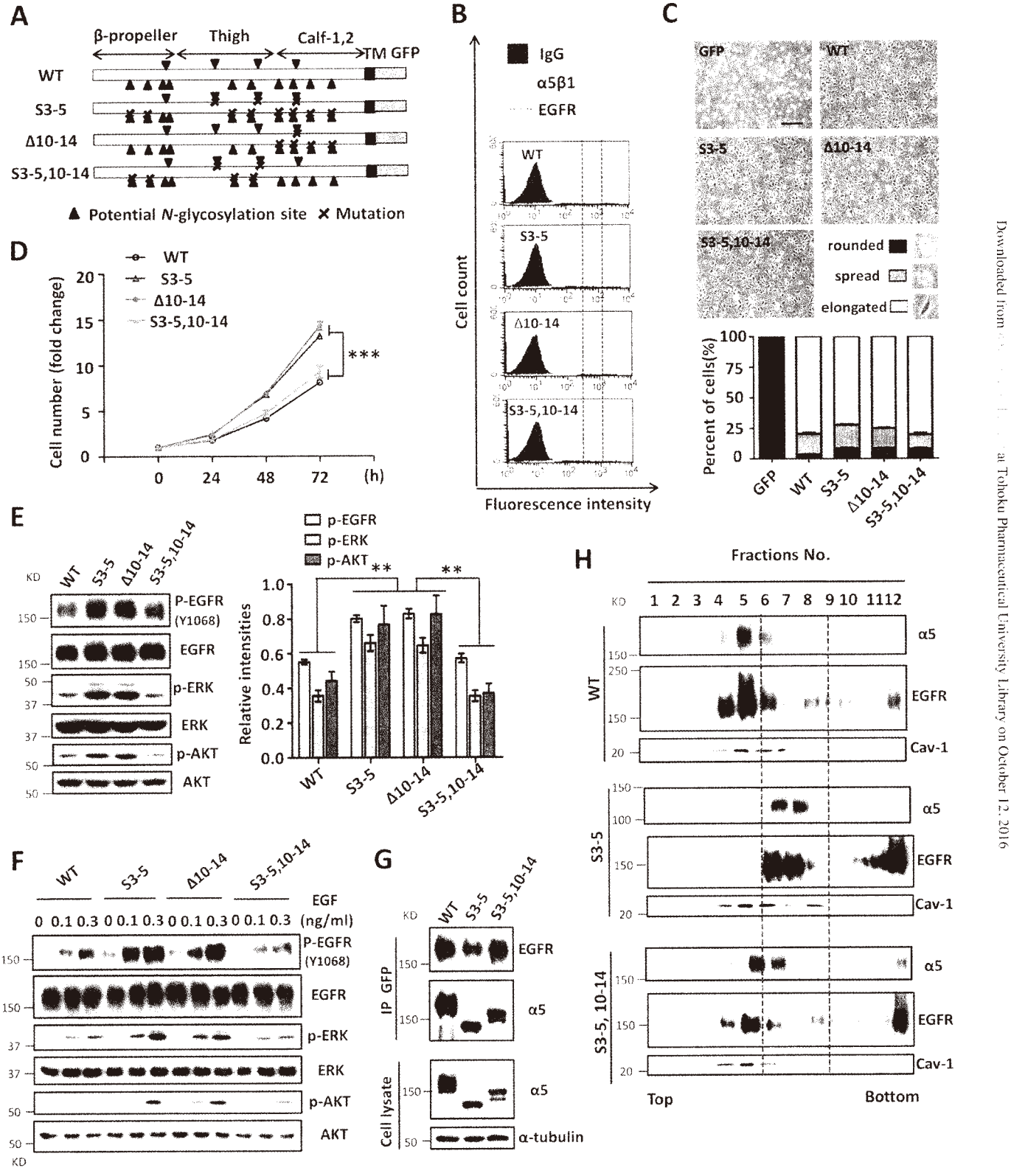

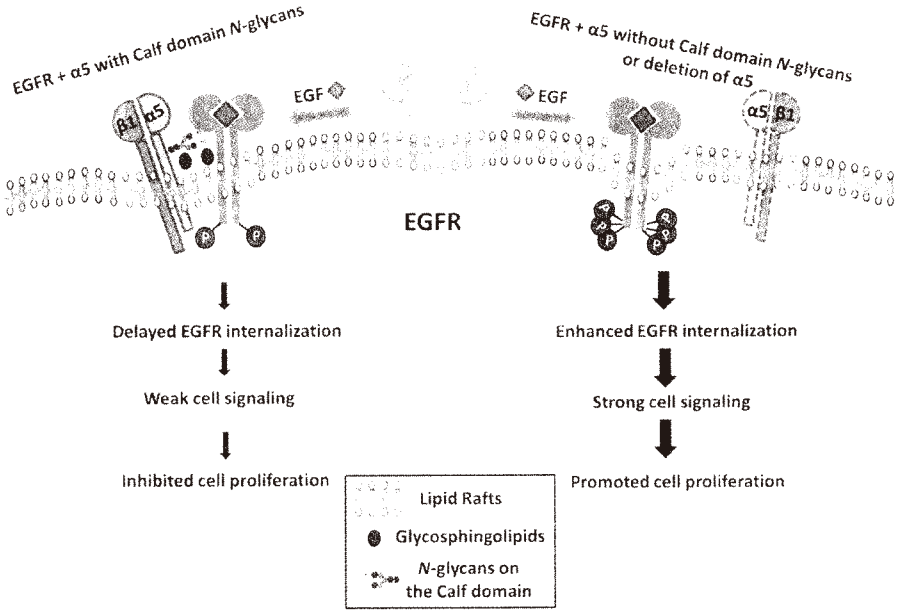

FIGURE 8. **Proposed molecular mechanism for the regulation of EGFR cellular signaling by the *N*-glycosylations of integrin α5.** In the integrin α5 with *N*-glycosylation on its Calf domain cells (*left*), integrin α5β1 forms a complex with EGFR as well as glycosphingolipids in the lipid raft, which may restrict the EGFR internalization and the related signaling upon EGF stimulation, resulting in an inhibition of cell proliferation. However, in the integrin α5-deficient or mutant (deletion of *N*-glycosylation on its Calf domain) cells (*right*), the majority of EGFR is located in lipid rafts without integrin α5, leading to a rapid activation and internalization of EGFR upon EGF stimulation. The *thick arrow lines* indicate a rapid EGF response and strong signal transduction, whereas the *thinner arrow lines* indicate that these events are inhibited.

integrin α1 also negatively regulated EGFR (26). We believe that the different effects of α5 on cell growth can be ascribed to distinct *N*-glycosylations, which may be altered in different cells and tissues and cancers. Further investigation is obviously needed to support this hypothesis.

The *N*-glycosylation of integrin α5 plays crucial roles in several biological functions, including cell adhesion and cell migration. However, little is known about the functioning of individual *N*-glycosylation. We previously underscored the importance of *N*-glycans on *N*-glycosylation potential sites 3–5 of α5 in its assembly of β1 (33). Although the interaction-mediated cross-talk between α5 and EGFR was described previously (41, 44), the precise underlying mechanisms of how α5 regulates EGFR signaling and the molecular basis for this interaction remain unclear. In the present study, we find that the *N*-glycosylation on the Calf domain is essential for integrin α5-EGFR complex formation and is a key regulator for EGFR-mediated signaling. Most studies have focused on the cytoplasmic domain of integrins for the regulation of cell functions. For example, Caswell *et al.* (56) reported that the Rab-coupling protein could mediate the complex formation between integrin α5 and EGFR through their cytoplasmic domains to regulate cell migration; Mattila *et al.* (26) described how integrin α1 negatively regulates EGFR-mediated cellular signaling through the activation of a protein tyrosine phosphatase in the cytosol. These theories are plausible because any output (downstream) must happen inside a cell. However, these explanations are insufficient to clarify the molecular mechanisms in detail. In the present study, we highlight an input (upstream), post-translational modification of the extracellular domains of α5 and show its importance in complex formation and cellular signaling. Similar to integrin α5, we previously showed how the *N*-glycosylation on integrin β4 regulates its association with EGFR

FIGURE 7. ***N*-Glycosylation on the Calf-1,2 domain of integrin α5 mediates its growth-inhibitory function.** *A*, schematic diagram of potential *N*-glycosylation mutational integrin α5 subunit (WT, S3–5, Δ10–14, and S3–5,10–14). *B*, the integrin α5 mutant cells express equally α5β1 and EGFR levels on cell surface, compared with the WT cells. The stable rescued CHO-B2 cell lines (10–14 and S3–5,10–14) were also established as described under "Experimental Procedures." The expression levels of both α5β1 and EGFR on cell surface were analyzed by flow cytometry analysis. The IgG was used as a control. *C*, the α5 mutant cells exhibited comparable abilities for cell spreading as WT ones. Cells were detached and then replanted on the FN-coated dishes. After incubation for 20 min, cells were fixed, and the images were taken. The percentages of the rounded, spread, and elongated cells were statistically analyzed (*bottom panel*, $n = 9$, from triplicate experiments). *D*, the S3–5,10–14, but not 10–14 cells exhibit a similar inhibitory ability for cell growth, compared with the WT cells. The cell growth abilities of WT, S3–5,10–14, and S3–5, 10–14 were analyzed as described in the legend to Fig. 1*C* ($n = 3$ individual experiments). *E*, the EGFR-related cellular signaling was revived in the S3–5,10–14 cells. Cell lysates from the indicated cells were subjected to WB with indicated antibodies (*left*). The relative ratios were statistically analyzed (*right*, $n = 3$ individual experiments). *F*, the response to EGF was decreased in S3–5,10–14 cells. Cells were serum-starved for 24 h, followed by a treatment with the indicated concentrations of EGF for 5 min, and then the resultant cell extracts were subjected to WB analysis with indicated antibodies. *G*, the interaction between integrin α5 and EGFR was also rescued in the S3–5,10–14 cells. The indicated cell extracts were immunoprecipitated with anti-GFP agarose, followed by anti-EGFR and α5 antibodies for WB (*top panels*). The whole cell extracts were also subjected to WB using the indicated antibodies (*bottom panels*; as an input). *H*, the localizations of EGFR and integrin α5 in the lower density lipid raft were also revived in the S3–5,10–14 cells. Distributions of integrin α5 and EGFR in lipid raft fractions were detected, as described in the legend to Fig. 6*D*. The localization shifts of integrin α5 and EGFR are highlighted with *gray dotted lines*. The caveolin-1 (*Cav-1*) was used to act as a positive control for lipid rafts. All values are means ± S.E. (*error bars*), Student's *t* test; **, $p < 0.01$; ***, $p < 0.001$. *Scale bar*, 120 μm.

and EGFR signaling (12). Recently, Paszek *et al.* (22) demonstrated that a bulky glycocalyx in ECM might facilitate integrin clustering and then promote a tumor phenotype by increasing integrin adhesion and signaling. Those results further support the notion that glycosylation plays an important role in protein-protein interaction (57).

It is worth noting that the *N*-glycans on the Calf domain of α5 represent a key switch for the regulation of EGFR-mediated signaling. Previous study of the crystal structure of the ectodomain of integrin α5β1 showed that the *N*-glycans on α5, particularly those surrounding the RGD-binding pocket, play an important role in its binding to FN (58). Thus, based on molecular modeling, we speculate that the *N*-glycans of a Calf domain may not participate in the cell adhesion process, but, instead, a location near the cell membrane suggests that they may be involved in the association with other molecules on the cell surface. In fact, restoration of all *N*-glycosylation sites on the Calf domain (sites 10–14) in an S3–5 mutant completely rescued the complex formation and the capacity for inhibitory effects of EGFR-mediated signaling, which were observed in wild-type α5-expressing cells. In consideration of the fact that the specific conformation of integrin α5β1 is essential for its mediated functions (59–61), future studies will require an extensive analysis of the structures of these *N*-glycosylation mutants as well as that of specific *N*-glycans on individual sites.

It is well known that an appropriate lipid raft formation is required for normal EGFR signaling transduction (62, 63). We demonstrate here that *N*-glycosylation on integrin α5 serves as a regulator for its association with EGFR and GM1, one of the gangliosides in lipid rafts, which regulates the EGF response. In fact, other gangliosides, such as GM3 and GD3, can also interact with the *N*-glycans on EGFR and regulate EGFR signaling, indicating the importance of the carbohydrate-to-carbohydrate interaction in cellular signaling (12, 18, 20, 62, 63). These results lead us to speculate that the *N*-glycans on the Calf domain may be the most suitable for those interactions among the α5, EGFR, and gangliosides at a distance. Of course, more evidence is needed to prove this hypothesis. Although the underlying mechanism for the complex formation that down-regulates EGFR internalization upon EGF stimulation remains unclear, the observation could partly explain why the cell growth was inhibited in the wild-type α5 cells because enhancement of EGFR internalization and recycling plays an important role in signal transduction for persistent proliferation and tumor carcinogenesis in cells (42, 64).

Given the existence of the mutations of several integrins and EGFR during pathological processes (65–67), particularly the *N*-glycosylation mutation of integrin α3 (68), and the apparent irregular expression of integrin α5 in multiple tumors (47, 53, 54), it is tempting to speculate that the *N*-glycosylation of integrin α5 may undergo mutations during tumorigenesis. Integrin α5 modified by different *N*-glycosylations exhibited different effects on cell proliferation and tumorigenesis, suggesting a possibility that the remodeling of *N*-glycosylation on this integrin may serve as a novel approach to tumor treatment. Furthermore, the present study clearly demonstrates how specific *N*-glycosylation on integrin α5 functions as a negative regulator for EGFR, which may provide a new perspective on the cross-talk between growth factor receptors and integrins.

Author Contributions—Q. H. performed all of the experiments with the help of T. I., T. F., S. H., and S. I. Q. H. and T. I. constructed the virus expression and the α5-knockout vectors. Q. H., T. I., and S. I. performed the cell-sorting experiments. Q. H., T. F., and S. H. contributed the generation of xenograft tumors. J. G. designed the experiment. Q. H. and J. G. analyzed the data, prepared the figures, and wrote the manuscript. All authors discussed the results and commented on the manuscript.

Acknowledgments—We thank Dr. Motoko Takahashi (Sapporo Medical University), Prof. Rudolf Juliano (School of Medicine, University of North Carolina, Chapel Hill, NC), and Prof. Jun Nakayama (Shinshu University Graduate School of Medicine) for kindly providing the cDNA of human EGFR, α5 subunit-deficient CHO-K1 cell line (CHO-B2), and U-251MG cell line, respectively.

References

1. Bogdan, S., and Klämbt, C. (2001) Epidermal growth factor receptor signaling. *Curr. Biol.* **11,** R292–R295
2. Citri, A., and Yarden, Y. (2006) EGF-ERBB signalling: towards the systems level. *Nat. Rev. Mol. Cell Biol.* **7,** 505–516
3. Hynes, N. E., and Lane, H. A. (2005) ERBB receptors and cancer: the complexity of targeted inhibitors. *Nat. Rev. Cancer* **5,** 341–354
4. Izumi, Y., Xu, L., di Tomaso, E., Fukumura, D., and Jain, R. K. (2002) Tumour biology: herceptin acts as an anti-angiogenic cocktail. *Nature* **416,** 279–280
5. Salomon, D. S., Brandt, R., Ciardiello, F., and Normanno, N. (1995) Epidermal growth factor-related peptides and their receptors in human malignancies. *Crit. Rev. Oncol. Hematol.* **19,** 183–232
6. Grandis, J. R., and Sok, J. C. (2004) Signaling through the epidermal growth factor receptor during the development of malignancy. *Pharmacol. Ther.* **102,** 37–46
7. Hampton, K. K., and Craven, R. J. (2014) Pathways driving the endocytosis of mutant and wild-type EGFR in cancer. *Oncoscience* **1,** 504–512
8. Mlcochova, J., Faltejskova, P., Nemecek, R., Svoboda, M., and Slaby, O. (2013) MicroRNAs targeting EGFR signalling pathway in colorectal cancer. *J. Cancer Res. Clin. Oncol.* **139,** 1615–1624
9. Sebastian, S., Settleman, J., Reshkin, S. J., Azzariti, A., Bellizzi, A., and Paradiso, A. (2006) The complexity of targeting EGFR signalling in cancer: from expression to turnover. *Biochim. Biophys. Acta* **1766,** 120–139
10. Coskun, Ü., Grzybek, M., Drechsel, D., and Simons, K. (2011) Regulation of human EGF receptor by lipids. *Proc. Natl. Acad. Sci. U.S.A.* **108,** 9044–9048
11. Guéguinou, M., Gambade, A., Félix, R., Chantôme, A., Fourbon, Y., Bougnoux, P., Weber, G., Potier-Cartereau, M., and Vandier, C. (2015) Lipid rafts, KCa/ClCa/Ca channel complexes and EGFR signaling: novel targets to reduce tumor development by lipids? *Biochim. Biophys. Acta* **1848,** 2603–2620
12. Kariya, Y., and Gu, J. (2011) *N*-Glycosylation of β4 integrin controls the adhesion and motility of keratinocytes. *PLoS One* **6,** e27084
13. Lajoie, P., Partridge, E. A., Guay, G., Goetz, J. G., Pawling, J., Lagana, A., Joshi, B., Dennis, J. W., and Nabi, I. R. (2007) Plasma membrane domain organization regulates EGFR signaling in tumor cells. *J. Cell Biol.* **179,** 341–356
14. Brown, D. A., and London, E. (2000) Structure and function of sphingolipid- and cholesterol-rich membrane rafts. *J. Biol. Chem.* **275,** 17221–17224
15. Simons, K., and Toomre, D. (2000) Lipid rafts and signal transduction. *Nat. Rev. Mol. Cell Biol.* **1,** 31–39

16. Lingwood, D., and Simons, K. (2010) Lipid rafts as a membrane-organizing principle. *Science* **327,** 46–50
17. Munro, S. (2003) Lipid rafts: elusive or illusive? *Cell* **115,** 377–388
18. Wang, J., and Yu, R. K. (2013) Interaction of ganglioside GD3 with an EGF receptor sustains the self-renewal ability of mouse neural stem cells *in vitro*. *Proc. Natl. Acad. Sci. U.S.A.* **110,** 19137–19142
19. Wang, X. Q., Sun, P., and Paller, A. S. (2005) Gangliosides inhibit urokinase-type plasminogen activator (uPA)-dependent squamous carcinoma cell migration by preventing uPA receptor/$\alpha\beta$ integrin/epidermal growth factor receptor interactions. *J. Invest. Dermatol.* **124,** 839–848
20. Yoon, S. J., Nakayama, K., Hikita, T., Handa, K., and Hakomori, S. I. (2006) Epidermal growth factor receptor tyrosine kinase is modulated by GM3 interaction with N-linked GlcNAc termini of the receptor. *Proc. Natl. Acad. Sci. U.S.A.* **103,** 18987–18991
21. Midgley, A. C., Rogers, M., Hallett, M. B., Clayton, A., Bowen, T., Phillips, A. O., and Steadman, R. (2013) Transforming growth factor-β1 (TGF-β1)-stimulated fibroblast to myofibroblast differentiation is mediated by hyaluronan (HA)-facilitated epidermal growth factor receptor (EGFR) and CD44 co-localization in lipid rafts. *J. Biol. Chem.* **288,** 14824–14838
22. Paszek, M. J., DuFort, C. C., Rossier, O., Bainer, R., Mouw, J. K., Godula, K., Hudak, J. E., Lakins, J. N., Wijekoon, A. C., Cassereau, L., Rubashkin, M. G., Magbanua, M. J., Thorn, K. S., Davidson, M. W., Rugo, H. S., Park, J. W., Hammer, D. A., Giannone, G., Bertozzi, C. R., and Weaver, V. M. (2014) The cancer glycocalyx mechanically primes integrin-mediated growth and survival. *Nature* **511,** 319–325
23. Wang, X. Q., Sun, P., and Paller, A. S. (2003) Ganglioside GM3 blocks the activation of epidermal growth factor receptor induced by integrin at specific tyrosine sites. *J. Biol. Chem.* **278,** 48770–48778
24. Yamada, K. M., and Even-Ram, S. (2002) Integrin regulation of growth factor receptors. *Nat. Cell Biol.* **4,** E75–E76
25. Larsen, M., Artym, V. V., Green, J. A., and Yamada, K. M. (2006) The matrix reorganized: extracellular matrix remodeling and integrin signaling. *Curr. Opin. Cell Biol.* **18,** 463–471
26. Mattila, E., Pellinen, T., Nevo, J., Vuoriluoto, K., Arjonen, A., and Ivaska, J. (2005) Negative regulation of EGFR signalling through integrin-α1β1-mediated activation of protein tyrosine phosphatase TCPTP. *Nat. Cell Biol.* **7,** 78–85
27. Miranti, C. K., and Brugge, J. S. (2002) Sensing the environment: a historical perspective on integrin signal transduction. *Nat. Cell Biol.* **4,** E83–E90
28. Schwartz, M. A., and Ginsberg, M. H. (2002) Networks and crosstalk: integrin signalling spreads. *Nat. Cell Biol.* **4,** E65–E68
29. Seguin, L., Kato, S., Franovic, A., Camargo, M. F., Lesperance, J., Elliott, K. C., Yebra, M., Mielgo, A., Lowy, A. M., Husain, H., Cascone, T., Diao, L., Wang, J., Wistuba, I. I., Heymach, J. V., Lippman, S. M., Desgrosellier, J. S., Anand, S., Weis, S. M., and Cheresh, D. A. (2014) An integrin β_3-KRAS-RalB complex drives tumour stemness and resistance to EGFR inhibition. *Nat. Cell Biol.* **16,** 457–468
30. Streuli, C. H., and Akhtar, N. (2009) Signal co-operation between integrins and other receptor systems. *Biochem. J.* **418,** 491–506
31. Liu, S., Calderwood, D. A., and Ginsberg, M. H. (2000) Integrin cytoplasmic domain-binding proteins. *J. Cell Sci.* **113,** 3563–3571
32. Isaji, T., Sato, Y., Fukuda, T., and Gu, J. (2009) *N*-Glycosylation of the I-like domain of β1 integrin is essential for beta1 integrin expression and biological function: identification of the minimal *N*-glycosylation requirement for $\alpha5\beta1$. *J. Biol. Chem.* **284,** 12207–12216
33. Isaji, T., Sato, Y., Zhao, Y., Miyoshi, E., Wada, Y., Taniguchi, N., and Gu, J. (2006) *N*-Glycosylation of the β-propeller domain of the integrin $\alpha5$ subunit is essential for $\alpha5\beta1$ heterodimerization, expression on the cell surface, and its biological function. *J. Biol. Chem.* **281,** 33258–33267
34. Kuwada, S. K., Kuang, J., and Li, X. (2005) Integrin $\alpha5/\beta1$ expression mediates HER-2 down-regulation in colon cancer cells. *J. Biol. Chem.* **280,** 19027–19035
35. Kuwada, S. K., and Li, X. (2000) Integrin $\alpha5/\beta1$ mediates fibronectin-dependent epithelial cell proliferation through epidermal growth factor receptor activation. *Mol. Biol. Cell* **11,** 2485–2496
36. Schreiner, C. L., Bauer, J. S., Danilov, Y. N., Hussein, S., Sczekan, M. M., and Juliano, R. L. (1989) Isolation and characterization of Chinese hamster ovary cell variants deficient in the expression of fibronectin receptor. *J. Cell Biol.* **109,** 3157–3167
37. Ran, F. A., Hsu, P. D., Wright, J., Agarwala, V., Scott, D. A., and Zhang, F. (2013) Genome engineering using the CRISPR-Cas9 system. *Nat. Protoc.* **8,** 2281–2308
38. Shalem, O., Sanjana, N. E., Hartenian, E., Shi, X., Scott, D. A., Mikkelsen, T. S., Heckl, D., Ebert, B. L., Root, D. E., Doench, J. G., and Zhang, F. (2014) Genome-scale CRISPR-Cas9 knockout screening in human cells. *Science* **343,** 84–87
39. Isaji, T., Im, S., Gu, W., Wang, Y., Hang, Q., Lu, J., Fukuda, T., Hashii, N., Takakura, D., Kawasaki, N., Miyoshi, H., and Gu, J. (2014) An oncogenic protein Golgi phosphoprotein 3 up-regulates cell migration via sialylation. *J. Biol. Chem.* **289,** 20694–20705
40. Mettouchi, A., Klein, S., Guo, W., Lopez-Lago, M., Lemichez, E., Westwick, J. K., and Giancotti, F. G. (2001) Integrin-specific activation of Rac controls progression through the G_1 phase of the cell cycle. *Mol. Cell* **8,** 115–127
41. Alam, N., Goel, H. L., Zarif, M. J., Butterfield, J. E., Perkins, H. M., Sansoucy, B. G., Sawyer, T. K., and Languino, L. R. (2007) The integrin-growth factor receptor duet. *J. Cell. Physiol.* **213,** 649–653
42. Gao, M., Patel, R., Ahmad, I., Fleming, J., Edwards, J., McCracken, S., Sahadevan, K., Seywright, M., Norman, J., Sansom, O., and Leung, H. Y. (2012) SPRY2 loss enhances ErbB trafficking and PI3K/AKT signalling to drive human and mouse prostate carcinogenesis. *EMBO Mol. Med.* **4,** 776–790
43. del Pozo, M. A., Alderson, N. B., Kiosses, W. B., Chiang, H. H., Anderson, R. G., and Schwartz, M. A. (2004) Integrins regulate Rac targeting by internalization of membrane domains. *Science* **303,** 839–842
44. Morozevich, G. E., Kozlova, N. I., Ushakova, N. A., Preobrazhenskaya, M. E., and Berman, A. E. (2012) Integrin $\alpha5\beta1$ simultaneously controls EGFR-dependent proliferation and Akt-dependent pro-survival signaling in epidermoid carcinoma cells. *Aging* **4,** 368–374
45. Lambert, S., Ameels, H., Gniadecki, R., Hérin, M., and Poumay, Y. (2008) Internalization of EGF receptor following lipid rafts disruption in keratinocytes is delayed and dependent on p38 MAPK activation. *J. Cell. Physiol.* **217,** 834–845
46. Kazui, A., Ono, M., Handa, K., and Hakomori, S. (2000) Glycosylation affects translocation of integrin, Src, and caveolin into or out of GEM. *Biochem. Biophys. Res. Commun.* **273,** 159–163
47. Samandari, E., Visarius, T., Zingg, J. M., and Azzi, A. (2006) The effect of γ-tocopherol on proliferation, integrin expression, adhesion, and migration of human glioma cells. *Biochem. Biophys. Res. Commun.* **342,** 1329–1333
48. Giancotti, F. G., and Ruoslahti, E. (1990) Elevated levels of the $\alpha5\beta1$ fibronectin receptor suppress the transformed phenotype of Chinese hamster ovary cells. *Cell* **60,** 849–859
49. Varner, J. A., Emerson, D. A., and Juliano, R. L. (1995) Integrin $\alpha5\beta1$ expression negatively regulates cell growth: reversal by attachment to fibronectin. *Mol. Biol. Cell* **6,** 725–740
50. Schirner, M., Herzberg, F., Schmidt, R., Streit, M., Schöning, M., Hummel, M., Kaufmann, C., Thiel, E., and Kreuser, E. D. (1998) Integrin $\alpha5\beta1$: a potent inhibitor of experimental lung metastasis. *Clin. Exp. Metastasis* **16,** 427–435
51. Zhou, G. F., Ye, F., Cao, L. H., and Zha, X. L. (2000) Over expression of integrin $\alpha5\beta1$ in human hepatocellular carcinoma cell line suppresses cell proliferation *in vitro* and tumorigenicity in nude mice. *Mol. Cell Biochem.* **207,** 49–55
52. Wang, Y., Shenouda, S., Baranwal, S., Rathinam, R., Jain, P., Bao, L., Hazari, S., Dash, S., and Alahari, S. K. (2011) Integrin subunits $\alpha5$ and $\alpha6$ regulate cell cycle by modulating the chk1 and Rb/E2F pathways to affect breast cancer metastasis. *Mol. Cancer* **10,** 84
53. Adachi, M., Taki, T., Higashiyama, M., Kohno, N., Inufusa, H., and Miyake, M. (2000) Significance of integrin $\alpha5$ gene expression as a prognostic factor in node-negative non-small cell lung cancer. *Clin. Cancer Res.* **6,** 96–101
54. Qian, F., Zhang, Z. C., Wu, X. F., Li, Y. P., and Xu, Q. (2005) Interaction between integrin α_5 and fibronectin is required for metastasis of B16F10 melanoma cells. *Biochem. Biophys. Res. Commun.* **333,** 1269–1275
55. Liu, D., Aguirre Ghiso, J., Estrada, Y., and Ossowski, L. (2002) EGFR is a

transducer of the urokinase receptor initiated signal that is required for *in vivo* growth of a human carcinoma. *Cancer Cell* **1,** 445–457
56. Caswell, P. T., Chan, M., Lindsay, A. J., McCaffrey, M. W., Boettiger, D., and Norman, J. C. (2008) Rab-coupling protein coordinates recycling of $\alpha5\beta1$ integrin and EGFR1 to promote cell migration in 3D microenvironments. *J. Cell Biol.* **183,** 143–155
57. Ono, M., Handa, K., Withers, D. A., and Hakomori, S. (2000) Glycosylation effect on membrane domain (GEM) involved in cell adhesion and motility: a preliminary note on functional $\alpha3$, $\alpha5$-CD82 glycosylation complex in ldlD 14 cells. *Biochem. Biophys. Res. Commun.* **279,** 744–750
58. Nagae, M., Re, S., Mihara, E., Nogi, T., Sugita, Y., and Takagi, J. (2012) Crystal structure of $\alpha5\beta1$ integrin ectodomain: atomic details of the fibronectin receptor. *J. Cell Biol.* **197,** 131–140
59. Mould, A. P., and Humphries, M. J. (2004) Regulation of integrin function through conformational complexity: not simply a knee-jerk reaction? *Curr. Opin. Cell Biol.* **16,** 544–551
60. Clark, K., Pankov, R., Travis, M. A., Askari, J. A., Mould, A. P., Craig, S. E., Newham, P., Yamada, K. M., and Humphries, M. J. (2005) A specific $\alpha5\beta1$-integrin conformation promotes directional integrin translocation and fibronectin matrix formation. *J. Cell Sci.* **118,** 291–300
61. Campbell, I. D., and Humphries, M. J. (2011) Integrin structure, activation, and interactions. *Cold Spring Harb. Perspect. Biol.* 10.1101/cshperspect.a004994
62. Miljan, E. A., Meuillet, E. J., Mania-Farnell, B., George, D., Yamamoto, H., Simon, H. G., and Bremer, E. G. (2002) Interaction of the extracellular domain of the epidermal growth factor receptor with gangliosides. *J. Biol. Chem.* **277,** 10108–10113
63. Handa, K., and Hakomori, S. I. (2012) Carbohydrate to carbohydrate interaction in development process and cancer progression. *Glycoconj. J.* **29,** 627–637
64. Tomas, A., Futter, C. E., and Eden, E. R. (2014) EGF receptor trafficking: consequences for signaling and cancer. *Trends Cell Biol.* **24,** 26–34
65. Camidge, D. R., Pao, W., and Sequist, L. V. (2014) Acquired resistance to TKIs in solid tumours: learning from lung cancer. *Nat. Rev. Clin. Oncol.* **11,** 473–481
66. Kawahara, E., Saito, A., Kobayashi, J., Maenaka, S., Minamoto, T., Imai, M. A., and Oda, Y. (2005) Adhesiveness of $\beta5$ integrin variant lacking FNK767–769 is similar to that of the prototype containing FNKFNK764–769. *Cell Biol. Int.* **29,** 521–528
67. Yoo, N. J., Soung, Y. H., Lee, S. H., Jeong, E. G., and Lee, S. H. (2007) Mutational analysis of proapoptotic integrin $\beta3$ cytoplasmic domain in common human cancers. *Tumori* **93,** 281–283
68. Nicolaou, N., Margadant, C., Kevelam, S. H., Lilien, M. R., Oosterveld, M. J., Kreft, M., van Eerde, A. M., Pfundt, R., Terhal, P. A., van der Zwaag, B., Nikkels, P. G., Sachs, N., Goldschmeding, R., Knoers, N. V., Renkema, K. Y., and Sonnenberg, A. (2012) Gain of glycosylation in integrin $\alpha3$ causes lung disease and nephrotic syndrome. *J. Clin. Invest.* **122,** 4375–4387

Integrin α5 Suppresses the Phosphorylation of Epidermal Growth Factor Receptor and Its Cellular Signaling of Cell Proliferation via *N*-Glycosylation

Qinglei Hang, Tomoya Isaji, Sicong Hou, Sanghun Im, Tomohiko Fukuda and Jianguo Gu

J. Biol. Chem. 2015, 290:29345-29360.
doi: 10.1074/jbc.M115.682229 originally published online October 19, 2015

THE JOURNAL OF BIOLOGICAL CHEMISTRY VOL. 289, NO. 50, pp. 34627–34641, December 12, 2014

β-Galactoside α2,6-Sialyltranferase 1 Promotes Transforming Growth Factor-β-mediated Epithelial-Mesenchymal Transition*

Received for publication, July 2, 2014, and in revised form, October 23, 2014 Published, JBC Papers in Press, October 24, 2014, DOI 10.1074/jbc.M114.593392

Jishun Lu[‡], **Tomoya Isaji**[‡], **Sanghun Im**[‡], **Tomohiko Fukuda**[‡], **Noritaka Hashii**[§], **Daisuke Takakura**[§], **Nana Kawasaki**[§], **and Jianguo Gu**[‡1]

From the [‡]*Division of Regulatory Glycobiology, Institute of Molecular Biomembrane and Glycobiology, Tohoku Pharmaceutical University, 4-4-1 Komatsushima, Aobaku, Sendai, Miyagi, 981-8558, Japan and the* [§]*National Institute of Health Sciences, 1-18-1, Kamiyoga, Setagaya, Tokyo, 158-8501, Japan*

Background: Molecular mechanisms underlying the effect of sialylation on tumor progression remain unclear.
Results: ST6GAL1 promoted the TGF-β-induced EMT through down-regulation of E-cadherin-mediated cell adhesion and up-regulation of integrin-mediated cell migration.
Conclusion: Expression of ST6GAL1 is critical for sufficient induction of EMT.
Significance: α2,6-Sialylation of *N*-glycans may play a role in EMT.

β-Galactoside α2,6-sialyltranferase 1 (ST6GAL1) catalyzes the addition of terminal α2,6-sialylation to *N*-glycans. Increased expression of ST6GAL1 has been reported in diverse carcinomas and highly correlates with tumor progression. Here, we report that *St6gal1* transcription and α2,6-sialylated *N*-glycans are up-regulated during TGF-β-induced epithelial-mesenchymal transition (EMT) in GE11 cells, requiring the Sp1 element within the *St6gal1* promoter. Knockdown of *St6gal1* strongly suppressed TGF-β-induced EMT with a concomitant increase in E-cadherin expression, a major determinant of epithelial cell adherens junctions. Conversely, overexpression of ST6GAL1 increased the turnover of cell surface E-cadherin and promoted TGF-β-induced EMT. Overexpressing β-galactoside α2,3-sialyltranferase 4 had little influence on EMT, indicating specificity for α2,6-sialylation. The basal mesenchymal phenotype of MDA-MB-231 human breast cancer cells was partially reversed by ST6GAL1 silencing. Moreover, ST6GAL1 knockdown inhibited the phosphorylation of Akt, but not Smad2, suggesting that ST6GAL1 contributes to EMT through a non-Smad signaling pathway. Taken together, our data indicate that ST6GAL1 promotes TGF-β-dependent EMT as well as maintenance of the mesenchymal state by growth signaling, providing a plausible mechanism whereby up-regulated ST6GAL1 may promote malignant progression.

Epithelial-mesenchymal transition (EMT)[2] is a cellular trans-differentiation process that allows fully polarized epithelial cells to undergo multiple biochemical changes, enabling them to acquire a mesenchymal identity and migrate to secondary sites (1, 2). Morphologically, EMT is characterized by a loss of cell adhesion and acquisition of cell motility. At a molecular level, it is characterized by a decreased expression of cell adhesion molecules and epithelial markers, such as E-cadherin and α3 integrin, and an increased expression of intermediate filament proteins and mesenchymal cell markers, including N-cadherin, α-smooth muscle actin (α-SMA), and vimentin. EMT has evolved as a critical developmental program (3, 4). However, this process is also recapitulated under pathological conditions, prominently in invasion and metastasis of carcinomas (5). A better understanding of the mechanisms involved in EMT is critical to develop efficacious treatments for tumor growth and metastasis.

TGF-β is a pluripotent cytokine and has received much attention as a major inducer of EMT during embryogenesis and cancer progression (6, 7). TGF-β induces EMT through activation of the Smad signaling pathway as well as non-Smad signaling cascades including MAPK/ERK, the Rho family of GTPases, and PI3K/Akt (8, 9). In the Smad-dependent pathway, TGF-β-induced activation of the receptor complex leads to phosphorylation of Smad2 and Smad3 at their C termini by TGF-β receptor I. The phosphorylated Smad proteins then form a trimer with Smad4 and translocate into the nucleus, where they associate and cooperate with other transcription factors to precisely regulate the target gene transcription (10). These reorchestrated target genes, as recently evidenced in several types of cancer cell lines undergoing EMT by mass spectrometry and microarray analysis, at least include the glycogenes involved in *N*-glycosylation, *O*-glycosylation, and sialylation (11–13), indicating the importance of cellular glycosylation pattern in both the transition to and the maintenance of the mesenchymal state.

Sialic acid is the most abundant terminal monosaccharide of glycoconjugates on the eukaryotic cell surface. It is known to be

* This work was supported in part by Grants-in-Aid for Scientific Research 21370059 (to J. G.) and 24570169 (to T. I.) and Grant-in-Aid for Challenging Exploratory Research 23651196 (to J. G.) from the Japan Society for the Promotion of Science, by Scientific Research on Innovative Areas Grants 23110002 (to J. G.) and 23110001 (to N. K.); and the Strategic Research Foundation Grant-aided Project for Private Universities from the Ministry of Education, Culture, Sports, Science and Technology of Japan.
[1] To whom correspondence should be addressed. Tel.: 81-22-727-0216; Fax: 81-22-727-0078; E-mail: jgu@tohoku-pharm.ac.jp.
[2] The abbreviations used are: EMT, epithelial-mesenchymal transition; FN, fibronectin; MAA, *M. amurensis* agglutinin; MET, mesenchymal-epithelial transition; α-SMA, α-smooth muscle actin; SNA, *S. nigra* lectin; ST3GAL4, β-galactoside α2,3-sialyltransferase 4; ST6GAL1, β-galactoside α2,6-sialyltranferase 1; DOX, doxycycline; FT, Fourier transform.

linked via an α2,3 or α2,6 bond to Gal/GalNAc or via an α2,8 bond to sialic acid in proteins through a group of sialyltransferases. Ample evidence demonstrates that sialylation plays fundamental roles in a wide range of normal biological processes, such as cell signaling, differentiation, growth, and apoptosis (14–17). Paradoxically, it has also been shown to contribute to cancer cell progression and metastasis by affecting cell adhesion, migration, and tumor growth (18, 19). Given the essentiality of phenotypic changes in cell adhesion, motility, and growth in EMT, we considered the possible involvement of sialylation in control of EMT.

For this purpose, we investigated the role of sialylation in TGF-β-induced EMT using the normal epithelial cell line, GE11, and mammary cancer cell line, MDA-MB-231 as the EMT and MET (mesenchymal-epithelial transition, the converse process of EMT) models, respectively. Here, we show for the first time that β-galactoside α2,6-sialyltranferase 1 (ST6GAL1), an enzyme that primarily creates terminal α2,6-sialic acid linkages on *N*-glycans, is specifically up-regulated during TGF-β-induced EMT in GE11 cells. Knockdown of *St6gal1* clearly inhibited EMT with a concomitant increase in E-cadherin. Overexpression of ST6GAL1, but not β-galactoside α2,3-sialyltranferase 4 (ST3GAL4) promoted EMT, indicating the specific role of ST6GAL1 during the EMT process. Furthermore, silencing ST6GAL1 partially reversed the basal mesenchymal phenotype of MDA-MB-231 human breast cancer cells. Together, our data show that ST6GAL1 plays a critical role in both the transition to and the maintenance of the mesenchymal state, which provides a plausible explanation for the up-regulated ST6GAL1 during malignant progression of multiple cancers.

EXPERIMENTAL PROCEDURES

Cell Line and Cell Culture—Epithelial GE11 cells, a β1 integrin-null cell line, were kindly gifted by Dr. Arnoud Sonnenberg (Division of Cell Biology, Netherlands Cancer Institute, Amsterdam). The 293T cells were provided from the RIKEN cell bank (Tsukuba, Japan). The phoenix cells and MDA-MB-231 cells were purchased from ATCC. All cells above were cultured in high glucose Dulbecco's modified Eagle's medium (DMEM) with 2 mM L-glutamine and 10% fetal bovine serum (FBS) under a humidified atmosphere containing 5% CO_2 at 37 °C. For the TGF-β-induced EMT model, 5×10^5 cells were plated on 10-cm dishes, followed by incubation with human recombinant TGF-β (PeproTech) at 5 ng/ml for 4 days as described previously (20).

shRNA-mediated Silencing of ST6GAL1 in GE11 Cells and MDA-MB-231 Cells—For the *St6gal1* knockdown in mouse GE11 cells, we utilized the doxycycline (DOX)-inducible shRNA expression system (Invitrogen) as described previously (21). Briefly, the shSt6gal1 targeting sequences (5′-CACCGCGCAAGACAGATGTGTGCTATGTGCTTTAGCACACATCTGTCTTGCGCC-3′ and 5′-AAAAGGCGCAAGACAGATGTGTGCTAAAGCACATAGCACACATCTGTCTTGCGC-3′) were first cloned into the pENTR/H1/TO vector. Then the pENTR/H1/TO-shRNA was recombined into a blasticidin-selectable CS-Rfa-ETBsd, a DOX-inducible shRNA lentiviral vector, by the Gateway™ cloning system (Invitrogen). The resulting vector was then transfected into 293T cells with packaging plasmids by the calcium phosphate for the preparation of viruses. GE11 cells were then infected by the obtained viruses and selected for stable integration with 12.5 μg/ml blasticidin. The shRNA-mediated silencing of *St6gal1* was induced by the addition of 1 μg/ml DOX in the established cell line, and the cells cultured by DOX-free medium were used as the control in the present study. Endogenous *ST6GAL1* in the human MDA-MB-231 cells was knocked down by introducing a shRNA sequence using lentiviral vectors from Sigma-Aldrich. The cells were selected by the addition of 3 μg/ml puromycin.

The Establishment of ST6GAL1- and ST3GAL4-overexpressing GE11 Cells—The previously constructed *ST6GAL1*- or *ST3GAL4*-overexpressing lentiviral vectors (CSIV-TRE-CMV-3xFLAG-*ST6GAL1*/*ST3Gal4*-KT) (21) were transfected into 293T cells with packaging plasmids by the calcium phosphate method for the preparation of viruses. The obtained viruses were then incubated with GE11 cells for 72 h. The infected cells were selected by the Kusabira Orange marker using FACS Aria II (BD Biosciences). The selected cells were transfected with the retrovirus containing the human β1 integrin overexpressed vector (pBABE-puro-β1 integrin). The established cells were further selected by the addition of 3 μg/ml puromycin and used in the present study.

Western Blot Analysis and Immunoprecipitation—Immunoblotting was carried out as described previously (20). Proteins were separated by SDS-PAGE. Samples were incubated at 4 °C overnight with appropriate primary antibodies: anti-E-cadherin (BD Biosciences), anti-N-cadherin (BD Biosciences), anti-α-SMA (Sigma), anti-β1 integrin (BD Biosciences), anti-Smad2 (cell Signaling), anti-phospho-Smad2 (Cell Signaling), anti-Akt (Cell Signaling), anti-phospho-Akt (Cell Signaling), anti-α-tubulin (Sigma), and anti-FLAG (Agilent). Proteins were visualized by chemiluminescence (ECL (Pierce) or Immobilon Western (Millipore)).

Flow Cytometry Analysis of Cells—Cells were grown to about 90% confluence, detached using trypsin containing 1 mM EDTA at 37 °C, and washed three times with cold PBS. Then cells were stained with the 10 μg/ml biotinylated *Sambucus nigra* lectin (SNA), which preferentially recognizes the α2,6-sialylated products or *Maackia amurensis* agglutinin (MAA), which preferentially recognized α2,3-sialylated products for 30 min on ice, followed by incubation with streptavidin-conjugate Alexa Fluor 647 (Invitrogen) for 30 min on ice. Finally, cells were washed three times with PBS and analyzed by flow cytometry (BD Biosciences).

Luciferase Assay—GE11 cells were transiently transfected with a reporter construct derived from basic vector pGL4.10 (Promega), which contained the different *St6gal1* promoters or their truncated fragments or mutated fragments. As an internal control, a *Renilla* luciferase construct (pGL4.82) was co-transfected. Transfected cells were treated with or without TGF-β for 72 h. The cells were lysed and subjected to a luciferase assay using a Dual-Luciferase reporter assay system (Promega) according to the manufacturer's instructions. Primers used to generate the different constructs are listed in Table 1.

N-Glycan Profiling by LC/MS—*N*-Glycan profiling was performed as reported previously (21). Briefly, the same amounts

of cell membrane fractions from GE11 cells treated with or without TGF-β were obtained by an ultracentrifugation and digested with *N*-glycosidase F. The released *N*-glycans were reduced with $NaBH_4$, and the resulting *N*-linked glycans were separated on a graphitized carbon column (Hypercarb, 150 × 0.1 mm, 5 μm; Thermo Fisher Scientific). Mass spectrometric analysis was performed using a Fourier transform ion cyclotron resonance/ion trap type mass spectrometer (FT-MS, LTQ-FT; Thermo Fisher Scientific). The resolution of FT-MS was 50,000, and the scan range was m/z 700–2,000. The monosaccharide compositions of the glycans were deduced from the accurate masses obtained by FT-MS and the product ion spectra.

Cell Surface Biotinylation and Immunoprecipitation—Cell surface biotinylation was performed as described previously (20). Briefly, cells were rinsed twice with ice-cold PBS and were then incubated with ice-cold PBS containing 0.2 mg/ml EZLink Sulfo-NHS-Biotin (Pierce) for 2 h at 4 °C. After incubation, 50 mM Tris-HCl (pH 8.0) was used for the initial wash to quench any unreacted biotinylation reagent. The cells were then washed three times with ice-cold PBS and solubilized in lysis buffer (10 mM Tris-HCl, pH 7.4, 150 mM NaCl, 1% Triton X-100). Insoluble material was removed by centrifugation at 15,000 rpm for 10 min at 4 °C. The supernatant (2 mg of protein) was incubated with streptavidin-agarose (15 μl in 50% slurry) (Upstate Biotechnology, Inc.) for another 3 h at 4 °C with rotation. After washing three times with lysis buffer, the immunoprecipitates were subjected to 7.5% SDS-PAGE, and the separated proteins were transferred to a PVDF membrane. The membrane was incubated with E-cadherin antibody for immunoblot analysis.

Immunofluorescence Staining—Cells cultured on pretreated glass bottom dishes were fixed with acetone/methanol and permeabilized with 0.2% Triton X-100. Antibodies against E-cadherin (BD Bioscience) were used, followed by the incubation with anti-mouse Alexa Fluor 488 secondary antibodies (Invitrogen) and Alexa Fluor 546 phalloidin (Invitrogen) or TO-PRO3 (Invitrogen).

RT-PCR for mRNA Expression Analysis—Total RNA was prepared with TRI reagent (Invitrogen), and 1 μg of total RNA was reverse-transcribed using a PrimeScript RT reagent kit with gDNA Eraser (Takara) according to the manufacturer's instructions. The sequences of the primers used for the PCR amplification were shown in Table 1. The glyceraldehyde-3-phosphate dehydrogenase (GAPDH) mRNA was used as a control in PCR runs, and the reaction products obtained were subjected to electrophoresis using 2% agarose gels containing ethidium bromide.

Cell Migration Assay—Cell Migration was examined with Transwells (BD BioCoat™ control inserts, 8.0-mm inserts; BD Biosciences) as described previously (20). Transwells were coated only on the bottom side with 10 μg/ml fibronectin (FN) at 4 °C overnight. Cells pretreated with or without TGF-β for 4 days were starved in serum-free medium for 12 h, trypsinized, and suspended with 0.5 mg/ml trypsin inhibitor (Nacalai Tesque) in DMEM. The suspended cells were centrifuged, and the supernatants were removed. The resulting cell pellets were resuspended with assay medium (serum-free DMEM) containing TGF-β and diluted to 1×10^5 cells/ml. To each FN-coated transwell, 500-μl aliquots of the cell suspension were added; the cells were then incubated at 37 °C for 4 h. After incubation, cells on the upper side were removed by scraping with a cotton swab. The membranes in the transwells were fixed with 4% paraformaldehyde and stained with 0.5% crystal violet overnight. Cells that had migrated to the lower side were counted using a phase-contrast microscope.

Metabolic Labeling—The pulse-chase experiment was performed as described previously (20). The cells grown at 90% confluence were washed three times with PBS and then starved for 30 min in DMEM without methionine and cysteine (Sigma). After starvation, the cells were pulse-labeled in 500 μl of DMEM containing 200 μCi of [^{35}S]methionine and cysteine (PerkinElmer Life Sciences) for 60 min and then changed with complete DMEM containing 10% FBS at the indicated times. The cells were lysed, and the cell lysates were immunoprecipitated with the anti-E-cadherin antibody and Dynabeads Protein G (Invitrogen). The immunoprecipitates were separated on 4–12% precast gels (Bio-Rad). After drying the gels, radioactive bands were visualized with a Fuji BAS 2500 BioImage analyzer.

Statistical Analysis—Statistical analyses were performed using either a one-tail unpaired Student's t test or one-way analysis of variance, using GraphPad Prism version 5.

RESULTS

St6gal1 and Its Products Were Specifically Up-regulated during the TGF-β-induced EMT in GE11 Cells—Considering the growing evidence for the involvement of sialylation in diverse cellular processes (*e.g.* growth, differentiation, and motility) characteristic of EMT (18, 22), we hypothesized a potential role of cell sialylation in the control of EMT. To test this idea, we initially utilized the established model of EMT, the mouse epithelial cell line, GE11, which undergoes progressive EMT upon TGF-β treatment and acquires a fibroblast-like morphology (20). First, RT-PCR analysis was performed to examine the changes in the expression of glycogenes involved in sialylation biosynthesis during the TGF-β-induced EMT. Interestingly, in contrast to the little difference in the expression of other glycogenes encoding the sialyltransferases, CMP-sialic acid transporter, and neuraminidases, the expression level of ST6GAL1 was significantly up-regulated after stimulation with TGF-β (Fig. 1*A*). These alterations in the expression of glycogenes were further reflected by their enzymatic products analyzed with flow cytometry, as seen in Fig. 1*B*; upon TGF-β treatment, the reactivity against SNA lectin, which specifically recognizes α2,6-sialylation, was greatly increased. In contrast, the reactivity against MAA lectin, which specifically recognizes α2,3-sialylation, showed a marginal change. Consistent with these observations, the complex type of *N*-glycan profiling of those cells by LC/MS showed that the ratios of sialylated *N*-glycans in the TGF-β-treated cells increased obviously, and the opposite asialo-*N*-glycans decreased apparently, when compared with untreated cells (Fig. 1*C*). Taken together, these results clearly demonstrated that *St6gal1* and α2,6-sialylation were specifically up-regulated during the TGF-β-induced EMT process in GE11 cells.

TABLE 1
Primers used for PCR and plasmid construction

	Sense primer (5′–3′)	Antisense primer (5′–3′)
Primers for RT-PCR		
Mouse *St3gal1*	ATGAGGAGGAAGACCCTCAAG	CCACCAGCCTCTTGTTCAAC
Mouse *St3gal2*	GATGAAGTGCTCTCTTCGGG	CAGGCACGATCTGGAACAGT
Mouse *St3gal3*	GTGAAGATGGGACTCTTGGT	ATTGCTCAGGTCGCTGCATG
Mouse *St3gal4*	AGCCATGCTTCCAGGGTGAG	CCTTGAAAGCTACCAGGACC
Mouse *St3gal5*	CTGCCGAGCAATGCCAAGTG	ATCCGGTCAGGGTCCACATA
Mouse *St6gal1*	ATGATTCATACCAACTTGAAG	GGTGCCCCATTAAACCTCAG
Mouse *St6gal2*	CTAGCCAGCAGGTTTTGTCCA	AGCATTCGTTGTCGCCATTG
Mouse *St6galnac1*	CATGACGAGATATTGCAGAGG	CTGCCTTGCTCTGAGGATTC
Mouse *St6galnac2*	AGACCCAGGTTCCCGCCAGG	AAGGAGGTCTTAGTGCCCAC
Mouse *St6galnac3*	ATGGATACATAAATGTGAGGACC	GTGGATACTGTAGCAGGCATCCA
Mouse *St6galnac4*	GTGGTCTACGGGATGGTCAG	GAGAGGCTGAGGCTCAAAGG
Mouse *CST*	AAAGTCGTGGTAGCGCAGAA	ACGTCACAACGATCCCTGAC
Mouse *Neu1*	TTCATCGCCATGAGGAGGTCCA	AAAGGGAATGCCGCTCACTCCA
Mouse *Neu2*	AGGAAGCTACAACGAAGCCACA	TTCTGAGCAGGGTGCAGTTTCC
Mouse *Neu3*	CTCAGTCAGAGATGAGGATGCT	GTGAGACATAGTAGGCATAGGC
Mouse *Neu4*	AGGAGAACGGTGCTCTTCCAGA	GTTCTTGCCAGTGGCGATTTGC
Mouse E-cadherin	CCCAAGCACGTATCAGGGTC	TCTGTGGCGATGATGAGAGC
Mouse N-cadherin	CTGACAATGGAATCCCGCCT	TCCCGCCGTTTCATCCATAC
Mouse *α-SMA*	CTGACAGAGGCACCACTGAA	ATCTCACGCTCGGCAGTAGT
Mouse *Sp1*	ACCATGAGCGACCAAGATCAC	TGGCACCCTGTGAAAGTTGT
Human *ST3GAL1*	GACTTGGAGTGGGTGGTGAG	ACAAGTCCACCTCATCGCAG
Human *ST3GAL2*	CTCTCGGGCAAGAGCTGTG	CTGCAGCATCATCCACCACC
Human *ST3GAL3*	CCTCTCCGCTGTGGTCATTT	GTCCAGCGGAGTCAAAGGAA
Human *ST3GAL4*	TGAGGGTGGCCCGAGG	CCGGGAGTAGTTGCCAAAGA
Human *ST3GAL5*	CCAATGCCAAGTGAGTACACC	TGAGCTCTCTTTACATGGTCAGG
Human *ST3GAL6*	CCACCCCTCACTTTAGCTCC	CAGGTGCCACCCAATAGACA
Human *ST6GAL1*	GAAAAATGGGCCTTGGCCTG	GAGCAGGAAAACAAGCCTGC
Human *ST6GAL2*	TGGGAAGAAGGCTGGTTCATT	TCGTCATCCTCCGGGTAGAA
Human *ST6GALNAC1*	AGCTCAACTACTCCTTGGTGC	CGAAAAGCTTCCTGGGGTCT
Human *ST6GALNAC2*	GCCAGGGACACCACATCATT	GAGGCGATGACTTGGTGAGA
Human *ST6GALNAC3*	AGTTGTGTCCCATACCAGCG	CTGCATGGTCACTCTGTACTGT
Human *ST6GALNAC4*	CATGAAGGCTCCGGGTCGG	CCATGTAGAGCGTGTCTCGG
Human *ST6GALNAC5*	AGGCTCCCAGATTGACCAGA	AGGGTGATTGGGATCCCTGC
Human *ST6GALNAC6*	CAACAAAGAGCAGCGGTCAG	ACAATCACACACTGGTGGCA
Human *CST*	GTGCTCAGGATTTGCAGTTCT	GAGTACCCAGGGCAAAGGTG
Human *Neu1*	TGAGAACGACTTCGGTCTGGTG	CCAGGAAACACCATCATCCTTG
Human *Neu3*	CACCTATGTGGGATCTCCAG	CACCTATGTGGGATCTCCAG
Human *Neu4*	CCGTCTTCCTCTTCTTCATCGC	CATTGCAGTAGAGGAAGCTGCC
Human E-cadherin	ACGCATTGCCACATACA	CGTTAGCCTCGTTCTCA
Mouse *α-SMA*	CCAGCGACCCTAAAGCTTCC	ACCATCACCCCCTGATGTCTG
Human *Sp1*	ACCATGAGCGACCAAGATCA	ATGTTGCCTCCACTTCCTCG
Primers for plasmid construction		
St6gal1-pro-344	TAGGTACCCCGACCAGCATGATGAACTA	CGAAGCTTATGCAGGGAATCTTGCAGTC
St6gal1-pro-625	CTGGTACCACCAGCAATTTTCTGCGTTC	CGAAGCTTAGAGCAAGCAAAACCCAAGA
St6gal1-pro-074	TAGGTACCACCGAGAGAGCACCTCATGT	CGAAGCTTATAGATGCTGAGGGCGAGAA
Pro-344-192	CAAGTCATGGTACCGGCCAGTTAGGCCAGAGAA	CCGGTACCATGACTTGTTTGATCAGGATCACCCT
Pro-344-69	GCCCAAATGGTACCGGCCAGTTAGGCCAGAGAAA	CCGGTACCATTTGGGCTTCCTTGCCTGCCGCATT
Pro-344-33	AAGCCTTTGGTACCGGCCAGTTAGGCCAGAGAAA	CCGGTACCAAAGGCTTGCTCTTTGTGGACAGACT
Pro-344-Sp1-mut	GCTCCGAACCAAAGGCTTGCTCTTTG	CCTTTGGTTCGGAGCAATGCGGCAGGC

The Sp1 Binding Site within St6gal1 Promoter-344 Was Required for Its Transcriptional Activation during TGF-β-induced EMT—The RT-PCR result above showed an enhanced transcription of *St6gal1* in TGF-β-induced EMT. Given the fact that three promoters exist in the mouse *St6gal1* gene, a Dual-Luciferase assay was carried out to determine the core promoter responsible for this enhancement. As shown in Fig. 2*A*, the activity of each promoter increased by 2–3-fold after treatment with TGF-β, indicating that all three promoters were involved in the induction of *St6gal1* expression in EMT. Subsequent sequence analysis of these promoters revealed the presence of several putative Sp1-binding elements and Smad-binding elements in each promoter (Fig. 2*A*). In fact, Sp1 and Smad proteins together have been reported to regulate the expression of vimentin, an important mesenchymal marker involved in cell migration, during TGF-β-induced EMT in pancreatic cancer cells (23). Here, to examine their roles in the regulation of *St6gal1* during the EMT process, we performed a luciferase assay by using the *St6gal1* promoter-344, which assumes highest activity under basal conditions among the three *St6gal1* promoters, and its truncated or mutated constructs as illustrated in Fig. 2*B*. The results showed that upon stimulation by TGF-β, the activity of Smad-binding element-deleted *St6gal1* promoter-344 still increased by ~1.5-fold, albeit it was decreased to some extent as compared with the full-length promoter (~2-fold). However, deleting or mutating the Sp1 elements in *St6gal1* promoter-344 completely abolished its response to TGF-β. These results suggest that the Sp1 element in *St6gal1* promoter-344 is necessary for its transcriptional activation during TGF-β-induced EMT in GE11 cells.

Silencing of St6gal1 Prevented the TGF-β-induced EMT in GE11 Cells—To directly assess the functional contribution of ST6GAL1 in TGF-β-induced EMT, we knocked down the endogenous *St6gal1* by RNA interference technology. Fig. 3*A* showed efficient shRNA-mediated silencing of *St6gal1* in TGF-β-treated GE11 cells. Upon TGF-β stimulation, the morphology of control cells alters from the typical "cobblestone" epithelial cell shape into the diffused fibroblast-like appearance (Fig.

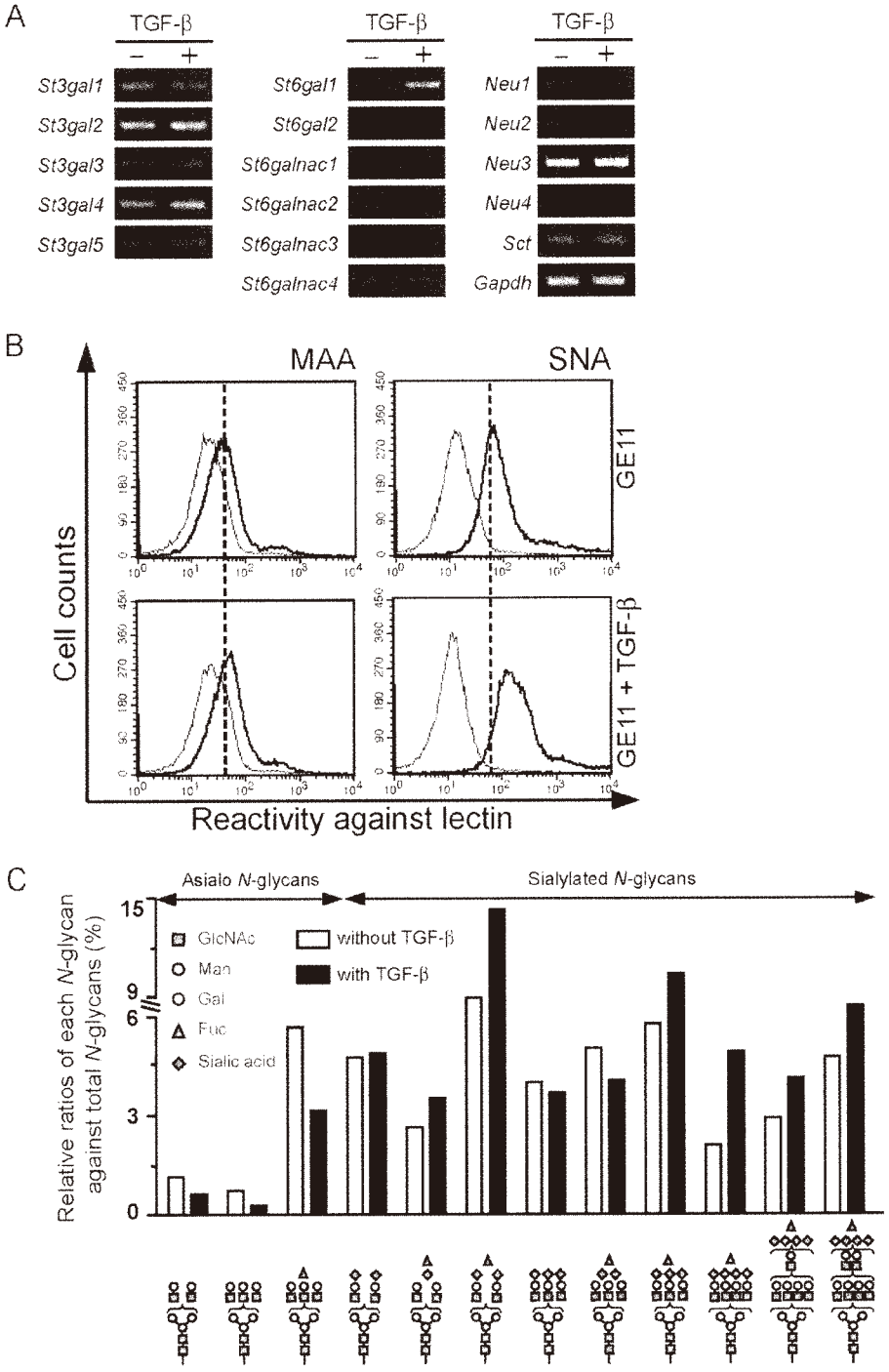

FIGURE 1. ***St6gal1* is specifically up-regulated at the transcriptional level during the TGF-β-induced EMT in GE11 cells.** *A*, RT-PCR using total RNA extracted from TGF-β-treated and -untreated cells was carried out to examine the expression levels of genes involved in protein sialylation. The expression level of *Gapdh* was used as a loading control. *Sct*, sialic acid transporter; *St3gal*, β-galactoside α2,3-sialyltransferase; *ST6Gal*, β-galactoside α2,6-sialyltransferase; *St6galnac*, α-*N*-acetylgalactosaminide α2,6-sialyltransferase; *Neu*, neuraminidase. *B*, cells treated with or without TGF-β were incubated with (*heavy line*) or without (*gray shadow*) biotin-conjugated MAA (recognizing α2,3-sialylated proteins) or biotin-conjugated SNA (recognizing α2,6-sialylated proteins), followed by incubation with streptavidin Alexa Fluor 647 conjugate, and subjected to FACS analysis. *C*, representative glycan profiling in the cells treated with or without TGF-β to compare the major complex type of *N*-glycans by LC/MS. Peak area of asialo- and sialylated *N*-glycans were calculated based on the extracted mass chromatograms acquired in positive and negative modes, respectively. The relative peak area of major *N*-glycans from those cells was presented as a percentage of the total peak area of the glycans. Glycan structures were deduced from the accurate masses and product ion spectra.

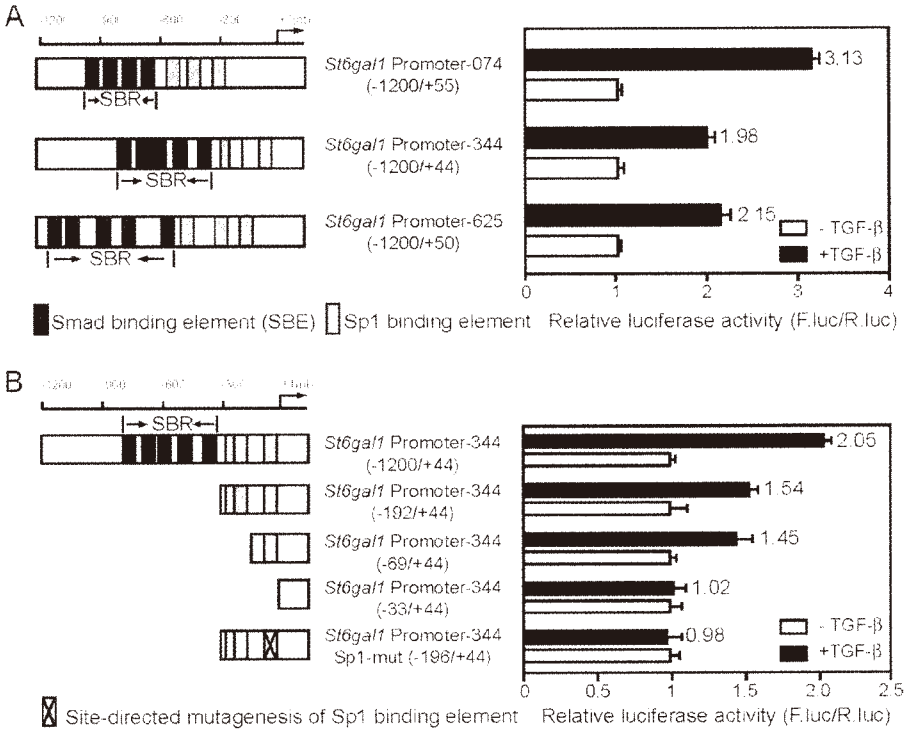

FIGURE 2. **The Sp1 binding site within *St6gal1* promoter-344 is required for its transcriptional activation during TGF-β-induced EMT.** *A* (*left*), representation of three *St6gal1* promoter constructs fused with the luciferase gene, respectively. The relative luciferase activity of each construct is indicated on the *right*. *B* (*left*), representation of the 5′-deleted mutants of *St6gal1* promoter-344 and site-directed mutagenesis of the indicated Sp1 element. The relative luciferase activity of each construct is indicated on the *right*. Each firefly luciferase construct was co-transfected into GE11 cells with a *Renilla* luciferase expression vector as an internal control. Following transfection, luciferase activity was measured after a 72-h incubation with or without TGF-β. The relative luciferase activity was normalized to the luciferase activity of the internal control, which contains the SV40 promoter-enhancer sequences upstream of the luciferase gene. The quantitative data for the relative luciferase activity (*right*) are presented as the means ± S.D. (*error bars*) from three independent experiments. *SBR*, Smad binding region.

3*B*). However, *St6gal1* knockdown cells still displayed a well organized epithelial morphology, indicating a reduced EMT phenotype. In agreement with these morphological changes, shRNA targeting *St6gal1* clearly prevented the loss of epithelial marker E-cadherin and, to a lesser extent, delayed the induction of mesenchymal marker α-SMA (Fig. 3, *C* and *D*). The decelerated loss of E-cadherin after knockdown of *St6gal1* was further confirmed by immunofluorescence analysis (Fig. 3*E*). Although it remains unclear why *St6gal1* knockdown did not affect the expression of N-cadherin, another mesenchymal marker, the results above strongly suggest that *St6gal1* is required for TGF-β-induced EMT. We then asked how *St6gal1* exerted its function in EMT. Considering that TGF-β induces EMT through activation of the Smad signaling pathway as well as non-Smad signaling cascades, including MAP-ERK, the Rho family of GTPases, and PI3K/Akt (8, 9), we first checked the phosphorylation level of Smad2, which acts as a major intracellular effector of Smad signaling. *St6gal1* knockdown did not affect the Smad signaling; as shown in Fig. 3*F*, no significant difference in the expression of phospho-Smad was observed between the *St6gal1* knockdown cells and control cells, indicating that *St6gal1* may contribute to EMT through non-Smad pathways. Given the recent reports showing that *St6gal1* promotes cell migration and invasion by activating PI3K/Akt signaling (21, 24), the activity of this signaling pathway was examined. The phosphorylation level of Akt was clearly decreased after knockdown of *St6gal1* in GE11 cells with or without TGF-β treatment, suggesting that silencing *St6gal1* was able to inhibit the PI3K/Akt signaling in TGF-β-induced EMT.

The Expression of ST6GAL1 Affected the Transcription and Turnover of E-cadherin on Cell Surface—E-cadherin is a transmembrane glycoprotein that plays a crucial role in EMT. Forced expression of E-cadherin has been showed to reverse the EMT in rat kidney fibroblast NRK49f cells (25). Interestingly, here, we found that knockdown of *St6gal1* resulted in an enhancement of E-cadherin transcription (Fig. 4*A*). This up-regulation of E-cadherin was further corroborated by the biotinylation data (Fig. 4*B*) and immunofluorescence staining analysis (Fig. 4, *C* and *D*), where it was seen that *St6gal1* knockdown cells showed a higher level of E-cadherin on the cell surface as compared with the control cells, even after the treatment with TGF-β for 48 h. In addition, considering the growing evidence for the involvement of ST6GAL1 in the cell surface retention of glycoproteins (26, 27), we were wondering whether this is also true for the E-cadherin in GE11 cells. To verify this, the pulse-chase experiment was performed using the ST6GAL1-overexpressing cells. As shown in Fig. 4, *E* and *F*, the decay rate of E-cadherin was increased after overexpression of ST6GAL1 in GE11 cells. The results above indicate that the increased expression of E-cadherin on the surface of *St6gal1* knockdown cells is due not only to its up-regulated transcription but also to its prolonged turnover.

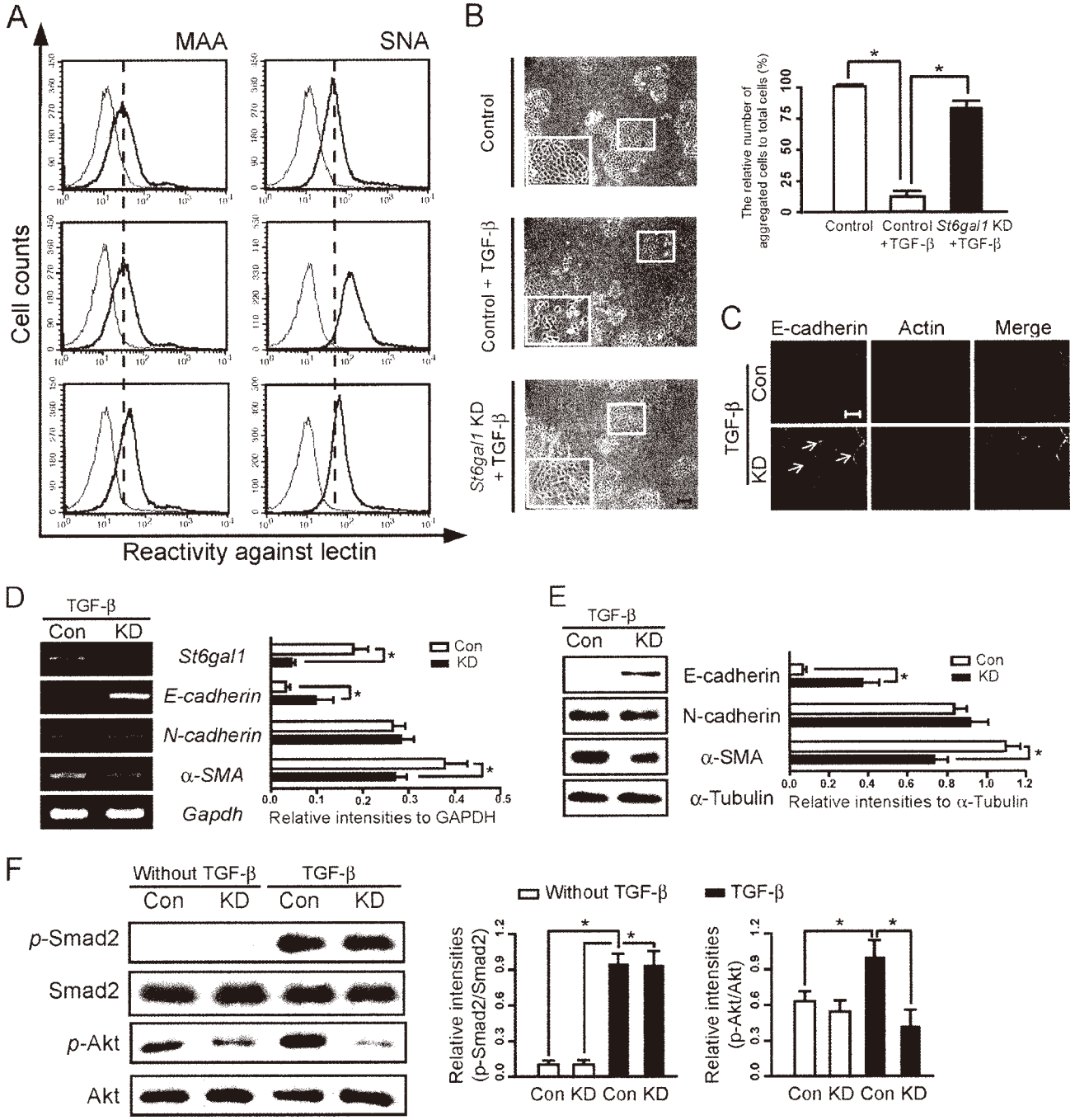

FIGURE 3. **Silencing of *St6gal1* prevents the EMT-associated morphological and molecular changes upon TGF-β stimulation in GE11 cells.** DOX-inducible shRNA-*St6gal1* GE11 cells were grown with or without DOX for 24 h and were then treated with TGF-β and incubated for another 72 h. *A*, the cells were collected and incubated with (*heavy line*) or without (*gray shadow*) biotin-conjugated SNA or biotin-conjugated MAA, followed by incubation with streptavidin Alexa Fluor 647 conjugate and subjected to FACS analysis to confirm the *St6gal1* knockdown efficiency. *B*, bright field pictures were taken to show the cell morphology. *Insets*, a representative cell morphology and its magnified view. *Scale bar*, 100 μm. The quantitative data for the number of aggregated cells relative to the total cells are presented as means ± S.D. (*error bars*) from three independent experiments (*, $p < 0.01$ by one-tailed unpaired Student's *t* test). *C*, to visualize the effects of *St6gal1* knockdown on the E-cadherin on cell surface, the indicated cells stimulated by TGF-β were stained with anti-E-cadherin antibody, followed by the incubation with fluorescent secondary antibody. Localization of F-actin was examined by staining with Alexa Fluor 546 phalloidin. *Scale bar*, 50 μm. The *arrows* indicate the E-cadherin expressed in the cell-cell contact. *D*, RT-PCR using total RNA extracted from those cells was carried out to examine the expression levels of E-cadherin, N-cadherin, and α-SMA. The expression level of *Gapdh* was used as a loading control. The quantitative data are presented as the means ± S.D. from three independent experiments (*, $p < 0.01$ by one-tailed unpaired Student's *t* test). *E*, cell lysates from those cells were immunoblotted with anti-E-cadherin, anti-N-cadherin, and anti-α-SMA antibodies. α-Tubulin was used as a loading control. The quantitative data are presented as the means ± S.D. from three independent experiments (*, $p < 0.01$ by one-tailed unpaired Student's *t* test). *F*, the indicated cell lysates were immunoblotted by phospho-Smad2, Smad2, phospho-Akt, and Akt antibodies. α-Tubulin was used as a loading control. The quantitative data are presented as means ± S.D. from three independent experiments (*, $p < 0.01$ by one-tailed unpaired Student's *t* test). *Con*, DOX-inducible shRNA-*St6gal1* GE11 cells; *St6gal1 KD*, DOX-inducible shRNA-*St6gal1* GE11 cells induced by DOX.

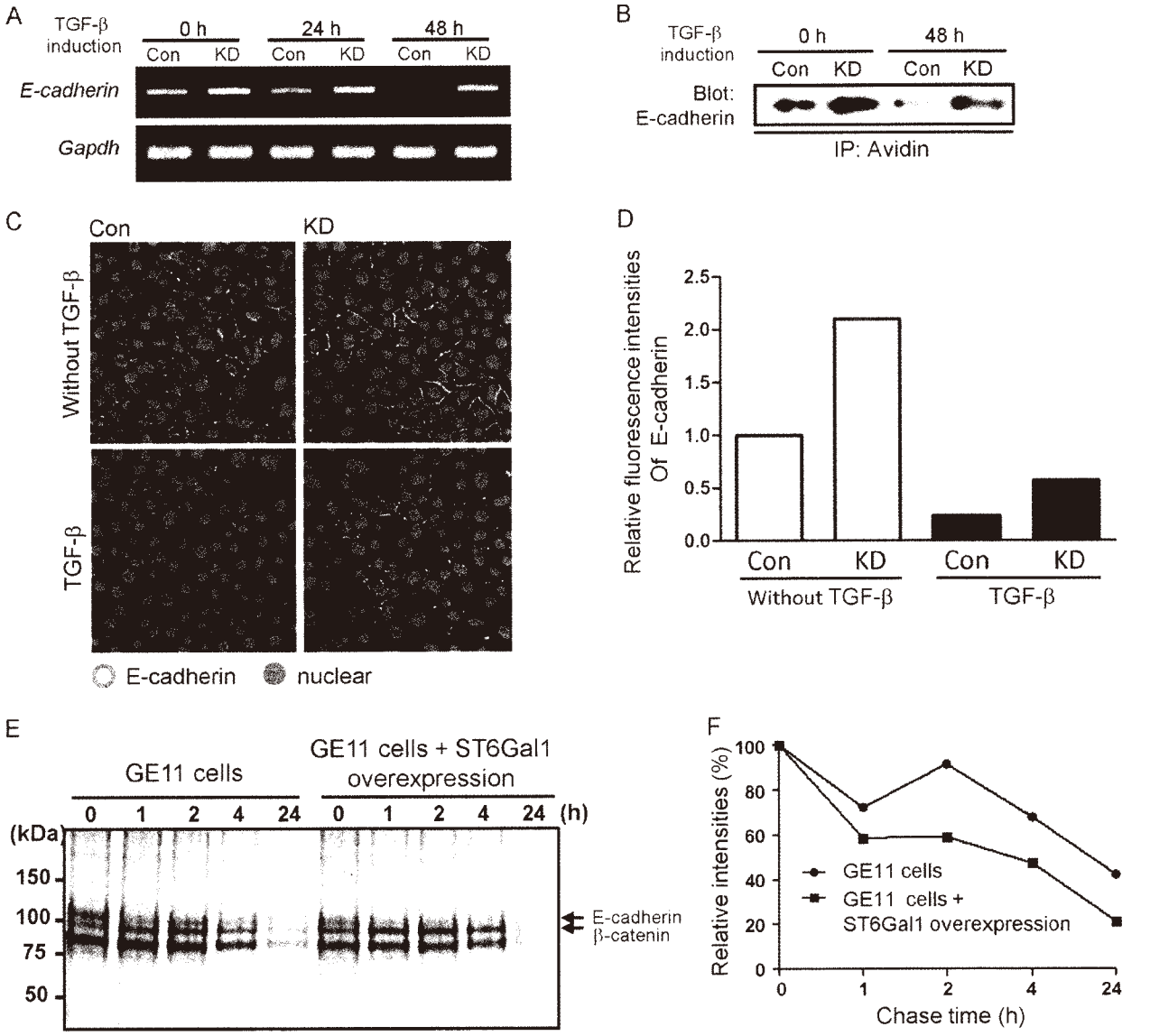

FIGURE 4. **The expression of ST6GAL1 affected the transcription and turnover of E-cadherin on the cell surface.** DOX-inducible shRNA-*St6gal1* GE11 cells were grown with or without DOX for 24 h and were then treated with TGF-β and incubated for another 48 h. *A*, time course analysis of the E-cadherin expression in cells treated with TGF-β for 0, 24, and 48 h by RT-PCR. The expression level of *Gapdh* was used as a loading control. *B*, cell surface biotinylation was performed as described under "Experimental Procedures." Equal amounts of the cell lysates were immunoprecipitated with avidin-agarose and immunoblotted with anti-E-cadherin antibody to examine the level of cell surface E-cadherin in the indicated cells. *C*, to directly visualize the effects of *St6gal1* knockdown on the E-cadherin on the cell surface, the indicated cells treated with or without TGF-β were stained with anti-E-cadherin primary antibody, followed by the incubation with fluorescent secondary antibody and TO-PRO-3. *D*, the relative fluorescence intensities of E-cadherin were quantified by the software ImageJ. *E*, the pulse-chase experiment was performed as described under "Experimental Procedures." The same amounts of the cell lysates were immunoprecipitated with anti-E-cadherin antibody at the indicated times. *F*, the relative E-cadherin intensities at each chasing point were quantified by the software ImageJ. The intensities of E-cadherin at the 0 h point of the ST6GAL1 overexpressed cells and control cells were set as 100%, respectively.

Overexpression of ST6GAL1, but Not ST3GAL4, Promoted the TGF-β-induced EMT—Although repression of ST6GAL1 activity by shRNA inhibited TGF-β-induced EMT, the influence could be due to potential off-target effects of the designed sequence. To rule out this possibility, we established a ST6GAL1-expressing GE11 cell line. The expression level of ST6GAL1 was verified by immunoblot analysis, and its enzymatic products were examined by FACS analysis (Fig. 5*A*). To evaluate the effects of the ST6GAL1 overexpression on TGF-β-induced EMT, RT-PCR (Fig. 5*C*) and Western blot (Fig. 5*D*) analyses were performed. The results showed that forced expression of ST6GAL1 promoted the loss of epithelial marker E-cadherin and accelerated the induction of mesenchymal marker α-SMA. Similar to the *St6gal1* knockdown cells, ST6GAL1-overexpressing cells exhibited no significant difference in the expression of N-cadherin from control cells. These results further corroborate that ST6GAL1 is required for the TGF-β-induced EMT in GE11 cells. ST6GAL1 mainly catalyzes the terminal α2,6-sialylation on *N*-glycans. This prompted us to ask whether α2,3-sialylation of *N*-glycans also plays a critical role in EMT. To address this question, we overexpressed ST3GAL4, which is primarily responsible for the α2,3-sialyla-

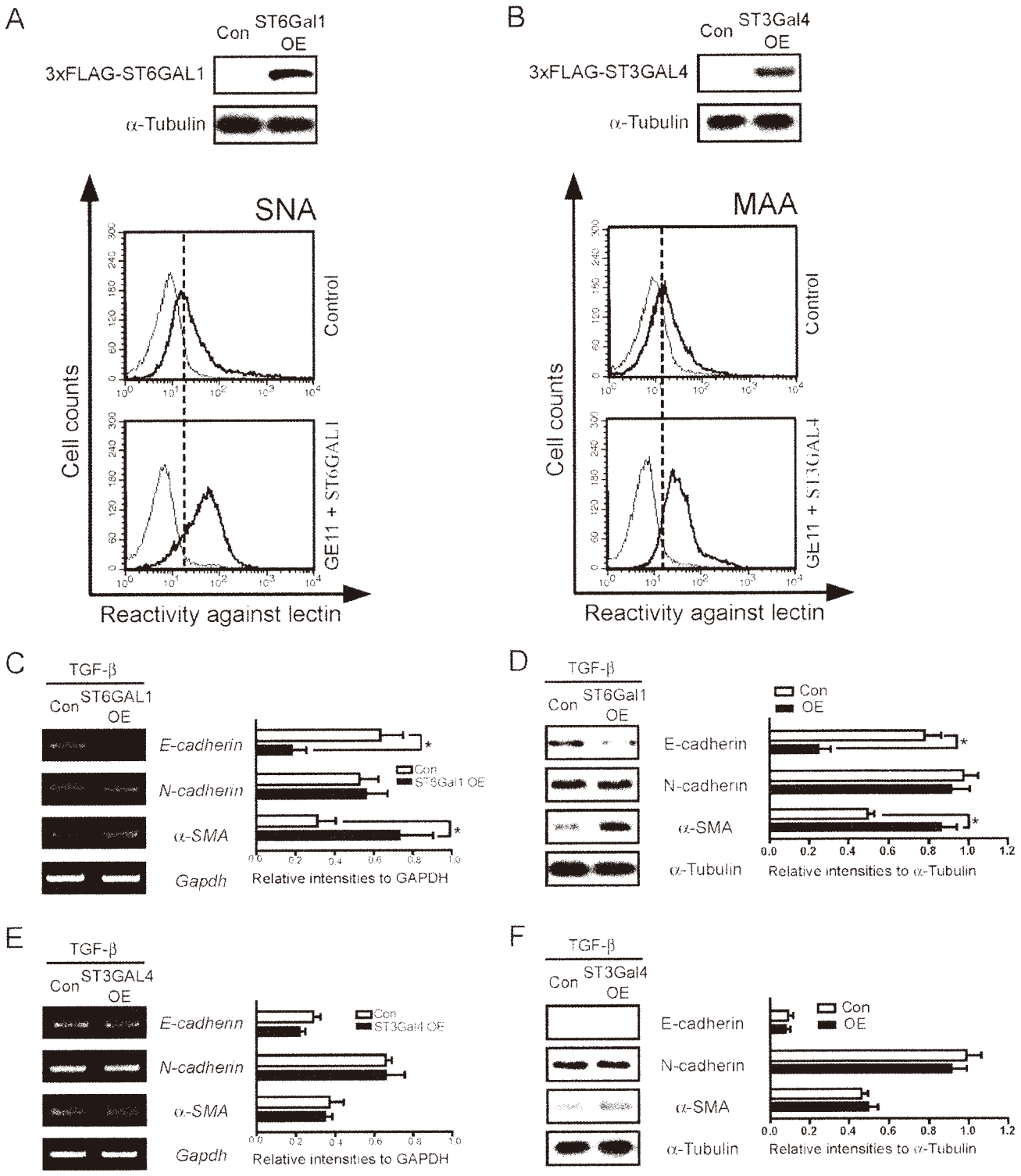

FIGURE 5. **Forced expression of ST6GAL1, but not ST3GAL4, promotes the EMT-associated molecular changes upon TGF-β stimulation in GE11 cells.** DOX-inducible *3xFLAG-ST6GAL1*- or *3xFLAG-ST3GAL4*-overexpressing GE11 cells were treated with or without 1 μg/ml DOX for 24 h, followed by the addition of TGF-β for another 48-h incubation. The expression level of *ST6GAL1* (*A*) and *ST3GAL4* (*B*) was confirmed by Western blot analysis using anti-FLAG antibody, and their enzymatic products were examined by FACS analyses using lectins, as described under "Experimental Procedures." *C* and *E*, RT-PCR analysis using the total RNA extracted from those cells was carried out to examine the expression levels of E-cadherin, N-cadherin, and α-*SMA*. The expression level of *Gapdh* was used as a loading control. The quantitative data are presented as means ± S.D. (*error bars*) from three independent experiments (*, $p < 0.01$ by one-tailed unpaired Student's *t* test). *D* and *F*, cell lysates from those cells were immunoblotted with anti-E-cadherin, anti-N-cadherin, and anti-α-SMA antibodies. α-Tubulin was used as a loading control. The quantitative data are presented as means ± S.D. from three independent experiments (*, $p < 0.01$ by one-tailed unpaired Student's *t* test).

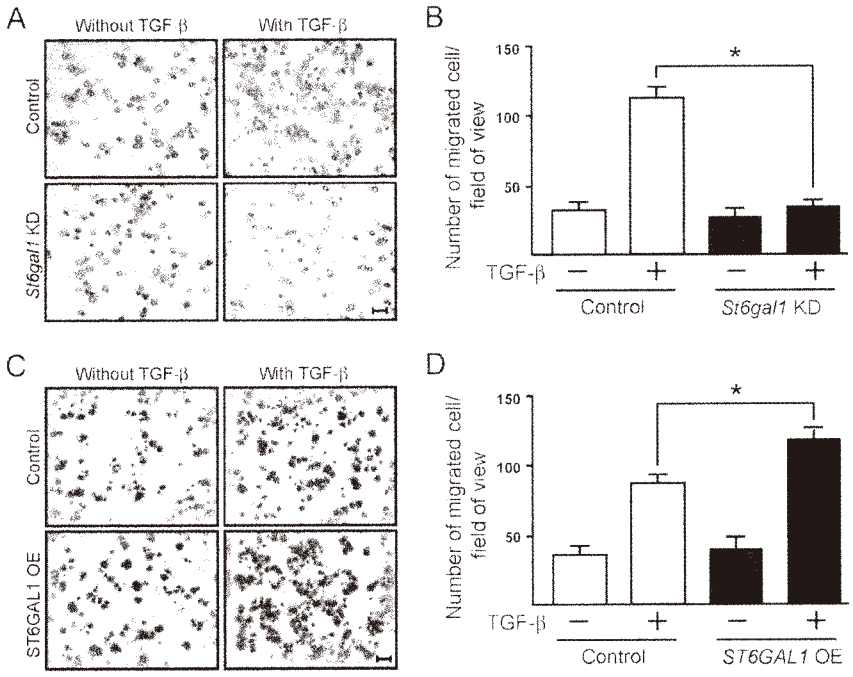

FIGURE 6. **Knockdown of *St6gal1* almost completely abrogates the TGF-β-induced cell migration, whereas the induction of TGF-β-mediated migration is significantly accelerated after overexpression of *ST6GAL1*.** The migratory ability of *St6gal1* knockdown cells (*A* and *B*) and *ST6GAL1*-overexpressing cells (*C* and *D*) toward FN was determined by a transwell assay. Cells that migrated through the transwell membrane were stained with 0.5% crystal violet. *A* and *C*, representative example recorded by phase-contrast microscopy. *Scale bar*, 100 μm. *B* and *D*, the migrated cells were counted under a microscope. The quantitative data were obtained from three independent experiments. The *p* values were calculated using one-tailed unpaired Student's *t* test. *Error bars*, S.D. *, $p < 0.01$.

tion of *N*-glycans, and replicated the experiments above. Fig. 5*B* showed the successful overexpression of ST3GAL4 and increased α2,3-sialylated products in GE11 cells. Subsequent RT-PCR (Fig. 5*E*) and Western blot (Fig. 5*F*) analyses indicated that there was little difference in the expression of EMT-associated molecules between ST3Gal4-overexpressing cells and control cells, highlighting the specific role of ST6GAL1 in control of EMT.

ST6GAL1 Was Required for the Cell Migration in TGF-β-induced EMT—A phenotypic hallmark of EMT is the stimulation of cell migration. Therefore, we assessed the migratory ability of GE11 cells by transwell analysis. As shown in Fig. 6, GE11 cells become highly migratory upon treatment with TGF-β. However, repression of ST6GAL1 expression significantly prevented TGF-β-induced increase in cell migration (Fig. 6, *A* and *B*). Conversely, overexpression of ST6GAL1 accelerated the induction of the TGF-β-mediated cell migration. These results indicated that ST6GAL1 is required for the enhancement of the cell migration during TGF-β-induced EMT.

ST6GAL1 Knockdown Induced MET-like Phenotypes in a Breast Cancer Cell Line—EMT illustrates the differentiation plasticity during the normal development and pathological process and is complemented by a reverse process called MET. To define the role of ST6GAL1 in MET, we knocked down endogenous *ST6GAL1* by RNA interference in the aggressive mesenchymal breast cancer cell line MDA-MB-231. Fig. 7, *A* and *B*, showed the successful silencing of *ST6GAL1* in this cell line. According to RT-PCR (Fig. 7*B*) and Western blot (Fig. 7*C*) analyses, we found that knockdown of *ST6GAL1* led to an increase in E-cadherin expression while decreasing the expression levels of the mesenchymal markers, such as α-SMA, β1 integrin, and FN. Furthermore, consistent with this reduced EMT, as shown at the expression level, repression of *ST6GAL1* activity significantly decreased the ability of MDA-MB-231 cells to migrate through the transwell membrane when compared with control cells (Fig. 7, *D* and *E*). These effects of ST6GAL1 knockdown on EMT in MDA-MB-231 cells, as in GE11 cells, were mediated via a non-Smad signaling pathway, because little difference in the expression level of phospho-Smad2 was observed between knockdown cells and control cells (Fig. 7*F*). Taken together, the results above suggest that the expression of ST6GAL1 plays an important role in EMT.

DISCUSSION

EMT is a cellular transdifferentiation process that plays critical roles in embryonic development and metastasis formation during malignant progression. The mechanisms underlying EMT have been extensively explored in the past decade. A vast amount of knowledge has been obtained from the research examining EMT at the mRNA and protein level. In the present study, we investigated the role of sialylation, a post-translational modification, in TGF-β-induced EMT and showed that ST6GAL1-mediated α2,6-sialylation is required for the sufficient induction of TGF-β-mediated EMT. In particular, we show here that *St6gal1* was specifically up-regulated during the TGF-β-induced EMT process in GE11 cells. Knockdown of *St6gal1*, interestingly, enhanced the transcription of E-cad-

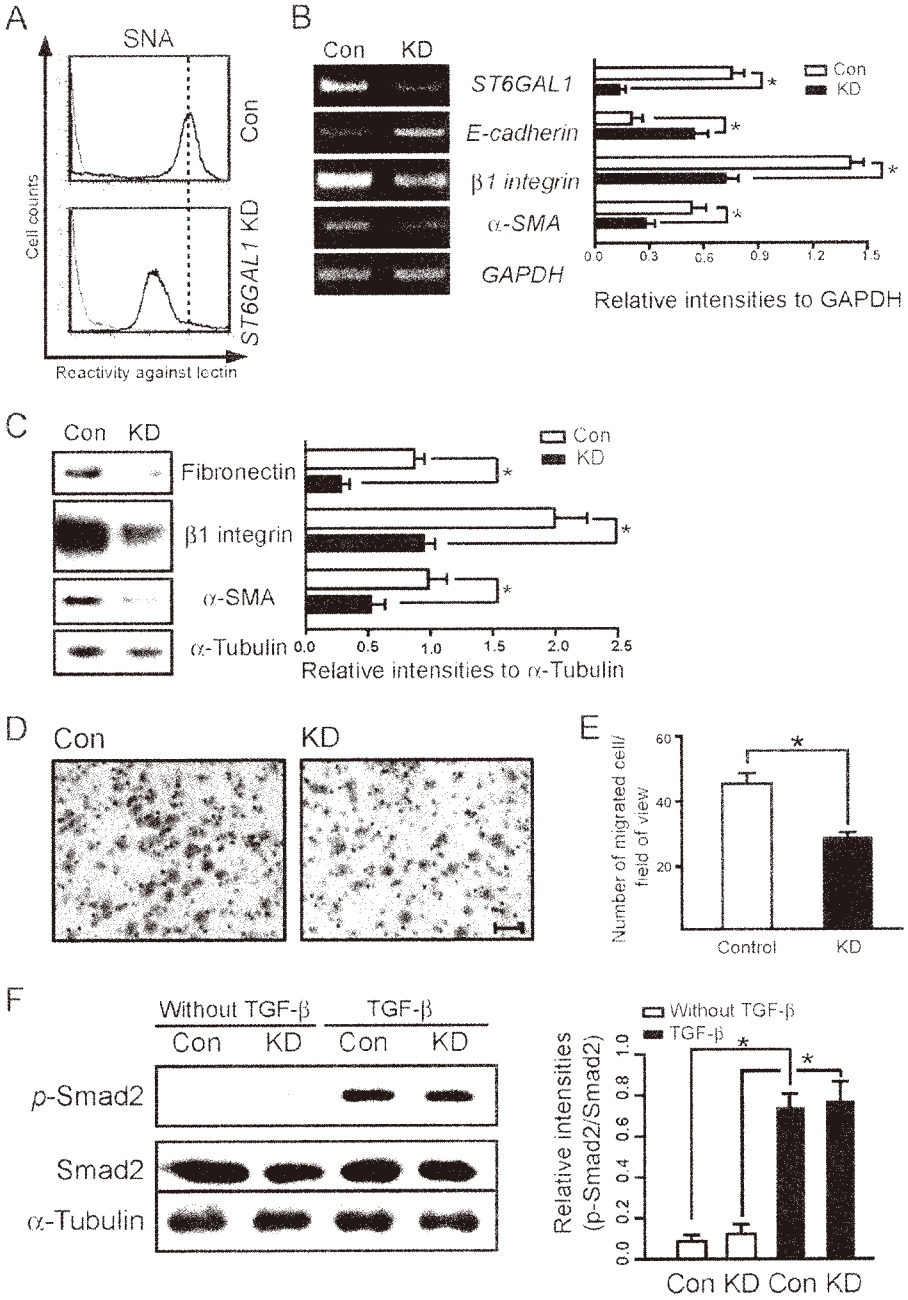

FIGURE 7. **Silencing *ST6GAL1* partially reverses the basal mesenchymal phenotype of MDA-MB-231 cells.** *A*, the indicated cells were collected and incubated with (*heavy line*) or without (*gray shadow*) biotin-conjugated SNA, followed by incubation with streptavidin Alexa Fluor 647 conjugate and subjected to FACS analysis to check the *St6gal1* knockdown efficiency. *B*, RT-PCR was carried out to examine the expression levels of *ST6GAL1*, E-cadherin, β1 integrin, and α-*SMA* in the indicated cells. The expression level of *GAPDH* was used as a loading control. The quantitative data are presented as means ± S.D. from three independent experiments (*, $p < 0.01$ by one-tailed unpaired Student's *t* test). *C*, cell lysates from those cells were immunoblotted (*IB*) with anti-fibronectin, anti-β1 integrin, and anti-α-SMA antibodies. α-Tubulin was used as a loading control. The quantitative data are presented as means ± S.D. from three independent experiments (*, $p < 0.01$ by one-tailed unpaired Student's *t* test). *D*, cell migration toward FN was determined by a transwell assay. A representative example was recorded by phase-contrast microscopy. *Scale bar*, 100 μm. *E*, the migrated cells were counted under a microscope. The quantitative data were obtained from three independent experiments. The *p* values were calculated using a one-tailed unpaired Student's *t* test. *Error bars*, S.D. *, $p < 0.01$. *F*, the indicated cell lysates was immunoblotted by anti-phospho-Smad2 and anti-Smad2 antibodies. α-Tubulin was used as a loading control. The quantitative data are presented as the means ± S.D. from three independent experiments (*, $p < 0.01$ by one-tailed unpaired Student's *t* test).

herin and strongly suppressed TGF-β-induced EMT, as evidenced not only by a prevention of the EMT-associated morphological and molecular changes but also by an inhibition of the TGF-β-mediated stimulation of cell migration. On the other hand, by using the MDA-MB-231 cells as a MET model, we observed that silencing *ST6GAL1* repressed the mesenchymal properties of this aggressive human breast cancer cell line and normalized these cells to an epithelial phenotype, indicating that ST6GAL1 is also important for maintenance of the cell mesenchymal state.

Roles of Sialylation in EMT

Our findings here that silencing of ST6GAL1 significantly inhibited the TGF-β-induced cell migration in GE11 cells as well as MDA-MB-231 cells indicate an important role of ST6GAL1 in the stimulation of cell migration. In line with our observations, much of the literature showed that ST6GAL1 promotes cell migration and invasion during cancer progression (28, 29). The function of ST6GAL1 in promoting cell migration might be partially mediated through affecting galectin-involved signalings because galectin-3 is highly correlated with cancer malignancy by regulating various biological processes (30, 31), and α2,6-sialylation of β1 integrin could impair their interaction with galectin-3, thereby facilitating cell migration (32). On the other hand, accumulating evidence suggested that ST6GAL1 renders the cells resistant to apoptosis. Bellis's group clearly demonstrated that ST6GAL1 serves as a major inhibitor of cell death pathways initiated by Fas, TNFR1, and galectins (14, 15, 33). Additionally, ST6GAL1 has also been shown to confer radiation resistance in colon cancer cell lines (34) as well as multidrug resistance in human acute myeloid leukemia (35). These studies imply that up-regulation of ST6GAL1 in TGF-β-induced EMT may also reduce the apoptosis sensitivity in response to various stimuli, thus extending the cell life span. Clearly, further investigation is needed to support this potential role of ST6GAL1 in EMT.

It is well known that E-cadherin is a major determinant for maintenance of the cell epithelial integrity and plays a crucial role in EMT. Loss of E-cadherin was sufficient to convert A549 NSCLC cells into the mesenchymal type (36). Conversely, forced expression of E-cadherin reversed the EMT in rat kidney fibroblast NRK49f cells (25). Here, we show that knockdown of ST6GAL1 up-regulated the transcription of E-cadherin, and overexpression of ST6GAL1 decreased the retention of cell surface E-cadherin, which provide a possible mechanism by which ST6GAL1 functions in EMT. Although it is difficult to give a plausible explanation for the up-regulated transcription of E-cadherin in ST6GAL1 knockdown cells based on the previous studies, the reduced retention of cell surface E-cadherin in ST6GAL1-overexpressing cells could be caused by the increased α2,6-sialylation of E-cadherin because growing evidence has shown that ST6GAL1 is involved in the cell surface retention of glycoproteins and E-cadherin is its direct substrate (26, 27). On the other hand, TGF-β triggers EMT mainly via the Smad signaling pathway. However, our data show that *St6gal1* knockdown did not affect this major TGF-β-Smad signaling. Instead, it inhibited the activity of the PI3K/Akt signaling cascade. In fact, activation of PI3K/Akt signaling plays a crucial complementary role in elaboration of the EMT process (37, 38). Treatment of cells with chemical inhibitors that selectively or specifically block this pathway dramatically affects the induction of the EMT phenotype. Accordingly, it can be concluded that the effects of ST6GAL1 on EMT induction and cell migration were also mediated through the PI3K/Akt signaling pathway. In agreement with this, several groups, including us, recently reported that ST6GAL1 promotes cell migration and invasion by activating PI3K/Akt signaling (21, 24), and this enhanced migratory response has been shown to be due, at least in part, to ST6GAL1-mediated sialylation of the β1 integrin receptor (19, 39, 40). Nonetheless, the GE11 cell utilized here is a β1 integrin-null cell line. This implies that there exist additional mediator proteins for promoting the cell migratory ability in TGF-β-induced EMT. Given the finding here that *St6gal1* knockdown reduced the fibronectin-mediated cell migration upon TGF-β stimulation, the candidate mediator may exist in fibronectin receptors. Besides α5β1 integrin, αvβ3 and αvβ6 serve as the important receptors for fibronectin as well, and both of them are deeply implicated in the promotion of cancer cell metastasis (41–44). Considering also a growing body of evidence for the cross-talk between αv integrins and TGF-β during EMT (45), it is reasonable to speculate that ST6GAL1 may affect the PI3K/Akt signaling pathway by modulating the sialylation status of αv integrin in GE11 cells. Meanwhile, apart from αv integrin, we could not rule out the possibility of the existence of additional mediators like receptor tyrosine kinases that participate in the PI3K/Akt or other non-Smad signaling transduction, because it has been shown that desialylation of insulin-like growth factor receptor quenches the Akt- and ERK-involved signaling in response to insulin-like growth factor II (46), and recently, overexpression of NEU1, which accounts for 70% of the sialidase activity of epithelial cells, diminished epidermal growth factor (EGF)-stimulated autophosphorylation of EGF receptor (47). Further investigation is obviously needed to elucidate the mechanistic roles of ST6Gal in TGF-β-induced EMT in more detail.

EMT is a complex and multifaceted process that requires a precise regulation of gene expression. Mounting evidence showed that this well orchestrated gene expression in EMT is achieved by the cooperative actions of a number of transcription factors. It has been shown, for instance, that transcription factors Sp1 and Smad form transcriptional complexes at the promoter binding region of vimentin and together regulate the expression of this critical EMT-associated protein (23). Likewise, we find that Sp1 and Smad proteins were also involved in the specific up-regulation of *St6gal1* during TGF-β-induced EMT. However, in contrast to the case of vimentin, in which Sp1 and Smad together act as a switch for vimentin expression, these two transcription factors may function to regulate the *St6gal1* expression independently, because deletion of the putative Smad binding sites within the *St6gal1* promoter only decreased the efficiency of *St6gal1* induction instead of completely abrogating its promoter activity. Recently, Sp1 and Smad proteins have been found to control the expression of tumor suppressor NDRG2 in a similar way during the TGF-β-induced EMT (48). These observations raise the question of how this regulatory strategy of *St6gal1/NDRG2* expression benefits the cells. One possible advantage is that it may favor the precise tuning and regulation of *St6gal1/NDRG2* levels to meet the requirements in different biological scenarios that they participate in. In agreement with this idea, Sp1 elements, but not together with Smad elements, within the human *ST6GAL1* promoter have been shown to be important for efficient transcription of *ST6GAL1* during the HL-60 cell differentiation induced by dimethyl sulfoxide (49). A detailed characterization of the *St6gal1* promoter in a different biological context is required for better understanding of its regulatory mechanisms.

In addition to *St6gal1*, we have previously reported that TGF-β also down-regulates the expression of *N*-acetylglucos-

aminyltransferase III (*Mgat3*), which is responsible for the synthesis of a bisecting *N*-acetylglucosamine (GlcNAc) in *N*-glycan, and up-regulates the expression of *N*-acetylglucosaminyltransferase V (*Mgat5*), which catalyzes the β1,6-GlcNAc branching in *N*-glycan in EMT (20). In fact, the introduction of a bisecting GlcNAc suppresses β1,6-GlcNAc branching formation because MGAT5 cannot utilize the bisected oligosaccharide as an acceptor (50–52), indicating the coordinated regulation of gene expression during EMT. Therefore, given the concomitant enhancement of ST6GAL1 in EMT, it is conceivable that the *N*-glycan structure remodeled by altered expression of MGAT3 and MGAT5 may facilitate (or at least not inhibit) the subsequent ST6GAL1-mediated sialylation. Consistent with this idea, Pinho *et al.* (53) reported that E-cadherin undergoes extensive modification of *N*-glycans with enhanced β1,6-GlcNAc branching and α2,6-sialylation during acquisition of the malignant phenotype in a canine mammary tumor cell line. Additionally, the increase in β1,6-GlcNAc branching and α2,6-sialylation in the mouse serum glycome has been shown to correlate with inflammation and ovarian tumor progression (54). In the past decade, growing evidence has shown that both ST6GAL1 and MGAT5 promote cell migration and invasion (19, 55). Based on the hypothesis above, it is highly possible that the enhanced migratory response of those cells with high expression of ST6GAL1 as well as MGAT5 is due, at least mainly, to the up-regulated α2,6-sialylation, and MGAT5 may act as an important coordinator for a better ST6GAL1-mediated sialylation. In agreement with this corollary hypothesis, we find here that despite the enhancement of MGAT5 expression in EMT in GE11 cells (data not shown), silencing of *St6gal1* almost completely inhibited the increased migratory ability upon TGF-β stimulation. Furthermore, this idea is further supported by a recent study (56) indicating that ST6GAL1 is responsible for the different invasive properties in the murine hepatocarcinoma Hca-F (high metastatic potential) and Hca-P (low metastatic potential) cells, although both *St6gal1* and *Gnt-V* are highly expressed in Hca-F cells as compared with in Hca-P cells.

It is worth noting that overexpression of ST6GAL1, but not ST3GAL4, was found to promote the TGF-β-induced EMT, although both of them catalyze the sialylation of *N*-glycan. This discrepancy in their function in EMT may be attributed to their different effects on the specific glycoproteins. As examples, α2,6-sialylation alters (i) the conformation of β1 integrin (57); (ii) clustering of CD45 (58), EGF receptor (59), and PECAM (27); and (iii) cell surface retention of PECAM (27) and the Fas death receptor (14), whereas little literature showed the involvement of ST3GAL4 in those aspects. Given that both of ST6GAL1 and ST3GAL4 create the sialylation with similar sugar size and negative charge on *N*-glycans, it is tempting to speculate that their different effects on the given glycoprotein may result from the different localization of the sialic acids that they add within the glycoprotein tertiary structure. Although it is difficult to determine due to technical challenges, a comparison of the crystal structure of the ST6GAL1 and ST3GAL1 revealed a significant difference in their glycan acceptor binding regions (60), which provides indirect evidence for the hypothesis above.

Recently, high expression of ST6GAL1 has also been identified in induced pluripotent stem cells and cancer stem cells and correlates with stem cell markers in normal tissues and colon cancer cell lines (61). Considering the emerging evidence that the EMT program may give rise to cancer stem cells or at least cells with stem cell-like properties (62), our research here provides further support for this concept and implies similar mechanistic roles of ST6GAL1 in TGF-β-induced EMT and cancer stem cells. Although these detailed mechanistic roles remain largely unknown, the current study clearly demonstrates the importance of ST6GAL1 in the sufficient induction of TGF-β-induced EMT and highlights the potential for targeting ST6GAL1 in clinical treatment.

Acknowledgments—We are grateful to Prof. K. Nagata and Dr. T. Kumagai (Tohoku Pharmaceutical University) for technical support for the Dual-Luciferase assay.

REFERENCES

1. Tarin, D., Thompson, E. W., and Newgreen, D. F. (2005) The fallacy of epithelial mesenchymal transition in neoplasia. *Cancer Res.* **65,** 5996–6000; discussion 6000–6001
2. Thiery, J. P., and Sleeman, J. P. (2006) Complex networks orchestrate epithelial-mesenchymal transitions. *Nat. Rev. Mol. Cell Biol.* **7,** 131–142
3. Greenburg, G., and Hay, E. D. (1982) Epithelia suspended in collagen gels can lose polarity and express characteristics of migrating mesenchymal cells. *J. Cell Biol.* **95,** 333–339
4. Hay, E. D. (1995) An overview of epithelio-mesenchymal transformation. *Acta Anat.* **154,** 8–20
5. Hugo, H., Ackland, M. L., Blick, T., Lawrence, M. G., Clements, J. A., Williams, E. D., and Thompson, E. W. (2007) Epithelial-mesenchymal and mesenchymal-epithelial transitions in carcinoma progression. *J. Cell. Physiol.* **213,** 374–383
6. Roberts, A. B., and Wakefield, L. M. (2003) The two faces of transforming growth factor β in carcinogenesis. *Proc. Natl. Acad. Sci. U.S.A.* **100,** 8621–8623
7. Kalluri, R., and Weinberg, R. A. (2009) The basics of epithelial-mesenchymal transition. *J. Clin. Invest.* **119,** 1420–1428
8. Valcourt, U., Kowanetz, M., Niimi, H., Heldin, C. H., and Moustakas, A. (2005) TGF-β and the Smad signaling pathway support transcriptomic reprogramming during epithelial-mesenchymal cell transition. *Mol. Biol. Cell* **16,** 1987–2002
9. Derynck, R., and Zhang, Y. E. (2003) Smad-dependent and Smad-independent pathways in TGF-β family signalling. *Nature* **425,** 577–584
10. Wu, G., Chen, Y. G., Ozdamar, B., Gyuricza, C. A., Chong, P. A., Wrana, J. L., Massagué, J., and Shi, Y. (2000) Structural basis of Smad2 recognition by the Smad anchor for receptor activation. *Science* **287,** 92–97
11. Maupin, K. A., Sinha, A., Eugster, E., Miller, J., Ross, J., Paulino, V., Keshamouni, V. G., Tran, N., Berens, M., Webb, C., and Haab, B. B. (2010) Glycogene expression alterations associated with pancreatic cancer epithelial-mesenchymal transition in complementary model systems. *PLoS One* **5,** e13002
12. Tan, Z., Lu, W., Li, X., Yang, G., Guo, J., Yu, H., Li, Z., and Guan, F. (2014) Altered *N*-glycan expression profile in epithelial-to-mesenchymal transition of NMuMG cells revealed by an integrated strategy using mass spectrometry and glycogene and lectin microarray analysis. *J. Proteome Res.* **13,** 2783–2795
13. Li, S., Mo, C., Peng, Q., Kang, X., Sun, C., Jiang, K., Huang, L., Lu, Y., Sui, J., Qin, X., and Liu, Y. (2013) Cell surface glycan alterations in epithelial mesenchymal transition process of Huh7 hepatocellular carcinoma cell. *PLoS One* **8,** e71273
14. Swindall, A. F., and Bellis, S. L. (2011) Sialylation of the Fas death receptor by ST6Gal-I provides protection against Fas-mediated apoptosis in colon carcinoma cells. *J. Biol. Chem.* **286,** 22982–22990

15. Liu, Z., Swindall, A. F., Kesterson, R. A., Schoeb, T. R., Bullard, D. C., and Bellis, S. L. (2011) ST6Gal-I regulates macrophage apoptosis via α2–6 sialylation of the TNFR1 death receptor. *J. Biol. Chem.* **286,** 39654–39662
16. Crespo, H. J., Cabral, M. G., Teixeira, A. V., Lau, J. T., Trindade, H., and Videira, P. A. (2009) Effect of sialic acid loss on dendritic cell maturation. *Immunology* **128,** e621–e631
17. Taniguchi, A., Higai, K., Hasegawa, Y., Utsumi, K., and Matsumoto, K. (1998) Differentiation elicits negative regulation of human β-galactoside α2,6-sialyltransferase at the mRNA level in the HL-60 cell line. *FEBS Lett.* **441,** 191–194
18. Büll, C., Boltje, T. J., Wassink, M., de Graaf, A. M., van Delft, F. L., den Brok, M. H., and Adema, G. J. (2013) Targeting aberrant sialylation in cancer cells using a fluorinated sialic acid analog impairs adhesion, migration, and *in vivo* tumor growth. *Mol. Cancer Ther.* **12,** 1935–1946
19. Seales, E. C., Jurado, G. A., Brunson, B. A., Wakefield, J. K., Frost, A. R., and Bellis, S. L. (2005) Hypersialylation of β1 integrins, observed in colon adenocarcinoma, may contribute to cancer progression by up-regulating cell motility. *Cancer Res.* **65,** 4645–4652
20. Xu, Q., Isaji, T., Lu, Y., Gu, W., Kondo, M., Fukuda, T., Du, Y., and Gu, J. (2012) Roles of *N*-acetylglucosaminyltransferase III in epithelial-to-mesenchymal transition induced by transforming growth factor β1 (TGF-β1) in epithelial cell lines. *J. Biol. Chem.* **287,** 16563–16574
21. Isaji, T., Im, S., Gu, W., Wang, Y., Hang, Q., Lu, J., Fukuda, T., Hashii, N., Takakura, D., Kawasaki, N., Miyoshi, H., and Gu, J. (2014) An oncogenic protein Golgi phosphoprotein 3 up-regulates cell migration via sialylation. *J. Biol. Chem.* **289,** 20694–20705
22. Ranjan, A., and Kalraiya, R. D. (2013) α2,6 sialylation associated with increased β1,6-branched *N*-oligosaccharides influences cellular adhesion and invasion. *J. Biosci.* **38,** 867–876
23. Jungert, K., Buck, A., von Wichert, G., Adler, G., König, A., Buchholz, M., Gress, T. M., and Ellenrieder, V. (2007) Sp1 is required for transforming growth factor-β-induced mesenchymal transition and migration in pancreatic cancer cells. *Cancer Res.* **67,** 1563–1570
24. Zhao, Y., Li, Y., Ma, H., Dong, W., Zhou, H., Song, X., Zhang, J., and Jia, L. (2014) Modification of sialylation mediates the invasive properties and chemosensitivity of human hepatocellular carcinoma. *Mol. Cell Proteomics* **13,** 520–536
25. Zheng, G., Lyons, J. G., Tan, T. K., Wang, Y., Hsu, T. T., Min, D., Succar, L., Rangan, G. K., Hu, M., Henderson, B. R., Alexander, S. I., and Harris, D. C. (2009) Disruption of E-cadherin by matrix metalloproteinase directly mediates epithelial-mesenchymal transition downstream of transforming growth factor-β1 in renal tubular epithelial cells. *Am. J. Pathol.* **175,** 580–591
26. Cha, S. K., Ortega, B., Kurosu, H., Rosenblatt, K. P., Kuro-O, M., and Huang, C. L. (2008) Removal of sialic acid involving Klotho causes cell-surface retention of TRPV5 channel via binding to galectin-1. *Proc. Natl. Acad. Sci. U.S.A.* **105,** 9805–9810
27. Kitazume, S., Imamaki, R., Ogawa, K., Komi, Y., Futakawa, S., Kojima, S., Hashimoto, Y., Marth, J. D., Paulson, J. C., and Taniguchi, N. (2010) α2,6-Sialic acid on platelet endothelial cell adhesion molecule (PECAM) regulates its homophilic interactions and downstream antiapoptotic signaling. *J. Biol. Chem.* **285,** 6515–6521
28. Zhu, Y., Srivatana, U., Ullah, A., Gagneja, H., Berenson, C. S., and Lance, P. (2001) Suppression of a sialyltransferase by antisense DNA reduces invasiveness of human colon cancer cells *in vitro*. *Biochim. Biophys. Acta* **1536,** 148–160
29. Lin, S., Kemmner, W., Grigull, S., and Schlag, P. M. (2002) Cell surface α2,6 sialylation affects adhesion of breast carcinoma cells. *Exp. Cell Res.* **276,** 101–110
30. Partridge, E. A., Le Roy, C., Di Guglielmo, G. M., Pawling, J., Cheung, P., Granovsky, M., Nabi, I. R., Wrana, J. L., and Dennis, J. W. (2004) Regulation of cytokine receptors by Golgi *N*-glycan processing and endocytosis. *Science* **306,** 120–124
31. de Oliveira, J. T., de Matos, A. J., Santos, A. L., Pinto, R., Gomes, J., Hespanhol, V., Chammas, R., Manninen, A., Bernardes, E. S., Albuquerque Reis, C., Rutteman, G., and Gärtner, F. (2011) Sialylation regulates galectin-3/ligand interplay during mammary tumour progression: a case of targeted uncloaking. *Int. J. Dev. Biol.* **55,** 823–834
32. Zhuo, Y., Chammas, R., and Bellis, S. L. (2008) Sialylation of β1 integrins blocks cell adhesion to galectin-3 and protects cells against galectin-3-induced apoptosis. *J. Biol. Chem.* **283,** 22177–22185
33. Zhuo, Y., and Bellis, S. L. (2011) Emerging role of α2,6-sialic acid as a negative regulator of galectin binding and function. *J. Biol. Chem.* **286,** 5935–5941
34. Lee, M., Lee, H. J., Bae, S., and Lee, Y. S. (2008) Protein sialylation by sialyltransferase involves radiation resistance. *Mol Cancer Res.* **6,** 1316–1325
35. Ma, H., Zhou, H., Song, X., Shi, S., Zhang, J., and Jia, L. (2014) Modification of sialylation is associated with multidrug resistance in human acute myeloid leukemia. *Oncogene* 10.1038/onc.2014.7
36. Bae, G. Y., Choi, S. J., Lee, J. S., Jo, J., Lee, J., Kim, J., and Cha, H. J. (2013) Loss of E-cadherin activates EGFR-MEK/ERK signaling, which promotes invasion via the ZEB1/MMP2 axis in non-small cell lung cancer. *Oncotarget* **4,** 2512–2522
37. Bakin, A. V., Tomlinson, A. K., Bhowmick, N. A., Moses, H. L., and Arteaga, C. L. (2000) Phosphatidylinositol 3-kinase function is required for transforming growth factor β-mediated epithelial to mesenchymal transition and cell migration. *J. Biol. Chem.* **275,** 36803–36810
38. Kattla, J. J., Carew, R. M., Heljic, M., Godson, C., and Brazil, D. P. (2008) Protein kinase B/Akt activity is involved in renal TGF-β1-driven epithelial-mesenchymal transition *in vitro* and *in vivo*. *Am. J. Physiol. Renal Physiol* **295,** F215–F225
39. Christie, D. R., Shaikh, F. M., Lucas, J. A., 4th, Lucas, J. A., 3rd, and Bellis, S. L. (2008) ST6Gal-I expression in ovarian cancer cells promotes an invasive phenotype by altering integrin glycosylation and function. *J. Ovarian Res.* **1,** 3
40. Shaikh, F. M., Seales, E. C., Clem, W. C., Hennessy, K. M., Zhuo, Y., and Bellis, S. L. (2008) Tumor cell migration and invasion are regulated by expression of variant integrin glycoforms. *Exp. Cell Res.* **314,** 2941–2950
41. Chen, Q., Manning, C. D., Millar, H., McCabe, F. L., Ferrante, C., Sharp, C., Shahied-Arruda, L., Doshi, P., Nakada, M. T., and Anderson, G. M. (2008) CNTO 95, a fully human anti αv integrin antibody, inhibits cell signaling, migration, invasion, and spontaneous metastasis of human breast cancer cells. *Clin. Exp. Metastasis* **25,** 139–148
42. Thomas, G. J., Lewis, M. P., Hart, I. R., Marshall, J. F., and Speight, P. M. (2001) αVβ6 integrin promotes invasion of squamous carcinoma cells through up-regulation of matrix metalloproteinase-9. *Int. J. Cancer* **92,** 641–650
43. Thomas, G. J., Lewis, M. P., Whawell, S. A., Russell, A., Sheppard, D., Hart, I. R., Speight, P. M., and Marshall, J. F. (2001) Expression of the alphav-beta6 integrin promotes migration and invasion in squamous carcinoma cells. *J. Invest. Dermatol.* **117,** 67–73
44. Sloan, E. K., Pouliot, N., Stanley, K. L., Chia, J., Moseley, J. M., Hards, D. K., and Anderson, R. L. (2006) Tumor-specific expression of αvβ3 integrin promotes spontaneous metastasis of breast cancer to bone. *Breast Cancer Res.* **8,** R20
45. Mamuya, F. A., and Duncan, M. K. (2012) aV integrins and TGF-β-induced EMT: a circle of regulation. *J. Cell Mol. Med.* **16,** 445–455
46. Hinek, A., Bodnaruk, T. D., Bunda, S., Wang, Y., and Liu, K. (2008) Neuraminidase-1, a subunit of the cell surface elastin receptor, desialylates and functionally inactivates adjacent receptors interacting with the mitogenic growth factors PDGF-BB and IGF-2. *Am. J. Pathol.* **173,** 1042–1056
47. Lillehoj, E. P., Hyun, S. W., Feng, C., Zhang, L., Liu, A., Guang, W., Nguyen, C., Luzina, I. G., Atamas, S. P., Passaniti, A., Twaddell, W. S., Puché, A. C., Wang, L. X., Cross, A. S., and Goldblum, S. E. (2012) NEU1 sialidase expressed in human airway epithelia regulates epidermal growth factor receptor (EGFR) and MUC1 protein signaling. *J. Biol. Chem.* **287,** 8214–8231
48. Shen, L., Qu, X., Ma, Y., Zheng, L., Chu, D., Liu, B., Li, X., Wang, M., Xu, C., Liu, N., Yao, L., and Zhang, L. (2014) Tumor suppressor NDRG2 tips the balance of oncogenic TGF-β via EMT inhibition in colorectal cancer. *Oncogenesis* **3,** e86
49. Taniguchi, A., Hasegawa, Y., Higai, K., and Matsumoto, K. (2000) Transcriptional regulation of human β-galactoside α2, 6-sialyltransferase (hST6Gal I) gene during differentiation of the HL-60 cell line. *Glycobiology* **10,** 623–628

50. Gu, J., Nishikawa, A., Tsuruoka, N., Ohno, M., Yamaguchi, N., Kangawa, K., and Taniguchi, N. (1993) Purification and characterization of UDP-*N*-acetylglucosamine: α-6-D-mannoside β 1–6*N*-acetylglucosaminyltransferase (*N*-acetylglucosaminyltransferase V) from a human lung cancer cell line. *J. Biochem.* **113,** 614–619
51. Schachter, H. (1986) Biosynthetic controls that determine the branching and microheterogeneity of protein-bound oligosaccharides. *Adv. Exp. Med. Biol.* **205,** 53–85
52. Schachter, H., Narasimhan, S., Gleeson, P., and Vella, G. (1983) Control of branching during the biosynthesis of asparagine-linked oligosaccharides. *Can. J. Biochem. Cell Biol.* **61,** 1049–1066
53. Pinho, S. S., Osório, H., Nita-Lazar, M., Gomes, J., Lopes, C., Gärtner, F., and Reis, C. A. (2009) Role of E-cadherin *N*-glycosylation profile in a mammary tumor model. *Biochem. Biophys. Res. Commun.* **379,** 1091–1096
54. Saldova, R., Piccard, H., Pérez-Garay, M., Harvey, D. J., Struwe, W. B., Galligan, M. C., Berghmans, N., Madden, S. F., Peracaula, R., Opdenakker, G., and Rudd, P. M. (2013) Increase in sialylation and branching in the mouse serum *N*-glycome correlates with inflammation and ovarian tumour progression. *PLoS One* **8,** e71159
55. Granovsky, M., Fata, J., Pawling, J., Muller, W. J., Khokha, R., and Dennis, J. W. (2000) Suppression of tumor growth and metastasis in Mgat5-deficient mice. *Nat. Med.* **6,** 306–312
56. Zhang, Z., Sun, J., Hao, L., Liu, C., Ma, H., and Jia, L. (2013) Modification of glycosylation mediates the invasive properties of murine hepatocarcinoma cell lines to lymph nodes. *PLoS One* **8,** e65218
57. Woodard-Grice, A. V., McBrayer, A. C., Wakefield, J. K., Zhuo, Y., and Bellis, S. L. (2008) Proteolytic shedding of ST6Gal-I by BACE1 regulates the glycosylation and function of α4β1 integrins. *J. Biol. Chem.* **283,** 26364–26373
58. Amano, M., Galvan, M., He, J., and Baum, L. G. (2003) The ST6Gal I sialyltransferase selectively modifies *N*-glycans on CD45 to negatively regulate galectin-1-induced CD45 clustering, phosphatase modulation, and T cell death. *J. Biol. Chem.* **278,** 7469–7475
59. Liu, Y. C., Yen, H. Y., Chen, C. Y., Chen, C. H., Cheng, P. F., Juan, Y. H., Chen, C. H., Khoo, K. H., Yu, C. J., Yang, P. C., Hsu, T. L., and Wong, C. H. (2011) Sialylation and fucosylation of epidermal growth factor receptor suppress its dimerization and activation in lung cancer cells. *Proc. Natl. Acad. Sci. U.S.A.* **108,** 11332–11337
60. Meng, L., Forouhar, F., Thieker, D., Gao, Z., Ramiah, A., Moniz, H., Xiang, Y., Seetharaman, J., Milaninia, S., Su, M., Bridger, R., Veillon, L., Azadi, P., Kornhaber, G., Wells, L., Montelione, G. T., Woods, R. J., Tong, L., and Moremen, K. W. (2013) Enzymatic basis for *N*-glycan sialylation: structure of rat α2,6-sialyltransferase (ST6GAL1) reveals conserved and unique features for glycan sialylation. *J. Biol. Chem.* **288,** 34680–34698
61. Swindall, A. F., Londoño-Joshi, A. I., Schultz, M. J., Fineberg, N., Buchsbaum, D. J., and Bellis, S. L. (2013) ST6Gal-I protein expression is upregulated in human epithelial tumors and correlates with stem cell markers in normal tissues and colon cancer cell lines. *Cancer Res.* **73,** 2368–2378
62. Mani, S. A., Guo, W., Liao, M. J., Eaton, E. N., Ayyanan, A., Zhou, A. Y., Brooks, M., Reinhard, F., Zhang, C. C., Shipitsin, M., Campbell, L. L., Polyak, K., Brisken, C., Yang, J., and Weinberg, R. A. (2008) The epithelial-mesenchymal transition generates cells with properties of stem cells. *Cell* **133,** 704–715

β-Galactoside α2,6-Sialyltranferase 1 Promotes Transforming Growth Factor-β -mediated Epithelial-Mesenchymal Transition

Jishun Lu, Tomoya Isaji, Sanghun Im, Tomohiko Fukuda, Noritaka Hashii, Daisuke Takakura, Nana Kawasaki and Jianguo Gu

J. Biol. Chem. 2014, 289:34627-34641.
doi: 10.1074/jbc.M114.593392 originally published online October 24, 2014

THE JOURNAL OF BIOLOGICAL CHEMISTRY VOL. 289, NO. 30, pp. 20694–20705, July 25, 2014

An Oncogenic Protein Golgi Phosphoprotein 3 Up-regulates Cell Migration via Sialylation*

Received for publication, December 12, 2013, and in revised form, May 22, 2014 Published, JBC Papers in Press, June 3, 2014, DOI 10.1074/jbc.M113.542688

Tomoya Isaji[‡], Sanghun Im[‡], Wei Gu[‡], Yuqin Wang[‡], Qinglei Hang[‡], Jishun Lu[‡], Tomohiko Fukuda[‡], Noritaka Hashii[§], Daisuke Takakura[§], Nana Kawasaki[§], Hiroyuki Miyoshi[¶], and Jianguo Gu[‡1]

From the [‡]Division of Regulatory Glycobiology, Institute of Molecular Biomembrane and Glycobiology, Tohoku Pharmaceutical University, Sendai, Miyagi 981-8558, [§]National Institute of Health Sciences, Setagaya, Tokyo 158-0098, and [¶]RIKEN BioResource Center, Tsukuba, Ibaraki 305-0074, Japan

Background: Molecular mechanisms of the effect of the GOLPH3 oncogenic protein on tumorigenesis remain unclear.
Results: GOLPH3 specifically up-regulates sialylation of integrin *N*-glycans, promotes sialylation-dependent cell migration, and affects AKT signaling.
Conclusion: GOLPH3 affects cell biological functions through a specific regulation of sialylation.
Significance: The sialylation of *N*-glycans is important for functions of GOLPH3.

Recently, the Golgi phosphoprotein 3 (GOLPH3) and its yeast homolog Vps74p have been characterized as essential for the Golgi localization of glycosyltransferase in yeast. GOLPH3 has been identified as a new oncogene that is commonly amplified in human cancers to modulate mammalian target of rapamycin signaling. However, the molecular mechanisms of the carcinogenic signaling pathway remain largely unclear. To investigate whether the expression of GOLPH3 was involved in the glycosylation processes in mammalian cells, and whether it affected cell behavior, we performed a loss-of-function study. Cell migration was suppressed in GOLPH3 knockdown (KD) cells, and the suppression was restored by a re-introduction of the *GOLPH3* gene. HPLC and LC/MS analysis showed that the sialylation of *N*-glycans was specifically decreased in KD cells. The specific interaction between sialyltransferases and GOLPH3 was important for the sialylation. Furthermore, overexpression of α2,6-sialyltransferase-I rescued cell migration and cellular signaling, both of which were blocked in GOLPH3 knockdown cells. These results are the first direct demonstration of the role of GOLPH3 in *N*-glycosylation to regulate cell biological functions.

Protein glycosylation is one of the most prevalent forms of post-translational modification, and altered glycosylation is a hallmark feature of cancers (1). Integrin is one of the major carriers of *N*-glycans in its governing of cell migration, proliferation, and differentiation (2). Integrin-mediated biological functions such as cell spreading and cell migration can be modulated as a consequence of an aberrant change in the *N*-glycosylation of integrins, which is often associated with the metastatic process. A series of studies (including by our group) have reported that alterations in the oligosaccharide portion of integrins that are modulated by the expression of each glycosyltransferase gene, such as *N*-acetylglucosaminyltransferases III (GnT[2]-III, also called MGAT3) and V (GnT-V, also called MGAT5), as well as by sialyltransferases, regulate cell malignant phenotypes such as integrin-mediated cell migration and cell spreading. For example, the expressions of GnT-V and β1,6-branched *N*-glycan levels are increased in highly metastatic tumor cell lines (3, 4), which enhances integrin-mediated cell migration. In contrast to GnT-V, the overexpression of GnT-III blocks branched *N*-glycan and results in an inhibition of integrin-mediated cell spreading and migration as well as in the phosphorylation of the focal adhesion kinase, thereby contributing to the suppression of cancer metastasis (5, 6).

Besides the branched *N*-glycans, the terminal sialic acids are believed to be common cancer-associated carbohydrate modifications (7). Sialic acids also are believed to be essential for the early development of vertebrates (8). Enhanced expression of α2,6-linked sialylation on *N*-glycans often correlates with human cancer progression, metastatic spread, a poor prognosis, and stem cell markers (7, 9, 10). Increased expression has been reported in carcinomas of the colon (11), breast (12), cervix (13), and ovary (9) and in some brain tumors (14). The expression level of the α2,6-sialyltransferase-I (*ST6GAL1*) gene is up-regulated by the Ras oncogene (15, 16). However, the molecular mechanism for the post-translational regulation of sialylations in cancer cells remains unclear.

The increased α2,6-linked sialylation on β1-integrins also has been reported in several transformed cell types and is postulated to alter integrin function by enhancing its activation state and binding to collagen (17–19). In these studies, increases in α2,6-linked

* This work was supported in part by Grants-in-aid for Scientific Research 21370059 (to J. G.) and 24570169 (to T. I.), Challenging Exploratory Research 23651196 (to J. G.) from the Japan Society for the Promotion of Science, Grants from the Scientific Research on Innovative Areas 23110002 (to J. G.), the Strategic Research Foundation Grant-aided Project for Private Universities from the Ministry of Education, Culture, Sports, Science and Technology of Japan, and The Mizutani Foundation for Glycoscience.
[1] To whom correspondence should be addressed. Tel.: 81-22-727-0216; Fax: 81-22-727-0078; E-mail: jgu@tohoku-pharm.ac.jp.

[2] The abbreviations used are: GnT, *N*-acetylglucosaminyltransferase; GCNT1, glucosaminyl(*N*-acetyl)transferase 1; FN, fibronectin; β4GALT1, β1,4-galactosyltransferase I; GOLPH3, Golgi phosphoprotein 3; MAM, *Maackia amurensis*; mTOR, mammalian target of rapamycin; PI4P, phosphatidylinositol 4-phosphate; ST6GAL1, α2,6-sialyltransferase-I; ST3GAL4, α-2,3-sialyltransferase-IV; EGFR, epidermal growth factor receptor; PA-*N*-glycan, pyridylaminated *N*-glycan; ANOVA, analysis of variance; FN, fibronectin; RCA-I, *R. communis* agglutinin I; FT, Fourier transform; ECM, extracellular matrix.

sialylation levels have been correlated with enhanced cell motility and invasiveness *in vitro*. Furthermore, the role of ST6GAL1 enzyme has been confirmed in *in vivo* growth and differentiation, for which β1-integrin function is important for tumorigenesis and in maintaining the proliferative state of tumor cells (20). Thus, the state of the *N*-glycans of integrin plays important roles in a poor prognosis for cancer, such as cell-cell adhesion, cell-extracellular matrix interaction, epithelial-mesenchymal transition, and metastatic ability.

Most of the glycosylation reactions happen in the Golgi apparatus. Recently, a Golgi phosphoprotein 3 (GOLPH3) was identified as an oncogenic protein in human solid tumors such as lung cancer, breast cancer, colon cancer, and melanoma, localized on the peripheral membrane of the trans-Golgi network and modulating a mammalian target of rapamycin (mTOR) signaling (21), budding of vesicles from the trans-Golgi, and recycling of transmembrane receptors (22). It is worth noting that the expression levels of GOLPH3 are highly related to the clinical stages of breast (23), esophageal (24), and lung (21) cancers and glioblastoma (25). The homolog of yeast GOLPH3, VSP74, is reportedly involved in the retention of mannosyltransferases at the Golgi, knockout of which results in the production of hypoglycosylated proteins (26). Recently, Ali *et al.* (27) reported that GOLPH3 regulates the Golgi retention of the *O*-glycan synthesis enzyme, core2 glucosaminyl(*N*-acetyl)transferase 1 (GCNT1), in mammalian cells because it has a similar sequence to the yeast's mannosyltransferases that are present in the cytoplasmic tail. However, the effects of GOLPH3 on *N*-glycanosylation remain mostly unclear.

In this study, we performed a knockdown and restoration of the *GOLPH3* gene in mammalian cells to investigate the effects of GOLPH3 on *N*-glycanosylation and its related biological functions. We found that GOLPH3 specially regulates sialylation of *N*-glycans and integrin-mediated cell migration, which may provide new insight into the functions of GOLPH3 in cancer.

EXPERIMENTAL PROCEDURES

Reagents and Antibodies—All reagents used were from Sigma and Nacalai Tesque, unless otherwise stated. The following antibodies were used: monoclonal antibodies against α5 (610634) and β1 (610468) from BD Biosciences; monoclonal antibody against α-tubulin (Sigma, T6199), β1 integrin for immunoprecipitation (TS2/16, ATCC); FACS or functional blocking (P5D2, DSHB); HA (Roche Applied Science, 1867423); antibody against FLAG for immunoblot (Sigma, F1804); immunoprecipitation (Sigma, A2220); polyclonal antibody against GOLPH3 (Abcam, ab82377); α3 integrin (Santa Cruz Biotechnology, Sc-6592); polyclonal antibody against EGFR (2232); AKT (9272); and monoclonal antibody against pAKT Ser-473 (4060) from Cell Signaling. Human EGF was purchased from PeproTech (AF-100).

Cell Lines and Cell Culture—The HeLa and 293T cells were provided from RIKEN Cell Bank (Japan). The Phoenix cells and MDA-MB231 cells were purchased from ATCC. All cell lines were maintained at 37 °C in Dulbecco's modified Eagle's medium (DMEM), supplemented with 10% fetal bovine serum (FBS), 100 units/ml penicillin G, and 0.1 mg/ml streptomycin, under a humidified atmosphere containing 5% CO_2, except for the virus production.

Knockdown Experiments—For small interfering RNA (siRNA) experiments, nontarget siRNA (D-001210-01-05, Dharmacon) and targeting *GOLPH3* siRNA (D-006414-03, Dharmacon) were transfected into HeLa cells by Lipofectamine 2000 (Invitrogen). For expressing short hairpin RNA, two vectors were used. One is pSUPER.retro.puro, which is a constitutive knockdown retrovirus vector. Another is CS-RfA-ETBsd (30) tetracycline-inducible knockdown lentivirus vector. Inserted oligonucleotide sequences were listed as follows: constitutive shRNA against *GOLPH3*, 5′-GATCCCCGAGAGGAAGGTTACAACTATTCAAGAGATAGTTGTAACCTTCCTCTCTTTTTC-3′ and 5′-TCAGAAAAAGAGAGGAAGGTTACAACTATCTCTTGAATAGTTGTAACCTTCCTCTCGGG-3′; control shRNA, 5′-GATCCCCTAGCGACTAAACACATCAATTCAAGAGATTGATGTGTTTAGTCGCTATTTTTC-3′ and 5′-TCAGAAAAATAGCGACTAAACACATCAATCTCTTGAATTGATGTGTTTAGTCGCTAGGG-3′; Tet-inducible shRNA against *GOLPH-292*, 5′-CACCGCATTGAGAGGAAGGTTACAATGATATGTGCATTGTAACCTTCCTCTCAATGCC-3′ and 5′-AAAAGGCATTGAGAGGAAGGTTACAATGCACATATCATTGTAACCTTCCTCTCAATGC-3′; and Tet-inducible shRNA against *GOLPH3-442*, 5′-CACCACGGTCCAGAACTGGATTGAATGATATGTGCATTCAATCCAGTTCTGGACCGT-3′ and 5′-AAAAACGGTCCAGAACTGGATTGAATGCACATATCATTCAATCCAGTTCTGGACCGT-3′. The production and infection of retro- and lentivirus were described under "Virus Infections."

Construction of cDNA and Expression Vectors—We used the Gateway™ cloning system from Invitrogen for all overexpression experiments. The Gateway™ entry vectors were constructed as follows. The cDNA of HA-tagged *GOLPH3* (a generous gift from Dr. Lynda Chin, Institute for Applied Cancer Science, University of Texas MD Anderson Cancer Center) (21) and HA-tagged, shRNA resistance *GOLPH3* were cloned by standard PCR protocols, into pENTR/D-TOPO (Invitrogen). The overlap extension PCRs were used to construct GOLPH3 mutants, which lacks a tetramer formation (Δ190–201) (28) or the binding to PI4P (R171A/R174A and W81A/R90A) (29). The cDNAs of human α2,3-sialyltransferase-IV (*ST3GAL4*), *ST6GAL1*, and β1,4-galactosyltransferase I (*β4GALT1*) (kindly provided by Dr. H. Narimatsu from National Institute of Advanced Industrial Science and Technology, Japan) were inserted into pENTR 1A tagged with 3×FLAG at the C terminus using the in-fusion method (Takara Bio). The overlap extension PCRs were utilized to construct the chimeric mutants (ST3GAL4(1–7) + β4GALT1(31–398) + 3×FLAG; β4GALT1(1–30) + ST3GAL4(8–360) + 3×FLAG; and ST6GAL1(1–16) + β4GALT1(24–398) + 3×FLAG) as illustrated in Fig. 5*A*, and ST6GAL1(1–113)-GFP replaced the catalytic domain of ST6GAL1 with GFP as reported previously (30). The resultant cDNAs in entry vectors were confirmed by DNA sequencing. The CSIV-TRE-RfA-CMV-KT lentiviral vector was constructed by replacement of the EF promoter with CMV in CSIV-TRE-RfA-EF-KT vector (31, 32) The expression vectors pEF puro-RfA and pcDNA3.1-RfA were constructed using the Gateway conversion kit (Invitrogen). Using LR clonase (Invitrogen), the subcloned cDNAs in entry vectors were transferred into pcDNA3.1-RfA for transient expression, CSIV-TRE-RfA-CMV-KT for the tetracycline inducible overexpression, and

TABLE 1
A combination of expression vectors in each experiment

Experiments	Knockdown	Overexpression
Fig. 1, *A* and *B*	siRNA[a]	
Fig. 1*C*	pSUPER.retro.puro[b]	
Fig. 2	pSUPER.retro.puro[b]	
Fig. 3, *A–C*	pSUPER.retro.puro[b]	pBABE hygro-RfA
Fig. 3, *D*, *E*, and *I–K*	CS-RfA-ETBsd[c]	CSIV-TRE-RfA-CMV-KT
Fig. 3, *F–H*	CS-RfA-ETBsd[c]	
Fig. 3*L*		CSIV-TRE-RfA-CMV-KT
Fig. 4*A*	siRNA[a]	CSIV-TRE-RfA-CMV-KT
Fig. 4*B*	siRNA[a]	CSIV-TRE-RfA-CMV-KT
Fig. 4, *C* and *D*	CS-RfA-ETBsd[c]	CSIV-TRE-RfA-CMV-KT
Fig. 5, *B* and *C*		pcDNA3.1-RfA
Fig. 5*D*	CS-RfA-ETBsd[c]	CSIV-TRE-RfA-CMV-KT
Fig. 5*E*	CS-RfA-ETBsd[c]	pEF puro RfA

[a] Nontarget siRNA or siRNA targeting GOLPH3 is shown.
[b] pSUPER.retro.puro containing shRNA against GOLPH3 or control is shown.
[c] CS-RfA-ETBsd containing Tet-inducible shRNA against GOLPH3 is shown.

pBABE hygro-RfA (33) or pEF puro-RfA for the stable expression. A combination of each vector with each experiment was summarized in Table 1.

Virus Infections—Viral infection was performed as described previously (33, 34). In brief, the lentivirus vectors (CSIV-TRE-RfA-CMV-KT or CS-RfA-ETBsd) were transfected into 293T cells with packaging plasmids by calcium phosphate. The pBABE hygro-RfA or pSUPER.retro.puro were transfected into Phoenix cells for the retrovirus. The target cells were cultured for 24 h to obtain virus media for infection. After infection for 72 h, cells were selected by the FACSAria II (BD Biosciences) to obtain Kusabira Orange-positive cells (CSIV-TRE-RfA-CMV-KT) or selected by puromycin (pSUPER.retro.puro), blasticidin (CS-RfA-ETBsd), or hygromycin (pBABE-hygro-RfA) to get resistant cells against these antibiotics.

Immunoprecipitation and Western Blot—Immunoprecipitation was performed as described previously with minor modifications (5, 33, 35). Briefly, cells were rinsed twice with ice-cold PBS. For β1 integrin, cells were solubilized in lysis buffer (20 mM Tris-HCl, pH 7.4, 150 mM NaCl, 1% Triton X-100), including protease and phosphatase inhibitors (Nacalai Tesque, Kyoto, Japan). The protein contents of lysates were determined by BCA assay (Pierce). The cell lysates were immunoprecipitated with anti-β1 antibody (TS2/16, Cell Resource Center for Biomedical Research, Tohoku University) and Ab-Capcher Protein A-R28 (Protenova, Tokushima, Japan) for 1 h at 4 °C with rotation, and then the immunocomplexes were washed. The immunoprecipitates were then treated with either neuraminidase (Seikagaku Corp., Tokyo, Japan) or *N*-glycosidase F (New England Biolabs, Beverly, MA) according to the manufacturer's instructions. Digested immunoprecipitates were then subjected to SDS-PAGE, and the separated proteins were transferred to a PVDF membrane (Millipore) and detected with anti-β1 antibody and anti-mouse IgG-conjugated HRP (Chemicon) using an Immobilon Western chemiluminescent HRP substrate (Millipore). For the association between glycosyltransferase and GOLPH3, cells were lysed with IP buffer (20 mM Tris-HCl, pH 7.4, 150 mM NaCl, 0.1% Triton X-100) that included protease inhibitors and were immunoprecipitated with FLAG-agarose. The immunocomplexes were washed with 20 mM Tris-HCl, 150 mM NaCl and were then subjected to SDS-PAGE, and the separated proteins were transferred to PVDF. The membrane was incubated using antibodies against FLAG, HA, or GOLPH3 and HRP-labeled secondary antibodies (anti-mouse, rat or rabbit IgG; Cell Signaling) for detection. The lectin precipitations were performed using either *Sambucus sieboldiana* agglutinin (SSA)-agarose (J-OILMILLS, J318) or *Maackia amurensis* agglutinin (MAM)-agarose (J-OILMILLS, J310), which specifically recognizes α2,6- or α2,3-sialylation, respectively. The precipitated glycoproteins were detected using either anti-α5, α3, β1 integrin. or EGFR antibody.

Cell Migration—Each Transwell (BD BioCoat™ control inserts, 8.0-μm inserts; BD Biosciences) was coated only on the bottom side with 10 μg/ml FN at 37 °C for 1 h. Cells were trypsinized, and the trypsin was neutralized with 1 μg/ml soybean trypsin inhibitor, and cells were resuspended in DMEM. The suspended cells were centrifuged, and the cell pellets were resuspended in an assay medium (0.1% BSA in DMEM containing 3% FBS) and diluted to 2×10^6 cells/ml; cell viabilities were confirmed by trypan blue staining. Cell suspensions of 500-μl aliquots were added to each FN-coated transwell, followed by incubation at 37 °C for 6 h for HeLa cells and 3 h for MDA-MB231 cells. After incubation, cells on the upper side were removed by scraping with a cotton swab. The membranes in the transwells were fixed with 4% paraformaldehyde and stained with 0.5% crystal violet for 30 min. Cells that had migrated to the lower side were counted using a phase-contrast microscope.

Video Microscope—A glass-bottom dish (Asahi Techno Glass, Japan) was precoated with 1 μg/ml LN-332 (36) (a precious gift from Dr. K. Miyazaki, Yokohama City University, Japan) and then blocked with 1% BSA for 1 h at 37 °C. A 200-μl aliquot of the cell suspension (4×10^4 cells/ml) in growth medium was added to each LN-332-precoated glass-bottom dish. Cell migration was monitored for 8 h using time-lapse video equipment (Carl Zeiss, Germany). After incubation for 1 h, images and movies were acquired using inverted microscopes (Axio Observer.D1, Carl Zeiss) every 5 min at 37 °C with 5% CO_2 in a heated chamber with temperature and CO_2 controller (Onpu-4 & CO2, Air Brown, Japan) during time-lapse imaging. Cell migration was evaluated using Axio Vision Rel. 4.7 (Carl Zeiss).

Preparation of Pyridylaminated N-Linked Oligosaccharide and Analysis of N-Glycans by the Reversed-phase HPLC—*N*-Glycan analysis was performed with minor modification as reported previously (37). The cells ($2–4 \times 10^7$ cells) were lysed by homogenization, and the *N*-glycans were then released with *N*-glycosidase F (Roche Applied Science) from 10 mg of proteins of cell lysates by incubation for 16 h. The pyridylaminated *N*-glycans (PA-*N*-glycans) were prepared according to the manufacturer's recommended procedure (pyridylamination manual kit, Takara Bio Inc., Shiga, Japan). Excess 2-aminopyridine was removed using a cellulose cartridge. The PA-*N*-glycans prepared from the cells were analyzed using a reversed-phase HPLC system (Shimazu Co., Kyoto, Japan) with an ODS80-TM column (4.6 × 150 mm; Tosoh Corp., Tokyo, Japan). Elution was performed at a flow rate of 1.0 ml/min at 55 °C using 20 mM ammonium acetate buffer, pH 4.0, as solvent A and the same buffer containing 1% 1-butanol as solvent B. The column was pre-equilibrated with 4% solvent B, and after injection of a sample, the PA-*N*-glycans were separated using

4% of solvent B for 10 min and then a linear gradient of 4–30% of solvent B for 60 min. PA-*N*-glycans were detected using a fluorescence detector at excitation and emission wavelengths of 320 and 400 nm, respectively. The elution time for each pyridylaminated *N*-glycan of HPLC was standardized using pyridylaminated $(NeuNAc\text{-}Gal\text{-}GlcNAc)_2Man_3(GlcNAc)_2$ and pyridylaminated $(Gal\text{-}GlcNAc)_2Man_3(GlcNAc)_2$ *N*-glycans (Takara Bio).

N-Glycan Profiling by LC/MS—*N*-Glycan profiling was performed with minor modification as reported previously (38). Cell pellets (1×10^7 cells) were homogenized in 2 ml of TBS (20 mM Tris-HCl, pH 7.4, 150 mM NaCl) containing protease inhibitor mixture (Nacalai Tesque) using a Potter-Elvehjem homogenizer. The homogenized cell lysates were centrifuged at $1000 \times g$ for 10 min at 4 °C, and the membrane fractions were obtained by an ultracentrifugation of the supernatants at $120{,}000 \times g$ for 80 min at 4 °C. *N*-Glycosidase F digestion was performed overnight on the membrane fraction at 37 °C, according to the manufacturer's recommended procedure. The released *N*-glycans were reduced in 500 μl of 0.5 M $NaBH_4$ at room temperature for 16 h, and neutralized using 5% acetic acid. The reduced *N*-linked glycans were recovered using a solid-phase extraction cartridge (EnviCarb C, Supelco, Bellefonte, PA) and were lyophilized. The reduced *N*-linked glycans were separated on a graphitized carbon column (Hypercarb, 150 × 0.1 mm, 5 μm; Thermo Fisher Scientific, Waltham, MA) at a flow rate of 500 nl/min in an UltiMate 3000 RSLCnano LC system (Dionex, Sunnyvale, CA). The mobile phases were 5 mM ammonium bicarbonate containing 2% acetonitrile (A buffer) and 5 mM ammonium bicarbonate containing 80% acetonitrile (B buffer). The glycans were eluted with a linear gradient of 5–55% of B buffer for 60 min. Mass spectrometric analysis was performed using a Fourier transform ion cyclotron resonance/ion trap-type mass spectrometer (FT-MS, LTQ-FT; Thermo Fisher Scientific). For mass spectrometry, the electrospray voltage was 2.5 kV in both the positive and negative ion modes. The resolution of FT-MS was 50,000, and the scan range was m/z 700–2000. The monosaccharide compositions of the glycans were deduced based on an accurate measurement of the mass, as obtained by FT-MS.

PCR for mRNA Expression Analysis—Total RNA was prepared with TRIzol (Invitrogen), and 1.0 μg of total RNA was reverse-transcribed using a SuperScript III first-strand synthesis system (Invitrogen) according to the manufacturer's instructions. PCR primers were as follows (sense and antisense, respectively): *ST3GAL3* (12), 5′-CGGATGGCTTCTGGAAATCTGT-3′ and 5′-TTGTGCGTCCAGGACTCTTTGA-3′; *ST3GAL4* (12), 5′-CCCAAGAACATCCAGAGCCTCA-3′ and 5′-CGTGGTGGGCTTCTGCTTAATC-3′; *ST6GAL1* (39), 5′-TATCGTAAGCTGCACCCCAATC-3′ and 5′-TTAGCAGTGAATGGTCCGGAAG-3′; *NEU1* (40), 5′-TGAGAACGACTTCGGTCTGGTG-3′ and 5′-CCAGGAAACACCATCATCCTTG-3′; and β-actin (12), 5′-GCACTCTTCCAGCCTTCC-3′ and 5′-GCGCTCAGGAGGAGCAAT-3′.

Flow Cytometric Analysis—Flow cytometric analysis was performed as described previously with minor modifications (5, 33, 35). Briefly, semi-confluent cells were detached from the culture dishes using trypsin containing 1 mM EDTA and were subsequently stained with or without the primary mouse anti-β1, followed by incubation with Alexa Fluor 647 goat anti-mouse IgG (Invitrogen). For lectin staining, cells were stained by biotinylated MAM or *Ricinus communis* agglutinin I (RCA-I), followed by incubation with Alexa Fluor 647-conjugated streptavidin. After washing three times with PBS, flow cytometric analysis was performed using a FACSCalibur flow cytometer and Cell Quest Pro software (BD Biosciences).

Xenograft Tumor Formation—To evaluate tumor formation in the wild-type and GOLPH3-KD HeLa cells, the athymic nude mice were given a subcutaneous injection of those cells. Briefly, the cells were plated on a 100-mm dish in complete medium. After treatment with PBS containing 1 mM EDTA, the cells were suspended to a single-cell level with DMEM. A total of 1×10^6 cells were subcutaneously injected into the NOD-athymic mice (5-week-old male BALB/c mice; Charles River Laboratories, Japan). 6 weeks after the injection, the tumor sizes were measured ($n = 5$ per group). Tumor volume was calculated using the formula $V = (L \times W^2) \times 0.5$ (where V = volume, L = length, W = width). The tumor weight was also measured after harvesting. All animal procedures were carried out according to experimental protocols approved by the Tohoku Pharmaceutical University Research Ethics Board.

Statistical Analysis—Statistical analyses were performed using either a Student's *t* test or one-way analysis of variance (ANOVA), using GraphPad Prism5.

Confocal Microscope—The expression vector of pEF puro ST6GAL1-GFP was transfected into the doxycycline-inducible GOLPH3 knockdown cells. After selection with 1 μg/ml puromycin, cells were grown on the coverslips (MatTek Corp., Ashland, MA) in the presence (KD) or absence of doxycycline for 72 h. The coverslips were rinsed twice with PBS and fixed with 4% paraformaldehyde for 10 min. The cells were then incubated with 0.1% Triton X-100 for 5 min at room temperature. Nonspecific interactions were blocked with 5% BSA at 37 °C for 60 min. After rinsing three times with PBS, cells were incubated with mouse anti-GM130, a Golgi marker, mAb (BD Biosciences, 610823) and then with secondary Alexa 568-labeled goat anti-mouse IgG and TO-PRO-3 (Molecular Probes) in the dark. Samples were analyzed by confocal microscopy using an FV-1000 confocal microscope (Olympus, Tokyo, Japan).

RESULTS

Expression of GOLPH3 Is Important for Integrin-meditated Cell Migration and Tumor Formation—GOLPH3 modulates the phosphorylation status of the AKT-mTOR signal pathway (21), which is a central regulator of cell growth, proliferation, differentiation, and survival. Recent studies have shown that mTOR also plays a critical role in the regulation of tumor cell motility, invasion, and cancer metastasis (41). However, the role of GOLPH3 in cancer cell migration and metastasis remains largely unknown.

To understand the effects of GOLPH3 expression on cell migration, we made knockdown HeLa cells by transfection with the siRNA-targeting *GOLPH3* gene, and examined cell migration using a Boyden chamber trans-migration assay. The knockdown efficiency of GOLPH3 was verified via immunoblotting analysis (Fig. 1*A*). As shown in Fig. 1*B*, the depletion of

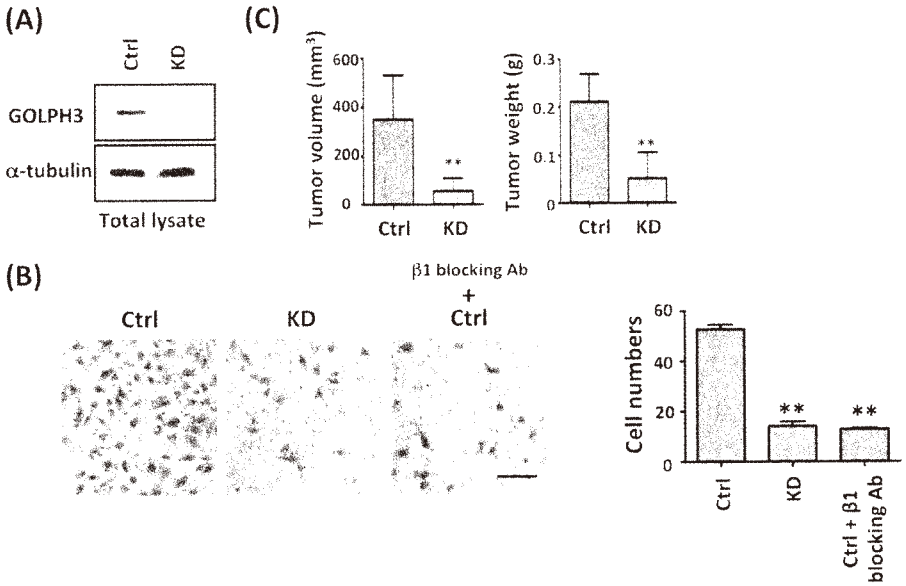

FIGURE 1. **Effects of knockdown of GOLPH3 on tumorigenicity and integrin-mediated cell migration.** *A*, expression levels of GOLPH3 in HeLa cells after transfection with *GOLPH3* siRNAs (*KD*) were compared with cells transfected with nontargeting siRNAs (*Ctrl*). *B*, cell migration toward FN was determined using the transwell assay as described under "Experimental Procedures." Cells that migrated were stained with crystal violet. Migrated cells were counted under a microscope. A representative example is shown in the *left panel*. The *scale bar*, 100 μm. The quantitative data (*right panel*) were obtained from three independent experiments. Data are presented as the means ± S.D. (**, $p < 0.001$ by one-way ANOVA with Tukey's post hoc test). *C*, xenograft model in nude mice. A total of 1×10^6 cells expressed shRNA for control (*Ctrl*) or *GOLPH3* (*KD*) were inoculated on the backs of nude mice by hypodermic injection. After inoculation for 6 weeks, tumor sizes were measured as described under "Experimental Procedures." The quantitative data for the tumor volume (*left panel*) and tumor weight (*right panel*) are presented as the means ± S.D. ($n = 5$; **, $p < 0.001$ by one-tail unpaired *t* test). *Ctrl*, control; *KD*, GOLPH3-knockdown; *β1*, integrin β1.

GOLPH3 dramatically inhibited cell migration on FN. The cell migration was completely suppressed by the addition of anti-β1 integrin-blocking antibody, suggesting that the expression of GOLPH3 plays an important role in integrin-mediated cell migration. In contrast to cell migration, there were no significant differences in cell viabilities between control and KD cells confirmed by trypan blue staining (data not shown). To determine the effects of GOLPH3 on tumor growth, wild-type or GOLPH3-KD cells were injected into 5-week-old male athymic mice, and tumor growth was monitored. As shown in Fig. 1*C*, control cells permitted the vigorous formation of tumors. However, the tumor formation was significantly suppressed in the KD cells, which was consistent with previous reports (21, 23). These results suggest that GOLPH3 involved tumor formation and malignant transformation both *in vitro* and *in vivo*.

Sialylation Was Decreased in the GOLPH3-Knockdown Cells—Several studies, including those conducted by our group, have reported that the *N*-glycans of integrins affect cell migration. For example, *ST6GAL1* knock-out mice experienced an enhanced epithelial tumor differentiation through the reduction of β1 integrin-mediated signaling (20). To further examine the effects of GOLPH3 on β1 integrin-mediated functions and *N*-glycosylation, we established stable GOLPH3 knockdown cell lines (Fig. 2*A*, *lower panels*). It is noteworthy that the band mobility of β1 integrin on SDS-PAGE differed between the control and the knockdown cells. To clarify whether the difference of β1 band mobility on SDS-PAGE was due to *N*-glycosylation or core protein degradation, the immunoprecipitated β1 integrins were treated with peptide:*N*-glycosidase F for deglycosylation. The treatment completely diminished the difference in the band mobility of β1 on SDS-PAGE between both cells, indicating that the knockdown of GOLPH3 affects the *N*-glycosylation of β1 integrin (Fig. 2*A*, *upper panels*). To further explore the difference in *N*-glycosylation, we analyzed pyridylaminated *N*-glycans that had been obtained from control and knockdown cells by using reversed-phase HPLC. It is interesting that the peaks eluting at around 50 min were dramatically decreased in the GOLPH3 knockdown cells, compared with those in control cells (Fig. 2*B*, *upper panel*). These peaks disappeared after digestion with sialidase (Fig. 2*B*, *middle panels*). After sequential treatments with sialidase and β-galactosidase, the elution patterns of the labeled *N*-glycans could not be distinguished between the GOLPH3 knockdown cells and the control cells (Fig. 2*B*, *middle* and *lower panels*). These results strongly indicated that GOLPH3 specifically affected sialylation on the *N*-glycans.

The sialylation of *N*-glycans is ordinarily accomplished using β-galactoside α-2,3-sialyltransferase-III, IV (ST3GAL3 and ST3GAL4), and β-galactoside α-2,6-sialyltransferase-I (ST6GAL1). In contrast, neuraminidase1 (NEU1) reduces the sialylation of *N*-glycan on the cell surface. We used RT-PCR to confirm whether the expression of GOLPH3 affected the gene expression levels of these sialyltransferases and sialidase. As shown in Fig. 2*C*, there were no significant differences between the control and the GOLPH3 knockdown cells, suggesting that the sialylation was regulated by GOLPH3 rather than by the gene expression of the sialytransferases and the sialidase.

Restoration of GOLPH3 Expression Rescued the Sialylation and Cell Migration, Which Were Blocked in the GOLPH3 Knockdown Cells—Many studies have suggested that sialylation played a crucial role in integrin-mediated cell migration

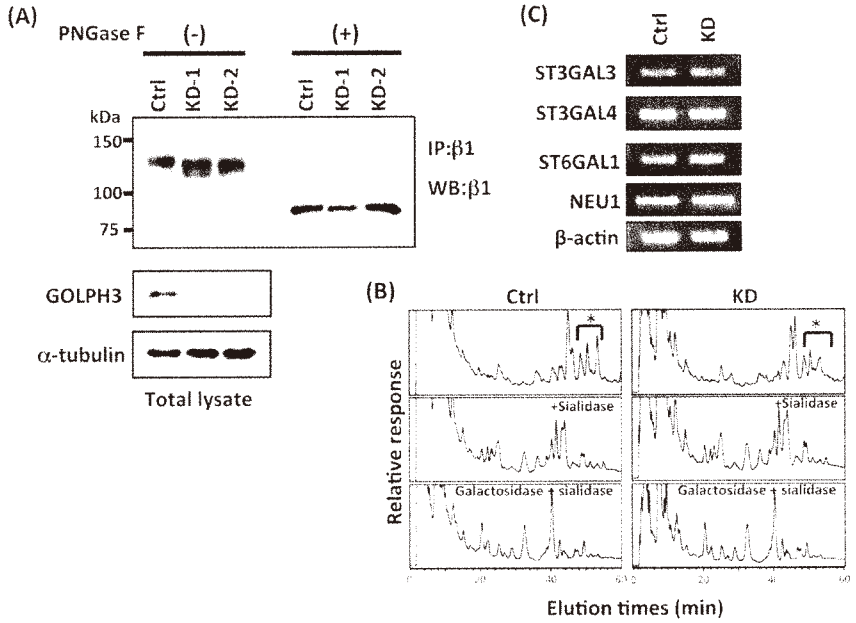

FIGURE 2. **Alteration of *N*-glycosylation in GOLPH3-knockdown cells.** *A*, total expression levels of β1 integrin were analyzed by Western blotting (*WB*). The same amounts of cell lysates (200 μg) were obtained from control and KD cells, which were picked up from HeLa cells expressed as shRNA for control (*Ctrl*) and *GOLPH3* (KD1,2) using the Phoenix system. Cell lysates were immunoprecipitated (*IP*) with anti-β1 antibody. The immunoprecipitates of β1 integrin were treated with (+) or without peptide:*N*-glycosidase F (*PNGase*) (−), and then immunoblotted with anti-β1 antibody (*upper panel*). The knockdown efficiency of GOLPH3 was confirmed by immunoblotting with anti-GOLPH3 antibody (*middle panel*). The α-tubulin was used as a loading control to warrant the same amounts of proteins to be used (*lower panel*). *B*, analysis of PA-*N*-glycans was by reversed-phase HPLC. Then *N*-glycans released from control or KD cells with peptide:*N*-glycosidase F were pyridylaminated as described under "Experimental Procedures." The PA-*N*-glycans (*upper panel*), sequentially digested with sialidase (*middle panel*) and β-galactosidase (*lower panel*), were subjected to reversed phase HPLC. The *asterisk* indicates the peaks for sialylated *N*-glycans. *C*, RT-PCR for mRNA expression of several sialyltransferases and sialidase as indicated. The β-actin was used as a loading control. *Ctrl*, control shRNA; *KD*, shRNA for *GOLPH3*-knockdown; *β1*, integrin β1.

(18, 20, 42). To clarify the relationships between GOLPH3 and sialylation, as described above, we overexpressed an shRNA-resistant *GOLPH3* gene in the GOLPH3-knockdown cells and then examined cell migration and *N*-glycan structures. As shown in Fig. 3*A*, the overexpression of GOLPH3 in the knockdown cells greatly rescued integrin-mediated cell migration on LN-332, which was blocked in the GOLPH3 knockdown cells. As expected, the mobility on SDS-PAGE for the β1 integrin band obtained from the rescue cells was slower than that from the KD cells and returned to a state similar to that of the control cells (Fig. 3*B*). It is noteworthy that the treatment with sialidase cancelled these differences.

To further confirm the difference, the *N*-glycan profiles of those three cells were compared using LC/MS. The data showed that sialylated *N*-glycans were decreased, and asialo-*N*-glycans were increased in KD cells, compared with those in the control cells (Fig. 3*C*), which was consistent with the results of HPLC analysis, as described in Fig. 2*B*. Furthermore, after the re-introduction of GOLPH3 (rescue cells), the expression pattern of sialylated and asialo-*N*-glycans in the KD cells was almost normalized to that of the control cells, suggesting that GOLPH3 specifically regulates sialylation of *N*-glycans. To examine directly the effects of GOLPH3 on sialylation, we designed a Tet-On expression system for knockdown and overexpression of GOLPH3. A positive correlation between the levels of the sialylated β1 integrin and the expression levels of GOLPH3 was also observed in the GOLPH3 knockdown and overexpression cells (Fig. 3*D*). However, the expression levels of GOLPH3 did not significantly affect β1 integrin expressed on the cell surface, which was confirmed by FACS analysis (Fig. 3*E*). The down-regulation of sialylation was also observed in GOLPH3 knockdown MDA-MB231 cells (Fig. 3*F*). Furthermore, a suppression of cell migration was also observed in GOLPH3 knockdown MDA-MB231 cells (Fig. 3*G*). To analyze overall sialylation, we performed FACS analysis. The down-regulation of sialylation was also observed in FACS analysis (Fig. 3*H*). The reactivity against MAM lectin was decreased, although the reactivity against RCA-I lectin was increased in GOLPH3 KD HeLa cells, compared with control cells. These results were consistent with the data analyzed by HPLC and MS (Figs. 2*B* and 3*C*). These results, taken together, strongly suggest that GOLPH3 influences sialylation.

To examine whether GOLPH3 specifically regulates the sialylation on β1 integrin, we also investigated other glycoproteins. It was interesting that a clear correlation of GOLPH3 expression with enhanced sialylation was also observed in α5 integrin but not in either α3 integrin or EGFR. A decreased GOLPH3 expression significantly suppressed both α2,6- and α2,3-sialylated integrin α5, although an increased GOLPH3 expression greatly enhanced both sialylations (Fig. 3*I*). The GOLPH3 expression did not affect the α2,3-sialylation of integrin α3 (Fig. 3*J*). Although it is possible that the overexpression of GOLPH3 could increase the sialylated EGFR, the knockdown of GOLPH3 only modestly affected the sialylation (Fig. 3*K*). Overexpression of GOLPH3 promoted cell migration as shown in Fig. 3*L*. Collecting these results suggests that the decreases in sialylation were different among different glycoproteins. Although the underlying molecular mechanism remains unclear, we could spec-

ulate that GOLPH3 differentially affects sialylation on target proteins.

Forced Expression of ST6GAL1 Rescued Cell Migration and AKT Phosphorylation, Which Were Blocked in KD Cells—As described above, the gene knockdown of GOLPH3 suppressed cell migration and sialylation, suggesting GOLPH3 is involved with cell migration via integrin and sialylations. GOLPH3 can also regulate downstream growth signaling in response to receptor tyrosine kinase activation (21, 43). Therefore, we hypothesized that GOLPH3 might affect the PI3K-AKT-

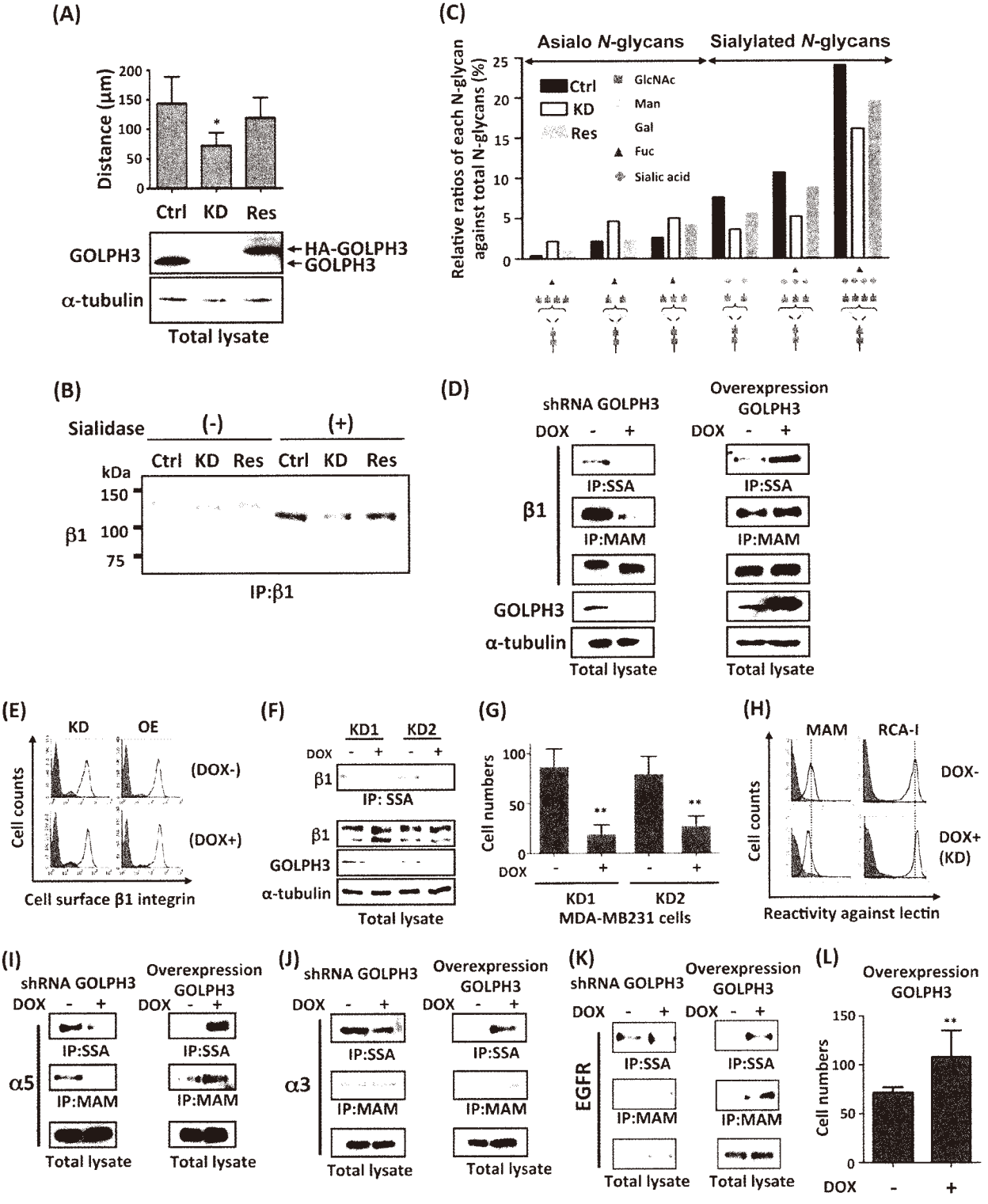

mTOR signaling pathway through the sialylations. In fact, many studies have reported that the sialylated β1 integrin plays important roles in its biological functions (18, 20, 44). Here, we examined whether a forced expression of sialyltransferases overcomes those phenotypes observed in GOLPH3 knockdown cells. As shown in Fig. 4, the overexpression of ST6GAL1 rescued not only integrin-mediated cell migration (Fig. 4*A*) but also EGFR-mediated AKT phosphorylation, both of which were suppressed in GOLPH3 knockdown cells (Fig. 4*C*). However, it is worth noting that the overexpression of ST3GAL4 could partly rescue EGFR-mediated AKT phosphorylation (data not shown) but not efficiently rescue the deficiencies of cell migration of GOLPH3 knockdown cells (Fig. 4*B*). The α2,6-sialylation status of β1 integrin was greatly increased in GOLPH3-KD cell by overexpression of ST6GAL1 (Fig. 4*D*). The total α2,6-sialylations levels confirmed by FACS analysis using SSA lectin were also increased (data not shown). These data suggest that the enhanced expression of sialylated *N*-glycans by GOLPH3 could be one of the mechanisms for its oncogenic signaling. GOLPH3 is known to regulate mTOR signaling (21). Unexpectedly, the treatment with rapamycin greatly up-regulated the expression of sialylated *N*-glycans on β1 integrin (Fig. 4*E*).

GOLPH3 Was Specifically Associated with Sialyltransferases—In yeast cells, Vps74p, which is a counterpart of GOLPH3, was associated with mannosyltransferase enzyme (26), coatomer (45), phosphatidylinositol 4-phosphate (PI4P) (29), and regulated *N*-glycan synthesis. Very recently, GCNT1 enzyme was reported to be one of the putative binding partners for GOLPH3 to retain its Golgi localization (27). To understand how GOLPH3 could regulate sialylation specifically, we tested whether GOLPH3 binds to sialyltransferase(s) such as ST3GAL4 and ST6GAL1, which mainly participate in the sialylation of *N*-glycans in HeLa cells. The co-immunoprecipitation showed that GOLPH3 specifically associated with ST3GAL4. Furthermore, the chimeric ST3GAL4 containing the cytoplasmic domain of β4GALT1 (Fig. 5*A*) lost its binding, although the chimeric β4GALT1 became associated when its cytoplasmic domain was replaced by ST3GAL4 (Fig. 5*B*). The association of GOLPH3 and ST6GAL1 was also observed (Fig. 5*C*). These results suggest that GOLPH3 is able to bind to a specific region within the cytoplasmic domains of sialyltransferases. In fact, GOLPH3 recognized PI4P via a positively charged binding pocket on the hydrophobic face of the protein (22, 29) for localization in the trans-Golgi. Vps74p oligomer is reported to be required for Golgi localization of glycosyltransferases in yeast cells (16). Therefore, we next sought to determine whether a lack of PI4P binding ability (R171A/R174A or W81A/R90A) (29) or the disruption of its oligomerization (Δ190–201) (16) rescued the aberrant sialylation observed in GOLPH3 knockdown cells. As expected, these GOLPH3 mutants could not rescue the sialylation levels of β1 integrin, suggesting the GOLPH3/sialyltransferase/PI4P participated in the regulation of α2,6-sialylations in a coordinated fashion (Fig. 5*D*). To examine the effects of GOLPH3 on localization of sialytransferases, we used a doxycycline-inducible system to establish the GOLPH3-KD cells expressed with ST6GAL1-GFP. To be consistent with the previous report (22), the localization of ST6GAL1-GFP did not apparently change in the presence or absence of doxycycline (Fig. 5*E*).

DISCUSSION

In this study, we found the following: (i) that GOLPH3 expression played an important role in integrin-mediated cell migration via the up-regulation of sialylation; (ii) that GOLPH3 was specifically associated with sialyltransferases and the regulated sialylation of *N*-glycans on β1 integrin; and (iii) that the expression of ST6GAL1 rescued the integrin-mediated cell

FIGURE 3. **Effects of restoration of GOLPH3 expression on β1 integrin-mediated cell migration and its *N*-glycosylation.** *A*, GOLPH3 knockdown cells as described in Fig. 2*A* were infected with retrovirus-expressing shRNA, a resistant *GOLPH3* gene, and then cultured in the presence of hygromycin to achieve 100% infection, which was used as rescued cells (*Res*). Cell migration on laminin 332 (*upper panel*) was monitored by time-lapse microscopy as described under "Experimental Procedures." Each *bar* represents the means ± S.D. of the migration distance of 10 cells in each assay (*, $p < 0.0001$, by one-way ANOVA with Tukey's post hoc test). The expression levels of GOLPH3 were compared among the control (*Ctrl*), the KD, and the rescued cells (*middle panel*), which were restored with the expression of GOLPH3 in KD cells. The α-tubulin was used as a loading control (*lower panel*). *B*, Western blotting for β1 integrin. The same amounts of cell lysates (200 μg) obtained from the indicated cells were immunoprecipitated (*IP*) with anti-β1 antibody, and the immunoprecipitates were digested with or without sialidase. After the treatment, the immunoprecipitates were then immunoblotted with β1 antibody. *Ctrl*, control shRNA; *KD*, GOLPH3-knockdown; *Res*, KD cells overexpressed a shRNA-resistant *GOLPH3* gene. *C*, comparison of major *N*-glycans from different cells by glycan profiling using LC/MS peak area of asialo and sialylated *N*-glycans were calculated using mass spectra obtained in positive and negative ion modes, respectively. The relative peak area of major *N*-glycans from the control, KD, and the rescued cells were expressed as a percentage of the total peak area of the glycans. Glycan structures were deduced by MS analysis. *D*, proteins extracted from HeLa cells that expressed a Tet-On expression system for shRNA of *GOLPH3*-292 (*left panel*) or the *GOLPH3* gene (*right panel*) using lentivirus systems as described under "Experimental Procedures" with or without doxycycline (*DOX*), were immunoprecipitated with the indicated lectin, resolved by SDS-PAGE, and then immunoblotted for β1 integrin antibody. Cell lysates were also Western blotted for the indicated antibodies. *SSA* is an α2,6-sialic acid-specific lectin, and MAM is an α2,3-specific lectin. *E*, HeLa cells that expressed Tet-inducible shRNA against *GOLPH3*-292 (*KD*; *left panel*) or *GOLPH3* gene (*OE*; *right panel*) were propagated with (*lower panel*) or without (*upper panel*) 1 μg/ml doxycycline for 72 h, detached with trypsin/EDTA, and washed with DMEM, including 10% FBS. After washing the cells were stained with (*solid line*) or without (*shadowed line*) anti-β1 antibody (P5D2) and then stained with anti-mouse IgG conjugated with Alexa Fluor 647. The expression levels of β1 integrin on the cell surface were analyzed using BD FACSCalibur, operated with BD CellQuest Pro software. *F*, MDA-MB231 cells expressed with the Tet-On system for shRNA of *GOLPH3*-292 (*KD1*) or *GOLPH3*-442 (*KD2*) using the lentivirus were cultured in the presence (+) or absence (−) with 1 μg/ml doxycycline for 72 h. Cell lysates were immunoprecipitated with the SSA lectin, resolved by SDS-PAGE, and then immunoblotted for β1 integrin antibody. Cell lysates were also Western-blotted for the indicated antibodies. *G*, cell migration on FN was determined using a transwell assay in GOLPH3 knockdown cells as described in *F*. The quantitative data were obtained from three independent experiments. Data are presented as the means ± S.D. (**, $p < 0.001$ by one-way ANOVA with Tukey's post hoc test). *H*, HeLa cells that expressed Tet-inducible shRNA against *GOLPH3*-292 were propagated with (*lower panel*, KD cells) or without (*upper panel*, control cells) 1 μg/ml doxycycline for 72 h. The detached cells were incubated with MAM lectin, which recognizes α2,3-sialylation glycans (*left panel*), and with RCA-I lectin, which specifically recognizes terminal galactose residue (*right panel*) or without (a *shadowed line*), and then incubated with streptavidin conjugated with Alexa Fluor 647. The reactivities against MAM and RCA-I lectin were analyzed using BD FACSCalibur, operated with BD CellQuest Pro software. *I–K* indicated the changes of sialylation levels on integrin α5, α3, and EGFR, respectively, in GOLPH3 knockdown and overexpression cells as described in *D*. *L*, HeLa cells expressed with the Tet-On system for overexpression of GOLPH3 as described in *D* were cultured in the presence (+) or absence (−) of doxycycline (*DOX*) at 1 μg/ml for 72 h. The cell migration on FN was determined using a transwell assay. Data are presented as the means ± S.D.; **, $p < 0.01$ by one-tail unpaired *t* test.

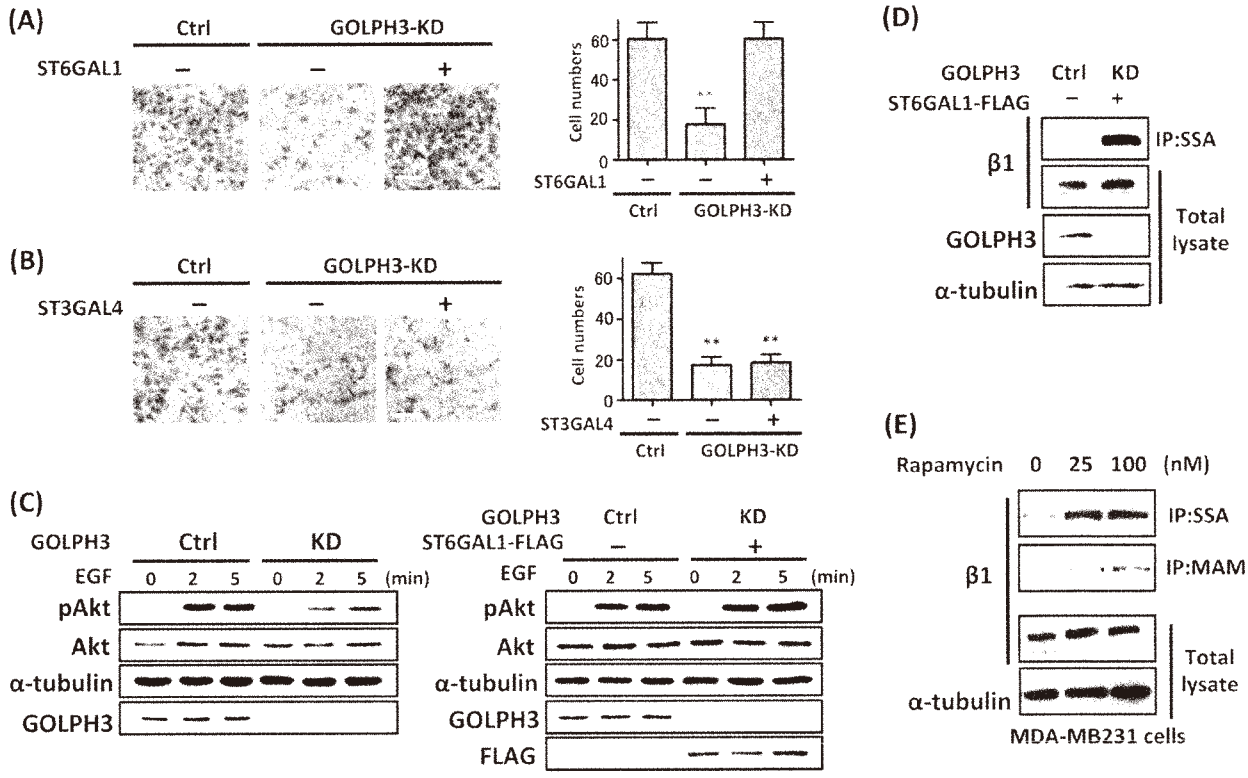

FIGURE 4. **Forced expression of ST6GAL1 led to a restoration of the cell migration and the phosphorylation of AKT, which were suppressed in the GOLPH3-knockdown cells.** The cell migration was examined by using the Boyden chamber described under "Experimental Procedures" in the presence (+) or absence (−) of doxycycline (*DOX*) at 1 μg/ml. The siRNAs of *GOLPH3* and control (*Ctrl*) were transiently transfected into cells containing the Tet-On expression system for ST6GAL1 (*A*) or ST3GAL4 (*B*). Migrated cells were then counted under a microscope. A representative example is shown in the *left panel*. The *scale bar*, 100 μm. The quantitative data were obtained from three independent experiments (*right panel*). Results are expressed as the mean number of cells migrated ± S.D. (**, $p < 0.001$ by one-way ANOVA with Tukey's post hoc test, $n = 5$). *C*, cells that expressed inducible shRNA against *GOLPH3* (*left panel*), with or without the forced expression of ST6GAL1 (*right panel*), were cultured in the presence (+) or absence (−) of DOX at 1 μg/ml for 72 h and then treated with (+) or without (−) EGF at 5 ng/ml for 2 or 5 min. Immunoblot analysis was performed with the indicated antibodies. *D*, HeLa cells that were expressed with Tet-On expression systems for both shRNAs of *GOLPH3*-292 and the ST6GAL1-FLAG genes were cultured in the presence (*right lane*) or absence (*left lane*) of DOX at 1 μg/ml for 72 h. The cell lysates were immunoprecipitated (*IP*) with SSA lectin. The immunoprecipitates and cell lysates were resolved on SDS-PAGE and blotted with several antibodies as indicated. *E*, inhibition of the mTOR signaling pathway by rapamycin induced the expression of sialylated β1 integrin. Proteins extracted from MDA-MB231 cells, which were treated with the indicated concentration of rapamycin for 72 h, were immunoprecipitated with SSA-agarose or MAM-agarose, resolved by SDS-PAGE, and then immunoblotted for β1 integrin antibody. Cell lysates were also Western blotted for the indicated antibody.

migration and the intracellular signaling of cancer cells, both of which were down-regulated in the GOLPH3-KD cells. These observations are the first to directly demonstrate the role of GOLPH3 in the *N*-glycosylation of glycoproteins to regulate the signaling events, which may influence mTOR signaling and tumor progression (Fig. 6).

Integrins are cell-surface glycoproteins that mediate cell-ECM interactions and link matrix proteins to the cytoskeleton (2). They play an important role in intracellular signal transduction (46), regulating various processes, such as cell proliferation, differentiation, apoptosis, and cell migration. Most integrins are major carriers of *N*-glycans, and changes in these structures can alter the cell-cell and cell-ECM interactions, thereby affecting cell adhesion, migration, and tumor malignancy. The β1 integrin heterodimerizes with one of 12 possible α subunits and mediates adhesion, spreading, and migration on multiple ligands, including collagen, laminin, and fibronectin (47, 48). A recent study on the crystal structure of α5β1 ectodomain showed that the RGD-binding pocket is surrounded by several *N*-glycan chains, leaving an exposed surface along the subunit interface (49). Computer modeling also showed that sialylation on an I-like domain may affect the signaling mediated by integrins (44). These results strongly support the notion obtained from this and previous studies, in which the alteration in the *N*-glycans of α5β1 on the cell surface could affect the biological function of the receptor (33, 35). In fact, the importance of individual *N*-glycans and the *N*-glycosylation sites of integrins have gradually become clearer. As described above, integrin is ideally suited to the influence of tumor cell behavior in diverse extracellular matrix milieus, and its *N*-glycosylation state is changed in physiological and pathological conditions such as tumorigenesis and cancer metastasis. However, the underlying molecular mechanism of these changes remains largely unexplained.

The original function of the GOLPH3 yeast homolog Vps74p as a protein that retains mannosyltransferases in the Golgi by interacting with a consensus amino acid sequence (26) had been observed in mammalian cells, in which GOLPH3 was bound to GCNT1 and regulated the cell-cell interaction through *O*-glycans (27). In this study, we found that GOLPH3 specifically associated with sialyltransferases and then affected the sialylation of *N*-glycans. Sialyltransferases, however, do not contain the consensus amino acid sequence that is shown in GCNT1, which suggests the existence of a novel molecular

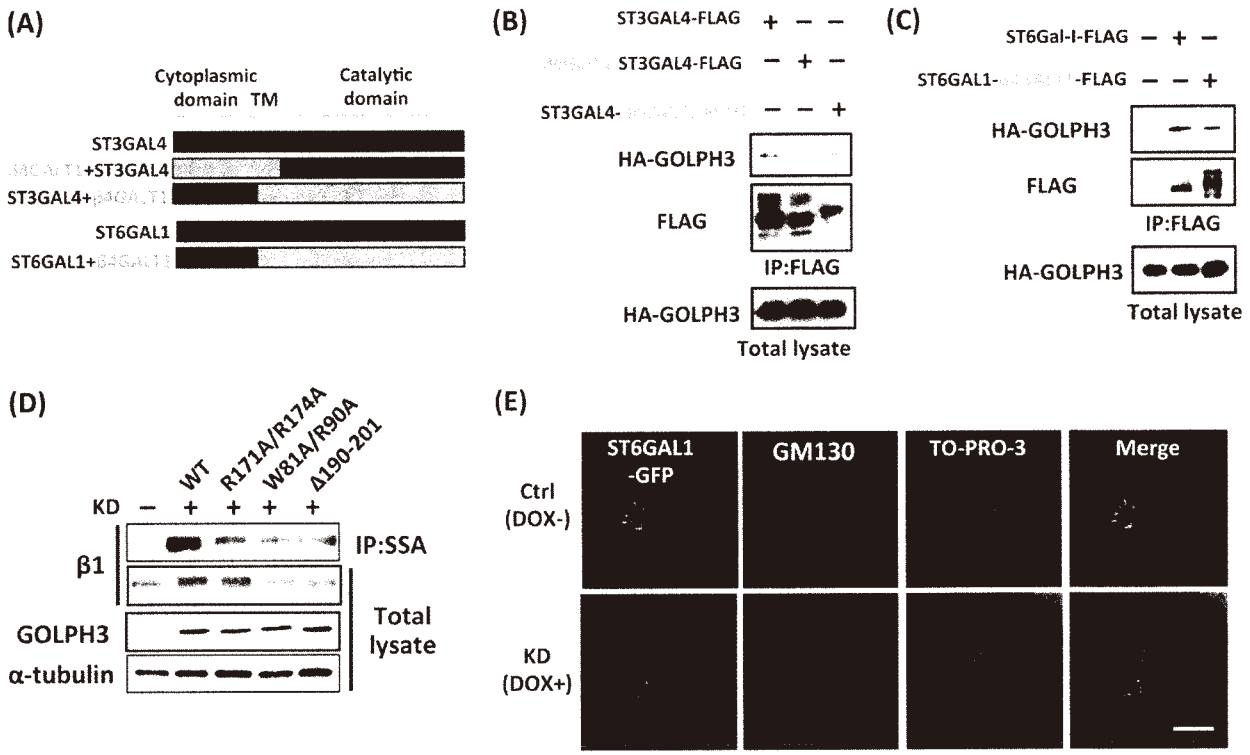

FIGURE 5. **GOLPH3 was associated with sialyltransferases through the cytoplasmic domain of sialyltransferase.** *A*, schematic diagram of sialyltransferases and chimeric constructs. GOLPH3 and the chimera of ST3GAL4 and β4GALT1 (*B*) or the chimera of ST6GAL1 and β4GALT1 (*C*) were transiently expressed in 293T cells. The cell lysates were immunoprecipitated (*IP*) with anti-FLAG and immunoblotted with anti-HA or anti-FLAG antibody. *D*, WT or GOLPH3 mutants (R171A/R174A, W81A/R90A, Δ190–201) shRNA-resistant in a Tet-inducible expression system were introduced into HeLa cells that expressed the Tet-inducible shRNA *GOLPH3*-292 (KD), as described under "Experimental Procedures." Cells were treated with 1 μg/ml of doxycycline for 72 h, lysed, and immunoprecipitated with SSA-agarose and immunoblotted with anti-β1 integrin. *E*, to examine the effects of GOLPH3 knockdown on localization of ST6GAL1, those ST6GAL1-GFP cells expressed with the doxycycline (*DOX*)-inducible GOLPH3 knockdown system were cultured for 72 h in the presence (KD) or absence (*Ctrl*) of DOX. Cells were stained with anti-GM130 primary antibody, TO-PRO-3, and fluorescent secondary antibodies. The cells were analyzed using an Olympus fluorescence microscope with 60×/1.35 NA oil immersion objective lens (FV1000 system). *Scale bar*, 10 μm.

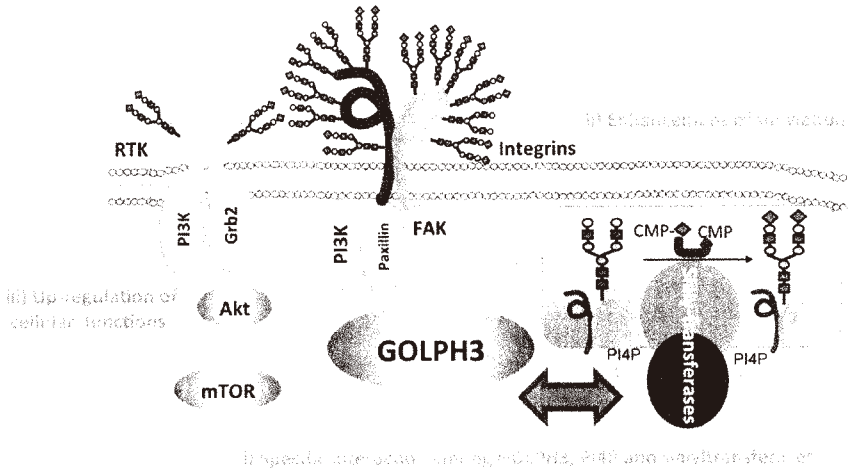

FIGURE 6. **Proposed molecular mechanism for the regulation of sialylation and cellular signaling by GOLPH3.** GOLPH3 has been known to modulate mTOR signaling (21). This study clearly showed that the interaction among GOLPH3, PI4P, and sialyltransferases might efficiently regulate α2,6-sialylation on several target proteins expressed on the cell surface, including integrins and some receptor tyrosine kinases (*RTK*). Then those resultant glycoproteins could cooperatively enhance integrin-mediated cell migration and activate cellular signal pathways such as the phosphoinositide 3-kinase (*PI3K*)-AKT-mTOR cascade. The possible molecular mechanism described here might partly explain the observation that the *GOLPH3* gene is usually amplified in many malignant tumors.

mechanism for the regulation by GOLPH3. Taken together, we could speculate that the direct or indirect association among GOLPH3, PI4P, and sialyltransferases efficiently regulates sialylation, especially α2,6-sialylation. For sialylation, an interaction with PI4P, which is enriched in the trans-Golgi apparatus, seems to be very important because the GOLPH3 mutant, which lacks PI4P binding ability, was unable to rescue the α2,6-sialylation of β1 integrin. The interaction between GOLPH3

and the cytoskeleton via unconventional myosin MYO18A and PI4P was reportedly involved in the exocytosis and maintenance of the Golgi (22). Here, we observed no significant change in the expression levels of β1 integrin on the cell surface with either the knockdown or the overexpression of GOLPH3 (Fig. 3*E*). However, we also could not detect any significant changes in the overall expression level of sialylated *N*-glycans between control and GOLPH3 overexpression cells (data not shown). The possible mechanisms could be explained as follows. First, the overexpression of GOLPH3 might selectively affect only a few glycoproteins, such as β1 integrin, and not all glycoproteins. Second, the overexpression of GOLPH3 might efficiently affect α2,6-sialylation, but not α2,3-sialylation, which is a larger portion of sialylation. In fact, it has been reported that the expression levels of α2,3-sialylation were much higher (~6.5-fold) than the α2,6-sialylation on α5β1 integrin obtained from placenta (50).

GOLPH3 has been known to modulate mTOR signaling and oversensitivity for rapamycin. High GOLPH3 expression correlates with the hyperactivation of mTOR signaling in human cancer cells. Unexpectedly, we found that treatment with rapamycin up-regulated the sialylation of β1 integrin (Fig. 4*E*). The details of the mechanism remain unclear. It could be speculated that cancer cells may escape from the apoptosis induction by rapamycin treatment and achieve cell survival and cell invasion through an up-regulation of sialylation. In fact, Ma *et al.* (51) reported that the expression ST6GAL1 was up-regulated in multidrug-resistant tumor cells. Thus, we believe that the induction of sialylation could allow tumor cells to acquire new potentials for malignancy and recurrence in some clinical cases. Furthermore, overexpression of ST6GAL1 efficiently rescued cell migration and AKT phosphorylation, which were blocked in the GOLPH3-knockdown cells (Fig. 6).

The results of this study clearly showed GOLPH3-mediated sialylation induction and the attendant biological functions. Specifically, β1 integrin was one of the important targets for sialylation. The knockdown of GOLPH3 resulted in the hyposialylation of β1 and subsequently decreased cell migration. The restoration of GOLPH3 and the up-regulation of ST6GAL1 expression significantly rescued the sialylation of β1 integrin and cell migration. Furthermore, overexpression of ST6GAL1 efficiently rescued cell migration and AKT phosphorylation, which were blocked in the GOLPH3-knockdown cells (Fig. 6). Indeed, elevated levels of ST6GAL1 and α2,6-sialylation have been observed in several types of tumors, including colon cancer (18, 52) and ovarian cancer (42, 53). The expression levels of ST6GAL1 mRNA and enzyme activities are known to be particularly enhanced in metastatic tumors, which were promoted by the Ras oncogene (15, 16). Consistently, *in vitro* cell culture studies have suggested that ST6GAL1 up-regulation contributes to cancer metastasis by regulating invasiveness and/or cell motility (18, 54), as observed in this study. It is worth noting that the effects of GOLPH3-mediated sialylation on cell migration and cellular signaling could not be excluded from other target proteins, such as EGFR. These results prompted us to speculate that the regulation of sialylation could be a plausible mechanism for the oncogenic GOLPH3 in various cancer tissues.

Acknowledgments—We thank Dr. Lynda Chin (Institute for Applied Cancer Science, University of Texas MD Anderson Cancer Center), Dr. K. Miyazaki (Yokohama City University, Japan), Dr. T. Miyagi (Tohoku Pharmaceutical University, Japan), and Dr. H. Narimatsu (National Institute of Advanced Industrial Science and Technology, Japan) for kindly providing HA-GOLPH3 expression vector, laminin 332, neuraminidase1 primers, and the cDNAs of ST3GAL4, ST6GAL1, and β4GALT1, respectively, for our initial work. We also acknowledge James L. McDonald for editing this manuscript.

REFERENCES

1. Varki, A., Kannagi, R., and Toole, B. P. (2009) in *Essentials of Glycobiology* (Varki, A., Cummings, R. D., Esko, J. D., Freeze, H. H., Stanley, P., Bertozzi, C. R. Hart, G. W., and Etzler, M. E., eds) pp. 617–632, Cold Spring Harbor Laboratory Press, Cold Spring Harbor, New York
2. Hynes, R. O. (1992) Integrins: versatility, modulation, and signaling in cell adhesion. *Cell* **69,** 11–25
3. Asada, M., Furukawa, K., Segawa, K., Endo, T., and Kobata, A. (1997) Increased expression of highly branched *N*-glycans at cell surface is correlated with the malignant phenotypes of mouse tumor cells. *Cancer Res.* **57,** 1073–1080
4. Pocheć, E., Lityńska, A., Amoresano, A., and Casbarra, A. (2003) Glycosylation profile of integrin α3β1 changes with melanoma progression. *Biochim. Biophys. Acta* **1643,** 113–123
5. Isaji, T., Gu, J., Nishiuchi, R., Zhao, Y., Takahashi, M., Miyoshi, E., Honke, K., Sekiguchi, K., and Taniguchi, N. (2004) Introduction of bisecting GlcNAc into integrin α5β1 reduces ligand binding and down-regulates cell adhesion and cell migration. *J. Biol. Chem.* **279,** 19747–19754
6. Zhao, Y., Nakagawa, T., Itoh, S., Inamori, K., Isaji, T., Kariya, Y., Kondo, A., Miyoshi, E., Miyazaki, K., Kawasaki, N., Taniguchi, N., and Gu, J. (2006) *N*-Acetylglucosaminyltransferase III antagonizes the effect of *N*-acetylglucosaminyltransferase V on α3β1 integrin-mediated cell migration. *J. Biol. Chem.* **281,** 32122–32130
7. Varki, A. (2007) Glycan-based interactions involving vertebrate sialic-acid-recognizing proteins. *Nature* **446,** 1023–1029
8. Schwarzkopf, M., Knobeloch, K. P., Rohde, E., Hinderlich, S., Wiechens, N., Lucka, L., Horak, I., Reutter, W., and Horstkorte, R. (2002) Sialylation is essential for early development in mice. *Proc. Natl. Acad. Sci. U.S.A.* **99,** 5267–5270
9. Dwivedi, C., Dixit, M., and Hardy, R. E. (1988) Plasma sialyltransferase as a tumor marker. *Cancer Detect. Prev.* **11,** 191–196
10. Swindall, A. F., Londoño-Joshi, A. I., Schultz, M. J., Fineberg, N., Buchsbaum, D. J., and Bellis, S. L. (2013) ST6Gal-I protein expression is upregulated in human epithelial tumors and correlates with stem cell markers in normal tissues and colon cancer cell lines. *Cancer Res.* **73,** 2368–2378
11. Dall'Olio, F., Chiricolo, M., Ceccarelli, C., Minni, F., Marrano, D., and Santini, D. (2000) β-Galactoside α2,6 sialyltransferase in human colon cancer: contribution of multiple transcripts to regulation of enzyme activity and reactivity with *Sambucus nigra* agglutinin. *Int. J. Cancer* **88,** 58–65
12. Recchi, M. A., Harduin-Lepers, A., Boilly-Marer, Y., Verbert, A., and Delannoy, P. (1998) Multiplex RT-PCR method for the analysis of the expression of human sialyltransferases: application to breast cancer cells. *Glycoconj. J.* **15,** 19–27
13. Chen, C. L., Lee, W. L., Tsai, Y. C., Yuan, C. C., Ng, H. T., and Wang, P. H. (2002) Sialyltransferase family members and cervix squamous cell carcinoma. *Eur. J. Gynaecol. Oncol.* **23,** 514–518
14. Kaneko, Y., Yamamoto, H., Kersey, D. S., Colley, K. J., Leestma, J. E., and Moskal, J. R. (1996) The expression of Galβ1,4GlcNAc α2,6 sialyltransferase and α2,6-linked sialoglycoconjugates in human brain tumors. *Acta Neuropathol.* **91,** 284–292
15. Le Marer, N., Laudet, V., Svensson, E. C., Cazlaris, H., Van Hille, B., Lagrou, C., Stehelin, D., Montreuil, J., Verbert, A., and Delannoy, P. (1992) The c-Ha-ras oncogene induces increased expression of β-galactoside α-2, 6-sialyltransferase in rat fibroblast (FR3T3) cells. *Glycobiology* **2,** 49–56
16. Seales, E. C., Jurado, G. A., Singhal, A., and Bellis, S. L. (2003) Ras oncogene

directs expression of a differentially sialylated, functionally altered β1 integrin. *Oncogene* **22,** 7137–7145
17. Chiricolo, M., Malagolini, N., Bonfiglioli, S., and Dall'Olio, F. (2006) Phenotypic changes induced by expression of β-galactoside α2,6 sialyltransferase I in the human colon cancer cell line SW948. *Glycobiology* **16,** 146–154
18. Seales, E. C., Jurado, G. A., Brunson, B. A., Wakefield, J. K., Frost, A. R., and Bellis, S. L. (2005) Hypersialylation of β1 integrins, observed in colon adenocarcinoma, may contribute to cancer progression by up-regulating cell motility. *Cancer Res.* **65,** 4645–4652
19. Chen, J. Y., Tang, Y. A., Huang, S. M., Juan, H. F., Wu, L. W., Sun, Y. C., Wang, S. C., Wu, K. W., Balraj, G., Chang, T. T., Li, W. S., Cheng, H. C., and Wang, Y. C. (2011) A novel sialyltransferase inhibitor suppresses FAK/paxillin signaling and cancer angiogenesis and metastasis pathways. *Cancer Res.* **71,** 473–483
20. Hedlund, M., Ng, E., Varki, A., and Varki, N. M. (2008) α2–6-Linked sialic acids on *N*-glycans modulate carcinoma differentiation *in vivo*. *Cancer Res.* **68,** 388–394
21. Scott, K. L., Kabbarah, O., Liang, M. C., Ivanova, E., Anagnostou, V., Wu, J., Dhakal, S., Wu, M., Chen, S., Feinberg, T., Huang, J., Saci, A., Widlund, H. R., Fisher, D. E., Xiao, Y., Rimm, D. L., Protopopov, A., Wong, K. K., and Chin, L. (2009) GOLPH3 modulates mTOR signalling and rapamycin sensitivity in cancer. *Nature* **459,** 1085–1090
22. Dippold, H. C., Ng, M. M., Farber-Katz, S. E., Lee, S. K., Kerr, M. L., Peterman, M. C., Sim, R., Wiharto, P. A., Galbraith, K. A., Madhavarapu, S., Fuchs, G. J., Meerloo, T., Farquhar, M. G., Zhou, H., and Field, S. J. (2009) GOLPH3 bridges phosphatidylinositol-4-phosphate and actomyosin to stretch and shape the Golgi to promote budding. *Cell* **139,** 337–351
23. Zeng, Z., Lin, H., Zhao, X., Liu, G., Wang, X., Xu, R., Chen, K., Li, J., and Song, L. (2012) Overexpression of GOLPH3 promotes proliferation and tumorigenicity in breast cancer via suppression of the FOXO1 transcription factor. *Clin. Cancer Res.* **18,** 4059–4069
24. Wang, J. H., Chen, X. T., Wen, Z. S., Zheng, M., Deng, J. M., Wang, M. Z., Lin, H. X., Chen, K., Li, J., Yun, J. P., Luo, R. Z., and Song, L. B. (2012) High expression of GOLPH3 in esophageal squamous cell carcinoma correlates with poor prognosis. *PLoS One* **7,** e45622
25. Zhou, J., Xu, T., Qin, R., Yan, Y., Chen, C., Chen, Y., Yu, H., Xia, C., Lu, Y., Ding, X., Wang, Y., Cai, X., and Chen, J. (2012) Overexpression of Golgi phosphoprotein-3 (GOLPH3) in glioblastoma multiforme is associated with worse prognosis. *J. Neurooncol.* **110,** 195–203
26. Tu, L., Tai, W. C., Chen, L., and Banfield, D. K. (2008) Signal-mediated dynamic retention of glycosyltransferases in the Golgi. *Science* **321,** 404–407
27. Ali, M. F., Chachadi, V. B., Petrosyan, A., and Cheng, P. W. (2012) Golgi phosphoprotein 3 determines cell binding properties under dynamic flow by controlling Golgi localization of core 2 *N*-acetylglucosaminyltransferase 1. *J. Biol. Chem.* **287,** 39564–39577
28. Schmitz, K. R., Liu, J., Li, S., Setty, T. G., Wood, C. S., Burd, C. G., and Ferguson, K. M. (2008) Golgi localization of glycosyltransferases requires a Vps74p oligomer. *Dev. Cell* **14,** 523–534
29. Wood, C. S., Schmitz, K. R., Bessman, N. J., Setty, T. G., Ferguson, K. M., and Burd, C. G. (2009) PtdIns4P recognition by Vps74/GOLPH3 links PtdIns 4-kinase signaling to retrograde Golgi trafficking. *J. Cell Biol.* **187,** 967–975
30. Schaub, B. E., Berger, B., Berger, E. G., and Rohrer, J. (2006) Transition of galactosyltransferase 1 from trans-Golgi cisterna to the trans-Golgi network is signal mediated. *Mol. Biol. Cell* **17,** 5153–5162
31. Karasawa, S., Araki, T., Nagai, T., Mizuno, H., and Miyawaki, A. (2004) Cyan-emitting and orange-emitting fluorescent proteins as a donor/acceptor pair for fluorescence resonance energy transfer. *Biochem. J.* **381,** 307–312
32. Kurita, R., Suda, N., Sudo, K., Miharada, K., Hiroyama, T., Miyoshi, H., Tani, K., and Nakamura, Y. (2013) Establishment of immortalized human erythroid progenitor cell lines able to produce enucleated red blood cells. *PLoS One* **8,** e59890
33. Isaji, T., Sato, Y., Fukuda, T., and Gu, J. (2009) *N*-Glycosylation of the I-like domain of β1 integrin is essential for β1 integrin expression and biological function: identification of the minimal *N*-glycosylation requirement for α5β1. *J. Biol. Chem.* **284,** 12207–12216
34. Sato, Y., Isaji, T., Tajiri, M., Yoshida-Yamamoto, S., Yoshinaka, T., Somehara, T., Fukuda, T., Wada, Y., and Gu, J. (2009) An *N*-glycosylation site on the β-propeller domain of the integrin α5 subunit plays key roles in both its function and site-specific modification by β1,4-*N*-acetylglucosaminyltransferase III. *J. Biol. Chem.* **284,** 11873–11881
35. Isaji, T., Sato, Y., Zhao, Y., Miyoshi, E., Wada, Y., Taniguchi, N., and Gu, J. (2006) *N*-glycosylation of the β-propeller domain of the integrin α5 subunit is essential for α5β1 heterodimerization, expression on the cell surface, and its biological function. *J. Biol. Chem.* **281,** 33258–33267
36. Kariya, Y., Ishida, K., Tsubota, Y., Nakashima, Y., Hirosaki, T., Ogawa, T., and Miyazaki, K. (2002) Efficient expression system of human recombinant laminin-5. *J. Biochem.* **132,** 607–612
37. Xu, Q., Isaji, T., Lu, Y., Gu, W., Kondo, M., Fukuda, T., Du, Y., and Gu, J. (2012) Roles of *N*-acetylglucosaminyltransferase III in epithelial-to-mesenchymal transition induced by transforming growth factor β1 (TGF-β1) in epithelial cell lines. *J. Biol. Chem.* **287,** 16563–16574
38. Kawasaki, N., Itoh, S., Hashii, N., Takakura, D., Qin, Y., Huang, X., and Yamaguchi, T. (2009) The significance of glycosylation analysis in development of biopharmaceuticals. *Biol. Pharm. Bull.* **32,** 796–800
39. Wang, P. H., Lee, W. L., Yang, Y. H., Chen, Y. L., Tsai, Y. C., and Yuan, C. C. (2007) α2,6-Sialyltransferase I expression in the placenta of patients with preeclampsia. *J. Chin. Med. Assoc.* **70,** 152–158
40. Miyagi, T., Wada, T., Yamaguchi, K., Shiozaki, K., Sato, I., Kakugawa, Y., Yamanami, H., and Fujiya, T. (2008) Human sialidase as a cancer marker. *Proteomics* **8,** 3303–3311
41. Liu, L., and Parent, C. A. (2011) Review series: TOR kinase complexes and cell migration. *J. Cell Biol.* **194,** 815–824
42. Christie, D. R., Shaikh, F. M., Lucas, J. A., 4th, Lucas, J. A., 3rd, and Bellis, S. L. (2008) ST6Gal-I expression in ovarian cancer cells promotes an invasive phenotype by altering integrin glycosylation and function. *J. Ovarian Res.* **1,** 3
43. Scott, K. L., and Chin, L. (2010) Signaling from the Golgi: mechanisms and models for Golgi phosphoprotein 3-mediated oncogenesis. *Clin. Cancer Res.* **16,** 2229–2234
44. Pan, D., and Song, Y. (2010) Role of altered sialylation of the I-like domain of β1 integrin in the binding of fibronectin to β1 integrin: thermodynamics and conformational analyses. *Biophys. J.* **99,** 208–217
45. Tu, L., Chen, L., and Banfield, D. K. (2012) A conserved N-terminal arginine-motif in GOLPH3-family proteins mediates binding to coatomer. *Traffic* **13,** 1496–1507
46. Schwartz, M. A., and Ginsberg, M. H. (2002) Networks and crosstalk: integrin signalling spreads. *Nat. Cell Biol.* **4,** E65–E68
47. Hynes, R. O. (2002) Integrins: bidirectional, allosteric signaling machines. *Cell* **110,** 673–687
48. Damsky, C. H., and Ilic, D. (2002) Integrin signaling: it's where the action is. *Curr. Opin. Cell Biol.* **14,** 594–602
49. Nagae, M., Re, S., Mihara, E., Nogi, T., Sugita, Y., and Takagi, J. (2012) Crystal structure of α5β1 integrin ectodomain: atomic details of the fibronectin receptor. *J. Cell Biol.* **197,** 131–140
50. Nakagawa, H., Zheng, M., Hakomori, S., Tsukamoto, Y., Kawamura, Y., and Takahashi, N. (1996) Detailed oligosaccharide structures of human integrin α5β1 analyzed by a three-dimensional mapping technique. *Eur. J. Biochem.* **237,** 76–85
51. Ma, H., Zhou, H., Song, X., Shi, S., Zhang, J., and Jia, L. (2014) Modification of sialylation is associated with multidrug resistance in human acute myeloid leukemia. *Oncogene*, 10.1038/onc.2014.7
52. Sata, T., Roth, J., Zuber, C., Stamm, B., and Heitz, P. U. (1991) Expression of α2,6-linked sialic acid residues in neoplastic but not in normal human colonic mucosa. A lectin-gold cytochemical study with *Sambucus nigra* and *Maackia amurensis* lectins. *Am. J. Pathol.* **139,** 1435–1448
53. Wang, P. H., Lee, W. L., Juang, C. M., Yang, Y. H., Lo, W. H., Lai, C. R., Hsieh, S. L., and Yuan, C. C. (2005) Altered mRNA expressions of sialyltransferases in ovarian cancers. *Gynecol. Oncol.* **99,** 631–639
54. Shaikh, F. M., Seales, E. C., Clem, W. C., Hennessy, K. M., Zhuo, Y., and Bellis, S. L. (2008) Tumor cell migration and invasion are regulated by expression of variant integrin glycoforms. *Exp. Cell Res.* **314,** 2941–2950

An Oncogenic Protein Golgi Phosphoprotein 3 Up-regulates Cell Migration via Sialylation

Tomoya Isaji, Sanghun Im, Wei Gu, Yuqin Wang, Qinglei Hang, Jishun Lu, Tomohiko Fukuda, Noritaka Hashii, Daisuke Takakura, Nana Kawasaki, Hiroyuki Miyoshi and Jianguo Gu

J. Biol. Chem. 2014, 289:20694-20705.
doi: 10.1074/jbc.M113.542688 originally published online June 3, 2014

Fish Physiol Biochem (2014) 40:1559–1572
DOI 10.1007/s10695-014-9948-1

Binding profiles and cytokine-inducing effects of fish rhamnose-binding lectins on Burkitt's lymphoma Raji cells

Masahiro Hosono · Shigeki Sugawara · Atsushi Matsuda · Takeo Tatsuta · Yasuhiro Koide · Imtiaji Hasan · Yasuhiro Ozeki · Kazuo Nitta

Received: 13 October 2013 / Accepted: 17 May 2014 / Published online: 27 May 2014

Abstract Rhamnose-binding lectin (RBL) is one of the animal lectin categories which take part in the innate immune responses of fish. *Osmerus lanceolatus* lectin (OLL) from shishamo smelt eggs is an RBL composed of two tandem-repeated domains, both of which are considered to be a carbohydrate-recognition domain. SAL, catfish (*Silurus asotus*) egg RBL composed of three domains, binds to Burkitt's lymphoma Raji cells through globotriaosylceramide (Gb3) carbohydrate chain and to reduce cell size and growth by altering membrane composition without causing cell death. In this experiment, we tried to compare the binding effects of these two RBLs on Raji cells. Flow cytometric and fluorescence microscopic analyses revealed that OLL also directly bound to and shrunk Raji cells with ten times less reactivity than SAL but reduced cell growth with decreasing cell viability. Anti-Gb3 antibody completely blocked the binding of SAL to Raji cells but not that of OLL. In addition, the direct bindings of OLL and SAL to Raji cells were comparably inhibited by melibiose, but lactose was more effective inhibitor for the binding of OLL than that of SAL. These results suggest that OLL has slightly different cell-binding property compared with SAL and binds not only to Gb3 but also to the other carbohydrate receptor-bearing β-galactoside chains. The quantitative RT-PCR analysis revealed that SAL induced the expression of TNF-α but not of IFN-γ, IL-1β, and IL-10. Thus, SAL-induced cytostatic effect on Raji cells might be partially caused by TNF-α-mediated signaling pathway.

Keywords Lectin · Fish eggs · Domain structure · Burkitt's lymphoma · Gb3 · TNF-α

Masahiro Hosono and Shigeki Sugawara have contributed equally to this article.

Electronic supplementary material The online version of this article (doi:10.1007/s10695-014-9948-1) contains supplementary material, which is available to authorized users.

M. Hosono (✉) · S. Sugawara · T. Tatsuta · K. Nitta
Division of Cell Recognition Study, Institute of Molecular Biomembrane and Glycobiology, Tohoku Pharmaceutical University, 4-4-1 Komatsushima, Aoba-ku, Sendai 981-8558, Japan
e-mail: mhosono@tohoku-pharm.ac.jp

A. Matsuda
Research Center for Medical Glycoscience (RCMG), National Institute of Advanced Industrial Science and Technology (AIST), 1-1-1, Umezono, Tsukuba, Ibaraki 305-8568, Japan

Y. Koide · I. Hasan · Y. Ozeki
Laboratory of Marine Biochemistry, Department of Environment Biosciences, International Graduate School of Arts and Sciences, Yokohama City University, 22-2 Seto, Kanazawa-ku, Yokohama 236-0027, Japan

Introduction

Animal lectins, carbohydrate-binding proteins, appear to have a wide variety of functions not only in the regulation of cell recognition, development, differentiation, and growth but also in defense, apoptosis, and protein quality control (Sharon and Lis 2004). Among them, one of the most striking biological effects of animal lectins is immune regulation (Kilpatrick 2002). It is well known that mannose-binding lectin (MBL), a member of C-type lectin family, acts as a pattern recognition receptor (PRR) which mediates direct killing through complement activation via MBL-associated serine proteases (MASPs) complexes (Thiel et al. 1997; Jack et al. 2001a, b) or through enhancing phagocytotic effect by acting as an opsonin (Kuhlman et al. 1989; Jack et al. 2001a, b; Neth et al. 2002).

A number of fish lectins have been found in eggs, serum, and skin mucus (Krajhanzl 1990; Ewart et al. 2001; Russell and Lumsden 2005; Vasta et al. 2011), and some have been characterized structurally (Vasta et al. 2011; Ogawa et al. 2011). Although their key role in an organization is still not clearly defined, lectins are thought to play a crucial role in the immune response. For instance, C-type lectins, galectins, intelectins, and pentraxins found in fish serum and skin mucus are thought to participate in the pattern-based recognition making up an innate immune response instead of the specific antibody against pathogens in adaptive immunity (Ewart et al. 2001; Russell and Lumsden 2005; Vasta et al. 2011). Fish eggs are a good source of lectins, especially those with affinity for L-rhamnose, termed rhamnose-binding lectins (RBLs) (Nitta et al. 2007; Ogawa et al. 2011). RBLs had been reported as an anti-B agglutinin early in the 1970s (Anstee et al. 1973), suggesting that they can recognize Galα-linked carbohydrate chain. Although a number of RBLs have been isolated and characterized so far, it has still been unclear why they bind to L-rhamnose, a rare sugar in vertebrates.

Recent studies have revealed that most of the RBLs consist of two or three domains containing conserved characteristic peptide motifs (Nitta et al. 2007; Ogawa et al. 2011) and have eight Cys residues at highly conserved positions which are estimated to form completed four disulfide bonds within each domain (Terada et al. 2007). The proposed carbohydrate-recognition domain (CRD), termed RBL CRD-like domain (RCLD) (Terada et al. 2007), is found not only in fish eggs but also in other organisms and species, e.g., ponyfish (*Leiognathus nuchalis*) skin mucus (Okamoto et al. 2005), sea urchin (*Anthocidaris crassispina*) eggs (Ozeki et al. 1991), marine bivalve (*Pteria penguin*) mantle (Naganuma et al. 2006), and colonial ascidian (*Botryllus schlosseri*) (Gasparini et al. 2008). Interestingly, latrophilin, a calcium-independent receptor for α-latrotoxin produced by black widow spiders, expressed in certain mammalian nervous cells involves RCLD itself in the extracellular N-terminal region (Krasnoperov et al. 1997; Lelianova et al. 1997).

It has been evidenced that one of the cellular receptor of RBLs is globotriaosylceramide (Gb3, Galα1-4Galβ1-4Glcβ1-1′Cer) located in the glycosphingolipid-enriched membrane microdomain (GEM) (Mori et al. 2000), also known as lipid rafts (Simons and Ikonen 1997). Gb3 also possesses Galα-linkage at the non-reducing end of its carbohydrate chain as well as human B antigen. Sugawara et al. (2005a, b) revealed that catfish (*Silurus asotus*) egg lectin (SAL) (Hosono et al. 1993, 1999) targeted Burkitt's lymphoma Raji cells expressing Gb3 and caused cytostatic effects on them but not on human myelogenous leukemia K562 cells lacking Gb3. SAL bound to Raji cells through a Gb3 carbohydrate chain and induced cell shrinkage with alteration of membrane structure, but not apoptosis (Sugawara et al. 2005a). In addition, SAL affected membranes by activating multidrug resistance 1 P-glycoprotein in GEM (Sugawara et al. 2005b). Similarly, Shirai et al. (2009) reported that chum salmon (*Oncorhynchus keta*) egg lectin (CSL) showed cytotoxicity on Gb3-expressing human colorectal adenocarcinoma Caco 2 cells but not on DLD-1 cells.

In our previous work, SAL and shishamo smelt (*Osmerus lanceolatus*) egg lectin (OLL) (Hosono et al. 1992) composed of three and two domains, respectively, showed an affinity for Gb3 by surface plasmon resonance (SPR) analysis and frontal affinity chromatography (FAC; Hosono et al. 2013). OLL and SAL shared similar structure (Fig. 1) and biochemical properties such as hemagglutination activity and sugar-inhibition pattern, whereas they differed slightly in carbohydrate-binding specificity (Hosono et al. 2013). To elucidate further the interaction between RBLs and tumor cells, in this study, we compared the binding profiles of OLL and SAL to Raji cells. It is

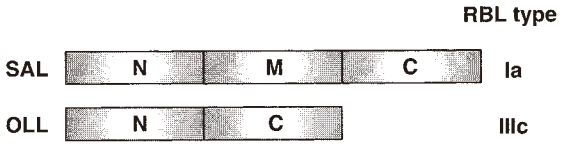

	OLL-N			
OLL-C	73	OLL-C		
SAL-N	37	42	SAL-N	
SAL-M	51	51	30	SAL-M
SAL-C	44	50	34	45

Fig. 1 Schematic depictions of SAL and OLL. Domain compositions of SAL and OLL were depicted by *twin-colored boxes* (*upper panel*). RBL type and domain characterization were referred from the classification reported by Ogawa et al. (2011). *N*, *M*, and *C* indicate N-terminal, middle, and C-terminal, respectively. Sequential identities (%) among all domains were noted in *lower panel*

also known that CSLs induce proinflammatory cytokines such as tumor necrosis factor (TNF)-α, interleukin (IL)-1β, and IL-8 in the peritoneal macrophage and in the fibroblastic-like cell line from rainbow trout (Watanabe et al. 2009). Thus, we attempted to know whether SAL provokes such effect on Raji cells.

Materials and methods

Materials

OLL and SAL were purified from eggs of shishamo smelt and catfish, respectively, as described previously (Hosono et al. 1992, 1993). Raji and K562 cells were obtained from the Cell Resource Center of the Biomedical Research, Institute of Development, Aging and Cancer, Tohoku University (Sendai, Japan) and Japanese Cancer Research Resources Bank (Tokyo, Japan), respectively. These cells were cultured in RPMI 1640 medium (Nissui, Tokyo, Japan) supplemented with 10 % fetal calf serum (FCS), penicillin (100 U/mL), and streptomycin (100 U/mL) and maintained at 37 °C in a 5 % CO_2 atmosphere.

Flow cytometric analysis

After Raji cells (1×10^5) were treated with OLL (10, 50, 100, and 200 μg/mL) or SAL (10, 50, and 100 μg/mL) at 4 °C for 30 min (final volume, 100 μL), and washed thrice with cold phosphate-buffered saline (PBS), cell size was measured by forward scatter light values using FACScalibur (Becton–Dickinson Co., Franklin Lakes, NJ). After the same treatment, apoptotic cells were detected by using a MEBCYTO apoptosis kit (MBL Co., Ltd, Nagoya, Japan) according to the manufacturer's protocol. Briefly, treated or untreated cells were suspended with the binding buffer (42.5 μL) and then incubated for 15 min at room temperature under darkness in the presence of 5 μL of fluorescein isothiocyanate-labeled annexin V (FITC-ANV) and 2.5 μL of propidium iodide (PI). After incubation, cells were analyzed by flow cytometry as described above.

Cell growth and viability

Cell viability was measured by the trypan blue dye exclusion test. A 50-μL aliquot of cell suspension was taken immediately after treatment with OLL and SAL as described above and then diluted with 50 μL of 0.4 % trypan blue solution. The numbers of stained and unstained (viable) cells were counted on a blood cell counting plate using an optical microscope. All treatments and cell counts were done in triplicate.

Binding assay

OLL and SAL were labeled with B-phycoerythrin (PE) and HiLyte Fluor 555 (HL) using a commercial labeling kit (Dojindo, Kumamoto, Japan), according to the instructions supplied. Raji and K562 cells were resuspended with 100 μL of PE- or HL-OLL (0.6 μM) and PE- or HL-SAL (0.6 μM) solution and incubated at 4 °C for 30 min with or without pretreatment with anti-Gb3 antibody (Seikagaku Corp., Tokyo, Japan). After being washed with cold PBS, cells were fixed in paraformaldehyde and analyzed under an Axioscope 2 fluorescence microscope (Carl Zeiss, Oberkochen, Germany). The binding inhibition assay was performed by flow cytometry using fluorescence-labeled RBLs. PE-OLL and PE-SAL were pre-incubated with lactose (Galβ1-4Glc) and melibiose (Galα1-6Glc) in a final volume of 100 μL at room temperature for 30 min. The solution was added to Raji cells (1×10^5), then incubated at 4 °C for 30 min. After a wash with cold PBS, cells were analyzed by using FACScalibur. Inhibitory values (%) were calculated

Table 1 Primer sequences of cytokine and TNF receptor genes

	Primer sequence	Fragment size (bp)
GAPDH	Sense 5′-AGCCACACGCTCAGACAC-3′; Antisense 5′-GCCCAATACGACCAAATCC-3′	66
INFγ	Sense 5′-GGCATTTTGAAGAATTGGAAAG-3′; Antisense 5′-TTTGGATGCTCTGGTCATCTT-3′	112
TNFα	Sense 5′-CAGCCTCTTCTCCTTCCTGAT-3′; Antisense 5′-GCCAGAGGGCTGATTAGAGA-3′	123
IL-1β	Sense 5′-TACCTGTCCTGCGTGTTGAA-3′; Antisense 5′-TCTTTGGGTAATTTTTGGGATCT-3′	76
IL-6	Sense 5′-GATGAGTACAAAAGTCCTGATCCA-3′; Antisense 5′-CTGCAGCCACTGGTTCTGT-3′	130
IL-8	Sense 5′-GAGCACTCCATAAGGCACAAA-3′; Antisense 5′-ATGGTTCCTTCCGGTGGT-3′	90
IL-10	Sense 5′-GATGCCTTCAGCAGAGTGAA-3′; Antisense 5′-GCAACCCAGGTAACCCTTAAA-3′	105
IL-11	Sense 5′-GGACAGGGAAGGGTTAAAGG-3′; Antisense 5′-GCTCAGCACGACCAGGAC-3′	109
IL-12B	Sense 5′-CCCTGACATTCTGCGTTCA-3′; Antisense 5′-AGGTCTTGTCCGTGAAGACTCTA-3′	75
TNFR1	Sense 5′-TGCTCCAAATGCCGAAAG-3′; Antisense 5′-AATGCCGGTACTGGTTCTTC-3′	100
TNFR2	Sense 5′-CTCCTTCCTGCTCCCAATG-3′; Antisense 5′-CACACCCACAATCAGTCCAA-3′	88

from the results of a flow cytometric analysis using the following formula:

$$\text{Inhibition } (\%) = (\text{Pg}-\text{P0}/\text{P1}-\text{P0}) \times 100$$

where Pg is a fluorescence peak (median) value from the test suspensions containing saccharide and labeled lectin. P1 is the peak value without saccharide which, in turn, means 0 % inhibition. Similarly, P0, without labeled lectin, means 100 % inhibition.

Quantitative reverse transcription polymerase chain reaction (qRT-PCR)

Raji cells (5×10^5) were cultured for 24 h in RPMI-1640 medium containing SAL (100 μg/mL) with or without saccharides (20 mM of lactose or melibiose) at 37 °C. Total cellular RNA was extracted from SAL-treated and SAL-untreated Raji cells using AllPrep RNA/Protein Kit (QIAGEN, Valencia, CA) according to the manufacturer's protocol. First-strand cDNA was synthesized from 1 μg of the total RNA using SuperScript® VILO™ cDNA synthesis Kit (Invitrogen, San Diego, CA). Expression levels of interferon (IFN)-γ, TNF-α, IL-1β, IL-6, IL-10, and IL-12B by qRT-PCR were performed with LightCycler 480 probe master kit and universal probe library (human) using a LightCycler 480 system (Roche Diagnostics, Indianapolis, IN). PCR primers for TaqMan/probe library assay were designed by the Universal Probe Library Assay Design Center (https://www.roche-applied-science.com/sis/rtpcr/upl/acenter.jsp) and listed in Table 1. Glyceraldehyde-3-phosphate dehydrogenase (GAPDH) gene was used as an internal control for gene expression analysis. The expression levels of target genes were normalized to the levels of GAPDH housekeeping gene.

Sodium dodecyl sulfate–polyacrylamide gel electrophoresis and Western blot analysis

Cell lysate was prepared using AllPrep RNA/Protein Kit as described above, then subjected to SDS-PAGE (10 % separation gel) and electrotransferred onto polyvinylidene difluoride (PVDF) membrane (pore size 0.45 μm) (Hybond-P; GE Healthcare Bio-Sciences AB, Uppsala, Sweden). The membrane was treated with blocking buffer (Blocking One; Nakarai Tesque Inc., Kyoto, Japan) for 1 h at room temperature and washed with Tris-buffered saline containing 0.05 % Tween-20. The primary antibodies used were directed to TNF-α (1:1,000, rabbit mAb, clone D5G9; Cell Signaling Technology Inc., Danvers, MA), and GAPDH (1:20,000, mouse mAb; clone 6C5; Ambion/Invitrogen, Carlsbad, CA) in the immunoreaction enhancer solution (Can Get Signal Solution 1; Toyobo Co., Osaka, Japan). At 16 h after incubation at 4 °C, the secondary antibody, horseradish peroxidase (HRP)-conjugated anti-mouse or anti-rabbit IgG (Chemicon International Inc., Temecula, CA), was diluted 1:20,000 in the same solution. The membrane was incubated for 1 h at room temperature and then exposed to X-ray film (Fuji Film Co., Tokyo, Japan) using ECL Prime detection reagent (GE Healthcare Bio-Sciences AB, Uppsala, Sweden).

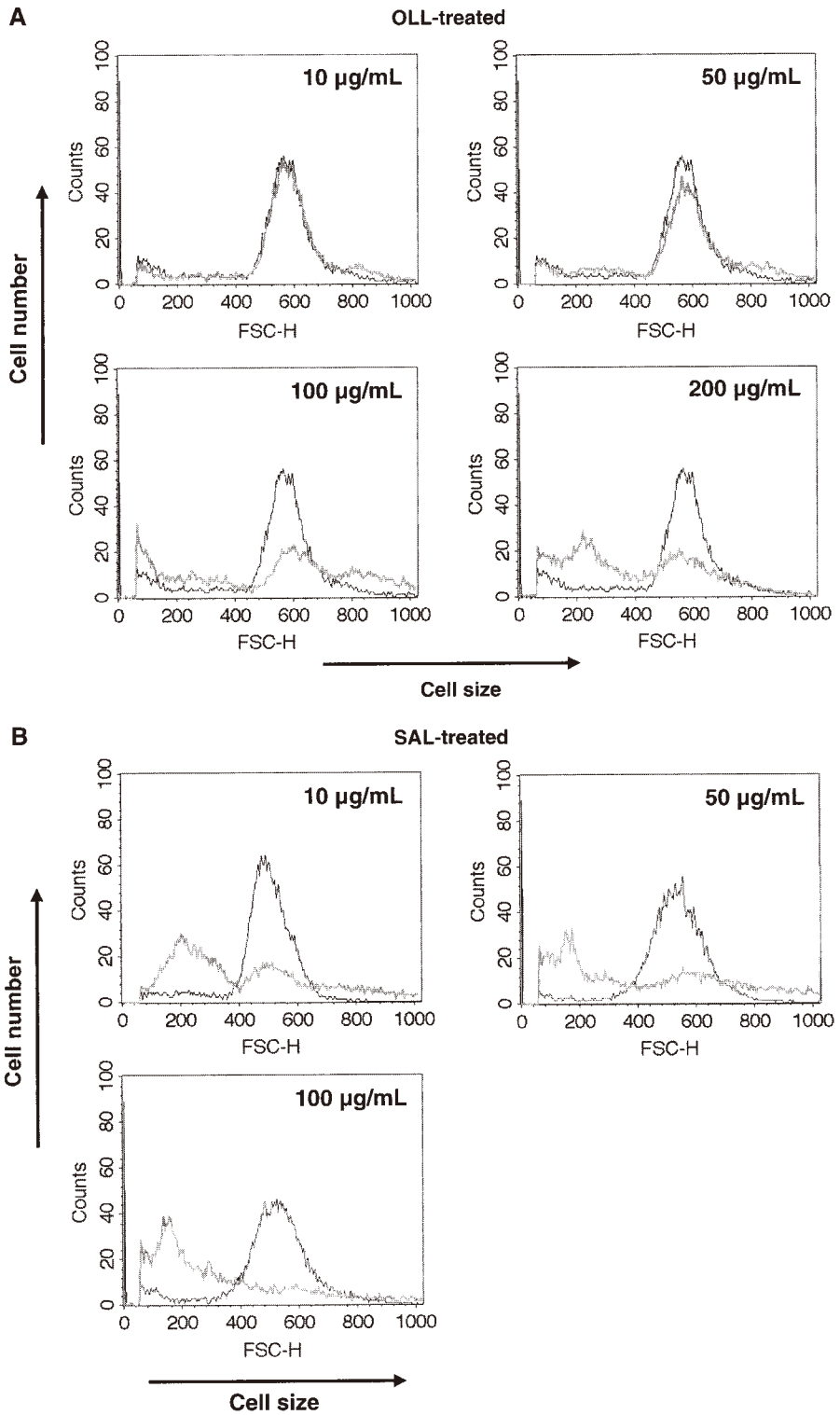

Fig. 2 OLL- and SAL-induced cell shrinkage. Raji cells were incubated with OLL or SAL at 4 °C for 30 min. After washing, cell size was measured by forward scatter light value of flow cytometric analysis. *Black line*, control; *green line*, RBL-treated

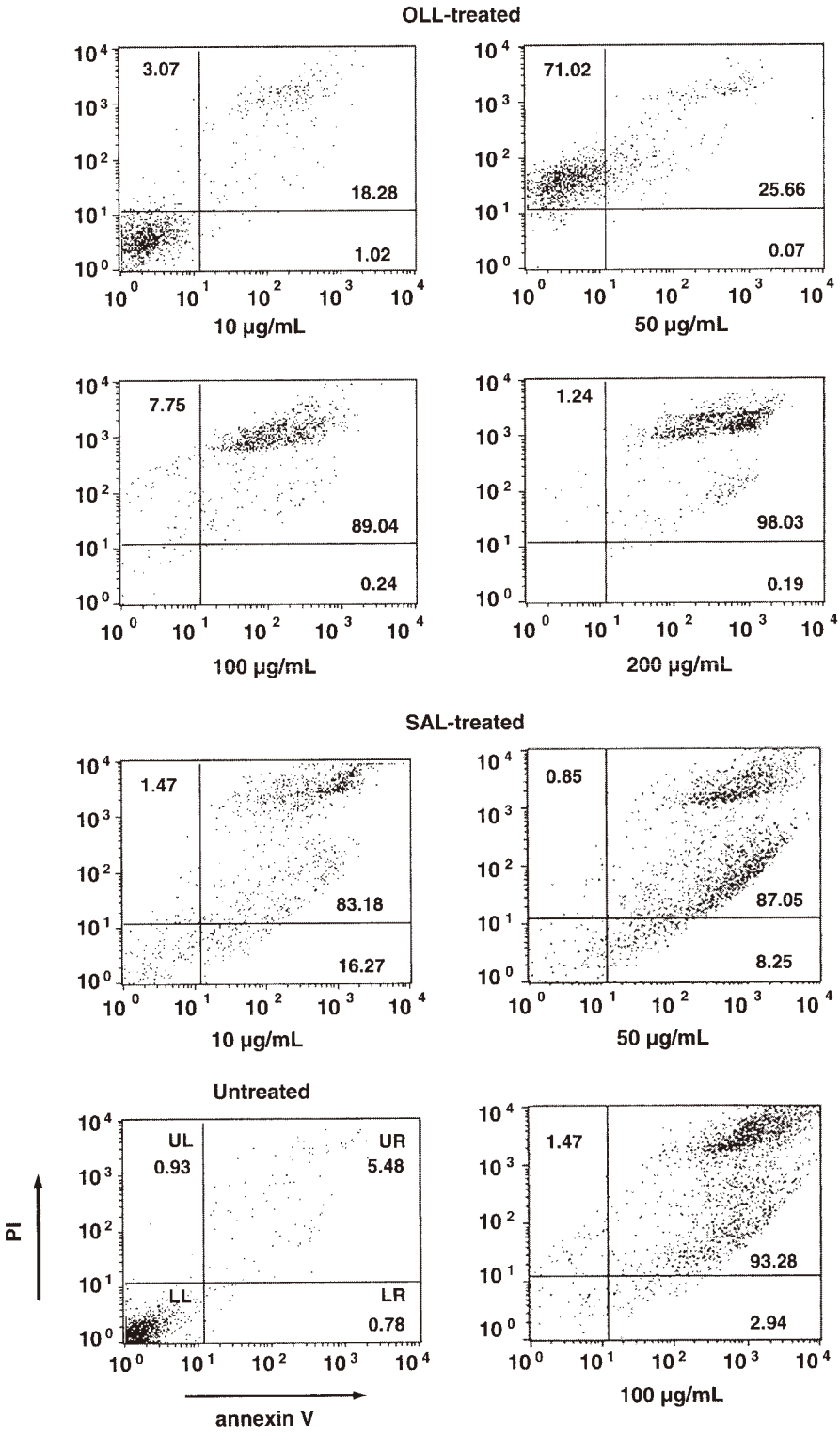

Fig. 3 Dose-dependent changes of FITC-annexin V binding and PI incorporation in OLL- and SAL-treated Raji Cells. Raji cells were incubated with OLL or SAL at 4 °C for 30 min. After washing, annexin V binding reflected by phosphatidylserine (PS) externalization and PI incorporation was detected by flow cytometry using a MEBCYTO apoptosis kit as described in the text. *Numbers* indicate the percentage of the cell population in each quadrant

Statistical analysis

Results were expressed in terms of mean ± standard error (SE) based on all experiments performed at least in triplicates. Statistical analysis was performed by using Student's *t*-test (two-tailed) and ANOVA. The criterion for statistical significance was $p < 0.01$.

Results

OLL induces cell shrinkage and membrane alteration as does SAL

Our previous study demonstrated that SAL comprised of three domains induced a reduction in the size of Raji cells at 4 °C for 30 min by binding to Gb3 on the cell surface (Sugawara et al. 2005a, b). To determine whether the number of RCLDs affects this ability or not, we examined OLL, a two domain-RBL, under the same conditions. As shown in Fig. 2, OLL-induced cell shrinkage at concentrations above 100 μg/mL. Since SAL showed similar activity at 10 μg/mL, the cell-shrinking effect of OLL was ten times weaker than that of SAL.

Sugawara et al. (2005b) reported that SAL causes time- and dose-dependent changes in FITC-ANV binding, and PI incorporation in Raji cells. According to the results of the flow cytometric analysis, OLL caused a dose-dependent change in the cell membrane from a normal state (AN−/PI−, the lower left quadrant, LL) to AN+/PI+ (the upper right quadrant, UR; Fig. 3). The concentration of OLL required to change more than 80 % of the cells from LL to UR was 100 μg/mL, whereas only 10 μg/mL of SAL could do that. Although the result coincided with the cell shrinkage noted above, OLL tended to lead the cells to UR through the upper left (AN−/PI+) area, in contrast with that SAL through the lower right (AN+/PI−) area (Sugawara et al. 2005b). The reason for this difference is still unclear but might be related to cell viability on treatment with these RBLs.

OLL-reduced viability of Raji cells

The flow cytometric analysis demonstrated that the OLL- and SAL-induced membrane alteration seemed to be lethal to Raji cells, because the presence of cells in the UR area is thought to reflect a state of late apoptosis or necrosis. However, Sugawara et al. (2005a) found that SAL scarcely induced cell death using the trypan blue dye exclusion test. To investigate whether OLL behaves as well as SAL or not, cell viability was measured by the same method. A remarkable (~50 %) loss of cell viability was observed on 48 h treatment with OLL (100 and 200 μg/mL), whereas more than 80 % of Raji cells were viable when the cells were treated with SAL (100 μg/mL; Fig. 4). On the other hand, the growth rate of Raji cells treated with OLL and SAL markedly decreased in a dose-dependent manner (Suppl. Fig. 1), suggesting that OLL exerted cytotoxicity to Raji cells in contrast with that SAL reduced growth without cell death.

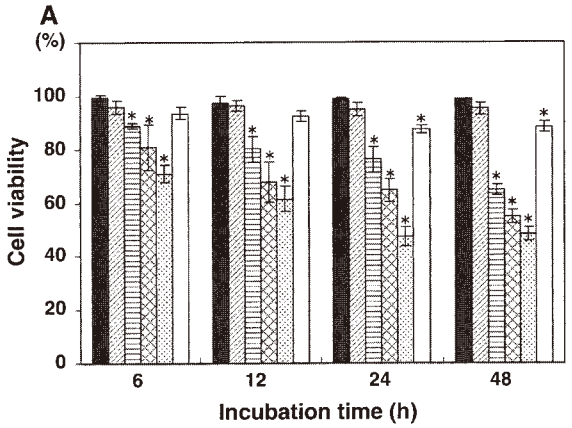

Fig. 4 Viability of OLL- and SAL-treated Raji cells. Raji cells (1×10^5/well) were treated with OLL (10 μg/mL, *stripped bar*; 50 μg/mL, *horizontally lined bar*; 100 μg/mL, *checked bar*; 200 μg/mL, *dotted bar*) or SAL (10 μg/mL, *open bar*). After 6, 12, 24, and 48 h, the cells were washed and stained with trypan blue. Each value represents the mean ± SD based on experiments done in quadruplicates. *Filled bar*, control. *$p < 0.01$ versus control

OLL directly binds to Raji cells

Although SAL changes the membrane of Raji cells by binding to Gb3 molecules on the cell surface, it does not bind to K562 cells lacking Gb3 and consequently causes neither AN binding nor PI incorporation (Sugawara et al. 2005a). We examined here the direct binding of OLL and SAL to their ligands at the surface of Raji and K562 cells by fluorescence microscopic analysis. PE- or HL-labeled OLL and SAL bound directly to Raji cells in the absence of anti-Gb3

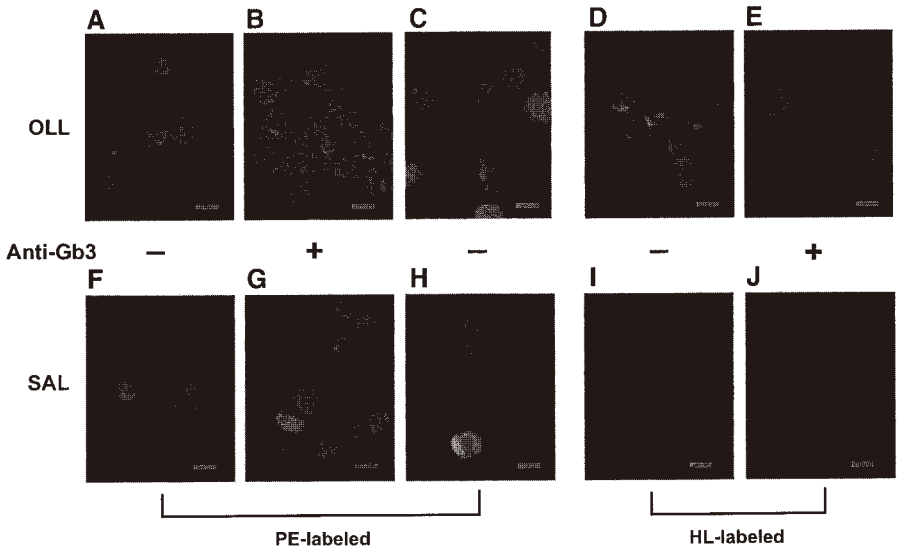

Fig. 5 Binding properties of OLL and SAL against Raji and K562 cells. Anti-Gb3 antibody-untreated (**a**, **c**, **d**, **f**, **h**, and **i**) or anti-Gb3 antibody-treated (**b**, **e**, **g**, and **j**) Raji cells and anti-Gb3 Ab-untreated K562 cells (**c**, **h**) were treated with PE- (**a**–**c**) and HL- (**d**, **e**) labeled OLL (0.58 μM) and PE- (**f**–**h**) and HL- (**i**, **j**) labeled SAL (0.63 μM) at 4 °C for 30 min. After washing, the cells were fixed with 4 % paraformaldehyde and stained with Hoechst 33258, and then observed by fluorescence microscope. The *scale bars* indicate 10 μm

antibody (Fig. 5a, d and f, i). Interestingly, anti-Gb3 Ab had distinct effects on OLL and SAL binding. OLL equally bound to Raji cells regardless of the anti-Gb3 Ab coexistence (Fig. 5a, b and d, e). In contrast, anti-Gb3 Ab fully blocked PE-SAL binding (Fig. 5f, g), but a small amount of fluorescence was observed in the HL-SAL binding (Fig. 5i, j). In addition, PE-SAL did not bind to K562 cells (Fig. 5h) as described above, whereas PE-OLL showed low binding to the cells (Fig. 5c).

Inhibitory properties of hapten disaccharides for the binding of RBLs

To examine the inhibitory effects of disaccharides including galactosyl α- and β-linkages, melibiose and lactose, respectively, a flow cytometric analysis was performed using PE-OLL and PE-SAL in the presence or absence of these saccharides. Both saccharides inhibited the binding between PE-RBL and Raji cells (Fig. 6). The IC_{50} values calculated from binding curves obtained were as follows: lactose for PE-OLL, 0.58 mM; lactose for PE-SAL, 1.38 mM; melibiose for PE-OLL, 0.013 mM; and melibiose for PE-SAL, 0.014 mM.

Induction of cytokine gene expression

Shiga-like toxins (Stxs), protein toxins belonging to the type 2 ribosome inactivating protein (RIP), are produced by enterohemorrhagic *E. coli* (Jacewics et al. 1986; Lindberg et al. 1987; Lingwood et al. 1987). The A subunit of Stx causes the cytotoxic effect as an 28S ribosomal RNA-targeting N-glycosidase (Endo et al. 1988; Saxena et al. 1989), and the pentameric B subunit is responsible for binding to Gb3 on the target cells (Lingwood 1996). Stx has also been shown to activate signaling pathway of monocyte THP-1 cells involving TNF-α expression (Foster and Tesh 2002) and to induce intracellular signals for cytoskeleton remodeling in human renal carcinoma ACHN cells (Takenouchi et al. 2004). We attempted to explore the alteration of cytokine gene expression in SAL-treated Raji cells. As results of the qRT-PCR analyses, the mRNAs of IL-6 and IL-12B were not amplified in Raji cells and, in addition, IFN-γ, IL-1β, and IL-10 showed no significant modulation in mRNA expression levels after treatment of SAL (Suppl. Fig. 2). In contrast, as shown in Fig. 7a, the level of TNF-α mRNA was significantly up-regulated by SAL, and the effect was abolished by the addition of melibiose but not by sucrose (Glcα1, β2Fru) as a negative control. The average of crossing point

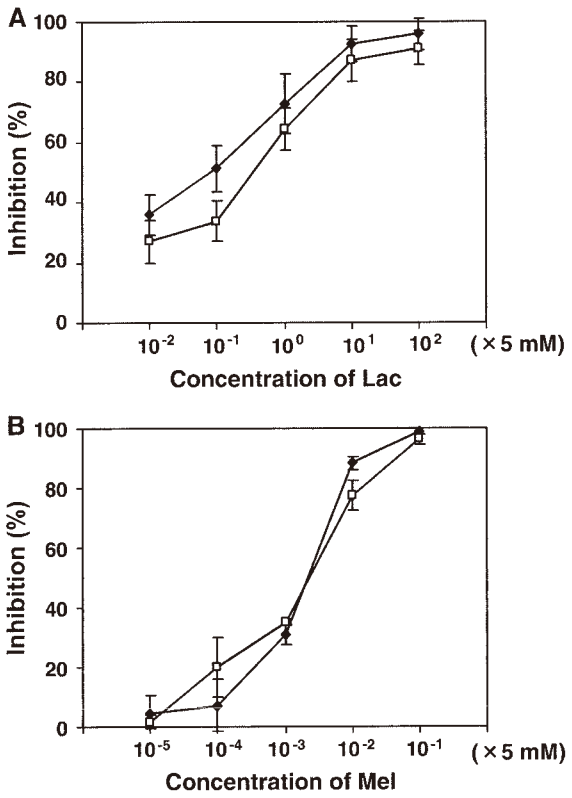

Fig. 6 Inhibition of RBLs-binding activity to Raji cells by saccharides. PE-OLL (*diamond*) or PE-SAL (*square*) was pre-incubated with lactose (Galβ1-4Glc) (**a**) or melibiose (Galα1-6Glc) (**b**) at room temperature for 20 min. Then, Raji cells (1×10^5) were treated with these mixtures at 4 °C for 30 min. After washing with PBS, PE-OLL or PE-SAL bound to Raji cells was detected by flow cytometry. Inhibition score (percent) was calculated from the difference among each median obtained from the fluorescence peak with the equation described in the text. Each value represents the mean ± SE based on experiments done in triplicate

values (TNF-α/GAPDH) from SAL-treated and SAL-untreated cells were 28.54 ± 0.37/20.63 ± 0.09 and 29.94 ± 0.66/21.03 ± 0.47, respectively. Similarly, Western blot analysis showed that the levels of membrane-bound TNF-α (mTNF-α) protein was significantly up-regulated by SAL treatment and the effect was also abolished by the addition of melibiose but not by sucrose (Fig. 7b). Those phenomena were observed concomitantly with agglutination of the cells (Fig. 7c), indicating that SAL-induced TNF-α expression in Raji cells could be occurred in association with its lectin activity. In addition, the expressions of TNF receptor (TNFR) 1 and 2 mRNA were detected in Raji cells by qRT-PCR analyses (Suppl. Table 1).

Discussion

Carbohydrate-based cell adhesion and signaling are involved in a variety of biological events which are crucial for the existence of cells. To date, several carbohydrate-related biological responses have been elucidated mainly in "protein quality control" in the endoplasmic reticulum including glycoprotein transport, refolding, and retaining (Hauri et al. 2000; Dahms and Hancock 2002; Helenius and Aebi 2004), following cytoplasmic degradation (Yoshida et al. 2005), and in "immunoresponse by pattern recognition or complement system" of innate immunity (Kawabata and Tsuda 2002; Endo et al. 2006). Since fish are directly and constantly in contact with pathogenic microorganisms in their environment, they exercise constitutive and responsive forces via innate immune system in skin mucus and in serum at the early infectious stage (Russell and Lumsden 2005; Magnadottir 2006; Vasta et al. 2011). In this aspect, some of the lectin families including C-type, pentraxin, F-type, galectin, and intelectin are thought to take part in and to achieve their effect (Vasta et al. 2011). Besides, the expression of certain fish lectins are up-regulated by infectious stimulation (Vasta et al. 2011; Wang et al. 2013; Yu et al. 2013), indicating that they might be involved in the innate response as a PRR.

RBLs are mostly composed of two or three tandem-repeated domain structures. Recent studies propose that a domain of RBL may function as a CRD (Terada et al. 2007). Only few findings have been reported so far concerning the intrinsic receptor for RBLs. Ozaki et al. (1983) revealed that the receptor for the amago (*Oncorhyncus rhodurus*) egg lectin was present on peritoneal macrophages after inflammatory stimulation and suggested that one of the physiological roles of RBL was likely to be in opsonization against pathogens. In fact, an antitumor effect termed lectin-dependent macrophage-mediated cytolysis was observed between macrophages and tumor cells treated with loach (*Misgurnus anguillicaudatus*) egg lectin, and these interactions disappeared in the presence of L-rhamnose and D-galactose (Yamazaki et al. 1984). On the other hand, the functional ligands/receptors of RBLs have been reported in the relationship between the hosts versus pathogenic bacteria (Vasta et al. 2011). Tateno et al. (2002) reported that RBLs from steelhead trout (*Oncorynchus mykiss*, STLs) bound to smooth-type lipopolysaccharides,

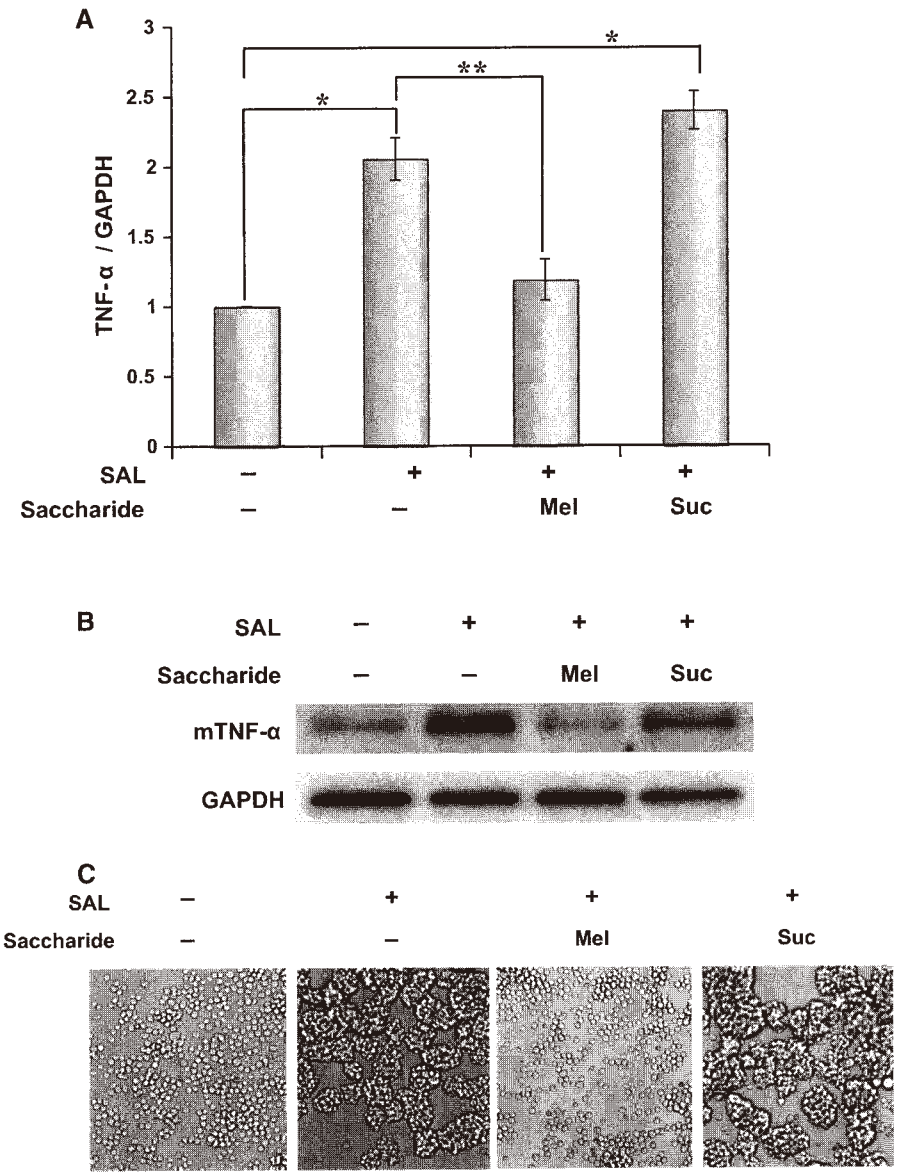

Fig. 7 SAL-induced TNF-α expression. **a** Alteration of TNF-α mRNA level in SAL-treated Raji cells. Cells (5×10^5) were exposed to SAL (100 μg/mL) with or without 20 mM of melibiose (Galα1-6Glc) and sucrose (Glcα1, β2Fru) for 24 h. Total RNAs was extracted from SAL-treated, SAL/saccharide co-treated and untreated Raji cells. Quantitative RT-PCR was performed using specific primers and GAPDH (control gene). Results are present onefold increase, and each value represents the mean ± SE of at least three independent experiments. Single asterisk indicates $p < 0.05$ compared with control value, and double asterisk indicates $p < 0.05$ compared with SAL-treated Raji cells. **b** Alteration of membrane-bound TNF-α (mTNF-α) in SAL-treated Raji cells. Cells were exposed to SAL (100 μg/mL) with or without 20 mM of melibiose and sucrose for 24 h. Whole cell extracts obtained from SAL-treated, SAL/saccharide co-treated and untreated Raji cells were subjected to immunoblot analysis using anti-TNF-α and anti-GAPDH antibodies. The detected protein bands estimated to be mTNF-α (25 kDa) and GAPDH (35 kDa) were indicated. **c** SAL-induced agglutination of Raji cells. Bright-field images of each condition were acquired an inverted microscope (model IX71, Olympus Co., Tokyo Japan) at a magnification of ×100

including L-rhamnose residue in their carbohydrate chains, of some bacteria. Beck et al. (2012) demonstrated that catfish RBL was up-regulated by *Flavobacterium columnare* in its susceptible fish and the hapten sugars of RBL, L-rhamnose, and D-galactose, reduced mortality caused by columnaris disease.

In our previous experiments concerning the carbohydrate-binding specificity of SAL and OLL for glycoconjugates, SAL preferentially bound to the α-galactoside rather than the β-galactoside (Hosono et al. 1993). In fact, both lectins strongly bound to the carbohydrate chains of glycoproteins but also glycolipids with non-reducing end Galα-linkages as determined by SPR and FAC (Hosono et al. 2013). However, OLL showed slightly different binding properties with a higher affinity for the Galβ-linkage in the SPR analysis, indicating that it recognized multiple carbohydrate chains. Indeed, a naturally occurring α-galactoside glycoconjugate, Gb3, is a good candidate for the receptor of RBLs (Sugawara et al. 2005b; Shirai et al. 2009; Watanabe et al. 2009). Gb3, also known as the centroblast-specific differentiation marker CD77 (Nudelman et al. 1983) or P^k antigen (Naiki and Marcus 1975), functions as a cell surface receptor for Stx1 B subunit as mentioned above and is thought to mediate certain apoptotic signals in Burkitt's lymphoma and Vero cells (Mangeney et al. 1993; Khine et al. 2004). Therefore, in our previous study, the cell biological influence of SAL was examined by using Burkitt's lymphoma Raji cells, and K562 cells which is a human erythroleukemia cell line not expressing Gb3 as a reference. SAL bound to Raji cells and induced cell shrinkage but not to K562 cells (Sugawara et al. 2005a). In addition, SAL led Raji cells to a double positive (AN+/PI+) state, termed "late apoptosis" or "necrosis," via the AN+/PI− state, termed "early apoptosis" (Sugawara et al. 2005a, b). Interestingly, ~70 % of cell viability remained after a 72-h treatment with SAL (Sugawara et al. 2005b).

In the present study, we showed that OLL-induced cell shrinkage and altered the membrane of Raji cells with less activity compared with SAL (Figs. 2, 3). In contrast, time- and dose-dependent decrease (up to 50 %) of cell viability was observed within 48 h of treatment with OLL (Fig. 4). The results of flow cytometric analysis demonstrated that OLL led Raji cells to the (AN+/PI+) state through the AN−/PI+ state unlike in the observation of SAL (Fig. 3). Although it is still unclear whether this discrepancy is caused by the difference in domain composition or carbohydrate-binding specificity between OLL and SAL, it might be partly due to the particular sequence of each lectin itself (Hosono et al. 2013).

To examine the cell-binding properties of RBLs, PE- or HL-labeled OLL and SAL were used for a fluorescence microscopic analysis. The molecular mass of these fluorochromes, B-phycoerythrin, and HiLyte-Fluor, is 240 and 1 kDa, respectively. Raji cells were constantly stained with PE- and HL-labeled OLL and SAL. Although the binding of SAL to Raji cells was completely inhibited by pre-treatment with anti-Gb3 antibody, the binding of OLL was not influenced by the antibody (Fig. 5). On the other hand, SAL did not bind to K562 cells while OLL partially bound to the cells. Thus, OLL directly binds to Raji cells as well as SAL, whereas the binding specificity is lower than that of SAL. The nonspecific binding of OLL to K562 cells and decrease in inhibitory effect by the specific antibody against Gb3 might be caused by the additional capacity of OLL to bind β-galactoside noted above. As a result of cytotoxic effect of OLL in contrast with SAL, taken together, the cell surface Gb3 of Raji cells might be a "safety" receptor for RBLs inducing a static state without cell death, and the cytotoxic effect induced by OLL is triggered through an another receptor including a β-galactoside carbohydrate chain.

To evaluate the participation of carbohydrates as a binding probe of RBLs to Raji cells, lactose and melibiose were added to the binding analysis by flow cytometry (Fig. 6). Comparing IC_{50} values revealed that melibiose inhibited the binding of both OLL and SAL to Raji cells 40 and 100 times higher than lactose, respectively. Although comparable inhibition was observed on addition of melibiose to OLL and SAL binding, the inhibitory activity of lactose for OLL was 2.4 times higher than that for SAL. These results also coincide with the findings noted above, i.e., OLL recognized not only Gb3 but also other carbohydrate receptors. Conversely, it should be noted again that Gb3 is assumed to be a "selective" receptor for RBL that contributes to cell shrinkage and growth inhibition without cell death.

A variety of lectins found in fish tissues and organisms have been known to recognize specific pathogens instead of immunoglobulin and then mediate diverse immune responses including opsonization, phagocytosis, cytokine induction, and so forth (Vasta et al. 2011). In catfish, multiple lectins have been isolated from eggs (Hosono et al. 1993), skin mucus (Tsutsui et al. 2011), and serum (Dutta et al. 2005; Ourth et al. 2007), which are egg RBL presented here, skin intelectin, and serum galactose- and mannose-binding lectin, respectively. Interestingly, even though

almost all RBLs are present mainly in ovary of a variety of fish, only ponyfish RBL was found in skin mucus (Okamoto et al. 2005). TNF-α, a pleiotropic cytokine produced by macrophages, monocyte, T cell, and NK cell, provokes multiple immunoregulatory responses and induces diverse effects on the target cells such as proapoptotic and proliferative effects (Aggarwal 2003; Jurisic et al. 2006). It is known that CSL-3 induces expression of TNF-α, IL-1β, and IL-8 in fish peritoneal macrophage cells and enhances their phagocytic effect (Watanabe et al. 2009). CSL-3 also induces apoptosis in Caco-2 cells through binding to Gb3 on the cell surface (Shirai et al. 2009). Moreover, not only Stx holotoxin but also its B subunit alone induce apoptosis in Gb3 expressing Burkitt's lymphoma cells (Mangeney et al. 1993), suggesting that Gb3 could be a negative signal receptor (Taga et al. 1997; Khine et al. 2004). On the other hand, in our previous experiment, we showed that SAL reversibly reduced proliferation of Raji cells without inducing apoptosis (Sugawara et al. 2005a, b), and here, we demonstrated that SAL induced the expression of TNF-α mRNA in Raji cells dependent on a carbohydrate-binding manner (Fig. 7a). It is still unclear what causes these apparently conflicted phenomena among Gb3-binding lectins. However, Raji cells are known to express mTNF-α and simultaneously both TNF receptor (TNFR) 1 and 2 on the cell surface (Jurisic et al. 2006; Zhang et al. 2008). Zhang et al. (2008) concluded interesting theory that endogenous (not exogenously added) mTNF-α on Raji cells may act as both "forward (death)"- and "reverse (survival)"-signaling mediator. When highly expressed mTNF-α behaves as a receptor, it promotes constitutive activation of NF-kB through reverse signaling and consequently causes cell survival, in contrast, when it behaves as a ligand, an opposite signal inducing cell death is triggered. As shown in Fig. 7b, mTNF-α was significantly increased in the protein level on SAL-treated Raji cells. Therefore, even though Gb3 exists on Raji cells as a negative (apoptosis inducing) receptor, mTNF-α enhanced by SAL could allow cells to avoid reaching apoptosis through "reverse signaling." Taken together, the interaction between RBLs and Gb3/TNF-α might affect the fate of cell death or survival.

As described above, several observations support the theory that Gb3 acts as the functional receptor of RBLs through innate immune responses. Indeed, highly selective-binding capacity of RBLs to the Gb3-sugar chain is suitable for the cell targeting. However, Watanabe et al. (2008) showed that *Glugea plecoglossi*, a pathogenic microsporidian of sweet fish (*Plecoglossus altivelis*) do not contain Gb3 molecules, whereas the spores are agglutinated by sweet fish egg lectin (SFL). In this case, RBL receptor of *G. plecoglossi* is not Gb3 but other glycoconjugates. These results are partially consistent with our present observation mentioned here (Fig. 5). Given that RBLs exert diverse effects on the Gb3-expressing target cells through their multiple sugar-binding capacities, they could function as a part of RRR.

In conclusion, we showed here that OLL directly but weakly bound to and shrunk Raji cells compared with SAL, and reduced cell growth with decreasing cell viability. Anti-Gb3 antibody could completely block the binding of SAL to Raji cells but not that of OLL. Thus, OLL has slightly different cell-binding property than SAL and might bind to not only Gb3 but also to the other glycoconjugates. SAL induced TNF-α expression but not IFN-γ, IL-1β, and IL-10 in Raji cells. Therefore, SAL-induced cytostatic effect on Raji cells might be partially caused by TNF-α-mediated signaling pathway.

Acknowledgments This work was supported by a Grant-in-Aid for Frontier Research Program for Private Universities from the Ministry of Education, Culture, Sports, Science, and Technology of Japan.

References

Aggarwal BB (2003) Signaling pathways of the TNF superfamily: a double-edged sword. Nat Rev Immunol 3:745–756

Anstee DJ, Holt PDJ, Pardoe GI (1973) Agglutinins from fish ova defining blood groups B and P. Vox Sang 25:347–360

Beck BH, Farmer BD, Straus DL, Li C, Peatman E (2012) Putative roles for a rhamnose binding lectin in *Flavobacterium columnare* pathogenesis in channel catfish *Ictalurus punctatus*. Fish Shellfish Immunol 33:1008–1015

Dahms NM, Hancock MK (2002) P-type lectins. Biochim Biophys Acta 1572:317–340

Dutta S, Sinha B, Bhattacharya B, Chatterjee B, Mazumder S (2005) Characterization of a galactose binding serum lectin from the Indian catfish, *Clarias batrachus*: possible involvement of fish lectins in differential recognition of pathogens. Comp Biochem Physiol C Toxicol Pharmacol 141:76–84

Endo Y, Tsurugi K, Yutsudo T, Takeda Y, Ogasawara T, Igarashi K (1988) Site of action of a Vero toxin (VT2) from

Escherichia coli O157:H7 and of Shiga toxin on eukaryotic ribosomes. RNA N-glycosidase activity of the toxins. Eur J Biochem 17:45–50

Endo Y, Takahashi M, Fujita T (2006) Lectin complement system and pattern recognition. Immunology 211:283–293

Ewart KV, Johnson SC, Ross NW (2001) Lectins of the innate immune system and their relevance to fish health. ICES J Mar Sci 58:380–385

Foster GH, Tesh VL (2002) Shiga toxin 1-induced activation of c-Jun NH2-terminal kinase and p38 in the human monocytic cell line THP-1: possible involvement in the production of TNF-α. J Leukoc Biol 71:107–114

Gasparini F, Franchi N, Spolaore B, Ballarin L (2008) Novel rhamnose-binding lectins from the colonial ascidian *Botryllus schlosseri*. Dev Comp Immunol 32:1177–1191

Hauri H, Appenzeller C, Kuhn F, Nufer O (2000) Lectins and traffic in the secretary pathway. FEBS Lett 476:32–37

Helenius A, Aebi M (2004) Roles of N-linked glycans in the endoplasmic reticulum. Annu Rev Biochem 73:1019–1049

Hosono M, Matsuda K, Kawauchi H, Takayanagi Y, Shiokawa H, Mineki R, Murayama K, Nitta K (1992) Comparison of N-terminal amino acid sequence of fish roe rhamnose-binding lectins. Biomed Res 13:443–449

Hosono M, Kawauchi H, Nitta K, Takayanagi Y, Shiokawa H, Mineki R, Murayama K (1993) Purification and characterization of *Silurus asotus* (Catfish) roe lectin. Biol Pharm Bull 16:1–5

Hosono M, Ishikawa K, Mineki R, Murayama K, Numata C, Ogawa Y, Takayanagi Y, Nitta K (1999) Tandem repeat structure of rhamnose-binding lectin from catfish (*Silurus asotus*) eggs. Biochim Biophys Acta 1472:668–675

Hosono M, Tatsuta T, Hikita T, Kominami J, Tsuruta-Nakamura S, Hirabayashi J, Kawser SMA, Ozeki Y, Hakomori S, Nitta K (2013) Domain composition of rhamnose-binding lectin from shishamo smelt eggs and its carbohydrate-binding profiles. Fish Physiol Biochem. doi:10.1007/s10695-013-9814-6

Jacewics M, Clausen H, Nudelman E, Donohue-Rolfe A, Keusch GT (1986) Pathogenesis of Shigella diarrhea. XI. Isolation of a shigella toxin-binding glycolipid from rabbit jejunum and HeLa cells and its identification as globotriaosylceramide. J Exp Med 163:1391–1404

Jack DL, Jarvis GA, Booth CL, Turner MW, Klein NJ (2001a) Mannose-binding lectin accelerates complement activation and increases serum killing of *Neisseria meningitidis* serogroup C. J Infect Dis 184:836–845

Jack DL, Read RC, Tenner AJ, Frosch M, Turner MW, Klein NJ (2001b) Mannose-binding lectin regulates the inflammatory response of human professional phagocytes to *Neisseria meningitidis* serogroup B. J Infect Dis 184: 1152–1162

Jurisic V, Bogdanovic G, Kojic V, Jakimov D, Srdic T (2006) Effect of TNF-α on Raji cells at different cellular levels estimated by various methods. Ann Hematol 85:86–94

Kawabata S, Tsuda R (2002) Molecular basis of non-self recognition by the horseshoe crab tachylectins. Biochim Biophys Acta 1572:414–421

Khine AA, Tam P, Nutikka A, Lingwood CA (2004) Brefeldin A and filipin distinguish two globotriaosyl ceramide/verotoxin-1 intracellular trafficking pathway involved in Vero cell cytotoxicity. Glycobiology 14:701–712

Kilpatrick DC (2002) Animal lectins: a historical introduction and overview. Biochim Biophys Acta 1572:187–197

Krajhanzl A (1990) Egg lectins of invertebrates and lower vertebrates: properties and biological function. Adv Lectin Res 3:83–131

Krasnoperov VG, Bitter MA, Beavis R, Kuang Y, Salnikow KV, Chepurny OG, Little AR, Plotnikov AN, Wu D, Holtz RW, Petrenko AG (1997) α-Latrotoxin stimulates exocytosis by the interaction with a neuronal G-protein-coupled receptor. Neuron 18:925–937

Kuhlman M, Joiner K, Ezekowitz RAB (1989) The human mannose-binding protein functions as an opsonin. J Exp Med 169:1733–1745

Lelianova VG, Davletov BA, Sterling A, Rahman A, Grishin EV, Totty NF, Ushkaryov YA (1997) α-Latrotoxin receptor, latrophilin, is a novel member of the secretion family of G protein-coupled receptors. J Biol Chem 272:21504–21508

Lindberg AA, Brown JE, Stromberg N, Westling-Ryd M, Schultz JE, Karlsson KA (1987) Identification of the carbohydrate receptor for Shiga toxin produced by *Shigella dysenteriae* type 1. J Biol Chem 262:1779–1785

Lingwood CA (1996) Role of verotoxin receptors in pathogenesis. Trends Microbiol 4:147–153

Lingwood CA, Law H, Richardson S, Petric M, Brunton JL, De Grandis S, Karmali M (1987) Glycolipid binding of purified and recombinant *Escherichia coli* produced verotoxin in vitro. J Biol Chem 262:8834–8839

Magnadottir B (2006) Innate immunity of fish. Fish Shellfish Immunol 20:137–151

Mangeney M, Lingwood C, Taga S, Caillou B, Tursz T, Wiels J (1993) Apoptosis induced in Burkitt's lymphoma cells via Gb3/CD77, a glycolipid antigen. Cancer Res 53:5314–5319

Mori T, Kiyokawa N, Katagiri Y, Taguchi T, Suzuki T, Sekino T, Sato N, Ohmi K, Nakajima H, Takeda T, Fujimoto J (2000) Globotriaosylceramide (CD77/GB3) in the glycosphingolipid-enriched membrane domain participate in B-cell receptor-mediated apoptosis by regulating Lyn kinase activity in human B cells. Exp Hematol 28:1260–1268

Naganuma T, Ogawa T, Hirabayashi J, Kasai K, Kamiya H, Muramoto K (2006) Isolation, characterization and molecular evolution of a novel pearl shell lectin from marine bivalve, *Pteria penguin*. Mol Divers 10:607–618

Naiki M, Marcus DM (1975) An immunochemical study of the human blood group P_1, P, and P^k glycosphingolipid antigens. Biochemistry 14:4837–4841

Neth O, Jack DL, Johnson M, Klein NJ, Turner MW (2002) Enhancement of complement activation and opsonophagocytosis by complexes of mannose-binding lectin with mannose-binding lectin-associated serine protease after binding to *Staphylococcus aureus*. J Immunol 169:4430–4436

Nitta K, Kawano T, Sugawara S, Hosono M (2007) Regulation of globotriaosylceramide (Gb3)-mediated signal transduction by rhamnose-binding lectin. Yakugaku Zasshi 127:553–561

Nudelman E, Kannagi R, Hakomori S, Lipinski M, Wiels J, Parsons M, Tursz T (1983) A glycolipid antigen associated with Burkitt lymphoma defined by a monoclonal antibody. Science 220:509–511

Ogawa T, Watanabe M, Naganuma T, Muramoto K (2011) Diversified carbohydrate-binding lectins from marine resources. J Amino acids. doi:10.4061/2011/838914

Okamoto M, Tsutsui S, Tasumi S, Suetake H, Kikuchi K, Suzuki Y (2005) Tandem repeat L-rhamnose-binding lectin from skin mucus of ponyfish, *Leiognathus nuchalis*. Biochem Biophys Res Commum 333:463–469

Ourth DD, Narra MB, Simco BA (2007) Comparative study of mannose-binding C-type lectin isolated from channel catfish (*Ictalurus punctatus*) and blue catfish (*Ictalurus furcatus*). Fish Shellfish Immunol 23:1152–1160

Ozaki H, Ohwaki M, Fukuda T (1983) Studies on lectins of amago (*Oncorhynchus rhodurus*) I. Amago ova lectin and its receptor on homologous macrophages. Dev Comp Immunol 7:77–87

Ozeki Y, Matsui T, Suzuki M, Titani K (1991) Amino acid sequence and molecular characterization of a D-galactose-specific lectin purified from sea urchin (*Anthocidaris crassispina*) eggs. Biochemistry 30:2391–2394

Russell S, Lumsden JS (2005) Function and heterogeneity of fish lectins. Veter Immunol Immunopathol 108:111–120

Saxena SK, O'Brien AD, Ackerman EJ (1989) Shiga toxin, Shiga-like toxin II variant, and ricin are all single-site RNA N-glycosidases of 28 S RNA when microinjected into Xenopus oocytes. J Biol Chem 264:596–601

Sharon N, Lis H (2004) History of lectins: from hemagglutinins to biological recognition molecules. Glycobiology 14: 53R–62R

Shirai T, Watanabe Y, Lee M, Ogawa T, Muramoto K (2009) Structure of rhamnose-binding lectin CSL3: unique pseudo-tetrameric architecture of a pattern recognition protein. J Mol Biol 391:390–403

Simons K, Ikonen E (1997) Functional rafts in cell membrane. Nature 387:569–572

Sugawara S, Sasaki S, Ogawa Y, Masahiro H, Nitta K (2005a) Catfish (*Silurus asotus*) lectin enhances the cytotoxic effects of doxorubicin. Yakugaku Zasshi 125:327–334

Sugawara S, Masahiro H, Ogawa Y, Takayanagi M, Nitta K (2005b) Catfish egg lectin causes rapid activation of multidrug resistance 1 P-glycoprotein as a lipid translocase. Biol Pharm Bull 28:434–441

Taga S, Carlier K, Mishal Z, Capoulade C, Mangeney M, Lecluse Y, Coulaud D, Tetaud C, Pritchard LL, Tursz T, Wiels J (1997) Intracellular signaling events in CD77-mediated apoptosis of Burkitt's lymphoma cells. Blood 90:2757–2767

Takenouchi H, Kiyokawa N, Taguchi T, Matsui J, Katagiri Y-U, Okita H, Okuda K, Fujimoto J (2004) Shiga toxin binding to globotriaocyl ceramide induces intracellular signals that mediate cytoskeketon remodeling in human renal carcinoma-derived cells. J Cell Sci 117:3911–3922

Tateno H, Ogawa T, Muramoto K, Kamiya H, Saneyoshi M (2002) Rhamnose-binding lectins from steelhead trout (*Oncorhynchus mykiss*) eggs recognize bacterial lipopolysaccharides and lipoteichoic acid. Biosci Biotechnol Biochem 66:604–612

Terada T, Watanabe Y, Tateno H, Naganuma T, Ogawa T, Muramoto K, Kamiya H (2007) Structural characterization of a rhamnose-binding glycoprotein (lectin) from Spanish mackerel (*Scomberomorous niphonius*) eggs. Biochim Biophys Acta 1770:617–629

Thiel S, Vorup-Jensen T, Stover CM, Schwaeble W, Laursen SB, Poulson K, Willis AC, Eggleton P, Hansen S, Holmskov U, Reid KBM, Jensenius JC (1997) A second serine protease associated with mannan-binding lectin that activates complement. Nature 386:506–510

Tsutsui S, Komatsu Y, Sugiura T, Araki K, Nakamura O (2011) A unique epidermal mucus lectin identified from catfish (*Silurus asotus*): first evidence of ontelectin in fish skin slime. J Biochem 150:501–514

Vasta GR, Nita-Lazar M, Giomarelli B, Ahmed H, Du S, Cammarata M, Parrinello N, Bianchet MA, Amzel LM (2011) Structural and functional diversity of the lectin repertoire in teleost fish: relevance to innate and adaptive immunity. Dev Comp Immunol 35:1388–1399

Wang L, Wang L, Zhang D, Li F, Wang M, Huang M, Zhang H, Song L (2013) A novel C-type lectin from crab *Eriocheir sinensis* functions as pattern recognition receptor enhancing cellular encapsulation. Fish Shellfish Immunol 34: 832–842

Watanabe Y, Shiina N, Shinozaki F, Yokoyama H, Kominami J, Nakamura-Tsuruta S, Hirabayashi J, Sugahara K, Kamiya H, Matsubara H, Ogawa T, Muramoto K (2008) Isolation and characterization of L-rhamnose-binding lectin, which binds to microsporidian *Glugea plecoglossi*, from ayu (*Plecoglossus altivelis*) eggs. Dev Comp Immunol 32: 487–499

Watanabe Y, Tateno H, Nakamura-Tsuruta S, Kominami J, Hirabayashi J, Nakamura O, Watanabe T, Kamiya H, Naganuma T, Ogawa T, Naude RJ, Muramoto K (2009) The function of rhamnose-binding lectin in innate immunity by restricted binding to Gb3. Dev Comp Immunol 33:187–197

Yamazaki M, Okutomi T, Sakakibara F, Kawauchi H, Mizuno D (1984) Macrophage-mediated tumor lysis induced by loach egg lectin. J Leukoc Biol 35:241–250

Yoshida Y, Adachi E, Fukiya K, Iwai K, Tanaka K (2005) Glycoprotein-specific ubiquitin ligases recognize N-glycans in unfolded substrates. EMBO Rep 6:239–244

Yu S, Yang H, Chai Y, Liu Y, Zhang Q, Ding X, Zhu Q (2013) Molecular cloning and characterization of a C-type lectin in roughskin sculpin (*Trachidermus fasciatus*). Fish Shellfish Immunol 34:582–592

Zhang H, Yan D, Shi X, Liang H, Pang Y, Qin N, Chen H, Wang J, Yin B, Jiang X, Feng W, Zhang W, Zhou M, Li Z (2008) Transmembrane TNF-α mediates "forward" and "reverse" signaling, inducing cell death or survival via the NF-κB pathway in Raji Burkitt lymphoma cells. J Leukoc Biol 84:789–797

Sialic acid-binding lectin (leczyme) induces apoptosis to malignant mesothelioma and exerts synergistic antitumor effects with TRAIL

TAKEO TATSUTA[1], MASAHIRO HOSONO[1], KOHTA TAKAHASHI[1], TAKASHI OMOTO[1], YUKIKO KARIYA[2], SHIGEKI SUGAWARA[1], SENITIROH HAKOMORI[3] and KAZUO NITTA[1]

[1]Division of Cell Recognition Study, Institute of Molecular Biomembrane and Glycobiology, Tohoku Pharmaceutical University, Aoba-ku, Sendai 981-8558; [2]Fukushima Medical University, Fukushima 960-1295, Japan; [3]Division of Biomembrane Research, Pacific Northwest Research Institute, WA 98122, USA

Received August 1, 2013; Accepted October 17, 2013

DOI: 10.3892/ijo.2013.2192

Abstract. Malignant mesothelioma is a highly aggressive tumor with poor prognosis. An effective drug for treatment of malignant mesothelioma is greatly needed. Sialic acid-binding lectin (SBL) isolated from oocytes of *Rana catesbeiana* is a multifunctional protein which has lectin activity, ribonuclease activity and antitumor activity, so it could be developed as a new type of anticancer drug. The validity of SBL for treatment of malignant mesothelioma was assessed using three malignant mesotheliomas and a non-malignant mesothlial cell line. Effectiveness of combinatorial treatment of SBL and tumor necrosis factor-related apoptosis inducing ligand (TRAIL) was also elucidated and characterized. SBL induced tumor-selective cytotoxicity that was attributed to induction of apoptosis. Combinatorial treatment of SBL and TRAIL showed synergistic apoptosis-inducing effect. Additional experiments revealed that Bid was the mediating molecule for the synergistic effect in SBL and TRAIL. These results suggested that SBL could be a promising candidate for the therapeutics for malignant mesothelioma. Furthermore, the combinatorial treatment of SBL and TRAIL could be an effective regimen against malignant mesothelioma.

Introduction

Malignant mesothelioma is a highly aggressive tumor with poor prognosis (1). It is commonly accepted that the development of malignant mesothelioma is closely associated with exposure to asbestos, radiation or simian virus 40 (2). Because of the fact that asbestos has been used in thousands of products for a long time all over the world, and estimated latency period between exposure to asbestos and diagnosis of mesothelioma is 20-40 years, and it is expected that the incidence of malignant mesothelioma increases dramatically over the next couple of decades (3,4). Malignant mesothelioma shows strong resistance to existing chemotherapy, irradiation therapy, and operative therapy and extremely poor prognosis with median survival and 5-year survival of <1 year and 1%, respectively (5,6). Because the benefits of single-agent first-line or second-line chemotherapy are limited, the current standard of care for first-line chemotherapy is cisplatin and pemetrexed (a folate inhibitor), the only first-line therapy approved by the US Food and Drug Administration for patients ineligible for surgery (7).

Sialic acid binding lectin (SBL) isolated from *Rana catesbeiana* is a multifunctional protein that has lectin activity, ribonuclease activity and antitumor activity. SBL selectively agglutinates tumor cells but not normal cells (8-10). The selective effect of SBL on cancer cells is due to its selective binding to tumor cells, because sialidase treatment of cells abolished the tumor cell agglutination and anti-proliferative effect induced by SBL (11). We previously reported the antitumor effect of SBL *in vitro* and *in vivo* (11-14), and the mechanism of SBL-inuduced apoptois was studied in human leukemia Jurkat cells (15,16). We studied the efficiency of SBL on treatment of malignant mesothelioma. We showed that SBL suppressed the cell proliferation of malignant mesothelioma and exerted synergistic apoptotic effect with tumor necrosis factor-related apoptosis inducing ligand (TRAL). The synergistic mechanism was analyzed and the potential of SBL as a new, active, anticancer reagent is suggested.

Materials and methods

Materials. SBL was isolated in sequential chromatography on Sephadex G-75, DEAE-cellulose, hydroxyapatite, and SP-Sepharose as described previously (17). Etoposide and anti-β-actin antibody were purchased from Sigma-Aldrich, (Tokyo, Japan). TRAIL was purchased from R&D Systems (Minneapolis, MN, USA). The antibodies utilized were:

Correspondence to: Dr Kazuo Nitta, Institute of Molecular Biomembrane and Glycobiology, Tohoku Pharmaceutical University, 4-4-1 Komatsushima, Aoba-ku, Sendai 981-8558, Japan
E-mail: knitta@tohoku-pharm.ac.jp

Key words: lectin, ribonuclease, leczyme, malignant mesothelioma, TRAIL, Bid, synergistic antitumor effect

anti-caspase-9 (MBL, Nagoya, Japan), anti-caspase-8, anti-caspase-3, anti-Bim, anti-Bik, anti-Bax and anti-Bid (Cell Signaling Technology, Beverly, MA, USA), anti-GAPDH (Ambion, Austin, TX, USA), anti-ERK1/2 (pT202/pY204), anti-ERK1, anti-JNK/SAPK (pT183/pY185), anti-JNK/SAPK, anti-p38 (pT180/pY182), and anti-p38 (BD Biosciences, Franklin Lakes, NJ, USA), horseradish peroxidase (HRP)-conjugated anti-mouse IgG (Zymed, South San Francisco, CA, USA), and HRP-conjugated anti-rabbit IgG (Cedarlane, Hornby, Ontario, Canada). Bid specific siRNA were obtained from Ambion.

Cell culture. Malignant mesothelioma cell line NCI-H28 and immortalized non-malignant mesothelial cell line Met-5A were purchased from American Type Culture Collection (ATCC; Manassas, VA, USA). Malignant mesothelioma cell lines ACC-MESO-1 and ACC-MESO-4 were obtained from Riken Cell Bank (Tsukuba, Japan). H28, MESO-1 and MESO-4 cells were cultured in RPMI-1640 medium supplemented with 10% fetal bovine serum (FBS). Met-5A was cultured in Medium 199 with Earle's balanced salt solution, 75 mM L-Gln, and 1.25 g/l sodium bicarbonate, supplemented with 3.3 nM epidermal growth factor (EGF), 400 nM hydrocortisone, 870 nM insulin, 20 mM HEPES, and 10% FBS. All cells were cultured with penicillin (100 U/ml) and streptomycin (100 μg/ml) at 37°C in 95% air and 5% CO_2 atmosphere.

Clonogenic assay. Cells were precultured for 24 h, and treated with SBL at various concentration for 48 h. Thereafter, the cells were trypsinized, and washed with phosphate-buffered saline (PBS), and plated in a 6-well plate (MESO-1, 500; MESO-4 and H28, 1,000; MeT-5A, 3,000 cells/well, respectively). After 12 days, the colonies were fixed with 2% paraformaldehyde, and stained with 0.1% crystal violet.

Analysis of Annexin V binding and propidium iodide (PI) incorporation. Annexin V binding and PI incorporation were detected with a MEBCYTO apoptosis kit (MBL). The cells were harvested and washed with PBS, then stained with fluorescein isothiocyanate (FITC)-labeled Annexin V and PI. Fluorescence intensity was determined using a FACScalibur flow cytometer (BD Biosciences).

Western blotting. Whole cell lysate was prepared by lysing the cells with extraction buffer [150 mM NaCl, 1% Triton X-100, 10 mM Tris-HCl (pH 7.5), 5 mM EDTA (pH 8.0), 1 mM phenylmethylsulfonyl fluoride (PMSF), 1 tablet/10 ml protease inhibitor cocktail (Roche Applied Science, Indianapolis, IN, USA)]. Soluble proteins were collected and concentrations were measured by DC protein assay kit (Bio-Rad, Richmond, CA, USA). Proteins were separated by SDS-PAGE and transferred to polyvinylidine difluoride (PVDF) membrane (GE Healthcare, Little Chalfont, UK). The membrane was blocked by 5% fat-free skim milk, then primary and secondary antibodies were added to the membrane, respectively. Bands of interest were detected using ECL Western blotting detection regents (GE Healthcare).

Calculation of CI values. To assess whether the combination effect is synergistic or additive, CI analysis was performed. CI, a numerical value calculated as described in equation below provides a quantitative measure of the extent of drug interaction.

$$CI = C_{SBL,X}/ IC_{X,SBL} + C_{TRAIL,X}/IC_{X,TRAIL}$$

$C_{SBL,X}$ and $C_{TRAIL,X}$ are the concentrations of SBL and TRAIL used in combination to achieve x% drug effect. $IC_{X,SBL}$ and $IC_{X,TRAIL}$ are the concentrations for single agents to achieve the same effect. When the concentration of SBL was set to 0.5 μM, treatment with TRAIL carried out in the range of 0.1-2.0 ng/ml, and when the concentration of TRAIL was set to 1 ng/ml, treatment with SBL carried out in the range of 0.1-2.0 μM. CI of <, = and >1 indicates synergy, addictively and antagonism, respectively.

Detection of the reduction of mitochondrial membrane potential (MMP). MMP was assessed using a fluorescent probe 5,50,6,60-tetrachloro-1,10,3,30-tetraethyl-benzamidazolocarbocyanin iodide (JC-1, AnaSpec, Fremont, CA, USA). Cells were cultured in the conditions of each experiment and then incubated with JC-1 (2 μM) dye diluted in culture medium at 37°C for 15 min. The cells were washed with PBS and analyzed using FACScalibur (Becton-Dickinson).

Knock-down of expression of Bid by siRNA treatment. Introduction of siRNA into H28 cells was performed by lipofection method. Bid specific siRNA (10 μM, sense; GGG AUGAGUGCAUCACAAATT, antisense; UUUGUGAUGC ACUCAUCCCTG) and Lipofectamine were mixed with Opti-MEM and added to the cells. After 4-h incubation, the medium was replaced with fresh medium and cells were cultured for 48 h. Thereafter, cells were harvested, plated in fresh dishes, and cultured for 24 h, and then siRNA was introduced again as above. The cells were used for the experiments 48 h from the final transfection.

Statistical analysis. Results were collected from three independent experiments, each performed in triplicate, and data are expressed as the mean ± SD. Statistical analysis was performed using GraphPad Prism 3.0 and comparisons were performed using Student's t-test, one-way or two-way analysis of variance (ANOVA), followed by Bonferroni's *post hoc* tests.

Results

SBL shows anti-proliferative effects on malignant mesothelioma cells but not on non-malignant mesothelial cells. Anti-proliferative effect of SBL to three malignant mesothelioma cell lines (H28, MESO-1 and MESO-4) and non-malignant mesothelial cells (Met-5A) was assessed by clonogenic assay. At the concentrations 5, 10 and 20 μM of SBL, the colony formations of MESO-1 and MESO-4 cells were <70, 30 and 5% and 20, 15 and 5%, respectively. In H28 cells, the colony formation was <5% at all concentrations tested, while the colony formation of Met-5A cells were higher at 90, 65 and 60%, respectively (Fig. 1). H28 cells were the most sensitive in the cell lines tested, and sensitivity was observed in the order MESO-1, MESO-4 and Met-5A cells. These results indicate that SBL has selective anti-proliferative effects on malignant mesothelioma cells.

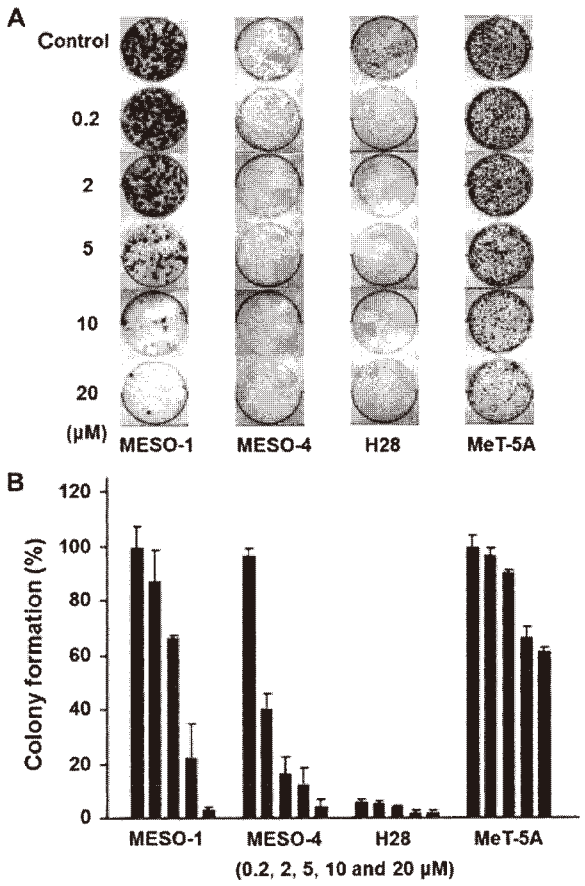

Figure 1. Effect of SBL on clonogenic potential of malignant mesothelioma cells and non-malignant mesothelial MeT-5A cells. (A) Cells were precultured for 24 h, then treated with increasing doses of SBL (0.2, 2, 5, 10 and 20 μM) for 48 h. After treatment, cells were washed with medium and plated in a 6-well plate (MESO-1, 500; MESO-4 and H28, 1,000; MeT-5A, 3,000 cells/well, respectively). After 12 days, the colonies were fixed with 2% paraformaldehyde, and stained with 0.1% crystal violet. (B) Assays were done in triplicate, and the average of colony counts is presented.

SBL induces apoptosis to malignant mesothelioma cells but not to non-malignant mesothelial cells. Next, we assessed whether the anti-proliferative effect on SBL to malignant mesothelioma cells is the resultant of apoptosis or not. Annexin V binding was observed in all three malignant mesothelioma cells from 24-h treatment of SBL in a time-dependent mannner, while Annexin V binding was not detected in Met-5A cells (Fig. 2A). Then, we analyzed activation of caspases in SBL-treated H28 and Met-5A cells by western blotting. Apparent activation of caspase-8, -9 and -3 was observed from 48-h treatment with SBL in H28, but not in Met-5A cells (Fig. 2B). Furthermore, to clarify the other factors involved in SBL-induced apoptosis, we assessed the expression of proapoptotic Bcl-2 protein members by western blotting. There were no alteration in expression of Bax, Bid, and Puma, but elevated expression of Bim was observed, and maximal at 24 h (Fig. 2C). Transient elevation of Bik expression was also observed as early as 6-h treatment with SBL. We also analyzed if mitogen-activated protein kinases (MAPKs) were activated in the process of SBL-induced apoptosis. Elevation of total p38 expression was observed from 24-h treatment with SBL. Phosphorylation of p38 and JNK was detected from 24- and 12-h treatment with SBL, respectively, in a time-dependent manner. On the other hand, phosphorylation of ERK was diminished from 12-h treatment with SBL. These results indicate that SBL induces apoptosis selectively to malignant cells. Moreover, it was considered that Bcl-2 family proteins such as Bim and Bik, and p38 and JNK may be involved in apoptotic signal caused by SBL.

Table I. Calculation for the combination of SBL and TRAIL.

Combination index (CI)	
SBL (0.5 μM)	TRAIL (1 ng/ml)
0.63	0.68

CI values of >1 and <1 indicate drug antagonism and synergism, respectively.

Combinatorial treatment with SBL and TRAIL shows synergistic cytotoxity to H28 cells attributed to enhancement of apoptosis. Studies were designed to investigate the effectiveness of combinatorial treatment with SBL and other anticancer reagents. Fas ligand and TNFα reportedly kill not only tumor cells but also normal cells, whereas, TRAIL is promising because of its high selectively to cancer cells. We analyzed if the antitumor effects were enhanced by combinatorial treatment with SBL and TRAIL. Twenty-four-hour treatment of SBL (5 μM) and TRAIL (2 ng/ml) alone resulted in loss of viability to 66.7 and 70.9%, respectively. Combinatorial treatment with SBL and TRAIL decreased the viability to 24.7% (Fig. 3A). When the concentration of SBL was set to 0.5 μM or TRAIL was 1 ng/ml, the CI values were 0.63 and 0.68, respectively, which indicate synergistic effect (Table I). To study the mechanism of synergistic effect of SBL and TRAIL, we tested whether apoptosis is enhanced in combinatorial treatment. Etoposide that enhances TRAIL-induced apoptosis, was assessed together as a positive control. Similarly to combinatorial treatment with etoposide and TRAIL, Annexin V binding was significantly increased in combinatorial treatment with SBL and TRAIL in H28 cells, whereas these effects were not observed in Met-5A cells (Fig. 3B). Furthermore, activation of caspase-8, -9 and -3 was significantly enhanced in combinatorial treatment with SBL and TRAIL (Fig. 3C in H28 cells). These results suggest that synergistic cytotoxicity of SBL and TRAIL are caused by the enhancement of apoptosis.

Synergistic effect of SBL and TRAIL is mediated by Bid. Next, we analyzed how the synergistic effects were induced in combinatorial treatment with SBL and TRAIL. Some anticancer reagents increase the expression of DR4 and DR5 and shows synergistic antitumor effect with TRAIL. We analyzed the expression of DR4 and DR5 in SBL-treated H28 cells by western blotting to elucidate the possibility if SBL could increase the expression of these receptors. Bortezomib that increases the expression of DR4 and DR5 was used as a positive control. We detected an increase of DR4 and DR5 expression in bortezomib-treated cells, but there are no increments of DR4 and DR5 expression in SBL-

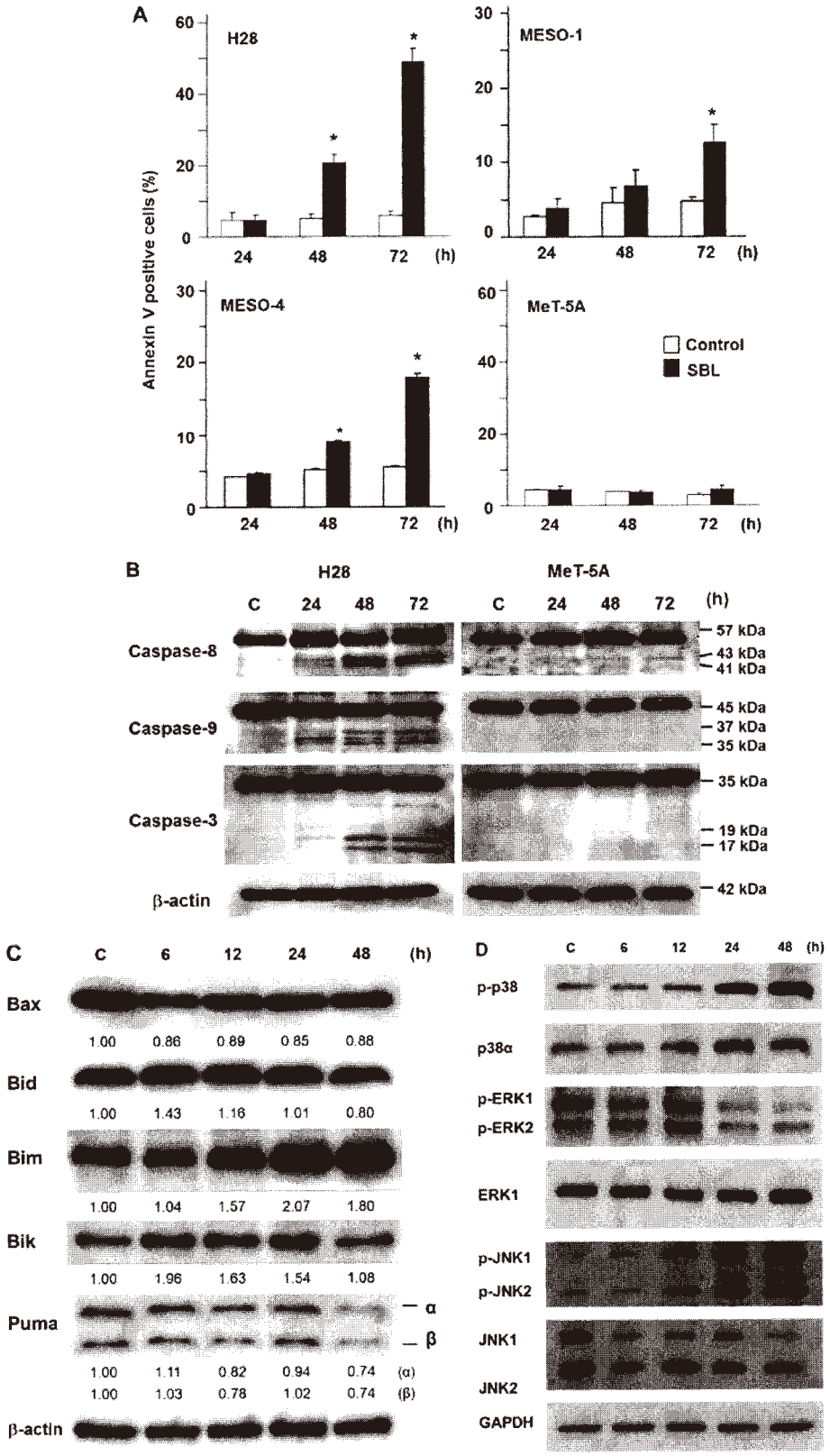

Figure 2. SBL induces apoptosis in malignant mesothelioma cells. (A) Binding of Annexin V in SBL-treated cells (H28, MESO-1, MESO-4 and MeT-5A). Cells were treated with SBL (5 μM) for the indicated time. The percentage of Annexin V-positive cells was determined using flow cytometric analysis. Data are expressed as the mean ± SD of three independent experiments. *P<0.05 versus control. (B) Caspase activation in SBL-treated H28 and MeT-5A cells. H28 and MeT-5A cells were treated with SBL (5 μM) for the indicated time. The activation of caspase-8, -9 or -3 was determined by western blotting. β-actin was used as a standard to ensure equivalent loading of cell extracts. (C) Effect of SBL on expression of proapoptotic Bcl-2 family proteins. H28 cells were treated with SBL (5 μM) for the indicated time. Expression of Bax and BH3-only proteins (Bid, Bim, Bik and Puma) was determined. Bands in the western blotting were quantified by densitometry and expressed as a ratio of intensity of bands to β-actin (respective bands/actin). (D) Phosphorylation pattern of MAPKs in SBL-treated H28 cells. H28 cells were treated with SBL (5 μM) for the indicated time. Expressions of each protein were detected by western blotting. GAPDH was used as a standard to ensure equivalent loading of cell extracts.

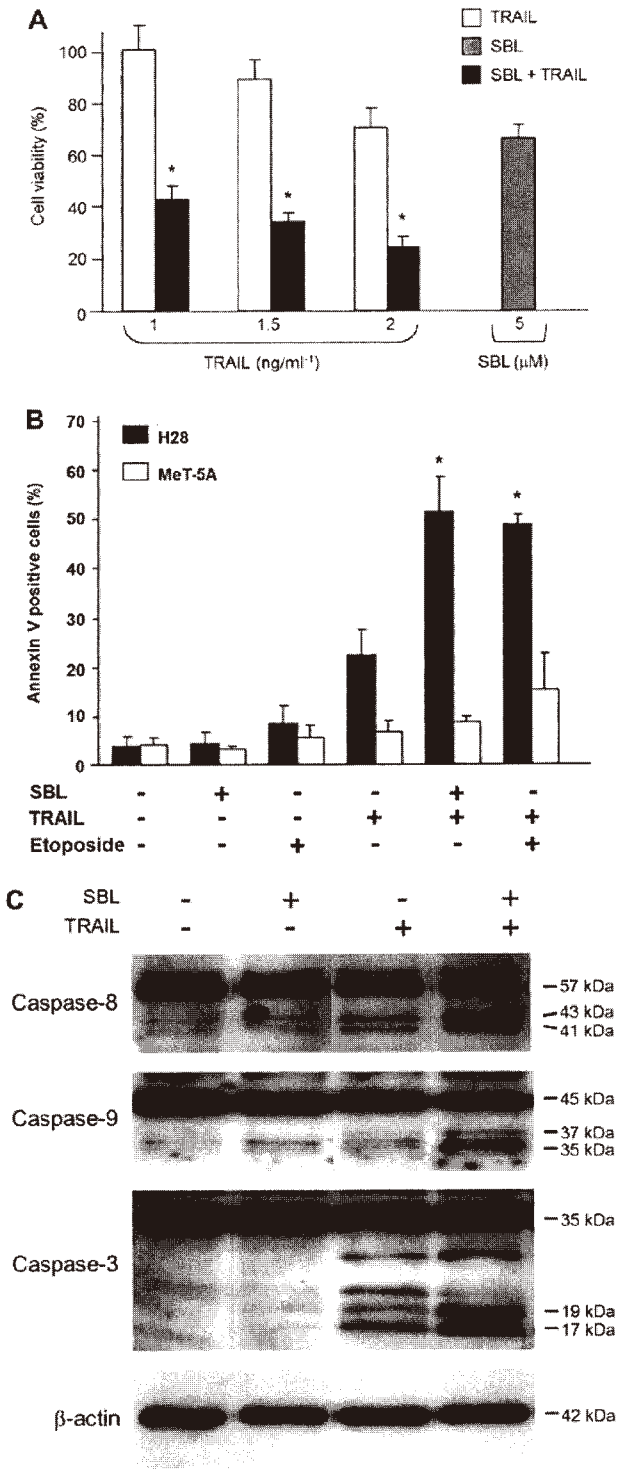

Figure 3. Combinatorial treatment with SBL and TRAIL shows synergistic cytotoxicity. (A) Cytotoxic effect of combination of SBL and TRAIL in H28 cells. Cells were treated with SBL (5 μM) and/or TRAIL (1, 1.5 and 2 ng/ml) in combination for 24 h. The viability was determined by WST-1 assay. Data are expressed as the mean ± SD from three independent experiments in triplicate. *P<0.05 versus SBL alone. (B) Binding of Annexin V in combination-treated cells. H28 or MeT-5A cells were treated with SBL (5 μM), etoposide (50 μM) and/or TRAIL (2 ng/ml) for 24 h. The percentage of Annexin V-positive cells was determined using flow cytometric analysis. Data are expressed as the mean ± SD of three independent experiments. *P<0.02 versus TRAIL alone. (C) Caspase activation in combination-treated H28 cells. Cells were treated with SBL (5 μM) and/or TRAIL (2 ng/ml) for 24 h. The activation of caspase-8, -9 or -3 was determined by western blotting. β-actin was used as a standard to ensure equivalent loading of cell extracts.

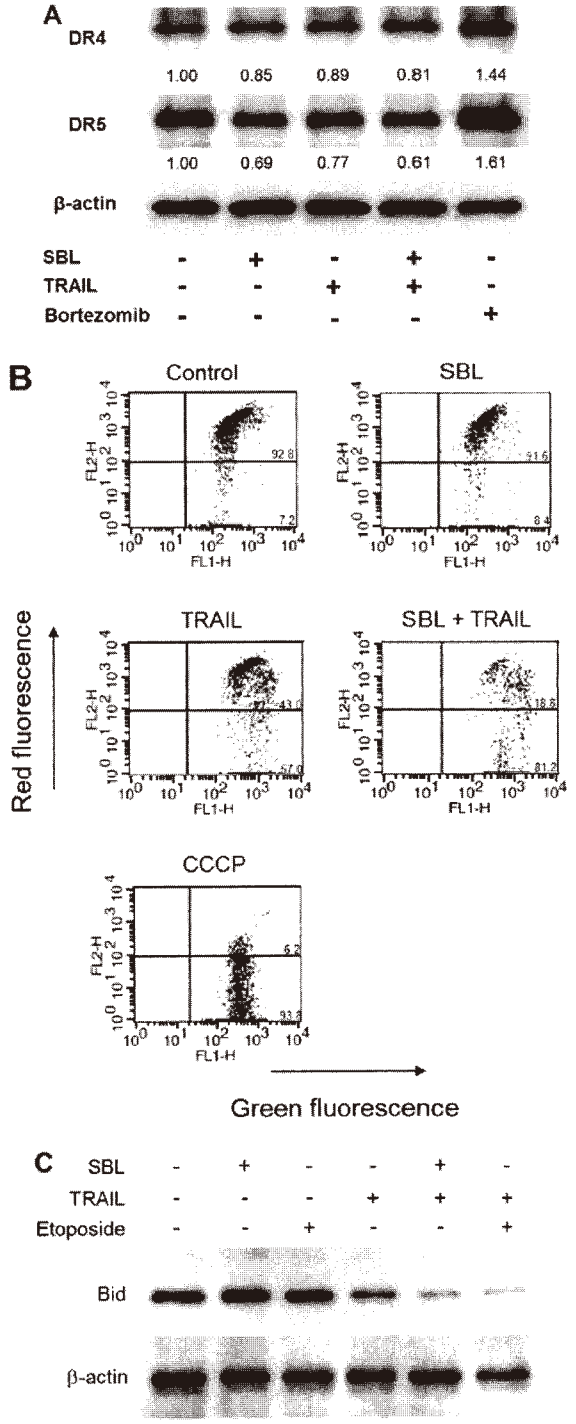

Figure 4. Mechanistic analysis of synergistic effect of SBL and TRAIL. (A) Effect of SBL on expression of DR4 and DR5. H28 cells were treated with SBL (5 μM) and/or TRAIL (2 ng/ml) in combination for 24 h. Expression of DR4 and DR5 was determined western blotting. Bortezomib (10 nM), known to upregurate DR4 and DR5, was used as positive control. Bands in the western blotting were quantified by densitometry, and expressed as a ratio of intensity of bands to β-actin (respective bands/actin). (B) Change of MMP in combination-treated H28 cells. Cells were treated with SBL (5 μM) and/or TRAIL (2 ng/ml) for 24 h and then exposed to JC-1 for 30 min. Change of MMP was determined using flow cytometric analysis. The percentage of cells divided into lower right-hand (LR) quadrant and upper right-hand (UR) quadrant is indicated. (C) Bid-mediated synergistic effect in combinatorial treatment with SBL and TRAIL. Bid cleavage in combination-treated H28 cells. Cells were treated with SBL (5 μM), etoposide (50 μM) and/or TRAIL (2 ng/ml) for 24 h. The cleavage of Bid was determined by western blotting. β-actin was used as a standard to ensure equivalent loading of cell extracts.

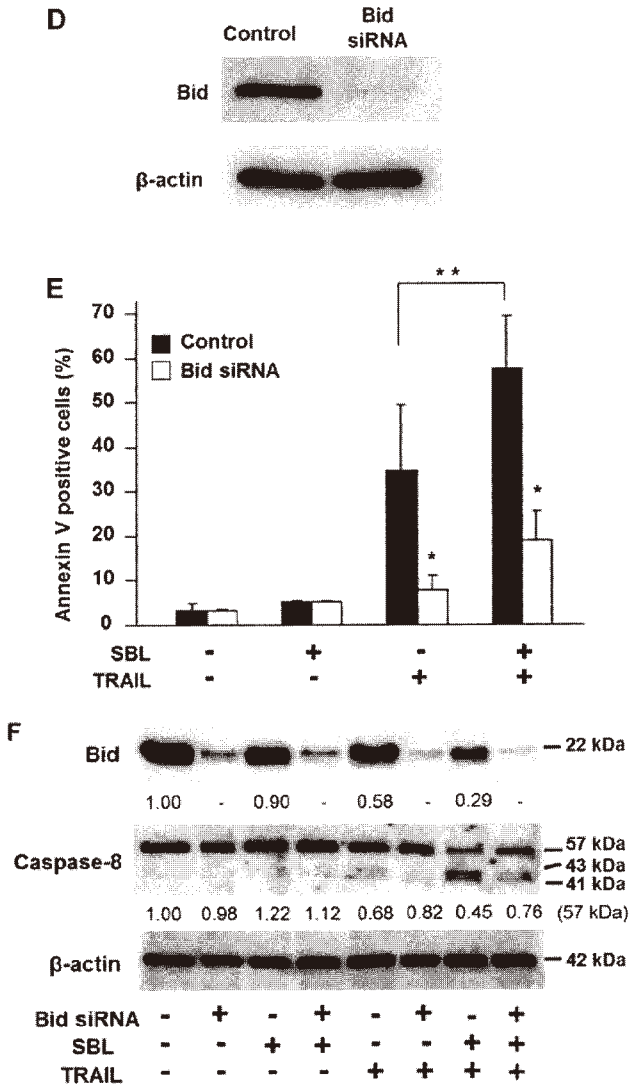

Figure 4. Continued. (D) RNA knock-down of Bid. H28 cells were subjected to two sequential rounds of transfection with Bid-specific siRNAs or vehicle (control). Bid expression is almost abrogated by the specific RNAi; there is no effect on expression of actin. (E) Effect of RNA knock-down of Bid on apoptotic facilitation between SBL and TRAIL in H28 cells. H28 cells subjected to two sequential rounds of Bid specific RNAi were treated with SBL (5 μM) and/or TRAIL (2 ng/ml) for 24 h. Percentage of Annexin V-positive cells was determined using flow cytometric analysis. Data are expressed as the mean ± SD of three independent experiments. P<0.02 versus control transfected with vehicle (*) or TRAIL alone (**). (F) Effect of RNAi knock-down of Bid on caspase-8 cleavage facilitated by combination of SBL and TRAIL in H28 cells. H28 cells transfected with Bid-specific siRNAs or vehicle were treated with SBL (5 μM) and/or TRAIL (2 ng/ml) for 24 h. Bid expression and caspase-8 activation was detected by western blotting. Bands in the western blotting were quantified by densitometry, and expressed as the ratio of intensity of bands to β-actin (respective bands/actin).

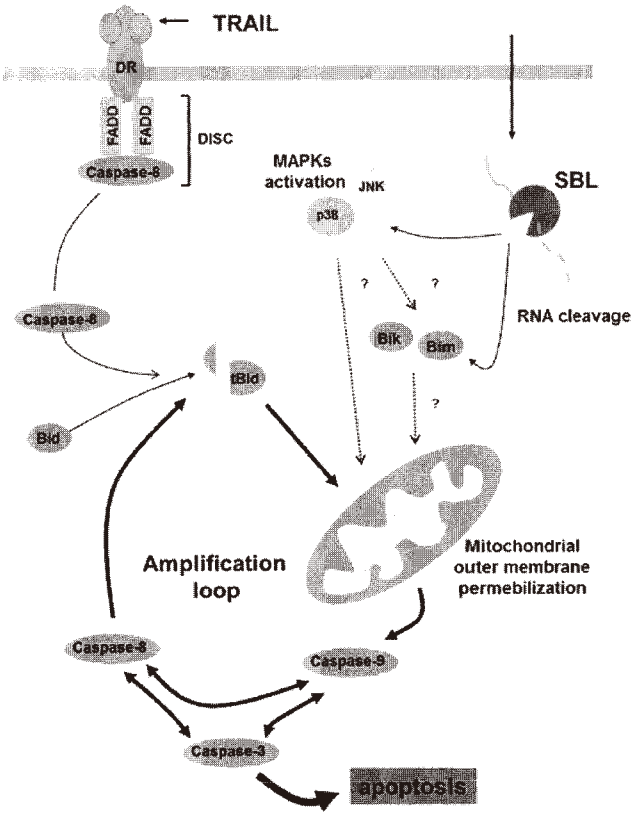

Figure 5. Proposed model for mechanism of apoptosis amplified by SBL and TRAIL in H28 cells. SBL catalyzes cleavage of cellular RNAs, and increases expression of Bik and Bim, phosphorylation of p38 and JNK MAPKs. On the other hand, TRAIL activates DR mediated by death-inducing signaling complex (DISC), which is formed by recruitment of Fas-associated death domain protein (FADD) and caspase-8. Caspase-8 activates Bid. These two signals induce apoptotic 'amplification loop' (thick line) associated with mitochondrial outer membrane permeabilization and caspase activation.

and/or TRAIL-treated cells (Fig. 4A). These results indicate that expression of DR4 and DR5 is not related to enhancement of apoptosis in combinatorial treatment with SBL and TRAIL.

Mitochondrial membrane depolarization is an indicator of apoptosis. We measured the MMP by using the mitochondrial membrane depolarization detector JC- 1. The mitochondrial membrane depolarization was significantly enhanced in combinatorial treatment with SBL and TRAIL, suggesting the involvement of mitochondrial perturbation in a synergistic mechanism (Fig. 4B).

Bid, a proapoptotic member of the Bcl-2 family, is cleaved by activated caspase-8, and then truncated Bid (tBid) translocates from the cytoplasm to the mitochondria, causing an efflux of cytochrome *c* from the mitochondria. We observed truncation of Bid in combinatorial treatment with SBL and TRAIL in H28 cells. Fig. 4C showed that tBid was significantly increased in combinatorial treatment with SBL and TRAIL, similarly to combinatorial treatment with etopside and TRAIL. Next, we assessed the contribution of enhanced Bid activation to synergistic effect of SBL and TRAIL by the knock-down of Bid. Enhancement of Annexin V binding in combinatorial treatment with SBL and TRAIL was significantly decreased by treatment of Bid siRNA (Fig. 4D and E). Furthermore, the enhanced activation of caspase-8 was also diminished by Bid siRNA (Fig. 4F). These results indicate that truncation of Bid is increased in combinatorial treatment with SBL and TRAIL and is plays an important role in synergistic apoptosis execution.

Discussion

In this study, we showed that SBL inhibited cell growth of the various malignant mesothelioma cells, but not of the non-

malignant mesothelial cells (Fig. 1). SBL-induced cytotoxity was accompanied by typical apoptotic changes, and these effects were only seen in malignant mesothelioma (Fig. 2). Thus, the new mechanistic and cancer selective properties of SBL can be assumed for the candidate for new kind of cancer therapy.

Combination therapy has been the standard of care, especially in cancer treatment, since it is a rational strategy to increase response and tolerability, and to decrease resistance. We studied here, the validity of the combinatorial treatment with SBL and TRAIL. TRAIL represents a promising candidate for the cancer therapy, because it causes apoptosis selectively to cancer cells (18,19). There are members of receptors for TRAIL including death receptors (DRs), DR4 and DR5, mediating induction of apoptosis, and the decoy receptors (DcR), DcR1 and DcR2 which fail to induce apoptosis (20-22). The selectivity of TRAIL to cancer cells is attributed to the fact that cancer cells have been shown to highly express the death receptors, whereas normal cells highly express the DcRs. However, many tumor cells are resistant to TRAIL in clinical trials. It is suggested that the low efficiency of TRAIL receptor agonists was due to the induced resistance (23-26). Efforts have been made to overcome the resistance and to improve the efficacy of TRAIL. There are reports that the apoptosis induced by TRAIL is enhanced by some other reagents (27,28). Bortezomib enhances the cytotoxity of TRAIL by increasing the expression of DR4 and DR5. We assessed the possibility that SBL is able to increase the expression of DR4 and DR5, and clarified that their expressions are not affected by SBL treatment (Fig. 4A). Engagement of death ligands to death receptors leads to activation of caspase-8, then activated caspase-8 transduces two different pathways dependent on cell types (29,30). In one pathway the activated caspase-8 directly activates effector caspases such as caspase-3 (31,32), in another pathway activated caspase-8 evokes mitochondrial perturbation through cleavage of Bid, and signal of apoptosis is amplified between caspase activation, mitochondria perturbation and Bid truncation (33). Cell types can be distinguished between type I cells using the former pathway (SKW6.4, H9) or type II cells using the latter pathway (Jurkat, CEM) (34). Etoposide was reported to sensitize malignant mesothelioma M28 cells to TRAIL-induced apoptosis, and this synergic effect requires amplification of death signals by cleavege of Bid, suggesting that M28 cells belong to type II cells (35). We investigated what the mediator of synergistic effect is between SBL and TRAIL. We found enhancement of apoptosis and mitochondrial depolarization in combination-treated H28 cells (Figs. 3 and 4B). Further study revealed increased cleavage of Bid, and it was important for amplification of apoptosis such as enhancement of caspase-8 activation in combination-treated cells (Fig. 4C-F). Our results also suggested that H28 cells belong to type II cells, because the cleavage of Bid enhances the apoptotic signals. Interestingly, Abayasiriwardana *et al* (36) reported that anisomycin, a translation inhibitor, lowers threshold for mitochondrial perturbation through Bim, and suggested that the contribution of JNK for the stability of Bim. Nikrad *et al* (37) and De Wilt *et al* (38) reported that bortezomib sensitizes cells to killing by TRAIL through not only the increment of expression of DR4 and DR5 but also the regulation of expression of Bcl-2 family including Bik and Bim. In the case of SBL, we detected elevated expression of Bik and Bim in SBL-treated cells. While anisomysin activated JNK and ERK but not p38 MAPKs (36), SBL activated JNK and p38 but not ERK (Fig. 2D). These observations suggest that Bcl-2 family proteins and MAPK signals play an important role in synergistic apoptotic cell death caused by combinatorial treatment.

In conclusion, SBL induced selective apoptosis to malignant mesothelioma cells. The combinatorial treatment with SBL and TRAIL induced synergistic apoptosis to malignant mesothelioma. The predicted mechanism is shown in Fig. 5. The synergistic effects were caused through enhancement of Bid cleavage and caspase activation. Bcl-2 family proteins and MAPKs may be involved in the synergistic mechanism. Eventually, apoptotic signal is amplified by amplification loop consisted of caspase activation and mitochondria perturbation and truncation of Bid. The cytotoxic effects of SBL and/or TRAIL were not observed in non-malignant mesothelial cells. Therefore, our results suggest that the combination of SBL and TRAIL can be an effective treatment for malignant mesothelioma.

Acknowledgements

This study was supported in part by Grant-in-Aid of the 'Academic Frontier' Project (2006-2011) and the 'Strategic Research' Project (2012-2017) for Private Universities from the Ministry of Education, Culture, Sports, Science and Technology of Japan.

References

1. Mutsaers SE: The mesothelial cell. Int J Biochem Cell Biol 36: 9-16, 2004.
2. Spugnini EP, Bosari S, Citro G, Lorenzon I, Cognetti F and Baldi A: Human malignant mesothelioma: molecular mechanisms of pathogenesis and progression. Int J Biochem Cell Biol 38: 2000-2004, 2006.
3. McCormack V, Peto J, Byrnes G, Straif K and Boffetta P: Estimating the asbestos-related lung cancer burden from mesothelioma mortality. Br J Cancer 106: 575-584, 2012.
4. Carbone M and Bedrossian CW: The pathogenesis of mesothelioma. Semin Diagn Pathol 23: 56-60, 2006.
5. Sugarbaker DJ and Norberto JJ: Multimodality management of malignant pleural mesothelioma. Chest 113: S61-S65, 1998.
6. Ceresoli GL, Locati LD, Ferreri AJ, Cozzarini C, Passoni P, Melloni G, Zannini P, *et al*: Therapeutic outcome according to histologic subtype in 121 patients with malignant pleural mesothelioma. Lung Cancer 34: 279-287, 2001.
7. Mossman BT, Shukla A, Heintz NH, Verschraegen CF, Thomas A and Hassan R: New insights into understanding the mechanisms, pathogenesis, and management of malignant mesotheliomas. Am J Pathol 182: 1065-1077, 2013.
8. Ceresoli GL, Zucali PA, Gianoncelli L, Lorenzi E and Santoro A: Second-line treatment for malignant pleural mesothelioma. Cancer Treat Rev 36: 24-32, 2010.
9. Liao YD, Huang HC, Chan HJ and Kuo SJ: Large-scale preparation of a ribonuclease from *Rana catesbeiana* (bullfrog) oocytes and characterization of its specific cytotoxic activity against tumor cells. Protein Expr Purif 7: 194-202, 1996.
10. Liao YD, Huang HC, Leu YJ, Wei CW, Tang PC and Wang SC: Purification and cloning of cytotoxic ribonucleases from *Rana catesbeiana* (bullfrog). Nucleic Acids Res 28: 4097-4104, 2000.
11. Nitta K, Ozaki K, Ishikawa M, Furusawa S, Hosono M, Kawauchi H, Sasaki K, *et al*: Inhibition of cell proliferation by *Rana catesbeiana* and Rana japonica lectins belonging to the ribonuclease superfamily. Cancer Res 54: 920-927, 1994.
12. Nitta K, Ozaki K, Tsukamoto Y, Furusawa S, Ohkubo Y, Takimoto H, Murata R, *et al*: Characterization of a *Rana catesbeiana* lectin-resistant mutant of leukemia P388 cells. Cancer Res 54: 928-934, 1994.
13. Nitta K, Ozaki K, Tsukamoto Y, Hosono M, Ogawakonno Y, Kawauchi H, Takayanagi Y, *et al*: Catalytic lectin (leczyme) from bullfrog (*Rana catesbeiana*) eggs. Int J Oncol 9: 19-23, 1996.

14. Nitta K: Leczyme. Methods Enzymol 341: 368-374, 2001.
15. Tatsuta T, Hosono M, Sugawara S, Kariya Y, Ogawa Y, Hakomori S and Nitta K: Sialic acid-binding lectin (leczyme) induces caspase-dependent apoptosis-mediated mitochondrial perturbation in Jurkat cells. Int J Oncol 43: 1402-1412, 2013.
16. Tatsuta T, Hosono M, Miura Y, Sugawara S, Kariya Y, Hakomori S and Nitta K: Involvement of ER stress in apoptosis induced by sialic acid-binding lectin (leczyme) from bullfrog eggs. Int J Oncol 43: 1799-1808, 2013.
17. Nitta K, Takayanagi G, Kawauchi H and Hakomori S: Isolation and characterization of *Rana catesbeiana* lectin and demonstration of the lectin-binding glycoprotein of rodent and human tumor cell membranes. Cancer Res 47: 4877-4883, 1987.
18. Wiley SR, Schooley K, Smolak PJ, Din WS, Huang CP, Nicholl JK, Sutherland GR, *et al*: Identification and characterization of a new member of the TNF family that induces apoptosis. Immunity 3: 673-682, 1995.
19. Ashkenazi A: Targeting death and decoy receptors of the tumour-necrosis factor superfamily. Nat Rev Cancer 2: 420-430, 2002.
20. Pan G, O'Rourke K, Chinnaiyan AM, Gentz R, Ebner R, Ni J and Dixit VM: The receptor for the cytotoxic ligand TRAIL. Science 276: 111-113, 1997.
21. Chaudhary PM, Eby M, Jasmin A, Bookwalter A, Murray J and Hood L: Death receptor 5, a new member of the TNFR family, and DR4 induce FADD-dependent apoptosis and activate the NF-kappaB pathway. Immunity 7: 821-830, 1997.
22. Kawauchi H, Sakakibara F and Watanabe K: Agglutinins of frog eggs: a new class of proteins causing preferential agglutination of tumor cells. Experientia 31: 364-365, 1975.
23. Kurbanov BM, Fecker LF, Geilen CC, Sterry W and Eberle J: Resistance of melanoma cells to TRAIL does not result from upregulation of antiapoptotic proteins by NF-kappaB but is related to downregulation of initiator caspases and DR4. Oncogene 26: 3364-3377, 2007.
24. Younes A, Vose JM, Zelenetz AD, Smith MR, Burris HA, Ansell SM, Klein J, *et al*: A Phase 1b/2 trial of mapatumumab in patients with relapsed/refractory non-Hodgkin's lymphoma. Br J Cancer 103: 1783-1787, 2010.
25. Herbst RS, Eckhardt SG, Kurzrock R, Ebbinghaus S, O'Dwyer PJ, Gordon MS, Novotny W, *et al*: Phase I dose-escalation study of recombinant human Apo2L/TRAIL, a dual proapoptotic receptor agonist, in patients with advanced cancer. J Clin Oncol 28: 2839-2846, 2010.
26. Soria JC, Mark Z, Zatloukal P, Szima B, Albert I, Juhasz E, Pujol JL, *et al*: Randomized phase II study of dulanermin in combination with paclitaxel, carboplatin, and bevacizumab in advanced non-small-cell lung cancer. J Clin Oncol 29: 4442-4451, 2011.
27. Duiker EW, Meijer A, van der Bilt AR, Meersma GJ, Kooi N, van der Zee AG, de Vries EG, *et al*: Drug-induced caspase 8 upregulation sensitises cisplatin-resistant ovarian carcinoma cells to rhTRAIL-induced apoptosis. Br J Cancer 104: 1278-1287, 2011.
28. Liu W, Bodle E, Chen JY, Gao M, Rosen GD and Broaddus VC: Tumor necrosis factor-related apoptosis-inducing ligand and chemotherapy cooperate to induce apoptosis in mesothelioma cell lines. Am J Respir Cell Mol Biol 25: 111-118, 2001.
29. Nagata S: Apoptosis by death factor. Cell 88: 355-365, 1997.
30. Scaffidi C, Fulda S, Srinivasan A, Friesen C, Li F, Tomaselli KJ, Debatin KM, *et al*: Two CD95 (APO-1/Fas) signaling pathways. EMBO J 17: 1675-1687, 1998.
31. Hasegawa J, Kamada S, Kamiike W, Shimizu S, Imazu T, Matsuda H and Tsujimoto Y: Involvement of CPP32/Yama(-like) proteases in Fas-mediated apoptosis. Cancer Res 56: 1713-1718, 1996.
32. Srinivasula SM, Ahmad M, Fernandes-Alnemri T, Litwack G and Alnemri ES: Molecular ordering of the Fas-apoptotic pathway: the Fas/APO-1 protease Mch5 is a CrmA-inhibitable protease that activates multiple Ced-3/ICE-like cysteine proteases. Proc Natl Acad Sci USA 93: 14486-14491, 1996.
33. Takahashi A, Hirata H, Yonehara S, Imai Y, Lee KK, Moyer RW, Turner PC, *et al*: Affinity labeling displays the stepwise activation of ICE-related proteases by Fas, staurosporine, and CrmA-sensitive caspase-8. Oncogene 14: 2741-2752, 1997.
34. Pespeni MH, Hodnett M, Abayasiriwardana KS, Roux J, Howard M, Broaddus VC and Pittet JF: Sensitization of mesothelioma cells to tumor necrosis factor-related apoptosis-inducing ligand-induced apoptosis by heat stress via the inhibition of the 3-phosphoinositide-dependent kinase 1/Akt pathway. Cancer Res 67: 2865-2871, 2007.
35. Broaddus VC, Dansen TB, Abayasiriwardana KS, Wilson SM, Finch AJ, Swigart LB, Hunt AE, *et al*: Bid mediates apoptotic synergy between tumor necrosis factor-related apoptosis-inducing ligand (TRAIL) and DNA damage. J Biol Chem 280: 12486-12493, 2005.
36. Abayasiriwardana KS, Barbone D, Kim KU, Vivo C, Lee KK, Dansen TB, Hunt AE, *et al*: Malignant mesothelioma cells are rapidly sensitized to TRAIL-induced apoptosis by low-dose anisomycin via Bim. Mol Cancer Ther 6: 2766-2776, 2007.
37. Nikrad M, Johnson T, Puthalalath H, Coultas L, Adams J and Kraft AS: The proteasome inhibitor bortezomib sensitizes cells to killing by death receptor ligand TRAIL via BH3-only proteins Bik and Bim. Mol Cancer Ther 4: 443-449, 2005.
38. De Wilt LH, Kroon J, Jansen G, De Jong S, Peters GJ and Kruyt FA: Bortezomib and TRAIL: a perfect match for apoptotic elimination of tumour cells? Crit Rev Oncol Hematol 85: 363-372, 2013.

Sialic acid-binding lectin (leczyme) induces caspase-dependent apoptosis-mediated mitochondrial perturbation in Jurkat cells

TAKEO TATSUTA[1], MASAHIRO HOSONO[1], SHIGEKI SUGAWARA[1], YUKIKO KARIYA[2], YUKIKO OGAWA[3], SENITIROH HAKOMORI[4] and KAZUO NITTA[1]

[1]Division of Cell Recognition Study, Institute of Molecular Biomembrane and Glycobiology, Tohoku Pharmaceutical University, Aoba-ku, Sendai 981-8558; [2]Fukushima Medical University, Fukushima 960-1295; [3]Divisions of Functional Morphology and Microbiology, Department of Pharmacy, Faculty of Pharmaceutical Science, Nagasaki International University, Sasebo, Nagasaki 859-3298, Japan; [4]Division of Biomembrane Research, Pacific Northwest Research Institute, Seattle, WA 98122, USA

Received June 29, 2013; Accepted August 6, 2013

DOI: 10.3892/ijo.2013.2092

Abstract. Sialic acid binding lectin (SBL) isolated from *Rana catesbeiana* oocytes is a multifunctional protein which has lectin activity, ribonuclease activity and antitumor activity. However, the mechanism of antitumor effects of SBL is unclear to date and the validity for human leukemia cells has not been fully studied. We report here that SBL shows cytotoxicity for some human leukemia cell lines including multidrug-resistant (MDR) cells. The precise mechanisms of SBL-induced apoptotic signals were analyzed by combinational usage of specific caspase inhibitors and the mitochondrial membrane depolarization detector JC-1. It was demonstrated that SBL causes mitochondrial perturbation and the apoptotic signal is amplified by caspases and cell death is executed in a caspase-dependent manner. The efficacy of this combinational usage was shown for the first time, to distinguish the apoptotic pathway in detail. SBL selectively kills tumor cells, is able to exhibit cytotoxicity regardless of P-glycoprotein expression and has potential as an alternative to conventional DNA-damaging anticancer drugs.

Introduction

Historically, replicative DNA was the main target of anticancer agents for many years, but because of the selectivity or occurrence of resistance to the drugs, agents which have new strategy such as molecular targeted therapy show promise for the treatment of cancer. Efforts to improve cancer therapy have focused on the development of more selective, biological mechanism-based agents that can overcome tumor resistance, as well as minimize toxic effects to normal cells (1).

Ribonucleases are enzymes which catalyze the degradation of RNA. RNases display various biological roles, including nutritional function, remobilization of phosphate, senescence, self-incompatibility, defensin-like activity and the conspicuous function in RNA metabolism (2,3). Some members of RNases are reported to exhibit angiogenic, neurotoxic, antitumor, or immunosuppressive activities (4). Bovine pancreatic ribonuclease A (RNase A), EC 3.1.27.5 (5), was the first RNase tested for a possible anticancer activity *in vitro* (6-8) and *in vivo* (9-12). While RNase A needed high amounts to observe the anticancer activity, more effective RNases have been reported in recent years. The proposed mechanism of ribonuclease-induced cytotoxicity is: i) cell surface binding and internalization, ii) translocation to the cytosol, iii) evasion of the cytosolic ribonuclease inhibitor protein (RI) and iv) degradation of cellular RNA. Differences in the efficiency of any of these steps could affect the cell susceptibility (13). One promising RNase for cancer therapeutic drug is onconase, a ribonuclease isolated from *Rana pipiens* oocytes. Onconase, manifests cytotoxic and cytostatic effects (14), presents synergism with several kinds of anticancer drugs (15-22) and at present is in phase II/III clinical trials as an anticancer drug (1,23). Onconase has demonstrated some advantages for potential clinical applications, including: a) evading human RNase inhibitors in cytosol, b) inhibitory activity against broad types of human tumors, c) without any untoward immune response and exerting only weak and reversible renal toxicity (24). The phase III clinical trial of onconase has prompted the genetic engineering of known RNases as well as a search for new medicinal RNases (3,12,24,25).

Sialic acid binding lectin (SBL) isolated from *R. catesbeiana* oocytes was found as a lectin, because SBL agglutinates various kinds of tumor cells and the agglutination was inhibited by sialoglycoprotein or ganglioside (26-28). Agglutination induced by SBL was observed in tumor cells, but not in normal

Correspondence to: Dr Kazuo Nitta, Institute of Molecular Biomembrane and Glycobiology, Tohoku Pharmaceutical University, 4-4-1 Komatsushima, Aoba-ku, Sendai 981-8558, Japan
E-mail: knitta@tohoku-pharm.ac.jp

Key words: lectin, ribonuclease, antitumor effect, leczyme, *Rana catesbeiana*, caspase pathway, mitochondria perturbation

red blood cells or fibroblasts (28). Amino acid sequence of SBL shows that it has homology to the member of RNase A superfamily and it has been revealed that SBL practically has pyrimidine base-specific ribonuclease activity (29-32). The antitumor effect of SBL was reported using P388 and L1210 murine leukemia cells *in vitro* and sarcoma 180, Ehrlich and Mep 2 ascites cells *in vivo* (33-35). RC-RNase isolated from *R. catesbeiana* is identical to SBL (36,37). It was also reported that RC-RNase seems to harbor a more specific anticancer activity compared with onconase (38).

However, the mechanism of antitumor effect of SBL is unclear and the validity for human leukemia cells has not been fully studied. We studied the antitumor effect of SBL using some human leukemia cell lines. We found that SBL shows cytotoxicity to some cell lines, including multiple drug resistant (MDR) cells. The mechanism of SBL-induced cytotoxicity is analyzed in detail by combinational usage of specific caspase inhibitors and mitochondrial membrane depolarization detector JC-1 and we clearly show that cytotoxicity is induced through caspase-dependent apoptosis in which mitochondrial perturbation occurs as upstream events. It is extrapolated that the novel mechanistic apoptosis inducing activity toward various human leukemia cells regardless of P-glycoprotein (P-gp) expression indicating that SBL is a new candidate as an alternative to conventional DNA-damaging anticancer drugs.

Materials and methods

Materials. SBL was isolated in sequential chromatography on Sephadex G-75, DEAE-cellulose, hydroxyapatite and SP-Sepharose as described previously (28). Etoposide (ETO), doxorubicin (DOX) and anti-β-actin antibody were purchased from Sigma-Aldrich (Tokyo, Japan). Tumor necrosis factor-related apoptosis inducing ligand (TRAIL) was purchased from R&D Systems (Minneapolis, MN, USA). Caspase inhibitors (zVAD-fmk, zIETD-fmk, zLEHD-fmk) and anti-caspase-9 antibody were purchased from Medical & Biological Laboratories Co., Ltd. (MBL, Nagoya, Japan). Anti-caspase-8 antibody, anti-caspase-3 antibody and anti-Bid antibody were purchased from Cell Signaling Technology (Beverly, MA, USA). Anti-cytochrome *c* antibody was purchased from Becton-Dickinson (Franklin Lakes, NJ, USA). Horseradish peroxidase (HRP)-conjugated anti-mouse IgG actibody and HRP-conjugated anti-rabbit IgG andibody was purchased from Zymed (South San Francisco, CA, USA) and Cedarlane Lab. Ltd. (Hornby, Ontario, Canada), respectively.

Cell culture. Human leukemia Jurkat T-cells, erythroleukemia K562 cells, Adriamycin-resistant and P-gp-overexpressing K562 cells (K562/ADR), Burkitt's lymphoma Raji cells and promyelocytic leukemia U937 cells were obtained from the Cell Resource Center of the Biomedical Research, Institute of Development, Ageing and Cancer, Tohoku University (Sendai, Japan). Cells were routinely kept in RPMI-1640 medium (Nissui Pharmaceutical Co. Ltd., Tokyo, Japan) supplemented with 10% fetal calf serum (FCS), penicillin (100 U/ml) and streptomycin (100 μg/ml) at 37°C in a 95% air and 5% CO_2 atmosphere.

RNA extraction and analysis. The cells were treated with SBL (2 μM) for indicated time. Total RNA of the cells was extracted with TRIzol reagent (Invitrogen, Carlsbad, CA, USA) according to the manufacturer's instructions. RNA (1 μg) was electrophoresed on 2% agarose gel containing formaldehyde (18%). The gels were visualized by ethidium bromide staining.

Measurement of cell viability. To determine the cytotoxicity, WST-8 assays (39), were done in accordance with the manufacturer's instructions. Briefly, the cells ($2x10^4$ cells/well) were plated into 96-well plates. Various concentration of reagents were added in triplicate to the cultures and incubated for indicated times before adding the WST-8 solution. The absorbance of the resulting product was measured 4 h later at a wavelength of 450 nm with back ground subtraction at 650 nm. The IC_{50} which shows the compound concentration required for 50% inhibition of the cell growth was calculated employing GraphPad Prism 3.0 software. Cell viability was determined by trypan blue dye exclusion assay. The cells ($2x10^5$ cells/ml) were cultured in 100 μl in 96-well plates. After treatment with SBL, the cells were stained with 0.25% trypan blue and both viable and non-viable cells were counted.

Observation of nuclear morphology. The cells ($2x10^5$ cells/ml) were cultured in 5 ml in 6-well plates. After treatment with SBL, the cells were collected by centrifugation and washed with PBS. Then the cells were fixed with 1% paraformaldehyde (100 μl) for 15 min at 4°C, and stained with Hoechst 33258 (50 μl, 1 mg/ml) for 15 min at 4°C. After three washes with PBS, the cells were mounted on slide glass using Prolong gold antifade reagent (Molecular Probes). The fluorescence was visualized with a fluorescence microscope, Zeiss Axioscope 2 (Carl Zeiss, Jena GmbH, Jena, Germany).

Detection of DNA fragmentation. The cells ($2x10^5$ cells/ml) were cultured in 100 μl in 96-well plates. After treatment with SBL, the cells were collected by centrifugation, washed with PBS, then lysed with cell lysis buffer [50 mM Tris-HCl (pH 6.8), 10 mM EDTA, 0.5% w/v sodium-N-lauroylsarcosinate]. The samples were incubated for 30 min with RNase A (final concentration, 500 μg/ml) at 50°C, before being digested for 30 min with proteinase K (final concentration, 500 μg/ml) at 50°C. Then the samples were electrophoresed on 1.8% agarose gel, DNA bands were visualized by ethidium bromide staining.

Flow cytometric analysis of Annexin V binding and propidium iodide (PI) incorporation. Annexin V binding and PI incorporation were detected with a MEBCYTO apoptosis kit (MBL) according to the manufacturer's instructions. The cells ($2x10^5$ cells/ml) were cultured in 1 ml in 24-well plates. Fluorescence intensity of fluorescein isothiocyanate (FITC)-Annexin V and PI was determined using a FACSCalibur flow cytometer (Becton-Dickinson).

Detection of caspase activity. Caspase activity was measured with caspase colorimetric protease assay kit (MBL) in accordance with the manufacturer's instructions. After treatment with SBL (2 μM) for indicated time, cells were lysed with cell lysis buffer and incubated for 10 min at 4°C. Then samples

Table I. Inhibitory effect of SBL, ETO and DOX on the viability of human leukemia cell lines.

Cell name	Characteristics	IC_{50} (mM)		
		SBL	ETO	DOX
Jurkat	T-cell leukemia	0.15±0.07	2.09±0.78	1.10±0.71
K562	Erythroleukemia	1.39±0.92	13.23±3.86	3.51±1.84
K562/ADM	P-glycoprotein-overexpressing K562 cells	0.36±0.18	N/A	N/A
U937	Promyelocytic leukemia	0.81±0.24	0.46±0.09	0.34±0.27
Raji	Burkitt's lymphoma	0.88±0.54	0.49±0.04	0.28±0.19

Cells were treated with SBL, ETO or DOX for 72 h. IC_{50} is the concentration which resulted in a 50% decrease in cell viability. Each value indicates the mean ± SD of three different experiments performed in triplicate.

were centrifuged at 12,400 rpm and supernatant was collected. Samples (50 μl, 1 μg/μl) were mixed with equal amount of 2X reaction buffer and substrates (DEVD-pNA for caspase-3, LEHD-pNA for caspase-9, IETD-pNA for caspase-8) were added at final concentration 200 μM. After incubation for 2 h at 37°C, the absorbance of the resulting product was measured at a wavelength of 405 nm.

Treatment of caspase inhibitors. The role of caspase activation in the process was studied by the addition of zVAD-fmk (pan-caspase inhibitor), zIETD-fmk (caspase-8 specific inhibitor) and zLEHD-fmk (caspase-9 specific inhibitor). Each caspase inhibitor (50 μM) was added to culture medium 30 min before the addition of reagents.

Western blotting. Whole cell lysate was prepared by lysing the cells with extraction buffer [150 mM NaCl, 1% Triton X-100, 10 mM Tris-HCl (pH 7.5), 5 mM EDTA (pH 8.0), 1 mM phenylmethylsulfonyl fluoride (PMSF), 1 tablet/10 ml protease inhibitor cocktail (Roche Applied Science, Indianapolis, IN, USA)]. Lysates of organelle (mitochondria) fraction or cytosol fraction were prepared by ProteoExtract Subcellular Proteome Extraction Kit (Merck Millipore, Billerica, MA, USA). Soluble proteins were collected and concentrations were measured by DC protein assay kit (Bio-Rad, Richmond, CA, USA) in accordance with instructions. Proteins were separated by SDS-PAGE and transferred to polyvinylidene difluoride (PVDF) membrane (GE Healthcare, Little Chalfont, UK). The membrane was blocked by 5% fat-free skim milk for 1 h. After the membrane was washed with TBST [20 mM Tris-HCl (pH 7.6), 137 mM NaCl, 0.05% Tween-20], primary and secondary antibodies were added to the membrane, respectively. The proteins on membrane were detected using ECL western blotting detection regents (GE Healthcare).

Detection of mitochondrial membrane potential (MMP) reduction. MMP was assessed using a fluorescent probe 5,50,6,60-tetrachloro-1,10,3,30-tetraethyl-benzamidazolocarbocyanin iodide (JC-1, AnaSpec, Fremont, CA, USA). Red emission from the dye is attributed to a potential-dependent aggregation of JC-1 in the mitochondria. Green fluorescence reflects the monomeric form of JC-1, appearing in the cytoplasm after mitochondrial membrane depolarization. Cells were cultured in condition of each experiment and then incubated with JC-1 (2 μM) dye diluted in culture medium at 37°C for 15 min. The cells were washed three times with PBS and analyzed immediately using FACSCalibur (Becton-Dickinson).

Statistical analysis. Results were collected from three independent experiments, each performed in triplicate and data are expressed as mean ± SD. Statistical analysis was performed using GraphPad Prism 3.0 and comparisons were made using one-way or two-way analysis of variance (ANOVA), followed by Bonferroni's *post hoc* tests.

Results

SBL shows cytotoxicity to some human leukemia cell lines including MDR cells. We have previously shown that SBL has antitumor activity against mouse leukemia cells *in vitro* and *in vivo* (33,34,40). In this study, antitumor activity of SBL for human leukemia cell line and the signaling mechanism was evaluated. To determine the effect of SBL on cell viability of some human leukemia cell lines, WST assay was performed. As shown in Table I, SBL shows cytotoxic effect for all cell lines tested at low concentration (0.15-1.39 μM) and the lowest IC_{50} value was observed in Jurkat cells (0.15 μM). The cytotoxic effect of SBL was observed regardless of the P-gp expression level, while ETO and DOX which are used clinically for leukemia as DNA damaging agent did not cause cytotoxic effect on P-gp-overexpressing K562 cells.

SBL degrades cellular RNA and inhibits cell proliferation of Jurkat cells. Because SBL has pyrimidine base-specific ribonuclease activity (31,32), we analyzed whether the cellular RNA is degraded by SBL or not. Total RNA extracted from SBL-treated Jurkat cells was analyzed by agarose gel electrophoresis and partial RNA degradation was found from 3-h treatment, then increased time-dependently (Fig. 1A). Next, the effects of SBL on Jurkat cell proliferation were analyzed in detail. Trypan blue dye exclusion assay showed that SBL (2 μM) exhibited cytotoxicity toward Jurkat cells from 24 h time-dependently and that SBL (0.2 μM or above) exhibited

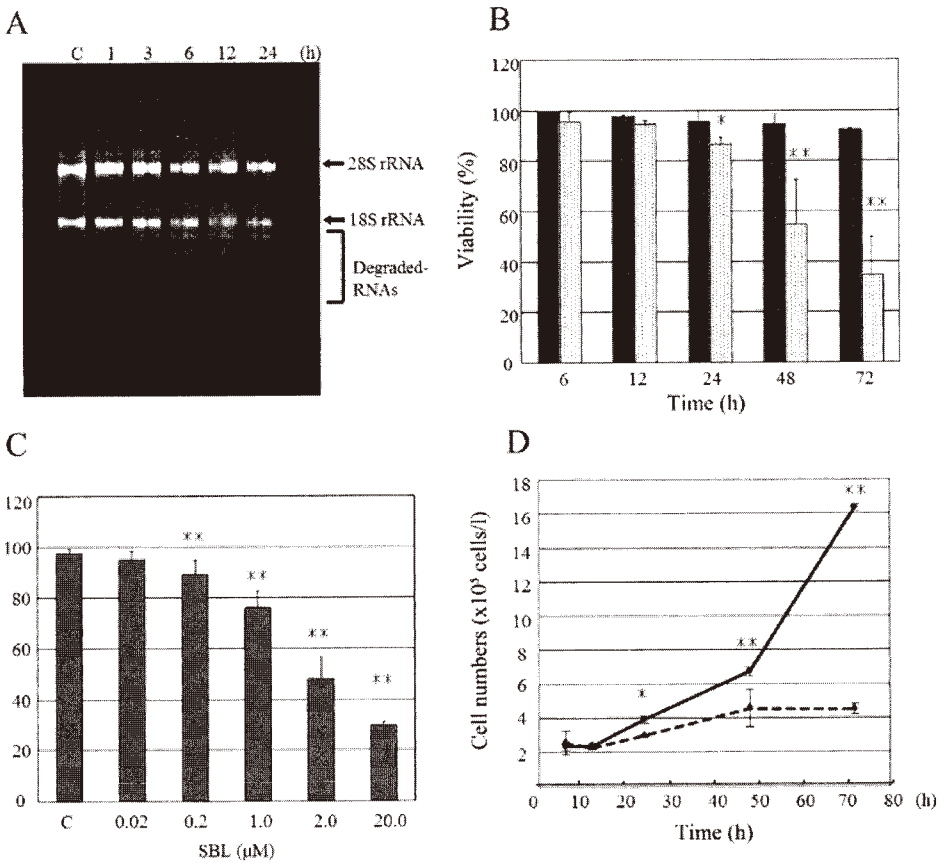

Figure 1. SBL degrades cellular RNA and inhibits cell proliferation of Jurkat cells. (A) Cells were treated with SBL (2 μM) for indicated time and RNA was extracted. Then, electrophoresis was performed on 1.5% agarose gel. C, control. Degraded RNAs were seen under 18S rRNA. (B) Cells were treated with (doted column) or without (filled column) SBL (2 μM) for indicated time. Cell viability was evaluated by trypan blue dye exclusion assay. (C) Cells were treated with SBL at various concentrations for 48 h. Cell viability was evaluated by the method described above. C, control. (D) Cells were treated with (dotted line) or without (solid line) SBL (2 μM) for indicated time and total cell number were counted. Each value represents the mean ± SD of three independent experiments. $^{*}p<0.05$ and $^{**}p<0.01$ vs. control.

cytotoxicity in 48-h treatment concentration-dependently (Fig. 1B and C). Furthermore, significant inhibition of Jurkat cell proliferation was observed from 24-h treatment (Fig. 1D).

SBL induces apoptosis in Jurkat cells. To study the mechanism involved in the cytotoxicity of SBL, first we investigated the morphological changes in SBL-treated Jurkat cells using Hoechst 33258. Exposure of SBL resulted in typical apoptotic morphological alterations, such as karyorrhexis, nuclear condensation and nuclear fragmentation (Fig. 2A). We further observed the apoptotic biological changes in SBL-treated Jurkat cells. Annexin-V binding which is attributed to externalization of phosphatidylserine (PS) was observed from 3-h treatment of SBL (Fig. 2B). Simultaneously, the activation of initiator caspase (-8 and -9) and effector caspase (-3) was observed from 3 or 6 h (Fig. 2C). Similarly, DNA fragmentation was observed in a dose-dependent manner (Fig. 2D). These data indicate that SBL induces apoptosis in Jurkat cells.

SBL-induced apoptosis is dependent on caspases and caspase-9 is activated more strongly than caspase-8. To analyze the detail of SBL-induced caspase activation, we performed experiments using caspase inhibitors. Pretreatment of z-VAD inhibited SBL-induced cell death (Fig. 3A) and completely blocked SBL-induced DNA fragmentation (Fig. 3B). Next, we analyzed activation pattern of caspase-8, -9 and -3 under the presence of specific inhibitors for each of the caspases (Fig. 4). Pretreatment of caspase-9 inhibitor, z-LEHD, inhibited activation of caspase-8. On the other hand, pretreatment of caspase-8 inhibitor, z-IETD, could not inhibit caspase-9 activation and the activation of caspase-9 was not affected even by the treatment of z-VAD or z-LEHD. Pretreatment of caspase-3 inhibitor, z-DEVD did not have an effect on activation of caspase-8 or -9. These data indicate that SBL induces caspase-dependent apoptosis and caspase-9 is activated strongly in SBL-induced apoptosis.

SBL induces activation of p38 and JNK, but not ERK. We monitored the activation of mitogen-activated protein kinases (MAPKs), extracellular signal-regulated kinases (ERKs), c-jun N-terminal kinase (JNKs)/stress-activated protein kinases and p38 in SBL-treated cells. Fig. 5 shows p38 kinase was activated as early as 1 h and sustained to 12 h. Furthermore, activation of JNK1/2 was observed from 1-h treatment and maximal at

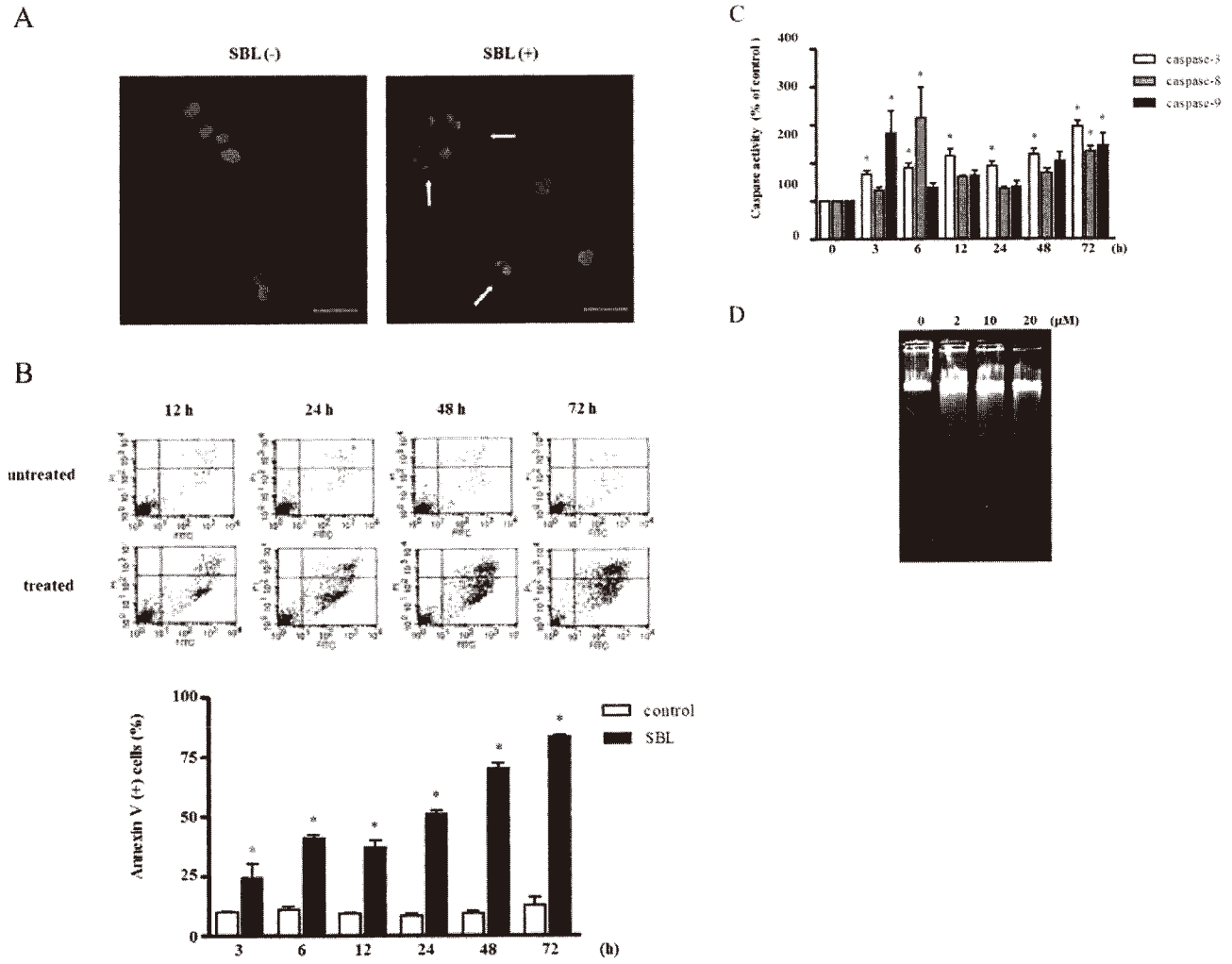

Figure 2. SBL induces apoptosis in Jurkat cells. (A) Morphological changes of nuclei in SBL-treated Jurkat cells. Cells were treated with SBL (2 μM) for 48 h and stained with Hoechst 33258. Nuclei were observed using a fluorescent microscope. SBL-untreated (left panel) and -treated (right panel) cells. Arrows indicate apoptotic nuclei. Magnification, x40 (scale, 10 μm). (B) Time-dependent changes of FITC-Annexin V binding and PI incorporation in SBL-treated Jurkat cells. Cells were treated with SBL (2 μM) for indicated time. Then, analysis of Annexin V-bound vs. PI incorporated cells was performed by FACSCalibur. In the lower panel, the percentage of Annexin V-positive cells is presented. Each value is the mean ± SE of three independent experiments. *$p<0.05$ vs. untreated cells. (C) Caspase activity of SBL-treated Jurkat cells. Cells were treated with SBL (2 μM) for indicated time. Then, the activity of each caspase was measured using fluorometric assay kit. (D) DNA fragmentation in SBL-treated Jurkat cells. Cells were treated with SBL at indicated concentrations for 48 h and DNA was prepared from the cells. DNA fragmentation was analyzed by agarose gel electrophoresis and stained with ethidium bromide.

6-9 h, whereas, activation of ERK was not observed in this condition. These results suggest that p38 and JNK may be involved in SBL-induced apoptotic signaling.

Mitochondrial perturbation occurs before activation of caspases. Because caspase-9 is known as initiator caspase in apoptosis through mitochondria pathway, we analyzed the mitochondrial perturbation in SBL-induced apoptosis. During apoptosis, loss of mitochondrial membrane potential (MMP) is observed. We detected mitochondrial membrane depolarization using JC-1 fluorescent dye in SBL-treated Jurkat cells and found that SBL caused mitochondrial membrane depolarization in a time-dependent manner (Fig. 6A). At the same time, release of cytochrome *c* from mitochondria to cytosol was also observed (Fig. 6B) and the cleavage of Bid, which causes an efflux of cytochrome *c* from the mitochondria, was observed from 6 h. These results show occurrence of mitochondrial perturbation in SBL-treated Jurkat cells.

To study the importance of mitochondrial perturbation in SBL-induced apoptosis, we analyzed cell viability and the mitochondrial depolarization under the presence of caspase inhibitors comparing with TRAIL and ETO known as inducer of apoptosis through death receptor pathway and mitochondrial pathway, respectively. At 48-h treatment with each of the reagents, pretreatment of z-VAD completely inhibited TRAIL-induced cytotoxicity, but did not or only partially inhibited SBL- or ETO-induced cytotoxicity (Fig. 7A). Similarly, mitochondrial depolarization caused by TRAIL was completely inhibited by z-VAD, while SBL or ETO-induced mitochondrial depolarization was not affected by z-VAD (Fig. 7B). Furthermore, z-IETD inhibited TRAIL-induced mitochondrial depolarization to similar extent with

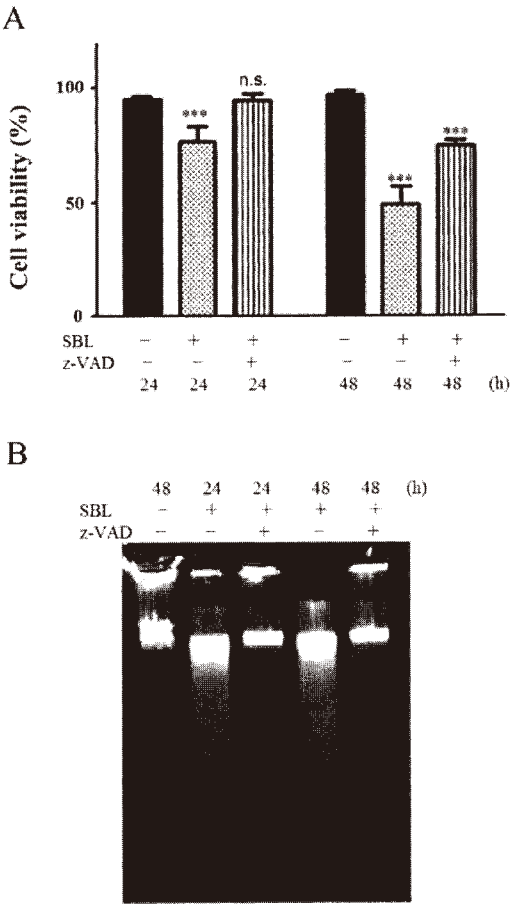

Figure 3. SBL-induced apoptosis is dependent on caspases. (A) Effect of z-VAD on SBL-induced cell death. Cells were treated with (striped column) or without (dotted column) z-VAD-fmk (50 μM) for 30 min and subsequently treated with SBL (2 μM) for indicated time. Cell viability was evaluated by trypan blue dye exclusion assay. Control (black column). Bars, mean ± SD. ***p<0.001. (B) Effect of z-VAD on DNA fragmentation in SBL-treated cells. Cells were treated with or without z-VAD-fmk (50 μM) for 30 min and subsequently treated with SBL (2 μM) for indicated time. Then, DNA was prepared from the cells. DNA fragmentation was analyzed by agarose gel electrophoresis and stained with ethidium bromide.

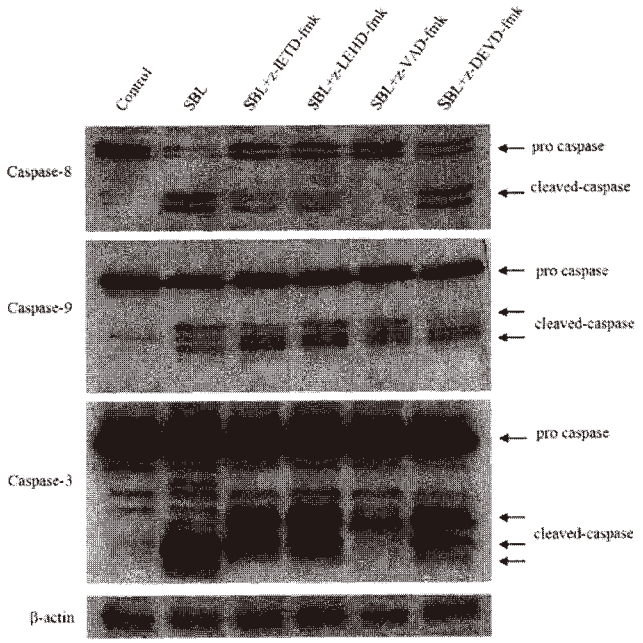

Figure 4. Effect of caspase inhibitors on SBL-induced caspase activation in Jurkat cells. Cells were treated with or without caspase inhibitor (50 μM) for 30 min and subsequently treated with SBL (2 μM) for 12 h. Then, whole cell lysate was separated by SDS-PAGE in 15% gel and subjected to western blot analysis using specific antibodies. β-actin was probed to demonstrate equal loading.

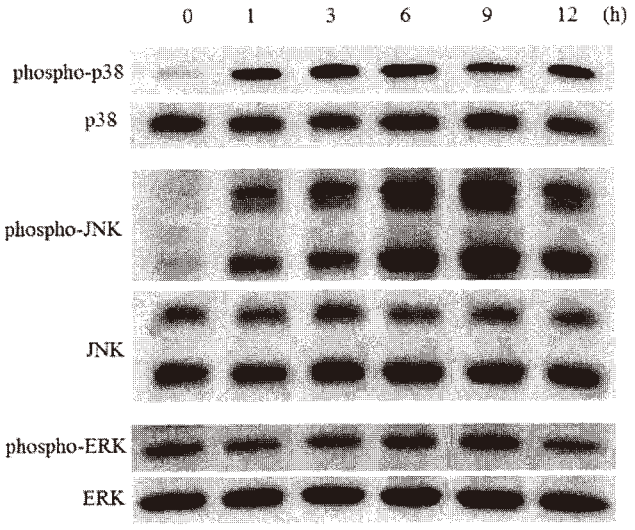

Figure 5. SBL induces activation of p38 and JNK but not activation of ERK. Cells were treated with SBL (2 μM) for indicated time and phosphorylation status of p38, JNK and ERK were determined by western blot analysis. Expression of total p38, JNK and ERK was also determined to confirm equal amount of protein loading in each lane.

z-VAD, whereas, z-LEHD was less effective. On SBL- or ETO-induced mitochondrial depolarization, neither IETD nor LEHD showed inhibitory effect like z-VAD (Fig. 7C). These results indicate that SBL-induced mitochondrial perturbation is not dependent on caspase activation. Thus, SBL invokes mitochondrial perturbation first and this process is followed by caspase activation and the amplification of death signal executes apoptotic cell death.

Discussion

SBL is a multifunctional protein which has lectin activity, ribonuclease activity and antitumor activity. The proposed mechanism of SBL-induced cell death is shown in Fig. 8. SBL binds to cell surface, internalizes into tumor cells and degrades cellular RNA and this ribotoxic stress triggers mitochondrial perturbation. The activation of p38 and JNK may be involved in the above process. Then, apoptotic signal is amplified by activation of caspase and leads to cell death.

SBL selectively agglutinates tumor cells, but not erythrocytes or fibroblasts (28). SBL shows cytotoxity to various tumor cells, but not to human primary WI-38 lung fibroblasts, normal mesothelial Met-5A cells (data not shown), human primary HFW fibroblasts, immortalized murine NIH- 3T3/3 cells (40), human primary HS-68 foreskin fibroblasts (37) or

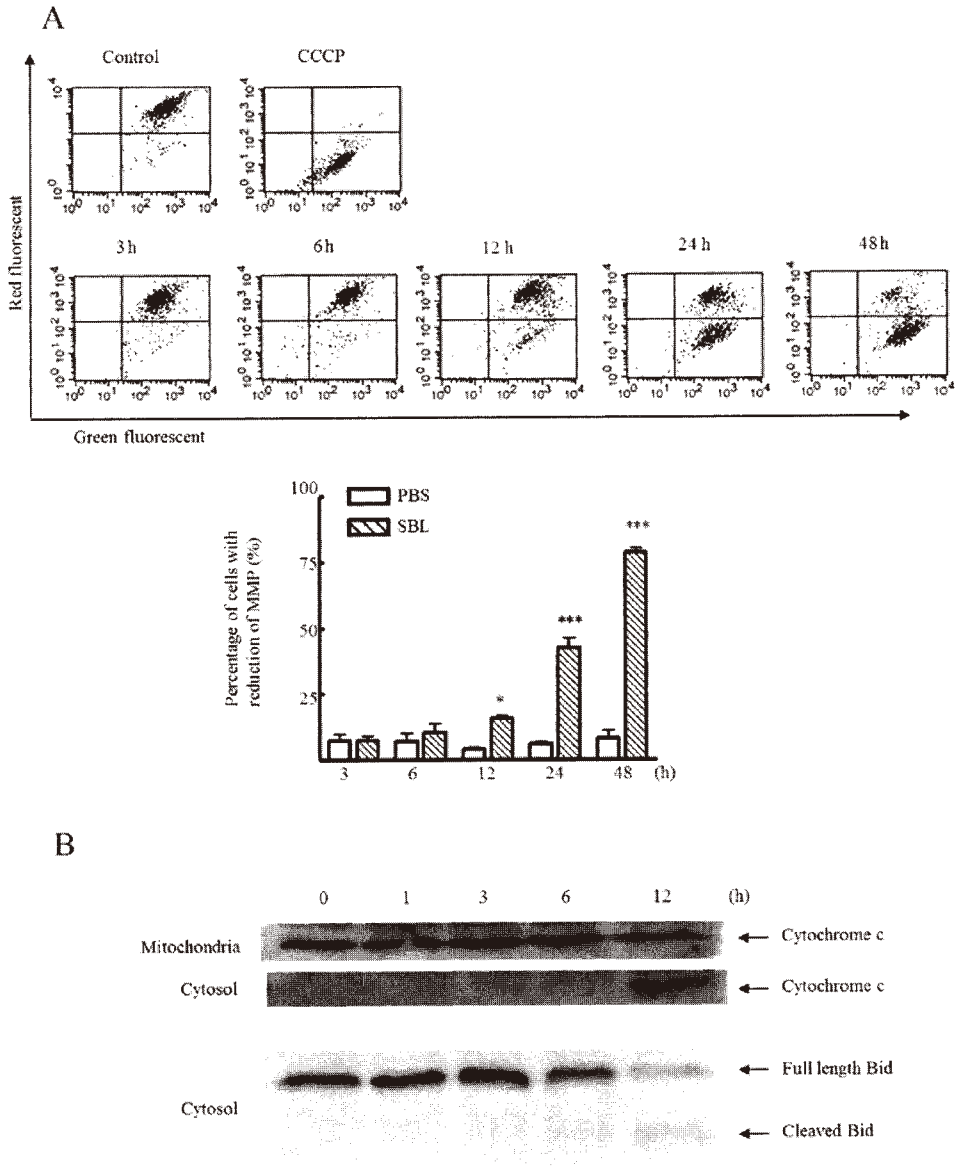

Figure 6. SBL induces mitochondrial perturbation in Jurkat cells. (A) Effect of SBL on MMP. Cells were treated with or without SBL (2 μM) for indicated time. Then, the cells were stained with JC-1 (mitochondria selective dye) and analyzed using FACSCalibur. In lower panel, the percentage of cells with reduced MMP (lower right quadrant of each dot plot) was represented. Each value represents the mean ± SD of three independent experiments. (B) Release of cytochrome *c* from mitochondria to cytosol and Bid cleavage in SBL-treated cells. Cells were treated with SBL (2 μM) for indicated time. Then, organelle and cytosol fractions were separated by SDS-PAGE in 15% gel and subjected to western blot analysis using anti-cytochrome *c* antibody and anti-Bid antibody.

hamster kidney BHK-21 cells (41). It seems that the selective effect of SBL on cancer cells is due to its selective binding to tumor cells, because sialidase treatment of cells abolished the tumor cell agglutination and also the antiproliferative effect induced by SBL (33).

In this study, we showed that SBL manifests cytotoxicity to some human leukemia cell lines including MDR cells, while conventional DNA-damaging agents, ETO and DOX which have been used clinically were not able to show cytotoxicity to MDR cells (Table I). The resistance of tumors occurs as a cross-resistance to a whole range of drugs with different structures and this phenomenon is called MDR. The cytotoxic drugs that are most frequently associated with MDR are hydrophobic and amphipathic natural products, such as the taxanes (paclitaxel and docetaxel), vinca alkaloids (vinorelbine, vincristine and vinblastine), anthracyclines (DOX, daunorubicin and epirubicin), epipodophyllotoxins (ETO and teniposide), antimetabolites (methorexate, fluorouracil, cytosar, 5-azacytosine, 6-mercaptopurine and gemcitabine), topotecan, dactinomycin and mitomycin *c* (42-46). Overexpression of ATP-binding cassette (ABC) transporters such as P-gp is known to be responsible for MDR (46). Cytotoxic RNase, PE5 (a variant of human pancreatic ribonuclease carrying a nuclear localization signal) reduced the expression level of the P-gp in MDR cell lines (47). It is believed that SBL displays novel mechanistic and tumor-selective cytotoxic effects regardless of P-gp expression and SBL is favorable as a new candidate anticancer drug.

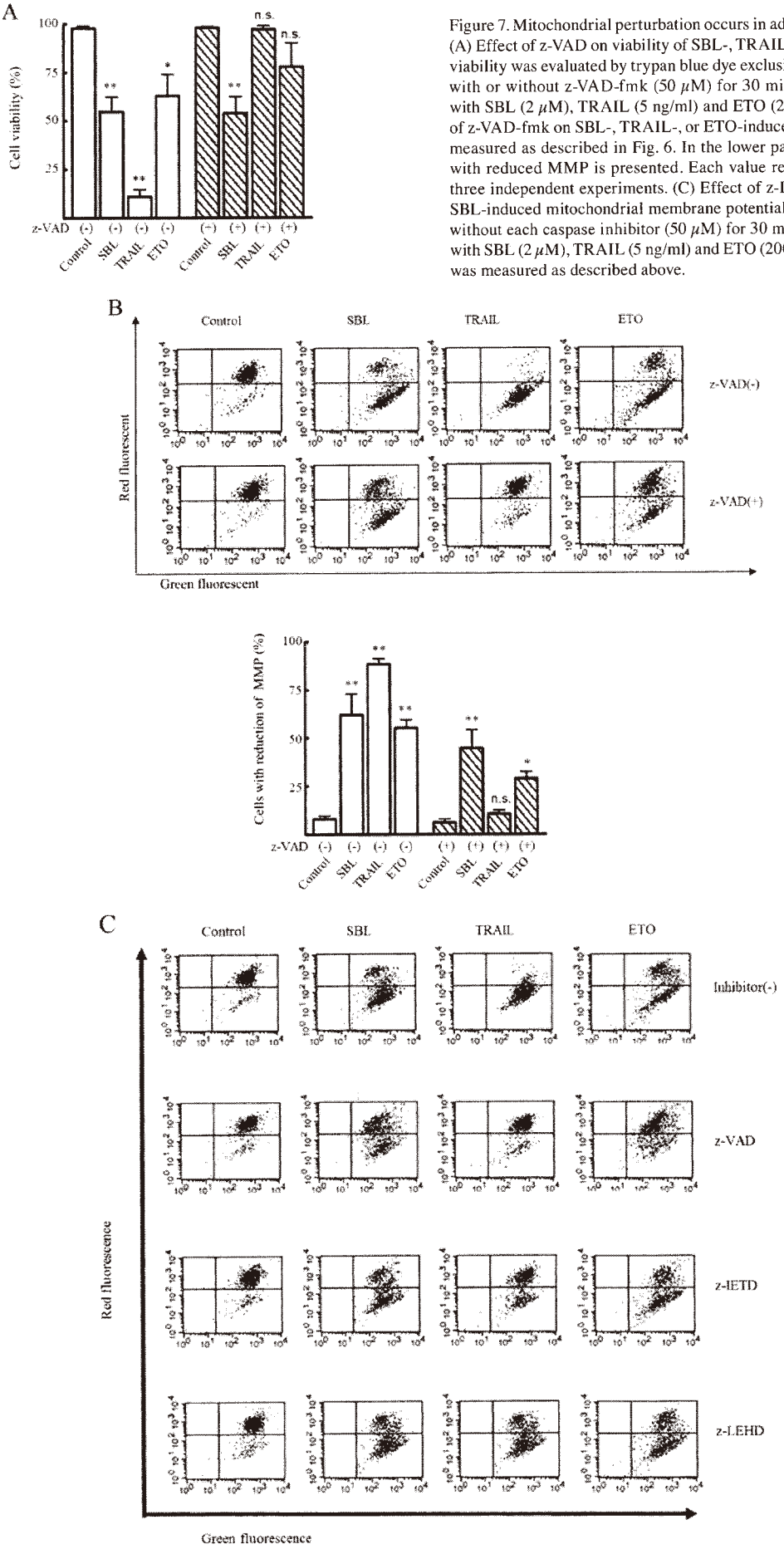

Figure 7. Mitochondrial perturbation occurs in advance of caspase activation. (A) Effect of z-VAD on viability of SBL-, TRAIL- or ETO-treated cells. Cell viability was evaluated by trypan blue dye exclusion assay. Cells were treated with or without z-VAD-fmk (50 μM) for 30 min and subsequently treated with SBL (2 μM), TRAIL (5 ng/ml) and ETO (200 μM) for 48 h. (B) Effect of z-VAD-fmk on SBL-, TRAIL-, or ETO-induced loss of MMP. MMP were measured as described in Fig. 6. In the lower panel, the percentage of cells with reduced MMP is presented. Each value represents the mean ± SD of three independent experiments. (C) Effect of z-IETD or z-LEHD on loss of SBL-induced mitochondrial membrane potential. Cells were treated with or without each caspase inhibitor (50 μM) for 30 min and subsequently treated with SBL (2 μM), TRAIL (5 ng/ml) and ETO (200 μM), for 48 h. Then, MMP was measured as described above.

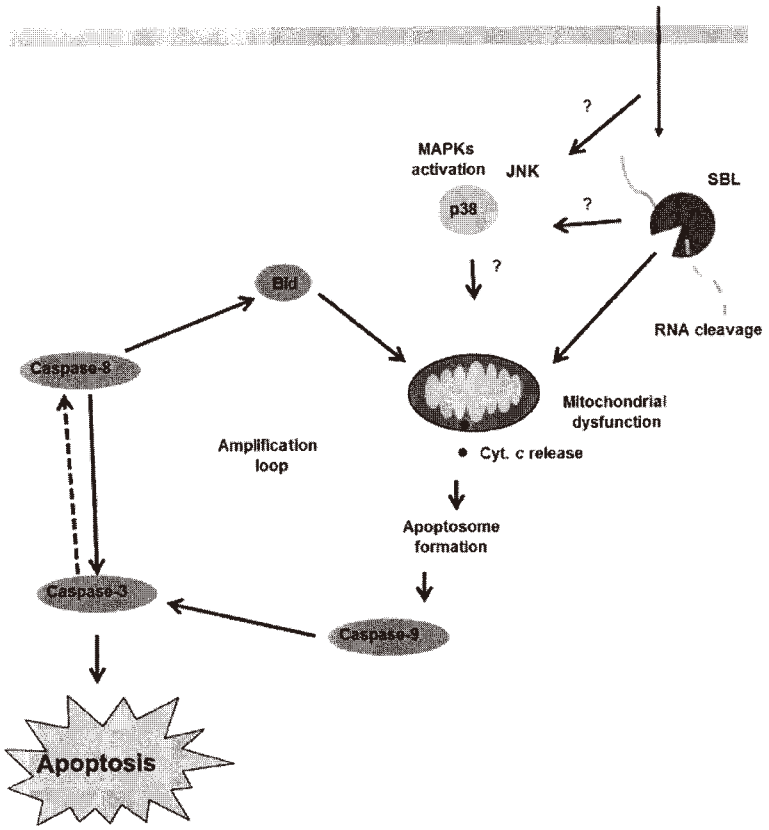

Figure 8. Proposed model for apoptotic mechanism induced by SBL in Jurkat cells. SBL binds to cell surface and internalizes into tumor cells. SBL degrades cellular RNA and this ribotoxic stress triggers mitochondrial perturbation. Then, apoptotic signal is amplified by caspase activation leading to cell death.

Apoptosis, also known as programmed cell death, plays a critical role in various biological phenomena, such as development, immunity and also cell death induced by chemotherapeutic drugs (48). Apoptosis may occur through death receptor-dependent (extrinsic) or independent (intrinsic or mitochondrial) pathways and the pathways finally activate the effector caspase-3, which leads to finally execution of apoptosis (49). During the execution phase of apoptosis, typical apoptotic changes such as chromatin condensation, nuclear collapse, internucleosomal DNA fragmentation are observed. A variety of studies have demonstrated that in cancer therapy, induction of apoptosis is a frequent outcome of effective therapy. In this study, we showed SBL-treated Jurkat cells present typical apoptotic morphological alterations, such as karyorrhexis, nuclear condensation and fragmentation (Fig. 2A) and apoptotic biological changes such as PS externalization, activation of caspases, and DNA fragmentation (Fig. 2B-D). This SBL-induced DNA fragmentation was completely blocked by z-VAD indicating that the cytotoxicity of SBL is induced through caspase-dependent apoptosis.

It has been reported that some chemotherapeutics and natural toxins which induce ribotoxic stress response activates MAPK (50,51). Regarding ribotoxic stress, He *et al* demonstrated ribotoxins, such as deoxynivalenol (DON), anisomycin, satratoxin G (SG) and ricin activate p38, JNKs and ERK in RAW264 mouse macrophage cell line (52). It was reported that activation of JNK is important for cytotoxicity of onconase using *jnk1*$^{-/-}$ *jnk2*$^{-/-}$ mouse embryo fibroblast (MEF) cells (53). Fang *et al* reported that RNase MC2 induces phosphorylation of p38, JNK and ERK in MCF-7 cells (3) and this RNase-mediated apoptotic signaling is contributed by dual phosphorylation of ERK and JNK in Hep G2 cells (54). Although it has been implicated largely that activation of p38 and JNK are proapoptotic (50,55) and that phosphorylation of ERK is linked with both antitumor activity (56) and tumor progression (57), some complicated results have been reported. Costro *et al* reported that PE5 kills adriamycin-resitant MCF-7 (MCF-7/ADR) cells through apoptosis associated with the inactivation of JNK, while onconase did not change the phosphorylation level of JNK in the cells (25). We showed that SBL is capable of inducing activation of p38 and JNK, but not ERK. The activation of p38 and JNK were observed as early as 1-h treatment with SBL suggesting that p38 and JNK may be activated upstream of mitochondrial perturbation. Although we tested the effects of p38 inhibitor (SP600125) and JNK inhibitor (SB203580), they did not affect the cytotoxicity induced by SBL (data not shown). There are some possible explanations for this phenomenon: i.e., binding to cell surface or the internalization into cytosol is able to display RNase activity of SBL, or the first cleavage of RNA, which is a non-detectable amount by electrophoresis can activate p38 and JNK. In addition, the activation of p38 and JNK may not be related to SBL cytotoxicity, or the inhibition of their activation may induce alternative death signals. The contribution of p38- and JNK-activation in SBL-induced cytotoxicity remains to be elucidated.

Wolf and Green reported that caspase-3 is capable of eliciting cleavage and activation of caspase-8 (58). Activation of caspase-8 results in the cleavage of Bid to produce a truncated form of the protein. Truncated Bid translocates from the cytoplasm to the mitochondria, where it appears to interact with and antagonize the actions of anti-apoptotic members of the Bcl-2 family, thereby causing an efflux of cytochrome *c* from the mitochondria (59-63). This, in turn, can result in the activation of caspase-9. Therefore, caspase-8 could amplify apoptotic signals through the continued release of cytochrome *c* and subsequent activation of caspase-9 and -3 (64). Once activating signals of apoptotic caspase are induced, the amplification signal can activate caspase-8, -9 and -3. In addition, the determination of exact time course of the sequential events is limited by detection sensitivity of experiments. These facts disturb discrimination of which pathway is involved in the stimuli. We utilized a combination of specific caspase inhibitors and mitochondrial membrane depolarization detector JC-1 to distinguish the SBL-induced signaling pathway comparatively with TRAIL and ETO. It was clearly shown that SBL-induced mitochondrial depolarization was not diminished by z-VAD, while TRAIL-induced mitochondrial depolarization was completely inhibited by z-VAD (Fig. 7A and B). These results indicate that cytotoxicity of SBL is induced through caspase-dependent apoptosis in which mitochondrial perturbation occurs as upstream events.

In conclusion, we report that SBL, a multifunctional protein shows cytotoxicity for some human leukemia cell lines including MDR cells (Fig. 8). The details of apoptotic signal induced by SBL was analyzed by combinational usage of specific caspase inhibitors and the mitochondrial membrane depolarization detector JC-1. The use of this combination was shown in detail to distinguish the apoptotic pathway. SBL displays novel mechanistic and tumor-selective cytotoxic effects regardless of P-gp expression and SBL has potential as an alternative molecule to conventional DNA-damaging anticancer drugs.

Acknowledgements

This study was supported by the 'Academic Frontier' Project for Private Universities from the Ministry of Education, Culture, Sports, Science and Technology of Japan.

References

1. Costanzi J, Sidransky D, Navon A and Goldsweig H: Ribonucleases as a novel pro-apoptotic anticancer strategy: review of the preclinical and clinical data for ranpirnase. Cancer Invest 23: 643-650, 2005.
2. Deshpande RA and Shankar V: Ribonucleases from T2 family. Crit Rev Microbiol 28: 79-122, 2002.
3. Fang EF, Zhang CZ, Fong WP and Ng TB: RNase MC2: a new *Momordica charantia* ribonuclease that induces apoptosis in breast cancer cells associated with activation of MAPKs and induction of caspase pathways. Apoptosis 17: 377-387, 2012.
4. D'Alessio G: New and cryptic biological messages from RNases. Trends Cell Biol 3: 106-109, 1993.
5. Raines RT: Ribonuclease A. Chem Rev 98: 1045-1066, 1998.
6. Ita M, Halicka HD, Tanaka T, Kurose A, Ardelt B, Shogen K and Darzynkiewicz Z: Remarkable enhancement of cytotoxicity of onconase and cepharanthine when used in combination on various tumor cell lines. Cancer Biol Ther 7: 1104-1108, 2008.
7. Rybak SM, Pearson JW, Fogler WE, Volker K, Spence SE, Newton DL, Mikulski SM, Ardelt W, Riggs CW, Kung HF and Longo DL: Enhancement of vincristine cytotoxicity in drug-resistant cells by simultaneous treatment with onconase, an antitumor ribonuclease. J Natl Cancer Inst 88: 747-753, 1996.
8. Kim DH, Kim EJ, Kalota A, Gewirtz AM, Glickson J, Shogen K and Lee I: Possible mechanisms of improved radiation response by cytotoxic RNase, Onconase, on A549 human lung cancer xenografts of nude mice. Adv Exp Med Biol 599: 53-59, 2007.
9. Halicka HD, Murakami T, Papageorgio CN, Mittelman A, Mikulski SM, Shogen K and Darzynkiewicz Z: Induction of differentiation of leukaemic (HL-60) or prostate cancer (LNCaP, JCA-1) cells potentiates apoptosis triggered by onconase. Cell Prolif 33: 407-417, 2000.
10. Tsai SY, Hsieh TC, Ardelt B, Darzynkiewicz Z and Wu JM: Combined effects of onconase and IFN-beta on proliferation, macromolecular syntheses and expression of STAT-1 in JCA-1 cancer cells. Int J Oncol 20: 891-896, 2002.
11. Mikulski SM, Viera A, Darzynkiewicz Z and Shogen K: Synergism between a novel amphibian oocyte ribonuclease And lovastatin in inducing cytostatic and cytotoxic effects in human lung and pancreatic carcinoma cell lines. Br J Cancer 66: 304-310, 1992.
12. Rutkoski TJ, Kink JA, Strong LE, Schilling CI and Raines RT: Antitumor activity of ribonuclease multimers created by site-specific covalent tethering. Bioconjug Chem 21: 1691-1702, 2010.
13. Haigis MC, Kurten EL and Raines RT: Ribonuclease inhibitor as an intracellular sentry. Nucleic Acids Res 31: 1024-1032, 2003.
14. Ledoux L and Brachet J: Remarks on preparations of ribonuclease from different manufacturing sources. Biochim Biophys Acta 16: 290, 1955.
15. Ledoux L.: Action of ribonuclease on neoplastic growth. II. Action on Landschutz ascites cells in vitro. Biochim Biophys Acta 20: 369-377, 1956.
16. Darzynkiewicz Z, Carter SP, Mikulski SM, Ardelt WJ and Shogen K: Cytostatic and cytotoxic effects of Pannon (P-30 Protein), a novel anticancer agent. Cell Tissue Kinet 21: 169-182, 1988.
17. Easty DM, Ledoux L and Ambrose EJ: The action of ribonuclease on neoplastic growth. III. Studies by interference microscopy. Biochim Biophys Acta 20: 528-537, 1956.
18. Telford IR, Kemp JF, Taylor EF and Yeaman MW: Effect of ribonuclease on survival of ascites tumor bearing mice. Proc Soc Exp Biol Med 100: 829-831, 1959.
19. Ledoux L: Action of ribonuclease on two solid tumours in vivo. Nature 176: 36-37, 1955.
20. Ardelt W, Mikulski SM and Shogen K: Amino acid sequence of an anti-tumor protein from *Rana pipiens* oocytes and early embryos. Homology to pancreatic ribonucleases. J Biol Chem 266: 245-251, 1991.
21. Ledoux L and Revell SH: Action of ribonuclease on neoplastic growth. I. Chemical aspects of normal tumour growth: the Landschutz ascites tumour. Biochim Biophys Acta 18: 416-426, 1955.
22. Aleksandrowicz J, Urbanczyk J, Ostrowska A and Sierko J: Further research on the activity of ribonucleases in the blood and urine of patients suffering from proliferative hemocytopathia. Blood 13: 652-664, 1958.
23. Vert A, Castro J, Ruiz-Martinez S, Tubert P, Escribano D, Ribo M, Vilanova M and Benito A: Generation of new cytotoxic human ribonuclease variants directed to the nucleus. Mol Pharm 9: 2894-2902, 2012.
24. Fang EF and Ng TB: Ribonucleases of different origins with a wide spectrum of medicinal applications. Biochim Biophys Acta 1815: 65-74, 2011.
25. Castro J, Ribo M, Navarro S, Nogues MV, Vilanova M and Benito A: A human ribonuclease induces apoptosis associated with $p21W^{AF1/CIP1}$ induction and JNK inactivation. BMC Cancer 11: 9, 2011.
26. Kawauchi H, Sakakibara F and Watanabe K: Agglutinins of frog eggs: a new class of proteins causing preferential agglutination of tumor cells. Experientia 31: 364-365, 1975.
27. Sakakibara F, Kawauchi H, Takayanagi G and Ise H: Egg lectin of *Rana japonica* and its receptor glycoprotein of Ehrlich tumor cells. Cancer Res 39: 1347-1352, 1979.
28. Nitta K, Takayanagi G, Kawauchi H and Hakomori S: Isolation and characterization of *Rana catesbeiana* lectin and demonstration of the lectin-binding glycoprotein of rodent and human tumor cell membranes. Cancer Res 47: 4877-4883, 1987.

29. Titani K, Takio K, Kuwada M, Nitta K, Sakakibara F, Kawauchi H, Takayanagi G and Hakomori S: Amino acid sequence of sialic acid binding lectin from frog (*Rana catesbeiana*) eggs. Biochemistry 26: 2189-2194, 1987.
30. Kamiya Y, Oyama F, Oyama R, Sakakibara F, Nitta K, Kawauchi H, Takayanagi Y and Titani K: Amino acid sequence of a lectin from Japanese frog (*Rana japonica*) eggs. J Biochem 108: 139-143, 1990.
31. Nitta K, Oyama F, Oyama R, Sekiguchi K, Kawauchi H, Takayanagi Y, Hakomori S and Titani K: Ribonuclease activity of sialic acid-binding lectin from *Rana catesbeiana* eggs. Glycobiology 3: 37-45, 1993.
32. Okabe Y, Katayama N, Iwama M, Watanabe H, Ohgi K, Irie M, Nitta K, Kawauchi H, Takayanagi Y, Oyama F, *et al*: Comparative base specificity, stability, and lectin activity of two lectins from eggs of *Rana catesbeiana* and *R. japonica* and liver ribonuclease from *R. catesbeiana*. J Biochem 109: 786-790, 1991.
33. Nitta K, Ozaki K, Ishikawa M, Furusawa S, Hosono M, Kawauchi H, Sasaki K, Takayanagi Y, Tsuiki S and Hakomori S: Inhibition of cell proliferation by *Rana catesbeiana* and *Rana japonica* lectins belonging to the ribonuclease superfamily. Cancer Res 54: 920-927, 1994.
34. Nitta K, Ozaki K, Tsukamoto Y, Furusawa S, Ohkubo Y, Takimoto H, Murata R, Hosono M, Hikichi N, Sasaki K, *et al*: Characterization of a *Rana catesbeiana* lectin-resistant mutant of leukemia P388 cells. Cancer Res 54: 928-934, 1994.
35. Nitta K, Ozaki K, Tsukamoto Y, Hosono M, Ogawakonno Y, Kawauchi H, Takayanagi Y, Tsuiki S and Hakomori S: Catalytic lectin (leczyme) from bullfrog (*Rana catesbeiana*) eggs. Int J Oncol 9: 19-23, 1996.
36. Liao YD: A pyrimidine-guanine sequence-specific ribonuclease from *Rana catesbeiana* (bullfrog) oocytes. Nucleic Acids Res 20: 1371-1377, 1992.
37. Liao YD, Huang HC, Leu YJ, Wei CW, Tang PC and Wang SC: Purification and cloning of cytotoxic ribonucleases from *Rana catesbeiana* (bullfrog). Nucleic Acids Res 28: 4097-4104, 2000.
38. Tang CH, Hu CC, Wei CW and Wang JJ: Synergism of *Rana catesbeiana* ribonuclease And IFN-gamma triggers distinct death machineries in different human cancer cells. FEBS Lett 579: 265-270, 2005.
39. Ishiyama M, Miyazono Y, Sasamoto K, Ohkura Y and Ueno K: A highly water-soluble disulfonated tetrazolium salt as a chromogenic indicator for NADH as well as cell viability. Talanta 44: 1299-1305, 1997.
40. Liao YD, Huang HC, Chan HJ and Kuo SJ: Large-scale preparation of a ribonuclease from *Rana catesbeiana* (bullfrog) oocytes and characterization of its specific cytotoxic activity against tumor cells. Protein Expr Purif 7: 194-202, 1996.
41. Hu CC, Lee YH, Tang CH, Cheng JT and Wang JJ: Synergistic cytotoxicity of *Rana catesbeiana* ribonuclease And IFN-gamma on hepatoma cells. Biochem Biophys Res Commun 280: 1229-1236, 2001.
42. Thomas H and Coley HM: Overcoming multidrug resistance in cancer: an update on the clinical strategy of inhibiting P-glycoprotein. Cancer Control 10: 159-165, 2003.
43. Ambudkar SV, Dey S, Hrycyna CA, Ramachandra M, Pastan I and Gottesman MM: Biochemical, cellular, and pharmacological aspects of the multidrug transporter. Annu Rev Pharmacol Toxicol 39: 361-398, 1999.
44. Krishna R and Mayer LD: Multidrug resistance (MDR) in cancer. Mechanisms, reversal using modulators of MDR and the role of MDR modulators in influencing the pharmacokinetics of anticancer drugs. Eur J Pharm Sci 11: 265-283, 2000.
45. Stavrovskaya AA: Cellular mechanisms of multidrug resistance of tumor cells. Biochemistry (Mosc) 65: 95-106, 2000.
46. Ozben T: Mechanisms and strategies to overcome multiple drug resistance in cancer. FEBS Lett 580: 2903-2909, 2006.
47. Castro J, Ribo M, Puig T, Colomer R, Vilanova M and Benito A: A cytotoxic ribonuclease reduces the expression level of P-glycoprotein in multidrug-resistant cell lines. Invest New Drugs 30: 880-888, 2012.
48. Elmore S: Apoptosis: a review of programmed cell death. Toxicol Pathol 35: 495-516, 2007.
49. Grutter MG: Caspases: key players in programmed cell death. Curr Opin Struct Biol 10: 649-655, 2000.
50. Mansouri A, Ridgway LD, Korapati AL, Zhang Q, Tian L, Wang Y, Siddik ZH, Mills GB and Claret FX: Sustained activation of JNK/p38 MAPK pathways in response to cisplatin leads to Fas ligand induction and cell death in ovarian carcinoma cells. J Biol Chem 278: 19245-19256, 2003.
51. Bunyard P, Handley M, Pollara G, Rutault K, Wood I, Chaudry M, Alderman C, Foreman J, Katz DR and Chain BM: Ribotoxic stress activates p38 and JNK kinases and modulates the antigen-presenting activity of dendritic cells. Mol Immunol 39: 815-827, 2003.
52. He K, Zhou HR and Pestka JJ: Mechanisms for ribotoxin-induced ribosomal RNA cleavage. Toxicol Appl Pharmacol 265: 10-18, 2012.
53. Iordanov MS, Wong J, Newton DL, Rybak SM, Bright RK, Flavell RA, Davis RJ and Magun BE: Differential requirement for the stress-activated protein kinase/c-Jun NH(2)-terminal kinase in RNA damage-induced apoptosis in primary and in immortalized fibroblasts. Mol Cell Biol Res Commun 4: 122-128, 2000.
54. Fang EF, Zhang CZ, Zhang L, Fong WP and Ng TB: In vitro and in vivo anticarcinogenic effects of RNase MC2, a ribonuclease isolated from dietary bitter gourd, toward human liver cancer cells. Int J Biochem Cell Biol 44: 1351-1360, 2012.
55. Dasmahapatra G, Lembersky D, Kramer L, Fisher RI, Friedberg J, Dent P and Grant S: The pan-HDAC inhibitor vorinostat potentiates the activity of the proteasome inhibitor carfilzomib in human DLBCL cells in vitro and in vivo. Blood 115: 4478-4487, 2010.
56. Chen J, Rusnak M, Luedtke RR and Sidhu A: D1 dopamine receptor mediates dopamine-induced cytotoxicity via the ERK signal cascade. J Biol Chem 279: 39317-39330, 2004.
57. Wilhelm SM, Carter C, Tang L, Wilkie D, McNabola A, Rong H, Chen C, Zhang X, Vincent P, McHugh M, Cao Y, Shujath J, Gawlak S, Eveleigh D, Rowley B, Liu L, Adnane L, Lynch M, Auclair D, Taylor I, Gedrich R, Voznesensky A, Riedl B, Post LE, Bollag G and Trail PA: BAY 43-9006 exhibits broad spectrum oral antitumor activity and targets the RAF/MEK/ERK pathway and receptor tyrosine kinases involved in tumor progression and angiogenesis. Cancer Res 64: 7099-7109, 2004.
58. Wolf BB and Green DR: Suicidal tendencies: apoptotic cell death by caspase family proteinases. J Biol Chem 274: 20049-20052, 1999.
59. Kuwana T, Smith JJ, Muzio M, Dixit V, Newmeyer DD and Kornbluth S: Apoptosis induction by caspase-8 is amplified through the mitochondrial release of cytochrome *c*. J Biol Chem 273: 16589-16594, 1998.
60. Li H, Zhu H, Xu CJ and Yuan J: Cleavage of BID by caspase 8 mediates the mitochondrial damage in the Fas pathway of apoptosis. Cell 94: 491-501, 1998.
61. Luo X, Budihardjo I, Zou H, Slaughter C and Wang X: Bid, a Bcl2 interacting protein, mediates cytochrome *c* release from mitochondria in response to activation of cell surface death receptors. Cell 94: 481-490, 1998.
62. Schendel SL, Azimov R, Pawlowski K, Godzik A, Kagan BL and Reed JC: Ion channel activity of the BH3 only Bcl-2 family member, BID. J Biol Chem 274: 21932-21936, 1999.
63. Wei MC, Zong WX, Cheng EH, Lindsten T, Panoutsakopoulou V, Ross AJ, Roth KA, MacGregor GR, Thompson CB and Korsmeyer SJ: Proapoptotic BAX and BAK: a requisite gateway to mitochondrial dysfunction and death. Science 292: 727-730, 2001.
64. Viswanath V, Wu Y, Boonplueang R, Chen S, Stevenson FF, Yantiri F, Yang L, Beal MF and Andersen JK: Caspase-9 activation results in downstream caspase-8 activation and bid cleavage in 1-methyl-4-phenyl-1,2,3,6-tetrahydropyridine-induced Parkinson's disease. J Neurosci 21: 9519-9528, 2001.

Cell Death and Differentiation (2012) 19, 170–179

www.nature.com/cdd

Plasma membrane-associated sialidase (NEU3) regulates progression of prostate cancer to androgen-independent growth through modulation of androgen receptor signaling

S Kawamura[1], I Sato[2], T Wada[2,3], K Yamaguchi[3], Y Li[4], D Li[4], X Zhao[4], S Ueno[3], H Aoki[1], T Tochigi[1], M Kuwahara[1], T Kitamura[5], K Takahashi[3,6], S Moriya[3,6] and T Miyagi*[,3,6]

Prostate cancers generally become androgen-independent and resistant to hormone therapy with progression. To understand the underlying mechanisms and facilitate the development of novel treatments for androgen-independent prostate cancer, we have investigated plasma membrane-associated sialidase (NEU3), the key enzyme for ganglioside hydrolysis participating in transmembrane signaling. We have discovered NEU3 to be upregulated in human prostate cancer compared with non-cancerous tissue, correlating with the Gleason score. *NEU3* silencing with siRNA in prostate cancer PC-3 and LNCaP cells resulted in increased expression of differentiation markers and in cell apoptosis, but decrease in Bcl-2 as well as a progression-related transcription factor, early growth response gene (*EGR-1*). In androgen-sensitive LNCaP cells, forced overexpression of NEU3 significantly induced expression of EGR-1, androgen receptor (AR) and PSA both with and without androgen, the cells becoming sensitive to androgen. The NEU3-mediated induction was abrogated by inhibitors for PI-3 kinase and MAP kinase and more specifically by their silencing in the absence of androgen, being confirmed by increased phosphorylation of AKT and ERK1/2 in *NEU3* overexpressing cells. NEU3 siRNA introduction caused reduction of cell growth of an androgen-independent PC-3 cells in culture and of transplanted tumors in nude mice. These data suggest that NEU3 regulates tumor progression through AR signaling, and thus be a potential tool for diagnosis and therapy of androgen-independent prostate cancer.
Cell Death and Differentiation (2012) **19**, 170–179; doi:10.1038/cdd.2011.83; published online 17 June 2011

Androgen receptor (AR) signaling has a central role in prostate cancer pathogenesis and progression, and androgen withdrawal is the main therapeutic options for treatment of advanced cases.[1,2] However, many prostate cancers eventually become androgen-independent, and this results in renewed growth and spread. The mechanism underlying the initial survival and subsequent growth of ablation-resistant prostate cancer cells is not fully characterized. However, several lines of evidence point to activation of AR signaling under androgen-independent conditions. Likely, mechanisms so far proposed include *AR* mutations, allowing receptors to be activated by new ligands,[3] *AR* gene overexpression causing AR oversensitive to low concentrations of androgen[4,5] and cross-stimulation of AR signaling by other growth factors.[6,7] It has been previously shown that early growth response gene 1 (*EGR-1*) is an important transcription factor involved in promoting prostate cancer progression,[8,9] its overexpression enhancing androgen-independent growth of prostate cancer cells by modulating androgen signaling through increased AR nuclear transition.[10] To facilitate the search for new effective therapeutic targets for androgen-independent prostate cancer, molecular mechanisms should be elucidated from various aspects. In this study, we focused on a human sialidase, a glycosidase catalyzing the removal of sialic acids from glycolipids and participating transmembrane signaling,[11,12] because the enzyme has been found to be upregulated in several human cancers and to suppress apoptosis of cancer cells.[13–15]

Alterations in glycosylation occur during tumorigenesis, and aberrant sialylation in particular has been implicated in the malignant phenotype with reference to metastatic potential and invasiveness.[16–18] Mammalian sialidase is the key enzyme for control of cellular sialic acid contents, through catalyzing the initial step in degradation of glycoproteins and glycolipids. Four types of human sialidases have been identified and characterized to date, designated as NEU1, NEU2, NEU3 and NEU4.[11,12] They differ in major subcellular localization and enzymatic properties including substrate specificity, and each has been found to have a unique functional role depending on its particular properties other than lysosomal catabolism. They behave in different manners during carcinogenesis.[19] Of the four types of sialidase,

[1]Department of Urology, Miyagi Cancer Center, Natori, Japan; [2]Division of Pathology, Miyagi Cancer Center Research Institute, Natori, Japan; [3]Division of Biochemistry, Miyagi Cancer Center Research Institute, Natori, Japan; [4]Department of Pathophysiology, Prostate Diseases Prevention and Treatment Research Center, Jilin University of Medical Sciences, Changchun, PRC, China; [5]Division of Cellular Therapy, Institute of Medical Science, University of Tokyo, Tokyo, Japan and [6]Division of Cancer Glycosylation Research, Institute of Molecular Biomembrane and Glycobiology, Tohoku Pharmaceutical University, Sendai, Japan
*Corresponding author: T Miyagi, Division of Cancer Glycosylation Research, Institute of Molecular Biomembrane and Glycobiology, Tohoku Pharmaceutical University, 4-4-1 Komatsushima, Aoba-ku, Sendai 981-8558, Japan. Tel: +81 22 727 0157; Fax: +81 22 275 2013; E-mail: tmiyagi@tohoku-pharm.ac.jp
Keywords: sialidase; prostate cancer; androgen receptor; EGR-1; PSA
Abbreviations: AR, androgen receptor; *EGR-1*, early growth response gene 1; DHT, dihydrotestosterone; EGFR, epidermal growth factor receptor
Received 03.1.11; revised 06.5.11; accepted 12.5.11; Edited by B Zhivotovsky; published online 17.6.11

plasma membrane-associated sialidase, NEU3, is unique in specifically hydrolyzing gangliosides, thought to participate in cell differentiation and transmembrane signaling.[11,12] In fact, recent observations have suggested an involvement of NEU3 in regulation of signal transduction through ganglioside modulation and interaction with some signaling molecules. NEU3 is upregulated in various human cancers, including colon,[13] renal[14] and ovarian cancers,[15] and contributes to the expression of malignant properties, including suppression of apoptosis by activating EGF receptor signaling,[20] and promotion of cell invasion and motility by affecting integrin-mediated signaling in the extracellular matrix in colon cancer cells[21] and by activating IL-6-mediated signaling via the PI3 kinase (PI3K)/Akt cascade in renal cancer cells.[14] Our present data show that upregulation of NEU3 is also observed in prostate cancer, activating AR signaling by increasing EGR-1, AR and PSA expression, possibly via epidermal growth factor receptor (EGFR) family activation, and causing androgen-independent proliferation of the cancer cells.

Results

NEU3 is upregulated in human prostate cancer. Relative mRNA levels of NEU3 measured by quantitative RT–PCR were 4.2 ± 2.5 and 1.2 ± 1.3 ($P<0.0001$) for 34 cancer and 35 non-cancerous samples, respectively, indicating that NEU3 in tumor specimens is significantly upregulated as compared with non-tumor prostate tissues (Figure 1a). The sialidase activity toward gangliosides showed a tendency to be increased in tumors, even in the limited number of specimens examined (Figure 1b). The mRNA levels positively correlated with the prostate cancer tissue grade, as assessed by Gleason score ($P<0.0001$) as shown in Figure 1c. Consistent with these data, immunohistochemistry with anti-NEU3 monoclonal antibody exhibited strong positive staining in prostate cancer tissues with a high Gleason score, whereas non-tumor prostate tissues were almost negative (Figure 1d).

NEU3 modulates expression of differentiation- and apoptosis-related molecules in human prostate cancer cell lines. To determine whether the increased NEU3 level in prostate cancer was reproducible *in vitro*, we analyzed two human prostate cancer cell lines, PC-3 and LNCaP. Androgen-insensitive and apoptosis-resistant PC-3 cells expressed a higher level of NEU3 than androgen-sensitive LNCaP cells, with reference to both sialidase activity and the mRNA level (Figure 2a). To examine whether the increased NEU3 expression affects promotion of prostate cancer progression, we then prepared *NEU3* overexpressing cells by retrovirus transfection and *NEU3* silencing cells with *NEU3* targeting siRNA. The sialidase activities after *NEU3* overexpression were 97.7 ± 14.1 U/mg and 104.5 ± 12.6 U/mg protein in PC-3 and LNCaP cells, respectively. After *NEU3* silencing, in comparison with control siRNA, the relative mRNA levels were $17.7 \pm 7.0\%$ and $19.6 \pm 8.5\%$, and the sialidase activities were 1.33 ± 0.51 U/g and 0.28 ± 0.11 U/g protein in PC-3 and LNCaP cells, respectively.

When the cell lines were treated with 5 mM sodium butyrate for 48 h, endogenous NEU3 was downregulated and the cells underwent differentiation and apoptosis. On the other hand, NEU3 overexpression resulted in suppression of apoptosis in both PC-3 and LNCaP cells, and furthermore, mock-transfected PC-3 cells seemed to be more resistant than that of LNCaP cells having a lower level of endogenous NEU3, as assessed by FACS analysis with AnnexinV Fluolostaining (Roche Diagnostics, Penzberg, Germany; Figure 2b). In the both cells, ectopic expression of *NEU3* caused decreased mRNA levels for keratin 17 and IL24 differentiation markers, and increased the level for antiapoptotic protein Bcl-2. Knockdown of *NEU3* led to essentially the opposite results (Figure 2c). These results indicate that NEU3 upregulation in prostate cancer might cause suppression of cell differentiation and apoptosis.

NEU3 enhances expression of AR signaling-related molecules. We next assessed expression levels of AR signaling-related molecules to observe whether NEU3 is involved in AR signaling pathway. NEU3 enhanced mRNA production for the progression-related transcription factor EGR-1 in both lines, and increased levels for AR and PSA in LNCaP cells, whereas *NEU3* knockdown lowered AR and PSA mRNA expression (Figure 3a). EGR-1 has been described to have a crucial role in prostate cancer progression and levels correlate positively with the tumor grade.[8,9] In addition to suppression of cell differentiation and apoptosis as shown in Figure 2, NEU3 might cause activation of the AR signaling pathway. When protein levels of AR and PSA were analyzed by immunoblotting in LNCaP cells cultured with charcol/dextran-stripped serum, the levels were increased not only by dihydrotestosterone (DHT) also by NEU3 even without DHT, and treatment with an anti-androgen drug bicalutamide returned these proteins to their basal levels (Figure 3b). On the other hand, *NEU3* silencing significantly reduced DHT-dependent increase in EGR-1, AR and PSA protein levels as well as basal levels of AR and PSA (Figure 3c). These results indicate that NEU3 promotes functional activation of androgen signaling in LNCap cells both in the presence and absence of androgen. To analyze glycolipid changes as a result of modulation of NEU3 expression, glycolipids extracted from the cells were subjected to thin-layer chromatography, because of special preference of the sialidase to gangliosides. As shown in Figure 3d, *NEU3* overexpression yielded an increase in lactosylceramide with a slight Gb3 increase as compared with control, but there was no detectable change before and after *NEU3* silencing. We also tried to detect a small change of cell surface gangliosides by FACS analysis with antibodies against GD1a, GM2, GM1 (Seikagaku Biobusiness, Tokyo, Japan) and GD2 (Upstate, Lake Placid, NY, USA), as a previous report suggested possible existence of these gangliosides in the cells.[22] However, all the antibodies failed to detect any significant change in either *NEU3* overexpressing or silencing cells (data not shown).

NEU3 activates AR signaling via PI3K and MAP kinase (MAPK) pathways. To gain insights into the signaling pathway involved in the NEU3-mediated induction of these

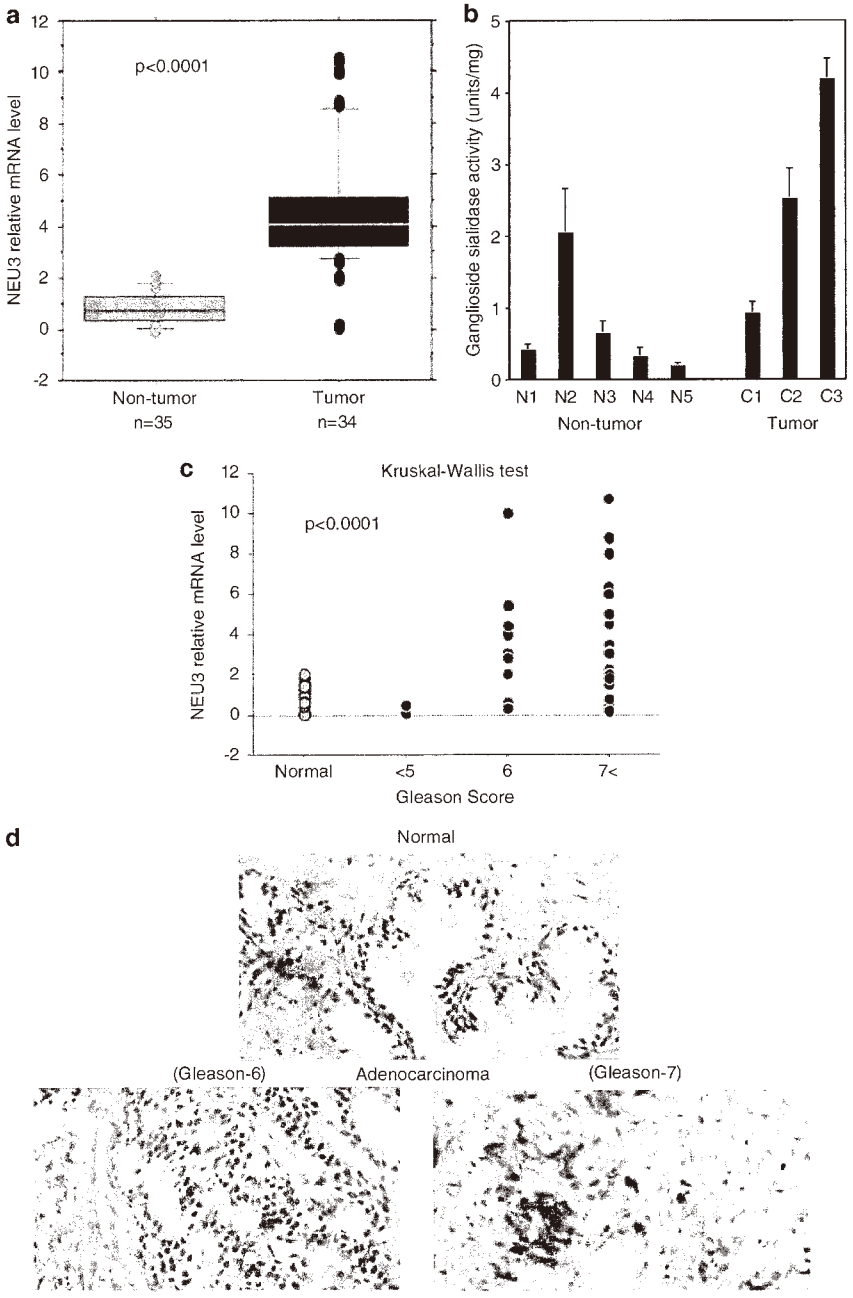

Figure 1 Upregulation of NEU3 in human prostate cancer. (**a**) Relative mRNA levels of NEU3 assessed by quantitative RT–PCR for 34 cancer and 35 non-cancerous samples. Box-and-whisker plots were used for statistical analysis. (**b**) Sialidase activity levels of cancer and non-cancerous samples assessed by fluorometric high-performance liquid chromatography with malononitrile. (**c**) Co-relationship between NEU3 level and prostate cancer grading, Gleason score. The data were statistically analyzed using the Kruskal–Wallis test. (**d**) Immunohistochemistry with anti-NEU3 monoclonal antibody for prostate cancer tissues with the high Gleason score and non-tumor prostate tissues

AR-related proteins, specific inhibitors of PI3K (LY294002) and MAPK (PD098059) pathways were used.[23] Treatment with LY294002 inhibited NEU3-induced EGR-1 and AR elevation, whereas PD098059 abolished the PSA increase (Figure 4a). To be more convincing, the siRNAs for PI3K p110α and for MAPKK (MEK1/2) were separately used to block specifically these expressions. In the cells of *PI3K* knocking down, NEU3-mediated AR induction was inhibited, and the cells bearing *MEK1* knockdown showed significantly lowered PSA expression as expected (Figure 4b). These results indicate that NEU3 induces and activates EGR-1 and AR through the PI3K pathway and PSA through the MAPK pathway, in an androgen-depleted environment. Consistent with these data, NEU3 significantly promoted

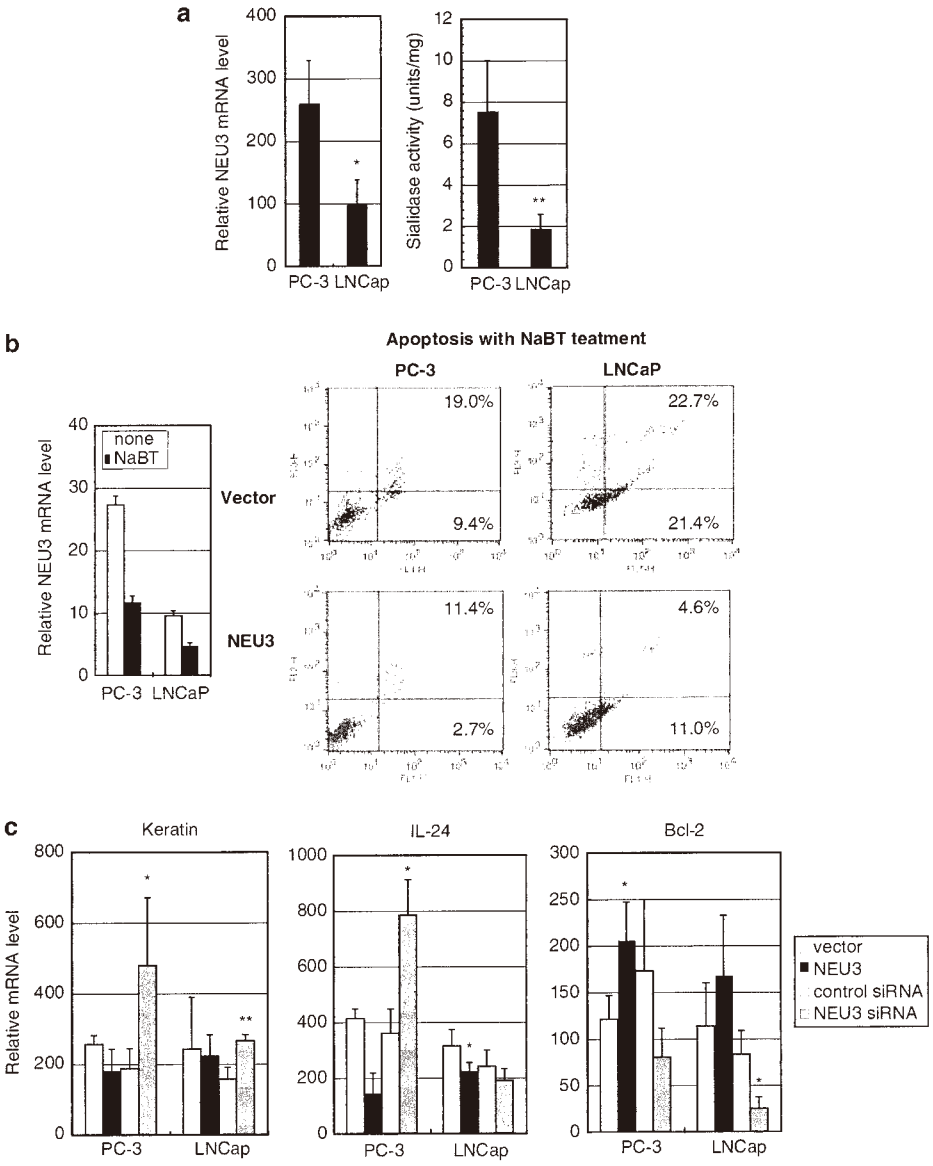

Figure 2 Altered expression of differentiation- and apoptosis-related molecules by NEU3 in human prostate cancer cell lines. (**a**) NEU3 expression in mRNA and sialidase activity levels in LNCaP cells and PC-3 cells. The data given are mean values from five to seven experiments ± S.D. *P*-values (**P* = 0.015, ***P* = 0.0003) were evaluated by the Student's *t*-test, and compared with PC-3 cells. (**b**) Apoptosis induction of PC-3 and LNCaP cells by treatment with sodium butyrate, and apoptosis suppression by NEU3 overexpression. Apoptosis was assessed by FACS analysis with AnnexinV. Results are representative of three independent experiments. (**c**) Measurement of mRNA levels of keratin 17 and IL24, and Bcl-2 in NEU3-silencing or -overexpressing cells. **P* < 0.05, ***P* < 0.01 compared with control siRNA or vector by the Student's *t*-test

phosphorylation of AKT and ERK in the same condition (Figure 4c). To elucidate further how NEU3 affects these pathways, upstream molecules were investigated. We previously demonstrated that NEU3 promotes phosphorylation of EGFR by enhancing dimerization in HeLa cells.[20] It has also been reported that the EGFR family modulates AR signaling and contributes androgen-independent tumor progression.[24–28] Expression levels of EGFR family were therefore evaluated as possible targets for NEU3 (Figure 4d). NEU3 was found to increase EGFR and ERBB2 in mRNA and protein levels together with AR and PSA elevation in LNCaP cells under androgen-deficient conditions, although they behaved differently in the presence of DHT. Phosphorylation level of ERBB2 was enhanced on a parallel with increase in the protein level, and DHT addition caused marked reduction of the phosphorylation. EGFR phosphorylation was not detectable under the condition as expected, but addition of EGF led to the higher phosphorylation level in *NEU3* overexpressing cells than the control cells (Figure 4e). Interestingly, ERK phosphorylation was always augmented by NEU3, independent of androgen or EGF. These results suggest

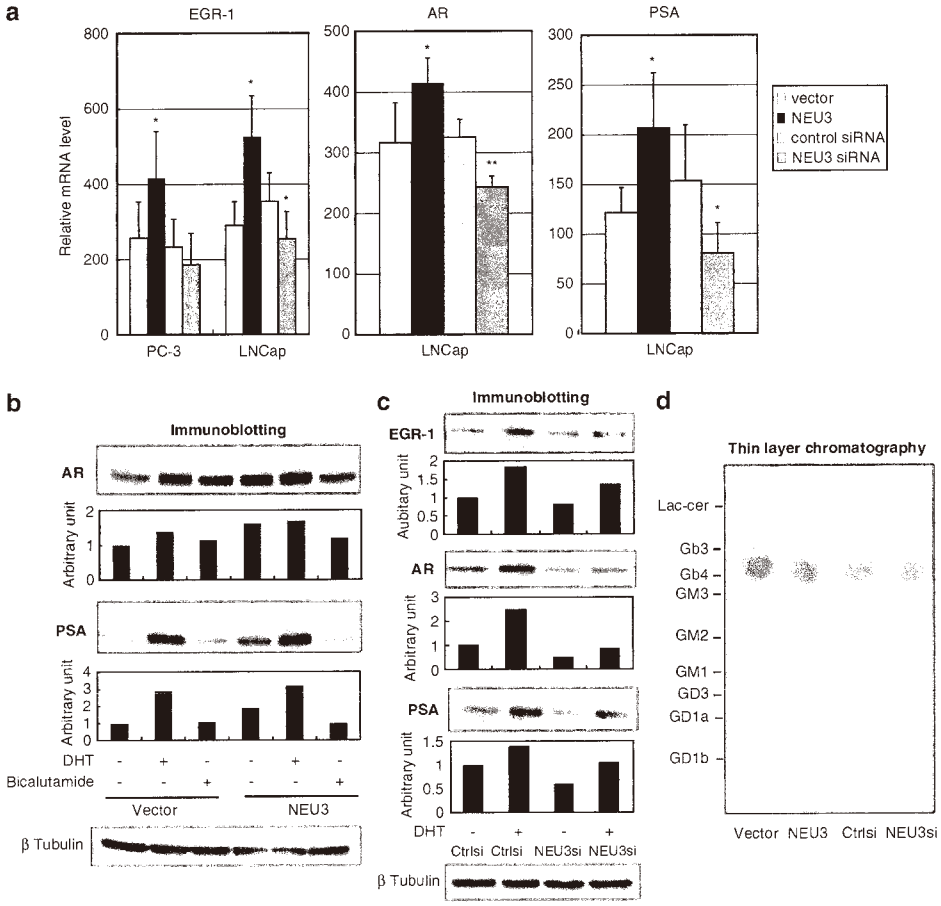

Figure 3 Altered expression of AR signaling-related molecules by NEU3 in LNCaP cells. (**a**) Altered mRNA expression of AR signaling-related molecules in NEU3-silencing or -overexpressing cells. $^{*}P < 0.05$, $^{**}P < 0.01$ compared with control siRNA or vector. EGR-1, AR and PSA levels were assessed by RT–PCR as described in Materials and Methods. (**b**) Protein levels of AR and PSA in the presence of DHT or bicalutamide in NEU3-overexpressing and control cells as assessed by immunoblotting with respective antibodies. (**c**) Protein levels of EGR-1, AR and PSA in the presence or absence of DHT in NEU3-silencing or control cells as assessed by immunoblotting. In **b** and **c**, the results are representative of three independent experiments. Quantitative data are presented as values relative to those in the cells treated with the vector or siRNA control in the absence of DHT and bicalutamide. (**d**) Thin-layer chromatography of glycolipids from NEU3-overexpressing and -silencing cells. After development, the glycolipids were visualized with orcinol–H_2SO_4. Results are representative of three independent experiments

that NEU3 activates AR signaling probably via induction of EGFR and/or ERBB2 under androgen-deficient conditions.

NEU3 potentiates DHT-dependent cell growth. To determine the effects of NEU3-mediated activation of AR signaling on cell proliferation, *NEU3* transfectants were cultured in the presence of 5 nM DHT or 5 μM antiandrogen bicalutamide (Figure 5a). DHT-induced LNCaP cell proliferation was remarkably increased as compared with the case with the vector control, and even 1 nM DHT caused significant stimulation of cell growth (data not shown), indicating that NEU3 enhances sensitivity to androgen, presumably via increase in numbers of ARs. Furthermore, interestingly, NEU3 stimulated cell growth even in the presence of bicalutamide. We do not know the mechanism of the NEU3 effects, but it has been suggested that increased AR expression converts even antagonists to weak agonists.[1,2] When AR were silenced to 10–15% the level of control cells, the cell growth rate was significantly reduced as compared with the cells having control AR shown in Figure 5a, implying AR dependence (Figure 5b). In *AR*-silenced cells, however, growth stimulation by NEU3 gradually occurred with an evident response to DHT after 3 days, even when decreased level of AR was sustained (to less than 15% of the control level for 5 days), possibly due to compensatory activation of AR signaling. To examine the possibility whether *AR* silencing gives any influence on expression levels of AR signaling related molecules, the protein and mRNA levels were evaluated in *AR* silencing LNCaP cells (Figure 5c). Under conditions in which AR and PSA was reduced profoundly, *AR* silencing stimulated ERK phosphorylation (left panel) and increased NEU3 and EGR-1 expression level (right panel), suggesting that the compensatory activation of AR signaling occurs as the results of NEU3 and EGR-1 elevation at the endogenous level. Reduced AR expression, including that following castration, thus might bring about NEU3 elevation, and finally end up with increased AR and continued cell growth. Taken together, NEU3 upregulation in prostate cancer

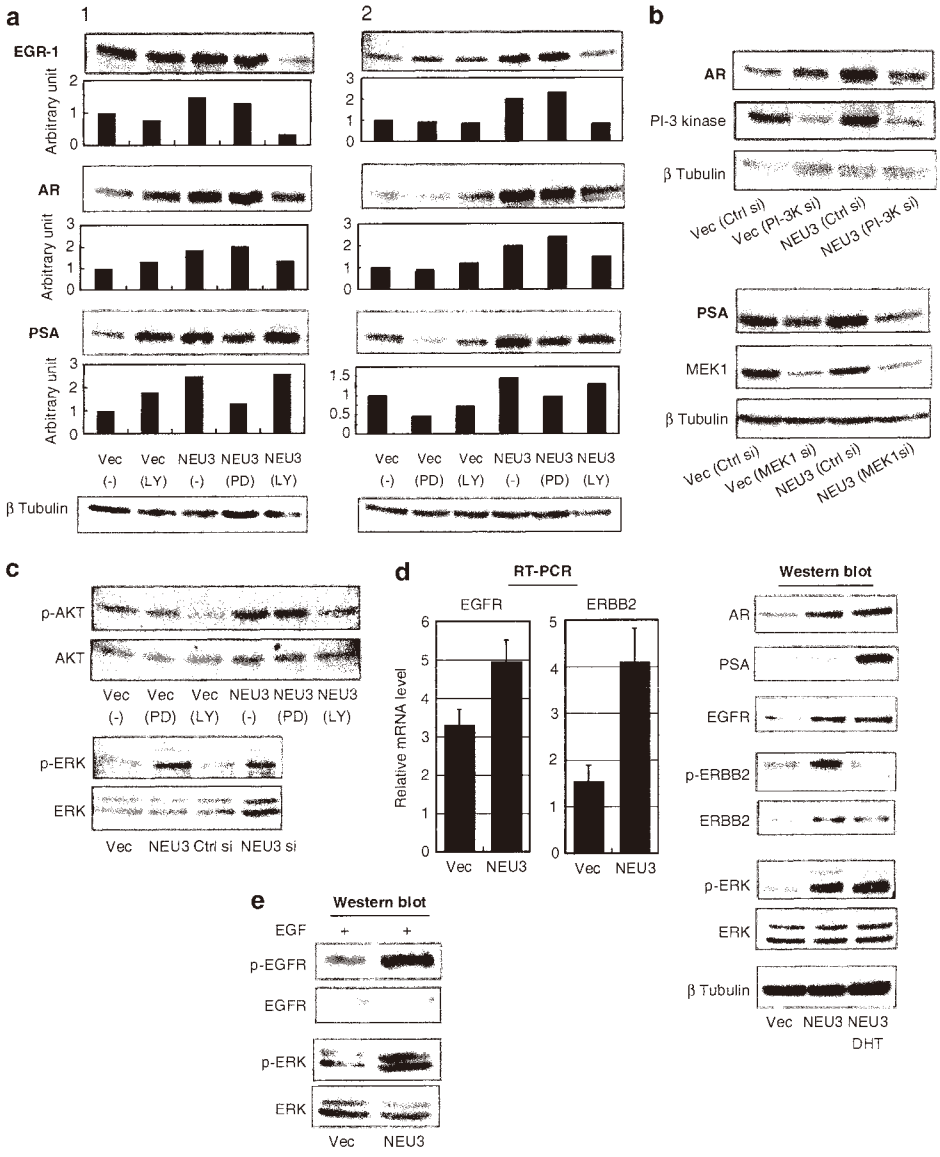

Figure 4 Activation of AR signaling by NEU3 via PI3K and MAPK pathway in LNCaP cells. (**a**) Effects of specific inhibitors of PI3K (LY294002) and MAPK (PD098059) on NEU-3-mediated increase in EGR-1, AR and PSA protein levels, as assessed by immunoblotting. The results are two representatives of four independent experiments. Quantitative data are presented as described in Figure 3. (**b**) Effects of silencing of PI3K and MAPKK on NEU-3-mediated increase in AR and PSA. The siRNAs for PI3K p110α and for MAPKK (MEK1/2) were separately introduced to block specifically these kinase expressions. Similar results were obtained in two independent experiments. (**c**) Increased phosphorylation of AKT and ERK by NEU3. (**d**) Increased expression of EGFR and ERBB2 by NEU3 as evaluated by RT–PCR (left panel) and immunoblotting (right panel), respectively. Enhanced phosphorylation of ERBB2 and ERK by NEU3 under androgen-depleted condition (left panel). (**e**) Phosphorylation of EGFR and ERK by NEU3 in the presence of EGF

indeed causes elevation of EGR-1, AR and PSA expression by activating AKT and ERK at least partly through EGFR family activation, leading to increasing sensitivity to low concentration of androgen and to progressive cell growth, under androgen-deficient conditions (Figure 5d). NEU3 upregulation may trigger off activation of AR pathway probably via EGFR family followed by ERK activation, leading to transcriptional activation of *NEU3* itself by SP1 transcription factor in positive feedback loop, as Sp1 is phosphorylated by ERK and *NEU3* is an SP1 target gene.[29]

***NEU3* gene silencing with siRNA suppresses prostate cancer growth.** To investigate the effects of siRNA-mediated *NEU3* silencing on prostate cancer growth and survival, NEU3 siRNA was introduced into the cells and xenografts. Figure 6a shows that *NEU3* silencing caused reduction in the number of viable cells of the both prostate cancer cell lines as measured by MTT assays, whereas they continued to proliferate after treatment with a control siRNA treatment. In LNCaP cells, *NEU3* silencing brought about decreased expression of EGR-1, AR and PSA as shown in

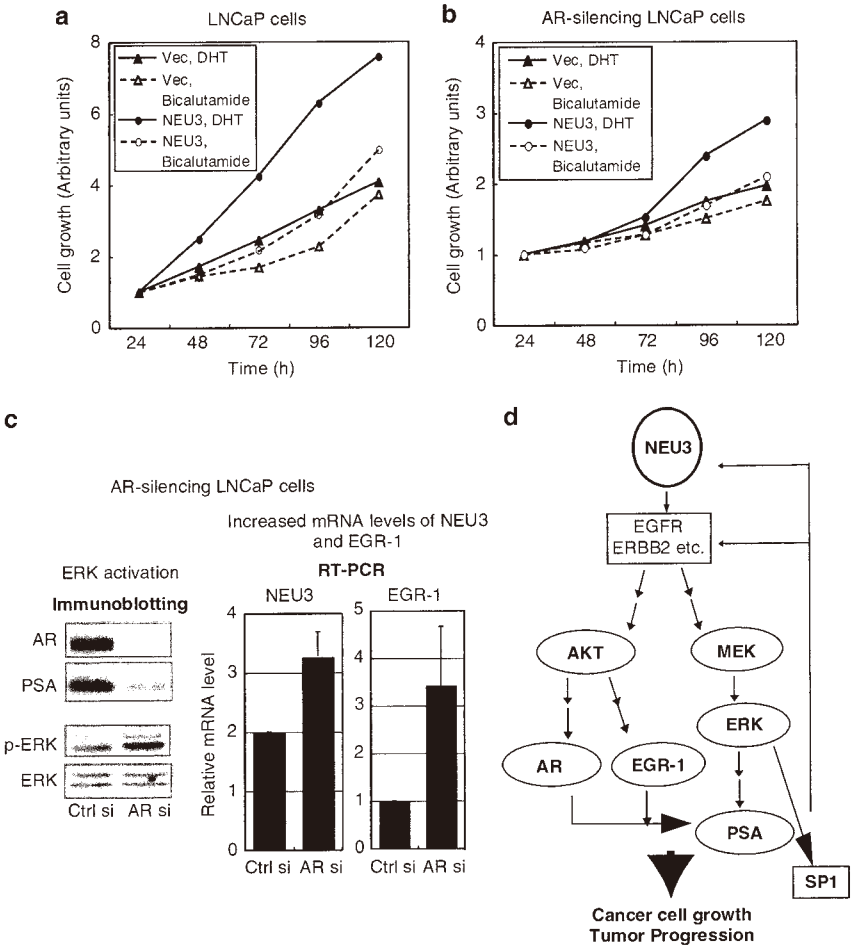

Figure 5 Acceleration of androgen-dependent cell growth by NEU3 in LNCaP cells. An increase in DHT-induced cell proliferation by NEU3 in LNCaP cells (**a**) and in *AR* silencing LNCaP cells (**b**), as determined by MTT assays. (**c**) Increased expression of NEU3 and EGR-1 (in RT–PCR, right panel) in *AR* silencing cells under conditions in which AR and PSA were reduced profoundly (in immunoblotting, left panel). Stimulated ERK phosphorylation seen by *AR* silencing (left panel). (**d**) Proposed model of a possible activation pathway of AR signaling regulated by NEU3 under androgen-deficient conditions

Figure 3c, contributing to the suppression of cell growth. The NEU3 siRNA-treated cells showed apoptosis at 72–96 h as assessed by a TUNEL assay (data not shown), as we previously described in HeLa cells.[20] To further test the utility of NEU3 siRNA as a therapeutic agent for prostate cancer *in vivo*, androgen-independent PC-3 cells, which feature higher NEU3 expression and stronger apoptosis-resistance than LNCaP cells, were implanted subcutaneously into nude mice. When the tumor volume reached at least 70–80 mm^3 at 3–4 weeks later, 10 mice for each group were administered NEU3 siRNA–atelocollagen complexes or atelocollagen[30,31] alone into the tumors. The volume of tumors injected with NEU3 siRNA was statistically less than that of control tumors, which continued to increase in size, and the 500 pmol dose siRNA was more effective than 250 pmol (Figure 6b). Immunohistological examination revealed suppressed NEU3 protein expression as well as lowered Ki-67 labeling together with more apoptotic cells in the siRNA-effective cases, whereas mitosis was observed frequently on HE staining and the Ki-67 labeling index was higher in control tumors (Figure 6c). These results indicate that the tumor reduction is probably due to inhibition of NEU3 expression.

Discussion

In this study, we demonstrated NEU3 expression to be markedly increased in human prostate cancers, and that upregulation caused suppression of cell differentiation and apoptosis. We also found that NEU3 activated AR signaling by increasing mRNA and protein levels of EGR-1, AR and PSA in LNCaP cells, to levels sufficient to maintain androgen-independent growth.[1] Silencing of the *NEU3* gene with an siRNA significantly inhibited prostate cancer cell growth, and administration of siRNA–atelocollagen complexes suppressed NEU3 protein expression, resulting in a decreased growth rate of nude mouse-transplanted tumors.

Our previous observations[20] revealed that *NEU3* silencing induces apoptosis with no specific stimuli, accompanied by decreased Bcl-xL and increased Bax mRNA levels as well as

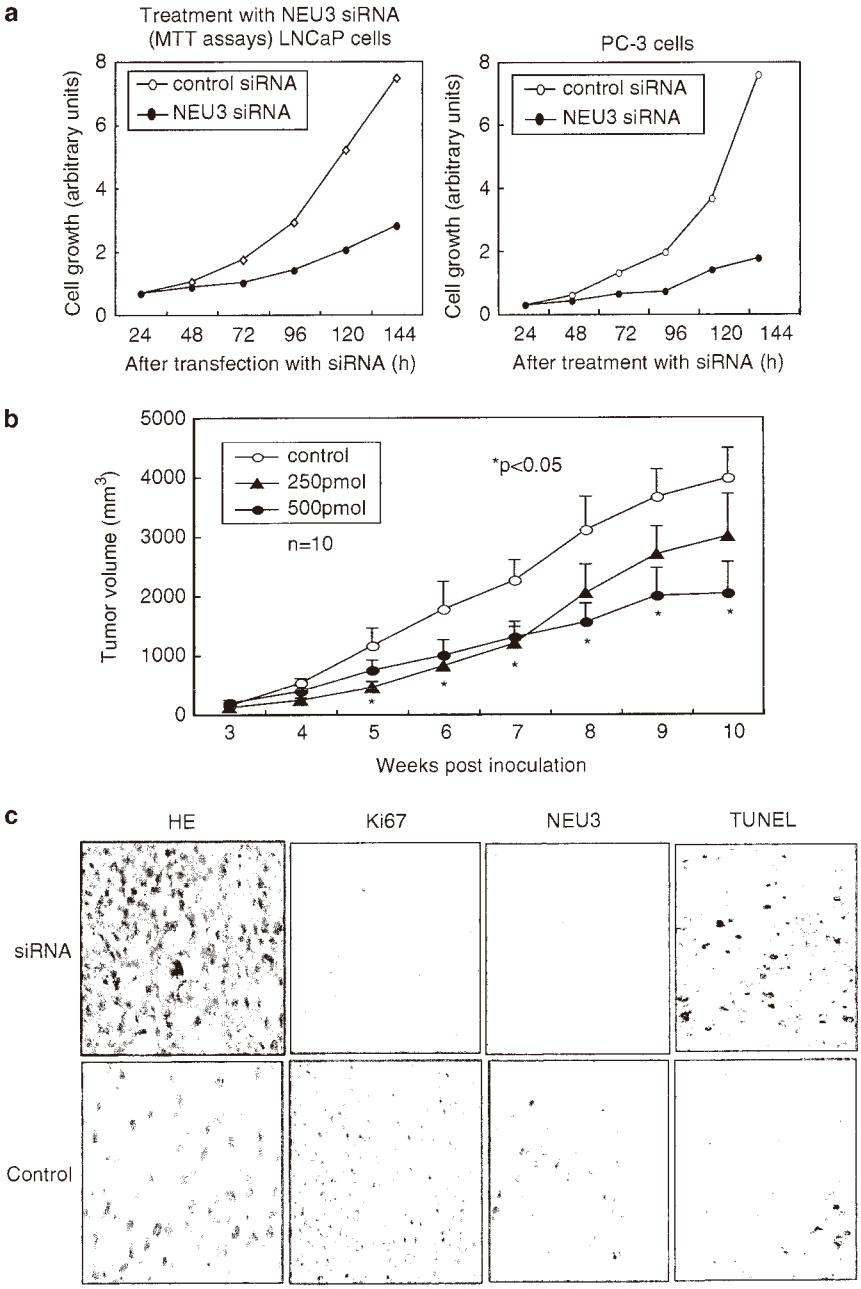

Figure 6 Suppression of prostate cancer growth *in vitro* and *in vivo* by treatment with NEU3 siRNA. (**a**) Reduction in the number of LNCaP and PC-3 cells by treatment with NEU3-specific siRNA, as assessed by MTT assays. (**b**) Reduction of the tumor volumes of xenografts implanted PC-3 cells by NEU3 siRNA treatment with atelocollagen. Different doses of NEU3 siRNA (0, 250 or 500 pmol) were injected into three groups of athymic nude mice ($n = 10$ for each condition) and the tumor diameters were measured and compared as described in Materials and Methods. The statistical analyses were performed using the Kruska–Wallis test. (**c**) HE staining (left panel) and immunohistological staining of tumor tissues from the mice with anti-Ki-67 and -NEU3 antibodies (two middle panels). Detection of apoptosis by TUNEL method in the tissues was carried out using an apoptosis detection kit (right panel)

caspase-3 activation in HeLa cells. The siRNA treatment here reduced invasiveness and motility of cancer cells, and interestingly, did not affect normal cells, even if NEU3 levels were efficiently suppressed. Furthermore, *NEU3* overexpression enhanced Ras activation and consequent stimulation of ERK and AKT, whereas the NEU3 siRNA inhibited Ras activity with downregulation of ERK and the AKT pathway. These results indicate that NEU3 has an important role in cancer cell survival, and its increased expression promotes malignancy probably by modulating Ras-mediated signaling.

In prostate cancer cells, consistent with other types of cancer, NEU3 activated the PI3K and MAPK pathways,

associated with increase in mRNA and protein levels of growth factor receptors including EGFR and ERBB2 under androgen-deficient conditions. For development of hormone-refractory progression, it has been reported that enhanced AR mRNA and protein expression is a critical factor in conversion to a hormone-refractory state in the majority of patients who do not have AR mutations[3] or amplification.[4,5] Other mechanisms include cross-talk between ARs and other signaling pathways, perhaps mediated by growth factor receptors such as EGFR and ERBB2. In this context, NEU3 might again be a pivotal molecule acting to upregulate growth factor receptors. We do not know the detailed mechanism of the NEU3-mediated upregulation at present. However, our recent studies suggest the possibility that NEU3 undergoes transcriptional activation by SP1 transcription factor,[29] which is positively regulated by several kinases including ERK[32] and involved in transcriptional regulation of genes implicated in cell growth and tumorigenesis including EGFR.[33] As proposed in Figure 5d, NEU3 upregulation may give rise to the increased expression of NEU3 itself and EGFR family by activating ERK and then SP1 in positive feedback loop. In addition to this transcriptional regulation, NEU3 may also positively regulate function of growth factor receptors probably through its association with the receptors and glycolipid changes as a result of its catalytic reaction.[12] Our previous results showed that NEU3 changed glycolipid pattern, such as an accumulation of lactosylceramide in colon cancer,[13] and in addition, NEU3 was co-immunoprecipitated with EGFR in HeLa cells.[20] The examination of glycolipid changes by thin-layer chromatography in this study also revealed an increase in lactosylceramide in *NEU3* overexpressing LNCap cells, although it is uncertain how the changes affect the growth factor receptors and it cannot be excluded the possibility of an involvement of other subtle glycolipid change.

In conclusion, our present observations strongly suggest that NEU3 is a pivotal molecule for regulation of progression of prostate cancer to androgen-independent growth. NEU3 might be used for the development of a new diagnostic approach capable of determining the malignant grade, and also as an excellent target for prostate cancer therapy by selective suppression of NEU3 using specific siRNAs.

Materials and Methods

Patient samples. The specimens of tumor and non-tumor prostate tissues were obtained by transrectal needle biopsy from 34 patients diagnosed with prostate cancer at various clinical stages and 35 non-cancer patients including examples with benign hyperplasia. Histopathological findings of the needle biopsy specimens confirmed the diagnosis for all patients by examination of the specimens from the almost identical portion. Informed consent was obtained from each to allow use of the specimens for research purposes, and the study was approved by the Committee on Human Rights in Research at Miyagi Cancer Center.

Cell lines and cell culture conditions. Human prostate cancer cell lines PC-3 (HSRRB, Osaka, Japan) and LNCaP-FGC (Cancer Cell Repository, Tohoku University, Sendai, Japan) were maintained in Ham F-12K containing 8% fetal bovine serum (FBS) and in RPMI 1640 containing 10% FBS, respectively. To assess AR signaling, LNCaP cells were cultured in phenol-red free RPMI 1640 medium supplemented with charcoal-stripped 10% FBS for 24–48 h, and treated with 1 or 5 nM DHT (Sigma, St Louis, MO, USA) or 5 μM bicalutamide (Toronto Research Chemicals Inc., Toronto, ON, Canada) for 24 h before harvesting. In some experiments, LNCaP cells were incubated in RPMI 1640 medium with 50 μM LY294002 and 20 μM PD098059 (inhibitors of PI3K and MAPK, respectively) for 24 h.

Transfections. For *NEU3* overexpression, the entire open reading frame (1.2 kb) of the human *NEU3* gene was inserted into a retrovirus vector pMXs-puro and the plasmid was introduced into PlatA, and target cells were then incubated with the culture media containing infectious viruses for two days and selected by cultivating in the presence of 1 μg/ml puromycin for 10–14 days as previously described.[34] siRNAs targeting *NEU3* and control scrambled siRNA were synthesized by Dharmacon Inc. (Thermo Fisher Scientific, Rockford, IL, USA) as described.[20] One of the siRNAs targeting *NEU3* (no. 3) was 5′-AAGG GAGTGTGGTAAGTTT-3′ beginning at nucleotide 839 of the *NEU3* open reading frame sequence, and the scrambled control was 5′-GCGATTAATGTAGGTT CGA-3′. The other siRNA targeting *NEU3* synthesized by iGENE Therapeutics (Tsukuba, Japan) was 5′-GGTTACAGTAGAATGTGAAGTGGCA-3′. These two types of siRNA targeting *NEU3* showed 75–95% *NEU3* reduction and almost same results in various experiments, and therefore, the former was routinely utilized. siRNAs targeting *AR* (On-Target plus SMART pool L-003400), *PIK3CA* (siGENOME SMART pool M-003018), and *MAP2K1* (siGENOME SMART pool M-003571) and a control siRNA (On-Target plus siControl Non-Targeting siRNA#2) were from Dharmacon Inc (Thermo Fisher Scientific). Transfection was performed by nucleofection or with a Lipofectamine RNAiMAX reagent (Invitrogen, Carlsbad, CA, USA), and cells were used for experimentation at 24–48 h thereafter.

Sialidase activity assays. Crude extracts were used for sialidase assays using bovine brain gangliosides GM3 (Alexis Biochemicals, Lansen, Switzerland) as the substrate in the presence of Triton X-100 as described elsewhere.[20] After incubation at 37 °C for 10–30 min, the amount of sialic acid released was determined by a modified thiobarbituric acid method or by fluorometric high-performance liquid chromatography with malononitrile.[35] One unit of activity was defined as the amount of enzyme that cleaved 1 nmol sialic acid from the substrates. Protein concentrations were determined by dye-binding assay (Bio-Rad Laboratories, Hercules, CA, USA).

Quantitative RT–PCR analysis. The mRNA levels of human NEU3 and other molecules were evaluated by quantitative RT–PCR (real-time PCR, Lightcycler, Roche Diagnostics) as described previously.[20] Total RNA was isolated from biopsy specimens, as well as from PC-3 and LNCaP cells with an RNeasy kit (Qiagen, Hilden, Germany), and first strand cDNAs synthesized by reverse transcription were used as templates for PCR. Human *NEU3* primers were 5′-AGGTCAGTCTCCAGTACCTTC-3′ (forward) and 5′-ACATCCAGCATCCTGACT GTAG-3′ (reverse). The others were: for *keratin 17*, 5′-GCTGGAGGTGAAGATCC GTGA-3′ (forward) and 5′-ATTGTCCACGGTGGCTGTGA-3′ (reverse); *IL24*, 5′-ACC CACAGCTATGCCTCTGATTG-3′ (forward) and 5′-TGTTAAATTGGCGAAAGC AGCTC-3′ (reverse); *Bcl-2*, 5′-GTACGACAACCGGGAGATAGTGAT-3′ (forward) and 5′-GCCTCCGTTATCCTGGATCCAGGT-3′ (reverse); *EGR-1*, 5′-CAGGGCTT TCGGACATGACA-3′ (forward) and 5′-GACTTGGCTCTGAGAACCTCCATC-3′ (reverse); *AR*, 5′-ACTTCACCGCACCTGATGTG-3′ (forward) and 5′-TTCCGAAGAC GACAAGATGGA-3′ (reverse); *PSA*, 5′-CAACCCTGGACCTCACACCTA-3′ (forward) and 5′-GGAAATGACCAGGCCAAGAC-3′ (reverse); *EGFR*, 5′-TGGTCCTTGGGA ATTTGGAA-3′ (forward) and 5′-GGGCAATGAGGACATAACCAG-3′ (reverse); *ERBB2*, 5′-TGGGAGCCTGGCATTTCTG-3′ (forward) and 5′-TCCGGCCATGC TGAGATGTA-3′ (reverse). To normalize for sample variation, human β-actin was assayed as an internal control. Densitometric analyses of PCR products were carried out with Quantity One 1D-analysis software (Bio-Rad Laboratories).

Immunoblotting. Cells were homogenized and solubilized in five volumes of ice-cold buffer (50 mM Hepes (pH 7.5), 150 mM NaCl, 1% NP-40, 0.25% deoxycholate, 2 mM EDTA, 10 mM NaF, 2 mM Na_3VO_4, 2 mM PMSF, 7.5 μg/ml aprotinin and 10 μg/ml leupeptin) for immunoblotting. The cell lysates were separated on SDS–PAGE under reducing conditions, and analyzed by immunoblotting with the respective antibodies using ECL Plus Western blotting reagent (GE Healthcare UK Ltd., Buckinghamshire, UK). Antibodies for EGR-1 and PSA were from Santa Cruz (Santa Cruz, CA, USA) and for AR from Upstate. Anti-Akt, anti-phospho-Akt (Ser473), anti-p44/42 MAPK, anti-phospho-p44/42 MAPK (Thr202/Tyr204) and anti-PI3K p110α (C73F8) antibodies were from Cell Signaling Technology (Danvers, MA, USA), and anti-MEK1 antibody was from BD Biosciences (San Jose, CA, USA).

Thin-layer chromatography. Glycolipids were extracted from LNCaP cells as described elsewhere,[14] fractionated by thin-layer chromatography on HPTLC

plates (Baker, Phillipsburg, NJ, USA) in C/M/0.5%. $CaCl_2$ (60 : 40 : 9, v/v/v) and visualized with orcinol–H_2SO_4.

Mouse models for tumor therapy. To generate tumor xenografts, PC-3 cells (6.0×10^6) were injected subcutaneously in 100 μl of serum-free F-12K medium through a 27-gauge needle into the lower flanks of 8-week-old athymic nude mice obtained from CLEA Japan Inc. (Tokyo, Japan). After 3–4 weeks when the tumor volume had reached at least 70–80 mm^3, the tumor-bearing nude mice were treated with NEU3 siRNA with atelocollagen (Koken Co. Ltd, Tokyo, Japan).[30,31] The concentration of atelocollagen was 1%, and different doses (0, 250, 500 pmol) of NEU3 siRNA (siSTABLE stability-enhanced oligonucleotide, Dharmacon Inc.) and one scrambled siRNA of the same type (500 pmol) were administrated into the tumors two times every week. Tumor diameters were measured at maximum length and width with digital calipers, and the tumor volume was calculated by the ellipsoid formula: volume = $(\text{width})^2 \times \text{length}/2$.[36] The data were statistically analyzed using the Kruskal–Wallis test for overall comparisons and the Tukey/Scheffe test for multiple pairwise comparisons. *P*-values < 0.05 were considered to be significant. All animal experiments in this study were performed in compliance with the guidelines of Laboratory Animal Research, Miyagi Cancer Center Research Institute.

Immunohistochemistry. Removed tissues were fixed in 10% neutral buffered formaldehyde 7 days, routinely processed for embedding in paraffin, and sectioned 2.5 mm thickness. To assess NEU3 and ki-67 expression, the sections were pretreated for antigen recovery by heating in 0.01 M citrate (pH 6.0) in microwave oven, and incubated with the anti-NEU3 monoclonal antibody prepared previously[37] and an anti-Ki67 antibody (Dako Cytomation, Dako, Glostrup, Denmark), respectively. Determination of cell apoptosis in tumor tissues was performed using an ApopTag plus peroxidase *in situ* apoptosis detection kit (Chemicon International Inc., Hants, UK) according to the manufacturer's instructions.

Conflict of Interest

The authors declare no conflict of interest.

Acknowledgements. We are grateful for Dr. Ochiya T (National Cancer Center, Tokyo) for his helpful suggestion for usage of atelocollagen. This work was supported in part by CREST of Japan Science and Technology Agency and by Grants-in Aid (on priority areas 20013047) for Scientific Research on Priority Areas in Cancer from the Ministry of Education, Culture, Sports, Science and Technology of Japan.

1. Heinlein CA, Chang C. Androgen receptor in prostate cancer. *Endocr Rev* 2004; **25**: 276–308.
2. Chen CD, Welsbie DS, Tran C, Baek SH, Chen R, Vessella R *et al.* Molecular determinants of resistance to antiandrogen therapy. *Nat Med* 2004; **10**: 33–39.
3. Taplin ME, Bubley GJ, Shuster TD, Frantz ME, Spooner AE, Ogata GK *et al.* Mutation of the androgen-receptor gene in metastatic androgen-independent prostate cancer. *N Engl J Med* 1995; **332**: 1393–1398.
4. Linja MJ, Savinainen KJ, Saramaki OR, Tammela TL, Vessella RL, Visakorpi T. Amplification and overexpression of androgen receptor gene in hormone-refractory prostate cancer. *Cancer Res* 2001; **61**: 3550–3555.
5. Edwards J, Krishna NS, Grigor KM, Bartlett JM. Androgen receptor gene amplification and protein expression in hormone refractory prostate cancer. *Br J Cancer* 2003; **89**: 552–556.
6. Bakin RE, Gioeli D, Sikes RA, Bissonette EA, Weber MJ. Constitutive activation of the Ras/mitogen-activated protein kinase signaling pathway promotes androgen hypersensitivity in LNCaP prostate cancer cells. *Cancer Res* 2003; **63**: 1981–1989.
7. Rahman M, Miyamoto H, Chang C. Androgen receptor coregulators in prostate cancer: mechanism and clinical implications. *Clin Cancer Res* 2004; **10**: 2208–2219.
8. Abdulkadir SA, Qu Z, Garabedian E, Song SK, Peters TJ, Svaren J *et al.* Impaired prostate tumorigenesis in Egr1-defficient mice. *Nat Med* 2001; **7**: 101–107.
9. Yang S-Z, Eltoum IA, Abdulkadir SA. Enhanced EGR-1 activity promotes the growth of prostate cancer cells in an androgen-deleted environment. *J Cell Biochem* 2006; **97**: 1292–1299.
10. Yang S-Z, Abdulkadir SA. Early growth response gene1 modulates androgen receptor signaling in prostate carcinoma cells. *J Biol Chem* 2003; **278**: 39906–39911.
11. Miyagi T, Wada T, Yamaguchi K. Review: roles of plasma membrane- associated sialidase NEU3 in human cancers. *Biochim Biophys Acta* 2008; **1780**: 532–537.
12. Miyagi T, Wada T, Yamaguchi K, Hata K, Shiozaki K. JB minireview: plasma membrane-associated sialidase as a crucial regulator of transmembrane signalling. *J Biochem* 2008; **144**: 279–285.
13. Kakugawa Y, Wada T, Yamaguchi K, Yamanami H, Ouchi K, Sato I *et al.* Up-regulation of plasma membrane- associated ganglioside sialidase (Neu3) in human colon cancer and its involvement in apoptosis suppression. *Proc Natl Acad Sci USA* 2002; **99**: 10718–10723.
14. Ueno S, Saito S, Wada T, Yamaguchi K, Satoh M, Arai Y *et al.* Plasma membrane-associated sialidase is up-regulated in renal cell carcinoma and promotes the interleukin-6 - induced apoptosis suppression and cell motility. *J Biol Chem* 2006; **281**: 7756–7764.
15. Nomura H, Tamada Y, Miyagi T, Suzuki A, Taira M, Suzuki N *et al.* Expression of NEU3 (plasma membrane-associated sialidase) in clear cell adenocarcinoma of the overy: its relationship with T factor of pTNM classification. *Oncol Res* 2006; **16**: 289–297.
16. Hakomori S. Glycosylation defining cancer malignancy: new wine in an old bottle. *Proc Natl Acd Sci USA* 2002; **99**: 10231–10233.
17. Varki NM, Varki A. Diversity in cell surface sialic acid presentations: implications for biology and disease. *Lab Invest* 2007; **87**: 851–857.
18. Lau KS, Dennis JW. N-glycans in cancer progression. *Glycobiology* 2008; **18**: 750–760.
19. Miyagi T. Aberrant expression of sialidase and cancer progression. *Proc Jpn Acad, Ser B Phys Biol Sci* 2008; **84**: 407–418.
20. Wada T, Hata K, Yamaguchi K, Shiozaki K, Koseki K, Moriya S *et al.* A crucial role of plasma membrane-associated sialidase in the survival of human cancer cells. *Oncogene* 2007; **26**: 2483–2490.
21. Kato K, Shiga K, Yamaguchi K, Hata K, Kobayashi T, Miyazaki K *et al.* Plasma membrane-associated sialidase (NEU3) differentially regulates integrin-mediated cell proliferation through laminin- and fibronectin-derived signaling. *Biochem J* 2006; **394**: 647–656.
22. Ravindranath MH, Muthugounder S, Presser N, Ye X, Brosman S, Morton DL. Endogenous immune response to gangliosides in patients with confined prostate cancer. *Int J Cancer* 2005; **116**: 368–377.
23. Manin M, Baron S, Goossens K, Beaudoin C, Jean C, Veyssiere G *et al.* Androgen receptor expression is regulated by the phosphoinositide 3-kinase/Akt pathway in normal and tumor epithelial cells. *Biochem J* 2002; **366**: 729–736.
24. Craft N, Shostak Y, Carey M, Sawyers CL. A mechanism for hormone-independent prostate cancer through modulation of androgen receptor signaling by the HER-2/neu tyrosine kinase. *Nat Med* 1999; **5**: 280–285.
25. Gregory CW, Fei X, Ponguta LA, He B, Bill HM, French FS *et al.* Epidermel growth factor increases coactivation of the androgen receptor in recurrent prostate cancer. *J Biol Chem* 2004; **279**: 7119–7130.
26. Berger R, Lin DI, Nieto M, Sicinska E, Garraway LA, Adams H *et al.* Androgen-dependent regulation of Her-2/neu in prostate cancer cells. *Cancer Res* 2006; **66**: 5723–5728.
27. Pignon J-C, Koopmansch B, Nolens G, Delacroix L, Waltregny D, Winkler R. Androgen receptor controls EGFR and ERBB2 gene expression at different levels in prostate cancer cell lines. *Cancer Res* 2009; **69**: 2941–2949.
28. Cai C, Portnoy DC, Wang H, Jiang X, Chen S, Balk SP. Androgen receptor expression in prostate cancer cells is suppressed by activation of epidermal growth factor receptor and ErbB2. *Cancer Res* 2009; **69**: 5202–5209.
29. Yamaguchi K, Koseki K, Shiozaki M, Shimada Y, Wada T, Miyagi T. Regulation of plasma membrane-associated sialidase *NEU3* gene by Sp1/Sp3 transcription factors. *Biochem J* 2010; **430**: 107–117.
30. Ochiya T, Takahama Y, Nagahara S, Sumita Y, Hisada A, Itoh H *et al.* New delivery system for plasmid DNA *in vivo* using atelocollagen as a carrier material: the Minipellet. *Nat Med* 1999; **5**: 707–710.
31. Takeshita F, Minakuchi Y, Nagahara S, Honma K, Sasaki H, Hirai K *et al.* Efficient delivery of small interfering RNA to bone-metastatic tumors by using atelocollagen *in vivo*. *Proc Natl Acad Sci USA* 2005; **102**: 12177–12182.
32. Wierstra I. Sp1: emerging roles – beyond constitutive activation of TATA-less housekeeping genes. *Biochem Biophys Res Commun* 2008; **372**: 1–13.
33. Safe S, Abdelrahim M. Sp transcription factor family and its role in cancer. *Eur J Cancer* 2005; **41**: 2438–2448.
34. Kitamura T, Koshino Y, Shibata F, Oki T, Nakajima H, Nosaka T *et al.* Retrovirus-mediated gene transfer and expression cloning: powerful tools in functional genomics. *Exp Hematol* 2003; **31**: 1007–1014.
35. Li K. Determination of sialic acids in human serum by reversed-phase liquid chromatography with fluorimatric detection. *J Chromatogr* 1992; **579**: 209–213.
36. Burfeind P, Chernicky CL, Rininsland F, Ilan J, Ilan J. Antisense RNA to the type I insulin-like growth factor receptor suppresses tumor growth and prevents invasion by rat prostate cancer cells *in vivo*. *Proc Natl Acad Sci USA* 1996; **93**: 7263–7268.
37. Wang Y, Yamaguchi K, Wada T, Hata K, Zhao X, Fujimoto T *et al.* A close association of ganglioside-specific sialidase, Neu3, with caveolin in membrane microdomains. *J Biol Chem* 2002; **277**: 26252–26259.

平成 24 年度～平成 28 年度私立大学戦略的研究基盤形成支援事業研究成果報告書

平成 29 年 5 月発行

編集　私立大学戦略的研究基盤形成支援事業(分子生体膜研究所)運営委員会

発行　東北医科薬科大学

〒981-8558　仙台市青葉区小松島 4-4-1

TEL　022-234-4181

印刷　株式会社東北プリント

平成24年度～平成28年度私立大学戦略的研究基盤形成支援事業研究成果報告書

平成29年５月発行

編集　私立大学戦略的研究基盤形成支援事業（創薬研究）運営委員会
発行　東北医科薬科大学
〒981-8558　仙台市青葉区小松島 4-4-1
TEL 022-234-4181
印刷　株式会社東北プリント